Government of **Western Australia**
Department of **Mines and Petroleum**

RECORD 2010/18

Fifth International Archean Symposium Abstracts

Edited by
IM Tyler and CM Knox-Robinson

5iaS 2010 Perth

Geo conferences (WA) Inc.


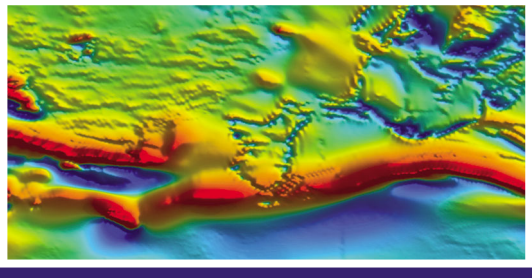


Geological Survey of Western Australia

Presented by Geoconferences (WA) Inc

Fifth International Archean Symposium

Burswood Entertainment Complex
5–9 September 2010
Perth, Western Australia

Abstracts

Edited by IM Tyler and CM Knox-Robinson

MINISTER FOR MINES AND PETROLEUM
Hon. Norman Moore MLC

DIRECTOR GENERAL, DEPARTMENT OF MINES AND PETROLEUM
Richard Sellers

ACTING EXECUTIVE DIRECTOR, GEOLOGICAL SURVEY OF WESTERN AUSTRALIA
Rick Rogerson

Disclaimer
The organisers of this conference have tried to ensure that the information in this volume is as accurate as possible. However, no guarantee can be made, or should be implied, that the information presented herein is totally accurate or complete. There you should not rely solely on this information when making a decision, commercial or otherwise.

The quality of the figures presented in this volume was dependent on the quality and format of the artwork supplied by the authors.

REFERENCE
The recommended reference for this publication is:
Tyler, IM and Knox-Robinson, CM 2010, Fifth International Archean Symposium Abstracts: Geological Survey of Western Australia, Record 2010/18, 410p.

National Library of Australia Card Number and ISBN 978-1-74168-314-1

Further details of geological publications and maps produced by the Geological Survey of Western Australia are available from:
Information Centre
Department of Mines and Petroleum
100 Plain Street
EAST PERTH, WESTERN AUSTRALIA 6004
Telephone: +61 8 9222 3459 Facsimile: +61 8 9222 3444
www.dmp.wa.gov.au/GSWApublications

TABLE OF CONTENTS

THEME 1:
PLANET FORMATION, CRUSTAL GROWTH AND THE EVOLVING LITHOSPHERE

KEYNOTE AND INVITED SPEAKERS

ORAL AND POSTER PRESENTATIONS

THEME 2:
DIVERSITY IN TECTONIC REGIMES

KEYNOTE AND INVITED SPEAKERS

ORAL AND POSTER PRESENTATIONS

THEME 3: UNIQUE MINERAL SYSTEMS?

KEYNOTE AND INVITED SPEAKERS

ORAL AND POSTER PRESENTATIONS

THEME 4: ESTABLISHING A HABITABLE PLANET

KEYNOTE AND INVITED SPEAKERS

ORAL AND POSTER PRESENTATIONS

SPONSORS

Geoconferences (WA) Inc acknowledges the generosity of the following sponsors of the 5IAS

GOLD SPONSORS

INDEPENDENCE GROUP NL
ABN 46 092 786 304

integra MINING Limited

SILVER SPONSORS

bhpbilliton
resourcing the future

Nickel West

SIPA Resources Ltd

Geological Survey of Western Australia

EVENT SPONSORS

digirock
EXPLORATION GEOLOGISTS

GOLD FIELDS

NEWMONT
ASIA PACIFIC

WORKSHOP SPONSOR

ANGLOGOLD ASHANTI
AUSTRALIA

EXHIBITION

Centre for EXPLORATION TARGETING

GENALYSIS
LABORATORY SERVICES

Intertek

Cryptodome's support is also acknowledged.

THEME 1

PLANET FORMATION, CRUSTAL GROWTH AND THE EVOLVING LITHOSPHERE

KEYNOTE & INVITED SPEAKERS

AN ISOTOPIC ROADMAP OF EARLY EARTH EVOLUTION- PROGRESS AND POTHOLES

T.I.S. Kemp

School of Earth & Environmental Science, James Cook University, Townsville, QLD 4811 Australia

A goal of isotope geochemistry is to chart the chemical evolution of the Earth and the solar system. The path to isotope enlightenment on the terrestrial front is littered with potholes and speed bumps, although our ability to navigate these is improving with rapid increases in analytical capability, and through refinements in approach.

The starting point for this ambitious journey is also the most poorly signposted - the Hadean Earth. In addition to (and perhaps accompanying) core formation, it is becoming increasingly apparent that major and long-lasting chemical differentiation of the silicate Earth occurred within the first few hundred million years of planetary accretion. In the absence of a geological record comparable to that available from other rocky bodies in the solar system (i.e. meteorites, lunar samples), investigation of these fundamental differentiation processes requires increased resolution of isotopic fine-print. In turn, this demands challenging analytical measurements that are continuously redefining the boundaries of precision and accuracy. An outstanding question, highlighted by Bennett et al. (2007), concerns the extent to which the Earth has progressively differentiated from an initially homogeneous composition (the traditional view) or become more homogeneous through time from an originally strongly differentiated state, the early-formed heterogeneities being gradually erased by crustal recycling and convective mantle stirring. There is also the growing possibility that the bulk Earth is not exactly equivalent to the familiar chondritic reference for isotope compositions, as has been demonstrated for major elements. This is a complication since chondrites are the commonly used baseline for assessing silicate differentiation.

The intention of this talk is to provide an overview of the current state of play with regard to understanding the differentiation and evolution of the major silicate reservoirs on the Earth throughout the Hadean and Archaean. Key questions are (1) when did differentiated crustal and mantle reservoirs appear on Earth (2) what were the composition and volume of these, (3) how long did they last, and (4) what were the geodynamic controls on differentiation, particularly the relative roles of fractional crystallisation in a global magma ocean versus the extraction of crustal material through mantle melting?

I will start by discussing developments in analytical tools that are used to decipher early Earth evolution. This will focus on the hafnium isotope analysis on zircon both in solution mode and by laser ablation, the latter becoming increasingly popular. The advantages and limitations of this technique will be highlighted. Then I will move on to the evidence for the appearance of differentiated reservoirs in the Earth. The principal evidence for an early 'depleted' reservoir comes from subtle variations in the $^{142}Nd/^{144}Nd$ ratio of mantle-derived and juvenile crustal rocks, suggesting the formation of a high Sm/Nd reservoir by 4.2 Ga, which is generally, but not always, assumed to be located in the mantle (e.g. Boyet and Carlson, 2005; Bennett et al. 2007). Evidence for the complementary low $^{142}Nd/^{144}Nd$ reservoir is beginning to emerge in Eoarchaean terranes (O'Neil et al. 2008) and ancient craton roots (Upadhyay et al. 2009), but the current mass balance either does not favour a chondritic bulk Earth composition for Nd isotopes, or signals the existence of a hitherto-unsampled hidden reservoir on Earth or elsewhere within the solar system with a $^{142}Nd/^{144}Nd$ ratio significantly lower than that of chondrites. There is some support for early incompatible element-depleted (high Sm/Nd) mantle from whole-rock $^{143}Nd/^{144}Nd$ data, but this is not corroborated by whole-rock Hf isotopes, which do not register a depleted (super-chondritic Lu/Hf) reservoir until sometime after 3.8 Ga, when large tracts of continental crust began to be stabilised. The apparent discord between two of the most powerful and generally coupled radiogenic isotope systems in the Eoarchaean has not been satisfactorily resolved. Some possibilities will be considered.

Evidence for an early 'enriched' and perhaps crustal reservoir comes from the Jack Hills zircons. An unradiogenic Hf isotope composition (i.e. low $^{176}Hf/^{177}Hf$ compared to chondrites) appears to be a robust feature of these grains, and testifies to the formation of some crust before 4.3 Ga (Amelin, 1999; Harrison et al, 2005, 2008; Blichert-Toft and Albarede, 2008; Kemp et al. 2010). In contrast, high $^{176}Hf/^{177}Hf$ values measured from some Jack Hills zircons are controversial and have been considered analytical artefacts. The evocative picture of a chemically-heterogeneous Hadean Earth where the generation of present-day volumes of continental crust and strongly depleted mantle was driven by plate tectonics (Harrison et al. 2005) appears to be collapsing into a rather simpler story involving the repeated remelting of a broadly basaltic crust formed at ~4.5 Ga. The sparse evidence for a depleted mantle (for Lu/Hf), and for juvenile input into this reservoir after 4.5 Ga implies that rather than being extracted from solid peridotite this enriched material represents the differentiated residua from crystallisation of one or more terrestrial magma oceans, and may have resided as a stable, but internally differentiating lid above quiescent mantle for 400 Ma. Most models postulate the complete disappearance of Hadean crust by 4.0 Ga but there is increasing evidence for its survival in the Pb, Nd and Hf isotope memory of the oldest cratons- this may be

the remnants of an originally voluminous reservoir that contains the 'missing' subchondritic $^{142}Nd/^{144}Nd$ needed to balance the ^{142}Nd excess in the present upper mantle. Should a widespread Hadean signature be established by other studies it would imply that Hadean lithosphere influenced the formation and evolution of presently preserved Archaean cratons. Hf isotope evidence from the Yilgarn Craton (Western Australia) suggests that Hadean protoliths were resampled during magmatic episodes as young as 2.65 Ga (Kemp et al. 2010). This craton must be considered a strong candidate to contain extant Hadean crust.

Further understanding of differentiation of the early Earth crust-mantle ensemble will require an interdisciplinary effort to formulate more refined physical models for planetary accretion, particularly regarding magma ocean formation and crystallisation and the petrological/geochemical consequences for the silicate Earth, additional improvements in analytical capability, experimental studies to constrain mechanisms of elemental fractionation both in different terrestrial environments and during planetary accretion, and a comprehensive search for the signature of Hadean crust in Archaean cratons and lithospheric mantle.

References

Amelin Y., Lee D-C., Halliday A.N. & Pidgeon R.T., 1999, Nature of the Earth's earliest crust from hafnium isotopes in single detrital zircons, Nature, 399, 252-255.

Bennett V.C., Brandon A.D. & Nutman,A.P., 2007, Coupled ^{142}Nd-^{143}Nd isotopic evidence for Hadean mantle dynamics, Science, 318, 1907-1910.

Blichert-Toft J. & Albarède F., 2008, Hafnium isotopes in Jack Hills zircons and the formation of the Hadean crust, Earth and Planetary Science Letters, 265, 686-702.

Harrison T.M., Blichert-Toft J., Muller W., Albarède F., Holden P. & Mojzsis S.J., 2005, Heterogeneous Hadean Hafnium: Evidence for Continental Crust at 4.4 to 4.5 Ga, Science, 310, 1947.

Harrison T. M., Schmitt A. K., McCulloch M. T. & Lovera O. M., 2008, Early (4.5 Ga) formation of terrestrial crust: Lu–Hf, $\delta^{18}O$, and Ti thermometry results for Hadean zircons, Earth and Planetary Science Letters, 268, 476-486.

Kemp A.I.S., Wilde S.A., Hawkesworth C.J., Coath C., Nemchin A.A., Pidgeon R.T., Vervoort J.D. & DuFrane S. A, 2010, Hadean crustal evolution revisited: new constraints from Pb-Hf isotope systematics of the Jack Hills zircons, Earth and Planetary Science Letters (in press).

O'Neil J., Carlson R.W., Francis D. & Stevenson R.K., 2008, Neodymium-142 evidence for Hadean mafic crust, Science, 321, 1828-1831.

Upadhyay D., Scherer E. & Mazger K., 2009, ^{142}Nd evidence for an enriched Hadean reservoir in cratonic roots, Nature, 459, 1118-1121.

WHAT CAN WE AGREE ON BEFORE 4 Ga?

J.W. Valley[1], C.B. Grimes[1,2], A-S. Bouvier[1,3], T. Ushikubo[1], D.M. Ortiz[1], A.J. Cavosie[4] & S.A. Wilde[5]

[1]Dept. of Geoscience, NASA Astrobiology Inst., WiscSIMS, Univ. of Wisconsin, Madison, WI 53706, USA
[2]Present address: Dept. of Geosciences, Mississippi State Univ., Mississippi State, MS 39762-5448, USA
[3]Present address: LPS, CEA-Saclay, 91191 Gif-sur-Yvette Cedex, France
[4]Department of Geology, University of Puerto Rico, Mayagüez, PR 00681, USA
[5]Dept. of Applied Geology, Curtin University of Technology, GPO Box U1987, Perth 6845, Australia

Detrital zircons from ~3 Ga Jack Hills sediments yield concordant U-Pb ages up to 4.4 Ga and provide evidence of conditions on the Early Earth. However, the parent rocks of these zircons have been destroyed and in the absence of known rocks older than 4 Ga, interpretations vary greatly in regard to pre-4 Ga surface conditions, composition of early magmas and crust, tectonic regimes, and implications for biology. Resolution of these controversies requires agreement on basic questions relating to the zircon record.

Are compositions of pre-4 Ga zircons reliably preserved? Froude et al. (1983) reported ages as old as 4.2 Ga and Wilde et al. (2001) found domains with isotopically concordant ages as old as 4.4 Ga. These ancient ages have now been verified in several labs. However, isotopically discordant domains with recent Pb loss are common, even in grains that also yield concordant ages. Nemchin et al. (2006a) conclude that the isotope geochemistry of most zircons is unreliable, but the process whereby oxygen isotopes would exchange in 10-20 μm domains of zircon that yield concordant U-Pb ages is not specified. Oxygen diffusion is very slow and diffusion distances are less than a few μm even in zircons from rocks that have undergone granulite-facies metamorphism and melting (Page et al. 2007). It is difficult to envision a process that would exchange oxygen without also causing Pb-loss and discordant ages. Experiments suggest that Li diffusion in zircon is significantly faster than oxygen and independent of REE content (Cherniak and Watson 2010). However, Ushikubo et al. (2008) report concentric, oscillatory Li banding in detrital zircons from granulite-facies metasediments that would be erased if diffusion was rapid. They suggest that [Li] exchange is retarded by slow diffusion of REEs that are linked to Li by charge-balanced coupled substitutions. For these reasons, careful documentation of in situ analysis spots is critical for interpreting age, isotope ratio and trace element data (Cavosie et al. 2006). In well-defined cases, detailed measurements and interpretations of carefully chosen natural samples may provide the most accurate description of isotopic and elemental behaviour in zircon.

Was the surface of Early Earth Hadean? Mildly elevated values of $\delta^{18}O$(Zrc) relative to mantle zircons (5.9-7.5 vs. 4.7-5.9‰, Figure 1) indicate that source magmas incorporated supracrustal material that had interacted with surface water at low temperatures during weathering or diagenesis. Thus, steam atmospheres condensed to liquid water oceans (possibly ice) before 4.3 Ga, and the period from 3.8 to 4.3 Ga was not distinctively "hell-like" (Valley et al. 2002). Cavosie et al. (2005) proposed that condensation of the first liquid water oceans, a worldwide event of tremendous geological consequence at ~4.3-4.4 Ga, should be accepted to mark the end of the Hadean and the start of the Archean Eon.

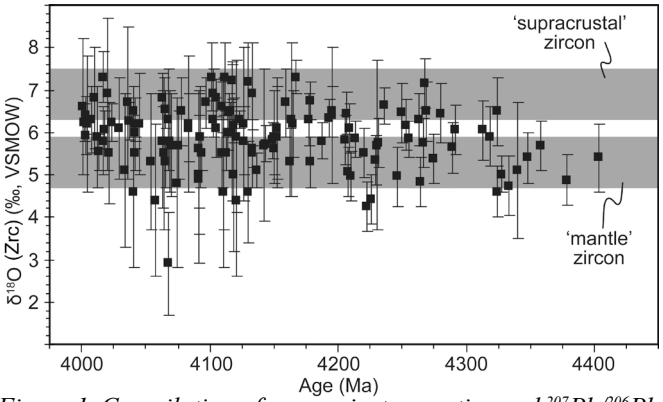

Figure 1. Compilation of oxygen isotope ratios and $^{207}Pb/^{206}Pb$ age (>85% concordant) for 4.4 to 4.0 Ga detrital zircons from the Jack Hills, Australia (data from: Peck et al. 2001, Wilde et al. 2001, Mojzsis et al. 2001, Cavosie et al. 2005, Nemchin et al. 2006a, Trail et al. 2007& Harrison et al. 2008). Uncertainty is plotted at 2σ quoted by authors. The $\delta^{18}O$(Zrc) value in high temperature equilibrium with the mantle is from Valley et al. (2005).

The pre-4 Ga zircons have been interpreted to indicate granitic parent magmas in continental or "proto-continental" crust based on mineral inclusions and REE, Ti, and isotope geochemistry (see Cavosie et al. 2007; Trail et al. 2007; Ushikubo et al. 2008; Harrison 2009).

Alternatively, the pre-4 Ga zircons have been interpreted to come from mafic magmas and more primitive crust analogous to zircons found: 1) on the Moon or 2) in modern oceanic crust, possibly in ophiolites formed at ocean ridges. 1) Nemchin et al. (2006c) reported values of $\delta^{18}O$(Zrc) from 5.5 to 7.2‰ for Apollo sample 14163 and concluded that mildly elevated values of $\delta^{18}O$(Zrc) exist on the Moon and thus that similar $\delta^{18}O$ values of pre-4 Ga zircons on Earth could form in the absence of either liquid water or felsic crust. However, Nemchin et al. (2006b) reported $\delta^{18}O = 5.49 \pm 0.13$‰ for a different suite of lunar zircons (14321) and Whitehouse and Nemchin (2009) show that the high values reported for 14163 resulted from poor sample preparation and that the correct $\delta^{18}O$ value is 5.70 ±0.07‰. Thus, zircons from the Moon do not show mildly elevated values of $\delta^{18}O$(Zrc) and this signature of liquid water is unique to Earth and includes many pre-4 Ga terrestrial zircons. 2) Coogan and Hinton (2006) state that pre-4 Ga zircons are geochemically similar to zircons that are reported

in many sections of young ocean-crust, and Rollinson (2008) speculated that the pre-4 Ga zircons would have elevated $\delta^{18}O$ if they crystallized from plagiogranite magmas formed by melting of altered mafic crust. These studies argue that the pre-4 Ga zircons came from mafic crust and provide no evidence of continental crust.

Three lines of geochemical evidence distinguish ocean-crust zircons from pre-4 Ga zircons, demonstrating that evolved gabbro and oceanic plagiogranite are not analogues to parental magmas of pre-4 Ga zircons (Figure 2). 1) Zircons from plagiogranite and gabbro consistently preserve mantle-like $\delta^{18}O$ (5.2±0.5‰, 221 zircons from 46 samples of in situ ocean crust, plagiogranites and gabbros, Cavosie et al. 2009, Grimes et al. 2010). No zircons with mildly elevated $\delta^{18}O$ values >6.0 have been found in ocean crust. This is in contrast to the Jack Hills zircons with ages >4 Ga, many of which record $\delta^{18}O$ from 6.0 to 7.5‰ (Figs. 1, 2a). Second, Grimes et al. (2007) demonstrated that the Jack Hills zircon suite is distinct from ocean-crust zircons formed at both fast and slow-spreading mid-ocean ridges. The U/Yb ratios of Jack Hills zircons resemble U/Yb in zircons from Phanerozoic and Archean age continental and island arc crust (Fig. 2c). Furthermore, concentrations of Li in normal magmatic ocean-crust zircons (typically <0.04 ppm) are several orders of magnitude lower than in Jack Hills zircons (10-60 ppm; Ushikubo et al., 2008, Bouvier et al. 2009, Grimes et al. 2010) (Fig. 2b). Based on the existing geochemical data, there is no known modern oceanic or ophiolitic analogue for the pre-4 Ga zircons. Neither plagiogranites nor evolved oxide-gabbro formed in oceanic environments are viable for the source of the Jack Hills zircons. In contrast, similarities are strong to Archean continental crust, esp. TTGs (Bouvier et al. 2009). These results support the suggestion that granitic (s.l.) "proto-continental" crust existed by 4.3 Ga, though the amounts of such crust are still uncertain.

Harrison (2009) suggests a fully developed continental crust with 'true' granites and plate tectonics by 4.4 Ga based largely on [Ti] and muscovite inclusions in zircon. However, [Ti] of zircons do not yield accurate estimates of crystallization temperature for granitic batholiths. Furthermore, [Ti] values for pre-4 Ga zircons are significantly higher than for many granites and are similar to zircons from many mafic plutons (Fu et al. 2008). Our EMPA analysis of muscovite inclusions shows that secondary fluorescence affects composition for small grains and SIMS measurements of $\delta^{18}O$ with a 5 μm spot show that some inclusions in pre-4 Ga zircons are compromised by metamorphic exchange (Ortiz 2010). Thus, we see no compelling evidence for true granites or high P/T metamorphism related to subduction.

Why are there no known rocks older than 4 Ga, but zircons have survived? Common thought suggests that rocks were destroyed by intense meteorite impacting and melting, but the new evidence for liquid water and weathering suggest the alternative possibility that a CO_2-rich atmosphere and extensive weathering may have disaggregated the protoliths.

When did Earth become habitable to life? Both O and Li isotope ratios suggest that conditions were sufficiently clement before 4.325 Ga, possibly as early as 4.4 Ga. The first life may have been almost 1 byr earlier than the first microfossil evidence.

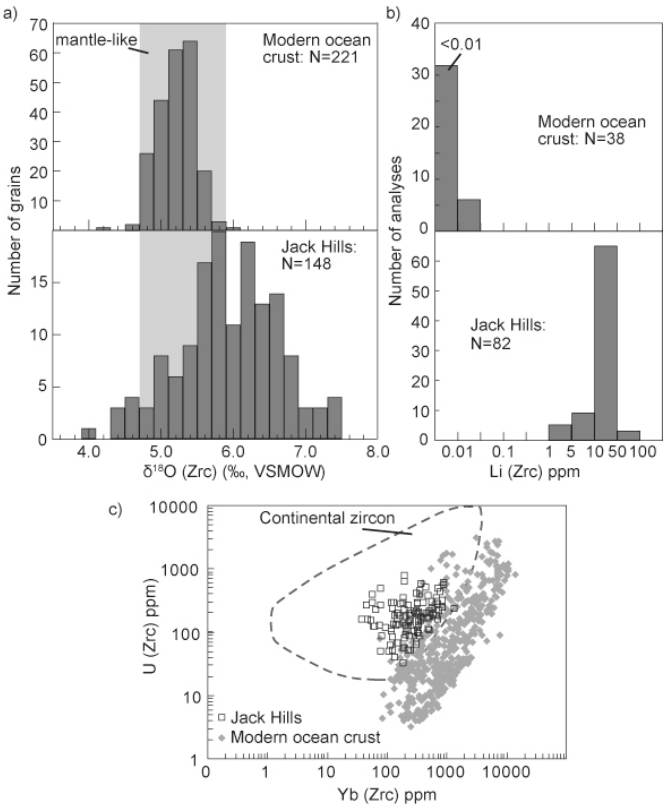

Figure 2. Trace element and oxygen isotope geochemistry of zircons from modern ocean-crust and >3.9 Ga detrital zircons from the Jack Hills. A) Histograms showing grain-averaged $\delta^{18}O$(Zrc) for individual zircons. Ocean-crust data are for magmatic zircons from plagiogranites and gabbros along the Mid-Atlantic and Southwest Indian Ridges (Cavosie et al. 2009, Grimes et al. 2010). Jack Hills values include domains with Pb/U age concordance >85% (see Fig.1). B) Lithium concentration in magmatic zircons (Ushikubo et al. 2008, Grimes et al. 2010). C) U vs. Yb diagram; ocean-crust zircon data and field for continentally-derived magmatic zircon from Grimes et al. (2009); Jack Hills zircon data are from Mass et al. (1992), Crowley et al. (2005), and Cavosie et al. (2006). (from Grimes et al. 2010)

Acknowledgements

This research was funded by NSF, ARC, and the NASA Astrobiology Institute.

References

Bouvier A-S., Ushikubo T., Kita N., Cavosie A.J., Kozdon R. & Valley J.W., 2009, Li isotopes in Archean zircons, American Geophysical Union Annual Meeting.

Cavosie A.J., Valley J.W. & Wilde S.A., 2005, Magmatic $\delta^{18}O$ in 4400-3900 Ma detrital zircons: A record of the alteration and recycling of crust in the Early Archean Earth and. Planetary Science Letters, 235, 663-681.

Cavosie A.J., Wilde S.A. & Valley J.W, 2005, A lower age limit for the Archean based on $\delta^{18}O$ of detrital zircons, Goldschmidt Conference, Geochimica et Cosmochimica Acta, 69, 10, S1, A391.

Cavosie A.J., Valley J.W., Wilde S.A. & Edinburgh Ion Microprobe Facility staff, 2006, Correlated microanalysis of zircon: $\delta^{18}O$ and U-Th-Pb isotopic constraints on the igneous origin of complex >3900 Ma detrital grains, Geochimica et Cosmochimica Acta, 70, 5601-5616.

Cavosie A.J., Valley J.W. & Wilde S.A., 2007, The oldest terrestrial mineral record: A review of 4400 to 4000 Ma detrital zircons from the Jack Hills, Western Australia, in *Earth's Oldest Rocks*, M.J. van Kranendonk, R.H. Smithies and V.C. Bennett (eds), Developments in Precambrian Geology 15, 91-111.

Cavosie, A.J., Kita N.T. & Valley J.W., 2009, Primitive oxygen isotope ratio recorded in magmatic zircons from the Mid-Atlantic Ridge, American Mineralogist 94, 926-934.

Cherniak D.J. and Watson E.B., 2010, Li diffusion in zircon, Contributions to Mineralogy and Petrology (in press).

Coogan L.A. and Hinton R.W., 2006, Do the trace element compositions of detrital zircons require Hadean continental crust? Geology, 34, 633-636.

Crowley J.L., Myers J.S., Sylvester P.J. & Cox R.A., 2005, Detrital zircon from the Jack Hills and Mount Narryer, Western Australia; Evidence for diverse >4.0 Ga source rocks, Journal of Geology 113, 239-263.

Fu B., Page F.Z., Cavosie A.J., Fournelle J., Kita N.T., Lackey J.S., Wilde S.A. & Valley J.W., 2008, Ti-in-zircon thermometry: applications and limitations, Contributions to Mineralogy and Petrology, 156, 197-215.

Froude, D.O., Ireland, T.R., Kinny, P.D., Williams, I.S., Compston, W., Williams, I.R. & Myers, J.S., 1983, Ion microprobe identification of 4100-4200 Myr-old terrestrial zircons, Nature, 304, 616–618.

Grimes C.B., John B.E., Cheadle M.J., Mazdab F.K., Wooden J.L., Swapp S. and Schwartz J.J., 2009, On the occurrence, trace element geochemistry, and crystallization history of zircon from in situ ocean lithosphere, Contributions to Mineralogy and Petrology, 158, 757-783.

Grimes C.B., Ushikubo T., John B.E. & Valley J.W, 2010, Uniformly mantle-like $\delta^{18}O$ in zircons from oceanic plagiogranites and gabbros, Contributions to Mineralogy and Petrology (in review).

Harrison T.M., 2009, The Hadean crust: evidence from >4 Ga zircons, Annual Reviews in Earth and Planetary Sciences, 37, 479-505.

Harrison T.M., Schmitt A.K., McCulloch M.T. & Lovera O.M., 2008, Early (≥4.5Ga) formation of terrestrial crust: Lu-Hf, $\delta^{18}O$, and Ti-thermometry results for Hadean zircons, Earth and Planetary Science Letters, 268, 476-486.

Maas R., Kinny P.D., Williams I.S., Froude D.O. & Compston W., 1992, The Earth's oldest known crust: A geochronological and geochemical study of 3900–4200 Ma detrital zircons from Mt Narryer and Jack Hills, Western Australia, Geochimica et Cosmochimica Acta, 56, 1281–1300.

Mojzsis, S.J., Harrison, T.M. & Pidgeon, R.T. 2001, Oxygen isotope evidence from ancient zircons for liquid water at the Earth's surface 4300 Myr ago, Nature, 409, 178–181.

Nemchin, A.A., Pidgeon, R.T. & Whitehouse, M.J., 2006a, Re-evaluation of the origin and evolution of >4.2 Ga zircons from the Jack Hills metasedimentary rocks, Earth and Planetary Science Letters, 244, 218–233.

Nemchin A.A., Whitehouse M.J., Pidgeon R.T. & Meyer C., 2006b, Oxygen isotope signature of 4.4-3.9 Ga zircons as a monitor of differentiation processes on the moon, Geochimica et Cosmochimica Acta, 70, 1864-1872.

Nemchin A.A., Whitehouse M.J., Pidgeon R.T. & Meyer C., 2006c, Heavy isotope composition of oxygen in zircon from soil sample 14163: Lunar perspective of an early ocean on the Earth, Lunar and Planetary Science, 1593.

Ortiz-Cordero D.M., 2010, Mineral Inclusions, in *Zircons: A Tool For Provenance Analysis of Sedimentary Rocks*, Unpublished MS Thesis, University of Wisconsin Madison.

Page F.Z., Ushikubo T., Kita N.T., Riciputi L.R. & Valley J.W., 2007, High precision oxygen isotope analysis of picogram samples reveals 2-μm gradients and slow diffusion in zircon. Am. Mineral, 92, 1772-1775.

Peck W.H., Valley J.W., Wilde S.A. & Graham C.M., 2001, Oxygen isotope ratios and rare earth elements in 3.3 to 4.4 Ga zircons: Ion microprobe evidence for high $\delta^{18}O$ continental crust and oceans in the Early Archean, Geochimica et Cosmochimica Acta, 65, 4215-4229.

Rollinson H., 2008, Ophiolitic trondhjemites: a possible analogue for Hadean felsic 'crust', Terra Nova, 20, 364-369.

Trail D., Mojzsis S.J., Harrison T.M., Schmitt A.K., Watson E.B. & Young E.D., 2007, Constraints on Hadean zircon protoliths from oxygen isotopes, Ti-thermometry, and rare earth elements, Geochemistry, Geophysics, Geosystems, 8.

Ushikubo T., Kita N.T., Cavosie A.J., Wilde S.A., Rudnick R.L. & Valley J.W., 2008, Lithium in Jack Hills zircons: Evidence for extensive weathering of Earth's earliest crust, Earth and Planetary Science Letters, 272, 666-676.

Valley J.W., Peck W.H., King E.M. & Wilde S.A., 2002, A Cool Early Earth, Geology, 30, 351-354.

Valley J.W., Lackey J.S., Cavosie A.J., Clechenko C.C., Spicuzza M.J., Basei M.A.S., Bindeman I.N., Ferreira V.P., Sial A.N., King E.M., Peck W.H., Sinha A.K. & Wei C.S., 2005, 4.4 billion years of crustal maturation: Oxygen isotopes in magmatic zircon, Contributions to Mineralogy and Petrology, 150, 561-580.

Whitehouse M.J. & Nemchin, A.A, 2009, High precision, high accuracy measurement of oxygen isotopes in a large lunar zircon by SIMS, Chemical Geology, 261, 32-42.

Wilde S.A., Valley J.W., Peck W.H. & Graham C.M., 2001, Evidence from detrital zircons for the existence of continental crust and oceans on the Earth 4.4 Gyr ago, Nature, 409, 175-178.

DIFFERENTIATION PROCESSES IN THE EARLY SOLAR SYSTEM

A.A. Nemchin

Department of Applied Geology, Curtin University of Technology, Kent Str. Bentley, WA 6102, Australia

Introduction

Differentiation is one of the most significant outcomes of planetary evolution. It is ultimately driven by the gravitational separation of phases with different densities. As a result all planetary bodies in the inner Solar System, which are, in general terms, similar in their chemical and mineral compositions, appear to have evolved along similar differentiation paths, resulting in the formation of an Fe-rich (probably metallic) core, Mg-rich (silicate) mantle and a residual reservoir enriched in the incompatible elements. In addition, some form atmospheres of various density and composition. The full differentiation record is either not preserved or not accessible for direct study on any of the planetary bodies in the Solar System. However, observed similarities provide an opportunity to reconstruct a complete picture from available pieces of information. Ultimate purpose of this reconstruction is not only a better comprehension of the history of the Solar System, but also an understanding of processes that drive evolution of the Earth.

Understanding differentiation on the planetary scale requires a perception of the timing involved in the formation of major reservoirs and their compositional characteristics. These characteristics are expected to vary from one planetary body to another as a result of difference in size, thermal history and volatile content, which determine degassing patterns, liquidus assemblages during melting, gravitational and temperature gradients etc. and as a result can push differentiation in a specific direction, defining subsequent history of a planetary body. The possibility of such variation must be also considered when applying information obtained from the study of one object in the Solar system to another.

The aim of this presentation is to provide a brief discussion of the main features of planetary differentiation based on the sampled part of the Solar System (other than Earth), which includes Earth's Moon, Mars and variety of small bodies from the asteroid belt.

Meteorites

Meteorites preserved a record of differentiation of the relatively small objects in the inner Solar System, such as asteroids, although, some like chondrites and a small proportion of achondrites remain virtually unchanged throughout their history (e.g. Krot et al. 2003) and show abundances of most elements similar to those observed in the solar atmosphere (with the exception of the few most volatile elements).

Differentiated achondrites show compositions that are highly fractionated relative to that of chondrites and textures that are indicative of magmatic crystallisation, although some are modified by metamorphic processes (e.g. Mittlefehldt, 2008). This group of meteorites consists of basalts and ultramafic cumulates that indicate differentiation somewhat similar to that observed during formation of oceanic crust from the mantle on Earth.

From the two main chemical groups of iron meteorites, the so-called magmatic iron meteorites are considered to form in the cores of asteroids (ten known groups forming in the cores of separate asteroids), while the origin of non-magmatic iron meteorites remains more controversial with the interpretation including crystallisation of a S-rich core (Kracher, 1982), partial asteroidal differentiation followed by impact mixing (Benedix et al., 2000), and formation in isolated impact melt pools (Wasson and Kallemeyn, 2002).

Extensive study of ^{182}Hf-^{182}W in magmatic iron meteorites (e.g. Kleine et al. 2005a; Lee 2005; Markowski et al., 2006) indicates that core formation in their parent bodies occurred less than 1 Ma after the formation of Ca-Al rich inclusions (~4568 Ma old), thought to be oldest objects in the Solar System (Connelly et al., 2008). In addition, several eucrites show internal isochron systematics in the Al–Mg (Srinivasan et al., 2007), Mn–Cr (Lugmair and Shukolyukov, 1998), and Hf–W (Kleine et al., 2005b) systems consistent with their eruption onto the surface of their parent body before 4560 Ma (i.e. less than 10 million years after the formation of the Solar System). All these data indicate that the full set of differentiation processes, including separation of cores and differentiation of mantles, has been in place on these small objects immediately after their formation. However, the degree of differentiation observed in the set of meteoritic samples is limited to the basalts as the most extreme differentiation product. Felsic or intermediate rocks have never been found in meteorites, with an exception of a pair of samples GRA 06128/06129, which are achondrites recently discovered in Antarctica and dominated by the sodic plagioclase. Two pyroxenes and Fe-rich olivine are the next most abundant mineral phases in these samples. According to Shearer et al. (2008) major and trace element characteristics of this meteorite, which are somewhat similar to terrestrial andesite, can be explained by very small degree melting of some primitive meteorites (chondrites) in a very volatile rich environment or by accumulation of plagioclase from a relatively felsic melt as a result of fractionation from a "magma ocean" (similar to anorthositic crust on the Moon) or in a large intrusion (i.e. layered complex). Day et al. (2009) suggested that GRA 06128/06129 is the result of a previously unrecognised style of formation of evolved crust. In addition to that, HFS (high field strength) element concentrations in this meteorite and

Os isotope compositions indicate that the core was not separated in the meteorite parent body prior to formation of the andesitic melt, indicating that significant differentiation of the silicate part of a planetary body can take place prior to core segregation (Day et al., 2009). Finally, observable excess of ^{26}Mg indicates that the rock was formed within a few million years of formation of the Solar System. Based on the ^{26}Al-^{26}Mg system and compared to the best estimates of the absolute time of CAI (Ca-Al rich inclusions) formation, the age of GRA 06128/06129 is determined as 4564.25 ± 0.21 Ma.

A combination of chronological data obtained for various meteorite groups suggests that the processes of early accretion and differentiation on some proto-planetary bodies had started immediately after the formation of the Solar System, while ^{26}Al was still abundant and could provide heat required for this differentiation. Differentiated meteorites originate from these relatively early accreted objects. The existence of undifferentiated meteorites with their younger ages suggests that at least some bodies in the Solar System accreted after a significant proportion of ^{26}Al had decayed, eliminating an important heat source. As a result, the oldest objects found in the Solar System, such as Ca-Al rich inclusions and chondrules, are preserved within these (undifferentiated) meteorites.

Mars

Mars was identified as the parent body of some meteorites by analogy of the data obtained from those meteorites with remote sensing data acquired by the spacecrafts sent to Mars in the 1970s (e.g., Viking). It is now widely accepted that about twenty meteorites, representing a few tens of kilograms of rock, come from Mars (e.g., McSween, 1985; 1994; Treiman et al., 2000). These meteorites are called SNC meteorites, standing for Shergotty-Nakhla-Chassigny, which are the names of the localities where the first described Martian meteorites were found. The SNC meteorites are mafic and ultramafic magmatic rocks (basalts, pyroxenites, lherzolites and dunites).

The presence of basalts and ultramafic rocks is in itself an indication of differentiation of the Martian mantle. In addition, Martian meteorites show measurable anomalies of both ^{182}W and ^{142}Nd, which are the products of now extinct parent isotopes ^{182}Hf and ^{146}Sm and, therefore, highlight early differentiation on Mars. In particular, all Martian meteorites show elevated ^{182}W/^{184}W ratios relative to chondrites, indicating core formation within about 20 million years and mantle differentiation within about 60 million years after CAI. The later is supported by the observed variations in ^{142}Nd. However, precision of these ages is limited by uncertainties in the estimates of parent to daughter ratios (e.g. Hf/W) in the bulk Martian mantle. In addition, some results (particularly Sm-Nd data, which reflect silicate differentiation) can be modified by the processes of mantle mixing and recycling. As a result of these uncertainties it is still not clear (1) if differentiation of the Martian core took place at the same time as on the asteroids or 10-20 million years later and (2) if core formation on Mars and differentiation of the Martian mantle are the result of the same process of global differentiation and occurred contemporaneously or whether there was a significant gap between these two differentiation events.

Regardless of uncertainties in both the W and Nd isotope systematics, preservation of anomalies in Martian rocks, even in the relatively young basalts, not only suggests early differentiation, but also indicates the preservation of reservoirs formed in the Martian mantle in a time interval less than ~ 60 million years after accretion. In other words, the early formed reservoirs in the Martian mantle remained isolated throughout the history of the planet, which suggests somewhat limited mantle mixing, for example compared to the Earth's mantle.

Similar to the differentiated meteorites originating from the asteroid belt, the most evolved rocks preserved in Martian meteorites are basalts. Felsic materials such as those found to dominate Earth's continental crust have never been recorded in Martian meteorites. Nevertheless, the compositional mapping of Mars at the 100-metre scale with the Mars Odyssey Thermal Emission Imaging System revealed the presence of a wide variety of igneous rocks on Mars including silica-rich dacites (e.g. Christensen et al., 2008), although the extent and distribution of felsic rocks, their precise nature and origin is difficult to determine from the currently available remote sensing data. Observed occurrences of quartz-bearing granitic rocks are rare and the Martian crust appears to be dominated by basalts.

Moon

Earth's Moon preserves the most complete record of planetary differentiation that can be constrained from the samples of lunar crust (anorthositic in composition), plutonic rocks and mare basalts, collected during the Apollo missions and also represented by the suite of lunar meteorites.

The leading model of lunar formation involves a collision of Earth with a Mars-size body (e.g., Canup and Asphaug, 2001), which produced a significant amount of debris believed to be dominated by the material derived from the impactor. Fast accretion of this debris generated enough heat to form a molten layer with a thickness of several hundred kilometres on the Moon, referred to as the Lunar Magma Ocean (LMO). Predicted sequence of LMO crystallisation (e.g. Shearer et al., 2006), which started with fractionation of Mg-rich olivine and pyroxene, followed by plagioclase (which floated forming lunar crust) and ilmenite cumulates resulted in the stratification of the lunar mantle, where heavier Fe-rich minerals resided above the Mg-rich cumulates and even heavier ilmenite-rich layers were positioned at the top of the mantle. It has also left a residual melt enriched in the incompatible elements. Crystallisation of this melt produced an enriched reservoir most likely located under the lunar anorthositic crust and referred to as KREEP (from the high abundance of K, REE and P).

Study of metals from lunar basalts (Touboul et al., 2007) indicates similarity of 182W/184W ratios in lunar rocks

and Earth's mantle, which contradicts predictions of the model of impact origin of the Moon that suggests that the Moon is mainly composed of impactor material (e.g. Canup, 2004), unless significant homogenisation of W between the impactor and the Earth occurred during the collision. Regardless of this difficulty, the time of formation of the Moon is estimated on the basis of W data as 62+90/-10 My after CAI formation (Touboul et al., 2007). Combined with the age of the oldest zircon (Nemchin et al, 2009), W data suggests that less than 100 Ma is required to crystallise the LMO and form the KREEP reservoir.

The specific sequence of crystallisation of LMO resulted in two main processes that probably determined subsequent evolution of the Moon and chemical characteristics of both highland and mare basalts. One was determined by the gravitational instability formed as a result of lighter Mg-rich phases accumulation in the lower part of the mantle beneath the heavier Fe-rich layers and ilmentite cumulates (e.g. Parmentier et al., 2002). This instability is believed to be resolved by a mantle overturn that followed LMO crystallisation. The second was driven by the overturn and resulted in dragging KREEP material into the lower mantle, possibly creating a heat source that supported mare volcanism and variably contaminating the source of mare basalts with incompatible elements. These processes demonstrate an initial stage of dissemination and recycling of enriched reservoir on a lunar scale.

Acknowledgements

I wish to acknowledge all the people I have worked with during the last ten years, who made my study of planetary materials an enjoyable experience.

References

Benedix G.K., McCoy T.J., Keil K. & Love S.G., 2000, A petrologic study of the IAB iron meteorites: Constraints on the formation of the IAB-winonaite parent body, *Meteoritics and Planetary Scence, 35,* 1127–1141.

Canup R.M. & Asphaug E., 2001, Origin of the Moon in a giant impact near the end of the Earth's formation, Nature, 412, 708–712.

Canup R.M., 2004, Dynamics of lunar formation, Annual Review of Astronomy and Astrophysics, 42, 441–475.

Christensen P.R., McSween, H.Y., Bandfield J.L., Ruff S.W., Rogers A.D., Hamilton V.E., Gorelick N., Wyatt M.B., Jakosky B.M., Kieffer H.H., Malin M.C. & Moersch J.E., 2005, Evidence for magmatic evolution and diversity on Mars from infrared observations, Nature, 436, 504-509

Connelly J., Amelin Y., Krot A.N. & Bizzarro M., 2008, Chronology of the solar system's oldest solids, The Astrophysical Journal, 675, L121–L124.

Day J.M.D., Ash R.D., Liu Y., Bellucci J.J., Rumble D., William F. McDonough W.F., Walker R.J. & Taylor L.A., 2009, Early formation of evolved asteroidal crust, Nature, 457, 179-182.

Kleine T., Mezger K., Palme H., Scherer E. & Muenker C., 2005a, Early core formation in asteroids and late accretion of chondrite parent bodies: Evidence from ^{182}Hf–^{182}W in CAIs, metal-rich chondrites and iron meteorites, Geochimica et Cosmochimica Acta, 69, 5805–5818.

Kleine T., Mezger K., Palme H., Scherer E. & Münker C., 2005, The W isotope composition of eucrite metals: constraints on the timing and cause of the thermal metamorphism of basaltic eucrites, Earth and Planetary Science Letters, 231, 41–52.

Kracher A., 1982, Crystallization of a S-saturated melt, and the origin of the iron meteorite groups IAB and IIICD, *Geophysical Research Letters, 9,* 412–415.

Krot A.N., Keil K., Goodrich C.A. & Scott E.R.D., 2003, Classification of meteorites, in *Treatise on Geochemistry Volume. 1*, Davis A.M., ed, Elsevier Pergamon, Amsterdam, 83-128

Lee D.C., 2005, Protracted core formation in asteroids: evidence from high precision W isotopic data, Earth and Planetary Science Letters, 237, 21–32.

Lugmair G.W. & Shukolyukov A., 1998, Early solar system time-scales according to ^{53}Mn–^{53}Cr systematic, Geochimica et Cosmochimica Acta, 62, 2863–2886.

Markowski A., Quitte G., Halliday A.N. & Kleine T., 2006, Tungsten isotopic compositions of iron meteorites: chronological constraints vs cosmogenic effects, Earth and Planetary Science Letters, 242, 1–15.

McSween H.Y., 1985, SNC meteorites: Clues to Martian petrologic evolution? Reviews of Geophysics, 23, 391-416.

McSween H.Y., 1994, What we have learnt about Mars from the SNC meteorites, Meteoritics, 29, 757-779.

Mittlefehldt D.W., 2008, Meteorites – A Brief Tutorial, Reviews in Mineralogy and Geochemistry, 68, 571-590.

Nemchin A., Timms N., Pidgeon R., Geisler T., Reddy S. & Meyer C., 2009, Timing of crystallization of the lunar magma ocean constrained by the oldest zircon, Nature Geoscience, 2, 133-136

Parmentier E.M., Zhong S., & Zuber M.T., 2002, Gravitational differentiation due to initial chemical stratification: origin of lunar asymmetry by the creep of dense KREEP? Earth and Planetary Science Letters, 201, 473-480.

Shearer C.K., Burger P.V., Neal C.R., Sharp Z., Borg L.E., Spivak-Birndorf L., Wadhwa M., Papike J.J., Karner J.M., Gaffney A.M., Shafer J., Weiss B.P., Geissman J. & Fernandes V.A., 2008, A unique glimpse into asteroidal melting processes in the early solar system from the Graves Nunatak 06128/06129 achondrites, American Mineralogist, 93, 1937–1940.

Shearer, C.K., Hess, P.C., Wieczorek, M.A., Pritchard, M.E., Parmentier, E.M., Borg, L.E., Longhi, J., Elkins-Tanton, L.T., Neal, C.R., Antonenko, I., Canup, R.M., Halliday, A.N., Grove, T.L., Hager, B.H., Lee, D-C. & Wiechert, U., 2006, Thermal and Magmatic Evolution of the Moon, in *New Views of the Moon*; Reviews in Mineralogy and Geochemistry, Mineralogical Society of America, 60, 365-518.

Srinivasan G., Whitehouse M.J., Weber I., & Yamaguchi A., 2007, The crystallization age of eucrite zircon, Science, 317, 345–347.

Touboul M., Kleine T., Bourdon B., Palme H. & Wieler R., 2007, Late formation and prolonged differentiation of the Moon inferred from W isotopes in lunar metals, Nature, 450, 1206–1209.

Treiman A.H., Gleason J.D. & Bogard D.D., 2000, The SNC meteorites are from Mars, Planetary and Space Science, 48, 1213-1230.

Wasson J. T. & Kallemeyn, G. W., 2002, The IAB iron-meteorite complex: A group, five subgroups, numerous grouplets, closely related, mainly formed by crystal segregation in rapidly cooling melts. *Geochimica et Cosmochimica Acta, 66,* 2445–2473.

ARCHAEAN GRANITOIDS RECORD A RANGE OF GEODYNAMICAL SITES FOR CRUSTAL GROWTH OR RECYCLING

J-F. Moyen

Department of Geology, University of Stellenbosch, South Africa.
Now at Université Jean-Monnet & CNRS UMR 6524. 23 rue du Docteur Michelon, 42023 Saint-Etienne, France.

Introduction

The tectonic environment of Archaean crustal growth (and recycling) has been the subject of considerable controversy, with strikingly different settings proposed. Regardless of the preferred model, however, different geodynamic sites are likely to display contrasting geothermal gradients, as well as varying possible sources, resulting in distinct granitoids types. This work examines the range of existing Archaean granitoids; their time distribution, and evolution; and the implications for Archaean crustal evolution.

The diversity of Archaean granitoids

The dominant type of Archaean plutonic rocks is represented by the TTG (Tonalite – Trondhjemite – Granodiorite) suite. They are assumed to represent up to 75% of the Archaean crust – although this proportion actually applies to the "Grey Gneiss Complexes" (Martin 1994). While Grey Gneisses are indeed chiefly of TTG composition, they do also comprise a range of other components, including different igneous rocks, restites and leucosomes, or even supracrustal layers (amphibolites or metapelites) that are not always recognized as such.

TTGs are sodic granitioids, dominated by plagioclase, quartz and biotite or amphibole. Their best-known geochemical feature is a fractionated REE pattern, although this is not in itself sufficient to characterize them (Martin 1994; Moyen 2009). TTGs are most likely formed by partial melting of a meta-mafic protolith (be it amphibolite or eclogite), in the garnet stability domain. The possible tectonic implications of TTG is discussed below.

A closely related type is represented by I-type plutons, with a plagioclase – K-feldspar – quartz – biotite mineralogy ("enriched TTG" for (Champion and Smithies 2007) and Bt-granites in (Moyen et al. 2003)). Geochemically, these rocks are very similar to the TTG proper, expect of course for overall higher LILE (including K) contents, and perhaps somewhat less fractionated REE patterns with occasionally a negative Eu anomaly. There is, in fact, no clear-cut boundary with the previous type, and all intermediate rocks do exist, with a range of LILE concentrations. The higher LILE contents do require a more enriched source, and the range of compositions from sodic to potassic is taken as reflecting a range of sources, from mafic, to intermediate (meta-andesites), to more felsic (tonalites) (Champion and Smithies 2007). In the East Pilbara, it was also demonstrated (Champion and Smithies 2007) that the potassic nature of the plutons is correlated with a less juvenile isotopic signature, pointing to a variation from juvenile, sodic magmas (generated from meta-basic rocks) to more potassic magmas, sourced from already formed continental crust and therefore corresponding to an increased crustal recycling. Since Archaean crust was probably never significantly thickened (maximum recorded pressures of 10—12 kbar); and since it is dominated by relatively unfertile lithologies; high temperatures at low pressures are required to generate large amounts of such melts, requiring either large-scale crustal collapse and thinning (post-collisional collapse?), or bulk crustal heating without thickening.

Peraluminous, S-type granitoids are uncommon in the Archaean, probably owing to the overall lack of large detrical sedimentary associations, the normal source for S-type granitoids (Clemens 2003). Most of the examples described are Late-Archaean, the oldest known having emplaced between 2.97 and 2.85 Ga South of the Murchison belt of South Africa (Jaguin et al., this volume).

As peraluminous granites derive from metasediments, their formation requires, at least, burial of supracrustal material to melting depth, typically 5—10 kbar for modern counterparts. This puts however little constrains on tectonic models.

"Mantle-derived" granitoids is used here to describe a group of rocks typified by their magnesio-potassic character, including elevated mg#'s and transition elements (Ni, Cr) contents, coupled with high LILE (including K) and REE, with "TTG like" fractionated patterns. They include (i) the "sanukitoid" suite proper, small monzodioritic to granodioritic plutons, stocks and dykes (and possibly their differentiation products), with a typical plagioclase – K-felsdpar – biotite – hornblende mineralogy; (ii) the large group of the "high-K calc-alkaline" (HKCA) granitoids, typically pink, K-fedspar porphyritic granites with a plagioclase – quartz – biotite ± hornblende matrix. Compared to the sanukitoids, they tend to be more potassic and richer in HFSE (and accordingly, they typically include large amounts of accessory minerals such as titanate).

Sanukitoids require an enriched mantle source. The most commonly proposed mechanism for enrichment is interactions between the mantle and "slab melts", i.e. felsic, TTG-like liquids generated by partial melting of meta-basic rocks (Martin et al. 2010). HKCA granitoids have a somewhat more complex origin; they are however always associated with enriched diorites, sharing many geochemical features with sanukitoids. They are therefore

thought to form via evolution of a dioritic magma (there is no agreement on the details of this "evolution", that could be fractionation, mixing with mantle-derived magmas, or remelting of underplated enriched diorites). The enriched diorites, in turn, form from a mantle source that has been enriched either by slab melts as in the case of sanukitoids (Moyen et al. 2001), or by a sedimentary component (Laurent et al., this volume).

Sanukitoids occur only in the late-Archaean; the oldest recorded example is ca. 2.95 Ga old in the Pilbara (Smithies and Champion 2000). HKCA granites are not always recognized as such in the literature; they also seem to be essentially restricted to the late-Archaean, although there may be older (ca. 3.2 Ga) such rocks in the Kaapvaal craton (Dalmein pluton, Usutu suite of Swaziland; Schoene et al. 2009).

The need for mantle enrichment by surface material (be it basalts or sediments) requires deep burial of hydrous rocks – ie rocks that once were at the surface. This is, essentially, suggestive of a subduction-type environment (although a continuous slab of downgoing material is not required).

Variable geotherms during the genesis of the TTG (and related) granitoids

The TTG suite is the most common granitic component in the Archaean. Despite its apparent homogeneity, it is actually a fairly diverse group, in which it is possible to identify, based on geochemical features, at least three main sub-types, that will be hereafter referred to as "low", "medium" and "high"-pressure TTG. The differences between the three groups are obvious for Al_2O_3, Na_2O, Sr and Y, La and Yb, Nb and Ta, Th, and ratios derived from these – i.e., for a very large range of elements (Figure 1) that includes the ones most commonly regarded as good geochemical tracers. The high-pressure group is characterized by elevated values in Al_2O_3, Na_2O, Sr; and low values in Y, Yb, Th, Ta and Nb. It is also somewhat more leucocratic than the other groups. The low-pressure rocks show opposite features, whereas the medium-pressure group is intermediate between the two.

All of these elements can somehow be related as good pressure indicators. Al_2O_3, Na_2O and Sr are sequestrated preferentially into plagioclase that is stable at pressures lower than ca. 15 kbar during melting of mafic lithologies. Y and Yb are compatible in garnet that is stable above 10-12 kbar. Nb and Ta values are controlled by rutile, stable above 16-18 kbar. These differences can be accounted for by melting of a source of similar trace elements composition, but over a range of pressures. At pressures of 10-12 kbar experimental studies show that melt coexists with an amphibole-plagioclase-pyroxene residuum with little garnet and no rutile; at ca. 15 kbar, the residuum would have no plagioclase but would comprise clinopyroxene, amphibole and significant amounts of garnet. Finally at 20 kbar or more, the melt would coexist with an eclogitic residuum, clinopyroxene (actually omphacite) and garnet with some rutile (Moyen and Stevens 2006).

The temperature of amphibolites/eclogites melting is nearly the same regardless of the pressure, therefore different depth of melting reflect very different geotherms, from less than 12 °C/km (comparable with modern subductions), to up to 30 °C/km (similar to rifts or oceanic plateaus). Even without making any assumptions about Archaean tectonic styles, this does at least demonstrate that different geodynamic environments existed concurrently – whatever they were.

In the modern Earth, granites mostly form in collision zones, principally by biotite incongruent melting (either metasediments, or older continental crust); thus, the modern potassic granites are essentially a consequence of the presence of biotite in the deep metamorphic crust. In contrast, in the young Earth, were continental crust was less abundant and large sediment accumulations nearly absent, similar settings would have involved mafic rocks dominated by amphibole. Thus, even if Archean melting occurred in settings as diverse as those that typify modern anatexis, most of the melts would nevertheless have been formed by incongruent melting of amphibole yielding sodic granitoids, apparently similar but with subtle differences.

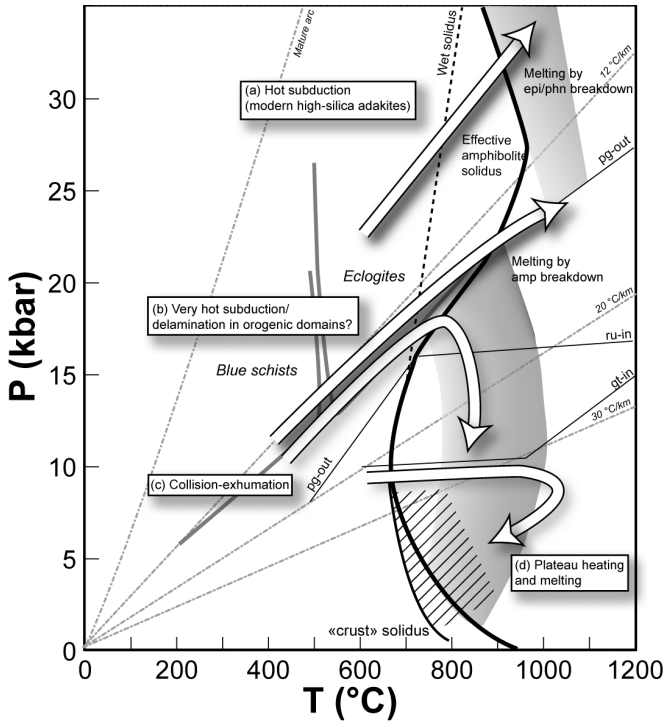

Figure 1. Schematic P—T diagram, summarizing the conditions required for the formation of the diverse types of TTG described in the text (grey, with the dark line being the amphibolites solidus). The PT range of formation of the potassic plagioclase-rich granitoids (and the solidus) are hatched. Geotherms required for each case are also figured (white arrows).

Discussion

Regardless of the models for Archaean global tectonics, the range of granitoids present does require a diversity of environments. Within the TTG group alone, geochemistry demonstrates the existence of geotherms varying from 10 to 30 °C/km, which can certainly not be achieved in

an unique environment. Likewise, the existence of the sanukitoids/HKCA does call for significant burial of surface matter into the mantle. On the other hand, the important volumes of potassic plagioclase-rich granitoids point to major intracrustal recycling and remelting of tonalitic to andesitic protoliths; this is difficult to achieve unless the crust as a whole was very hot. Collectively, Archaean granitoids do therefore demonstrate the existence of diverse geodynamic settings.

In the early and mid-Archaean, the range of granitoid types is restricted to the TTG and related (plagioclase-rich) granitoids. Even then, however, the existence of distinct sub-components of the TTG group demonstrates the existence of distinct tectonic environments.

As Earth's differentiation progresses, the continental crust evolves and large sedimentary associations become common; in general the crust becomes more diverse, and more sources can be tapped to form granitoids. At the same time, deep recycling (subduction?) becomes more significant. This translates in the onset of new granitoid types (peraluminous granites and "mantle derived" HKCA/sanukitoids.

Collectively, Archaean granitoids record a double evolution: towards a more diverse and in general biotite-richer crust, on one hand; towards a tectonic setting dominated by more common subductions, probably stable over longer periods and with cooler geotherms, on the other hand. This evolution occurs on a craton by craton basis; in the Kaapvaal craton for instance, it is essentially achieved at ca. 3.0 Ga whereas it may not occur before 2.7 or even 2.5 Ga in other places. During the Archaean, individual regions of Earth are progressively "transformed" from an ancient to a modern type of tectonics; the change was fully achieved somewhere in the Early Proterozoic.

References

Champion D. C. & Smithies R. H., 2007, Geochemistry of Paleoarchean granites of the East Pilbara Terrane, Pilbara Craton, Western Australia: implications for early Archean crustal growth, in *Earth's Oldest rocks*, Van Kranendonk M. J., Smithies R. H. and Bennett V. eds, Developments in Precambrian Geology 15, Elsevier, 369-410.

Clemens J. D., 2003, S-type granitic magmas: petrogenetic issues, models and evidence, Earth-Science Reviews, 61, 1-18.

Jaguin J., Moyen J.-F., Boulvais P. & Poujol M., 2010, Mid-Archean granites south of the Murchison greenstone belt, South Africa: The oldest large biotite-muscovite leucogranite bodies, 5th IAS meeting, Perth. This volume.

Laurent O., Martin H., Moyen J.-F., Doucelance R. & Paquette J. L., 2010, Genesis and significance of high-K series at the Archaean-Proterozoic boundary, 5th IAS meeting, Perth. This volume.

Martin H., 1994, The Archean grey gneisses and the genesis of the continental crust, in *Archean crustal evolution*, Condie K. C. (ed.), Developments in Precambrian Geology 11, Elsevier, 205-259.

Martin H., Moyen J.-F. & Rapp R., 2010, Sanukitoids and the Archaean-Proterozoic boundary, Transactions of the Royal Society of Edinburgh, Earth Science (in press).

Moyen J. F., Martin H. & Jayananda M., 2001, Multi-element geochemical modelling of crust-mantle interactions during late-Archaean crustal growth: the Closepet granite (South India), Precambrian Research, 112, 87-105.

Moyen J.-F., Martin H., Jayananda M. & Auvray B., 2003, Late Archaean granites: a typology based on the Dharwar Craton (India), Precambrian Research, 127, 103-123.

Moyen J.-F. & Stevens G., 2006, Experimental constraints on TTG petrogenesis: implications for Archean geodynamics, in *Archean geodynamics and environments*, Benn K., Mareschal J.-C. and Condie K. C. eds, American Geophysical Union, 164, 149-178.

Moyen J.-F., 2009, High Sr/Y and La/Yb ratios: The meaning of the "adakitic signature", Lithos 112, 556-574.

Schoene B., Dudas F. O. L., Bowring S. A. & De Wit M., 2009, Sm-Nd isotopic mappig of lithospheric growth and stabilization in the eastern Kaapvaal craton, Terra Nova, 21, 219-228.

Smithies R. H. & Champion D. C., 2000, The Archaean high-Mg diorite suite: Links to Tonalite-Trondhjemite-Granodiorite magmatism and implications for early Archaean crustal growth, Journal of Petrology, 41, 1653-1671.

CALC-ALKALINE DACITES FROM ICELAND AND THEIR RELEVANCE FOR MODELS OF EARLY ARCHAEAN CRUSTAL EVOLUTION

M.Willbold[1,2,3], E. Hegner[2], A. Stracke[3,4] & A. Rocholl[2]

[1] Department of Earth Sciences, University of Bristol, Wills Memorial Building, Queens Road, Bristol, BS8 1RJ, United Kingdom
[2] LMU München, Department für Geowissenschaften, Luisenstraße 36, D-80333 München, Germany
[3] Max-Planck-Institut für Chemie, Postfach 3060, D-55020 Mainz, Germany
[4] ETH Zürich, Institut für Isotopengeologie und Mineralische Rohstoffe, Clausiusstraße 25, 8092 Zürich, Switzerland

Introduction

Early Archaean tonalite-trondhjemite-granodiorite assemblages (TTG) represent the oldest felsic rocks on Earth and make up the lithological backbones of Precambrian terrains. Identifying the geodynamic setting in which these rocks were formed will enable us to understand crucial aspects of the early chemical and physical evolution of our planet. Geological and structural evidence for geodynamic processes that operated in the early Earth are mostly obliterated by intensive late- or post-Archaean tectonic events. Primarily based on the characteristic trace element composition of early Archaean TTG, it is commonly assumed that they formed in convergent plate margin settings. This inference mainly hinges on the observation that only rocks from subduction zone settings, such as modern adakites, show the key-chemical signatures of early Archaean TTG, in particular their high La/Nb, Pb/Ce, La/Yb, and Sr/Y ratios (Martin, 1986; Martin et al., 2005). However, this view has recently been challenged by geological and experimental evidence suggesting that the tectonic processes were dominated by either vertical tectonic processes or crustal stacking in the early Archaean (Van Kranendonk et al., 2007; Nair & Chacko, 2008). Both scenarios imply that early Archaean TTG represent partial melts of a thick mafic proto-crust. It is widely accepted that such internal crustal differentiation cannot produce the continental trace element signatures found in Archaean TTG (de Wit, 1998). In this contribution, we present geochemical data for modern dacites and associated mafic crustal xenoliths from Iceland. The dacites show geochemical signatures similar to early Archaean TTG and hence allow us to assess whether partial melting of thick mafic plateaus can produce TTG-like trace element patterns and to discuss possible implications for models of early Archaean crustal evolution.

The Króksfjördur calc-alkaline dacites and related mafic crustal xenoliths

The Tertiary basaltic to felsic Króksfjördur volcanic complex in NW Iceland developed in a swarm of fissures close to the Icelandic rift about 10 Ma ago (Pedersen & Hald, 1982; Jónasson et al., 1992). Dacites collected from the volcanic complex comprise pitchstones and lavas. The massive, black pitchstones contain phenocrysts of plagioclase and augite set in a devitrified glass matrix. The light-grey and fine-grained lavas have phenocrysts of hornblende, plagioclase, augite, ilmenite and quartz. Coarse to medium-grained gabbroic xenoliths were recovered from one outcrop of dacitic lavas and from an outcrop of pumice tuff (Jónasson et al., 1992; Willbold et al., 2009). All xenoliths are fresh and display annealed high-temperature mineral assemblages comprising plagioclase + clinopyroxene + Fe-Ti oxides ± amphibole ± olivine ± orthopyroxene. Average trace element compositions of the Króksfjördur calc-alkaline dacites and the mafic crustal xenoliths are shown in Fig. 1.

Continental geochemical signatures of the Króksfjördur calc-alkaline dacites

The dacites show a number of pertinent chemical characteristics similar to early Archaean TTGs. They are calc-alkaline (Jónasson et al., 1992; Willbold et al., 2009) with molar Na/K ratios of 3.6 ± 0.3 (1 SD) similar to the values of early Archaean tonalites. They are enriched in Al_2O_3 (14.8 ± 0.3 wt.%), lack a pronounced Eu anomaly (Fig. 1a) and have low Nb concentrations (11 ± 1 µg/g). In addition, they are characterised by high Mg numbers of 42 ± 2, low MgO (1.31 ± 0.15 wt.%) and have low Sr concentrations (283 ± 84 µg/g) for a given Na_2O+CaO value of 7.8 ± 0.2 wt.%. Most notably, however, the Króksfjördur calc-alkaline dacites are almost indistinguishable from Archaean TTG associations in that they show similar positive Pb anomalies in primitive mantle-normalised trace element diagrams (Pb/Ce = 0.11 ± 0.02; Fig. 1) and depletions in Nb and Ta relative to La (La/Nb = 2.5 ± 0.4). Moreover, the Króksfjördur calc-alkaline dacites as well as the Archaean TTG associations have characteristically low Nb/Ta ratios (9.3 ± 1 and 13 ± 3, respectively), which are different from those in modern primitive arc-derived andesites (Nb/Ta = 17 to 51 at TiO_2 = 0.6 to 0.7 wt.%; Kelemen et al., 2004).

A petrogenetic model for the Króksfjördur calc-alkaline dacites

The major element composition of the Króksfjördur calc-alkaline dacites is similar to that of TTG-like melts produced in dehydration melting experiments of mafic materials between 0.1 and 0.3 GPa (Beard & Lofgren, 1991) suggesting that the Króksfjördur calc-alkaline dacites formed by water-undersaturated partial melting of the Icelandic crust (Pedersen & Hald, 1982; Jónasson et al., 1992; Willbold et al., 2009). In Fig. 1, modelled trace element abundances for the Króksfjördur calc-alkaline dacites are compared with average Archaean TTG assuming that the chemical composition of the

source rock for the Króksfjördur calc-alkaline dacites is similar to that of the associated crustal xenoliths. The results corroborate the notion that dehydration melting at crustal levels and subsequent fractional crystallisation can account for the typical TTG-like composition of the dacites, in particular their distinctive Pb, Nb, Ta, and Ti anomalies and low Nb/Ta ratios (Fig. 1). Consequently, these chemical features of TTG assemblages do not necessarily require geochemical processes commonly associated with plate subduction and hence support models invoking melting of, for example, basaltic plateaus (Kröner & Layer, 1992; Hamilton, 1998; Bédard, 2006; Smithies et al., 2007; Van Kranendonk et al., 2007). In contrast to high-Al_2O_3 TTG suites, the Króksfjördur calc-alkaline dacites do not show a pronounced depletion of heavy rare-earth elements (REE) relative to light REE (Drummond & Defant, 1990). It has been postulated that the high Sr/Y and La/Yb ratios in Archaean TTG are due to melting of garnet-bearing eclogitic or amphibolitic protoliths (Martin, 1986; Drummond & Defant, 1990; Martin et al., 2005). Our calculations show that an increase of the modal abundance of residual garnet results in progressively higher Sr/Y ratios and lower Yb concentrations in the melts, similar to those of early Archaean TTG (Fig. 1b). More importantly, all other trace element characteristics in the Króksfjördur calc-alkaline dacites, notably the low Nb/Ta, and high Pb/Ce and La/Nb ratios are retained.

Implications for early Archaean crustal evolution

By accepting the Króksfjördur calc-alkaline dacites as an opportunity to study early Archaean TTG genesis we do not necessarily imply that the latter were formed in a geodynamic setting *identical* to that of Iceland. In contrast to the early Archaean (assuming that modern-style plate-tectonics had not been operating), the Iceland plateau does not remain stationary with respect to a deep-seated heat source and therefore the conditions for its widespread melting are not ideal. The interaction between the Iceland mantle plume and the Atlantic mid-ocean ridge, however, makes Iceland unique among all oceanic plateaus or ocean island chains. The heat flow in the Icelandic crust is considerably higher than the average present-day global heat flux and resembles somewhat better the one in the early Archaean (e.g. see Herzberg, 1992). The excess heat drives large hydrothermal systems and facilitates intense hydratisation of the Icelandic crust. This stabilises amphibole, which, during prograde metamorphism, releases water and triggers dehydration melting. The high heat flow also promotes its melting (i.e. its granitisation) as testified by the unusually high abundance of felsic volcanic rocks on Iceland when compared to other modern oceanic plateaus (e.g. Jónasson, 2007). As such, the processes that formed the Króksfjördur calc-alkaline dacites may be interpreted as a modern analogue of early Archaean processes involved in the formation of Archaean TTG. Recent findings suggest that early Archaean magmatism in the Pilbara craton of NW Australia may have been predominantly tholeiitic similar to the situation on Iceland (Smithies et al., 2007). An increase in the abundance of TTG-like magmas in the Pilbara craton from the Palaeoarchaean to the Mesoarchaean may be due to increasing rates of crustal melting probably similar to the process that formed the Króksfjördur calc-alkaline dacites.

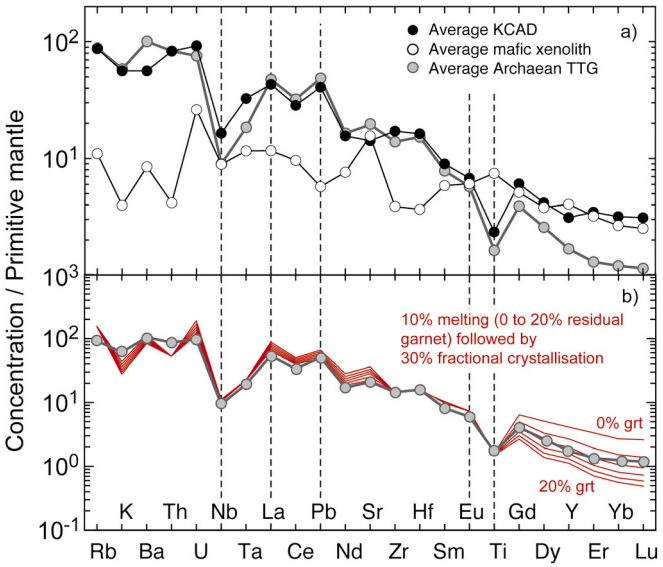

Figure 1 a) Average primitive mantle-normalised (McDonough & Sun, 1995) trace element patterns of Króksfjördur calc-alkaline dacites (KCAD), related crustal mafic xenoliths, and average Archaean TTG (Kemp & Hawkesworth, 2003). Although the KCAD were not formed in the garnet-stability field and lack TTG-like depletions in heavy rare-earth elements (Gd to Lu), there is good agreement for key-chemical characteristics such as enrichment in Pb, depletion in Nb, Ta, and Ti, as well as lack of a Eu anomaly. b) Modelled melt compositions assuming a two-stage forward modelling approach, involving high-pressure dehydration melting of a mafic crust chemically similar to mafic crustal xenoliths associated to the KCAD. Note the good agreement between modelled melt compositions and average TTG. Also shown is the effect of different amounts of residual garnet (0 to 20% modal abundance; 4% increments) on the modelled melt compositions. In the model, garnet subsequently replaces plagioclase and amphibole during prograde metamorphism and melting (Percival, 1983; Rapp & Watson, 1995). The results show that, if garnet would have been present in the source of the KCAD, the characteristically high Sr/Y, La/Yb ratios, and low Yb concentrations would have been reproduced together with the arc-like trace element characteristics as found in TTG.

Acknowledgements

This work was funded by the German Research Council (DFG) grant He 1857/12 to E. Hegner and by a Max-Planck-Gesellschaft fellowship awarded to M.Willbold.

References

Beard J.S. & Lofgren G.E., 1991, Dehydration melting and water-satured melting of basaltic and andesitic greenstone and amphibolites at 1, 3, and 6.9 kb, Journal of Petrology, 32, 365–401.

Bédard J.H., 2006, A catalytic delamination-driven model for coupled genesis of Archean crust and sub-continental lithospheric mantle, Geochimica et Cosmochimica Acta, 70, 1188–1214.

de Wit M.J., 1998, On Archean granites, greenstones, cratons and tectonics: does evidence demand a verdict?, Precambrian Research, 91, 181–226.

Drummond M.S. & Defant M.J., 1990, A model for Trondhjemite-Tonalite-Dacite genesis and crustal growth via slab melting: Archean to modern comparisons, Journal of Geophysical Research, 95, 21503–21521.

Hamilton W.B., 1998, Archean magmatism and deformation were not products of plate tectonics, Precambrian Research, 91, 143–179.

Herzberg C., 1992, Depth and degree of melting of komatiite, Journal of Geophysical Research, 97, 4521–4540.

Jónasson K., 2007, Silicic volcanism in Iceland: composition and distribution within the active volcanic zones, Journal of Geodynamics, 43, 101–117.

Jónasson K., Holm P.M. & Pedersen A.K., 1992, Petrogenesis of silicic rocks from the Króksfjördur central volcano, NW Iceland, Journal of Petrology, 33, 1345–1369.

Kelemen P.B., Hanghoj K. & Greene A.R., 2004, One View of the Geochemistry of Subduction-related Magmatic Arcs, with an Emphasis on Primitive Andesite and Lower Crust, in Treatise on Geochemistry, Holland H.D. & Turekian K.K., eds, Elsevier, Amsterdam, 593–659.

Kemp A.I.S. & Hawkesworth C.J., 2003, Granitic perspectives on the generation and secular evolution of the continental crust, in Treatise on Geochemistry, Holland H.D. & Turekian K.K., eds, Elsevier, Amsterdam, 349–410.

Kröner A. & Layer P.W., 1992, Crust formation and plate motion in the Early Archean, Science, 256, 1405–1411.

Martin H., 1986, Effect of steeper Archean geothermal gradient on the geochemistry of subduction-zone magmas, Geology, 14, 753–756.

Martin H., Smithies, R.H. Rapp, R., Moyen J.-F. & Champion D., 2005, An overview of adakite, tonalite-trondhjemite-granodiorite (TTG), and sanukitoid: relationships and some implications for crustal evolution, Lithos, 79, 1–24.

McDonough W. & Sun S.S., 1995, The composition of the Earth, Chemical Geology, 120, 223–253.

Nair R. & Chacko T., 2008, Role of oceanic plateaus in the initiation of subduction and origin of continental crust, Geology, 36, 583–586.

Pedersen A.K. & Hald N., 1982, A cummingtonite-porphyritic dacite with amphibole rich xenoliths from the Tertiary central volcano at Króksfjördur, NW Iceland, Lithos, 15, 137–159.

Percival J.A., 1983, High-grade metamorphism in the Chapleau-Foleyet area, Ontario, American Mineralogist, 68, 667–686.

Rapp R.P. & Watson E.B., 1995, Dehydration Melting of Metabasalt at 8-32kbar: Implications for Continental Growth and Crust-Mantle Recycling, Journal of Petrology, 36, 891–931.

Smithies R.H., Champion, D.C. & Van Kranendonk, M.J., 2007, The oldest well-preserved felsic volcanic rocks on Earth: geochemical clues to the early evolution of the Pilbara supergroup and implications for the growth of a Paleoarchean protocontinent, in Earth's oldest rocks, Van Kranendonk M.J., Smithies R.H. & Bennett V.C., eds, Elsevie,r339-369.

Van Kranendonk M.J., Smithies R.H., Hickman A.H. & Champion D.C., 2007, Review: secular tectonic evolution of Archean continental crust: interplay between horizontal and vertical processes in the formation of the Pilbara Craton, Australia, Terra Nova 19, 1–38.

Willbold M., Hegner E., Stracke A. & Rocholl A., 2009, Continental geochemical signatures in dacites from Iceland and implications for models of early Archaean crust formation, Earth and Planetary Science Letters, 279, 44–52.

GEOCHEMICAL AND ISOTOPIC CHARACTERISTICS OF THE NUVVUAGITTUQ BELT: IMPLICATIONS FOR EARTH'S EARLY CRUST

J. O'Neil[1], R.W. Carlson[1] & D. Francis[2]

[1]Department of Terrestrial Magnetism, Carnegie Institution of Washington, 5241 Broad Branch Road, N.W., Washington, DC 20015 USA
[2]Earth & Planetary Sciences Department, McGill University, Montreal, Qc, Canada, H3A 2A7

Introduction

Until recently, the only Hadean samples available were detrital zircons from the Jack Hills conglomerate (~4.4 Ga; Wilde et al., 2001). Although these zircons provide invaluable information about the early Earth, their host rocks have been destroyed, leaving no direct samples of the Earth's primordial crust. Other than these detrital zircons, rare occurrences of Eoarchean crust provide the only compositional constraints on the nature of the Earth's early crust. Thus a period of over 500 million years of the Earth's history is unrepresented in the rock record and the nature of the Earth's early crust and the processes responsible its formation remain largely speculation. Moreover, although primary crust forming today is mafic in composition, our knowledge of the Earth's early crust is largely based on felsic rocks because they are the most likely host rocks for the zircons that provide old U-Pb ages. These granitic rocks cannot, however, have been directly produced from melting of the primordial mantle and must have been derived from the melting of an older mafic precursor. This emphasises the need to focus on the mafic component in Eoarchean/ Hadean terrains in order to constrain the composition of Earth's early crust. Unfortunately, mafic rocks are more likely to undergo compositional modification during the extensive metamorphism experienced by all Eoarchean/ Hadean rocks, and they tend to be devoid of zircon, thus necessitating the use of other geochronometers.

Recent ^{142}Nd studies on the Nuvvuagittuq greenstone belt showed that the dominant lithology of the belt, known as the "faux-amphibolite", have a deficit in 142Nd of 7 to 15 ppm compared to the terrestrial Nd standard (O'Neil et al., 2008). The magnitude of the deficit correlates with the Sm/Nd ratio of the samples and thus suggests that the faux-amphibolite formed at ~4.28 Ga, making it the only know remnant of Hadean crust preserved on Earth.

Geological setting

The Nuvvuagittuq greenstone belt is located in the Northeastern Superior Province on the east coast of Hudson Bay, Canada and is composed of a ~10 km^2 Eoarchean to Hadean volcano-sedimentary sequence (O'Neil et al., 2007, 2008). The Nuvvuagittuq faux-amphibolite consists of gneisses ranging from cummingtonite amphibolite to garnet-biotite schist composed of variable proportions of cummingtonite + biotite + quartz, ± plagioclase ± garnet ± anthophyllite ± cordierite. The faux-amphibolite is intruded by numerous ultramafic and gabbroic sills. The Nuvvuagittuq greenstone belt also contains chemical sedimentary rocks, which include a finely-banded iron formation and a more massive silica-formation, which together define an easily recognizable stratigraphic horizon that can be traced around the entire belt.

The oldest U-Pb dates from the Nuvvuagittuq greenstone belt have been obtained in rare thin intrusive felsic bands of tonalitic composition. Zircons from these felsic bands have yielded U-Pb ages of 3817 ± 16 (David et al., 2009) and 3751 ± 10 Ma (Cates and Mojzsis, 2007) that are interpreted to be their crystallization age. ^{147}Sm-^{143}Nd whole rock isochrons obtained on a differentiated sill and a highly deformed gneissic gabbro sill intruding the faux-amphibolite give ages of 3840 ± 280 Ma and 4023 ± 110 Ma respectively, which support an older age for the faux-amphibolite (O'Neil et al., 2008), which they intrude. The Nuvvuagittuq greenstone belt is surrounded by 3660 Ma tonalites (David et al., 2009) interpreted to have been produced by the melting of the belt's mafic rocks (Adams et al., 2009; David et al., 2009). The faux-amphibolite have been metamorphosed to at least upper amphibolite facies conditions (O'Neil et al., 2007; Cates and Mojzsis, 2009; Scher and Minarik 2009) and preliminary ^{147}Sm-^{143}Nd analyses on garnets from the faux-amphibolite are consistent with an age of 2700 Ma for the garnet formation. The Nuvvuagittuq belt is also intruded by 2686 ± 4 Ma pegmatites (David et al., 2009). These geochronological constraints suggest that the Nuvvuagittuq greenstone belt recorded more than 1.5 billion years of Earth's history (~4.3 to 2.7 Ga) in a critical time period of its early stages.

Mafic Hadean crust

The faux-amphibolites generally have a mafic composition, and range from basalt to andesite in terms of their silica contents (SiO_2 = 42-68 wt.%), with a concomitant decrease in MgO content (16.7-2.2 wt.%) with increasing SiO_2. The faux-amphibolites can be divided into a high-Ti and a low-Ti chemical groups that define distinct trends in a plot of TiO_2 vs Zr. These groups are stratigraphically separated by the banded iron formation in the Nuvvuagittuq greenstone belt. At what is interpreted as the base of the sequence, the high-Ti faux-amphibolite is mainly basaltic in composition and generally has lower Al_2O_3 and higher TiO_2 contents, whereas the low-Ti faux-amphibolite is characterized by high Al_2O_3 and low TiO_2 contents and exhibits a wider range of composition from basaltic to andesitic. The low-Ti faux-amphibolite can also be further subdivided into a depleted and an enriched subgroup based on the abundance of high field strength elements (HFSE) and

rare earth elements (REE). The high-Ti faux-amphibolite is characterized by relatively flat-REE patterns as opposed to the enriched low-Ti faux-amphibolite that has LREE-enriched profiles with flat HREE, and the depleted low-Ti faux-amphibolite that have U-shaped REE profiles. The three different geochemical groups of faux-amphibolite have compositional analogues in three types of ultramafic sills exhibiting the same stratigraphic succession. Type-1 ultramafic sills, analogues of the high-Ti faux-amphibolite, intrude the belt below the BIF, whereas Type-2 and Type-3 ultramafic sills, analogues of the depleted and the enriched low-Ti faux-amphibolites, respectively, are located above the BIF. The early high-Ti faux-amphibolites share geochemical characteristics with tholeiitic volcanic suites with low Al_2O_3 and high TiO_2 contents and are consistent with crystal fractionation at low pressures under dry conditions. In contrast, the low-Ti faux-amphibolites are geochemically similar to calc-alkaline volcanic suites. Their high Al_2O_3 and low TiO_2 contents for the andesitic compositions suggest the early crystallization of Fe-Ti oxides and late appearance of plagioclase and are more consistent with fractionation at elevated water pressures. The faux-amphibolite comprises an anthophyllite-biotite assemblage seen locally in both the high and low-Ti faux-amphibolites that are characteristically very low in Ca and high Mg contents. Many samples have CaO contents < 1 wt.%. Such low Ca contents are unlikely to represent the original composition of their igneous precursors and are interpreted to reflect intensive weathering. They also commonly have enriched LREE profiles and negative Eu anomalies. The geochemical composition of the cordierite-anthophyllite faux-amphibolite is consistent their protoliths being mafic volcanics hydrothermally altered by seawater.

A new series of faux-amphibolite was analysed for its ^{142}Nd isotopic composition. All samples yielded low $^{142}Nd/^{144}Nd$ ratios and have deficits in ^{142}Nd ranging from -7.5 to -18.5 ppm compared to terrestrial standard (figure 1).

This is comparable to the ^{142}Nd deficit measured previously for the faux-amphibolite (O'Neil et al., 2008). The $^{142}Nd/^{144}Nd$ ratios for the faux-amphibolite correlate positively with their Sm/Nd ratios producing a slope corresponding to an age of 4276^{+61}_{-104} Ma for all faux-amphibolite, including the three different geochemical groups. However, as observed before, the lowest $^{142}Nd/^{144}Nd$ ratios were found in the enriched low-Ti faux-amphibolites. A line fitting only the enriched low-Ti faux-amphibolites corresponds to an age of 4263^{+41}_{-64} Ma. Preliminary data suggest that the ultramafic rocks have no deficit in ^{142Nd}, which is expected given their near chondritic Sm/Nd ratios. Including the enriched low-Ti faux-amphibolites and the corresponding co-genetic ultramafic sills gives a ^{146}Sm-^{142}Nd age of 4310^{+43}_{-61} Ma.

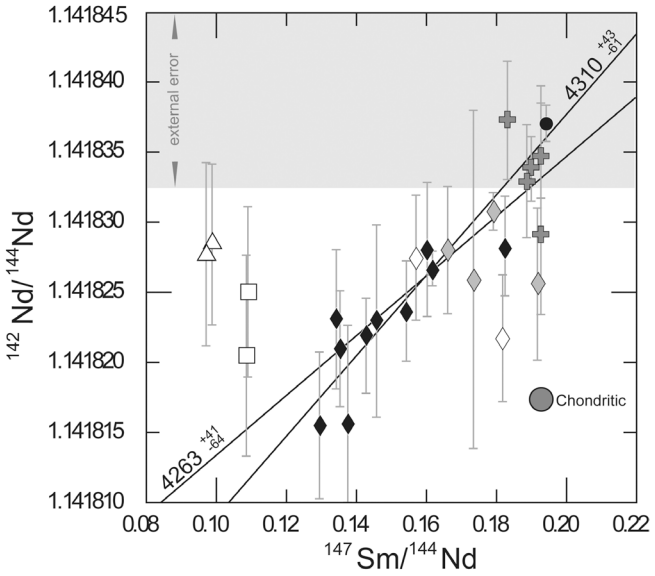

Figure 1: $^{142}Nd/^{144}Nd$ versus $^{147}Sm/^{144}Nd$ isochron diagram for the Nuvvuagittuq rocks. The horizontal grey band shows the ±6 ppm external precision obtained on the terrestrial standard. Symbols are: open diamond = high-Ti faux-amphibolite; grey diamond = depleted low-Ti faux-amphibolite; black diamond = enriched low-Ti faux-amphibolite; black circle = Type 2 ultramafic; grey plus = gabbro; open triangle = felsic band; open square = tonalite. The best fit line through the enriched low-Ti faux-amphibolite data corresponding to an age of 4263^{+41}_{-64} Ma. A line including Type-2 ultramafic sill corresponds to an age of 4310^{+43}_{-61} Ma.

Conclusion

The ^{142}Nd isotopic composition and the geochemistry of the faux-amphibolite along with the occurrence of low CaO cordierite-anthophyllite assemblages are consistent with its protolith being Hadean basaltic to andesitic hydrothermally altered volcanic rocks recording an evolution from "tholeiitic to "calc-alkaline" magmatism. This geochemical succession seen in the Nuvvuagittuq greenstone belt is typical of the volcanic successions of many younger Archean greenstone belts. Regardless of the exact tectonic setting, this volcanic succession suggests that the geological processes responsible for the formation and evolution of Archean greenstone belts were active as early as 4.3 Ga.

Acknowledgements

We would like to acknowledge the people from the Pituvik Landholding Corporation for their support for the logistical aspect in the field. We also thank the people and municipality of Inukjuak for their hospitality. This research was supported by the National Science Foundation (NSF-EAR-0910442) and the National Science and Engineering Research Council of Canada (NSERC) Discovery Grants to Francis (RGPIN 7977-00).

References

Adam, J., Rushmer, T.A., O'Neil, J. & D. Francis, D., 2009, Hadean Boninites and TTG Genesis, Eos, Transactions, American Geophysical Union, 90, Fall Meeting Supplement, Abstract V13C-2042.

Cates, N.L. & Mojzsis, S.J., 2007, Pre-3750 Ma supracrustal rocks from the Nuvvuagittuq supracrustal belt, northern Quebec, Earth and Planetary Science Letters, 25, .9-21.

Cates, N.L. & Mojzsis, S.J., 2009, Metamorphic zircon, trace elements and Neoarchean metamorphism in the ca. 3.75 Ga Nuvvuagittuq supracrustal belt, Quebec (Canada), Chemical Geology, 261, 98-113.

David, J., Godin, L., Stevenson, R., O'Neil, J. & Francis, D., 2009, U-Pb ages (3.8-2.7 Ga) and Nd isotope data from the newly identified Eoarchean Nuvvuagittuq supracrustal belt, Superior Craton, Canada, Geological Society of America Bulletin, 121, 150-163.

O'Neil, J., Carlson, R.W., Francis, D. & Stevenson, R.K., 2008, Neodymium-142 Evidence for Hadean Mafic Crust, Science, 321, 1828-1831.

O'Neil, J., Maurice, C., Stevenson, R.K., Larocque, J., Cloquet, C., David, J. & Francis, D., 2007, The Geology of the 3.8 Ga Nuvvuagittuk (Porpoise Cove) Greenstone Belt, northern Superior Province, Canada, in *Earth's Oldest Rocks*, M.J. Van Kranendonk, R.H. Smithies & V.C. Bennett, eds, Developments in Precambrian Geology 15, Elsevier BV.

Scher, S. & Minarik, W., 2009. Thermobarometry in the Hadean: The Nuvvuagittuq Greenstone Belt, Eos, Transactions, American Geophysical Union, 90, Joint Assembly. Supplement, Abstract V23C-05.

Wilde, S.A., Valley, J.W., Peck, W.H. & Graham, C.M., 2001, Evidence from detrital zircons for the existence of continental crust and oceans on the Earth 4.4 Gyr ago, Nature, 409, 175-178.

THE EVOLUTION AND EXTENT OF ARCHEAN CONTINENTAL LITHOSPHERE: IMPLICATIONS FOR TECTONIC MODELS

W.L. Griffin[1], S.Y. O'Reilly[1], J.C. Afonso[1] & G.C. Begg[1,2]

[1]GEMOC, Macquarie University, NSW 2109, Australia
[2]Minerals Targeting International, West Perth, WA 6005, Australia

The composition of the subcontinental lithospheric mantle (SCLM), as sampled by xenoliths in volcanic rocks, shows a broad correlation with the tectonothermal age of the overlying crust. Archean cratons have variably depleted SCLM; the SCLM beneath Phanerozoic crust is dominated by compositions that are only moderately depleted compared to the Primitive Upper Mantle; the SCLM of Proterozoic cratons is generally intermediate between these extremes. These variations have been interpreted as suggesting a gradual secular change in SCLM-forming processes (eg Griffin et al., 2003). However, recent developments in seismic tomography and the integrated modeling of geophysical and petrological data (Afonso et al. 2008; Begg et al. 2009; Griffin et al. 2009) have stimulated a major re-evaluation of the original composition and present extent of Archean SCLM.

Most estimates of the composition of Archean SCLM have been based on suites of xenoliths, mainly from kimberlites. These estimates (Table 1) represent depleted garnet lherzolites with high orthopyroxene/olivine. However, these estimates suffer from important sampling biases. The high opx/ol is a feature of xenoliths from the Kaapvaal craton of South Africa, and especially the large dumps from the diamond mines of the Kimberley area, which have supplied ca 85% of the analyses of kimberlite-borne xenoliths in the literature. It is now clear that such high opx/ol is rare in xenolith suites from other cratons. Equally importantly, the published database is strongly biased toward garnet peridotites, because these are the samples for which P-T estimates can be derived using mineral compositions (cpx-opx or gnt-ol for T, and gnt-opx for P).

The previous estimates of Archean SCLM compositions have other problems as well. Advances in the modelling of geophysical data (Deen et al., 2006; Afonso et al. 2008) have shown that it is difficult to account for the high shear-wave velocities measured in the cores of large cratons, if the cratonic roots consist of "typical" depleted garnet lherzolites. These compositions would also predict deeper geoid anomalies and higher elevations than are observed over the cratons. Detailed regional seismic tomography studies of cratons (e.g. Kaapvaal Seismic Project) have outlined high-velocity volumes separated by zones of lower velocity. Combining the tomographic maps with GIS data, it is apparent that kimberlites *preferentially intrude the lower-velocity margins* of the cratons and of sub-blocks within them. This means that that most cratonic xenolith suites represent this low-velocity material, and the high-velocity cratonic SCLM is under-represented in published xenolith databases.

Xenolith suites contain a rich array of rock types, but with little information on their spatial relationships. In recent years several studies of tectonically emplaced peridotite massifs have recognised that these large slabs of SCLM originally were highly depleted, but have experienced refertilisation by the introduction of mafic melts. For example, Le Roux et al. (2007) have demonstrated that the type Lherzolite of the Lherz massif is a metasomatic rock; its protolith was a highly depleted dunite/harzburgite. Similarly, the well-studied garnet peridotites of the Western Gneiss Region of Norway represent relatively small refertilised zones within large volumes of dunite (Beyer et al. 2004, 2006). The refertilisation processes that add Ca, Al and Fe to the SCLM and produce garnet lherzolites also impart a higher density and lower seismic velocity. This explains why the kimberlites, which preferentially sample the low-velocity margins of cratonic blocks, carry a relatively high proportion of garnet lherzolite xenoliths.

We therefore have suggested (Griffin et al., 2009) that most Archean SCLM originally consisted of highly depleted dunites/harzburgites, similar to the Archean orogenic massifs of western Norway. The revised "primitive SCLM" composition (Table 1) has a lower opx/ol ratio than previous estimates, as well as lower Ca and Al, and higher Mg#. Incorporation of such rocks in the cold upper parts of the cratonic SCLM satisfies both the seismic and the gravity data, suggesting that large volumes of these depleted rocks are preserved in the cores of cratons, where they will be poorly sampled by volcanic eruptions.

The roots of most Proterozoic shields generally show somewhat lower seismic velocities than those beneath Archean cratons, and this observation has been interpreted as indicating that the Proterozoic roots were originally less depleted than Archean roots. However, isotopic studies are increasingly demonstrating that these Proterozoic cratons (as distinct from Proterozoic mobile belts) contain significant amounts of Archean material (Figure 1), especially in the lower crust (Belousova et al. 2009; Zheng et al. 2004, 2006, 2008). It seems probable that this Archean crust was underlain by Archean SCLM, and the seismic velocities beneath Proterozoic cratons are similar to those in the metasomatised parts of the Archean SCLM. We therefore now interpret most of the SCLM beneath Proterozoic cratons as consisting of refertilised Archean SCLM.

The extremely depleted Archean SCLM (Table 1), and even its metasomatised variants, are buoyant relative to the asthenosphere (Poudjom Djomani et al., 2001), and

Table 1. Average compositions for xenoliths, Norwegian exposed peridotites and the revised Archean SCLM.

	Average Low-T xenolith	**Average Low-T xenoliths**	**Average dunite/ harzburgite**	**Average lherzolite**	**"Primitive" Archean SCLM**
	Kaapvaal Craton	Slave Craton Canada	Almklovdalen Norway	Almklovdalen Norway	**Calculated**
SiO_2	46.5	42.9	42.8	43.81	**42.9**
TiO_2	0.05	0.00	0.01	0.03	**0.01**
Al_2O_3	1.40	1.10	0.14	2.2	**0.30**
Cr_2O_3	0.34	0.50	0.32	0.41	**0.40**
FeO	6.6	7.2	6.5	7.3	**6.5**
MnO	0.10	0.10	0.11	0.12	**0.15**
MgO	43.8	47.2	49.2	43.8	**49.2**
CaO	0.88	0.60	0.09	1.66	**0.10**
Na_2O	0.10	0.12	0.16	0.27	**0.10**
NiO	0.29	0.31	0.34	0.31	**0.34**
Mg#	92.2	92.1	93.1	91.5	**93.1**
Cr/ (Cr+Al)	0.14	0.10	0.35	0.04	**0.23**

would not be likely to "delaminate" or be subducted. Thus we would expect most of the SCLM generated in Archean time to be still on the surface of the Earth. Mapping of the SCLM worldwide combining global seismic tomography with isotopic data on the age of deep crust and SCLM (see below) suggests that ca 70% of the existing SCLM is Archean in origin. This is consistent with modelling of GEMOC's worldwide database of zircon Hf-isotope data, which suggests that ca 70% of the continental crust had been generated by the end of Archean time (Belousova et al., in prep).

Rather than a gradual evolution in SCLM-forming processes, we suggest a sharp dichotomy between Archean and younger tectonic regimes. Highly depleted peridotites can be found in modern tectonic environments, including subduction zones. However, Archean SCLM is unique in one important respect: whereas Phanerozoic peridotites have 8±1 wt% FeO regardless of their degree of depletion, Archean SCLM typically has significantly lower FeO (mean 6.5%; Table 1). These compositions (Table 1) imply very high degrees of melt extraction (ca 50%) at high T and P, a process with enormous energy requirements. We suggest that these highly depleted rocks were formed in mantle overturns, or very large plumes, and that these geodynamic mechanisms were restricted to the Archean.

The timing of melt extraction from a peridotitic residue can be estimated from Re-Os studies, but the Os-isotope

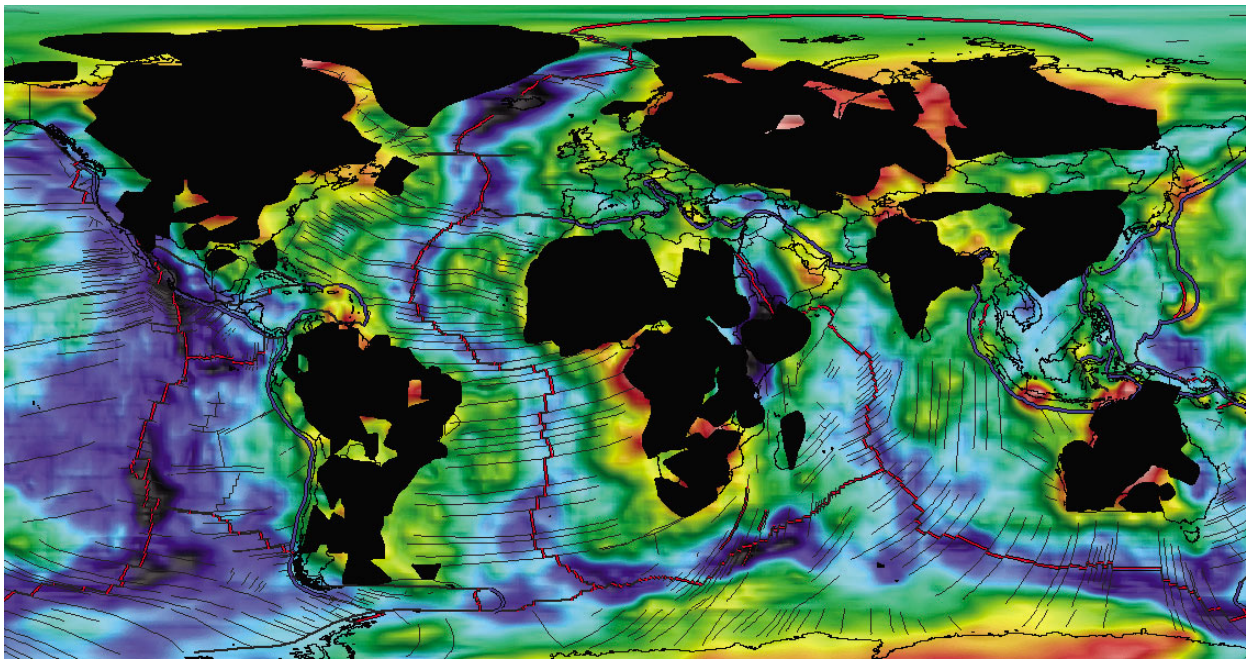

Figure 1. Interpreted extent (conservative) of original Archean SCLM (black) superimposed on a global Vs tomography image (100-150 km depth) provided by Steve Grand (University of Texas, NM). Cool colors are low Vs.

systematics of SCLM peridotites are controlled by the presence of sulfide phases, and any sample may contain >1 generation of sulfides (Alard et al. 2002). Whole-rock Os-isotope data therefore can only provide minimum ages for melt extraction. The analysis of Os isotopes in single sulfide grains (Pearson et al., 2002, Griffin et al. 2004) can avoid the mixing problem, but if all sulfides were removed from the dunite residues along with the melts, the analysis of sulfide grains may date only the re-introduction of subsequent fluids. With these caveats, it probably is significant that Os T_{RD} model ages for sulfides in xenoliths from several cratons show a major peak around 3 Ga, and there are no T_{RD} >3.5 Ga in either the sulfide dataset or among published whole-rock analyses. This suggests to us that most of the Archean SCLM was formed between 3-3.5 Ga ago; we have no evidence of Hadean SCLM, and the existing Archean SCLM may represent a tectonic/dynamic regime that operated in a short transition period between the Hadean and the NeoArchean regimes.

It is important to recognise that the widely studied garnet lherzolite xenoliths, from kimberlites (the major source of our knowledge about the ancient SCLM composition) are metasomatised rocks, rather than primitive melt-residues; their compositions (whether major- or trace-element) thus cannot be used to model their conditions of formation. Specifically, they do not provide evidence for shallow melting, the existence of Archean plate tectonics, or the generation of the cratonic SCLM by underthrusting of ocean-ridge peridotites (e.g. Canil 2002) as traditionally thought. The production of Archean SCLM through large-scale plume/overturn mechanisms may well have coexisted with a regime similar to modern plate tectonics. However, as in the modern situation, oceanic lithosphere generated by melt extraction at mid-ocean ridges would be unstable on cooling, and would rarely be preserved.

Acknowledgements

The ideas presented here have been developed through discussions with numerous colleagues over many years. Steve Grand provided an updated version of his global seismic tomography model and helped us to understand many aspects of its use to investigate the lithosphere. The analytical data were obtained using instrumentation funded by ARC LIEF, and DEST Systemic Infrastructure Grants, industry partners and Macquarie University. The research was supported by ARC and Macquarie University grants to S.Y. O'Reilly and W.L. Griffin, and collaborative research with industry partners, especially Western Mining Resources and BHP-Billiton.

References

Afonso J.C., Fernandez M., Ranalli G., Griffin W.L. & Connolly J.A.D., 2008, Integrated geophysical-petrological modeling of the lithosphere and sublithospheric upper mantle: methodology and applications, Geochemistry, Geophysics, Geosystems 9, Q05008, doi:10.1029/2007GC001834.

Alard O., Griffin W.L., Pearson N.J., Lorand J.-P. & O'Reilly S.Y., 2002, New insights into the Re-Os systematics of subcontinental lithospheric mantle from in-situ analysis of sulfides, Earth and Planetary Science Letters, 203, 651-663.

Begg G.C., Griffin W.L., Natapov L.M., O'Reilly S.Y., Grand S.P., O'Neill C.J., Hronsky J.M.A., Poudjom Djomani Y., Swain C.J., Deen T. & Bowden P., 2009, The lithospheric architecture of Africa: Seismic tomography, mantle petrology and tectonic evolution, Geosphere, 5, 23-50.

Belousova E.A., Reid A.J., Griffin W.L. & O'Reilly S.Y., 2009, Rejuvenation vs recycling of Archean crust in the Gawler Craton, South Australia: Evidence from U-Pb and Hf isotopes in detrital zircon, Lithos, 113, 570-582.

Beyer E.E., Brueckner H.K., Griffin W.L., O'Reilly S.Y. & Graham S., 2004, Archean mantle fragments in Proterozoic crust, Western Gneiss Region, Norway, Geology, 32, 609-612.

Beyer E.E., Griffin W.L. & O'Reilly S.Y., 2006, Transformation of Archean lithospheric mantle by refertilisation: Evidence from exposed peridotites in the Western Gneiss Region, Norway, Journal of. Petrology, 47, 1611-1636.

Canil D. 2002, Vanadium in peridotites, mantle resdox and tectonic environments: Archean to present, Earth Planetary Science Letters, 195, 75-90.

Deen, T., Griffin, W.L., Begg, G., O'Reilly, S.Y. & Natapov L.M., 2006, Thermal and compositional structure of the subcontinental lithospheric mantle: Derivation from shear-wave seismic tomography, Geochemistry, Geophysics and Geosystems, doi:10.1029/2005GC001164.

Griffin W.L., O'Reilly S.Y., Abe N., Aulbach S., Davies R.M., Pearson N.J., Doyle B.J. & Kivi K., 2003, The origin and evolution of Archean lithospheric mantle, Precambrian Research, 127, 19-41.

Griffin W.L., Graham S., O'Reilly S.Y. & Pearson N.J., 2004, Lithosphere evolution beneath the Kaapvaal Craton. Re-Os systematics of sulfides in mantle-derived peridotites, Chemical Geology, 208, 89-118.

Griffin,W.L., O'Reilly S.Y., Afonso J.C. & Begg G., 2009, The composition and evolution of lithospheric mantle: A re-evaluation and its tectonic implications, Journal of Petrology, 50, 1185-1204.

Le Roux V., Bodinier J-L., Tommasi A., Alard O., Dautria J.M. &Riches A.J.V., 2007, The Lherz spinel peridotite: Refertilized rather than pristine mantle,. Earth and Planetary Science Letters, 259, 599-612.

Pearson N.J., Alard O., Griffin W.L., Jackson S.E. & O'Reilly S.Y., 2002, In situ measurement of Re-Os isotopes in mantle sulfides by Laser Ablation Multi-Collector Inductively-Coupled Mass Spectrometry: analytical methods and preliminary results, Geochimica et Cosmochimica Acta, 66, 1037-1050.

Poudjom Djomani Y.H., O'Reilly S.Y., Griffin W.L. & Morgan P., 2001, The density structure of subcontinental lithosphere: Constraints on delamination models, Earth and Planetary Science Letters, 184, 605-621.

Zheng J., Griffin W.L., O'Reilly S.Y., Lu F., Wang C., Zhang M., Wang F. & Li H., 2004, 3.6 Ga lower crust in central China: new evidence on the assembly of the North China Craton,. Geology, 32, 229-232.

Zheng J.P., Griffin W.L., O'Reilly S.Y., Zhang M., Pan Y., Pearson N.J. and Lin G., 2006, Widespread Archean basement beneath the Yangtze Craton, Geology, 34, 417-420.

Zheng J.P., Griffin W.L., O'Reilly S.Y., Hu B.Q., Zhang M., Pearson N.J., Lu F.X. & Wang F.Z., 2008, Continental collision and accretion recorded in the deep lithosphere of central China, Earth and Planetary Science Letters, 269, 496-506.

ISOTOPIC CONSTRAINTS ON FORMATION OF HADEAN-ARCHEAN MANTLE AND CRUST

S.B. Shirey & R.W. Carlson

Carnegie Institution of Washington, Department of Terrestrial Magnetism, 5241 Broad Branch Road, NW, Washington DC 20015 USA

Introduction

Early ^{147}Sm-^{143}Nd isotopic data on Eoarchean to Neoarchean juvenile granitoids and Lu-Hf isotopic data on their separated zircon fractions were used to define the Earth's earliest mantle composition leading to these basic conclusions: a) the earliest Archean mantle was already depleted in highly incompatible elements; b) Nd isotopic compositions of some granitoids are inexplicably high; c) fidelity of some whole-rock Sm/Nd ratios through billions of years of crustal residence can be problematic; and d) prior creation and separation of substantial volumes of continental crust is a possible explanation for early mantle depletion (e.g. Armstrong, 1991). Much more detail on Hadean processes now can be obtained from the significant advances in the last two decades: a) refinement of the Lu-Hf decay constant; b) detailed study of the Hadean zircon population; c) the widespread application of the ^{146}Sm-^{142}Nd system in concert with the ^{147}Sm-^{143}Nd system.

Implications for the Hadean from the present oceanic mantle

The isotopic and trace element composition of the present oceanic mantle and its evolution with time carry implications for the terrestrial mantle in the Hadean. The secular increase in the Nb/Th of the depleted mantle from around 8 at 3 Ga to around 18 today (e.g. Collerson & Kamber, 1999), geodynamic modelling of mantle convection (e.g. Christensen & Hofmann, 1994; Davies, 2002), and the 1.8 Ga mean age of the oceanic basalt Pb isotope data array (e.g. Hofmann, 2003) make it likely that the isotopic heterogeneity of the present oceanic mantle is direct evidence for the incorporation of recycled oceanic lithospheric mantle, some of which could be as ancient as Eoarchean (Shirey et al., 2008). Any recycling of Hadean continental crust would have been volumetrically swamped by oceanic lithosphere recycling. Furthermore, the continental crust is so rich in key lithophile elements (e.g. Rb, Ba, Sr, Pb, LREE) that mass balance dictates its recycling into the mantle would be easily apparent (Carlson and Shirey, 1988). Although recycled continental material is present in the modern mantle, forming the EM1 and EM2 end members, it is a relatively rare component and suggestive of only minimal masses of recycled material (e.g. Hofmann, 1997; Hofmann, 2003). Therefore in the Hadean, it is likely that intramantle processes and recycling of oceanic lithosphere dominated the geochemical evolution of the mantle (Carlson & Shirey, 1988; Shirey et al., 2008).

Mantle compositions prior to the appearance of the first preserved crust

The earliest Eoarchean juvenile rocks and Hadean zircons with highest bona fide Hf isotopic compositons can be used to track the characteristics of their sources in the mantle, thus defining the Earth's Hadean mantle composition (c.f. review of Hawkesworth et al., 2010). Using the recent determinations of the Lu decay constant (e.g. Scherer et al., 2001) to calculate initial Hf isotopic compositions, the Hf and Nd isotopic compositions of the inferred Hadean mantle do not show the typical 1:2 ratio of ε_{Nd}:ε_{Hf} that is evident for the Earth's mantle after 2.5 Ga and is expected for typical melting in the shallow mantle or for fractional crystallization (Vervoort & Blichert-Toft, 1999). ε_{Hf} has a time-averaged chondritic composition whereas ε_{Nd} displays time-averaged depleted (e.g high Sm/Nd) growth (Fig. 1A,B). Continental crustal rocks such as tonalite-trondhjemite-granodiorite (TTG) are known to be derived from the mantle by a multiple-step melting process that starts with mantle-derived basalt which are then remelted one or more times (e.g. Martin et al., 2005). Trace element partition coefficients for the residual mineral assemblages of such low-pressure melting always produce higher Sm/Nd and Lu/Hf in the residues and would lead to a mantle whose Hf isotopic composition is more depleted compared to Nd by about factor of two. Therefore, the Nd and Hf isotopic composition of the inferred Hadean mantle cannot be due chiefly to prior crustal extraction even with a mafic intial stage and requires intramantle fractionation such as with a transient magma ocean.

Recent high-precision $^{142}Nd/^{144}Nd$ measurements of meteorites and a variety of terrestrial samples show that the Earth's mantle has a range of nearly 40 ppm in $^{142}Nd/^{144}Nd$, a signature that must have been created in the first 100 Ma of Earth history when ^{146}Sm was actively decaying to ^{142}Nd. Boyet & Carlson (2005; 2006) proposed the separation of an early enriched reservoir (EER) from the magma ocean that must have formed just after Earth's accretion. Separation of an EER also should have produced a depleted terrestrial mantle with an ε_{Hf} isotopic composition as depleted as or more depleted than the Nd isotopic depletion of the mantle. Since this depletion is not seen, another explanation is required. Using high pressure partition coefficients for Lu, Hf, Sm, and Nd in Ca-silicate and Mg-silicate perovskite (Corgne et al., 2005; Liebske et al., 2005) settling from this magma ocean has a negligible affect on Sm/Nd but a large effect on Lu/Hf (Caro et al., 2005). This would have lowered the bulk Lu/Hf of the upper mantle enough to bring its bulk evolution through the field of oldest juvenile continental crustal rocks (Fig. 1C) without having much effect on the Nd isotopic evolution of the mantle. Thus, prior to the onset of Eoarchean crustal preservation at 3.9 Ga, the Hadean mantle bears the integrated geochemical effect of magma ocean crystallization and oceanic lithosphere recycling.

Table 1. A possible summary of Hadean through Archean events, with supporting evidence and chief effect on the mantle, compiled from the literature and modified from Shirey et al. (2008).

Time (Ga)	Event	Supporting evidence	Effect
4.57	accretion	meteorites	chondritic composition Earth
4.57- 4.54	core formation first magma ocean separation of early enriched reservoir (EER)	composition, Hf-W modelling, energetics 142Nd & 143Nd, composition	depleted mantle signatures
4.5-4.4	giant impact to form Moon second magma ocean perovskite fractionation mantle overturn?	composition, modelling modelling Lu-Hf, Sm-Nd hypothesis	mantle with Hf composition different from Nd
4.4-3.9	oceanic lithosphere (non-continental)	Hadean zircons, O, Lu-Hf	oceanic lithosphere recycling with little crustal preservation
3.9	onset of subduction?, and first continental crust	arc-like rocks, ophiolites	preserved cratonic nucleii
3.5	first mantle keels and permanent crust extraction	Nb/Th, Sm-Nd, xenoliths	start of continental crust-derived mantle depletion
2.5-3.1	terranes with direct subduction imprints	preserved arcs, geophysics	present style tectonics and mantle evolution

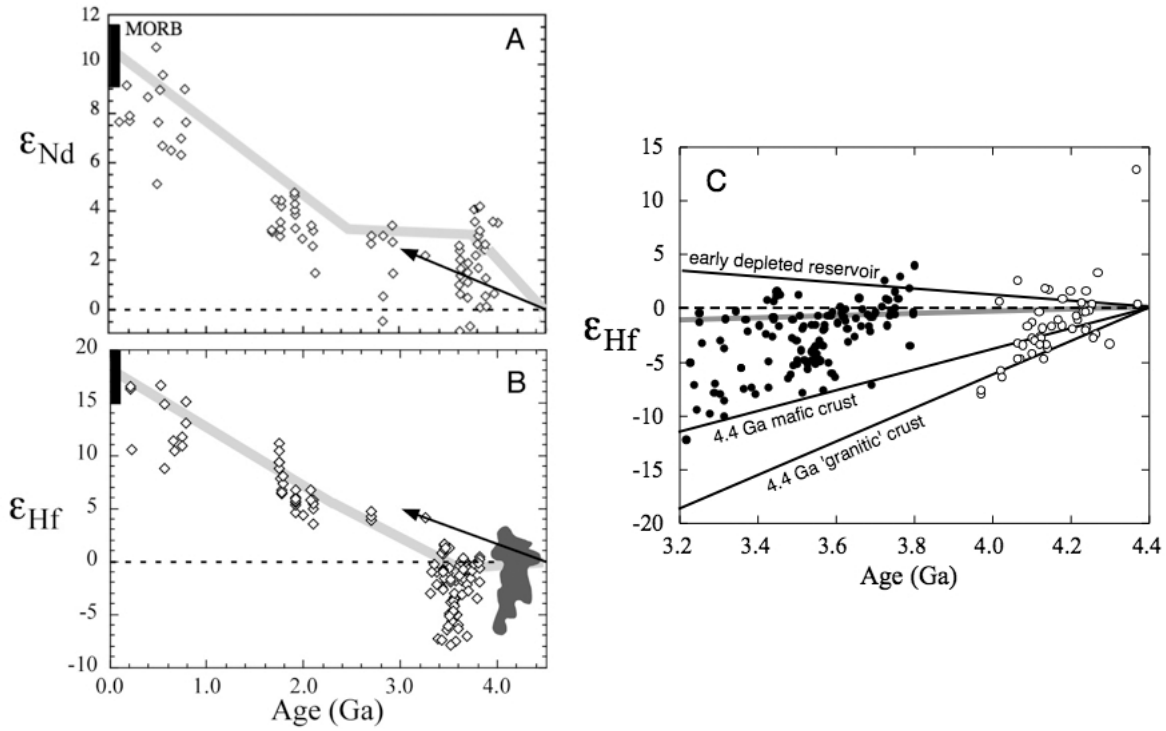

Figure 1A,B. Nd and Hf isotopic composition of Archean to recent mantle-derived rocks, granitoids and Hadean zircons versus age that define the possible evolution of the early mantle. Hadean zircons are the dark grey field in B. Mantle-derived rocks and juvenile granitoids are the open diamonds in A and B younger than 3.2 Ga. Juvenile granitoids, granitoids involving reworked crust, and separated zircons from these rocks are shown by open diamonds older than 3.2 Ga in A and B. The dashed line represents chondritic evolution, the grey thick line the evolution of mantle sources for juvenile rocks, and the arrow the growth of a depleted mantle generated by a process such as early continental crust removal. Figure 1C. Initial Hf isotope systematics of Hadean zircon (white) and Eoarchean zircon and whole rocks (black) after Kramers (2007), Kamber (2007), and Shirey et al. (2008) which is basically the data older than 3.2 Ga from Fig. 1B. Early depleted reservoir evolution (separation at 4.5 Ga) after Boyet & Carlson (2005) projects to modern N-MORB Hf isotope composition. Two types of early Hadean (4.4. Ga) crustal reservoirs were modelled to separate from chondritic composition with $^{176}Lu/^{177}Hf$ of 0.021 (basaltic) and 0.012 ('granitic'). Note that all initial Hf isotope compositions of Eoarchean zircons from Acasta, Southwest Greenland, Barberton, North China, Yangtze and the Western Superior cratons (black) fall into the fields defined by the early depleted reservoir and the mafic Hadean crust. Also, the bulk of the depleted 'juvenile' whole rock data (highest 1/3 of black circles) straddle estimates of mantle evolution (grey line) following Ca-silicate and Mg-silicate perovskite fractionation from the Mars-sized object impact generated magma ocean (Caro et al., 2005). Hf data in B, C has been recalculated using the decay constant of Scherer (2001) and is consistent with the chondritic composition for $^{176}Hf/^{177}Hf$ and $^{176}Lu/^{177}Hf$ given in Bouvier et al. (2008). A,B is modified from Bennett (2003), and A,B,C are after Shirey et al. (2008) which give primary data sources from the literature.

Evolution of the mantle-crust system once continental preservation begins

Continental cratons with stable mantle keels that often have some vestige of a subduction imprint began to appear by at least 3.5 Ga (Shirey et al., 2004; Westerlund et al., 2006). While a role for plumes seems necessary for the older lithospheric components of some cratons, by 3 Ga this subduction imprint is evident throughout the continental lithospheric mantle from the abundance of eclogitic sulfide bearing diamonds (e.g. Shirey et al., 2001) and surface-derived stable isotopic signatures in eclogites (e.g. Jacob, 2004) and eclogitic sulfides (e.g. Farquhar et al., 2002). Unless such mantle keels are removed by recent tectonic activity such as the North China craton (e.g. Gao et al., 2002), they underlay most other Archean to Proterozoic terranes. After about 3 Ga, juvenile crustal rocks began to show derivation from progressively depleted mantle with typical igneous ε_{Nd}:ε_{Hf} = 1:2 (Fig. 1A,B) suggesting that extraction of continental crust by plate-tectonic-like geologic processes progressively depleted the mantle from this time onward. While Neoarchean subduction appears geochemically analogous to present subduction, it can not easily explain many features of cratons and granite-greenstone crust such as: a) crustal differentiation with mantle keels of comparable age to the crust in place; b) superposition of plume-derived and subduction-derived magmas; and c) radial, non-accretionary internal distribution of geologic ages. This does not rule out subduction as an Archean process but rather shows that we must seek more imaginative models of crustal differentiation.

Speculations on the delay of crustal preservation

Hadean zircons have the trace element composition and inclusion mineral assemblages typical of continental zircons (Grimes et al., 2007; Hopkins et al., 2008). However, they could have been derived from a continent-absent, mafic to ultramafic protocrust (Kamber et al., 2003; Kramers, 2007; O'Neil et al., 2008) that was multiply remelted between 4.4 and 4.0 Ga under wet conditions to produce evolved felsic rocks whose compositions mimic continental crust (e.g. Darling et al., 2009; Shirey et al., 2008). Such crust may have been recycled in transitory, small-scale fashion that would not have required a global system of tectonic plates. If the mafic-ultramafic protocrust followed a post giant impact magma ocean overturn, then a stable, cool-bottom mantle might have resulted and the transition to plate tectonics could have been the result of mantle heating from radioactive decay (Elkins-Tanton, 2008; Kramers, 2007). If, alternatively, the mafic-ultramafic protocrust was produced by traditional mantle convection with no global overturn, then the transition to plate tectonics might have marked the cooling of the mantle to the point where large lithospheric plates could have been formed on a global scale. Cessation of the late heavy meteorite bombardment also contributed creating an environment that allowed lithospheric plates to stabilise.

References

Armstrong R.L., 1991, The persistent myth of crustal growth, Australian Journal of Earth Sciences, 38, 613–630.

Bennett V.C., 2003, Chapter 2.13 - Compositional evolution of the mantle, in *Treatise on geochemistry: Vol. 2, The Mantle,* Carlson, R.W., ed., New York, Elsevier, 493–519.

Bouvier A., Vervoort J. & Patchett P., 2008, The Lu-Hf and Sm-Nd isotopic composition of CHUR: Constraints from unequilibrated chondrites and implications for the bulk composition of terrestrial planets Earth and Planetary Science Letters, 273, 48–57.

Boyet M. & Carlson R.W., 2005, ^{142}Nd evidence for early (>4.53 Ga) global differentiation of the silicate Earth, Science, 309, 576–581.

Boyet M. & Carlson R.W., 2006, A new geochemical model for the Earth's mantle inferred from ^{146}Sm-^{142}Nd systematics: Earth and Planetary Science Letters, v. 250, p. 254-268.

Carlson, R.W. & Shirey S.B., 1988, Magma oceans, ocean ridges, and continental crust; relative roles in mantle differentiation, LPI Contribution, 681, 13–14.

Caro G., Bourdon B., Wood B.J. & Corgne A., 2005, Trace-element fractionation in Hadean mantle generated by melt segregation from a magma ocean, Nature, 436, 246–249.

Christensen U.R. & Hofmann A.W., 1994, Segregation of subducted oceanic crust in the convecting mantle Journal of Geophysical Research, 99, 19, 867–19,884.

Collerson K.D. & Kamber B.S., 1999, Evolution of the continents and the atmosphere inferred from Th-U-Nb systematics of the depleted mantle, Science, 283, 1519–1522.

Corgne A., Liebske C., Wood B.J., Rubie D.C. & Frost D.J., 2005, Silicate perovskite-melt partitioning of trace elements and geochemical signature of a deep perovskitic reservoir, Geochimica et Cosmochimica Acta, , 69, 485–496.

Darling J., Storey C. & Hawkesworth C., 2009, Impact melt sheet zircons and their implications for the Hadean crust, Geology, 37, 927.

Davies G.F., 2002, Stirring geochemistry in mantle convection models with stiff plates and slabs, Geochimica et Cosmochimica Acta, 66, 3125–3142.

Elkins-Tanton L.T., 2008, Linked magma ocean solidification and atmospheric growth for Earth and Mars, Earth and Planetary Science Letters, 271, 181-191.

Farquhar J., Wing B.A., McKeegan K.D., Harris J.W., Cartigny P. & Thiemens M.H., 2002, Mass-independent sulfur of inclusions in diamond and sulfur recycling on early Earth, Science, 298, 2369–2372.

Gao S., Rudnick R., Carlson R., McDonough W. & Liu Y., 2002, Re-Os evidence for replacement of ancient mantle lithosphere beneath the North China craton, Earth and Planetary Science Letters, 198, 307–322.

Grimes C.B., John B.E., Kelemen P.B., Mazdab F.K., Wooden J.L., Cheadle M.J., Hanghoj K. & Schwartz J.J., 2007, Trace element chemistry of zircons from oceanic crust: A method for distinguishing detrital zircon provenance, Geology, 35, 643-646.

Hawkesworth C., Dhuime B., Pietranik A., Cawood P., Kemp A. & Storey C., 2010, The generation and evolution of the continental crust, Journal of the Geological Society, 167, 229.

Hofmann A.W., 1997, Mantle geochemistry: the message from oceanic volcanism, Nature, 385, 219–229.

Hofmann A.W., 2003, Chapter 2.03 - Sampling mantle heterogeneity through oceanic basalts: isotopes and trace elements, in *Treatise on Geochemistry: Vol. 2, The Mantle,* Carlson R.W., ed., New York, Elsevier, 61–101.

Hopkins M., Harrison T.M. & Manning C.E., 2008, Low heat flow inferred from >4 Gyr zircons suggests Hadean plate boundary interactions, Nature, 456, 493.

Jacob D.E., 2004, Nature and origin of eclogite xenoliths from kimberlites, in *8th International Kimberlite Conference,* Mitchell R.H., Gruetter H.S., Heaman L.M., Scott Smith B.H. & Stachel T., eds., Victoria, BC, Lithos, 77, 295–316.

Kamber B.S., 2007, The enigma of the terrestrial protocrust: evidence for its former existence and the importance of its complete disappearance, in *Earth's Oldest Rocks,* Van Kranendonk M.J., Smithies R.H. & Bennett, V.C., eds,New York, Elsevier, 75–89.

Kamber B.S., Collerson K.D., Moorbath S. & Whitehouse M.J., 2003, Inheritance of early Archaean Pb-isotope variability from long-lived Hadean protocrust, Contributions to Mineralogy and Petrology, 145, 25–46.

Kramers J.D., 2007, Hierarchical Earth accretion and the Hadean Eon, Journal of the Geological Society of London, 164, 3–17.

Liebske C., Corgne A., Frost D.J., Rubie D.C. & Wood B.J., 2005, Compositional effects on element partitioning between Mg-silicate perovskite and silicate melts, Contributions to Mineralogy and Petrology, 149, 113–128.

Martin H., Smithies R.H., Rapp R., Moyen J.-F. & Champion D., 2005, An overview of adakite, tonalite-trondhjemite-granodiorite (TTG), and sanukitoid; relationships and some implications for crustal evolution: Lithos, 79, 1–24.

O'Neil J., Carlson R., Francis D. & Stevenson R., 2008, Neodymium-142 evidence for hadean mafic crust: Science, 321, 1828.

Scherer E., Muenker C. & Mezger K., 2001, Calibration of the lutetium-hafnium clock, Science, 293, 683–687.

Shirey S.B., Carlson R.W., Richardson S.H., Menzies A.H., Gurney J.J., Pearson D.G., Harris J.W. & Wiechert U., 2001, Archean emplacement of eclogitic components into the lithospheric mantle during formation of the Kaapvaal Craton, Geophysical Research Letters, 28, 2509–2512.

Shirey S.B., Kamber B.S., Whitehouse M.J., Mueller P.A. & Basu A.R., 2008, A review of the isotopic and trace element evidence for mantle and crustal processes in the Hadean and Archean: Implications for the onset of plate tectonic subduction, in *When Did Plate Tectonics Begin on Earth?* Condie K. & Pease V., eds, Boulder, CO, Geological Society of America Special Paper 440, 1–29.

Shirey S.B., Richardson S.H. & Harris J.W., 2004, Integrated models of diamond formation and craton evolution, Lithos, 77, 923–944.

Vervoort J.D. & Blichert-Toft J., 1999, Evolution of the depleted mantle; Hf isotope evidence from juvenile rocks through time, Geochimica et Cosmochimica Acta, 63, 533–556.

Westerlund K.J., Shirey S.B., Richardson S.H., Carlson R.W., Gurney J.J. & Harris J.W., 2006, A subduction origin for Early Archean peridotitic diamonds and harzburgites from the Panda kimberlite, Slave craton: Implications from Re-Os isotope systematic, Contributions to Mineralogy and Petrology, 152, 275–294.

THEME 1

PLANET FORMATION, CRUSTAL GROWTH AND THE EVOLVING LITHOSPHERE

ORAL & POSTER ABSTRACTS

POTENTIAL CHANGES IN THE SOURCE OF GRANITOIDS IN THE ARCHEAN: THE Si ISOTOPE PERSPECTIVE

K. Abraham[1,2], A. Hofmann[3], S.F. Foley[1], D. Cardinal[2] & L. André[2]

[1]Earth System Science Research Centre, Institute for Geosciences, University of Mainz, Becherweg 21, Mainz, D-55099, Germany
[2] Section of Mineralogy−Petrography−Geochemistry, Royal Museum for Central Africa, Leuvensesteenweg 13, Tervuren, B 3080, Belgium
[3] School of Geological Sciences, University of KwaZulu-Natal, Durban, P/Bag X54001, South Africa

Introduction

Earth´s oldest crust constitutes rocks of the tonalite-trondhjemite-granodiorite (TTG) series tectonically interleaved with, or intrusive into, greenstone belts. The petrogenesis of TTGs, their geodynamic environment, their rate of formation, and lack of importance in post-Archean times is still a matter of debate. In order to investigate the different hypotheses for their origin we combine silicon isotopes with major and trace element analyses on different generations of intrusive units from 3.55 to 3.10 Ga from the Barberton Mountain Land, South Africa.

In contrast to the Archean, today's continental crust is more potassic in composition and shows differences in trace element characteristics (*e.g.* the enrichment of incompatible elements and a significant Eu anomaly). Processes that lead to this changeover from "sodic" to more "potassic" crust are the subject of considerable interest. With the investigation of the variations in Si isotope composition among the different generations of plutons in the Barberton Mountain Land (BML) we investigate the capability of silicon isotopes to trace this change to potassium rich plutonism. The BML is particularly suitable in this regard, because of its pristine character. Furthermore, the BML represents one of relatively few localities around the world (also Singhbhum craton, India), where the emplacement of K-rich plutons started earlier (~3.1 Ga) than in other places (~2.6 Ga).

Silicon isotopes could give further constraints on essential questions regarding the source of granitoids by discriminating between possible sources. The proposed geodynamic processes for the origin of TTGs are either melting of a subducted slab or melting of the lower part of thick, mafic crust in an intra-plate setting. Comparison of the isotope signatures of the TTG amongst different reservoirs provides further information about the possible contribution of sediments (cherts) and silicified basalts of the Archean ocean floor, or from the mantle, and thus about the sources of TTG genesis.

Results from experimental petrology indicate that TTG rocks are produced by partial melting of a mafic source within the garnet stability field. The role of water during this process, determining whether the source consists of amphibolite (Foley *et al.,* 2002) or eclogite (Rapp *et al.,* 2003), can be tested by silicon isotopes, since Si isotopic variations originating from interaction with water have a much larger range than those of magmatic processes.

However, knowledge about mineral/melt Si isotope fractionation is very limited. Therefore we performed Si isotope analyses on different parts of migmatites from Finland (Nehring *et al.,* 2009) to estimate a preliminary range of Si isotope fractionation during partial melt processes.

Geology

Nine samples were taken from at least four different generations of plutons (Figure 1) from the Barberton Mountain Land, South Africa. In general, the intrusive units can be subdivided in two major types of igneous rocks (Lowe & Byerly, 2007): The "sodic" TTG group (tonalite-trondhjemite-granodiorite) and the later "potassic" GMS group (granite-monzonite-syenite). The former rocks are generated in a time span between 3.5 to 3.2 Ga, whereby the latter formed about 3.1 Ga (Kamo & Davis 1994). The emplacement of different plutons is mostly coeval with different deformation events (D1 to D4) during the formation of the Barberton Mountain Land. We refer to Moyen *et al.* (2007) and references therein for a more detailed geological overview of the study area.

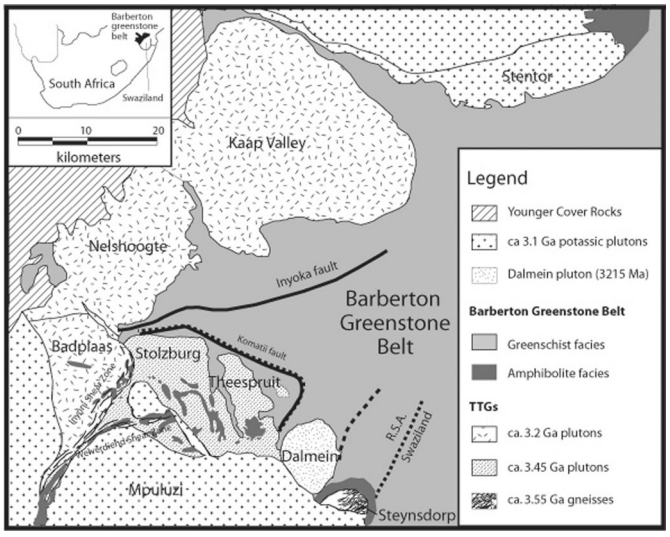

Figure 1. Simplified geological map of the Barberton Mountain Land (BML; South Africa), showing the nine different plutons investigated (adapted from Moyen et al., 2007).

Results

The TTG group rocks are all trondhjemitic or tonalitic in composition and show no discernible temporal variation in major and trace element composition. The two granites of the GMS group can be distinguished from the TTG group by their potassium content (average K_2O: TTG=1.8%; GMS=4.1%). Additionally, they show typical differences to the TTG indicated by major and trace element composition (e.g. higher Rb/Sr ratio) and more fractionated rare earth elements (REE) with a small negative Europium anomaly and higher La/Yb_N.

Silicon isotope variations are presented in per mil variation relative to the NBS28 quartz standard. Details about the preparation procedure and the analytical method can be found in Abraham *et al.,* 2008. Overall, the plutons show very limited variation ($\delta^{30}Si$= -0.17‰ to +0.05‰, average $\delta^{30}Si$= -0.06‰, n=9). The isotope composition of the Barberton plutons is comparable with granitoids analyzed so far, which range between -0.8‰ and +0.4‰ (average $\delta^{30}Si$= -0.10‰, n=44; Douthitt, 1982, Ding *et al.,* 1996). André *et al.* (2006) identified slightly heavier $\delta^{30}Si$ values ($\delta^{30}Si$= -0.04‰ to +0.41‰, average $\delta^{30}Si$= +0.23‰, n=5) in high-grade early Archean tonalitic crustal gneisses (Amîtsoq, Isua). A small but progressive temporal increase in $\delta^{30}Si$ between the different pluton generations in Barberton (average $\delta^{30}Si$ values from the first to the fourth generation, $\delta^{30}Si$= -0.17‰, $\delta^{30}Si$= -0.11‰, $\delta^{30}Si$= -0.05‰ and $\delta^{30}Si$= +0.01‰, respectively) is apparent, but is not much larger than the average standard deviation between the replicates (0.071‰).

Preliminary results for leucosomes, melanosomes and mesocratic parts of two different migmatites from Finland indicate a small range of fractionation during the melting process: $\Delta_{leuco\text{-}melano}{}^{30}Si$=0.23‰ and $\Delta_{leuco\text{-}melano}{}^{30}Si$=0.33‰, showing that the leucocratic melt is isotopically heavier than the restite.

Discussion

Our knowledge about silicon isotopes in felsic igneous rocks is still very limited due to the small number of studies conducted to date (Douthitt, 1982; Ding et al., 1996, Andrè et al., 2006). The different processes that account for Si isotope fractionations during granitoid genesis are summarized here.

Si isotope fractionation during magmatic differentiation, partial melting and fractional crystallization

In general, the isotope fractionation during magmatic differentiation is expected to be small because of the high temperatures. Grant (1954) suggested on the basis of theoretical calculations that equilibrium Si isotope fractionation should depend on the degree of polymerization of the silicate unit. This is confirmed by observations on natural rocks, since felsic igneous rocks (~0‰) show slightly heavier isotope composition than mafic rocks (-0.3‰) (Douthitt, 1982, Ding *et al.,* 1996). Due to the fact that $\delta^{30}Si$ generally increases with silicon contents of rocks, it was assumed that with progressive magmatic differentiation the isotope signature should evolve to higher values. However, recent theoretical calculations on equilibrium isotopic fractionation of oxygen and silicon for several minerals, displaying various degrees of polymerization of silicate tetraedra (Méheut *et al.,* 2009), indicate that the fractionation factor of Si in equilibrium does not strictly follow the degree of polymerisation of silicate tetraedra previously suggested.

There is only limited knowledge about Si isotope fractionation during partial melting. Given that migmatites and felsic igneous rocks fall in the same $\delta^{30}Si$ range, it has been hypothesized that the $\delta^{30}Si$-values remain unchanged during the formation of migmatites (Ding *et al.,* 1996, André *et al.,* 2006). However, our preliminary results on migmatites of Finland suggest that there is a variation (max. $\Delta^{30}Si$=0.33‰) for the partial melting process.

Fractional crystallization of minerals can lead to a change in isotope composition of the melt. In general, the equilibrium isotope fractionation between silicate minerals pairs in igneous rocks (feldspar-hornblende, quartz-feldspar, and feldspar-pyroxene) generates only small isotope fractionations of 0.2-0.5‰ (Ding *et al.,* 1996), so that the resulting variation is expected to be small. This result is justified by theoretical calculations (Méheut *et al.,* 2009). As deduced by Epstein & Taylor (1970), the isotope fractionation sequence, meaning the preference for ^{30}Si, among coexisting mineral phases is (pyroxene, biotite, hornblende) < (plagioclase, K-feldspar) < (quartz, cristobalite). The fractional crystallization of mafic minerals would lead to an evolution to higher values in the residual (quartz- and plagioclase-rich) melt. It is known that trondhjemite can result from fractional crystallization of a tonalite parental magma. Operation of this process would lead to relatively higher $\delta^{30}Si$ in trondhjemites and lower $\delta^{30}Si$ in tonalites within the different Barberton TTG plutons.

The water content and the involvement of sediment in the source

The resemblance of Archean K-rich granites (3.1 Ga) with Middle Paleozoic (0.45 to 0.34 Ga) granites from Australia (Douthitt, 1982) and young (<0.5 Ga) granitoids from China (Ding *et al.,* 1996), suggests that the processes which would lead to a large fractionation of silicon isotopes, such as the influence of water during magma genesis or the assimilation of other material (sediments such as clays with strong negative ^{30}Si values) are affecting late Archean and Phanerozoic granitoids equally. Douthitt (1982) detected no difference between S-type (supracrustal source) and I-type (igneous source) granitoids, which hints at no significant effect of the involvement of sedimental material on the Si isotope signature.

Si isotope fractionation during diffusion

The experimentally determined thermal Si isotopic fractionation in molten basalt is Ω_{Si} = 0.6, whereby the parameter Ω_i defines the isotopic fractionation in per mil per 100 °C per atomic mass unit (Richter *et al.,* 2009). Thus, in a temperature gradient, the cold end-member of

the molten basalt would become enriched in $\delta^{30}Si$, with a surprisingly large degree of isotope fractionation.

Temperature differences in the source of granitoids

Magmatic differentiation and fractional crystallization of tonalitic parental magmas causes enrichment in sodium. Thus K_2O-rich granites must emerge from different source rocks to tonalites. It is generally known that granitic melts form at lower temperatures (650°C-700°) than tonalitic melts (Wyllie, 1977). The enrichment of ^{30}Si by diffusion in cold melts (Richter et al., 2009) fits very well with the different formation temperatures. The overall increase in ^{30}Si from early ($\delta^{30}Si$=-0.17) to late granitoids ($\delta^{30}Si$=+0.01) in Barberton and the concomitant K_2O-enrichment may reflect different formation temperatures for the different granitoid generations. This means that K-rich melt, which emerges at colder temperatures shows higher isotope composition than Na-rich melt. The slightly higher isotope composition of 3.8 Ga Amîtsoq gneisses (average $\delta^{30}Si$=+0.23‰, n=5), might be attributed to higher strain or other formation conditions during the early Archean.

Conclusion

There is an overall slight increase in $\delta^{30}Si$ with time in different generations of plutons in the BML. The Si isotope variation reflects different temperature conditions in the source of granitoids, with K-rich, heavy $\delta^{30}Si$ granitoids emerging at lower temperatures. We confirm that the Si-isotope signatures of K-rich granites of different origins show no clear difference and that this similarity extends back to 3.1 Ga.

Acknowledgements

K. Abraham would like to acknowledge the «Deutsche Forschungsgemeinschaft» and the Royal Museum for Central Africa for funding.

References

Abraham K., Opfergelt S., Fripiat F., Cavagna A.J., de Jong J.T.M., Foley F., André L. & Cardinal D., 2008, $\delta^{30}Si$ and $\delta^{29}Si$ determinations on USGS BHVO-1 and BHVO-2 reference materials with a new configuration on a Nu Plasma Multi-Collector ICP-MS, Geostandards and Geoanalytical Research, 32, 193-202.

André L., Cardinal D., Alleman L.Y. & Moorbath S., 2006, Silicon isotopes in ~3.8 Ga West Greenland rocks as clues to the Eoarchean supracrustal Si cycle, Earth and Planetary Science Letters, 245, 162-173.

Ding T., Jiang S., Wan D., Li Y., Li J., Song H., Liu Z. & Yao X., 1996, in Silicon isotope geochemistry, 1-125 Geological Publishing House, Beijing, China.

Douthitt C.B., 1982, The geochemistry of stable isotopes of silicon, Geochimica et Cosmochimica Acta, 46, 1449−1458.

Epstein S., & Taylor H.P.J., 1970, Stable isotopes, rare gases, solar wind, and spallation products: $^{18}O/^{16}O$, $^{30}Si/^{28}Si$, D/H, $^{13}C/^{12}C$ studies of lunar rocks and minerals, Science, 167, 533-535.

Foley S., Tiepolo M. & Vannucci R., 2002, Growth of early continental crust controlled by melting of amphibolite in subduction zones, Nature, 417, 637-640.

Grant F.S., 1954, The geological significance of variations in the abundances of the isotopes of silicon in rocks, Geochimica et Cosmochimica Acta, 5, 225-242.

Kamo S.L., & Davis D.W., 1994, Reassessment of Archean crustal development in the Barberton Mountain Land, South Africa, based on U-Pb dating, Tectonics, 13, 167-192.

Lowe D.R. & Byerly G.R., 2007, An overview of the geology of the Barberton greenstone belt and vicinity: implications for early crustal development, in Earth's Oldest Rocks, Van Kranendonk M.J., Smithies R.H. & Bennett V.C., eds, Developments in Precambrian Geology, 15, 481-526, Elsevier, Amsterdam.

Méheut M., Lazzeri M., Balan E. & Mauri F., 2009, Structural control over equilibrium silicon and oxygen isotopic fractionation: A first-principles density-functional theory study. Chemical Geology, 258, 28-37.

Moyen J-F., Stevens G., Kisters A.F.M. & Belcher R.W., 2007, TTG plutons of the Barberton Granitoid-Greenstone Terrain, South Africa, in Earth´s Oldest Rocks, Van Kranendonk M.J., Smithies R.H. & Bennett V.C., eds, Developments in Precambrian Geology, 15, 607-667, Elsevier, Amsterdam.

Nehring F., Foley S.F., Hölttä P. & Van den Kerkhof, A.M., 2009, Internal differentiation of the Archean continental crust: fluid-controlled partial melting of granulites and TTG-amphibolite associations in Central Finland, Journal of Petrology, 50, 3-35.

Rapp R., Shimizu N. & Norman M.D., 2003, Growth of early continental crust by partial melting of eclogite, Nature, 425, 605-609.

Richter F.M., Watson E.B., Mendybaev R, Dauphas N., Georg B., Watkins J. & Valley J., 2009, Isotopic fractionation of the major elements of molten basalt by chemical and thermal diffusion. Geochimica et Cosmochimica Acta 73, 4250-4263.

Wyllie P.J., 1977, Crustal anatexis: an experimental review, Tectonophysics, 13, 41-71.

ZIRCON GEOCHRONOLOGY AND GEOCHEMISTRY OF THE TTG SUITES OF THE RIO MARIA GRANITE-GREENSTONE TERRANE: IMPLICATIONS FOR THE GROWTH OF THE ARCHEAN CRUST OF THE CARAJÁS PROVINCE, BRAZIL

J.A.C. Almeida[1,2], R. Dall'Agnol[1,2], M.A. Oliveira[1,2], M.J.B. Macambira[2,3], M.M. Pimentel[4], O.T. Rämö[5], F.V. Guimarães[1,2] & A.A.S. Leite[1]

[1]Group of Research on Granite Petrology, Institute of Geosciences, Federal University of Pará, Brazil
[2]Graduated Program on Geology and Geochemistry, Institute of Geosciences, Federal University of Pará
[3]Isotope Geology Laboratory, Institute of Geosciences, Federal University of Pará
[4]Geochronology Laboratory, Institute of Geosciences, University of Brasilia
[5]Department of Geology, University of Helsinki

Introduction

The TTG suites are the most voluminous granitoid rocks exposed in the Mesorchean Rio Maria granite-greenstone terrane (RMGGT) in the southern part of the Carajás province, the largest Archean domain of the Amazonian craton (Althoff et al. 2000, Souza et al. 2001, Dall'Agnol et al. 2006, Almeida et al., unpubl.).

Results

Extensive field work in key areas of the RMGGT, integrated with petrographic, geochemical, andgeochronological studies, the latter employing the Pb-Pb evaporation and U-Pb LA-ICP-MS on zircon techniques, indicates that the TTG magmatism record in the RMGGT can be divided into three episodes: (I) A first event at 2.96±0.2 Ga (the older rocks of the Arco Verde tonalite and the Mogno trondhjemite), (II) a second one at 2.93±0.1 Ga (Caracol tonalitic complex, Mariazinha tonalite, and the younger rocks of the Arco Verde tonalite), and (III) finally, a restricted event at 2.86±0.1 Ga (Agua Fria trondhjemite). The new data demonstrate that the Mogno trondhjemite is significantly older than previously admitted, reveal the existence of a new TTG suite (Mariazinha tonalite) and indicate that the volume of TTG suites formed during the ~2.87 Ga event was limited. The Arco Verde tonalite yielded significant age variations (2.98 to 2.93 Ga) but domains with different ages could not be individualized so far. Isotopic data suggest that the tonalitic-trondhjemitic crust of the RMGGT derived from sources geochemically similar to the metabasalts of the Andorinhas supergroup extracted from the mantle during the Mesoarchean (3.0 to 2.9 Ga) and with short time of crustal residence.

These rocks are composed essentially of tonalite and trondhjemite with quartz and plagioclase as essential minerals, biotite as main mafic minerals and titanite, allanite, epidote, apatite and zircon as primary accessory minerals. Small amounts of K-feldspar are occasionally found. In terms of chemistry, the TTG of the RMGGT exhibit SiO_2 content between 65 and 75 wt% and are metaluminous to peraluminous, sodic granitoids, impoverished in K_2O ($K_2O/Na_2O<0.5$) and Rb. Almost all analyzed samples of the TTGs suites of the TGGRM belong to the high-Al group, but there are significant contrasts in Al_2O_3 and Sr between different TTG units. Based on the trace elements behavior, the Rio Maria TTG granitoids were divided into three groups: 1) high-La/Yb group, with high Sr/Y and Nb/Ta ratios, derived from magmas generated at relatively high pressures (>1.5 GPa) from sources leaving garnet and amphibole as residual phases; 2) medium-La/Yb group which magmas formed at intermediate pressure conditions (~1.0-1.5 GPa), but still in the garnet stability field; and 3) low-La/Yb group, with low Sr/Y and Nb/Ta ratios, crystallized from magmas generated at lower pressures (~1.0 GPa), from an amphibolitic source that left plagioclase as a residual phase.

In contrast to Barberton (Moyen et al. 2007) and similar to Pilbara (Champion & Smithies 2007) TTGs, there is no discernible correlation between geochemical series and either the TTGs units of the RMGGT or the ages of those units. In a Sr vs. SiO2 diagram (Fig. 1), most of the TTGs of the RMGGT is concentrated in the field of high-Al, high-Sr of Pilbara and in the low-Sr sub-series of Barberton. However, a large number of samples of the Arco Verde tonalite plot in the the low-Al, low-Sr field of Pilbara and the Mogno trondhjemite samples tend to plot along the border between the low-Sr and high-Sr sub-series of Barberton.

The three distinct TTG geochemical groups distinguished in the RMGGT [low-, medium- and high-(La/Yb)] can be most probably correlated to depth or pressure of their magma genesis. In the RMGGT, the high- to medium-(La/Yb) dominant TTGs are similar in Sr and SiO2 contents to the high-Al, high-Sr group of Pilbara, to the low-Sr sub-series of Barberton and to both Sr groups of Karelian and Kola cratons (Fig. 1). These rocks include samples of all TTG units and were probably formed in the stability field of garnet at pressures of 1.0 to >1.5 GPa. In order to explain their geochemical characteristics, the low-Al, low-Sr, low-(La/Yb) TTGs, dominant in the Arco Verde tonalite, should be formed at comparatively lower pressures (≤ 1.0 GPa) in the stability field of plagioclase. Finally, the high-(La/Yb) TTGs of the Mogno trondhjemite, which compositions straddle the limit between the low-Sr and high-Sr fields of Barberton TTGs (Fig. 1), should be derived from magmas formed

in the garnet stability field at relatively higher pressure (≥1.5 GPa) and probably at somewhat lower temperature (< 1000°C; cf. Moyen et al., 2007). The Mariazinha tonalite magma is also formed at relatively higher pressures compared to the dominant TTGs of RMGGT, but it should result from a larger degree of partial melting compared to the Mogno trondhjemite magma to explain its lower silica contents. This implies a higher melting temperature for the Mariazinha tonalite magma, estimated at ≥1100°C.

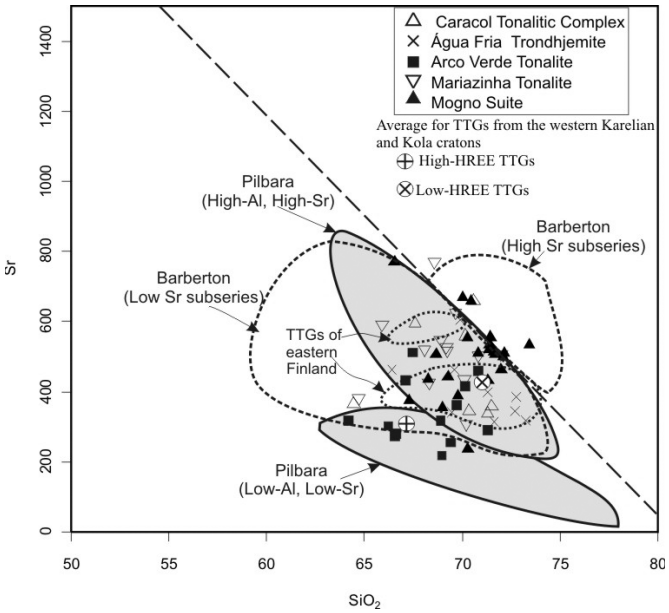

Figure1. SiO vs Sr diagram showing the distribution of samples of the TTG suites of the Rio Maria granite-greenstone terrane and the fields for TTG series of Pilbara craton (Champion & Smithies 2007), Barberton granite-greenstone terrane (Moyen et al. 2007) and eastern Finland (Martin 1987). The average composition of TTGs from the western Karelian and Kola cratons (Halla et al. 2009) is also shown for comparison.

These three geochemical groups do not have a straight correspondence with the three episodes of TTG generation and a same TTG unit can be composed of rocks of different groups. However, rocks of the high-La/Yb group are related dominantly to the Mogno trondhjemite and Mariazinha tonalite; those of the medium-La/Yb group are common in the Mogno trondhjemite and Arco verde tonalite but dominate in the Agua Fria trondhjemite and Caracol tonalitic complex; finally, the low La/Yb group is composed essentially of rocks of the Arco Verde tonalite.

A model involving a subduction zone underneath a thick oceanic plateau (Halla et al., 2009) was envisaged to explain the tectonic evolution of the RMGGT. In this context, the low-La/Yb group was formed from magmas originated by the melting of the base of a thickened basaltic oceanic crust at comparatively lower pressures (ca. 1.0 GPa), whereas the medium- and high-La/Yb groups were derived from the slab melting at increasing different pressures (1.0-1.5 and ≥ 1.5 GPa, respectively). Part of these TTG magmas react during their ascent with the mantle wedge being totally consumed and leaving a metassomatized mantle. 50 m. y. later, at ca. 2870 Ma, thermal events, possibly related to the slab-break-off and asthenosphere mantle upwelling or to the action of a mantle plume, may have induced the melting of the metassomatized mantle and the generation of sanukitoid magmas. These magmas may have heated the base of the Archean continental crust and could have lead to the local melting of the basaltic crust forming the Água Fria trondhjemite magma.

Acknowledgements

This research received financial support from CNPq (R. Dall'Agnol – Grants 0550739/2001-7, 476075/2003-3, 307469/2003-4, 484524/2007-0; PRONEX – Proc. 66.2103/1998-0, M. A. Oliveira – doctor schollarship; J. A. C. Almeida – doctor schollarship), CAPES (F. V. Guimarães, master scollarship), and Federal University of Pará (UFPA). This paper is a contribution to the Brazilian Institute of Amazonia Geosciences (INCT program –CNPq/MCT/FAPESPA – Proc. 573733/2008-2).

References

Almeida J.A.C., Dall'Agnol R., Oliveira M.A., Macambira M.J.B., Pimentel M.M., Rämö O.T., Guimarães F.V. & Leite A.A.S., unpubl., Zircon geochronology and geochemistry of the TTG suites of the Rio Maria granite-greenstone terrane: Implications for the growth of the Archean crust of Carajás Province, Brazil,. Submitted to Precambrian Res.

Althoff F.J., Barbey P. & Boullier A.M., 2000, 2.8–3.0 Ga plutonism and deformation in the SE Amazonian craton: the Archean granitoids of Marajoara (Carajás Mineral province, Brazil), Precambrian Research, 104, 187-206.

Champion, D.C. & Smithies, R.H., 2007, Geochemistry of Paleoarchean Granites of the East Pilbara Terrane, Pilbara Craton, Western Australia: Implications for Early Archean Crustal Growth, in *Earth's Oldest Rocks*, Van Kranendonk M.J., Smithies R.H. & Bennett V.C., eds., Developments in Precambrian Geology 15, Elsevier, Amsterdam, 369-410.

Dall'Agnol R., Oliveira M.A., Almeida J.A.C., Althoff F.J., Leite A.A.S., Oliveira D.C. & Barros, C.E.M., 2006, Archean and Paleoproterozoic granitoids of the Carajás metallogenetic province, eastern Amazonian craton, in Symposium on Magmatism, Crustal Evolution, and Metallogenesis of the Amazonian Crato,. Abstracts Volume and Field Trips Guide, Dall'Agnol R., Rosa-Costa L.T., Klein E.L., eds, Belém, PRONEX-UFPA/SBGNO, 99-150.

Halla J., van Hunen J., Heilimo E. & Hölttä P., 2009. Geochemical and numerical constraints on Neoarchean plate tectonics, Precambrian Research, 179, 155-162.

Martin H., 1987, Petrogenesis of Archaean trondhjemites, tonalites and granodiorites from eastern Finland: major and trace element geochemistry. Journal of Petrology, 28, 921-953.

Moyen J.-F., Stevens G., Kisters A.F.M. & Belcher R.W., 2007, TTG plutons of the Barberton granitoid-greenstone terrain, South Africa, in *Earth's Oldest rocks*, Van Kranendonk M.J., Smithies R.H. & Bennet V.C, eds, Developments in Precambrian geology 15, Elsevier, 606-668.

Souza Z.S., Potrel H., Lafon J.M., Althoff F.J., Pimentel M.M., Dall'Agnol R. & Oliveira C.G., 2001, Nd, Pb and Sr isotopes of the Identidade Belt, an Archaean greenstone belt of the Rio Maria region (Carajas Province, Brazil): Implications for the Archaean geodynamic evolution of the Amazonian Craton, Precambrian Research, 109, 293-315.

GEOCHRONOLOGY AND GEOCHEMISTRY OF THE RIO MARIA TTG SUITES, AMAZONIAN CRATON

J.A.C. Almeida[1,2], R. Dall'Agnol[1,2], M.A. Oliveira[1,2], M.J.B. Macambira[2,3], M.M. Pimentel[4], O.T. Rämö[5], F.V. Guimarães[1,2] & A.A.S. Leite[1]

[1]Group of Research on Granite Petrology, Institute of Geosciences, Federal University of Pará, Brazil
[2]Graduated Program on Geology and Geochemistry, Institute of Geosciences, Federal University of Pará
[3]Isotope Geology Laboratory, Institute of Geosciences, Federal University of Pará
[4]Geochronology Laboratory, Institute of Geosciences, University of Brasilia
[5]Department of Geology, University of Helsinki

Introduction

The TTG suites are the most voluminous granitoid rocks exposed in the Mesorchean Rio Maria granite-greenstone terrane (RMGGT) in the southern part of the Carajás province, the largest Archean domain of the Amazonian craton (Althoff et al. 2000, Souza et al. 2001, Dall'Agnol et al. 2006, Almeida et al. submitted).

Results

Extensive field work in key areas of the RMGGT, integrated with petrographic, geochemical, and geochronological studies, the latter employing the Pb-Pb evaporation and U-Pb LA-ICP-MS on zircon techniques, indicates that the TTG magmatism record in the RMGGT can be divided into three episodes: (I) A first event at 2.96±0.2 Ga (the older rocks of the Arco Verde tonalite and the Mogno trondhjemite), (II) a second one at 2.93±0.1 Ga (Caracol tonalitic complex, Mariazinha tonalite, and the younger rocks of the Arco Verde tonalite), and (III) finally, a restricted event at 2.86±0.1 Ga (Agua Fria trondhjemite). The new data demonstrate that the Mogno trondhjemite is significantly older than previously admitted, reveal the existence of a new TTG suite (Mariazinha tonalite) and indicate that the volume of TTG suites formed during the ~2.87 Ga event was limited. The Arco Verde tonalite yielded significant age variations (2.98 to 2.93 Ga) but domains with different ages could not be individualized so far. Isotopic data suggest that the tonalitic-trondhjemitic crust of the RMGGT derived from sources geochemically similar to the metabasalts of the Andorinhas supergroup extracted from the mantle during the Mesoarchean (3.0 to 2.9 Ga) and with short time of crustal residence.

These rocks are composed essentially of tonalite and trondhjemite with quartz and plagioclase as essential minerals, biotite as main mafic minerals and titanite, allanite, epidote, apatite and zircon as primary accessory minerals. Small amounts of K-feldspar are occasionally found. In terms of chemistry, the TTG of the RMGGT exhibit SiO_2 content between 65 and 75 wt% and are metaluminous to peraluminous, sodic granitoids, impoverished in K_2O ($K_2O/Na_2O<0.5$) and Rb. Almost all analyzed samples of the TTGs suites of the TGGRM belong to the high-Al group, but there are significant contrasts in Al_2O_3 and Sr between different TTG units. Based on the trace elements behavior, the Rio Maria TTG granitoids were divided into three groups: 1) high-La/Yb group, with high Sr/Y and Nb/Ta ratios, derived from magmas generated at relatively high pressures (>1.5 GPa) from sources leaving garnet and amphibole as residual phases; 2) medium-La/Yb group which magmas formed at intermediate pressure conditions (~1.0-1.5 GPa), but still in the garnet stability field; and 3) low-La/Yb group, with low Sr/Y and Nb/Ta ratios, crystallized from magmas generated at lower pressures (~1.0 GPa), from an amphibolitic source that left plagioclase as a residual phase.

In contrast to Barberton (Moyen et al. 2007) and similar to Pilbara (Champion & Smithies 2007) TTGs, there is no discernible correlation between geochemical series and either the TTGs units of the RMGGT or the ages of those units. In a Sr vs. SiO2 diagram (Fig. 1), most of the TTGs of the RMGGT are concentrated in the field of high-Al, high-Sr of Pilbara and in the low-Sr sub-series of Barberton. However, a large number of samples of the Arco Verde tonalite plot in the low-Al, low-Sr field of Pilbara and the Mogno trondhjemite samples tend to plot along the border between the low-Sr and high-Sr sub-series of Barberton.

The three distinct TTG geochemical groups distinguished in the RMGGT [low-, medium- and high-(La/Yb)] can be most probably correlated to depth or pressure of their magma genesis. In the RMGGT, the high- to medium-(La/Yb) dominant TTGs are similar in Sr and SiO2 contents to the high-Al, high-Sr group of Pilbara, to the low-Sr sub-series of Barberton and to both Sr groups of Karelian and Kola cratons (Fig. 1). These rocks include samples of all TTG units and were probably formed in the stability field of garnet at pressures of 1.0 to >1.5 GPa. In order to explain their geochemical characteristics, the low-Al, low-Sr, low-(La/Yb) TTGs, dominant in the Arco Verde tonalite, should be formed at comparatively lower pressures (≤ 1.0 GPa) in the stability field of plagioclase. Finally, the high-(La/Yb) TTGs of the Mogno trondhjemite, which compositions straddle the limit between the low-Sr and high-Sr fields of Barberton TTGs (Fig. 1), should be derived from magmas formed in the garnet stability field at relatively higher pressure (≥1.5 GPa) and probably at somewhat lower temperature (< 1000°C; cf. Moyen et al., 2007). The Mariazinha tonalite magma is also formed at relatively higher pressures compared to the dominant TTGs of RMGGT, but it should result from a larger degree of partial melting compared to the Mogno trondhjemite magma to explain its lower silica contents. This implies a higher melting temperature for the Mariazinha tonalite magma, estimated at ≥1100°C.

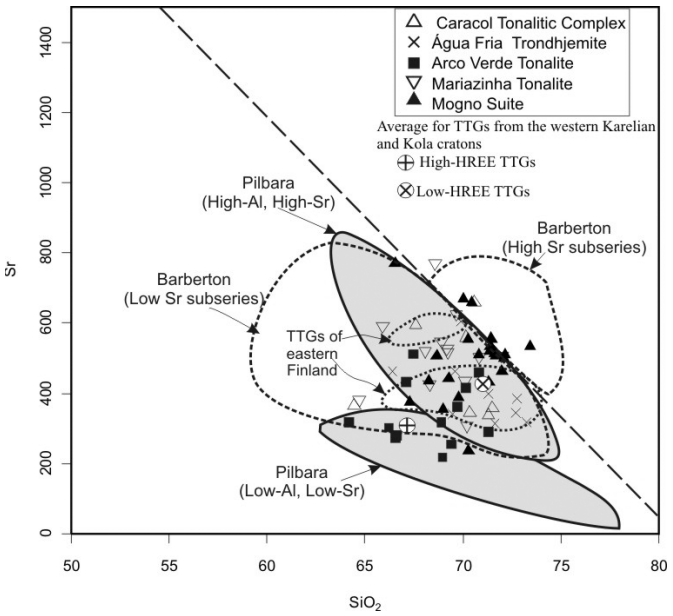

Figure 1. SiO vs Sr diagram showing the distribution of samples of the TTG suites of the Rio Maria granite-greenstone terrane and the fields for TTG series of Pilbara Craton (Champion & Smithies 2007), Barberton granite-greenstone terrane (Moyen et al. 2007) and eastern Finland (Martin 1987). The average composition of TTGs from the western Karelian and Kola cratons (Halla et al. 2009) is also shown for comparison.

These three geochemical groups do not have a straight correspondence with the three episodes of TTG generation and a same TTG unit can be composed of rocks of different groups. However, rocks of the high-La/Yb group are related dominantly to the Mogno trondhjemite and Mariazinha tonalite; those of the medium-La/Yb group are common in the Mogno trondhjemite and Arco verde tonalite but dominate in the Agua Fria trondhjemite and Caracol tonalitic complex; finally, the low La/Yb group is composed essentially of rocks of the Arco Verde tonalite.

A model involving a subduction zone underneath a thick oceanic plateau (Halla et al., 2009) was envisaged to explain the tectonic evolution of the RMGGT. In this context, the low-La/Yb group was formed from magmas originated by the melting of the base of a thickened basaltic oceanic crust at comparatively lower pressures (ca. 1.0 GPa), whereas the medium- and high-La/Yb groups were derived from the slab melting at increasing different pressures (1.0-1.5 and ≥ 1.5 GPa, respectively). Part of these TTG magmas react during their ascent with the mantle wedge being totally consumed and leaving a metasomatized mantle. 50 m. y. later, at ca. 2870 Ma, thermal events, possibly related to the slab-break-off and asthenosphere mantle upwelling or to the action of a mantle plume, may have induced the melting of the metasomatized mantle and the generation of sanukitoid magmas. These magmas may have heated the base of the Archean continental crust and could have lead to the local melting of the basaltic crust forming the Água Fria trondhjemite magma.

Acknowledgements

This research received financial support from CNPq (R. Dall'Agnol – Grants 0550739/2001-7, 476075/2003-3, 307469/2003-4, 484524/2007-0; PRONEX – Proc. 66.2103/1998-0, M. A. Oliveira – doctor scholarship; J. A. C. Almeida – doctor schollarship), CAPES (F. V. Guimarães, master scholarship), and Federal University of Pará (UFPA). This paper is a contribution to the Brazilian Institute of Amazonia Geosciences (INCT program –CNPq/MCT/FAPESPA – Proc. 573733/2008-2).

References

Almeida J.A.C., Dall'Agnol R., Oliveira M.A., Macambira M.J.B., Pimentel M.M., Rämö O.T., Guimarães F.V. & Leite A.A.S., submitted, Zircon geochronology and geochemistry of the TTG suites of the Rio Maria granite-greenstone terrane: Implications for the growth of the Archean crust of Carajás Province, Brazil, Submitted to Precambrian Research.

Althoff F.J., Barbey P. & Boullier A.M., 2000, 2.8–3.0 Ga plutonism and deformation in the SE Amazonian craton: the Archean granitoids of Marajoara (Carajás Mineral province, Brazil), Precambrian Research, 104, 187–206.

Champion D.C. & Smithies R.H., 2007, Geochemistry of Paleoarchean Granites of the East Pilbara Terrane, Pilbara Craton, Western Australia: Implications for Early Archean Crustal Growth, in *Earth's Oldest Rocks*, Van Kranendonk M.J., Smithies R.H. & Bennett V.C., eds, Developments in Precambrian Geology 15, Elsevier, Amsterdam, 369–410.

Dall'Agnol R., Oliveira M.A., Almeida J.A.C., Althoff F.J., Leite A.A.S., Oliveira D.C. & Barros, C.E.M., 2006, Archean and Paleoproterozoic granitoids of the Carajás metallogenetic province, eastern Amazonian craton, in Symposium on Magmatism, Crustal Evolution, and Metallogenesis of the Amazonian Craton. Abstracts Volume and Field Trips Guide, Dall'Agnol R., Rosa-Costa L.T., Klein E.L., eds, Belém, PRONEX-UFPA/SBGNO, 99–150.

Halla J., van Hunen J., Heilimo E. & Hölttä P., 2009, Geochemical and numerical constraints on Neoarchean plate tectonics. Precambrian Research, 179, 155–162.

Moyen J-F., Stevens G., Kisters A.F.M. & Belcher R.W., 2007, TTG plutons of the Barberton granitoid-greenstone terrain, South Africa, in *Earth's Oldest Rocks*, Van Kranendonk M.J., Smithies R.H. & Bennett V.C., eds, Developments in Precambrian Geology 15, Elsevier, Amsterdam, 606–668.

Souza Z.S., Potrel H., Lafon J.M., Althoff F.J., Pimentel M.M., Dall'Agnol R. & Oliveira C.G., 2001, Nd, Pb and Sr isotopes of the Identidade Belt, an Archaean greenstone belt of the Rio Maria region (Carajas Province, Brazil): Implications for the Archaean geodynamic evolution of the Amazonian Craton, Precambrian Research, 109, 293–315.

THE TIMING OF VOLATILE ADDITION TO EARTH - CONSTRAINTS FROM HIGH TEMPERATURE METAL-SILICATE PARTITIONING OF SIDEROPHILE VOLATILE ELEMENTS

C. Ballhaus[1], C. Münker[2], R. Fonseca[1], A. Rohrbach[3], V. Laurenz[1] & K-P. Jochum[4]

[1]Steinmann-Institut, Universität Bonn (Germany)
[2]Geowissenschaften, Universität zu Köln (Germany)
[3]Erdwissenschaften, ETH Zürich (Switzerland)
[4]Max-Planck-Institut für Chemie, Mainz (Germany)

Introduction

It has been known for some time that relative to CI chondrite and the sun, the Earth is depleted in moderately to highly volatile elements (Palme & O'Neill 2003). For a given element, the degree of depletion correlates with its condensation temperature, which is defined as the temperature at which 50 percent of the element has condensed to a solid phase, commonly calculated for 10^{-4} bar total pressure. Elements more volatile than Si are depleted relative to CI, and together with the highly volatile elements they define a log-linear trend in concentration-temperature space that is known as the volatility trend (Fig. 1).

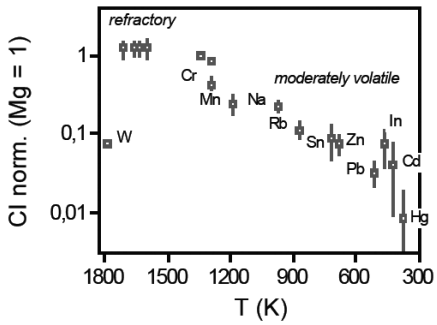

Figure 1. Selected refractory and moderately volatile elements relevant for the study. Concentrations from Palme & O'Neill (2003), condensation temperatures from Lodders & Fegley (1998)

Several explanations have been given as to how the volatility trend developed. One possibility discussed but now largely discarded (Palme & O'Neill 2003, p. 28) is that Earth was initially more volatile-rich, but then lost some volatiles by a thermal event, e.g. by impact heating. Alternatively, much of the Earth could have been accreted in a hot region of the solar nebula, from material that was pre-depleted in volatile elements by nebular fractionation processes (Palme & O'Neill 2003). And a third option is that the volatile elements are part of an element inventory that was brought in during later stages of Earth's accretion, added to an Earth that was much more refractory than it is today (O'Neill 1991, Albarede 2009). O'Neill (2008) hypothesized that this volatile-enriched material could have come from beyond the snow line of the solar system, i.e. from the asteroid belt between Jupiter and Mars. The implication of this model is that with respect to Earth's composition, the volatility trend would infact be a volatile enrichment trend.

For understanding early Earth's evolution, it is important to distinguish among these alternatives. If it can be shown that the bulk of the volatile elements were indeed added later than the refractory element inventory of the Earth, we might question that mantle degassing was a major source for Earth's hydrosphere and atmosphere (Albarede 2009). The option that komatiites may have been wet melts (Parman et al. 1997, Grove et al. 2002) would also have to be reconsidered. But how can we distinguish between these alternative accretion modes? One possibility is by experiment. The volatility trend includes lithophile elements as well as elements with potentially siderophile and chalcophile affinities, e.g. Ga, Sn, Pb, Cd and Hg, none of which are depleted relative to the lithophile elements with the same condensation temperatures. If we can demonstrate by experiment that some elements along the volatility indeed have siderophile affinities, even though their concentrations in the mantle were unaffected by core formation, then the only remaining explanation is that the moderately volatile elements must have been added when core formation was largely complete.

Experiments reported here were performed from 1600 to 2300°C in a piston-cylinder (1 GPa) and a multi-anvil press (5-6 GPa), using sintered MgO as capsule material. The silicate material was a fertile mantle composition that was doped with a range of refractory to moderately volatile, potentially siderophile elements in the hundreds of ppm range, including Cr, W, Zn, Cd, and Pb. The metal phase was pure Fe. Phases at run conditions were a magnesiowüstite-saturated silicate melt and an Fe-dominated metallic melt. Major and trace elements of the quench products were analyzed by EPMA and laser-ablation ICP mass spectrometry, respectively.

Partition coefficients are shown in Fig. 2. All elements studied become increasingly siderophile as the experimental run temperature increases. This phenomenon is known as thermal reduction and arises because the free energies of formation of the respective oxides increase with increasing temperature. The effect is small for Cr and W, moderate for Cd, but very large for Pb whose D (metal/silicate) increases from ~ 0.2 at 1400°C (Lagos et al. 2008) to > 100 at 2100°C.

Theoretically we can use the ranges in D to constrain the temperature of core formation. Chromium and tungsten

belong to the refractory elements that were added to Earth in the early accretionary phase, to be later depleted by core formation. The CI-normalized abundances of these elements in the mantle could be reconciled with Ds (metal/silicate) of around 1.5 (Cr) and ~ 10 (W), which upon consultation of Fig. 2 would afford temperatures around 2100 to 2300°C. Note that this temperature estimate assumes that silicate and metal maintained equilibrium throughout core formation (cf. Wetherill 1975), which may not be so if in the later stages of core formation, accretion was dominated by the addition of fragments already differentiated with respect to metal and silicate (O'Neill 2008). For Cd und Pb, this temperature does not provide a realistic match. If we were to assume that Cd and Pb equilibrated with metal at 2100°C, both elements would lie in Fig. 1 two orders of magnitude below the volatility trend, and not right on it.

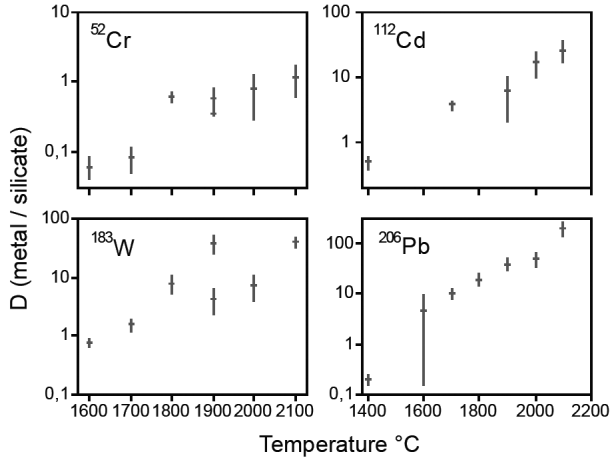

Figure 2. Experimentally determined metal-silicate partition coefficients, of selected siderophile elements from Fig. 1. The 1400°C datapoint is from Lagos et al. (2008).

Out of all alternative origins summarized above, the only feasible option is that the moderately volatile element inventory was added to Earth at a time when core formation was near-complete. Cadmium and lead may be quite siderophile at high temperature, however, that affinity is of little consequence for the abundances of Cd and Pb in the mantle. Our data provide independent experimental support for O'Neill's (1991) and Albarede's (2009) models that Earth's accretion progressed in discrete stages, starting with highly refractory material from the inner solar system, followed by volatile-enriched fractions derived from beyond the asteroid belt, and completed by a late chondritic veneer. Our experiments also imply that the 238U/204Pb ratio of bulk Earth must be much higher than previously assumed (Allegre et al. 1995), as the early components from the inner solar system were so refractory that they could hardly have contained any Pb. Hence, the only Pb fraction that may now be residing in Earth's core is that radiogenic Pb fraction that was generated by in-situ decay of U and Th from the early, highly refractory portion of the Earth. Whether such early loss of radiogenic Pb may in part explain the lead paradox, i.e. why Earth's mantle comes to lie to the right of the geochron, remains to be evaluated. Any such model would critically depend on the degree of equilibration between silicate and metal equilibrated during early core formation, in particular if the efficiency with which radiogenic lead could have been collected by a segregating Fe-dominated core melt varied with time.

References

Albarede F., 2009, Volatile accretion history of the terrestrial planets and dynamic implications, Nature, 461, 1227-1233.

Allegre C.J., Manhes G. & Göpel C., 1995, The age of the Earth. Geochimica et Cosmochimica Acta, 59, 1445-1456.

Grove T. L., Parman S. W., Nuka P., DeWit M. &, Dann J., 2002, Influence of H2O on the development of spinifex textures in komatiites. Geochimica et Cosmochimica Acta, 66, 294.

Lagos M., Ballhaus C., Münker C., Wohlgemuth-Ueberwasser C. & Berndt J., 2008, Is the Earth's missing lead in the core? Nature, 456, 89-92.

Lodders K., Fegley B., 1998, The Planetary Scientist's Companion. Oxford University. Press New York, 371p.

O'Neill, H.St.C., 1991, The origin of the Moon and the early history of the Earth -a chemical model. Part 2: The Earth. Geochimica et Cosmochimica Acta, 55, 1159-1172.

O'Neill, H.St.C., Palme, H., 2008, Collisional erosion and the non-chondritic composition of the terrestrial planets, Philosphical Transactions of the Royal Society, A 366, 4205-4238.

Palme H. & O'Neill H.St.C., 2003, Cosmochemical estimates of mantle composition, in *Treatise on Geochemistry Vol. 2, The Mantle and Core*, Carlson R.W., ed., 1-38.

Parman S. W., Dann J. C., Grove T. L. & deWit M. J., 1997, Emplacement conditions of komatiite magmas from the 3.49 Ga Komati Formation, Barberton Greenstone Belt, South Africa, Earth and Planetary Science Letters, 150, 303-323.

Wetherill G.W., 1975, Radiometric chronology of the early solar system. Annual Review of Nuclear. Sciience, 25, 283-328.

NORTH-EAST SUPERIOR PROVINCE ULTRAPLUTONIC TERRANES: GENESIS OF TTG AND ENDERBITE BY PROGRESSIVE CRUSTAL MATURATION

J.H. Bédard

Geological Survey of Canada, 490 de la Couronne, Quebec, PQ, G1K 9A9, Canada

There is no consensus on the processes responsible for genesis of the Archean cratonic crust, which is dominated by tonalite-trondhjemite-granodiorite: (TTG). The NE Superior Province (NESP) is divided into two, isotopically-defined terranes (Boily et al., 2009), that were assembled prior to the paroxysmal NeoArchean event at 2.74-2.72 Ga. This event (50% of outcrop surface) is dominated by TTG and enderbite (pyroxene-tonalite/trondhjemite) and in both terranes occurred at 2.74-2.72 Ga. Enderbitic rocks make up 20% of the surface outcrop. All rocks have high light/heavy rare-earth element ratios (L/HREE), high large ion lithophile element (U-Th-Rb-Cs-La: LILE) contents, positive Sr-Pb anomalies, and negative Nb-Ta-Ti anomalies (Boily et al., 2009). Enderbites have compositions that broadly overlap with the field of TTGs (Fig.1), with slightly smaller enrichment in LILE. Reintegrated pre-exsolution antiperthite grains plotted on a 5 kbar solvus yield 550-870ºC for tonalite-trondhjemite, and 810-1045ºC for enderbites (Bédard, 2003). Amphibole barometry implies fairly uniform 3-5 Kb emplacement pressures. Greenstone belt relics occur as amphibolite to granulite facies slivers, but once formed an extensive cover sequence (Maurice et al., 2009) before it foundered into the middle crust. Younger granitoids show increasing K-enrichment with time, leading to the production of late monzonites, leucogranites, and granite-granodiorite plutons with associated shoshonite plutons (Bédard et al., 2003). Such typical Archean TTG signatures and trends are commonly explained by melting of subducted oceanic crust. However, near-ubiquitous inherited zircon cores

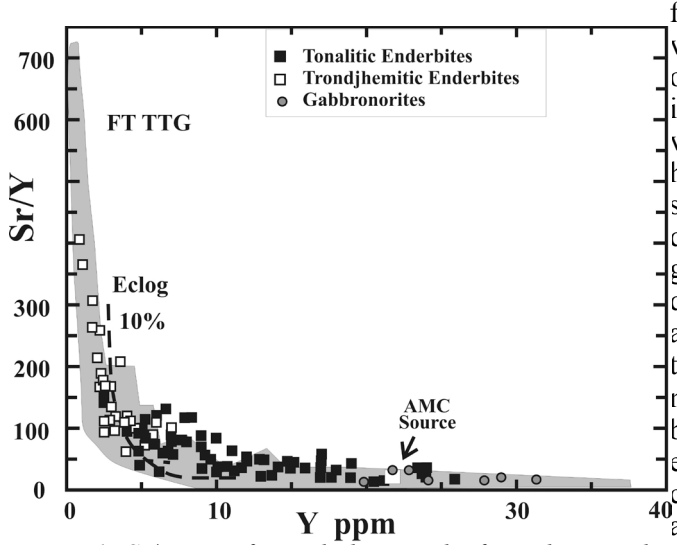

Figure 1. Sr/Y vs Y for enderbitic rocks from the Douglas Harbour Domain of the NESP, compared to the field of TTG.

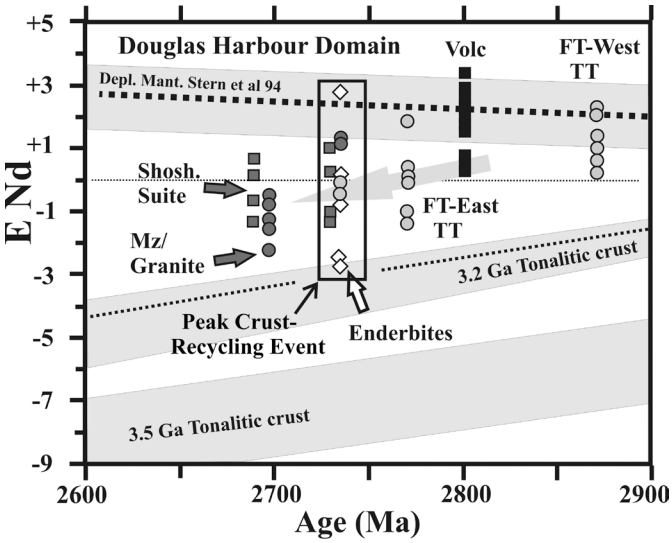

Figure 2. Epsilon Nd vs crystallization age for rocks in the Douglas Harbour domain of the NESP. Adapted from Boily et al. (2009).

and progressively more negative Nd-isotopic signatures in younger NESP TTGs (Fig. 2) imply extensive recycling of older felsic crust. The geochemistry of parental ancestral tonalites and trondhjemites can be modeled by 5-30% melting of a source similar to locally-occurring tholeiitic metabasalts, with residues of rutile-bearing eclogite, garnet-websterite, or hornblende-garnet websterite. Geochemical variations and models imply that the genesis of the trondhjemite to tonalite series is dominated by partial melting, with only 25% of the geochemical variation possibly being accounted for by fractional crystallization. The compositional variations among the enderbite suite largely mimic that of TTGs (Fig.1), with progressive HREE depletion with increasing SiO_2. Two scenarios seem plausible to explain voluminous enderbites. 1) As lower crustal metabasites heat up they may dehydrate rather than melt at the wet solidus. Higher temperatures would be needed reach the dry solidus and generate abundant felsic melt. Melting at greater depth (P=5-7 kbar and T ca 1000ºC) in the more dehydrated part of the lower crust would thus generate a high-temperature water-undersaturated tonalitic to dioritic melt parental to this suite. A spectrum of mineralogically diverse plutonic rocks (ex: hornblende-biotite tonalite, clinopyroxene-hornblende-tonalite, enderbite) with essentially the same chemical composition could thus be produced by melting at different depths and temperatures in a foundering lower crust with a heterogeneous distribution of water. 2) The similarity of geochemical signatures between the enderbites and

TTGs is paradoxical, since the two suites have different mineral parageneses. A possible explanation may be that the enderbite series formed by near-bulk volatile-free remelting of previously formed and differentiated TTGs. This second scenario is more consistent with inherited Zr cores and Nd isotopic data, and mitigates the source volume problem. In either scenario, the extensive TTG/pyroxene-TT episode at 2.74-2.72 Ga seems difficult to explain using the adakite model (melting of subducted oceanic crust). Given a 10 km thick oceanic crust that melts 10%, with a convergence rate of 1.2 cm/y, a 20 my time window implies that 40 subduction zones were simultaneously active so as to generate 10,000 km^3 of TTG (50% of a 40km-thick continental crustal block 500x500km in size). A major, craton-wide heating event related to a major, basaltic underplating event appears to be required to generate such volumes of magma, and only major mantle upwellings such as plumes seem adequate to the task.

References

Bédard J.H., 2003, Evidence for regional-scale, pluton driven, high-grade metamorphism in the Minto Block, northern Superior Province, Canada, Journal of Geology, 111, 183-205.

Bédard, J.H., Brouillette, P., Madore, L. & Berclaz, A., 2003, Archean cratonization and deformation in the northern Superior Province, Canada: an evaluation of plate tectonic vs vertical tectonic models, Precambrian Research, 127, 61-87.

Maurice, C., David, J., Bédard, J.H. & Francis, D., 2009, Evidence for a widespread mafic cover sequence in the Northeastern Superior Province of Canada, Precambrian Research, 168, 45-65.

Boily, M., Leclair, A., Maurice, C., Bédard, J.H., Berclaz, A. & David, J., 2009, Paleo- to Mesoarchean basement recycling and terrane definition in the Northeastern Superior Province, Québec, Canada, Precambrian Research, 168, 23-44.

CALC-ALKALINE INTERRUPTIONS OF A THOLEIITIC SEQUENCE, CHIBOUGAMAU, ABITIBI BELT: REMELTING OF A MATURING JUVENILE OCEANIC PLATEAU

J.H. Bédard[1], F. Leclerc[2,3], L.B. Harris[2] & P. Roy[3]

[1] Geological Survey of Canada, 490 de la Couronne, Québec, PQ, G1K 9A9, Canada.
[2] Institut National de la Recherche Scientifique - Eau, Terre et Environnement, 490 de la Couronne, PQ, G1K 9A9, Canada.
[3] Ministère des Ressources naturelles et de la Faune du Québec, 400 boul. Lamaque, Val-d'Or, PQ, J9P 3L4, Canada.

It has been proposed that Archaean greenstones are tectonic collages of juvenile arc terranes and oceanic crust. An alternate view proposes essentially in-situ growth and maturation of oceanic plateaux. In the Chibougamau area (NE Abitibi belt), the Obatogamau (tholeiitic) and Waconichi (calc-alkaline: ca 2727/8 Ma) formations constitute a first volcanic cycle (Fig.1), while the Bruneau Member. (mostly tholeiitic) and Blondeau (mostly calc-alkaline) Formation. constitute a second. The Lac Doré Layered Complex (LDC, 2727/8 Ma) intrudes the first cycle. The Bruneau Member/ Blondeau Formation contact is intruded by tholeiitic to calc-alkaline layered sills at 2717 Ma (Bédard et al., 2009). Tholeiitic diabasic sills are common everywhere below this contact, and probably fed basaltic volcanism (Bédard et al., 2009). The LDC is split by the tonalitic Chibougamau pluton (2714 Ma) in an anticlinal core, and cobbles from this tonalite show up in the unconformably overlying Opemisca Group conglomerates.

Obatogamau Formation tholeiites have near-constant, low MgO (ca 5%, Fig.1, stage 1a) suggesting a near-steady-state plumbing system, with mantle inputs balanced by fractional crystallization. Lower Obatogamau Formation lavas have higher Th, suggesting localized contamination, but isotopic data preclude involvement of old crust. David Member lavas (Stage 1b) show upwardly decreasing Zr/Y, TiO_2 and P_2O_5, suggesting progressive depletion of source mantle. Although they occupy the same stratigraphic level as the Obatogamau Formation, David Member basalts have distinct geochemical signatures, and may be a distinct shield volcano. Alternatively, there may have been differential erosion north and south of the LDC?

The Waconichi Formation records the arrival of voluminous felsic magmas. Near the LDC, and associated with Cu-rich VMS deposits, are soda-rhyolites with enriched, flat REE patterns (Type 3), probably generated by low-pressure anatexis of local tholeiitic basalts (Fig.2A), presumably above the LDC chamber. Distally to the LDC, the Waconichi Formation is composed of intermediate to felsic tuffs with steeply fractionated L/HREE (Types 1-2). These tuffs are underlain by a thin set of intermediate lavas (hybrids?) that are underlain in turn by a thin chert-exhalite unit that rests on Obatogamau Formation/David Member basalts. The highly fractionated L/HREE profiles of

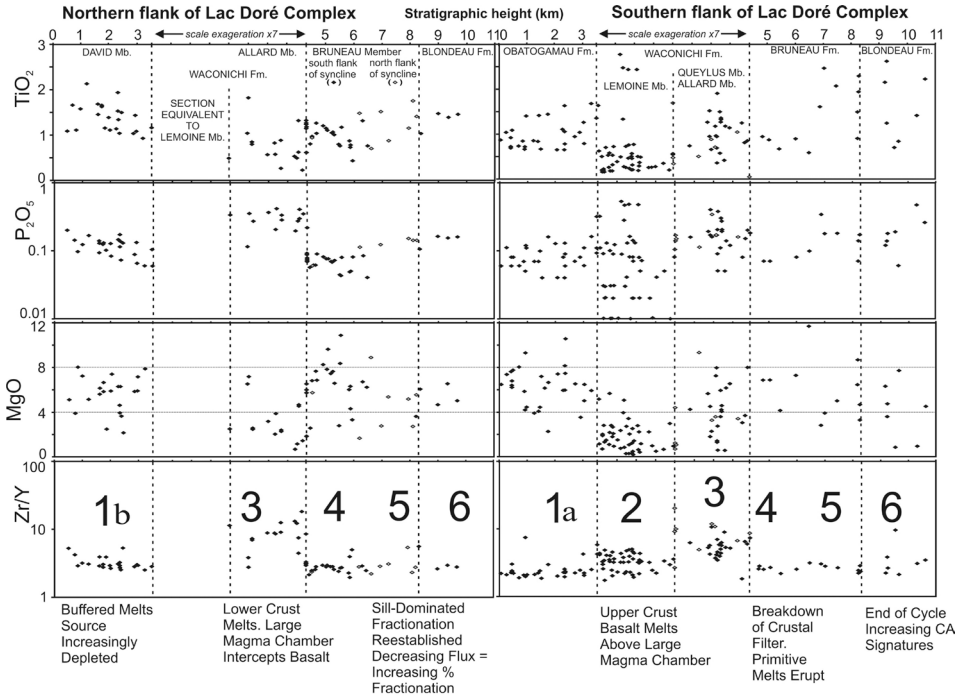

Figure 1. Composite stratigraphic column for either flank of the Lac Doré Complex, showing the main evolutionary stages. Note that the thickness of the ca 1km thick Waconichi Fm has been exaggerated. Adapted from Leclerc et al. (2010).

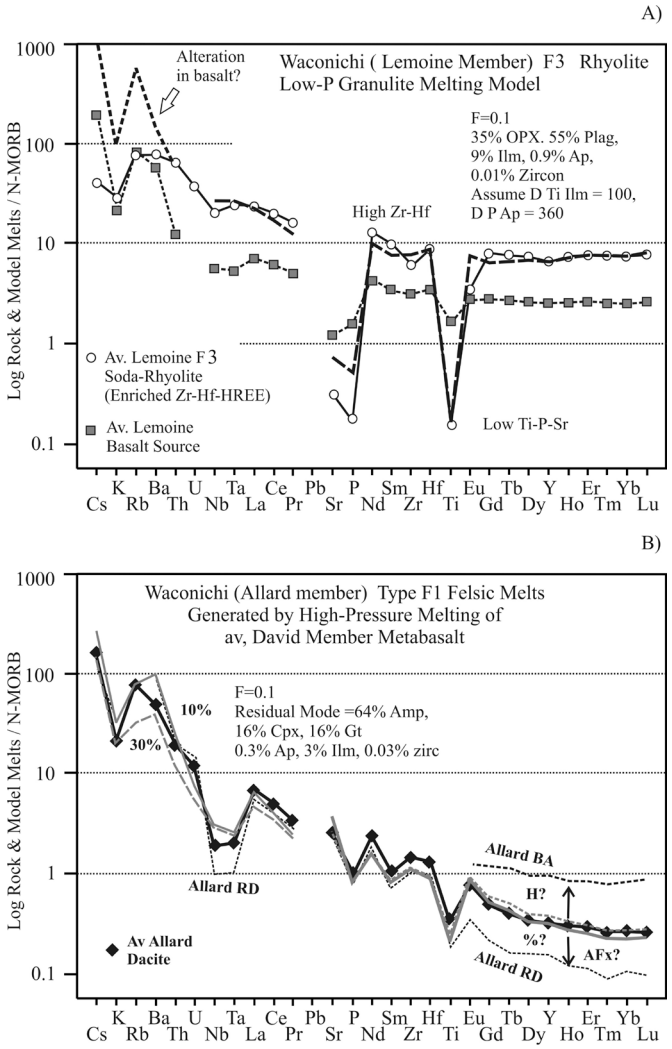

Figure 2. Equilibrium melting models using parameterized D datasets showing possible model for the generation of: A) Type 3 soda-rhyolites by high-T low-P anatexis of locally-occurring metabasalts in the roof zone of the LDC. These lavas only occur in the vicinity of this contact. Misfits in LILE elements probably reflect alteration of the basalt used as the source. B) Type 1 dacitic melts by high-P anatexis of av. David basalt. 10 and 30% melting curves are shown. The compositions of Allard average basaltic andesite (BA) and rhyodacite (RD) are sketched in. There remains considerable uncertainty about why a spectrum of HREE abundances is observed, whether this reflects variations in % melting, hybridization with incoming basalt, or amphibole fractionation.

the Type 1-2 tuffs require a garnet-bearing residue (Fig.2B), and geochemical modeling implies that local basalts are plausible sources. The absence of interbedded basalts in the upper Waconichi Formation tuffs suggests an efficient crustal filter was established, preventing eruption of basalt (stages 2-3 on Fig.1). Calculated model melts from LDC cumulates resemble Type 1-2 magmas (Bédard et al., 2009), and since the LDC and Waconichi Formation are coeval, the LDC may be the exhumed magma chamber in which these melts accumulated and differentiated.

The lowermost Bruneau Member basalts are MgO-rich (<12 wt %, stage 4), but give way up-section to evolved lavas (MgO ca 5%, stage 5) with Zr/Y, TiO_2 and P_2O_5 contents that define continuations of the Obatogamau Formation/David Member trend (Fig.1). This suggests that the nature of the parental basaltic melt did not change significantly during the Waconichi Formation eruption event. We interpret the Waconichi Formation as the result of the establishment of a major felsic crustal magma chamber (LDC) that prevented eruption of basalt. The high-MgO pulse of the lower Bruneau Member would represent a sudden breakdown of this largely-congealed crustal filter, allowing unfractionated mantle melt to pass unhindered through the crust. The disappearance of high-MgO lavas in the upper Bruneau Member, and progressive upward decrease in MgO and increase in TiO_2 and P_2O_5 of the basalts, suggest that a crustal plumbing system was re-established and that unfractionated melts were no longer able to erupt.

Volcanics in the upper Bruneau Member and Blondeau Formation show great diversity (stages 5-6), and an increasing proportion of evolved melts, with intimate mixtures of tholeiitic and calc-alkaline stems. This suggests that; a) the mantle flux into the crustal plumbing system could no longer buffer melt compositions; b) mantle-derived melts became increasingly fractionated with time; c) that crustal inputs became more significant, although isotopic data imply a near-juvenile source.

Geochemical signatures imply that calc-alkaline magmas punctuated a tholeiitic magma system, and were largely the result of remelting of previously erupted tholeiitic basalts. Geochemical signatures (Th/Yb vs Nb/Yb, Pearce, 2008) suggest that calc-alkaline magmatism does not represent the results of source metasomatism, as in arcs, but AFC/mixing processes.

References

Bédard J.H., Leclerc F., Harris L. & Goulet N., 2009, Intra-sill magmatic evolution in the Cummings Complex, Abitibi greenstone belt: Tholeiitic to calc-alkaline magmatism recorded in a subvolcanic conduit system, Lithos, 111, 47-71.

Leclerc, F., Bédard J.H., Harris L.B., Goulet, N. & McNicoll, V., 2010, Revision of the Roy Group stratigraphy in the Chibougamau area (Abitibi Subprovince, Southeastern Superior craton) B implications for Archaean volcanism and VHMS exploration, Submitted to Canadian Journal Earth Sciences.

Pearce, J.A., 2008, Geochemical fingerprinting of oceanic basalts with applications to ophiolite classification and the search for Archean ophiolites, Lithos, 100, 14-48.

THE TERRANECHRON® APPROACH TO CRUSTAL EVOLUTION STUDIES AND IMPLICATIONS FOR CONTINENTAL GROWTH

E.A. Belousova[1], W.L. Griffin[1], G. Begg[1,2] & S.Y. O'Reilly[1]

[1]GEMOC, National Key Centre, Department of Earth and Planetary Sciences, NSW 2109, Australia
[2]Minerals Targeting International., West Perth WA, 6005, Australia

Introduction

To understand the genesis of a block of crust and the nature of crust-mantle interaction, we need to know not only the age distribution of the magmatic rocks but also the nature (juvenile/mantle or ancient/crustal) of the magmatic protoliths. TerraneChron® is a specifically developed methodology to study the evolution and growth of the continental crust through time. It allows the evaluation of how much new crust was formed, and how much older crust was recycled, thus providing essential information on the rate at which the continental crust has grown at different stages of Earth's history. This approach is based on the integrated in situ analysis of zircons for U-Pb and Hf isotopic composition using laser-ablation microprobe techniques. The methodology is typically applied to zircons from drainage samples judiciously collected within defined catchments that sample areas of the crust formed in different tectonic settings, but also uses separated zircons from host rocks for groundtruthing.

Application to crustal evolution studies and mineral exploration

Most mineral exploration models require an understanding of the geological evolution of the crust in the area of interest; critical information includes the timing of magmatic events and the types and sources of the magmas. Acquiring this type of information in unmapped regions, or even checking the reliability of existing data, can be very costly in both time and money. However, TerraneChron® has provided a rapid and cost-effective solution to this problem.

Sampling Strategy

The methodology can be applied to zircons separated from single rocks or to zircons from drainage samples collected within a defined catchment (on scales of 10 - 1000 km, depending on the objective). The use of drainage samples has many advantages: nature has separated and concentrated a statistically more meaningful sample than is achievable by conventional single rock sampling and methods, and this can provide a more comprehensive coverage of rock types from the drainage area (Griffin et al., 2006; Belousova et al., 2009). These sediment samples also may provide zircons from source rocks that no longer outcrop, or even exist as intact rock units; these grains carry valuable information on crustal history.

Analytical Techniques

The U-Pb analyses are done by LAM-ICPMS techniques, which provide rapid and cost-effective age determinations with precision equivalent to the ion microprobe (e.g. Jackson et al., 2004). The Hf-isotope data are collected by LAM-multicollector (MC)-ICPMS (e.g. Griffin et al., 2000). Hf isotopes provide information on the source of the magmatic rock from which each zircon crystallised; they tell whether the magmatism involved a juvenile source (e.g. melting of young mantle-derived magmas, if only pre-existing crust was involved (i.e. crustal reworking), or a combination of these processes. The analysis of trace elements provides information about the composition of the magmatic rock that precipitated the zircon (e.g. Belousova et al., 2002). Thus the TerraneChron® approach provides more layers of information than the conventional approach based on U-Pb age spectra.

Event Signatures and Terrane Correlation

The comparison of large volumes of data on the ages and Hf-isotope compositions of zircons can be simplified by reducing the data to 'Event Signature' curves that show the main features of crustal evolution (Griffin et al., 2006; O'Reilly et al., 2008). Figure 1 illustrates the principle; the mean crustal residence time of the magma sources involved at each stage of the area's evolution is given by the difference between the mean crystallisation age of the magmas (the U/Pb age of the zircons) and the mean T_{DM} model age of those zircons. In this plot (Figure 1), reworking of older crust produces a downward trend with decreasing age, while juvenile inputs (leading to a lower mean source age) produce rising trends with decreasing age. Trends of intermediate slope imply contributions from both juvenile and pre-existing crustal sources.

Event Signatures reveal the timing and geochemical patterns of mantle magmatic events and crustal orogenesis that have affected each terrane sampled. Figure 1 compares the curve for the Gawler Craton with those for the Mount Isa Inlier, the Broken Hill area and the Georgetown Inlier. Although all these areas have strong evidence for Archean basement, the Broken Hill curve is significantly different from the other three curves before ca. 1800 Ma. The near-parallelism of curves for the Gawler Craton, the Mount Isa Block and the Georgetown Inlier implies a similarity in their early evolution (e.g. before ca. 1800 Ma). After ca. 1800, the Mount Isa and Broken Hill areas show remarkably parallel development (Figure 1): both underwent melting of the older crust from ca. 1800-1750 Ma, then experienced a major juvenile addition around 1650 Ma.

Testing models for Continental crustal growth

A worldwide database of 12,375 TerraneChron® analyses of zircon (Belousova et al., unpubl.), largely from detrital

sources, has been generated at GEMOC since 2000. To this dataset we have added U-Pb and Hf-isotope data available from a number of recent publications (4,070 analyses from rock samples and sediments). This large volume of data (n=16,445) makes it feasible to examine processes of crustal evolution on a global scale, and to test existing models for the growth of continental crust through time.

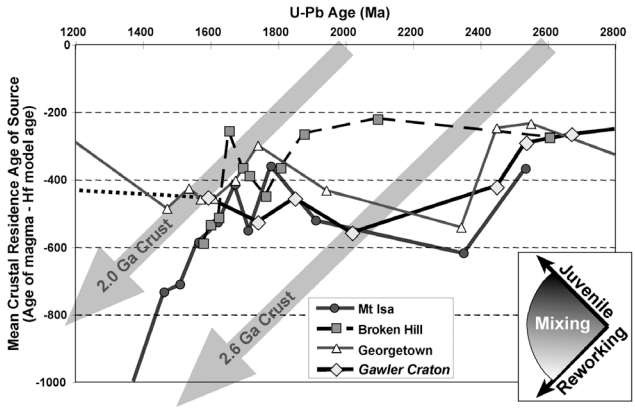

Figure 1. Comparison of 'Event Signatures' for the Gawler Craton with the Curnamona Craton, Mount Isa Block, and Georgetown Inlier (Belousova et al., 2009).

Figure 2 shows the distribution of U-Pb ages in the GEMOC TerraneChron® database (blue line) compared to the data from other studies. Previous studies (e.g. Iizuka et al., 2005) have shown that the distribution of zircon ages in a large sample from the Mississippi River accurately reflected the relative areas of the igneous provinces in the drain-age area. The data of Campbell & Allen (2008) are shown separately as a green line; these represent detrital zircons collected from the mouths of 40 of the world's largest rivers and thus provide a broad global picture of the age distribution, but unfortunately they are not accompanied by Hf-isotope data. A good correlation between the major peaks in the TerraneChron® and Campbell & Allen (2008) datasets indicates that the TerraneChron® dataset is broadly representative of the worldwide distribution of crustal age provinces.

To understand the growth rate of the continental crust it is critical to evaluate the proportion of juvenile material added to the crust at each point during its evolution. The amount of juvenile material produced at any given time is commonly underestimated, because some of that material was later reworked, and the record of the original juvenile material is lost during subsequent crustal evolution. The approach proposed in this study attempts to offset this effect, and "restore" an indication of the true juvenile input using the integrated dataset.

The age data alone would support an Episodic Growth model, but the Hf-isotope data (Figure3) reveal that most of the magmatic rocks represented in the major "episodes" were derived by the recycling of pre-existing crust, especially after ca. 2.5 Ga; the juvenile contribution represents a small proportion of most magmatic episodes. Modelling of the ages of the recycled components emphasises the repeated reworking of Archean components, supporting an Early Growth model.

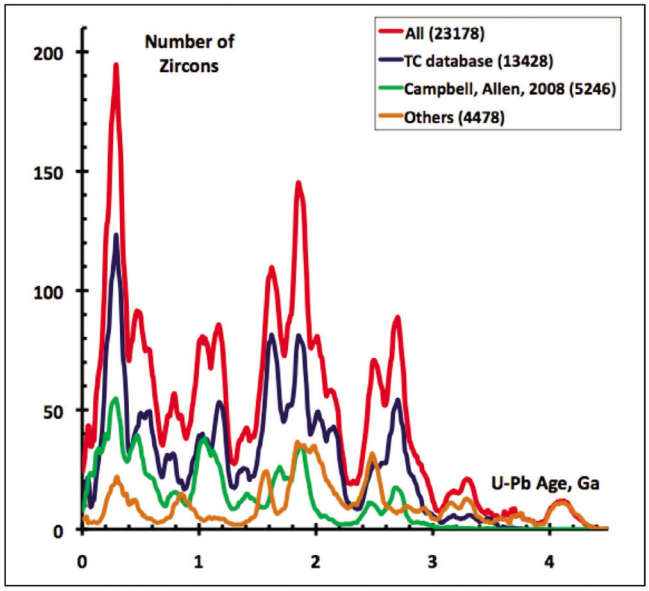

Figure 2. Comparison of zircon U-Pb age distributions for data collected from different sources. The red curve shows distribution of ages in a worldwide data set including grains with ages but no Hf-isotope data. The TerraneChron® (TC) database (blue curve) is from GEMOC; data of Campbell & Allen (2008; green curve) are detrital zircons from the mouths of 40 of large rivers.

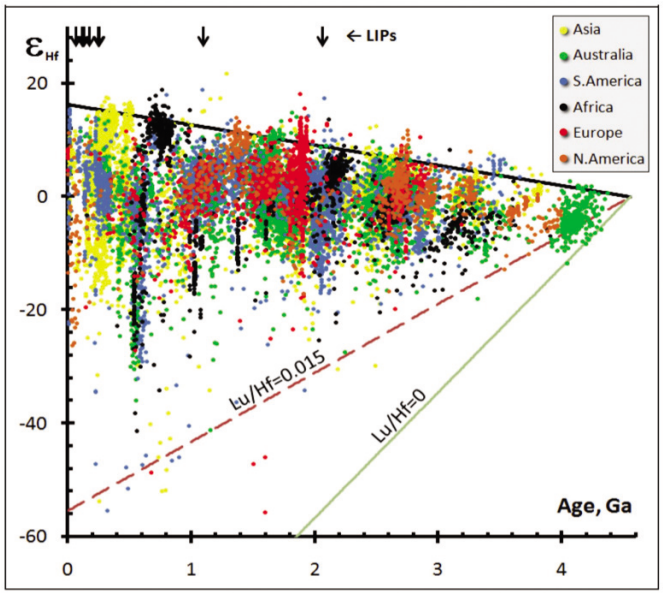

Figure 3. Plot of εHf vs. age showing data plotted by continent (Belousova et al., unpubl.).

Acknowledgements

Funding for this work came from collaborative projects with industry (including WMC, BHPB, DeBeers, Newmont, Gold Fields), Macquarie. University External Collaborative Research Grants and ARC Discovery and Linkage grants. The analytical data were obtained using instrumentation funded by ARC LIEF, and DEST Systemic Infrastructure Grants, industry partners and Macquarie. University. The research was supported by ARC and Macquarie. University grants to S.Y. O'Reilly and W.L. Griffin, and collaborative research with industry partners, especially Western Mining Resources and BHP-Billiton.

References

Belousova E.A., Griffin W.L., O'Reilly S.Y. & Fisher N.I., 2002, Igneous Zircon: Trace element composition as an indicator of host rock type, Contributions to Mineralogy and Petrology, 143, 602–622.

Belousova E.A., Reid A.J., Griffin W.L. & O'Reilly S.Y., 2009, Rejuvenation vs. Recycling of Archean Crust in the Gawler Craton, South Australia: Evidence from U-Pb and Hf-isotopes in Detrital Zircon, Lithos, 113, 570–582.

Campbell I.H. & Allen C.M., 2008, Formation of supercontinents linked to increases in atmospheric oxygen, Nature Geoscience, 1, 554–558.

Griffin W.L., Pearson N.J., Belousova E.A., Jackson S.E., O'Reilly S.Y., van Achterberg E. & Shee S.R., 2000, The Hf isotope composition of cratonic mantle: LAM-MC-ICPMS analysis of zircon megacrysts in kimberlites. Geochimica et Cosmochimica Acta, 64, 133–147

Griffin W.L., Belousova E.A., Walters S.G & O'Reilly S.Y., 2006, Archean and Proterozoic Crustal Evolution in the Eastern Succession of the Mt Isa District, Australia: U-Pb and Hf-isotope studies of detrital zircons, Australian Journal of Earth Sciences, 53, 125–150.

Iizuka T., Hirata T., Komiya T., Rino S., Katayama I., Motoki A. & Maruyama S., 2005, U–Pb and Lu–Hf isotope systematics of zircons from the Mississippi River sand: implications for reworking and growth of continental crust, Geology, 33, 485–488.

Jackson S.E., Pearson N.J., Griffin W.L. & Belousova E.A., 2004, The application of laser ablation-inductively coupled plasma-mass spectrometry to in-situ U-Pb zircon geochronology, Chemical Geology, 211, 47–69.

O'Reilly S.Y., Griffin W.L., Pearson N.J., Jackson S.E., Belousova E.A., Alard O. & Saeed A., 2008, Taking the pulse of the earth: linking crust and mantle events, Australian Journal of Earth Sciences, 55, 983–995.

THE HADEAN EARTH AS VIEWED FROM THE EOARCHEAN ROCK ISOTOPIC RECORD

V.C. Bennett

Research School of Earth Sciences, The Australian National University, Canberra, ACT 0200

Introduction

The processes of early terrestrial chemical differentiation, including the origin of continental crust, are key questions in twenty-first century Earth science. Geochemical relationships show that the crust and mantle have been strongly linked for at least the last billion years (e.g., Hofmann, 1988), probably through plate tectonics processes, but how and when this linkage occurred and what the Earth was like for the first 3.5 billion years continues to be vigorously debated. Harrison et al, (2005) among others, championed the very early advent of modern-style subduction and voluminous continental crust containing abundant low-temperature granite, based on the geochemistry of ca. 4 Ga detrital zircons from the Jack Hills, Western Australia. Whereas the composition and geology of 3.85-3.60 Ga rocks from Archean crustal terranes implies a much different style of tectonism involving sequential, first billion years continental crust growth from arcs dominated by basaltic-dacitic rocks (e.g. Nutman, 2006). Plausible crustal growth curves range from extensive formation of continents in the Hadean immediately after formation of the Earth (e.g. Armstrong, 1981), to punctuated periods of intermittent bursts of continental growth (e.g., McCulloch & Bennett, 1994), to relatively late additions of granitic crust in modern arc systems. Understanding the timing and mechanism of early continental growth has wide ranging implications including for volatile recycling and evolution of the atmosphere, mantle dynamics, design of resource exploration models in Precambrian terranes, and linking biologic and lithospheric evolution patterns.

The first 100 million years: Timing and extent of early chemical differentiation on the Earth from ^{142}Nd and ^{143}Nd isotopic variations

Recognising ^{142}Nd isotopic variations in terrestrial rocks (which can only arise from events occurring during the lifetime of now extinct ^{146}Sm [$t_{1/2}$=103 myr]) has been an on-going quest starting with Harper and Jacobsen, 1992. The significance of ^{142}Nd variations is that they unequivocally reflect early silicate differentiation processes operating in the first 500 myr of Earth history, the key time period between accretion and the beginning of the rock record. The establishment of the existence of ^{142}Nd variations, (e.g., Caro et al, 2003, 2006, Boyet et al, 2004, Bennett et al, 2007) in ancient Earth materials has opened a new range of questions including, how widespread is the evidence of early differentiation, how do ^{142}Nd compositions vary with time, rock type and geographic setting, and, combined with other types of isotopic and geochemical data, what can ^{142}Nd isotopic variations reveal about the timing and mechanisms of early terrestrial differentiation? To explore these questions we are determining high precision ^{142}Nd, ^{143}Nd and ^{176}Hf isotopic compositions from the oldest well-preserved (3.63- 3.87 Ga), rock suites from the extensive early Archean terranes worldwide including those of southwest Greenland, western Australia, Antarctica and North China craton. Our results (Fig. 1) demonstrate both the persistence and systematic dilution of Hadean isotopic signatures in Archean rocks from southwest Greenland, as well as the distinct isotopic characteristics of coeval ca. 3.73 Ga rocks from Western Australia.

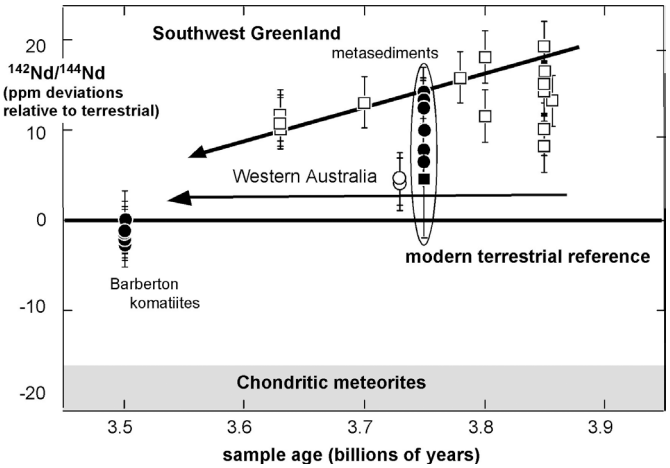

Figure 1. ^{142}Nd/^{144}Nd variations (expressed as ppm differences from modern terrestrial compositions) as a function of age in early Archean rocks from southwest Greenland (Itsaq complex), western Australia (Yilgarn Craton) and South Africa (Barberton). (From Bennett et al, 2007).

Additionally, the combined ^{143}Nd- ^{142}Nd data from this samples forms a self-consistent dataset, with the Itsaq samples having both higher ^{142}Nd/^{144}Nd and initial ^{143}Nd/^{144}Nd isotopic compositions than the Narryer gneisses. The relative isotopic differences preserved in contemporaneous samples from two widely separated terranes points to the existence of diverse mantle sources at 3.7 Ga. The Narryer gneisses either formed from a mantle source with a lower average Sm/Nd than the Itsaq source, or the Narryer mantle was partially remixed with a more LREE enriched source prior to 3.7 Ga, but after ^{146}Sm was largely decayed.

Additionally, data from the coupled short and long half-life ^{146}Sm-^{142}Nd and ^{147}Sm-^{143}Nd decay schemes allows direct calculation of a mantle source differentiation age (cf. Harper & Jacobsen, 1992). Assuming a 20 ppm terrestrial offset from average chondritic compositions (e.g. Boyet & Carlson, 2005) and a solar system initial ^{146}Sm/^{144}Nd of 0.0075, with solar system evolution starting at 4.567 Ga, our combined ^{143}Nd- ^{142}Nd data from the oldest (ca. 3.85 Ga) measured terrestrial samples directly date formation of differentiated silicate reservoirs in the first 30-60 myr of Earth history (Boyet &

Carlson, 2005; Bennett et al., 2007). This very early age makes it difficult to attribute early continent formation as the primary mechanism of Sm/Nd fractionation.

Mass of hadean continents from combined ^{176}Hf and ^{142}Nd isotopic data

In Phanerozoic mantle and mantle-derived samples, including primitive granitoids, initial Hf and Nd isotopic compositions are well correlated (e.g. Vervoort & Blichert-Toft, 1997). This is not the case for Eoarchean samples. For example the most positive initial Hf isotopic compositions from zircons from three of the same samples (Hiess et al, 2009) yielding positive ^{142}Nd anomalies (Bennett et al, 2007) are all within error of chondritic values (calculated using λ^{176}Lu= 1.867 x 10^{-11} yr^{-1}). These results are in agreement with previously published whole rock and bulk zircon results for Archean samples from west Greenland, when all are calculated using the same decay constant and chondritic parameters. Overall the data from Eoarchean rocks span a much narrower range and are distinct from the more heterogeneous initial εHf values exhibited by the 4.0- 4.4 Ga Jack Hills zircons (Bennett et al., submitted).

To generate the ^{142}Nd excesses (up to 18 ppm) in the source region of the tonalites requires chemical differentiation of their mantle source starting at ~4.51 Ga, with the depleted mantle source having a high Sm/Nd=0.390, that is about 20% higher than chondrites (=undifferentiated mantle). However, these same Eoarchean rocks all have initial ^{176}Hf/^{177}Hf compositions very close to chondritic compositions. This requires a source with a long-term chondritic Lu/Hf ratio. This trace element signature is distinct from that of the modern upper mantle, which is characterized by both long-term high Lu/Hf and Sm/Nd evolving to the characteristic radiogenic Hf and Nd isotopic compositions of modern basalts. There is a general consensus that the depleted chemical signature of the present day upper mantle largely reflects extraction of continental crust (e.g. Hofmann, 1988). This is demonstrated by the complementarity of trace element signatures with, for example, the continents being light rare earth element enriched and the mantle having a complementary light rare earth element depleted pattern. Thus the high Sm/Nd and Lu/Hf of the mantle is balanced by the low Lu/Hf and Sm/Nd of the continental crust. In contrast the apparent chemical pattern of the Hadean mantle as determined by our isotopic analysis

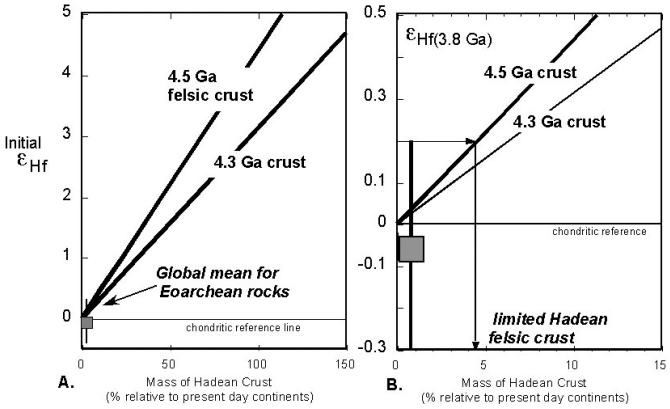

Figure 2a. Model results of initial Hf isotopic compositions of Eoarchean rocks (given as εHf=parts in 10,000 variation relative to a primitive mantle reference) as a function of mass of Hadean (either 4.5 Ga or 4.3 Ga) continental crust. (From Bennett et al., submitted). B. Detailed view of Fig. 2a.

of the oldest Archean rocks requires high Sm/Nd but chondritic Lu/Hf. High Sm/Nd in the Hadean mantle could potentially be achieved by extraction of large volumes of continental crust, but this would also generate high ^{176}Hf, which are not observed. From mass balance considerations neither modern average continental crust, nor ancient continental crust as represented by tonalites can be the complementary reservoir for early mantle depletion. This then implicates alternative models of early differentiation such as might occur by mineral fractionation at depth in a terrestrial magma ocean (Caro et al., 2005).

Moreover, owing to the efficacy of continental crust extraction in fractionating Lu/Hf in the mantle, the near-chondritic Hf isotopic compositions of Archean tonalites (e.g. Hiess et al, 2009) can provide quantitative limits on the amount of Hadean crust that could have been produced and preserved. This is shown in Figure 2a, b, where based on various model assumptions as outlined in Bennett et al, (submitted) the initial εHf as recorded in zircons from Eoarchean rocks can be directly related to the age and amount of preserved Hadean continental crust. The box in Figure 2a and the more detailed Figure 2b represents our best esimtate of the isotopic composition of the Eoarchean mantle. As such this would indicate that the size of Hadean continents formed and preserved to 3.8 Ga were much less than 5% of the present day continental mass.

References

Armstrong R.L., 1981, Radiogenic isotopes: The case for crustal recycling on a near steadystate no-continental-growth Earth, Philosophical Transactions of the Royal Society of London, A301, 443–472.

Bennett V.C., Brandon A.D. & Nutman A.P., 2007, Coupled ^{142}Nd-^{143}Nd isotopic evidence for Hadean mantle dynamics. Science, 318, 1907–1910.

Boyet M. & Carlson R.W., 2005, ^{142}Nd evidence for early (>4.53 Ga) global differentiation of the silicate Earth Science, 309, 567–589

Boyet M., Blichert-Toft J., Rosing M., Storey C.D., Télouk M. & Albarede F., 2004, ^{142}Nd evidence for early Earth differentiation, Earth and Planetary Science Letters, 214, 427–442.

Caro G., Bourdon B., Birck J.-L. & Moorbath S., 2003, ^{146}Sm-^{142}Nd evidence from Isua metamorphosed sediments for early differentiation of the Earth's mantle, Nature**,** 423, 428–432.

Caro G., Bourdon B., Birck J.-L. & Moorbath S., 2006, High-precision ^{142}Nd/^{144}Nd measurements in terrestrial rocks: Constraints on the early differentiation of the Earth's mantle. Geochimica et Cosmochimica Acta, 70, 164–191.

Hofmann A.W., 1988, Chemical differentiation of the earth: The relationship between mantle, continental crust, and oceanic crust, Earth and Planetary Science Letters, 90, 297–314.

Harper Jr. C.L. & Jacobsen, S.B., 1992, Evidence from coupled ^{147}Sm-^{143}Nd and ^{146}Sm-^{142}Nd systematics for very early (4.5-Gyr) differentiation of the Earth's mantle, Nature, 360, 728–732.

Harrison T.M., Blichert-Toft J., Muller W., Albarède F., Holden P. &Mojzsis S.J., 2005, Heterogeneous Hadean hafnium: evidence of continental crust at 4.4 to 4.5 Ga, Science**,** 310, 1947–1950.

Hiess J., Bennett V.C. Nutman A.P. & Williams I.S., 2009, In situ U–Pb, O and Hf isotopic compositions of zircon and olivine from Eoarchaean rocks, West Greenland: New insights to making old crust Geochimica et Cosmochimica Acta 73 4489–4516.

McCulloch M.T. & Bennett, V.C., 1994, Progressive growth of the Earth's continental crust and depleted mantle: Geochemical constraints. Geochimica et Cosmochimica Acta, 58(21 SU -): 4717–4738.

Nutman A.P., 2006, Antiquity of the Oceans and Continents, Elements, 2, 223–227.

Vervoort J.D. and Blichert-Toft J., 1999, Evolution of the depleted mantle: Hf isotope evidence from juvenile rocks through time, Geochimica et Cosmochimica Acta, 63, 533–556.

GEOCHEMICAL AND Sr-Nd ISOTOPE CONSTRAINTS ON THE PETROGENESIS OF GRANITOIDS FORM NORTHWESTERN PART OF THE DHARWAR CRATON, SOUTHERN INDIA: EVIDENCE FOR CRUSTAL ACCRETION AND GEODYNAMIC IMPLICATIONS

S. Dey

Department of Applied Geology, Indian School of Mines, Dhanbad – 826 004, India
e-mail:geodeys@gmail.com

Granite-greenstone belts provide vital clues of Archaean crust formation events, although the precise mechanism and geodynamic setting are still topics of intensive debate. Geodynamic models suggested explaining Archaean crust formation in different cratons can be broadly divided into two groups viz. subduction-related accretion and mantle plume-related growth. Similar divergence of views exists for the actual geodynamic setting during the late Archaean evolution of the Dharwar craton (DC), southern India. To further constraint the mechanism of crust generation, granitoids in three areas across the northwestern part of the Dharwar Craton (DC) are studied. They are divided into four suites viz. the 'western' and 'eastern' tonalite-trondhjemite-granodiorite (TTG) gneisses, biotite monzogranites and porphyritic biotite granodiorites.

The western TTG gneisses are part of the middle Archaean gneissic complex in Western Dharwar craton (WDC) and are metaluminous, low-Al tonalitic to trondhjemitic in composition, characterized by moderate to high SiO_2, low K_2O, Rb and Ba. The eastern TTG gneisses occur in the late Archaean Eastern Dharwar craton (EDC) and are metaluminous trondhjemites and granodiorites, spatially associated but presumably somewhat older than the biotite monzogranites and porphyritic biotite granodiorites. These TTG gneisses are pre- to syn-tectonic, and show variable SiO_2 and Al_2O_3, enriched LREE and depleted HREE with slightly negative to no Eu anomaly. These granitoids show unusual chemistry in containing higher FeO(T), K_2O, Ba, Cr and Ni compared to the classical TTGs.

The biotite monzogranites are mostly post tectonic and display evolved calc alkaline composition with high SiO_2, K_2O, LILE and LREE, depleted to undepleted HREE and strongly negative to no Eu anomalies. The porphyritic granodiorites exhibit post-tectonic calc-alkaline, sanukitoid-like character with expanded SiO_2, higher TiO_2, P_2O_5, Sr, Ba, Cr and Ni, and lower Rb. Compared to typical sanukitoids they, however, uniquely display considerably higher K_2O, ΣREE and Th. In εNd vs. $I^{87}Sr/^{86}Sr$ correlation diagram the monzogranites plot in the field of late Archaean juvenile gneisses whereas the porphyritic granodiorites fall nearer to the mantle array.

The western gneisses are similar to typical Archaean TTGs and probably derived from a depleted metabasalt source presumably in the middle Archaean period. The late Archaean evolution of the terrain is explained by a subduction environment characterized by a slab (oceanic plate) dipping westerly below a middle Archaean continent (i.e. WDC). Slab-derived fluids/melts had been continuously metasomatizing the overlying mantle wedge. In the initial stage, the eastern gneisses were produced by melting of slab basalt followed by slight contamination from metasomatized mantle wedge, and then accreted into the crust. Subsequent slab break-off due to terrain accretion and resultant upwelling of hot mantle asthenosphere possibly shifted the locale of magma generation to the overlying extremely metasomatized mantle wedge. As a result, the porphyritic granodiorites were formed and intruded into the crust. This, in turn, triggered melting of the gneisses accreted earlier (i.e. mostly eastern gneisses) and generated the evolved monzogranites.

Monzogranites occurring east of the Hungund-Kushtagi schist belt of EDC show higher εNd but lower T_{DM} ages than those occurring west. This indicates that that the schist belt represents a suture zone along which terrains of different histories were brought in juxtaposition by horizontal plate-tectonic process (accretion). The terrain on the eastern side of the schist belt had only juvenile late Archaean component whereas that on the west had mixed juvenile and middle Archaean components.

SECULAR COOLING OF THE SOLID EARTH, ARCHAEAN EMERGED LAND SURFACE, AND CRUSTAL GROWTH MODELS

N.E. Flament[1,2], N. Coltice[1] & P.F. Rey[2]

[1]Laboratoire de Sciences de la Terre, UMR CNRS 5570, Université de Lyon, Lyon, France
[2]Earthbyte Group, School of Geosciences, The University of Sydney, Australia

Introduction

In the long term, the evolution of the area of emerged land at the surface of the Earth is controlled by the growth of the continental crust, by the shape of the continents, and by the secular cooling of the Earth's mantle that imposes changes in the isostatic balance between continents and oceans. The area of emerged land is of fundamental importance to the geochemical coupling between the mantle, the continental crust and the hydrosphere. Yet, Precambrian sea levels remain geologically poorly constrained, and their modelling is made difficult by the lack of consensus on continental growth curves (e.g. Rino et al. 2004) and by the interdependency between the thermal evolution of the Earth and continental growth (Spohn & Breuer, 1993). In this contribution, we first estimate sea level and area of emerged land for a possible range of Archaean mantle temperatures and continental volume (Flament et al. 2008). We show that sea levels were high in the Archaean, and that the area of emerged land was small compared to present-day. We then investigate the sensitivity of sea level and of the area of emerged land to continental growth models. For this purpose, we developed an integrated model to calculate mantle temperature (Labrosse & Jaupart 2007), continental hypsometry (Rey & Coltice 2008), sea level, emerged land surface (Flament et al. 2008) and oceanic $^{87}Sr/^{86}Sr$ for a given continental growth model. We show that the predicted Archaean area of emerged land, of less than 5% of Earth's surface, does not closely depend on contrasted continental growth models. In addition, our modelling results reconcile early continental growth models with the evolution of oceanic $^{87}Sr/^{86}Sr$, suggesting that there could be no need for delayed continental growth models.

Emerged land area as a function of mantle temperature and continental area

Possible range of Archaean conditions

Petrological and geochemical data both suggest that the mantle was hotter in the Archaean. However, how much hotter depends on the water content of komatiites, which is subject to debate (e.g. Arndt et al. 1998). Following the recent review of arguments on Archaean mantle temperature by Labrosse & Jaupart (2007), we propose that the Archaean mantle was 200 ± 100ºC hotter than present.

Continental area in the Archaean is poorly constrained because of the lack of consensus on continental growth curves. We propose that the Archaean continental area was between 20 and 80% of the present-day continental area.

Sea level/continental freeboard

We developed a model to evaluate the area of emerged continental crust as a function of mantle temperature, continental area and continental hypsometry. For constant continental hypsometry, comparing results for three thermal evolution models, we find that a constant continental freeboard (± 200 m) is possible throughout Earth's history as long as the potential temperature of the upper mantle never exceeded its present value by more than 110–210°C (as first pointed by Galer, 1991). This implies either a limited secular cooling of the planet or, most likely, a change in continental freeboard since the Archaean.

Continental hypsometry and area of emerged land

As for the area of emerged land, our calculations for constant continental hypsometry suggest that less than ~ 12% of Earth's area were emerged in the Archaean (Flament et al. 2008), compared to 27.5% at present. Moreover, in the Archaean, the strength of the continental lithosphere would have been reduced because of a greater radioactive heat production. This would have limited crustal thickening in a context of continental collision (Rey & Coltice, 2008), resulting in less pronounced topography. Taking this effect into account, we show that the continents were mostly flooded until the end of the Archaean, and that only 2-3% of Earth's area (approximately the size of South America) consisted of emerged land by 2.5 Ga (Fig. 1). These results are consistent with the widespread occurrence of submarine continental flood basalts in the Archaean (Arndt, 1999; Kump & Barley, 2007) and with the appearance and strengthening of the geochemical fingerprint of felsic sources in the sedimentary record from 2.5 Ga.

Continental growth, emerged land area, and evolution of oceanic $^{87}Sr/^{86}Sr$

An integrated model, from the mantle to the surface

In order to investigate the influence of continental growth models on the area of emerged land and on the evolution of oceanic $^{87}Sr/^{86}Sr$, we developed an integrated model based on the empirical thermal evolution model of Labrosse & Jaupart (2007). In this model, the continental elevation is deduced from the results of Rey & Coltice (2008). This allows us to calculate both sea level and area of emerged land using the model of Flament et al (2008). We calculate the evolution of $^{87}Sr/^{86}Sr$ in the mantle, continents and oceans, using a geochemical box model in which the continental runoff depends on the area of emerged land and on the maximum continental elevation. Calculations are carried out for two contrasted continental growth models, a late continental growth

model broadly similar to the models of Taylor & McLennan (1985) and of Veizer & Jansen (1979), and an early continental growth model similar to that proposed by Armstrong (1981).

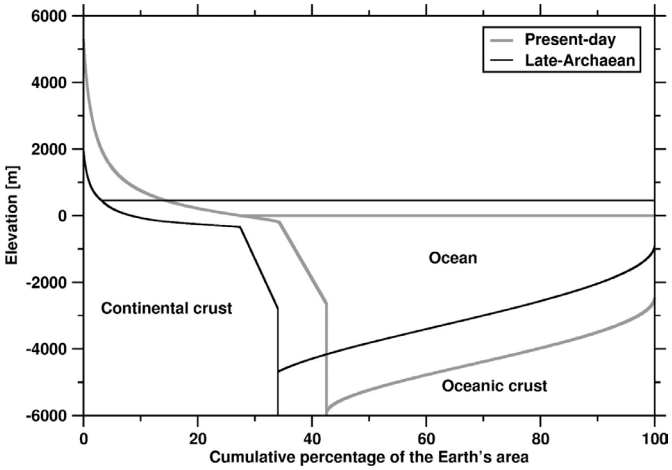

Figure 1. Modelled hypsometry and sea level for the present-day (dark grey) and for possible late-Archaean conditions (black), with a mantle 150°C hotter than present, 80% of the present continental mass, and a lower maximum continental elevation (~ 3500 m compared to 8850 m today). The oceanic part of the hypsometry is flipped to better illustrate tectonic processes. Archaean sea level and bathymetry are calculated using the thermal evolution model of Labrosse & Jaupart (2007).

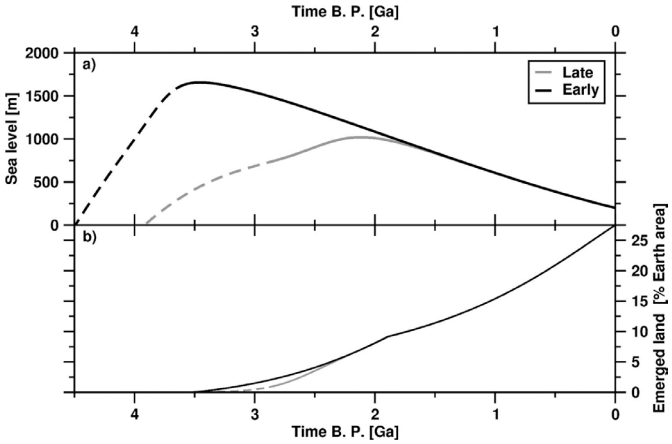

Figure 2. (a) Calculated sea level and (b) emerged land area for a late continental growth model (dark grey) and an early continental growth model (black). Dashed lines indicate uncertain modeling result, due to the unrealistic early warming period predicted by the thermal evolution model of Labrosse & Jaupart (2007).

Results and discussion

Our results suggest that contrary to sea level, the area of emerged land does not closely depend on continental growth models (Fig. 2). We find that less than 5% of Earth's area was emerged in the Archaean (Fig. 2). Furthermore, we show that the oceanic $^{87}Sr/^{86}Sr$ predicted for the early crustal growth model is consistent with the available data on marine carbonates (Shields & Veizer, 2002) when a smaller emerged area and/or lower continental elevations are accounted for (Fig. 3). This result invalidates the common argument that delayed continental growth curves are required to account for the observed trend in oceanic $^{87}Sr/^{86}Sr$.

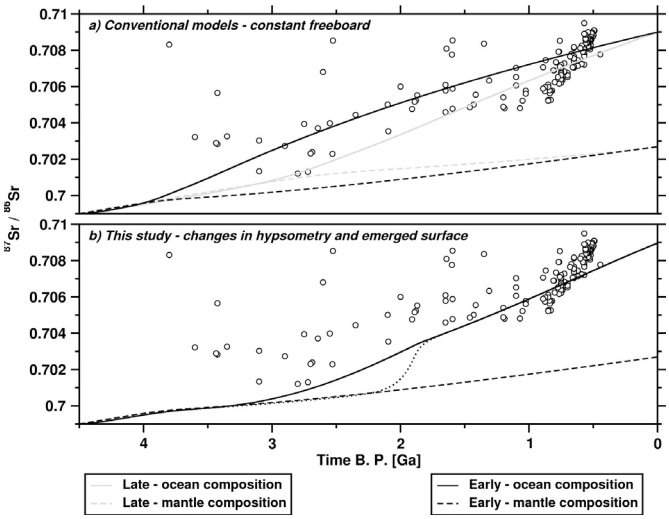

Figure 3. Calculated evolution of the $^{87}Sr/^{86}Sr$ of seawater (plain curves) and of the mantle (dashed curves) a) for both late (dark grey) and early (black) continental growth models, under the conventional hypotheses of constant continental hypsometry and constant freeboard; b) for the early continental growth model, taking the emerged surface from Figure 2 (plain curve). The effect of a change in continental hypsometry is illustrated by the dotted. Empty black circles are $^{87}Sr/^{86}Sr$ data on marine carbonates from the compilation of Shields & Veizer (2002).

Conclusion

For reasonable Archaean mantle temperature and continental area, we predict an emerged land area of less than 12% of Earth's surface. This estimate decreases to less than 5% of the Earth's surface when lower Archaean continental elevations are taken into account. The investigation of the influence of two contrasted continental growth models (early and late) on the evolution of the area of emerged land shows that the area of emerged land does not closely depend on continental growth. When a smaller area of emerged land is taken into account, our calculations reconcile early continental growth models with the evolution of oceanic $^{87}Sr/^{86}Sr$, suggesting that there could be no need for late continental growth models.

References

Armstrong R. L., 1981, Radiogenic isotopes: the case for crustal recycling on a near-steady-state no-continental growth Earth, Philosophical Transactions of the Royal Society of London, Series A, 301, 443–471.

Arndt N.T., Ginibre C., Chauvel C., Albarède F., Cheadle M., Herzberg C., Jenner G. & Lahaye, Y., 1998, Were komatiites wet? Geology, 26, 739–742.

Arndt N. T., 1999, Why was flood volcanism on submerged continental platforms so common in the Precambrian? Precambrian Research, 97, 155–164.

Flament N., Coltice N. & Rey P.F., 2008, A case for late-Archaean continental emergence from thermal evolution models and hypsometry, Earth and Planetary Science Letters, 275, 326–336.

Galer S.J.G., 1991, Interrelationships between continental freeboard, tectonics and mantle temperature, Earth and Planeary Science Letters, 105, 214–228.

Kump L. R. & Barley M. E, 2007, Increased subaerial volcanism and the rise of atmospheric oxygen 2.5 billion years ago, Nature, 448, 1033–1036.

Labrosse S. & Jaupart C., 2007, Thermal evolution of the Earth: Secular changes and fluctuations of plate characteristics, Earth and Planetary Science Letters, 260, 465–481.

Rey P.F. & Coltice, N., 2008, Neoarchean strengthening of the lithosphere and the coupling of the Earth's geochemical reservoirs, Geology, 36, 635–638.

Rino S., Komiya T., Windley B.F., Katayama I., Motoki A. & Hirata T., 2004, Major episodic increases of continental crustal growth determined from zircon ages of river sands; implications for mantle overturns in the early Precambrian, Physics of Earth and Planetary Interiors, 146, 369–394.

Shields G. & Veizer J., 2002, Precambrian marine carbonate isotope database: Version 1.1, Geochemistry, Geophysics, Geosystems, 3, 1031.

Spohn T. & Breuer, D., 1993, Mantle differentiation through continental crust growth and recycling and the thermal evolution of the Earth, in *Evolution of the Earth and planets*, Takahashi, E., Jeanloz, R., and R. Rudie, eds, AGU Geophysical Monograph, Washington DC, 55–71.

Taylor S.R. & McLennan S.M., 1985, *The continental crust: its composition and evolution*, Blackwell Scientific Publications, 328p.

Veizer J. & Jansen S.L., 1979, Basement and sedimentary recycling and continental evolution, Journal of Geology, 87, 341–370.

EOARCHAEAN MANTLE SLIVERS IN THE ISUA SUPRACRUSTAL BELT: LINKS TO THE 3720-3710 Ma ISLAND ARC ROCKS

C.R.L. Friend[1] & A.P. Nutman[2]

[1]45, Stanway Road, Headington Oxford OX3 8HU, UK
[2]School of Earth and Environmental Sciences, University of Wollongong, Wollongong, Australia

Introduction

Discovery of preserved slivers of Eoarchaean mantle intercalated with metabasaltic rocks would have major significance for several reasons. Most early mantle geochemical modelling studies are based on indirect sampling through the use of two-stage recycled penecontemporaneous mafic crust in the form of juvenile tonalites (e.g. Bennett *et al*. 1993, 2007). There are also the important tectonic implications for finding a surviving piece of relatively intact Eoarchaean mafic crust and mantle rocks; an ophiolite complex.

The Eoarchaean Isua supracrustal belt (Greenland) is an important component of the Itsaq Gneiss Complex (Nutman et al. 1996). Being the largest unit of pre-3700 Ma supracrustal rocks it has attracted a range of different scientific studies, some of which are controversial. It is now certain that the belt is composite, and contains tectonically juxtaposed fragments of unrelated volcanic-sedimentary packages of different age. Two distinct, tectonically assembled, rock packages are dated at *c*. 3800 Ma and *c*. 3700 Ma (Nutman *et al*. 1997). Whilst this interpretation was originally controversial, there is now at least the acceptance that the belt comprises several different tectonic packages, the configuration of which is debated (e.g. Komiya et al. 1999; Myers 2001; Nutman et al. 2002) The northwest arm of the Isua supracrustal belt is a tectonic assemblage of strongly deformed, amphibolitized pillow lavas and lesser amounts of gabbro (island arc tholeiite, picrite and boninite protoliths), felsic schists (andesite-dacite protoliths), chemical sedimentary rocks and depleted mantle dunite of different ages. The key to interpreting these data is discovering rare low strain zones which give vital evidence for understanding the rocks (Nutman & Friend 2009).

The rocks described here all come from the younger package which is well constrained geochronologically. The age of the unit is constrained by an amphibolite-ultramafic schist tectonic contact that is cut by a 3717 ± 6 Ma mafic tonalite intrusion (Grimes & Dunning 2002, Friend & Nutman, submitted) which makes some of the alteration very early. Some layered gabbro preserves an amphibolitized igneous texture and contains high Th/U igneous zircons. The dominant amphibolites are interpreted as island arc basalts (Polat & Hofmann 2003) and are consequently just older than the 3717±11 Ma gabbros (Friend & Nutman, submitted) that cut them. There are also thin felsic layers interpreted as acid volcanic and chemical sediment layers associated with some of the mafic volcanic rocks.

The ultramafic schists within this package (Fig. 1) have in the past been written off as either being too highly altered to obtain reliable protolith information or, as all representing cumulate rocks (bases of layered gabbro intrusions). However, contained within the altered ultramafic schists two lenses of magnesian, dunite ultramafic rocks up to *c*. 300m long have been discovered. These lenses have depleted Mg-Si-Al chemistry and can be considered as candidates for mantle rocks and are compositionally very distinct from the layered ultramafic rocks that certainly are present in the Isua supracrustal belt. One ultramafic lens comprises clean overall massive dunite with varying textural relations in Fo_{92} olivine, chromite and very minor amounts of clinopyroxene. The other lens contains olivine (Fo_{96}) with intergrowths of Ti-humite group minerals, chromite and rare orthopyroxene. These lenses were tectonically intercalated with island arc and picrite rocks by 3717 Ma, when mafic tonalites were intruded across tectonic contacts. Ti-humite group minerals were first recorded by Dymek et al. (1988a, b), from a layer of highly altered ultramafic schist (Fig. 1).

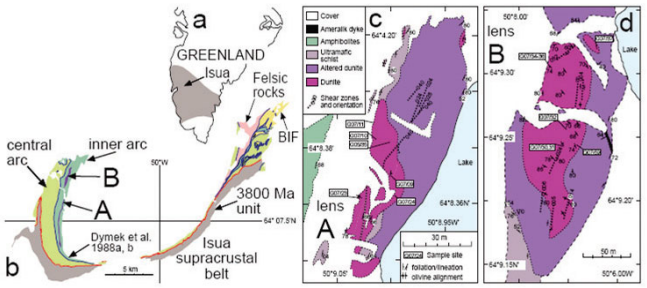

Figure 1. Location of the two ultramafic lenses A and B in West Greenland. a) The position of the Archaean craton (shaded) with the position of the Isua supracrustal belt. b) Summary of the structure of the Isua supracrustal belt. The c. 3700 Ma tectonic package is divided into the central and inner arcs by internal tectonic contacts. The c. 3800 tectonic package is grey. The locations of the two lenses A and B in the western arm of the belt are indicated. c) Detail of lens A. d) Detail of lens B.

This assemblage of mantle ultramafic and island arc gabbros and pillowed basaltic rocks and chemical sediment, some of which preserve seawater-like signatures (e.g. Friend et al. 2007) is interpreted as a 3720-3700 Ma-old supra-subduction zone ophiolite. It is proposed that the ultramafic rocks are different tectonic slivers of a *c*. 3720 Ma sub-arc mantle wedge, which is the environment where their high temperature (>1000°C) chemical and textural variations developed, with superimposed regional crustal metamorphism

is lower amphibolite facies (600-500°C). Minerals from the ultramafic lenses have been analysed using LAICPMS. In Lens A, olivines (Fo_{92}) show very low REE abundances with a slight progressive enrichment in HREE with distinct negative Ta, Zr and Eu anomalies and no significant Ti anomaly. In Lens B olivine (Fo_{96}) have a depleted but markedly different pattern that is enriched in the HREE which rises from 0.05 to 2x primitive mantle and with marked positive Ta, Zr and negative Ti anomalies. The TiCh/TiCl minerals have proven to preserve strong +ve anomalies in the HFS elements Ta, Zr and negative Ti anomalies. Patterns for TiCh/TiCl are depleted and have a distinctly downwards hooked pattern in the HREE. They have marked positive anomalies in Ta, Nb, Zr and Ti. The minerals in lens B thus appear consistent with strong partitioning of Ti. The composition of these minerals matches those found in Phanerozoic exhumed mantle suites, interpreted to display varying degrees of sub-arc metasomatism. It is argued that there is a relationship with the typically HFSE-depleted signatures identified in the island arc basaltic and picritic rocks (Polat & Hofmann 2003; Appel et al. 2009), to which this ultramafic rock is adjacent, and it is proposed to preserve evidence for the separation of this basaltic arc material. If so, this is the first time that direct evidence for geochronologically controlled mantle and crustal materials has been documented in ~3700 Ma crust.

Recently the Isua belt has been described as containing an 'ophiolite' Furnes et al. (2007a,b) that is then described in more detail and ascribed an age of 3800Ma (Furnes et al. 2008). The rocks described to make up this dissected 'ophiolite' come from the 3800 Ma and 3720 Ma tectonic slices as well as using some of the <3500 Ma Ameralik dykes (e.g. White et al. 2000; Nutman et al. 2004). Consequently this interpretation fails the basic test for an ophiolite in which the rocks have to be roughly synchronous in age.

Convincing sheeted dyke complexes have not been found in the Isua 3720-3710 Ma assemblage, therefore it is not an intact section through an ophiolite. This is because this assemblage was repeatedly partitioned by Archaean shear zones. None-the-less, assembling the detailed geochemistry from the island arc basaltic material (Polat & Hofmann 2003) with the data from the ultramafic rocks, an argument can be made that this assemblage resembles a supra-subduction ophiolite (e.g. references in Pearce, 2003; Dilek & Polat 2008). It is thus contended that this geochemically and geochronologically controlled assemblage supports continuity of crust-formation processes at convergent plate boundaries for almost 4 billion years.

Acknowledgements

We thank Ole Christiansen of NunaMinerals A/S for long term logistic help.

References

Appel P.W.U., Polat A. & Frei R., 2009, Dacitic ocelli in mafic lavas, 3.8-3.7 Ga Isua greenstone belt, West Greenland: Geochemical evidence for partial melting of oceanic crust and magma mixing, Chemical Geology, 258, 105–124.

Bennett V.C., Nutman A.P. & McCulloch M.T., 1993, Nd isotopic evidence for transient, highly depleted mantle reservoirs in the early history of the Earth, Earth and Planetary Science Letters, 119, 299–317.

Dilek Y. & Polat A., 2008, Suprasubduction zone ophiolites and Archean tectonics, Geology, 36, 431–432.

Dymek R.F., Brothers S.C. & Schiffries C.M., 1988a, Petrogenesis of ultramafic rocks from the 3800 Ma Isua supracrustal belt, West Greenland, Journal of Petrology, 29, 1353–1397

Dymek R.F., Brothers S.C. & Schiffries C.M. 1988b. Titanian chondrodite- and titanian clinohumite-bearing metadunite from the 3800 Ma Isua supracrustal belt, West Greenland: Chemistry, petrology and origin, American. Mineralogist, 73, 547–558.

Friend C.R.L. & Nutman A.P., submitted, Eoarchean ophiolites? New evidence for the debate on the Isua supracrustal belt, southern West Greenland. American Journal of Science.

Friend C.R.L., Bennett V.C., Nutma, A.P. & Norman, M.D., 2007, Palaeoarchaean seawater signatures from chemical (meta) sedimentary rocks, southern West Greenland, southern West Greenland. Contributions to Mineralogy and Petrology, DOI 10.1007/S00410-007-0239-z.

Furnes H., Rosing M., Dilek Y. & de Wit M., 2009, Isua supracrustal belt (Greenland) – A vestige of a 3.8 Ga suprasubduction zone ophiolite, and implications for Archean geology. Lithos, doi:10.1016/j.lithos.2009.03.043.

Furnes H., de Wit M., Staudigel H., Rosing M. & Muehlenbachs K., 2007a, A vestige of Earth's oldest ophiolite, Science, 315, 1704–1707.

Furnes H., de Wit M., Staudigel H., Rosing M. & Muehlenbachs K., 2007b, Response to comments on "A vestige of Earth's oldest ophiolite", Science, 318, 746e.

Grimes S.W. & Dunning G.R., 2002, A 3714 Ma pluton intruding the Isua greenstone belt, southwest Greenland; the world's oldest volcano-sedimentary section (or, at least part of it) gets older, Geological Society of America 2002 annual meeting, Geological Society of America Abstracts with Programs, 34, 365.

Komiya T., Maruyama S., Masuda T, Appel P.W.U. & Nohda S., 1999, Plate tectonics at 3.8-3.7 Ga: Field evidence from the Isua accretionary complex, southern West Greenland, Journal of Geology, 107, 515–554.

Myers J.S., 2001, Protoliths of the 3.8–3.7 Ga Isua greenstone belt, West Greenland. Precambrian Research, 105, 129–141.

Nutman A.P. & Friend C.R.L., 2007, Comment on "A vestige of Earth's oldest ophiolite". Science, 318, 746c.

Nutman A.P. & Friend C.R.L., 2009, New 1:20,000 geological maps, synthesis and history of the Isua supracrustal belt and adjacent orthogneisses, southern West Greenland: A glimpse of Eoarchaean crust formation and orogeny, Precambrian Research, 172, 189–211.

Nutman A.P., Friend C.R.L. & Bennett, V.C., 2002, Evidence for 3650-3600 Ma assembly of the northern end of the Itsaq Gneiss Complex, Greenland: Implication for early Archean tectonics, Tectonics, 21, article 10.1029/2000TC001203.

Nutman A.P., Friend C.R.L. & Bennett, V., 2004, Dating of the Ameralik dyke swarms of the Nuuk district, southern West Greenland: Mafic intrusion events starting from c. 3510 Ma, Journal of the Geological Society, London, 161, 421–430.

Nutman A.P., Bennett V.C., Friend C.R.L. & Rosing M.T., 1997, ~3710 and ≥3790 Ma volcanic sequences in the Isua (Greenland) supracrustal belt; structural and Nd isotope implications, Chemical Geology, 141, 271–287.

Nutman A.P., Friend C.R.L., Bennett V.C. & McGregor V.R., 2004, Dating of the Ameralik dyke swarms of the Nuuk district, southern West Greenland: mafic intrusion events starting from *c*. 3510Ma, Journal of the Geological Society of London, 161, 421–430.

Nutman A.P., Friend C.R.L., McGregor V.R., Bennett V. & Kinny P.D., 1996, The Itsaq Gneiss complex of southern West Greenland: the World's most extensive record of early crustal evolution (3900-3600 Ma): Precambrian Research, 78, 1–39.

Pearce J.A., 2003, Supra-subduction zone ophiolites: The search for modern analogues. Geological Society of America Special Paper, 373, 269–293.

Polat, A. & Hofmann A.W., 2003, Alteration and geochemical patterns in the 3.7-3.8 Ga Isua greenstone belt, West Greenland, Precambrian Research, 126, 197–218.

White, R.V., Crowley J.L., & Myers J.S., 2000, Earth's oldest well-preserved mafic dyke swarms in the vicinity of the Isua greenstone belt, southern West Greenland, Geology of Greenland Survey Bulletin, 186, 65–72

REE AND HFSE FRACTIONATION DUE TO PROTRACTED FLOW OF BASINAL BRINES: BELT-PURCELL SUPERGROUP

I. González-Álvarez[1,2,3] & R. Kerrich[4]

[1]ABM Resources NL, Nedlands 6009, Perth, Western Australia
[2]Centre for Exploration Targeting, School of Earth and Environment, University of Western Australia, Crawley 6009, Western Australia
[3]Now at: CSIRO, Australian Resources Research Centre, Geology and Geochemistry, Kensington, WA 6151, Australia
[4]Department of Geological Sciences, University of Saskatchewan, Saskatoon, SK S7N 5E2, Canada

Abstract
Argillites, sandstones and carbonate-rich units throughout the Belt-Purcell Supergroup sequence record three types of REE patterns. T1 with a Post-Archaean Upper Continental Crust (PA-UCC) Rare Earth Element (REE; prefix L, M and H designate light-, medium-, and heavy-REE, respectively) pattern, T2 and T3 REE patterns both feature enriched and fractionated HREE, but T2 exhibits LREE depletion. Relative to T1, T2 comprises low-ΣLREE/ΣHREE (average ΣREE=15) and T3 high-ΣLREE/ΣHREE (average ΣREE=24), with both T2 and T3 displaying progressive enrichment of HREE and erratic ratios of Zr/Hf, Ti/Sm, Y/Ho, Y/Yb and Al/Yb. Such fractionations are more pronounced in sandstones due to greater hydraulic conductivity facilitating post-depositional fluid flow.

Collectively, T2 and T3 patterns cannot be explained by means of sedimentary processes involving provenance, weathering or sedimentary sorting. Therefore REE as well as REE/High Field Strength Elements (HFSE) and HFSE/HFSE fractionation patterns in the argillites, sandstones and carbonate-rich units are interpreted as post-depositional processes superimposed on a PA-UCC provenance signature, specifically to pervasive and episodic migration of oxidizing-alkaline diagenetic basinal brines in the Belt-Purcell Supergroup. These brines originated from large scale geothermal events at ~1 Ga.

Introduction
REE and HFSE (Nb, Ta, Zr, Hf) as well as other trace elements (e.g., Sc, Th, Ti and Al) preserve their primary elemental ratios in sedimentary sequences under a large spectrum of conditions. However, some fractionation of trace elements during the sedimentary process due to weathering, sedimentary sorting, diagenesis and metamorphism, or some combination of these processes, have been described in several studies (e.g., Rudnick & Gao, 2003).

The Mesoproterozoic Belt-Purcell Supergroup of Montana and British Columbia is up to 17 km thick and includes siliciclastic- and carbonate-dominated formations. Some siliciclastic formations have extensive dolomite-rich domains (Whipple et al., 1984). Geochemically and geochronologically argillites in the lower sequence, devoid of dolomite, have trace element patterns ~1 when normalized to PA-UCC (Rudnick & Gao, 2003), whereas sandstones have parallel patterns diluted by the addition of quartz. Detrital monazite ages are dominantly ~1.8 Ga. Therefore, both lines of evidence support a dominantly Palaeoproterozoic provenance. However, a systematic fractionation of REE and HFSE has been recorded spanning the complete sedimentary sequence and extending to three locations. Other studies on monazite grains from the argillitic and sandtone units from the lower part of the sequence have identified post-depositional age monazites that differ in texture and composition from their detrital counterparts, and have ages spanning 1.2-0.3 Ga. This was interpreted to record intermittent, large scale, advection of basinal brines through the basin (González-Álvarez et al., 2006). This study evaluates mobility of trace elements, specifically REE and HFSE, during post-depositional events associated with these brines.

Geologic setting
The Belt-Purcell Supergroup is a Mesoproterozoic (~1,500 Ma), dominantly siliciclastic sedimentary sequence in western Laurentia, outcropping from southwestern Montana, United States, to southeastern British Columbia, Canada. The stratigraphic sequence records ~75 Ma of deposition and displays a maximum thickness of ~17-22 km (Chandler, 2000 and references therein). The Belt-Purcell basin is interpreted as an intracratonic basin that originated by rifting. According to Ross & Villeneuve (2003) there was an active extensional basin to the west based on several lines of evidence including predominant sediment input from the west and rapid rates of subsidence, coupled with large-scale facies pattern changes.

The Belt-Purcell Supergroup is divided into four principal stratigraphic divisions: (1) the lower Belt, mainly deltaic, fine-grained turbiditic facies, and carbonate-rich shallow water deposits; (2) the Ravalli Group, shallow to subaerial deposits; (3) the middle Belt, carbonate-rich shallow water deposits; and (4) the Missoula Group, mainly alluvial deposits (e.g., Whipple et al., 1984).

The Belt-Purcell Supergroup is predominantly siliciclastic with bimodal argillites and sandstones. Two main carbonate-rich units are extensively developed spatially throughout the basin in the lower and middle Belt. Siliciclastic and carbonate-rich units in the Belt-Purcell sequence grade progressively into each other, such that the carbonate units include variable proportions

of detrital siliciclastics. Metamorphic grade is lower greenschist facies at the three localities sampled for this study.

Indications of trace element mobility in previous studies in the Belt-Purcell Supergroup

Throughout the stratigraphic sequence and at the three localities sampled argillites display three types of REE patterns (Fig. 1): (1) T1 REE pattern is nearly flat at PA-UCC, where quartz content controls absolute REE abundances; average ΣLREE/ΣHREE = 21, which is identical to PA-UCC. Relative to PA-UCC, multi-element normalized diagrams show: (a) variable Th/U ratios (1.3 to 6.2) stemming largely from a wide range of U concentrations; (b) zero to minor negative anomalies at Nb-Ta and Zr-Hf relative to neighbouring REE, likely from winnowing of the heavy minerals titanite and zircon; and (c) zero to minor positive anomalies at Y relative to Yb where Y/Yb ratios are 8.2 to 9.5 compared to a ratio of 9 in PA-UCC. (2) T2 argillites generally slope upward from La to Lu on PA-UCC normalized plots, and accordingly have a lower average ΣLREE/ΣHREE ratio (at 15) than T1. On multi-element diagrams, T2 shares the unfractionated Nb/Ta and Zr/Hf ratios with T1, but includes positive and negative anomalies at Zr-Hf, and consistently lower Y/Yb (average 8.9) and Al/Yb ratios (average ~48,000 versus PA-UCC value of 66,000) consistent with relative HREE addition. (3) T3 displays overall systematic LREE enrichment compared to T2, with high-ΣLREE/ΣHREE = 24. T3 REE patterns include some erratic patterns that would correspond to transitions between T1 and T2 (Fig. 1). Sandstones and carbonate-rich units present the same three REE patterns.

Provenance, weathering and sedimentary sorting are primary sedimentary processes that can imprint specific trace element signatures. The process of sedimentation averages the chemical composition of wide areas of exposed crust. Many studies envision the Belt-Purcell Basin to have been in-filled by a Mississippi-scale river system that drained mainly sands and fine-grained sediment, from different catchments (Ross & Villeneuve, 2003). The catchment area was dominantly Palaeoproterozoic with minor Archaean contributions (Ross & Villeneuve, 2003). T1 Argillites have Th/Sc-Sc and Cr-Ni systematics plotting in the post-Archaean field, and detrital monazite ages are ~1,900-1,680 Ma (González-Álvarez et al., 2006). The geochemical characteristics of T1 argillites support a predominantly Proterozoic source for the Belt-Purcell Supergroup at the three sampled locations. T2 and T3 REE patterns cannot be explained on the basis of the original provenance signature. Weathering can produce fractionation of REE in regolith relative to the parent rock. This is expressed as LREE enrichment but depletion in HREE due to preferential removal of HREE by complexation reactions, and a positive Ce anomaly also develops. Such effects are not present in PA-UCC. Sedimentary sorting and deposition of minerals enriched in HREE could generate the observed T2 low-ΣLREE/ΣHREE pattern. Zircon is the most likely candidate, having normalized HREE>MREE>LREE. However, the absolute content of Zr in T1 and T2 argillites is comparable, but the Zr-Yb correlation is lower at 0.6 for the latter, ruling out zircon accumulation as the cause of HREE enrichment. Therefore REE and HFSE fractionation post-deposition due to basinal brine activity is hypothesized to explain the T2 and T3 REE patterns in argillites and sandstones throughout the stratigraphic sequence.

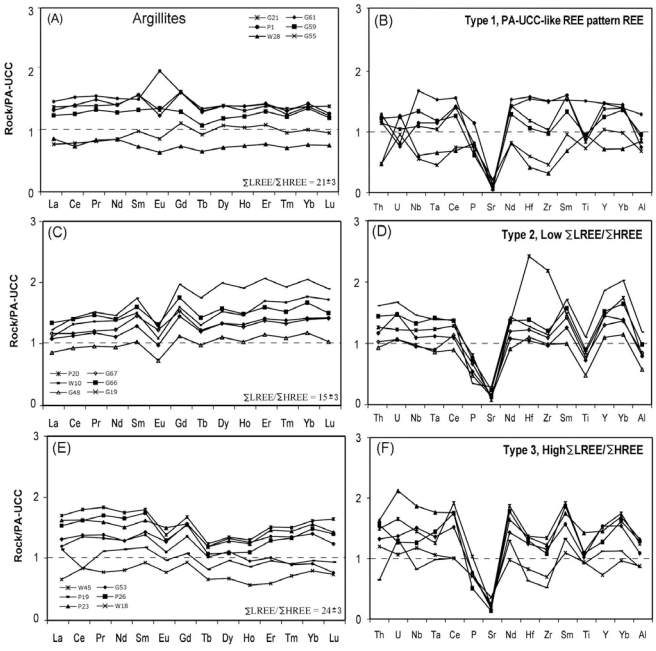

Figure 1. (A), (C) and (E) T1, T2 and T3 argillite REE patterns and (B), (D) and (F) T1, T2 and T3 argillite multi-element patterns (modified from González-Álvarez and Kerrich, 2010).

Generally, Al, Ti, REE, HFSE, Y and Sc are considered immobile during hydrothermal activity and metamorphism. However, REE and HFSE can appear to be both mobile and fractionated under specific conditions of Eh, pH and temperature. Enrichments of U, Y and HREE proximal to unconformity U deposits in the Mesoproterozoic Athabasca basin, and fractionation of REE and HFSE in Magadi-type cherts from the East African Rift, both resulted from the activity of low-temperature alkaline oxidizing brines. Preferential aqueous solubility of HREE occurs in the presence of bicarbonate complexes and the transformation of smectite to illite enriches fluids in HREE. The trace element signature of the sedimentary package in the Belt-Purcell Supergroup supports these parameters and similar alkaline and oxidizing conditions of the brines.

Source of the fluids and circulation paths

The brines in the Belt-Purcell basin may have come from three main sources: (1) meteoric water from the continent; (2) sea-water from the basin itself as recorded at the Sullivan Deposit in the lower Belt-Purcell sequence in British Columbia; or (3) diagenetic water extracted from the transformation from smectite to illite in the lower and middle part of the sequence due to burial pressure. The stratigraphic thickness implies burial pressures and temperatures for most of the sequence equivalent to greenschist facies (~350 ^{o} -500^{o} C and ~3-12 kbars).

Major mineral composition for the argillites which dominate most of the Belt-Purcell sequence is an assemblage of quartz with minor plagioclase and

microcline, in a matrix of smectite, chlorite and/or illite-mica, depending upon their stratigraphic level.

In addition, at burial depths of >3-4 km temperature and pressure conditions cause dehydration of smectite which becomes an important source of fluid (Saffer et al., 2008 and references therein). In this reaction smectite converts to illite, as studied in the Nankai subduction zone, where the reaction occurs at ~2,000 m of burial and ~60° C, releasing Fe, Mg and water.

From the evidence of diagenetic monazite, argillites and sandstones were permeable units throughout the sequence, over > 1 Ga, to allow trace element mobility. Sandstone units ~10s m in thickness in the Belt-Purcell sequence can be traced uniformly for 100s of km, such as for the Appekunny Formation. This may have created the more complex and erratic trace element patterns in the sandstone units due to higher fluid-rock interaction, reported previously by González-Álvarez & Kerrich (2010).

Composition and driving forces of the brines

Paleomagnetic, paleoclimatic and sedimentary data are consistent with deposition at low latitudes between 10° and 35°. Evidence for hot climate during deposition of the Belt-Purcell Supergroup is halite casts and abundant scapolite. Evaporites are a potential source of salinity for brines which also raised the alkalinity of the fluid, coupled with the conversion of smectite into illite, which released Mg into the fluid.

Interaction between mafic melts and carbonates results in the release of large amounts of CO_2. Magmatic episodes are represented by tholeiitic gabbros and diorites, mafic lava flows as well as volcanic ash deposits present in the lower, middle and upper part of the Belt-Purcell stratigraphic sequence (e.g., Whipple et al., 1984). Mafic intrusion events present in the Belt-Purcell sequence that interacted with the carbonate-rich units releasing CO_2 within the system are: (1) the Moyie sills intruding the lower part of the sequence into the Aldrigde Formation laterally turning into the carbonate-rich Waterton Formation; (2) the Purcell sill intruding the carbonate-bearing Helena Formation; and (3) volcanic unit at the Missoula Group. CO_2 addition would confer oxidizing conditions to the brines.

The main tectono-thermal events recorded in the Belt-Purcell Supergroup are: (1) intracontinental rifting at ~1,500 Ma accompanied by heat flow during thinning of the lithosphere, and (2) extensional events during the break-up of Rodinia at ~850 Ma. These large-scale events, among others such as Grenvillian activity, may have reactivated the brines by intrabasinal and distal tectonic events.

Conclusions

The Belt-Purcell Basin had large volumes of diagenetic brines, and heat and/or peaks in tectonic stress, that resulted in intermittent fluid flow over >1 Ga. Metre thick, permeable and stratigraphically continuous sandstone units, shear zones and faults could have formed the plumbing system in the basin for advection of these fluids. Evaporitic units coupled with Mg released from smectite-illite transformations in the argillitic packages throughout the sequence would confer an alkaline characteristic to the fluids. This, coupled with CO_2 release from the interaction of the mafic intrusions and carbonate units and the CO_2 directly released from magmatic pulses associated to the rift nature of the basin, would confer an oxidizing signature to the brines. The fingerprints of the circulation of these alkaline oxidizing brines had important geochemical effects on element mobility in the sedimentary units, causing fractionation of REE and HFSE. Secondary monazite grains suggest the fluids were active for ~1 Ga.

Acknowledgements

The staff of Waterton-Glacier International Peace Park is thanked for their enduring support. R. Kerrich acknowledges NSERC MFA support of the ICP-MS facility, and the George McLeod endowment to the Department of Geological Sciences, University of Saskatchewan, Canada. T. Prokopiuk is thanked for his comments on the article.

References

Chandler F.W., 2000, The Belt-Purcell basin as a low-latitude passive rift: implications for the geological environment of Sullivan type deposits, In: *The Geological Environment of the Sullivan Deposit, British Columbia*. Lydon, J.W., Höy, T., Slack, J.F., Knapp, M.E., (eds.), Geological Association of Canada, Mineral Deposits Division Special Publication, 1, 82–112.

González-Álvarez I., Kusiak M.A. & Kerrich R., 2006 A trace element and chemical Th-U total Pb dating study in the lower Belt-Purcell Supergroup, western North America: provenance and diagenetic implications, Chemical Geology, 230, 140–160.

González-Álvarez I. & Kerrich R., 2010, REE and HFSE mobility due to protracted flow of basinal brines in the Mesoproterozoic Belt-Purcell Supergroup, Laurentia, Precambrian Research, doi:10.1016/j.precamres.2009.12.008

Ross G.M. & Villenueve M.E., 2003, Provenance of the Mesoproterozoic (1.45 Ga) Belt basin (western North America): another piece in the pre-Rodinia paleogeographic puzzle, Geological Society of America, 115, 1191–1217.

Rudnick, R.L. & Gao, G., 2003, The composition of the continental crust, In: *The crust*, *Treatise on Geochimistry, Volume 3*, Rudnick, R.L. ed, Elsevier, Oxford, New York, pp. 1-64.

Saffer M.D., Underwood M.B. & McKiernan A.W., 2008, Evaluation of factors controlling smectite transformation and fluid production in subduction zones: Application to the Nankai Trough, Island Arc, 17, 208–230.

Whiple J.W., Connor J.J., Raup O.B. & McGrimsey R.G., 1984, Preliminary report on the stratigraphy of the Belt Supergroup, Glacier National Park and adjacent Whitefish Range, Montana, in *Northwest Montana and Adjacent Canada*, McBane, J.D. & Garrison, P.B., eds., Montana Geological Society Guidebook, 1984 Field Conference and Symposium, 33–50.

WESTERN KARELIAN GRANITOID MAGMATISM AND CRUSTAL EVOLUTION

E. Heilimo[1], P. Mikkola[2], J. Halla[3] & P. Hölttä[4]

1Department of Geosciences and Geography, P.O. Box 64, FIN-00014 University of Helsinki, Finland
2Geological Survey of Finland, P.O. Box 1237, 70211 Kuopio, Finland
3Geological Museum, Finnish Museum of Natural History, P.O. Box 11, FIN-00014 University of Helsinki, Finland
4Geological Survey of Finland, P.O. Box 96, FIN-02151 Espoo, Finland

Introduction

The Archean Karelian Province of the Fennoscandian Shield is one of the largest exposed fragments of Archean crust in the world and has been the target of renewed interest over the last 10 years. Western part of the Province is located on the border of north western Russia and Finland. New, partly unpublished geochemical data divide the granitoids into four groups: tonalite-trondhjemite-granodiorites (TTG), sanukitoids (high-Mg granitoids), quartz diorites and anatectic leucogranitoids. New isotopic data provide constraints on the ages and potential sources of different granitoids.

TTGs: high- and low-HREE TTG subgroups

TTG granitoids form 80% of the exposed crust in Karelia. This voluminous and long-lived (2.95-2.75 Ga) series can be subdivided into two groups: dominating (1) low-HREE (heavy rare earth elements) TTGs and (2) rarer high-HREE TTGs (Halla et al. 2009). Differences in the major element compositions of low- and high-HREE TTGs are small. The low-HREE TTG group shows slightly higher SiO_2 (68–76 wt.%) and lower MgO contents (<1.2 wt.%) compared with the larger SiO_2 range (60–74 wt.%) and extended MgO range of the high-HREE group. The high-HREE group shows higher contents of mantle compatible elements (V, Cr, Ni, and Co) as well as a slight tendency to higher Mg# values compared with those of the low-HREE group.

The HREE composition of low-HREE TTG group [average $(Gd/Er)_N = 3.97$] is consistent with high-pressure partial melting (>2.0 GPa) of a garnet-bearing basaltic source, whereas the high-HREE group [average $(Gd/Er)_N = 1.88$] suggests low-pressure melting (1.0 GPa) of a garnet-free basaltic crust and interaction with the mantle. One possible tectonic scenario for the genesis of the two groups is an incipient hot subduction zone underneath a thick oceanic plateau/protocrust. Deep melting in the lower part of thick basaltic oceanic crust (stacked crust or plateau) could produce low-HREE TTGs, whereas melting of subducting slab and possible interactions with the mantle wedge in shallow depths would be capable of generating high-HREE TTGs. (Halla et al. 2009)

Sanukitoids

Neoarchean (2.72-2.70 Ga) late to post-tectonic, relatively small volume sanukitoids are variable-sized, and textured intrusions of diorites, tonalites, and granodiorites. The major and trace element geochemistry of the intrusions show typical sanukitoid affinities: a mantle signature (high content of MgO, Ni, Cr and high Mg#) and enrichment in LILE (especially K_2O, Ba, and Sr). The intrusions form a distinctive series that can be clearly distinguished from TTG groups by their high Ba–Sr signature, low Na_2O/K_2O ratio, and uniform HREE pattern. The sanukitoid series in Finland can be compositionally constrained as follows: SiO_2=55–70 wt.%, K_2O=1.5–5.0 wt.%, Na_2O/K_2O=0.5–3, MgO=1.5–9 wt.%, Mg#=45–65, Ba+Sr>1400 ppm, and $(Gd/Er)_N$=2–6. The probable source of sanukitoid series is enriched subcontinental lithosphere mantle. The accumulation of K_2O, Ba, and Sr in the mantle source may have occurred as a consequence of multiple metasomatic events: subduction related fluids/melts and possibly asthenospheric upwelling. The slab breakoff at the end-stage of subduction is a viable trigger for the sanukitoid magmatism. (Heilimo et al. 2010, submitted)

Quartz diorites

Neoarchean quartz diorites (2.72-2.70 Ga) are a series of rocks from diorites to tonalites, being distinctly more mafic (SiO_2=50-65 wt. %, MgO=2.5-6.5 wt. %) than TTGs. They show some geochemical similarities with the sanukitoid suite, yet Cr, Ni, Ba and K_2O contents are lower than in sanukitoids with similar SiO_2 contents and fractionation of LREE [$(La/Sm)_N$] is weaker (averages 3.0 vs [sanukitoids] = 5.0). Like partly coeval sanukitoids, the quartz diorites are interpreted as partial melts of mantle, but the link between these two is not yet well defined. Quartz diorites are more common in western half of Western Karelia, but locally the suites overlap spatially. (Mikkola et al. submitted)

Anatectic leucogranitoids

At 2.7-2.68 Ga whole Western Karelia was migmatized and intruded by leucogranitoids presenting the last major Archean magmatic event (Käpyaho et al. 2006, 2007, Mikkola et al. submitted). Unlike the previous magmatic episodes the leucogranitoids are interpreted as partial melts of pre-existing crust, without significant addition of juvenile material. Based on composition, ages of inherited zircons and Sm-Nd isotopes older TTGs are the most potential source, but locally also middle and lower crust amphibolites can be regarded as a possible source. In trace and major element composition leucogranitoids are very heterogeneous, common nominators are the leucocratic (average MgO=0.37 wt. %) and silica rich character (average SiO_2=73.4 wt. %). Migmatite leucosomes, dykes and intrusions are interpreted as a result of same extended event as they cannot be differentiated from each other chemically and the obtained ages overlap (Käpyaho et al. 2006, 2007, Mikkola et al. submitted).

Zircon O-isotopes

Zircon oxygen data from the TTGs (mean $\delta^{18}O$=6.10±0.19 ‰) shows that they were derived from sources with isotope composition similar to unaltered MORB. Leucogranitoids and leucosomes define a slightly higher average, 6.42 ± 0.10 ‰, but the shift from TTGs is interpreted as result of fractionation during anatexis and does not require input from source with higher $\delta^{18}O$ values (Mikkola et al. submitted). Surprisingly the oxygen isotope compositions of zircons from sanukitoids of the western an eastern part of the province scattered and yielded values from 5.02 ± 0.26 ‰ to 6.58 ± 0.29 ‰. These results are not in line with the interpretation that the sanukitoids show higher $\delta^{18}O$ values than TTGs as a result of source metasomatised by fluids and melts from subducted sediments. Instead they may support more complex enrichment processes in the mantle, including asthenospheric upwelling as an agent in metasomatism (Heilimo et al. 2010).

Time line

Paleoarchean (~3.5 Ga) and early Mesoarhean (>3.1 Ga) rocks are known from small subareas of the western Karelian Province, but Sm-Nd model ages, Pb-Pb data and inherited zircon cores indicate the existence of such crust in larger areas (Käpyaho et al. 2006, Mikkola et al. submitted). The fragmentary character of data and ages continues to 2.83-2.78 which marks a more voluminous period of crustal growth via major TTG and minor felsic volcanic activity (Käpyaho et al. 2006, Mikkola et al. submitted). This was followed at 2.79-2.77 Ga by mafic-ultramafic main phase of greenstone belt volcanism, (Papunen et al. 2009) and the last phase of TTG magmatism at 2.76-2.75 Ga, possibly extending to 2.72 Ga (Mikkola et al. submitted). Mantle derived sanukitoids and quartz diorites both intruded at 2.72-2.70 Ga, just prior to crustal anatexis at 2.7 Ga caused by collisional tectonics (Kontinen & Paavola 2006). Collision thickened the crust and caused migmatization and intrusion of anatectic leucogranitoids without significant input from mantle. The produced melts concentrated in crustal scale shear zones leaving unmigmatized domains of TTGs between intensively deformed and migmatized areas. Regardless of tectonic setting after the greenstone belt volcanism, the igneous magmatism developed from one consisting solely of TTG types to one consisting of compositionally diverse types e.g. TTGs, sanukitoids, quartz diorites and anatectic leucogranites.

Acknowledgements

This study has been supported by the Geological Survey of Finland, and the University of Helsinki.

References

Halla J., van Hunen J., Heilimo E. & Hölttä P., 2009, Geochemical and numerical constraints on Neoarchean plate tectonics, Precambrian Research 174, 155–162.

Heilimo E., Halla J. & Hölttä P., 2010, Geochemical Constraints on the Origin of the Neoarchean Sanukitoid Series in the Western Karelian Province (Finland). Lithos, in press.

Heilimo E., Halla J. & Huhma H., submitted, U–Pb SIMS geochronology of sanukitoid affinity intrusions in the Finnish part of the Karelian Province, submitted to Lithos.

Käpyaho, A. Mänttäri, I. & Huhma, H., 2006, Growth of Archaean crust in the Kuhmo district, Eastern Finland: U−Pb and Sm−Nd isotope constraints on plutonic rocks, Precambrian Research 146, 95–119.

Käpyaho A., Hölttä P. & Whitehouse M.J., 2007, U–Pb zircon geochronology of selected Archaean migmatites in eastern Finland, Bulletin of the Geological Society of Finland 79, 95–115. Full text: http://www.geologinenseura.fi/bulletin/Volume79/Kapyaho_etal_2007.pdf

Kontinen A. & Paavola J. 2006. A preliminary model of the crustal structure of the eastern Finland Archaean complex between Vartius and Vieremä, based on constraints from surface geology and FIRE 1 seismic survey, Geological Survey of Finland, Special Paper 43, 223–240. Full text: http://arkisto.gtk.fi/sp/sp43/sp43.pdf.

Mikkola P., Huhma H., Heilimo H. & Whitehouse M., Submitted, Archean crustal evolution of the Kianta Complex, Karelia; constraints from geochemistry and isotopes from Suomussalmi, Finland, submitted to Lithos.

Papunen H. Halkoaho T. & Luukkonen E. 2009, Archaean evolution of the Tipasjärvi-Kuhmo-Suomussalmi Greenstone Complex, Finland, Geological Survey of Finland. Bulletin 403. 68p. Full text: http://arkisto.gtk.fi/bul/bt403.pdf.

GEOCHEMISTRY AND RADIOGENIC ISOTOPE CHARACTERISTICS OF THE FORT HOPE GREENSTONE BELT, NORTHWESTERN ONTARIO: DEVELOPMENT OF A CONTINENTAL ARC ON THE MARGINS OF A SUPERCONTINENT

P. Hollings[1] & G. Stott[2]

[1] Department of Geology, Lakehead University, 955 Oliver Road, Thunder Bay, Ontario, P7B 5E1, Canada
[2] Precambrian Geoscience Section, Ontario Geological Survey, 933 Ramsey Lake Road, Sudbury, Ontario, P3E 6B5, Canada

Introduction

The Uchi subprovince of the Superior Province (Figure 1) is unusual in that it incorporates over 300 million years of discontinuous volcanic activity. It forms a long, linear domain, well over 600 km, along the southern margin of a Mesoarchean terrane. As such it offers an excellent opportunity to evaluate the nature of continental growth processes in the Archean (Hollings & Kerrich, 1999; Percival et al. 2006), the styles of Archean plate tectonics (e.g. Wyman & Hollings, 2006) and the evolution of these processes over time. In general the older sequences have been interpreted as the result of rifting of passive margins of an older cratonic nucleus (c.f., Davis et al., 1988; Tomlinson et al., 1996), likely related to the impingement of a mantle plume on the continental lithosphere (e.g. Hollings et al., 1999) and are included within the NCT of Thurston et al. (1991). In contrast, the younger assemblages of the Uchi comprise a mix of allochthonous and autochthonous volcanic sequences (Stott & Corfu, 1991; Hollings & Kerrich, 2006).

Regional Geology

The Miminiska-Fort Hope greenstone belt is located towards the eastern end of the Uchi subprovince and has been the subject of relatively little detailed mapping or other geological studies. Detailed geological mapping was undertaken by Wallace (1978, 1981a, b) in the south of the belt and by Prest (1944) in the northern portion. Based primarily on U/Pb zircon age determinations and regional correlations with the central Uchi and the Pickle Lake belt (Young 2006), we tentatively identify one portion of the northern part of the belt that could be correlated with the (~2.89 to 2.86 Ga) Pickle Crow assemblage of the Pickle Lake belt., The older assemblages comprise predominantly tholeiitic pillow basalts with rare felsic pyroclastic flows. In contrast, the

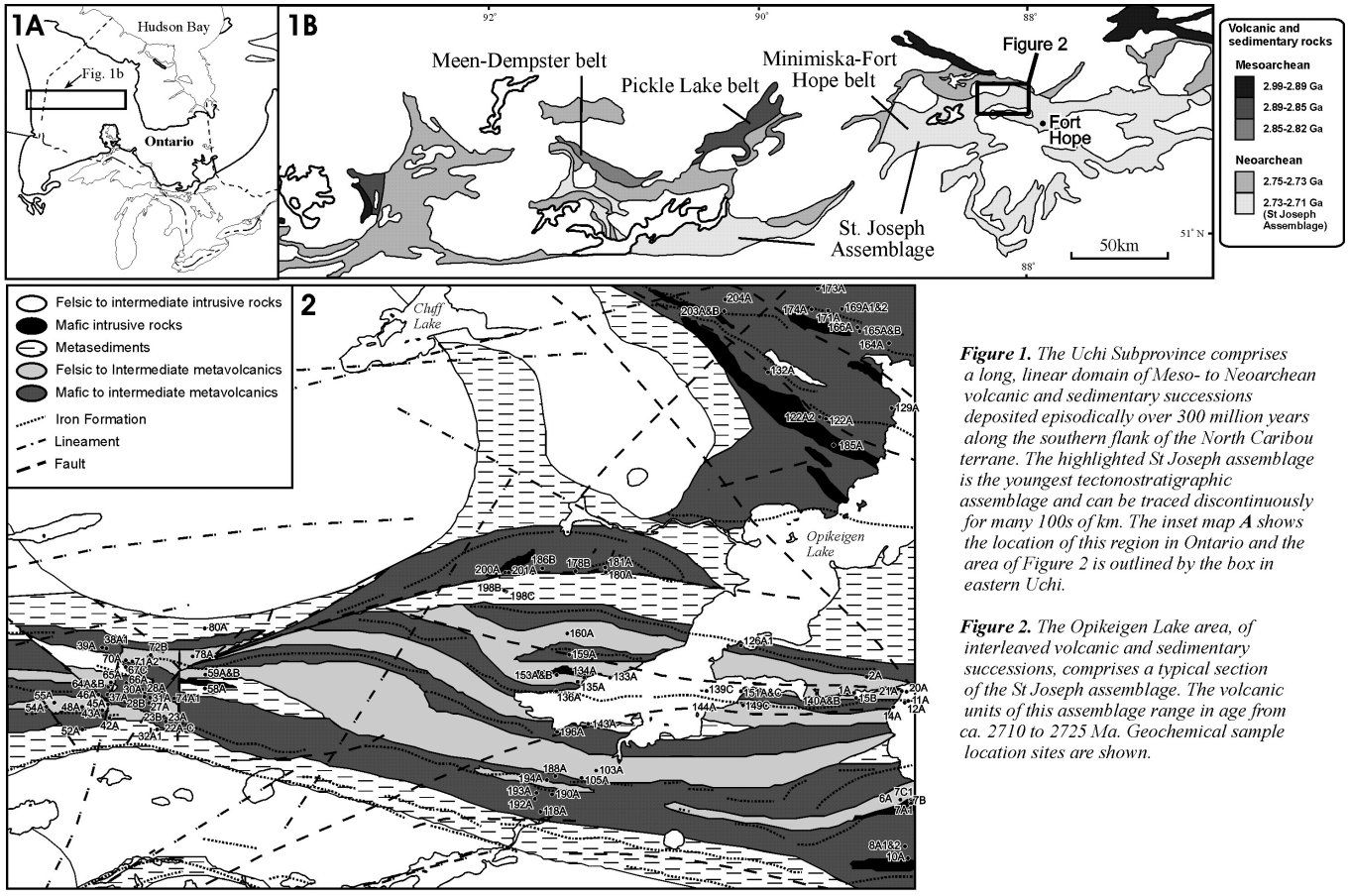

Figure 1. *The Uchi Subprovince comprises a long, linear domain of Meso- to Neoarchean volcanic and sedimentary successions deposited episodically over 300 million years along the southern flank of the North Caribou terrane. The highlighted St Joseph assemblage is the youngest tectonostratigraphic assemblage and can be traced discontinuously for many 100s of km. The inset map* ***A*** *shows the location of this region in Ontario and the area of Figure 2 is outlined by the box in eastern Uchi.*

Figure 2. *The Opikeigen Lake area, of interleaved volcanic and sedimentary successions, comprises a typical section of the St Joseph assemblage. The volcanic units of this assemblage range in age from ca. 2710 to 2725 Ma. Geochemical sample location sites are shown.*

southern portion of the Fort Hope belt includes felsic pyroclastic rocks with ages of 2723-2716 Ma (Corfu & Stott 1993) and younger clastic sediments. Based on the reported ages and the presence of tholeiitic and calc-alkaline basalt flows overlain by intermediate to felsic pyroclastic units (Wallace, 1981a) Stott & Corfu (1991) proposed that this assemblage was an extension of the St Joseph assemblage of the Lake St Joseph greenstone belt. Wallace (1978) conducted the first detailed mapping of the Opikeigen Lake area (Figure 2). He reported the presence of abundant massive and pillowed lavas and flow breccias in east-trending belts throughout the area. Algoma-type iron formation occurs as minor bands intercalated with the mafic volcanics (Wallace, 1978). Mafic tuffs between 0.3 and 1.5 m thick are intercalated throughout the volcanic pile as are felsic to intermediate pyroclastic tuffs, massive flows and autobreccias (Wallace, 1978). More recently the Norton Lake area was subject to detailed mapping as part of a Master's thesis by Johnson (2005) whereas the Opikeigen Lake area was mapped in detail by Hall (2005) with more recent compilation by Madon et al. 2009.

Results

The volcanic rocks of the Fort Hope belt range in composition from basalts to rhyolites. Some mafic volcanic rocks of the St Joseph assemblage are characterised by pronounced LREE depletion (La/Sm_n = 0.54-0.95) comparable to modern Mid-Ocean Ridge basalts, with $\varepsilon_{Nd(T=2700Ma)}$ ranging from 0.83-3.03; whereas other mafic volcanic rocks of this assemblage are characterised by depleted to weakly LREE enriched primitive mantle normalized patterns and negative Nb anomalies (La/Sm_n = 0.56-3.63; Nb/Nb* = 0.21-0.69) with $\varepsilon_{Nd(T=2700Ma)}$ ranging from 0.29-2.09. The intermediate to felsic volcanic rocks are characterised by LREE enrichment and negative Nb anomalies similar to modern supra-subduction sequences. The complexity of the mafic rock chemistry of the St Joseph assemblage is consistent with a backarc origin, upon which was constructed the largely pyroclastic calc-alkalic volcanic successions observed along the length of the southern edge of the Uchi domain.

Implications

Previous Hf isotopic work (Corfu & Stott, 1996), field relations (Stott & Corfu, 1991) and geochemistry (Hollings & Kerrich, 2006) in the central Uchi complement the available geochemical data for the St Joseph assemblage in the Fort Hope area. The evidence suggests that the Uchi domain was constructed largely as an episodic, parautochthonous succession of intra-oceanic arcs and backarc basins, initially composed of relatively juvenile, mantle-derived material, with evidence of progressive crustal contamination from older basement on the southern margin of the Mesoarchean North Caribou terrane. During the circa 2700 Ma Uchian orogeny, these assemblages were telescoped and interleaved, with especially notable interleaving of the St Joseph assemblage volcanics and younger clastic sedimentary panels that form the southernmost margin of the North Caribou terrane. This collisional orogenesis was concurrent with the intrusion of large, continental arc plutons most prominently inboard from the southern margin and suggests plate tectonic processes were similar to those occurring today.

Acknowledgements

P.H. acknowledges support from an NSERC Discovery Grant.

References

Corfu F. & Stott G.M., 1993, U-Pb geochronology of the central Uchi Subprovince, Superior Province, Canadian Journal of Earth Sciences, 30, 1179–1196.

Corfu F. & Stott G.M., 1996, Hf isotopic composition and age constraints on the evolution of the Archean central Uchi Subprovince, Ontario, Canada, Precambrian Research, 78, 53–63.

Davis D.W., Sutcliffe R.H. & Trowell N.F., 1988, Geochronological constraints on the tectonic evolution of alate Archaean greenstone belt, Wabigoon subprovince, Northwest Ontario, Canada, Precambrian Research, 39, 171–191.

Desrochers J.-P., Hubert C., Ludden J.N. & Pilote P., 1993, Accretion of Archean oceanic plateau fragments in the Abitibi greenstone belt, Canada, Geology, 21, 452–454.

Hall L.A.F., 2005, Precambrian geology, Opikeigen Lake area, Ontario Geological Survey, Preliminary Map P.3269, scale 1:20,000.

Hollings P., Wyman D. & Kerrich R., 1999, Komatiite - basalt - rhyolite volcanic associations in Northern Superior Province greenstone belts: Significance of plume-arc interaction in the generation of the proto continental Superior Province, Lithos, 46, 137–161.

Hollings P. & Kerrich R., 2006, Light rare earth element depleted to enriched basaltic flows from 2.8-2.7 Ga greenstone belts of the Uchi Subprovince, Ontario, Canada, Chemical Geology, 227, 133–153.

Madon Z.B., McIlraith S.J. & Stott G.M. 2009, Geological compilation of the Miminiska Lake – Fort Hope area, eastern Uchi domain, Ontario Geological Survey, Preliminary Map P.3611, scale 1:250 000.

Percival J.A., Sanborn-Barrie M., Stott G.M., Helmstaedt H., Skulski T. & White D.J., 2006, Tectonic evolution of the western Superior Province, Canada, Canadian Journal of Earth Sciences, 43, 1085–1117.

Prest V.K., 1944, Geology of the Fort Hope area, Ontario Department of Mines, Annual Report, 1942, 51, pt.3, 1–28.

Stott G.M. & Corfu F., 1991, Uchi Subprovince, in *Geology of Ontario*, Ontario Geological Survey, Special Volume 4, Part 1, 145–236.

Sun S.-s. and McDonough W.F., 1989, Chemical and isotopic systematics of oceanic basalts: implications for mantle composition and processes, in *Magmatism in the Ocean Basins*, Geological Society of London, Special Publication, 42, 313–345.

Thurston P.C., Osmani I.A & Stone D., 1991, Northwestern Superior Province: Review and terrane analysis, in *Geology of Ontario*, Ontario Geological Survey, Special Volume 4, Part 2, 81–144.

Tomlinson K.Y., Thurston P.C., Hughes D.J. & Keays R.R., 1996, The central Wabigoon region: Petrogenesis of mafic-ultramafic rocks in the Steep Rock, Lumby Lake and Obonga greenstone belts (Continental rifting and rifting in the Archean), in *1996 Western Superior Transect Second Annual Workshop*, Harrap R.M. and Helmstaedt H., eds, Lithoprobe Report 53, 65–73.

Wallace H., 1978, Geology of the Opikeigen Lake area, Ontario Geological Survey, Report 185, 58p.

Wallace H., 1981a, Geology of the Minimiska Lake area, Ontario Geological Survey, Report 214, 96p.

Wallace H., 1981b, Geology of the Attwood Lake area. Ontario Geological Survey, Report 203, 49p.

Wyman D.A. & Hollings P., 2005, Late Archean convergent margin volcanism in the Superior Province: A comparison of the Blake River Group and Confederation Assemblage, in *Archean Geodynamics and Environments*, AGU Geophysical Monograph Series, 164, 215–237.

Young M.D., McNicoll V., Helmstaedt H., Skulski T. & Percival J.A. 2006, Pickle Lake revisited: New structural, geochronological and geochemical constraints on greenstone belt assembly, western Superior Province, Canada, Canadian Journal of Earth Sciences, 43, 821–847.

U-Pb-Hf-O CHARACTER OF NEOARCHEAN BASEMENT TO THE PINE CREEK OROGEN, NORTH AUSTRALIAN CRATON

J.A. Hollis[1], L.M. Glass[1], C.J. Carson[2], A.I.S Kemp[3], G. Yaxley[4], R. Armstrong[4] & A. Scherstén[5]

[1]Northern Territory Geological Survey, PO Box 3000, Darwin NT 0801, AUSTRALIA
[2]Geoscience Australia, PO Box 378, Canberra ACT 2601, AUSTRALIA
[3]School of Earth and Environmental Sciences, James Cook University, Townsville QLD 4811, AUSTRALIA
[4]PRISE, The Australian National University, Research School of Earth Sciences, Building 61, Mills Road, Acton ACT 0200, AUSTRALIA
[5]Geological Survey of Denmark and Greenland, Oester Voldgade 10, Copenhagen-K 1350, DENMARK

Introduction

Neoarchean basement to Palaeoproterozoic strata is sparsely exposed in the North Australian Craton (NAC), with most known exposures in the Pine Creek Orogen (PCO). However the ubiquitous occurrence of Neoarchean zircon in detrital spectra of Palaeoproterozoic strata in basins throughout the NAC bears testament to the apparent abundance of exposed Neoarchean crust during the Palaeoproterozoic. Detrital spectra in the various Palaeoproterozoic basins show a striking resemblance in their dominant age peaks at ~2500 Ma and ~1865 Ma. Potential erosive source rocks of ~2500 Ma age are known from granites and granitic gneisses of the Rum Jungle and Nanambu complexes and the Kukalak Gneiss in the PCO, and from the Billabong Complex in the Tanami Region. However relatively little is known of the isotopic nature of this Neoarchean basement and how these widely distributed gneisses of similar magmatic age might be related. Recently older Neoarchean rocks have also been reported from the PCO (2671 Ma and 2640 Ma Arrarra Gneiss; Hollis et al., 2009).

In this contribution we report Hf and O zircon isotopic data for three Neoarchean granites and granitic gneisses from the PCO, with U-Pb magmatic ages of 2671, 2640 and 2527 Ma. We also report data for a sample of intrusive granodiorite of 1867 Ma Nimbuwah Complex, and U-Pb and Hf detrital zircon data for Palaeoproterozoic sandstone from a basal unit of the PCO stratigraphy. These data yield information on the timing and nature of Archean crust formation in the NAC. They also provide a basis for investigating possible relationships with other Archean basement rocks of the NAC and their potential as erosive sources to Palaeoproterozoic sedimentary rocks.

Regional geology

The PCO is exposed over 47 500 km^2 and comprises a thick (>4km) succession of Palaeoproterozoic clastic, carbonate and carbonaceous sedimentary and volcanic rocks unconformably overlying Neoarchaean (~2670–2500 Ma) granitic and gneissic basement. The PCO has been broadly subdivided into 3 regions: the amphibolite- to granulite-facies Litchfield Province in the west; the greenschist-facies Central Domain (including the Rum Jungle region and South Alligator Valley), and the amphibolite-facies Nimbuwah Domain in the east. In addition to differences in metamorphic grade and structural styles, these regions are also distinct in the timing and nature of metamorphism and the timing and chemistry of the main phases of magmatism.

Exposed Neoarchean felsic basement to the Palaeoproterozoic PCO includes the Rum Jungle Complex in the Central Domain and the Nanambu Complex, Kukalak Gneiss and Arrarra Gneiss in the Nimbuwah Domain. Neoarchaean basement is also present under Cretaceous cover in the Central Domain, (Woolner Granite) and in the northern part of the Nimbuwah Domain (Kukalak Gneiss). Archean basement has not been recognised in the Litchfield Province. The oldest known basement is the subcropping Woolner Granite (2674 ± 3 Ma, Glass et al. 2010, Williams & Compston, 1983) in the Central Domain, which has been intersected in drillholes, and which has the same magmatic age as exposed Arrarra Gneiss (2671 ± 3 Ma, Hollis et al., 2009, Carson et al., in press) in the Nimbuwah Domain. Magmatism at ~2500 Ma is common to both the Central and Nimbuwah domains: the Rum Jungle Complex (2545–2521 Ma, Cross et al., 2005); and the Nanambu Complex (2520 ± 3 Ma, Hollis et al., 2009) and Kukalak Gneiss (2527 ± 3 Ma, 2510 ± 4 Ma, Hollis et al., 2009) respectively. Magmatism at 2640 ± 5 Ma is also recorded in the Arrarra Gneiss (Hollis et al., 2009, Carson et al., in press).

The ~1865 Ma Nimbuwah Event affected only the Nimbuwah Domain. Regional moderate to high-pressure amphibolite-facies metamorphism is thought to have been induced by emplacement of granodioritic plutons of the Nimbuwah Complex at depth into Neoarchaean basement and the overlying Palaeoproterozoic succession at 1868–1860 Ma (Worden et al., 2008a, Hollis et al., 2009). This was coincident with the development of NW-vergent folds and thrusts in the Nimbuwah Domain, and with felsic volcanism in the Central Domain and Litchfield Province (~1863 Ma, Worden et al., 2008a,b). This was followed by syn- to post-tectonic granite emplacement at ~1830–1800 Ma.

Methodology

SHRIMP U-Pb data for magmatic samples were collected on the SHRIMP IIe at Geoscience Australia, Canberra. Analytical procedures were reported in Hollis et al. (2009) and Carson et al. (in press). U-Pb data for a sedimentary sample were obtained via laser ablation-sector field-

inductively coupled plasma-mass spectrometry (ICPMS) at the Geological Survey of Denmark and Greenland in Copenhagen using a NewWave Research/Merchantek 213 nm laser coupled to an Element2 ICPMS. Analytical procedures and results were reported in Hollis et al. (2010). Oxygen data were collected using SHRIMP II at the Research School of Earth Sciences, Australian National University (ANU), Canberra. Analyses were made on the same spots previously analysed for U-Pb. Hf data for magmatic samples were collected using an Eximer UV laser and Thermo-Scientific Neptune MC-ICPMS at ANU. Where possible analyses were made on the same spots analysed previously for U-Pb and O. Hf data for the sedimentary sample was collected using a Coherent 193 nm ArF GeoLas micro-sampling system and Neptune MC-ICPMS at the Advanced Analytical Centre at James Cook University, Townsville. Analyses were made adjacent to spots previously analysed for U-Pb in domains with similar internal morphology. εHf values were calculated using the chondritic values of Blichert-toft & Albarede (1997), Lu decay constant of Scherer et al. (2001) and a Depleted Mantle model of Griffin et al. (2000)

U-Pb-Hf-O character of Archean basement and Palaeoproterozoic Nimbuwah Complex

SHRIMP U-Pb zircon data for seven granite and granitic gneiss samples of exposed and sub-surface Neoarchean basement to the Palaeoproterozoic PCO has revealed common ~2670 Ma and ~2530–2500 Ma magmatism in the Nimbuwah and Central domains (Williams & Compston 1983, Hollis et al. 2009, Carson et al., in press, Glass et al., 2010). Felsic magmatism at ~2640 Ma has also been recognised in the Nimbuwah Domain (Hollis et al., 2009). Three of the samples from the Nimbuwah Domain were investigated further using Hf and O isotopes. An 1867 Ma sample of the Nimbuwah Complex (Carson et al., in press) was also investigated to establish if Palaeoproterozoic magmatism involved reworking of Archean basement.

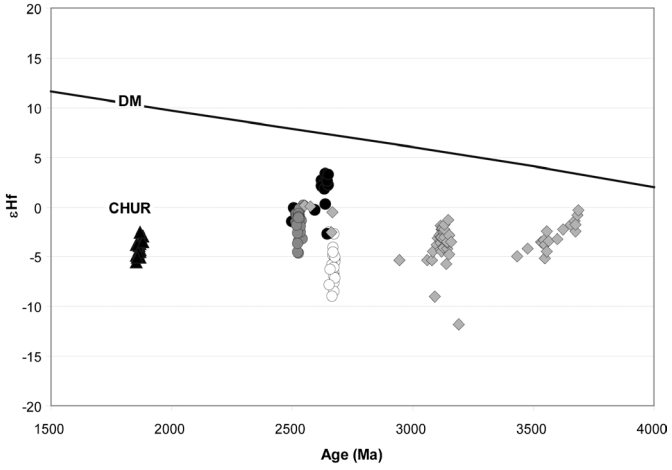

Figure 1. Plot of εHf vs age for magmatic zircons from 2671 Ma Arrarra Gneiss (open circles), 2640 Ma Arrarra Gneiss (black circles), 2527 Ma Kukalak Gneiss (grey circles), 1867 Ma Nimbuwah Complex (black triangles), and detrital zircon from Crater Formation (grey diamonds). Reference Depleted Mantle (DM) and CHondritic Uniform Reservoir (CHUR) evolution lines are shown.

The oldest sample of the Arrarra Gneiss (2671 Ma) yields unradiogenic and variable Hf signature (εHf -2.5 to -8.9, Figure 1) with dominantly mantle-like $\delta^{18}O$ (5.5–6.7‰ with only two grains > 6.5‰, Figure 2). This suggests that the rock was derived from melting of a mix of mantle-derived 3650–3200 Ma sources with relatively limited reworking of supracrustal material with elevated $\delta^{18}O$. The younger component of the Arrarra Gneiss (2640 Ma) has tightly clustered Hf data with a more radiogenic signature (εHf dominantly 3.4 to 1.9, Figure 1), which is consistent with the mantle-like $\delta^{18}O$ data (typically 5.2–5.8‰, Figure 2). This indicates probable derivation dominantly from a ~3000 Ma mantle source. Hf data for the 2527 Ma Kukalak Gneiss clusters below CHUR (-4.6 to 0.2, Figure 1). Oxygen data indicate a significant reworked supracrustal component ($\delta^{18}O$ 6.7–8.9‰, Figure 2). Combined with the relatively clustered εHf data, this is consistent with derivation primarily from reworked material with an average crustal residence age of ~3100–3000 Ma. A sample of 1867 Ma Nimbuwah Complex has clustered εHf of -2.5 to -5.5 (Figure 1) with O signatures dominantly indicative of reworked supracrustal sources (6.2–8.9‰, Figure 2). This is consistent with derivation from reworked sources of a similar origin with an average crustal residence age of ~2800–2700 Ma.

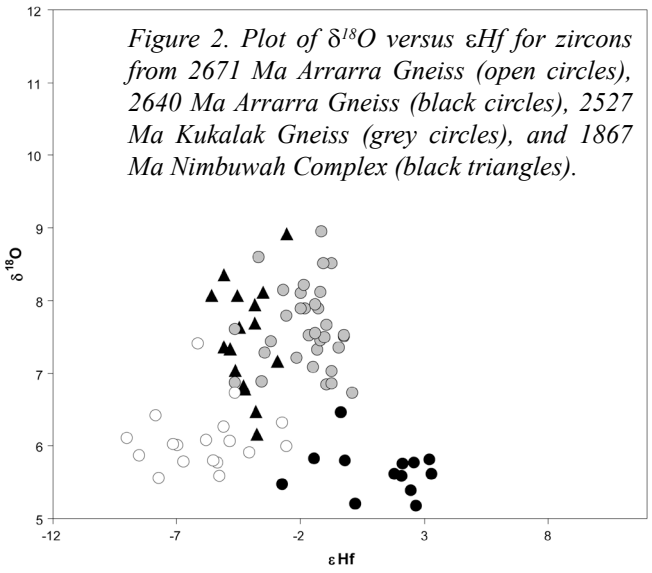

Figure 2. Plot of $\delta^{18}O$ versus εHf for zircons from 2671 Ma Arrarra Gneiss (open circles), 2640 Ma Arrarra Gneiss (black circles), 2527 Ma Kukalak Gneiss (grey circles), and 1867 Ma Nimbuwah Complex (black triangles).

U-Pb and Hf character of basal Palaeoproterozoic Pine Creek Orogen strata

The Crater Formation is a basal unit of the Palaeoproterozoic strata of the Central Domain of the PCO and unconformably overlies the Neoarchaean (~2535–2520 Ma) Rum Jungle Complex. It forms part of the Woodcutters Supergroup, which is typically dominated by a near unimodal ~2500 Ma detrital age peak. The Crater Formation sample is distinct in having a dominant Mesoarchean age peak at 3125 Ma with smaller peaks at ~3550 Ma and ~3680 Ma, and only four Neoarchean grains (~2670 Ma and ~2550 Ma, Figure 3). Magmatic source rocks of these ages are unknown in the NAC.

The oldest two populations at ~3550 Ma and ~3680 Ma have εHf of -5.1 to -0.3, that lie on the same evolutionary trend from a single ~4000 Ma depleted mantle source (Figure 1). Only a small degree of mixing with other crustal sources is indicated by the small deviation away from this evolutionary trend. The dominant ~3125 Ma peak falls below CHUR at -5.7 to -1.2, indicating derivation from mixed sources with average crustal residence ages in the range 3700–3500 Ga (Figure 1). The moderately radiogenic nature of the ~2670–2550 Ma grains suggests they were also derived from a mixture of juvenile material and older continental crust.

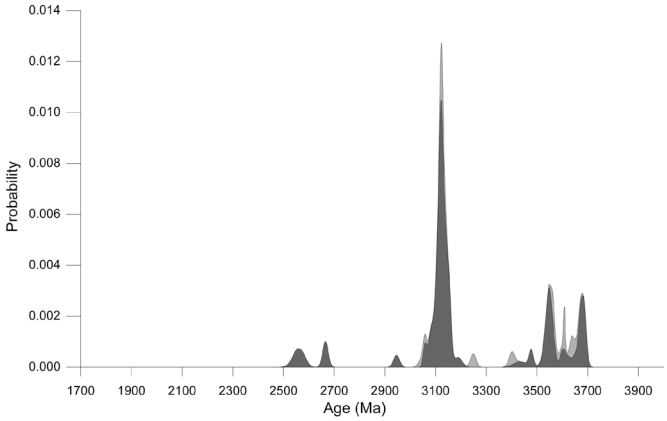

Figure 3. Probability density plot of 70 analyses on 70 grains from the Crater Formation. Less than 10% discordant analyses are shown in dark grey. Pale grey areas represent >10% discordant data.

Implications for crust formation in the Pine Creek Orogen, North Australian Craton

The U-Pb-Hf-O data indicate complexity in the isotopic character of Neoarchaean basement within the PCO with sources likely to have been extracted from the mantle at various times in the period 3700–3000 Ma. In particular there are indications of juvenile magmatism at ~ 3650–3200 Ma and ~3000 Ma. Similarly the Hf isotopes for ~3125 Ma zircons from the Crater Formation are consistent with derivation from mantle sources in the older of these age ranges. Meso- and Eoarchean detrital zircon grains from the Crater Formation point to an older, ~4000 Ma, mantle source not recognised in the magmatic samples.

The unradiogenic and variable εHf signatures, combined with elevated $\delta^{18}O$, for the 2527 Ma Kukalak Gneiss and 1867 Ma Nimbuwah Complex samples are consistent with an increased contribution from assimilation and crustal reworking processes during crust formation in the late Neoarchean and Palaeoproterozoic.

The small size of the dataset presented here should be considered in assessing the more general significance of these conclusions to the evolution of the NAC.

Acknowledgements

JAH and LMG publish with the permission of the Director, Northern Territory Geological Survey; CJC publishes with the permission of the Chief Executive Officer, Geoscience Australia. This publication is a product of the National Geoscience Agreement.

References

Blichert-Toft J. & Albarede F., 1997, The Lu-Hf geochemistry of chondrites and the evolution of the mantle-crust system, Earth and Planetary Scence. Letters, 148, 243–258. Erratum, Earth and Planetary Scence. Letters, 1998, 154, 349.

Carson C.J., Hollis J.A., Glass L.M., Close D.F., Whelan J.A., Wygralak A., in press. Summary of results, Joint NTGS-GA geochronology project: East Arunta, Pine Creek and Murphy Inlier regions, July 2007 – June 2009, Northern Territory Geological Survey, Record.

Cross A.J., Claoué-Long J.C., Scrimgeour I.R., Ahmad M. & Kruse P.D., 2005, Summary of results, Joint NTGS-GA geochronology project: Rum Jungle, basement to southern Georgina Basin and eastern Arunta Region 2001-2003, Northern Territory Geological Survey, Record 2005–006.

Glass L.M., Hollis J.A. & Carson C.J., 2010, Archaean and Palaeoproterozoic crustal evolution processes in the Pine Creek Orogen: U-Pb, Hf, O, Nd isotopic data and geochemistry, in *Annual Geoscience Exploration Seminar (AGES) 2010. Record of abstracts*, Northern Territory Geological Survey, Record 2010-002.

Griffin W.L., Pearson N.J., Belousova E., Jackson S.E., van Achterbergh E., O'Reilly S.Y. & Shee S.R., 2000, The Hf isotope composition of cratonic mantle: LAM-MC-ICPMS analysis of zircon megacrysts in kimberlites, Geochimica et Cosmochimica Acta, 64, 133–147.

Hollis J.A., Carson C.J. & Glass L.M., 2009, SHRIMP U–Pb zircon geochronological evidence for Neoarchean basement in western Arnhem Land, northern Australia, Precambrian Research, 174, 364–380.

Hollis J.A., Beyer E.E., Whelan J.A., Kemp A.I.S., Scherstén A. & Greig A., 2010, Summary of results. NTGS laser U-Pb and Hf geochronology project: Pine Creek Orogen, Murphy Inlier, McArthur Basin and Arunta Region, July 2007–June 2008, Northern Territory Geological Survey, Record 2010–001.

Scherer E., Münker C. & Mezger K, 2001. Calibration of the lutetium-hafnium clock. Science 293, 683–687..

Williams I.S. & Compston W., 1983, Ion microprobe U-Pb dating of zircons from granitoids recovered in core from drill holes P4/1D, P11/1, P12/11 and P14/1, Woolner, Northern Territory, in *Annual Report for EL 3478 "Woolner",* Manning E.R., Richardson B.R. & Starkey L.J., Appendix 3. Mobil Energy Minerals Australia Inc. Northern Territory Department Geological Survey, Open File Company Report CR1983-0231.

Worden K.E., Carson C.J., Close D.F., Donnellan N. & Scrimgeour I.R., 2008a, Summary of results, Joint NTGS-GA geochronology project: Tanami Region, Arunta Region, Pine Creek Orogen and Halls Creek Orogen correlatives, January 2005–March 2007, Northern Territory Geological Survey, Record 2008–003.

Worden K.E., Carson C.J., Scrimgeour I.R., Lally J., & Doyle N., 2008b, A revised Palaeoproterozoic chronostratigraphy for the Pine Creek Orogen, northern Australia: Evidence from SHRIMP U-Pb zircon geochronology, Precambrian Research 166, 122–144.

CONTRASTING ARCHAEAN CRUSTAL RECORDS IN WESTERN PART OF THE NAPIER COMPLEX, EAST ANTARCTICA

K. Horie[1], T. Hokada[1], Y. Hiroi[2], Y. Motoyoshi[1] & K. Shiraishi[1]

1 National Institute of Polar Research, 10-3, Midori-cho, Tachikawa 190-8518, Japan
2 Department of Earth Sciences, Chiba University, Yayoicho, Inage-ku, Chiba 263-8522, Japan

Introduction

The Napier Complex in East Antarctica has attracted considerable interest from a viewpoint of its long Archaean crustal history from 3800 Ma to 2500 Ma (e.g., Harley & Black 1997) and >1000˚C ultrahigh-temperature (UHT) metamorphism on a regional scale (e.g., Sheraton et al., 1987; Harley & Hensen 1990). The Fyfe Hills and Mt. Cronus regions in the western part of the Napier Complex are the areas where ancient >3800-3600 Ma zircon ages have been obtained. Compston & Williams (1982) reported the preliminary data giving >3800 Ma SHRIMP zircon upper intercept ages for granitic orthogneiss from Fyfe Hills. Asami et al. (2002) reported >3600 Ma zircon ages using electron microprobe for a quartzo-feldspathic gneiss from Mt. Cronus. For both areas, 3000 Ma or younger protolith ages are also reported in the literature. It is quite important to confirm the reported early Archaean crustal ages to make more detailed discussion about the Archean crustal history of the Napier Complex. In addition, the timing of ultrahigh-temperature metamorphism is argued to be either >2550 Ma or ~2480 Ma (e.g., Kelly & Harley, 2005).

Samples and Analytical Procedures

We have studied three samples (2 felsic orthogneiss, 1 quartzite) from Fyfe Hills and two samples (paragneiss and quartzite) from Mt. Cronus. The studied samples were collected by Y.H. during field work with the 2004-2005 Japanese Antarctic Research Expedition. Zircon grains were concentrated using conventional mineral-separation techniques, including crushing and pulverizing, followed by separation using methylene iodide. *In-situ* U–Pb analyses were performed using a Sensitive High Resolution Ion Microprobe (SHRIMP II) at the National Institute of Polar Research, Japan. An O_2^- primary ion beam of 2.5-3.0 nA was used to sputter an analytical spot of ~ 25 μm diameter on the polished mount. The procedures for Pb and U isotopic analyses of zircon are after Horie et al. (2006).

Results and Discussion

The felsic orthogneiss of Fyfe Hills yielded two age peaks centered at ca. 2740 and ca. 2530 Ma. Another orthogneiss shows two major age populations centered at ca. 2530 and ca. 2480 Ma with inheritance at ca. 2800 and ca. 2635 Ma. U–Pb data for the quartzite from Fyfe Hills are scattered from ca. 3045 to ca. 2400 Ma and show peaks around 3020, 2940, 2875, 2760, 2680, 2520, and 2440 Ma. On the other hand, paragneiss and quartzite from Mt. Cronus yielded several age peaks centered around 3015, 2870, 2760, 2680, 2580, and 2490 Ma.

Thus, there is no evidence of older than Paleoarchean for both areas. We could suggest that the magmatic protoliths of some of orthogneiss from Fyfe Hills were formed at 2740 Ma. The paragneiss in the same area was sourced from 3020–2760 Ma sediments. Both orthogneiss and paragneiss record a metamorphic age at ~2520 Ma. Contrary to this, sedimentary sources of pargneisses in Mt. Cronus range from 3015Ma to 2580 Ma with a metamorphic age of ~2490 Ma.

Our new data suggest that ancient >3800-3600 Ma ages are not always dominant in these area, and that the newly obtained 3000-2600 Ma protolith ages are somewhat similar with those reported for the other areas (e.g., Mt. Riiser-Larsen, Tonagh Island) in the Napier Complex. Also interesting is that recorded protolith and metamorphic age components for these two areas, Fyfe Hills and Mt. Cronus - about 50km away from each other, differ systematically. The data can provide insight into the Archaean crustal development in this part of Antarctica and also time constraints for the process of ultrahigh-temperature metamorphism.

References

Asami M., Suzuki K. & Grew E.S., 2002, Chemical Th–U-total Pb dating by electron microprobe analysis of monazite, xenotime and zircon from the Archean Napier Complex, East Antarctica: evidence for ultra-high-temperature metamorphism at 2400 Ma, Precambrian Research 114, 249–275.

Compston W. & Williams I.S., 1982, Protolith ages from inherited zircon cores measured by a high mass-resolution ion microprobe. Fifth International Conference on Geochronology, Cosmochronology and Isotope Geology, Abstracts, 63–64.

Harley S.L. & Hensen B.J., 1990, Archaean and Proterozoic high-grade terranes of East Antarctica (40–80°E): a case study of diversity in granulite facies metamorphism, in *High-temperature Metamorphism and Crustal Anatexis*. Ashworth J.R. & Brown M., eds, Unwin Hyman, London 320–370.

Harley S.L. & Black L.P., 1997, A revised Archaean chronology for the Napier Complex, Enderby Land, from SHRIMP ion-microprobe studies, Antarctic Science 9, 74–91.

Horie K., Hidaka H. & Gauthier-Lafaye F., 2006, Elemental distribution in zircon: Alteration and radiation-damage effects, Physics and. Chemistry of the Earth, 31, 587-592.

Kelly N.M. & Harley S.L., 2005, An integrated microtextural and chemical approach to zircon geochronology: refining the Archaean history of the Napier Complex, east Antarctica, Contributions to Mineralogy and. Petrology, 149, 57–84.

Sheraton J.W., Tingey R.J., Black L.P., Offe L.A. & Ellis D.J., 1987, Geology of Enderby Land and western Kemp Land, Antarctica, Australia Bureau of Mineral Resources, Bulletin, 223, 1–51.

U-Pb AGE, TRACE ELEMENTS AND Nd ISOTOPES OF MONAZITES FROM METASEDIMENTS IN MT. NARRYER, WESTERN AUSTRALIA

T. Iizuka & M.T. McCulloch[1]

Research School of Earth Sciences, Australia National University
[1]Now at School of Earth and Environment, University of Western Australia

Introduction

Knowledge of early crustal evolution is central to deciphering the evolution of the young Earth. Metasediments from the Mt. Narryer region in the Yilgarn Craton of Western Australia are of particular importance for the study of early crustal evolution, because they yield Hadean (>4.03 Ga) detrital zircons (Froude et al., 1983), that contribute to our understanding of early crustal evolution. To better understand the tectonothermal and pre-depositional history of the Earth's earliest crystal fragments, a comprehensive study has been carried out on monazites from Mt. Narryer metasediments rocks.

Monazite, a LREE phosphate mineral, is ubiquitous as an igneous accessory phase in low-Ca felsic rocks and as a secondary accessory phase in a wide range of metamorphic rocks. Monazite can be precisely dated by the U-Th-Pb system, thereby providing timing constraints on igneous and metamorphic events. Its geochemical features also reflect the nature of tectonothermal history that its host/source rocks experienced. In addition, its initial Nd isotopic ($^{143}Nd/^{144}Nd$) compositions provide constraints on whether the source magma is of juvenile 'mantle' origin or reflects a more extensive crustal reworking history. In this study, we have conducted back scattered electron (BSE) imaging, in situ U-Pb isotopic dating, geochemical and Sm-Nd analyses of monazites from Mt. Narryer metasediments.

Samples and methods

The Mt. Narryer supracrustal belt is a narrow (~2.5 km) linear belt over a distance of 21 km. The supracrustal belt dominantly comprises quartzite, quartz-pebble meta-conglomerate, and polymictic meta-conglomerate with pebbles of quartz, BIF, and paragneiss. The sedimentary rocks experienced metamorphism at upper amphibolite to granulite facies conditions, as indicated by the mineral parageneses of sillimanite-cordierite-garnet in quartzite. They also experienced at least two periods of deformation (Williams and Myers, 1987). The southern sector of the belt is divided into five lithostratigraphic units designated A to E, from oldest to youngest (Myers et al., 1990). Hadean detrital zircons with U-Pb ages up to 4.28 Ga have been identified in meta-sedimentary rocks from Units B to E (Froude et al., 1983; Crowley et al., 2005; Pidgeon & Nemchin, 2006).

Monazite grains were separated from 5 metasedimentary rock samples that we collected: Meta-quartzite MN051 and meta-conglomerate MN074 from Unit C, meta-conglomerates MN080 and 090 from Unit D, and meta-quartzite MN100 from Unit E. U-Pb isotopic and geochemical data were obtained in situ by laser ablation-inductively coupled plasma quadrupole mass spectrometry (LA-ICPQMS) at the Australian National University (ANU). The Sm-Nd isotopic analyses were performed in situ by LA-multiple collector-ICPMS at the ANU.

Results

Based on the BSE images, the internal structures of the grains were classified into the following five types: (i) homogeneous, (ii) core-rim structure, (iii) patchy structure, (iv) mosaic structure (fine scale patchy structure relative to analytical spatial resolution), and (v) oscillatory-zoning.

U-Pb isotopic data

Most monazites studied here provide concordant U-Pb isotopic ages. The $^{207}Pb/^{206}Pb$ age populations of monazites yielding concordant or <5% discordant U-Pb ages are shown in histograms (Fig. 1). The monazite age populations of all Mt. Narryer samples studied here show a dominant peak at 2.7–2.6 Ga. The BSE images indicate that some of the 2.7–2.6 Ga monazites formed by recrystallization of older monazites. The oscillatory-zoned grains from sample MN074 gave $^{207}Pb/^{206}Pb$ ages of 3.6 Ga and around 3.3 Ga. No monazites older than ~3.65 Ga have been found.

Geochemical data

The monazite grains with ages of 2.7–2.6 Ga are extremely depleted in HREE and show moderate negative Eu anomalies, while those older than 2.8 Ga have variable patterns and are less depleted in HREE. The oscillatory-zoned monazites are characterized by pronounced negative Eu anomalies and less HREE depletion. Notably, younger monazites tend to have higher Gd/Lu (i.e., HREE depletion) and that the increase of the ratio occurred at ~3.3–3.2 and 2.7–2.6 Ga.

Sm-Nd isotopic data

All monazite grains analyzed for Sm-Nd isotopes exhibit negative εNd(t) values, indicating that their sources were older crustal materials, rather than juvenile magmas. In addition, younger monazites display more negative εNd(t) values.

Constraints on the tectonothermal history

The geochronological data, combined with the BSE images, reveal that many of older monazite grains recrystallized at 2.7–2.6 Ga (Fig. 1), similar to the ages

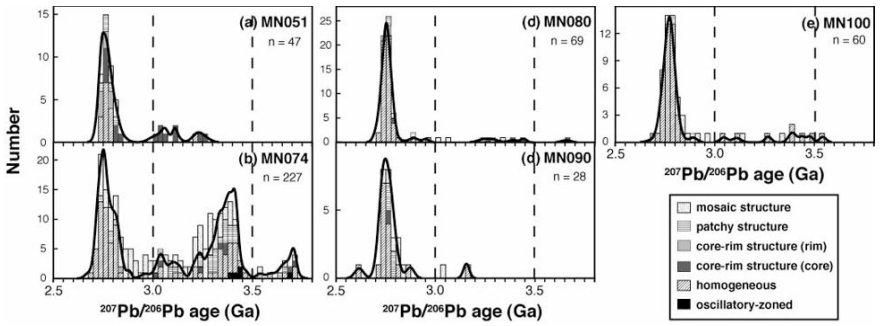

Figure 1. 207Pb/206Pb age histograms of concordant and <5% discordant monazites for sample (a) MN051, (b) MN074, (c) MN080, (d) MN090, (e) MN100. Columns are coded according to internal structure under BSE imagery. Bold lines illustrate relative age probability for analyses of no-mosaic-zoned sites.

of the hornblendes from amphibolites (Kinny et al., 1990) and zircon overgrowths (Trail et al., 2007) from metasediments in the belt. In addition, our geochemical data reveal that the 2.7–2.6 Ga monazites generally have REE patterns with prominent HREE depletion compared to older monazites from the same samples. The HREE depletion in monazite is generally attributed to its formation in equilibrium with garnet that strongly partitions HREE (e.g., Bea and Montero, 1999). Indeed, stronger depletion of HREE in monazite is observed for samples richer in garnet. Therefore, our results, coupled with the reported hornblende ages, provide compelling evidence for high-grade metamorphism that resulted in garnet formation at 2.7–2.6 Ga in the Mt. Narryer region.

The monazite geochemical data also highlight that the degree of HREE depletion in monazites from samples MN074 and 080 was high at not only 2.7–2.6 Ga, but also ~3.3–3.2 Ga. The most notable geochemical feature of samples MN074 and 080 is its high-Fe and -Mn bulk composition. Fe and Mn activities control metamorphic reactions including garnet (e.g., Spear, 1993). Fe- and Mn-rich rocks contain abundant garnets that grew at early stages of regional metamorphism, whereas Fe-poor and/or Mg-rich rocks never develop garnet. Considering this, the HREE depletion in ~3.3–3.2 Ga monazites can be interpreted as reflecting that the Mt. Narryer meta-sediments experienced an earlier metamorphic event leading to metamorphic monazite and garnet formation at ~3.3–3.2 Ga. Indeed, we found that some garnets from sample MN074 are chemically zoned: the cores have lower Y and M- and HREE and higher Ti contents relative to the rims. The zoning profile can be most simply explained by two distinct episodes of metamorphic garnet growth. Hence, we interpret that Mt. Narryer meta-sediments experienced at least two metamorphic events; one at ~3.3–3.2 Ga and another at 2.7–2.6 Ga, when peak granulite-facies metamorphism occurred.

Our results thus provide new constraints on timing of deposition of the Mt. Narryer sediments. Given that oscillatory-zoning is a typical structure in igneous monazites and that the oscillatory-zoned monazites exhibit striking negative Eu anomalies and a high range of HREE and Th contents (features which are commonly observed in igneous monazite; Rasmussen & Muhling, 2009), the youngest crystallization age of the oscillatory-zoned monazites can be interpreted as a maximum estimate for the deposition age. The youngest concordant oscillatory-zoned monazite has a ^{207}Pb/^{206}Pb age of 3296 ± 38 Ma, in good agreement with the youngest detrital zircon age of 3281 ± 14 Ma (Kinny et al., 1990). On the other hand, a younger limit is obtained from the metamorphic age at ~3.3–3.2 Ga, even though the analytical uncertainty of the present dating technique does not allow resolution of the timing of the metamorphic event from the ages of the youngest detrital grains. Accordingly, the deposition age of the Mt. Narryer sediments is now constrained to between 3.28 and 3.20 Ga.

Insights into the sediment provenance

Despite the significant metamorphic monazite growth, a relatively high proportion of detrital monazite survives in Fe- and Mn-rich sample MN074. This is likely because the high Fe and Mn bulk composition resulted in the efficient shielding of early formed monazite by garnet. The preservation of detrital monazite permits us to assess the provenance of the Mt. Narryer sediments. The age population of detrital (≥3.28 Ga) monazites from sample MN074 defines two peaks at ca. 3.6 and 3.3 Ga (Fig. 1). These peaks are concurrent with those in the age populations of detrital zircons from Mt. Narryer meta-sediments (Crowley et al., 2005; Pidgeon & Nemchin, 2006, and references therein), and also with the protolith ages of the surrounding granitoids (3.68–3.60 Ga Meeberrie and 3.38–3.35 Ga Dugel gneisses) as well as deformed granite (3.30–3.28 Ga). Importantly, some ca. 3.6 and 3.3 Ga monazites have oscillatory-zoning and euhedral shape. In addition, some grains contain zircon inclusions, while the most abundant inclusions observed in <3.2 Ga metamorphic monazites are quartz. These observations suggest that some of the ca. 3.6 and 3.3 Ga monazites are of igneous, rather than metamorphic origin.

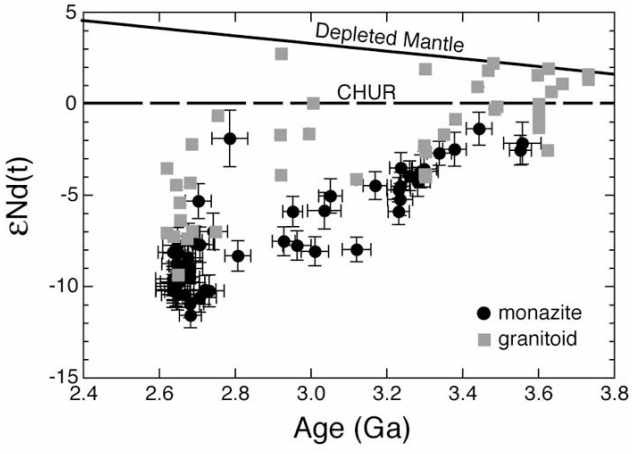

Figure 2. Plot of ^{207}Pb/^{206}Pb age vs. εNd(t) for monazite from Mt. Narryer metasedimentary rocks (black circle). Nd isotopic data of the surrounding granitoids are also shown (grey square).

To further constrain the nature of the ca. 3.6 and 3.3 Ga igneous source rocks, we have compared REE and Nd isotopic data of the monazites with those of the surrounding granitoids. The REE profiles of melts in equilibrium with the oscillatory-zoned, euhedral and zircon-bearing monazites were calculated using the partitioning coefficients between monazite and silicate melt. The melts that equilibrated with the ca. 3.6 and 3.3 Ga monazites have $[La/Yb]_N$ (normalized to chondrite) of ca. 34–36 and 14–21, respectively. These values correspond well to those of the contemporaneous Meeberrie ($[La/Yb]_N$ = 34) and Dugel ($[La/Yb]_N$ = 16 and 216) granitic gneisses in the Narryer Gneiss Complex (Myers, 1988; Maas & McCulloch, 1991). In addition, εNd(t) values of the >3.28 Ga monazites are similar to those of the contemporaneous surrounding granitoids (Nutman et al., 1993) (Fig. 2). These observations clearly indicate that the Mt. Narryer sediments were partly derived from the Meeberrie and Dugel granitic gneisses.

No monazites with ages older than 3.65 Ga have been found from the Mt. Narryer meta-sediments. This may suggest that the source rocks of the >3.65 Ga detrital zircons were not low-Ca felsic rocks and hence contained little monazite, or alternatively that although the source rocks may have contained monazite, this phase completely dissolved/recrystallized during metamorphism after 3.65 Ga or was eliminated during prolonged sedimentary recycling. The implication of the latter scenario is that Hadean zircons most likely experienced significant metamorphism and/or prolonged sedimentary recycling prior to their deposition.

Acknowledgements

We are grateful to K.D. Collerson, T. Komiya, T. Shibuya, T. Ohta, H. Ozawa, E. Sugimura for assistance during our field seasons in the Narryer Gneiss Complex, and to L. Kinsley, G. Mortimer and C. Allen for analytical support.

References

Bea F. & Montero P., 1999. Behavior of accessory phases and redistribution of Zr, REE, Y, Th and U during metamorphism and partial melting of metapelites in the lower crust: An example from the Kinzigite Formation of Ivrea-Verbano, NW Italy. Geochimica et Cosmochimica Acta, 63, 1133–1153.

Crowley J.L., Myers J.S., Sylvester P.J. & Cox R.A., 2005, Detrital zircons from the Jack Hills and Mount Narryer, Western Australia: Evidence for diverse >4.0 Ga source rocks. Journal of Geology, 113, 239–263

Froude D.O., Ireland T.R., Kinny P.D., Williams I.S. & Compston W., 1983, Ion microprobe identification of 4,100–4,200 Myr-old terrestrial zircons, Nature, 304, 616–618.

Kinny P.D., Wijbrans J.R., Froude D.O., Williams I.S. & Compston W., 1990, Age constraints on the geological evolution of the Narryer Gneiss Complex, Western Australia, Australian Journal of Earth Sciences, 37, 51–69.

Maas R. & McCulloch M.T., 1991, The provenance of Archean clastic metasediments in the Narryer Gneiss Complex, Western Australia: Trace element geochemistry, Nd isotopes, and U-Pb ages for detrital zircons, Geochimica et Cosmochimica Acta, 55, 1915–1932.

Myers J.S., 1988, Early Archaean Narryer Gneiss Complex, Yilgarn Craton, Western Australia, Precambrian Research, 38, 297–307.

Myers J.S., Williams I.R., Kinny P.D., Nutman A.P., Pidgeon R. & Wilde S.A., 1990, Excursion 1: Narryer Gneiss Complex, In Ho S.E., Glover J.E., Myers J.S., Muhling J.R., eds *Third International Archean Symposium, Perth, Excursion Guidebook,* Geology Department and University Extension University of Western Australia Publication, 21, 61–95.

Nutman A.P., Bennett V.C., Kinny P.D. & Price R., 1993, Large-scale crustal structure of the northwestern Yilgarn Craton, Western Australia: Evidence from Nd isotopic data and zircon geochronology. Tectonics, 12, 971–981.

Pidgeon R.T.& Nemchin A.A., 2006, High abundance of early Archean grains and the age distribution of detrital zircons in a sillimanite-bearing quartzite from Mt Narryer, Western Australia. Precambrian Research 150, 201–220.

Rasmuseen B. & Muhling J.R., 2009, Reactions destroying detrital monazite in greenschist-facies sandstones from the Witwatersrand basin, South Africa. Chemical Geology, 264, 311–327.

Spear F.S., 1993. *Metamorphic phase equilibria and pressure-temperature-time paths*, Mineralogical Society of America, 799p.

Trail D., Mojzsis S.J. & Harrison T.M., 2007, Thermal events documented in Hadean zircons by ion microprobe depth profiles. Geochimica et Cosmochimica Acta., 71, 4044–4065.

Williams I.R. & Myers J.S., 1987, Archaean geology of the Mount Narryer region, Western Australia, West Australian Geological Survey, Report 22, 32p.

ISOTOPIC GEOCHEMISTRY OF THE NORTHERN GOLDFIELDS, YILGARN CRATON, WESTERN AUSTRALIA: SETTING THE SCENE FOR KOMATIITE EMPLACEMENT

C. Isaac[1], M. Fiorentini[1], K.F. Cassidy[2], T.C. McCuaig[1], N. Thebaud[1], E. Belousova[3], C. Perring[4], S. Wyche[5] & C. Kirkland[5]

[1] Centre for Exploration Targeting, M006, The University of Western Australia, 35 Stirling Hwy., Crawley, WA, Australia, 6009
[2]Bare Rock Geological Services Pty Ltd, Fremantle, WA, 6160
[3] GEMOC ARC National Key Centre, Department of Earth and Planetary Sciences, Macquarie University, NSW, Australia, 2109
[4] BHP Billiton, Level 41 Central Park 152-158 St Georges Tce., Perth, WA, Australia 6000
[5]Geological Survey of Western Australia; Department of Mines and Petroleum, Mineral house, 100 Plain St., East Perth, WA, Australia 6004

Introduction

The genesis of individual komatiite-hosted nickel-sulphide (KANS) deposits in Archean granite-greenstone terranes has been widely debated and is reasonably constrained (Barnes, 2006). However, the reasons why KANS deposits cluster and why mineralised komatiites are preferentially emplaced within specific lithospheric environments are not well understood. In this study, we investigate the early craton-scale lithospheric architecture that favoured the emplacement of large komatiite systems and the development of nickel-sulphide deposits and camps in the Yilgarn Craton of Western Australia. Our focus is on the 2.8-2.7 Ga greenstone belts of the northern portion of the Eastern Goldfields Superterrane (the Northern Goldfields), from the areas of Leonora and Laverton in the south to the northern edge of the craton (Fig. 1a).The ultramafic rocks in the study area comprise komatiites and komatiitic basalts, the latter of which have not been found anywhere else in the Yilgarn Craton. The purpose of this study is to examine the processes (both shallow and deep-seated) operating during the Archean and relate these processes to the emplacement of komatiites, komatiitic basalts and what role, if any it may have played in mineralisation of nickel-sulphide deposits.

Over the course of this study, Lu-Hf and Sm-Nd isotope systematics in conjunction with U-Pb sensitive high-resolution ion microprobe (SHRIMP) geochronology will be used to discern the characteristics of the deeper lithosphere through much of the Archean (>3.0–<2.6 Ga). The Sm-Nd map of Champion & Cassidy (2007) is one of the first forays into large scale lithospheric mapping, the result being a portrait of the ages of the various parts of the Yilgarn Craton (Fig. 1b). However, Sm-Nd analyses, which are performed by dissolution of whole rock powder, can only provide information about the time of formation of the rock. This is useful when performed on komatiites (providing their age can be estimated by other means, as komatiites are normally zircon poor) and on felsic rocks as well. However, the fact that plutons older than 2.72 Ga have yet to be discovered in the Eastern Goldfields restricts information that can be derived from Sm-Nd isotopes to the mid-to-late Archean. Zircons do take up Sm and Nd into their structure, but few Sm-Nd studies have been conducted on zircons, and the results have been somewhat erratic (Kinny & Maas, 2003). The Lu-Hf isotopic system behaves very similarly to the Sm-Nd isotopic system, Lu and Hf are also taken into the structure of zircon in measurable concentrations, and the database of successful Lu-Hf analyses is much larger (Kinny & Maas, 2003). Because of this, the Lu-Hf system is more suitable for estimating crustal setting further back in time using inherited zircons from granite plutons and felsic volcanics from the Yilgarn. Analyses of Lu-Hf and U-Pb on a given spot (core/rim) of a zircon will give information on the type (evolved/thicker/cooler versus younger/thinner/hotter) of lithosphere sampled by the pluton the zircon was in at a given time in geologic history. Examining zircon populations of various felsic rocks across the north Eastern Goldfields will help show the type of lithosphere sampled at different places and points in time in the history of accretion of the Yilgarn. Whole rock Sm-Nd provides an estimate of crustal residence time for a given melt and will allow us to compare the behaviour of Lu-Hf.

In addition, mass-independent sulphur isotopes on sulphides from VMS deposits, felsic volcanics and nickel-sulphide deposits will be used as a proxy for surface processes. More information on the tectonic setting of komatiites can be found by looking at sulphur isotopes. Work done by Farquhar & Wing (2003) revealed that $\delta^{33}S$ isotopes are most pronounced in the Archean, the result of interactions of sulphur compounds with ultraviolet radiation. The mass-independent fractionation of ^{33}S has revealed that isotopic fluctuation of sulphur was controlled by atmospheric conditions prior to 2.45 Ga, after which biological processes and oxidation overtook S sequestering (Farquhar & Wing, 2003). The interaction with UV causes fractionation into a light $\delta^{33}S$ that is taken up by as oceanic sulphate and a heavier $\delta^{33}S$ that is absorbed into subaerial sediments (Farquhar & Wing, 2003).This affords a unique signature to rocks greater than 2.45 Ga. One debate regarding komatiite hosted sulphide nickel deposits is how to achieve sulphur saturation once the komatiite erupts. Typically it has been assumed that sulphur was picked up from sediments that the komatiites came into contact with that was responsible for sulphur saturation (Lesher et al., 2001). However, Bekker et al.

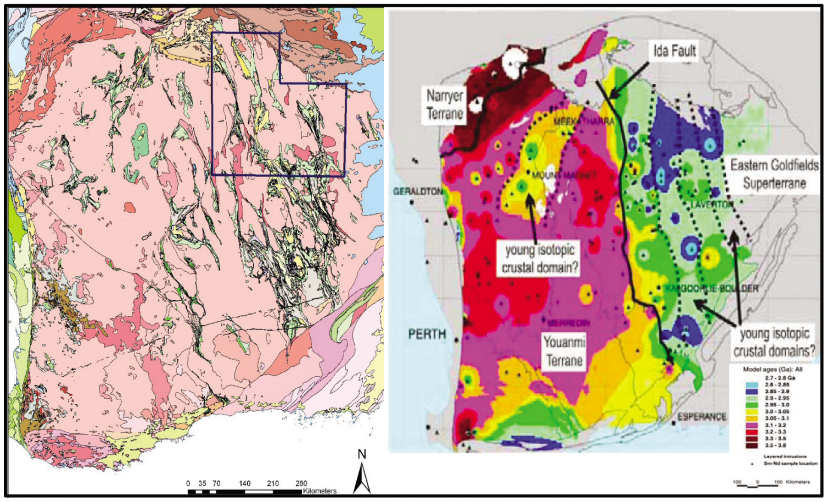

Figure 1: a) (left image): Geological map of the Yilgarn Craton, Western Australia. Study area is outlined in blue. b) (right image): Sm-Nd map of the Yilgarn from Champion & Cassidy (2007).

(2009) have suggested that alternate sources of sulphur such as volcanogenic massive sulphide could be an alternate source for additional sulphur for contamination and boosting S contents of komatiites to saturation. Mass-independent sulphur isotopes may be capable of resolving this ambiguity, as sediments derived from small continents will likely have a heavier (i.e. positive) $\delta^{33}S$ signature than those derived from marine settings (Farquhar & Wing, 2003). Additional sulphur isotopic studies from felsic volcanics and other deposits may help better estimate water depth and thus tectonic setting of their locations.

To date, work on this project has focused on samples of granites that were previously analysed for U-Pb SHRIMP ages (Nelson, 1997; Nelson, 1998). Preliminary analyses give εHf values ranging between -7 and +8, with the majority being between 0 and +5. These results exhibit a range of signatures between juvenile and reworked older source material, with the majority having a juvenile signature close to CHUR. These preliminary Lu-Hf data agree with the interpretation by Champion & Cassidy (2007) That prior to 2.68 Ga magmatism was primarily syn-volcanic, with crustal recycling starting after 2.68 Ga. The results of this in-depth study will expand considerably on the work done by Champion and Cassidy, provide a new powerful tool for exploration and much needed detail on a previously poorly studied portion of the Yilgarn.

Acknowledgements

The Authors wish to acknowledge that this project is funded by the ARC Nickel Linkage Project LP0776780

References

Barnes S, 2006. Komatiites: Petrology, volcanology metamorphism and geochemistry in *Nickel Deposits of the Yilgarn Craton: Geology, Geochemistry and Geophysics Applied to Exploration*, Barnes S.J., ed, Society of Economic Geologists Special Publication 13, 13–50, Johnson Printing.

Bekker A., Barley M.E., Fiorentini M.L., Rouxel O.J,, Rumble D., Beresford S.W., 2009, Atmospheric sulphur in Archean Komatiite-hosted Nickel deposits, Science, 326, 1086–1089.

Champion & Cassidy, 2007, An overview of the Yilgarn Craton and its crustal evolution, in *Proceedings of Geoconferences (WA) Inc. Kalgoorlie '07 Conference, 25-27 September 2007, Kalgoorlie, Western Australia*, Bierlein F.P. & Knox-Robinson C.M., eds, Geoscience Australia Record 2007/14, 8–13.

Farquhar J. & Wing B.A., 2003. Multiple sulphur isotopes and the evolution of the atmosphere, Earth and Planetary Science Letters, 213, 1–13.

Kinny P.D. & Maas R., 2003, Lu-Hf and Sm-Nd isotope systems in zircon, in *Zircon*, Hanachar J.M. & Hoskin P.W.O., eds, Reviews in Mineralogy and Geochemistry, 53, 327–341.

Lesher C.M., Burnham O.M. & Keays R.R., 2001, Trace-element geochemistry and petrogenesis of baren and ore-associated komatiites, The Canadian Mineralogist, 39, 673–696.

Nelson D.R., 1997, Compilation of SHRIMP U-Pb zircon geochronology data, 1996, Geological Survey of Western Australia, Record 1997/2, 189p.

Nelson, D.R., 1998, Compilation of SHRIMP U-Pb zircon geochronology data, 1997, Geological Survey of Western Australia, Record 1998/2, 189p.

AGE AND SIGNIFICANCE OF VOLUMINOUS MAFIC–ULTRAMAFIC MAGMATIC EVENTS IN THE MURCHISON DOMAIN, YILGARN CRATON

T.J. Ivanic[1], M.T. Wingate[1], M.J. Van Kranendonk[1,2], C.L. Kirkland[1] & S. Wyche[1]

[1]Geological Survey of Western Australia, Dept. of Mines and Petroleum
[2]Also at: School of Earth and Geographical Sciences, the University of Western Australia

Introduction

Late Archean mafic–ultramafic rocks in layered intrusions comprise approximately 40% by volume of greenstones within the northern Murchison Domain (northwestern Youanmi Terrane) of the Yilgarn Craton, Western Australia. The largest of these layered intrusions is the predominantly gabbroic Windimurra Igneous Complex, which outcrops over an area of ~2500 km^2; the nearby Narndee Igneous Complex covers an area of 700 km^2. However, these mafic-ultramafic igneous complexes have been dissected by large-scale, strike-slip shear zones and are intruded by Neoarchean granitic rocks, so that the full original extent of any single complex is unknown. Collectively these intrusions have an areal extent of 250 x 400 km, which is similar in extent to the Bushveld Igneous Complex, South Africa (Fig. 1, inset). These intrusions are host to V and PGE mineralization and are an important component of Murchison Domain evolution.

Supracrustal rocks that host the layered mafic–ultramafic complexes form part of the 2950-2700 Ma Murchison Supergroup (Van Kranendonk & Ivanic, 2009). Whereas c. 2950 Ma greenstones occur in the southern part of the Murchison Domain (Yeats et al., 1996; Wang et al., 1998), greenstones in the northern part of the domain were deposited in three magmatic cycles, between 2825 and 2700 Ma. The 2825-2800 Ma Norie Group is intruded, at its base, by syn-volcanic and younger granitic rocks. The younger 2800-2740 Ma Polelle and 2735-2700 Ma Glen groups have disconformable to unconformable contacts on the older greenstones. The groups are dominated by mafic and ultramafic volcanic rocks, but also include locally thick felsic volcanic units, as well as banded iron-formation and clastic sedimentary rocks (Watkins & Hickman, 1990; Van Kranendonk, 2008; Van Kranendonk & Ivanic, 2009).

The Norie and Polelle Groups host mafic–ultramafic complexes of different age, emplaced as shallow-level subvolcanic sills during eruption of the overlying volcanic units (Van Kranendonk &Ivanic, 2009). The older, structurally lowermost sills include thick layered mafic-ultramafic igneous complexes with evidence of multiple magma pulses and complex cyclical layering, whereas the younger sills are generally thinner and composed of a single magma pulse.

Previous geochronology, as well as new results from precise ion microprobe (SHRIMP) U–Pb ages of zircon and baddeleyite integrated with the geology and areal extent of the mafic–ultramafic intrusive suites across the

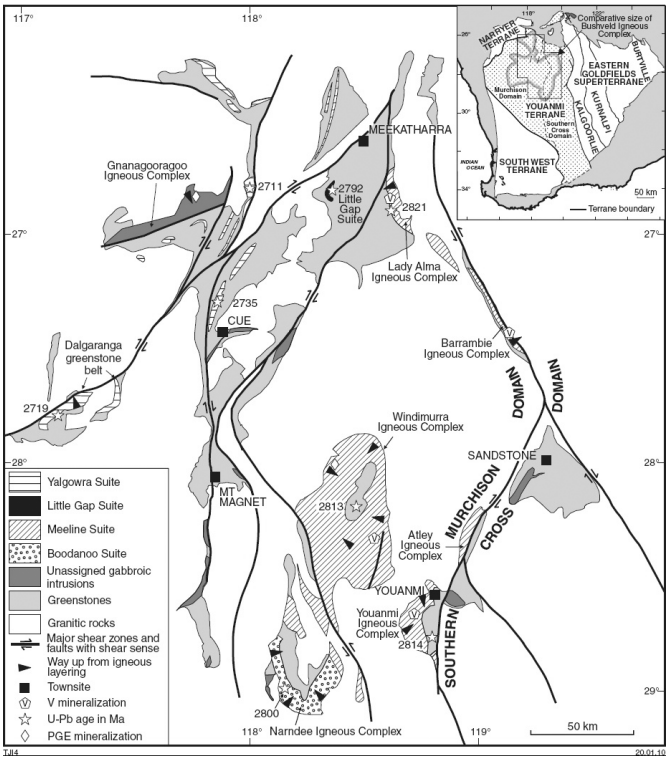

Figure 1. Map of the mafic–ultramafic suites and igneous complexes of the northern Youanmi Terrane relative to greenstones and granites, modified from Tyler and Hocking (2007).

Murchison Domain produce a stratigraphic context, assist in estimating their original size and volume, and provide important constraints for the tectonic development of the craton.

Layered mafic–ultramafic igneous suites

Five mafic-ultramafic components have been identified in the Murchison Domain: (1) the c. 2815 Ma Meeline Suite, which includes the Windimurra and Youanmi Igneous complexes; (2) the 2800 ± 6 Ma Boodanoo Suite, which includes the Narndee Igneous Complex; (3) the 2792 ± 5 Ma Little Gap Suite; (4) the c. 2745 Ma Gnanagooragoo Igneous Complex; and (5) the 2735–2710 Ma Yalgowra Suite of layered gabbroic sills. The intrusions are typically layered, tabular bodies of gabbroic rock with ultramafic basal units, which in places are greater than 6 km in thickness and 85 km in diameter, although these are minimum dimensions as they have been dismembered by younger deformation. Outcrop patterns, aeromagnetic surveys, and gravity data indicate that most intrusions form large tabular bodies; i.e. sills, laccoliths, or lopoliths. The largest mafic–ultramafic layered intrusions of the Meeline and

Boodanoo Suites — the Windimurra, Narndee, and Youanmi Igneous Complexes — preserve a large part of their original intrusion morphology, with relatively shallowly inward-dipping concentric layers. This contrasts with the majority of the other mafic–ultramafic intrusive rocks in the northern Murchison Domain, which are steeply dipping, parallel to greenstone bedding, and deformed into parallelism with major shear zones (Fig. 1). The margins of some of the larger igneous complexes are sheared and intruded by granitic rocks, so that information concerning the nature of the contact relationships with greenstones has been obscured.

The Windimurra Igneous Complex is the largest of the Meeline Suite and its age is estimated at c. 2815 Ma. It is the largest exposed mafic–ultramafic intrusion in Australia. The coherent main body of the complex is 85 km north–south and 37 km east–west and extending over an area of 2500 km^2 (Ahmat, 1986). This complex shows multiple discordant features in its igneous layering, which is indicative of highly unstable conditions during magma emplacement, possibly reflecting intrusion during lithospheric extension. The Narndee Igneous Complex is the only hydrous complex identified in the Murchison Domain and contains a significant quantity of hornblende gabbro (Scowen, 1991). Geochronology yields a U–Pb crystallization age of baddeleyite at 2800 ± 6 Ma. In these two suites there is geochemical evidence for multiple pulses of magma (e.g. Ahmat, 1986; Scowen, 1991; Nebel et al., this volume). Two leucocratic sill tops from the Yalgowra Suite gave ages of 2735 ± 6 Ma and 2711 ± 2 Ma. However, this magmatic younger episode appears to have been much less volumetrically significant than the c. 2800 Ma magmatism.

Igneous complexes of the Meeline Suite are host to significant vanadium mineralization in the upper parts of the layered series. There is, at least minor, Ni–Cu–PGE mineralization in sulphides, primarily in the basal parts of the Meeline and Boodanoo Suites, and in the Gnanagooragoo Igneous Complex (Parks, 1998). Minor Ni–Cu–PGE is also found in lateritic formations overlying ultramafic parts of these suites/complexes.

Conclusions

Collectively, the areal distribution, thickness, and volume of mafic–ultramafic magma in Murchison Domain intrusive complexes is similar to that in the 2.06 Ga Bushveld Igneous Complex, and indicates a major addition of mantle-derived magma to Murchison Domain crust over a 115 million year period. All suites are contemporaneous with packages of high-Mg tholeiitic lavas and/or felsic volcanic rocks in greenstone belts (Fig. 2). The distribution, ages, and compositions of the earlier mafic-ultramafic rocks are most consistent with genesis in a mantle plume setting.

Significantly, mafic–ultramafic magmatism in the northern Murchison Domain overlaps in time with that of the Southern Cross Domain and also the Burtville Terrane of the Eastern Goldfields Superterrane (Fig. 2), now separated by over 500 km. This suggests the possibility of a shared history over at least 100 Ma (c. 2820-2710 Ma) and possibly longer.

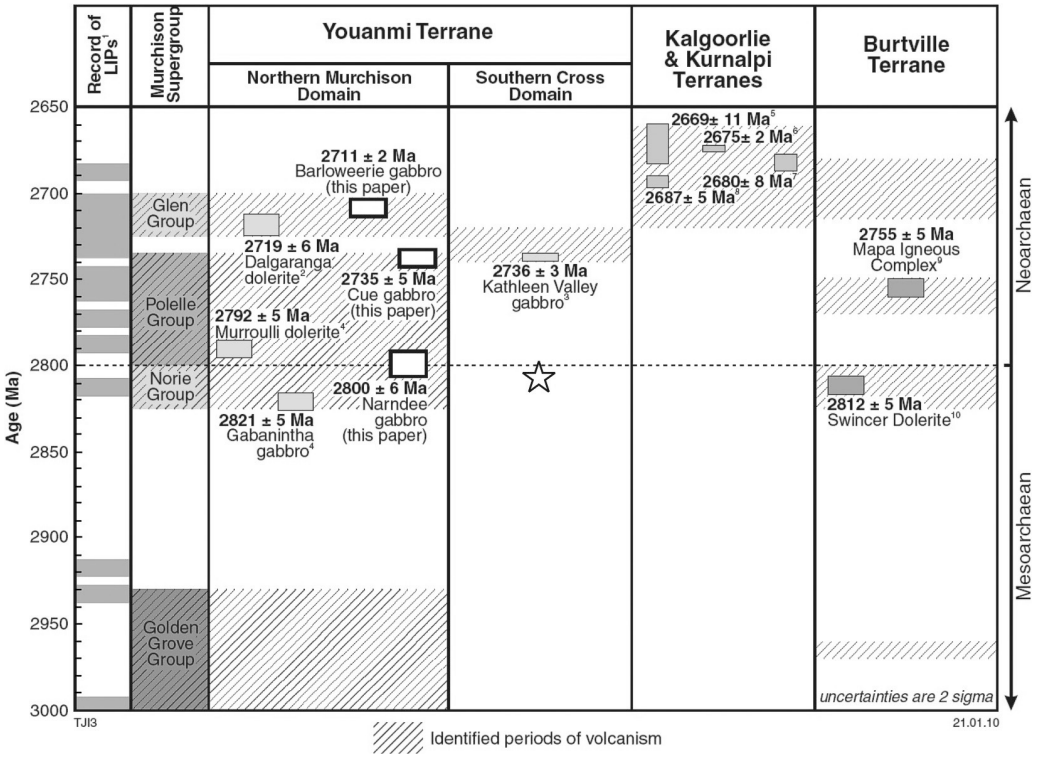

Figure 2. Summary of age determinations for mafic intrusions in Youanmi Terrane compared to Kalgoorlie, Kurnalpi, and Burtville Terranes. [1]An extract from the global mafic magmatism "bar code" (Ernst et al. 2005) is shown on the left. Ages: [2]Pigeon and Hallberg (2000), [3]Liu et al. (2002), [4]Wang (1998), [5]Compston et al. (1986), [6]Woods (1997), [7]Carey (1994), [8]Kent & MacDougall (1995), [9]GSWA 185976, (Wingate et al., in press a), [10]GSWA 185968 (Wingate et al., in press b). Star indicates new data from c. 2800 Ma gabbro in the northern part of the Southern Cross Domain (Riganti et al., this volume).

Acknowledgements

Zircon and baddeleyite analyses were conducted using the SHRIMP ion microprobes at the John de Laeter Centre for Mass Spectrometry at Curtin University of Technology, in Perth, Australia. Staff at the Geological Survey of Western Australia, Carlisle Laboratory, are thanked for their diligent efforts in separating the minute amounts of zircon and baddeleyite from geochronology samples. The authors publish with permission of the Executive Director of the Geological Survey of Western Australia.

References

Ahmat A.L., 1986, Petrology, structure, regional geology and age of the gabbroic Windimurra complex, Western Australia, University of Western Australia, 279p (unpublished).

Campbell I.H. & Hill R.I., 1988, A two-stage model for the formation of the granite-greenstone terrains of the Kalgoorlie-Norseman area, Western Australia, Earth and Planetary Science Letters 90, 11–25.

Compston W., Williams I.S., Campbell I.H. & Gresham J.J., 1986, Zircon xenocrysts from the Kambalda volcanics: age constraints and direct evidence for older continental crust below the Kambalda Norseman greenstones, Earth and Planetary Science Letters 76, 299–311.

Ernst R., Buchan K. & Campbell I., 2005, Frontiers in Large Igneous Province research, Lithos 79, 271–297.

Kent A.J.R, MacDougall I., 1995, ^{40}Ar-^{39}Ar and U-Pb age constraints on the timing of gold mineralization in the Kalgoorlie goldfields, Western Australia, Economic Geology 90, 845–859.

Nebel O., Mavrogenes J.A., Arculus R.J., Ivanic T.J. & Langford R., 2010, Geochemical depth-profiling of late-stage melts from the ~ 2.8 Ga Windimurra Igneous Complex, Western Australia, this volume.

Parks J., 1998, The Weld Range platinum group element deposit, in *Geology of Australian and Papua New Guinean mineral deposits*, Berkman D.A. & Mackenzie D.H. eds, The Australian Institute of Mining and Metallurgy, Melbourne. 279–286.

Pigeon R. T., & Hallberg J. A., 2000, Age relationships in supracrustal sequences of the northern part of the Murchison Terrane, Archaean Yilgarn Craton, Western Australia: a combined field and zircon U-Pb study, Australian Journal of Earth Sciences, 47, 153–165.

Riganti A., Wingate M.T., Wyche S., 2010, New geochronology for the northern Southern Cross Domain, this volume.

Scowen P., 1991, The geology and geochemistry of the Narndee intrusion: Australian National University, PhD thesis, 214p (unpublished).

Tyler I. M. & Hocking R. M., 2007, 1:500,000 Geological Map of Western Australia, Geological Survey of Western Australia.

Van Kranendonk, M.J., 2008, New evidence on the evolution of the Cue–Meekatharra area of the Murchison domain, Yilgarn Craton, Geological Survey of Western Australia, Annual Review 2006-07, 39-49

Van Kranendonk M.J. & Ivanic T.J., 2009, A new lithostratigraphic scheme for the northeastern Murchison Domain, Yilgarn Craton, Geological Survey of Western Australia, Annual Review 2007–08, 34–53.

Wang Q., 1998, Geochronology of the granite-greenstone terranes in the Murchison and Southern Cross Provinces of the Yilgarn Craton, Western Australia, Unpublished Ph.D. thesis. Australian National University, Canberra, 186p.

Wang, Q., Schiøtte, L. & Campbell, I.H., 1998,. Geochronology of supracrustal rocks from the Golden Grove area, Murchison Province, Yilgarn Craton, Western Australia, Australian Journal of Earth Sciences, 45, 571–577.

Watkins K. & Hickman A., 1990, Geological evolution and mineralization of the Murchison province, Geological Survey of Western Australia, Bulletin 127, 267p.

Wingate M.T.D., Kirkland C.L. & Pawley M.J., in press a, 185968, leucogabbro, Mount Sefton, Geochronology Record 869, Geological Survey of Western Australia.

Wingate M.T.D., Kirkland C.L. & Pawley M.J., in press b, 185976, leucogabbro, Mount Warren, Geochronology Record 870, Geological Survey of Western Australia.

Yeats C.J., McNaughton N.J. & Groves, D.I., 1996, SHRIMP U-Pb geochronological constraints on Archaean volcanic-hosted massive sulphide and lode gold mineralization at Mount Gibson, Yilgarn Craton, Western Australia, Economic Geology 91, 1354–1371.

MID-ARCHEAN GRANITES SOUTH OF THE MURCHISON GREENSTONE BELT, SOUTH AFRICA: THE OLDEST LARGE BIOTITE-MUSCOVITE LEUCOGRANITE BODIES

J. Jaguin[1], J-F. Moyen[2], P. Boulvais[1] & M. Poujol[1]

[1] Géosciences Rennes, UMR 6118, Campus de Beaulieu, 35000 Rennes, France
[2]Departement of Geology, University of Stellenbosch, South Africa
Now at the Université Jean Monnet, laboratoire magmas et volcans, département de géologie, 23 rue du Docteur Paul Michelon, 42023 Saint Etienne, France and CNRS, UMR 6524, LMV, F-63038 Clermont—Ferrand, France

Introduction

Peraluminous leucogranites, defined by the presence of at least one high-Al mineral such as muscovite or garnet, are of primordial importance because they normally form during continental collisions by partial melting of aluminous sediments (Zen, 1988, e.g. Clemens, 2003). However, the earliest such plutons reported so far are late-Archaean, in the Superior Province of Canada, with some rare occurrences of minor intrusions, plugs or dykes of minor volumetric importance. Our work evidences the occurrence of large (10's of km) plutons of Ms-Bt and Grt-Bt mid-Archaean leucogranites, emplacing during a protracted period near the Murchison Greenstone Belt (MGB) of South Africa.

Geological setting

The Mesoarchean Murchison Greenstone Belt (MGB) is a volcanic and -sedimentary belt located in the northeastern part of the Kaapvaal Craton in South Africa (Fig. 1). The belt forms an East-Northeasterly trending sequence, 140 km long along strike for a maximum width of 20 km. Most of the belt was accreted between 3.09 and 2.97 Ga (Poujol, 1996), and was deformed probably soon after that time.

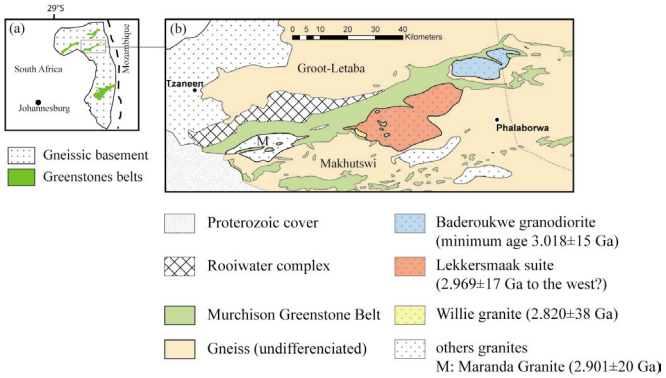

Figure 1. (a) Localisation of the MGB on the East part of the Kaapvaal Craton (b) Map of the belt and surrouding gneisses and granitoids.. Also reported ages of crystallization of granitoids in Ga (Maranda: Poujol et al, 1996; Willie, Discovery (West of Lekkersmaak) and Baderoukwe: Poujol, 2001).

To the North, the belt is in tectonic contact with the composite Groot-Letaba gneisses, along the Letaba Shear zone. The poorly exposed Groot-Letaba gneiss yield an age of 3.171±6 Ga (Brandl & Kröner, 1993). They are therefore likely older than the belt itself, and probably form a polyphased, composite basement.

South of the belt, similar gneisses (the Makhutswi gneisses) yielded an age of 3.063±12Ga (Poujol & Robb, 1999). However, the MGB is rarely in actual contact with the gneisses, and is bounded by a series of intrusive granitic bodies, from East to West the Baderoukwe pluton, Lekkersmaak suite and Maranda granite.

The Lekkersmaak suite

The Lekkersmaak suite is a generic term encompassing all potassic granitoids on the Southern edge of the belt between Gravelotte and Phalaborwa. It comprises a range of intrusive rocks including:

1. Large plutons (probably two distinct plutons, see Fig. 1). They are fine-grained, yellowish leucogranites dominated by quartz and K-feldspar. Typically, they are two-mica leucocgranites (biotite + muscovite), although either mica may be locally absent. In a few localities, garnet is also present as a magmatic mineral, and they can be associated with tourmaline-bearing pegmatoids.
2. A smaller intrusive, known as the Discovery pluton, is associated with emerald mineralization immediately South of the town of Gravelotte. The Discovery pluton outcrops mainly as aplitic dykes, and is composed of quartz, K-feldspar and minor biotite and muscovite.
3. The Willie granite is a small pluton intrusive into the two larger units of the Lekkersmaak suite. It is a coarse-grained to porphyritic pluton, with mostly muscovite and subordinate biotite.
4. Ms-bearing pegmatites are ubiquitous in the area, and extend to the South to the village of Mica, where muscovite bearing pegmatites are mined.

Geochronology: a protracted history of peraluminous magmatism

Existing geochronological data for these rocks are scarce, and we are in the process of re-dating the two mica granites. Excluding old, unreliable Rb-Sr ages, only two of the facies have been dated:
The Discovery granite yielded an age of 2.969±17 Ga (upper intercept age, Poujol, 2001) and the Willie granite

was dated at 2.820±38 Ga (Poujol, 2001). The latter age is of critical importance. As the Willie granite is clearly cutting across the two large fine grained plutons of the Lekkersmaak suite, this puts a minimum age constrain for these intrusions, that must be older than 2.850 Ga. We speculate that they may have formed concurrently with the Discovery pluton, which we regard as a manifestation of the same plutonic event, at ca. 2.96 Ga – the age of the end of the accretion of the MGB, and probable age of the main tectono-metamorphic event in the belt.

A younger age (Burger & Walraven, 1974) of 2.690 Ga was obtained on coarse-grained, muscovite-free rocks near the core of the Lekkersmaak pluton. As this age is inconsistent with field relations, and was obtained on a markedly different facies (not peraluminous), we regard it as not representative of the Lekkersmaak suite as a whole; rather, it certainly corresponds to the intrusion of the younger Mashishimale pluton that intruded at 2.698±21 Ga (Poujol, 2001) immediately to the South.

The range of ages available on the leucogranites shows that those rocks are among the first occurrence of 2 mica granites.

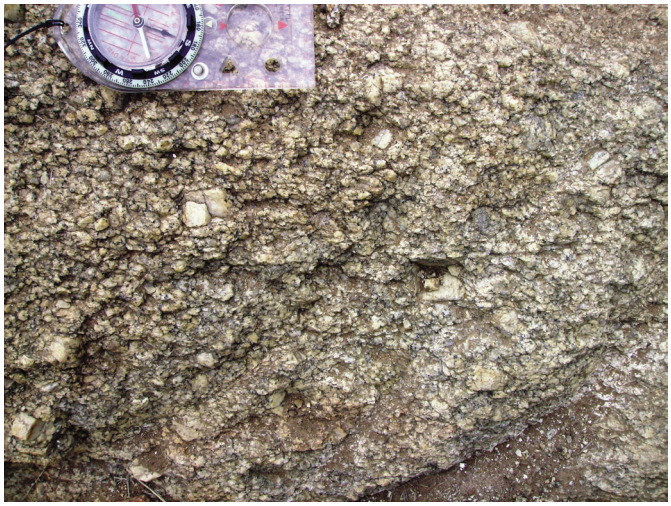

Figure 2: picture of the Willie granite, showing centimetric feldspars.

Discussion and conclusion

Although the occurrence of biotite in granite is common at all times of the crust history, the occurrence of muscovite is uncommon at these early times. This mineral highlights the high content in Al and K of the magma that is link to a crustal fusion of sediments (e.g. Zen, 1988). In the modern Earth, this only happens during continental collision (S-type plutons).

In the MGB area, a series of mid-Archaean events record a sort of "proto-collision". Structural data show that the belt accreted in a sinistral transpressive regime, with top to the south movement. Metamorphic conditions recorded in the belt (Block & Moyen,. this volume) are greenschist to amphibolites facies, with clockwise P-T-t loops, consistent with crustal thickening; the geotherm recorded by the peak metamorphic assemblages is consistent with the geotherm required for the melting of the sedimentary pile and the generation of Bt-Ms leucogranites from metapelite. Furthermore, these peraluminous granites have a metapelite protolith, similar in composition to the La France Domain schists (Block & Moyen, this volume). Sr and Nd isotope characterisation is programmed and will allow to discuss this specific point in more details. . Besides, ^{39}Ar-^{40}Ar dating on muscovite and U-Pb dating on zircon and monazite is now in progress and will allow to precise the timing of events (emplacement, deformation).

On the other hand, it must be noted that the "peraluminous" event south of the MGB was long-lived, as it covered a period spanning from at least 2690 to 2850 Ma, i.e. 120 Ma long. This long-term activity is not typical for modern collision belts, where the peraluminous magmatism lasts only a few Ma to tens of Ma.

None of this represents a proper, Himalayan type collision. It is however, a crustal response to convergence, resulting in some (limited) crustal thickening, with the usual associated magmatic and metamorphic manifestations: barrovian series and Bt-Ms leucogranites.

References

Block S. & Moyen J.F., 2010, the Murchison Greenstone Belt, South Africa: Accreted Slivers with contracting metamorphic conditions, this volume.

Brandl G. & Kröner A., 1993, Preliminary results of single zircon studies from various archaean rocks of the Northeastern Transvaal, in 16th colloquium of African Geology, Mines G.S.A., ed, Mbabane Zwaziland, 54–56.

Burger A.J. & Walraven F., 1979, Summary of age determination carried out during the period April 1977 to March 1978: Annals of the Geological Survey of South Africa, 12, 209–218.

Clemens J. D., 2003, S-type granitic magmas - petrogenetic issues, models and evidence, in Earth Science Reviews, 61, 1-18.

Poujol, M., Robb, L.J., Respaut, J.P. & Anhaeusser, C.R., 1996, 3.07-2.97 Ga Greenstone Belt formation in the northeastern Kaapvaal Craton: Implications for the origin of the Witwatersrand Basin, Economic Geology, 91, 1455–1461.

Poujol M., Robb L.J., 1999, New U-Pb zircon ages on gneisses and pegmatite from south of the Murchison greenstone belt, South Africa, South African Journal of Geology, 102, 93–97.

Poujol M., 2001, U-Pb isotopic evidence for episodic granitoid emplacement in the Murchison greenstone belt, South Africa, Journal of African Earth Sciences, 33, 155–163.

Vearncombe J. R., Barton J. M., Jr, Cheshire P. E., De Beer J. H., Stettler E. H. & Brandl G., 1992, Geology, geophysics and mineralization of the Murchison schist belt, Rooiwater complex and surrounding granitoids, Memoirs of Geological Survey of South Africa (now Council for Geosciences), 139.

Zen E., 1988, Phase relations of peralumionous granitic rocks and their petrogenetic implications, in Annual Review of Earth and Planetary Sciences 1988, 16, 21–51.

WHAT DO CURRENT GEOPHYSICAL MODELS OF ARCHEAN LITHOSPHERE REALLY TELL US? - AN EXAMPLE FROM SOUTHERN AFRICA

A.F. Kobussen, J.C. Afonso, W.L. Griffin & S.Y. O'Reilly

GEMOC ARC National Key Centre, Dept. of Earth and Planetary Sciences, Macquarie University NSW 2109, Australia

Introduction

Modern geophysical methods can be used to characterise the compositional and thermal state of Archean lithospheric mantle with increasing precision. However, these models are snapshots of the current lithospheric conditions, and may not adequately reflect the recent evolutionary history of the lithosphere. The common practice of interpreting geophysical models of Archean lithosphere in a uniformitarianist fashion may therefore not properly account for previous thermal or tectonic activity beneath a region.

Kaapvaal cratonic lithosphere samples

The Kaapvaal Craton in southern Africa is undoubtedly the most studied of the Archean-age cratons. Hundreds of occurrences of kimberlites and related rocks provide geographically extensive suites of mantle xenoliths and xenocrysts that have been actively studied for decades. In addition, there have been a number of detailed seismic and magnetotelluric surveys of the craton and surrounding regions. Comparisons of these data provide a method for tracking the evolution of the lithospheric mantle from the time of the kimberlite eruption to the present. The Kaapvaal cratonic lithosphere samples used for this study were brought to the surface during two episodes of kimberlite magmatism approximately 119 and 90 Ma (Figure 1).

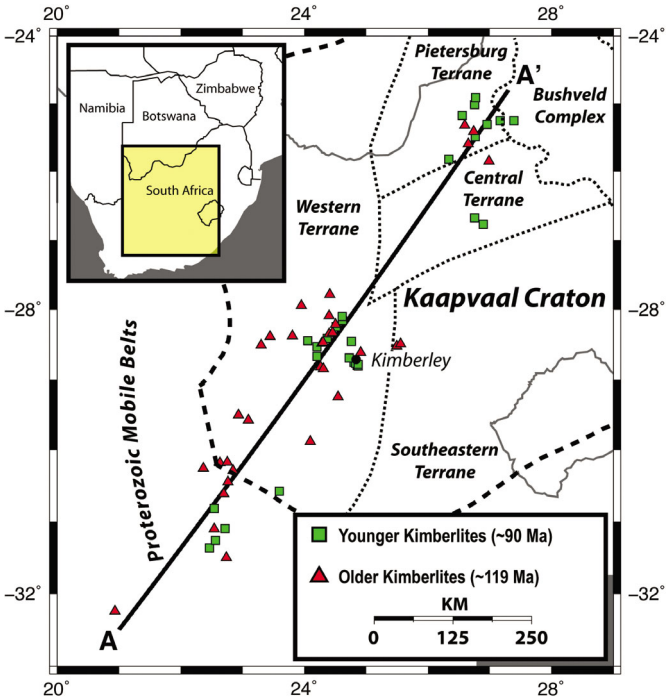

Figure 1. A simplified tectonic map of southern Africa showing the locations of kimberlite hosts used in this study. Section line A-A' refers the vertical sections shown in Figures 2 and 3.

Transforming garnet data into seismic data

Garnet xenocrysts collected from these kimberlite occurrences in the course of diamond exploration provide a geographically extensive sample of mantle material from each time period. Using the garnet geotherm method (Ryan et al. 1996), a pressure and temperature (P-T) is calculated for each garnet. Combining P-T data with whole-rock compositional estimates derived from garnet chemistry (Griffin et al. 1999, O'Reilly & Griffin 2006) supplies the information required to directly calculate seismic velocities.

Seismic velocities for the upper mantle are calculated from the garnet data using components of the LitMod - Perple_X computer codes (Afonso et al. 2008, Connolly 2009). The stable mineral assemblage at a given depth is estimated using a Gibbs free-energy minimization algorithm (Connolly 2005, 2009) within the system CaO-FeO-MgO-Al_2O_3-SiO_2 (CFMAS). The elastic moduli of the bulk rocks are computed using the elastic moduli of each end-member mineral, the pressure, and the temperature. The mole fraction of each end member (e.g. forsterite) present in each stable phase (e.g. olivine) is calculated as part of the Gibbs free-energy minimization algorithm mentioned above. The resulting elastic moduli of each stable mineral phase are then calculated as the mean values of the end-member moduli weighted by their respective mole proportions. Finally, the elastic moduli of the bulk rock are calculated using the Voigt-Reuss-Hill averaging scheme. Anharmonic seismic velocities obtained in this way are then corrected for anelastic effects due to grain size and seismic wave frequency. The shear-wave seismic velocities derived from the older and the younger set of garnet xenocrysts are shown in Figure 2.

Modern vs. ancient seismic signals

There are significant reductions in upper mantle seismic velocities between the eruption of the older and younger set of kimberlites, particularly below 175 km in the southwestern half of the profile. These reductions are largely expected in light of large-scale changes to the composition and thermal state of the lithospheric mantle recorded in xenoliths and xenocrysts during the same period (Bell et al. 2003, Kobussen et al. 2009). The very low velocities derived from the younger garnet xenocrysts indicate a strong seismic low-velocity zone beneath the southwestern and northeastern corner, but not the central part of the profile.

Modern tomographic models of the same region indicate a slightly different picture. Figure 3 is a section through

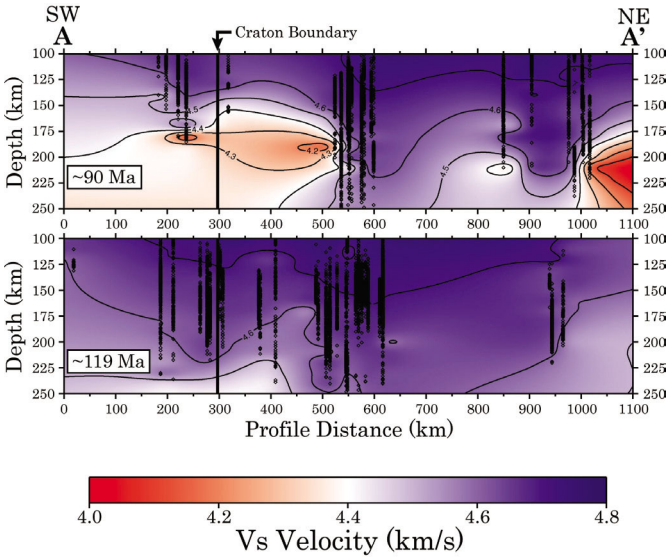

Figure 2. Garnet-derived S-wave velocities for the older (bottom) and younger set of garnet xenocrysts along profile A-A' in Figure 1. The heavy vertical black line shows the craton boundary as mapped at the surface. Individual garnet xenocrysts are shown as open symbols at the points where they project onto the cross-section. For contouring methods, see Kobussen et al. (2009).

the Kaapvaal Craton along the same profile shown in Figure 2. In comparison to the younger garnet-derived model, velocities in the modern tomographic model are higher at depths below 175 km in the southwestern and extreme northeastern corner of the profile. However, the velocities from the tomography are lower in the central parts of the section at depth.

The changes in seismic velocity among these three profiles suggest a consistent evolutionary trend in the thermal and chemical state of the lithospheric mantle beneath southern Africa. In the oldest image, the garnet-derived S-wave velocities are consistent with a thick lithosphere in a state of near thermal equilibrium. Conversely, S-wave velocities derived from the younger set of garnet xenocrysts suggest extreme local thermal disequilibrium, as evidenced by the very irregular pattern of seismic velocities and anomalously low velocities at ~175-220 km depth in the southwestern half and northeastern corner of the profile. Directly adjacent to the very low velocities are relatively high velocities in the centre of the profile. In the modern tomographic image, the thermal disequilibrium recorded in the younger garnets has dissipated into a broad low-velocity zone beneath the entire craton. Independent thermal modelling (Nyblade & Sleep 2003) confirms that relatively warm lithosphere

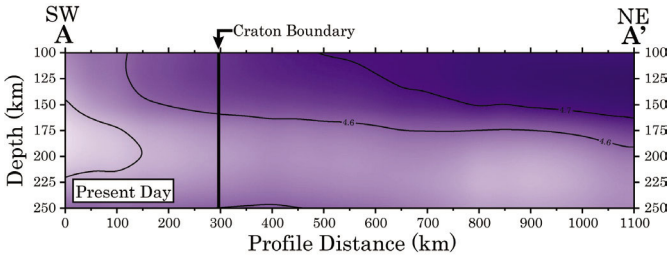

Figure 3. A section through a modern tomographic surface-wave model (S. Fishwick, pers. comm.) along profile A-A' in Figure 1. The colour scale is the same as Figure 2.

must remain beneath southern Africa to explain the anomalously high topography of the Southern African Plateau. Our own preliminary thermal modelling also indicates that the irregular thermal anomaly recorded by the younger set of garnets would dissipate into a broad zone of relatively higher temperatures at 175-250 km, consistent with the tomographic model.

Conclusions

Modern geophysical models of cratonic lithosphere provide only a snapshot of the current compositional and thermal conditions of a region. Without greater context on the recent tectonothermal history of the lithosphere, it is difficult to understand the meaning of these images in terms of geological processes. In the case of southern Africa, seismic images calculated from two suites of garnet xenocrysts of differing age indicate there has been significant thermal and metasomatic activity in the lithosphere in the recent past, and the effects of this activity are still evident in modern seismic images. It therefore can be misleading to assume modern geophysical images of lithosphere necessarily represent a steady-state regime. It is also problematic to try to constrain modern seismic models with ancient xenoliths due to the likely change in the thermal and/or compositional state of the lithosphere since the removal of the xenoliths from the mantle.

Acknowledgements

S. Fishwick kindly provided his tomographic model of southern Africa for comparison to the garnet-derived velocity models. DeBeers Group Services contributed substantial financial, logistical, and information resources. ARC Discovery and Linkage Grants to SYO'R and WLG provided additional financial support. AK was supported by a Macquarie University postgradute scholarship and a Commonwealth IPRS scholarship. This study used instrumentation funded by ARC LIEF and DEST Systemic Infrastructure Grants, Macquarie University and industry. Oliver Gaul and Norman Pearson assisted with analytical work.

References

Afonso J.C., Fernàndez, M., Ranalli G., Griffin W.L., & Connolly J.A.D., 2008, Integrated geophysical-petrological modeling of the lithosphere and sublithospheric upper mantle: Methodology and applications, Geochemistry, Geophysics, Geosystems, 9, doi:10.1029/2007GC001834.

Bell D.R., Schmitz M.D., & Janney P.E., 2003, Mesozoic thermal evolution of the southern African mantle lithosphere, Lithos, 71, 273–287.

Connolly J.A.D., 2005, Computation of phase equilibria by linear programming: A tool for geodynamic modeling and its application to subduction zone decarbonation, Earth and Planetary Science Letters, 236, 524–541.

Connolly J.A.D., 2009, The geodynamic equation of state: What and how, Geochemistry, Geophysics, Geosystems, 10, doi:10.1029/2009GC002540.

Griffin W.L., O'Reilly, S.Y. & Ryan C.G., 1999, The composition and origin of subcontinental lithospheric mantle, in *Mantle petrology: field observations and high pressure experimentation: a tribute to Francis F. (Joe) Boyd*, Fei, Y., Bertka C.M. & Mysen B.O., eds, The Geochemical Society of London, Special Publication No. 6, 13–45.

Kobussen A.F., Griffin W.L. & O'Reilly S.Y., 2009, Cretaceous thermo-chemical modification of the Kaapvaal cratonic lithosphere, South Africa, Lithos, 112S, 886–895.

Nyblade A.A., & Sleep N.H., 2003, Long lasting epeirogenic uplift from mantle plumes and the origin of the Southern African Plateau, Geochemistry, Geophysics, Geosystems, 12, doi:10.1029/2003GC000573.

O'Reilly S.Y. & Griffin, W.L., 2006, Imaging global chemical and thermal heterogeneity in the subcontinental lithospheric mantle with garnets and xenoliths: Geophysical implications, Tectonophysics, 416, 289–309.

Ryan C.G., Griffin,W.L. & Pearson N.J., 1996, Garnet geotherms: Pressure-temperature data from Cr-pyrope garnet xenocrysts in volcanic rocks, Journal of Geophysical Research, 101, 5611–5625.

REE MOBILIZATION AND LOW-TEMPERATURE MONAZITE IN BASINAL BRINE ENVIRONMENTS

M.A. Kusiak[1], I. González-Álvarez[2, 3], R. Kerrich[4] & P. Konečny[5]

[1]Institute of Geological Sciences, Polish Academy of Science, Warsaw, Poland
[2]ABM Resources NL, Perth, Western Australia
[3]Centre for Exploration Targeting, School of Earth and Environment, Univ. of Western Australia
[4]Department of Geological Sciences, University of Saskatchewan, Saskatoon, Canada
[5]Štátny Geologický Ústav Dionýza Štúra, Bratislava, Slovakia

Introduction

The stability of monazite, a light rare earth element (LREE) phosphate with Ce predominance, in silicate melts depends on numerous compositional parameters such as SiO2, CaO and P2O5 activities, oxygen fugacity, peraluminosity, and the ratios and contents of the lanthanides and actinides (Förster 1998). At low temperature (low-T) conditions of diagenesis and metamorphism monazite is generally considered unstable, and replaced by allanite or a new low-T monazite generation (e.g. Overstreet 1967; Wing et al. 2003, Rasmussen & Muhling 2007). Several studies report that monazite can crystallize under subgreenschist and low-temperature blueschist conditions (Rasmussen et al. 2001), or during diagenesis (Evans et al. 2002). Th, Ca and Y are incompatible in the monazite structure at low-T conditions (~350°C), and middle rare earth elements (MREE) occupy the structure (Rasmussen and Muhling 2009).

Two monazite populations have been described in the Belt-Purcell Supergroup : the first has detrital textures, ages >1.4 Ga, lower ΣLREE/ΣHREE, and higher ThO2 and Y contents; whereas the second has euhedral textures, ages up to ~1 Ga post-deposition, and lower ThO2 and Y, but higher ΣLREE/ΣHREE contents than detrital counterparts (González-Álvarez et al., 2006). This study presents new data for the population of secondary monazites that includes monazite-(Nd) in a sedimentary sequence associated with basinal brine activity and discusses its implications for constraining conditions during brine-rock interactions.

Geologic Setting

The Belt-Purcell Supergroup (BPS) is a Mesoproterozoic sedimentary sequence up to 17 km thick deposited in a time span of ~75 Ma that outcrops in Western Laurentia. The BPS is divided into four main stratigraphic units: (1) the lower Belt, mainly deltaic, fine-grained turbiditic facies, and carbonate-rich shallow water deposits; (2) the Ravalli Group (the Appekunny and Grinnell formations), from shallow marine to alluvial deposits; (3) the middle Belt, characterized by carbonate-rich shallow marine facies ; and (4) the Missoula Group, alluvial deposits (e.g., Whipple et al. 1997). Metamorphic grade trends from subgreenschist facies in the northeast to amphibolite facies in the lowest part of the sequence southwest due to the burial and higher heat flow produced by local plutons. Metamorphic grade is lower greenschist facies at the Red Rock canyon locality sampled for this study.

The Grinnell formation

This study focused on samples collected from the Grinnell Formation (Ravalli Group) which overlies the Appekunny Formation and is dominantly made of red and green argillites (a combination of siltite, mudstone and very fine-grained sandstone) with intermittent ~1 meter thick sandstone units (quartz-arenites, sub-arkoses and sub-litharenites).

Results

Monazite grains were analyzed using a Cameca SX-100 electron microprobe equipped with four wavelength-dispersive type spectrometers, at the Electron Microprobe Laboratory in Štátny Geologický Ústav Dionýza Štúra in Bratislava, Slovakia. The accelerating voltage was 15 kV, probe current 180 nA, and beam diameter 2-3 µm. The following crystals were used to analyse different groups of elements: (1) TAP: Al, Si, As; (2) LPET: P, Pb, Th, U, Y, S, Ca, Sr; and (3) LLIF: REE, Fe.

Microanalyses show that variations in the BSE (back-scattered electron) contrast are influenced by variations of LREE contents (mainly by La and Nd). Monazites from the Grinnell Formation (GFm) record a significant fractionation of La, Pr and Nd. In the zoned grains, the core is commonly rich in Pr, Nd, Sm and Eu, whereas the rim has higher La and Ce content (Figure 1). REE content is highly variable: (1) La2O3 ranges from 3.26 to 19.15 wt.%; (2) Ce2O3 from 12.37 to 36.02 wt.%; (3) Pr2O3 from 0.07 to 5.03 wt.%; (4) Nd2O3 from 5.17 to 30. 94 wt.%; (5) Sm2O3 from 0.01 to 6.20 wt.%; (6) Eu2O3 from 0.03 to 0.62 wt.%; (7) Gd2O3 from 0.41 to 2.44 wt.%; and (8) Yb2O3 up to 0.91 wt.%.

Most monazite grains described in this study have relative enrichment of MREE compared to published analyses of detrital monazites (e.g. González-Álvarez et al. 2006). Based on the IMA nomenclature, several monazite grains were classified as monazite-(Nd) which is the monazite with predominant Nd instead of Ce. Ratios of Nd/La and Nd/Ce for such monazite-(Nd) are >3 and ~0.8-1.6 respectively, whereas average values for monazite-(Ce) (define) are ~1 for Nd/La and ~0.4-0.5 for Nd/Ce. Monazite-(Nd) from the Grinnell Formation have Sm contents distinctly dominant over the La and Gd contents (Figure 2). The Pr/La ratio >1 is similar to the monazites-(Nd) reported by Greaser & Schwander (1987), whereas Dy and Er contents in monazite-(Ce) from the Grinnell Formation are enriched. Differences in HREE content (Dy-Yb) are negligible between the

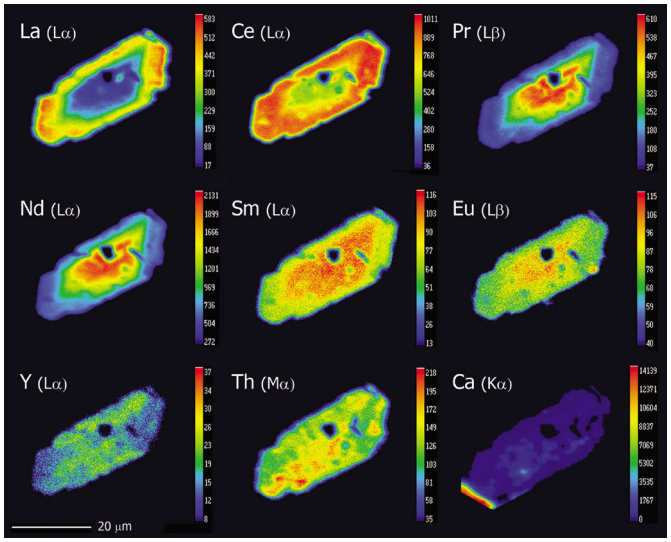

Figure 1. X-ray element maps for La, Ce, Pr, Nd, Sm, Eu, Y, Th, Ca in a strongly zoned monazite crystal from the RRC905 sample.

monazite-(Ce) and monazite-(Nd) in the analyzed grains. Y2O3 content varies from ~0.03 to 3.39 wt. % with higher content for those grains where the Nd/La ratio is ~1. In most of the grains, the ThO2 and UO2 contents are around 1.5 wt. % and below 0.5 wt. % respectively. Thorium content is always higher in the core. There is no correlation between Th and U. Pb concentration in most of the analyses is at the range of detection limit, with maximum values up to 0.79 wt.%. All these chemical features make dating of diagenetic monazite difficult or unreliable.

Discussion and Conclusions

REE minerals rich in Nd or La can be formed under strongly oxidizing conditions (Clark 1984). Ce is removed from the system by oxidation together with other elements (e.g., Fe, Al, Mn and Ti). Lack of Ce ion availability could allow other LREE or/and MREE ions present in solution to enter the monazite structure as predominant cations. This would yield a possible scenario for the formation of monazite-(Nd) enriched in MREE.

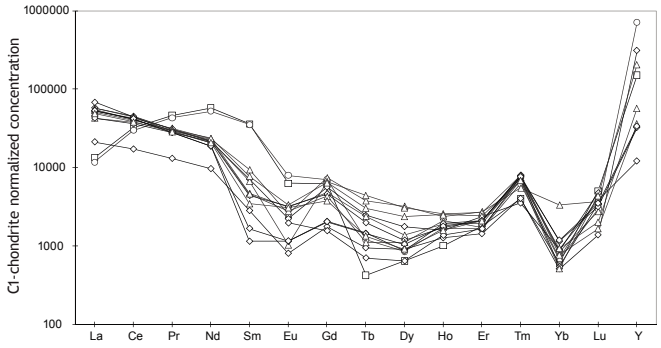

Figure 2. Monazite compositional variation diagram, showing differences between monazite-(Nd) (open circles and squares) and monazite-(Ce).

Various studies suggest that REE can be redistributed in sedimentary environments, and that growth of diagenetic monazite could be associated with diagenetic activity (e.g., Milodowski & Zalasiewicz 1991; Lev et al. 1999; Schandl et al. 2004). Protracted flow of oxidizing basinal brines preferentially through permeable units has been suggested to explain the presence of diagenetic monazite in sandstone units of the Belt-Purcell Supergroup (González-Álvarez et al. 2006). Ce, La and Nd are the first LREE removed during monazite alteration by weathering and/or hydrothermal events. Monazite Th-silicate-bearing samples show that the remnants of monazite crystals are enriched in Nd, implying that Nd remains in the monazite during its alteration (Papoulis et al. 2004). However, Poitrasson et al. (1996) showed contrasting behavior of monazite in the presence of co-existing hydrothermal fluids. The previous study described a decrease in Nd in the altered parts of the monazite compared with an increase in Th. This was interpreted to result from the higher solubility of lanthanides in the hydrothermal fluids that could be absorbed by kaolinite and dickite. Authigenic illite/smectite mixed-layer clays preferentially extract LREE relative to MREE producing a MREE-enriched fluid (Sethi et al. 1998), which may explain the lack of Ce in the fluid and preference for Nd for crystallizing monazite. Authigenic illite is widespread in the Grinnell Formation.

In the previous study of the Grinnell Formation secondary diagenetic monazite grains were distinguished and interpreted to have post-depositional chemical ages of ~1400 Ma to ~500 Ma. These monazite grains are euhedral, and display different Y, ThO_2 and LREE/HREE contents than their detrital counterparts (González-Álvarez et al. 2006). In addition, post-Belt depositional ages have been interpreted as reflecting episodic brine activity that redistributed and fractionated REE and HFSE (high field strength elements) over ~1000 Ma (González-Álvarez & Kerrich, 2010).

These observations indicate that secondary monazite cannibalized previous detrital monazite, and that the oxidizing fluids transported REEs into the sediments from an external source and redistributed these elements within the basin. González-Álvarez et al. (2006) described rims on detrital monazite in the Appekunny Formation as well as complete secondary monazites with no zonation and post-depositional ages in the same stratigraphic unit and location. This suggests that in some cases, detrital monazites were stable through recristallization stages preserving in part the detrital signature. However, complete new monazite grains co-exist with detrital monazites with no rims in the same stratigraphic units. How secondary, detrital and detrital-with secondary rims could co-exist remains an open question. Different permeabilities in the same stratigraphic unit could have been a factor, as well as local changes in the composition (Eh-pH values) of the brines carrying the REEs. A possible source of the brines could be from dissolution of evaporitic units in the Belt-Purcell sequence, which would result in alkaline fluids. Oxidizing conditions may have been attained, evidenced by CO_2 generation within sedimentary basins by reactions between clays and carbonate (Hutcheon 1989), that removed Ce. Low-T secondary monazite provides an efficient proxy to constrain the secular evolution of basinal fluids in sedimentary environments.

Acknowledgements

This research was carried out thanks to the Foundation for Polish Science "Homing" grant to M.A. Kusiak. T. Prokopiuk is thanked for his insights.

References

Clark A.M., 1984, Mineralogy of the rare earth elements, in *Rare earth element geochemistry*, ed.: Henderson P., Developments in Geochemistry, 2, 33–61.

Evans J.A., Zalasiewicz J.A., Fletcher I., Rasmussen B. & Pearce N.J.G., 2002, Dating diagenetic monazite in mudrocks: constraining the oil window? Journal of the Geological Society of London, 159, 619–622.

Förster H.J., 1998, The chemical composition of REE-Y-Th-U-rich accessory minerals in peraluminous granites of the Erzgebirge-Fichtelgebirge region, Germany, Part I: The monazite-(Ce)-brabanite solid solution series, American Mineralogist, 83, 259–272.

González-Álvarez I., Kusiak M.A. & Kerrich R., 2006, A trace element and chemical Th-U total Pb dating study in the Lower Belt-Purcell Supergroup, Western North America: provenance and diagenetic implications, Chemical Geology, 230, 140–160.

González-Álvarez I. & Kerrich, R., 2010, REE and HFSE mobility due to protracted flow of basinal brines in the Mesoproterozoic Belt-Purcell Supergroup, Laurentia, Precambrian Research, *in press*.

Graeser S. & Schwander, H., 1987, Gasparite-monazite-(Nd): two minerals to the monazite group from the Alps. Schweizerische Mineralogische und Petrographische Mitteilungen, 67, 103–113.

Lev S.M., McLennan S.M. & Hanson G.N., 1999, Mineralogic controls on REE mobility during blackshale diagenesis, Journal of Sedimentary Research, 69, 1071–1082.

Milodowski A.E. & Zalasiewicz, J.A., 1991, Redistribution of rare earth elements during diagenesis of turbidite/hemipelagite mudrock sequences of Llandovery age from central Wales, in *Developments in Sedimentary Provenance Studies,* Morton, A.C., ed,. Geoleological Society of America Special Publication 57, 101–124.

Overstreet W.C., 1967, The geologic occurrence of monazite. U.S. Geological Survey Professional Papers, 530, 1-327.

Papoulis D., Tsolis-Katagas P. & Katagas C., 2004, Monazite alteration mechanisms and depletion measurements in kaolins, Applied Clay Science, 24, 271–285.

Rasmussen B., Fletcher I.R. & Muhling J.R., 2007, In situ U-Pb dating and element mapping of three generations of monazite: Unravelling cryptic tectonothermal events in low-grade terranes, Geochimica et Cosmochimica Acta 71, 670–690.

Poitrasson F., Oelkers E., Schott J. & Montel, J.M., 2004, Experimental determination of synthetic $NdPO_4$ monazite end-member solubility in water from 21ºC to 300ºC: Implications for rare earth element mobility in crustal fluids, Geochimica et Cosmochimica Acta, 68, 2207–2221.

Rasmussen B. & Muhling J.R., 2007, Monazite begets monazite: evidence for dissolution of detrital monazite and reprecipitation of syntectonic monazite during low-grade regional metamorphism, Contribution to Mineralogy and Petrology, 154, 675–689.

Rasmussen B. & Muhling, J.R., 2009, Reactions destroying detrital monazite in greenschist facies sandstones from the Witwaterstrand basin, South Africa, Chemical Geology, 264, 311–327.

Rasmussen B., Muhling J.R., Fletcher I.R. & Wingate M.T.D., 2006, In situ SHRIMP U-Pb dating of monazite integrated with petrology and textures: Does bulk composition control whether monazite forms in low-Ca pelitic rocks during amphibolite facies metamorphism? Geochimica et Cosmochimica Acta 70, 3040–3058.

Schandl E.S. & Gorton, M.P., 2004, A textural and geochemical guide to the identification of hydrothermal monazite: criteria for selection of samples for dating epigenetic hydrothermal ore deposits. Economic Geology, 99, 1027–1035.

Sethi P.S, Hanningan R.E. & Leithold E.L., 1998, Rare-Earth Element Chemistry of Cenomanian-Turonian Shales of the North American Greenhorn Sea, Utah, in *Shales and Mudstones II,* Schieber J., Zimmerle W. & Sethi P.S., eds, Stuttgart, 195–208.

Whipple J.W., Binda P.L. & Windston D., 1997, Geologic guide to Glacier National Park, Montana and areas adjacent to Watertoon, Alberta, Belt Symposium III, in *Guidebook to the Belt-Purcell Supergroup, Glacier National Park and vicinity, Montana and adjacent Canada,* Link P.K. (ed.), Geologic Field Trip Guidebook for the Belt Symposium III, Belt Association, Pocatello, Idaho, 125–155.

Wing B.A., Ferry J.M. & Harrison, T.M., 2003, Prograde destruction and formation of monazite and allanite during contact and regional metamorphism of pelites: petrology and geochronology, Contributions to Mineralogy and Petrology, 145, 228–250.

ORIGIN AND SIGNIFICANCE OF HIGH-K SERIES AT THE ARCHAEAN-PROTEROZOIC BOUNDARY

O. Laurent[1,2,3], H. Martin[1,2,3], J.F. Moyen[2,3,4], R. Doucelance[1,2,3] & J.L. Paquette[1,2,3]

[1]Clermont Université, Université Blaise Pascal, Laboratoire Magmas et Volcans, BP 10448, F-63000 Clermont-Ferrand, France
[2]CNRS, UMR6524, LMV, F-63038 Clermont-Ferrand, France
[3]IRD, R 163, LMV, F-63038 Clermont-Ferrand, France
[4]Université Jean Monnet, Laboratoire Magmas et Volcans, Département de Géologie, 23 rue du Docteur Paul Michelon 42023 Saint-Étienne, France

Introduction

The Archaean-Proterozoic transition represents a fundamental change in the petrogenetic processes giving rise to the Earth's juvenile continental crust. During the Archaean, crustal rocks are dominated by juvenile tonalite-trondhjemite-granodiorite (TTG) series, formed by partial melting of hydrous garnet- and amphibole-bearing metabasalts. In contrast, since ~ 2.5 Ga, most of the granitoids form by recycling of older continental material; less common juvenile magmas are represented by "classical" arc series (BADR: basalt-andesite-dacite-rhyolite, or plutonic equivalents): they are generated in subduction settings by partial melting of the mantle wedge, previously hybridized by fluids coming from dehydration of the downgoing slab. This study focuses on particular late-Archaean granitoids called sanukitoids, in order to better constrain the petrogenetic changes occuring at the Archaean-Proterozoic boundary and to assess their potential geodynamic causes. Sanukitoids occur as dioritic, monzodioritic and granodioritic plutons, identified in almost all Archaean terranes throughout the world, and emplaced exclusively between 2.75 and 2.50 Ga. They share chemical features with both TTG and BADR series, suggesting that they have witnessed the evolution of the continental juvenile magmatism, from archaic to modern processes.

We specifically studied the late-Archaean (~ 2.6 Ga: Barton et al. 1994 ; Kröner et al. 1999 ; Zeh et al. 2007) Bulai pluton, a calc-alkaline batholith intrusive in the Central Zone of the Limpopo Belt in north-eastern South Africa. This composite pluton is made up of large volumes of porphyritic granodiorites with subordinate enclaves and dykes which have monzodioritic and enderbitic compositions, reminiscent of the petrography of sanukitoids. The Bulai pluton is intrusive within a complex Archaean supracrustal sequence that underwent two granulite-facies structural-metamorphic overprints, at ~ 2.65 and ~ 2.0 Ga respectively.

Sm–Nd and U–Pb data – effects of the granulite facies overprint

In the Bulai pluton, there is very little structural field evidence for subsolidus deformation, but all rocks display extensive granoblastic textures, suggesting that the thermal peak of the Paleoproterozoic (~ 2.0 Ga) metamorphic event induced annealing, almost complete for the finest-grained samples. In addition, 4 Sm–Nd internal isochrons (whole rock and separated minerals), indicate significantly younger ages (1.9–2.3 Ga) than the supposed time of emplacement of the pluton (~2.6 Ga). These results provide evidence for chemical re-equilibration and open-system conditions, at least at the grain-size scale, during the Paleoproterozoic granulite-facies overprint.

On the other hand, an external Sm–Nd isochron (10 whole-rock samples; Fig. 1) yields an imprecise age of 2729 ± 170 Ma, consistent with the magmatic age. Moreover, new U–Pb LA-ICP-MS dating on separated zircons of three samples of the Bulai pluton yielded $^{207}Pb/^{206}Pb$ ages of 2599 ± 11 Ma, 2592 ± 9 Ma and 2589 ± 12 Ma, for two granodiorites samples and one monzodioritic dyke, respectively (Fig. 1). These ages are within error of each other and in reasonable agreement with the published ages (between 2572 ± 4 Ma and 2612 ± 7 Ma: Barton et al. 1994, Kröner et al. 1999, Zeh et al. 2007), confirming that emplacement of the Bulai pluton took place between 2.58 and 2.61 Ga. No influence of the Paleoproterozoic (~ 2.0 Ga) metamorphic overprint was recorded by the zircons of the granitoids, which do not show any younger rim.

This demonstrate that while small-scale chemical and isotopic re-equilibration took place during the younger granulite-facies metamorphism, the Bulai rocks behaved as closed-systems at the sample scale, which is of primary importance to assess their petrogenesis by studying the whole-rock major-and trace-elements compositions.

Whole-rock geochemistry

The whole-rock major- and trace-element composition of the Bulai pluton has unequivocal affinities with "high-Ti" late-Archaean sanukitoids (Martin et al. 2009). It belongs to a high-K (2–6 wt.% K_2O) calc-alkaline differentiation suite, with metaluminous affinities ($0.7 < A/CNK < 1$) and relatively high Mg# (0.4–0.6). Bulai rocks are "juvenile" with ε_{Nd} ranging between -1 and 0.5. In addition, they are very rich in all incompatible trace elements; the most mafic terms (monzodioritic enclaves and enderbites) are the most enriched, with primitive mantle-normalized LILE and LREE contents up to 300. These characteristics preclude crustal involvement in the genesis of these magmas and point to an enriched mantle source for the mafic end-member of the Bulai batholith.

Chondrite normalized, REE patters are strongly fractionated ($[La/Yb]_N$ ~ 25–80), mainly due to high LREE contents (La_N ~ 250–630). The Bulai magmas, in particular the mafic ones, are also characterized by high

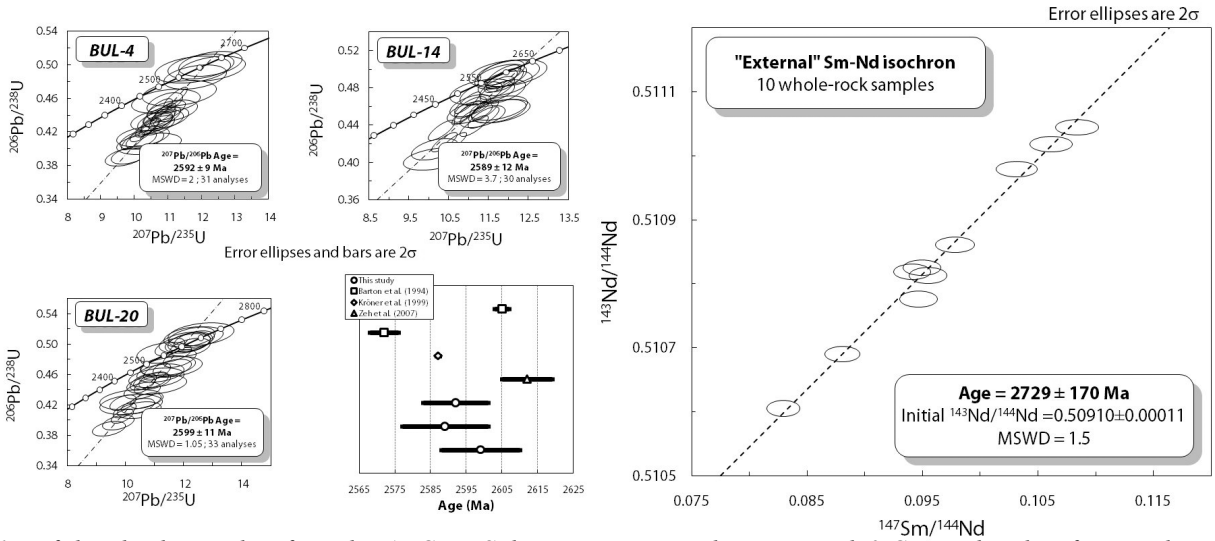

Figure 1. Left-hand side: results of U–Pb LA-ICP-MS dating on separated zircons, with 3 Concordia plots for samples BUL-4, BUL-20 (granodiorites) and BUL-14 (monzodiorite dyke). We also compared these new data with the emplacement ages obtained by Barton et al. (1994), Kröner et al. (1999) and Zeh et al. (2007). Right-hand side: Sm–Nd external isochron established with 10 whole-rock compositions. The age calculated is consistent, within error, with the emplacement ages obtained by U–Pb zircon dating.

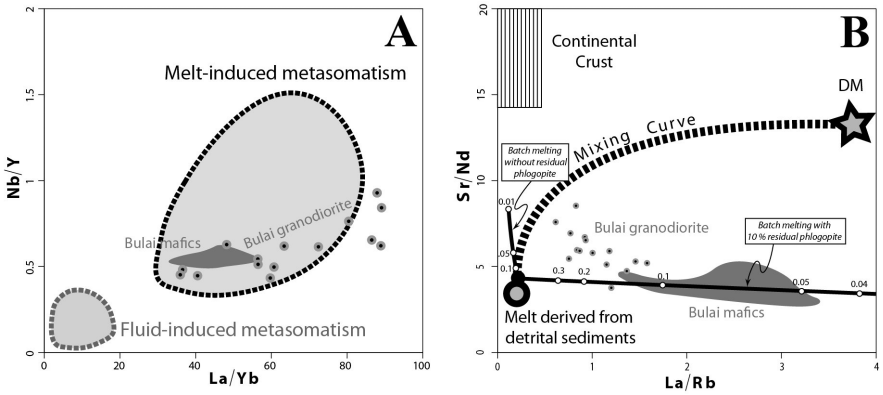

Figure 2: (A) Nb/Y vs. La/Yb diagram. The Bulai mafic facies (grey field) and granodiorites (dots) plot within the field of arc magmas which source is a melt-metasomatized mantle. Fields are from Martin et al. (2009). (B) Sr/Nd vs. La/Rb diagram. The black dot on the mixing curve represent the composition of a hybrid mantle, resulting from binary mixing of 30% melt derived from terrigenous sediments with a depleted mantle composition (DM). Melting of this hybrid composition would explain the composition of the Bulai mafics only if 10% phlogopite is present in the residue to account for high La/Rb. Also note that the granodiorite compositions plot along a rough trend pointing towards the continental crust average, suggesting that the geochemical variability of the Bulai suite result from interactions at crustal levels (AFC…). Partition coefficients are from Johnson & Plank (1999) and Adam & Green (2006).

HFSE contents (Nb ~ 15–45 ppm ; Y ~ 10–90 ppm ; up to 770 ppm Zr), such that despite rather high LILE contents, elements such as Sr (340–980 ppm) show a strong negative spike in mantle-normalized patterns. High HFSE contents and high Nb/Y, together with fractionated REE patterns indicate that the metasomatic agent is a silicic melt rather than a hydrous fluid (Fig. 2A). This is also supported by high Nb/Ta (20–34) and extreme enrichment in all trace elements in general excepted fluid-mobile elements (in particular U, Pb and Cs) which are depleted in comparison with other elements.

Petrogenesis of the Bulai pluton

The low silica mafic rocks from the Bulai derived from an enriched (metasomatized) mantle. High La/Rb, Th/Rb, Nb/Zr and low Sr/Nd (< 9) in these rocks suggest that the metasomatic agent was a felsic melt generated by melting of terrigenous sediments. Simple geochemical modeling indicates that mixing of a liquid generated by 20–30% melting of terrigenous sediments with a mantle peridotite depleted in most incompatible trace elements, in the proportions 10:90 to 35:65, generates a hybrid composition with Sr/Nd ratios in good agreement with the ones of the Bulai rocks (Fig. 2B). Melting of the resulting metasomatic mantle would produce magmas which closely match with the Bulai mafics field only if residual phlogopite is involved (Fig. 2B).

We tested this hypothesis with a more robust geochemical modeling, in the form of a Monte-Carlo-type numerical simulation where the source composition, the partition coefficients and the melting rate are randomly chosen within a determined range. The results are in good agreement with the preliminary hypothesis, as the trace elements patterns of the mafic facies of the Bulai pluton match the compositional range obtained for low-degree melting of a garnet- and phlogopite-bearing lherzolite, resulting from the interaction of a sediment-derived melt with depleted mantle in the proportion 1:2 (Fig. 3).

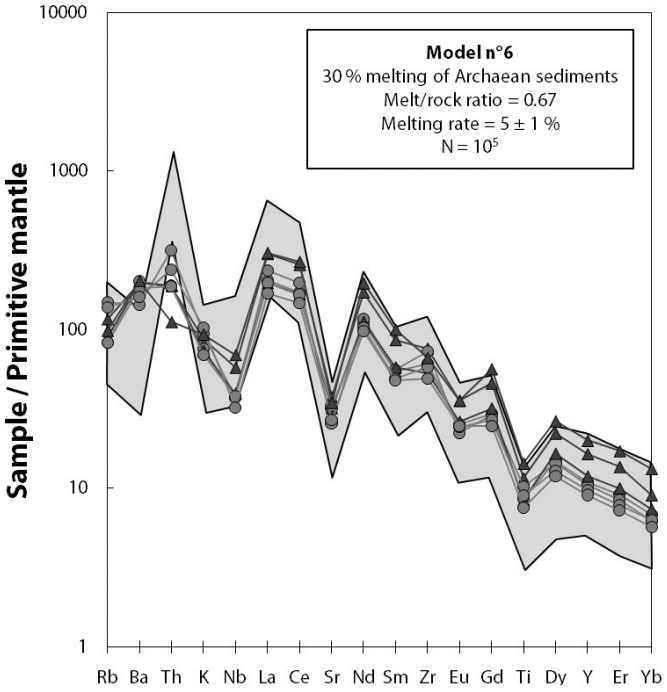

Figure 3. trace-elements pattern of the Bulai mafic enclaves (triangles) and enderbites (circles). The patterns are similar (except for Th) with the compositional range of modeled liquids derived from low degree (~ 5%) melting of a garnet- and phlogopite-bearing lherzolite, represented by the light grey field. The melt/rock ratio is the ratio between the mass fractions of sediment-derived melt and initial depleted peridotite during the metasomatic event. Partition coefficients are from Adam & Green (2006).

Therefore, the composition of the mafic facies of the Bulai pluton can be achieved by a two-stage process: 1) a liquid produced by melting of terrigenous sediment interacts with mantle peridotites; 2) Low-degree (< 10%) melting of the resulting hybrid mantle, with residual phlogopite, gives rise to the Bulai mafic magmas. Subsequent evolution of the Bulai "primary" melt at crustal levels, and possibly interactions with existing continental crust (via fractional cryustallization, remelting of underplated Bulai mafics or mixing/AFC with crustal melts) probably generated the range of observed Bulai rocks.

Discussion and conclusion

Comparison with Archaean sanukitoids s.s. and implications for continental crust petrogenesis

Based on experimental (Rapp et al. 1999) and geochemical (Martin et al. 2009) data, sanukitoids s.s. are thought to form by a similar process, with TTG-like "slab melts" interacting with the overlying mantle wedge. On the other hand, our geochemical study failed to demonstrate any significant role played by melting of subducted metabasalts; the Bulai rocks are better explained if the mantle metasomatic agent is a melt from terrigenous sediments. Interactions of such a liquid with mantle peridotites implies that the sedimentary layer is located under a mantle slice, such as a sedimentary veneer on a subducted slab. This would point to lower thermal regimes compared to "proper" Archaean sanukitoids, as metasediments melt at ~ 50 to 100°C cooler than metabasalts at slab pressures. This conclusion is supported by the fact that Bulai trace element patterns are similar to those of sub-actual potassic magmas generated in magmatic arc environments by interactions between mantle and terrigenous sediments (e.g. Sunda arc ; Elburg et al. 2002). Thus, the Bulai magmas witness the time when the temperature of the subducted slab was too cold to allow melting of the metabasaltic layer, but still hot enough to generate subsequent melts from the sedimentary veneer.

Both lines of evidence imply that the geodynamic changes that took place at the Archaean-Proterozoic transition, as recorded by sanukitoid-related rocks, are the result of progressive and global cooling of Earth. Involvement of subducted sediments is a common feature of sub-actual subduction zone settings, but not during the Archaean, although it is a more fertile lithology than metabasalts. Therefore, this also suggests that recycling of continental material within the mantle initiates roughly at the Archaean-Proterozoic transition.

Acknowledgements

This project is funded by the international program !Khure. We also wish to thank C. Bosq for support during sample preparation, and the Department of Geology of the Stellenbosch University (South Africa) for fieldwork assistance.

References

Adam J. & Green T., 2006, Trace element partitioning between mica- and amphibole-bearing garnet lherzolite and hydrous basanitic melt: 1. Experimental results and the investigation of controls on partitioning behaviour, Contributions to Mineralogy and Petrology, 152, 1–17.

Barton J.M., Holzer L., Kamber B., Doig R., Kramers J.D. & Nyfeler D., 1994, Discrete metamorphic events in the Limpopo Belt, southern Africa: implications for the application of P-T paths in complex metamorphic terrains, Geology, 22, 1035–1038.

Elburg M.A., Van Bergen M., Hoogewerff J., Foden J., Vroon P., Zulkarnain I. & Nasution A., 2002, Geochemical trends across an arc-continent collision zone: magma sources and slab-wedge transfer processes below the Pantar Strait volcanoes, Indonesia, Geochimica et Cosmochimica Acta, 66, 2771–2789.

Johnson M.C. & Plank T., 1999, Dehydration and melting experiments constrain the fate of subducted sediments, Geochemistry, Geophysics, Geosystems, 1, 1007–1033.

Kröner A., Jaeckel P., Brandl G., Nemchin A.A. & Pidgeon R.T., 1999, Single zircon ages for granitoid gneisses in the Central Zone of the Limpopo Belt, Southern Africa and geodynamic significance, Precambrian Research, 93, 299–337.

Martin H., Moyen J.F. & Rapp R.P., 2009, The sanukitoid series: magmatism at Archean-Proterozoic transition, Earth and Environmental Science Transactions of the Royal Society of Edinburgh, 100, 1–19.

Rapp R.P., Shimizu N., Norman M.D., Applegate G.S., 1999, Reaction between slab-derived melts and peridotite in the mantle wedge: experimental constraints at 3.8 GPa, Chemical Geology, 160, 335–356.

Zeh A., Gerdes A., Klemd R. & Barton J.M., 2007, Archean to Proterozoic Crustal Evolution in the Central Zone of the Limpopo Belt (South Africa-Botswana): Constraints from Combined U–Pb and Lu–Hf isotope Analyses of Zircon, Journal of Petrology, 48, 1605–1639.

GROWTH OF EARLY CONTINENTAL CRUST BY WATER-PRESENT ECLOGITE MELTING

A. Laurie & G. Stevens

Department of Earth Science, University of Stellenbosch, Matieland 7602, South Africa

Introduction

The Tonalite, Trondhjemite and Granodiorite (TTG) series of rocks are sodic granitoids which make up approximately 90% of the Archaean continental crust (e.g. Jahn et al. 1981). Consequently, studies which have focused on the petrogenesis of these rocks form the basis for our understanding of the creation of Earth's continental crust. Considerations of the major and trace element geochemistry of the high-Al type TTG (Barker & Arth 1976), indicates that these magmas form by partial melting of a slightly enriched MORB-like source (Smithies et al. 2009, Moyen et al. 2006) at pressures high enough to ensure a garnet-amphibolite or eclogitic mineralogy in the source (e.g. Drummond & Defant 1990, Rapp et al. 2003). Melting of such sources at high pressures produces the petrogenetically important features of TTG geochemistry; i.e. high Sr contents and low Nb/Ta ratios that are respectively interpreted to indicate an absence of plagioclase and the presence of rutile in the residuum (Foley et al. 2002); High La/Yb ratios interpreted to reflect a substantial fraction of garnet (>15%) in the residuum (e.g. Moyen et al. 2006). Consequently, the most commonly accepted geodynamic model for TTG genesis involves the partial melting of Archaean oceanic crust within subduction zones (e.g. Condie 1981). Other aspects of TTG geochemistry such as high average Ni and Cr contents are interpreted to reflect interaction of the magmas with the mantle wedge. These averages increase as the rocks become younger and this is proposed to reflect changes in subduction zone geometry, with the increasing subduction angle that results from cooling of the mantle during the Archaean producing deeper melting and thicker mantle wedge for the TTG magmas to traverse. Clearly, trace element geochemistry is very important in our interpretations of how TTG magmas arise. Despite this importance, few experimental studies have measured trace element compositions of TTG melts and none, to our knowledge, has measures a full suite of major, trace and REE chemistry.

In general, TTG magmas have been assumed to arise through fluid-absent partial melting and a substantial body of experimental data relevant to this process exists (see Moyen et al. 2006 for review). However, models which propose TTG formation by this mechanism in a subduction zone environment, fail to account for the substantial amount of water that must be lost from the subducting slab prior to the onset of fluid-absent melting. These fluids appear not to metasomatise the overlying mantle wedge in a fashion similar to that which occurs in Phanerozoic subduction zones, as no significant products of mantle melting (andesites and diorites) are produced concurrently with TTGs. A potential solution to this problem is to consider the possibility of TTG production by fluid-present melting, as proposed by Drummond & Defant (1990). However, relatively little good experimental data relevant to this process exists, as few studies have conducted water-present partial melting experiments on metamafic rocks within the relevant pressure range. Additional complications arise in that much of this range is above the stability limits of plagioclase, thus issues of the mineralogical appropriateness of the starting material are also raised. This study investigates the role of high pressure water-present melting of an appropriate source rock in the production of TTG melts, with the aim of characterising, as far as possible, the major, trace and REE chemistry of the melts. This requires (1) the construction of a pseudosection to constrain the mineralogy of the starting material to be used in the experiments and the details of water loss from the slab; (2) experimental investigation of the water-present melting behaviour of the appropriate high-pressure metamafic assemblages; and (3) a thermal structural model of a potential Archaean subduction, from which information on the P-T paths followed by different levels within the upper slab can be extracted.

The nature of Archaean oceanic crust and subduction process

Archaean oceanic crust is proposed to be slightly thicker than modern oceanic crust (e.g. Furnes et al. 2007) and is proposed to have a similar profile of hydration therefore the upper 3-4km are hydrothermally altered (e.g. Bickle et al. 1994). It is commonly accepted that Archaean mantle was hotter that at subsequent times (e.g. Vlaar et al. 1993), promoting a longer ridge system and several small and fast moving plates. Thus we propose that modern young and fast subduction zones are the most appropriate analogue from which conditions within Archaean subduction zones can be estimated. A thermal structural model for an Archaean subduction zone has been based on the SE Costa Rican young and fast subduction zone (Peacock et al. 2005), but with a slightly thicker oceanic crust and a hotter mantle (Fig. 1a). The resultant thermal structural model is defined by the same fundamental characteristics as the Costa Rican model, i.e. strong temperature gradients in the upper portions of the slab, while within the underlying central and lower crust; cool temperatures persist until deep within the mantle. As a result, the top of the slab follows a markedly inflected PT path characterised by a period of near isobaric heating upon progression beyond the wedge tip, following which the hottest upper portions of the slab will overly cool portions of the slab which are undergoing substantial dehydration. Migration of this slab water upwards will allow for interaction with the hot upper portions of the slab. The PT path followed

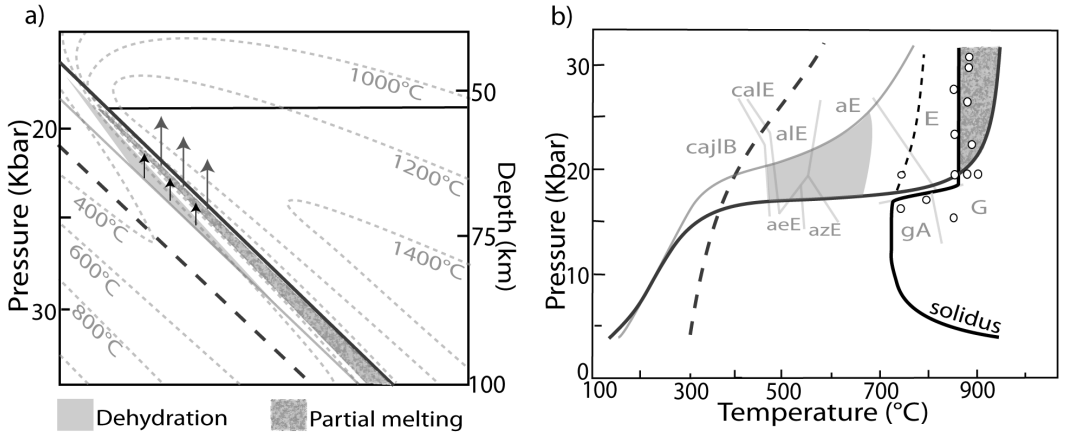

Figure 1. a) Thermal-structural model of a proposed young and fast Archaean subduction zone. The Bold lines represent the top of convecting mantle–wedge (solid black horizontal line); the top (solid) and the base (dashed) of a ~10km thick subducting Archaean oceanic crust. The solid grey line delineates 3km below the slab top, which represents the depth to which the slab is hydrated. The light grey shaded area indicates where prograde dehydration reactions release ~20molar% water. The small black arrows indicate movement of slab water. The dark grey mottled area indicates the area within the slab which is above water-present solidus temperatures, determined by this study (see (b)); and where melting of the slab will occur if water is added and quartz is not exhausted. Big grey arrows indicate movement of TTG partial melts. b) P-T diagram illustrating modelled P-T paths of subducting oceanic crust (Bold grey curves (as described in (a)) within a proposed young and fast Archaean subduction zone; the experimental runs conducted by this study (open circles); and the metamafic water-present solidus (thick black curve) which was redefined for pressures above plagioclase stability. PT paths are superimposed on a NCFMASHTO pseudosection which was produced using the DSE1 composition. Metamorphic facies abbreviations: A, amphibolite; B, blueschist; E, eclogite; G, granulite. Mineral abbreviations: a, amphibole; c, chlorite; e, epidote; g, garnet; j, jadeite; l, lawsonite; z, zoisite.

by the upper surface of the slab, in combination with a pseudosection constructed using a MORB composition (DSE1) (Fig. 1b) indicates an amphibole-eclogite or eclogite pre-anatectic assemblage. Similarly, the pseudosection predicts that the hydrated upper 3km of the slab intercept dehydration reactions where 20mol% water is released within a temperature band between 450ºC and 650ºC.

High-pressure water-present eclogite melting

Water-saturated partial melting experiments were conducted between 15 and 30kbar, and 750ºC and 900ºC (Fig. 1b), using a Holloway design non-end-loaded 10mm piston cylinder apparatus. The starting material was a Dabie Shan MORB eclogite (DSE1) with the peak metamorphic mineral assemblage: Grt + Qtz + Omp + Rt. In experiments conducted above 18kbar partial melting occurred at temperatures between 850ºC and 870ºC and the melting reaction is characterised by the breakdown of the jadeite molecule in the pyroxene: Qtz + Cpx_1 + H_2O = Melt + Cpx_2 + Grt. This study indicates that the solidus is located some 150ºC higher than the currently accepted high pressure portion of the water-present metamafic solidus (between 690ºC and 750ºC at 18kbar) (e.g. Lambert & Wyllie 1973, Liu et al. 1993), yet is at similar temperatures to the well defined lower pressure portion of this solidus, which is characterised by the haplotonalitic melting reaction: Qtz + Pl + H_2O = Melt (Johannes et al. 1993). This discrepancy is proposed to result from the fact that the previous studies have used natural volcanic rocks or low grade metamafic rock starting materials for their experiments. Consequently, these plagioclase-bearing starting materials have melted metastably. The textures and mineral compositions of the run products in this study indicate a reasonable approach to equilibrium. Consequently the solidus shifts approximately 150ºC from between 690ºC and 750ºC below 18kbar to between 850ºC and 870ºC above 18kbar. These two steep sections of the solidus in PT space are linked by a relatively flat portion where the melting reaction occurs in response to the re-emergence of plagioclase in the assemblage (Fig. 1b). Additionally, the run products which have partially melted, are characterised by good melt-residuum segregation textures**,** which are assumed to have formed as a consequence of the water-saturated nature of the experiments and the capsule design employed. This provides the unique opportunity to analyse the major, trace and RE element compositions of the melt using a combination of SEM -ED and –WD spectrometry with a cryostage to cool the sample to -180ºC during analyses, as well as laser ablation ICP-MS analyses, without having to use crushed crystalline materials as melt traps (e.g. Hermann et al. 2006).

The melts have the compositions of sodic, trondhjemites and metaluminous to peraluminous. They K_2O-poor (as a consequence of the MORB starting material) and are leucocratic with highly fractionated REE pattern and are HREE depleted. They have trace element compositions and ratios very similar to average TTG values (Fig. 2), despite being shown in previous modelling studies to be unlikely to result from melting of an eclogitic source (Foley 2002). The melts also have Ni and Cr contents (14ppm and 39ppm respectively) that are comparable to average TTG values (Ni_{ave} 14ppm and Cr_{ave}= 29ppm (Martin 1994)). This indicates that the high Ni and Cr signature of TTGs may be source-controlled and result from melting of Ni- and Cr-bearing omphacite. This challenges the notion that this aspect of TTG geochemistry indicates interaction of the magma with the mantle wedge.

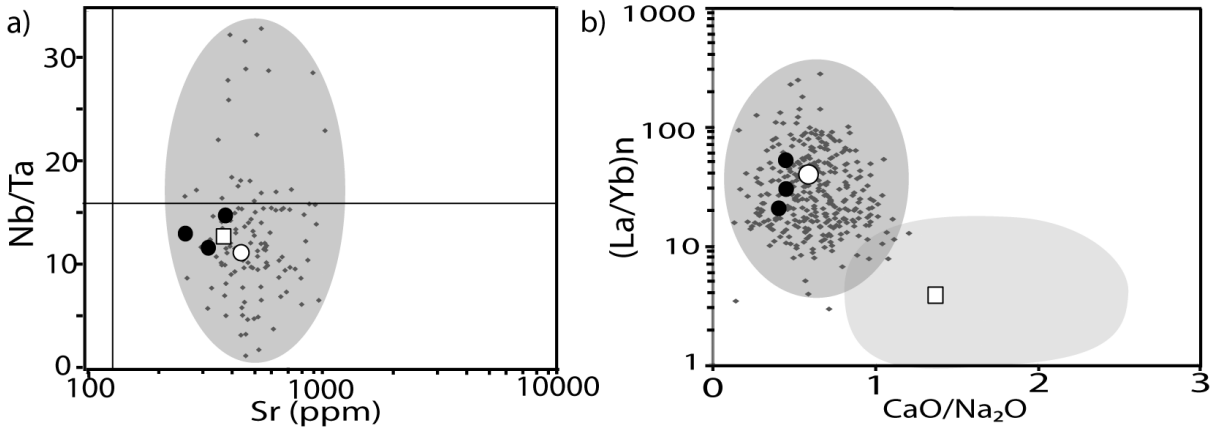

Figure 2. a) Nb/Ta ratios versus Sr contents; and b) La_n/Yb_n ratios versus CaO/Na_2O ratios of Archaean TTG gneisses (grey diamonds) compared to experimental melts produced by this study (black circles). The melts produced in this study plot within the range of Archaean TTG gneisses (grey shaded area) and are TTG-like in terms of major and trace element chemistry. Open circle = average TTG composition; open square = bulk continental crust. The intersection of the black lines indicates primitive mantle values and the light grey shaded area in b) represent arc-related calc-alkaline granitoids for reference.

Conclusions

The melts produced in this experimental study are similar to TTGs in terms of major, trace and REE chemistry. Therefore TTG magma generation by high pressure water-present melting of an eclogitic source appears to be a viable model for TTG genesis and represents an attractive alternative hypothesis to water-absent melting processes, as the process allows zones of upper-slab anatexis to function as capture sites for water released from the cooler slab. The position of the high pressure metamafic rock solidus has been experimentally redefined and has been shown to have a pronounced inflection to higher temperatures (~150ºC) at the position of the plagioclase-out reaction. This experimental result can only be achieved by using an appropriate high-pressure mineral assemblage as a starting material, as at pressures above the plagioclase-out reaction, plagioclase-bearing starting materials melt metastably at temperatures above the projection of the haplogranitic water-present solidus. The new solidus is used in conjunction with models for the likely PT paths followed by crust within an Archaean subduction zone, as well as the water release from this crust, to illustrate that fluid-present melting of the slab was likely to be an unavoidable process within the context of Archaean subduction zones, but is unlikely to occur to a significant degree in the modern Earth, even in the hottest known subduction zones. As the shape of the water-present solidus mimics the form of the PT paths followed by upper levels within the subducting slab, the viability of the anatectic process is very dependant on the temperature in the mantle wedge. Cooling of the upper mantle by only a small amount in the late Archaean acted to "turn off" water-present melting of the slab, allowing water to metasomatise the mantle wedge and induce calc-alkaline magmatism in association with volcanic arcs.

Acknowledgements

This research was supported by NRF funding to GS as part of the SARChI program. J.D. Clemens provided the DE1 starting material and J-F Moyen provided Archaean TTG database.

References

Barker F. & Arth J.G., 1976, Generation of trondhjemitic–tonalitic liquids and Archaean bimodal trondhjemite–basalt suites, Geology, 4, 596– 600.

Bickle M.J., Nisbet E.G. & Martin A., 1994, Archean greenstone belts are not oceanic crust, Journal of Geology 102, 121–138.

Condie K.C., 1981, *Archaean Greenstone Belts*, Elsevier, Amsterdam. 434p.

Drummond M.S. & Defant M.J., 1990, A model from trondhjemitetonalite-dacite genesis and crustal growth via slab melting: Archean to modern comparisons, Journal of Geophysical Research, 95, 21503–21521.

Foley S.F., Tiepolo M. & Vannucci R., 2002, Growth of early continental crust controlled by melting of amphibolite in subduction zones, Nature, 417, 837–840.

Furnes H., de Wit M., Staudigel H., Rosing M. & Muehlenbachs K., 2007, A vestige of earth's oldest ophiolite, Science, 315, 1704, DOI: 10.1126/science.1139170.

Grove T.L., Till C.B., Lev, E., Chatterjee N. & Me'dard E., 2009, Kinaematic variables and water transport control the formation and location of arc volcanoes, Nature, 459, 694–697.

Hermann J., Spandler C., Hack A. & Korsakov A.V., 2006, Aqueous fluids and hydrous melts in high-pressure and ultra-high pressure rocks: Implications for element transfer in subduction zones, Lithos, 92, 399–417.

Jahn B.M., Glikson A.Y., Peucat J.J. & Hickman A.H., 1981, REE geochemistry and isotopic data of Archaean silicic volcanics and granitoids from the Pilbara Block, western Australia: implications for the early crustal evolution, Geochimica et Cosmochimica Acta, 45, 1633–1652.

Johannes W. & Holtz J., 1996, *Petrogenesis and experimental petrology of granitic rocks*, Minerals and Rocks Series Vol. 22. xiii + 335p. Berlin: Springer-Verlag.

Lambert I.B. & Wyllie P.J., 1972, Melting of gabbro (quartz eclogite) with water excess to 35 kbar, with geological application, Journal of Geology, 80, 693–703.

Liu J., Bohlen S.R. & Ernst W.G., 1993, Stability of hydrous phases in subducting oceanic crust, Earth and Planetary Science Letters 143 (I 996) 16 1-17 1.

Martin H. & Moyen J-F., 2002, Secular changes in TTG composition as markers of the progressive cooling of the Earth, Geology, 30, 319–322.

Martin H., 1994, The Archean grey gneisses and the genesis of the continental crust., in *Archean crustal evolution*, Condie, K.C., ed, Elsevier, Amsterdam, 205–259.

Moyen J-F. & Stevens G., 2006, Experimental constraints on TTG petrogenesis: Implications for Archean geodynamics, in *Archean geodynamics and environments*, Benn, K., et al., eds, American Geophysical Union Geophysical Monograph 164, 149–175.

Peacock S.M., van Keken P.E., Holloway S.D., Hacker B.R., Abers G.A. & Fergason R.L., 2005, Thermal structure of the Costa Rica – Nicaragua subduction zone, Physics of the Earth and Planetary Interiors, 149, 187–200.

Rapp R.P., Shimizu N. & Norman M.D., 2003, Growth of early continental crust by partial melting of eclogite, Nature, 425, 605–609.

Smithies R.H., Champion D.C. & Van Kranendonk, 2009, Formation of Paleoarchean continental crust infracrustal melting of enriched basalt, Earth and Planetary Science Letters, 281, 298–306.

Vlaar N.J., van Keken P.E. & van den Berg A.P., 1994, Cooling of the Earth in the Archaean: Consequences of pressure-release melting in a hotter mantle, Earth and Planetary Science Letters, 121, 1–18.

GEOCHRONOLOGICAL AND GEOCHEMICAL STUDY OF PALAEOPROTEROZOIC GRANITIC GNEISSES AND THEIR CLINOPYROXENITE ENCLAVES FROM NW FUJIAN, SE CHINA: IMPLICATIONS FOR THE CRUSTAL EVOLUTION OF THE CATHAYSIA BLOCK

L. Li[1], M. Sun[1], Y. Wang[2], G. Xing[3], G. Zhao[1], K. Cai[1], X. Xia[1], Y.i Zhang[2] & J. Wong[1]

[1]Department of Earth Sciences, University of Hong Kong, Pokfulam Road, Hong Kong
[2]Key Laboratory of Isotope Geochronology and Geochemistry, Guangzhou Institute of Geochemistry, Chinese Academy of Sciences, Guangzhou, P.R. China
[3]Nanjing Institute of Geology and Mineral Resources, Nanjing, P.R. China

LA-ICP-MS U-Pb zircon dating of two granitic gneissic samples in northwestern Fujian Province, Southeast China gave Palaeoproterozoic to Neoarchean ages (1.9 to 2.6 Ga) for the rounded zircon cores and Palaeoproterozoic upper intercept ages (1851 ± 21 Ma, 1857 ± 29 Ma respectively) for zoned rims. These rims have oscillatory growth zoning and possess εHf values between -8.8 and +3.7 and T_{DM} model ages between 2.1 and 2.6 Ga. These granitic gneisses are peraluminous (A/CNK=0.94- 1.28), characterized by high SiO_2 (68.1-72.1 wt. %), K_2O (2.14-6.26 wt. %) and low CaO (0.98-1.65 wt. %), MgO (0.45-1.41 wt. %), FeOt (1.52-4.57 wt. %), TiO_2 (0.2-0.5 wt. %) and P_2O_5 (0.06-0.16 wt. %) contents. These samples also show relatively low REE contents and moderate LREE/HREE fractionation and display obvious negative anomalies in Nb, Ta, Sr, P and Ti. All these features indicate that the precursor magmas of these granitic gneisses were likely formed by partial melting of sedimentary rocks with a little juvenile materials input.

Clinopyroxenite enclaves are found in these granitic gneisses. These clinopyroxenites typically have high MgO (19.4~21.3 wt. %), Ni (298~412 ppm) and Cr (1411~2424 ppm), but low contents of TiO_2 (0.29~0.32 wt. %), and are characterized by high CaO/Al_2O_3 (4.1~5.3), low Al_2O_3/TiO_2 ratios (8.7~9.5) and HREE depletion which are similar to the typical features of the Al-depleted type komatiites. The geochemical characteristics of these clinopyroxenites, such as high $(Gd/Yb)_N$ and low HREE, Y, Zr and Hf, suggests partial melting of the upper mantle source with residual garnet.

The occurrence of clinopyroxenite in the granitic gneisses, combined with previous U-Pb and Nd-Hf isotopic studies for the granitic gnesisses and amphibolites in this region, provide constraints on the crustal evolution and mantle feature of the Cathaysia Block. It is therefore proposed that the Cathaysia Block was most likely formed at 1.85 Ga through granitic magma emplacement as the result of recrystallization of crustal materials derived from Palaeoproterozoic to Neoarchean sources, probably triggered by underplating of magma from the upper mantle.

Acknowledgements

The authors appreciate the assistance of X.P. Xia and X. Fu in ICP-MS and XRF analyses, M.N. Dai for Hf analysis. J.F. Gao, Y.H. He and S.H. Yang are thanked for their helpful discussion and A.M. Zhang and F.F. Zhang for help in the field. This study was financially supported by research grants from the Hong Kong Research Grant Council (HKU 7041/05), the National Nature Sciences Foundation of China (40721063, 40825009, 40830319), the Chinese Academy of Science (KZCX2-YW-128, KZCX1-YW-15-1) and the Chinese Ministry of Land and Resources (200811015). A HKU postgraduate studentship to Longming Li is gratefully acknowledged.

References

Xu X.S., O'Reilly S.Y., Griffin, W.L., Wang, X.L., Pearson, N.J. &, He, Z.Y., 2007, The crust of Cathaysia: Age, assembly and reworking of two terranes, Precambrian. Research, 158, 51–78.

Wan Y.S. Liu D.Y., Xu M.H., Zhuang J.M., Song B., Shui Y.R. & Du L.L., 2007, SHRIMP U-Pb zircon geochronology and geochemistry of metavolcanic and metasedimentary rocks in Northwestern Fujian, Cathaysia Block, China: Tectonic implications and the need to redefine lithostratigraphic units, Gondwana Research,12, 166–183.

Zhuang J.M., Huang Q.Z., Deng B.Z., Guo B.& Jie Y.J., 2000, Study on the subdivision of units of lithology and stratum of Precambrian metamorphic rocks in Fujian Province, Publishing House of Xiamen University, Xiamen. 1–94. (in Chinese)

Ma J.Q., 2002, Discussion on some fundamental geology problems and their studying orientation, Fujian Province, Geology of Fujian, 4, 200–205. (in Chinese with English abstract)

THE PGE BUDGET OF THE KAAPVAAL AND KARELIAN SUB-CONTINENTAL LITHOSPHERIC MANTLE

W.D. Maier[1], P. Peltonen[2], I. McDonald[3], S.J. Barnes[4], S-J. Barnes[5], C. Hatton[6] & F. Viljoen[7]

[1]Department of Geosciences, University of Oulu, Linnanmaa, 90014 Oulu, Finland.
Geological Survey of Finland, Betonimiehenkuja 4, Espoo 02151, Finland.
[3]School of Earth, Ocean & Planetary Sciences, Cardiff University, Cardiff CF10 3YE, UK
[4]CSIRO, 26 Dick Perry Ave., Kensington 6151, WA, Australia.
[5]Sciences Appliques, Université du Québec à Chicoutimi, Chicoutimi G7H 2B1, Qc, Canada.
[6]Council for Geoscience, Private Bag X112, Pretoria 0001, South Africa
[7]Department of Geology, University of Johannesburg, Auckland Park 2006, South Africa

Introduction and analytical procedure

The Kaapvaal craton represents the best studied cratonic nucleus on Earth, owing to an abundance of mantle xenoliths in kimberlites. Study of mantle xenoliths from the Karelian craton has begun during the last decade, after the discovery of several diamondiferous kimberlites (Peltonen et al., 1999). Many mantle xenoliths derived from the Kaapvaal and Karelian sub-continental lithospheric mantle (SCLM) are depleted in basaltic components (e.g. Al_2O_3, CaO, Sc). Based in part on Re/Os studies, this has been modeled by predominantly Archean extraction of komatiitic magma (Boyd, 1989; Griffin et al. 2009; Walker et al., 1989; Peltonen et al., 2003). Subsequently, the SCLM of both cratons has seen multiple episodes of refertilisation with LREE-LILE enriched fluids and/or alkaline basaltic and kimberlitic melts of asthenospheric and lithospheric derivation (Erlank et al., 1987; Peltonen et al., 1999).

One of the problems in constraining the origin of the SCLM is that our knowledge of its composition is almost entirely based on xenoliths brought to surface by kimberlite, and the assumption that such xenoliths are representative of the craton as a whole. Moreover, relatively few (<60) Kaapvaal xenoliths have been analysed for the complete PGE spectrum, mostly from Premier (Maier et al., 2005) and Lesotho (Pearson et al., 2004). In the present study, we aim to establish whether it is possible to produce a representative average PGE composition of the Archean SCLM of the Kaapvaal craton. This could potentially allow us to constrain any potential secular variation in the composition of the mantle (c.f. Maier et al., 2009). We have thus determined whole rock PGE contents of more than 103 xenoliths from 15 kimberlite pipes on the Kaapvaal craton. In order to evaluate inter-cratonic PGE variability we have also determined PGE in 20 xenoliths from 5 pipes in the Karelian craton. The PGE in most Kaapvaal samples were determined by ICP-MS after nickel sulfide fire assay and tellurium co-precipitation at Cardiff University. The PGE in the samples from Gibeon, Lesotho, and Premier were analysed by the same method, but at the Geological Survey of Finland. It has been suggested that the Ni-sulfide collection method underestimates Pt and Ir values by approximately 15 relative percent (Lorand et al., 2008), but this has been disproved recently (Savard et al., in press).

Results

The samples have highly variable concentrations of Pt and Pd, but average Pt and Pd contents of the peridotites are similar in both cratons examined and they also show considerable similarity with SCLM peridotites from the Slave craton (Irvine et al., 2003). In most Kaapvaal and Karelian peridotites Pt and, in particular, Pd is strongly depleted relative to the IPGE. Average Pt/Pd ratios in the samples are twice those of PUM (Pt/Pd = 2.2 - 2.3, vs 1.07 in PUM), but in our Lesotho xenoliths Pt/Pd is much higher. Rhodium is less depleted relative to PUM than Pt and Pd. All PPGE are depleted relative to shallow mantle rocks (basalt-borne xenoliths) and modern orogenic peridotites. The concentrations of the IPGE in our xenoliths are equally highly variable (Fig. 1), but on average these elements occur in similar concentrations in the Kaapvaal and Karelian (and Slave) cratons, and modern primitive mantle. Amongst the few Kaapvaal and Karelia samples with higher Ir and Ru contents than PUM, most are from Jagersfontein (Fig. 1). Several samples have negative Ru anomalies, and a small number are highly depleted in all PGE (< 0.1 x PUM). The correlation between PGE and indices of melt depletion (i.e. Al_2O_3) is poor. This may be due to contamination with host kimberlite or mantle metasomatism by silicate and/or sulfide melt (Pearson et al., 2004; Maier et al., 2005). We found no systematic variation in PGE contents and distribution patterns between xenoliths from Group 1 and Group 2 kimberlite pipes, or between on-craton and off-craton (Gibeon, Markt, Melon Wold) localities.

Review of previous work

Past PGE studies on mantle xenoliths from the Kaapvaal and other cratons showed a pattern of distinct depletion in Pt and Pd, and to a lesser degree Rh, relative to the IPGE (Os-Ir-Ru) and primitive mantle values (e.g. Pearson et al., 2004; Maier et al., 2005). The data were interpreted to reflect incompatible behaviour of Pt, Pd and, somewhat less so, Rh, during mantle melting, and compatible behaviour of the IPGE. The IPGE and Rh are largely hosted by monosulfide solid solution (mss) included within olivine, whereas Pt and Pd tend to be mainly hosted by interstitial Cu-rich sulfides (Alard et al. 2001). The mss may represent residual sulfide shielded from dissolution during mantle melting by the olivine, whereas the Cu sulfides crystallized from metasomatic fluids/melts.

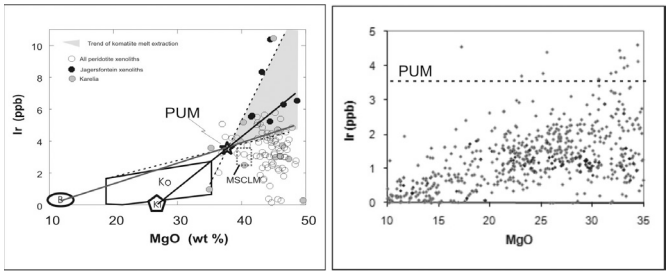

Figure 1a: Iridium and Ru contents of Kaapvaal and Karelian mantle xenoliths, plotted vs MgO. Extraction of basaltic (B) or komatiitic (Ko) magma results in Ir and Ru contents higher than PUM. Refertilisation with basalt or kimberlite (K) can lower Ir and Ru contents, but results in lower than observed MgO contents. MSCLM=modern sub-continental mantle. b: PGE contents in terrestrial basalts and komatiites. See text for explanation. Data from Barnes and Fiorentini (2008) and Maier et al. (2009).

Modelling of melting of sulfide-bearing mantle (e.g. Mungall 2007) suggests that much of the variance in PPGE abundance in the mantle restite occurs within a critical melting range, corresponding to the final disappearance of sulfide. Hence, there should be a broadly bimodal "all or nothing" distribution of PPGE contents of mantle samples, ranging from those with close to their original endowment, representing samples containing residual sulfide but largely independent of how much, to those highly depleted in Pt and Pd representing complete extraction of the sulfide component. IPGE variation in mantle restites should be more complex, and more sensitively dependent on degree of mantle melting, depending on the degree to which the IPGE-rich MSS is shielded by unmelted olivine. This combination of factors leads to the observed patterns of wide continuous variation in IPGE, coupled with discontinuous wholesale depletion of PPGE.

It remains puzzling why there are no terrestrial magmas with IPGE contents higher than PUM. Such magmas should have formed in response to high degree melting and complete dissolution of mantle sulfides. In general, it is our impression that quantitative modeling of PGE behaviour during melting and refertilisation of the SCLM has so far been moderately successful, partly because the nature of the metasomatic agents (particularly their PGE contents) and the high pressure D values of the PGE (Righter et al., 2008) remain incompletely understood, because of retention or entrainment of refractory IPGE-rich pahses, and because multiple events of melting and refertilisation that occurred over a span of 3 billion years are difficult to unravel. An alternative approach to improve the understanding of the petrogenesis of the mantle consists of compiling the bulk composition of the mantle (e.g. Becker et al. 2006). Their estimate differs from previous estimates mainly in that it has almost twice the amount of Pd (~7 as opposed to ~4). It has recently met with some sceptisism (e.g. Lorand et al., 2008) on the grounds that mantle samples may have had their PGE (particularly PPGE) contents modified by processes of mantle metasomatism.

PGE mass balance of the SCLM

We want to take a step back and examine whether a purely mass balance approach can provide some constraints on the PGE budget of the Archean (i.e. rather than the modern) mantle. Maier et al. (2009) suggested that the early Archean mantle had lower PGE contents than the modern mantle. If this were true, then PUM estimates would be of limited use in constraining core-mantle differentiation. Knowledge of the composition of the Archean mantle comes mainly from SCLM derived xenoliths, and interpreting these samples is more complicated than modern samples of oceanic mantle because the former underwent much longer and more complex melting and refertilisation histories that may have affected their PGE contents. In order to gain as representative a composition as possible the sample population has to be large, and we also have to consider the composition of Archean mantle derived magmas (Fig. 2).

The two most important results of our study may be summarised as following: *Firstly*, the modern mantle (as represented by PUM estimates) and most mantle-derived magmas have Pt/Pd approximately at unity, yet our SCLM xenoliths have average Pt/Pd significantly above unity. In other words, there is a mass balance mismatch between the potential starting composition, the extracted magmas and the residues. Three possible explanations may be considered. (i) The Archean mantle may have had Pt/Pd ratios > 1 (i.e. different to modern mantle), and thus partial melts with Pt/Pd around unity that were produced by relatively more compatible behaviour of Pt could produce residues with Pt/Pd above unity. (ii) The Archean mantle, the partial melts, and the residues all had Pt/Pd at unity, but Pt was reintroduced into the mantle by metasomatising alkaline magmas, potentially enriched in Pt and Au (McInnes et al., 1999). However, the source of the Pt remains enigmatic as a complimentary Pt depleted crustal reservoir is not known. (iii) Palladium could have been preferentially removed from the mantle by S undersaturated fluids or melts, whereas Pt and Au were preferentially retained in refractory alloys (Alard et al., 2000). However, we know of no complimentary, sufficiently large crustal reservoir that is pervasively enriched in Pd.

Secondly, the average IPGE contents of the Kaapvaal and Karelian (and Slave) SCLM are broadly similar to PUM (Fig. 1). This result is particularly remarkable because basaltic and komatiitic magmas contain IPGE contents systematically and significantly below PUM (Fig. 2), due to the compatible behaviour of the IPGE during mantle melting. As a result, IPGE contents in residual mantle samples should be higher than in PUM, no matter how complex the melting and refertilisation history of the mantle was. Several possible explanations may be considered to explain this mismatch. (i) Most of our samples represent mantle that has been refertilised by alkaline or basaltic melts. If these magmas were IPGE poor, as expected for small degree melts, this could have led to dilution of IPGE contents. However, significant resetting would require introduction of tens of percent of metasomatic material, inconsistent

with the relatively high MgO contents of the samples (Fig. 1). (ii) The missing IPGE of the SCLM could be hosted in chromite pods that were disaggregated during kimberlite ascent. However, chromite control of the IPGE is inconsistent with the lack of correlation between Cr and IPGE in our samples. (iii) Some of the more IPGE depleted samples could represent cumulates from magmas ascending through the mantle (Niu et al., 1997), or from the oceanic lithosphere subsequently accreted to the craton roots (Peltonen et al., 1999; Canil and Lee, 2009). (iv) The SCLM could represent buoyant residues of originally more fertile mantle residues from which Fe-rich components had segregated gravitationally (Arndt et al., 2009). However, it is not apparent why the IPGE would be preferentially concentrated in the more Fe rich component. (v)The Archean mantle could have been depleted in IPGE relative to modern mantle. This model is consistent with low PGE contents in early- to mid Archean komatiites from the Kaapvaal and Pilbara cratons (Maier et al., 2009), possibly due to the length of time rerquired for refertilisation of the mantle with late veneer. (vi) The present PUM estimate could be too high. This is suggested by the fact that the IPGE contents of modern sub-oceanic mantle, as sampled by orogenic peridotite massifs, are also lower than expected from melt residues; Many oceanic peridotites are residues of ca 8-18% melting of MORB basalt (Lorand et al. 2008) and thus, if the IPGE behaved in a compatible manner, the peridotites should have ca 10-20% higher IPGE contents than PUM. The observed levels are slightly below PUM (Fig. 1) suggesting that current PUM estimates of the IPGE are ca. 10-20% too high. The mass balance mismatch is less significant than in the case of the Archean mantle, but larger than analytical error.

Griffin et al. (2009) recently argued that kimberlites preferentially sample refertilised and thus non-representative sections of the sub-continental lithospheric mantle. If this were true then our estimate of the composition of the SCLM would be erronous. The model of Griffin et al. (2009) can be tested by a detailed examination of PGE contents in the Jormua ophiolite of Finland, believed to represent a contiguous sub-continental mantle section (Peltonen et al. 2003). This work is in progress, with preliminary data from more than 20 samples showing broadly similar PGE concentration patterns as the Karelian and Kaapvaal xenoliths.

Summary

PGE data from more than 120 samples of kimberlite-hosted mantle peridotite xenoliths indicate that the SCLM contains significantly lower Pt and Pd contents than the presently accepted PUM estimate, and broadly similar IPGE contents. The Pt and Pd depletion can largely be explained by the incompatible behavior of these elements during mantle melting with complete consumption of sulfides. In contrast, experimental results and data from terrestrial mantle-derived magmas indicate that the IPGE behave in a compatible manner during mantle melting. Therefore, these elements should be significantly enriched in mantle residues. The mismatch is consistent with a relatively PGE depleted Archean mantle resulting from sluggish refertilization with late veneer. Alternatively, many SCLM samples could represent cumulates.

References

Alard O., et al., 2000, Nature, 407, 891–894.
Arndt N.T., et al., 2009, Lithos, 109, 61–71.
Barnes S.J. & Fiorentini M.L., 2008, Chemical Geology, 257, 44–58.
Becker H., et al., 2006, Geochimica et Cosmochimica Acta, 70, 4528–4550.
Boyd F.R., 1989, Earth and Planetary Science Letters 96, 15–26.
Canil D., Lee C-T.A., 2009, Geology, 37, 667–670
Erlank A.J., et al. 1987., in Mantle metasomatism, Hawkesworth C.J. & Menzies M.A., eds, Academic Press, London, 221–311.
Griffin W.L., et al., 2008, Journal of Petrology, 50, 1185–1204.
Irvine G.J., et al., 2003, Lithos, 71, 461–488
Lorand J.-P., et al., 2008a, Chemical Geology, 248, 174–194.
Lorand J.-P., et al., 2008b, Elements, 4, 247–252.
Maier W.D., et al., 2005. South African Journal of Geology, 108, 413–428.
Maier W.D., et al., 2009, Nature, 460, 620–623.
Mungall J.E., 2007, in The Crust, *Treatise on Geochemistry* Volume 3, Rudnick R., ed, Chapter 21. Elsevier, 1–33.
Niu Y., et al., 1997, Earth and Planetary Science Letters, 152, 251–265.
Pearson D.G., et al., 2004, Chemical Geology, 208, 29–59.
Peltonen P., et al., 1999, in Proceedings of the 7th International Kimberlite Conference, Gurney J.J., et al., eds, 664–676.
Peltonen P. ,et al., 2003, Geology, 31, 645–648.
Righter, K. et al. 2008. Nature Geoscience.
Walker R.J., et al., 1989, Geochimica et Cosmochimica Acta 63, 1583–1595.

IMPLICATIONS OF CARBON DIOXIDE INCLUSIONS IN JACK HILLS ZIRCONS

M. Menneken[1], T. Geisler[1,2], A.A. Nemchin[3], B. Gasharova[4] & M. Grange[3]

[1]Institute für Mineralogie, Westfälische Wilhelms-Universität Münster, Corrensstraße 24, 48149 Münster, Germany
[2]Mineralogie, Department für Geowissenschaften, Universität Hamburg, Grindelallee 48, 20146 Hamburg, Germany
[3]Western Australian School of Mines, Curtin University of Technology, Bentley, Western Australia, 6102, Australia
[4]ANKA, Karlsruhe Institut of Technology, Institut für Synchrotronstrahlung, Hermann-von-Helmholtz-Platz 1, 76344 Eggenstein-Leopoldshafen, Germany

Introduction

Unravelling Earth's earliest evolution has been mainly based on detrital zircon grains from Jack Hills, Western Australia, since grains of Hadean age were discovered in 1986 by Compston & Pidgeon. About 10 % of the detrital zircon population is of Hadean age (e.g. Pidgeon & Nemchin, 2006), with the oldest grain so far discovered, being as old as 4.4 Gyr (Wilde, 2001). Jack Hills zircons therefore are the oldest preserved vestige of Earth. As they do not represent complete rocks, conclusions about their host rock have to be drawn by isotope chemistry, crystal chemistry, morphology, mineral inclusions, and internal structures of these individual zircon crystals.

So far, quartz, K-feldspar, plagioclase, chloritised biotite, chlorite, amphibole, apatite, monazite, xenotime and rutile have been identified (Maas et al. 1992, Peck et al. 2001, Menneken et al. 2007). Most of these phases have been reported to occur as polyphase inclusions. As inclusions in minerals are supposed to represent the composition of the melt or fluid they crystallized from, this inclusion assemblage suggests a granitic origin. However, the additional identification of diamond and graphite inclusions in zircons of all age groups is not consistent with a magmatic origin. Here we report the identification of CO_2 inclusions in Jack Hills zircon grains. Their discovery may shed new light on the origin of the diamond and graphite inclusions and therefore also on the origin of the Jack Hills zircon grains themselves.

Methods

An Yvon Jobin HR800 Raman spectrometer has been used to identify inclusions. CO_2 inclusions were identified by two intense Raman bands near 1289 and 1392cm^{-1} (called Fermi diad, Fig. 1). The exact position and the frequency difference Δ of the upper and lower band of the Fermi diad depends on the internal pressure of the inclusion. We used the experimental calibration of Yamamoto & Kagi (2006) to convert Δ values to the CO_2 density. In one zircon we have mapped the distribution of CO_2 inclusions by synchrotron infrared spectroscopy at the ANKA beamline in Karlsruhe, Germany.

The internal growth texture of the host zircons was visualized by cathodoluminecence (CL) imaging and individual growth zones were dated by sensitive high-resolution ion microprobe (SHRIMP) or laser ablation inductively-coupled plasma mass-spectrometry (LA-ICP-MS). Their Ti concentration was additionally measured by SHRIMP and LA-ICP-MS to be able to apply the Ti-in zircon thermometer (Watson & Ferry, 2007).

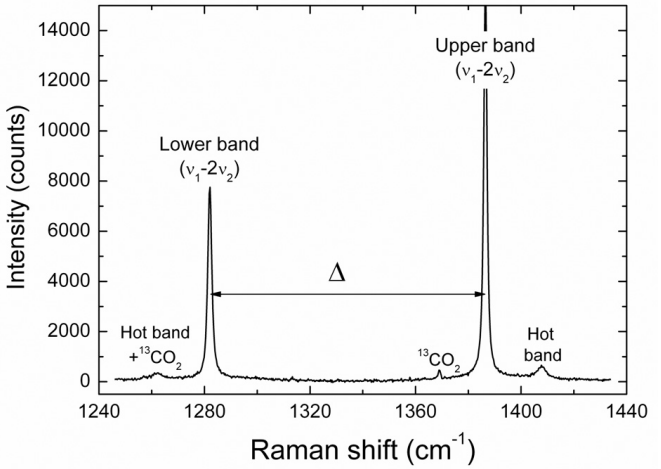

Figure 1. Raman spectra of a CO_2 inclusion. The width Δ between the Fermi diad was used to calculate the internal pressure of the CO_2 inclusions.

Results

Until now we could identify inclusions of CO_2 in five zircon grains from Jack Hills. One grain contains more than 30 identified CO_2 inclusions, of which one also contains some O_2. Additionally, traces of N_2 have been detected in one inclusion of another grain. No other fluid or gas species could be identified in any of the grains so far. We also identified apatite, quartz, and diamond/graphite (grain JH15-142, Menneken et al. 2007) in some of these zircon grains. The CL images of the host zircons reveal a variety of internal growth textures such as oscillatory and sector zoning as well as chaotic and banded textures, crosscutting primary growth zones. One grain exhibits some brighter CL zones along empty inclusion trails, which were opened in the process of polishing and might have contained even more CO_2 inclusions. The U-Pb ages of the CO_2-bearing zircon grains cluster between 3.4 Ga and 3.6 Ga, except for grain JH15-142 that yielded two different $^{206}Pb/^{207}Pb$ ages of ca. 3.9 and 4.1 Ga (Menneken et al. 2007). This grain yielded the highest Ti-in-zircon temperatures of up to 869 ± 10°C. All other grains give temperatures between 650 and 720°C, in agreement with previous results (Watson & Harrison 2005). The densities of the CO_2 inclusions obtained from the Δ values vary from 0.33 g/cm³ up to 1.08 g/cm³.

Discussion and conclusion

According to Roedder (1984) inclusions can be used directly to determine the conditions that prevailed at the time of host mineral growth, if

1. the fluid trapped upon sealing of the inclusion was a single, homogeneous phase,

2. the cavity in which the fluid is trapped does not change in volume after sealing,
3. nothing is added or lost from the inclusion after sealing,
4. the effects of pressure are insignificant or are known, and
5. the origin of the inclusion is known.

Although we could not detect any traces of H_2O in none of the investigated inclusions, the identification of additional O_2 by its Raman band at 1555 cm^{-1} in one inclusion indicates the initial presence of H_2O, as to our knowledge O_2 can only be produced by hydrolysis of H_2O due to gamma radiation, possibly resulting from U and Th decay in the host zircon. The resulting H_2 and the primary H_2O could have been diffused out of the inclusion (rule 3), since hydrogen species disappear more easily than carbonic ones during post-metamorphic annealing (Touret, 2000), which usually leads to a relative enrichment of CO_2 in H_2O-CO_2 composite inclusions. Furthermore, it has to be taken into consideration that the volume of the inclusion might have changed after trapping (rule 2). Whereas the uplift of the host grain will have resulted in relaxation of the crystal structure, the resulting volume change, which is not very large due to the low compressibility of zircon, might have been balanced by the swelling of the zircons crystal structure due to metamictisation. However, a large density increase as a result of zircon metamictisation is relatively unlikely, since the Raman spectra of the host zircons do not indicate a high degree of metamictisation. It is therefore safe to assume that the actual measured densities of the CO_2 inclusions represent minimum densities.

To be able to deduce the *P-T-t* conditions of primary zircon growth or zircon re-equilibration by using the densities of the CO_2 inclusion obtained by Raman spectroscopy, the Ti-in-zircon temperature, and the U-Pb age, the CO_2 inclusions have to be located in the same growth zone from which the U-Pb age and the Ti temperature was obtained from. However, some CO_2 inclusions are aligned along distinct healed cracks that are visible by bright CL bands along the cracks. Since these zones are less than 2 µm thick, U-Pb- or Ti measurements of these areas was not possible. Nevertheless, for most host zircon grains we could relate the U-Pb and Ti-data to zones where their CO_2 inclusions are located. An example is shown in Fig. 2, where a single CO_2 inclusion, showing a negative zircon crystal shape, is located in a zircon that shows oscillatory and sector zoning.

Those densities of the inclusions that could clearly be linked to zircon data vary from 0.42 g/cm³ up to 0.95 g/cm³. Using the Ti in zircon temperatures, minimum pressures of zircon crystallisation between 1.0 – 4.7 kbar

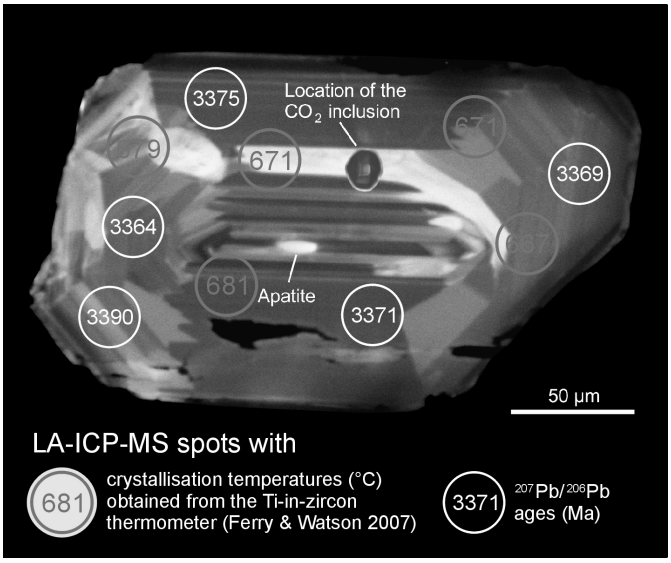

Figure 2. Cathodoluminescence image with U-Pb-ages and Ti-in-zircon temperatures of grain JH21-1 obtained by LA-ICPMS and a superimposed transmitted light image of its CO_2 inclusion.

at temperatures of about 700 °C were estimated using the equation of state of CO_2 (Span & Wagner, 1996). These *P-T* estimates correspond to amphibolite to granulite facies conditions. Granulites are well known to contain fluid inclusions of pure CO_2 (Touret, 2009). However, CO_2-rich inclusions can be found in all metamorphic grade rocks, in lower grade rock (greenschist facies) almost exclusively along major shear zones, in higher grades above the beginning of migmatites melting, with a sudden and marked increase when entering the granulite domain (Touret, 2000). Present day granulite facies conditions can be found in the lower continental crust. In many granulites, the oxygen fugacity conditions derived from compositions of Ti-Fe oxides are within the graphite stability field (Touret, 2009, and references therein). This is consistent with the identification of graphite inclusions in Jack Hills zircons (Menneken et al. 2007). However, graphite in granulites seems to remain exceptional.

Until now, fluid inclusions have not been reported in zircon grains from Jack Hills. This is most likely due to the main use of X-ray micro-analyses to identify inclusions in most cases. However, this could also indicate that the zircon grains from different samples from the Jack Hills metaconglomerate differ in their inclusion mineralogy. This would be in agreement with the fact that we could not identify CO_2 in all zircon mounts investigated so far.

Acknowledgements

We acknowledge financial support from the Deutsche Forschungsgemeinschaft through grant GE1094/14-1.

References

Compston W. & Pidgeon R.T., Jack Hills, evidence of more very old detrital zircons in Western Australia, Nature, 321, 766–769.

Ferry J.M. & Watson E.B., 2007, New thermodynamic models and revised calibrations for the Ti-in-zircon and Zr-in-rutile thermometers, Contributions to Mineralogy and Petrology, 154, 429–437.

Maas et al., 1992, The Earth's oldest known crust: A geochronological and geochemical study of 3900-4200 Ma old detrital zircons from Mt. Narryer and Jack Hills, Western Australia, Geochimica et Cosmochimica Acta, 56, 1281–1300.

Menneken, M., et al. 2007, Hadean diamonds in zircon from Jack Hills, Western Australia, Nature 448, 917–920.
Peck W.H., Valley J.W., Wilde S.A. & Graham C.M., 2001, Oxygen isotope ratios and rare earth elements in 3.3 to 4.4 Ga zircons: Ion microprobe evidence for high $\delta^{18}O$ continental crust and oceans in the Early Archean, Geochimica et Cosmochimica Acta, 65, 4215–4229.
Pidgeon R.T. & Nemchin A.A., 2006, High abundance of early Archaean grains and the age distribution of detrital zircons in a sillimanite-bearing quartzite from Mt Narryer, Western Australia, Precambrian Research, 150, 201–220.
Roedder E, 1984, *Fluid inclusions. Reviews in Mineralogy, volume 12*, Mineralogical Society of America, Washington.
Span R. & Wagner W., 1996, A new equation of state for carbon dioxide covering the fluid region from the triple point temperature to 1100 K at pressures up to 800 MPa, Journal of Physical and Chemical Reference Data, 25, 1509–1596.
Touret J.L.R., 2000, Fluids in metamorphic rocks, Lithos, 55, 1–25.
Touret J.L.R., 2009, Mantle to lower-crust fluid/melt transfer through granulite metamorphism, Russian Geology and Geophysics, 50, 1052–1062.
Wilde S.A., Valley J.W., Peck W.H. & Graham C.M., 2001, Evidence from detrital zircons for the existence of continental crust and oceans on the Earth 4.4 Gyr ago, Nature, 409, 175–178.
Yamamoto J. & Kagi H., 2006, Extended micro-Raman densimeter for CO2 applicable to mantle-originated fluid inclusions, Chemistry Letters, 35, 610–611.

LITHOSPHERIC CONTROLS ON THE LOCALIZATION OF KOMATIITE-HOSTED NICKEL-SULFIDE DEPOSITS

D.R. Mole[1], M. Fiorentini[1], N. Thebaud[1], C. McCuaig[1], K.F. Cassidy[1], S.J. Barnes[2], E.A. Belousova[3], I. Mudrovska[1] & M. Doublier[4]

[1]Centre for Exploration Targeting, University of Western Australia, 35 Stirling Highway, Crawley, 6009, Western Australia
[2]CSIRO Earth Science & Resource Engineering, 26 Dick Perry Ave, Kensington WA 6151, Australia
[3]Centre for Geochemical Evolution and Metallogeny of Continents, Macquarie University, Macquarie, NSW 2109, Australia
[4]Geological Survey of Western Australia, 100 Plain Street, East Perth, WA 6004, Australia

Introduction

Since the nickel boom of the 1960s, research into komatiite-hosted nickel sulphide systems has focused on the deposit and mine-scale environment (e.g. Gresham & Loftus-Hills, 1981; Beresford et al. 2002). This has led to a greater understanding of the geochemical, physical and stratigraphic interactions favourable to the formation of nickel sulphide systems. However, very few projects have looked at komatiite systems on a regional-craton scale. In this project, we look to investigate how geotectonic setting, nature of the lithosphere and 4D lithospheric architecture affect the characteristics and prospectivity of komatiites in the Archaean greenstone belts of the South Yilgarn, and how these interactions may localise komatiite systems to form large, world-class Ni deposits or 'camps'.

The importance of early lithospheric architecture on the formation and evolution of a terrane has been highlighted in recent studies by Champion & Cassidy (2007), Foley (2008) and Begg et al. (2009). Champion & Cassidy (2007) used an integrated isotopic (Sm-Nd), geochemical and geochronological approach to constrain the 4D history of the Yilgarn craton. This project takes this work further by using LA-ICP-MS Lu-Hf analyses and U-Pb SHRIMP dating to document lithospheric evolution through time. This method, based on the Terrachron® technique (Griffin et al. 2004) developed at GEMOC, is innovative as it creates a number of 'time-slices' which represent the Lu-Hf lithospheric architecture at a given time period. The study area for this project comprises the south-central Yilgarn Craton, from the Marda region in the north down to Ravensthorpe, including the western region of the Eastern Goldfields.

Results

In order to analyse the data spatially and temporally, the Lu-Hf data were placed in a 'time-slice' based on U-Pb age and plotted as a geo-referenced contour map. This allowed the documentation of changing lithospheric architecture in space and time. The results for each time-slice are presented below.

2.6-2.7 Ga time-slice

This time-slice corresponds to that of the Sm-Nd map of Champion & Cassidy (2007) and also Ni mineralisation in the Eastern Goldfields. Although the data points are widely distributed, the general trends agree closely with that of the Sm-Nd work. The Youanmi Terrane (YT) is comprised of much older, more re-worked crust, with a strong crustal Hf signature, particularly around the Marda region. In contrast, the Eastern Goldfields Superterrane (EGST) shows a much more juvenile, depleted mantle (DM)-derived signature.

2.7-2.8 Ga time-slice

Moving back 100 Ma, this timeslice shows that the YT appears to have two distinct isotopic regions. The region at the centre of the terrane, covering the Marda greenstone sequence, is extremely evolved (εHf = -6.02 to -0.88). This indicates that the crust of the Marda region is long-lived, crustally-derived and has

been significantly reworked since its formation. In contrast, the crust south of the Marda region, encompassing the Forrestania, Lake Johnston and Ravensthorpe greenstone belts, shows a more juvenile signature (εHf = +0.66 to -1.2). There is only one sample from the EGST in this time-slice, in the far north of the craton (Mt Keith). This sample continues the trend shown in the 2.6-2.7 Ga time-slice, in that the EGST consists of crust which is much more juvenile (εHf = +2) and DM-derived than that of the YT.

2.8-3.1 Ga time-slice

This time-slice, although consisting of only 5 sample points, gives a first indication of the lithospheric architecture of the south-central Yilgarn at 2.8-3.1 Ga – the period of komatiite emplacement and Ni mineralisation in the YT. The region around the Marda complex remains extremely evolved, with εHf of -4.63 and -5.6, indicating that even at 2.8-3.1 Ga, this region had undergone significant crustal re-working and evolution. The region south of the Marda complex, as at 2.7–2.8 Ga, is much more juvenile than the northern region, and is also more juvenile than the same area at the younger time-slice, with εHf values of +2 to +2.5.

Discussion

The results of the first stage of this project have significant implications for crustal and cratonic evolution in the south-central Yilgarn, and indeed the craton as a whole. There also appears to be a strong spatial and temporal correlation between the location and character of magmatic events and the lithospheric architecture.

Craton evolution in space and time

The time-slices of lithospheric architecture presented in Figure 1 document the evolution of the central Yilgarn, particularly the YT, through the Late Archean from 3.1 to 2.6 Ga, and show a number of key features:

1. The crust of the Marda region is highly evolved for

the entire period of 3.1-2.6 Ga, indicating that the crust of this area is long-lived and much older than the surrounding material. This reinforces the work of previous studies (Chen et al. 2003; Wyche et al. 2004) which indicate that this central region may form the cratonic nuclei of the Yilgarn. The discovery of very old (4350-3130 Ma) detrital zircons in the basal quartzite of greenstones in this region also supports this (Compston et al. 1984; Wyche et al. 2004).

2. The results also confirm that the isotopic signatures of the EGST and YT at 2.6-2.7 Ga are fundamentally different, as first shown by the Sm-Nd map of Champion & Cassidy (2007). The YT consists of much older, long-lived crustally-derived material, whereas the EGST is made up of younger, DM-derived crust. This supports the idea that the YT and EGST evolved separately and were tectonically juxtaposed at some point during the Late Archean (Champion & Sheraton, 1997).
3. A key observation is the identification of a younger, more juvenile region in the YT, south of the Marda region. The time-slices show that at 2.8-3.1 Ga, the crust of this region is very juvenile, showing DM-derived εHf (+2 to +2.5) values. As the area youngs to 2.7-2.8 Ga, it evolves isotopically, indicating crustal melting and re-working has occurred. As the region youngs by a further 100 Ma to 2.6-2.7 Ga, the region evolves further and becomes fully cratonised to the rest of the YT. The changing lithospheric architecture of this area through time indicates that it evolved differently to the central YT and may represent a new domain in terms of crustal genesis, history and evolution.

Lithospheric architecture: implications for magmatism and Ni-Cu-PGE prospectivity

Using this time-resolved Lu-Hf lithospheric architecture, we investigated the variations in komatiite properties, geochemistry and prospectivity within the new crustal framework, focusing on the 2.9 Ga komatiite systems of the YT. The 2.8-3.1 Ga time-slice constrains the lithospheric architecture at the time of komatiite emplacement in this region, and consists of the evolved, crustally-derived central region covering the Marda and northern Southern Cross greenstone belts, and the juvenile, DM-derived southern region encompassing Forrestania, Lake Johnston and Ravensthorpe greenstone belts. A number of significant correlations were noted between the komatiites, greenstone packages and lithospheric architecture of these distinct areas:

1. The greenstone sequences as a whole are dominated by tholeiitic magmatism, however the volume of komatiite increases in the juvenile southern region (Perring et al. 1995; Witt, 1998), whereas belts of the more evolved northern area are almost completely mafic in nature (Chen et al. 2003). This indicates lithospheric architecture may control melt fractionation and geochemistry, and subsequently temperature.
2. Komatiites occurring in the central belts are generally made up of thin sheet flows, with no thick cumulate bodies (Chen et al. 2003). However in the more juvenile southern region, komatiites are much thicker and feature channelized flows with thick dunite/cumulate bodies (Perring et al. 1995; Witt, 1998). This indicates that lithospheric architecture may control the volume of a magmatic event.
3. In terms of Ni-Cu-PGE prospectivity, the belts in the central, more evolved region are currently unprospective, with no known deposits. The southern, more juvenile region contains a number of historical (RAV 1-8) and active (Flying Fox, Spotted Quoll) komatiite-hosted nickel sulphide deposits. Hence lithospheric architecture appears to acts as a first-order control on nickel sulphide prospectivity.

These observations suggest that lithospheric architecture exerts a significant control on the properties of magmas. We propose that this is due to the coupling of lithospheric architecture and geometry. Figure 2 shows a cross-section of inferred lithospheric geometry (at 2.8-3.1 Ga) using εHf as a proxy for lithosphere thickness. When a plume impinges on this geometry a number of scenarios can occur: (1) In regions of thick lithosphere (e.g. Marda area), smaller volumes of melt are generated due to high pressures and these melts are obstructed by thick ensialic crust, leading to significant assimilation and fractional crystallisation (AFC). Resultant lavas in this area are likely to be less voluminous, lower-Mg and hence

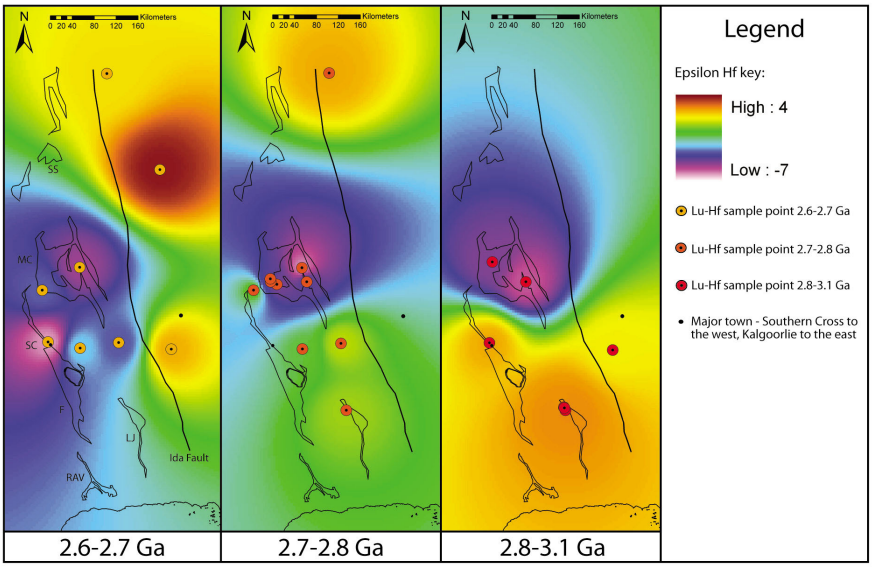

Figure 1. Lu-hf (εHf) lithospheric architecture time-slices for 2.6-2.7 Ga, 2.7-2.8 Ga and 2.9-3.1 Ga.

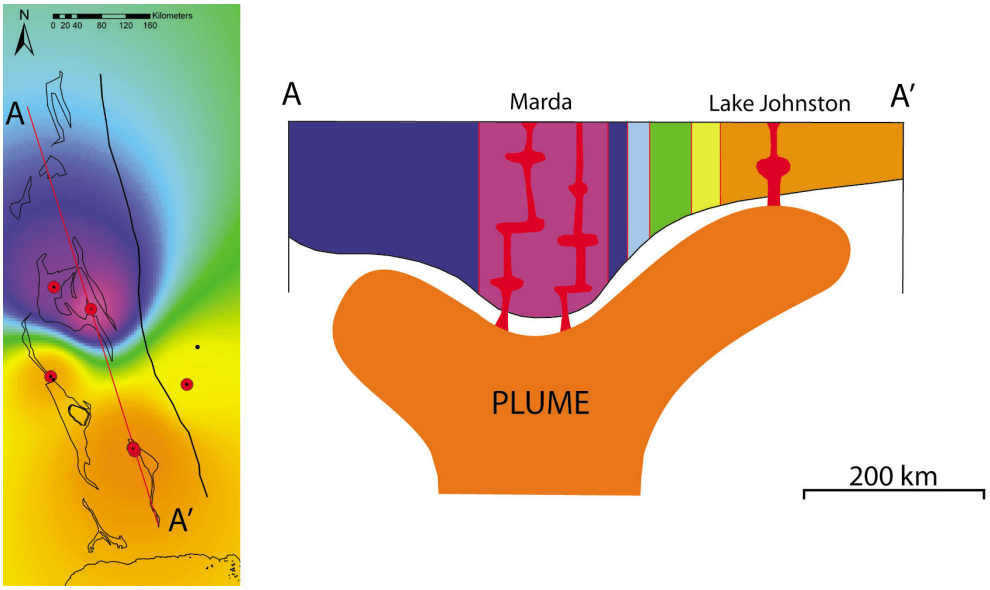

Figure 2. Cross-section through the Lu-Hf lithospheric architecture at 2.8-3.1 Ga.

cooler. This correlates well with the tholeiite-dominated sequence observed in the Lower sequence of the Marda greenstone belt. Such igneous environments are not favourable to the formation of nickel sulphide deposits. (2) In regions of thin lithosphere (e.g. Forrestania), the plume can rise to shallower levels and larger volumes of melt are generated. These melts have a less obstructed route to the surface and therefore experience less AFC. As a result, erupted melts are more voluminous, have higher Mg and are hotter. This correlates with observations in the southern belts of komatiite-abundant greenstone sequences with thick cumulate piles (Perring et al. 1995) (indicating high effusion rate), conducive to the formation of nickel sulphide deposits, verified by the presence of multiple komatiite-hosted nickel sulphide deposits (i.e. Digger Rocks, Flying Fox, Maggie Hays).

Conclusion

The new time-resolved Lu-Hf lithospheric architecture of the South Yilgarn has demonstrated significant potential to delineate crustal domains and elucidate crustal and cratonic history of the south Yilgarn, notably identifying the different genesis and crustal history of the south YT compared to the central YT. This study has also shown that lithospheric architecture appears to play a significant first-order control on the location, character, geochemistry and prospectivity of a komatiite system.

Acknowledgements

We would like to acknowledge the ARC Linkage grant and industry sponsors BHP Nickel West, Norilsk and St Barbara Ltd for providing funding for this project. The Geological Survey of Western Australia (GSWA) is also acknowledged for logistical support in the field, provision of archived samples and technical expertise.

References

Begg G.C., Griffin W.L., Natapov L.M., O'Reilly S.Y., Grand S.P., O'Neill C.J., Hronsky J.M.A., Djomani Y.P., Swain C.J., Deen T. & Bowden P., 2009, The lithospheric architecture of Africa: Seismic tomography, mantle petrology, and tectonic evolution, Geosphere, 5, 23–50.

Beresford S., Cas R., Lahaye Y. & Jane M., 2002, Facies architecture of an Archean komatiite-hosted Ni-sulphide ore deposit, Victor, Kambalda, Western Australia: implications for komatiite lava emplacement, Journal of Volcanology and Geothermal Research, 118, 57–75.

Champion D.C. & Sheraton J.W., 1997, Geochemistry and Nd isotope systematics of Archaean granites of the Eastern Goldfields, Yilgarn Craton, Australia: implications for crustal growth processes, Precambrian Research, 83, 109–132.

Chen S.F., Riganti A., Wyche S., Greenfield J.E. & Nelson D.R., 2003, Lithostratigraphy and tectonic evolution of contrasting greenstone successions in the central Yilgarn Craton, Western Australia, Precambrian Research, 127, 249–266.

Compston W., Williams I.S., Froude D.O., Kinney P.D. & Ireland T.R., 1984, Zircon U-Pb age determinations by ion microprobe on pre-greenstone rocks from the northwest and central Yilgarn Block, W Australia. Terra Cognita, 4, 208.

Foley S.F., 2008, Rejuvenation and erosion of the cratonic lithosphere, Nature Geoscience, 1, 503–510.

Gresham J.J. & Loftus-Hills G.D., 1981, The geology of the Kambalda nickel field, Western Australia, Economic Geology, 76, 1373–1416.

Griffin W.L., Belousova E.A., Shee S.R., Pearson N.J., & O'Reilly S.Y., 2004, Archean crustal evolution in the northern Yilgarn craton: U-Pb and Hf isotope evidence from detrital zircons, Precambrian Research, 131, 231–282.

Perring C.S., Barnes S.J. & Hill R.E.T., 1995, The physical volcanology of Archaean komatiite sequences from Forrestania, Southern Cross Province, Western Australia, Lithos, 34, 189–207.

Witt W.K., 1998, Geology and mineral resources of the Ravensthorpe and Cocanarup 1:100,000 sheets. Geological Survey of Western Australia, Report 54.

Wyche S., Nelson D.R. & Riganti A., 2004, 4350-3130 Ma detrital zircons in the Southern Cross Granite-greenstone terrane, Western Australia: implications for the early evolution of the Yilgarn Craton, Australian Journal of Earth Sciences 51, 31–45.

CONSTRUCTION AND ATTEMPTED DESTRUCTION OF AN ARCHEAN TERRANE IN NORWAY

P.I. Myhre[1], F. Corfu[2] & S.G. Bergh[1]

[1]Department of Geology, University of Tromsø, N-9037 Tromsø, Norway
[2]Department of Geosciences, University of Oslo, N-

Introduction

The West Troms Basement Complex (WTBC) is a c. 100 km^2 large Neoarchean to Paleoproterozoic terrane in northern Norway. It is presently located on the western margin of Fennoscandia (figure 1, modified from Hölttä et al (2008)) separated from the remainder of the Precambrian craton by Caledonian nappes mainly consisting of Neoproterozoic-Paleozoic rocks of allochtonous to parautocthonous nature. In the west, the WTBC borders a passive continental margin consisting of Mesozoic-Cenozoic downfaulted rocks. The present tectonic position is that of a horst. The region is usually not included as a part of the Fennoscandian shield despite its proximity (Koistinen et al. 2001). The reason for this is the possibility that WTBC may be a Caledonian exotic terrane with respect to the Fennoscandian shield.

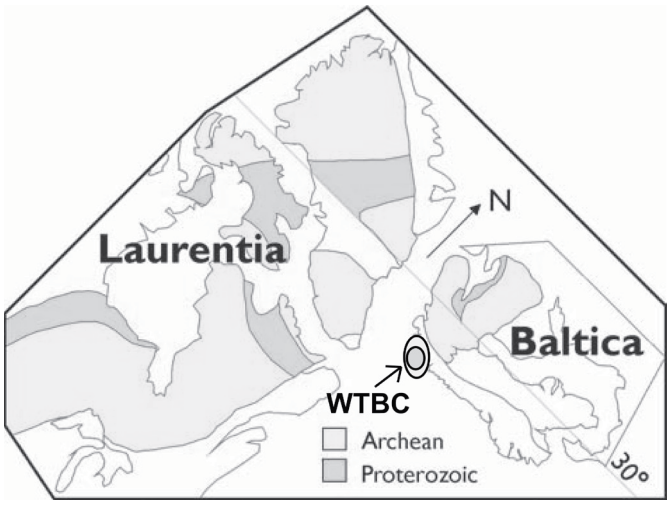

Figure 1. Positions of Fennoscandia (Baltica) and Laurentia at 2450 Ma (Hölttä et al 2008) with the present-day position of WTBC superimposed.

Regional geology

The WTBC is made up of Neoarchean para- and orthogneisses (Corfu et al. 2003), Neoarchean greenstone belts, Paleoproterozoic supracrustal belts and voluminous 1800-1750 bimodal intrusions (figure 1, Bergh et al in press). Several mafic dyke swarms are present, one of which intruded at c. 2400 Ma (Kullerud et al. 2006). The Neoarchean rocks were involved in extensive Paleoproterozoic (Svecofennian) deformation concentrated along 5 or 6 deformation belts with supracrustal rocks and along intra-block ductile shear zones producing a regional lens-shaped structural pattern with NW-SE trending regional fabrics.

Results

In an ongoing effort to establish a detailed tectonostratigraphy of the WTBC we present field mapping and U-Pb geochronology from four tonalites, three migmatite neosomes, a felsic volcanic and a mafic dyke, all with Neoarchean ages (table 1).

These rocks can be considered polymetamorphic, recording several Neoarchean tectono-thermal events, and having experienced Svecofennian and Caledonian orogenies. As a consequence, zircons are commonly discordant due to inheritance and disturbance of their U-Pb-systems. We have sought to overcome this complexity by using a combination of TIMS, CA-TIMS and SIMS analytical approaches and careful image-aided characterisation of the zircon populations. It appears that some of the complex zircon systematics are due to exposure to temperatures below the self-annealing temperature, followed by reburial and annealing, presumably in the Paleoproterozoic, when several unconformities were present in the WTBC (e.g. Bergh et al (2007). The results are shown in table 1. Most notably, the data shows that Neoarchean rocks are present in the entire WTBC. The oldest rocks are present in Ringvassøya and Vannøya in the northern part of the WTBC (figure 2), where tonalites with ages of c. 2885 Ma (Bergh et al. 2007) and c. 2840 Ma (table 1, (Zwaan et al. 1998) are overthrust by a greenstone belt containing felsic volcanics of c. 2850 Ma (table 1). The tonalites have inherited zircons as old as c. 2975 Ma. These rocks are also the least affected by Svecofennian thermal events. C. 2825 Ma inherited zircons are also present in tonalites in the remainder of the WTBC (Senja, table 1). The next important rock-forming event took place at c. 2730 Ma with the formation of tonalite, diorite and precursor rocks of neosomes found in four localities, followed at 2700 – 2650 Ma by the emplacement of granitoid rocks and anatexis as recorded by a granite, a tonalite, a neosome and by inherited zircon in a neosome. This period concluded with the intrusion of mafic dykes in Kvaløya at c. 2660 Ma. The last Neoarchean thermal event is recorded by neosomes with ages of 2600-2575 Ma in two localities.

Implications

As illustrated in figure 1 there are several possible correlatives of the WTBC in the North Atlantic realm, due to its present-day position at the edge of the a craton (figure 1). Areas with similar aged rocks include the Nagssugtoqidian orogen in Greenland (Nutman et al. 2008, Connelly & Mengel 2000), the Lewisian Complex (e.g. Kinny et al. 2005, Corfu et al. 1998) and the Fennoscandian shield (e.g. Hölttä (2008). Today is evidently not the first time the WTBC has been in a position of cratonic divergence: the mafic dykes intruding at 2660 Ma (table 1) and 2400 Ma (Kullerud et al. 2006)

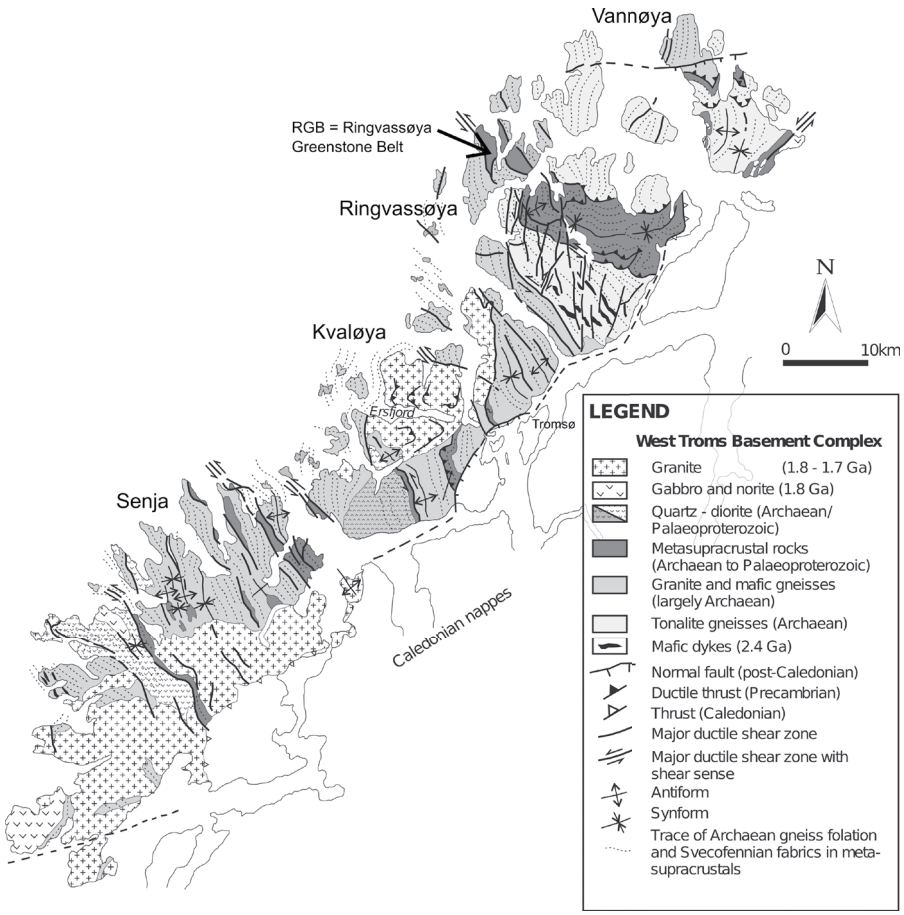

Figure 2. Map of the West Troms Basement Complex (WTBC) with the largest islands indicated (from Bergh et al in press).

Table 1. Geochronogram presenting the results from this study.

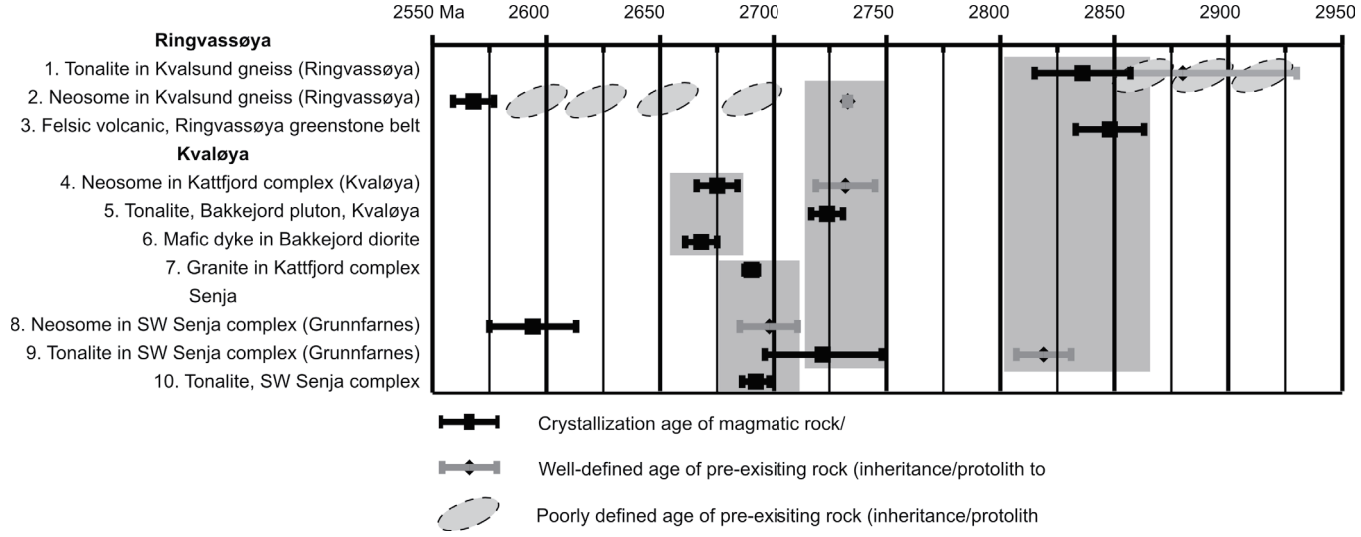

indicate divergent continental systems, and perhaps also the c. 2220 Ma (Bergh et al. 2007) and c. 1970 Ma (Myhre et al., subm.) intrusive/extrusive/siliciclastic sequences. Thus, the WTBC constitutes another piece in the puzzle of Neoarchean and Paleoproterozoic supercratons/ supercontinents.

Acknowledgements

We wish to acknowledge K. Kullerud, K.B. Zwaan, E.J.K Ravna and P.E.B. Armitage for contributing samples, field data and observations relevant to this project through many years of field work and mapping efforts in the WTBC.

References

Bergh S.G., Kullerud K., Corfu F., Armitage P.E., Davidse, B., Johansen H.W., Pettersen T. & Knudsen S., 2007, Low-grade sedimentary rocks on Vanna, North Norway: A new occurrence of a Palaeoproterozoic (2.4-2.2 Ga) cover succession in northern Fennoscandia, Norwegian Journal of Geology, 87, 301–318.

Bergh S.G., Kullerud K., Armitage P.E.B., Zwaan, K.B., Corfu F., Ravna E.J.K. & Myhre P.I. in press: Neoarchaean through Svecofennian tectono-magmatic evolution of the West Troms Basement Complex, North Norway, Norwegian Journal of Geology.

Connelly J.N. & Menge F.C., 2000, Evolution of Archean components in the Paleoproterozoic Nagssugtoqidian orogen, West Greenland. Geological Society of America Bulletin, 112, 747–763.

Corfu F., Armitage P.E., Kullerud K. & Bergh S.G., 2003, Preliminary U-Pb geochronology in the West Troms Basement Complex, North Norway:archean and Palaeoproterozoic events and younger overprints, Geological Survey of Norway Bulletin, 441, 61–72.

Corfu F., Crane A., Moser D. & Rogers G., 1998, U-Pb zircon systematics at Gruinard Bay, northwest Scotland: implications for the early orogenic evolution of the Lewisian complex, Contributions to Mineralogy and Petrology, 133, 329–345.

Hölttä P., Balagansky V., Garde,A.A., Mertanen,S., Peltonen P., Slabunov A., Sorjonen-Ward P. & Whitehouse M., 2008. Archean of Greenland and Fennoscandia, Episodes, 31, 13–19.

Kinny P., Friend C. & Love G., 2005, Proposal for a terrane-based nomenclature for the Lewisian Gneiss Complex of NW Scotland, Journal of the Geological Society of London, 162, 175–186.

Koistinen T., Stephens M., Bogatchev V., Nordgulen Ø., Wennerström M. & Korhonen, J., 2001, Geological map of the Fennoscandian Shield. Geological Survey of Finland, Espoo; Geological Survey of Norway, Trondheim; Geological Survey of Sweden, Uppsala; Ministry of Natural Resources of Russia, Moscow.

Kullerud K., Skjerlie K.P., Corfu F. & de la Rosa J.D., 2006, The 2.40 Ga Ringvassøy mafic dykes, West Troms Basement Complex, Norway: The concluding act of early Palaeoproterozoic continental breakup,. Precambrian Research, 150, 183–200.

Myhre P., Corfu F. & Bergh S., submitted, Palaeoproterozoic (2000-1950 Ma) Pre-Orogenic Supracrustal Sequences in the West Troms Basement Complex, northern Norway, Precambrian Research.

Nutman A.P., Kalsbeek F. & Friend C.R.L., 2008, The Nagssugtoqidian orogen in South-East Greenland: Evidence for Paleoproterozoic collision and plate assembly, American Journal of Science 308(4), 529–572.

Zwaan K., Fareth E. & Grogan P., 1998, Bedrock map Tromsø. Geological Survey of Norway, Trondheim

COMBINED ZIRCON U-Pb-Hf-O ANALYSES FROM ARCHAEAN TTG GNEISSES IN SOUTHERN WEST GREENLAND.

T. Næraa[1,2], A. Scherstén[3], J.E. Hoffmann[4] & A.I.S. Kemp[5]

[1]Geological Survey of Denmark and Greenland – GEUS, Øster Voldgade 10, 1350 København K, Denmark.
[2]Natural History Museum of Copenhagen, Copenhagen University, Øster Voldgade 3-7, 1350 København K, Denmark.
[3]Dept. of Earth & Ecosystem Sciences, Lund University, Sölvegatan 12, 223 62 Lund, Sweden
[4]Rheinische Wilhelms-Universität Bonn, Steinmann Institut, Institut für Mineralogie; Poppelsdorfer Schloss, 53115 Bonn, Germany
[5]School of Earth and Environmental Sciences, James Cook University, Townsville 4811 Australia.

Introduction

Archaean high-grade terranes are dominated by tonalite-trondhjemite-granodiorite (TTG) gneisses. The timing for the generation (distinct events or continuous), differentiation and stabilization of these early crustal segments are poorly understood. In this study we analysed zircon U-Pb-Hf-O isotopes from strongly deformed and, in some cases, migmatised gneisses. All of these gneisses have been overprinted by one or several tectonometamorphic events, including intrusion of pegmatites or sheets of granitic composition, migmatisation (migmatitic veining), lower grade metamorphic overprinting and metasomatism/leaching (relative silica increase). Any of these overprinting processes might have been repeated several times. The studied gneisses were sampled across a proposed terrane boundary in the Nuuk region of southern West Greenland. The protolith ages of the gneisses range from Palaeoarchaean to Neoarchean and formed in accretionary events, where these terranes were juxtaposed and amalgamated by ~2.7 Ga when a major regional tectonothermal event affected all gneisses. These gneisses have potentially recorded many of the thermal processes that have occurred in the continental crust of the study area and thus can be used to evaluate the processes that differentiate continental crust. Further, as we combine data from several isotopic systems we can monitor the processes of decoupling and/or disturbance of the isotopic systems in the zircon grains.

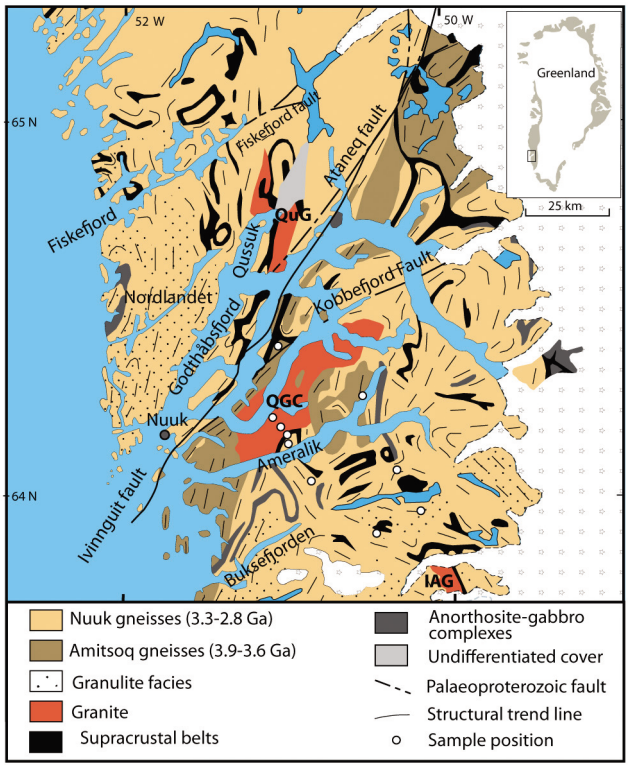

Figure 1. Geological map of the southern Nuuk region (modified from Escher &Pulvertaft 1995). QGC=Qôrqut Granite Complex, QuG=Qugssuk Granite, IAG=Ilivertalik granite/charnockite. Sample locations are indicated.

Regional Geology

The Archean crust in the Nuuk region is dominated by TTG gneisses with subordinate greenstone belts, anorthosites and granites (Escher & Pulvertaft 1995) (fig. 1). Igneous crystallisation ages of the gneiss protoliths range from ~3.85 to ~2.7 Ga, generally clustering in two periods, at ~3.85 to 3.6 Ga and at 3.3 to 2.7 Ga (Garde 1997; Nutman & Friend 2007, and references there in). More evolved granites generally intruded late during the two igneous periods and may in some instances be related to peak metamorphism at ~3.6, ~3.0, ~2.8 and ~2.7 Ga (Griffin et al. 1980; Garde 1997; Friend et al. 1996; Pidgeon & Kalsbeek 1978). The ~2.7 Ga event is a major regional tectonothermal event that induced large scale deformation, anatexis and emplacement of crustally- derived granites, and is generally interpreted as a major accretion event (Friend et al. 1996).

Results and interpretations

The zircon U/Pb-Hf data from this study distinguish, at the first level of order, 3 crust forming periods (fig. 2). Gneiss protolith ages of these periods are ~3.86-3.55, ~3.25, at ~2.87-2.7 Ga (reported protolith ages are the best estimate for the igneous crystallisation, model Hf ages are not reported). The oldest group of gneisses has a protolith age range of 190 Myr, and might be further subdivided into two periods at 3.87-3.82 Ga and 3.7-3.55 Ga. Zircon populations group into ages of 3.87, 3.82, 3.7 and 3.65-3.55 Ga, and in the oldest groups of gneisses, rims with ages of ~3.6 Ga and ~2.7 Ga is common. The most juvenile gneisses from this period have $\varepsilon Hf_{(t)}$ protolith values that fall within ±1 epsilon unit from CHUR; the 3.7-3.55 Ga protoliths have lower $\varepsilon Hf_{(t)}$ values (~-1) than the 3.82-3.86 Ga gneisses (~0) (fig. 2). This difference in $\varepsilon Hf_{(t)}$ values is not significant but

suggests increased input of recycled crust into the later crust forming plutonic bodies. The growth zoned cores of oldest zircon population (3.87 Ga) have a $\delta^{18}O$ value of 6, whereas the younger (3.55 to 3.7 Ga) populations show a scatter from 5 to 8.5. Some of the individual gneisses contain several zircon populations with distinct initial $\varepsilon Hf_{(t)}$ values and distinct zircon U/Pb ages, where related zircon textures suggest that the populations are igneous. These observations suggest that mixing of distinct zircon populations are common and could either be explained by inheritance or by magmatic sheeting of the crust with subsequent strong deformation which have homogenised the gneisses to a hand sample level. One gneiss sample, with foliation parallel leucocratic veins, represents a example of the latter, here two zircon populations with distinct initial $\varepsilon Hf_{(t)}$ at ~3.7 and ~3.6 Ga also have distinct zircon texture and $\delta^{18}O$ values. Scaling such primary heterogeneity up to tens of meters and subsequently deforming the heterogeneous crust unit into homogeneous banded gneiss could be used as model for forming gneisses with multi component zircon populations.

In the next crust forming event, the gneiss protolith age of the 4 investigated rocks are 3.25 Ga. At this age the gneisses divide into two distinct groups based on their initial $\varepsilon Hf_{(t)}$ values, one group with $\varepsilon Hf_{(t)}$ values around +1 (for seemingly juvenile components) and on group with $\varepsilon Hf_{(t)}$ around -8.5 (for remelted existing crust). No prominent mixing between the two reservoirs is observed. It follows that at this period crust formed out of reservoirs with a very different crustal residence time. There is no distinction in $\delta^{18}O$ of the two reservoirs, with a mean value of 5.8±0.4. Both units have been overprinted by metamorphism and Pb-loss induced decupling of the U/Pb and Lu/Hf is pronounced.

The youngest crust forming period in the region started at ~2.88 Ga and apparently continued for 50-60 Myr. These gneisses show a distinction between juvenile rocks with $\varepsilon Hf_{(t)}$ values at ~+1-2 and rocks that show mixing trends toward recycled crustal reservoir. This distinction is also observed in the $\delta^{18}O$ composition, with higher $\delta^{18}O$ values tor the rocks with a recycled component. Two metamorphic events at ~2.8 and ~2.7 Ga have overprinted many of the earlier formed crust units. The metamorphic grains/rims have $\varepsilon Hf_{(t)}$ values ranging -22 to -4, most of the low $\varepsilon Hf_{(t)}$ can be explained by Pb-loss induced decupling of the U/Pb and Lu/Hf isotopes. However some of the metamorphic domains have a more radiogenic Hf signature. Crustal derived granites with $\varepsilon Hf_{(t)}$ down to ~-9 intruded the crust during the 2.7 Ga event. The granite contains a inherited zircon population with age of ~2.88 and a corresponding $\varepsilon Hf_{(t)}$ value of ~1.

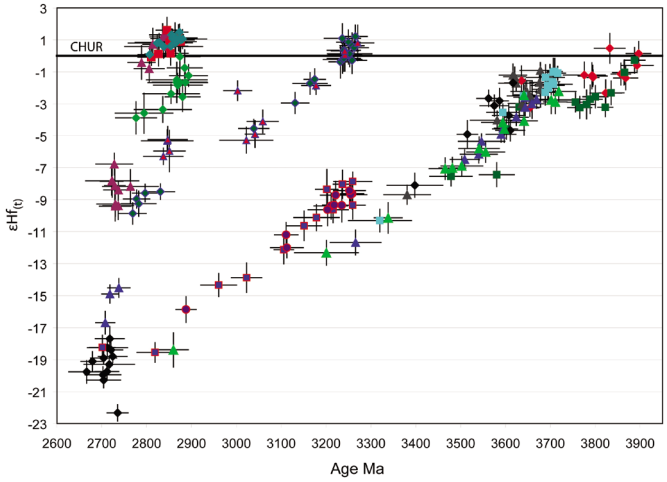

Figure 2. $\varepsilon Hf_{(t)}$ vs. time diagram with zircon isotope data from his study. CHUR=CHondrite Uniform Reservoir. 3 first order periods of crust formation are observed. Pb-loss decoupling of the U/Pb and Lu/Hf isotopes are observed a steep trend lines.

Discussion and summary

Our data support a model where the processes of crustal growth and reworking are episodic with apparently limited interaction between discrete crustal segments (at least until 2.88 Ga, where some mixing is evident). In the group of Eo- to Palaeoarchaean gneisses, crustal growth continued for ~190 Myr, the multi component zircon populations (from individual samples) that seemingly were established at or before 3.6 Ga, suggest that reworking and/or mixing of crustal units could have been pronounced during this period. Remelting of parts of this old crustal reservoir occurred on a minor scale during the next two growth episodes, it is however only towards the end of the ~1.2 Ga period that the tectonomagmatic processes have mixed different levels of the different crust reservoirs. The process of stabilisation finally stopped at ~2.7 Ga, after ~1.2 Gyr, with a major thermal event that affected a large part of the Archaean crust in southern West Greenland.

References

Escher J. C. & Pulvertaft,T.C.R., 1995, Geological map of Greenland, 1:2 500 000, Geological Survey of Greenland.

Garde A.A., 2007, A mid-Archaean island arc complex in the eastern Akia terrane, Godthåbsfjord, southern West Greenland. Journal of the Geological Society of London, 164, 565–579.

Friend C.R.L., Nutman A.P., Baadsgaard H., Kinny P.D. & McGregor V.R., 1996, Timing of late Archaean terrane assembly, crustal thickening and granite emplacement in the Nuuk region, southern West Greenland, Earth and Planetary Science Letters, 142. 353–365.

Griffin W.L., McGregor V.R., Nutman A.P., Taylor P.N. & Bridgwater, D., 1980, Early Archaean granulite-facies metamorphism south of Ameralik, West Greenland, Earth and Planetary Science Letters 50, 59–74.

Nutman A.P. & Friend, C.R.L., 2007, Adjacent terranes with ca. 2715 and 2650 Ma high-pressure metamorphic assemblages in the Nuuk region of the North Atlantic Craton, southern West Greenland: Complexities of Neoarchaean collisional orogeny, Precambrian Research, 155, 159–203.

Pidgeon R.T. & Kalsbeek F., 1978, Dating of igneous and metamorphic events in the Fiskenaesset region of southern West Greenland, Canadian Journal of Earth Sciences 15, 2021–2025.

MESOARCHEAN SANUKITOID ROCKS OF THE RIO MARIA TERRANE, BRAZIL

M.A. Oliveira[1,2], R. Dall'Agnol[1,2], B. Scaillet[3], J.A.C. Almeida[1,2], F.J. Althoff[1,4] & A.A.S. Leite[1,2]

[1]Group of Research on Granite Petrology, Institute of Geosciences, Federal University of Pará, Brazil
[2]Graduated Program on Geology and Geochemistry, Institute of Geosciences, Federal University of Pará
[3]CNRS/INSU, Université d'Orléans, Université François Rabelais Tours, Institut des Sciences de la Terre d'Orléans, 1a rue de la Férollerie, 45071 Orléans cedex 2, France.
[4]Faculdade de Geologia – Universidade Federal do Espírito Santo, Campus de Alegre – ES.

Introduction

We report petrographical, geochemical and mineralogical data on the 2.87 Ga Rio Maria sanukitoid suite which is exposed in large domains of the Rio Maria Granite-Greenstone Terrane, southeastern Amazonian craton, Brazil. It is intrusive in the greenstone belts of the Andorinhas Supergroup, in the Arco Verde, Mariazinha, and Caracol tonalite, and Mogno trondhjemite. Archean potassic leucogranites, Água Fria trondhjemite, and the Paleoproterozoic granites of Jamon Suite are intrusive in the rocks of the Rio Maria suite (Oliveira et al. 2009).

Petrography

The dominant rocks have granodiorite to subordinate monzogranitic compositions, with minor proportions of intermediate quartz-diorites or quartz-monzodiorites rocks, in addition to mafic end members occurring as layered rocks or as enclaves (Fig. 1). The granodiorites display medium- to coarse- even-grained textures and show generally a gray color with greenish shades due to strongly saussuritized plagioclase, and weak WNW-ESE striking foliation.

Geochemistry

The Rio Maria suite has clear geochemical characteristics of Sanukitoids rocks (high Mg#, elevated Cr and Ni contents, LREE enrichment, and high Ba and Sr contents relative to typical calc-alkaline series (Fig. 2). The significant geochemical contrasts between the occurrences of the granodiorites in different areas suggest that this unit corresponds in fact to a granodioritic suite of rocks derived from similar but distinct magmas. In spite of their broad geochemical similarities, granodiorites, intermediate rocks, and mafic enclaves show some significant differences in their REE patterns (Fig. 3) and in the behavior of Rb, Ba, Sr, and Y, suggesting that these rocks are not related by a fractional cristallization process.

Mineral Chemistry and Parameters of Crystallization

In the rocks of the Rio Maria suite, the mineral assemblage is dominated by amphibole-plagioclase-biotite and epidote minerals, all of inferred magmatic origin, pyroxenes being notably absent. Textural and compositional criteria indicate that amphibole is a principal mineral on the liquidus of all the Rio Maria rocks. To derive crystallisation conditions (Oliveira et al. submitted), the phase assemblages, proportions and compositions of the natural rocks were compared with experimental works carried out on similar magma compositions. The comparison shows that the parental magmas were water-rich, with more than 7 wt% dissolved H_2O near liquidus, with crystallisation temperature in the range 950-680°C. The Mg/(Mg+Fe) ratios of both amphibole and biotite indicate fO_2 conditions in the range NNO + 0.5 up to NNO + 2.5, therefore pointing to both water-rich and oxidizing conditions for sanukitoid magmas (Fig. 4a, c).

Analyses of amphibole aluminium content in cumulate rocks, indicate in addition a high pressure crystallisation stage, around 700-1000 MPa, prior to emplacement in the upper crust at around 200 MPa (Fig. 4b, d). Sanukitoid magmas share therefore two of the principal characteristics of modern arc magmas, elevated redox

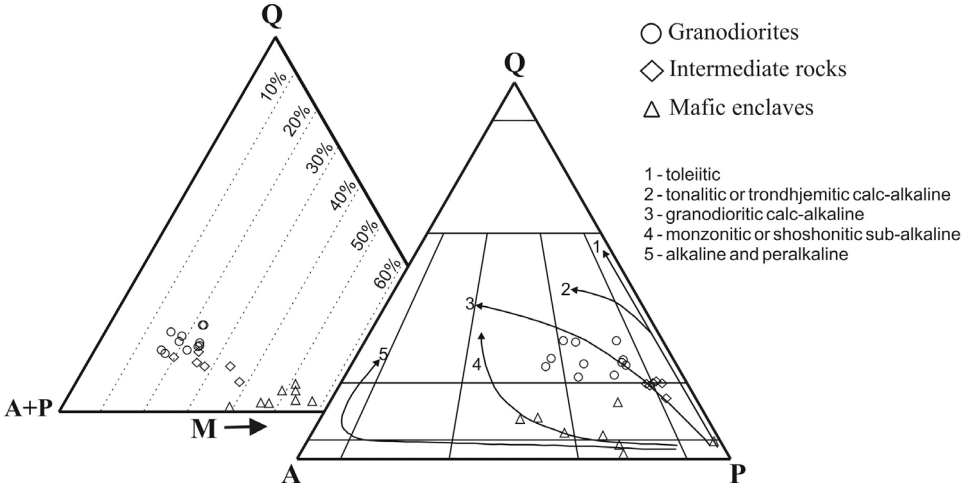

Figure 1. QAP and Q-(A+P)-M plots for the rocks of the Rio Maria suite (Bannach area). Data sources: Granodiorites and intermediate rocks (Oliveira et al. 2009); Mafic enclaves (Oliveira et al. submitted).

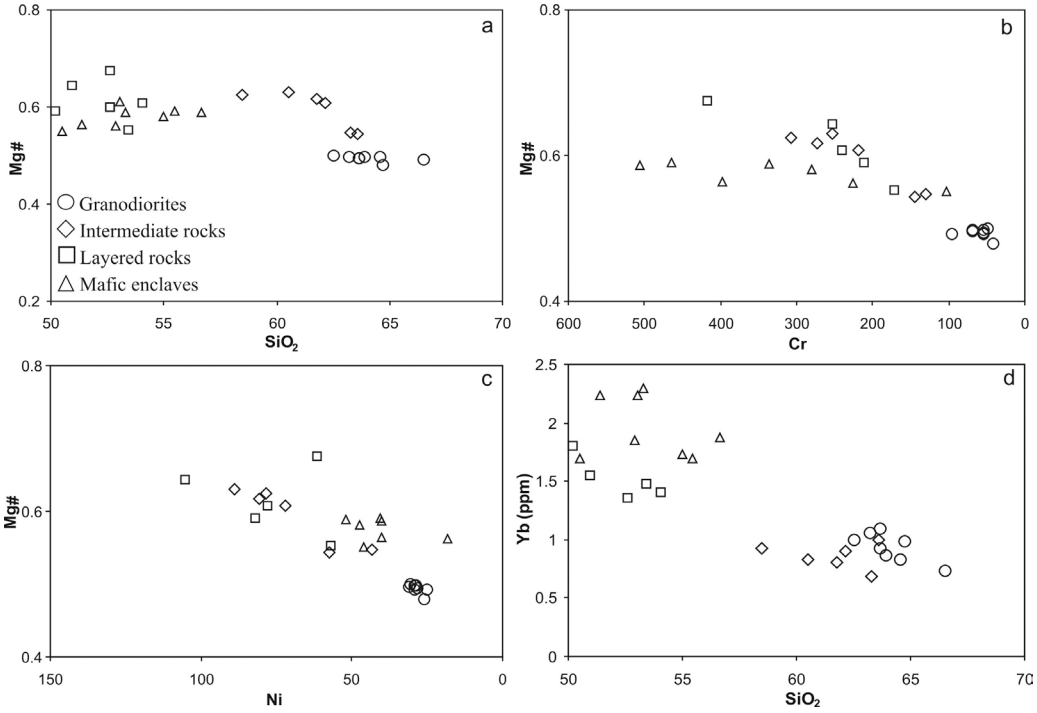

Figure 2 - (a) Mg# vs. SiO_2; (b) Mg# vs. Cr; (c) Mg# vs. Ni; (d) Yb vs. SiO_2 diagrams for the different rocks of the Rio Maria suite (Bannach area).

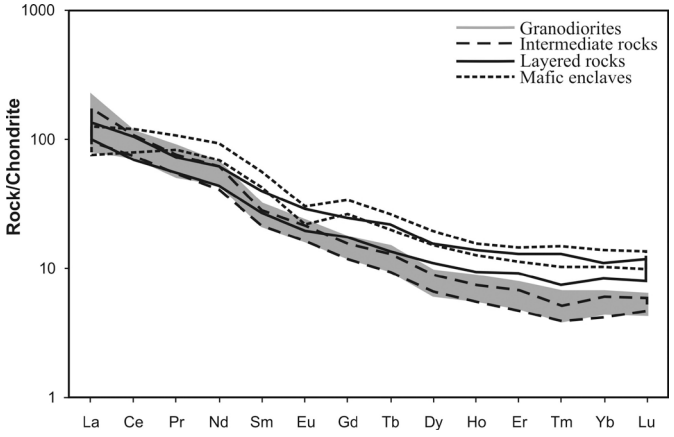

Figure 3 - Chondrite-normalized REE patterns for the rocks of the Rio Maria suite of Bannach area (normalization values from Evensen et al., 1978).

sate and volatile contents, which suggest that they may have formed in a geodynamic environment broadly similar to present-day subduction zones.

Conclusions and Perspectives

Geological and mineralogical studies on the Rio Maria Archean sanukitoid rocks opposed to experimental results obtained in rocks or synthetic materials of similar compositions allowed us to make quantitative estimates of the parameters of crystallization of their magmas. These rocks were derived from cogenetic but not comagmatic magmas that should have evolved under similar conditions. We conclude that the Rio Maria magmas were water-rich, with > 7 wt. % estimated water contents, and evolved in oxidizing conditions above the condition of NNO buffer, probably in between NNO + 0.5 to NNO + 2.5. These conditions allowed the crystallization of amphibole as the liquidus phase and inhibited clinopyroxene and orthopyroxene. Those magmas should begin to crystallize at a temperature estimated at 950 °C, crystallizing essentially amphibole.

The magma ascent was rapid and the proportion liquid/crystals in the magma were high to explain the high level of emplacement of the Rio Maria suite and the limited deformational structures observed on their rocks. After magma ascent to upper crustal levels, plagioclase begun to crystallize (cf. the evolution proposed for the Pinatubo dacite; Prouteau & Scaillet 2003). At lower temperatures, a peritectic reaction involving amphibole + plagioclase + magnetite + ($K\text{-feldspar}_{melt}$) resulted in the presence of biotite and magmatic epidote. The stability of epidote in those conditions was ensured by the oxidized character of the Rio Maria magmas. Their final emplacement should have occurred at ca. 200 MPa and any early precipitated amphibole possibly re-equilibrated extensively at these conditions, except for the coarse amphibole crystals, such as that found in the cumulate rocks. It is assumed in the proposed evolution scenario that the different magmas which have formed the Rio Maria sanukitoid evolved in similar conditions and ascended in the crust together or almost simultaneously, at short intervals of geological time.

The P-T-H_2O-fO_2 estimates reached above for the Rio Maria suite point therefore to oxidized and wet conditions for their precursor magmas, two features characteristic of present-day arc magmas, including those with a strong slab melt signature, such as Pinatubo. The immediate, and perhaps principal, implication is that Sanukitoid petrogenesis at Rio Maria is indeed compatible with a subduction zone geodynamic setting during the Archean in this area. It remains, however, to be demonstrated whether such arc attributes are specific to Rio Maria magmas or characterize Sanukitoid occurrences worldwide. The origin of the primary or primaries magmas of the Rio Maria sanukitoid rocks deserve complementary data and approaches and should be the focus of future studies.

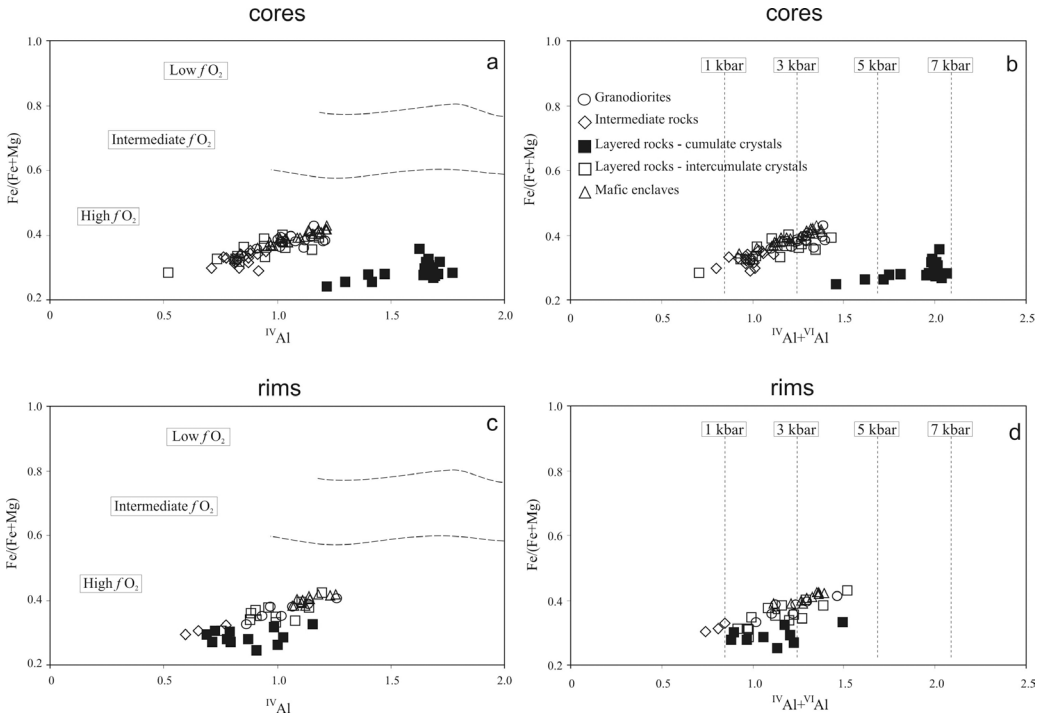

Figure 4 - (a, c) amphibole Fe/(Fe+Mg) x ^{IV}Al diagrams (Anderson & Smith, 1995) showing the possible oxygen fugacity conditions during the crystallization of rocks of the Rio Maria suite (Bannach area); (b, d) amphibole Fe/(Fe+Mg) x Al_{tot} diagrams (Anderson & Smith, 1995) showing the possible crystallization pressures for amphibole of the Rio Maria suite.

Acknowledgements

S. R. F. Vlach, E. Ruberti, and M. Mansueto are acknowledged for support on electron microprobe analyses (Institute of Geosciences of São Paulo University). This research received financial support from CNPq (Roberto Dall'Agnol – Grants 0550739/2001-7, 476075/2003-3, 307469/2003-4; Marcelo Augusto de Oliveira – master, doctor, and DCR scholarship), FAPESPA (Fundação de Amparo a Pesquisa do Estado do Pará: Marcelo Augusto de Oliveira – Financial support), and Federal University of Pará (UFPA). This abstract is a contribution to the Brazilian Institute of Amazonia Geosciences (INCT program – CNPq/MCT/FAPESPA – Process no 573733/2008-2).

References

Anderson J.L & Smith D.R., 1995, The effects of temperature and fO2 on the Al-in-hornblende barometer, American Mineralogist 80, 549–559.

Evensen N.M., Hamilton P.T. & O'Nions R.K., 1978, Rare earth abundances in chondritic meteorites, Geochemica et Cosmochemica Acta, 39: 55–64.

Oliveira M. A., Dall'Agnol R., Althoff, F. J. & Leite, A.A.S. 2009, Mesoarchean sanukitoid rocks of the Rio Maria Granite-Greenstone Terrane, Amazonian craton, Brazil, Journal of South American Earth Sciences, 27, 146–160.

Oliveira M.A. Dall'Agnol, R. & Scaillet, B., submitted, Petrological constraints on crystallization conditions of Mesoarchean sanukitoid rocks, southeastern Amazonian craton, Brazil, Journal of Petrology.

Prouteau G. & Scaillet B., 2003, Experimental constraints on the origin of the 1991 Pinatubo dacite, Journal of Petrology, 44, 2203–2241.

PERSISTENCE OF ARCHEAN LITHOSPHERIC MANTLE BENEATH CONTINENTS AND OCEANS

S.Y. O'Reilly[1], W.L. Griffin[1], M. Zhang[1] G.C. Begg[1,2] & J. Hronsky[1,3]

[1]GEMOC, Macquarie University, NSW 2109, Australia
[2]Minerals Targeting International, 17 Prowse Street, West Perth, WA 6005, Australia
[3]Western Mining Services (Australia) Pty Ltd, 17 Prowse Street, West Perth, WA 6005, Australia

Summary

High-resolution global seismic tomography (Vs) models reveal high-velocity domains beneath cratonic crust in Africa that extend to depths of 300-400 km. These high-velocity domains show a distinct contrast with the characteristics of "normal" asthenosphere and are interpreted as depleted, buoyant roots that formed in the Archean and have been metasomatised over time, but have remained attached to the overlying crust. Such deep roots are impediments to free horizontal convection in the upper mantle. As a result, movement of magmas and other fluids in such regions may be more vertically constrained (a shallow lava lamp regime). This process creates a geodynamic environment conducive to interaction of such magmas with the boundaries of deep mantle domains that would carry old "crustal" geochemical signatures.

The tomographic models and the recent world magnetic-anomaly map show that these continental roots, overlain by thinned continental crust, locally extend well out under the deep Atlantic Ocean basin. However, such high-velocity domains are not confined to the basin margins, but are scattered randomly through the basin, some quite distant from the continental margins of South America and Africa. These high-velocity domains are interpreted to be remnant lithospheric fragments isolated by disruption of the ancient continental regions during rifting. This interpretation is supported by the old Os depletion ages of mantle peridotites from mid-ocean ridges and oceanic islands.

Archean mantle characteristics

Archean subcontinental lithospheric mantle (SCLM) is distinctive in its highly depleted composition, commonly strong stratification, and the presence of rock types absent in younger SCLM. Is Archean SCLM part of a compositional continuum that shows a secular evolution varying broadly with the age of the last major tectonothermal event in the overlying crust, or was the Archean mantle formed in a different way in a distinctive tectonic regime? Did subduction play a major role in Archean SCLM formation? What is the composition of original Archean mantle and how much persists today?

The "typical" Archean mantle composition used in geochemical/geophysical modelling is a depleted garnet lherzolite. This composition is derived from peridotite xenoliths in kimberlites, mainly from the SW Kaapvaal Craton, and a few from Siberia. However, most such "typical" Archean xenoliths have experienced repeated metasomatism, leading to a progression from dunite/harzburgite through "depleted" lherzolite to "fertile" lherzolite, mirroring the secular evolution of the SCLM as a whole (Griffin et al., 2009), and this is discussed in more detail in Griffin et al. (2010).

Archean lithosphere is significantly less dense than asthenosphere at any depth, whereas young (Phanerozoic) lithosphere is initially less dense due to thermal buoyancy, but on cooling becomes denser and thus gravitationally unstable. Original (unmetasomatised) Archean lithosphere is depleted (Mg-rich and low in basaltic components such as Al, Ca, Fe), consists dominantly of dunite and Ca-poor harzburgite (e.g. Griffin & O'Reilly, 2007) and has high seismic wave velocities mainly due to the high content of Mg-rich olivine (Fo_{92-94}). Young lithosphere is fertile (higher in Al, Ca and Fe) with more Fe-rich olivine (Fo_{88} average) and higher modal pyroxene, resulting in lower seismic velocity (O'Reilly et al., 2001). These compositional variations alone can account for up to 25% of the observed seismic velocity differences between cratonic and tectonically active regions. However, the combined effects of composition and tectonic environment are intrinsically additive; the Mg-rich cratonic SCLM is also the coolest, and the young tectonic SCLM with its Fe-rich olivine and high pyroxene content is warmer. Thus the separate effects of composition and temperature on seismic wave speed are reinforced in Earth's different tectonic regimes (e.g. Poudjom Djomani et al., 2001; O'Reilly et al., 2001; Deen et al., 2006).

Evidence for deep cratonic roots beneath Africa

Figure 1 shows a series of tomographic slices through the African continent from 100-175 km, 175-250km, 250-325km and 325 – 400km using a high-resolution global tomography model derived from SH body wave travel times based on the approach of Grand (2002) and fully described by Begg et al. (2009) and O'Reilly et al. (2009). The vertical resolution is estimated as 75-150 km in either direction. Note the colour reversal with red spectrum for fast and blue for slow velocities. The clear demarcation of cratonic domains persists in the 175-250km layer that extends to the lower level accepted for most subcontinental lithospheric mantle. At 250-325km, the cratons maintain coherence and relative velocity contrast at depths below traditional Archean SCLM regions. At 325-400 km, domains beneath the cratons still show higher Vs than the Earth model. Even allowing for considerable vertical smearing of velocity, the higher-velocity roots beneath the cratons extend almost to the transition zone (410 km discontinuity).

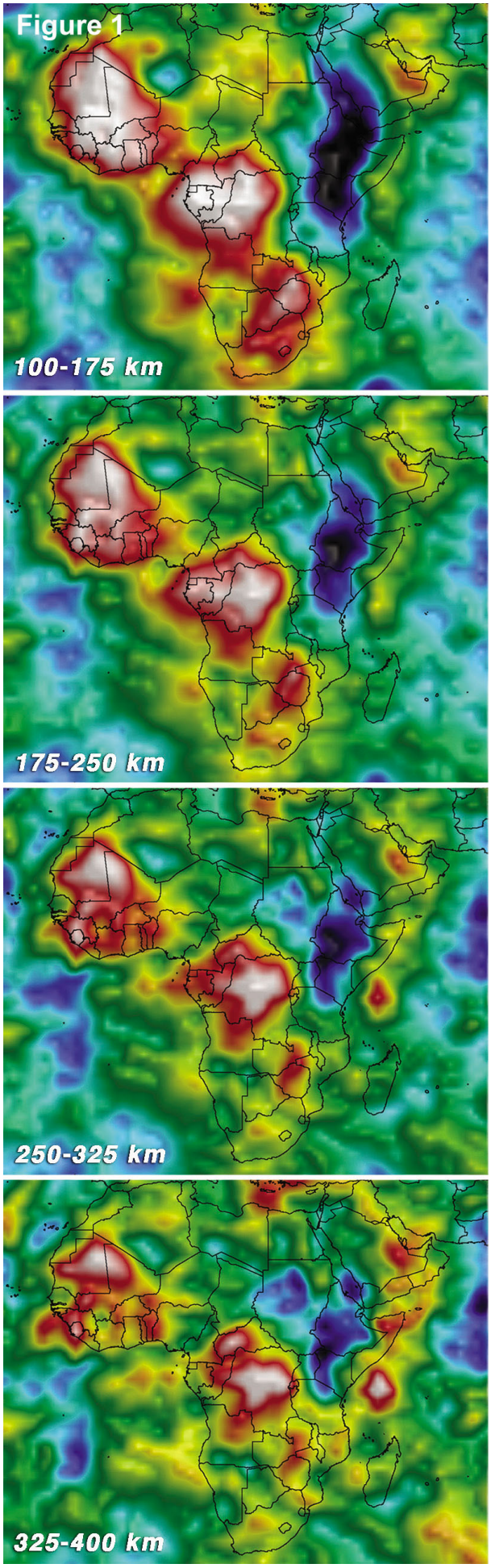

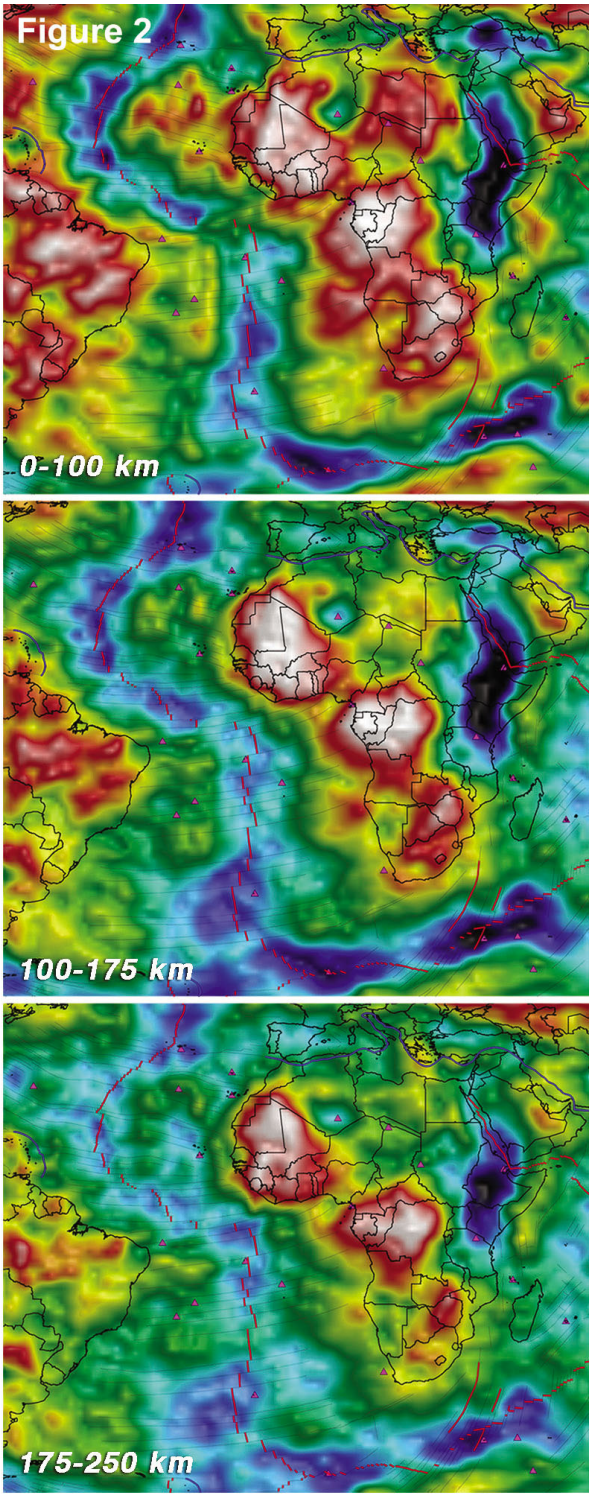

Figure 1. Tomographic model images (Vs models) for four depth slices through the lithospheric mantle an upper mantle beneath Africa. See text for explanation and discussion. Note that red colours indicate higher velocities and cool colours lower velocities.

Figure 2. Tomographic model images at three depth slices for the Atlantic Ocean Basin (see text for details of the model). Note that "hot" (red-white) colours indicate higher velocities and cool colours lower velocities.

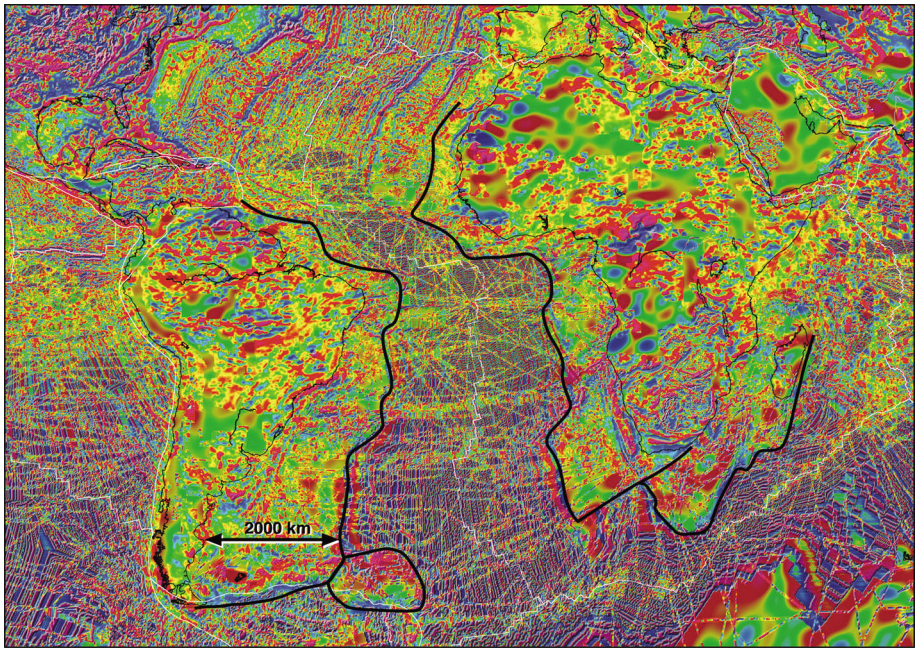

Figure 3. Modified extract from the global magnetic anomaly map (Korhonen et al., 2007) showing the Atlantic Ocean Basin and Atlantic coasts of South Africa and South America. Black lines outline the regions with crustal rather than oceanic magnetic characteristics.

Ancient continental lithosphere domains in the Atlantic oceanic region

Figure 2 shows tomographic slices through the oceanic lithosphere and upper mantle of the Atlantic Ocean Basin at 0-100km, 100-175km and 175-250km. In the 0-100km section, high-velocity regions are obvious. Some are apparently continuous with continental regions (especially off the southwestern African and southeastern South American coasts) and some occur as discrete "blobs" extending towards the mid-ocean ridge from the continental margins such as those between the mid-Atlantic Ridge and the northwest African coast. In the layer from 100-175km, these fast domains persist, and some also show velocity contrasts in the 175-250km layer.

We suggest that these high-velocity volumes represent remnants of depleted (buoyant) ancient continental lithosphere, fragmented and stranded during the rifting process at the opening of the ocean basin. The high-velocity domains extending out from the coastlines are not uniformly distributed along the basin edge. The most marked high-velocity regions off SE South America and northwest and southwest Africa appear continuous with their respective continental deep structure as seen in the tomographic models. The new global magnetic-anomaly map (Figure 3) shows that these regions have a complex magnetic signature that is consistent with extended continental crust, and distinct from that of oceanic lithosphere. The seismic data suggest that this thinned continental crust is underlain by Archean to Proterozoic SCLM that has been mechanically disrupted and thinned during the formation of the ocean basins partly by listric detachment of continental crust from the underlying continental SCLM. Re-Os data on sulfides from mantle xenoliths from Cape Verde support this concept. Their depleted mantle model ages of 2.7 – 3.5 Ga (Coltorti et al., 2010) suggest that these xenoliths are disrupted fragments of the West African cratonic SCLM.

Conclusions

The roots of ancient cratons may extend to near the transition zone, representing persistence of parts of these buoyant domains since their formation in the Archean. Throughout this time, rifting and reassembly may modify the original boundaries and the deep roots may be progressively modified, especially along domain margins, by interaction with ascending melts during tectonic events, and by percolation of fluids.

Opening of ocean basins may be largely by listric faulting, leaving significant continental lithospheric wedges at rifted margins, and stranding buoyant domains of ancient lithosphere in the upper part of the new oceanic crust-mantle system (Figure 4), where they would "surf the convecting mantle".

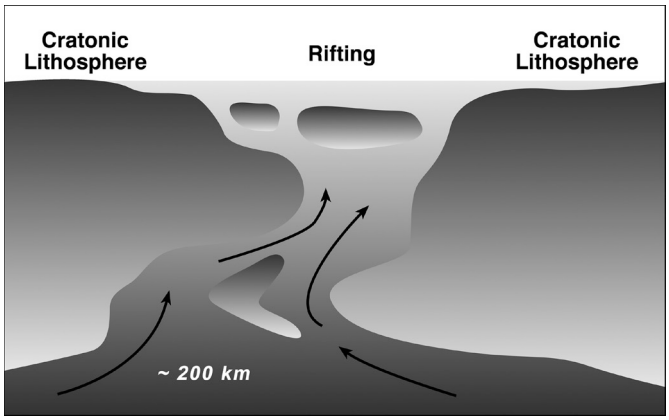

Figure 4. Cartoon depicting listric faulting of cratonic margins during ocean-basin formation, and stranding of buoyant ancient mantle remnants in the oceanic domain.

Acknowledgements

The ideas presented here have been developed through discussions with numerous colleagues over many years. Steve Grand provided an updated version of his global seismic tomography model and helped us to understand many aspects of its use to investigate the lithosphere. The analytical data

were obtained using instrumentation funded by ARC LIEF, and DEST Systemic Infrastructure Grants, industry partners and Macquarie University. The research was supported by ARC and Macquarie University grants to S.Y. O'Reilly and W.L. Griffin, and collaborative research with industry partners, especially Western Mining Resources and BHP-Billiton

References

Begg G.C., Griffin W.L., Natapov L.M., O'Reilly S.Y., Grand S.P., O'Neill C.J., Hronsky J.M.A., Poudjom Djomani Y., Swain C.J., Deen T. & Bowden P., 2009, The lithospheric architecture of Africa: Seismic tomography, mantle petrology and tectonic evolution. Geosphere 5, 23–50.

Coltorti M., Bonadiman C., O'Reilly S.Y., Griffin W.L. & Pearson N.J., 2008, Buoyant ancient continental mantle embedded in oceanic lithosphere (Sal island, Cape Verde Archipelago). Lithos doi:10.1016/j.lithos.2009.11.005.

Deen T., Griffin W.L., Begg G., O'Reilly S.Y. & Natapov L.M., 2006, Thermal and compositional structure of the subcontinental lithospheric mantle: Derivation from shear-wave seismic tomography. Geochemistry, Geophysics, Geosystems, doi:10.1029/2005GC001164.

Grand S., 2002, Mantle shear-wave tomography and the fate of subducted slabs, Philisophical Transactions of the Royal Society of London, A360, 2475-2491.

Griffin, W.L. & O'Reilly, S.Y., 2007, The earliest subcontinental mantle, in *The Earth's Oldest Rocks.* Van Kranendonk M.J., Smithies R.H. & Bennett V.C., eds, Elsevier, Amsterdam, 1013–1035.

Griffin W.L., O'Reilly S.Y., Afonso J.C. & Begg G., 2009, The composition and evolution of lithospheric mantle: A re-evaluation and its tectonic implications, Journal of Petrology, 50, 1185–1204.

Griffin W.L, O'Reilly S.Y., Afonso J.C. & Begg G.C., 2010, The evolution and extent of Archean continental lithosphere: implications for tectonic models, this volume

O'Reilly S.Y., Griffin W.L., Poudjom Djomani Y.H. & Morgan P., 2001, Are lithospheres forever? Tracking changes in subcontinental lithospheric mantle through time, GSA Today, 11, 4–10.

O'Reilly S.Y., Zhang M., Griffin W.L, Begg G. & Hronsky J., 2009, Ultradeep continental roots and their oceanic remnants: a solution to the geochemical "crustal reservoir" problem? Lithos, 112, 2, 1043–1054.

Poudjom Djomani Y.H., O'Reilly S.Y., Griffin W.L. & Morgan P., 2001, The density structure of subcontinental lithosphere: Constraints on delamination models, Earth and Planetary Science Letters, 184, 605–621.

MANTLE GEOCHRONOLOGY AND THE AGE OF THE SUB-CRATONIC LITHOSPHERE

N.J Pearson[1], W.L. Griffin[1], S.Y. O'Reilly[1] & O. Alard[2]

[1]GEMOC Key Centre, Department of Earth and Planetary Sciences, Macquarie University, NSW 2109, Australia
[2]CNRS, Université de Montpellier, 34095 Montpellier Cedex 05, France

Introduction

High precision *in situ* analysis of trace-element compositions and isotope ratios has revolutionised geochronology and geochemistry over the past decade. Most of the advances are due to the proliferation of laser-ablation microprobe inductively coupled plasma mass spectrometry (ICP-MS) and the rapid development of the multi-collector (MC-) ICP-MS. One of the main benefits of *in situ* analysis is that it allows the isotopic data to be interpreted in a microstructural context and to be integrated with geochemical data from other microanalytical techniques. This approach not only provides age information but helps to constrain the nature of the source rocks and to unravel the processes that have subsequently modified it.

Knowledge of the age, composition and evolution of the sub-continental lithospheric mantle (SCLM) is essential to an understanding of continental dynamics and the long-term stability of cratons. The combination of U-Pb dating of zircons and model ages derived from Hf isotopes has been demonstrated to be a powerful technique for understanding crustal evolution (e.g. Griffin et al., 2004a). Unfortunately the occurrence of zircon in mantle peridotites is rare and it is usually interpreted to be a product of metasomatism (e.g. Konzett et al., 2000; Zheng et al., 2006).

Re-Os Isotopes in Peridotites

Re-Os isotopic analyses of mantle-derived peridotites have contributed much of what is currently known about the age of the SCLM. ^{187}Re is the parent element of ^{187}Os (β-decay, $t^{1/2} = 1.666\ 10^{-11}a^{-1}$) and because it is moderately incompatible it is largely extracted from the mantle into basaltic melts during the formation of mafic crust. In contrast, Os is strongly compatible and it is concentrated in the residual mantle. Since the first application of Re-Os to dating mantle lithosphere formation (Walker et al., 1989) the assumption has been made that the model ages represent the age of primary melt depletion and lithosphere stabilisation.

Most of the initial information on the age of the SCLM has been provided by analysis of the whole-rock Re-Os isotopic system in mantle-derived peridotites, sampled as exposed massifs and xenoliths brought up by volcanic eruption. Model ages from xenoliths from beneath the Siberian, Kaapvaal and Slave cratons indicate that parts of the sub-continental lithospheric mantle are as old as the overlying Archean crust. Nevertheless, the significance of younger ages in the Re-Os dataset for cratonic xenoliths remains unclear. Do the younger ages represent melt extraction events or are they result of disturbance of the Re-Os system during metasomatism? This question has been investigated by applying *in situ* analytical techniques.

Sulfide is the dominant host for Os and the other platinum group elements (PGE) in mantle-derived peridotites, contributing between 80-100% of the whole-rock budget of these elements. *In situ* LAM-ICPMS analysis of PGEs shows that multiple generations of sulfide occur within many peridotites as evidenced by the variations in PGE patterns with micro-structural context (Alard et al., 2000). Inclusions of sulfide in primary silicates are characterised by high Os (20-1000 ppm) but low Pd/Ir (0.001-1), whereas interstitial sulfides and those associated with metasomatic phases typically have low Os (<30 ppm), Ir but high Pd/Ir ratios (up to 1000).

The development of *in situ* analysis techniques for Re-Os isotopes using laser ablation MC-ICP-MS enables the determination of ^{187}Os/^{188}Os in single sulfide grains (Pearson et al., 2002). Analyses of enclosed and interstitial sulfides in peridotite xenoliths show that the two types of sulfide differ significantly in their Re-Os systematics. Enclosed sulfides, such as those occurring in macrocrystic olivine in kimberlites, typically have unradiogenic Os compositions. Interstitial sulfides typically have ^{187}Os/^{188}Os ranging from asthenospheric (0.127) to highly radiogenic values (0.175). Analyses of multiple sulfide grains from single samples of spinel peridotite define mixing trends that may have either positive or negative slopes. In such samples it is clear that the whole-rock Re-Os signature reflects a mixing of several sulfide populations (Alard et al., 2002; Pearson et al., 2002). The observed trends also indicate the mobility of radiogenic Os, but not Re, and the disturbance of the Re-Os isotopic system during metasomatism.

Archean Lithospheric Mantle

In situ Re-Os isotopic analysis of sulfide phases in peridotite xenoliths from kimberlites in the Kaapvaal Craton has been used to determine the history of the SCLM and to establish links with crustal events (Griffin et al., 2004b). Samples from the Western Terrane (Finsch, Kimberley and Jagersfontein) and from the Southeastern Terrane (Northern Lesotho pipes) were included in the study to investigate the stabilization of the craton. Sulfides with the compositional features of both the 'enclosed' and 'interstitial' types of Alard et al. (2000) are present but both types may occur enclosed in primary silicates. This reflects the recrystallization in the SCLM and the presence of multiple generations of sulfides with widely varying Os contents, Re/Os and ^{187}Os/^{188}Os. The oldest sulfide ages are preserved in the most depleted peridotites, typically at shallower levels of the SCLM. Sulfide addition accompanies metasomatism

by asthenosphere-derived silcate melts and fluids, and there is an associated decrease in the maximum sulfide T_{RD} model ages. The Re-Os model ages of the whole-rock samples therefore represent mixtures and because the model age of whole-rock sample is younger than the maximum sulfide T_{RD} it is unlikely to date any specific geological event.

The age distribution of sulfides with $^{187}Os/^{188}Os$ <0.08, interpreted as MSS residual from melting (or last affected by metasomatism), show distinct differences between the terranes: Western Terrane, 2.9-3.2 Ga; Southeastern Terrane, 3.0-3.6 Ga. The peaks correlate with the oldest crustal ages in each terrane and indicate that the formation of the SCLM was earlier than, or contemporaneous with, the earliest crustal formation. Each terrane appears to have carried its own SCLM keel at the time of craton assembly. Distinct model-age peaks reflect the timing of the suturing of terranes (2.65, 2.75 Ga), and later rifting/collision of the western margin of the Kalahari Supercraton (1.8-2.2 Ga, ca 1 Ga). The sulfide age data push back the mean age of SCLM stabilization of the Kaapvaal Craton and suggest that the bulk of the Kaapvaal SCLM had formed prior to 3 Ga.

The age structure of the SCLM beneath the Udachnaya kimberlite pipe in the eastern Siberian craton has been studied using *in situ* Re-Os analysis of sulfides enclosed in olivine (Griffin et al., 2002). The olivine grains were selected from coarse (5-8 mm) mineral concentrate and their composition and grain size suggest derivation from the 'megacrystalline dunites' that occur at depths of 150-180 km. The sulfide inclusions range in size from 20-250 μm and several olivine grains contained multiple sulfide inclusions. Typically the sulfides consist of interfingered Ni-rich and Fe-rich MSS, surrounded by discontinous zones of pentlandite and an outer zone of chalcopyrite. No alloys were observed in section although irregular signals during laser ablation indicate the presence of Pt-rich nuggets.

The Os, Pt and Re contents of the sulfides allow the recognition of 5 populations with the compositional features: Group 1(67-6009 ppm Os; Os/Pt 256; Re/Os 0.0006); Group 2 (320-20000 ppm Os; Os/Pt <1.8; Re/Os 0.0007); Group 3A (40-225 ppm Os; Os/Pt <1-7; Re/Os 0.003); Group 3B (3-85 ppm Os; Os/Pt 9.5; Re/Os 0.006); Group 3C (~8 ppm Os; Os/Pt 1.1; Re/Os 0.067). The Os isotopic data for most sulfides from Groups 1, 2 and 3A give T_{RD} and T_{MA} ages > 2.5 Ga. Although Proterozoic model ages are derived from some Group 3A and 3B sulfides, most of the Group 3 sulfides have $^{187}Os/^{188}Os$ above the present-day CHUR, giving negative T_{RD} ages. In some cases where multiple sulfide inclusions occur in a single olivine grain, the sulfides belong to the same group and are similar in isotopic composition. In other olivine grains the sulfides are from different groups and have widely varying isotopic compositions and Re/Os ratios. In general these do not yield Re-Os isochrons with meaningful ages and initial ratios, implying that the inclusions represent different generations of sulfides.

The distribution of T_{MA} ages indicates that the SCLM beneath the Udachnaya pipe formed during the period 3.0-3.5 Ga, culminating with a major lithosphere-forming event at 2.9 Ga. It is suggested that partial melting of eclogites (3.2 to 2.9 Ga) produced melts with high $^{187}Os/^{188}Os$ and high Re/Os. Varying degrees of interaction between these melts and the Os-rich MSS produced the range of observed Os isotope compositions.

The T_{MA} age distribution plot for sulfides from peridotite xenoliths from the Slave Craton has a pronounced peak at 2.7 Ga (Aulbach et al., 2004). Thus the sulfide age distributions for the Kaapvaal, Siberian and Slave Cratons all have distinct modes between 2.7 and 3.0 Ga, suggesting that c.2.7 Ga corresponds to the timing of final stabilization of the lithospheric mantle beneath those cratons that still exist.

Discussion

The development of the *in situ* analysis method of mantle sulfides has shown that Re-Os isotope systematics in mantle-derived peridotites are complex. The microanalytical technique has demonstrated that different generations of sulfide, recognised on the basis of mineralogy and PGE compositions, have very different Os-isotope composition and that Os is mobile during metasomatism. The *in situ* data indicate that whole-rock Re-Os analyses of mantle-derived peridotites reflect the mixing of several generations of sulfides and that the interpretation of these data in terms of depletion ages may be ambiguous. Evidence for the scale of this mixing is shown by the range of Os isotope compositions for sulfide inclusions in single olivine grains. Thus analysis of separated olivine might overcome the effects of recent Re addition but may still give an $^{187}Os/^{188}Os$ for a mixture of different generations of sulfide. At best whole-rock T_{RD} ages provide minimum estimates for the age of melting in cratonic peridotites.

Meaningful interpretation of Re-Os data in terms of mantle events requires understanding of the occurrence and mobility of sulfides in mantle peridotites. Heterogeneity of Os isotopes in the convecting mantle is used as evidence to negate the significance of the age of a single sulfide grain (Pearson & Wittig, 2008; Rudnick & Walker, 2009). Because sulfide is one of the first phases to enter the melt during peridotite melting, then all of the sulfide present in highly depleted cratonic peridiotites might be metasomatic and could have mixed isotopic signatures. The whole-rock derived depletion ages for these samples will have little significance, especially if there are multiple generations of sulfide. It is important to note that the oldest sulfide model ages should also be considered to be minimum depletion ages. Although Os isotope ratios in low-Os sulfides may be less precise than conventional techniques, the *in situ* analyses provide the spatial context to recognise different sulfide generations and provide more readily interpretable depletion ages.

References

Alard O., Griffin W.L., Lorand J.P., Jackson S.E. & O'Reilly S.Y., 2000, Non-chondritic distribution of the highly siderophile elements in mantle sulfides Nature, 407, 891–894.

Alard O., Griffin W.L., Pearson N.J., Lorand J.-P. & O'Reilly S.Y., 2002, New insights into the Re-Os systematics of sub-continental lithospheric mantle from in situ analysis of sulphides, Earth & Planetary Science Letters, 203, 651–663.

Aulbach S., Griffin W.L., Pearson N.J., O'Reilly S.Y., Doyle, B.J. & Kivi K., 2004, Mantle formation and evolution, Slave Craton: from HSE abundances and Re-Os systematics of sulfide inclusions in mantle xenocrysts, Chemical Geology, 208, 61–88.

Griffin W.L., Spetsius Z.V., Pearson N.J. & O'Reilly S.Y., 2002, In-situ Re-Os analysis of sulfide inclusions in kimberlite olivine: New constraints on depletion events in the Siberian lithospheric mantle, Geochemistry, Geophysics, Geosystems, 2002-11-21.

Griffin W.L., Belousova E.A., Shee S.R., Pearson N.J. & O'Reilly S.Y. 2004a, Crustal evolution in the northern Yilgarn Craton: U-Pb and Hf-isotope evidence from detrital zircons. Precambrian Research, 127, 231–282.

Griffin W.L., Graham S., O'Reilly S.Y. & Pearson N.J., 2004b, Lithospheric evolution beneath the Kaapvaal Craton: Re-Os systematics of sulfides in mantle-derived peridotites, Chemical Geology, 208, 89–118.

Konzett J., Armstrong R.A. & Gunther D., 2000, Modal metasomatism in the Kaapvaal craton lithosphere: constraints on timing and genesis from U–Pb zircon dating of metasomatized peridotites and MARID-type xenoliths, Contributions to Mineralogy and Petrology 139, 704–719.

Pearson N.J., Alard O., Griffin W.L., Jackson S.E. & O'Reilly S.Y., 2002, In situ measurement of Re-Os isotopes in mantle sulfides by laser ablation multicollector-inductively coupled plasma mass spectrometry: Analytical methods and preliminary results, Geochimica et Cosmochimica Acta, 66, 1037–1050.

Pearson D.G. & Wittig N., 2008, Formation of Archaean continental lithosphere and its diamonds: the root of the problem, Journal of the Geological Society of London 165, 123–141.

Rudnick R.L. & Walker R.J., 2009, Interpreting ages from Re-Os isotopes in peridotites. Lithos, 112S, 1083–1095.

Walker R.J., Carlson R.W., Shirey S.B. & Boyd F.R., 1989, Os, Sr, Nd, and Pb isotope systematics of southern African peridotite xenoliths: implications for the chemical evolution of the subcontinental mantle, Geochimica et Cosmochimica Acta, 53, 1583–1595.

Zheng J., Griffin W.L., O'Reilly S.Y., Zhang,M. & Pearson N., 2006, Zircons in mantle xenoliths record the Triassic Yangtze-North China continental collision, Earth and Planetary Sciences, 247, 130–142.

CONSTRAINTS ON AGES OF GREENSTONE MAGMATISM IN THE NORTHERN PART OF THE SOUTHERN CROSS DOMAIN, YILGARN CRATON

A. Riganti[1], S. Wyche[1], M.T.D. Wingate[1], C.L. Kirkland[1] & S.F.Chen[2]

[1]Geological Survey of Western Australia, 100 Plain Street, East Perth, WA 6004, Australia
[2]P.O. Box 68, Victoria Park, WA 6979, Australia

Introduction

The northern Southern Cross Domain forms part of the Youanmi Terrane within the Archean Yilgarn Craton (Cassidy et al., 2006). Like the Eastern Goldfields Superterrane to the east and the Murchison Domain to the west, the northern Southern Cross Domain is characterized by the presence of multiply deformed greenstone belts separated by extensive tracts of variably deformed granite and granitic gneiss. However, in contrast to the adjoining regions, reconstruction of the greenstone stratigraphy and tectonic history has been notably hindered by the lack of exposure, structural discontinuity, and scarcity of suitable units for isotopic dating.

Advances in targeting mafic rocks for SHRIMP (sensitive high-resolution ion microprobe) U–Pb geochronology have opened up fresh opportunities to elucidate the geological evolution of the northern Southern Cross Domain. Newly obtained geochronology data from key areas of the domain provide robust constraints on the ages of the greenstones, and raise intriguing questions about the relationships of these greenstones with similar rocks in other parts of the Yilgarn Craton.

Regional geological setting and previous age constraints

The northern part of the Southern Cross Domain in the central part of the Yilgarn Craton comprises a number of discrete greenstone belts with common lithostratigraphic elements and structural histories, which most likely represent dismembered remnants of a wider succession (Riganti et al., 2007). Structural complexity, limited exposure, and lack of age control from the mafic sequence have precluded the establishment of detailed stratigraphic successions within the belts, as well as correlations between them. However, an overall regional stratigraphic sequence for the greenstones has quartzite and quartz–mica schist at the base, and an overlying mafic succession dominated by tholeiitic basalts with minor spinifex-textured komatiitic basalts and layered gabbroic sills, and subordinate ultramafic rocks (Chen et al., 2003). Banded iron-formation (BIF) and chert are abundant at lower to middle stratigraphic levels, whereas felsic intercalations within the mafic rocks are generally rare, and typically deeply weathered. In parts of the domain, the mafic-dominated succession is unconformably overlain by weakly metamorphosed felsic to intermediate volcanic rocks, followed by clastic metasedimentary rocks.

In the mapping program carried out by the Geological Survey of Western Australia (GSWA) in the northern central Yilgarn Craton between 1997 and 2005, all attempts to directly date igneous rocks from the greenstone succession proved unsuccessful, leaving the age of the greenstones poorly constrained within an interval of about 400 million years. Quartzite at the base of the exposed greenstone succession in the Maynard Hills and Illaara greenstone belts yielded 4.35 to 3.13 Ga detrital zircons indicating greenstone deposition on, or adjacent to, continental crust, and constraining the maximum depositional age of the greenstones to 3131 ± 3 Ma (Wyche et al., 2004). A Sm–Nd isochron age for basaltic rocks in the Marda–Diemals belt suggested a greenstone age of 3050 ± 100 Ma (Fletcher et al., 1984). Porphyritic microgranite at Deception Hill yielded an interpreted SHRIMP U–Pb zircon age of 3023 ± 10 Ma but contained a smaller component of zircons at 2787 ± 26 Ma, with the latter ascribed to radiogenic Pb loss (Nelson, 1999). However, the stratigraphic position of this intrusion with respect to the greenstone succession is unknown, and data from several similar intrusions in the region suggest that the older zircons may be inherited.

In the Marda–Diemals greenstone belt, the mafic sequence is unconformably overlain by the felsic to intermediate Marda Complex, in which greenstone-derived basal conglomerates and sandstones are overlain by andesite, rhyolite, and rhyolitic ignimbrite, dated at c. 2732 Ma (Riganti & Chen, 2002; Nelson, 2001a). In the same area, clastic sedimentary rocks of the Diemals Formation have a maximum age of c. 2729 Ma (Nelson, 2001b). Farther north, in the Gum Creek greenstone belt, the poorly exposed upper part of the succession also contains c. 2720 Ma felsic volcanic (Bodorkos et al., 2006) and clastic sedimentary rocks.

Given the limited direct age constraints available, the greenstones in the northern Southern Cross Domain were generally regarded as representing a 3.0 Ga mafic succession followed by a cycle of felsic magmatism and sedimentation at 2.7 Ga (Chen & Wyche, 2001), by analogy with similar ages previously reported for the adjacent Murchison Domain and in the southern part of the Southern Cross Domain (e.g. Wang et al. 1996; Pidgeon & Wilde, 1990). This assumption was largely based on lithological similarities and/or comparable tectono-structural histories with these parts of the Youanmi Terrane, as well as the isotopically distinct signatures from other terranes of the Yilgarn Craton (based on Sm–Nd isotopes; e.g. Champion & Cassidy, 2007).

New geochronology data

In recent years, significant advances in the ability to identify Zr-rich rocks in the field using a portable XRF analyser have allowed the targeting of mafic samples that contain sufficient zircon or baddeleyite for isotopic dating, thus opening up the possibility of obtaining crystallization ages directly from greenstones in the northern Southern Cross Domain. In order to further maximise the chances of obtaining suitable minerals, gabbroic rocks with late-stage, felsic differentiates were the target of choice in the attempt to date the greenstones.

Medium- to coarse-grained mafic rocks are a relatively common component of the greenstone succession in the region, where they form both discrete sill-like units, and coarser intervals and lenses within finer-grained, extrusive mafic rocks. One of the best-preserved sills, the Grass Flat Gabbro, is exposed west of Diemals Homestead, on the limbs of the Watch Bore Syncline (GSWA, 2008). The Grass Flat Gabbro consists of two major layered sills, each up to 1 km in thickness (Wyche et al., 2001). The lower sill intruded between chert and BIF horizons and typically contains more felsic zones with sparse acicular clinopyroxene crystals, up to 20 cm long, in a medium- to coarse-grained plagioclase-rich matrix. Locally preserved igneous layering, defined by differentiation of leucocratic and melanocratic gabbro, is concordant with bedding in underlying shale. The upper sill, in the core of the syncline, is concordant with both underlying and overlying spinifex-textured komatiitic basalts. The gabbroic rocks may be co-magmatic intrusive equivalents of the mafic extrusive greenstones they intrude, although this has not been demonstrated.

Four samples were collected for SHRIMP geochronology from the Grass Flat Gabbro, targeting outcrops with the highest Zr contents based on multiple portable-XRF analyses. One sample (GSWA 185990), which indicated about 400 ppm Zr, yielded abundant, variably metamict, euhedral zircons with high and variable Th/U ratios. The data are concordant to moderately discordant, and four concordant analyses indicate a mean $^{207}Pb/^{206}Pb$ date of 2807 ± 10 Ma, interpreted as the age of crystallization (Wingate et al., in press, c).

This new result for the Grass Flat Gabbro has important implications for the mafic magmatic history of the northern Southern Cross Domain. It revises the minimum age for the mafic sequence from c. 2732 Ma to c. 2807 Ma, and raises questions about the accepted division of greenstone magmatism into a 3.0 Ga mafic and 2.7 Ga felsic cycle for the area.

Regional implications

Evaluated in a broader regional context, the new 2807 Ma age for northern Southern Cross Domain greenstones introduces a critical missing link to the understanding of the crustal history of the Yilgarn Craton. A wealth of geochronological data recently acquired by GSWA (GSWA, 2009) has led to a significant re-assessment of the Archean greenstone magmatic evolution of other parts of the Youanmi Terrane and farther afield in the Yilgarn Craton (Van Kranendonk & Ivanic, 2009; Hall et al., 2009; Romano & Doublier, 2010; Ivanic et al., in press). The Murchison Domain and the Burtville Terrane (and possibly the southern part of the Southern Cross Domain) have been recognized to have similar components in their magmatic histories between c. 2820 and 2710 Ma. In particular, mafic to ultramafic magmatism between c. 2820 and c. 2800 Ma is becoming more widely recognized across the Yilgarn Craton:

In their stratigraphic re-evaluation of the Murchison Domain, Van Kranendonk and Ivanic (2009) identified three main stages of volcanism and sedimentation. Of these, the basal Norie Group consists of mafic volcanic rocks, that erupted between 2820 and 2800 Ma, overlain by felsic volcaniclastic sedimentary rocks intercalated with BIFs. Mafic–ultramafic layered intrusions into the sequence above (Ivanic et al., in press) include, among others, those of the Meeline Suite (e.g. the Windimurra, Atley, Barrambie, Lady Alma, and Youanmi Igneous Complexes), emplaced between c. 2820 and c. 2800 Ma, and the c. 2800 Boodanoo Suite (e.g. Narndee Igneous Complex). Greenstone magmatism continued between c. 2785 and c. 2734 Ma with the Polelle Group that comprises mafic volcanic rocks, felsic volcanic and volcaniclastic sedimentary rocks, and BIF. The c. 2724–2700 Ma Glen Group contains coarse clastic sedimentary rocks and basalts deposited prior to the onset of voluminous granitic magmatism.

In the southern part of the Southern Cross Domain, the interpreted age of felsic volcanic rocks from the Honman Formation in the Lake Johnston greenstone belt has been reduced from c. 2921 Ma to at least c. 2856 Ma (Romano & Doublier, 2010), and komatiitic units previously considered older than 2900 Ma are now regarded as intrusive (Heggie et al., in press), and therefore younger (i.e. <2856 Ma) components of the greenstone sequence. Leucogabbro from mafic sills in the northeast Yilgarn Craton (Burtville Terrane) has been dated at 2812 and 2755 Ma (Wingate et al., in press, a, b).

U–Pb and recently acquired Lu–Hf data also show evidence of a conspicuous 2.8 Ga juvenile crustal addition across the Yilgarn Craton (GSWA, unpublished data).

Although not identified in the northern Southern Cross Domain, old (>2900 Ma) greenstones are recognized in southern parts of the Southern Cross Domain (e.g. 2934 ± 7 Ma in the Southern Cross greenstone belt: Mueller & McNaughton, 2000), and in the Murchison Domain (c. 2950 Ma for greenstones in the Mount Gibson – Golden Grove area: Yeats et al., 1996; Wang et al., 1998), and have recently been identified in the Burtville Terrane (2961 ± 5 Ma in the Ulrich Range: Hall et al., 2009).

The new 2807 Ma age for the intrusion of the Grass Flat Gabbro in the Marda–Diemals greenstone belt does not preclude the possibility that the mafic–ultramafic volcanic component of this and other belts in the northern Southern Cross Domain are older than 2900 Ma, but does nonetheless establish an important stage of crustal development previously unidentified in this part of the Domain. It shows that c. 2820–2800 Ma mafic magmatism occurred in the northern part of the Southern Cross Domain at the same time as in adjacent parts

of the Youanmi Terrane and in the Burtville Terrane, supporting the proposition that these crustal fragments shared a common history prior to c. 2800 Ma. It is likely that the widespread mafic magmatic event that produced the Grass Flat Gabbro is related to the development of a large-scale mantle plume (cf. Ivanic et al., in press).

Given the similarity in age, the possibility that the Grass Flat Gabbro represents a stratigraphic equivalent of rocks of the Meeline or Boodanoo Suite of the Murchison Domain needs to be tested with more detailed geochemistry than is currently available. Similarly, geochronological data for the northern Southern Cross Domain need to be refined (e.g. age of the Deception Hill Microgranite) to better constrain the age and character of magmatism at the Paleoarchean–Mesoarchean boundary in this part of the Yilgarn Craton.

Acknowledgements

Zircon analyses were conducted using the SHRIMP ion microprobes at the John de Laeter Centre of Mass Spectrometry at Curtin University of Technology in Perth, Australia. The authors publish with permission of the Executive Director of the Geological Survey of Western Australia.

References

Bodorkos S., Love G.J., Nelson D.R. & Wingate M.T.D., 2006, 179239: porphyritic metadacite, Montague Well; Geochronology Record 647, Geological Survey of Western Australia, 4p.

Cassidy K.C., Champion D.C., Krapez B., Barley M.E., Brown S.J.A., Blewett R.S., Groenewald P.B. & Tyler I.M., 2006, A revised geological framework for the Yilgarn Craton, Western Australia, Geological Survey of Western Australia, Record 2006/8, 8p.

Chen S.F., Riganti A., Wyche S., Greenfield J.E. & Nelson D.R., 2003, Lithostratigraphy and tectonic evolution of contrasting greenstone successions in the central Yilgarn Craton, Western Australia, Precambrian Research, 127, 249–266.

Chen S.F. & Wyche, S. (compilers), 2001, Archaean granite–greenstones of the central Yilgarn Craton, Western Australia — a field guide, Geological Survey of Western Australia, Record 2001/14, 76p.

Champion D.C. & Cassidy K.C., 2007, An overview of the Yilgarn Craton and its crustal evolution, in *Proceedings of Geoconferences (WA) Inc. Kalgoorlie '07 Conference,* F.P. Bierlein & C.M. Knox-Robinson, eds, Geoscience Australia, Record 2007/14, 8–13.

Fletcher I.R., Rosman K.J.R., Williams I.R., Hickman A.H. & Baxter J.L., 1984, Sm–Nd geochronology of greenstone belts in the Yilgarn Block, Western Australia, Precambrian Research, 26, 333–361.

Geological Survey of Western Australia, 2008, Central Yilgarn, 2008 update, Geological Survey of Western Australia, 1:100 000 Geological Information Series.

Geological Survey of Western Australia, 2009, Compilation of geochronology data, June 2009 update, Geological Survey of Western Australia.

Hall C.E., Pawley M.J., Doublier M.P., Romano S.S., Wyche S. & Wingate M.T.D., 2009, The Burtville Terrane, northeast Yilgarn Craton: does it really belong in the Eastern Goldfields Superterrane? Geological Survey of Western Australia, Annual Review 2007–08, 1–3.

Heggie G.J., Fiorentini M.L., Barnes S.J., Barley M.E. & Gregory I. in press, Stratigraphy and stratigraphic control on the style of komatiite emplacement in the 2.9 Ga Lake Johnston Greenstone Belt, Yilgarn Craton, Western Australia, Precambrian Research.

Ivanic T.J., Wingate M.T.D., Van Kranendonk M.J., Kirkland C.L. & Wyche, S., in press, Age and significance of voluminous mafic-ultramafic magmatic events in the Murchison Domain, Yilgarn Craton, Precambrian Research.

Mueller A.G. & McNaughton N.J., 2000, U–Pb ages constraining batholith emplacement, contact metamorphism, and the formation of gold and W–Mo skarns in the Southern Cross area, Yilgarn Craton, Western Australia, Economic Geology, 95, 1231–1258.

Nelson D.R., 1999, 142920: quartz-feldspar porphyry, Deception Hill; Geochronology Record 342, Geological Survey of Western Australia, 5p.

Nelson D.R., 2001a, 168960: meta-ignimbrite, Marda Tank; Geochronology Record 194, Geological Survey of Western Australia, 4p.

Nelson D.R., 2001b, 168962: metasandstone, Yarbu Mine; Geochronology Record 196, Geological Survey of Western Australia, 4p.

Pidgeon R.T. & Wilde S.A., 1990, The distribution of 3.0 Ga and 2.7 Ga volcanic episodes in the Yilgarn Craton of Western Australia, Precambrian Research, 48, 309–325.

Romano S.S. & Doublier M.P., 2010, Geology of the Lake Johnston greenstone belt, Youanmi Terrane, Yilgarn Craton, Geological Survey of Western Australia, Record 2010/2, 4–6.

Riganti A. & Chen S.F., 2002, Geology of the Jackson 1:100 000 sheet: Geological Survey of Western Australia 1:100 000 Geological Series Explanatory Notes, 51p.

Riganti A., Wyche S. & Chen S.F., 2007, A new lithostructural framework for the central Yilgarn Craton, Geological Survey of Western Australia, Annual Review 2005–06, 72–76.

Van Kranendonk M.J. & Ivanic, T.J., 2009, A new lithostratigraphic scheme for the northeastern Murchison Domain, Yilgarn Craton, Geological Survey of Western Australia Annual Review, 2007–08, 35–53.

Wang Q., Schiøtte L. & Campbell I.H., 1996, Geochronological constraints on the age of komatiites and nickel mineralisation in the Lake Johnston greenstone belt, Yilgarn Craton, Western Australia, Australian Journal of Earth Sciences, 43, 381–385.

Wang Q., Schiøtte L. & Campbell I. H., 1998, Geochronology of supracrustal rocks from the Golden Grove area, Murchison Province, Yilgarn Craton, Western Australia, Australian Journal of Earth Sciences, 45, 571–577.

Wingate M.T.D., Kirkland C. L. & Pawley M. J. in press a, 185968, leucogabbro, Mount Sefton, Geochronology Record 869, Geological Survey of Western Australia.

Wingate M.T.D., Kirkland C.L. & Pawley M. J., in press b, 185976, leucogabbro, Mount Warren, Geochronology Record 870, Geological Survey of Western Australia.

Wingate M.T.D., Kirkland C.L., Riganti A., & Wyche S., in press c, 185990, gabbro, Grass Flat Bore; Geochronology Record 868, Geological Survey of Western Australia.

Wyche S., Chen S.F., Greenfield J.E. & Riganti A., 2001, Geology of the Johnston Range 1:100 000 sheet, Western Australia Geological Survey, 1:100 000 Geological Series Explanatory Notes, 31p.

Wyche S., Nelson D.R. & Riganti A., 2004, 4350–3130 Ma detrital zircons in the Southern Cross Granite–Greenstone Terrane, Western Australia: implications for the early evolution of the Yilgarn Craton, Australian Journal of Earth Sciences, 51, 31–45.

Yeats C.J., McNaughton N.J. & Groves D.I., 1996, SHRIMP U–Pb geochronological constraints on Archean volcanic-hosted massive sulfide and lode gold mineralization at Mount Gibson, Yilgarn Craton, Western Australia, Economic Geology, 91, 1354–1371.

2.69 Ga PARINGA BASALTS: CRUSTAL RECYCLING INTO THE ASTHENOSPHERE SOURCE

N. Said[1] & R. Kerrich[2]

[1]Centre for Exploration Targeting, School of Earth and Environment, The University of Western Australia, 35 Stirling Hwy, Nedlands, WA 6009
[2]Department of Geological Sciences, University of Saskatchewan, Saskatoon, SK, Canada S7N 5E2

Introduction

Neoarchean greenstone terranes globally record two prevalent volcanic associations: komatiites-tholeiitic basalts and bimodal tholeiitic to calc-alkaline basalts-dacites. Komatiites and associated basalts are generally interpreted as products of anomalously hot mantle plumes, erupted in ocean basins or continental margins (Arndt, 2008). Where crustally uncontaminated, both the komatiite-basalt association record prevalently depleted mantle asthenosphere signatures in terms of trace element, and Nd and Hf isotopes (Bennett, 2003), in conjunction with dominantly positive Nb anomalies, where Nb/Th ratios are greater than the primitive mantle value of 8. The tholeiitic to calc-alkaline association is generally considered to be arc-related (Wyman & Kerrich 2009).

A few studies have reported Archean isotopically, or trace-element, enriched volcanic sequences that appear not related to crustal contamination. Tomlinson et al. (1998) documented LREE-depleted Al-undepleted komatiitic basalts with ε_{Nd} values of ~-2 interpreted in terms of recycled older crust in the asthenosphere source. Polat (2009) interpreted transitional- to alkali-basalts of the 2.7 Ga Wawa greenstone terrane of Ontario, Canada, as ocean island basalts, and Smithies et al. (2004) inferred LREE-enriched mantle sources for the 3.0-2.95 Ga igneous suites of the Malina Basin, Pilbara craton.

Two types of Paringa basalts (depleted and enriched) occur towards the top of the volcanic stratigraphy of the Kambalda Sequence in the Neoarchean Kalgoorlie Terrane, Yilgarn craton. The depleted examples record LREE depletion with positive ε_{Nd} values, whereas enriched counterparts preserve coherent fractionated LREE patterns in conjunction with negative ε_{Nd} values. Enriched Paringa basalts have previously been interpreted as crustally contaminated komatiites (Lesher & Arndt 1995) or boninites (Redman & Keays 1985).

Therefore, these coexisting basalts provide a window into compositionally and isotopically heterogeneous, depleted to enriched asthenospheric mantle domains, or alternatively provide context for assessing varied intensities of crustal contamination. The results are used to evaluate the geodynamic setting in which the Paringa Basalts were erupted.

Geochemical Results

Depleted Paringa basalts are compositionally restricted, with Mg# between 61 and 57, and Ni between 166 and 73 ppm. On REE and primitive mantle normalised diagrams (Fig. 1) they are characterised by: (1) near-flat REE patterns with a small range of LREE depletion [$(La/Sm)_N$=1.01-0.76]; (2) absence of Ce or Eu anomalies; (3) Nb/Th ratios of 8.7-12, variably greater than the primitive mantle value of 8; and (4) no negative primitive-mantle normalised Nb, P, or Ti anomalies relative to neighbouring REE. They have compositions similar to Neoarchean tholeiitic basalts associated with komatiites, and ε_{Nd} 2.7 Ga values of +1.3 to + 2.2 are in keeping with the majority of crustally uncontaminated Neoarchean basalts and komatiites. Enriched counterparts of the Paringa Basalt are compositionally varied, with Mg# 76-53 and Ni 391-73 ppm. On REE and primitive-mantle normalised diagrams (Fig.1), they feature: (1) systematically fractionated LREE [$(La/Sm)_N$=2.1-3.1]; (2) near flat HREE, (3) absence of Ce or Eu anomalies; (4) low Nb/Th ratios of 0.7-1.6 ; and (5) strong negative primitive- mantle normalised Nb, P and Ti anomalies. Epsilon Nd values are -1.7 to -4.4; and there is no correlation of ε_{Nd} with indices of crustal contamination such as $(La/Sm)_N$ or Nb/Th ratios (Fig. 2).

Assimilation-fractional crystallisation (AFC) modelling was conducted using a komatiite as parental liquid. Contaminants used in this modelling were local trondhjemite-tonalite-dacite (TTD) Black Flag Group (BFG), high-Ca granites of the Yilgarn craton, and average Archean upper-, middle-, and lower continental crust of Taylor & McLennan (1985). None of the average Archean crustal compositions match the AFC trends, nor does the BFG. High-Ca granites do match the trends, as does average modern upper crustal composition but the High-Ca granites have depleted mantle Nd-isotope compositions. There are numerous additional problems with the AFC model in the genesis of the enriched Paringa basalts, including: (1) coherent REE patterns, uniform interelement ratios [Zr/Nb (18-21, La/Sm_N (2.2-3.1)], and isotopic signatures over a range of Mg#, and Nb-, P-, and Ti-anomalies that do not increase systematically with Th or $(La/Sm)_N$ as expected for crustal contamination; (2) Enriched Paringa basalts do not have the pronounced Zr-Hf/MREE anomalies of other crustally contaminated basalts of the Kambalda Sequence; (3) The Black Flag Group TTD dacites, presumably derived from continental crust beneath the Archean Kalgoorlie Terrane, or melts of such crust, has $\varepsilon_{Nd} \geq 0$, and hence cannot be a realistic contaminant; (4) There are no known lithological units of AUCC in the Kalgoorlie Terrane, that have $\varepsilon_{Nd} < 0$; and (5) Recent precise U-Pb zircon dating (e.g. Kositicin et al. 2008) has shown that the Paringa Basalt is younger than the Kambalda Komatiite by at least 10 Ma.

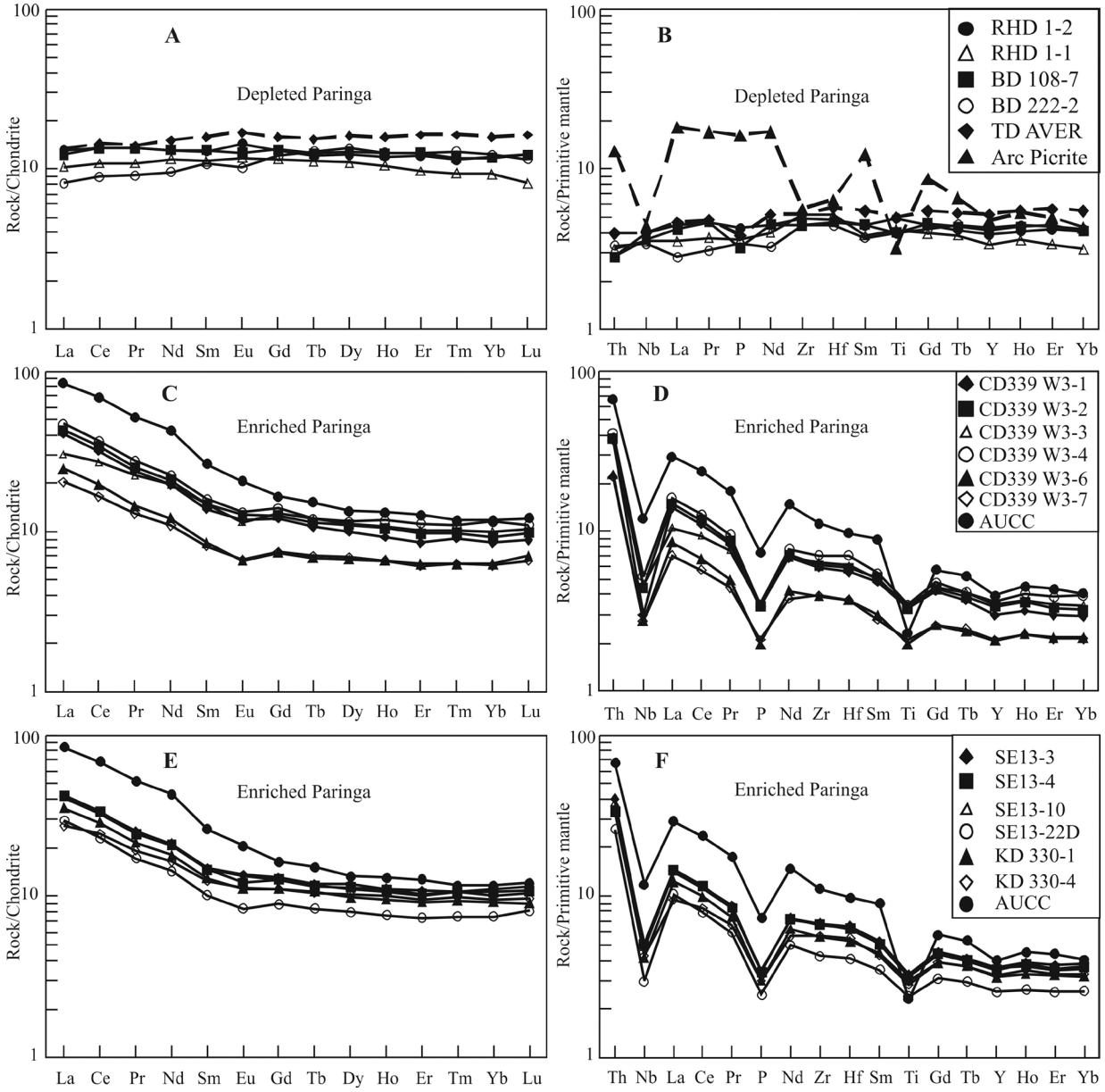

Figure 1. Chondrite and primitive mantle normalised trace element plots for the Paringa Basalts. Normalising values from Sun & McDonough (1989). Average uncontaminated Tisdale tholeiitic basalts (TD) from Kerrich et al. (1999). Archean upper continental crust (filled circle) from Taylor & McLennan (1985). In B an average Archean arc picrites is from Polat & Kerrich (2006).

Implications

Enriched Paringa basalts are compositionally distinct from Mg-rich continental flood basalts that feature greater contents of Ti, and other incompatible elements, with fractionated HREE, or boninites, picrites, or medium-K basalts from intraoceanic arcs. Rather, these basalts are interpreted to result from recycling of older continental crust into the mantle source of the plume from which the Kambalda Sequence komatiites and basalts were erupted. This enriched region could either be an independent plume, or an enriched "streak" in the Kalgoorlie Terrane plume. Alternatively, foundering of older crust into the shallow asthenosphere, or delamination of older subduction-modified continental mantle lithosphere, are consistent both with the negative ε_{Nd}-values and deep negative Nb, P, and Ti anomalies. Crustally uncontaminated depleted Paringa basalts have systematically positive Nb anomalies and LREE depletion in conjunction with positive ε_{Nd} values of depleted mantle asthenosphere. The two distinct compositional and isotopic types record a heterogeneous mantle plume, possibly erupted at a rifted craton margin where some units of the Kambalda Sequence record in contrast contamination during eruption.

References

Arndt N.T., 2008, *Komatiite*. Cambridge University Press. Cambridge.

Bennett V.C., 2003, Compositional evolution of the Mantle, in *Treatise of Geochemistry 2*, Carlson, R.W. eds, , 493–519.

Kerrich R., Polat A., Wyman D. & Hollings P., 1999, Trace element systematics of Mg-, to Fe-tholeiitic basalt suites of the Superior Province: implications for Archean mantle reservoirs and greenstone belt genesis, Lithos, 46, 163–187.

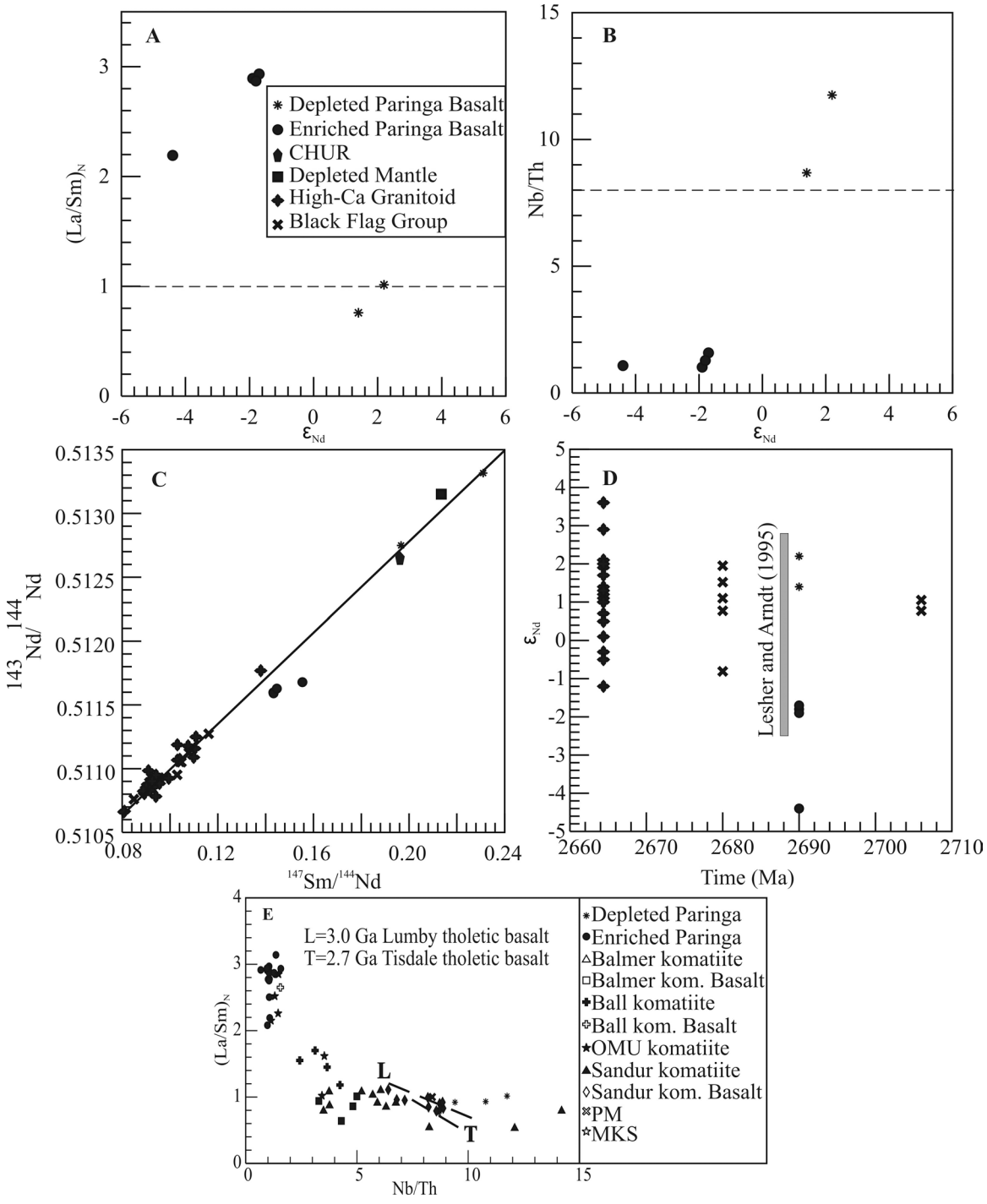

Figure 2. Variations of (La/Sm)N and Nb/Th versus εNd (A,B), $^{147}Sm^{144}/Nd$ versus $^{143}Nd^{144}/Nd$ (C); Age versus εNd(D); and Nb/Th versus La/Sm)N (E) for the Paringa Basalts. LU=Lumby uncontaminated tholeiitic basalts; LU= Lumby contaminated tholeiitic basalts are from Kerrich et al. (1999). In F the range of εNd values for the Kambalda Sequence in an earlier study is depicted as a vertical line (Lesher & Arndt 1995).

Kositcin N., Brown S.J.A., Barley M.E., Krapez B., Cassidy K.F. & Champion D.C., 2008, SHRIMP U-Pb zircon age constraints on the Late Archean tectonostratigraphic architecture of the Eastern Goldfields Superterrane, Yilgarn Craton, Precambrian Research, 161, 5–33.

Lesher C.M. & Arndt N.T., 1995. REE and Nd isotope geochemistry, petrogenesis and volcanic evolution of contaminated komatiites at Kambalda, Western Australia, Lithos, 34, 127–157.

Polat A., 2009, The geochemistry of Neoarchean (ca. 2700 Ma) tholeiitic basalts, transitional to alkaline basalts, and gabbros, Wawa Subprovince, Canada: Implications for petrogenetic and geodynamic processes, Precambrian Research, 168, 83–105.

Polat A. & Kerrich, R., 2006, Reading the geochemical fingerprints of Archean hot subduction volcanic rocks: evidence for accretion and crustal recycling in a mobile tectonic regime, in *Archean Geodynamics and Environments*, Benn K., Mareschal J.D. & Condie, K.C., eds, Geophysical Monograph Series, 164, 189–213.

Redman B.A. & Keays R.R., 1985, Archean basaltic volcanism in the Eastern Goldfields, Yilgarn Block, Western Australia, Precambrian Research, 30, 113–152.

Smithies R.H., Champion D.C., Sun S-s., 2004, Early evidence for LILE enriched mantle source regions: diverse magmas from the c. 3.0 Ga Mallina Basin, Pilbara Craton, NW Australia, Journal of Petrology, 45, 1515–1537.

Sun S-s. & McDonough W.F., 1989. Chemical and isotopic systematics of oceanic basalts: implications for mantle composition and processes, in *Magmatism in the Ocean Basins*, Saunders A.D. & Norry, M.J. eds, Geological Society of London Special Publication 42, 313–345.

Taylor S.R. & McLennan S.M., 1985, *The Continental Crust: Its Composition and Evolution*. Blackwell Scientific Publications, Oxford. 312p.

Tomlinson K.Y., Stevenson R.K., Hughes D.J., Hall R.P., Thurston P.C. & Henry P., 1998. The Red Lake greenstone belt, Superior province: Evidence of plume-related magmatism at 3 Ga and evidence of an older enriched source, Precambrian Research, 89, 59–76.

Wyman D. & Kerrich R., 2009. Plume and Arc magmatism in the Abitibi subprovince: implications for the origin of continental lithospheric mantle, Precambrian Research, 168, 4–22.

PALEO-ARCHAEAN RHYOLITES AND THE SOURCE OF POTASSIUM IN THE PROTO-CONTINENTAL CRUST

C.J.M.G. Sanchez-Garrido[1], G. Stevens[1], J-F. Moyen[1,*], H. Martin[2,3,4], R. Doucelance[2,3,4,], C. Harris[5] & R.A. Armstrong[6]

[1] Department of Earth Sciences, University of Stellenbosch, South Africa Private Bag X-1, Matieland 7602, South Africa;
[2] Clermont Université, Université Blaise Pascal, Laboratoire Magmas et Volcans, BP 10448, F-63000 Clermont-Ferrand;
[3] CNRS, UMR 6524, LMV, F-63038 Clermont-Ferrand;
[4] IRD, R 163, LMV, F-63038 Clermont-Ferrand, France;
[5] Department of Geological Sciences University of Cape Town, Louis Ahrens Building, Library Road, Rondebosch, 7701, South Africa;
[6] Research School of Earth Sciences, the Australian National University, Canberra, A.C.T. 0200 Australia;
** now at Département de Géologie, Université Jean-Monnet Faculté des Sciences, 23 rue du Docteur Michelon, 42023 Saint Etienne, France*

Introduction

Seventy five percent of Earth's continental crust is considered to have formed during the Archaean (4.0—2.5 Ga), as sodic Tonalite-Trondhjemite-Granodiorite (TTG) granitoids (Taylor & McLennan, 1995). These rocks arose through the partial melting of subducted hydrated oceanic crust and consequently, their formation constitutes continental crustal growth. The granitoid rock associations formed over the last 2.5 Gyr of Earth's history are predominantly calc-alkaline in chemistry and are mainly the products of crustal recycling. This implies that the bulk chemistry of the continental crust was largely shaped during the Archaean. Here we present evidence of a range of unusually low-Ca, high-K, peraluminous Archaean granites and rhyolites in the Barberton Greenstone Belt (BGB), which are preserved potentially only as clasts within the basal conglomerates of the 3.225 to 3.215 Ga Moodies group. This work aims to define the geochemistry of these granites, explore their relationship to the TTG plutons and investigation their contribution to the chemistry of the Archean upper crust from the Barberton area.

Geological setting and sample description

The Barberton Greenstone Belt accreted over the interval. 3.5 Ga to < 3.2 Ga and is surrounded by TTG granitoids formed over the same period. These cluster in three age groups at ca. 3.51—3.55 Ga, 3.45 Ga and 3.27—3.21 Ga, which are proposed to coincide with the accretionary episodes. The greenstone belt itself consists of 3 lithostratigraphic units: the Onverwacht Group, a mafic-ultramafic units interbedded with thin layers of chemical sediments; the Fig Tree Group, shallow-marine sediments and intermediate to felsic volcaniclastic rocks; and, the Moodies group, a coarse clastic sedimentary succession formed as a consequence of the topographic relief erected during the 3230 Ma collisional event (Heubeck & Lowe, 1994). The TTGs and the greenstone belt have been intruded by younger K-rich granites of the Granodiorite-Monzogranite-Syenite suite (GMS) between 3.20 and 3.10 Ga ago. The granitic and rhyolitic clasts of this study occur within the basal conglomerate of the Moodies group. Two main populations of clasts have been observed and sampled: i.e. volcanic and plutonic clasts, which represent material formed at surface or within shallow level magma chamber. Both varieties are characterised by the same range of compositions and alteration is moderate to low, as evidenced by the preservation of delicate igneous textures (i.e. graphic intergrowth between quartz and K-feldspar) and by a Chemical Index of Alteration (Nesbitt & Lowe, 1982) which varies from 50.06 to 65.08.

Geochronology, geochemistry and petrogenesis of the clasts

U-Pb SHRIMP analysis of zircons from 22 clasts revealed that the granites and rhyolites crystallised concurrently during each of the 3 episode of TTG magmatism in the Barberton Greenstone Belt (3519-3554 Ma, 3438-3486 Ma and 3210-3295 Ma) (Figure 1A). The age relationship between the TTGs and the clasts suggests that these rock types are either co-genetic, i.e. linked by a magmatic evolution process; or are coeval, i.e. formed in the same tectonic environment.

The clasts are characterised by high K_2O+Na_2O/CaO ratios (average 67.10) which reflect very low CaO contents (average 0.29 wt%), they have flat HREE profiles (average La_N/Yb_N 12.08) and high Ni and Cr contents (averages of 43.6 and 26.5 ppm respectively). Certain features in the chemistry of the clasts would appear to rule out a co-genetic relationship with the TTGs. In particular, the lack of deep Eu anomaly (Eu/Eu*) and the absence of correlation between Eu/Eu* and the Sr, or CaO content, in combination with the low CaO content, indicates that these magmas were not derived from a TTG-like source by a process involving fractionation of plagioclase. Similarly, the high Ni and Cr content of the granitic magmas, when compared to the TTGs, indicate that they were not derived from a TTG-like composition via a process involving separation of the granitic magma from pyroxene and/or amphibole-bearing residue. Consequently, we conclude that the granites were not produced by partial melting or fractional crystallisation of a protolith or magma of TTG composition. Thus, the TTG and granitic magmatisms were coeval in each of three episodes of accretionary related magmatism in the belt and it is concluded that the granites were formed in association with the subduction zones that generated the TTGs.

Radiogenic and stable isotopes

Study of Sm-Nd isotopes of both TTG and clasts (Figure 1B) are in agreement with the above. Epsilon Nd (ε_{Nd}) and depleted mantle Nd model ages (T_{DM}) of the two older groups of the clasts (3.45 and 3.54 Ga) are reasonably similar to the ε_{Nd} of the TTGs of the same age. This indicates that their precursor was extracted from the DM at the same time. However the ε_{Nd} of the clasts do not plot on the ε_{Nd} evolution vector of the TTG which exclude once again the TTG as a potential source for the clasts.

Epsilon Nd values of the clasts indicate that their precursor was extracted from a LREE depleted source (depleted mantle or newly extracted basalts). The lack of heterogeneity in the chemistry of the clast as well as the lack of positive correlation between $^{147}Sm/^{144}Nd$ and ε_{Nd} argue that the scatter of the ε_{Nd} seems to reflect the isotope heterogeneity of the source of the clasts, and exclude the hypothesis of mixing between juvenile material early extracted from a depleted mantle source and an older recycled crustal component (for the 2 older

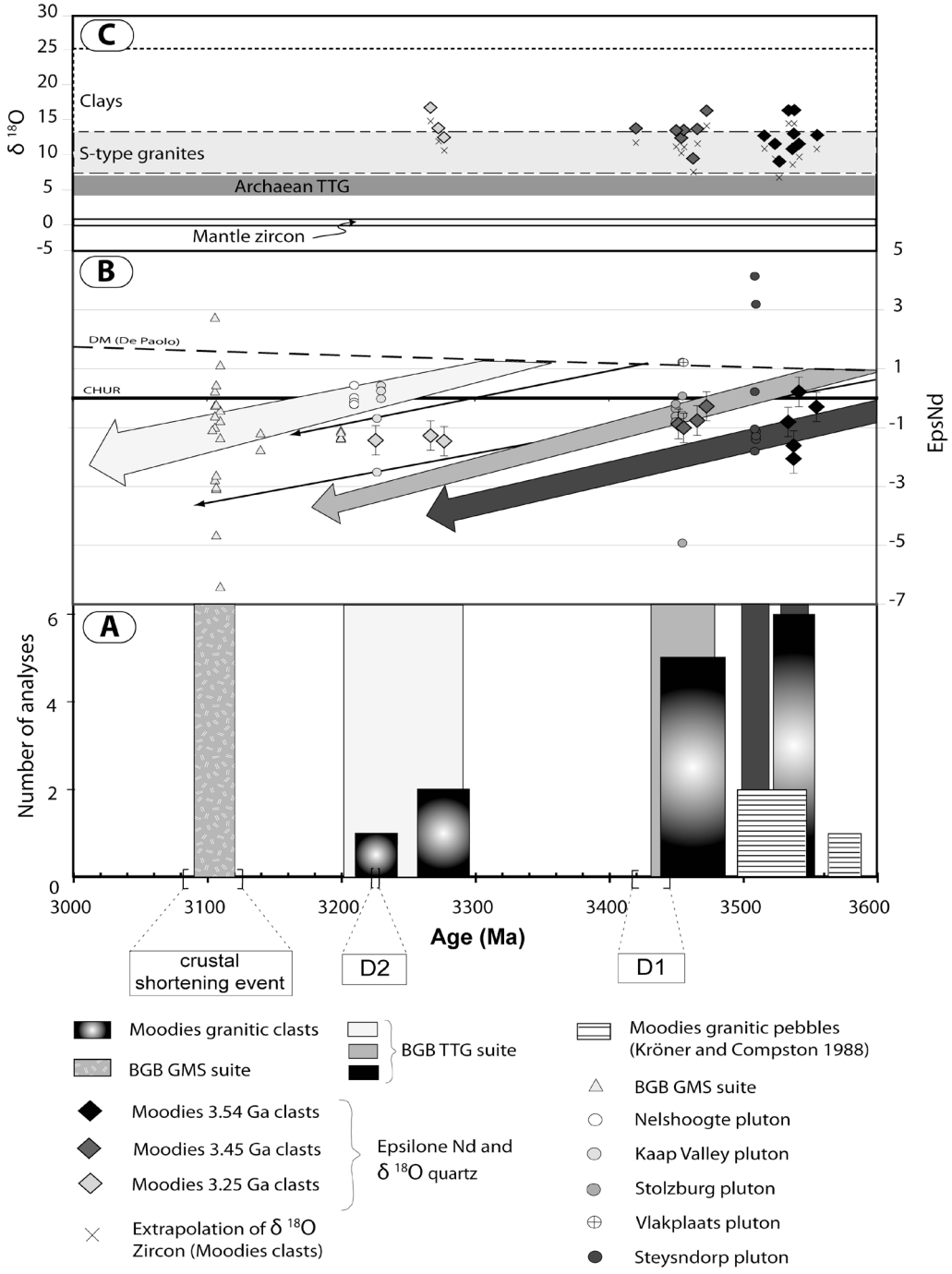

Figure 1A. A histogram representing the frequency of occurrence of crystallization ages in the granitic clasts (this study and Kröner and Compston 1988) as well as the TTGs and the late K-rich granites (Granodiorite-Monzogranite-Syenite (GMS) suite) occurring in the BGB. The major tectonic events affecting the BGB are represented along the age axis. The D1 event has been proposed to record processes within an active oceanic arc margin, the D2 event represents terrain amalgamation during an accretionary orogeny. This was accompanied by TTG formation during the 3226-3229 Ma periods. The 3126-3084 Ma event is thought to represent transcurrent shearing in an intraplate compressional context, but is accompanied by substantial mantle heat addition to the base of the crust and widespread granitic magmatism.

Figure 1B. Diagram showing the Epsilon Nd of the clasts, TTG and GMS suite as a function of their crystallisation ages.

Figure 1C. Summary of the δ18O values of the quartz phenocrysts from the clasts. Rock types plotted for reference are from Valley et al (2005).

groups of clasts). The increasing difference between the age of crystallisation of the clast and their T_{DM} age appear to reflect an increase amount of old material in the clasts genesis. The younger population of clasts (3.26 Ga) is a good example of that, as they also have a positive correlation between $^{147}Sm/^{144}Nd$ and ε_{Nd}. Importantly the chemistry of the clasts (REE pattern) proves that this old material is not TTG-like.

$\delta^{18}O$ in quartz phenocrysts from the clasts were analyzed using conventional laser fluorination. The quartz crystals have high $\delta^{18}O$ values for Archaean granites, ranging from 9.02 to 16.75‰. The extrapolated values for the magmatic zircon in equilibrium with the quartz phenocrysts are consequently significantly higher that typical for Archaean granitoids (6.76 to 14.46 ‰) (Figure 1C). The $\delta^{18}O$ values of the granites are similar to those of typical S-type granites and are evidence of clay-rich nature of the sediments from which the magmas were derived.

Origin of the clasts

From the earlier discussion it is clear that the chemistry of the clasts is not associated with a process of magmatic evolution. Consequently, the rock compositions should reflect the chemical characteristics of the magmas in the source. The peraluminous nature of the granites (A/CNK average:1.08, but up to 1.48), coupled with their increasing peraluminosity with maficity, high $\delta^{18}O$ values of the quartz phenocrysts and their accessory mineral suite typical of S-type granites (zircons, apatite, monazite, titanite and rutile) points toward a clay-rich sedimentary component in the source of the granites. The eruptive and high-level intrusive nature of the granites indicates that they formed via a fluid absent melting process.

In the subduction setting accounting for the formation of the TTG in the BGB there would appear to be two potential options for the source of the granites. A recent experimental study (Schmidt et al, 2004) has demonstrated that in such a setting even mafic sources can produce granitic melts, if they contain any significant K_2O fraction as, at high pressure, this stabilises phengite: the Archaean oceanic crust (which has been demonstrated to be K enriched compared to MORBs, due to its derivation from a less depleted mantle) thus constitutes a potential source. Alternatively, the magmas may have been produced by the melting of a metasedimentary source that may have occurred as a Ni and Cr-bearing clay-rich sedimentary veneer on the oceanic crust. Rocks with suitable compositions occur as thin layers within the Theespruit Formation in the BGB. The experiments of Schmidt et al (2004) allow these hypotheses to be tested. Fluid-absent melting of the mafic potential source, via consumption of phengite, will result in K-rich granitic melt that is significantly more enriched in CaO compared to the clasts (by a factor of > 5). In other hand, melting of metapelitic material under the same conditions produced granitic melt in very good agreement with the chemical characteristics of the clasts. The presence of rutile in some clasts provides a constraint on the pressure of the source as in such metasedimentary compositions rutile is stable above 1.5 GPa at 850 degrees ˚C, decreasing to 1 GPa at 1000 ˚C. Finally, a minimum estimate of the magma temperature (up to 855 ˚C) is given by the zircon solubility temperature. Consequently, we conclude that the clasts formed by fluid-absent melting of an originally clay-rich sediment derived from the weathering of the K-rich Archaean oceanic crust, at pressures in excess of 1.5 GPa.

Conclusion

This study demonstrates that each of three episodes of Archaean subduction in the BGB have produced both sodic TTG and granitic contributions to the crust. Melting of originally clay-rich oceanic sediments, consumed during the destruction of oceanic lithosphere, produced potassic upper crustal rocks without the staging of K_2O in the TTG reservoir. In the BGB, this occurred during three cycles of arc magmatism leading to a significant accumulation of K-rich sediments in the upper crust concurrent with the accretionary event which precedes cratonization. The southern facies of the Fig Tree sediments which formed as a consequence of the impending accretion event (Lowe & Nocita, 1999) have low La_N/Yb_N (6.39) and high $K_2O + Na_2O/CaO$ ratios (80.60) (Hoffman, 2005). This indicates that this substantial accumulation of potassic sediments was derived predominantly from material similar to the granites documented in this study and not TTG material.

Acknowledgements

G. S. acknowledges the NRF funding through the SARChI Programme. This project is partially funded by a joint French-South Africa Research program (!Khure CNRS & NRF) grant to G. S., , J.-F. M. and H. M.

References

Heubeck C. & Lowe, D.R., 1994, Late syndepositional deformation and detachment tectonics in the Barberton Greenstone Belt, South Africa, Tectonics 13, 1514–1536.

Hofmann A., 2005, The geochemistry of sedimentary rocks from the Fig Tree Group, Barberton greenstone belt: implications for tectonic, hydrothermal and surface processes during mid-Archean times, Precambrian Research, 143, 23–49.

Kröner A. & Compston W, 1988, Ion microprobe ages of zircons from early Archaean granite pebbles and greywacke, Barberton greenstone belt, Southern Africa. Precambrian Research, 38, 367–380.

Lowe D.R. & Nocita, B.W., 1999, Foreland basin sedimentation in the Mapepe Formation, southern-facies Fig Tree Group, in *Geologic evolution of the Barberton Greenstone Belt, South Africa,* Lowe D.R. and Byerly G., eds, Boulder, Colorado, Geological Society of America Special Paper 329.

Nesbitt H. W. & Young G. M., 1982, Early Proterozoic climates and plates motions inferred from major element chemistry of lutites, Nature 299, 715–717.

Schmidt M. W., Vielzeuf D., Auzanneau E., 2004, Melting and dissolution of subducting crust at high pressures: the key role of white mica. Earth and Planetary Science Letters, 228, 65–84.

Taylor S. R. & McLennan S. M., 1995, The geochemical evolution of the continental crust, Reviews of Geophysics, 33, 241–265.

Valley J. W. et al., 2005, 4.4 billion years of crustal maturation: oxygen isotope ratios of magmatic zircon, Contributions to Mineralogy and Petrology, 150, 561–580.

Nd-Sr ISOTOPIC AND TRACE ELEMENT CHARATERISTICS OF LOW Ti-P-K BASALTS FROM THE MAHAKOSHAL GREENSTONE BELT, CENTRAL INDIA

R.V.R. Talusani

Division of Earth Sciences, The University of New England, Armidale, NSW 2351, Australia.

Continental rift zones are long, narrow tectonic depressions in the earth's surface where the lithosphere has been modified by extension. The dynamics and evolution of rift zones has been the subject of intense study and debate for many years and still remains the focus of active investigation. Magmatism in the rift zones has important implications for crustal and mantle evolutionary models.

The late Archean-Paleoproterozoic Mahakoshal greenstone belt (MGB) is a 500 km long, 5 to 40 km wide, ENE-trending rift zone in central India. The MGB is an intracontinental mantle-activated aborted rift filled with a thick volcano-sedimentary sequence metamorphosed to the greenschist facies. The rocks have undergone polyphase deformation and are traversed by ENE-trending thrust faults and minor north striking, high-angle normal faults. The geology, metamorphism and structural setting of the MGB are detailed in some previous studies (Roy & Bandyopadhyay 1990, Roy et al. 2002, Nair et al. 1995, Talusani 2001), but limited information exists on the geochemistry of magmatic rocks of the MGB. For this reason, geochemistry of the basalts of the MGB has been investigated. The igneous rocks of the MGB record different stages of magmatic history and provide an excellent opportunity to study the tectonomagmatic evolution of Late Archaean crust and mantle. Magmatism is represented by ultramafic rocks, basalts, rhyolites, diorites and granites. Low Ti-P-K basalts occur near Katni in the central part of the MGB. These basalts are undeformed but slightly altered.

The Katni basalts define a good correlation between MgO and most major and trace elements. Some of these variations can be explained by fractional crystallization model. These basalts display depleted isotopic and trace element compositions. The initial $^{87}Sr/^{86}Sr$ ratios (0.70310 – 0.70465) of the Katni basalts are indicative of minimal crustal contamination of the mantle melt. The ε_{Nd} values (+3.4 to +5.6) obtained point to a depleted mantle source. The Katni basalts have near horizontal REE patterns, NMORB-like trace element patterns, high Zr/Nb ratio (~26) and ε_{Nd} values range from +3.4 to +5.6, indicative of their derivation from a depleted mantle source.

Modeling calculations were carried out to quantitatively evaluate the source mineralogy and the amount of partial (batch) melting. Partial melting modeling suggests that these basalts were derived by about 6% melting of peridotite containing no garnet. The primary magmas were derived from a relatively shallow mantle source. The overall uniform geochemical character of the Katni basalts indicates that they are likely to be from a single source and were emplaced in a mid-continental rift setting. The geochemical and Nd-Sr isotopic variations observed in these rocks are best explained by a model involving limited amount of lithospheric mantle involvement in addition to the dominant asthenospheric mantle components.

References

Nair K.K.K., Jain S.C. & Yedekar D.B., 1995, Stratigraphy, structure and geochemistry of the Mahakoshal greenstone belt, Memoir of the Geological Society of India, 31, 403–432.

Roy A. & Bandyopadhyay B.K., 1990, Tectonic and structural pattern of the Mahakoshal belt of central India: A discussion, Geological Survey of India Special Publication, 28, 226–240.

Roy A., Hanuma Prasad M. & Devarajan M.K., 2002, Low pressure metamorphism, deformation and syntectonic granite emplacement in the Palaeoproterozoic Mahakoshal supracrustal belt, central India, Gondwana Research, 5, 489–500.

Talusani R.V.R., 2001, Possible Carlin-type disseminated gold mineralization in the Mahakoshal fold belt, central India, Ore Geology Reviews, 17, 241–247.

THE PALEOARCHEAN GEODYNAMO, SOLAR WIND AND MAGNETOPAUSE

J.A. Tarduno[1,2], R.D. Cottrell[1], M.K. Watkeys[3], A. Hofmann[3], P.V. Doubrovine[1,4], E. Mamajek[2], D. Liu[5], D.G. Sibeck[6], L.P. Neukirch[2] & Y Usui[1]

[1]Department of Earth & Environmental Sciences, University of Rochester, Rochester, NY, 14627, USA
[2]Department of Physics and Astronomy, University of Rochester, Rochester, NY, 14627, USA
[3]School of Geological Sciences, University of KwaZulu-Natal, Durban 4000, South Africa
[4]Physics of Geological Processes, University of Oslo, Oslo 0316, Norway
[5]Beijing SHRIMP Centre, Chinese Academy of Geological Sciences, Beijing 100037, China
[6]Code 674, NASA/Goddard Space Flight Center, Greenbelt, MD, 20771, USA

Introduction

The onset and nature of the geomagnetic field is important for understanding the evolution of the core, atmosphere and life on Earth. The geomagnetic field shelters the atmosphere from erosion by the solar wind. In the case of the early Earth, the magnetic field would have had to balance the greatly enhanced solar wind pressure associated with the young rapidly-rotating Sun. The interplay between the magnetic field and radiation from the young Sun controls the loss of light elements and, ultimately, water and therefore can be thought of as a fundamental stage in the development of a habitable planet.

The geomagnetic field could have started shortly after core formation, especially in the case of relatively small present core-mantle boundary heat flow (~3 TW, Aubert et al., 2009). However, two recent hypotheses have called for a much later onset age of the geodynamo. Ozima et al, (2005) hypothesized that lunar nitrogen values reflected transport from Earth's atmosphere by the solar wind at 3.8-3.9 Ga in the absence (or with a very weak) geomagnetic field. Labrosse et al. (2007) predicted a delayed onset of the geodynamo, to ages as young as 3.4 Ga, on the basis of a model for cooling of a dense liquid layer at the base of the early Earth's magma ocean. If present heat flow at the CMB is high (~11 TW), the model of Aubert et al. (2009) predicts dynamo onset at ~3.75 Ga.

Investigating the early magnetic field to examine these predictions is difficult because of the ubiquitous metamorphism that has affected Paleoarchean rocks. Secondary thermoviscous magnetizations are expected to dominate in bulk whole rock samples of this age. Another concern is the potential for chemical remagnetization associated with Fe remobilization. The paleomagnetic challenge is one of finding natural magnetic carriers that can see through the metamorphism.

Methods

The paleomagnetism group at the University of Rochester has developed a new approach for paleointensity measurement using single silicate crystals (Cottrell & Tarduno, 1999) and in the past decade have used it to explore variations in long-term geomagnetic field behavior (e.g. Tarduno et al., 2001; Tarduno et al., 2006). Single silicate minerals can carry minute magnetic inclusions with the magnetic domain state and composition requirements to see through the metamorphism. Silicate crystal hosts that have been measured are typically ~1 mm in size, and are clear under low magnification (i.e. crystals with larger multidomain magnetic inclusions carrying secondary magnetizations are excluded). Measurement requires high sensitivity magnetometers. In the Rochester laboratory, this requirement is met by a 2G 3-component DC 755R SQUID Magnetometer with high resolution sensing coils and a new 2G 3-component DC SQUID Magnetometer with a 6.3 mm diameter room-temperature access bore optimized for singe crystal studies.

Oriented crystals are not required for paleointensity analyses, but they are needed for constraining paleolatitude, which is in turn needed for the calculation of dipole moments from a field values recorded at a given site. Methods using thin sections, grain isolation and CO_2 laser heating have been developed to obtain paleointensity and paleolatitude information from oriented silicate grains (Tarduno et al., 2007).

Results

Some of the least metamorphosed Paleoarchean rocks are found in the Barberton Greenstone Belt, having peak temperatures less than or equal to ~350 degrees C. Single silicate crystals (quartz and feldspar) hosting single domain-like magnetite inclusions separated from 3.2 billion-year-old plutons of the Kaapvaal craton South Africa have yielded paleointensity values based on thermoremanent magnetizations (i.e. magnetizations acquired on primary cooling) (Tarduno et al., 2007). These records suggest an intensity that is within 50% of the modern field value.

Dacite clasts from sedimentary rocks of the Barberton Greenstone Belt pass a conglomerate test, indicating magnetization prior to 3.42 Ga (Usui et al., 2009). The ~3.45 Ga dacite parent body for the clasts, however, reveals a high unblocking temperature magnetization with a scatter much higher than that seen in younger rocks. The simplest explanation of the large dispersion of magnetic directions is that it reflects the presence of multidomain magnetic grains in the whole rock samples studies that are susceptible to carrying magnetic overprints. However, the scatter could reflect magnetization in the absence of a geodynamo, in a field related to solar wind interaction with the atmosphere. A good discriminator of external versus internal terrestrial

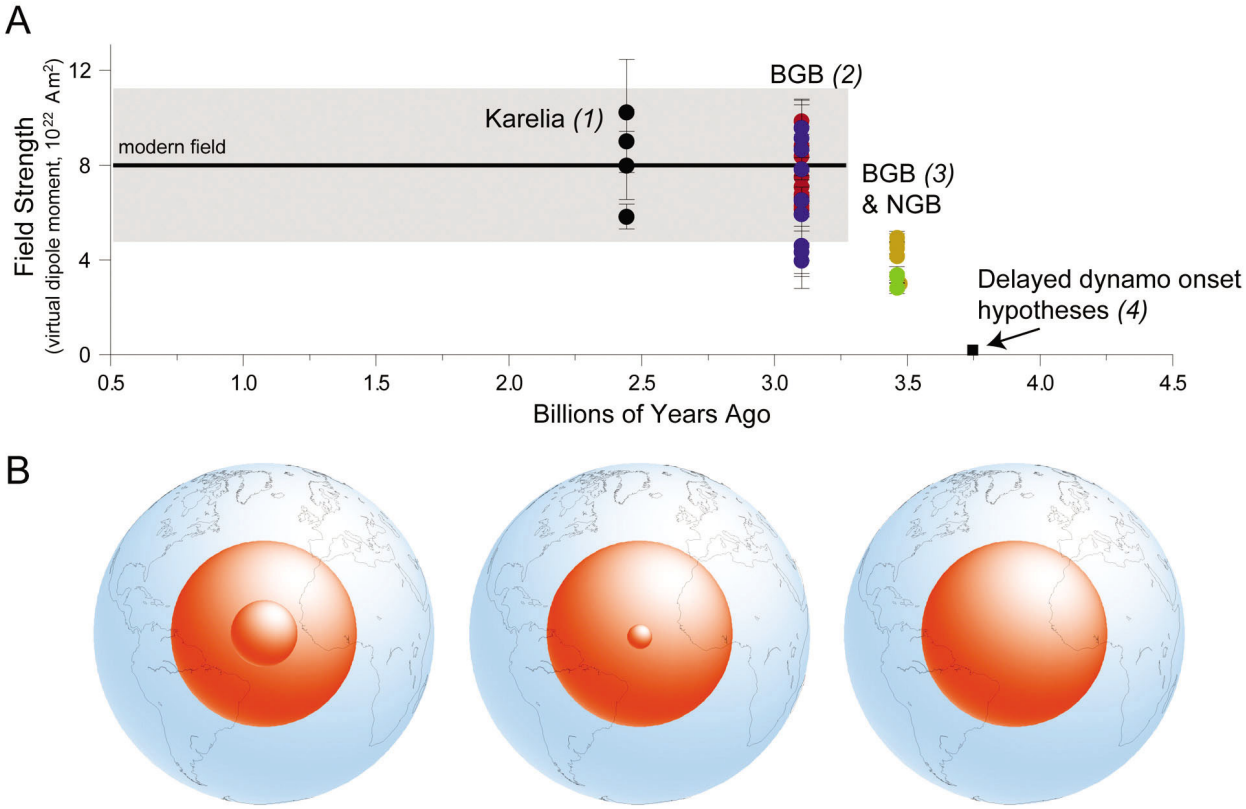

Figure 1. A. Summary of paleointensity data available from single silicate crystals. Locality abbreviations: BGB, Barberton Greenstone Belt, South Africa; NGB, Nondweni Greenstone Belt, South Africa. Also show is delayed geodynamo onset model. Data and model sources are as follows: (1) Smirnov et al., 2003 (2) Tarduno et al., 2007) (3) Tarduno et al. (2010) (4) Ozima et al., 2005; Labrosse et al., 2007; Aubert et al., 2009. B. Schematic evolution of inner core growth after Smirnov et al., 2003.

fields is paleointensity. Using modern Venus as an example of a planet lacking a dynamo, we expect that solar wind/atmosphere interaction will create a field that is much more variable, and more than an order of magnitude weaker than the post 3.2 Ga dynamo-driven field recorded on Earth.

We have tested the non-dynamo magnetization scenario by sampling dacites from two Kaapvaal craton localities in the Barberton Greenstone Belt and the Nondweni Greenstone Belt (dated at ~3.4 Ga). Thellier-Coe paleointensity data that meet acceptance criteria from quartz phenocryts show average field strengths that are unexpected from magnetization mechanisms in the absence of a geodynamo. Instead, these data extend the record of a geodynamo back in time 250 million years, from 3.2 Ga to ~3.45 Ga (Tarduno et al., 2010) (Figure 1).

Implications and future work

The field measured for 3.4 to 3.45 Ga is ~30-50% weaker than that of present-day and when combined with a greater solar wind pressure suggests steady-state Paleoarchean magnetopause standoff distances ≤ 5 Earth radii, similar to values observed during recent coronal mass ejection events. Aurora would have been at lower latitudes and polar cap area is predicted to have been up to 3 times greater than today. Heating, expansion and volatile loss from the exosphere is implied, affecting long-term atmospheric composition.

On-going efforts to test for the presence of an even older Paleoarchean-Hadean geodynamo, using extant rocks, and crystals (e.g. quartz and zircons) hosting magnetic inclusions from sedimentary rocks (sites from southern Africa, India and Australia) will be discussed.

Acknowledgements

We are grateful to the late William Goree for his encouragement and design of the small bore SQUID magnetometer and to the staffs of William Goree Inc and Applied Physics for final construction of the instrument. Supported by the US NSF and the John Simon Guggenheim Foundation (to JAT).

References

Aubert J.S. Labrosse C. Poitou, 2009, Modelling the paleo-evolution of the geodynamo, Geophysical Journal International, 179, 1414–1438.

Cottrell R.D & J.A. Tarduno, 1999, Geomagnetic paleointensity derived from single plagioclase crystals, Earth and Planetary Science Letters, 169, 1–5.

Labrosse S., Hernlund J.W. & Coltice N., 2007, A crystallizing dense magma ocean at the base of Earth's mantle, Nature, 450, 866–869.

Ozima, M., Seki K., Terada N., Miura Y.N., Podosek F.A. & H. Shinagawa, 2005, Terrestrial nitrogen and noble gases in lunar soils, Nature, 436, 655–659.

Smirnov A.V., Tarduno J.A. & Pisakin B.N., 2003, Paleointensity of the early geodynamo (2.45 Ga) as recorded in Karelia: A single crystal approach, Geology, 31, 415–418.

Tarduno J.A., Cottrell R.D. & Smirnov A.V., 2001, High geomagnetic field intensity during the mid-Cretaceous from Thellier analyses of single plagioclase crystals, Science, 291, 1779–1783.

Tarduno J.A, Cottrell R.D & Smirnov A.V., 2006, The paleomagnetism of single silicate crystals: Recording the geomagnetic field during mixed polarity intervals, superchrons and inner core growth, Reviews of Geophysics, 44, Art. No. RG1002.

Tarduno J.A., Cottrell R.D., Watkeys M.K. & Bauch D., 2007, Geomagnetic field strength 3.2 billion years ago recorded by single silicate crystals, Nature, 446, 657–660.

Tarduno J.A., Cottrell R.D., Watkeys M., Hofmann A., Doubrovine P.V., Mamajek E., Liu D., Sibeck D.G., Neukirch L., Usui Y., in press, Geodynamo, solar wind and magnetopause 3.45 billion years ago, Science.

Usui Y., Tarduno J.A., Watkeys M.K., Hofmann A. & R.D. Cottrell, 2009, Evidence for a 3.45 billion-year-old magnetic remanence: Hints of an ancient geodynamo from conglomerates of South Africa, Geochemistry, Geophysics, Geosystems, 10, Q09707.

EVIDENCE OF HADEAN CRUST IN THE PILBARA CRATON

S.G. Tessalina[1]*, B. Bourdon[2], M. Van Kranendonk[3#], J-L. Birck[4] & P. Philippot[1]

[1]Equipe Géobiosphère Actuelle et Primitive, Institut de Physique du Globe, IMPMC, CNRS & Université Paris Diderot, 4 Place Jussieu, 75252 Paris Cedex 05, France
**Present address: GEMOC, Earth and Planetary Sciences, Macquarie University 2109 Australia [2]Institute of Isotope Geochemistry and Mineral Resources, Department of Earth Sciences, ETH Zürich, CH-8092 Zürich, Switzerland*
[3]Geological Survey of Western Australia, 100 Plain St., East Perth, Western Australia, 6004 Australia
 # also at: School of Earth and Environment, the University of Western Australia, 35 Stirling Hwy., Crawley WA, 6009 Australia
[4]Equipe Géochimie et Cosmochimie, Institut de Physique du Globe, CNRS & Université Paris Diderot, 4 Place Jussieu, 75252 Paris Cedex 05, France

Introduction

Application of the ^{146}Sm-^{142}Nd and ^{147}Sm-^{143}Nd chronometers and U-Pb systematics to ancient rocks has shown that the differentiation of Earth's mantle into depleted and enriched reservoirs may have been initiated within the first 100-200 million years of Earth history (Caro et al. 2006, Kamber et al. 2003, Mojzsis et al. 2001). However, there is only limited evidence for the nature and composition of a complementary enriched crustal reservoir before 4.0 Ga (O'Neil et al. 2008, Upadhyay et al. 2009). In order to learn more about the nature of early crust on earth, we have undertaken new trace element and Sm-Nd isotope analyses on a suite of unweathered samples of well-preserved, low-grade basalt, sedimentary and hydrothermal rocks collected from two closely spaced drill holes through the c. 3.48 Ga Dresser Formation, Warrawoona Group in the North Pole Dome area of the Pilbara Craton, Western Australia (Pilbara Drilling Project).

Geological setting and sampling

The Dresser Formation (Warrawoona Group, Pilbara Craton) at North Pole in Western Australia consists of metabasalts and metakomatiites interleaved with three beds of cherty metasedimentary rocks that have experienced low-grade metamorphism (Van Kranendonk et al. 2008, Buick & Dunlop 1990). The lowermost chert unit is intercalated with several barite horizons and is overlain by silicified volcanogenic and bedded carbonate**.** This succession of chert, barite, volcanoclastic sandstone and carbonate is called the chert-barite unit and is connected to a network of barite-silica feeder veins intrusive to the underlying volcanic rocks and sedimentary unit. These intrusive barite and silica veins are thought to represent the conduits for hydrothermal fluid circulation (Thorpe et al. 1992, Buick & Dunlop 1990, Van Kranendonk 2006).

The tectonic setting of the Warrawoona Group has been interpreted as a thrust stack of remnants of oceanic crust (Kato & Makamura 2003), a volcanic-arc or near-arc sequence (Barley 1993), an oceanic plateau (Condie 1997), or a volcanic plateau built on a substrate of continental crust (Green et al. 2000, Van Kranendonk et al. 2007). The evidence supporting contamination of mantle-derived melts by older crust is based on the trace element composition of volcanic rocks (Green et al. 2000), the presence of inherited and detrital zircons, and xenoliths of older felsic crust (Van Kranendonk et al. 2007, Smithies et al. 2009) and high-μvalues of Pb isotopes (Bickle 1983).

Studied samples were collected from two closely spaced drill holes through the chert-barite unit and overlying (pillow basalt) and underlying (komatiite) volcanic units (Van Kranendonk et al. 2008, Philippot et al. 2009). The analyzed drill core samples include bedded carbonates, bedded barite, silica veins, pillow basalts and komatiites. All samples show various degrees of hydrothermal silicification, carbonation and pyritization. In addition to these, we analyzed three samples of komatiitic basalts and two black silica veins collected several hundred meters below the drill core sections from surface outcrops. The samples collected deeper in the volcanic succession are better preserved and less affected by hydrothermal circulation than those from the drill cores.

Results

^{147}Sm-^{143}Nd systematics

With the exception of one bedded carbonate, all the analysed samples fit on a Sm-Nd whole-rock isochron with a best-fit age of 3.492 ± 0.1 Gyr and an initial ε_{Nd} value of –3.3 ± 1.0 (Tessalina et al. in press). The Sm-Nd isochron age is in good agreement with a Pb-Pb age on galena of 3.490 Gyr from hydrothermal barite in this unit (Thorpe et al. 1992), a zircon U-Pb age of 3.480 Gyr recently obtained from a volcanoclastic layer of the same drill core (Van Kranendonk et al. 2008), and regional age control from underlying and overlying volcanics and related intrusions in the North Pole Dome between 3.515 to 3.458 Gyr (Thorpe et al. 1992, Van Kranendonk et al. 2007, Buick et al. 1995). These age data imply that the volcanic and sedimentary rocks, and associated hydrothermal precipitates, evolved as a closed system since deposition and that the chert-barite unit was deposited simultaneously with widespread and voluminous hydrothermal circulation. These results also preclude significant hydrothermal alteration associated with ca 2.7 Ga volcanism as hypothesized by Buick and Dunlop (1990), as this later event would have modified the Sm/Nd ratio and affected the isochron (Polat et al. 2003).

Nb-Th-U systematics

Nb-Th-U systematics have proven useful for reconstruction of the temporal evolution of continental

crust as a function of depleted mantle chemistry (Collerson & Kamber 1999). These elements are highly incompatible during mantle melting, as well as relatively immobile during metamorphism and alteration. Trace element ratios of such highly incompatible elements are classically used in geochemistry (rather than absolute abundances) because these ratios are good indicators of source rather than processes. Moreover, U and Th occur in low concentrations in mantle melts, and even minor contamination of these melts with crust or lithospheric mantle material (in which Th and U are more abundant) will significantly decrease the Nb/U and Nb/Th ratios of the final products. In addition, Nb/Th and Nb/U ratios in Archean mantle-derived basalts reflect, to a first order, the chemistry of the depleted mantle melt source (Collerson & Kamber 1999).

North Pole basalts have an average Nb/U ratio of 26.5, similar to early Archean mantle-derived rocks (28.0 ± 6.7, Collerson & Kamber 1999) and the primitive mantle value (30 ± 3, Hofmann et al. 1986), but significantly different from continental crust (Nb/U = 9.7). The average Nb/Th ratio of North Pole basalts (6.65) is lower than the average value of Early Archean mantle-derived rocks (8.5 ± 1.4).

Discussion

The negative ε_{Nd} value of -3.3 ± 1.0 indicates the involvement of older, enriched material in the Dresser Formation succession. The involvement of different possible crustal contaminants in North Pole basalts may be tested by combined analysis of trace-element data and Nd isotopic compositions: these possible contaminants include local Archean granodiorite (Green et al. 2000), average Early Archean Upper continental crust (Condie 1993), or Archean basaltic material (Condie 1993).

Even assuming that the mantle source had a Nb/U ratio similar to that of the least contaminated basalt from the underlying Coonterunah Subgroup, with Nb/U = 40.6 (Green et al. 2000), the assimilation of about 4-21% of Archean granodiorite, or about 4-11 % of average Early Archean Upper Crust, and/or 20-35% of Archean basalt is required to approach the composition of the North Pole Dome basalts.

Once the percentage of assimilated crust is estimated, one can reconstruct its $^{147}Sm/^{144}Nd$ and $^{143}Nd/^{144}Nd$ ratios and therefore estimate a model age of crust extraction, assuming that the primitive mantle melt has a komatiitic composition and that the final contaminated melt has a North Pole Dome basalt composition. The corresponding ages of crustal extraction from a chondritic mantle reservoir can then be determined. For the three types of contaminant, the Nd model ages range between 4.32 Ga for Archean granodiorite and upper continental crust, and 4.51 Ga for the Archean basalt. This extracted primitive crust apparently has been preserved within the deeper parts of the lithosphere, in the substrate for Pilbara volcanic plateau magmatism, or as kernels within a developing subcontinental lithospheric mantle, until sampled by volcanism at 3.49 Ga. The preservation of Hadean fragments within the lithospheric mantle has already been proposed to explain the low $^{142}Nd/^{144}Nd$ composition of the Proterozoic Khariar nepheline syenite complex, India (Upadhyay et al. 2009).

Based on the Nb-Th-U systematics, North Pole basalts are distinct from modern intraplate magmas (e.g. Ocean Island Basalt) and oceanic arc magmas, but are similar to average Archean basalt. This suggests that an appropriate contaminant involved in the source of North Pole basalt could be of basaltic origin. Contamination by continental crust or granodiorite cannot be ruled out, however. This would imply that by ~4.3 Ga, the extracted crustal component was already significantly differentiated, a scenario supported by the occurrence of 4.2 to 4.4 billion year old detrital zircons of the Jack Hills conglomerate, Western Australia (Mojzsis et al. 2001, Wilde et al. 2001). Our recognition of a Hadean crustal contaminant in Pilbara crustal rocks suggest that the evolution of the Pilbara crust commenced much earlier than previously thought and that the preserved <3.53 Ga volcanic edifice was built on a substrate of older mafic crust (over 4.3 Ga) but the origin of this crust solely based on our Nd isotope inference cannot be ascertained.

Conclusions

We report new ^{147}Sm-^{143}Nd data from weakly metamorphosed Paleoarchean basalt and layered chert-barite successions of the Dresser Formation, Pilbara Craton, Western Australia. A Sm-Nd isochron from basaltic, sedimentary and hydrothermal rocks at 3.49 ± 0.10 Ga is in good agreement with previous Pb-Pb and zircon U-Pb ages obtained on the same rocks. This indicates that the ^{147}Sm-^{143}Nd radioactive system has not been reset since the Paleoarchean. Initial ε_{Nd} values of –3.3 ± 1.0 indicate the involvement of an older protolith in the formation of the studied rocks. Modelling of trace element and isotopic compositions suggests that this older component was crustal and separated from the convective mantle over 4.3 billion years ago.

In conclusion, our new Sm-Nd isotopic data, combined with Th-U-Nb systematics, support the existence of an enriched Hadean crust during the early evolution of the Pilbara Craton. This crust may represent a cryptic relic of Hadean crust formed on an early magma-ocean Earth. The indication of Hadean primitive crust supports a model of basaltic crust formation on early Earth. Long term residence of differentiated material in the lithosphere with no, or limited, recycling in the deep mantle via subduction processes, could be a characteristic of late Hadean to early Archean geodynamics.

Acknowledgements

We thank the Institut de Physique du Globe de Paris, the Institut des Sciences de l'Univers (INSU) and the Geological Survey of Western Australia for supporting the Pilbara Drilling Project. P.P. acknowledges financial support from the Agence Nationale de la Recherche (ANR-Blanc).

References

Barley M.E., 1993, Volcanic, sedimentary and tectonostratigraphic environments of the ~3.46 Ga Warrawoona Megasequence: a review, Precambrian Research, 60, 47–67.

Bickle M.J., 1983, A 3500 Ma plutonic and volcanic calc-alkaline province in the Archaean East Pilbara Block, Contributions to Mineralogy and Petrology, 84, 25–35.

Buick R. & Dunlop J.S.R., 1990, Evaporitic sediments of early Archaean age from the Warrawoona Group, North Pole, Western Australia, Sedimentology, 37, 247–277.

Buick R. et al., 1995, Record of emergent continental crust approximately 3.5 billion years ago in the Pilbara Craton of Australia, Nature, 375, 574–577.

Caro G., Bourdon B., Birck J.-L. & Moorbath S., 2006, High-presicion 142Nd/144Nd measurements in terrestrial rocks: Constraints on the Early differentiation of the Earth's mantle, Geochimica et Cosmochimica Acta, 70, 164–191.

Collerson K.D. & Kamber B.S., 1999, Evolution of the continents and the atmosphere inferred from Th-U-Nb systematics of the depleted mantle, Science, 283, 1519–1522.

Condie K.C., 1997, Plate Tectonics and Crustal Evolution, Butterworth-Heinemann, Oxford.

Condie K.C., 1993, Chemical composition and evolution of the upper continental crust: contrasting results from surface samples and shales, Chemical Geology, 104, 1–37.

Green M.G., Sylvester P.J. & Buick R., 2000, Growth and recycling of Early Archaean continental crust: Geochemical evidence from the Coonterunah and Warrawoona Groups, Pilbara Craton, Australia, Tectonophysics, 322, 69–88.

Kamber B.S., Collerson K.D., Moorbath S. & Whitehouse M., 2003, Inheritance of early Archean Pb-isotope variability from long-lived Hadean protocrust, Contributions to Mineralogy and Petrology, 145, 25–26.

Kato Y. & Makamura K., 2003, Origin and global tectonic significance of Early Archean cherts from the Marble Bar greenstone belt, Pilbara Craton, Western Australia, Precambrian Research, 125, 191–243.

Mojzsis S.J., Harrison T.M. & Pidgeon R.T., 2001, Oxygen-isotope evidence from ancient zircons for liquid water at the Earth's surface 4,300 Myr ago, Nature, 409, 178–181.

O'Neil J.R., Carlson R.W., Francis D. & Stevenson R.K., 2008, Neodimium-142 evidence for Hadean mafic crust, Science, 321, 1828–1831.

Philippot P. et al., 2009, Drilling Archean stratigraphic horizons: Pilbara Craton, Western Australia and Barberton Belt, South Africa, Comptes Rendus Palevol, 8, 649–663.

Polat A., Hofmann A.W., Münker C., Regelous M. & Appel P.W.U., 2003, Contrasting geochemical patterns in the 3.7-3.8 Ga pillow basalt cores and rims, Isua greenstone belt, Southwest Greenland: implications for postmagmatic alteration processes, Geochimica et Cosmochimica Acta, 67, 441–457.

Smithies R.H., Champion D.C. & Van Kranendonk M., 2009, Formation of Paleoarchean continental crust through infracrustal melting of enriched basalt, Earth and Planetary Science Letters, 281, 298–306.

Tessalina S.G., Bourdon B., Van Kranendonk M., Birck J.-L., Philippot P., 2010, Influence of Hadaean crust evident in basalts and cherts from the Pilbara Craton, Nature Geosciences, in press

Thorpe R.I., Hickman A.H., Davis D.W., Moretnsen J.K. & Trendall A.F., 1992, Constrains to model for Archaean lead evolution from precise U-Pb geochronology from the Marble Bar region, Pilbara Craton, Western Australia. in The Archaean: Terrains, processes and metallogeny, Glover J.E.H., Ho S., eds, Vol. 22, Geology Department and University Extension, The University of Western Australia publication, 395–408.

Upadhyay D., Scherer E.E. & Mezger K., 2009, 142Nd evidence for an enriched Hadean reservoir in cratonic roots, Nature, 459, 1118–1120.

Van Kranendonk M., Hickman A.H. & Smithies R.H., 2007, The East Pilbara Terrane of the Pilbara Craton, Western Australia: Formation of a continental nucleus through repeated mantle plume magmatism. in Earth's Oldest Rocks, M. Van Kranendonk, M.J. Smithies, R. H. & Bennett V. eds., Vol. 15, Elsevier, Amsterdam, 307–337.

Van Kranendonk M., Philippot P., Lepot K., Bodorokos S. & Pirajno F., 2008, Geological setting of Earth's oldest fossils in the c. 3.5 Ga Dresser Formation, Pilbara Craton, Western Australia, Precambrian Research, 167, 93–124.

Van Kranendonk M.J., 2006, Volcanic degassing, hydrothermal circulation and the flourishing of early life on Earth: A review of the evidence from c.3490-3240 Ma rocks of the Pilbara Supergroup, Pilbara Craton, Western Australia, Earth-Science Reviews, 74, 197–240.

Wilde S.A., Valley J.W., Peck W.H. & Graham C.M., 2001, Evidence from detrital zircons for the existence of continental crust and oceans on the Earth 4.4 Gyr ago, Nature, 409, 175–178.

GROWTH AND EVOLUTION OF ARCHEAN CRUST IN SOUTH CHINA

S-B. Zhang[1], Y-F. Zheng[1] & G. Zhao[2]

[1] School of Earth and Space Sciences, University of Science and Technology of China, Hefei 230026, China
[2] Department of Earth Sciences, The University of Hong Kong, Pokfulam Road, Hong Kong

While Archean rocks are widely present in North China, Sm-Nd isotopic studies have shown that the Precambrian basement of South China consists mainly of Paleoproterozoic rocks, with only sporadic occurrences of Archean rocks at a few localities. The Yangtze craton is one of the major crustal blocks in South China. To improve the understanding of growth and evolution history of the Yangtze craton, a combined study of zircon U-Pb dating, O and Lu-Hf isotope analyses was carried out on the Kongling Complex in the Yangtze Gorge, the oldest basement in South China.

The Kongling Complex consists of granitoid gneisses (basement rocks), supracrustal rocks (upper unit) and some mafic rocks occurring as lenses, boudins or layers. It is divided into two parts by the Neoproterozoic Huangling batholith. The basement rocks are mainly TTG rocks with minor granites. Three groups of U-Pb ages were obtained for zircons from seven basement rocks in the northern and southern parts of the Kongling Complex, including migmatites, gneisses and granites. The first group of 2.90 to 3.00 Ga represents the emplacement time of magmatic plutons except one granite body with an age of 2.85 Ga. The second group of 3.12 to 3.35 Ga was obtained from residual cores of zircons from some migmatites and gneisses. The third group of about 1.98 Ga was obtained from zircon overgrowth in migmatite. Metamorphic ages similar to the third group were also obtained from metasedimentary rocks and amphibolites, suggesting cratonization of the Yangtze craton at this time. These ages indicates a tectonothermal event in the mid-Paleoproterozoic in the Yangtze craton, consistent with contemporaneous global events during the assembly of supercontinent Columbia. The O isotope compositions of basement rocks are similar to those of typical Archean TTG rocks, with most zircon $\delta^{18}O$ values lower than 6‰. The O isotopic ratios for the metasedimentary rocks are obviously higher, consistent with its sedimentary sources. Zircon Lu-Hf isotopes were measured for the three groups of zircons from the migmatites, gneisses and granites. The ~2.9 Ga zircon grains from different rocks have similar Hf isotope compositions, with $\varepsilon_{Hf}(t)$ values of -2.1 to -5.2 and Hf model ages of 3.4 to 3.5 Ga. The Hf isotopic ratios of 13 residual zircon cores are lower than the ~2.9 Ga grains. The weighted mean of their $\varepsilon_{Hf}(t)$ values is -1.6, corresponding to a Hf model age of 3.55 Ga. The Hf isotopic results suggest that the growth of Yangtze continental nucleus began as early as 3.5 Ga. $\varepsilon_{Hf}(t)$ values for the Paleoproterozoic zircons from the migmatite and metasedimentary rocks are variably negative and Hf model ages are Archean. The migmatites, gneisses and granites of the Kongling Complex have similar Rb-Sr and Sm-Nd isotope compositions. The $\varepsilon_{Nd}(t)$ values at t = 2.9 Ga are all around zero, from -1.9 to +2.6. Therefore, the initial growth of the Yangtze continental crust started no later than 3.5 Ga and suffered reworking in the middle Paleoproterozoic after the growth in the Archean.

U-Pb dating and Lu-Hf isotope analyses on detrital zircons from the Liantuo Formation, whose deposition occurred at about 750 Ma, give similar information on the early history of the Yangtze craton. Totally 106 grains were analysed for zircon U-Pb ages and 39 grains were further analyzed for their Lu-Hf isotopes. Four populations of ages are recognized, namely >3.0Ga, ~2.95Ga, ~1.95 Ga and 820-750 Ma. One grain shows a concordant U-Pb age of 3.8 Ga and an $\varepsilon_{Hf}(t)$ value of -0.8 with a Hf model age of 4.0 Ga, representing the oldest crustal relict in the Yangtze craton. The 3.3 Ga zircons have positive $\varepsilon_{Hf}(t)$ values as high as 4.2, providing compelling evidence for the growth of juvenile crust in the Paleoarchean. All the zircons have Archean Hf model ages, with prominent peaks at 3.2 to 3.6 Ga, indicating an important period of crustal growth in the Paleoarchean. The other three zircon populations at ~2.95 Ga, ~1.95 Ga and 820-750 Ma have negative $\varepsilon_{Hf}(t)$ values and are consistent Archean Hf model ages, suggesting multi-stage episodic reworking of Archean crust in South China.

FORWARD MODELLING OF PETROLOGICAL CRUST-FORMING PROCESSES ON THE EARLY EARTH

K. Ziaja, S. Buhre, S.F. Foley & R.W. White

Earth System Science Research Centre, Institute for Geosciences, University of Mainz, Becherweg 21, D-55099 Mainz, Germany

Introduction

The timing of the onset of the modern style of plate tectonics on Earth is still debated, and the tectonic style must have evolved as the planet cooled (Stern 2007). Furthermore, the bulk compositions of rocks involved in early Earth processes must have changed as well. Present day subduction involves MORB with 4-8 wt% MgO, whose metamorphic products during subduction are, presuming hydrothermal alteration close to the mid-ocean ridge, amphibolite, garnet-amphibolite and eclogite. The formation of early continental crust, comparable to tonalite-trondhjemite-granodiorite gneisses (TTG), requires hydrothermal alteration of oceanic crust, which transforms to garnet-amphibolite before melting (Foley et al. 2002). Due to higher heat flow and higher degrees of melting, the Archaean oceanic crust was probably thicker than today (Bickle et al. 1994) and had a bulk composition that was more magnesium-rich. This crust may have been so thick that it could not be subducted as a coherent unit. There may have been delamination and metamorphism of only the lower ultramafic part of the oceanic crust, which had not experienced hydrothermal alteration. Experiments on a komatiite (17.5% MgO) from Gorgona island, Columbia, showed that the metamorphic products of picrites and ultramafic cumulates are plagioclase-free pyroxenites and that the incoming of garnet lies at higher pressures than those for MORB (Foley et al. 2003), suggesting that there may be important differences in magmatic processes in subduction zones as a function of time. Partial melts of these (garnet-) amphibole-pyroxenites would have led to basaltic to nephelinitic melts that do not resemble TTG (Foley et al. 1999). In the late Archean the oceanic crust became thinner due to the progressive cooling of the Earth, and it became possible to subduct the whole crust (Abbott & Mooney 1995), including hydrothermally altered rocks, thus producing TTG by melting of garnet-amphibolite during subduction. The thinning of oceanic crust must have been caused by a compositional change in the bulk compositions of the rocks involved in these processes. Here, forward modelling, combining mineral equilibria calculations and high-pressure experiments, is used to locate this first-order transition from plagioclase-free to plagioclase-dominated melting conditions in modelled Archaean oceanic crust (MAOC) containing rocks with varying MgO.

Thermodynamic modelling

Mineral equilibria calculations were undertaken in the NCFMASHTO system (Na_2O – CaO – FeO – MgO – Al_2O_3 – SiO_2 – H_2O – TiO_2 with "O" as a factor for the amount of Fe^{3+}) using the Software THERMOCALC 3.33 (Powell & Holland 1988) and the internally consistent data set tcds55 (Holland & Powell 1998). Several P-T pseudosections, with intermediate MgO contents between the Gorgona komatiite and MORB composition were modelled, assuming water-saturated conditions. The bulk compositions for the Gorgona komatiite, picrites from the Deccan Traps (Shirey et al. 1994) and Keweenawan (Krishnamurthy et al. 2000) and a MORB (Diener et al. 2007, Sun & McDonough 1989) are given in Table 1.

MORB (Fig. 1a) shows a field of various garnet-amphibolite-assemblages at high temperatures (700-900°C) up to 17 kbar, which include plagioclase, amphibole and garnet; the dominating assemblage is garnet – hornblende – diopside – plagioclase – quartz – rutile – H_2O. Mineral abbreviations are those used in Diener et al. (2007). The low-T boundary is marked by the incoming of garnet at low P, and plagioclase at medium to high P. The plagioclase-stability line describes the transition to eclogite at high P-T and the solvus top between diopside and omphacite is located at 625 °C and 17 kbar. The effect of higher MgO is seen in the pseudosection modelled for bulk composition B (Keweenawan, Fig. 1b), note the different pressure range compared to Fig. 1a. The amphibolite assemblage mentioned before is still stable but within a smaller P-T window because garnet stability is restricted to slightly higher pressures than for MORB. Additionally, orthopyroxene is stable at high T. The assemblage garnet – hornblende – diopside/omphacite – rutile – quartz – H_2O covers a wide range from 12 to 25 kbar, in which the clinopyroxenes are not

Table 1. The bulk compositions in wt % and mol % used in constructing the phase diagrams in Figure 1.

Rock composition	SiO_2	Al_2O_3	CaO	MgO	FeO	Na_2O	TiO_2	O	Unit
MORB (A)	51.61	15.19	11.21	8.38	9.59	2.66	1.37		wt %
(Fig. 1a)	53.40	9.26	12.43	12.93	8.29	2.66	1.07	0.5	mol %
Keweenawan (B)	49.16	13.03	10.01	11.23	11.85	2.64	1.19	0.5	wt %
(Fig. 1b)	50.34	7.86	10.98	17.15	10.13	2.62	0.92	0.5	mol %
Deccan Traps (C.)	47.41	10.07	13.19	13.20	11.11	1.65	2.00		wt %
(Fig. 1c)	47.63	5.96	14.20	19.77	9.32	1.61	1.51	0.5	mol %
Gorgona (D)	46.30	10.10	10.20	17.50	11.57	1.24	0.66		wt %
(Fig. 1d)	46.01	5.92	10.86	25.93	9.60	1.20	0.49	0.2	mol %

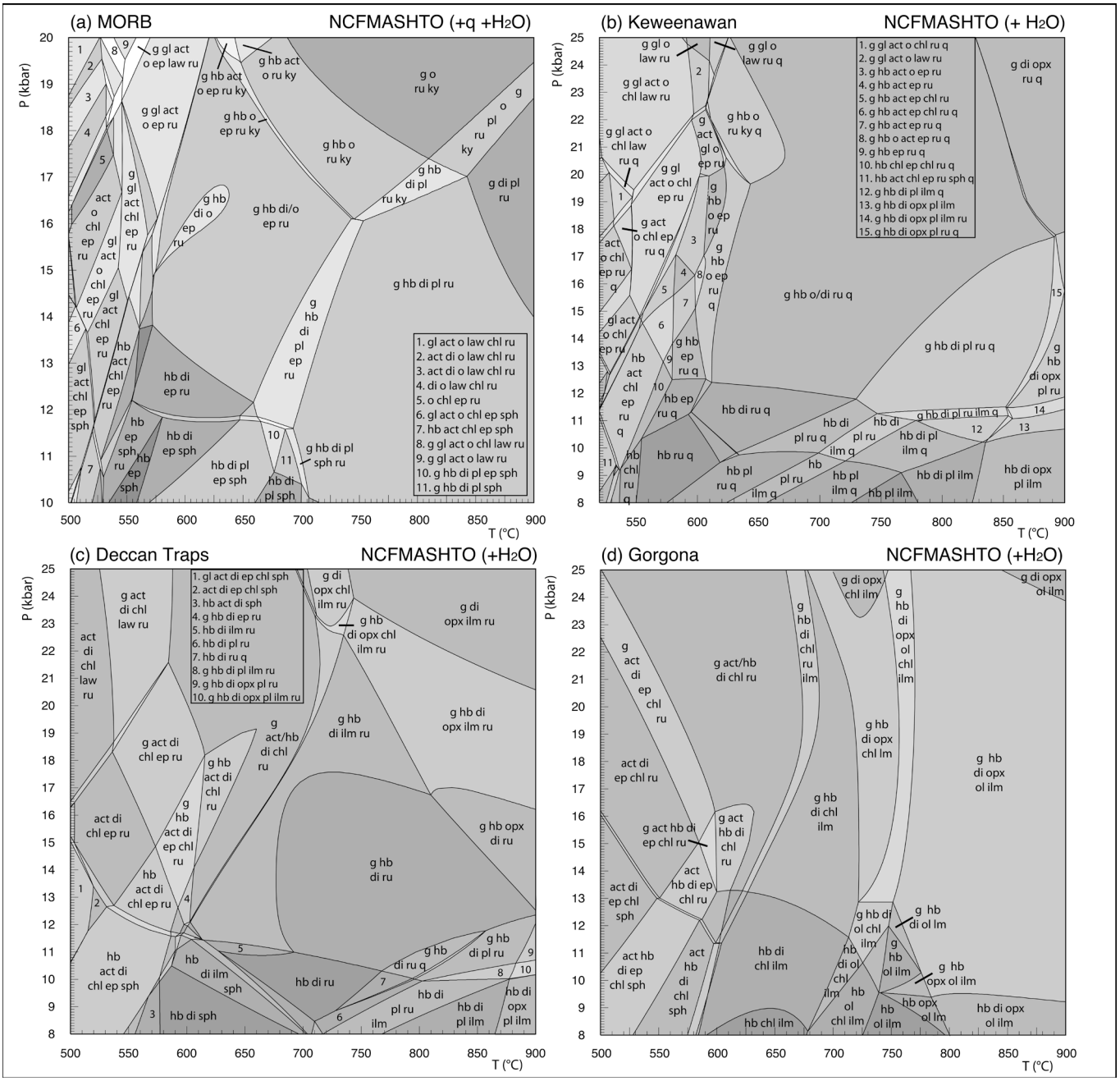

Figure 1. P-T pseudosections for metamorphosed (a) MORB, (b) Keweenawan, (c) Deccan Traps and (d) Gorgona.

further distinguishable above the solvus at high P-T. This assemblage, as well as the assemblage without garnet, occur also in the pseudosection for composition C (Deccan Traps picrite, Fig. 1c), but they are reduced to a small, ellipsoidal P-T area around 800 °C and 11 kbar. In Fig. 1c garnet-amphibolite stability is restricted within a narrow range between 800 – 900°C and 10 – 12 kbar but it is unlikely that the melting would be so constrained, especially at these pressures. The low-T assemblages in the Deccan Traps composition are stable in the pseudosection for the Gorgona komatiite (Figure 1d) as well. In the latter, orthopyroxene appears at lower temperatures and olivine is stable in the pseudosection at T above ca. 750 °C, creating the main differences between these two pseudosections. The incoming of garnet is at approximately 10 kbar for both. Hornblende – diopside – orthopyroxene – olivine – ilmenite – H_2O garnet broadly correspond to the (garnet-) amphibole-pyroxenite as described in Foley et al. (2003), and covers nearly the complete field in excess of 750 °C.

The trend of metamorphosed products of MORB via picrite to komatiite show a change from amphibolites to pyroxenites delineated by the changing stability of the main marker minerals plagioclase and garnet. With increasing MgO the field of garnet-amphibolite decreases, firstly due to the decreasing stability of garnet at lower pressures (Figs 1a-1b), and secondly owing to the restriction of plagioclase stability to lower pressures in the Deccan Traps, and its complete disappearence in the Gorgona-pseudosection. Assemblages without amphibole are always located in the upper right corner of the pseudosections, shrinking with increasing MgO of the bulk composition until only a small amphibole-free assemblage is located in Figure 1d. The amphibole-out reaction is accompanied by water-release and may be an indication for the onset of melting. Unfortunately, there is no melting model for metabasic rocks in THERMOCALC and the solidus is not shown in the pseudosections. Adopting the haplogranite melt-model of White et al. (2007) in the system FMASH (FeO – MgO – Al_2O_3 – SiO_2 – H_2O)

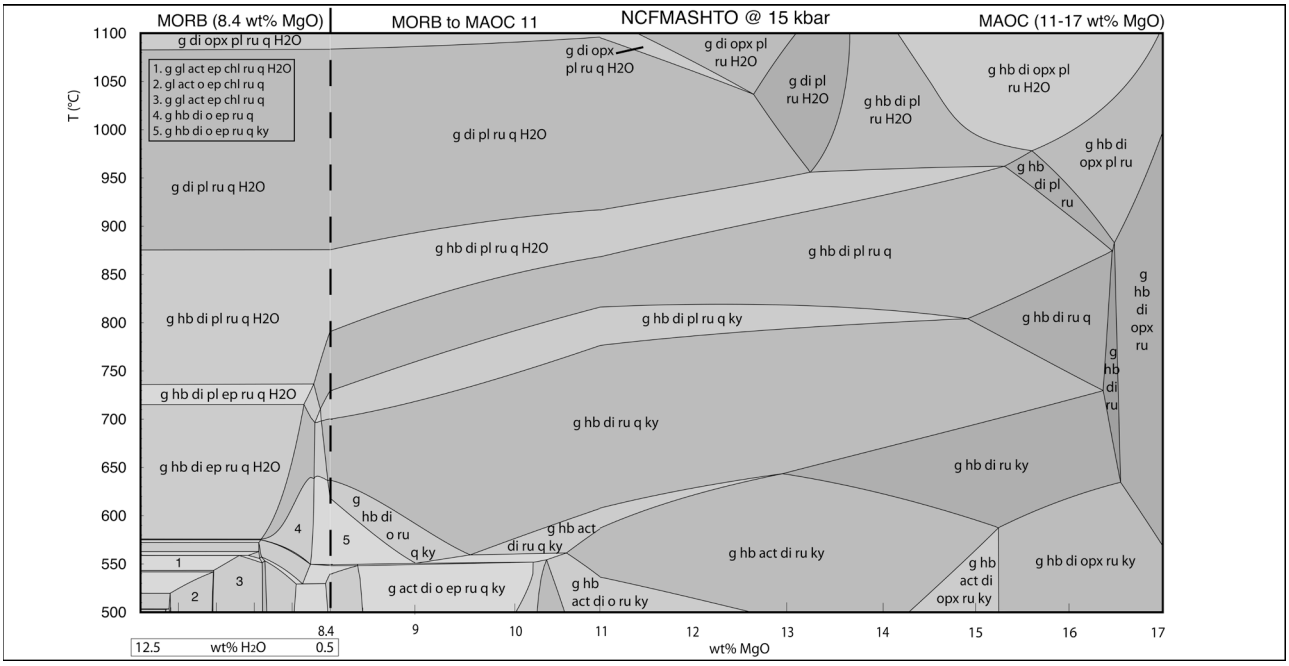

Figure 2. T-X pseudosection at 15 kbar covering the range from a water-saturated MORB to MAOC with 17 wt% MgO.

suggests that the melting of the modelled rocks would begin at 950 °C for MORB to 1050 °C for Gorgona at 10 kbar. These calculations should be treated as highly uncertain due to the different chemical system and rock-type for which the model is developed, but the agreement with the few experimental solidus determinations in Foley et al. (2003) is good.

Model Archaean Oceanic Crust (MAOC)

The solidus for different relevant model Archaean oceanic crust compositions (MAOC) will be determined in a series of high pressure experiments at pressures up to 20 kbar. The MgO range for the chosen bulk compositions, all prepared as oxide mixes, was deduced from the findings of the P-T pseudosections in Figure 1. The basic bulk composition (11 wt% MgO) itself was calculated on the basis of an experimental partial melt composition from MORB pyrolite (Falloon & Green 1988). This model rock was further modified by adding calculated amounts of olivine to produce three compositions with different magnesium contents (11, 13, 15 wt%). In order to ensure comparability, the other oxides in the system were kept constant relative to each other and 0.5 wt% of water was added as $Mg(OH)_2$.

Pseudosections for each MAOC-composition, and with a low water-content for the bulk compositions in Table 1, were modelled. H_2O-bearing assemblages at high P-T equal the assemblages modelled under water-saturated conditions, but the low-T assemblages display a simplification where H_2O does not form a discrete fluid phase. A comparison of the latter pseudosections with those for MAOC also indicates differences due to changes in concentrations of the other oxides. A coupled T-X pseudosection at 15 kbar is shown in Figure 2. The left hand part illustrates the effect of water from a water-saturated MORB towards a MORB including 0.5 wt% H_2O (dotted line). All assemblages at the left side are water-bearing, and the H_2O-out line develops as a positively sloped boundary until H_2O is stable only above 800°C in the MORB with 0.5 wt% H_2O. The right hand part illustrates the changes from MORB to MAOC-compositions, the latter with increasing MgO from 11 to 17 wt%. Many assemblages are stable over a wide range of bulk compositions. With higher MgO, the stability of the assemblages shifted towards higher T and new fields become stable.

Preliminary Results

The first experiments performed on MAOC were at 10 kbar/1050 °C, 10 kbar/1100 °C and 15 kbar/1100 °C. Clinopyroxene was stable at 10 and 15 kbar, and orthopyroxene at 10 kbar for each composition. Plagioclase occured at 10 kbar, but not in the high-MgO MAOC, whereas garnet was identified at 15 kbar in the two most MgO-rich MAOCs. Amphibole was stable at 10 kbar/1050 °C and at 15 kbar in the high-MgO composition. In all experiments a melt was formed and for this reason the results could not be compared directly to the P-T pseudosections. In the latter, more phases are stable compared to the experiments. This deviation may be attributed to the presence of a melt phase in the experiments that cannot be modelled with THERMOCALC. Furthermore, the mineral models do not encompass all the element substitutions that can occur in nature. Phases appearing in the P-T pseudosections and not in the experiments may have been involved in melting and reacted out. Plagioclase, garnet and amphibole bearing assemblages, precursors for garnet-amphibolite and TTG-production through melting, were not yet found together in an experimental assemblage. Garnet, amphibole and clinopyroxene are stable together at 15 kbar in the high-magnesium MAOC-composition, whose assemblage is close to the garnet-amphibole-pyroxenite described in Foley et al. (1999). Further experiments are needed to determine the solidus of the different MAOC-compositions.

Acknowledgements

We wish to acknowledge the Mainz Earth System Science Research Centre “Geocycles” for financial support.

References

Bickle M.J., Nisbet E.G. & Martin A., 1994, Archean greenstone belts are not oceanic crust, Journal of Geology, 102, 121–138.

Diener J.F.A., Powell R., White R.W. & Holland T.J.B., 2007, A new thermodynamic model for clino-and orthoamphiboles in the system Na_2O-CaO-FeO-MgO-Al_2O_3-SiO_2-H_2O-O, Journal of Metamorphic Geology, 25, 631–656.

Falloon T.J. & Green, D.H., 1988, Anhydrous Partial Melting of Peridotite from 8 to 35kb and the Petrogenesis of MORB, Journal of Petrology, Special Lithosphere Issue, 379–414.

Foley S.F, Musselwhite D.S. & van der Laan S.R., 1999, in *Proceedings of the 7th Kimberlite Conference Volume 1*, Gurney J.J., Gurney J.L., Pascoe M.D. & Richardson S.H., eds, Red Roof Design, Cape Town, 238–246.

Foley S. F., Tiepolo M., & Vannucci R., 2002, Growth of early continental crust controlled by melting of amphibolite in subduction zones, Nature, 417, 837–840.

Foley S. F., Buhre S., & Jacob D. E., 2003, Evolution of the Archean crust by delamination and shallow subduction, Nature, 421, 249–252.

Holland T.J.B. & Powell R., 1998, An internally consistent thermodynamic data set for phases of petrological interest, Journal of Metamorphic Geology, 16, 309–343.

Krishnamurthy P., Gopalan K. & Macdougall J.D., 2000, Olivine Compositions in Picritie Basalts and the Deccan Volcanic Cycle, Journal of Petrology, 41, 1057–1069.

Powell R. & Holland T.J.B., 1988, An internally consistent dataset with uncertainties and correlations: 3. Applications to geobarometry, worked examples and a computer program, Journal of Metamorphic Geology, 6, 173–204.

Shirey S. B., Klewin K.W., Berg J.H. & Carlson R.W., 1994, Temporal changes in the sources of flood basalts: Isotopic and trace element evidence from the 1100 Ma old Keweenawan Mamainse Point Formation, Ontario, Canada, Geochimica et Cosmochimica Acta, 58, 4475–4490.

Stern R.J., 2007, When and how did plate tectonics begin? Theoretical and empirical considerations, Chinese Science Bulletin, 52, 578–591.

White R.W., Powell R & Holland T.J.B., 2007, Progress relating to calculation of partial melting equilibria for metapelites, Journal of Metamorphic Geology, 25, 511–527.

THEME 2

DIVERSITY IN TECTONIC REGIMES

KEYNOTE & INVITED SPEAKERS

A 4-D, CRATON-SCALE FRAMEWORK FOR THE SUPERIOR PROVINCE, CANADA

J.A. Percival

Geological Survey of Canada, Ottawa, Ontario

The Superior Province - a large, complex, metallogenically diverse craton - has become relatively well understood through a century of research and exploration, including recent widespread mapping, geochronology, tracer isotope geochemistry and deep-probing geophysical imaging. Views of its orogenic evolution have evolved toward a plate-tectonic framework over the past two decades as a result of recognition of numerous isotopically, chronologically and geophysically unique continental and oceanic terranes (Fig. 1), juxtaposed on a 2000-km length scale during five distinct orogenic events that produced orogenic flysch basins and terrane imbrication on the crustal scale. Disparate fragments of Mesoarchean to Eoarchean continental crust (3.9-2.8 Ga) and intervening tracts of Neoarchean oceanic crust (2.77-2.70 Ga) were assembled through successive accretionary and collisional events between 2.72 and 2.68 Ga, resulting in the first-order easterly alignment of terranes and transcurrent faults characteristic of the southern part of the province (Percival et al. 2006a). Continental blocks retain evidence for distinct pre-2.8 Ga evolution (Stott & Corfu 1991; Boily et al. 2009), including widespread evidence of volcanic-dominated rift (breakup) sequences (Thurston 2002; Percival et al. 2006b). Neoarchean volcano-plutonic rocks of arc affinity dominate oceanic and continent-margin settings, suggestive of widespread subduction of oceanic crust prior to accretion events (e.g. Polat et al. 2009). Back-arc or rifted arc settings in the 2.735-2.70 Ga calc-alkaline sequences represent the main hosts to volcanogenic massive sulphide deposits.

The 3.0 Ga North Caribou superterrane (Fig. 1) appears to have acted as a nucleus during collision with the

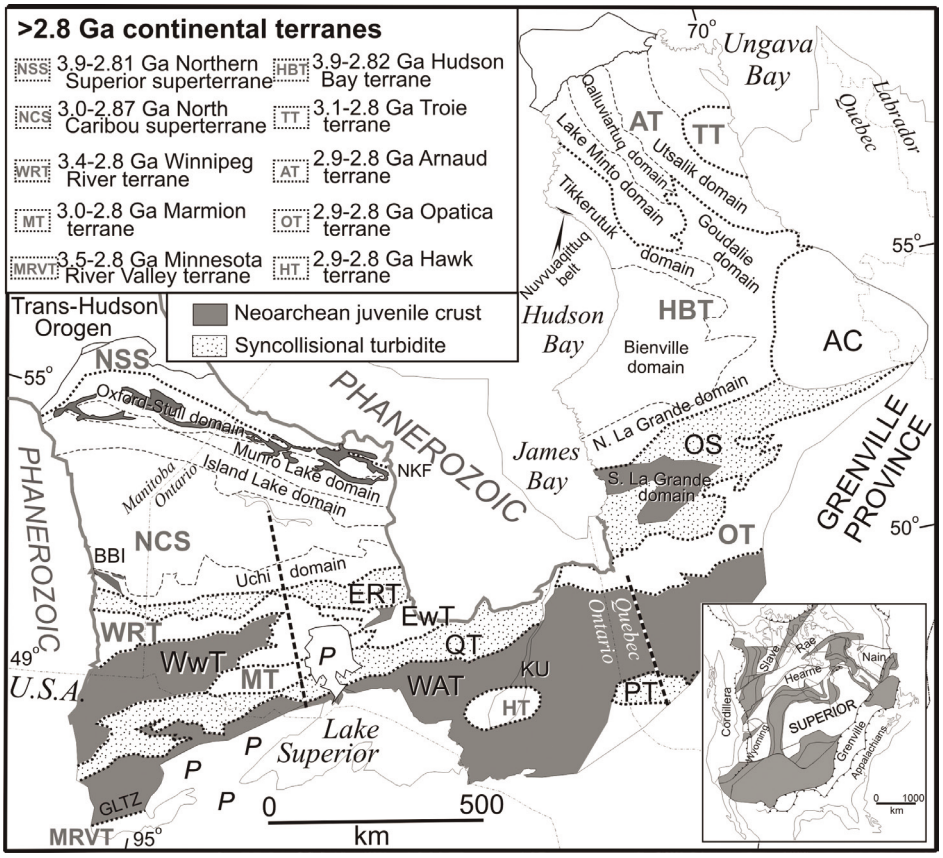

Figure 1. Tectonic framework for the Superior Province, showing age range of continental domains (identified in legend), distribution of juvenile oceanic domains, syncollisional turbidite basins, and Proterozoic cover (P). Subdivisions of the Superior Province modified after Percival et al. (2006a) and Boily et al. (2009). Dashed lines show locations of seismic profiles in White et al. (2003, western Superior) and Ludden & Hynes (2000, southeastern Superior). Abbreviations: AC: Ashuanipi complex; AT: Arnaud terrane; ERT: English River metasedimentary terrane; EwT: Eastern Wabigoon terrane; HBT: Hudson Bay terrane; HT: Hawk terrane; KU: Kapuskasing uplift; MRVT: Minnesota River Valley terrane; MT: Marmion terrane; NCS: North Caribou superterrane; NSS: Northern Superior superterrane; OnT: Opinaca metasedimentary terrane; OT: Opatica terrane; PT: Pontiac metasedimentary terrane; QT: Quetico metasedimentary terrane; TT: Troie terrane; WAT: Wawa-Abitibi terrane; WRT: Winnipeg River terrane; WwT: Western Wabigoon terrane; Inset: tectonic map of North America (after Hoffman 1989) showing location of the Superior Province.

Northern Superior superterrane on the north, at about 2.72 Ga, and with the Winnipeg River terrane on the south (ca. 2.72-2.70 Ga), the latter trapping synorogenic turbidites in the English River basin. Docking of the juvenile Wabigoon terrane further to the south occurred at ca. 2.71-2.70 Ga (Percival et al. 2004), followed by collision of the Abitibi-Wawa terrane and syntectonic deposition of Quetico basin turbidites. The final event welded the Minnesota River Valley terrane to the southern Superior margin and tectonically underplated a wedge of probable oceanic crust beneath it (White et al. 2003). In two regional Lithoprobe transects (White et al., ibid; Ludden & Hynes, 2000), prominent crustal reflectivity and mantle lithospheric features dip gently northward to central North Caribou latitudes before reversing dip further to the north.

In the eastern Superior Province, structural trends swing through a broad oroclinal flexure to northerly as the background erosion level increases. The ancient Hudson Bay terrane (3.8-2.9 Ga), which may connect with the Northern Superior superterrane beneath Hudson and James bays, and the <2.9 Ga Arnaud terrane to the east underwent severe reworking during 2.78-2.68 Ga magmatism (Percival et al. 2001; Boily et al. 2009). Polyphase deformation and high-grade metamorphism (2.73-2.68 Ga) in the northeastern Superior Province (Lin et al. 1996; Skulski & Percival 1996; Percival & Skulski 2001) cannot be directly related to accretion events recognized in the southern Superior because correlative units do not extend through the oroclinal bend. Whether the elongate supracrustal and plutonic belts of this region developed in a subduction regime (e.g. Percival et al. 2001; Percival & Mortensen 2002) or through plume-driven processes (e.g. Bédard 2006; Maurice et al. 2009) remains a subject of debate.

Several late-tectonic events recognized across the Superior Province characterize the cratonization process between 2.69 and 2.60 Ga. Deposition of "Timiskaming-type" conglomerates, alkaline magmatism, emplacement of crust-derived granites, regional metamorphism, transcurrent faulting, hydrothermal fluid circulation, lode gold localization and post-orogenic cooling express thermal relaxation and stabilization of a refractory lithospheric mantle keel. These late-tectonic events are thermomechanically consistent with a process of mantle lithosphere inversion described by Percival & Pysklywec (2007).

The progressive accretion of continental and oceanic domains on a 2000 km length scale, coupled with three-dimensional evidence for terrane stacking, provide compelling evidence that plate-tectonic-like processes drove assembly of the Superior Province, albeit modified by late strain and magmatism.

Acknowlegments

Data collection and synthesis activities have been supported by the Geological Survey of Canada through the NATMAP and Targeted Geoscience Initiative programs. Lithoprobe was jointly funded by the Natural Science and Engineering Research Council and Natural Resources Canada. The synthesis has benefited from numerous discussions with colleagues, collaborators and students.

References

Bédard J.H., 2006, A catalytic delamination-driven model for coupled genesis of Archaean crust and sub-continental lithospheric mantle, Geochimica et Cosmochimica Acta, 70, 1188-1214.

Boily M., Leclair A., Maurice C., Bédard J.H. & David J., 2009, Paleo- to Mesoarchean basement recycling and terrane definition in the Northeastern Superior Province, Québec, Canada, Precambrian Research, 168, 23-44.

Hoffman P.F. 1989, Precambrian geology and tectonic history of North America in *The geology of North America - an overview*, A.W. Bally, and A.R Palmer, eds, Geological Society of America, The Geology of North America, A, 447-512.

Lin S., Percival, J. A. & Skulski, T., 1996, Structural constraints on the tectonic evolution of a late Archean greenstone belt in the northeastern Superior Province, northern Quebec (Canada), Tectonophysics, 265, 151-167.

Ludden J. & Hynes A., 2000, The Lithoprobe Abitibi-Grenville transect: two billion years of crust formation and recycling in the Precambrian shield of Canada, Canadian Journal of Earth Sciience, 37, 459-476.

Maurice C., David J., Bédard J.H. & Francis, D., 2009, Evidence for a widespread mafic cover sequence and its implications for continental growth in the Northeastern Superior Province, Precambrian Research. 168, 45-65.

Percival J.A. & Mortensen J.K., 2002, Water-deficient calc-alkaline plutonic rocks of Northeastern Superior Province, Canada: significance of charnockitic magmatism, Journal of Petrology, 43, 1617-1650.

Percival J.A., and Pysklywec R., 2007, Are Archean lithospheric keels inverted? Earth and Planetary Science Letters, 254, 393-403.

Percival J.A. & Skulski T., 2000, Tectonothermal evolution of the northern Minto block, northeastern Superior Province, Canada, Canadian Mineralogist, 38, 345-378.

Percival J.A., Stern R.A. & Skulski T., 2001, Crustal growth through successive arc magmatism: Reconnaissance U-Pb SHRIMP data from the northeastern Superior Province, Canada, Precambrian Research, 109, 203-238.

Percival J.A., McNicoll V., Brown J.L. & Whalen J.B., 2004, Convergent margin tectonics, central Wabigoon subprovince, Superior Province, Canada, Precambrian Research, 132, 213-244.

Percival J.A., Sanborn-Barrie M., Stott G., Helmstaedt H., Skulski T. & White, D.J., 2006a, Tectonic evolution of the Western Superior Province from NATMAP and Lithoprobe studies, Canadian Journal of Earth Sciences, 43, 1085-1117.

Percival J.A., McNicoll V. & Bailes A.H., 2006b, Strike-slip juxtaposition of ca. 2.72 Ga juvenile arc and >2.98 Ga continent margin sequences and its implications for Archean terrane accretion, western Superior Province, Canada, Canadian Journal of Earth Sciences, 43, 895-927.

Polat A., Kerrich R., and Windley B.F., 2009, Archean crustal growth processes in the southern Superior Province and southern West Greenland: geodynamic and magmatic constraints, in *Accretionary Orogens in Space and Time*, Cawood P. A. & Kröner, A., eds, Geological Society of London, Special Publication 318, 155-191.

Skulski T. & Percival, J.A., 1996, Allochthonous 2.8 Ga oceanic plateau slivers in a 2.72 Ga continental arc sequence: Vizien greenstone belt, northeastern Superior Province, Canada, Lithos, 37, 163-179.

Stott G.M. & Corfu F., 1991, Uchi subprovince, in *Geology of Ontario*, Thurston P.C., Williams H.R., Sutcliffe R.H. & Stott G.M., eds,. Ontario Geological Survey Special Volume 4, Part 1, 145-238.

Thurston P.C., 2002, Autochthonous development of Superior Province greenstone belts? Precambrian Research, 115, 11-36.

White D.J., Musacchio G., Helmstaedt H.H., Harrap R.M., Thurston P.C., van der Velden A. & Hall, K., 2003, Images of a lower-crustal oceanic slab: Direct evidence for tectonic accretion in the Archean western Superior province, Geology, 31, 997-1000.

USING THE PALEOPROTEROZOIC LIP RECORD TO RECONSTRUCT A LATE ARCHEAN SUPERCONTINENT(S)

R.E. Ernst[1] & W. Bleeker[2]

[1]Dept. Earth and Environmental Sciences, University of Waterloo, Waterloo, N2L 3G1, Canada, & Ernst Geosciences; Richard.Ernst@ErnstGeosciences.com;
[2]Geological Survey of Canada, 601 Booth Street, Ottawa, Ontario, K1A 0E8, Canada; wbleeker@nrcan.gc.ca

Introduction

The approximately 35 Archean cratons embedded in younger continents represent fragments of a late Archean – earliest Paleoproterozoic supercontinent (Kenorland) or several independent continents (supercratons) (e.g. Bleeker 2003). Determining the cratonic arrangements and their paleogeography is of fundamental significance for all aspects of late Archean geology, such as: the geodynamic setting and origin of greenstone belts, the scale and distribution of major faults and orogenic belts, the distribution of metallogneic belts, and the comparison of all these aspects in late Archean time with presumed equivalent magmatic, sedimentary and structural aspects in the younger record. Despite much effort, the configuration of an earliest Paleoproterozoic supercontinent(s) (and indeed other proposed pre-Pangea supercontinents, Nuna and Rodinia) is poorly understood and the most definitive technique, paleomagnetism, has been hampered by poor geochronology of the units most suitable for paleomagnetic studies (namely dolerite dykes and sills).

Herein we report on a path forward. New developments in the separation of baddeleyite and ability to precisely date small sizes of baddeleyite and zircon are allowing more accurate and precise ages to be reliably obtained for large igneous province (LIP) events and especially their dolerite dyke swarms that are widespread on all main tectonic elements ('puzzle pieces') of the Earth's past plates. Precisely-dated events can be assembled on a timeline into a LIP 'barcode' (not unlike a supermarket

Table 1. The use of Large Igneous Provinces (LIPs) in paleocontinental reconstructions

#	Technique	Description
1	Comparison of magmatic "barcodes" between crustal blocks	The sharply pulsed LIP record of a crustal block can be summarized on a timeline as a barcode. Given the large "footprint" of LIP events, originally neighbouring crustal blocks will share essential elements of their LIP record and hence their magmatic barcode. A comparison of barcodes thus provides a powerful technique in identifying blocks that were "nearest neighbours".
2	Reconstructing the geometry of dyke swarms	Reconstruction of crustal blocks to restore fragmented giant dyke swarms to their original geometry, either a linear pattern or a radiating pattern.
3	Locating and matching plume centres	The distribution of layered intrusions and the geometry of dyke swarms can be used to locate igneous or plume centres ("hotspots") of a LIP event. Once such centres are identified on more than one block, but of the same age, a likely reconstruction would involve overlapping the plume centres.
4	Paleomagnetic studies	Compare paleomagnetic directions of similar or identical age LIP components (dykes, flows, etc.) on different crustal blocks to determine their original orientation (relative to north arrow, i.e. "azimuthal orientation") and paleo-latitude, and to construct and compare apparent polar wander paths.
5	Geochemical fingerprinting	Compare major and trace element compositions and ratios, and isotope geochemistry, of LIP units on different blocks to identify likely matches. Geochemistry cannot identify a former connection definitively, but a major contrast in geochemical fingerprints between LIP fragments on different blocks can rule out a direct correlation.
6	Timing of breakup on a particular margin	LIPs commonly are associated with rift-drift transition and continental breakup (e.g., the 55 Ma magmatic pulse in the North Atlantic), thus initiating passive margin development. Margins with comparable rift-drift transitions, marked and dated by voluminous magmatism, could be conjugate margins.
7	Timing of accretion and assembly	Prior to accretion of different crustal blocks, their histories and LIP record (magmatic barcodes) may be different and largely independent, but they will start to share events after accretion and assembly. In this way, the approximate timing of accretion of different blocks may be determined.

barcode or a DNA fingerprint) that characterizes each 'puzzle piece' and which can be compared with the barcodes of other cratons. By matching these 'barcodes' and using the precise 'piercing points' provided by regional radiating and linear dyke swarms, we can compare and reconstruct the 'puzzle pieces' into past continents and supercontinents (Bleeker & Ernst 2006; http://www.largeigneousprovinces.org/06may.html)

A summary of the ways in which the LIP record can be used in paleocontinental reconstruction is summarized in Table 1 which is extracted from Ernst & Bleeker (2010) and Ernst & Srivastava (2008)

Figure 1 shows the current barcode status of the main 'puzzle pieces' between 2.6 Ga and 1.8 Ga. From this summary it is clear that some cratons such as the Superior and Karelia cratons are relatively well-barcoded, whereas most other cratons are poorly constrained; they have many magmatic units remaining to be precisely dated. In order to use the LIP methodologies for reconstructing paleocontinents, it is necessary to substantially upgrade the LIP barcodes for all remaining main cratonic puzzle pieces.

As a contribution to this effort, a group of mining and oil companies is contributing over $1,000,000 for a 5-year global project focussed on U-Pb baddeleyite and zircon dating of LIPs units (especially their dyke swarms and sill provinces) around the world and back to 2.7. Ga (www.supercontinent.org). In addition to a robust geochronology team (aiming to produce at least 250 new precise ages), we have also assembled an international team of 40+ collaborators to obtain the critical geochronology samples (1-2 kg in size) from all regions (from all relevant "puzzle pieces"), and we are collaborating in the interpretation of these results with complementary expertise from related fields such as paleomagnetism and geochemistry. This project, inspired by basic academic research, is being sponsored by mining and oil companies because of the growing realization that deciphering past arrangements of continents and supercontinents and their paleogeographies is feasible and provides a competitive advantage in searching for new resources.

Some progress has already been achieved during the Project planning phase. A ca. 2.7 -2.1 Ga reconstruction places Wyoming, Hearne, Karelia and Kola cratons from west to east along the southern Superior craton (Bleeker and Ernst 2006). Additional LIP correlations support a position of Zimbabwe against the eastern Superior craton with the Yilgarn craton also nearby (Söderlund et al. 2010). The latter result is being further evaluated by additional dating, but if confirmed, would contribute to resolving the debate on the origin of 2.7 Ga greenstone

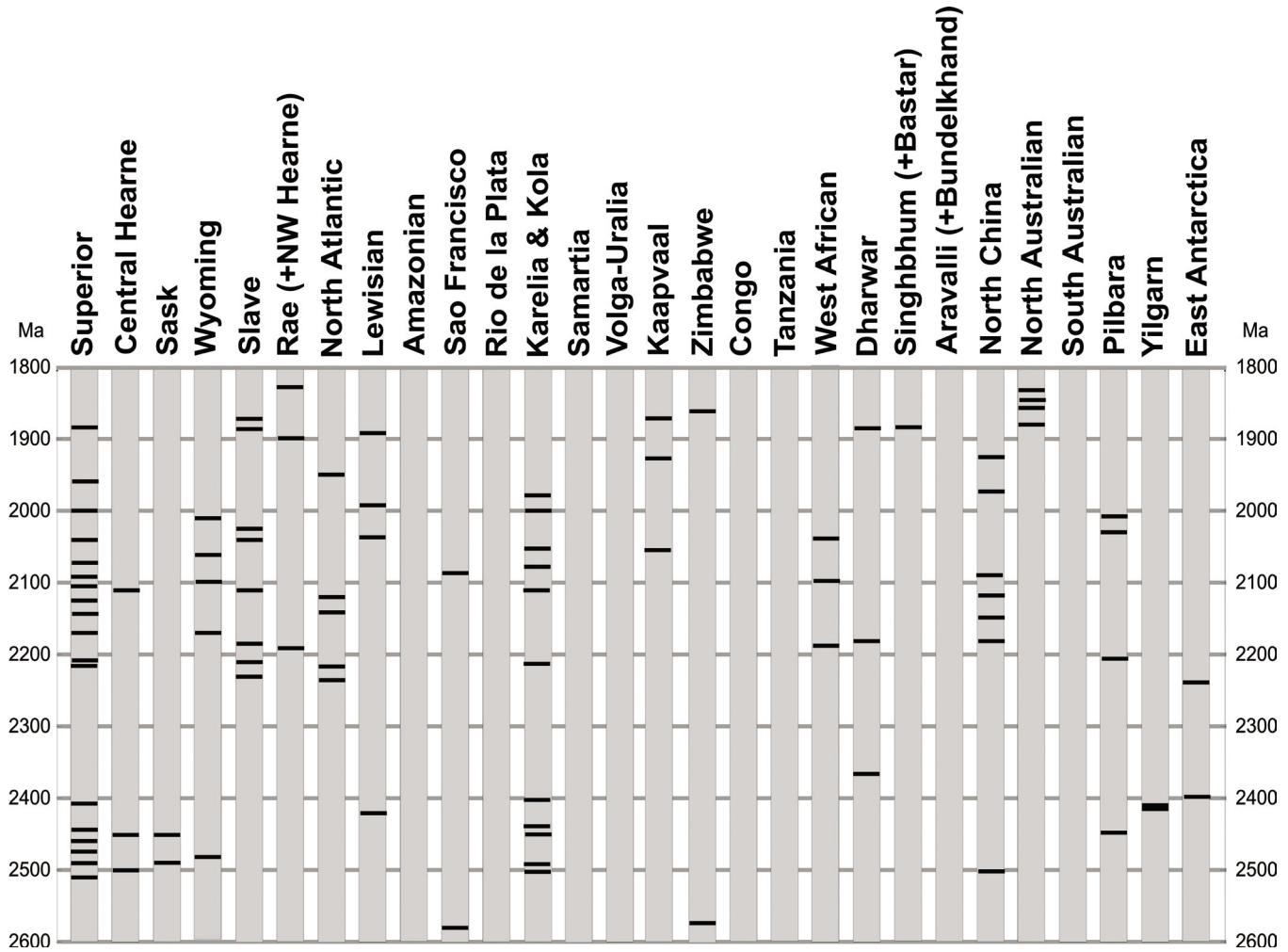

Figure 1. Large Igneous Provinces (LIP) barcode status for each of the main cratonic puzzle pieces. Note that most are currently poorly populated, which can be solved by a U-Pb geochronology campaign on the many undated magmatic units in each puzzle piece.

belts: widespread global event or more localized magmatic node(s) associated with a continent which subsequently fragmented and dispersed the 2.7 Ga greenstone belts. The preliminary proposed nearest neighbour relationship for the major ca. 2.7 Ga greenstone belts in Superior, Karelia, Zimbabwe and Yilgarn cratons favours regional magmatic node interpretation.

There are several Paleoproterzoic LIP barcode events already recognized to have considerable regional importance in the rifting and progressive breakup of late Archean supercontinent(s) (e.g. Ernst and Bleeker 2010; Buchan et al. 2010):
1) 2505 Ma Mistassini event of southeastern Superior craton which is also widespread in Karelia, and present in the Zimbabwe and Hearne cratons;
2) 2445 - ca. 2480 Ma Matachewan event of the Superior craton which is linked to layered intrusions both in southern Superior craton (East Bull Lake Intrusive Suite) and is also present in Baltica and Wyoming.
3) 2410 Ma Widgiemooltha event of the Yilgarn craton which is also present in Zimbabwe and in Karelia and eastern Superior cratons;
4) 2370 Ma Bangalore event, so far only recognized in the Dharwar craton;
5) 2210 Ma Ungava-Nipissing event of eastern Superior craton, which is also present in the Karelia and Pilbara cratons;
6) 2170 Ma Biscotasing event of eastern Superior craton, which is also present in the Wyoming and Dharwar cratons;
7) 2100-2070 Ma Marathon – Fort Frances events of the southern Superior craton, which are also present in Hearne, Slave, Karelia and other blocks. This event seems to be linked with the final breakup of Karelia-Kola, Hearne and Wyoming from southern Superior craton.
8) 2060 Ma Bushveld event, so far only recognized in the Kaapvaal craton; and
9) ca. 1900-1860 Ma magmatic events present on many cratons including Superior, Slave, Wyoming, and which appear to be post-breakup and to have been emplaced during a time transitional to the next supercontinent, Nuna (Columbia).

References

Bleeker W., 2003, The late Archean record: a puzzle in ca. 35 pieces, Lithos, 71, 99-134.

Bleeker W. & Ernst R.E., 2006, Short-lived mantle generated magmatic events and their dyke swarms: The key unlocking Earth‘s paleogeographic record back to 2.6 Ga, in *Dyke Swarms - Time Markers of Crustal Evolution*, Hanski E., Mertanen S., Rämö T. & Vuollo. J. Eds, Taylor and Francis/Balkema, London, 3-26.

Buchan K.L., Ernst R.E., Bleeker W., Davis W.J., Villeneuve M., van Breemen O., Hamilton M.A. & Söderlund U., 2010, Proterozoic Magmatic Events of the Slave Craton, Wopmay Orogen and Environs, Geological Survey of Canada Open File 5985.

Ernst R.E. & Bleeker W., 2010, Large igneous provinces (LIPs), giant dyke swarms, and mantle plumes: significance for breakup events within Canada from 2.6 Ga to present. Canadian Journal of Earth Sciences, in press.

Ernst R.E. & Srivastava R.K., 2008, India’s place in the Proterozoic world: constraints from the large igneous provinces (LIP) record, in *Indian Dykes: Geochemistry, Geophysics, and Geochronology*, Srivastava R.K., Sivaji Ch. & Chalapathi Rao N.V., eds, Narosa Publishing House Pvt. Ltd, New Delhi, India, 41-56.

Söderlund U., Hofmann, A. Klausen, M.B., Olsson J.R. & Ernst, R.E., 2010, Towards a complete magmatic barcode for the Zimbabwe craton: baddeleyite U-Pb dating of regional dolerite dike swarms and sill provinces, Precambrian Research, in press.

FALSIFICATION OF THE PLATE TECTONIC HYPOTHESIS FOR GENESIS OF ARCHAEAN VOLCANIC AND PLUTONIC ROCKS, AND AN OUTLINE OF POSSIBLE ALTERNATIVE MECHANISMS

J.H. Bédard

Geological Survey of Canada, 490 de la Couronne, Québec, PQ, G1K 9A9, Canada.

Archaean TTG-greenstone dome-and-keel associations (TTG = tonalite-trondhjemite-granodiorite) do not occur at modern convergent margins. Conversely, andesitic strato-volcanoes and thrust-and-fold belts which typify modern Andean margins and collisional orogens are untypical of Archaean terranes. How then can the genesis of Archaean cratons be attributed to convergent margin settings? Basaltic plateau maturation above major mantle upwelling zones is a possible alternative setting (Fig.1). The Abitibi belt is a possible example of the early stages of maturation, with ubiquitous juvenile Nd isotopic signatures that imply the absence of older crust, and only ca 50my of evolution being preserved. Calc alkaline volcanic facies increase in abundance up-section. Trace element modeling implies that the Type I-II soda-rhyolites are geochemical equivalents of TTG plutons and formed by high-pressure anatexis of typical Archaean basalts; Type III soda rhyolites are low-

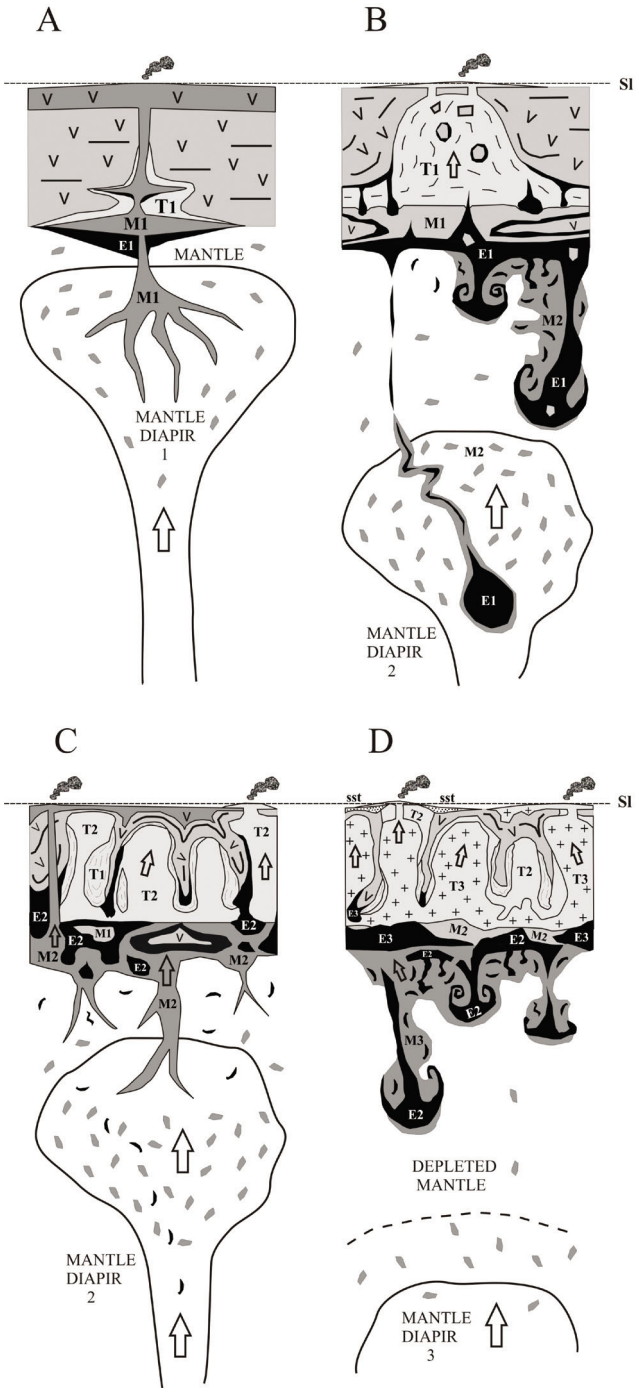

Figure 1. Cartoon illustrating the catalytic delamination-driven tectonomagmatic model, adapted from Bédard (2006). A) Large mantle plume releases melt (M1) that constructs a thick volcanic crust. Underplating magma causes melting at the base of the crust to form a 1st generation of tonalitic melt (T1) with complementary eclogitic to pyroxenitic restites (E1). B) As M1-magmatism wanes, the underplated melt layer cools and crystallizes. Buoyant tonalitic melt (T1) rises into the volcanic carapace, initiating a 1st cycle of partial crustal convective overturn. Dense restites and cumulates (E1) delaminate into the mantle. Large bodies of E1 travel fast and escape into the deep mantle, and may guide ascent of mantle diapirs. Smaller delaminated bodies mix into the shallow upper mantle and trigger the formation of a 2nd generation of mantle melt (M2). The M2 label here represents melt-enriched domains. C) The 1st generation crustal restites are largely destroyed as M2 melts are generated, collect and ascend. New melt from a 2nd mantle diapir also contribute to M2. Eruptions of M2 fill troughs in the surface. Mantle melt (M2) that underplates the crust generates a 2nd generation of tonalite melt (T2) by melting relicts of lava (v) and of the underplated M1 magma, yielding a 2nd generation of restites and cumulates (E2). Older tonalites (T1) are extensively remobilized at this time, and also contribute to T2. The voluminous T2 tonalites are buoyant and trigger a 2nd cycle of partial crustal convective overturn. D) As M2-magmatism wanes, the underplated layer cools and crystallizes. The restites and cumulates (E2) delaminate into the mantle, triggering the formation of a 3rd generation of mantle melts (M3), and destroying the 2nd generation restites. Melting of underplated M2 melt and relict lavas generate a 3rd generation of tonalitic to granodioritic melt (T3), also yielding a 3rd generation of restites and cumulates (E3). Older tonalitic rocks (T1 and T2) are extensively remobilized and largely constitute T3. The voluminous T3 tonalites/granodiorites are buoyant and trigger a 3rd cycle of partial convective overturn in the crust. Tonalitic bodies that protrude above sea level (sl) are eroded to form sandstones (sst) and conglomerates.

pressure melts of similar source basalts; while andesites are mixtures of basalt and high-P felsic anatectic melts. Geochemical trends imply that AFC/mixing processes best explain magmatic Th/Yb-Nb/Yb systematics (Fig.2); with source enrichment signatures typical of modern subduction-related magmas rarely appearing. A more advanced stage of crustal maturation is represented by the NE Superior, which is dominated by TTGs and enderbitic (px-TTG) plutons. Nd-isotopic and zircon xenocryst data imply repeated and large-scale remelting of older TTGs to generate younger ones, with the high-T enderbites representing near-total remelts. Almost 50% of the Minto crust (ca 500x500km) was reworked in a narrow 20my timespan. The subduction-slab melting model cannot generate such volumes so quickly. If a hypothesis of progressive maturation and recycling of an initially basaltic crust is retained, then large volumes of eclogitic restites must form and be removed. Garnet saturation requires in-situ plateau thicknesses ca 50km, which may be possible above larger and hotter Archaean plumes. Alternatively, much of the melting could be linked to delamination, taking place as cold, dense metabasites founder into the mantle. Heat transfer into 3-D sinking blobs is more efficient than transfer into a subducting slab. Foundering metabasites would have the requisite O-C-isotopic signatures, contain carbon that would become diamonds, and could melt and also degass, transferring LILE and felsic melt to the surrounding mantle, mimicking subduction-related magmatism (boninites, shoshonites, sanukitoids). Disaggregation of restitic eclogite blobs into depleted px-gt-free harzburgite would generate excess opx by reaction, raise mg#, and refertilize source mantle with Al and Ca, allowing and possibly triggering new pulses of basaltic/komatiitic magmatism. This catalytic recycling model explains coupled genesis of Archaean crust and ultra-depleted mantle. This family of hypotheses does not exclude terrane covergence and suturing. However, numerical modeling implies that oceanic slabs would probably drip into a hotter Archean mantle. The adakite model for TTG genesis also implies slab softening. Since plate-tectonics is largely driven by the pull of cooling and densified subducting slabs, the driving force for Archeaen plate motions should be absent or weak. Thus, soft-docking of weak crustal terranes should be the rule, yielding the most common Archaean tectonic style (steep widespread fabrics, low metamorphic grades, TTG-cored antiforms that may trigger partial convective overturn).

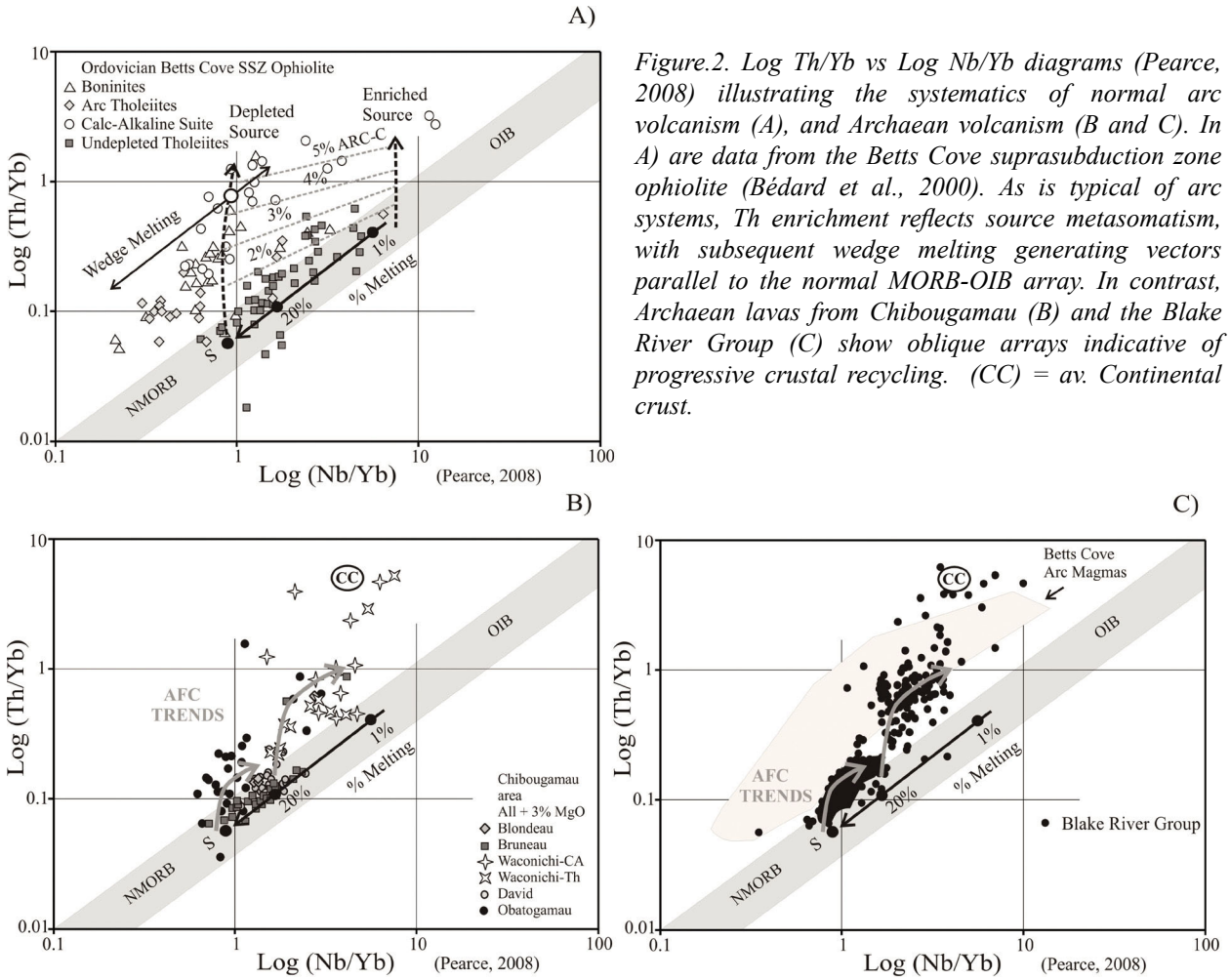

Figure.2. Log Th/Yb vs Log Nb/Yb diagrams (Pearce, 2008) illustrating the systematics of normal arc volcanism (A), and Archaean volcanism (B and C). In A) are data from the Betts Cove suprasubduction zone ophiolite (Bédard et al., 2000). As is typical of arc systems, Th enrichment reflects source metasomatism, with subsequent wedge melting generating vectors parallel to the normal MORB-OIB array. In contrast, Archaean lavas from Chibougamau (B) and the Blake River Group (C) show oblique arrays indicative of progressive crustal recycling. (CC) = av. Continental crust.

References

Bédard J.H., Lauzière K., Tremblay A., Sangster A., Douma S.L. & Dec, T., 2000, The Betts Cove Ophiolite and its cover rocks, Geological Survey of Canada, Bulletin 550, 76pp.

Bédard J.H., 2006, A catalytic delamination-driven model for coupled genesis of Archaean crust and sub-continental lithospheric mantle, Geochimica et Cosmochimica Acta, 70, 1188-1214.

Pearce, J.A., 2008, Geochemical fingerprinting of oceanic basalts with applications to ophiolite classification and the search for Archean ophiolites, Lithos, 100, 14-48.

THE FUNDAMENTAL ARCHITECTURE OF THE SOUTH-CENTRAL ABITIBI GREENSTONE BELT, SUPERIOR CRATON, CANADA, AND THE LOCALIZATION OF WORLD-CLASS Au DEPOSITS

W. Bleeker & O. van Breemen

Bleeker, W., Geological Survey of Canada, 601 Booth Street, Ottawa, ON, K1A 0E8; van Breemen, O., Geological Survey of Canada, 601 Booth Street, Ottawa, ON, K1A 0E

Resolving early thrust architecture in polydeformed granite-greenstone terrains is notoriously difficult. The history of geological thought on the Abitibi greenstone belt exemplifies this as no other, having oscillated between end member interpretations of regional layer-cake stratigraphy and that of a collage of micro-terranes separated by thrusts and sutures. Although micro-terrane models perhaps downplayed some known stratigraphic relationships, the "splitter's approach" has been useful in systematizing all the assemblages and drawing attention to their boundary relationships. Since then, the pendulum has swung back (too far?) to a regional layer-cake model. However, given the polyphase deformation history and the obvious complexity of the Abitibi greenstone belt, it seems likely that, ultimately, a realistic model for the tectonostratigraphic architecture of the Abitibi will lie somewhere in the middle between these end members, incorporating the strongest observations from both sides of the debate but excluding the weakest. At a philosophical level, this is typical for polarized debates on complex problems involving large and somewhat fuzzy datasets.

Here we present a model that stakes out this middle ground, arguing that the south-central Abitibi greenstone belt likely consists of at least three ~100-km-scale tectonostratigraphic terranes that were imbricated early in the deformation history, immediately after or even during deposition of dominantly deep water turbiditic greywackes (the "Porcupine-type" sediments).

At the lowest structural level occurs (1) the large "Timmins-Swayze terrane", characterized by the classical ca. 2750-2685 Ma cyclic stratigraphy of the area south of Timmins and west into the Swayze area. The oldest volcanic rocks and banded iron formations are a key component of this terrane. A particularly prominent iron formation, marking the sequence boundary between the classical Deloro and Tisdale Groups, forms a key marker unit in this terrane, extending from the Swayze belt to possibly as far east as the Adams Mine area and as far south as Temagami. The terrane is capped by the flyschoid sediments of the Porcupine assemblage. The Timmins-Swayze terrane was overridden by (2) the "Kidd-Munro terrane" along the regional "Pipestone Thrust". We now have sufficient data to demonstrate a regional, pre-folding, "old-over-young" relationship along this thrust contact, with the entire ca. 2718-2712 Ma Kidd-Munro assemblage, hosting not only the giant Kidd Creek VMS deposit, but also the classical Pyke Hill komatiites, sitting on top of younger turbidites. Thrust emplacement was towards the west and south. At the highest structural level, there may be (3) a third major thrust slice emplacing the younger 2703-2695 Ma Blake River assemblage. Defining stratigraphic elements of one terrane are lacking in the others; for instance, there are no Kidd-Munro age rocks in the Timmins-Swayze terrane, and Tisdale age volcanic rocks are absent in type sections of the Kidd-Munro assemblage.

Possibly, climactic Kidd-Munro volcanism (2716-2714 Ma), characterized by komatiites and high-silica rhyolites, is represented by distal chemical sedimentation in the main iron formation of the Timmins-Swayze terrane, an idea that could be tested by searching for a felsic tuff component and 2716-2714 Ma zircons in this regional iron formation. If no such link exists, there is even less relationship between these two terranes and thrust displacement on the fundamental Pipestone Thrust correspondingly larger. The present situation is that all three terranes are severely telescoped and sitting structurally on top of each other. Each has its own stratigraphy, metallogenic endowment, and "centre of gravity" in terms of map distribution.

Following upright folding of the imbricated terranes ("D1", quotes indicating a broad event involving high-level thrusting and at least two phases of folding), there was a sudden flare-up of alkaline magmatism, starting just prior to 2680 Ma and likely accompanied by a very significant phase of extension. After this extension, the folded terranes were re-imbricated, thick-skin style, with folding and thrust burial ("D2") of terrestrial, syn-orogenic, clastic rocks (Timiskaming-type sediments). The major "breaks" (e.g. the Destor-Porcupine and Cadillac-Larder Lake- Matachewan Fault Zones), periodically spaced, were conceived as crustal- if not lithospheric-scale extensional faults that were then inverted as south-over-north, high-angle D2 thrusts, with Timiskaming conglomerates and sandstones preserved in footwall synclines. Finally, the breaks evolved into transpressional zones dominated by strike-slip deformation, first sinistral and then dextral. Net displacements on these breaks are south-side up, exposing plutons and deeper stratigraphy to the south, and tens of kilometers sinistral strike-slip.

The superposition of these events, especially the extensional event and its magmatism, followed by thick-skin re-imbrication, and strike-slip, has been critical in the generation of world-class Au deposits. Extension and magmatism thinned the lithosphere, and created the deep fluid pathways, even though most of the gold was emplaced later during re-imbrication and the evolution to strike-slip. All critical elements of this complex story are duplicated in several other world-class Au districts, particularly in the Yilgarn. For instance, the New Holland camp of the Eastern Goldfields is essentially a carbon copy of the Timmnins area and there are many others. Recognizing the essential elements of this complex story, and their critical superposition in time and space, allows for detailed targeting in the search for large productive gold camps.

THE RISE OF THE CONTINENTS AND THE SHIFT TO MODERN EARTH

P.F. Rey[1], N. Coltice[2] & N.E. Flament[1]

[1]Earthbyte Group, School of Geosciences, The University of Sydney, Australia
[2]Laboratoire de Sciences de la Terre, UMR CNRS 5570, Université de Lyon, France

Introduction

Terrestrial planets evolve via partial melting and gravitational differentiation whereas experiencing slow secular cooling. Mass and energy transfers across their various envelopes depend on the mode of convective motion, which may involve stagnant or mobile lid systems, for which plate tectonics is one possible mode. Modes of convective motion may involve gravitational instabilities, switches between various modes of convection and thermal catastrophes due to feedback between plate aggregation and mantle temperature (Coltice et al., 2007, 2008). Hence, from 4.54 to 2.5 Ga the Earth differentiation may not have followed a linear and smooth path, but rather a chaotic storyline involving sudden crises that punctuated periods of relative quietness. In this contribution, we focus on the Earth secular cooling and its long-term effect on (1) the geochemical coupling between the crust and other geochemical reservoirs, and (2) the stabilization of the Earth geodynamics. Secular cooling has the double effect to strengthen the Earth lithosphere and to promote continental emergence. Strengthening results from the exponential dependence of viscosity to temperature, while emergence is a response of the deepening of the ocean basins as the deep mantle cools down, which lowers the mean sea level. Both effects conspire to enhance weathering and erosion of the continents and therefore to enhance the geochemical coupling between the continents and other Earth's envelopes.

Earth secular cooling

Figure 1 shows the evolution of heat flow at the surface of Archean cratons. Disregarding the heat production in the mantle, we use the U, Th, and K concentrations of present-day average Archean crust determined by Taylor & McLennan (1995), and we use for the mantle heat flow the parameterization of Grigné et al. (2005), assuming a 200ºC drop in mean mantle temperature since 3.5 Ga. The decrease through time is due to the decay of radiogenic elements and cooling of the Earth's interior. The impact of the Earth secular cooling on the continental geotherm of Archean cratons is shown in figure 2, using the temperature at the Moho as a proxy for the geotherm.

At present, Archean cratons are cold and strong. However back in the Archean, they were much warmer and therefore weaker. The Earth progressive cooling led to a non-linear increase in the averaged strength of the continental lithosphere. Figure 3 shows that there is an acceleration of the strengthening of the continental lithosphere during the Neoarchean (2.8 to 2.5 Ga ago). This non-linear evolution is due to the preferential strengthening the upper part of the lithospheric mantle

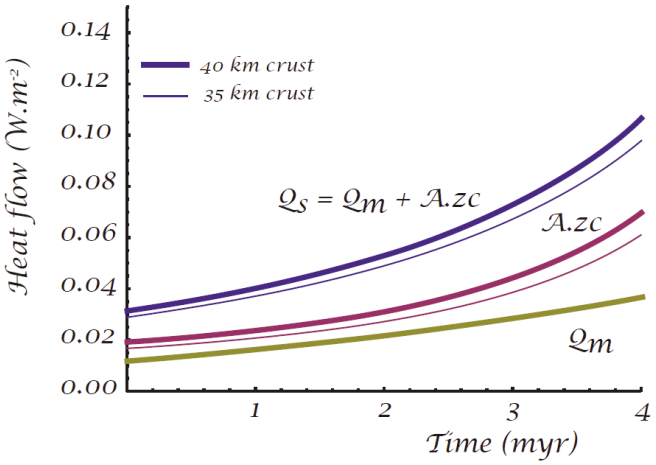

Figure 1. Secular evolution of surface heat flow. The surface heat is the sum of radiogenic heat in the crust (A.zc) and input heat flow from the mantle (Q_m).

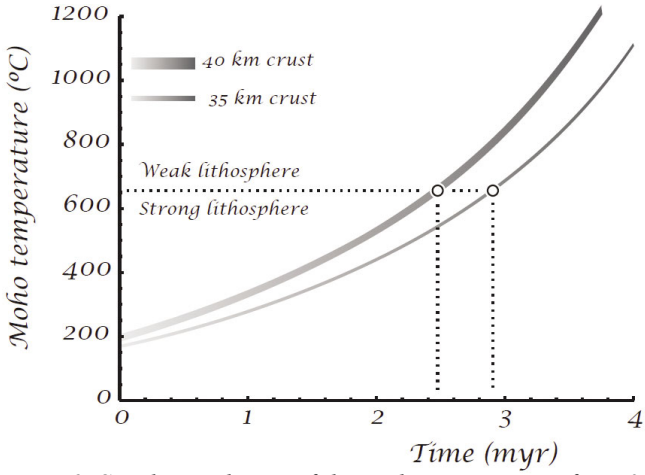

Figure 2. Secular evolution of the Moho temperature for a 35 km and 40 km thick continental crust.

for Moho temperature ≤ ca. 650ºC. Plotting the vertically integrated strength as a function of depth (Fig. 4) reveals that it is the strengthening of the upper mantle that explains the bulk of the strengthening of the continental lithosphere as the Moho temperature drops below 650ºC. Although the secular cooling of the Earth may have occurred at a constant rate, the strengthening of the lithosphere may have recorded a strong acceleration during the Neoarchean.

The rise of orogenic plateaux

Stronger lithospheres offer more resistance to gravitational forces. Hence, orogenic plateaux can grow higher on stronger crusts than they can on weaker crusts. A simple triaxial model is used in figure 5 to show the evolution of the elevation of orogenic plateaux as a function of the Moho temperature (our proxy for the

continental geotherm). Archean continents were unlikely to support orogenic plateaux higher than 2000m (Rey & Coltice, 2008). In the Archean, orogenic crusts would have reached their plateau elevations much earlier during convergence compared to modern plateaux, with most of the convergence being accommodated via the widening of the plateau rather than its rise.

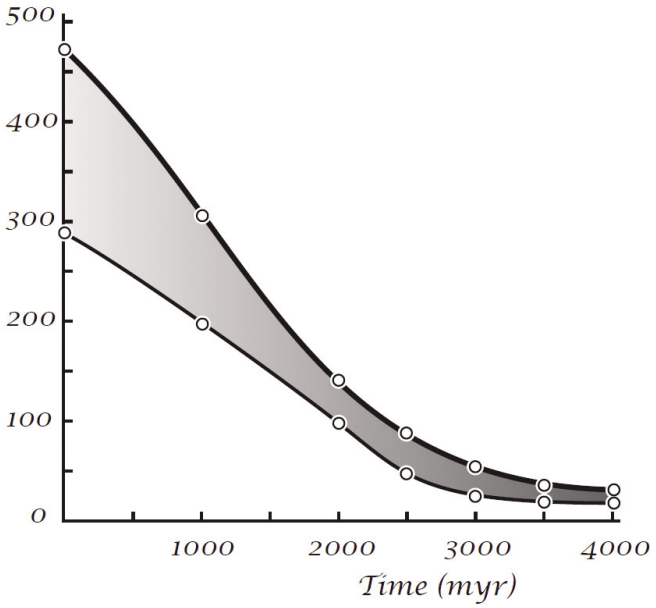

Figure 3. Secular evolution of the integrated strength of the lithosphere. Note the sudden change in the rate of strengthening from 3Ga.

At the Earth's surface, the area of emerged continental crust, therefore the area of continents exposed to weathering and erosion, is a function of mantle temperature, continental area and hypsometry. Since in the Archean the Earth's hypsometry involved a much reduced elevation peak, our results suggest that the area of emerged land was much reduced in the Archean. Flament et al. (2008) developed a model that evaluates the area of emerged continental crust as a function of mantle temperature, continental area and hypsometry. They found that the continents were mostly flooded until the end of the Archean, with only 2-3% of Earth's area (approximately the size of South America) consisting of emerged land.

The shift to modern Earth

The strengthening and emergence of the continents, and the rise of orogenic plateaux, may have enhanced continental erosion and therefore the geochemical coupling between the felsic crust and the atmosphere/ocean system, and may have enhanced the coupling between the crust and the mantle via subduction of continental detrital sediments. In the Neoarchean, exogenic envelopes recorded major shifts in composition that are consistent with the progressive exposure of large areas of felsic crust at the Earth's surface. The change of the average composition of the surface of emerged land is recorded on continents by the composition of black shales, and in the ocean by the strontium isotopic composition of carbonates and the phosphorus concentration of banded iron formations. Neoarchean black shales and carbonates record a shift from compositions buffered by mafic lithologies to compositions buffered by felsic lithologies

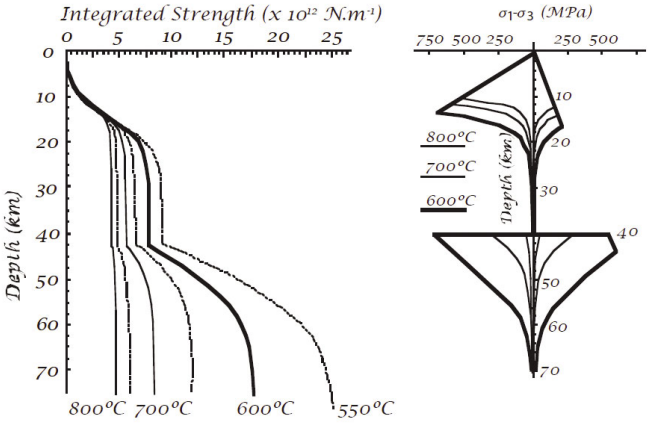

Figure 4. Left: Vertically integrated strength as a function of depth. This graph is produced by integrating the rheological profiles on the right.

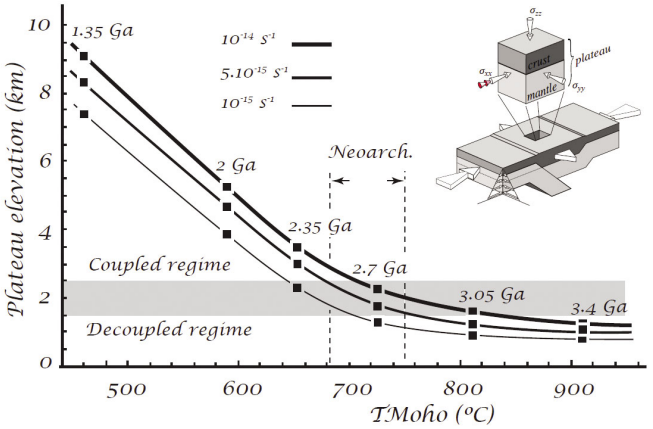

Figure 5. Secular evolution of the elevation of orogenic plateaux. The three curves are for different initial strain rates. Note the sudden rise of plateaux from 3Ga.

(Taylor & McLennan, 1985; Veizer & Compston, 1976; Shields & Veizer, 2002), whereas banded iron formations indicate that the pre–2 Ga ocean was strongly depleted in phosphorus, an element strongly partitioned into the felsic continental crust (Bjerrum & Canfield, 2002). In addition, oxygen isotopic data on detrital magmatic zircons show that the incorporation of crustal sediments in silicic magma, an indication of intracrustal recycling, did not appear before the Neoarchean (Valley et al., 2005; Kemp et al., 2006). Oxygen and silica isotopes in cherts point toward a drop in the Earth's surface temperature in the Neoarchean, at a time when oxygenation reached a critical level (Robert & Chaussidon, 2006). Silicate weathering and erosion being a very efficient sink for atmospheric CO_2, we propose that the strengthening and emergence of the continental lithosphere in the Neoarchean was a very important factor contributing to both the cooling of the Earth's surface and oxygenation of the Earth's atmosphere.

This Neoarchean transition from primitive to modern Earth has often been presented in the context of a major pulse of crustal growth and differentiation (Taylor & McLennan, 1985, 1995), superplume activity (Condie, 2004), and/or mantle overturn and orogenic crisis (Stein & Hofman, 1994; Breuer & Spohn, 1995). However, in the context of continental strengthening, we propose

that the Earth's exogenic and endogenic geochemical reservoirs became strongly coupled when a significant portion of the felsic crust, hitherto hidden under greenstone covers and/or under sea level, permanently reached the Earth's surface and when sharper mountain belts and high orogenic plateaus were able to sustain higher erosion rates and fluxes toward the oceans.

Stabilization of the Earth geodynamics

A consequence of the possible late Archean emergence of continents, and rise of orogenic plateaux, is the necessary increase of the rate of crustal recycling back into the mantle via subduction of large volumes of detrital sediments. Once can speculate that this recycling would have slowed down significantly the rate of crustal growth, hence stabilizing the fraction of continents at the Earth's surface. The recycling of sediments may have also contributed to the re-hydration of the mantle and lowered its viscosity. The subduction and dehydration of wet sediments may also have contributed to the decoupling between the upper plate and the lower plate along the Benioff plane hence stabilizing asymmetric subduction.

Conclusions

The pre–Neoarchean geological record points toward a minor role of continental weathering and erosion in the cycling of atmospheric carbon and that of incompatible elements trapped in the continental crust. A large number of global anomalies in the Neoarchean point toward a major period of reorganization in the Earth's endogenic and exogenic envelopes. To understand this critical period of the Earth's history, the long-term evolution related to the progressive cooling and differentiation of the Earth's envelopes must be considered separately from shorter pulses related to superplume events (Condie, 2004) and mantle instabilities (Stein & Hofmann, 1994; Breuer & Spohn, 1995). As the rheology of rocks is exponentially sensitive to temperature, we argue that the secular cooling of the Earth was associated with a rapid strengthening and emergence of its continental lithosphere, and the rise of orogenic plateaux. Our numerical experiments show that the strengthening of the continental lithosphere went through a rheological threshold in the Neoarchean. At that time, the strength of the continents reached a level enabling significant crustal thickening and topographic heights. This in turn increased drastically erosion and the geochemical coupling between the felsic crust, the atmosphere, the hydrosphere, and the mantle.

References

Bjerrum C.J. & Canfield D.E., 2002, Ocean productivity before about 1.9 Gyr ago limited by phosphorus adsorption onto iron oxides, Nature, 417, 159–162.

Breuer D. & Spohn T., 1995, Possible flush instability in mantle convection at the Archean-Proterozoic transition, Nature, 378, 608–610.

Coltice N., Phillips B.R., Bertrand H., Ricard Y. & Rey P., 2007, Global warming of the mantle at the origin of flood basalts over supercontinents, Geology 35, 391–394.

Coltice N., Bertrand H., Rey P., Jourdan F., Phillips B.R., Ricard Y., 2008, Global warming of the mantle beneath continents back to the Archean, Gondwana Research doi:10.1016/j.gr.2008.10.001.

Condie K.C., 2004, Supercontinents and superplume events: distinguishing signals in the geologic record, Physics of Earth and Planetary Interiors, 146, 319–332.

Flament N., Coltice N. & Rey P. F., 2008, A case for late-Archaean continental emergence from thermal evolution models and hypsometry, Earth and Planetary Science Letters, 275, 326–336.

Grigné C., Labrosse S. & Tackley P.J., 2005, Convective heat transfer as a function of wavelength: Implications for the cooling of the Earth, Journal of Geophysical Research, 110, B3, B03409, doi: 10.1029/2004JB003376.

Kemp A.I.S., C.J. Hawkesworth, B.A. Paterson & P.D. Kinny, 2006, Episodic growth of the Gondwana supercontinent from hafnium and oxygen isotopes in zircon, Nature, 439, 580–583.

Rey P. F. & Coltice N., 2008, Neoarchean strengthening of the lithosphere and the coupling of the Earth's geochemical reservoirs, Geology, 36, 635–638.

Robert F.M. & Chaussidon 2006, A palaeotemperature curve for the Precambrian oceans based on silicon isotopes in cherts, Nature, 443, doi:10.1038/nature05239.

Shields G. & Veizer, J., 2002, Precambrian marine carbonate isotope database: Version 1.1. Geochemistry, Geophysics, Geosystems, 3, 1031.

Stein M. & Hofmann A.W., 1994, Mantle plumes and episodic crustal growth. Nature, 372, 63–68.

Taylor, S. R., S. M., McLennan, 1985. *The continental crust, its composition and evolution*, Blackwell, London, 312p.

Taylor S. R. & McLennan S. M., 1995, The geochemical evolution of the continental crust. Reviews of Geophysics, 33, 241–265.

Valley J., Lackey J., Cavosie A., Clechenko C., Spicuzza M., Basei M., Bindeman I., Ferreira V., Sial A., King E., Peck W., Sinha A. & Wei, C., 2005, 4.4 billion years of crustal maturation: oxygen isotope ratios of magmatic zircon, Contributions to Mineralogy and Petrology, 150, 561–580.

Veizer, J. & Compston, W., 1976, $^{87}Sr/^{86}Sr$ in Precambrian carbonates as an index of crustal evolution, Geochimica et Cosmochimica Acta, 40, 905–914.

THE METAMORPHIC RECORD OF A PALEOARCHEAN CRUSTAL COLLISION

G. Stevens[1], J-F. Moyen[1*] & C. Lana[1]

[1]Department of Earth Science, Stellenbosch University, Private Bag X1, 7602, Stellenbosch, South Africa; [*] now at Département de Géologie, Université Jean-Monnet Faculté des Sciences, 23 rue du Docteur Michelon, 42023 Saint Etienne, France

Introduction

The role of subduction zone processes in the formation and evolution of Archean crust is a topic of substantial controversy. On the one hand, evidence for TTG formation by the partial melting of a high-pressure garnet-amphibolite or eclogite source, appears to present a strong argument for subduction of oceanic crust as the driving mechanism in producing the Archean continental crust (e.g. Foley, 2002; Rapp et al., 2003). On the other hand, Stern (2005) has argued that subduction zones have existed on Earth only since Neoproterozoic times, as this is when blueschists and complete ophiolite sections appear in the rock record. However, the duality of metamorphic PT regimes that may constitute evidence for plate tectonics stretches back to Neoarchean times, with rocks that undergo untrahigh temperature metamorphism reflecting settings analogous to modern backarcs, whilst eclogite to high-pressure granulite series rocks reflect the consequences of crustal convergence (Brown, 2006). Brown (2006) proposes that the earlier Archean metamorphic record is characterised by rocks of the rather "ordinary" moderate pressure – high temperature facies series, reflecting an absence of subduction zones. The geology of the Barberton greenstone belt (BGB) and surrounding granitoid rocks covers a substantial portion of this earlier Archean record and provides a potentially unique opportunity to investigate metamorphic processes associated with a Paleoarchean subduction zone. This arises because the greenstone belt contains clear evidence for accretionary processes, with major fault bounded blocks consisting sequences that are different in age and stratigraphy (e.g. de Ronde and de Wit (1994); Lowe, (1994)). Additionally, the main collisional event at ca 3230 Ma was preceded by the formation of a convergence-related magmatic arc in the interval 3290 to 3230 Ma (Kisters et al 2010), and resulted in high-pressure garnet-epidote-amphibolite facies metamorphism in the rocks of the Stolzburg terrane (Fig. 1) which constitute the lower plate in the collisional process. Along the Inyoni shear zone (Fig. 1), where the Stolzburg terrane is in contact with the rocks of the magmatic arc (Badplaas domain), peak recorded metamorphic conditions within metamafic rocks of ca 1.2 GPa and 550°C developed during decompression (Moyen et al., 2006). Similarly, rocks of the Theespruit formation, close to the extensional detachment with the greenstone belt, also record a relatively high-pressure history of decompression, with peak recorded PT conditions being preserved by assemblages that form part of an exhumation fabric (Diener et al, 2005; Lana et al, 2009). Thus, these metamorphic rocks that record the lowest dP/dT values known for the Paleo- and Mesoarchean (as low as 480°C/GPa), potentially have a higher pressure history that is yet to be revealed. This study explores material from Stolzburg terrane in an attempt to reveal this history.

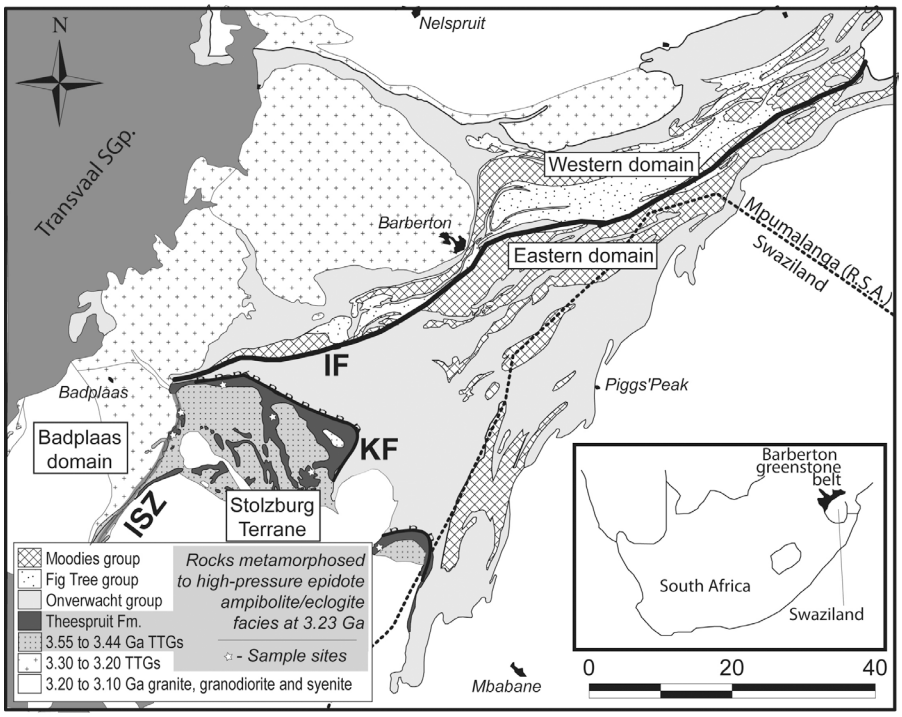

Figure 1. A map of the BGB and surrounding granitoids. The rocks of the Western and Eastern domain were juxtaposed along the Inyoka fault (IF) during 3.23 Ga collision. As a consequence, rocks of the lower plate (Theespruit Formation and 3.45 to 3.55 Ga. TTG plutons of the Stolzburg terrane) underwent high-pressure, low temperature metamorphism. The Stolzburg terrane was exhumed relative to the low grade metamorphic rocks of the greenstone belt along the Komati fault (KF) and is separated from the magmatic arc rocks of the Badplaas domain by the Inyoni shear zone (ISZ).

Garnet-bearing rocks of the Stolzburg terrane

This work focuses on three varieties of garnet developed within rocks of mafic to intermediate composition in the Stolzburg terrane. Firstly, within the cores of rootless folds in metamafic rocks of the Inyoni shear zone, garnet is developed as porphyroblasts up to 8mm in diameter, that are characterized by poikiloblastic cores with quartz, epidote and chlorite inclusions. The crystals display core to rim growth zonation, characterized predominantly by decreasing spessartine and increasing almandine contents towards the rims. The garnets display low Mg#s (typically < 11) and high grossular contents (36 to 40%) and occur in a matrix of hornblende, plagioclase clinopyroxene and epidote, which defines a fabric that post-dates garnet growth. Pseudosection modelling of the stability field of this assemblage, when combined with isopleths of garnet composition, indicates that the garnet is likely to have formed at a substantially higher pressure than the range within which the matrix assemblage is stable. Conditions of garnet growth of P > 1.4 GPa and T < 610°C are indicated, which are above the modelled upper limit of plagioclase stability in these rocks. These garnet crystals display REE patterns with no significant Eu anomaly (Eu/Eu* = 0.9 to 1.2), whilst the matrix plagioclase displays a typical significant positive Eu anomaly. This is interpreted to support the suggestion that the garnet composition formed from an assemblage that lacked plagioclase.

In rocks of intermediate composition within the Inyoni shear zone, garnet exists that has clearly formed via plagioclase breakdown. In these rocks, garnet is euhedral and largely free of inclusions and has low Mg#s (< 10) and high, but variable grossular contents (from 30 to > 40). Two generations of epidote occur, an earlier, more aluminous and less Fe-rich variety and a subsequent more Fe-rich variety that has formed with garnet. The garnet and epidote occur within a matrix of albitic plagioclase, collectively pseudomorphing domains previously occupied by clasts of originally more calcic plagioclase. Pseudosection modelling of these rocks indicates that the garnets formed at pressures of 1.3 GPa and upwards, with temperature constrained to below 600°C. At this temperature, 1.3 GPa is the modelled limit of plagioclase stability in these rocks, and the textures are interpreted to reflect the breakdown calcic plagioclase, with actinolite, to form garnet and epidote as the upper limit of plagioclase stability was approached.

In rocks of the Theespruit formation (Fig 1) large and complexly zoned garnet crystals are developed in aluminous horizons within rocks of both mafic and intermediate composition. These garnets range in size from 5 to 25mm and are characterised by intensely poikiloblastic cores, typically with inclusion trails of ilmenite defining a fabric that is at an oblique angle to the later matrix fabric that wraps around the garnet. The core domains are mantled by a thick rim (2 to 8mm) of second generation of garnet containing substantially fewer inclusions. The chemistry of these crystals displays complex zonation patterns. The core domains are characterised by relatively flat Mg# (4 to 5) and grossular content zonation (~ 10%), with spessartine content being high in the centre of the core (7%) and decreasing systematically outwards the outside, yet rising sharply again towards this internal contact. Mg# and grossular-content also increase over this interval. The mantle of the garnet is characterised by increasing grossular content (to 25%) and Mg# (to 9), whilst spessartine content decreases to low values (2%) towards the rim. Apart from the ilmenite inclusions, the core domain contains inclusions of chlorite, epidote and polymineralic inclusions of chlorite, albite and K-feldspar. These are interpreted to reflect the breakdown products of original phengite inclusions. The matrix of the rock contains the low-temperature amphibolite facies assemblage: hornblende, biotite, ilmenite, quartz, plagioclase, epidote and chlorite. Chlorite in these rocks contains a significant MnO content (up to 1 wt %). Consequently, the increase in MnO content towards the core-mantle interface of the garnet is interpreted to reflect the breakdown of chlorite to produce garnet, with a concurrent increase in pressure, as reflected in the concurrent increase in grossular content. The core domains of these garnets display chondrite normalised REE patterns with slight positive Eu anomalies. This is interpreted to reflect the absence of plagioclase in the assemblage associated with this generation of garnet. In some crystals the rim domains display slight negative Eu anomalies, whilst in garnet from other layers this is absent. Pseudosection modelling of these rocks, using a bulk composition for the rims that has been corrected by subtraction of the garnet core component, indicates that garnet records prograde growth form approximately 0.8 GPa and 500°C, to 1.1 to 1.2GPa at 590°C

Conclusions

Domains within the Stolzburg terrane that have largely escaped resetting to the lower-pressure amphibolite facies conditions established as a result of orogenic collapse, contain evidence for metamorphism under conditions transitional between the high pressure garnet-epidote amphibolite facies and the low-temperature eclogite facies. These metamorphic conditions are only slightly hotter (50 to 100°C) than those that would be developed at equivalent pressures within modern, warm subducting slabs (Fig. 2). These rocks contain evidence for a plagioclase-free prograde path in rocks that probably had feldspar-free protoliths. In rocks with plagioclase in the protolith, plagioclase reacts with ferromagnesian minerals to produce garnet, albite and epidote bearing assemblages. This incipient eclogite facies metamorphism constitutes clear evidence for a subduction process leading to collision at 3.23 Ga. Figure 2a illustrates 2 two important aspects of what should be expected of the Archean rock record associated with subduction. Firstly, conditions in the subducting slab were too hot to produce blueschists. This is evidenced by that fact that even modern warm subduction scenarios may not produce blueschists and generally do not produce slab melts. Melting of the slab requires even hotter conditions in the subducted slab. Consequently, the high pressure greenschist facies – epidote amphibolite facies – eclogite facies progression defines the Archean subduction related metamorphic facies series. Secondly, the fact that this progression intersects both the water saturated basalt

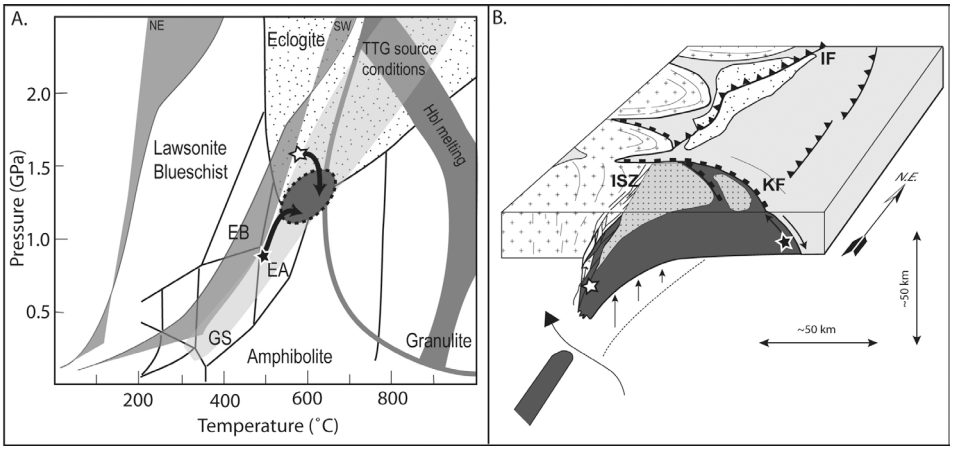

Figure 2: A. Metamorphic conditions determined in this study (arrows and dashed ellipse), compared with those in the warm SW Japan and cool NE Japan subducting slabs. The edges of the slab PT fields marked by the solid lines represent the top of the slab in each case. Abbreviated facies notations as follows: EA, epidote amphibolite; EB, epidote blueschist; GS, greenschist (After Peacock and Wang, 1999). The light grey band represents the proposed Archean subduction metamorphic facies series, which results in slab melting under eclogite facies conditions. B. A cartoon indicating culmination of subduction in the BGB by collision at 3.23 Ga. The high-pressure Stolzburg terrane, portions of which were transported down the subduction channel, is being exhumed due to orogenic collapse. The high pressure domain is rising relative to the lower grade greenschist facies rocks of the greenstone belt, via deformation along the Komati fault, and relative to the magmatic arc rocks of the Badplaas domain, via deformation accommodated within the Inyoni shear zone. The black star represents a sample from the Theespruit formation that has followed an epidote-amphibolite facies evolution, the white star represents a sample from the Inyoni shear zone that has been metamorphosed through the lower temperature portion of the eclogite facies. The key for Figure 1 applies.

solidus and the field of fluid-absent hornblende melting, results in slab melting to produce TTG magmas. This traps slab water and transfers it to the overlying crust, thereby limiting hydration of the overlying mantle wedge. In the modern earth it is melting of this hydrated mantle that produces magmas that transfer heat to the crust in back-arc settings. Consequently, the Archean subduction related metamorphic signature does not have an ultrahigh temperature metamorphic counterpart. This arose only once the Earth was cool enough to limit slab melting, allowing for more hydration of the mantle.

Acknowledgements

GS acknowledges NRF and DST funding via the South African Research Chair initiative.

References

de Ronde C.E.J. & de Wit, M.J., 1994, The tectonic history of the Barberton greenstone belt, South Africa: 490 million years of Archaean crustal evolution, Tectonics, 13, 983.1005.

Diener J.F.A., Stevens G., Kisters A.F.M. & Poujol M., 2005, Metamorphism and exhumation of the basal parts of the Barberton greenstone belt, South Africa: Constraining the rates of Mesoarchean tectonism, Precambrian Research, 143, 87.112.

Foley S.F., Tiepolo M., Vannucci R., 2002, Growth of early continental crust controlled by melting of amphibolite in subduction zones, Nature, 417, 837.840.

Jahn B-M., Liu X., Yui T-F., Morin N. & Coz B-L., 2005, High-pressure/ultrahigh-pressure eclogites from the Hong'an Block, East-Central China: Geochemical characterization, isotope disequilibrium and geochronological controversy, Contributions to Mineralogy and Petrology, 149, 499.526.

Kamo S.L. & Davis D.W., 1994, Reassessment of Archaean crustal development in the Barberton Mountain Land, South Africa, based on U-Pb dating, Tectonics, 13, 167.192.

Kisters A.F.M., Belcher R., Dziggel A. & Poujol M., 2010, Continental growth and convergence-related arc plutonism in the Mesoarchaean: Evidence from the Barberton granitoid-greenstone terrain, South Africa, Precambrian Research, in press. doi:10.1016/j.precamres.2010.01.002

Kisters A.F.M., Stevens G., Dziggel A. & Armstrong R.A., 2003, Extensional detachment faulting and core-complex formation in the southern Barberton granite-greenstone terrain, South Africa: Evidence for a 3.2 Ga orogenic collapse, Precambrian Research, 127, 355.378.

Lana C., Kisters A.F.M. & Stevens G., 2009, Exhumation of Mesoarchean TTG gneisses from the middle crust: Insights from the Steynsdorp core complex, Barberton granitoid-greenstone terrain, South Africa, GSA Bulletin; 122, 183.197.

Lowe D.R., 1994, Accretionary history of the Archaean Barberton greenstone belt (3.55–3.22 Ga), southern Africa, Geology, 22, 1099.1102.

Moyen J-F., Stevens G. & Kisters A.F.M., 2006, Record of mid-Archaean subduction from metamorphism in the Barberton terrain, South Africa, Nature, 442, 559.562.

Peacock S.M. & Wang K., 1999, Seismic consequences of warm versus cool subduction metamorphism: Examples from southwest and northeast Japan, Science, 286, 937.939.

Rapp R.P., Shimizu N. & Norman M.D., 2003, Growth of early continental crust by partial melting of eclogite, Nature, 425, 605.609.

Stern R.J., 2005, Evidence from ophiolites, blueschists, and ultrahigh-pressure metamorphic terranes that the modern episode of subduction tectonics began in Neoproterozoic time, Geology, 33, 557.560,

TWO TYPES OF PALEOARCHEAN CONTINENTAL CRUST; OCEANIC-TYPE PLATEAUX AND SUBDUCTION ZONE COLLAGES ON EARLY EARTH

M.J. Van Kranendonk[1,2]

1Geological Survey of Western Australia, 100 Plain St., East Perth, Western Australia, 6004, Australia. Email: martin.vankranendonk@dmp.wa.gov.au
2also at; School of Earth and Environment, the University of Western Australia, 35 Stirling Hwy., Crawley WA, 6009 Australia

Introduction

Over 4.5 billion years, Earth evolved from a molten ball to a cooler planet with large continental plates, but how and when continents grew and plate tectonics started remain poorly understood. In this paper, I review the evidence that 3.5-3.2 Ga continental nuclei in the Pilbara, Australia and eastern Kaapvaal Craton, southern Africa, formed as thick oceanic plateaux over hot, upwelling mantle and survived due to contemporaneous development of thick, buoyant, unsubductable mantle roots. These nuclei are distinct from, but complimentary to, high-grade gneiss terranes that formed over shallow subduction zones on a vigorously convecting early Earth with small plates. Steep, "modern" subduction did not commence until 3.2 Ga, when plate size may have increased as a function of secular planetary cooling and the development of thick protocontinental nuclei that helped deflect plates downward.

Oceanic plateaux

The Paleoarchean East Pilbara Terrane (Pilbara Craton, Australia) and the Barberton Greenstone Belt (BGB) and surrounding granitic rocks of the eastern Kaapvaal Craton (southern Africa) have remarkably similar histories from ca. 3.53-3.22 Ga, yet diametrically opposed tectonic interpretations (de Wit et al., 1992; Van Kranendonk et al., 2007). Previously, several lines of evidence have been cited to support subduction-accretion in the development of Pilbara and Kaapvaal lithosphere: 1) 20-km thick sequences of dominantly pillowed basalt ± komatiite, interpreted as stacked oceanic crust(de Wit et al., 1987, 1992); 2) Calc-alkaline felsic volcanics and voluminous TTG, interpreted as subduction-related arc magmas and/or melts of stacked oceanic lithosphere (de Wit et al., 1992; Barley, 1993); 3) Local recumbent isoclinal folds, thrust faults and moderate-pressure metamorphism (P = 4-6 kb), interpreted as products of Alpine-style orogeny (Bickle et al., 1985; de Wit et al., 1992) ; 4) Moderate- to high-P (8-15 kb), moderate-T (600-700ºC) assemblages in narrow greenstone septae southwest of the BGB, used to infer subduction, terrane accretion and/or crustal stacking through orogeny at 3230 Ma (Moyen et al., 2006); 5) Granite domes as post-collisional extensional metamorphic core complexes (Kisters & Anhaeusser, 1995; Zegers et al., 2001) ; 6) Thick subcontinental lithospheric mantle (SCLM), interpreted to have formed through tectonic underplating of subducted oceanic lithosphere (Helmstaedt & Gurney, 1995).

However, several recent studies, together with new considerations presented here, suggest that Paleoarchean Pilbara and Kaapvaal lithosphere developed as oceanic-type plateaux, without the direct influence of subduction-accretion processes.

Thick greenstone successions

Geological mapping and U-Pb zircon dating indicate that the >20 km thick greenstone successions are upward-younging, geochemically variable, and unaffected by large-scale tectonic duplication (Lowe & Byerly, 2007; Van Kranendonk et al., 2007). Evidence for contamination of even the stratigraphically lowest basaltic rocks by older – in part sialic – crust is widespread (Van Kranendonk et al., 2007, 2009). Basaltic compositions are similar to plateau-type volcanics, rather than MORB and komatiites derive from deep melting within a mantle plume, rather than shallow melting of wet mantle (Herzberg et al., 2007). In Pilbara, deposition was through lateral accumulation in extensional basins developed on older protocrust and it has been shown that regional low-grade, contact-style, metamorphism of greenstones is uniquely explained by syn-depositional doming and basin formation during episodic, long-lived crustal development (Van Kranendonk et al., 2002, 2007).

Felsic volcanics as products of fractionation/contamination

Evidence from Pilbara felsic volcanics, including magma mingling and the presence of hybrid basaltic andesites, combined with low La/Nb ratios and tholeiitic major element trends, indicate derivation through a combination of fractional crystallisation and crustal contamination in large tholeiitic magma chambers (Smithies et al., 2007).

TTG as products of infracrustal melting

Widespread, voluminous TTG derive from contemporaneous high- and low-pressure infracrustal melting of mafic rocks within >50 km thick crust (Champion & Smithies, 2007) rather than from subducted oceanic lithosphere. Isotopic and geochronological data from c. 3.46 Ga Pilbara TTG indicate they formed from a >3.5 Ga source composed of enriched basalt or hybrid basalt-TTG (Smithies et al., 2009).

Melt-depleted SCLM

Studies of mantle xenoliths and xenocrysts from diamondiferous kimberlites in Pilbara and Kaapvaal suggest that the SCLM consists dominantly of highly depleted dunite-harzburgite residues from unusually high-degree partial melting events typically attributed to mantle plumes (Griffin & O'Reilly, 2007). The

progressive change in the compositions of low-Ti basalts and komatiites over time in Pilbara, the presence of 3.33 Ga ultra-depleted komatiites in Kaapvaal (Wilson et al., 2003), and Mesoarchean Sm-Nd, Rb-Sr and Re-Os dates on silicate inclusions in diamonds all are consistent with the *in situ* development of the lithospheric keel through melt-depletion of subcontinental mantle *during* plume-derived crust formation at 3.5-3.2 Ga (Smithies et al., 2005, 2009).

Partial convective overturn

The Pilbara dome-and-keel architecture consists of steeply-dipping greenstone keels and multicomponent granitic complexes that contain distinctive structural and metamorphic features that are uniquely indicative of a process known as partial convective overturn (PCO: Collins et al., 1998; Sandiford et al., 2004; Van Kranendonk et al., 2004). Structures and metamorphic assemblages previously ascribed to Alpine-style orogeny there have been shown to result from shortening within the restraining bend of a late kinematic (2.94 Ga) strike-slip shear zone (Van Kranendonk et al., 2004). BGB exhibits a similar dome-and-keel architecture, with cleavage triple points between granite domes, upright folds that plunge radially inwards towards the centre of the BGB, and extensional detachments along the amphibolite-greenschist facies transition with granite-up/greenstone-down displacement. A moderate-P metamorphic rind with steeply-dipping, concentric foliations and steeply-plunging mineral lineations in greenstone septae wrapped around granitic domes are consistent with PCO and the diapiric rise of granites at 3225-3216 Ma (Van Kranendonk et al., 2009).

A major difference is that BGB is interpreted to have been affected by an immediately preceding episode of subduction and arc-arc collision at 3230 Ma (de Wit et al., 1992; de Ronde & Kamo, 2000; Moyen et al., 2006). However, several features cast significant doubt on the arc-accretion model.

1. An inferred thrust fault near the base of the greenstones has been discounted and shown to be an extensional fault, unrelated to crustal thickening (Kisters & Anhaeusser, 1995; Van kranendonk et al., 2009). Combined with upward-younging stratigraphy, these data preclude significant tectonic thickening in crust formation.
2. Extension-related structures in higher-grade rocks outside the belt (vertically rodded, high-grade supracrustal remnants around domical granites) developed at the same time (3230 Ma) as compression-related structures (upright folds, recumbent isoclinals folds, thrusts), at lower metamorphic grade, inside the belt. These contemporaneous, but distinctly different, structural styles are also atypical of subduction-accretion zones, but characteristic of PCO, where extension develops in rising, more buoyant material, and compression in the denser, sinking greenstones resulting from bed-length shortening between rising domes.
3. The 3230 Ma, high-P assemblages recorded southwest of the BGB occur in subvertically-lineated, L>S supracrustal remnants wrapped around older granitic rocks that show evidence of diapiric emplacement. These structures are atypical of subduction-accretion complexes, but diagnostic of PCO, and thus the metamorphism must also relate to PCO. This is supported by the fact that even the highest-P assemblages are not equivalent to geotherms found in modern subduction-collision zones; these conditions may only directly relate to the lineated supracrustal remnants and not to the surrounding, much hotter, granites.
4. The higher-P assemblages grade across strike to lower P-T assemblages in the BGB (Cloete, 1993), with no evidence of crustal stacking or inverted metamorphic isograds to explain the higher pressures. Greenstone assemblages at granite margins exhibit evidence of isothermal burial (Van Kranendonk et al., 2009), consistent with greenstone sinking across granite margins made relatively cool by conductive transfer of heat through granite crests.

Model of crust formation

The following model applies to Pilbara and Kaapvaal lithosphere. In early stages, a thick proto-crust was produced through voluminous melting of a primitive asthenospheric source, possibly including zones enriched in recycled felsic crust. This process resulted in an oceanic-type plateau around 35 km thick, of dominantly enriched basalt as well as low-Al TTG bodies produced within areas of extensive basaltic under- and intraplating. Evidence from xenocrystic and detrital zircons, and from Sm-Nd isotopic data indicates a long history of early crustal development, back to ca. 4.3 Ga (Van Kranendonk et al., 2009; Tessalina et al., 2010).

Continued melting of upwelling mantle between 3.5-3.42 Ga resulted in massive eruption and intraplating of komatiite, komatiitic basalt, and tholeiitic basalts, building a crust ≥50 km thick (Champion & Smithies, 2007; Van Kranendonk et al., 2007). Large tholeiitic magma chambers fractionated and were contaminated by older felsic crust, resulting in calc-alkaline intermediate to felsic volcanics. Continued addition of mantle heat resulted in widespread high and low-pressure melting of older enriched basalt and earlier formed TTG to produce large volumes of TTG. Early on, accumulation of voluminous buoyant residues from mantle (plume?) melting may have been hindered by the sinking of eclogitic residues complementary to extensive TTG formation. As a result, eclogite was lost from this proto keel, although some may have been retained to catalyse the remelting processes that produced low-Ti basalts and ultimately led to the ultra-depletion of the SCLM keel (Smithies et al., 2005; Griffin & O'Reilly, 2007). Subsequent voluminous magmatism led to extreme melt depletion of the SCLM and development of a thick lithospheric keel.

Onset of PCO was initiated through extensive partial melting of mid-crustal TTG, at least partly in response to the build-up of radiogenic heat within the granites (Sandiford et al., 2004). In BGB, this resulted in felsic volcanism, crustal extension and deposition of the Fig Tree Group. Cold greenstone fingers dripped down from

the base of the succession into partially melted granitic mid-crust, resulting in high-P, but relatively low-T, metamorphism of greenstones and the diapiric rise of granitic domes. Subsequent, more extensive partial melting facilitated wholescale sinking of greenstones by 3230 Ma. Greenstone sinking was facilitated across extensional detachments, with strain concentrated along the greenschist/amphibolite-facies transition, resulting in exhumation of deeper-level granitic rocks on greenstone belt margins. Uplift of granitic rocks was accompanied by erosion and unconformable deposition of the Moodies Group during contractional deformation driven by shortening across the sinking greenstone belt.

Subduction zone collages

The North Atlantic Craton (NAC) represents the type example of a high-grade gneiss terrain, consisting of a sea of tonalitic gneisses with sparely distributed, generally highly dismembered, panels of greenstones and layered anorthosite-gabbro intrusions (Bridgwater et al., 1974; Myers, 1984; Windley & Garde, 2009). Detailed mapping and geochronology has shown that the apparently monotonous high-grade gneisses are derived from several distinct tectonostratigraphic terranes, ranging from Eo- to Neoarchean in age and assembled during at least two main tectonic episodes in the Paleo- and Neoarchean (Nutman et al., 1989, 2002, 2009).

A key feature of the NAC is the recognition of lithotectonic terranes, each with distinct early crustal histories and some also with distinct metamorphic grade and supracrustal assemblages (Nutman et al., 1989, 2002; Windley & Garde, 2009). Significantly, these terranes are separated by thin mylonite zones that, together with the terranes themselves, have been affected by recumbent isoclinal folds and later upright folds associated with Neoarchean terrane accretion: even the best preserved and largest panel of supracrustal rocks at Isua consists of two lithologically and geochronologically distinct packages, intruded by TTG of different age, and separated by a thin zone of highly strained metasedimentary rocks (Nutman et al., 2002, 2009). Another key feature is the huge volumes of TTG crust that is universally agreed to have formed from melting of basalt at lower crustal, to subcrustal depths, probably within shallow subduction zones (Drummond and Defant, 1990). These TTG were emplaced into supracrustal rocks during thrusting and large-scale recumbent isoclinal folding that predated and accompanied episodes of terrane accretion (Myers, 1984; Nutman et al., 1989). A third key feature is the boninitic geochemical signature of pillowed metabasalts at Isua, which suggest formation in an intra-oceanic arc setting (Polat et al., 2002). Combined, these data provide key indications of subduction zone processes in the formation of the North Atlantic Craton during at least two accretionary events in the Paleo- and Neoarchean. Significantly, all crust older than c. 3.5 Ga consists of HGTs, and it is quite likely that the subduction-accretion mechanism identified for the NAC was responsible for the formation of all these pieces of ancient crust.

Tectonics on Early Earth

As with modern Earth, Paleoarchean Earth formed continental crust over zones of upwelling mantle and zones of downwelling oceanic lithosphere, albeit with differences in overall composition and tectonic style from modern counterparts.

Acknowledgements

Lengthy discussions with Hugh Smithies, Allen Nutman, John Myers and Alf Kröner helped stimulate my interest in this topic. This paper is published with permission of the Executive Director, Geological Survey of Western Australia.

References

Barley M.E., 1993, Volcanic, sedimentary and tectonostratigraphic environments of the ~3.46 Ga Warrawoona Megasequence: a review, Precambrian Research, 60, 47–67.

Bickle M.J., Morant P., Bettenay L.F., Boulter C.A., Blake T.S. & Groves D.I., 1985, Archaean tectonics of the Shaw Batholith, Pilbara Block, Western Australia: structural and metamorphic tests of the batholith concept, in *Evolution of Archean Supracrustal Sequences*, Ayers L.D., Thurston P.C., Card K.D. & Weber W., eds, Geological Association of Canada, Special Paper 28, 325–341.

Bridgwater D., McGregor V.R. & Myers J.S., 1974, A horizontal tectonic regime in the Archaean of Greenland and its implications for early crustal thickening, Precambrian Research, 1, 179–197.

Champion D.C. & Smithies R.H., 2007, Geochemistry of Paleoarchean granites of the East Pilbara Terrane, Pilbara Craton, Western Australia: implications for early Archean crustal growth, in *Earth's Oldest Rocks*, Van Kranendonk M.J., Smithies R.H. & Bennet V. eds, Elsevier, Amsterdam, 369–409.

Cloete M., 1993, Burial metamorphism in the 3.47 Ga Barberton Greenstone Belt, South Africa, in *Low temperature metamorphism: Processes, Products and economic significance*, Vergara M. & Klem U. eds, Department of Geology, University of Santiago, Chile, 1–7.

Collins W.J., Van Kranendonk M.J. & Teyssier C., 1998, Partial convective overturn of Archaean crust in the east Pilbara Craton, Western Australia: Driving mechanisms and tectonic implications, Journal of Structural Geology, 20, 1405–1424.

de Ronde C.E.J. & Kamo S.L., 2000, An Archaean arc-arc collisional event: a short-lived (ca 3 Myr) episode, Weltvereden area, Barberton greenstone belt, South Africa, Journal of African Earth Sciences, 30, 219–248.

de Wit M.J., Hart R.A. & Hart R.J., 1987, The Jamestown Ophiolite Complex, Barberton Mountain Belt: a section through 3.5 Ga oceanic crust, Journal of African Earth Sciences, 5, 681–730.

de Wit M.J., Roering C., Hart R.J., Armstrong R.A., de Ronde C.E.J., Green R.W.E., Tredoux M., Peberdy E. & Hart R.A., 1992, Formation of an Archaean continent, Nature, 357, 553–562.

Drummond M.S. & Defant M.J., 1990, A model for trondhjemite-tonalite- dacite genesis and crustal growth via slab melting: Archean to modern comparisons, Journal of Geophysical Research, 95, 21503–21521.

Griffin W.L. & O'Reilly S.Y., 2007, Cratonic lithospheric mantle: Is anything subducted? Episodes, 1, 43–53.

Helmstaedt H. & Gurney J.J., 1995, Geotectonic controls of primary diamond deposits: implications for area selection, Journal of Geochemical Exploration, 53, 125–144.

Herzberg C., Asimow P.D., Arndt N., Niu Y., Lesher C.M., Fitton J.G., Cheadle M.J. & Saunders A.D., 2007, Temperatures in ambient mantle and plumes: constraints from basalts, picrites, and komatiites, Geochemistry, Geophysics, Geosystems, 8, 1–34.

Kisters A.F.M. & Anhaeusser C.R., 1995, Emplacement features of Archaean TTG plutons along the southern margin of the Barberton greenstone belt, South Africa, Precambrian Research, 75, 1–15.

Lowe D.R. & Byerly G.R., 2007, An overview of the geology of the Barberton greenstone belt and vicinity: Implications for early crustal development, in *Earth's Oldest Rocks*, Van Kranendonk M.J., Smithies R.H., Bennet V., eds, Elsevier, Amsterdam, 481–526.

Moyen J-F., Stevens G. & Kisters A.F.M., 2006, Record of mid-Archaean subduction from metamorphism in the Barberton terrain, South Africa, Nature, 442, 559–562.

Myers J.S., 1984, Archean tectonics in the Fiskenaesset region of southwest Greenland, in *Precambrian Tectonics Illustrated*, Kröner A. & Greiling R., eds, E. Schweizerbart'sche Verlagsbuchhandlund, Germany, 95–112.

Nutman A.P., Friend C.R.L., Baadsgaard H. & McGregor V.R., 1989, Evolution and assembly of Archean gneiss terranes in the Godthåbsfjord region, southern west Greenland: structural, metamorphic, and isotopic evidence, Tectonics, 8, 573–589.

Nutman A.P., Friend C.R.L. & Bennett V.C., 2002, Evidence for 3650-3600 Ma assembly of the northern end of the Itsaq Gneiss Complex, Greenland: Implication for early Archaean tectonics, Tectonics 21, 10.1029/2000TC001203.

Nutman A.P., Friend C.R.L. & Paxton S., 2009, Detrital zircon sedimentary provenance ages for the Eoarchean Isua Supracrustal Belt southern West Greenland: Juxtaposition of an imbricated ca. 3700 Ma juvenile arc against an older complex with 3920-3760 Ma components, Precambrian Research, 172, 212–233.

Polat A., Hofmann A.W. & Rosing M.T., 2002, Boninite-like volcanic rocks in the 3.7-3.8 Ga Isua greenstone belt, West Greenland: geochemical evidence for intra-oceanic subduction zone processes in the early Earth, Chemical Geology, 184, 231–254.

Sandiford M., Van Kranendonk M.J. & Bodorkos S., 2004, Conductive incubation and the origin of dome-and-keel structure in Archean granite-greenstone terrains: a model based on the eastern Pilbara Craton, Western Australia, Tectonics 23, DOI: 10.1029/2002TC001452.

Smithies R.H., Van Kranendonk M.J. & Champion D.C., 2005, It started with a plume – early Archaean basaltic proto–continental crust, Earth and Planetary Science Letters, 238, 284–297.

Smithies R.H., Champion D.C. & Van Kranendonk M.J., 2007, The oldest well-preserved volcanic rocks on Earth: geochemical clues to the early evolution of the Pilbara Supergroup and implications for the growth of a Paleoarchean continent, in *Earth's Oldest Rocks*, Van Kranendonk M.J., Smithies R.H. & Bennet V. eds, Elsevier, Amsterdam, 339–367.

Smithies R.H., Champion D.C. & Van Kranendonk M.J., 2009, Formation of Paleoarchean continental crust through infracrustal melting of enriched basalt, Earth and Planetary Science Letters, 281, 298–306.

Tessalina S.G., Bourdon B., Van Kranendonk M. & Philippot, P., 2010, 147Sm-143Nd and Nb-Th-U evidence for Hadean mafic crust in the Pilbara Craton, Western Australia, Nature Geoscience, 3, 214–217.

Van Kranendonk M.J., Hickman A.H., Smithies R.H., Nelson D.N. & Pike G., 2002, Geology and tectonic evolution of the Archaean North Pilbara terrain, Pilbara Craton, Western Australia, Economic Geology, 97, 695–732.

Van Kranendonk M.J., Collins W.J., Hickman A.H. & Pawley M.J., 2004, Critical tests of vertical vs horizontal tectonic models for the Archaean East Pilbara Granite-Greenstone Terrane, Pilbara Craton, Western Australia, Precambrian Research, 131, 173–211.

Van Kranendonk M.J., Hickman A. & Smithies R.H., 2007, The East Pilbara Terrane of the Pilbara Craton, Western Australia: Formation of a continental nucleus through repeated mantle plume magmatism, in *Earth's Oldest Rocks*, Van Kranendonk M.J., Smithies R.H. & Bennet V., eds, Elsevier, Amsterdam, 307–337.

Van Kranendonk M.J., Kröner A., Hegner E. & Connelly J., 2009, Age, lithology and structural evolution of the c. 3.53 Ga Theespruit Formation in the Tjakastad area, southwestern Barberton Greenstone Belt, South Africa, with implications for Archean tectonics, Chemical Geology, 261, 114–138.

Wilson, A.H., Shirey, S.B. & Carlson, R.W., 2003, Archaean ultra-depleted komatiites formed by hydrous melting of cratonic mantle, Nature, 423, 858–861.

Windley B.F. & Garde A., 2009. Arc-generated blocks with crustal sections in the North Atlantic Craton of West Greenland: Crustal growth in the Archean with modern analogues, Earth-Science Reviews, 93, 1–30.

Zegers T.E., Nelson D.R., Wijbrans J.R. & White S.H., 2001, SHRIMP U-Pb zircon dating of Archean core complex formation and pancratonic strike-slip deformation in the East Pilbara Granite-Greenstone Terrain, Tectonics, 20, 883–908.

TECTONIC IMPLICATIONS OF RECENT ADVANCES IN YILGARN STRATIGRAPHY

S. Wyche

Geological Survey of Western Australia, 100 Plain St, East Perth, WA, 6004, Australia

Introduction

Local and regional stratigraphies described in the first-generation 1:250,000-scale geological mapping in the Yilgarn Craton were based mainly on mapped outcrop distribution. However, much of the geology is poorly exposed and deeply weathered, and so field relationships are difficult to establish in many places. The second generation of field mapping, at 1:100,000 scale, has been able to take advantage of an accumulating dataset, acquired partly through government- and industry-sponsored research projects, that includes geophysical data such as aeromagnetics, gravity, radiometrics, deep-crustal seismic reflection, and magnetotellurics; precise SHRIMP geochronology; spectral data; and high-quality geochemical and isotope data. These new data have provided the basis for the first craton-wide syntheses of stratigraphy and magmatic evolution.

Based on the new mapping, Cassidy et al. (2006) subdivided the Yilgarn Craton into six terranes, the easternmost three of which constituted the Eastern Goldfields Superterrane. Subsequent revision has further subdivided the Eastern Goldfields Superterrane (Fig. 1; Pawley et al. 2009). The Narryer and South West Terranes in the west of the craton are dominated by granite and granitic gneiss with minor supracrustal greenstones, whereas the Youanmi Terrane and the Eastern Goldfields Superterrane contain substantial greenstone belts separated by granite and granitic gneiss. The Ida Fault, which marks the boundary between the western Yilgarn Craton and the Eastern Goldfields Superterrane, is a major structure that extends to the base of the crust (Swager et al. 1997).

Oldest Yilgarn

Evidence of very old crust-forming events is widespread in the Yilgarn Craton. Detrital zircon populations at Jack Hills and Mount Narryer in the Narryer Terrane (Crowley et al. 2005), and the Maynard Hills in the Youanmi Terrane (Wyche 2007), include zircons older than 4000 Ma that pre-date any known rocks on Earth. The character and chemistry of the detrital zircons at Jack Hills and Mount Narryer suggest that they are derived from a range of early-formed crust types including granite and intermediate rocks, and may show evidence of early hydration (Cavosie et al. 2007). The oldest rocks identified in the Yilgarn Craton are c. 3730 Ma migmatitic gneiss and layered mafic rocks, also in the Narryer Terrane (Kinny & Nutman 1996).

Other evidence of early Yilgarn crust includes common >3000 Ma xenocrystic zircons in various rock types across the craton (e.g. Hill et al. 1989). Also, Sm–Nd (Champion & Cassidy 2007) and Lu–Hf isotope data show evidence of at least two early stages of mantle extraction in the Youanmi Terrane, at c. 4200 Ma and c. 3800 Ma. This is followed by a more complex, craton-wide history after c. 3200 Ma.

Yilgarn greenstone successions

Oldest Yilgarn supracrustal rocks

The supracrustal rock record in the Yilgarn Craton dates back to c. 3000 Ma. Preserved greenstone successions contain >2900 Ma mafic and felsic volcanic rocks in both the western part of the craton at Golden Grove (Wang et al. 1998) and Mount Gibson (Yeats et al. 1996) where they are associated with VMS-style mineralization, and in the Burtville Terrane in the northeastern part of the craton (Pawley et al. 2010). There are no regional-scale studies of these rocks that allow them to be put into a tectonic context.

c. 2820 Ma – c. 2735 Ma

Greenstone successions in the Yilgarn Craton are dominated by rocks that formed after c. 2820 Ma. Recent Lu–Hf isotope data indicate craton-wide magmatism beginning at c. 2820 Ma that involved both the development of juvenile crust, and the reworking of older crust.

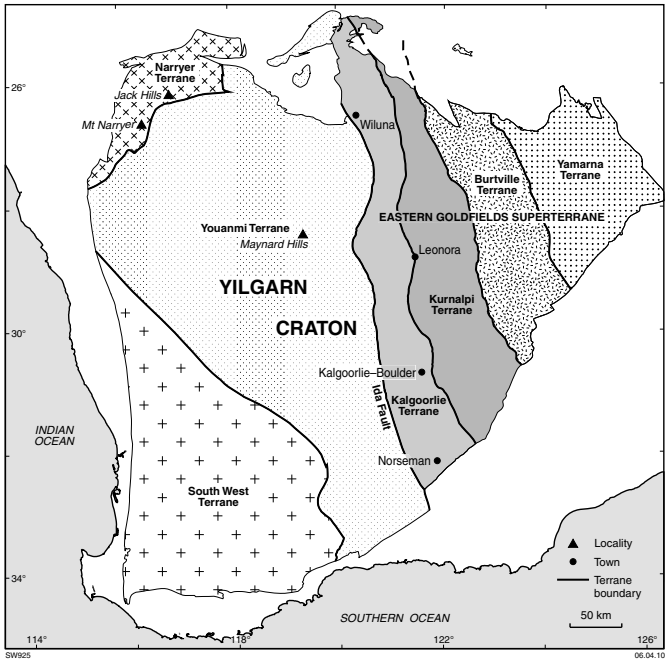

Figure 1. Tectonic subdivision of the Yilgarn Craton showing towns and localities referred to in the text, modified after Cassidy et al. (2006)

Consistent with new Lu–Hf data, recent mapping in the northwestern Youanmi Terrane has demonstrated the existence of several cycles of mafic to felsic volcanism, with the first cycle beginning c. 2820 Ma. Mafic–ultramafic magmatism, likely due to a major plume event, produced large layered intrusions between c. 2820

Ma and c. 2800 Ma (Van Kranendonk & Ivanic 2009), coinciding with similar magmatism in other parts of the craton at this time (Pawley et al. 2010; Riganti et al. 2010). This was followed by a protracted cycle of mafic to calc-alkaline volcanism and associated sedimentary rocks in the northwestern Youanmi Terrane, from c. 2800 Ma until c. 2735 Ma. Calc-alkaline magmatism was dominant after c. 2760 Ma, and broadly coincided with a period of mafic TTG and high-HFSE granite magmatism (Van Kranendonk & Ivanic 2009). Lu–Hf data show that this was a period of crustal recycling, with a prominent c. 2750 Ma peak of very old crust. A similar cycle has been recognized in the Burtville Terrane, with calc-alkaline volcanism prominent at c. 2770 Ma (Pawley et al. 2010). There is also evidence of a significant episode of mafic magmatism at c. 2735 Ma in the eastern Youanmi Terrane, and at c. 2755 Ma and c. 2735 Ma in the eastern part of the Eastern Goldfields Superterrane (Pawley et al. 2010).

c. 2720 Ma – c. 2640 Ma

The youngest identified volcanic cycle in the northwest Yilgarn, between c. 2720 Ma and c. 2700 Ma (Van Kranendonk & Ivanic 2009), broadly coincided with calc-alkaline volcanism in the Kurnalpi Terrane of the Eastern Goldfields Superterrane. The calc-alkaline volcanic centres in the Kurnalpi Terrane, interpreted by Barley et al. (2008) as intra-arc volcanic complexes outboard to the east of a westward-dipping subduction zone, partly overlap in age, and are locally intercalated with, komatiites in the western part of the Eastern Goldfields Superterrane. These komatiites are preserved in a distinct north-northwesterly trending belt, about 600 km long and up to 100 km wide, between Norseman and Wiluna. Their age is well constrained between c. 2710 Ma and c. 2700 Ma (Kositcin et al. 2008). They commonly show evidence of contamination by older crust, and are locally intrusive into, and probably coeval with, felsic volcanic rocks. The Norseman–Wiluna komatiites are not only younger than those in the Youanmi Terrane, but also differ in character in that komatiites of the Youanmi Terrane include both Al-depleted and Al-undepleted varieties, whereas those in the Norseman–Wiluna successions are exclusively Al-undepleted (Barnes 2006).

Between c. 2692 Ma and c. 2680 Ma, volcanic centres in the central-western part of the Kurnalpi Terrane deposited bimodal (basalt–rhyolite) and calc-alkaline intermediate–silicic volcanic and associated intrusive and sedimentary rocks. Barley et al. (2008) interpreted these 'Gindalbie' successions as representing an arc-rift environment. Gindalbie-style volcanism overlapped with, and was succeeded by, TTG volcanism and associated sedimentary rocks and mafic intrusions represented by the Black Flag Group in the Kalgoorlie Terrane. The deposition of the Black Flag Group between c. 2690 Ma and c. 2660 Ma coincided with voluminous high-Ca TTG granite magmatism in the Eastern Goldfields Superterrane (Champion & Cassidy 2007). Krapež & Hand (2008) interpret the Black Flag Group (their Kalgoorlie Sequence) as representing a strike-slip intra-arc basin. Felsic volcanic and associated plutonic rocks with TTG affinities of this age have also been recorded in a poorly exposed bimodal greenstone succession in the Yamarna Terrane in the far east of the Eastern Goldfields Superterrane. Limited SHRIMP geochronology indicates that they range in age between c. 2683 Ma and c. 2658 Ma (Pawley et al. 2010).

The youngest supracrustal rocks in the Yilgarn Craton are the so-called 'late-stage basins' in the Eastern Goldfields Superterrane that rest unconformably on all earlier greenstone successions. Likely deposited in a very short time (c. 10 m.y.) after c. 2665 Ma, they preserve fluvial and deep-marine facies that Krapež & Barley (2008) interpret as deposits formed in a tectonic-escape corridor after arc closure. Blewett & Czarnota (2007) interpret the basins as forming during extension associated with granite doming.

Conclusions

While the very early tectonic history of the Yilgarn Craton remains largely unresolved, recent mapping, combined with interpretation of new geophysical, geochemical, geochronological, and spectral datasets, has resulted in stratigraphic interpretations that give new insights into the later history of the craton. A major thermal event after c. 2820 Ma is consistent with the development of a craton-scale mantle plume. The consequences of this event are seen in the rock record for the next 70 m.y. or so, with mafic–felsic greenstone cycles in the western and far eastern part of the craton involving substantial recycling of older crustal material at various times. An arc-like greenstone succession in the Eastern Goldfields, after c. 2720 Ma, is punctuated by a major, discrete episode of komatiite magmatism at c. 2705 Ma.

Acknowledgements

This contribution is published with the permission of the Executive Director, Geological Survey of Western Australia.

References

Barley M.E., Brown S.J.A., Krapež B. & Kositcin N., 2008, Physical volcanology and geochemistry of a Late Archaean volcanic arc: Kurnalpi and Gindalbie Terranes, Eastern Goldfields Superterrane, Western Australia, Precambrian Research, 46, 53–76.

Barnes S.J., 2006, ed., *Nickel deposits of the Yilgarn Craton: geology, geochemistry, and geophysics applied to exploration*, Society of Economic Geologists, Special Publication 13.

Blewett R. & Czarnota K., 2007, An new integrated tectonic framework for the Eastern Goldfields Superterrane, in *Proceedings of Geoconferences (WA) Inc. Kalgoorlie '07 Conference*, Bierlein F.P. & Knox-Robinson C.M., eds, Geoscience Australia, Record 2007/14, 8-13.

Cassidy K.F., Champion D.C., Krapež B., Barley M.E., Brown S.J.A., Blewett R.S., Groenewald P.B. & Tyler, I.M., 2006, A revised geological framework for the Yilgarn Craton, Western Australia, Geological Survey of Western Australia, Record 2006/8.

Champion D.C. & Cassidy K.C., 2007, An overview of the Yilgarn Craton and its crustal evolution, in *Proceedings of Geoconferences (WA) Inc. Kalgoorlie '07 Conference*, Bierlein F.P. & Knox-Robinson C.M., eds, Geoscience Australia, Record 2007/14, 8–13.

Cavosie A.J., Valley J.W. & Wilde S.A., 2007, The oldest terrestrial mineral record: a review of 4400 Ma to 4000 Ma detrital zircons from Jack Hills, Western Australia, in *Earth's Oldest Rocks*, Van Kranendonk M.J., Smithies R.H. & Bennett V.C., eds, Developments in Precambrian Geology, 15, Elsevier, 91–111.

Crowley J.L., Myers J.S., Sylvester, P.J. & Cox R.A., 2005, Detrital zircon from the Jack Hills and Mount Narryer, Western Australia: evidence for diverse >4.0 Ga source rocks, Journal of Geology, 11, 239-263.

Hill R.I., Campbell I.H. & Compston W., 1989, Age and origin of granitic rocks in the Kalgoorlie–Norseman region of Western Australia — Implications for the origin of Archaean crust, Geochimica et Cosmochimica Acta, 53, 1259–1275.

Kinny P.D. & Nutman A.P., 1996, Zirconology of the Meeberrie Gneiss, Yilgarn Craton, Western Australia: an early Archaean migmatite, Precambrian Research, 78, 165–178.

Kositcin N., Brown S.J.A., Barley M.E., Krapež B., Cassidy K.F. & Champion D.C., 2008, SHRIMP U-Pb zircon age constraints on the Late Archaean tectonostratigraphic architecture of the Eastern Goldfields Superterrane, Yilgarn Craton, Western Australia, Precambrian Res. 161, 5–33.

Krapež B. & Barley M.E., 2008, Late Archaean synorogenic basins of the Eastern Goldfields Superterrane, Yilgarn Craton, Western Australia Part III. Signatures of tectonic escape in an arc-continent collision zone, Precambrian Research, 161, 183-199.

Krapež B. & Hand J.L., 2008, Late Archaean deep-marine volcaniclastic sedimentation in an arc-related basin: the Kalgoorlie Sequence of the Eastern Goldfields Superterrane, Yilgarn Craton, Western Australia, Precambrian Research, 161, 89–113.

Pawley M.J., Romano S.S., Hall C.E., Wyche S. & Wingate M.T.D., 2009, The Yamarna Shear Zone: a new terrane boundary in the northeastern Yilgarn Craton, Geological Survey of Western Australia, Annual Review 2007-08, 26-32.

Pawley M.J., Wyche S., Hall C.E., Romano S.S. , Doublier M.P., Wingate M.T.D. & Kirkland C.L, 2010, Episodic crustal growth in the northeast Yilgarn Craton, Western Australia: implications for craton evolution, ,this volume.

Riganti A., Wyche S., Wingate M.T.D., Kirkland C.L. & Chen S.F, 2010, constraints on ages of greenstone magmatism in the northern part of the Southern Cross Domain, Yilgarn Craton, this volume.

Swager C.P., Goleby B.R., Drummond B.J., Rattenbury M.S. & Williams P.R., 1997, Crustal structure of granite–greenstone terranes in the Eastern Goldfields, Yilgarn Craton, as revealed by seismic profiling, Precambrian Research, 83, 43–56.

Van Kranedonk M.J. & Ivanic T.J. 2009, A new lithostratigraphic scheme for the northeastern Murchison Domain, Yilgarn Craton, Geological Survey of Western Australia, Annual Review 2007-08, 34–53.

Wang Q., Schiøtte L. & Campbell I.H., 1998, Geochronology of supracrustal rocks from the Golden Grove area, Murchison Province, Yilgarn Craton, Western Australia, Australian Journal of Earth Sciences, 45, 571–577.

Wyche S., 2007, Evidence of pre-3100 Ma crust in the Youanmi and South West Terranes, and the Eastern Goldfields Superterrane, of the Yilgarn Craton, in *Earth's Oldest Rocks*, Van Kranendonk M.J., Smithies R.H. & Bennett V.C., eds, Developments in Precambrian Geology, 15, Elsevier, 113-123.

Yeats, C.J., McNaughton, N.J. and Groves, D.I., 1996, SHRIMP U-Pb geochronological constraints on Archean volcanic-hosted massive sulfide and lode gold mineralization at Mount Gibson, Yilgarn Craton, Western Australia, Economic Geology, 91, 1354-1371.

THEME 2

DIVERSITY IN TECTONIC REGIMES

ORAL & POSTER ABSTRACTS

THE MURCHISON GREENSTONE BELT, SOUTH AFRICA: ACCRETED SLIVERS WITH CONTRASTING METAMORPHIC CONDITIONS

S. Block[1,3] & J-F. Moyen[2,3]

[1] ENS Lyon, 46 Allée d'Italie 69007 Lyon France
[2] Department of Geology, University of Stellenbosch, South Africa
[3]Now at Université Jean Monnet, Laboratoire Magmas et Volcans, Département de Géologie, 23 rue du Docteur Paul Michelon 42023 Saint-Étienne, France and CNRS, UMR6524, LMV, F-63038 Clermont-Ferrand, France

Metamorphism provides key information to unravel tectonic histories, and is commonly used to constrain the evolution of orogenic domains in the Proterozoic and Phanerozoic. However, it has been comparatively underused in the study of Archaean terranes, and only a few studies (Stevens & Moyen 2007) present comprehensive descriptions of structural and metamorphic histories of Archaean domains. This study presents the results of reconnaissance work on the Mesoarchaean Murchison Greenstone belt, South Africa.

Regional geology:

The Murchison Greenstone Belt (MGB) is a 3.09–2.97 Ga old volcano-sedimentary belt (Poujol et al., 1996) situated in the northern part of the Archaean Kaapvaal craton of South Africa. It is an isoclinally folded sequence, striking ENE and elongated for 140km. From north to south, it is formed of the following units:

- The Silwana amphibolites, occurring as a 0.1 to 1.5 km wide band only in the Eastern half of the MGB.
- The Rubbervale formation, a unit of schists derived from felsic volcanoclastics, up to 10 km wide throughout the belt.
- The main domain, that comprises mostly mafic and ultramafic metamorphic volcano-sedimentary lithologies, 10-15 km wide;
- The La France Domain, a 2-3 km wide sliver of aluminous schists and quartzites in the central portion of the MGB.

To the North, the belt is in tectonic contact with amphibolite-facies basement gneisses, containing Hbl-pg-ep-cpx amphibolite pods. The southern limit of the belt corresponds to the intrusive contact of the Ms-Bt granites of the Lekkersmaak suite (Jaguin et al., this volume) (Fig. 1).

Structures

The structures of the belt are briefly summarized here. The main fabric of the belt is a regional sub-vertical to steeply north-dipping cleavage that carries a steep easterly plunging stretching lineation. The sense of shear is always sinistral/top to the south, corresponding to a transpressive, sinistral dominant setting throughout the belt.

To the north, high strain, sinistral transpressive shear zone bounds the belt, which is in tectonic contact with the northern granitoid basement. A major transpressive sinistral fault, the Letaba shear zone, consistent with the top to the south structural features of the northern MGB, brings the locally garnet-bearing Silwana amphibolites against low grade ultramafic and mafic greenschists of the core of the belt. Within the belt, a local high strain mineralised zone, known as the antimony line, also displays top to the South structural features. The La France formation is separated by a fault zone from the rest of the belt (although the outcrop is poor in this region). The Southern contact of the belt is intrusive, and the metasediments of the La France formation are intruded by Bt-Ms leucogranites of the AGE Lekkersmaak suite (Jaguin et al. this volume, Vearncombe 1992, Poujol et al. 2001).

Metamorphic assemblages and P—T conditions

A reconnaissance study of the belt has identified the following metamorphic units, which are currently studied in greater details:

The Silwana amphibolites

The Silwana amphibolites are hornblende-plagioclase-epidote amphibolites, locally garnet-bearing in favourable (Al and Fe rich) lithological bands typically 10 cm thick. They display layered modal variations that may represent metamorphically transformed primary mineral layering. The isogranular texture suggests a high temperature recrystallisation, although the absence of melting puts an approximate upper limit for temperature at around 750°C. Similar amphibolites were studied in the Barberton Greenstone Belt, to the South of the MGB, where P–T quantifications yielded pressures of over 8 kbar (Moyen et al. 2006; Stevens et al. this volume).

The main domain

The main body of the belt is made of a variety of low grade, greenschist facies, mafic and ultramafic metamorphic rocks. The most representative lithologies are chlorite schists, talc-chlorite schists, and chlorite-muscovite-actinolite schists, with variable amounts of carbonates and quartz. Carbonate schists containing chlorite, fuchsite, muscovite and talc are also common throughout the belt. All of this corresponds to greenschist facies assemblages. Some quartz-rich aluminous lithologies, which form prominent ridges corresponding to folds in the vicinity of the Antimony line, show staurolite, suggesting that portions of the main domain may have reached slightly higher, upper-greenschist to lower-amphibolite metamorphic conditions. Pressures between 4 and 5 kb, and temperatures up to 400°C are plausible

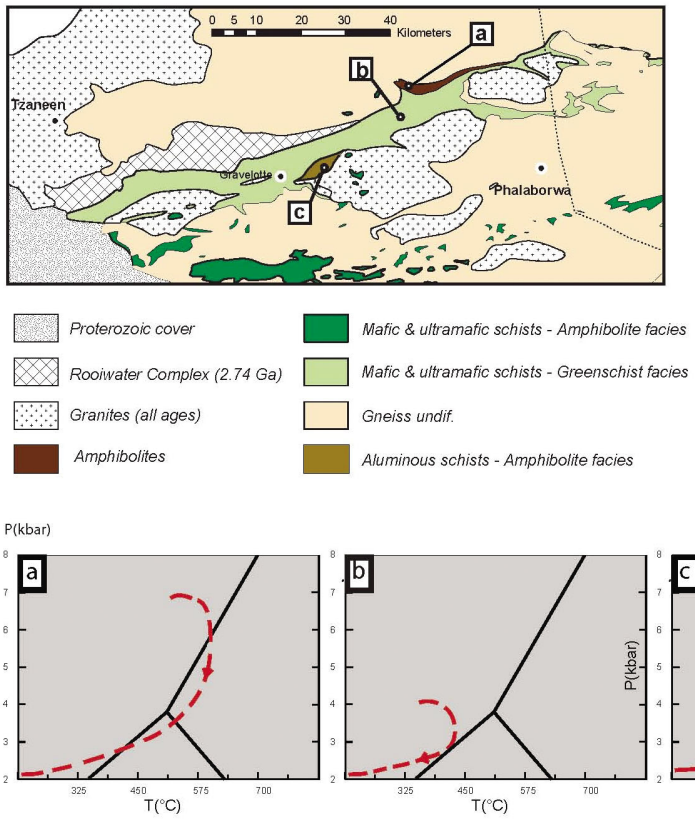

Figure 1. Simplified geological map of the Murchison Greenstone Belt. Approximate PT paths followed by the MGB units inferred from observed mineral assemblages (dashed lines) and preliminary results (full line).

estimates for these rocks; the metamorphic conditions in this domain may be somewhat variable, possibly owing to post-peak metamorphic continued deformation.

The La France Domain

The La France Domain is a small unit made of quartzites and aluminous schists. The aluminous schists display a biotite-chlorite-muscovite-quartz metamorphic banding. The generalised occurrence of biotite distinguishes the La France aluminous schists from other lithologies of the MGB. The schists are also kyanite-, staurolite- or garnet-bearing in a few localities, although the three minerals do not occur together in the same sample: the rocks are either st (locally st-garnet) or ky (locally ky-grt) schists. These minerals all occur in two distinct habits. Kyanite occurs either as needles parallel to the metamorphic fabric, or as protruding minerals overgrowing the banding. Staurolite can be found as euhedral crystals overgrowing the banding or as deformed, sigma-shaped minerals. A first generation of garnet overgrows the metamorphic fabric, while a second generation rims the former one. A second generation of biotite, as well as tourmaline, are occasionally observed to overgrow the banding. Finally, retrograde assemblage (especially around ky and st) are ms- and bi-bearing.

Therefore, three successive assemblages are present in the La France schists (Table 1).

So far, only the PT conditions of samples presenting the kyanite-staurolite assemblage were quantified. Pseudosections were built using the program Perplex (Conolly et al.), using the mineral thermodynamic models of Powell & Holland 2002 for most minerals, and van Hinsberg for Trm. We estimated the PT conditions by extracting isopleths for the composition of key minerals and comparing with analysed values. An imprecise value of P = 5-8 kbar and T = 540°C +- 30 was obtained for the peak M_2 assemblage.

The succession of the three assemblages, especially the fact that M_1 is, at least locally, chl-ky before reaching the garnet field, suggest a clockwise P–T loop, with burial before heating to the peak and near isothermal exhumation.

Discussion

Regional vs. Contact metamorphism

The Murchison Schist Belt displays two small, amphibolite facies, outer domains juxtaposed on either side of a large, greenschist facies, central domain (figure). Such a disposition is common in Archaean greenstone belts, and is typically explained as contact metamorphism related to the emplacement of the nearby plutons. However, our preliminary results rule out this hypothesis: (1) the difference between the core and the edge is not only one of temperature, but also of pressure; (2) the apparent geotherms are lower (higher P for lower T) in the outside domains than in the main body of the belt; in particular, the Ky-Gt-St assemblage of the La France aluminous schists is inconsistent with contact metamorphism induced by the intrusion of the Lekkersmaak suite pluton (sillimanite and/or cordierite bearing assemblages would be more likely). (3) in places, the plutons intrude greenschist-facies portions of the MGB, without any contact metamorphism. (4) The contacts between different metamorphic "grades" are typically sharp and not progressive, with gently changing conditions from the rim to the interior of the belt; (5)

Table 1. Three successive assemblages in La France Schists.

Assemblage	Minerals	Note
M_1	Bi_1-q-ms_1-chl-st_1 Bi_1-q-ms_1-chl-ky_1	Forms the metamorphic fabric; pre to syn-tectonic
M_2	St_2-ky_2+-grt_1 (core)+-bi_2+-trm	Large crystals, overgrowing the fabric
M_3	Ms_2-grt_2-bi_3(rim)	Retrograde

the metamorphic minerals commonly form a prominent fabric in the rock and do not suggest static heating. Therefore, the metamorphism of the MGB is more likely related to regional tectono-metamorphic events.

A stack of contrasted units

Our study shows that the MGB is made of different metamorphic units with distinct peak PT conditions. The contacts between the units are sharp. A clear transpressive sinistral shear zone brings the Silwana amphibolites against the greenstones of the main domain to the North of the MGB, and it corresponds to a metamorphic break of up to 4–5 kbar, across a less than 100 m wide contact zone. The contact between the La France domain and the main domain is obscured, but demonstrably occurs through a mineralized crushed zone (where the disused La France gold mine was once located) less than 200 m wide, without any progressive change of metamorphic conditions either side of the tectonic zone; rather, the at least 200 °C and 2–4 kbar break occurs all in 200 m. Thus, we infer that a major fault separates the La France Domain from the main domain of the MGB. The MGB therefore appears to have been formed by tectonic accretion and stacking of contrasted units metamorphosed at different crustal levels, in a globally transpressive sinistral tectonic environment.

Tectonic processes

The MGB is bounded to the South by peraluminous granites of the Lekkersmaak suite (Jaguin et al., this volume). Such peraluminous granites have a metapelite protolith, similar in composition to the La France Domain schists. It is therefore tempting to propose that the stacking demonstrated here operated on a crustal level, with metasediments similar to these of the La France domain being buried deep enough to permit melting and formation of the Lekkersmaak granitoids. In the modern Earth, such a process would be typical of collisional plate boundaries.

On the other hand, the pressures recorded in the MGB are not extremely high; a clear oceanic suture is missing; and the tectonic regime is a sinistral transpression, rather than thrusting on shallow-dipping planes.

The tectonic regime that formed the Murchison Schist Belt therefore appears to be intermediate between two conceptual "end members". There are no evidence to support a thrust belt model where nappe tectonics juxtapose and stack together crustal scales metamorphosed along HP, LT gradients. But the MGB cannot be represented as a homogeneously warm and ductile crust that systematically accommodated shortening by strike-slip faults. The probable mechanism accounting for the formation of the MGB lies somewhere in the middle. In a uniquely Archaean way, convergence would be accommodated by crustal transpression and moderate thickening and metamorphism.

References

Conolly J.A.D., 2005, Computation of phase equilibria by linear programming: a tool for geodynamic modeling and its application to subduction zone decarbonation, Earth and Planetary Science Letters, 236, 524–541.

Jaguin J., Moyen J.-F., Boulvais P. & Poujol M., 2010, Mid-Archaean granites South of the Murchison Greenstone Belt, South Africa : the earliest massive biotite-muscovite leucogranites, this volume.

Moyen J.-F., Stevens G. & Kisters A.F.M., 2006, Record of mid-Archaean subduction from metamorphism in the Barberton terrain, South Africa, Nature, 443, 559–562.

Poujol M., Robb, L.J., Respaut J.P. & Anhaeusse, C.R., 1996, 3.07–2.97 Ga greenstone belt formation in the northeastern Kaapvaal Craton: Implications for the origin of the Witwatersrand Basin, Economic Geology, 91, 1455–1461.

Poujol M. 2001, U-Pb isotopic evidence for episodic granitoid emplacement in the Murchison greenstone belt, South Africa, Journal of African Earth Sciences, 33, 155–163.

Powell R., Holland T.J.B. & Worley B., 1998,. Calculating phase diagrams involving solid solutions via non-linear equations, with examples using THERMOCALC, Journal of Metamorphic Geology, 16, 577–588.

Stevens G., Moyen J.-F. & Lana C., 2010, Paleoarchean subduction-zone metamorphism: Evidence from the Barberton greenstone belt, this volume.

van Hinsberg V. & Schumacher J., 2007, Intersector element partitioning in tourmaline: a potentially powerful single crystal thermometer, Contributions to Mineralogy and Petrology, 153, 289–301.

Vearncombe J.R., Barton J.M. Jr., Cheshire P.E., De Beer J.H., Stettler E.H. & Brandl G., 1992 Geology, geophysics and mineralization of the Murchison schist belt, Rooiwater complex and surrounding granitoids, Memoirs, Geological Survey of South Africa (now Council for Geosciences), 139.

PALEOARCHEAN TO NEOARCHEAN GRANITOIDS AND MIGMATITES DEFINING THE LAYERED CRUSTAL STRUCTURE OF VOLGO-URALIA

S.V. Bogdanova[1], B. De Waele[2], E.V. Bibikova[3], E.A. Belousova[4], A.V. Postnikov[5] & L.P. Popova[5]

[1]Department of Earth & Ecosystem Sciences, Lund University, Solvegatan 12, SE-22362 Lund, Sweden
[2] SRK Consulting, 10 Richardson Street, West Perth WA 6005
[3]Vernadsky Institute of Geochemistry and Analytical Chemistry, RAS, Kosygin street 19, 119991 Moscow, Russia
[4] GEMOC ARC National Key Centre, Department of Earth and Planetary Sciences, Macquarie University, Sydney NSW 2109, Australia
[5]Gubkin State University of Oil and Gas, Leninsky pr. 65, 117296 Moscow, Russia

Introduction

Volgo-Uralia is one of the three major crustal segments of the Precambrian East European Craton. It occupies its entire eastern third and is the least known because of a thick Neoproterozoic to Phanerozoic sedimentary cover. However, geophysical data and thousands of deep drillings into the crystalline basement of this high- potential oil and gas province provided valuable information on the crustal structure as well as rock relationships and abundances (Bogdanova, 1986; Muslimov & Lapinskaya, 1996). Volgo-Uralia is a high-grade terrain comprising both Archean and Paleoproterozoic rock belts bounded by zones of shearing. The recent seismic-reflection profile "TATSEIS" (Trofimov, 2006), has revealed an up to 60 km thick strongly stacked crust, in which a "transparent" layer forms upper part of the crystalline crust within the so-called "Bakaly granitoid block". The present study targeted the Bakaly granitoids and associated migmatites for which the U-Pb zircon ages, Lu-Hf isotopic characteristics of the dated zircons, and the rock Sm-Nd isotopic compositions and chemistries were determined. These demonstrate a multistage evolution and recycling of the Archean crust between 3.3 and 2.6 Ga, and a collisional origin of the up to 20 km thick upper crustal layer in Volgo-Uralia.

General

In Volgo-Uralia, granulite- and amphibolite-facies supracrustal and plutonic rocks make up a number of infracrustal belts that trend NE-SW to ENE-WSW. These belts are bounded by zones of strong thrusting and shearing, which also accommodate ca. 2.6 Ga gabbro-anorthositic to monzogranitic intrusions. Altogether, the crust is considered to have been formed mostly during a collisional event at ca. 2.7 Ga. Large Paleoproterozoic belts of metasedimentary and igneous origins surround the Neoarchean proto-craton of Volgo-Uralia and partly branch into its interiors. Seismic profiling and the presence of Paleoproterozoic supracrustal rocks, which werepervasively deformed, migmatized and metamorphosed at conditions up to the granulite facies between ca. 2.1 and 1.8 Ga ago, suggest that the crust and upper mantle consist of both Paleoproterozoic and strongly reworked Archaean rocks (Bogdanova et al. 2005). The Neoarchean shear zones appear to have been reactivated in the Paleoproterozoic. The latest deformation and metamorphic reworking occurred at ca. 1.8 Ga.

The Bakaly granitoids

The Bakaly granitoid complex forms a separate block in eastern Volgo-Uralia. It comprises various mostly plagioclase-rich granitoids, granitic gneisses and migmatites, previously considered to be Neoarchean on the basis of a few TIMS zircon ages (Bibikova et al., 1994). Together, the various granitoids constitute a separate geophysical domain marked by mosaics of mostly negative gravity and magnetic anomalies. As recorded by ca. 800 drillings, this pattern is created by small (70 to 200 km^2) granitic cupolas mostly consisting of K-rich adamellites and granites, and associated migmatites with narrow granodioritic rims. Four different granitoid suites are recognized in the Bakaly block, that also differ in age.

The 3.3-3.2 Ga Tashliar suite

A 3266±7 Ma old monzodiorite and a 3237±11 Ma old quartz-monzonitic mesosome in a migmatite with a leucosome vein aged 2710±19 Ma, contain zircons with $\varepsilon_{Hf}(T)$ values ranging between 0.1 and (-) 3.7, which correspond to Hf T(DM) crustal ages of ca. 3.5-3.8 Ga. Nd T(DM) dating of these rocks yielded similar 3.5-3.7 Ga ages for the protoliths. Together with the presence of a 3544-Ma zircon xenocryst in a Neoarchean Bakaly granitoid, this indicates that the crustal history of Volgo-Uralia began in Paleoarchean, possibly even in Eoarchean times. These oldest rocks of the Bakaly block are characterized by high abundances of TiO_2 (up to 0.8 %), P_2O_5 (up to 0.7%), Nb (up to 11 ppm), Y (18-27 ppm), Zr (290-450 ppm), and total REE up to 1000 ppm at $(La/Yb)_N$ ratios of up to 70, all suggesting their affinity to alkaline igneous series. The extent and tectonic setting of this igneous suite, which forms a separate tectonic block among the other granitoids, is difficult to assess, but it may have been intruded in association with a mantle upwelling event and wider spread.

The 2.72- 2.65 Ga Bakaly (Bak-1) and (Bak-2) suites

These two Neoarchean Bakaly suites, one comprising dominant quartz dioritic and tonalitic gneisses (Bak-1), and the other K-rich granodiorites, granites and migmatites (Bak-2), are considered to have been formed sequentially during between ca. 2.72 and 2.65 Ga. Both comprise gneissic as well as massive granitoids, and migmatites that are made up of paleosomes, mesosomes and mostly vein leucosomes occurring

in various proportions and representing a range of compositions. The thicknesses of some individual zones of migmatization may exceed 50 m. A gently dipping foliation is characteristic, documented from most drill-cores of the Bakaly granitoids. The Bak 1 quartz diorites and tonalites form numerous sheet-like bodies with thickness up to 20 m. These follow NE-trending deformation zones and have, in turn, are discordantly intruded by Bak-2 granitoids. The latter often compose separate massifs and K-feldspar-rich leucosomes. Both suites scatter chemically due to various protoliths having been involved in melting at different depths, the degrees of melting, and variations of water contents. The host rocks are metasedimentary and metavolcanic gneisses, and amphibolites. The 2.7 Ga Bak-1 rocks with 66 to 72% SiO_2 resemble somewhat Neoarchean TTG (tonalite-trondhjemite-granodiorite) granitoids (Martin, 1994). They have higher Ba (up to 925 ppm), Th (up to 20 ppm), TiO_2 (up to 0.5 %), LILE and LREE at lower #Mg (<37). However, in the dated Bak-1 quartz diorite, the $\varepsilon_{Nd}(T)$ value is –1.3, the $\varepsilon_{Hf}(T)$ of the zircons ranging between 0.2 and -2.5, which corresponds to protolith model ages of 3.4-3.2 Ga and indicates a crustal not juvenile origin of the Bak-1 granitoids. In contrast to the Bak-1 suite, the Bak-2 granodioritic (± tonalitic)-granitic suite generally follows a calc-alkaline trend. These granitoids are often leucocratic, rich in K-feldspar, and some bear two micas and garnet like typical S-type granites. The Bak-2 granitoids differ from the Bak-1 rocks by much higher LILE, Th (up to 50 ppm), LREE and total REE (110-600 ppm) at widely ranging $(La/Yb)_N$ ratios (30-145), which reflect different depths of melting. Among the Bak-2 rocks, the oldest is the 2710±19 Ma vein leucosome in the Tashliar 3.2 Ga mesosome, and the youngest S-type garnet-bearing granite with an age of 2648±33 Ma. Metamorphic overgrowths of the latter age have been found on zircons from the dated Bak-1 quartz diorite. The Bak-2 S-type granite contains zircons with very variable Hf characteristics: the $\varepsilon_{Hf}(T)$ values range between 0.5 and -20, and the T(DM) crustal ages from 3.1 to 4.4 Ga, which can be related to a metasedimentary protolith deposited after ca. 3.1 Ga. In a 2663±33 Ma old granite, zircons with $\varepsilon_{Hf}(T)$ values from +5.0 to -0.3 indicate involvement of mantle-derived melts contaminated by crustal materials. This rock features Hf T(DM) ages between 2.8 and 3.2 Ga.

The 2.6 Ga Aktanysh monzonitic suite

Several small intrusions of quartz-monzonitic and quartz-syenitic to granitic compositions occur in connection with the NE-trending fault zones, which also accommodate gabbro-anorthosite intrusions with ages of ca. 2620 Ma. With a best crystallization age of 2600±11 Ma, they terminated the Archean magmatic evolution in the Bakaly block. The 2.6 Ga granitoids differ markedly from the Bakaly granitoids by their higher abundances of Ti, HFSE (Nb, Ta, Zr and Hf), Y and total REE up to 340 ppm at low $(La/Yb)_N$ ratios of 6 to 20, indicating a shallow derivation. The Hf T(DM) ages of zircons from the 2.6 Ga monzonitic rocks vary between 3.6 and 3.3 Ga, and are thus similar to the source ages of the Bak-1 granitoids. These zircons are characterized by negative $\varepsilon_{Hf}(T)$ values, some as low as -7. Such data suggest that the melts of the 2.6-Ga monzonitic rocks were derived largely from the re-melting of 3.3-3.0 Ga crust, probably with an incorporation of older (up to ~3.6 Ga) crustal materials. The presence of zircon xenocrysts of 3076±9 and 3034±23 Ma confirms this conclusion.

The origin of the Bakaly Archean granitoids and their role in the formation of the Volgo-Uralian crustal structure

The presently available data suggest the following stages of Archean crustal evolution in Volgo-Uralia:

- Before 3.3-3.2 Ga, continental cores/microcontinents with crustal ages from ca. 3.8 to 3.4 Ga were formed, as evidenced by the Tashliar 3.3-3.2 Ga monzonitic rocks. To produce their melt(s), a mantle-crust interaction cannot be ruled out;
- The 3.2-2.8 Ga period was one of plate-tectonic geodynamics with the formation of granite-greenstone terrains resembling Proterozoic and Phanerozoic accretionary belts. They comprise juvenile island arcs, back arcs and continental magmatic arcs, and featuring TTG granitoid magmatism. The TTG associations of different age were major predecessors of the Bakaly granitoids,
- At 2.72-2.65 Ga, collisional tectonics with associated strong deformation, metamorphism, and remelting of the early crust occurred in Volgo-Uralia and defined the successive formation of the Bak-1 and Bak-2 granitoids, gneisses and migmatites. Compositional variations of these rocks appear to image a heterogeneous collisional structure in which the various rock complexes were stacked tectonically. This event was linked to the worldwide Neoarchean supercontinent assembly(ies) (Bleeker, 2003),
- At ca. 2.62-2.60 Ga, intrusions of gabbro-anorthosites and monzonitic granitoids generated due to remelting of the Archean crust and possible mantle underplating took place along the major shear zones related to post-collisional extension.

The Bakaly granitoid block represents part of an up to 20 km thick upper crustal layer (Trofimov, 2006) exposed at the top of the crystalline basement. This seismically "transparent" layer occupies ca. 25% of the total thickness of the Archean-to-Paleoproterozoic crust in Volgo-Uralia. It is composed essentially of Bakaly-type granitoids and migmatites formed during a quite short period of ca. 30 Ma. Similar layers are known from other collisional orogens like, for instance, the Himalayan, where a zone of crustal melting and seismic "transparency" has been discovered by the INDEPTH transect (Nelson et al, 1996). A dominant process in the development of the crustal layering and the formation of the upper crustal layers in the crust of Volgo-Uralia was recurrent recycling of Archean crust.

Acknowledgements

S. Bogdanova thanks the Gledden Visiting Senior Fellowships at the University of Western Australia, which provided funding for the SHRIMP datings of the Volgo-Uralian rocks. The financial contribution of the Swedish Science Research

Council to SB's project is also acknowledged. E. Bibikova acknowledges the financial support of the Russian Foundation of Basic Research, project № 05-00226, and Isotopic Program 4 RAS. The help of Z.-X. Li in the conduction of some of the SHRIMP analyses is much appreciated. Graham Begg generously supported the Hf isotopic studies of zircons by E. Belousova.

References

Bibikova E.V., Kirnozova T.I., Popova L.P., Postnikov A.V., Makarov V.A. & Kremenetsky, A.A., 1994, U-Pb ages and correlation magmatic rocks of granulite- and amphibolite-facies complexes in the Volgo-Uralian Province of the East European Craton, Stratigraphy, Geological Correlation, 2, 3–7.

Bleeker W., 2003, The late Archean record: a puzzle in ca. 35 pieces, Lithos, 71, 99–134.

Bogdanova S., De Waele B., Bibikova E., Postnikov A. & Popova L., 2005, Volgo-Uralia: SHRIMP evidence of strong Palaeoproterozoic reworking of Archaean crust, in *Supercontinents and Earth Evolution Symposium 2005,* Wingate M.T.D & Pisarevsky, S.A., eds, Geological Society of Australia, Abstracts 81, 118.

Bogdanova S.V., 1986, *The Earth's Crust of the Russian Platform in the Early Precambrian (as exemplified by the Volgo-Uralian segment)*. Nauka, Moscow, 1–224 (in Russian).

Bogdanova S.V., De Vaele B., Bibikova E.V., Belousova E.A., Postnikov A.V., Fedotova A.A. & Popova L.P., submitted, Volgo-Uralia: the first U-Pb, Lu-Hf and Sm-Nd isotopic evidence of preserved Paleoarchean crust, American Journal of Science.

Martin H., 1994, The Archean grey gneisses and the genesis of continental crust, *Archean Crustal Evolution,* K.C. Condie, ed, Developments in Precambrian Geology, 205–259.

Muslimov, R.K. & Lapinskaya, T.A., eds, 1996, *The Crystalline Basement in Tatarstan and Problems of its Oil and Gas Deposits*, Denta, Kazan (in Russian), 488p.

Nelson K.D., Zhao W., Brown L.D., Kuo J., Che J., Liu X., Klemperer S.L., Makovsky Y., Meissner R., Mechie J., Kind, R., Wenzel F., Ni J., Nabelek J., Leshou C., Tan H., Wei W., Jones A.G., Booker J., Unsworth M., Kidd W.S.F., Hauck M., Alsdorf D., Ross A., Cogan M., Wu C., Sandvol E. & Edwards M., 1996, Partially molten middle crust beneath southern Tibet: Synthesis of project INDEPTH results, Science, 274, 1684–1688.

Trofimov V.A., 2006, Deep CMP Seismic Surveying along the Tatseis-2003 Geotraverse across the Volga-Ural Petroliferous Province, Geotectonics (Geotektonika), 4, 249–262.

WHEN DID ONE-SIDED SUBDUCTION BEGIN ON EARTH? THE METAMORPHIC RECORD AND MODELLING

M. Brown

Laboratory for Crustal Petrology, Department of Geology, University of Maryland, College Park, MD 20742, USA (mbrown@umd.edu)

Introduction

Earth is a self-organized system with an irreversible evolution continuously dissipating energy to space. Secular change implies that the mantle most likely was warmer in the past. A warmer mantle will affect mantle dynamics, the degree of mantle melting and the strength of the lithosphere, with consequences for the viability of one-sided subduction. Given the limited geological record for the Hadean and early Archean, to improve our understanding of geodynamics during the early Precambrian will require that we combine geological information with results of well-constrained experiments using numerical modelling.

Metamorphism and geodynamics

At convergent plate boundaries subduction of the lithosphere is asymmetric—the subducted slab sinks under the overriding plate, which moves horizontally. One-sided subduction generates lower thermal gradients in the subduction channel and higher thermal gradients in the arc–backarc or orogenic hinterland of the overriding plate. This duality of thermal regimes is the hallmark of one-sided subduction and paired metamorphic belts are the characteristic imprint of this thermal structure in the geological record (Brown 2006, 2010). If subduction is terminated by collision, the resulting suture zone between the subduction channel and the overriding plate will be characterized by thermal gradients that evolve from lower (subduction-related) to intermediate (collision-related) values. Peak mineral assemblages in high-grade (high-temperature) metamorphic rocks are robust recorders of pressure (P) and temperature (T) because prograde dehydration and melting reactions liberate fluid or generate melt that most likely will be lost leaving behind nominally anhydrous mineral assemblages that are difficult to retrogress or overprint without fluid ingress. When combined with precise age information, P–T retrieved from these high-grade (high-temperature) metamorphic rocks may be inverted to yield apparent thermal gradients for 'peak' or close-to-peak metamorphic conditions at a particular time in Earth history (Brown 2007). In turn this information may be used to infer geodynamics (Brown 2008, 2009).

Aims and caveats

The aims of this work are to: 1) invert the record of crustal metamorphism as a proxy for earlier thermal environments to reveal the geodynamic history of Earth; and, 2) test the outcome using 2-d petrological–thermomechanical numerical modelling. To achieve the first aim requires: 1) retrieval of reliable P–T–t information from rocks; 2) identification of types of metamorphism based on natural groups within these data and relating them to geodynamic settings; and, 3) identification of patterns of age distribution in the data and relating them to global tectonic cycles. There are two caveats. First, metamorphic imprints in the continents record discrete 'events' (kinematic or subduction-to-collision) whereas subduction on a timescale shorter than that of global tectonic cycles is continuous. Second, the record of crustal metamorphism is a function of what is preserved and exhumed—if the preservation and/or exhumation potential of some types of metamorphic rock was poor earlier in Earth history, the record may be biased.

Classification of metamorphic rocks

Approximately 140 metamorphic belts have been classified based on 'peak' P–T (Brown 2007) into three types as follows (Fig. 1): 1) high pressure to ultrahigh pressure metamorphism (HPM–UHPM), characterized by lawsonite blueschist and lawsonite eclogite or UHPM eclogite (UHPM eclogites are those metamorphosed at P exceeding the stability of Qtz, recognized by the presence of Coe or Dia, or by equivalent P–T conditions determined using robust thermobarometry), where T is that registered at maximum P, and the 'age' of metamorphism is around peak P; 2) medium temperature eclogite and high pressure granulite metamorphism (E-HPGM), characterized by P–T conditions where eclogites and high-pressure granulites co-exist according to bulk composition (at P between Sil=Ky and Qtz=Coe and T above ~650°C, which is intermediate between HPM–UHPM and G–UHTM), where peak T generally was reached after maximum P, and the 'age' of metamorphism is around or slightly post peak T; and, 3) granulite to ultrahigh temperature metamorphism (G-UHTM), characterized by granulite or UHTM granulite (UHTM granulites are those metamorphosed at T >900°C at P of Sil stability, recognized by robust thermobarometry or the presence of a diagnostic assemblage in an appropriate bulk composition and oxidation state, e.g. Opx + Sil + Qtz, Spr + Qtz or Spl + Qtz), where P is that registered at maximum T, and the 'age' of metamorphism is inferred to be close to or more likely slightly post peak T.

The metamorphic record

Phanerozoic sutures are marked by early HPM and/or UHPM with apparent thermal gradients <350°C/GPa (Fig. 2a) and maximum P >2.7GPa, and later E-HPGM with apparent thermal gradients of 350–750°C/GPa (Fig. 2a). G-UHTM with apparent thermal gradients of 800–1300°C/GPa (Fig. 2a) is rare at the surface, but may be inferred at depth in the hinterland of some

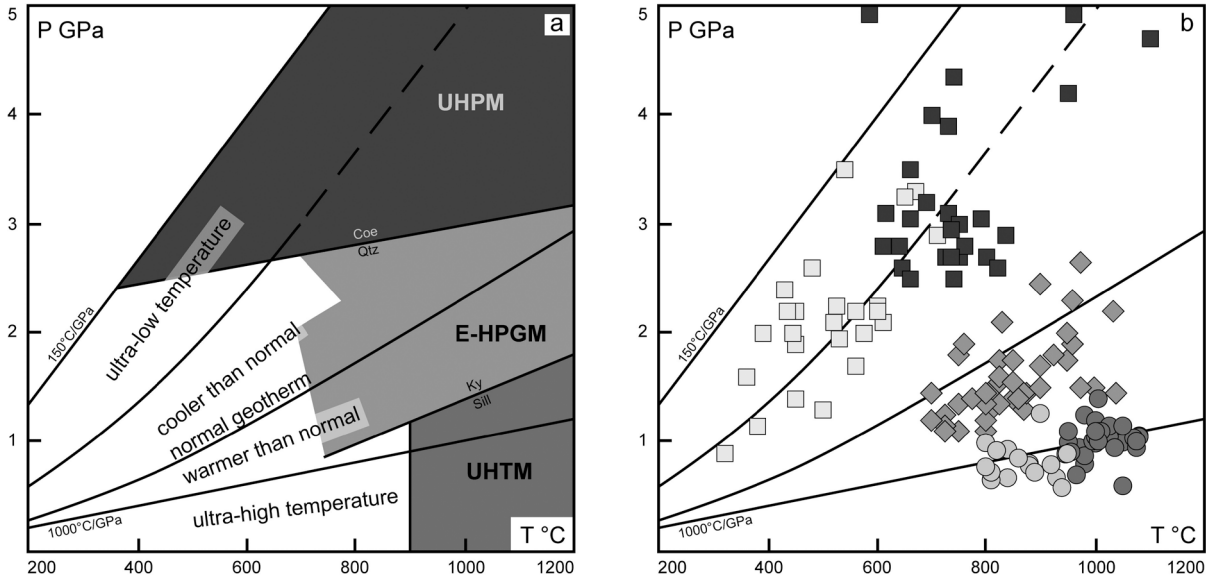

Figure 1. a. A division of P-T space based on whether thermal conditions implied by peak metamorphic mineral assemblages in orogenic crust were warmer or cooler than a normal (conductive) continental geotherm. For thermal conditions warmer than a normal continental geotherm, a thermal gradient of ~1,000ºC/GPa is the practical limit for a conductive response; metamorphic belts that record apparent thermal conditions hotter than this plot in the 'ultra-high temperature' P-T field. For thermal conditions cooler than a normal continental geotherm, a two-fold division is shown into a 'cooler than normal' and an 'ultra-low temperature' P-T field. b. Peak P-T values for 140 metamorphic belts (from Brown 2007) in relation to a normal (conductive) continental geotherm. Each datum records a point on a metamorphic (transient) geotherm, and the different apparent thermal gradients implied by each of the three main types of extreme metamorphic belt, G-UHTM (circles), E-HPGM (diamonds) and HPM-UHPM (squares), are inferred to reflect different thermal regimes and tectonic settings.

active orogens. For the Precambrian, two regimes may be distinguished. Mesoarchean–Neoproterozoic sutures are marked by E-HPGM, where the maximum *P* jumps from <1 GPa to around 2 GPa from the Mesoarchean to the mid-Paleoproterozoic. Apparent thermal gradients for E-HPGM are generally in the range 350–700°C/GPa (Fig. 2b). G-UHTM is also first registered in the Neoarchean, with apparent thermal gradients that are generally in the range 800–1,300°C/GPa (Fig. 2b). The appearance of E-HPGM and G-UHTM registers a change in geodynamics that generated sites of lower heat flow, inferred to be associated with subduction, and sites of higher heat flow, corresponding to be arcs–backarcs and orogenic hinterlands. In contrast, Eoarchean–Mesoarchean crust registers *P–T* conditions characteristic of low-to-moderate-*P*–moderate-to-high-*T* metamorphism. Granulites and 'wet' melting are common, and in high-grade terranes multiple episodes of anatexis occur over 10s to >100Ma. Apparent thermal gradients are warm (800–1,000°C/GPa, maximum *T* not extreme) in both greenstone belts and high-grade terranes, and as retrieved from inclusion assemblages in Hadean zircons (1,000°C/GPa; Hopkins et al. 2009), although metamorphism in Barberton at *ca*. 3.2 Ga presages cooler environments (450–700°C/GPa; *P* up to 1.2–1.5 GPa; Moyen et al. 2006). Neither extreme crustal temperatures nor pressures are documented before the Mesoarchean–Neoarchean; there is no imprint of subduction of continental crust to and return from mantle conditions.

Paired metamorphic belts

Classic paired metamorphic belts in which an inboard higher thermal gradient metamorphic belt is juxtaposed against an outboard lower thermal gradient metamorphic belt along a tectonic contact are found in Phanerozoic accretionary orogens of the circum-Pacific. The concept of paired metamorphic belts may be generalized and extended more widely than in the original proposition to subduction-to-collision orogenic systems in addition to accretionary orogenic systems. In this wider application, paired metamorphic belts are "penecontemporaneous belts of contrasting type of metamorphism that record different apparent thermal gradients, one warmer and the other colder, juxtaposed by plate tectonics processes" (Brown 2009, 2010). This extends the original concept and makes it more useful in the context of our better understanding of the relationship between thermal regimes and geodynamics.

Numerical modelling

Results from 2-d petrological–thermomechanical numerical modelling experiments of ocean plate subduction at a convergent plate boundary show that Precambrian geodynamic regimes depend primarily on upper-mantle temperature (T_{UM}), with a transition from 'no subduction' at T_{UM} >250–200K higher than present through a 'pre-subduction' regime to a one-sided subduction regime at T_{UM} <175–160K higher than present (Sizova et al. 2010). This change in behavior is related to a reduced weakening by decreased percolation of melt from the sub-lithospheric mantle at lower T_{UM}. Prior to the Mesoarchean a 'pre-subduction' regime may have operated in which convergence forced an ocean plate under a continental plate without the formation of a pronounced mantle wedge or backarc basin. As mantle temperature declined melt-related weakening was less and stronger plates stabilized one-sided subduction during the Mesoarchean–Neoarchean.

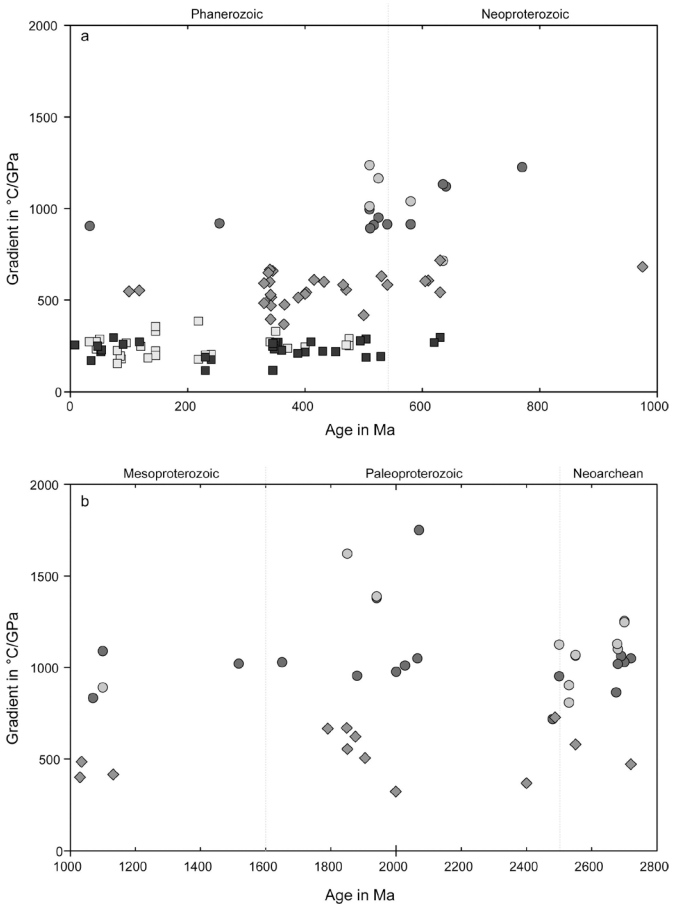

Figure 2. Apparent thermal gradient in ºC/GPa plotted against age of metamorphism in Ma (data from Brown 2007) for the three types of extreme metamorphic belt, G-UHTM (circles), E-HPGM (diamonds) and HPM-UHPM (squares), for two time intervals, a. Phanerozoic and Neoproterozoic, and b. Mesoproterozoic to Neoarchean.

Concluding remarks

The first imprint of one-sided subduction in the geological record is the appearance of two contrasting types of metamorphism—G-UHTM and E-HPGM—in the late-Archean crust; this manifests the onset of a 'Proterozoic plate tectonics regime'. Results of 2-d numerical experiments show the degree of lithosphere weakening induced by sub-lithospheric melts is the crucial control on the geodynamic regime. The lower melt flux as the ΔT for the upper mantle decreased below 175K resulted in stronger plates and stabilized one-sided subduction. This first-order transition probably occurred sometime during the Mesoarchean Era. There are many other changes that occurred during the Mesoarchean–Neoarchean Eras consistent with a transition to one-sided subduction, including differences in the style and chemistry of volcanism and plutonism, the end of the flat Earth and the appearance of passive margins, and the formation of supercratons and beginning of the Proterozoic supercontinent cycle (Condie & Pease 2008). The change to one-sided subduction may have begun locally in the Mesoarchean–Neoarchean Eras and become global in the Paleoproterozoic Era; this was a landmark event in Earth history. The 'Proterozoic plate tectonics regime' evolved during a Neoproterozoic transition to the 'modern plate tectonics regime' characterized by colder subduction imaged by the formation and exhumation of HPM–UHPM rocks.

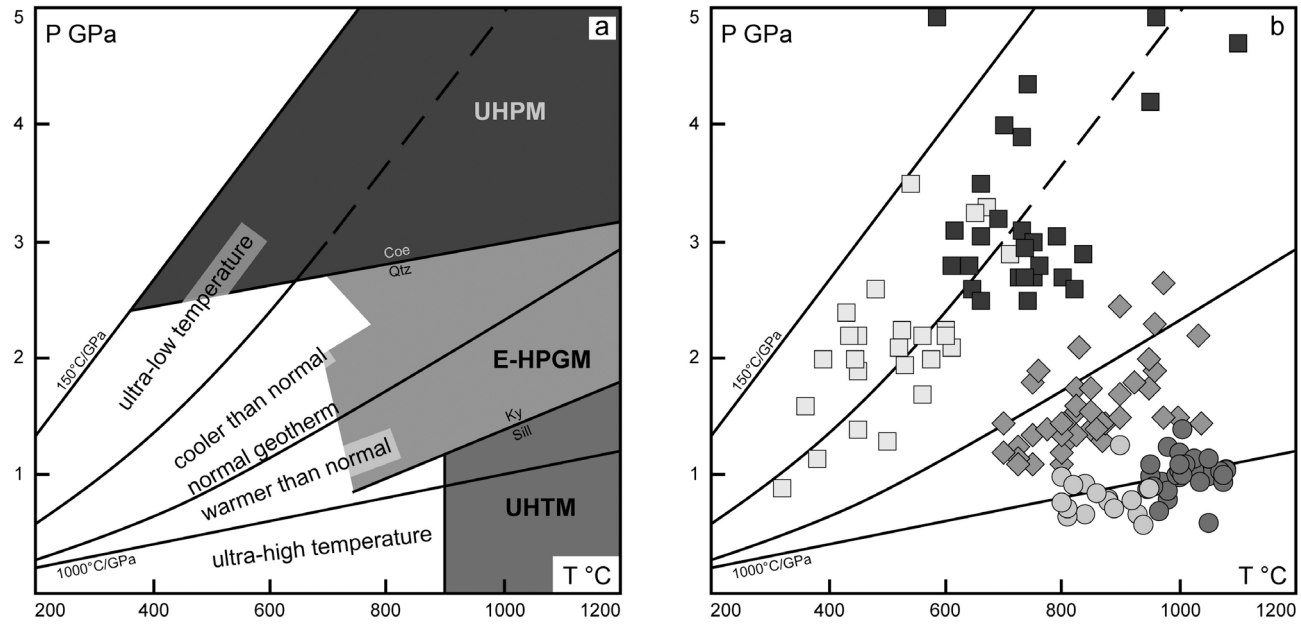

Figure 3. Snapshots from numerical experiments in which the upper-mantle temperature and the crustal radiogenic heat production are varied independently (where ΔT is the difference between the prescribed upper mantle temperature and the present value of 1360K at 70km depth, and H_r is the prescribed value of average crustal radiogenic heat production as a function of the present value H_r^o). The experiments show different tectonic regimes: a. the 'modern subduction' regime (ΔT = 0–175K) characterized by one-sided subduction; b. a 'pre-subduction' regime (ΔT = 175–250K) in which oceanic lithosphere may underthrust the continental crust but does not subduct; and, c. a 'no-subduction' regime (ΔT ≥ 250K) in which the lithosphere is too weak to underthrust. For further details of the experiments including color figures see Sizova et al. (2010).

References

Brown M., 2006, Duality of thermal regimes is the distinctive characteristic of plate tectonics since the Neoarchean, Geology, 34, 961–964.

Brown M., 2007, Metamorphic conditions in orogenic belts: A record of secular change, International Geology Review, 49, 193–234.

Brown M., 2008, Characteristic thermal regimes of plate tectonics and their metamorphic imprint throughout Earth history: When did Earth first adopt a plate tectonics mode of behavior? in *When Did Plate Tectonics Begin on Planet Earth?* Condie K. & Pease V., eds, Geological Society of America Special Paper, 440, 97–128.

Brown M., 2009, Metamorphic patterns in orogenic systems and the geological record, in Earth *Accretionary Systems in Space and Time*, Cawood P.A. & Krőner A., eds, Geological Society, London, Special Publications, 318, 37–74.

Brown M., 2010, Paired metamorphic belts revisited, Gondwana Research, doi:10.1016/j.gr.2009.11.004.

Condie K. & Pease V. 2008, When Did Plate Tectonics Begin on Planet Earth? Geological Society of America Special Paper, 440, 1–294.

Hopkins M., Harrison T.M. & Manning, C.E., 2009, Hadean thermobarometry revisited, AGU Fall Meeting 2009, abstract V12B-08.

Moyen J.-F., Stevens G. & Kisters A., 2006, Record of mid-Archaean subduction from metamorphism in the Barberton terrain of South Africa, Nature, 442, 559–562.

Sizova E., Gerya T., Brown M. & Perchuk L., 2010, Subduction styles in the Precambrian: Insight from numerical experiments, Lithos, http://dx.doi.org/10.1016/j.lithos.2009.05.028.

MESOARCHEAN CRUST IN THE EASTERN GAWLER CRATON, SOUTH AUSTRALIA: LOCATION, AGE, COMPOSITION AND POSSIBLE CORRELATIONS

G.L. Fraser[1], N.L. Neumann[1], S. McAvaney[2], M. Szpunar[2], A. Reid[2] & D. Champion[1]

[1]Onshore Energy and Minerals Division, Geoscience Australia, GPO Box 378, Canberra, ACT, 2617
[2]Geological Survey Branch, Primary Industries and Resources South Australia, GPO Box 1671, Adelaide, SA, 5001

Introduction

Crust predating 3.0 Ga within the Australian continent has previously been identified only in relatively restricted areas of the Yilgarn and Pilbara Cratons of Western Australia. Here we report the discovery of early Mesoarchean (~3150 Ma) rocks in the eastern Gawler Craton of South Australia. Rocks of broadly Mesoarchean age have been inferred by some authors to exist at depth beneath the Gawler Craton (Creaser & Fanning, 1993; Daly & Fanning, 1993), but no rocks of this age have been identified previously at the surface. The newly identified Mesoarchean granites and gneisses crop out across at least ~20 x 30 km and, on the basis of inherited zircon and Nd-isotopic compositions, are inferred to be present at depth beneath a region of at least ~1500 km^2.

Results

On northeastern Eyre Peninsula, South Australia, south of the town of Iron Knob, the Cooyerdoo Granite crops out as subhorizontal platforms and small tors on the eastern side of the Middleback Ranges. Four samples of the Cooyerdoo Granite, collected across a north-south distance of ~10 km, each yield zircon populations dominated by a youngest concordant age component at ~3150 Ma that we interpret as the igneous crystallisation age (Fraser et al., submitted). Three of these four samples also contain pre-3150 Ma zircon, interpreted as inherited xenocrysts, ranging in age between ~3200 and 3300 Ma. An additional sample from an unnamed gneissic granite, collected a few kilometres west of Iron Knob also contains abundant oscillatory-zoned zircon with an age of ~3150 Ma, as well as compositionally and texturally distinct zircon with high U content and very low Th/U occurring as overgrowths and individual grains with an age of ~2500 Ma. This sample is interpreted as an equivalent of the Cooyerdoo Granite that has experienced high-grade metamorphism at ~2500 Ma. Each of these five samples yields depleted-mantle Nd-model ages between ~3300 and 3400 Ma, consistent with the age of inherited zircon components, and suggesting granite derivation from crust of late-Paleoarchean age. Compositionally, the Cooyerdoo Granite is very similar to post-tectonic, potassic granites of the Yilgarn and Pilbara Cratons, having elevated LILE and LREE content, and low Na/K. In the Yilgarn and Pilbara Cratons, granites of this composition are interpreted to have been derived from melting of pre-existing TTG crust (Champion & Smithies, 2001, 2007; Van Kranendonk et al., 2007), and we suggest a similar origin for the Cooyerdoo Granite. The combination of granite chemistry, inherited zircon ages and Nd-model ages suggests the presence of ~3300 to 3400 Ma TTG-like crust within at least parts of the eastern Gawler Craton, which was melted to form the Cooyerdoo Granite at ~3150 Ma.

Interpretation and Discussion

The Cooyerdoo Granite is relatively enriched in heat producing elements, yielding calculated modern-day heat production values between ~3.0 and 8.4 μWm^{-3} and a mean value of ~5.0 μWm^{-3}. The presence of relatively radiogenic Archean crust in the eastern Gawler Craton provides at least a partial explanation for the extremely radiogenic character of Paleo- to Mesoproterozoic granites that intrude this region. For example, the Paleoproterozoic Burkitt Granite, and Mesoproterozoic Charleston Granite yield heat production values of ~17 μWm^{-3} and ~11 μWm^{-3}, respectively. Both can now be shown to intrude through, and based on their evolved Nd-isotopic compositions appear to be partially derived from, relatively radiogenic Mesoarchean crust.

Evidence for Mesoarchean crust has not been identified west of the Kalinjala Mylonite Zone, which we suggest may form the western boundary of this ancient crustal block. The northern extent of this ancient crust is obscured by the extensive cover of the flat-lying Mesoproterozoic Gawler Range Volanics, and its eastern extent is covered by Paleoproterozoic metasedimentary rocks. The southern extent of Mesoarchean crust is unclear, although we note that the geology of southeastern Eyre Peninsula is dominated by Paleoproterozoic (~1850 Ma) granitoids of the Donington Suite that do not contain Archean inherited zircons or highly evolved Nd-isotopic signatures, suggesting they are not derived from, or contaminated by, Mesoarchean material. Consequently, we tentatively suggest that the Mesoarchean crust present on northeastern Eyre Peninsula may pinch out to the south, perhaps between splays of the Kalinjala Mylonite Zone.

Despite the geochemical similarities between the Cooyerdoo Granite and post-tectonic Archean granites of the Yilgarn and Pilbara Cratons, no direct age equivalents of the Cooyerdoo Granite exist within the Yilgarn or Pilbara, as far as we are aware. To the south of the Gawler Craton, across the Gondwana break-up margin in East Antarctica, ~3150 Ma zircons have been identified in gneisses from the Miller Range (Goodge and Fanning, 1999; Goodge et al., 2001) and from the southern Prince Charles Mountains (Boger et al., 2001, 2006). These age similarities suggest that discontinuous

fragments of Mesoarchean crust may be present more widely within the East Antarctic and Gawler Cratons, which together formed the Mawson Continent (Fanning et al., 1996).

Acknowledgements

We thank the local landholders for access to their properties in and around the Middleback Ranges. Chris Foudoulis is thanked for sampling assistance in the field, and for provision of high-quality zircon separates. Keith Sircombe and Patrick Burke provided assistance with SHRIMP analyses in the Geoscience Australia Geochronology Laboratory, and Liz Webber and Bill Pappas (Geoscience Australia) provided geochemical analyses. G. F., N. N. and D. C. publish with the permission of the Chief Executive Officer, Geoscience Australia.

References

Boger S.D., Wilson C.J.L. & Fanning C.M., 2001, Early Paleozoic tectonism within the East Antarctic craton: the final suture between east and west Gondwana? Geology, 29, 463–466.

Boger S.D., Wilson C.J.L. & Fanning C.M., 2006, An Archean province in the southern Prince Charles Mountains, East Antarctica: U-Pb zircon evidence for c. 3170 Ma granite plutonism and c. 2780 Ma partial melting and orogenesis, Precambrian Research, 145, 207–228.

Creaser R.A. & Fanning C. M., 1993, A U-Pb zircon study of the Mesoproterozoic Charleston Granite, Gawler Craton, South Australia, Australian Journal of Earth Sciences, 40, 519–526.

Champion D.C. & Smithies R.H., 2001, Archean granites of the Yilgarn and Pilbara cratons, Western Australia, 4th International Archaean Symposium 2001, Extended Abstracts, AGSO, Record 2001/37.

Champion D.C. & Smithies, R.H., 2007, Three billion years of granite magmatism: Palaeo-Archaean to Permian granites of Australia, Sixth International Hutton Symposium, Origin of granites and related rocks, University of Stellenbosch, South Africa, July 2007. Presentation available at:
http://www.ga.gov.au/minerals/research/pubs/presentations/hutton_symp_2007.jsp#dload

Daly S.J. & Fanning C.M., 1993, Archaean, in *The Geology of South Australia. Vol 1 The Precambrian*, Drexel J. F., Preiss W. V. & Parker A. J., eds, Geological Survey of South Australia, Bulletin 54.

Fanning C.M., Moore D.H., Bennett V.C. & Daly S.J., 1996, The "Mawson Continent": Archaean to Proterozoic crust in East Antarctica and the Gawler Craton, Australia. A cornerstone in Rodinia and Gondwana, Geological Society of Australia Abstracts, 41, 135.

Fraser G., McAvaney S., Neumann N., Szpuna M. & Reid, A, Discovery of early Mesoarchean crust in the eastern Gawler Craton, South Australia. Submitted to Precambrian Research.

Goodge J.W. & Fanning C.M., 1999, 2.5 b.y. of punctuated Earth history as recorded in a single rock, Geology, 27, 1007–1010.

Goodge J.W., Fanning C.M. & Bennett V.C., 2001. U-Pb evidence of ~1.7 Ga crustal tectonics during the Nimrod Orogeny in the Transantarctic Mountains, Antarctica: implications for Proterozoic plate reconstructions, Precambrian Research, 112, 261–288.

LITHOSPHERIC LATERAL HETEROGENEITY IN THE SUB-CONTINETAL LITHOSPHERIC MANTLE – EFFECTS AND CONSEQUENCES

W. Gorczyk[1], B. Hobbs[12], A. Ord[2], K. Gessner[2] & T. Gerya[3]

[1.] CSIRO Exploration and Mining, Perth, Australia.
[2] School of Earth and Environment, The University of Western Australia, Perth, Australia.
[3.] Dept. of Geosciences, ETH-Zurich, Switzerland.

Introduction

The seismic structure of the sub-continental lithospheric mantle (SCLM) is known to be heterogeneous, resulting in strong vertical and lateral variations in rheological properties. Lithospheric discontinuities (sharp changes in the thermal and/or compositional structure) are thought to be long lived and are mostly correlated with major tectonic boundaries(Begg et al., 2009). SCLM underneath continents is constructed of blocks with different thermal and compositional characteristics, due to strong depletion or extensive metasomatism, during tectonic processes. Boundaries between the mosaic of continental blocks are the locus for repeated emplacement of ascending magmas, infiltrated by silicate melts together with H_2O and CO_2 fluids (Coltorti & Gregoire, 2008) leading to metasomatism and weakening of the SCLM.

This paper explores the control that mantle heterogeneity exerts on the thermal and chemical evolution during deformation subsequent to the development of the heterogeneity. We explore the behaviour of the lithosphere in a compressional regime with variable lateral and vertical heterogeneities in rheological properties (Fig. 1). These variations may have been

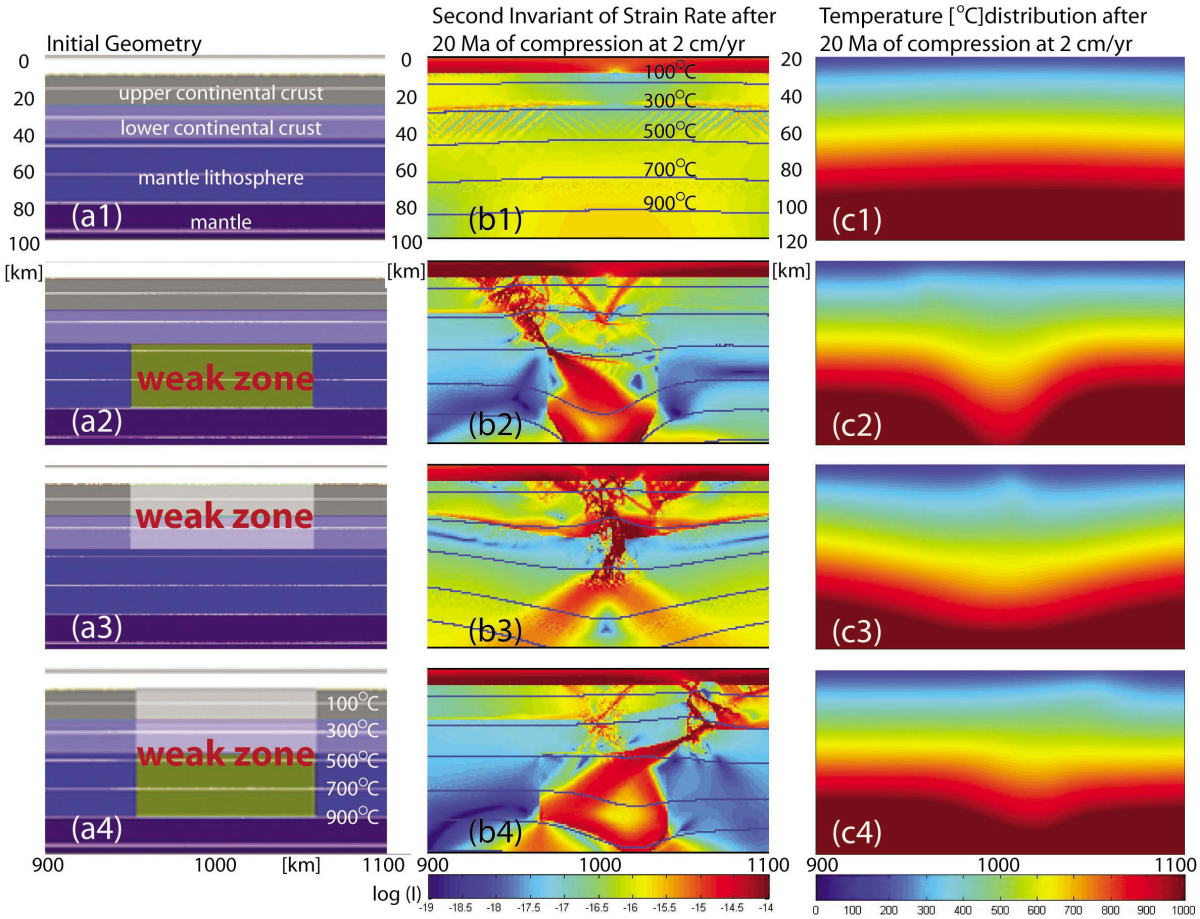

Figure 1. Control of complexity in mantle deformation by initial heterogeneity of mantle strength. (a) Four simple models of initial heterogeneity. From the top: (a1) no heterogeneity, (a2) a weak zone only in the sub-crustal mantle lithosphere, (a3) a weak zone only in the crust, (a4) a weak zone through the entire lithosphere. (b) Plots of shear strain rate and isotherms after 20 Ma of shortening at 2 cm/yr. From the top: (b1) homogeneous deformation, (b2) deformation concentrated in the crust above the sub-crustal weak zone and extending into the mantle, (b3) deformation concentrated in the crustal weak zone, (b4) deformation extending through the lithosphere. (c) Plots of temperature distribution after 20 Ma of shortening at 2 cm/yr: (c1) regular temperature distribution, (c2) initial stage of mantle lithosphere delamination, (c3) synclinal temperature distribution – no delamination, (c4) initial stage of mantle lithosphere delamination.

caused for instance by amalgamation of micro-continents such as is thought to be characteristic of the Eastern Goldfields (Standing, 2008) in the Yilgarn and of the Amadeus Basin (Hand & Sandiford, 1999) The models presented here are simplistic but illustrate the basic principles. The code used in this study is based on a conservative finite-difference, multi-grid, marker in cell method (Gerya & Yuen, 2003). Devolatilisation reactions and melting can affect the physical properties of rocks and are incorporated in a self-consistent manner. We use a petrological-thermomechanical modelling approach with all rock properties including mechanical properties calculated in the Lagrangian scheme for rock markers at every time step based on Gibbs free energy minimization (Connolly, 2005) as a function of the local pressure, temperature and rock composition.

Results and Discussion

The results illustrate that initial structural complexity is necessary for and has a dramatic effect on subsequent fault development, the growth of deep basins, core complex formation, melting and devolatilisation within the lithosphere. The lowered plastic yield stress in the weak zones (Fig. 1) nucleates localised deformation and creates conditions for delamination via a Rayleigh-Taylor instability. Above the site of localised delamination of the mantle lithosphere, a series of deep crustal faults develop that may extend into the upper mantle. These deep structures can act as the pathways for mantle derived $CO_2 \pm H_2O$ fluids which are a possible source for major mineral deposits and alkaline igneous complexes. Isotherms are commonly elevated throughout the lithosphere in the hanging wall of deep through-going structures and are depressed in the footwalls. This means that some architectures favour devolatilisation and melting in the hanging wall and hence are optimal for mineralisation development. We discuss models that discriminate between architectures that favour fluid migration and those that are likely to be barren. A large spectrum of behaviour occurs that results from minor changes in the orientation and strength of the weak zones.

References

Begg G.C., Griffin W.L., Natapov L.M., O'Reilly S.Y., Grand S.P., O'Neill C.J., Hronsky J.M.A., Djomani Y.P., Swain C.J., Deen T., & Bowden P., 2009, The lithospheric architecture of Africa: Seismic tomography, mantle petrology, and tectonic evolution, Geosphere, 5, 23–50.

Coltorti M., & Gregoire M., 2008, Metasomatism in oceanic and continental lithospheric mantle: introduction, Geological Society of London, Special Publications, 293, 1–9.

Connolly J.A.D., 2005, Computation of phase equilibria by linear programming: a tool for geodynamic modelling and an application to subduction zone decarbonation, Earth and Planetary Science Letters, 236, 524–541.

Gerya T.V., & Yuen D.A., 2003, Characteristics-based marker-in-cell method with conservative finite-differences schemes for modelling geological flows with strongly variable transport properties, Physics of the Earth and Planetary Interiors, 140, 293-318.

Hand M., & Sandiford M., 1999, Intraplate deformation in central Australia, the link between subsidence and fault reactivation, Tectonophysics, 305, 121-140.

Standing J.G., 2008, Terrane amalgamation in the Eastern Goldfields Superterrane, Yilgarn Craton, Evidence from tectonostratigraphic studies of the Laverton Greenstone Belt, Precambrian Research, 161, 114–134.

THERMOBAROMETRIC EVOLUTION OF EAST YILGARN CRUST: CONSTRAINTS ON NEOARCHAEAN TECTONICS AND GOLD MINERALIZATION

B. Goscombe[1], R. Blewett[2], K. Czarnota[2], D. Foster[3] & B. Wade[4]

[1]Integrated Terrane Analysis Research (ITAR), 18 Cambridge Rd. Aldgate SA 5154.
[2]Geoscience Australia, GPO Box 378, Canberra ACT 2601.
[3]Dept. of Geological Sciences, University of Florida, Gainesville, Florida 32611, USA.
[4]Adelaide Microscopy, University of Adelaide, Adelaide SA 5005.

Introduction

The East Yilgarn crust experienced at least five distinct thermal regimes at different times in its evolution (Goscombe et al., 2007, 2009). M1 is recorded by moderate-P (7.5 kb), low-T/depth ratio (20 ºC/km) metamorphism at approximately 2710-2695 Ma accompanying formation of the volcanic sequences and before the high-Ca granite bloom. M1 parageneses are spatially restricted to crustal shear systems and are interpreted to have formed during partial downward advection of magmatic arc margins during docking events, followed by rapid isothermal decompression. Significantly these parageneses predate the granite bloom and doming events and formed in a horizontal tectonics setting (i.e. plate tectonics) and not vertical tectonics settings such as keels adjacent to diapiric domes. Rare low-P (2.5-5.0 kb) granulite parageneses (Ma) are interpreted to have formed in high heat flow settings within the magmatic arcs.

A regional M2 thermal anomaly produced low-P (3.5-5.0 kb), high-T/depth ratio (30-40 ºC/km) metamorphism (M2) associated with emplacement of large volumes of high-Ca granite at 2685-2655 Ma. M2 is associated with termination of volcanism and through-going subduction, with compression at 2670 Ma resulting in minor crustal thickening and tight clockwise P-T paths. The regional M2 thermal anomaly softened the crust, priming it for a marked response from a stress switch to extension at 2665-2645 Ma (M3a). M2 crustal thickening was insufficient to induce gravitationally driven extension, consequently M3a lithospheric extension is interpreted as far field imposed stress such as slab roll-back. Similar horizontal to vertical $\sigma 1$ stress switches are a common feature of Phanerozoic accretionary orogens due to changes in outboard subduction zone dynamics. M3a parageneses indicate a low-P (4.0 kb), very high-T/depth ratio (40-50 º/km) thermal anomaly superimposed on regional M2. The M3a thermal anomaly is spatially restricted to arcuate zones associated with post-volcanic siliciclastic rift basins in the upper-plate of crustal scale extensional shear zones. The extensional upper-plate setting is confirmed by M3a parageneses tracking anti-clockwise P-T paths.

It could be argued that the East Yilgarn Craton would not be as endowed in world class gold mineralization without the late orogenic switch from compression during M2 to lithospheric extension during M3a. All of the processes, architectures and juxtapositions required for world class gold deposits, formed during the M3a period and are a natural response to this significant stress switch. M3a lithospheric extension thinned the crustal lithosphere resulting in a higher flux of energy from the mantle lithosphere that then drove many of the key processes leading to mineralization. Lithospheric extension was heterogeneous, resulting in basinal rifts and partitioned zones of high heat flux resulting in steep thermal gradients that drove fluid flow. The extensional stress field also modified fluid flow trajectories, giving both horizontal and downward paths in part (Sheldon et al., 2007), allowing the mixing of multiple fluid sources in the upper crust. Extensional rifting dropped basinal fluids into the upper crust significantly increasing the ambient fluid volume and introducing a new fluid type into the crust. Lithospheric extension and associated deep penetrating structures facilitated both the generation of mafic granitoid, syenite, lamprophyre and carbonatite melts and dry strongly reduced fluids in the mantle (Walshe et al., 2008a) and transport of these up into the upper crust. These mantle derived melts and fluids are possibly a major primary source of the gold and mixing of this distinct fluid type with ambient hydrous fluids in the upper crust ultimately resulted in precipitation and mineralization. Lithospheric extension both created and reactivated older crustal shear zones, generating suitable structural architectures such as extensional growth faults and footwall domes. These architectures allowed the focusing of fluids from different sources facilitating mixing and ultimately mineralization, both during M3a lithospheric extension and during subsequent reactivation of these structures in D4 and D5 with remobilization associated with low-grade hydrothermal alteration events (M3b) to 2620 Ma. M3a lithospheric extension and consequent high heat flow and decompressing lower-plate domes, facilitated crustal melting and emplacement of low-Ca granites in the upper-crust, which extended the M3a thermal anomaly and perturbed isotherms, further influencing fluid flow and mineralization.

Acknowledgements

Sponsors of the pmd*CRC Y4 project, the Geological Survey of Western Australia, Geoscience Australia and Adelaide Microscopy are gratefully acknowledged for support and contributions. Martin Van Kranendonk, Steve Wyche, Heather Sheldon, Kevin Cassidy, Dave Champion, Paul Henson are thanked for helpful discussions.

References

Goscombe B., Blewett R.S, Czarnota K., Maas R. & Groenewald B.A., 2007, Broad thermobarometric evolution of the Eastern Goldfields Superterrane, Proceedings of Geoconferences (WA) Inc. Kalgoorlie ’07 Conference, Geoscience Australia, Record 2007/14, 33–38.

Goscombe B.D., Blewett R.S., Czarnota K., Groenewald B.A. & Maas R., 2009, Metamorphic evolution and integrated terrane analysis of the Eastern Yilgarn Craton: Rationale, Methods, Outcomes and Interpretation, Geoscience Australia, Record 2009/23.

Sheldon H.A., Barnicoat A.C., Zhang Y. & Ord A., 2007, Metamorphism in the Eastern Yilgarn Craton: implications for fluid flow and mineralization, Proceedings of Geoconferences (WA) Inc. Kalgoorlie’07 Conference, Geoscience Australia Record 2007/14, 138–142.

Walshe J.L., Neumayr P., Cleverley J., Petersen K., Andrew A., Whitford D., Carr G.R., Kendrick M., Young C. & Halley S., 2008, Multiple fluid resivoirs in Eastern Yilgarn gold systems, pmd*CRC Y4 Project Final Report.

2.7 Ga KAMBALDA SEQUENCE: PLUME IMPINGEMENT AT A RIFTED CRATON MARGIN

R. Kerrich[1] & N. Said[2]

[1]*Department of Geological Sciences, University of Saskatchewan, Saskatoon, SK, Canada S7N 5E2*
[2]*Centre for Exploration Targeting, School of Earth and Environmental Sciences, The University of Western Australia, 35 Stirling Hwy, Nedlands, WA 6009*

Introduction

Neoarchean greenstone terranes globally record two prevalent volcanic associations: komatiites-tholeiitic basalts and bimodal tholeiitic to calc-alkaline basalts-dacites. Komatiites and associated basalts are generally interpreted as products of anomalously hot mantle plumes, erupted in ocean basins or continental margins (Kerrich et al., 1999; Manikyamba et al., 2008). Where there is a combination of field, trace element, and isotopic evidence for the absence of crustal contamination, basalts are tholeiitic with near-flat REE patterns over a range of REE abundances, and both komatiites and basalts share dominantly positive Nb anomalies The tholeiitic to calc-alkaline association is generally considered to be arc-related (Wyman & Kerrich, 2009, and references therein).

Several classic papers report geochemical data for ultramafic and basalt volcanic sequences of the Yilgarn craton, including the Kalgoorlie Terrane. Sun & Nesbitt (1978) described LREE depleted spinifex textured peridotite (STP) flows, and basalts, from the Yilgarn craton and other Archean greenstone belts. They interpreted the LREE characteristics in terms of a two stage process: removal of an incompatible element enriched melt followed by second stage melting of the depleted residue. Three basaltic magma series were defined by Redman & Keays (1985) for Yilgarn craton greenstone belts. High magnesium series- , and low magnesium series basalts (HMSB, LMSB) were accounted for by mantle source regions variably depleted in incompatible elements, whereas siliceous high magnesian series basalts (SHMSB or SHMB) were derived from an incompatible element enriched mantle. Alternatively, Sun et al. (1989) interpreted SHMB as crustally contaminated komatiites. Lesher & Arndt (1995) further constrained these models for the 2.7 Ga Kambalda Sequence with combined trace element and Sm-Nd isotope data, documenting progressive crustal contamination of liquids erupted from a mantle plume up the volcanic stratigraphy in the Kalgoorlie Terrane. Said & Kerrich (2009) proposed an additional process, that the enriched Paringa basalt represented crust recycled into it's mantle source, rather than contamination during eruption, as well as crustal contamination of some basalts. Sylvester et al. (1997) reported high-precision trace element data, specifically Nb/Th ratios, in crustally uncontaminated Lunnon basalts of the Lower Basalt Unit, to address the question of the extent and timing of extraction of continental crust from mantle asthenosphere.

The ~ 2.7 Ga Kambalda Sequence of the Kalgoorlie Terrane includes stratigraphically Lower and Upper Basalt Units separated by the Kambalda Komatiite Unit (Fig. 1). This paper reports new high-precision major and trace element, and Sm-Nd isotope data, for six basalt formations or suites defined in the Lower Basalt Unit, as well as the underlying autochthonous Penneshaw Formation, to build on earlier work, and address primary asthenosphere melts versus crustally contaminated counterparts. Specifically, we address the magnitude and significance of positive Nb anomalies, building on the work of Sylvester et al. (1997). These results are used to evaluate the geodynamic setting in which the Lower Basalts were erupted and contribute to the issue of continental growth.

Geochemical Results

Basaltic flows of the Woolyeneer Formation, and Lunnon and Wongi Basalts, are compositionally restricted tholeiites with Mg# and Ni contents of 56-52, 110 ppm, 57-51, 190-160 ppm, and 63, 300-210 ppm, respectively. Heavy-REE (HREE) are flat at 4-6 times chondrite (Fig.1), with mild LREE-depletion at $(La/Sm)_N$=0.77-0.94, and Nb/Th ratios of 8-17 signifying these basalts were erupted through the autochthon without crustal contamination as there is no correlation of Nb/Th with $(La/Sm)_N$. These basalts are further characterized by the absence of significant anomalies of Zr-Hf/MREE, where Zr/Hf and Zr/Sm ratios are close to the respective PM values of 36 and 25. The Scotia Basalt is distinctive in having a range of HREE fractionation where $(Gd/Yb)_N$=1.1-1.4 indicative of melting over a range of depths from above to below the garnet stability field at ~ 90 km (Fig.1).

Basalts of the Burbanks and Penneshaw Formations have major element compositions akin to the Woolyeneer Formation, but near flat REE at 9-11 times chondrite. Both formations have two populations: the most primitive have greater Th contents but Nb/Th<8, whereas the more evolved show lower Th in conjunction with Nb/Th>8, in keeping with the hottest liquids having assimilated crust but the evolved flows being uncontaminated (Fig. 1). Missouri basalts are all crustally contaminated (Fig. 1). Collectively, the uncontaminated Woolyeneer, Lunnon, Wongi, Scotia basalts and Burbanks Formation have ε_{Nd} values spanning from 4.5 to 1.5, whereas ε_{Nd} values for the contaminated Missouri Basalt and Penneshaw Formation span between 2 and 1; there is a weak trend of ε_{Nd} with Nb/Th.

Implications

Crustally uncontaminated basalts have systematically positive Nb anomalies relative to Th in conjunction with slight trace element depletions of within plate depleted

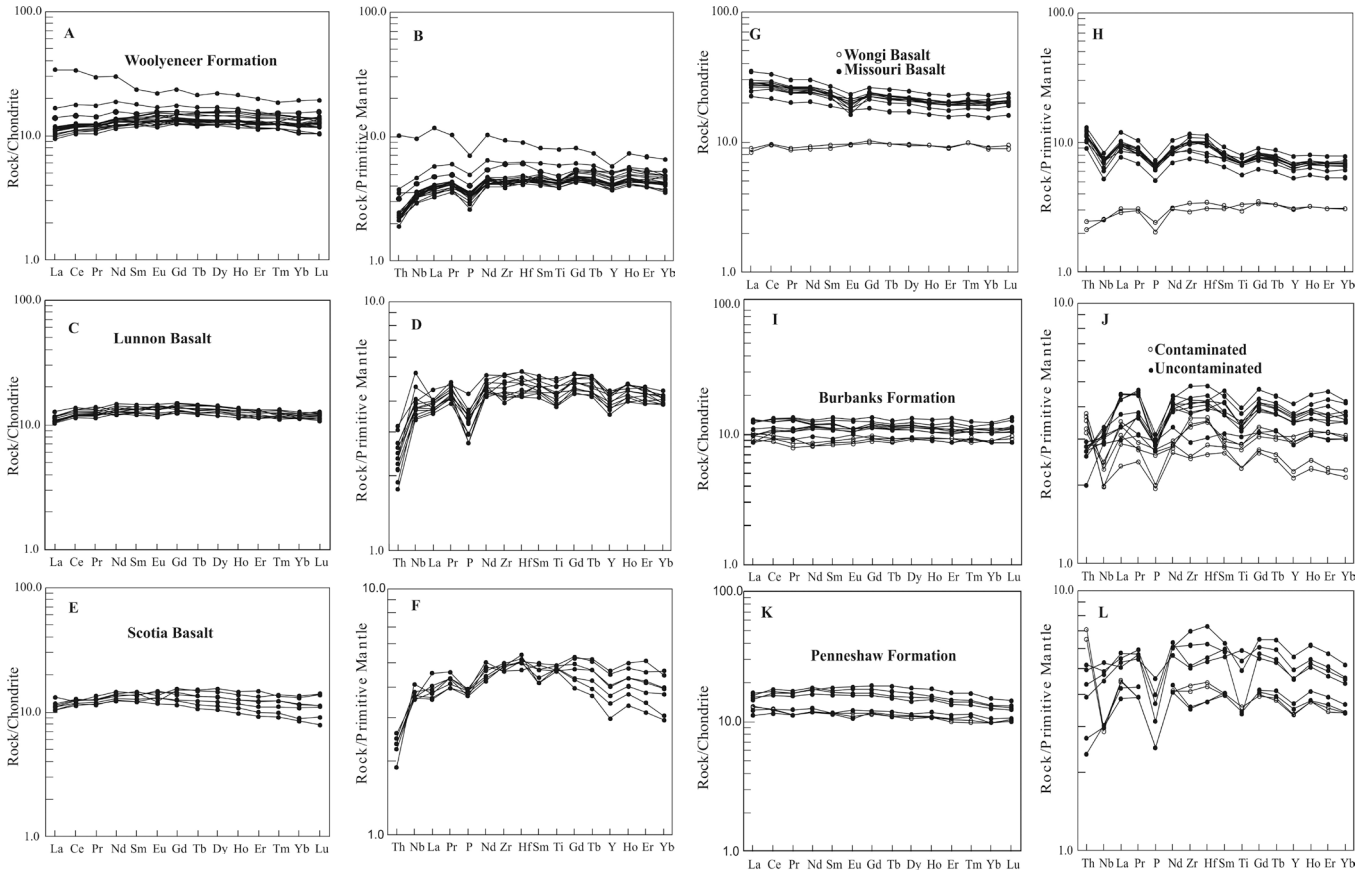

Figure 1. Chondrite and Primitive mantle normalised plots. Normalising values from Sun & McDonough (1989).

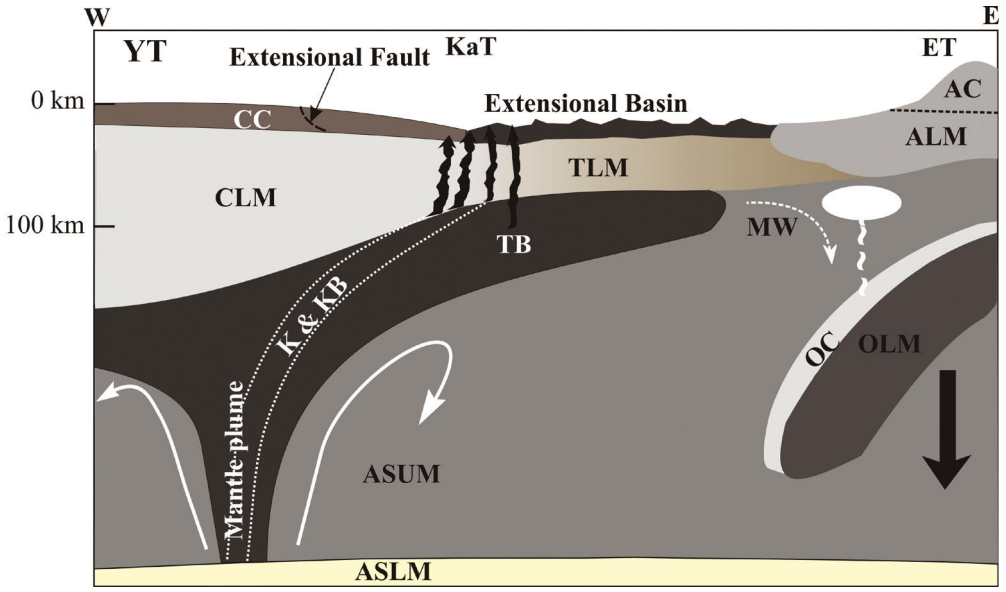

Figure 2. Model of Plume magmatism at a rifted cratonic margin for the Kambalda Sequence. AC=arc crust, ALM=arc lithospheric mantle, ASLM=asthenospheric lower mantle; ASUM=asthenospheric upper mantle, CC=continental crust, CLM=continental lithospheric mantle, K=komatiite, KB=komatiitic basalt, MW=mantle wedge, OC=oceanic crust, OLM= oceanic lithospheric mantle, TB=tholeiitic basalt, TLM=transitonal lithospheric mantle, YT=Youanmi Terrane; KaT=Kalgoorlie Terrane, ET=Eastern Terrane.

asthenosphere signatures. Some of the examined basalts record crustal contamination. Collectively, taken with field evidence for synvolcanic extension, these results are consistent with eruption of a mantle plume through, or more likely, impinging at the margin of rifted cratonic lithosphere mantle. Mantle plumes are deflected towards the margins of cratonic mantle roots where decompressional melting may occur over a range of depths, where hotter liquids assimilated crust but cooler liquids did not (cf. Sleep et al., 2002; Fig. 2). This process most likely accounts for the presence of both crustally contaminated and uncontaminated komatiite-basalt sequences. Accordingly, the Lower Basalt formations collectively record both craton margin as well as oceanic aspects of a mantle plume. Uncontaminated basalts have REE and multielement patterns akin to Phanerozoic intraoceanic plateau basalts, and differ from Phanerozoic continental flood basalts in lower TiO_2 contents and mostly flat HREE,

References

Kerrich R., Polat A., Wyman D. & Hollings P., 1999, Trace element systematics of Mg-, to Fe-tholeiitic basalt suites of the Superior Province: implications for Archean mantle reservoirs and greenstone belt genesis, Lithos 46, 163–187.

Lesher C.M. & Arndt N.T., 1995, REE and Nd isotope geochemistry, petrogenesis and volcanic evolution of contaminated komatiites at Kambalda, Western Australia, Lithos 34, 127–157.

Manikyamba C., Kerrich R., Khanna T.C., Satyanarayanan M. & Krishna A.K., 2008. Geochemical systematics of komatiite-tholeiite and adakitic-arc basalt associations: The role of mantle plume and convergent margin in formation of the Sandur Superterrane, Dharwar craton, India. Lithos, 155-172.

Redman B.A. & Keays R.R., 1985, Archean basaltic volcanism in the Eastern Goldfields, Yilgarn Block, Western Australia Precambrian Research, 30, 113–152.

Said N. & Kerrich R., 2009, Geochemistry of Coexisting Depleted and Enriched Paringa Basalts, in the 2.7 Ga Kalgoorlie Terrane, Yilgarn Craton, Western Australia: Evidence for a Heterogeneous Mantle Plume Event, Precambrian Research, 174, 287–309.

Sleep N.H., Ebinger C.J. & Kendall J.M., 2002, Deflection of, mantle plume material by cratonic keels, in *The Early Earth: physical, chemical and biological development,* Fowler C.M.R., Ebinger C.J. & Hawkesworth C.J., eds, Geological Society of London, Special Publication 199, 135–150.

Sun S-S. & Nesbitt R.W., 1978, Petrogenesis of Archean ultrabasic and basic volcanic — Evidence from rare earth elements, Contributions to Mineralogy and Petrology, 65, 301–325.

Sun S-S., Nesbitt R.W. & McCulloch M.T., 1989, Geochemistry and petrogenesis of Archean and early Proterozoic siliceous high-magnesian basalts, in *Boninites*, Crawford A.J. ed, Unwin Hyman, London, 149–173.

Sylvester P.J., Campbell I.H. & Bowyer D.A., 1997, Niobium/Uranium evidence for early formation of the continental crust, Science 275, 521–523.

Wyman D. & Kerrich R., 2009. Plume and Arc magmatism in the Abitibi subprovince: implications for the origin of continental lithospheric mantle, Precambrian Research, 168, 4–22.

DETRITAL ZIRCON EVIDENCE FOR THE CRATONIZATION OF THE NORTH CHINA CRATON

C. Liu[1], G. Zhao[1], M. Sun[1], F. Wu[2], J. Yang[2] & C. Yin[1]

[1]Department of Earth Sciences, The University of Hong Kong, Pokfulam Road, Hong Kong
[2]State Key Laboratory of Lithospheric Evolution, Institute of Geology and Geophysic, Chinese Academy of Sciences, P.O. Box 9825, Beijing 100029, China

Introduction

There is a broad consensus that the basement of the North China Craton was formed by amalgamation of the Eastern and Western Blocks along the Trans-North China Orogen (Fig. 1; Guo et al., 2005; Kröner et al., 2006; Kusky & Li, 2003; Li & Kusky, 2007; Liu et al., 2006; Wilde & Zhao, 2005; Wu et al., 2005; Zhao et al., 2005). However, a major debate has surrounded the timing and tectonic processes involved in the collision of the two blocks. Some researchers have suggested eastward-directed subduction with the collision at ~1.85 Ga (Kröner et al., 2006; Wilde & Zhao, 2005; Zhang et al., 2007; Zhao et al., 2005), whereas others have proposed westward-directed subduction with collision at ~2.5 Ga (Kusky & Li, 2003; Li & Kusky, 2007). The ~1.85 Ga collision model is mainly based on the following lines of evidence: (1) high-pressure granulites and retrograded ecologites in the Trans-North China Orogen are strongly deformed gabbroic dykes that were emplaced at ~1.92 Ga and experienced high-pressure metamorphism at ~1.85 Ga (Kröner et al., 2006); (2) ductilely deformed Paleoproterozoic granitoid gneisses in the orogen were emplaced between 2.36 Ga and 2.02 Ga, indicating that the main deformation in these areas is not Archean but Paleoproterozoic in age (Kröner et al., 2005); and (3) metamorphic zircons are present in both the Archean and Paleoproterozoic rocks of the orogen and yield consistent metamorphic ages of ~1.85 Ga (Guo et al., 2005; Liu et al., 2006; Zhao et al., 2008). In contrast, one of the major argument for the ~2.5 Ga collision model is the existence of the end-Archean (~2.5 Ga) Qinglong foreland basin, which extends N to NE up to 1600 km long along the eastern side of the Central Orogenic belt (Kusky & Li, 2003; Li & Kusky, 2007). Li & Kusky (2007) divided this foreland basin into the northern, middle and southern sectors, of which the northern sector is represented by the Qinglong Group in the eastern Hebei area, the middle sector includes the Gaofan and Hutuo Groups in the Wutaishan area and the Wanzi Group in the Taihangshan area, and the southern sector is represented by the Songshan Group in the Songshan area. However, these authors did not carry out detailed dating work on detrital zircons from these groups, which can provide constraints on the maximum depositional age of these groups, and thus it still remains unknown whether or not these groups were deposited in the Qinglong foreland basin at ~2.5 Ga. In this study, U-Pb isotopic compositions were analysed for detrital zircons of sandstone from the Hutuo and Yejishan Groups in the middle sector in order to determine the maximum depositional age and source rocks of the foreland basin, which can provide a significant constraint on the timing of the collision between the Eastern and Western Blocks along the Trans-North China Orogen.

Geological setting

The Wutai-Hengshan-Fuping mountain belt is situated in the central part of the Trans-North China Orogen (Fig. 1) and displays a NE-SW trending linear transecting the orogen. Unconformably overlying both the Wutai and Fuping Complexes is the Hutuo Group, which has been considered to be the youngest lithostratigraphic unit in the Hengshan-Wutai-Fuping belt. The Hutuo Group mainly locates to the south of the Wutai Complex, covering nearly one quarter the area of the belt. The group can be subdivided into three lithostratigraphic units. The lower Doucun Subgroup includes the Sijizhuang, Nantai and Dashiling Formations, consisting of basal conglomerate, quartzite, slate phyllite and volcaniclastic rocks, metamorphosed to greenschist facies. The middle Dongye Subgroup, which can be subdivided into the Qingshicun, Wenshan, Hebiancun, Yaochi, Beidaxing and Tianpengnao Formations, consists of clastic sediments, dolomite, marble and metavolcanic rocks metamorphosed to sub-greenschist to greenschist facies. The upper Guojiazhai Subgroup, which includes the Xiheli, Heishanbei and Diaowangshan Formations, is composed of clastic sediments, sandstones and another unit of conglomerate, which were interpreted as quick deposition of molasses formation (Bai et al., 1986). The Hutuo Group's total thickness has been estimated to be greater that 10km (Tian et al., 1991) and the structural and metamorphic studies in this region suggested that the Hutuo Group is characterized by semi-brittle folding to brittle faults and is considered as being involved into the orogenic event with the above three complexes, displaying similar structural geometries with the underlying Wutai Group (Tian et al., 1991).

The Lüliang Complex is located at the western margin of the middle segment of the Trans-North China Orogen and consists of Paleoproterozoic granitoid plutons and supracrustal rocks (Geng et al., 2006; Zhao et al., 2008). The supracrutal rocks have been divided into three major stratigraphic units: Jiehekou, Lüliang and Yejishan Groups (Geng et al., 2006). The Yejishan Group, also called the Lanhe or Heichashan Group in the Chinese literature, is exposed along a narrow, northeast-southwest-trending belt that extends from Dongmafang, through Yejishan and Heichashan, to Fangshan. The group is composed of three major units: the lower Qingyangshuwan Formation, the middle Bailongshan Formation and the upper Chengdaogou Formation. The Qingyangshuwan Formation consists of subgreenschist-facies metamorphosed feldspar-quartz sandstones, siltstones and thin beds of marbles, which is considered to have been deposited in littoral to shallow marine sedimentary environment. The Bailongshan Formation comprises weakly metamorphosed massive

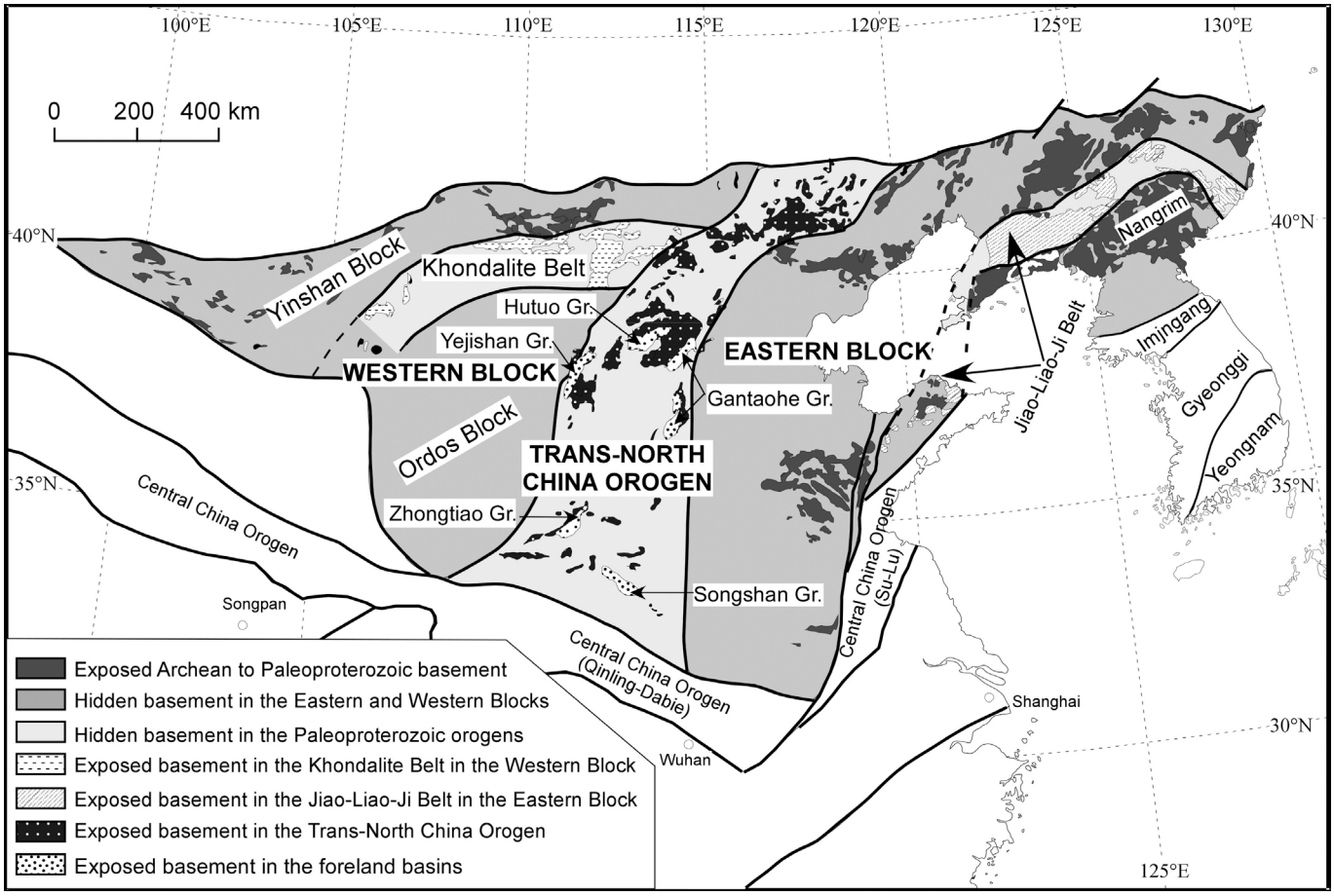

Figure 1. Tectonic subdivision of the North China Craton, modified from Zhao et al. (2005). Also shown are locations of the Paleoproterozoic foreland basins.

basalts and pillowed basalts with subordinate dacites, andesites, rhyolites and interbeds of siltstones and marbles followed upward by flysch-like thin-bedded fine-grained sandstones and siltstones, suggesting they formed under a deep water sedimentary environment. The Bailongshan Formation is unconformably overlain by the Chengdaogou Formation, which consists of thick layer conglomerates and coarse-grained sandstones with large-scale tabular oblique bedding and mud crack structures (Liu et al., 2009). These sedimentary rocks are similar to the Hutuo Group, which is interpreted as have developed in a foreland basin (Bai et al., 1986; Kusky & Li, 2003; Li & Kusky, 2007; Wilde et al., 2005; Zhao et al., 2001). Therefore, the ages of detrital zircons from the Hutuo and Yejishan Groups will place a powerful constraint on the controversial issue of whether the collision between the Eastern and Western Block along the Trans-North China Orogen occurred at the end-Archean (~2.5 Ga) or at the late Paleoproterozoic (~1.85 Ga).

Depositional ages of the Hutuo and Yejishan Groups and their constraints on the timing of final amalgamation of the North China Craton

In this study, the youngest concordant zircon grain of 1919±29 Ma achieved from the Hutuo Group does not belong to any significant age population, so without other independent information on the geology of likely provenance terrains this age can not be estimated as a reliable maximum depositional age for the Hutuo Group (Fig. 2a). However, this zircon age is the same with the emplacement ages of high-pressure granulite facies mafic dykes near Dashiyun in the Hengshan Complex (1915±4 Ma and 1914±2 Ma; Kröner et al., 2006) within their errors. The scarcity of magmatic zircon in the mafic dykes also explains why we only achieved single grain of this age. The electronic microprobe dating of monazite from prolonged granitic intrusion along the foliation of the Longquanguan ductile shear zone located between the Wutai and Fuping Complexes shows that the major deformation episode took place at 1877-1846 Ma (Zhao et al., 2006), which puts a firm minimum age on deposition of the deformed Hutuo Group.

237 detrital zircon grains from the lower, middle and upper sequences of the Yejishan Group were dated in this study. Although the ages of these detrital zircons cannot be applied to determination of depositional age of the Yejishan Group, the youngest ages around ~1843 Ma, as shown in Fig. 2b, can be used to constrain the maximum depositional time of the group if such aged zircons did not form during the metamorphism of the group. As mentioned before, the Yejishan Group only underwent greenschist facies metamorphism, which precludes the possibility that the ~1843 Ma zircons formed during the metamorphism of the Yejishan Group. Therefore, the youngest ages of ~1843 Ma can be regarded as the maximum depositional age of the Yejishan Group. On the other hand, the minimum depositional age of the metamorphosed and deformed Yejishan Group can be constrained by the emplacement ages of the unmetamorphosed and undeformed post-collisional

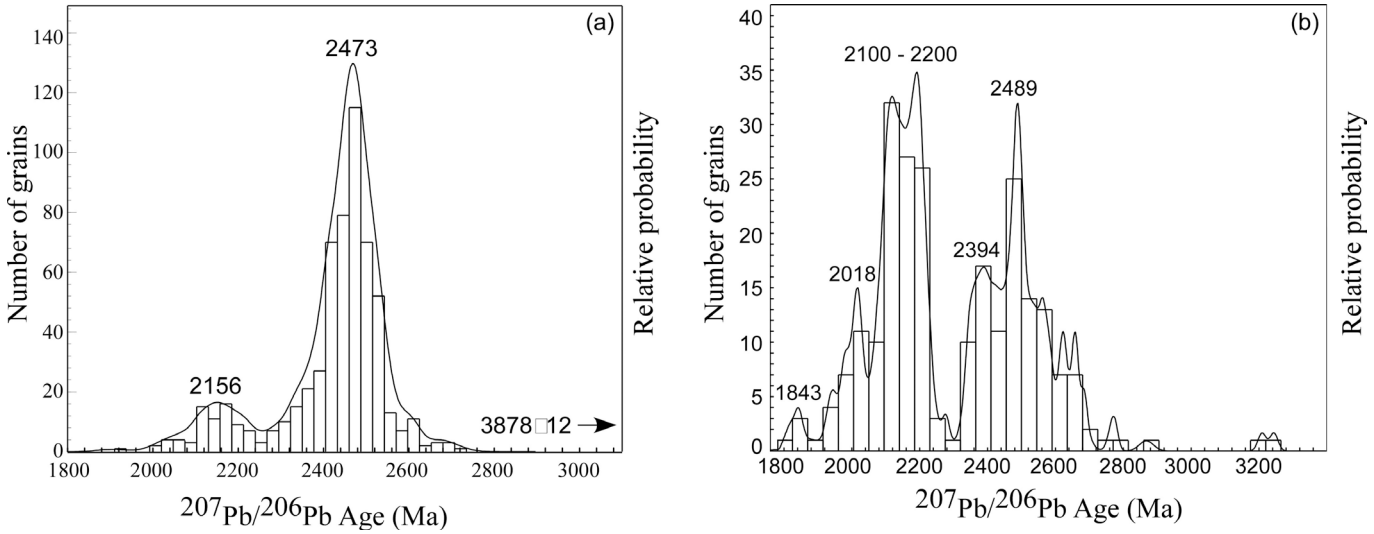

Figure 2. Histograms for the distribution of all $^{207}Pb/^{206}Pb$ ages obtained for detrital zircons from the (a) Hutuo Group and (b) Yejishan Group.

granites in the Lüliang Complex, including the 1815±5 Ma Luyashan charnockite, 1807±10 Ma Luchaogou porphyritic granite, 1798±11 Ma Guandishan massive granite and 1790±14 Ma Tangershan massive granite. Taken together, the depositional age of the Yejishan Group can be approximately bracketed between 1840-1800 Ma.

The determination of depositional ages of the Yejishan and Hutuo Groups places a rigorous constraint on the timing of the collision between the Eastern and Western Blocks along the Trans-North China Orogen to form the coherent basement of the North China Craton. As mentioned in the introduction, there are two contrasting schools of thought regarding the timing of the collision between the two blocks, with one arguing that the final collision occurred at ~2.5 Ga (Kusky & Li, 2003, Li & Kusky, 2007), whereas the other believes that it occurred at ~1.85 Ga (Zhao et al., 2001, 2005; Wilde et al., 2002; Kröner et al., 2005, 2006; Guo et al., 2005; Liu et al., 2006, Zhang et al., 2007, 2009). The major argument for the first model is that a series of foreland basins in the Trans-North China Orogen was speculated to have developed at the ~2.5 Ga (Kusky & Li, 2003; Li & Kusky, 2007). However, this is not supported by the data presented in this study, which indicate that the foreland basin at the middle sector of in the Trans-North China Orogen developed in the period 1.92-1.80 Ga, not at about 2.5 Ga. In contrast, our new data are well consistent with the model that the collision between the Eastern and Western Blocks to form the Trans-North China Orogen occurred at ~1.85 Ga (Zhao et al., 2001, 2005; Wilde et al., 2005; Kröner et al., 2005, 2006; Guo et al., 2005; Liu et al., 2006, Zhang et al., 2007).

Acknowledgements

This research was financially supported by Hong Kong RGC GRF grants (7063/06P, 7066/07P and 7053/08P). We thank Liewen Xie, Yueheng Yang, and Yanbing Zhang for their laboratory assistance. A HKU postgraduate studentship to Chaohui Liu is greatly acknowledged.

References

Bai J., 1986, The Precambrian crustal evolution of the Wutaishan area. In: J. Bai (Ed.), The Early Precambrian Geology of Wutaishan, Tianjin Science and Technology Press, Tianjin, 376–383.

Geng Y.S., Yang C.H. & Wan Y.S., 2006, Paleoproterozoic granitic magmatism in the Luliang area, North China Craton: constraint from isotopic geochronology, Acta Petrologica Sinica 22, 305–314.

Guo J.H., Sun M., Chen F.K. & Zhai M.G., 2005, Sm-Nd and SHRIMP U-Pb zircon geochronology of high-pressure granulites in the Sanggan area, North China Craton: timing of Paleoproterozoic continental collision, Journal of Asian Earth Sciences, 24, 629–642.

Kröner A., Wilde S.A., Li J.H. & Wang K.Y., 2005, Age and evolution of a late Archean to Paleoproterozoic upper to lower crustal section in the Wutaishan/Hengshan/Fuping terrain of northern China, Journal of Asian Earth Sciences 24, 577–595.

Kröner A., Wilde S.A., Zhao G.C., O'Brien P.J., Sun M., Liu D.Y., Wan Y.S., Liu S.W. & Guo J.H., 2006, Zircon geochronology and metamorphic evolution of mafic dykes in the Hengshan Complex of northern China: Evidence for late Palaeoproterozoic extension and subsequent high-pressure metamorphism in the North China Craton, Precambrian Research 146, 45–67.

Kusky T.M. & Li J.H., 2003, Paleoproterozoic tectonic evolution of the North China Craton, Journal of Asian Earth Sciences 22, 383–397.

Li, J.H. & Kusky, T., 2007, A late Archean foreland fold and thrust belt in the North China craton: Implications for early collisional tectonics, Gondwana Research, 12, 47–66.

Liu S.W., Zhao G.C., Wilde S.A., Shu G.M., Sun M., Li Q.G., Tian W. & Zhang J., 2006, Th-U-Pb monazite geochronology of the Luliang and Wutai Complexes: Constraints on the tectonothermal evolution of the Trans-North China Orogen, Precambrian Research, 148, 205–224.

Liu S.W., Li Q.G. & Zhang L.F., 2009. Geology, geochemistry of metamorphic volcanic rock suite in Precambrian Yejishan Group, Luliang mountains and its tectonic implications, Acta Petrologica Sinica, 25, 547–560.

Tian Y.Q., 1991, *Geology and Gold Mineralization of Wutai-Hengshan Greenstone Belt*, Shanxi Science and Technology Press, Taiyuan (in Chinese).

Wilde S.A. & Zhao G.C., 2005, Archean to Paleoproterozoic evolution of the North China Craton, Journal of Asian Earth Sciences, 24, 519–522.

Wu F.Y., Zhao G.C., Wilde S.A. & Sun D.Y., 2005, Nd isotopic constraints on crustal formation in the North China Craton, Journal of Asian Earth Sciences, 24, 523–545.

Zhang J., Zhao G.C., Li S.Z., Sun M., Liu S.W., Wilde S.A., Kröner A. & Yin C.Q., 2007, Deformation history of the Hengshan Complex: Implications for the tectonic evolution of the Trans-North China Orogen, Journal of Structural Geology, 29, 933–949.

Zhao, G.C., 2001, Palaeoproterozoic assembly of the North China Craton, Geological Magazine, 138, 87–91.

Zhao G.C., Sun M., Wilde S.A. & Li S.Z., 2005, Late Archean to Paleoproterozoic evolution of the North China Craton: key issues revisited, Precambrian Research, 136, 177–202.

Zhao G.C., Wilde S.A., Sun M., Li S.Z., Li X.P. & Zhang J., 2008, SHRIMP U-Pb zircon ages of granitoid rocks in the Luliang Complex: Implications for the accretion and evolution of the Trans-North China Orogen, Precambrian Research, 160, 213–226.

Zhao L., Zhang J.J. & Liu S.W., 2006, Syn-deformational granites of the Longquanguan ductile shear zone and their monazite electronic microprobe dating, Acta Petrologica et Mineralogica, 20, 210–218 (in Chinese).

TEMPORAL CONSTRAINTS ON THE EVOLUTION OF THE SINGBHUM CRUSTAL PROVINCE FROM U-Pb SHRIMP DATA

R. Mazumder[1], S. Reddy[2] & C. Clark[2]

[1]Geological Studies Unit and Fluvial Mechanics Laboratory, Indian Statistical Institute, 203, B.T. Road, Kolkata 700108, India. mrajat@isical.ac.in
[2]The Institute for Geoscience Research, Dept of Applied Geology, Curtin University of Technology, GPO Box U1987, Perth, WA 6845, Australia.

The Singhbhum Crustal Province (SCP), eastern India, is among one of the few Precambrian terrains in the world that records purported sedimentation and volcanism in varying tectonic regimes from the Mesoarchaean to Neoproterozoic eras. However a lack of precise age data from the SCP, particularly U-Pb, is a major impediment in constraining the tectonic evolution of the SCP and its regional and intercontinental correlation. 45 new SHRIMP II U-Pb zircon analyses from the Singhbhum Granite Phase III, the youngest basement on which younger supracrustal successions are deposited, are variably discordant and define a single trend with upper and lower age intercepts of 893 ± 43 Ma and 3302 ± 13 Ma, respectively. A subset of 11 analyses of <5% discordant analyses give a $^{207}Pb/^{206}Pb$ age of 3288 ± 8 (2σ) Ma. The youngest Proterozoic alkaline rock bodies in the SCP succession (Sushina nepheline syenite) yields an age of 922.4 ± 10.4 Ma (2σ) that is within error of the lower intercept from the Singhbhum Granite Phase III isotopic distribution. Our internally consistent data record part of both the original basement history during the Mesoarchaean as well as that of the youngest Neoproterozoic alkaline magmatism in the SCP and pin the stratigraphic evolution of the SCP.

Samples from the Dhalbhum and Chandil Formations volcanic rocks commonly contain multiple populations of grains with a range of Palaeoproterozoic to Neoarchaean ages. However, a single sample of Chandil Formation Rhyolite contains a single, largely concordant, igneous population that record an age of 1629 ± 5 Ma(2σ) . This age is similar to the youngest ages recorded in other sample population from other volcanic rocks of the Chandil Formation and stratigraphically lower Dhalbhum Formation (youngest grain population ~1740 Ma). These data constrain the intervening Dalma Volcanics to be late Paleoproterozoic in age (1740-1630 Ma). These data indicate that much of the volcanic succession recorded in the SCP represents a geologically brief (~100 Ma) episode of both acidic and basic magmatism.

In a reconstructed Gondwana, the Singhbhum Craton is inferred to lie adjacent to the Vestfold Hills in East Antarctica and along the northern margin of a wide region of Neoproterozic orogenesis that marks one of the major Gondwana forming collision zones. The correlation is based primarily on the similarities between the Eastern Ghats in India and the Ruker Terrain in East Antarctica and the assumption that the relationships of the terranes within India and Antarctica today are unchanged. However prior to the amalgamation of Gondwana the relative position of the Singhbhum Craton relative to the East Antactic terranes is poorly constrained. Recent detrital zircon studies of the Vestfold Hills indicate that during deposition of the Chelnok Supracrustals, zircons were being sourced from regions with ages of 3.7, 3.2 and 2.8 Ga. Two of these ages (3.2 and 2.8 Ga) are ages of volcanism and granite emplacement suggesting that the Vestfold Hills may have sourced material from the Singhbhum craton and was therefore proximal to India for a long period of time prior to the amalgamation of Gondwana. Whether the Singhbhum Craton was part of proto-Antarctica or vice-versa needs further detailed geochronological investigation.

AN ARCHAEAN SUPERCONTINENT "SIWA": SPATIO-TEMPORAL AND PALAEOMAGNETIC EVIDENCE

S. Mohanty

Department of Applied Geology, Indian School of Mines, Dhanbad 826004, India

Introduction

Application of the concepts of plate tectonics for identification of supercontinents during Archaean and Palaeoproterozoic time is facilitated by several key attributes. By using palaeomagnetic and spatio-temporal attributes, it is demonstrated here that the South Indian and Yilgarn cratons were juxtaposed with each other at ~2400 Ma. This supercontinental block is termed here as "SIWA" – an acronym for South India and Western Australia.

Palaeomagnetic attributes

Analysis of palaeomagnetic data of key poles of ~2400 Ma mafic dykes from the Dharwar craton of South India and the Yilgarn craton of Western Australia (Halls et al. 2007) led to the suggestion that the South Indian block and the Western Australia were located at high latitude (Fig. 1a). The present analysis takes the antipodal point of the Widgiemooltha dyke (used by Halls et al. 2007) which is possibly equivalent to the YA dyke of the Perth area analysed by Giddings (1976), and suggests to place the Western Australia along the east coast of India (Fig. 1b). In this configuration the Yilgarn craton is proposed to be placed at the position of the Eastern Ghats, a Mesoproterozoic to Neoproterozoic orogenic belt on the east coast of India. The proposed configuration shows very good geometrical matching of the boundaries of >2400 Ma terranes (Fig. 1c). The orientation of mafic dykes in the South Indian and Yilgarn cratons show identical orientation patterns. The orientations of magnetic north directions determined from the palaeomagnetic data for ~2400 Ma mafic dykes of Dharwar and Yilgarn cratons also show identical orientation in this configuration (Fig. 1c). Thus, palaeomagnetic information indicates proximity of South India and Western Australia at ~2400 Ma.

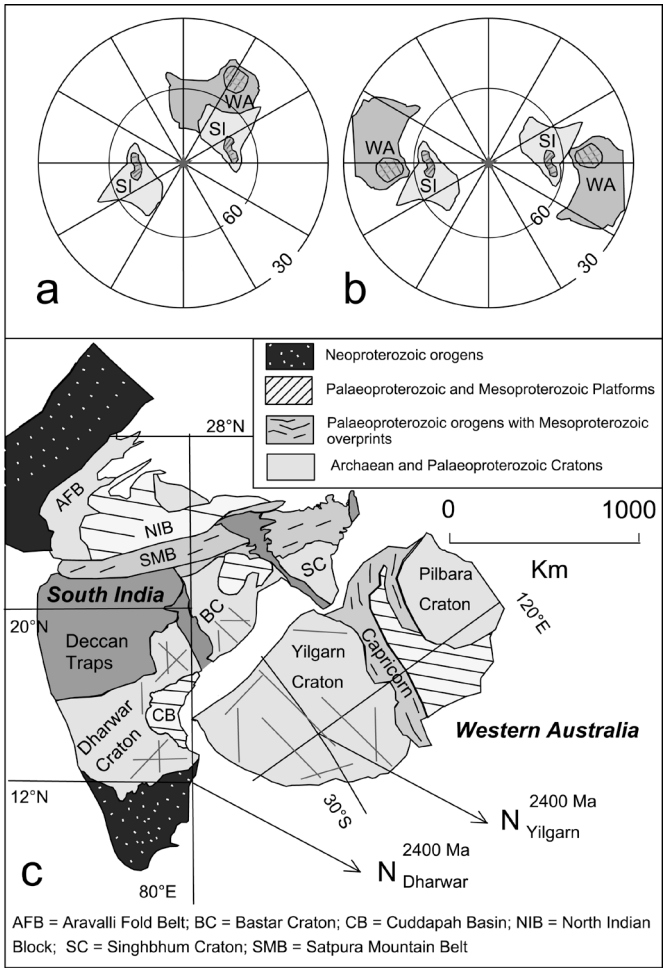

Spatio-temporal attributes

Detailed examination of the evolutionary history of the South Indian and Western Australian cratons indicate that both the blocks have >3400 Ma age TTG suite of rocks as the oldest components. These ancient basement gneisses were followed by the development of older greenstone terranes (containing flood basalts and BIF succession) between 3400 and 3300 Ma, which were affected by high-grade (amphibolites-granulite) metamorphism at ~3300 Ma and granite plutons at ~3100 Ma. An auriferous younger greenstone succession (containing flood basalts, acidic flows and BIF) along with granites developed in the South Indian and Yilgarn cratons between 2900 and 2600 Ma. The late Archaean events of both these cratonic blocks include intrusions of high-K granites of 2540 to 2460 Ma age, and high to medium grade metamorphism. Intrusions of mafic dyke swarms mark an extensional regime at ~2400 Ma, possibly related to the breaking of the supercontinent. Two more swarms of mafic dykes in the South Indian cratons belong to ~2100 Ma and ~1900 Ma age. These dyke swarms were possibly related to the prolonged breaking process. Comparison of spatio-temporal data of the North Indian block and the Western Australian block led Mohanty (2010) to suggest that the Satpura orogeny of Central India is coeval with the Capricorn orogeny between the Yilgarn and Pilbara cratons. Therefore, the final breaking of "SIWA" at ~2000 Ma led to the development of the Cuddapah basin at the margin of the South Indian craton, and amalgamation of Yilgarn and Pilbara cratons along the Glenburgh orogen.

Figure 1. An Archaean Supercontinent "SIWA" at ~2400 Ma. (a) South polar projection of South India (SI) and Western Australia (WA) based on palaeomagnetic data for 2367 Ma mafic dykes of Dharwar craton and 2415 Ma Widgiemooltha dyke (after Halls et al. 2007). (b) Modified south polar projection by taking antipodal data of Widgiemooltha dyke and by placing Australia along the east coast of India at ~2400 Ma (present work). (c) The proposed model, showing geometrical matching of craton margin configuration, dyke orientations and palaeo-north directions.

Conclusions

Analysis of palaeomagnetic and spatio-temporal data from the South Indian and Yilgarn cratons indicate their joint evolution at least up to 2400 Ma. The mafic dyke swarms of both the blocks show matching orientations in the reconstructed geometry. However, these dykes are of at least three different ages. More detailed geochronological and palaeomagnetic studies of these dyke swarms would constrain the dispersal event of the supercontinent.

References

Giddings J.W., 1976, Precambrian paleomagnetism in Australia I: basic dykes and volcanic from the Yilgarn Block, Tectonophysics, 30, 91–108.

Halls H.C., Kumar A., Srinivasan R. & Hamilton M.A., 2007, Paleomagnetism and U-Pb geochronology of easterly trending dykes in the Dharwar craton, India: feldspar clouding, radiating dyke swarms and the position of India at 2.37 Ga, Precambrian Research, 155, 47–68.

Mohanty S., 2010, Tectonic evolution of the Satpura Mountain Belt: a critical evaluation and implication on supercontinent assembly, Journal of Asian Earth Sciences, in press.

TECTONIC EVOLUTION OF THE NORTH ATLANTIC CRATON AND THE FORMATION OF CONTINENTAL CRUST 3.8-2.6 Ga

J.S. Myers

Two main features dominated the tectonic evolution of the Earth and the nature of continental crust: gravity and heat loss. Gravity led to relatively uniform stratification of the Earth. Heat loss was more heterogeneous and manifest through rising magma, plumes and Mantle convection. These led to sub-horizontal movements of coherent slabs of the Earth's crust, plate tectonics, further enhancing stratification caused by gravity and the most prominent feature of continental crust, sub-horizontal layering on all scales from tens of km to mm thick over hundreds to thousands of km².

Sub-horizontal layering and the processes by which it formed are well illustrated in the Archean gneiss complex of southwest Greenland, the best known part of the North Atlantic Craton. Key elements of this complex that best reveal the tectonic processes through time are the 3.8-3.7 Ga Isua greenstone belt, 3.1 Ga Ivisaartoq greenstone belt, and 2.9 Ga Fiskenæsset and Nunataarsuk anorthosite complexes. These units contain remnants of primary stratigraphy from which it is possible to determine original way-up of rock sequences, the evolution of thrust belts, and the facing directions of the first, recumbent, fold structures.

Although similar tectonic processes occurred between at least 3.8 and 2.6 Ga, there were two distinct patterns of crustal growth. One resembles that of post-Archean plate tectonics in which continental crust was generated and tectonically reworked in relatively narrow, steeply dipping arcs or linear belts of great lateral extent that developed along, or were accreted to, continental margins. The other formed by the intrusion of sills of granitoid magma into basaltic rocks and sub-horizontal translation and stacking as sub-horizontal slabs over hundreds of km². Within the Archean gneiss complex of southwest Greenland there was no temporal evolution in these patterns of crustal growth. Both kinds of plate tectonic process coexisted throughout the Archean.

The Isua greenstone belt (Myers 2001, 2009, Nutman & Friend 2009) formed by amalgamation of >3.8 Ga basaltic rocks and a 3.8 Ga tonalite batholith with >3.7 Ga basaltic arcs and 3.7 Ga tonalite before 3.66 Ga. The rocks were repeatedly intercalated by thrusts and folded into recumbent isoclinal folds before the intrusion of dolerite and norite dykes at 3.5 Ga. They were further stacked in a thrust belt followed by the intrusion of a tonalite batholith at 3.0 Ga into a 3.07 Ga volcanic arc of basalt and andesite (Garde 2007).

The Ivisaartoq greenstone belt (Chadwick 1990, Mader 2005, Polat et al. 2007) comprises two units of mainly basaltic amphibolite that formed in different geological environments. One unit is interpreted as a remnant of a juvenile island arc formed in a supra-subduction zone in oceanic crust (Polat et al. 2007) whereas the other is interpreted as volcanic deposits erupted through and onto older continental crust (Mader 2005). The first unit was folded into recumbent isoclinal folds and the second unit was heterogeneously deformed before the two slabs of crust were tectonically juxtaposed at 3 Ga and further deformed together.

The Fiskenæsset and Nunataarsuk anorthosite complexes have the best preserved and best exposed igneous stratigraphy of any Archean anorthosite complexes known on Earth. The stratigraphy and structure of the Fiskenæsset complex were discovered in the 1970's (Myers 1985) but those of Nunataarsuk were only recently determined by detailed mapping (Myers unpublished, Geological Survey of Denmark and Greenland, Copenhagen). Each complex was intruded as multiple pulses of magma to form a sill <1 km thick extending over several hundred km² in basaltic volcanic rocks. The Nunataarsuk complex was folded into recumbent isoclinal folds, cut by thrusts and imbricated about 100 million years before the intrusion of sheets of tonalite, whereas the Fiskenæsset complex was cut by thrusts and imbricated for the first time during the intrusion of tonalite along thrust planes. In both cases the anorthosite complexes were overwhelmed by tonalite that forms 80% of the Archean gneiss complex in these regions. However, the tonalite was intruded as sheets sub-parallel to the igneous stratigraphy of the anorthosite complexes. The anorthosite complexes now occur as thin layers and trains of inclusions of parts of the igneous stratigraphy that was disrupted in an orderly way by thrust complexes. The thrust complexes are especially well preserved in the Nunataarsuk anorthosite complex on the nunatak of Nunataarsuk where there was little disruption by granitoid magma and this will be a focus of the presentation. There the first major episode of folding, imbrication and thrust stacking was followed >200 million years later at 2.65 Ga by a second, similar, episode but at this time thrusting was accompanied by the intrusion of sheets of granite and granitic pegmatite along the thrust planes.

These complex flat-lying structures were folded by two sets of large-scale upright open folds with orthogonal axial surfaces that produced dome-and-basin fold interference structures. The recumbent isoclinal folds and thrust structures of the Fiskenæsset complex were also refolded by similar large-scale upright open folds with orthogonal axial surfaces.

Each anorthosite complex now extends over several hundred km² and comprises individual layers of igneous stratigraphy that can be followed around recumbent

isoclinal folds with amplitudes of >30 km. Nowhere is a deep crustal section exposed and therefore all the rocks in each region appear to reflect a relatively thin slab of crust dominated by sub-horizontal intrusions, recumbent isoclinal folds and thrust complexes, bounded by sub-horizontal detachments both above and below.

These conclusions support previous general concepts that the gneiss complex of southwest Greenland is composed of a number of different fragments of continental crust: terranes of Friend et al. (1988) and Friend & Nutman (2005) and tilted crustal blocks of Windley & Garde (2009), but are different in detail. The models of Friend et al. (1988) and Friend & Nutman (2005) are largely based on the ages of rock units rather than on structures, and the model of Windley & Garde (2009) lacks attention to detail and is over simplistic, largely based on the presence or absence of prograde granulite facies metamorphism overprinting the youngest fold structures. Their interpretation that the style of deformation changes downwards within the crustal blocks from metavolcanic belts with only one episode of isoclinal folding to gneisses with polyphase fold interference structures is unsupported by the structure of regions containing the Fiskenæsset and Nunataarsuk anorthosite complexes. Likewise their proposed block boundaries in some parts of these regions cut across, rather than divide, rock units and structures.

The structure and tectonic evolution of the Fiskenæsset and Nunataarsuk anorthosite complexes indicate that parts of the gneiss complex of southwest Greenland reflect tilted, perhaps imbricated, sheets or slabs of crust a few km thick, rather than comprising tilted blocks exposing crustal sections of microcontinents. Each slab represents a relatively thin sheet of continental crust thickened by recumbent isoclinal folding and thrust stacking. These slabs of crust are not necessarily different tectonostratigraphic terranes or parts of different continents.

The Mesoarchean (Gradstein et al. 2004) slabs of continental crust containing the Fiskenæsset and Nunataarsuk anorthosite complexes largely formed through the intrusion of sub-horizontal, thin sheets of granitoid magma, mainly tonalite, over hundreds of km². This process of crustal growth was most prevalent in the Archean and subsequently little known. However, in contrast, the crustal slabs containing the Eoarchean Isua and Mesoarchean Ivisaartoq greenstone belts evolved by accretion of volcanic arcs against older rafts of continental crust, a process that is well known throughout time.

Acknowledgements

Thanks are expressed to the Geological Survey of Denmark and Greenland, the Greenland Bureau of Minerals and Petroleum, the Isua Multidisciplinary Research Project supported by the Danish National Science Research Council and Commission for Scientific Research in Greenland, and the Natural Sciences and Engineering Research Council of Canada for supporting fieldwork in Greenland.

References

Chadwick B., 1990, The stratigraphy of a sheet of supracrustal rocks within high-grade orthogneisses and its bearing on Late Archaean structure in southern West Greenland, Journal of the Geological Society of London, 147, 639–652.

Friend C.R.L & Nutman A.P., 2005, New pieces to the Archaean terrane jigsaw puzzle in the Nuuk region, southern West Greenland: steps in transforming a simple insight into a complex regional tectonothermal model, Journal of the Geological Society of London, 162, 147-162.

Friend C.R.L., Nutman A.P. & McGregor V.R., 1988, Late Archaean terrane accretion in the Godthåb region, southern West Greenland, Nature, 335, 535–538.

Garde A.A., 2007, A mid-Archaean island arc complex in the eastern Akia terrane, Godthåbsfjord, southern West Greenland, Journal of the Geological Society of London, 164, 565–579.

Gradstein F.M., Ogg J.G., Smith A.G., Bleeker W. & Lourens L.J., 2004, A new geologic time scale with special reference to Precambrian and Neogene, Episodes, 27, 83–100.

Mader M.M., 2005, From genesis to juxtaposition: the evolution of the Ivisârtoq greenstone belt, southwest Greenland, Unpubl MSc Thesis, Memorial University, Canada.

Myers J.S., 1985, Stratigraphy and structure of the Fiskenæsset Complex, southern West Greenland, Grønlands Geol. Unders., Bulletin. 150.

Myers J.S., 2001, Protoliths of the 3.8-3.7 Ga Isua greenstone belt, West Greenland, Precambrian Research, 105, 129-141.

Myers J.S., 2009, The nature and evolution of the Earth's oldest continental crust – interpreting the field evidence at Isua in Greenland, in *Evolution of the continental crust*, Abstracts, 17, Geological Society of London.

Nutman A.P. & Friend C.R.L., 2009, New 1:20,000 scale geological maps, synthesis and history of investigation of the Isua supracrustal belt and adjacent orthogneisses, southern West Greenland: a glimpse of Eoarchaean crust formation and orogeny, Precambrian Research, 172, 189–211.

Polat A., Appel P.W.U., Fryer B., Windley B., Frei R., Samson I.M. & Huang H., 2009, Trace element systematics of the Neoarchean Fiskenæsset anorthosite complex and associated meta-volcanic rocks, SW Greenland: evidence for a magmatic arc origin, Precambrian Research, 175, 87–115.

Windley B.F. & Garde A.A., 2009, Arc-generated blocks with crustal sections in the North Atlantic craton of West Greenland: crustal growth in the Archean with modern analogues, Earth-Science Reviews, 93, 1–30.

ABORTED CRATONISATION OF JUVENILE EOARCHAEAN CRUST - ITSAQ GNEISS COMPLEX (GREENLAND): IMPLICATION FOR ANCIENT CRUSTAL PRESERVATION

A.P. Nutman[1] & C.R.L. Friend[2]

[1]School of Earth and Environmental Sciences, University of Wollongong, Wollongong, Australia
[2]45, Stanway Road, Headington Oxford OX3 8HU, UK

The Eoarchaean Itsaq Gneiss Complex (Greenland) consists of 3890-3690 Ma convergent plate boundary magmatic assemblages (tonalites intruded into arc picrites-basalts-andesite-dacites and rare rhyolites, layered gabbros, dunite slivers and chemical sediments) that were amalgamated by 3660 Ma. From shortly after the last amalgamation event, crustal heating coupled with extension initiated a >100 m thick detachment (3640-3600 Ma) of lower amphibolite facies low $\delta^{18}O$ mylonite filled with tectonised granite (sensu stricto) sheets and lithons. This is preserved locally at the northwestern edge of the Isua area. This separated the Complex at 3640-3600 Ma into an upper plate (most of the Isua area) with low-amphibolite to locally upper greenschist metamorphism and intruded by discrete low $\delta^{18}O$ granite sheets, from most of the rest of the Complex, which lies in the lower plate with repeated upper-amphibolite to granulite facies metamorphism, intense ductile deformation, migmitization and anatexis producing granites, coeval with several episodes of gabbro-diorite intrusion. Low $\delta^{18}O$ signatures have not yet been detected in these lower crustal migmatites. This extension had finished by *c*. 3590 Ma, because by then 3620-3600 Ma detrital sedimentary rocks had been infolded with migmatised orthogneisses and metamorphosed. The >3600 Ma Uivak (Labrador) and Narryer (Western Australia) Gneiss Complexes have similar histories to the lower plate in the Itsaq Gneiss Complex. We propose that early Archaean regimes of protracted (≥50 million years) largely extensional deformation greatly thinned the affected ancient crust, laying it bare for easier destruction by later tectonic forces and incorporation into younger magmatic rocks. This mechanism would reduce the chances of survival of ancient crust and obliterated most of the structural geological record related to juvenile crust formation in arc-like convergent plate boundary settings, only a short time before. A young analogue could be the Mesozoic-Holocene decratonisation of the North China Craton that was initiated shortly after Mesozoic terrane amalgamation with tectonic thickening.

EPISODIC CRUSTAL GROWTH IN THE NORTHEAST YILGARN CRATON, WESTERN AUSTRALIA: IMPLICATIONS FOR CRATON EVOLUTION

M.J. Pawley[1], S. Wyche[2], C.E. Hall[1], S.S. Romano[2], M.P. Doublier[1], M.T.D. Wingate[2] & C.L. Kirkland[2]

[1]Geological Survey of Western Australia, PO Box 1664, Kalgoorlie, WA 6433, Australia
[2]Geological Survey of Western Australia, 100 Plain Street, East Perth, WA 6004, Australia

Introduction

The rocks in the northeast Yilgarn Craton, Western Australia, have been the subject of a recent mapping program by the Geological Survey of Western Australia in the first detailed study of this area. Early results have indicated that the Burtville Terrane, proposed by Cassidy et al. (2006), actually represents two terranes with distinct greenstone stratigraphies that are separated by the Yamarna Shear Zone (Pawley et al. 2009). The new subdivision consists of a western Burtville Terrane, comprising greenstone rocks that are older than c. 2740 Ma, and a younger, eastern Yamarna Terrane that comprises mainly <2720 Ma greenstones. In this abstract, the term "northeast Yilgarn Craton" will apply to the combined Burtville and Yamarna Terranes.

The compilation of greenstone and granite U–Pb SHRIMP zircon geochronology in the northeast Yilgarn Craton indicates there were four main periods of crustal growth in the Burtville Terrane between c. 2970 and 2635 Ma, with only the youngest episode recorded in the rock record of the Yamarna Terrane. This abstract will present the age distribution and characteristics of the main episodes of crustal growth in the northeast Yilgarn Craton, compare these episodes with the rest of the Yilgarn Craton, and propose a broad geodynamic model for the eastern part of the craton to explain the rock distribution.

c. 2969–2910 Ma

The oldest rocks recognized in the northeast Yilgarn Craton are found at Mount Strawbridge in the northern Burtville Terrane. This area includes a metamorphosed succession of tholeiitic basalt with minor felsic volcanic rocks and quartzite. A metadacite from this area has a SHRIMP U–Pb zircon age of 2961 ± 5 Ma (193363; GSWA in prep.), and detrital zircons from a quartzite from near the dacite have an almost continuous age spectrum from 2969 to 2910 Ma (185979; GSWA in prep.). Felsic intrusive rocks of this age have also been recognized from within the Burtville Terrane, including a 2932 ± 3 Ma metagranite (179449; GSWA in prep.), and a 2939 ± 6 Ma orthogneiss (GA 2001969122; Dunphy et al. 2003). Young granites in the Burtville Terrane have populations of xenocrystic zircons that range from 2960 to 2921 Ma.

Rocks with similar ages are observed elsewhere in the Yilgarn Craton. The Penneshaw Formation in the southern Kalgoorlie Terrane has been dated at c. 2950–2930 Ma (Nelson, 1997), and likely represents a basement fragment underlying the <2720 Ma Kambalda Sequence (Kositcin et al. 2008). A meta-conglomerate from Dingo Range in the Kurnalpi Terrane, the adjacent terrane to the west of the Burtville Terrane, contains a population of c. 2970–2930 Ma detrital zircons (GA 2001967056; Dunphy et al., 2003). In the southern Youanmi Terrane, in the western part of the Yilgarn Craton, porphyritic microgranites have been dated at 2921 ± 4 Ma in the Parker Dome (Wang et al. 1996), and 2934 ± 7 Ma in the Ghooli Dome (Mueller and McNaughton, 2000). Evidence of c. 2960–2920 Ma volcanism and granite magmatism has also been reported in the western part of the Youanmi Terrane (Van Kranendonk & Ivanic 2009).

c. 2810–2800 Ma

Magmatism at c. 2810–2800 Ma has been recognized in several areas across the northeast Yilgarn Craton. In the northwestern Burtville Terrane, a sequence of basalt and komatiitic basalt overlain by intermediate to felsic volcaniclastic rocks is dated at 2805 ± 5 Ma, and intruded by minor intermediate and felsic porphyries dated at 2804 ± 6 Ma, (Kositcin et al. 2008). The 2812 ± 5 Ma Swincer Dolerite (Wingate et al. in press a), intruded a package of tholeiitic basalts with minor komatiitic basalt (now metamorphosed to tremolite schists) in the eastern part of the Burtville Terrane to form a series of sub-volcanic sills. Non-outcropping c. 2711 Ma orthogneiss from the northern Yamarna Terrane, sampled from drill core, has a population of xenocrystic zircons dated at c. 2815–2800 Ma (Cassidy 2007b).

Rocks of this age have been found in the Kurnalpi Terrane at Windarra, where a basalt sequence, with minor ultramafic and felsic volcaniclastic rocks, has been dated at c. 2810–2790 Ma (Kositcin et al. 2008). A mafic layered intrusion central-eastern Youanmi Terrane has an emplacement age of c. 2807 Ma (Riganti et al. this volume). In the northwestern Youanmi Terrane, supracrustal rocks of the Norie Group were deposited between c. 2814 and c. 2800 Ma, and mafic and ultramafic layered intrusions of the Boodanoo and Meeline Suites were emplaced at c. 2800 Ma (Van Kranendonk & Ivanic 2009).

c. 2775–2735 Ma

Between c. 2775 and c. 2735 Ma, there are three main periods of greenstone deposition across the northeast Yilgarn Craton. The first stage, which occurred across the Burtville Terrane at c. 2775–2760 Ma, resulted in the felsic volcanic and volcaniclastic rocks of the c. 2770 Ma Palkapiti Formation (183118 and 178112; GSWA in prep.) in the east, which overlies ultramafic and mafic volcanic rocks, clastic sedimentary rocks, and

banded iron-formation. Felsic magmatism at this time is indicated by a 2761 ± 11 Ma metagranite in the eastern Burtville Terrane (185969; GSWA in prep.). A dacitic volcaniclastic rock of the Hanns Jasper Formation in the southern part of the Burtville Terrane has been dated at 2774 ± 5 Ma (193362; GSWA in prep.), and in the same area, there are orthogneisses with protolith ages ranging from 2770 to 2765 Ma, which likely represent the magmatic equivalent of the dacitic rocks. The c. 2711 Ma orthogneiss in the Yamarna Terrane has a population of c. 2775–2770 Ma xenocrystic zircons (Cassidy 2007b).

Magmatism between c. 2775 and c. 2760 Ma is common across the Yilgarn Craton. In the Kalgoorlie Terrane, porphyry with an age of 2770 ± 3 Ma (Dunphy et al. 2003) intruded the greenstones near Wiluna. Farther west, the Polelle Group, in the western Youanmi Terrane, was undergoing a transition from mafic volcanism of the Meekatharra Formation to felsic volcanism of the Greensleeves Formation (Van Kranendonk and Ivanic, 2009). Also in the western Youanmi Terrane, granites of the Cullculli Suite of the Annean Supersuite range in age from c. 2800 to c.2750 Ma (Van Kranendonk & Ivanic, 2009). In the southern part of the Youanmi Terrane, a granite gneiss from the Ghooli Dome has been dated at 2775 Ma (Mueller & McNaughton, 2000).

The second stage resulted in mafic magmatism across the Burtville Terrane at c. 2755 Ma. The 2755 ± 5 Ma Mapa Igneous Complex is a layered mafic intrusion that intruded mafic volcanic rocks in the northeastern part of the Burtville Terrane (Wingate et al. in press b). A hornblende plagiogranite from the northwestern Burtville Terrane, also dated at 2755 ± 5 Ma, is interpreted to be the fractionated felsic component of a layered gabbro (Fletcher et al. 2001) that intruded metamorphosed mafic and ultramafic volcanic rocks. A c. 2751 Ma xenocrystic zircon was found in the c. 2711 Ma orthogneiss from the Yamarna Terrane (Cassidy, 2007b).

The c. 2755 Ma rocks in the northeast Yilgarn Craton are contemporaneous with felsic volcanic and volcaniclastic rocks of the Greensleeves Formation in the Polelle Group, and the Annean Supersuite, both in the western Youanmi Terrane (Van Kranendonk & Ivanic 2009).

The final stage of magmatism between c. 2775 Ma and c. 2735 Ma, that between c. 2740 and c. 2735 Ma, includes both mafic and felsic magmatism. The 2737 ± 26 Ma Argus Igneous Complex (185970; GSWA in prep.) is a small, layered anorthosite and gabbro sill that is hosted by highly strained mafic rocks in the hangingwall of the Yamarna Shear Zone, which probably represents a piece of the Burtville Terrane that was tectonically interleaved into the Yamarna Terrane. In the southern part of the Burtville Terrane, an orthogneiss has a protolith age of 2738 ± 3 Ma (193410; GSWA in prep.). In the Yamarna Terrane, a 2740 Ma xenocrystic zircon has been found in a dacite of the Toppin Formation.

The c. 2740–2735 Ma magmatism in the northeast Yilgarn Craton is contemporaneous with several rock units from other parts of the craton. These include the 2736 ± 3 Ma Kathleen Valley Gabbro from the eastern Youanmi Terrane (Liu 2007), c. 2735 Ma felsic magmatic and volcanic rocks of the Marda Volcanic Complex in the southern Youanmi Terrane (Chen et al. 2003), and a 2735 ± 5 Ma pegmatoidal leucogabbro from the western Youanmi Terrane (185922; GSWA in prep.).

c. 2715–2635 Ma

The latest period of Yilgarn magmatism was long-lived with several stages. The oldest rocks include granite gneisses from the Yamarna Terrane, such as the 2706 ± 22 Ma Rason gneiss (Cassidy 2007a) and the 2711 ± 6 Ma Throssell orthogneiss (Cassidy 2007b). This c. 2711 Ma orthogneiss contains all of the >2740 Ma zircon xenocrysts so far recognized in the Yamarna Terrane. In the southern Burtville Terrane, granite veins in basalts of the Irwin Hills greenstone belt have been dated at 2716 ± 5 Ma (GSWA 182603; in prep.), and the Burtville granodiorite has been dated at 2716 ± 4 Ma (GA 2001969033A; Dunphy et al. 2003). Abundant zircon xenocrysts of this age have been found in the Burtville Terrane granites, with the xenocrysts extending down to 2686 Ma, suggesting that c. 2705–2686 Ma rocks: 1) have not been sampled; 2) are not exposed at current exposure levels; or 3) were extensively recycled and not preserved.

The c. 2715–2705 Ma rocks in the northeast Yilgarn Craton are contemporaneous with the c. 2715–2704 Ma Kurnalpi Sequence of the Kurnalpi Terrane, and the c. 2715–2692 Ma Kambalda Sequence, farther west in the Kalgoorlie Terrane (Kositcin et al. 2008), and the c. 2724–2700 Ma Glen Group and c. 2716–2694 Ma Austin Downs Supersuite in the western Youanmi Terrane (Van Kranendonk & Ivanic 2009).

The next stage involved volcanism in the Yamarna Terrane, where a bimodal greenstone package includes the 2683 ± 5 Ma felsic Toppin Formation (183150; GSWA in prep.). Widespread felsic magmatism across the northeast Yilgarn Craton at this time produced the abundant c. 2681–2658 Ma granites. These include the "syn-tectonic granites", such as the c. 2662 Ma Point Salvation Monzogranite that forms the footwall to the Yamarna Shear Zone (179446; GSWA in prep), and the 2666 ± 8 Ma Ngarrutji Monzogranite (185972; GSWA in prep.) that was contemporaneous with folding of the Mount Venn Igneous Complex.

The c. 2683–2658 Ma rocks are contemporaneous with the later stages of felsic volcanism in the west of the Kurnalpi Terrane, deposition of the felsic volcanic and volcaniclastic rocks of the c. 2686–2666 Ma Kalgoorlie Sequence (Kositcin et al. 2008) in the Kalgoorlie Terrane, and felsic magmatism of the Tuckanarra Suite and early Jungar Suite in the western Youanmi Terrane (Van Kranendonk & Ivanic 2009).

A suite of c. 2650 to c. 2634 Ma granites in the northeast Yilgarn Craton includes dykes that cut the orthogneisses, and "post-tectonic" plutons such as the 2643 Ma Wartu Monzogranite (179449; GSWA in prep.) that intrudes and truncates the pervasive, ductile foliation in the

Mount Venn greenstone belt in the eastern Burtville Terrane. These granites correspond with the later stages of low-Ca magmatism that has been recognized across the craton (Champion & Sheraton 1997).

Implications for geodynamics in the eastern Yilgarn Craton

The compilation of the geochronology in the northeast Yilgarn Craton stresses the importance of the Yamarna Shear Zone as a terrane boundary that separates the older Burtville Terrane from the younger Yamarna Terrane to the east.

The compilation also reveals a fundamental pattern to the distribution of rocks in the Yilgarn Craton. It indicates that the Burtville and Youanmi Terranes possess similar rock types of the same age, suggesting a shared, episodic geological history that extends from c. 2940 Ma to c. 2635 Ma. In contrast, the Yamarna Terrane to the east has affinities with the <2720 Ma Kalgoorlie and Kurnalpi Terranes, located between the Burtville and Youanmi Terranes. This suggests that the Burtville and Youanmi Terranes may have been contiguous for a large part of their history, and possibly broke apart during the c. 2720 Ma plume-related extension that resulted in the deposition of the Kambalda and Kurnalpi Sequences in the Kalgoorlie and Kurnalpi Terranes. Extension to the east at this time, accommodated along the Yamarna Shear Zone, resulted in the deposition of the greenstone package containing the c. 2683 Ma Toppin Formation. The presence of xenocrystic zircon populations and older basement fragments, such as the Penneshaw Formation, in the younger terranes represent fragments the Burtville and Youanmi Terranes within the younger arc-like successions. The current configuration of the crustal blocks supports the arc accretion model of Barley et al. (2003), where it was suggested that the Burtville Terrane was a continental-rift fragment that was re-accreted onto the "ancestral" Yilgarn Craton, although they did not examine the origin of the older rift fragment and its relation to the rest of the craton, or recognize the presence of the younger Yamarna Terrane.

Acknowledgements

Zircon analyses were conducted using the SHRIMP ion microprobes at the John de Laeter Centre of Mass Spectrometry at Curtin University of Technology in Perth, Australia. The authors publish with permission of the Executive Director of the Geological Survey of Western Australia.

References

Barley M.E., Brown S.J.A., Cas R.A.F., Cassidy K.F., Champion D.C., Gardoll S.J. & Krapež B., 2003, *An integrated geological and metallogenic framework for the eastern Yilgarn Craton: Developing geodynamic models of highly mineralised Archaean granite–greenstone terranes*, AMIRA Project P624.

Cassidy K.F., 2007a, GA Sample ID 98967050B: Geoscience Australia's geochronology database, July 2007 data release, http://www.ga.gov.au/oracle/ozchron.

Cassidy K.F., 2007b, GA Sample ID 98967052B: Geoscience Australia's geochronology database, July 2007 data release, http://www.ga.gov.au/oracle/ozchron.

Cassidy K.F., Champion D.C., Krapež B., Barley M.E., Brown S.J.A., Blewett R.S., Groenewald P.B. & Tyler I.M., 2006, A revised geological framework for the Yilgarn Craton, Western Australia, Geological Survey of Western Australia, Record 2006/8, 8p.

Champion D.C. & Sheraton J.W., 1997, Geochemistry and Nd isotope systematics of Archaean granites of the Eastern Goldfields, Yilgarn Craton, Australia: implications for crustal growth processes, Precambrian Research, 83, 109–132.

Chen S.F., Riganti A., Wyche S., Greenfield J.E. & Nelson D.R., 2003, Lithostratigraphy and tectonic evolution of contrasting greenstone successions in the central Yilgarn Craton, Western Australia, Precambrian Research, 127, 249–266.

Dunphy J.M., Fletcher I.R., Cassidy K.F. & Champion D.C., 2003, Compilation of SHRIMP U–Pb geochronological data, Yilgarn Craton, Western Australia, 2001–2002, Geoscience Australia, Record 2003/15, 139p.

Fletcher I.R., Dunphy J.M., Cassidy K.F. & Champion D.C., 2001, Compilation of SHRIMP U–Pb geochronological data, Yilgarn Craton, Western Australia, 2000–2001, Geoscience Australia, Record 2001/47, 111p.

Kositcin N., Brown S.J.A., Barley M.E., Krapež B, Cassidy K.F. & Champion D.C., 2008, SHRIMP U–Pb zircon age constraints on the Late Archaean tectonostratigraphic architecture of the Eastern Goldfields Superterrane, Yilgarn Craton, Western Australia, Precambrian Research, 161, 5–33.

Liu S., 2007, GA Sample ID 97965402: Geoscience Australia's geochronology database, July 2007 data release, http://www.ga.gov.au/oracle/ozchron.

Mueller A.G. & McNaughton N.J., 2000, U–Pb ages constraining batholiths emplacement, contact metamorphism, and the formation of gold and W-Mo skarns in the Southern Cross area, Yilgarn Craton, Western Australia, Economic Geology, 95, 1231–1257.

Nelson D.R., 1997, Evolution of the Archaean granite–greenstone terranes of the Eastern Goldfields, Precambrian Research, 83, 57–81.

Pawley M.J., Romano S.S., Hall C.E., Wyche S. & Wingate M.T.D., 2009, The Yamarna Shear Zone: a new terrane boundary in the northeastern Yilgarn Craton, Geological Survey of Western Australia, Annual Review 2007–08, 26–32.

Riganti A., Wyche S., Wingate M.T.D., Kirkland C.L. & Chen S.F., 2010, Constraints on ages of greenstone magmatism in the northern part of the Southern Cross Domain, Yilgarn Craton,, this volume.

Van Kranendonk M.J. & Ivanic T.J., 2009, A new lithostratigraphic scheme for the northeastern Murchison Domain, Yilgarn Craton, Geological Survey of Western Australia, Annual Review 2007–08, 35–53.

Wang Q., Schiøtte L. & Campbell I.H., 1996, Geochronological constraints on the age of komatiites and nickel mineralization in the Lake Johnston greenstone belt, Yilgarn Craton, Western Australia, Australian Journal of Earth Sciences, 43, 381–385.

Wingate M.T.D., Kirkland C. L. & Pawley M. J., in press a, 185968, leucogabbro, Mount Sefton; Geological Survey of Western Australia, Geochronology Record 869.
Wingate M.T.D., Kirkland C.L. & Pawley M. J., in press b, 185976, leucogabbro, Mount Warren; Geological Survey of Western Australia, Geochronology Record 870.

NEW CONSTRAINTS ON THE TECTONICS OF THE ARCHAEAN-PALEOPROTEROZOIC TRANSITION FROM THE GAWLER CRATON, SOUTH AUSTRALIA

A.J. Reid[1], E.A. Jagodzinski[1] & G.L. Fraser[2]

[1]Geological Survey Branch, Primary Industries and Resources South Australia, GPO Box 1671, Adelaide, SA, 5001
[2]Onshore Energy and Minerals Division, Geoscience Australia, GPO Box 378, Canberra, ACT, 2617

Introduction

A Neoarchaean, ~2900–2700 Ma, supercontinent dubbed Kenorland is now preserved as relic terranes within the extensive Proterozoic cratons of North America and correlative terranes in Baltica (Williams et al., 1991; Aspler & Chiarenzelli, 1998). This continent is likely to have developed as a result of the major juvenile crust formation event of this time, which is recorded in extensive calc-alkaline magmatism, including mafic and ultramafic material present in many Neoarchaean cratons (Barley et al., 1998). Contractional deformation and post-orogenic magmatism over the interval ~2600-2560 Ma is a characteristic of a number of terranes including, for example the Yilgarn and Wyoming cratons, which has been taken to indicate Kenorland was effectively cratonised at this time.

In a number of terranes such as the Kaapvaal and Pilbara cratons, and the Gawler Craton, South Australia, however, the post ~2600 Ma time interval is not characterised by termination of sedimentary basins but rather by ongoing sedimentation and or the initiation of new basins, together with associated intrusive and extrusive magmatism. Substantive differences such as these in the temporal evolution of many of the Neoarchaean terranes led Aspler & Chiarenzelli (1998) to propose there may have been more than one 'supercontinent' during the Neoarchaean. Furthermore, while widespread ~2450 Ma mafic and ultramafic magmatism in many North American terranes appear to indicate rifting across Kenorland (Heaman, 1997), it appears, that not all the Neoarchaean terranes were undergoing rifting at this time. A number of terranes including the Dhawar Craton, India (Clark et al., 2009) and the Sask Craton, Canada (Rayner et al., 2005) and the Gawler Craton, indicate that contractional orogenesis was in fact underway ~2480-2400 Ma within some terranes.

The Gawler Craton, South Australia, preserves extensive sedimentary sequences and associated magmatic rocks that span the interval covering the Archaean-Palaeoproterozoic transition, with bimodal calc-alkaline volcanism and associated sedimentation occurring over the interval ~2560-2480 Ma. The pervasive high geothermal gradient metamorphism within the Gawler Craton in the earliest Palaeoproterozoic, ~2470-2420 Ma (Fanning et al., 2007; Jagodzinski et al., 2009) suggests the Gawler Craton is potentially a correlative of the Dhawaar Craton, Sask Craton and other similar terranes, in terms of timing of magmatic and orogenic events (Payne et al., 2009).

We report new zircon U-Pb ion probe data collected in a new study of Neoarchaean to Earliest Palaeoproterozoic metasedimentary and meta-igneous rocks of the Gawler Craton, South Australia (Jagodzinski et al., 2009); an important time interval for the development of the Gawler Craton that has been investigated by relatively few geochronological studies. The new data show that the interval ~2560-2480 Ma was characterised by deposition and associated magmatism. This was terminated by contractional deformation and high geothermal gradient metamorphism over the interval ~2470-2410 Ma.

Geology of the Neoarchaean-earliest Palaeoproterozoic of the Gawler Craton

Neoarchaean to early Palaeoproterozoic rocks within the Gawler Craton are spatially organised into two belts, the Mulgathing and Sleaford complexes (Reid & Daly, 2009), which are likely to represent portions of a formerly contiguous belt now disrupted by Palaeo- and Mesoproterozoic tectonism and magmatism (Daly et al., 1998; Hand et al., 2007). These complexes contain coeval felsic and mafic–ultramafic (including komatiites) volcanic rocks and clastic and chemical sedimentary sequences. The recent discovery of 3150 Ma orthogneiss in the eastern Gawler Craton (Fraser et al., 2008; Fraser et al., in press) has confirmed the long held inference that the Neoarchaean rocks of the Gawler Craton were deposited, at least in part, onto a pre-existing Mesoarchaean basement (Creaser & Fanning, 1993).

Development of the volcano-sedimentary basin

Prior to this study, the late Archaean volcano-sedimentary sequences of the Mulgathing and Sleaford complexes were believed to have formed during the interval *ca* 2555–2510 Ma, prior to onset of the Sleafordian Orogeny at *ca* 2460 Ma (Daly & Fanning, 1993; Fanning et al., 2007). The youngest interpreted maximum depositional age for paragneisses of the Mulgathing Complex was inferred to be ~2512 Ma (Swain et al., 2005). The existing data suggest a hiatus of about 50 Ma prior to onset of the Sleafordian Orogeny, which is accompanied by *ca* 2460 Ma magmatism in the Mulgathing Complex (Fanning et al. 2007). Two significant results emerge from the new data reported in Jagodzinski et al. (2009); (1) the Mulgathing Complex contains sedimentary sequences younger than *ca* 2510 Ma; and (2) rather than a hiatus in magmatic activity, there was continuous magmatism between *ca* 2510 Ma and 2460 Ma.

Constraints on the timing of deposition of the metasediments

Three paragneisses were analysed in this study: the Christie Gneiss in its type area at Mt Christie (R1562985), at Golf Bore (R1565736) and southeast of Tarcoola (R1562450). All three samples contain a *ca* 2515 Ma detrital zircon population, as previously recorded in other samples dated from the Mulgathing Complex (Swain et al., 2005; McFarlane et al., 2007). However, at Mt Christie, the paragneiss contains two younger detrital zircon populations at 2499 ± 4 Ma and 2485 ± 4 Ma. The ~2485 Ma age peak is also quite prominent in sample R1562450, and on closer inspection of the published datasets, a similar ~2485 Ma zircon population, albeit minor, is also present.

Where this 2485 Ma peak is defined by only 2 or 3 analyses it is easy to overlook its geological significance and assume it represents zircon cores that were partially reset or underwent partial Pb loss during the Sleafordian Orogeny. However, the robust ~2485 and 2499 Ma populations at Mt Christie cannot be so easily dismissed. It is clear that at least some, possibly all of the metasedimentary sequences in the Mulgathing Complex are significantly younger than previously interpreted, with basin development extending into the late Palaeoproterozoic and closing the gap between the cessation of sedimentation and onset of orogenesis.

Magmatism in the Mulgathing Complex

As with sedimentation, the interval of known magmatism can now be expanded into the late Palaeoproterozoic. Prior to this study, the youngest known pre-Sleafordian granites of the Mulgathing Complex were the *ca* 2509 Ma dykes and veins intruding the Lake Harris komatiites (Fanning et al. 2007). The six meta-igneous rocks analysed in this study are all younger, yielding ages ranging between *ca* 2480-2495 Ma. This continuum of magmatism from *ca* 2510 to 2460 Ma indicates a high geothermal gradient is likely to have been operative during both the formation of the rift basin and during its subsequent inversion. A high geothermal gradient, together with the strong possibility of plate margin magmatism, and a strong mantle magmatic input is a recipe for a complex, active geotectonic environment, which may find correlatives with other Neoarchaean-Palaeoproterozoic worldwide.

Acknowledgements

Sue Daly is acknowledged for her work on the Archean of the Gawler Craton over many years within the Geological Survey of South Australia.

References

Aspler L.B. & Chiarenzelli J.R., 1998, Two Neoarchean supercontinents? Evidence from the Paleoproterozoic, Sedimentary Geology, 120, 75–104.

Barley M., Krapez B., Groves D.I. & Kerrich R., 1998, The late Archaean bonanza: metallogenic and environmental consequences of the interaction between mantle plumes, lithospheric tectonics and global cyclicity, Precambrian Research, 91, 65–90.

Clark C., Collins A.S., Kinny P.D., Timms N.E. & Chetty T.R.K., 2009, SHRIMP U-Pb age constraints on the age of charnockite magmatism and metamorphism in the Salem Block, southern India, Gondwana Research, 16, 27–36.

Creaser R.A. & Fanning C.M., 1993, A U-Pb zircon study of the Mesoproterozoic Charleston Granite, Gawler Craton, South Australia, Australian Journal of Earth Sciences, 40, 519-526.

Daly S.J. & Fanning C.M., 1993, Archaean, in *The geology of South Australia; Volume 1, The Precambrian*. J.F. Drexel, Preiss W.V. & Parker A.J., eds, Geological Survey of South Australia, Bulletin 54, Adelaide, South Australia, Australia, 32–49.

Daly S.J., Fanning C.M. and Fairclough M.C., 1998, Tectonic evolution and exploration potential of the Gawler Craton, South Australia, AGSO Journal of Australian Geology & Geophysics, 17, 145–168.

Fanning C.M., Reid A. & Teale G., 2007, A geochronological framework for the Gawler Craton, South Australia, South Australia, Geological Survey, Bulletin 55.

Fraser G., Foudoulis C., Neumann N., Sircombe K., McAvaney S., Reid A. & Szpunar M., 2008, Foundations of South Australia discovered, AusGeo News, 92, 10–11.

Fraser G., McAvaney S., Neumann N., Szpunar M. & Reid A., in press, Discovery of early Mesoarchean crust in the eastern Gawler Craton, South Australia, Precambrian Research.

Hand M., Reid A. & Jagodzinski E., 2007, Tectonic framework and evolution of the Gawler Craton, South Australia, Economic Geology, 102, 1377–1395.

Heaman L.M., 1997, Global mafic magmatism at 2.45 Ga: remnants of an ancient large igneous province, Geology, 25, 299–302.

Jagodzinski E., Reid A. & Fraser G., 2009, Compilation of SHRIMP U-Pb geochronological data for the Mulgathing Complex, Gawler Craton, South Australia, 2007–2009, South Australia, Department of Primary Industries and Resources. Report Book 2009/16.

McFarlane C.R.M., Mavrogenes J.A. & Tomkins A.G., 2007, Recognizing hydrothermal alteration through a granulite facies metamorphic overprint at the Challenger Au deposit, South Australia, Chemical Geology, 243, 64–89.

Payne J.L., Hand M., Barovich K., Reid A.J. & Evans D.A.D., 2009, Correlations and reconstruction models for the 2500-1500 Ma evolution of the Mawson Continent, in *Palaeoproterozoic supercontinents and global evolution* Reddy S.M., Mazumder R., Evans D.A.D. & Collins A.S., eds,. Geological Society of London, 319–355.

Rayner N.M., Stern R.A. & Bickford M.E., 2005, Tectonic implications of new SHRIMP and TIMS U-Pb geochronology of

rocks from the Sask Craton, Peter Lake Domain, and Hearne margin, Trans-Hudson Orogen, Saskatchewan, Canadian Journal of Earth Sciences, 42, 635–657.

Reid A.J. & Daly S.J., 2009, The Mulgathing and Sleaford complexes of the Gawler Craton: a historical perspective of the geology and mineral potential, MESA Journal, 52, 4–12.

Swain G., Woodhouse A., Hand M., Barovich K., Schwarz M. & Fanning C.M., 2005, Provenance and tectonic development of the late Archaean Gawler Craton, Australia; U-Pb zircon, geochemical and Sm-Nd isotopic implications. Precambrian Research, 141, 106–136.

Williams H., Hoffman P.F., Lewry J.F., Monger J.W.H. & Rivers, T., 1991, Anatomy of North America: thematic geologic portrayals of the continent, Tectonophysics, 187, 117–134

AGE CONSTRAINTS IN THE SOUTHERN PART OF THE SOUTHERN CROSS DOMAIN OF THE YILGARN CRATON

S.S. Romano[1*], M.P. Doublier[1], D. Mole[2], N. Thébaud[2], M.T.D. Wingate[1] & C.L. Kirkland[1]

[1]Geological Survey of Western Australia, Mineral House, East Perth, Western Australia, 6004 (sandra.romano@dmp.wa.gov.au)
[2]Centre for Exploration Targeting, School of Earth and Environment (M006) University of Western Australia, Crawley, Western Australia, 6009

Introduction

The Lake Johnston (Figure 1a) and Southern Cross greenstone belts in the southern part of the Southern Cross Domain of the Archean Yilgarn Craton host significant nickel and gold deposits. Based on several U–Pb SHRIMP zircon ages, parts of the greenstone belt successions have been interpreted to be older than 2.9 Ga (Wang et al., 1996; Mueller & McNaughton, 2000). One consequence of this interpretation has been that the Barberton-type komatiites in the Lake Johnston greenstone belt have been regarded as old (>2.9 Ga) komatiite-hosted nickel deposits (Barnes, 2006). New field mapping, geochemical and geochronological studies, challenge this established interpretation, and encourage a re-assessment.

Lake Johnston greenstone belt

The lowest exposed part of the Lake Johnston greenstone belt stratigraphy is the submarine volcanic Maggie Hays Formation (Gower & Bunting, 1976). It is composed of a thick package of strongly deformed, pillowed and massive basalts that are overlain by a mixed sequence of mafic pyroclastic rocks, hyaloclastite, and basaltic lava flows. Thin, quartz-rich sedimentary interbeds become more abundant towards the top of the succession. The package is intruded by dolerite, pyroxenite, gabbro, leucogabbro, and undifferentiated ultramafic rocks. The latter might be related to the ultramafic rocks of the Honman Formation (Gower & Bunting, 1976), but this has not been demonstrated. In the southern part of the greenstone belt, the Lake Medcalf mafic to ultramafic igneous complex (Gower & Bunting, 1976) intrudes the Maggie Hays Formation. A newly acquired gravity survey over the Lake Johnston area indicates a substantial areal extent of mafic intrusive rocks (Figure 1b).

Porphyritic intermediate volcanic rocks of the Honman Formation, which overlies the Maggie Hays Formation, have yielded SHRIMP U–Pb zircon ages of 2921 ± 4 Ma and 2903 ± 5 Ma (Wang et al., 1996). An additional small zircon population of c. 2856 Ma, with high Th/U–ratios of c. 5, was interpreted by Wang et al., (1996) to be of metamorphic origin. Although not necessarily conclusive, many studies suggest that metamorphic zircons tend to have low Th/U–ratios (<0.2), whereas higher ratios are more common in igneous zircons (Hoskin and Black,

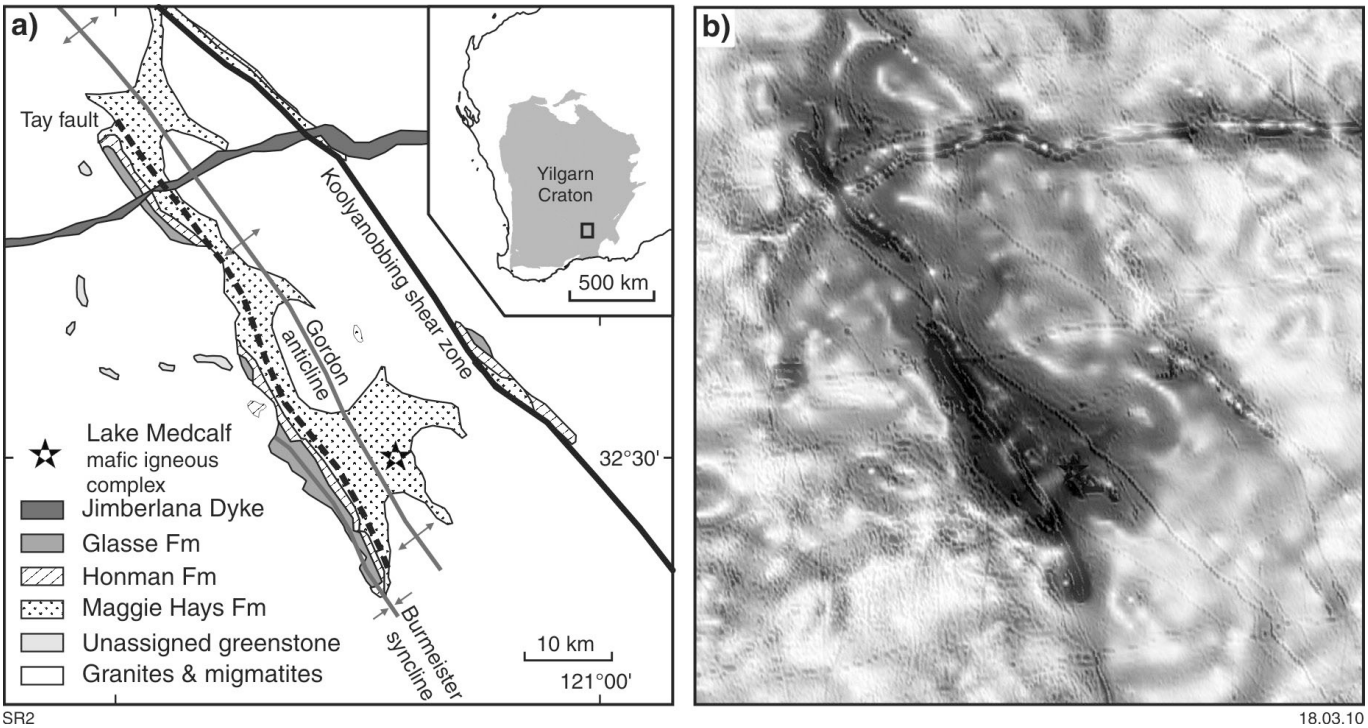

Figure 1. a) Geological map of the Lake Johnston greenstone belt (modified after Buck et al., 1998); b) Combined gravity/ magnetic image of the Lake Johnston greenstone belt. The gravity high in the south eastern part of the Lake Johnston belt is related to the mafic intrusive rocks (e.g. Lake Medcalf mafic igneous complex). The extent differs from the previously mapped occurrence of mafic intrusive rocks.

2000). Thus, it is possible that the c. 2.9 Ga zircons are xenocrystic and that the 2856 Ma zircons date the volcanism rather than a metamorphic event. Additional evidence for a younger age of the Honman Formation is given by felsic volcaniclastic rocks overlying volcanic rocks that have a maximum depositional age of c. 2873 Ma (Thébaud et al., 2009). A mixed succession of banded iron-formation, clastic sedimentary rocks, and minor felsic volcanic rocks of unknown age lie stratigraphically above the felsic volcaniclastic rocks (Heggie et al., in press). Whereas there are ultramafic rocks present at all levels in the Honman Formation, extrusive (i.e. olivine spinifex-textured) komatiites are found only at the top of the formation. If the apparently intrusive ultramafic rocks lower in the succession are intrusive equivalents of the spinifex-textured komatiites at the top of the formation, then the felsic volcanic rocks pre-date the ultramafic event.

The Honman Formation is overlain by the Glasse Formation (Gower & Bunting, 1976), which is characterized by massive basalt with several amygdale-rich horizons, and minor ultramafic intrusive rocks. The context of the ultramafic rocks within the Glasse Formation is unclear.

Southern Cross greenstone belt

The structurally lowest exposed unit in the Southern Cross greenstone belt is represented by a thin layer of muscovite schist and quartzite, which is strongly sheared along the margin of the Ghooli Dome (Bloem et al., 1997). In the Illaara and Maynard Hills greenstone belts in the northern part of the Southern Cross Domain, similar rocks have been interpreted to represent reworked Mesoarchean crust (Wyche et al., 2004).

The basal, probably metasedimentary unit is unconformably overlain by a volcanic succession that is up to 5 km thick. The lower part of the volcanic succession is formed by tholeiitic and komatiitic basalts, and the upper part is dominated by komatiite. Several layers of banded iron-formation are interbedded with the volcanic rocks, and minor amounts of gabbro intrude the sequence. U–Pb zircon ages from quartz porphyry sills from the Southern Star (2934 ± 7 Ma; interpreted as a magmatic age; Mueller & McNaughton, 2000) and Copperhead deposits (2912 ± 5 Ma; interpreted as a minimum age; Mueller & McNaughton, 2000), suggest that at least parts of the volcanic pile formed prior to 2.9 Ga.

A thick sedimentary succession rests unconformably on the volcanic rocks. The basal part of the sedimentary package is marked by black shale, followed by a mixed succession of psammites, pelites, and minor quartzite and conglomerate. Recent SHRIMP U–Pb zircon age from the lower part of the sedimentary succession indicates a maximum depositional age of 2702 ± 17 Ma (Thébaud & Miller, 2009).

These recent findings show that the belt also contains a much younger component, which has not been previously recognized, and suggest a substantial depositional hiatus in the Southern Cross greenstone belt. However, the source and maximum age of deposition of the sedimentary rocks, in the Southern Cross greenstone belt remains poorly constrained: they appear to be younger than sedimentary rocks of the Diemals Formation (maximum depositional age of 2729 ± 9 Ma: Nelson, 2001a) and also felsic volcanic rocks of the Marda Complex (2732 ± 3 Ma: Nelson, 2001b) to the north. Moreover, the c. 2702 Ma age (Thébaud & Miller, 2009) is within the age ranges of various felsic volcanic components of the Eastern Goldfields Superterrane to the east (Kositcin et al., 2008).

Granites and adjacent greenstones

The Lake Johnston greenstone belt is flanked by large granite domes. One of the external domes to the west of the greenstone belt yielded a SHRIMP U–Pb zircon age of 2770 ± 4 Ma (this study). Thus, it is significantly older than the smaller scale internal granites, which have U–Pb crystallizaton ages of 2718 ± 6 Ma (Wingate et al., in press), and 2714 ± 11 Ma (this study), and may represent an earlier stage of granite doming. The Ghooli Dome, a major dome structure within the Southern Cross greenstone belt exhibits younger magmatism dated at 2691 ± 7 Ma (SHRIMP U–Pb zircon; Dalstra et al. 1998), but also retains evidence of earlier c. 2770 granite magmatism (Mueller & McNaughton, 2000).

Poorly exposed greenstone remnants outcrop along the margins of granite domes west of the Lake Johnston greenstone belt. Mapping and studies of drill chips show a succession of banded iron-formation, mafic extrusive rocks, dolerite, and ultramafic rocks. This association is not exclusive to the Lake Johnston belt succession: similar rock associations have been described in the adjacent Forrestania greenstone belt to the west (Perring et al., 1995). However, a new magnetotelluric survey of the Lake Johnston area indicates that a major fault separates the Forrestania greenstone belt to the west, from both the Lake Johnston greenstone belt and the greenstone remnants which lie to the east. Hence, a relation of the greenstone fragments to the Lake Johnston greenstone belt appears more likely. However, the timing, off-set and regional importance of this structure needs further investigation.

Conclusion

Recent mapping and new geochronological data from the Lake Johnston and Southern Cross greenstone belts indicate that the stratigraphy of the southern part of the Southern Cross Domain is more complex than previously thought, and needs re-assessment. Dating of different stratigraphic levels and lithologies will allow a better correlation of the greenstone successions within the region. New geochronology data indicate a complex age pattern for felsic plutonic rocks, with pre 2.7 Ga granites appearing to prevail in the Lake Johnston area. Together with the newly acquired magnetotelluric and gravity surveys, these ages should assist in the development of a 3D architecture and geodynamic model for the region (see also contribution by Thébaud et al., this volume).

Acknowledgements

Zircon U–Pb analyses were conducted using the SHRIMP ion

microprobes at the John de Laeter Centre of Mass Spectrometry at Curtin University of Technology in Perth, Australia. The authors publish with permission of the Executive Director of the Geological Survey of Western Australia.

References

Barnes S.J., 2006, Komatiite-hosted nickel sulphide deposits: geology, geochemistry, and genesis in *Nickel deposits of the Yilgarn Craton: geology, geochemistry, and geophysics applied to exploration*, Barnes S.J, ed, Society of Economic Geologists, Special Publication, 13, 51–118.

Bloem E.J.M., Dalstra H.J., Ridley J.R. & Groves D.I., 1997, Granitoid diapirism during protracted tectonism in an Archaean granitoid-greenstone belt, Yilgarn Block, Western Australia, Precambrian Research, 85, 147–171.

Buck P.S., Vallance S.A., Petting C.S., Hill R.E. & Barnes S.J., 1998, Maggie Hays nickel deposit, in *Geology of Australian and Papua New Guinean Mineral Deposits,* Berkman D.A. & Mackenzie D.H., eds, 357–364.

Dalstra H.J., Bloem E.J.M., Ridley J.R. and Groves D.I., 1998, Diapirism synchronous with regional deformation and gold mineralisation, a new concept for granitoid emplacement in the Southern Cross Province, Western Australia, Geologie en Mijnbouw, 76, 321–338.

Gower C.F. & Bunting J.A., 1976, Lake Johnston, Western Australia, Geological Survey of Western Australia, 1:250 000 Geological Series Explanatory notes, 27p.

Heggie G.J., Fiorentini M.L., Barnes S.J., Barley M.E. & Gregory I., in press, Stratigraphy and stratigraphic control on the style of komatiite emplacement in the 2.9 Ga Lake Johnston Greenstone Belt, Yilgarn Craton, Western Australia, Precambrian Research.

Hoskin P.W.O. & Black, L.P., 2000, Metamorphic zircon formation by solid-state recrystallization of protolith igneous zircon, Journal of Metamorphic Geology, 18, 423–439.

Kositcin N., Brown S.J.A., Barley M.E., Krapež B., Cassidy K.F. & Champion D.C., 2008, SHRIMP U-Pb zircon age constraints on the late Archaean tectonostratigraphic architecture of the Eastern Goldfields Superterrane, Yilgarn Craton, Western Australia, Precambrian Research, 161, 5–33.

Mueller A.G. & McNaughton N.J., 2000, U-Pb ages constraining batholith emplacement, contact metamorphism, and the formation of gold and W-Mo skarns in the Southern Cross area, Yilgarn Craton, Western Australia, Economic Geology, 95, 1231–1258.

Nelson D.R. 2001a, 168962: metasandstone, Yarbu Mine; Geochronology Record 196, Geological Survey of Western Australia, 4p.

Nelson D.R. 2001b, 168960: meta-ignimbrite, Marda Tank; Geochronology Record 194, Geological Survey of Western Australia, 4p.

Perring C.S., Barnes S.J. & Hill R.E.T., 1995, The physical volcanology of Archean komatiite sequences from Forrestania, Southern Cross Province, Western Australia, Lithos, 34, 189–207.

Thébaud N. & Miller J., 2009, U-Pb age constrain on the siliciclastic sediments from the upper supracrustal cover in the Southern Cross greenstone belt, Youanmi Terrane, Western Australia in *Smart Science for Exploration and Mining,* Williams P.J., ed, Proceedings of the Tenth Biennial SGA Meeting, Townsville, 960–962.

Thébaud N., Fiorentini M., McCuaig C., Miller J., Barnes S., Joly A. & Doublier M., 2009, Tectonostratigraphic controls on the localization of Achaean komatiite-hosted nickel-sulphide deposits and camps in the Yilgarn Craton, Goldschmidt Conference Abstract 2009, A1323.

Wang Q., Schiøtte L. & Campbell I.H., 1996, Geochronological constraints on the age of komatiites and nickel mineralisation in the Lake Johnston greenstone belt, Yilgarn Craton, Western Australia, Australian Journal of Earth Sciences, 43, 381–385.

Wingate, M.T.D., Kirkland, C.L., & Romano, S.S., in press, 182308: foliated metagranite, Lake Johnston; Geochronology Record 872, Geological Survey of Western Australia.

Wyche S., Nelson D.R. & Riganti A., 2004, 4350–3130 Ma detrital zircons in the Southern Cross Granite–Greenstone Terrane, Western Australia: implications for the early evolution of the Yilgarn Craton, Australian Journal of Earth Sciences, 51, 31–45.

TECTONO-METAMORPHIC HISTORY OF SOME GREENSTONE BELTS OF THE SE KAAPVAAL CRATON

L. Saha[1], A. Hofmann[1], H. Xie[2] & E. Hegner[3]

[1]School of Geological Sciences, University of KwaZulu-Natal, Private Bag X54001, Durban 4000, South Africa
[2]Beijing SHRIMP Center, Chinese Academy of Geological Sciences, 26 Baiwanzhuang Road, Beijing 100037, China
[3]Department für Geo- und Umweltwissenschaften, Ludwig-Maximilians-Universität, Theresienstr. 41, 80333 München, Germany

Introduction

In the context of ongoing debate on the origin and evolution of Archaean crust, the Barberton granitoid-greenstone terrain of the Kaapvaal craton (South Africa) has emerged as one of the classic areas for geological studies. This terrain preserves some of the oldest, well preserved supracrustal components (~3.5 Ga) on Earth. Intensive geochronological, geochemical and metamorphic studies on different units of the Barberton greenstone belt and associated granitoids and gneisses have helped to gain some basic understanding about early crust-forming processes during Archaean times (Lowe & Byerly, 2007; Schoene et al., 2008). Several greenstone belts described south of Barberton include the Dwalile, Assegaai, De Kraalen, Witrivier, Commondale, and Nondweni greenstone belts that are at least 3.2 Ga old and are tectonically interleaved with tonalite-trondhjemite-granodiorite (TTG) gneisses. These greenstone belts are intruded by a large variety of granitoids (Hunter & Wilson, 1988; Brandl et al., 2006) and preserve evidence of strong deformation and high-grade metamorphism. In spite of potential correlation of these greenstone belts with several units from the Barberton greenstone belt (Sleigh, 1988; Verbeek, 1991), they have attained less scientific interest, possibly due to their poor exposure and higher metamorphic grade.

Exposed in the area around Piet Retief town, the Assegaai, De Kraalen and Witrivier greenstone belts preserve very distinct supracrustal sequences that show evidence of multiple episodes of deformation and high-grade (upper amphibolite to granulite facies) metamorphism. The minimum age of these greenstone belts has previously been determined to be ~3.25 Ga (Farrow et al., 1990), on the basis of Rb-Sr whole rock data of the intrusive Anhalt trondhjemite.

Lithology of Assegaai, De Kraalen and Witrivier greenstone belts

The supracrustal rocks of the Assegaai greenstone sequence include (a) talc-tremolite schists and amphibolites, (b) banded quartzites, (c) ferruginous rocks, (d) mica schists, (e) calc-silicate rocks and (f) pelitic schists. Ultramafic schists and amphibolites are the dominant lithology in the area, with the latter locally showing strongly deformed pillow structures. The supracrustal rocks of the De Kraalen greenstone belt predominantly consist of meta-BIF, calc-silicate gneisses, quartzites, amphibolites and other mafic-ultramafic rocks. Most of the mafic-ultramafic rocks form an interlayered sequence of meta-dunite, meta-websterite, and gabbro-norite. The presence of cumulate textures and the lack of pillow structures indicate that these rocks are possibly intrusive into the other supracrustal rocks (Verbeek, 1991). Some of the ultramafic rocks are, however, devoid of any cumulate texture and, together with amphibolites, may represent part of an extrusive sequence associated with the metasedimentary rocks. The Witrivier greenstone belt occurs south of the De Kraalen belt and predominantly consists of mafic-ultramafic schists, amphibolites and calc-silicates.

Geochronology

Previous workers (Sleigh, 1988; Verbeek, 1991) suggested the presence of older continental basement to the greenstone belts compositionally similar to the bimodal mafic-felsic Ngwane Gneiss of the Ancient Gneiss Complex in Swaziland. Similar layered gneisses were also reported from Commondale by Smith (1987). To find evidence for the presence of older basement for the Assegaai supracrustal rocks we dated zircons from granitoid gneisses previously mapped as potential basement rocks (Sleigh, 1988). The age spectra (~3.19-3.22 Ga) for these samples however indicate their relationship with the intrusive Anhalt trondhjemite suite. $\varepsilon_{Nd(t)}$ values for these rocks are slightly negative with t_{DM} ages of 3.38 Ga, indicating derivation from slightly older crust.

Metamorphism of the Assegaai, De Kraalen and Witrivier greenstone belts

Detailed petrographic analyses of different supracrustal units from the Piet Retief area revealed that while most of the supracrustal rocks from the Assegaai greenstone belt preserve peak metamorphic mineral assemblages representative of amphibolite-facies conditions, some calc-silicates and amphibolites from De Kraalen and Witrivier greenstone belts preserve garnet+clinopyroxene±plagioclase+quartz or clinopyroxene+plagioclase+quartz-bearing peak metamorphic assemblages, indicating a higher grade of metamorphism. Garnet+clinopyroxene+plagioclase+quartz-bearing assemblages in calc-silicates from De Kraalen and Witrivier greenstone belts are replaced by amphiboles. The primary igneous assemblage of olivine±orthopyroxene in meta-dunite and clinopyroxene in meta-websterite in De Kraalen greenstone belt are also replaced by amphiboles, indicating that peak metamorphism was followed by an amphibolite facies event. Within the amphibolites from the Assegaai greenstone belt, the peak metamorphic assemblage

is represented by hornblende+plagioclase+quartz. The peak metamorphic assemblage from Assegaai metapelites consists of garnet+staurolite+biotite+quartz. Metamorphic assemblages consisting of talc+chlorite in the ultramafic schists, chlorite±albite in the metapelites of Assegaai greenstone belt, albite+epidote in the calc-silicates from De Kraalen and Witrivier greenstone belts represent the final retrograde event.

The petrographic observations helped to distinguish three metamorphic events: M_1, M_{2A} and M_{2B}. M_1 is represented by formation of garnet+clinopyroxene in the calc-silicates of De Kraalen and Witrivier greenstone successions and by formation of clinopyroxene in the amphibolites of De Kraalen greenstone belt. M_{2A} represents a major amphibolite facies event that led to formation of amphiboles in the calc-silicates, mafic and ultramafic rocks in the Assegaai, De Kraalen and Witrivier greenstone belts and formation of garnet+staurolite+quartz-bearing assemblage in Assegaai metapelites. M_{2B} represents the final retrograde event (albite-epidote facies condition) that affected all units from the greenstone belts.

P-T estimates for M_1 were made using THERMOCALC and conventional thermobarometry (Ellis & Green, 1974, Krogh, 1988). Such calculations show that the De Kraalen supracrustal rocks were metamorphosed at 14-15 kbar and 550-600 ºC, while the Witrivier supracrustal rocks were metamorphosed at ~14 kbar, 750 ºC during M_1. M_{2A} P-T conditions of ~8 kbar, 625 ºC were obtained from isopleth thermobarometry of one of the metapelite samples of the Assegaai greenstone succession (Figure 1a). In the absence of any representative mineral assemblages for thermobarometry, P-T conditions for M_{2B} was constrained solely on the basis of mineral assemblage. The presence of albite+epidote in the calc-silicates and amphibolites, and albite+chlorite in metapelites indicates that the final retrogression (M_{2B}) occurred under albite-epidote facies condition.

Discussion

The De Kraalen and Witrivier supracrustal rocks were subjected to high-pressure granulite facies metamorphism (M_1) at about ~14-15 kbar, during which the temperature conditions for the Witrivier supracrustals reached >750 ºC. This high pressure event was followed by a major amphibolite facies event (M_{2A}) at ~ 7-8 kbar, 600 ºC that affected the supracrustal rocks of all greenstone belts uniformly and obliterated evidence of M_1 assemblages from most lithologies. We conclude that the De Kraalen and Witrivier greenstone belts followed a clockwise P-T path representative of collisional tectonic regimes (Figure 1b). The De Kraalen and Witrivier supracrustal sequences were buried to depths of 30-45 Kms (during M_1) and were later exhumed and juxtaposed against the Assegaai greenstone succession (during M_2). The time frame of the M_{2A} event can be placed at ca. 3.20 Ga, on the basis of field relationships of partial melt veins in 3.22-3.19 Ga granitoids, indicating that exhumation was accompanied by widespread intrusion of tonalite-trondhjemite plutons.

Conclusions

A high pressure metamorphic event (~14 kbar, 600 ºC) at 3.2 Ga has been recorded from the Stolzburg granitoid-gneiss terrain south of the Barberton greenstone belt (Moyen et al., 2006). Our observation of a 3.2 Ga high-pressure event from the southeastern Kaapvaal craton lends support to the model that convergent

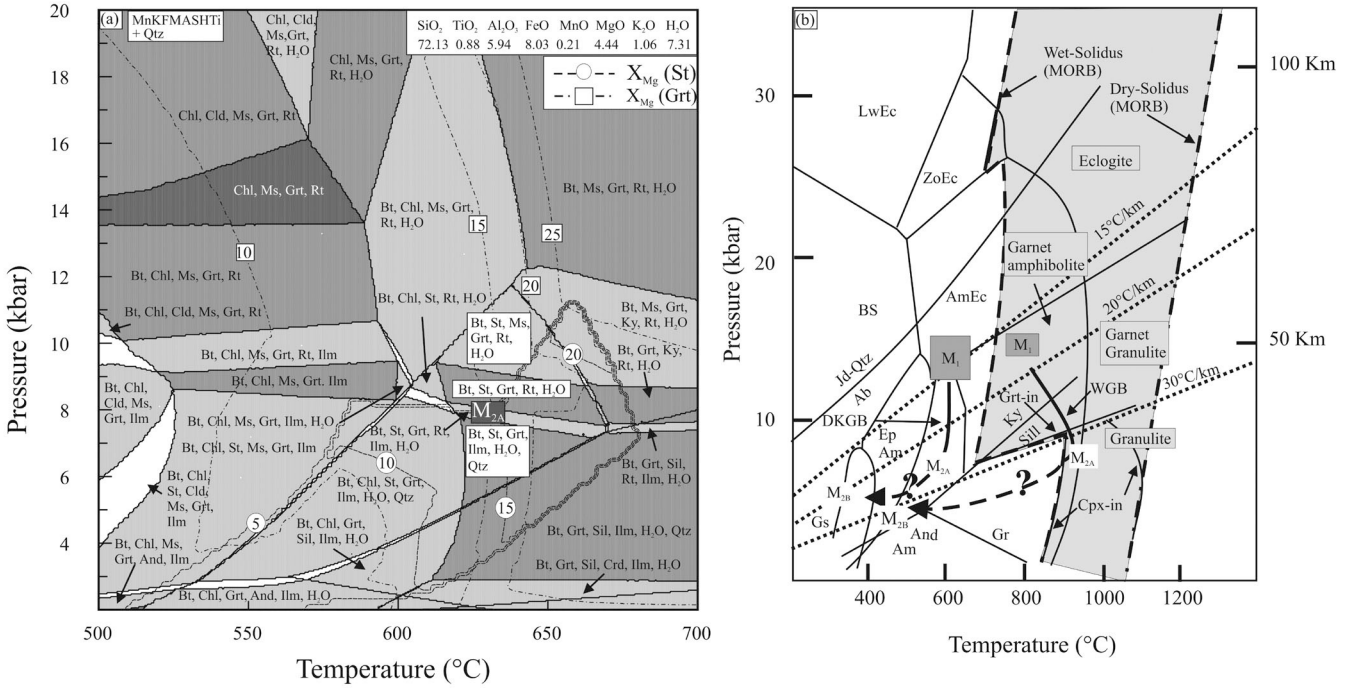

Figure 1. (a) P-T pseudosection of metapelite from the Assegaai greenstone belt (constructed using PERPLEX), showing the peak metamorphic condition of M_{2A} (black box) at ~ 8 kbar, 625 ºC. Mineral abbreviations used are after Kretz (1983). (b) Diagram summarizing the Archaean P-T history of the De Kraalen (DKGB) and Witrivier (WGB) greenstone belts. Grey boxes indicate P-T conditions of the high-pressure metamorphic event (M_1), and white boxes indicate P-T conditions of M_{2A-B}. Note that these boxes are schematic. Arrows indicate clockwise P-T paths of decompression for the high pressure rocks. Dashed portions of the P-T paths are uncertain due to lack of representative assemblages for barometry.

tectonic processes similar to those associated with modern collisional tectonic regimes in the vicinity of subduction zones were operating at that time. Although a subduction zone model is compelling, other models are possible. Ongoing structural-metamorphic work in the southeastern part of the Kaapvaal craton may help to distinguish between the different processes.

Acknowledgements

We thank Qing Ye and Hui Zhou in the Beijing SHRIMP Center for sample mount preparation and cathodoluminescence imaging. Financial support was provided by a UKZN post-doctoral fellowship to LS and by the South African National Research Foundation (NRF) and the German Ministry of Education and Research (BMBF) grants to AH and EH (grant SUA 08/038).

References

Ellis D.J. & Green D.H., 1979, Experimental study of the effect of Ca upon garnet–clinopyroxene Fe–Mg exchange equilibria, Contributions to Mineralogy and Petrology, 71, 13–22.

Farrow D.J., Harmer R.E., Hunter D.R. & Eglington B.M., 1990, Rb-Sr and Pb-Pb dating of the Anhalt Leucotonalite, northern Natal, South African Journal of Geology, 93, 696–701.

Kretz R., 1983, Symbols of rock-forming minerals, American Mineralogist, 68, 277–279.

Krogh E.J., 1988, The garnet-clinopyroxene Fe-Mg geothermometer-a reinterpretation of existing experimental data, Contributions to Mineralogy and Petrology, 99, 44–48.

Lowe D.R. & Byerly G.R., 2007, An overview of the geology of the Geology of the Barberton Greenstone Belt and vicinity: Implications for Early Crustal Development, in, *Earth's oldest rocks,* Van Kranendonk M.J., Smithies R.H. & Bennett V., eds, 481–526, Elsevier, Amsterdam.

Moyen J.-F., Stevens G. & Kisters A.F.M., 2006, Record of mid-Archaean subduction from metamorphism in the Barberton terrain, South Africa, Nature, 443, 559–562.

Schoene B., de Wit M. & Bowring S.A., 2008, Mesoarchean assembly and stabilization of the eastern Kaapvaal craton: a structural-thermochronological perspective, Tectonics, 27, doi:10.1029/2008TC002267.

Sleigh D.W.W., 1988, The Geology of the Archaean Terrane in the Piet Retief District, Transvaal, Unpublished MSc thesis, University of Natal, Pietermaritzburg.

Smith R.G., 1987, Geochemistry and Structure of the Archaean Granitoid-Supercrustal Terrane, Southeastern Transvaal and Northern Natal, Unpublished PhD thesis, University of Natal, Pietermaritzburg.

Verbeek J.A., 1991, The Geology and Geochemistry of the Archaean Granitoid-Supracrustal Terrane, Southeast of Piet Retief, Transvaal, Unpublished PhD thesis, University of Natal, Pietermaritzburg.

ARCHEAN EVOLUTION OF THE BELOMORIAN PROVINCE: FROM AN OCEAN TO A COLLISION OROGEN

A.I. Slabunov

Institute of Geology, Karelian Research Centre, Russian Academy of Sciences, (slabunov@krc.karelia.ru)

The eastern Fennoscandian (Baltic) Shield consists dominantly of Archean bedrock that can be divided into the Karelian, Murmansk, Belomorian (BP), Kola, and Norrbotten provinces (Fig. 1a), each having a distinct crustal growth and subsequent reworking history. The two former provinces and the latter one are Neoarchean cratons and the Belomorian and Kola provinces are mobile belts. A series of complexes, uncommon to the Archean and essential for understanding Archean geodynamics, were revealed in BP (Fig. 1b).

The thickness of the earth's crust of the BP is estimated at 40 km in the central part. It increases to 46 km in the NW part at the contact with the East Lapland terrain of the Karelian craton and decreases to 38 km at the boundary with the Kola province (Sharov et al., in press). In the lower crust of the BP there is no layer with numerous reflecting surfaces characteristic of a craton. Seismic and geological data show that the boundaries between the provinces are mostly tectonic in nature, the present structural architecture being built by both Archean and Paleoproterozoic events. Seismic (CDP) profiling data (Berzin et al. 2001; Sharov et al., in press) show (Fig. 1c) that the internal structure of BP reflects nappe tectonics; in Archean time, a collage of numerous slabs was formed, and in Paleoproterozoic time BP was thrusted on to the Karelian craton and, in turn, was thrusted by rocks of the Kola province.

The BP (Fig. 1b) consists dominantly of Meso- and Neoarchean rock associations. Neoarchean granitoids predominate. However, ophiolites, eclogite-bearing metamélange, island-arc volcanics, fore-arc basin sediments, oceanic plateau-type rocks, collisional granites, kyanite-faces metamorphic rocks, volcanogenic coarse-grained clastic rocks, subalkaline granitoids and leucogabbro (Slabunov et al. 2006 and references therein) are present among supracrustal rock associations. Rocks of the Belomorian province were subjected to multiple metamorphism in Archean and Paleoproterozoic time at moderately high to high pressures and were deformed considerably.

Neoarchean granitoids make up about 80% of the BP. The Sm–Nd model ages of all the granitoids without exception vary from 2.93 to 2.72 Ga and almost overlap the ages of magmatic crystallization. The latter is in the range 2.70–2.78 Ga. 2.83–2.80 Ga tonalites and quartz diorites are scarce in the Central Belomorian and the North Belomorian terrain. About 2.77 Ga ago hypersthene diorite, enderbite and charnockite massifs were formed in the Central Belomorian domain (Slabunov et al., 2006 and references therein). Also present in the latter are exotic 2875 Ma granitoids (kyanite-bearing trondhjemites or "frozen adakites") interpreted as melts from eclogites (Shchipansky et al. 2005).

The youngest 2.68–2.64 Ga granitoids form small tonalite, trondhjemite and diorite veins in the northern BP, subalkaline granite massifs in the southern BP and postkinematic plagiomicrocline granites in the West BP.

Highly metamorphosed supracrustal complexes make up not more than 20% of the BP, but as they are likely to host ore and are crucial for the understanding of the formation and evolution of the structure, they are given close attention. Four generations of greenstone complexes are distinguished: 2.88–2.82 Ga, 2.8–2.75 Ga, ca. 2.75 Ga and not later than 2.66 Ga, and one paragneiss complex in which sediments were formed 2.89-2.82 Ga ago.

The oldest (ca 2.88-2.86 Ga) rocks in the BP occur as 1) fragments of the oceanic crust of the Central Belomorian greenstone belt (GB); 2) a basalt–komatiites (oceanic plateau-type) association in the Keret GB; 3) island-arc volcanics of the Keret GB; 4) metagraywacke (fore-arc basin sediments) of the Chupa paragneiss belt.

The Central Belomorian GB is composed of amphibolites (metabasalts and metagabbros) together with ultramafic rocks (metamorphosed harzburgite, dunite and orthopyroxenite), and rare Co and Ni-rich pyrites. Some mantle normalized trace element patterns of the CBMZ metaperidotite show U-shapes typical of ophiolitic mantle peridotites. The Sm-Nd systematics of metabasalts from the belt (εNd at 2.85 Ga = + 2.3) and the absence of inherited zircons in it (Slabunov et al. 2009) show that the protolith of these rocks was not contaminated by old crustal material, which also suggests that they were produced in an oceanic setting (Slabunov et al. 2006). This complex can be correlated using petrogeochemical and isotopic (Sm-Nd) characteristics with similar oceanic rocks and ophiolites and is considered a fragment of Mesoarchean oceanic crust.

The Mesoarchean (2.88-2.82 Ga) greenstone complex of the Keret GB (Slabunov, 2008) is composed of three highly metamorphosed volcanogenic associations, with scarce relics of komatiitic-basaltic, andesitite-basaltic-rhyolitic and basaltic-andesite-basaltic lava assemblages with graywacke. The basalt-komatiite assemblage corresponds in geochemical characteristics to oceanic-plateau rocks. The andesite-bearing associations can be correlated using petrogeochemical (Th>Nb<La) characteristics with island-arc volcanics.

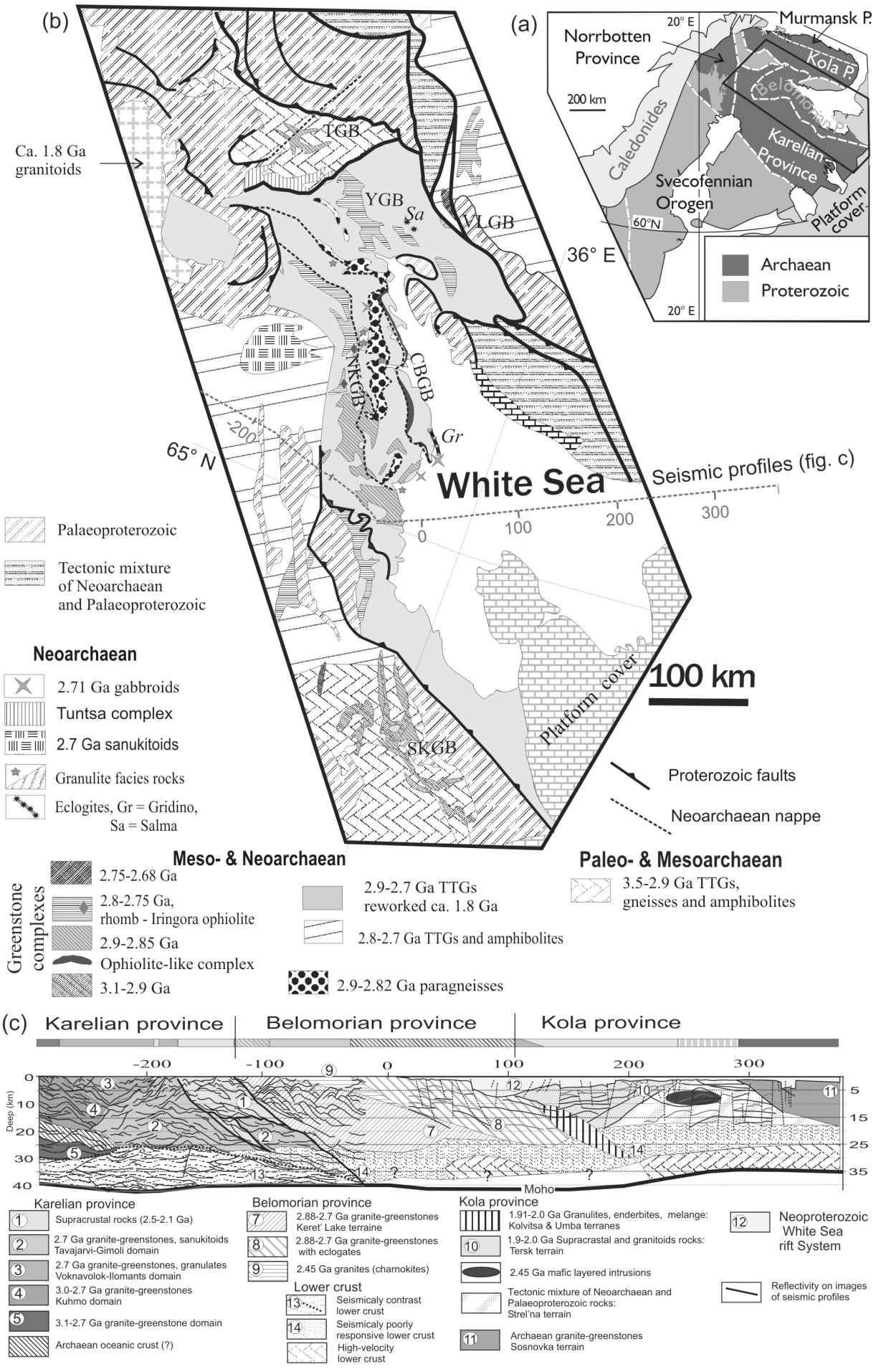

Figure 1. (a) Principal tectonic units of the Fennoscandian Shield (Hölttä et al. 2008). (b) Geological scheme of the Belomorian province, Fennoscandian Shield (Slabunov 2008), (c) Geological deep section along seismic profiles DSS–CDP Kalevala-Kem'-White Sea (Sharov et al., in press).

The U–Pb age of intermediate to felsic volcanics is estimated at 2877–2829 Ma (andesite tuffs) and 2829 Ma (neck-facies dacites), and the Sm–Nd model age of the andesite (T_{DM} = 2.80 Ga, ε_{Nd} = +2.8) is similar (Bibikova et al. 2004 and references therein), suggesting an ensimatic character for the island-arc system discussed.

The Chupa paragneiss belt is built up by migmatized (kyanite)-garnet-biotite gneisses with scarce unmigmatized fine-grained garnet-biotite gneiss bodies with banded-textured relics. Based on their petrochemical characteristics, particularly enrichment in Ni, V, Co, Cr, they are interpreted as metagraywackes generated by erosion of felsic (dacites), mafic and ultramafic rocks in a fore-arc basin environment. The time of deposition of the sedimentary rocks, from which the paragneisses were formed, fits the interval 2.9–2.84 Ga, because the age of detrital zircons is 3.2–2.89 Ga and that of early metamorphogenic zircon is 2820±15 Ma (Bibikova et al. 2004).

The Keret GB is the oldest fragment of continental crust in the BP and was formed in the Mesoarchean as a result of accretion of oceanic, volcanic arc and fore-arc associations.

The significant constituents of the western BP (Fig. 1b) are Neoarchean greenstone complexes of the Tikshozero belt and those of the Khizovaara structure of the Keret GB. They consist of various 2.8-2.78 Ga (Bibikova et al., 2003) volcanics of calc-alkaline and adakitic types and can be correlated with island-arc, suprasubduction zone ophiolites (Iringora complex), metagraywackes and komatiitic-basaltic associations (Kozhevnikov, 2000, Shchipansky et al., 2004). Two rare ophiolite and quartzite-bearing associations form parts of these belts (Kozhevnikov, 2000 and references therein). The above rock associations form a complex accretionary collage against the oldest continental crustal block.

The 2.75 Ga complex (Chelozero Formation) consists largely of arc-type metavolcanics with volcanic-sedimentary rocks, metabasalts and high-Mg basic rocks (Slabunov et al. 2006 and references therein).

Neoarchean (2720 Ma, Volodichev et al. 2004, Kaulina & Apanasevich, 2005) eclogites were found in two areas of the BP. In the Gridino area, an eclogite-bearing mélange forms tectonic slate (Slabunov et al. 2006). Eclogites correspond to tholeiite-series MORB and oceanic-plateau basaltic rocks. The Gridino eclogite consists of omphacite with 27-31% Jadeite, 20-22% homogeneous garnet – Prp (F=0.67-0.68), accessory rutile and zircon. The eclogites were formed at *T*=740-865°C and *P*=14.0-17.5 kbar (Volodichev et al. 2004). Eclogite-bearing mélange was formed during subduction or collision.

From 2.72–2.71 Ga onwards, collision tectonics took place in all parts of the BP forming nappe structures (Miller & Milkevich 1995), high pressure metamorphism (kyanite–orthoclase subfacies: T = 650–700°C; P = 12–13 kbar, Volodichev 1990) and granite formation (migmatite fields and leucogranite massifs with the geochemical characteristics of collisional S-type granites were formed); granite-gneiss domes were formed at the same time in the western part of the structure.
2701 Ma leucogabbro massifs were probably formed during the collision orogen collapse stage. Volcanogenic molasse (with subalkaline volcanic rock and polymictic conglomerate lenses) of the Voche-Lambina GB was produced at the same time (Mitrofanov & Pozhelenko, 1991).

The crustal evolution of the BP during the period 2.9-2.66 Ga is similar to the evolution of Phanerozoic collision orogens.

References

Bibikova E.V., Glebovitskii V.A., Claesson S., Miller Yu.V., Kirnozova T.I., Myskova T.A., L'vov A.B. & Makarov V.A., 2001, New isotopic data on the protolith age and evolutionary stages of the Chupa Formation, Belomorian Belt, Geochemistry International (Moscow), 39(Suppl. 1), 12–17.

Bibikova E.V., Samsonov A.V., Shchipansky A.A., Bogina M.M., Gracheva T.V. & Makarov V.A., 2003, The Hisovaara structure in the Northern Karelian greenstone belt as a Late Archean accreted island arc: isotopic geochronological and petrological evidence, Petrology (Moscow), 11(3), 261–290.

Berzin R.G., Suleimanov A.K., Zamozhnyaya N.G., Andryushchenko Y.N. & Stupak V.M., 2001, Geophyzical investigations on regional profile 4B SVEKALAPKO, in *Deep Structure and Crustal Evolution of the Eastern Fennoscandian Shield: Kem'Kalevala Reflection Profile*, Sharov, N.V., ed, 39–63, Karelian Sci. Centre RAS, Petrozavodsk. [In Russian].

Hölttä P., Balagansky V., Garde A., Mertanen S, PeltonenP., Slabunov A., Sorjonen-Ward P. & Whitehouse M., 2008, Archean of Greenland and Fennoscandia, Episodes, Special Issue, 31 (1), 13–19.

Kaulina T. & Apanasevich E., 2005, Late archaean eclogites of the Kola Peninsula (NE Baltic shield): U-Pb and Sm-Nd data, 7nd International Eclogite Conference, Seggau (Austria), Mitt. Österr. Miner. Ges. 150, 64.

Kozhevnikov V.N., 2000, *Archean greenstone belts of the Karelian Craton as accretionary orogens,* 223, Karelian Res. Centre, Petrozavodsk. [in Russian].

Miller Yu.V. & Mil'kevich R.I., 1995, The fold-and-nappe structure of the Belomorian zone and its relationship with the Karelian granite–greenstone domain, Geotectonics, 6, 80-93.

Mitrofanov F.P. & Pozhilenko V.I. , eds, 1991, *The Voche-Lambina Archean Geodynamic Testing Site in the Kola Peninsula,* 196, Kola Sci. Center, Acad. Sci. USSR, Apatity. [in Russian].

Sharov N.V., Slabunov A.I., Isanina E.V., Krupnova N.A., Roslov Y.V. & Shchiptsova N.I., 2010, Seismic simulation of the Earth's crust on the profiles DSS –CDP Kalevala-Kem'-White Sea, Geophysical Journal (Ukraina). (In press)

Shchipansky A.A., Konilov A.N., Mints M.V., Dokukina K.A. & Sokolikova S.Y., 2005, Late Archean Salma eclogites, Belomorian mobile belt, Kola Peninsula, Russia: petrogenesis, age and implication for the geodynamic interpretation of early continental crust-forming environments, in *The Belomorian mobile belt and its analogues: geology, geochronology, geodynamics and metallogeny, Field trip guied book and Extended abstracts*, Karelian Sci. Centre RAS, Petrozavodsk, 324–327.

Shchipansky A.A., Samsonov A.V., Bibikova E.V., Babarina I.I., Konilov A.N., Krylov K.A., Slabunov A.I. & Bogina M.M., 2004, 2.8 Ga boninite-hosting partial suprasubduction ophiolite sequences from the North Karelian greenstone belt, NE Baltic Shield, Russia, in *Precambrian Ophiolites and Related Rocks*, Kusky T., Veenstra V. & Condie K., eds, Amsterdam: Elsevier, 425–487.

Slabunov A.I., 2008, *Geology and geodynamics of Archean mobile belts (example from the Belomorian province of the Fennoscandian Shield)*, KarRC, RAS, Petrozavodsk. [in Russian] , 298.

Slabunov A.I., Lobach-Zhuchenko S.B., Bibikova E.V., Sorjonen-Ward P., Balagansky V.V., Volodichev O.I., Shchipansky A.A., Svetov S.A., Chekulaev V.P., Arestova N.A. & Stepanov V.S., 2006, The Archean nucleus of the Fennoscandian (Baltic) Shield, in *European Lithosphere Dynamics*, Gee D.G. & Stephenson R.A., eds, Geological Society of London, Memoir, 32, 627–644.

Slabunov A.I., Stepanova A.V. & Bibikova E.V., 2009, Mesoarchean segment of ocean crust (Central-Belomorian Greenstone Belt of the Belomorian Province), in *Archean granite-greenstone systems and their younger analogues, Extended abstracts and Guidebook of field trips*, Karelian Res. Centre, RAS, Petrozavodsk, 154–156.

Volodichev O.I., 1990, *The Belomorian complex of Karelia: geology and petrology*, Nauka, Leningrad. [in Russian], 248.

Volodichev O.I., Slabunov A.I., Bibikova E.V., Konilov A.N. & Kuzenko T.I., 2004, Archean eclogites in the Belomorian mobile belt, Baltic Shield, Petrology, 12, 540–560.

EVOLUTION OF A CONTINENTAL MARGIN: THE MESOPROTEROZOIC BALTICA–LAURENTIA MARGIN

T. Slagstad[1], N. Culshaw[2], M. Marker[1] & T. Røhr[1]

[1]Geological Survey of Norway, 7491 Trondheim, Norway
[2]Department of Earth Sciences, Dalhousie University, Halifax, NS, Canada, B3H 3J5

Introduction

Baltica and Laurentia are generally interpreted to have been contiguous throughout the Late Palaeo- and Mesoproterozoic Eras (Fig. 1), thus representing one of the oldest, and longest-lived Andean-type margins in the world. This interpretation is based on scant palaeomagnetic evidence, the quality of which is debated (e.g., Romer 1996), as well as correlation of major geological events (e.g., Bingen et al. 2002, Åhäll & Connelly 2008). However, detailed knowledge is lacking from parts of the margin, hampering a more comprehensive understanding of its evolution and along-strike variation in terms of the nature and timing of tectonic events. In particular, data from the period 1500 Ma (the last known, major magmatic event, Bingen et al. 2005) to ca. 1050–1000 Ma (initiation of the main Sveconorwegian orogenic phase, Bingen et al. 2008) — covering almost the entire Mesoproterozoic Era — are scarce from Baltica. Here, we present new geochronological and geochemical data from the Sveconorwegian Province in southwest Norway and the southwestern Grenville Province in Ontario. The new data allow us to discuss and refine interpretations for the Mesoproterozoic tectonomagmatic evolution of the Baltica–Laurentia margin at a relatively high level of detail, and elucidate some of the processes that operated along the margin.

Andean setting at 1500 Ma

Amalgamation of the core of the Fennoscandian Shield was complete by ca. 1850 Ga, and was followed by subduction-related magmatism and accretion along its southwestern margin until ca. 1500 Ma (Bingen et al. 2005, Åhäll & Connelly 2008, this work), apparently accompanied by continental back-arc rapakivi magmatism up to several 100 km inboard of the margin (Åhäll et al. 2000). A similar Late Palaeoproterozoic evolution has also been suggested for Laurentia (Karlstrom et al. 2001). At ca. 1470 Ma, a major magmatic province, the Eastern Granite-Rhyolite Province, formed in Laurentia by partial melting of pre-existing continental crust (Van Schmus et al. 1996). The tectonic setting in which this province formed has long been debated, however, recent geochemical, age and Sm–Nd isotopic data from the Central Gneiss Belt in the Grenville Province in Ontario suggest it formed inboard of an extensional, active continental margin (Slagstad et al. 2009). Extension both within and behind the arc was accompanied by mafic underplating, which in turn induced partial melting in the overlying mature to juvenile continental crust. The data thus indicate simultaneous reworking and formation of new crust along the Laurentian margin. A similar evolution appears to have taken place in southwest Baltica, where recent work shows that continental-margin magmatism, represented by abundant calc-alkaline, mainly intermediate to felsic magmatic rocks, continued until at least 1490 Ma, and was accompanied by crustal melting and rhyolitic magmatism to the northeast, in the Rjukan Group (Menuge & Brewer 1996). Lithologically and temporally similar rocks to the Rjukan Group are found in the Wakeham Group in eastern Quebec (van Breemen & Corriveau 2005). This indicates that a similar tectonic regime operated along much of the Baltica–Laurentia margin at roughly the same time, implying a link to continental-margin processes, most likely related to slab roll back.

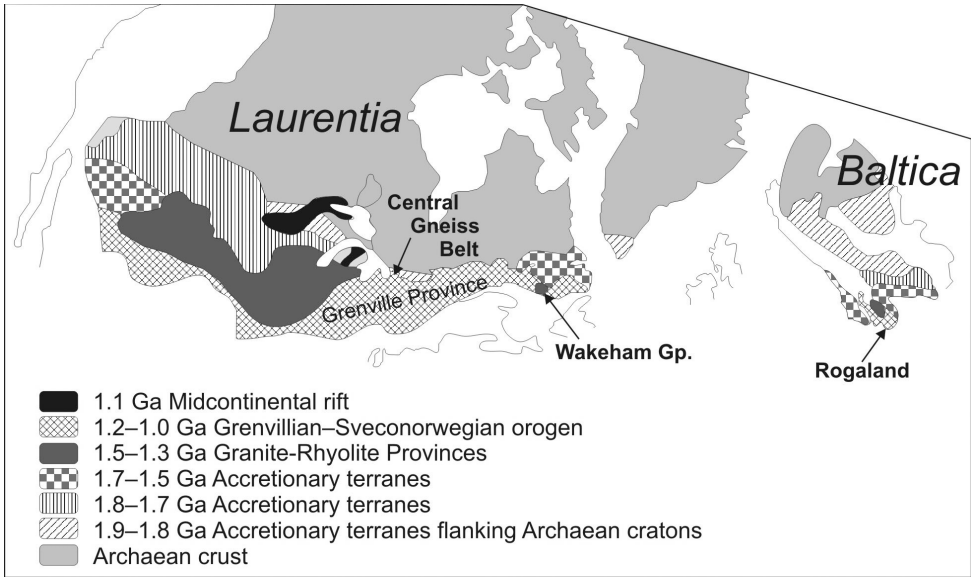

Figure 1. The figure shows the configuration of Baltica and Laurentia between ca. 1.8 and 1.2 Ga, modified after Menuge & Brewer (1996).

Mesoproterozoic (1500–1200 Ma) evolution

This time period is relatively well understood in Laurentia, and appears to be characterised by formation of successively younger arcs and back-arcs formed southeast and outboard of the Laurentian margin. Geochemical, Sm–Nd isotopic and detrital zircon data from amphibolites and metasedimentary rocks in the Sand Bay, Lower-and Upper Lighthouse, and Parry Island gneiss associations (Central Gneiss Belt) show that they were deposited on thinned continental crust in back-arc and intra-arc/arc-rift settings after ca. 1350 Ma. The detrital zircon data show that these rocks can be correlated with the Composite and Frontenac Arc Belts, overlying the Central Gneiss Belt, where arc- and back arc-related magmatism continued in until ca. 1200 Ma (e.g., Carr et al. 2000). The investigated rocks are associated with anorthosite, and we speculate that deep-crustal and supracrustal magmatic products of back-arc rifting were juxtaposed during attempted subduction of the attenuated continental crust. These events were roughly coeval with formation of the Southern Granite-Rhyolite Province in a similar tectonic setting to the southwest on the Laurentian margin (Mosher 1998).

In the county of Rogaland, in southwest Baltica, there is evidence of magmatism from ca. 1260 to 1200 Ma (Bingen et al. 2002, Brewer et al. 2004), which Brewer et al. (2004) interpreted to reflect continental extension in a back-arc setting. However, evidence of arc magmatism during the Mesoproterozoic is restricted to the ca. 1200 Ma Tromøy arc (Knudsen & Andersen 1999), in the interior of the Sveconorwegian orogen. Thus, although the Laurentian and Baltican margins are typically considered to have been contiguous at this time (e.g., Bingen et al. 2002, Johansson 2009) rocks signalling widespread formation of arcs/back-arcs along the Baltican margin appear to be missing. New geochemical and age data from southwest Norway suggest that continental extension during the 1260–1200 Ma period was accompanied by deposition of immature sediments (pelites) and mafic, MORB-type amphibolite, followed by deposition of quartzite, calc-silicate gneiss and impure marble. In addition to typical 'Baltican' zircons in the age range 1900–1700 Ma, these sediments contain abundant zircons ranging in age from 1500 to 1200 Ma, with peaks at ca. 1350 and 1500 Ma. The 1500 Ma zircons were derived from the presumed basement in the region, whereas no obvious source has been identified for the younger grains. We speculate that the younger zircons may reflect arc and back-arc magmatism near the Baltican margin, similar to that proposed for the Laurentian margin, and plan to undertake Hf-isotope analyses of these zircons to shed light on their origin. Recent field work in Rogaland shows that the 1500 Ma arc-related orthogneisses were deformed prior to intrusion of mafic dykes with MORB compositions. The dykes cross-cut the gneissic fabric in the rocks, but over a distance of a few kilometres become transposed into parallelism with the fabric in the orthogneiss. The transposition is most likely related to Sveconorwegian deformation at ca. 1000 Ma, and indirect evidence suggests that intrusion of the mafic dykes took place around 1220 Ma. This implies a deformational event between 1500 and 1220 Ma. We tentatively interpret this event to reflect accretion along the Baltican margin, suggesting that the margin oscillated between extension and compression. A similar change in setting has previously been proposed for the Laurentian margin (Rivers & Corrigan 2000).

From Andean- to SW Pacific-type continental margin

A change in tectonic regime, from mainly continental, Andean-type arc magmatism, to oceanic arc and back-arc magmatism, appears to have taken place between 1500 and 1400 Ma along the Baltica–Laurentia margin. Detrital zircon data from the Central Gneiss Belt show that the oceanic arcs/back-arcs received variable input of continental material, either from the continent itself or from rifted and thinned continental fragments. The detrital zircon data from Baltica also suggest proximity to continental crust, with deposition of sediments derived from Palaeoproterozoic ('Baltica') as well as Mesoproterozoic (oceanic arcs) sources. Thus, the post-1500 Ma Baltica–Laurentia margin probably resembled the present-day southwest Pacific margin, suggesting a change in the overall tectonic setting at ca. 1500 Ma. Formation of arcs and intra-arc/back-arc basins over a period of several 100 million years implies the presence of a very long-lived ocean, wide enough to deliver old and cool oceanic crust to the margin. The data from Baltica and Laurentia also suggest several episodes of back-arc magmatism, up to 500–1000 km inboard from the margin. This contrasts with modern-day plate margins, where back-arc magmatism is generally located less than a few hundred kilometres from the margin.

References

Åhäll K.-I. & Connelly J.N., 2008, Long-term convergence along SW Fennoscandia: 330 m.y. of Proterozoic crustal growth, Precambrian Research, 161, 452–472.

Åhäll K.-I., Connelly J.N. & Brewer T.S., 2000, Episodic rapakivi magmatism due to distal orogenesis?: Correlation of 1.69–1.50 Ga orogenic and inboard, "anorogenic" events in the Baltic Shield, Geology, 28, 823–826.

Bingen B., Nordgulen Ø. & Viola G., 2008, A four-phase model for the Sveconorwegian orogeny, SW Scandinavia, Norwegian Journal of Geology, 88, 43–72.

Bingen B., Mansfeld J., Sigmond E.M.O. & Stein H.J., 2002, Baltica-Laurentia link during the Mesoproterozoic: 1.27 Ga development of continental basins in the Sveconorwegian Orogen, southern Norway, Canadian Journal of Earth Sciences, 39, 1425–1440.

Bingen B., Skår, Ø., Marker M., Sigmond E.M.O., Nordgulen Ø., Ragnhildstveit J., Mansfeld J., Tucker R.D. & Liégeois J.-P., 2005, Timing of continental building in the Sveconorwegian orogen, SW Scandinavia, Norwegian Journal of Geology, 85, 87–116.

Brewer T.S., Åhäll K.-I., Menuge J.F., Storey C.D. & Parrish R.R., 2004, Mesoproterozoic bimodal volcanism in SW Norway, evidence for recurring pre-Sveconorwegian continental margin tectonism, Precambrian Research, 134, 249–273.

Carr S.D., Easton R.M., Jamieson R.A. & Culshaw N.G., 2000, Geologic transect across the Grenville orogen of Ontario and New York, Canadian Journal of Earth Sciences, 37, 193–216.

Johansson Å. 2009, Baltica, Amazonia and the SAMBA connection–1000 million years of neighbourhood during the Proterozoic? Precambrian Research, 175, 221–234.

Karlstrom K.E., Åhäll K.-I., Harlan S.S., Williams M.L., Mclelland J. & Geissman J.W., 2001, Long-lived (1.8-1.0 Ga) convergent orogen in southern Laurentia, its extensions to Australia and Baltica, and implications for refining Rodinia, Precambrian Research, 111, 5–30.

Knudsen T.-L. & Andersen T., 1999, Petrology and geochemistry of the Tromøy Gneiss Complex, south Norway, and alleged example of Proterozoic depleted lower continental crust, Journal of Petrology, 40, 909–933.

Menuge J.A. & Brewer T.S., 1996, Mesoproterozoic anorogenic magmatism in southern Norway, in *Precambrian Crustal Evolution in the North Atlantic Region*, Brewer, T.S., ed. Geological Society of London Special Publication 112, 275–295.

Mosher S., 1998, Tectonic evolution of the southern Laurentian Grenville orogenic belt, Geological Society of America Bulletin, 110, 1357–1375.

Rivers T. & Corrigan D., 2000, Convergent margin on southeastern Laurentia during the Mesoproterozoic: Tectonic implications, Canadian Journal of Earth Sciences, 37, 359–383.

Romer R., 1996, Contiguous Laurentia and Baltica before the Grenvillian-Sveconorwegian orogeny? Terra Nova, 8, 173–181.

Slagstad T., Culshaw N.G., Daly J.S. & Jamieson R.A., 2009, Western Grenville Province holds key to midcontinental Granite-Rhyolite Province enigma, Terra Nova, 21, 181–187.

Van Breemen O. & Corriveau L., 2005, U-Pb age constraints on arenaceous and volcanic rocks of the Wakeham Group, eastern Grenville Province, Canadian Journal of Earth Sciences, 42, 1677–1697.

Van Schmus,- W.R., Bickford M.E. & Turek A. 1996, Proterozoic geology of the east-central Midcontinent basement, in *Basement and Basins of Eastern North America*, van der Pluijm, B.A. & Catacosinos, P.A. eds., Geological Society of America Special Paper, 308, 7–32.

GLOBAL TRANSITION FROM GREENSTONE MAGMATISM TO CRATONISATION INVOLVED TWO CYCLES OF PYROCLASTIC VOLCANISM AND EXHUMATION

R.J. Squire[1], R.A.F. Cas[1] & I.H. Campbell[2]

[1]School of Geosciences, Monash University, Clayton, VIC, 3168
[2]Research School of Earth Sciences, The Australian National University, CANBERRA, ACT, 0200

Introduction

Archean cratons around the world contain voluminous greenstone lavas overlain by thick (up to 5 km) piles of felsic clastic detritus that record the transition from mafic-ultramafic volcanism to cratonisation. Unfortunately, an inability to clearly subdivide the superficially similar felsic clastic successions and correlate them between the various geological terranes and domains comprising the cratons has led to uncertainty about the timing and nature of their palaeogeographic and palaeotectonic evolution. This problem is further magnified when attempts are made to correlate the events associated with cratonisation at a global scale. To help address this problem, we present a review of the provenance characteristics, including detrital-zircon geochronology, for the late Archean felsic clastic successions of the eastern Yilgarn Craton. Our data show that the post-greenstone clastic successions may be subdivided into two major cycles that both commenced with voluminous pyroclastic volcanism and ended with widespread erosion associated with granite emplacement. Similar, albeit diachronous, cycles appear to be present in other late Archean cratons around the world suggesting the involvement of similar processes at a global scale. This refined interpretation provides a more robust framework for correlating the magmatic, sedimentary and deformational histories of the numerous cratons and will lead to an improved understanding of the palaeogeographic and palaeotectonic evolution of Earth's late Archean crust.

Post-greenstone clastic successions of the Eastern Goldfields Superterrane

The Eastern Goldfields Superterrane (EGST), which is located in the eastern part of the Yilgarn Craton (Fig. 1), Australia, is dominated by rocks generated between about 2715 and 2620 Ma. These late Archean successions are subdivided into three volcano-sedimentary packages that formed at ~2715−2690 Ma (the Kambalda Sequence, Swager et al., 1992), ~2690−2660 Ma (the Kalgoorlie Sequence, Hand et al., 2002; Krapež & Hand, 2008) and ~2660−2650 Ma (the late-basin (or late-stage basin) sequences, Krapež et al., 2008). Here, we are interested in the successions of the Kalgoorlie and Late Basin Sequences.

Krapež and Hand (2008) subdivided the thick packages of predominantly felsic clastic rocks overlying the greenstone lavas (i.e., the Black Flag Group) into four unconformity-bound sequences interpreted to span from about 2690 to 2658 Ma. The underlying greenstone

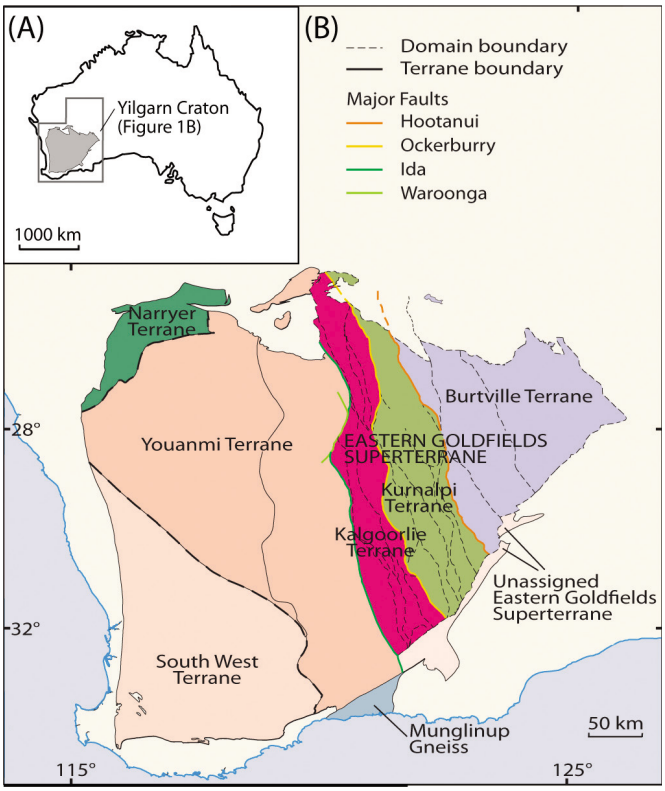

Figure. 1. Simplified geological map of the Yilgarn Craton. After Champion and Cassidy (2007).

units constrain the maximum depositional age to about 2690 Ma and a SHRIMP U−Pb zircon age of 2658 ± 3 Ma for the intrusive Mount Shea porphyry (Krapež et al., 2000) was used to indicate the minimum age. Although the source of the detritus was interpreted to include lavas, ash fallout deposits, pyroclastic flows, hydroclastic debris and subaerially reworked epiclastic, pyroclastic and hyrdroclastic units, it is unclear how the provenance of these successions relate to the three orogenic episodes that span the same interval (D1, D2 and D3, Blewett et al., under review) or the two major peaks in felsic magmatism in the region at about 2685 and 2665 Ma (Campbell and Hill, 1988; Champion and Cassidy, 2007). The highest erosion rates on Earth today occur on the flanks of subaerial volcanoes draped in recently erupted pyroclastic debris and in tectonically active continent−continent collision zones (Koppes and Montgomery, 2009). If similar environments were present during deposition of the Black Flag Group, as are commonly interpreted (e.g., Krapež et al., 2008; Krapež and Hand, 2008), their markedly different provenance should enable them to be distinguished (or correlated).

But this is not the case. Several units contain single populations of detrital zircons, suggesting provenance was from a remarkably homogenous source, whereas others display a broad mix of ages up to about 2800 Ma (Table 1, Krapež et al., 2000; Fletcher et al., 2001; Dunphy et al., 2003; Kositcin et al., 2008; Squire et al., under review).

A similar problem exists for the late-basin units that overlie the Black Flag Group. Krapež et al. (2008) suggested that deformational fabrics and intrusive relationships within rocks of the Kalgoorlie Sequence indicated that deposition probably occurred within five million years of about 2658 Ma. However, some units are dominated by a single population of zircons with a mean age of ~2670–2660 Ma (e.g., Navajo and Merougil Sequences, Krapež et al., 2000; Fletcher et al., 2001) and are dominated by volcanic quartz. In contrast, other units contains a broad spread of detrital-zircon ages, including several old grains up to about 3500 Ma (e.g., the Kurrawang Formation, Mt Belches Sandstone and the Wallaby Conglomerate, Krapež et al., 2000; Kositcin et al., 2008) and volcanic quartz is rare. Although Kositcin et al. (2008) noted the coincidence of the ~2665 Ma detrital-zircon population and a known peak in felsic magmatism (Champion and Cassidy, 2007), the palaeogeographic and palaeotectonic significance of the marked switch in provenance between the Late Basin units was not discussed.

Correlations of successions

The Black Flag Group is subdivided into an early Black Flag Group and late Black Flag Group based on marked differences in detrital-zircon age populations (Table 1), composition of the detritus and structural setting of the host basin (Squire et al., under review). The early Black Flag Group involved rapid reworking and redeposition of feldspar-rich pyroclastic debris generated at about 2690–2680 Ma. This event, and dolerite magmatism at about 2680 Ma (e.g., the Golden Mile Dolerite, Rasmussen et al., 2009), were generated during regional D_1 extension (Blewett et al., under review). In contrast, the predominantly coarse clastic facies of the late Black Flag Group were deposited in extensional basins at the margins of granite domes (e.g., Kanowna Belle, Agnew and Wallaby). Although minor felsic volcanism probably occurred coincident with this event from about 2675–2665 Ma, most of the detritus was sourced from the nearby substrate during regional doming (i.e., granite emplacement), which is reflected by detrital-zircon age populations (Table 1) and clast compositions. Blewett et al. (under review) interpreted this event as occurring during D_2, although the evidence for this remains equivocal.

The beginning of Late Basin deposition is heralded by the influx of the quartz-rich successions containing a single detrital-zircon age population at about 2665–2660 Ma such as the Merougil Group (Table 1). This event occurred broadly coincident with the peak in high-Ca granite magmatism and the compositional characteristics of these rocks (i.e., the dominance of volcanic crystal debris) suggest that they were sourced from a large quartz-rich pyroclastic eruption, although the sedimentary facies suggest reworking in subaerial and submarine environments prior to final deposition. Rare

Table 1. Subset of U–Pb detrital-zircon age data from the Kalgoorlie and Kurnalpie Terranes in the Yilgarn Craton. Samples containing less than 13 concordant results are not included in this table or the discussion. Source of data: A = Kositcin et al., (2008); B = Sircombe et al. (2007); C = Krapež et al. (2000); D = Dunphy et al. (2003); E= Fletcher et al. (2001). Abbreviations: n, number of concordant analyses; KT, Kalgoorlie Terrane; KuT, Kurnalpie Terrane; Form., Formation; sst., sandstone; congl., conglomerate. From Squire et al. (under review).

UNIT, TERRANE	LOCATION	SAMPLE	DESCRIPTION
Single population of detrital zircons with weighted mean age of ~2690-2680 Ma (CYCLE ONCE; early Black Flag Group)			
Black Flag Group, KT	North of St Ives	E321	2678 ± 6 Ma (n=18); feldspar-rich volcanic sandstone; (A)
Black Flag Group, KT	North of St Ives	E322	2676 ± 4 Ma (n=13); feldspar-rich volcanic sandstone; (A)
Spargoville Sequ., KT	Widgiemooltha	E7	2686 ± 3 Ma (n=18); dacitic breccia; (C)
Unnamed sst., KT	Lawlers, Agnew	E396	2689 ± 4 Ma (n=20); volcanic sandstone; (A)
Unnamed sst., KuT	Maggies Dam	E350	2676 ± 4 Ma (n=13); volcanic sandstone; (A)
Broad or mixed peak(s) ranging up to about 2800 Ma (CYCLE ONE: late Black Flag Group)			
Unnamed sst., KT	Widgiemooltha	E203	possibly bi-modal (peaks ~2687 & 2731 Ma); (n=26); volcanic sst; (A)
Golden Valley Congl., KT	Kanowna Belle	2004967308	possible dominant component ~2668 Ma; (n=32); volcanic sst.; (B)
Unnamed sst., KT	3-in-Hand, Kundana	2004967367	possible dominant component ~2696 Ma; (n=42); volcanic sst; (B)
Black Flag Group, KT	Eight Mile Dam	EMD2	possibly bi-modal (peaks ~2728 & 2666 Ma); (n=36); volcanic sst; (C)
Fifima Sst., KT	Genesis, Agnew	2001967052C	Broad spread; one old grain ~2816 Ma; (n=38); volcanic sst; (D)
Unnamed breccia, KuT	Granny Smith	E401	Insufficient data to pick clear peaks; (n=14); volcanic breccia; (A)
Unnamed sst, KuT	Yandal Station	E229	Broad spread; (n=40); volcanic sandstone; (A)
Unnamed sst, KuT	Twin Peaks	E314	Broad spread; (n=30); volcanic sandstone; (A)
Yilgangi Congl., KuT	Yilgangi	E337	Broad spread; possible peak ~2664 Ma; (n=41); volcanic sandstone; (A)
Single population of detrital zircons with weighted mean age of ~2670-2660 Ma (CYCLE TWO; Merougil Group)			
Merougil Sst., KT	St Ives	MB	2664 ± 6 Ma; (n=15); quartz-rich sandstone; (C)
Merougil Sst., KT	St Ives	MQ	2671 ± 6 Ma; (n=16); quartz-rich sandstone; (C)
Killaloe Form., KT	Buldania	BF-1	2667 ± 6 Ma; (n=31); quartz-rich sandstone; one old grain; (C)
Penny Dam Congl., KuT	Penny Dam	KU-2	2671 ± 3 Ma; (n=39); quartz-rich sandstone; (C)
Navajo Sst., KT	West of Kalgoorlie	2000967013	2657 ± 4 Ma; (n=29); quartz-rich sandstone; (E)
Broad spread, including several zircons between about 2800 & 3500 Ma (CYCLE TWO; Kurrawang Group)			
Kurrawang Form., KT	Kalgoorlie	KU-1	Broad spread with several >3 Ga zircons ;(n=35); quartz-rich sst.; (C)
Kurrawang Form., KT	Davyhurst	2004967366	Broad spread with several >3 Ga zircons ;(n=59); quartz-rich sst.; (B)
Jones Creek Congl., KT	Jones Creek	E178	Broad spread with several >3 Ga zircons ;(n=36); quartz-rich sst.; (C)
Mount Belches Sst, KuT	Mount Belches	KU-3	Broad spread with several >3 Ga zircons ;(n=48); quartz-rich sst.; (C)
Wallaby Congl., KuT	Wallaby	E319	Broad spread with several >3 Ga zircons ;(n=41); quartz-rich sst.; (A)
Unnamed sst., KuT	Lancefield	E313	Broad spread with several >3 Ga zircons ;(n=35); quartz-rich sst.; (A)

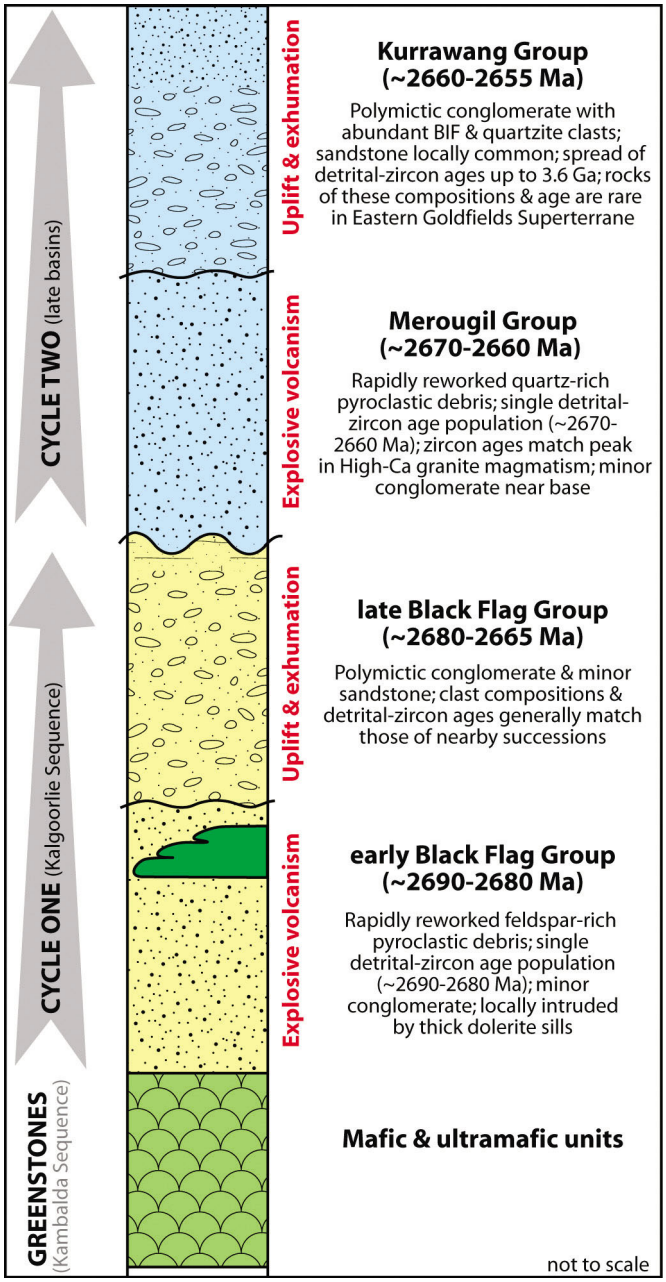

Figure 2. Sedimentary cycles for the post-greenstone successions in the Yilgarn Craton: Cycle One includes units of the Black Flag Group; Cycle Two includes the Merougil and Kurrawang Groups. From Squire et al. (under review).

conglomerate facies with clasts of diverse provenance near the base of the Merougil Group indicated local reworking in the lowermost part of this unit in the early stages of deposition, although for most of the units the restricted volcanic provenance suggests that deposition occurred soon after the eruption. The Kurrawang Group records the final depositional event of the EGST at about 2660–2655 Ma. The abundance of granitic, BIF and quartzite clasts in this unit, together with common detrital zircons aged 3500–2800 Ma, indicate the involvement of ancient continental c Mile Dolerite at about 2680 Ma. Uplift of these and surrounding successions during nascent granite doming created extensional basins (e.g., Wallaby, Kanowna Belle and Agnew) into which predominantly coarse conglomeratic and breccia facies of the 'late Black Flag Group' were deposited at about 2675–2665 Ma. The beginning of Cycle Two is heralded by the sudden influx of voluminous quartz-rich pyroclastic debris of the Merougil Group at about 2665–2660 Ma. These successions were deposited in northwest-trending basins that appear to truncate, and thus post-date, the Cycle One units. The mean ages of the detrital zircons from the Merougil Group match closely the age of the peak in high-Ca granite magmatism in the Yilgarn Craton and thus probably represent the surface expression of the same igneous event. Deposition of polymictic conglomerate units dominated by clasts of banded iron formation (BIF), granite and quartzite and unusually old detrital zircons represent the final stages of deposition associated with Cycle Two.

The refined depositional history of the EGST presented here is not only important for aiding palaeotectonic and palaeogeographic reconstructions of the Yilgarn Craton but will benefit similar correlations in late Archean Terranes from elsewhere in the world. For example, in Canada the Slave and Superior Cratons display evidence for remarkably similar cycles despite a diachroneity between both cratons and the Yilgarn Craton (Bleeker, 2003). Similar relationships appear to be present in Africa, although additional provenance data are required for many of the post-greenstone successions to confirm these observations. Once done, a more robust understanding of the cratonisation of the late Archean cratons will lead to an improved understanding of the palaeogeographic and palaeotectonic evolution of Earth at this time.

Acknowledgements

We thank Gold Fields Australia, Geological Survey of Western Australia, Barrick, the pmd*CRC and MERIWA for supporting the various research projects that have contributed to this study. In particular, we would like to thank D. Keys, S. Wyche, C. Hall, M. Pawley and C. Spaggiari for valuable discussions and input on the topic.

References

Bleeker W., 2003, The late Archean record: a puzzle in ca. 35 pieces. Lithos, 71, 99–134.

Blewett R.S., Czarnota K. & Henson P.A., under review, Structural-event framework for the Eastern Yilgarn Craton, and its implications for orogenic gold, Precambrian Research.

Campbell I.H. & Hill R.I., 1988. A two-stage model for the formation of the granite-greenstone terrains of the Kalgoorlie-Norseman area, Western Australia. Earth and Planetary Science Letters, 90, 11–25.

Champion D.C. & Cassidy K.F., 2007, An overview of the Yilgarn Craton and its crustal evolution, in Proceedings of Geoconferences (WA) Inc. Kalgoorlie '07 Conference, Bierlein F.P. & Knox-Robinson C.M., eds, Geosciences Australia, Record 2007/14, Kalgoorlie, Western Australia, 8–13.

Dunphy J.M., Fletcher I.R., Cassidy K.F. & Champion D.C., 2003. Compilation of SHRIMP U-Pb geochronological data, Yilgarn Craton, Western Australia 2001-2002, Geoscience Australia, Record 2003/15, 139.

Fletcher I.R., Dunphy J.M., Cassidy K.F. & Champion D.C., 2001, Compilation of SHRIMP U−Pb geochronology data, Yilgarn Craton, Western Australia, 2000−01, Geoscience Australia Record 2001/47, 111p.

Hand J.L., Cas R.A.F., Ong L., Brown S.J.A., Krapež B., Barley M.E. & 2002, Syn- and post-eruptive volcaniclastic sedimentation in Late Archaean subaqueous depositional systems of the Black Flag Group, Eight Mile Dam, Kalgoorlie, Western Australia, in Precambrian sedimentary environments: a modern approach to ancient depositional systems, Altermann, W. & Corcoran, P.L., eds, Blackwell Science Ltd, Oxford, UK, 2002, 235–258.

Koppes M.N. & Montgomery D.R., 2009, The relative efficacy of fluvial and glacial erosion over modern to orogenic timescales, Nature Geoscience 2, 644–647.

Kositcin N., Brown S.J.A., Barley M.E., Krapež B. Cassidy, K.F. & Champion, D.C., 2008, SHRIMP U-Pb zircon age constraints on the late Archaean tectonostratigraphic architecture of the Eastern Goldfields Superterrane, Yilgarn Craton, Western Australia, Precambrian Research 161, 5–33.

Krapež B., Barley M.E. & Brown S.J.A., 2008, Late Archaean synorogenic basins of the Eastern Goldfields Superterrane, Yilgarn Craton, Western Australia. Part I. Kalgoorlie and Gindalbie Terranes, Precambrian Research 161, 135–153.

Krapež B., Brown S.J.A., Hand J., Barley M.E. & Cas R.A.F., 2000, Age constraints on recycled crustal and supracrustal sources of Archaean metasedimentary sequences, Eastern Goldfields Province, Western Australia: evidence from SHRIMP zircon dating, Tectonophysics, 322, 89–133.

Krapež B. & Hand J.L., 2008, Late Archaean deep-marine volcaniclastic sedimentation in an arc-related basin: The Kalgoorlie Sequence of the Eastern Goldfields Superterrane, Yilgarn Craton, Western Australia, Precambrian Research 161, 89–113.

Rasmussen B., Mueller A.G. & Fletcher I.R., 2009, Zirconolite and xenotime U−Pb age constraints on the emplacment of the Golden Mile Dolerite sill and gold mineralization at the Mt Charlotte mine, Eastern Goldfields Province, Yilgarn Craton, Western Australia, Contributions to Mineralogy and Petrology, 157, 559–572.

Sircombe K., Cassidy K.F., Champion D.C. & Tripp G.I., 2007, Compiliation of SHRIMP U-Pb geochronological data, Yilgarn Craton, Western Australia, 2004-2006, Geoscience Australia, Record, 2007/01, 182.

Squire R.J., Allen C.M., Cas R.A.F., Campbell I.H., Blewett R.S. & Nemchin, A.A., under review. Transition from greenstone volcanism to cratonisation in the eastern Yilgarn Craton, Western Australia, revealed by provenance characteristics of late Archean sedimentary successions, Precambrian Research.

Swager C.P., Witt W.K., Griffin T.J., Ahmat A.L., Hunter W.M., McGoldrick P. & Wyche S., 1992, Late Archaean granite-greenstones of the Kalgoorlie Terrane, Yilgarn Craton, Western Australia, in, The Archaean — Terrains, Processes and Metallogeny, Glover, J.E., Ho, S.E., eds, Geology Department and University Extension Services, University of Western Australia Publication 22, 107–122.

DETRITAL ZIRCON SHRIMP U-Pb AGE OF THE 2.3 GA DIAMICTITES OF THE METEORITE BORE MEMBER IN THE SOUTH PILBARA, WESTERN AUSTRALIA

M. Takehara[1], M. Komure[1], S. Kiyokawa[1], K. Horie[2] & K. Yokoyama[3]

[1]Department of Earth and Planetary Sciences, Kyushu University, Hakozaki, Higashi-ku, Fukuoka, 812-8581, Japan, [2]National Institute of Polar Research, 10-3, Midoricho, Tachikawa, Tokyo, 190-8518, Japan [3]National Museum of Nature and Science, 3-23-1, Hyakunincho, Shinjuku-ku, Tokyo, 169-0073, Japan

Introduction

The Meteorite Bore Member, which is a part of the Turee Creek Group in the upper most Mount Bruce Supergroup, is composed of more than 300m thick diamictites within a shale-rich sedimentary sequence. Dropstones and striated clasts in the diamictites suggest that the Meteorite Bore Member is composed of low-latitude glacial deposits (Trendall & Blockley, 1970, Martin, 1999). The depositional age of the Meteorite Bore Member is constrained to 2.4-2.3 Ga by the underlying 2449 Ma Woongarra Rhyolite of the upper part of Hamersley Group (Barley et al., 1997), and by the overlying 2209 Ma Cheela Springs Basalt of the Wyloo Group (Martin et al., 1998). Moreover, similar deposits are present in the Huronian Group, Canada and the Transvaal Group, South Africa, evidence of an early Proterozoic ''Snowball earth'' event (Kirschvink et al., 2000). This is thought to be one of the important events in forming the Great Oxidation event and in constructing a supercontinent in early Proterozoic (e.g. Eyles, 2008). Martin (1999) carried out a detailed lithological study in the Meteorite Bore Member. Based on lithology, distribution of rock types and lateral variation, he reconstructed the paleotopography of the Pilbara Craton at the time of Paleoproterozoic glaciation. The purpose of this study is to understand the clast composition and to date detrital zircon in the matrix of the Meteorite Bore Member, to gain a more detailed understanding of the paleogeography of the Pilbara Region around 2.3 Ga. Therefore we studied the Meteorite Bore Member in the Meteorite Bore area where the diamictite bed is thickest.

Lithology

The Meteorite Bore Area is located on the south limb of the Hardey Syncline in the southern Hamersley Basin, formed during the 2.2 Ga Ophthalmian Orogeny. An axial-planar cleavage is well developed throughout the whole area. The Meteorite Bore Member is mainly composed of poorly sorted, mud matrix-supported conglomerates. Although the conglomerates are deformed and the matrix is strongly foliated, the grains are well preserved. The conglomerates consist mainly of cobbles, with boulders up to 300 mm in diameter present. They are mainly composed of felsic volcanic rock and medium to coarse-grained sandstones, with minor amounts of BIF, chert, dolerite and mudstone clasts.

Outsized Clasts

The distribution of outsized clasts in the mud matrix is similar to the results of Martin (1999). The clasts mainly consist of fine sandstone, felsic volcanic rock (rhyolite) and small amount of BIF, chert, dolerite, conglomerate, mudstone and quartz pebbles. We carried out whole rock XRF analysis of the clasts of felsic volcanic rock in the Meteorite Bore Member and in the Woongarra Rhyolite. Major element composition of these samples fit in the rhyolite field. The spider diagrams of N- MORB normalized trace elements show the same pattern.

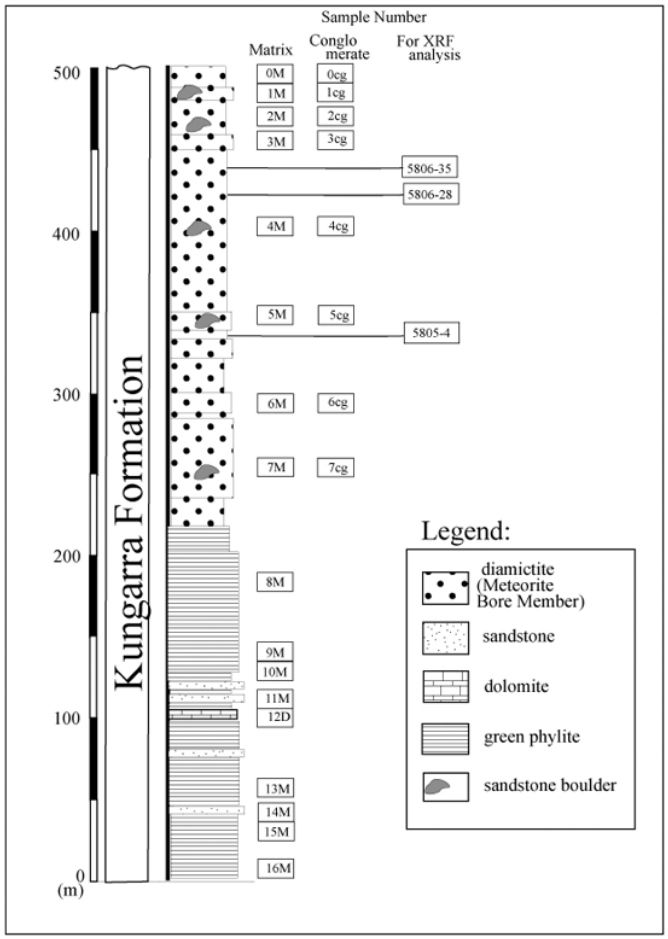

Figure l. Stratigraphic sections of green phyllite and overlying diamictite in the Meteorite Bore area, Southern Pilbara. Shown are the sample numbers for the detrital zircon U-Pb dating and whole rock XRF analysis. M: Samples of matrix, cg: Samples of clasts, D: Samples of dolomites, and 5806-35,5806-28,5805-4: Samples for XRF analysis.

U-Pb SHIRIMP Zircon age

The U–Pb age dating of detrital zircon from the matrix of the diamictites using SHRIMP provided critical information for the provenance of the Meteorite Bore Member. Most of the zircon ages clustered within the

range of approximately 2490-2420 Ma, with a few ages corresponding to older zircons. The probability distribution in the range of 2490-2420 Ma included two obvious peaks of the zircon ages at 2468 and 2438 Ma.

Origin of clasts and Paleotopography

Based on the clast lithology and matrix zircon dating, the diamictites of the Meteorite Bore Member are derived mainly from the Woongarra Rhyolite. Matrix detrital zircon ages of 2490 Ma match the depostional age of the Brockman Iron Formation. However, banded iron formation clasts are not well preserved. A minor amount of banded iron formation among the clasts might be from the Boolgeeda Iron Formation, in the upper-most Hamersley Group. The erosion surface in the Pilbara to the north must have reached down to the lower part of the Woongarra Rhyolite, which in the Hardey Syncline area is stratigraphically 1500 m below the Meteorite Bore Member. The Meteorite Bore Member at the Hardy Syncline area was thought to be deposited in a foreland basin, known as the McGrath trough (e.g. Horwitz, 1982), deepening to the south. This suggested the northern Pilbara was uplifted at least 500 to 1000 m and eroded between 2.4 and 2.3 Ga. After the glaciation, sedimentary facies quickly changed to red bed sandstones, with the MacGrath trough covered by a very shallow ocean.

Acknowledgements

We thank Y.Tsutsumi and M.Shigeoka for helping with the analysis at the National Science Museum. We acknowledge support from JSPS foundation (No.1434053).

References

Barley M.E., Pickard A.L. & Sylvester P.J., 1997, Emplacement of a large igneous province as a possible cause of banded iron formation 2.45 billion years ago, Nature, 385, 55–58.

Horwitz R.C., 1982, Geological History of the Early Proterozoic Paraburdoo hinge zone, Western Australia, Precambrian Research, 19, 191–200.

Kirschvink J.L., Gaidos E.J., Bertani L.E., Beukes, N.J., Gutzmer J., Maepa L.N. & Steinberger R.E., 2000, The Paleoproterozoic Snowball Earth: extreme climatic and geochemical global change and its biological consequences, National Academy of Sciences, Proceedings, 97, 1400–1405.

Martin D.McB., 1999, Depositional setting and implications of Paleoproterozoic glaciomarine sedimentation in the Hamersley Province, Western Australia, Geological Society of America Bulletin, 111, 189–203.

Martin D.McB., Li Z.X., Nemchin A.A. & Powell C.McA., 1998, A pre-2.2 Ga age for giant hematite ores of the Hamersley province, Australia, Economic Geology, 93, 1084–1090.

Trendall A.F. & Blockley J.G., 1970, The iron formations of the Precambrian Hamersley Group, Western Australia; With special reference to the associated crocidolite, Geological Survey of Western Australia Bulletin, 119, 366p.

MID CRUSTAL METAMORPHIC EVIDENCE FOR MANTLE HEATING OF THE KAAPVAAL CRATON AT 2.73 Ga

J. Taylor[1], G. Stevens[1] & C. Lana[1]

[1]*Department of Earth Science, University of Stellenbosch, Matieland 7602, South Africa*

Introduction

In comparison with the well established geodynamic framework that exists for the Barberton Greenstone Belt (BGB), the tectonometamorphic history of the 3.7-3.2 Ga Ancient Gneiss Complex (AGC) of Swaziland, located S and SE of the BGB (Fig. 1), is poorly constrained. The AGC was accreted onto the eastern margin of the greenstone belt at ~3.23 Ga (Schoene et al. 2008) and as it is an allochthonous terrane, may record aspects of crustal evolution that the BGB does not. In general, the AGC is characterised by higher metamorphic grades than the low-grade rocks of the Barberton terrane. In south-central Swaziland, pelitic granulites and orthogneisses preserve evidence of a period of high temperature metamorphism and deformation that was accompanied by abundant in situ crustal anatexis. Of the limited studies that have focussed on these rocks, none have successfully establish the setting and regional context for the high-grade metamorphism (Wilson & Jackson 1988, Kröner et al. 1993, Condie et al. 1996). The granulites are restricted to three main areas (Fig. 1), however the metamorphic relationship between the areas is undetermined and it remains ambiguous whether they record the same high-grade event. For example, area A is comprised of migmatitic paragneisses overlying basement orthogneisses that crop out along the Mkhondo River in south-central Swaziland where the timing of the metamorphism has been constrained to ca 2.73 Ga (zircon U-Pb SHRIMP age, Taylor et al. 2010). Areas B and C are dominated by paragneisses that crop out along the Luboya and Matsanjeni Rivers E and NE of area A, where an age of 3.3 Ga (mean 207Pb/206Pb zircon evaporation age) has been proposed for the timing of the metamorphism (Kröner et al. 1993). In addition, a wide range of peak metamorphic pressure-temperature (P-T) estimates have been proposed for these rocks. Thus, the primary aims of the current study are to establish the regional context for the granulite facies metamorphism in the three areas by providing better constraints on the conditions and timing of the metamorphism and deformation, and to explore the broader implications of this for the tectono-metamorphic evolution of the Kaapvaal craton.

Conditions of metamorphism, anatexis and deformation

Area A

The supracrustal sequence in area A is characterised by a thick succession of migmatitic, metapelitic garnet-cordierite-biotite-feldspar ± orthopyroxene bearing gneisses, metapsammitic cordierite-biotite-feldspar gneisses, metaquartzites, minor BIF and mafic amphibolite gneisses. As garnet is developed in conjunction with leucosomes at the sites of melting, partial melting in the metapelites involved incongruent, fluid absent melting of biotite via the reaction Bt + Qtz + Pl → Grt + Crd + Kfs + Melt. Mineral equilibria modelling of the dominant metamorphic assemblage in the metapelites, Grt + Bt + Crd + Pl + Kfs + Ilm + Qtz + Melt in NCKFMASHTO (Thermocalc v3.30, Holland & Powell 1998), constrains the conditions of peak metamorphism in area A to 830-855ºC at 4.4-6.4 kbars (Fig. 1). The cooling path is constrained by overlapping the mineral assemblage stability fields with measured mineral compositions in the rock. Deformation in area A is dominated by open, upright folding during NE-SW directed compression, resulting in folds that plunge shallowly towards the NW (Fig. 1). The high-grade fabric is parallel to the layering/compositional banding, and garnet-bearing leucosomes associated with melt segregation are in turn developed parallel to the fabric/layering and are themselves undeformed. Therefore the dominant style of deformation in area A, D1, was characterised by NE-SW directed compression and coincided with high-grade metamorphism and melting.

Areas B & C

In area B, fluid absent melting of biotite and sillimanite via the reaction Bt + Qtz + Pl + Sil → Grt + Crd + Kfs + Melt was responsible for the bulk of the melt. The area is dominated by garnet-cordierite-biotite-sillimanite-feldspar-spinel bearing metapelites and minor garnet-biotite-feldspar metapsammites. Mineral equilibria modelling of the assemblage Grt + Bt + Crd + Sil + Kfs + Ilm + Qtz + Melt using a typical metapelite composition constrains peak metamorphism in Area B to 800-875ºC at 5.5-7.3 kbars (Fig. 1). The cooling path is constrained by the overlap between the mineral assemblage stability fields and measured mineral compositions in the rock

Area C consists of a compositionally diverse suite of metapelitic, metapsammitic and quartzofeldspathic gneisses displaying various degrees of in situ partial melting. Typical peak metamorphic assemblages in the metapelites and metapsammites include garnet-biotite-feldspar ± orthopyroxene, cordierite-biotite-sillimanite-feldspar and cordierite-biotite-orthopyroxene-feldspar. Modelling of the assemblage Grt + Bt + Opx + Pl + Kfs + Ilm + Qtz + Melt using a metapsammite composition and measured Ca in Grt compositional isopleths, constrains peak metamorphism in area C to 830-870ºC at 6.5-7.6 kbars, however, a relatively ill-constrained cooling path is defined. In contrast, modelling of the assemblage Crd + Bt + Sil + Pl + Kfs + Rt + Qtz + Melt produces poor peak P-T constraints but a well-constrained cooling path, identical to the cooling path followed by area B (Fig. 1).

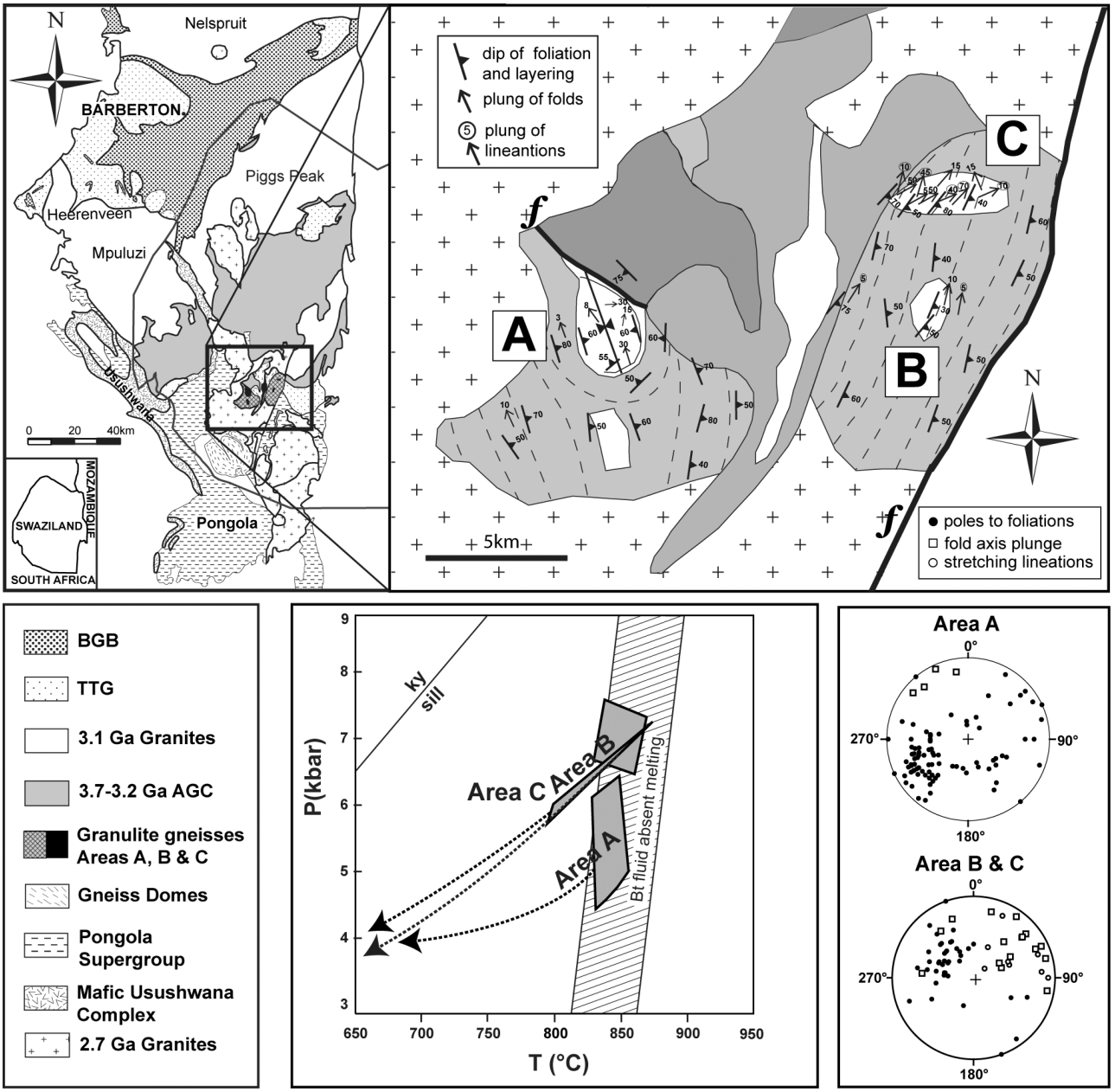

Figure 1. Schematic geological map of the Ancient Gneiss Complex (AGC) showing the location of, and structural and metamorphic data for, the granulite gneisses from study areas A, B & C.

In contrast to area A, the style of deformation in areas B and C was dominated by constrictional compression producing tube-like folds that plunge shallowly to the NE, strong mineral stretching lineations and rodding L-tectonite fabrics that plunge shallowly to the NE (Fig. 1). The folds are defined by the anatectic leucosomes themselves, and the peritectic mineral phases in them display a strong solid-state fabric that is parallel to the trend of the folds. Thus we interpret the dominant style of deformation in areas B and C, D2, to have immediately post-dated high-grade metamorphism and melting and the deformation to be associated with exhumation and uplift of the terrane.

Discussion and conclusions

Relating the three granulite terranes

Results from this study indicate that areas A, B and C underwent mid- to shallow crustal, granulite facies metamorphism at similar peak conditions (Fig. 1); that anatexis was associated with the production of significant volumes of S-type granitic melt; and that the areas subsequently followed similarly shaped cooling paths during exhumation. Area A experienced syn-peak metamorphic, NE-SW directed compressional D1 deformation. Areas B and C experienced syn- to post-peak, D2 deformation related to exhumation and uplift. Thus the combined metamorphic and structural data indicates that the three areas are related and formed part of one mid- to shallow crustal, Archaean granulite gneiss terrane.

Conclusions on the origin and setting for the high-grade metamorphism

Regardless of tectonic setting, the low-medium P, high T metamorphic conditions described for the granulite terrane was associated with an elevated apparent geotherm (±50°C/km) that necessitates the addition of mantle heat to the crust. In a recent study by Taylor et al. (2010), U-Pb SHRIMP dating of zircon from an in situ anatectic leucosome constrained the timing of the granulite facies metamorphism in area A to ca 2.73 Ga. This age corresponds with a number of regionally

significant, tectono-magmatic events on the Kaapvaal craton during the Neoarchaean. Firstly, it approximates the proposed age for continental collision and granulite-facies metamorphism in the Southern Marginal Zone of the Limpopo Belt at ca 2.7-2.6 Ga (Fig. 1) (Smit & Van Reenen 1997, Kreissig et al. 2001). In light of the syn- to post-peak deformation recorded in areas A, B and C, orogenic collapse and extension of hot over-thickened crust associated with the Limpopo Orogony seems plausible at first. However, the lack of extensive regional deformation, metamorphism and uplift that one would expect in areas such as the BGB and AGC, renders this hypothesis less likely. In fact, late D3 deformation in the BGB at ~3.10-3.07 Ga is the last penetrative deformation event recorded in the belt (Belcher & Kisters 2006), and thermochronology suggests that the BGB has not experienced temperatures in excess of 300°C since ~3.10 Ga (Schoene et al. 2008). In addition, the principal D1 compressive stresses that were active in area A are orthogonal to the trend of the Limpopo Belt, and, the age of ca 2.73 Ga for the metamorphism predates peak metamorphism in the Southern Marginal Zone by some 20-30 million years (Kreissig et al. 2001).

A second, more plausible theory is that granulite facies metamorphism in the AGC was coeval with a period of regional crustal anatexis, evidenced by extensive flood basalt volcanism on the craton at 2.71 Ga (the Ventersdorp Supergroup LIP, Armstrong et al. 1991) and widespread, intracratonic granitic magmatism. A significant proportion of these granites intruded the AGC and areas surrounding the Pongola Basin at ~2.72 Ga (Fig. 1). The elevated crustal geotherm at the time may therefore be related to underplating of the crust by Ventersdorp related magmas. D1 deformation in area A may be explained via comparison with the deformational styles in the Pongola and Central Rand depositional basins. The Pongola Supergroup, a Late Archaean supracrustal succession characterising the southeastern Kaapvaal craton and a proposed correlative of the Witwatersrand Supergoup, is dominated by major, upright, NW-SE trending folds (Gold & Von Veh 1995), ± parallel to the D1 folds. Similarly, a NE-SW directed compressive stress field is proposed to have existed during the later stages of Witwatersrand Basin development (Stanistreet & McCarthy 1991), and resulted in both the NW striking synsedimentary folds and block faulting that is characteristic of the Central Rand Basin.

Implications for the Kaapvaal craton crust

The granulites described in this study offer unique insight into the mid-crust of the Kaapvaal craton during the Neoarchaean, where the metamorphism is interpreted to reflect a period of anomalously high heat flow within the Kaapvaal craton crust. An increase in the heat input from the mantle via magmatic under- or intraplating is proposed to explain the observed thermal anomaly, with the Ventersdorp lavas being the eruptive manifestation of these mantle derived melts. We suggest the formation of a Ventersdorp aged plume marginal to the craton, which coincided with a globally recognized ~2.7 Ga mantle plume event. The high-T metamorphism provides evidence for significant mid-crustal heating, anatexis and, thus, rheological weakening of the crust. Mobilisation of the mid-crust as gneissic domes and syn-sedimentary basement uplift was concurrent with sedimentation of auriferous reefs of the Upper Central Rand Group of the Witwatersrand Supergroup and played an important role in the recycling of gold-rich horizons within the 2.89-2.71Ga Central Rand Basin (Tweedie 1986).

Acknowledgements

The authors gratefully acknowledge South African National Research Foundation (NRF) grant funding to Professor Gary Stevens via the SARChI programme, as well as a PhD Bursary to Jeanne Taylor.

References

Armstrong R.A., Compston W., Retief E.A., Williams I.S. & Welke H.J., 1991, Zircon Ion Microprobe studies bearing on the age and evolution of the Witwatersrand Triad, Precambrian Research, 53, 243–266

Belcher R.W. & Kisters A.F.M., 2006, Progressive adjustments of ascent and emplacement controls during incremental construction of the 3.1 Ga Heerenveen batholith, South Africa, Journal of Structural Geology, 28, 1406–1421

Condie K.C., Kröner A. & Milisenda C.C., 1996, Geochemistry and geochronology of the Mkhondo suite, Swaziland: Evidence for passive-margin deposition and granulite facies metamorphism in the late Archaean of southern Africa, Journal of African Earth Science, 22, 483–506

Gold D.J.C & Von Veh M.W., 1995, Tectonic evolution of the Late Archaean Pongola-Mozaan basin, South Africa, Journal of African Earth Science, 21, 203–212

Holland T.J.B. & Powell R., 1998, An internally consistent thermodynamic data set for phases of petrological interest, Journal of Metamorphic Geology, 16, 309–343

Hunter D.R., Kröner A., Maphalala R. & Milisenda C.C., 1993, The Ancient Gneiss Complex, in The Ancient Gneiss Complex: Overview papers and guidebook for excursion, Kröner A., ed, Swaziland Geological Survey Mines Department Bulletin, 11, 62p.

Kreissig K., Holzer L., Frei R., Villa I.M., Kramers J.D., Kröner A., Smit C.A. & Van Reenen D., 2001, Geochronology of the Hout River Shear Zone and the metamorphism in the Southern Marginal Zone of the Limpopo Belt, Southern Africa, Precambrian Research, 109, 145–173

Kröner A., Wendt J.I., Milisenda C.C., Compston W. & Maphalala R., 1993, Zircon geochronology and Nd isotopic systematic of the Ancient Gneiss Complex, Swaziland, and implications for crustal evolution, in The Ancient Gneiss Complex: Overview papers and guidebook for excursion, Kröner A., ed, Swaziland Geological Survey Mines Department Bulletin, 11: 62p

Schoene B., de Wit M.J. & Bowring S.A., 2008, Mesoarchaean assembly and stabilization of the eastern Kaapvaal craton: a structural-thermochronological perspective, Tectonics, 27, 1–27

Smit C.A. & Van Reenen D., 1997, Deep crustal shear zones, high-grade tectonics, and associated metasomatic alteration in the Limpopo Belt, South Africa: implications for deep crustal processes, Journal of Geology, 105, 37–57

Stanistreet I.G. & McCarthy T.S., 1991, Changing tectono-sedimentary scenarios relevant to the development of the Late Archaean Witwatersrand Basin, Journal of African Earth Science, 13, 65-81

Taylor J., Stevens G., Armstrong R. & Kisters A.F.M., 2010, Granulite facies anatexis in the Ancient Gneiss Complex, Swaziland, at 2.73 Ga: Mid-crustal metamorphic evidence for mantle heating of the Kaapvaal craton during Ventersdorp magmatism, Precambrian Research, 177, 88–102

Tweedie E.B., 1986, The Evander Goldfield, in Mineral Deposits of Southern Africa I, Anhaeusser C.R. & Maske S., eds, Geological Society of South Africa, 705–730.

Wilson A.C. & Jackson M.P.A., 1988, Mantled gneiss domes in southern Swaziland and the concept of ‘stable’ Pongola cratonic cover, South Africa Journal of Geology, 91, 404–414

NATURE AND EVOLUTION OF THE ARCHEAN CRUST OF THE SÃO FRANCISCO CRATON: A REVIEW

W. Teixeira[1], L.S. Marques[2] & C.R. Petroni[1]

[1]Instituto de Geociências, the University of São Paulo
[2]Instituto de Astronomia, Geofísica e Ciências Atmosféricas, the University of São Paulo

Introduction and Precambrian Framework

The São Francisco craton (SFC) in the eastern South American continent and its extension in its African counterpart (West Congo Craton; WC) offers an ideal environment for the study of Archean geology, including aspects leading to the understanding of the geodynamics of early Earth's crust. A number of ancient granite-greenstone sequences occur interspersed in a terrain mostly comprising a wide variety of gneisses, migmatites and granitoid rocks, all of which provide a unique geologic record extending from 3.8 to 2.6 Ga. More than 300 U-Pb ages and Sm/Nd data (age histograms; Nd isotopic trends versus time) compiled from key basement units were interpreted together with the REE patterns, supported by geologic correlations, to reveal a complex and protracted Archean magmatic and metamorphic evolution. Most of the information is based on relevant published information during the last two decades, but some particular correlations based on unpublished data are also included, when appropriate. Tectonic inferences dealing with the composition and nature of the continental crust, as well as the extent and age of the Archean components are also addressed.

The SFC encompasses Archean terrains and segments of a Paleoproterozoic collisional orogeny. Basement exposures along the central part of the Craton were tectonically affected by a zone of 1.8-1.2 Ga extensional grabens and intracratonic basins known in the northern part as the Paramirim aulacogen (Fig. 1). The northern part of the SFC resulted from the accretion of at least three Archean blocks (Gavião, Jequié, Serrinha; Figure 1, inset) and intervening coeval fragments (e.g., North Gabon, Chaillu massives; WC), all assembled during a Paleoproterozoic collisional orogeny (2.3-1.9 Ga). Each one of the Archean blocks exhibits a distinct origin and tectonic history, as demonstrated by radiometric ages, isotopic signatures and geochemical characteristics of respective rocks. The Gavião block underwent polycyclic evolution from very old juvenile components dated between 3400 and 3000 Ma, with partial melting episodes at ca. 2.8-2.7 Ga. It is made up of amphibolite facies TTG suites and associated greenstone belts - some of them originated in continental settings, as suggested by age provenance studies and the isotopic constraints which are compatible with crustal contamination. The Sete Voltas and Boa Vista/Mata Verde mantled gneissic domes, which form the basement of the one metavolcanic-sedimentary sequence, represent the oldest well-dated Archean crust of the South American continent. Whereas the plutonic precursors of the old TTG suite were emplaced at 3.42 Ga, the T_{DM} ages (3.7-3.6 Ga) are interpreted as the protolith age, or rather their contamination by even older crust. The Jequié block comprises partly migmatised charnockite and enderbite corresponding to calc-alkaline plutons (3.0-2.9 Ga) and mega-enclaves of supracrustal rocks that have been intensely deformed and re-equilibrated in granulite facies during the Paleoproterozoic collisional event. Granitoid intrusions as old as 2.8-2.6 Ga are also present. The T_{DM} ages (3.4-3.0 Ga) indicate the heterogeneous protoliths from which the Jequié rocks derived whereas four major accretion/differention events were identified by U-Pb data: 2800 Ma, 2700 Ma, 2640 Ma and 2500 Ma. This suggests the Jequié block was formed by a multi-episodic collage of primitive Archean arcs coupled with reworking events, driven by oceanic crust subduction processes underneath the Gavião block. In the Serrinha block amphibolite facies orthogneiss, tonalite and migmatite are widespread, showing a magmatic and metamorphic history from 3195 to 2924 Ma with inherited Pb age components as old as 3314 Ma. This block similarly experienced Paleoproterozoic deformation and metamorphism, and hosts Paleoproterozoic greenstone belts and crustally derived granitoid intrusions (2.1 Ga). These plutons display strongly negative ε_{Ndt} values (up to -10), Archean T_{DM} ages (2.87-3.27 Ga), and U-Pb inherited zircon ages as old as 3650 Ma. The Serrinha block probably represents a Mesoarchean extension of the Congo paleocontinent that was amalgamated to the proto-SCF in Paleoproterozoic times.

The crystalline basement in the southern part of the SFC (Fig. 1, inset) comprises distinct Archean metamorphic terrains (e.g., Campo Belo, Belo Horizonte, Bonfim, Passa Tempo) and Paleoproterozoic assemblages that include metavolcanic-sedimentary sequences and plutonic rocks. These younger units are genetically related to 2.3-1.9 Ga continental and intra-oceanic arcs that have been successively accreted (together with Archean fragments) during long-lived convergence between the São Francisco and the West Congo paleocontinents, similar to the tectonic architecture of the northern segment. The Campo Belo complex, as an independent block, is made up of amphibolite facies gneissic-granitoid suites and migmatites, as well as orthoamphibolites and/or ultramafic rocks which may contain lenticular bodies of metabasites and are often cut by granitic aplites. At least one coeval greenstone belt (3.12-3.00 Ga) crops out in this block whereas relicts of low grade metamorphosed volcano-sedimentary sequences, some of which bearing graphite deposits, are also recognized. The Campo Belo rocks display U-Pb ages of ca 3205-3000 Ma, 2840 Ma (migmatitic event) and 2650 Ma, the youngest one referred to a major the period of crustal reworking and high grade

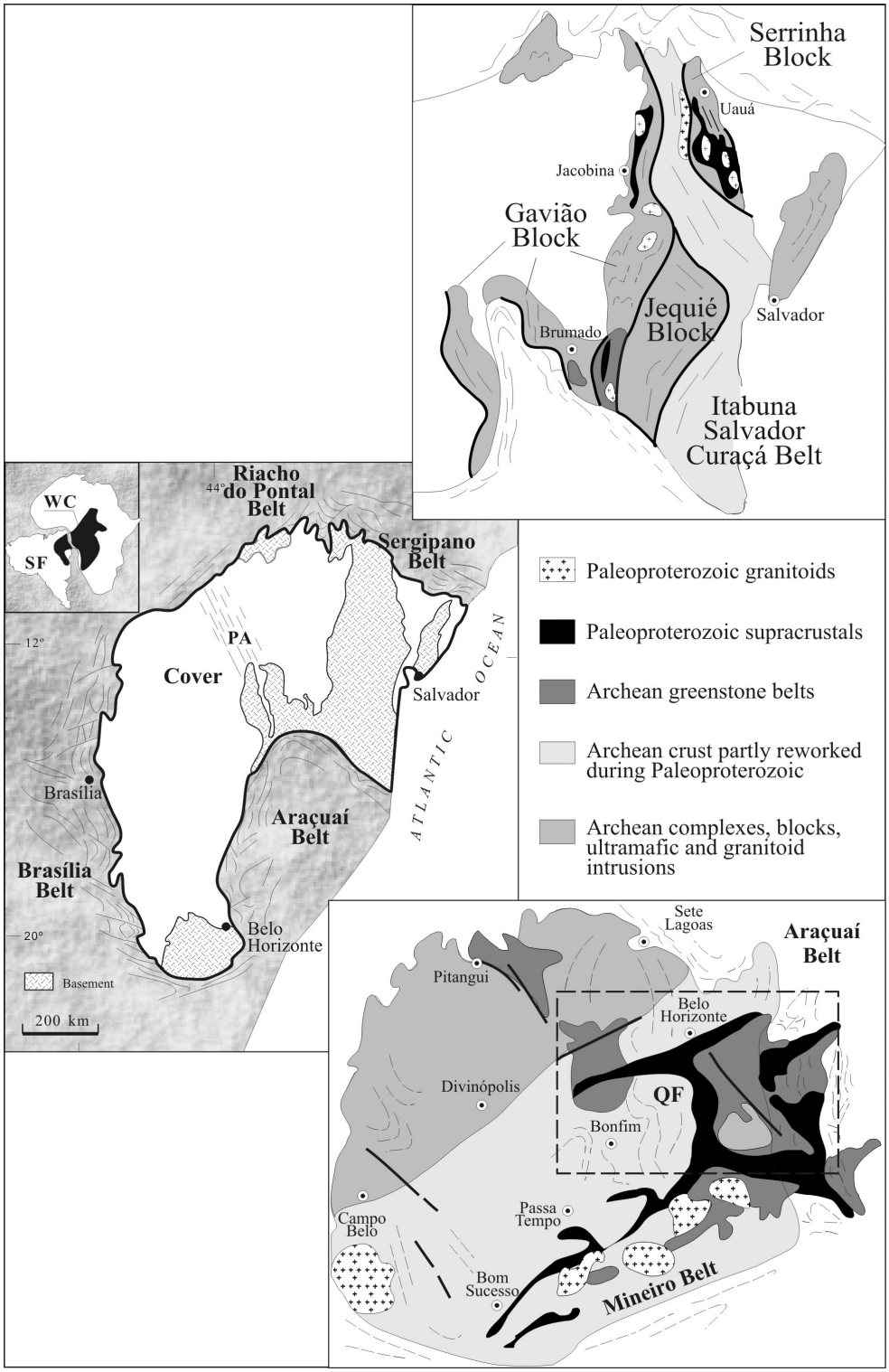

Figure 1. Tectonic framework of the São Francisco Craton, highlighted by the Archean and Paleoproterozoic segments (insets), the Paramirim Aulacogen (PA) and the Neoproterozoic cover (in blank). Neoproterozoic belts marginal to the Craton are also shown. Keys: WC (West Congo), SF (São Francisco), QF (Quadrilátero Ferrífero).

metamorphism (see afterwards). A large mafic-ultramafic layered body and basic-noritic dikes (ca. 2.7 Ga) crosscut the country rocks. They are tectonically linked with the late stage cratonization of the Campo Belo complex. Whereas the oldest age (3205 Ma) is interpreted to be a relict age component in the investigated migmatite; the 3000 Ma age refers to the main magmatic event that formed the regional orthogneisses. This interpretation agrees well with most of the T_{DM} ages (3.07-2.90 Ga) and the available juvenile-like ε_{Ndt} and μ_1 single stage Pb signatures. The Campo Belo orthogneisses have TTG composition and show chemical affinities with HSA-type (high SiO_2) adakites, in agreement with derivation in a magmatic arc setting.

In contrast with the Campo Belo block the nearby Passa Tempo complex encompasses hypersthenes-bearing gneissic rocks with subordinate NW- or EW trending mafic-ultramafic bodies and granodioritic to alkali-granitic, weakly foliated, and light-colored granitoid rocks. These granitoid plutons are the product of migmatisation that followed regional granulite-facies metamorphism with minimum ages of 2600 Ma and 2622 Ma, respectively. Particularly the

lithogeochemistry of the TTG-type granitoids suggests an origin by partial melting of hydrated basaltic crust in a subduction environment. The Belo Horizonte complex encompasses granodioritic and granitic gneisses containing amphibolites xenoliths, as well as migmatites. The regional foliation is broadly coeval with migmatization, as indicated by leucosomes both parallel and secant to the foliation. Chemical analyses of the less migmatized gneiss reveal a predominant trondhjemitic composition. The migmatization event took place at 2860 Ma and compares well with the age of the Campo Belo migmatite (see above). Additional ages are 2776 and 2712 Ma, while the inherited zircon grains yield ages of ca. 3030, 2920 and 2880 Ma. These ages together with the T_{DM} ones (3.4-3.1 Ga) suggest the existence of older protoliths and a protacted evolution for the Belo Horizonte complex. One supracrustal assemblage has coreless zircon from felsic volcanics 3029 Ma old, suggesting it is contemporary with greenstone belt rocks recognized in the Campo Belo complex (see above).

In the Quadrilátero Ferrífero (QF, figure 1) the Rio das Velhas orogeny (2780-2700 Ma) signals the most important magmatic and tectono-metamorphic event during which the Bonfim metamorphic complex and the Rio das Velhas greenstone belt were formed. The complex is made up of in situ anatexis of gneisses (with amphibolite protoliths as old as 2.9 Ga), calc-alkaline and tholeiitic intrusions, regionally marked by N–S mylonitic foliation and transpression motions. The Bonfim rocks have T_{DM} ages ranging from 3.1 to 2.8 Ga with crustal-like ε_{Ndt} parameters. Additional U-Pb ages in granitoid rocks (2720-2700) and metamorphic complexes in the vicinity of QF (e.g., Caeté; 2776 Ma) suggest their genetic relationship with the Rio das Velhas event. Felsic volcanics of the Rio das Velhas greenstone belt yield 2751-2792 Ma suggesting period of about 40 Ma for such magmatism. Additional provenance age studies (detrital zircons) indicate that most of the Rio das Velhas basin was filled during approximately 30 m. y. (between 2746 and 2717 Ma), reinforcing the contemporaneous evolution with the Bonfim block. Noteworthy are a few detrital zircons from the lower formation of the Rio das Velhas greenstone belt that have single cores with minimum ages of 3809 Ma and 3539 Ma. This offers a clue for the possible presence of Paleoarchean crust in SFC as source area for the greenstone belt sediments. However, the continental growth in the southern part of the SFC was more voluminous in the Mesoarchean and Neoarchean (3200-2600 Ma), as suggested by the extensive geochronological record available for different metamorphic complexes. Most workers envisage an active continental margin model for the evolution of the Bonfim block, which involved reworking of high Al_2O_3 tonalite/trondhjemite crust followed by intrusion of mafic, andesitic dikes, calc-alkaline tonalites and late K-rich granites, as supported by detailed geologic mapping. Most important, the 2780-2700 Ma evolution marks the final assembly and stabilization of the continental lithosphere of the proto-SFC, now reduced to a small exposure (c. 10,000 km^2) due to the succeeded Paleoproterozoic evolution (see figure 1; inset) and extensive Neoproterozoic sedimentation. Magmatic activity postdating this event is represented by crust-derived granitoid rocks (2610-2555Ma) occurring in the Belo Horizonte, Bonfim and Passa Tempo complexes (see above). They are homogeneous, weakly deformed or not deformed at all during the late Archean, although mainly affected by the Paleoproterozoic tectonism (see below). Chemically these plutons are calc-alkaline and slightly peraluminous granites, yielding variably REE contents from weak to strong fractionated patterns and mostly with significant negative Eu anomalies.

Summary and tectonic implications

Interpretation of T_{DM} age histograms and U-Pb ages suggest that early to mid Archean continental lithosphere underlies much of the SFC, with an estimated extension ca. 1200 km long and 500 km wide. The observed internal variation of the age patterns in space and time seems to be primary related to a mosaic of independent terrains with reasonable sizes (a few hundred of kilometers), each one with its particular evolution, but the bulk Archean core acting as a stable foreland during the long-lived convergence of the São Francisco and West Congo paleocontinents at Paleoproterozoic times. Such a dynamics is supported by the anatomy and regional structures of the Paleoproterozoic arcs (figure 1) that also led to remobilization of the recognized Archean fragments (e.g., Serrinha, Jequié, Barbacena), as well as of the 3.7-3.6 Ga mantled gneiss domes.

The most representative age records in the SFC are ca. 3200-3000 Ma, 2900-2800 Ma and 2780-2600 Ma, thus indicating the polycyclic nature of the Archean dynamics. About 75% of the available ε_{Ndt} constraints suggest that reworking of pre-existent crust has played an important role rather than accretion/differentiation processes during much of the Archean evolution, including evidence from the oldest mantled gneissic domes. This assessment is consistent with the observed chemical characteristics of the basement rocks that are compatible with TTG suites, showing strong fractionation of HREE, LREE enrichment and light Eu anomalies. Particularly the Archean granitoid rocks exhibit chemical affinity with HSA-type adakites. The oldest age interval is well recorded in the Campo Belo and Gavião blocks where the ca. 3.1-3.0 Ga greenstone belts crop out. The Campo Belo TTG suites display comparable U-Pb and T_{DM} ages (3.07-2.90 Ga) that together with the available juvenile-like ε_{Ndt} and μ_1 single stage Pb signatures point to a juvenile derivation in a magmatic arc setting, in agreement with the chemical affinities with adakites. The Gavião block was similarly assembled by accretion of TTG suites and greenstone belts, but during episodic processes related with a much broader time interval (ca. 3.4 and 3.0 Ga). Major and trace element petrogenetic modeling suggests that the pre-existing grey gneiss may be the source which melting generated the precursor magmas to produce the younger trondhjemitic grey gneiss and granodiorite by subduction of the oceanic lithosphere. This is also supported by the intensive migmatization that affected the old gneiss before the emplacement of the 3.1 Ga plutons. The 2900-2800 Ma event, recorded in the northern and southern parts of the SFC, included partial melting of the established sialic crust that has age components of

ca. 3.6-3.8 Ga. Significant amount of crustal reworking predominate in the late Archean (2780-2600 Ma) over practically all the basement terrains, as highlighted by the available crustal like ε_{Ndt} parameters calculated for the U-Pb crystallization ages in the Bonfim complex. This is compatible with an active continental margin scenario for the related Rio das Velhas orogeny (2.78-2.70 Ga). In this regard the nearby Passa Tempo complex records a granulitic metamorphism (minimum age of 2.62 Ga) which may be linked with the collision between the Bonfim and Campo Belo blocks, as also supported by the petrogenetic characteristics of the TTG-type granitoids.

To conclude, the Archean geodynamic scenario of the SFC is consistent with a progressive transition from an early oceanic regime that predominated in Mesoarchean times with development of successive island arcs (e.g., Jequié, Serrinha, Campo Belo, Belo Horizonte blocks) toward an active continental margin setting in the late Archean. The latter environment is consistent with geochemical and isotopic characteristics of the Bonfim rocks, tectonically related with the Rio das Velhas orogeny.

3D THERMAL-MECHANICAL MODELS OF ARCHEAN DOME AND KEEL FORMATION: INSIGHTS FROM SOUTHERN CROSS DISTRICT

N.Thébaud[1], G. Duclaux[2], K. Gessner[1] & M. Doublier[3]

*[1] Centre for Exploration Targeting, School of Earth and Environment (M006) University of Western Australia, Crawley, Western Australia, 6009 (*correspondence: nthebaud@cyllene.uwa.edu.au)*
[2] CSIRO Australian Resources Research Centre 26 Dick Perry Ave., Kensington 6151 Western Australia
[3] Geological Survey of Western Australia, P.O. Box 1664 Kalgoorlie Western Australia 6433

Introduction

The kinematic interaction between Archaean greenstone belts and adjacent granitoids is crucial for understanding the crustal evolution; and has been the subject of ongoing debate (e.g. Van Kranendonk et al. 2004). Processes proposed to explain Archaean dome and keel deformation patterns include (i) folding interferences, (ii) crustal extension following gravitational collapse, (iii) metamorphic core complex formation, (iv) gravity driven deformation associated with exhumation of late-Archaean granitoids relative to a supracrustal cover, or a combination of two or more of these processes (e.g. Collins 1998; Van Kranendonk 2004). Folding interference (Snowden 1984; Blewett 2002) and core complex models (e.g. Williams & Curie 1993) are typically associated with incremental polyphase deformation processes. In contrast, gravity driven deformation processes attributed to both magmatic diapirism and/or to ballooning plutonism are considered part of a continuum, protracted by the atypical Archaean thermal regime (e.g. Collins et al. 1998).

In addition to magmatic deposits, Archaean greenstone belts host large gold deposits, and gold mineralisation is largely structurally controlled (e.g. Groves et al. 1998; Bierlein et al. 2006). It is thus important to resolve the regional and local tectonic evolution of a granite-greenstone terrane, not only to understand the evolution of the early earth but also to constrain the formation and localization of major lode gold deposits. Recent research in the Yilgarn Craton and the Pilbara Craton has highlighted the importance of the granitoid domes as a heat engine and possible fluid source for mineralised gold system (e.g. Neumayr et al. 2008).

Finite strain distribution, metamorphic history, and the relative timing of granitoid emplacement relative to orogenic events are parameters that are critical to distinguish between different processes associated with the granite-greenstone formation. However, over the past decades studies based on field observations in various Archaean cratons failed to unify the views with regards to the Archean dome and keel formation. One of the reasons for ongoing debate are contrasting views on how to relate structural data measured at the outcrop scale with regional tectonic processes. A common approach is to interpret each locally observed fabric to be significant at a regional scale, and from this construct a polyphase deformation history at the terrane scale. Another approach considers that rheological contrasts between different geologic units and strain localisation along shear zones and faults may lead to the development of local fabrics that are part of a continuum, and therefore some of these local observations can be of limited terrane-scale significance. The latter case has not always been considered in regional tectonic model such as in the Southern Cross district.

In this contribution we want to test the hypothesis that structural complexity may be scale-dependant and that local fabric relationships may not be significant at the regional scale. We propose that our ability to resolve the tectonic evolution of the granite-greenstone interaction relies on our capability to predict and document the stress and strain evolution of different rheological units, as well as the thermal history in three dimensions through time.

In this paper we present preliminary results of a set of 3D thermal-mechanical numerical simulations generated as first pass experiments to test the physical robustness of various conceptual tectonic models. We aim to compare the results obtained with the tectono-stratigraphic evolution documented for the Southern Cross district. The Southern Cross district is part of the Youanmi Terrane with greenstones mostly deposited between 3.0 and 2.8 Ga in the South East of the Yilgarn Craton of Western Australia (Mueller & McNaughton 2000). Structural investigations of the finite strain pattern and metamorphic zoning documented in the Southern Cross district are well preserved and document a complex structural and metamorphic history that spanned from ca. 2.77 Ga to 2.63 Ga (Bloem et al. 1997; Mueller & McNaughton 2000). The results of previous investigations pointed toward a deformation history associated with the combination of a regional shortening event simultaneous with the granitoid emplacement by diapirism and/or ballooning plutonism (Bloem et al. 1997).

Simulations setup and preliminary results

The 3D strain pattern evolution associated with dome and keel structures was modeled using Gale. This open-source code employs a Lagrangian integration point particle-in cell scheme (Moresi et al. 2003), which combines a deformable mesh of computational points and a dense arrangement of mobile material points. The boundaries of the deformable mesh conform to the boundaries of the material as the simulation progresses, but the interior is constrained to remain as regular as possible. The particles track history-dependent properties such as instantaneous

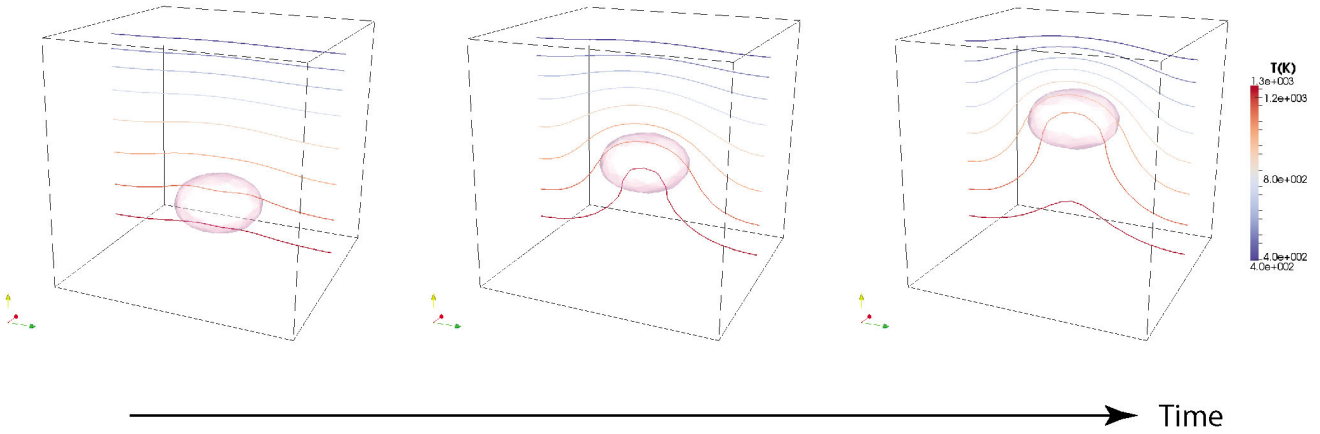

Figure 1. Thermal evolution through time of the gravity driven buoyant ascent of low density radiogenic intrusion (in pink on the figure).

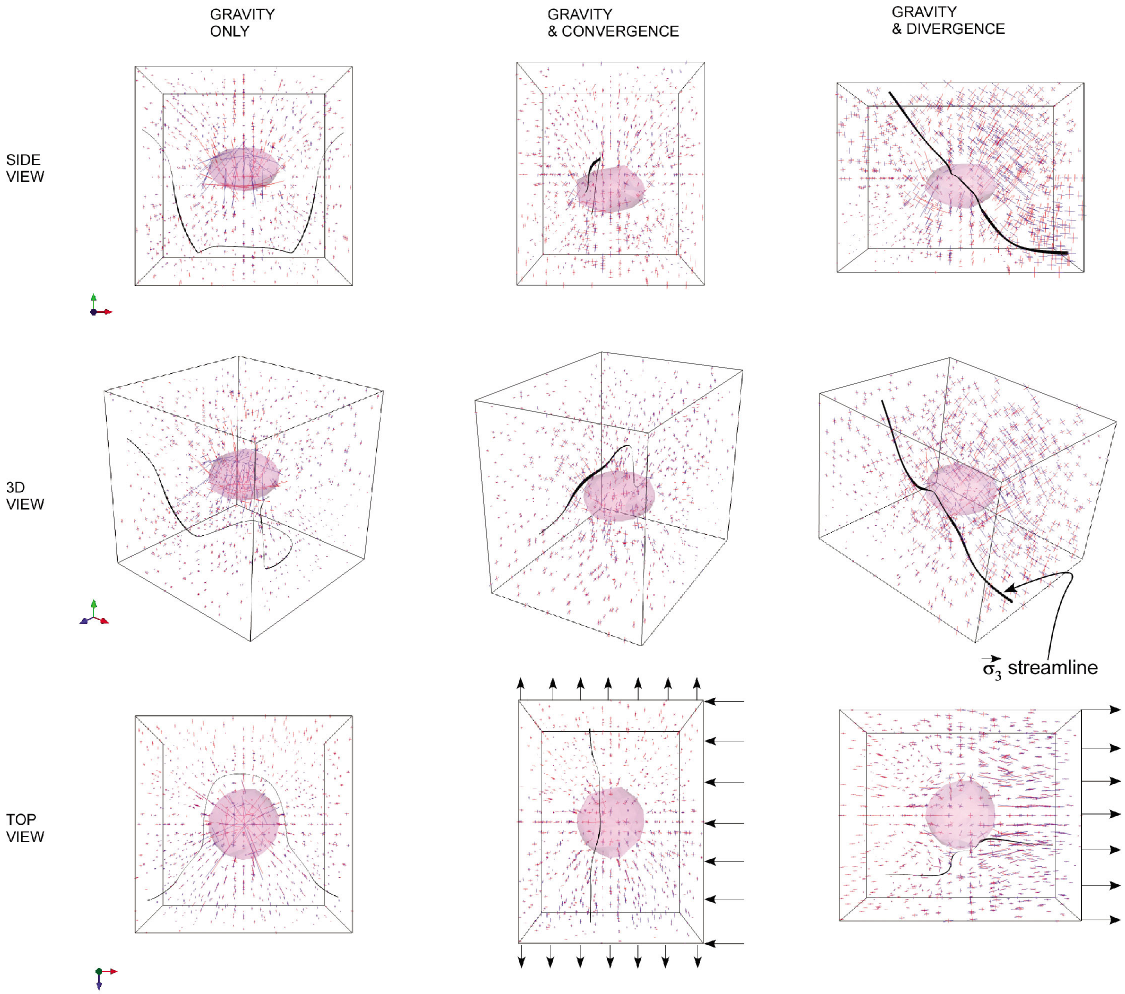

Figure 2. Simulation scenarios tested. The left column presents 3 different views of the purely gravity driven experiment results; the second raw presents the same set of views for the convergence experiment results; and the right raw presents similar views for a set of divergence experiment results. The surface shape of the granitic body is represented in pink; the 3 stress eigenvectorss are also plotted, with Sigma 1 (the maximum stress vector) in red, and Sigma 3 (the minimum stress vector) in blue. We also plotted a minimum stress eigenvector streamline. This later features illustrates the variation of sigma 3 orientation through space, following the trajectory of sigma 3 vectors in the model at a particular instant. The minimum stress vector also underlines the direction of opening of veins when this process occurs (Ramsay and Huber 1987).

and finite strain for purely viscous and strain-softening materials. This technique overcomes common limitations of continuum gridbased models such as strain limits due to a deforming mesh, or inaccuracies due to remeshing. For simplification, in the set of experiment detailed below, we did not consider neither the effect of thermal expansion, nor the dependency of viscosity with temperature or strain rate. More complex constitutive laws for materials with temperature dependant rheologies (dislocation creep mechanism) will also be investigated.

The model is comprised of a cube with each side 100 km long filled by a moderately viscous material (1E21 Pa.s) with a density of 2900 kg/m^3 and a low internal heat production (0.02 microW/m^3), representing a metasomatised greenstone type material. In the lower part of this greenstone matrix we included an approximatively 20 km radius flat shaped ellipsoid of low density (2700 kg/m^3) viscous material (1E23 Pa.s) with higher internal heat production (2 microW/m^3), representing a large granitic body. We tested different scenarios with: (1) a purely gravity driven set of experiments where the buoyant ascent of the low density material is constrained by Navier-Stokes equations only, (2) a set of models in convergence associated with lateral escape, and (3) a set of models in divergence (Fig. 2).

The results of these generic simulations are illustrated in Figure 1 and 2. Figure 1 illustrates the thermal evolution through time of a raising highly radiogenic intrusion through a greenstone medium. As the highly radiogenic intrusion raise, heat producing elements are transported toward the surface. As a result, the isotherms are disturbed and the geotherm strongly increase above and at the direct vicinity of the intrusion. Figure 2, displays a set of snapshot realized after 40 time steps for the 3 scenarios described above. This figure illustrates the extremely diverse local stress fields modeled (1) through space in a particular simulation, and (2) between the different simulations. We also noticed the variation of the the local stress fields through time. Indeed, as the granitic body migrates upward in the model it creates large radial stress disturbances resulting in local stress directions change. A minimum stress streamline (Fig. 2) is displayed for each model. This feature follows the trajectory of σ_3 vectors in the model at a particular instant. Its curved propagation through space emphasizes changes of the local stress field. Structural geologists refer to the minimum stress vector direction as the direction of opening of veins when this process occurs. This also demonstrates the extreme variation of stress field (1) within a particular model, and (2) between the different models. The resulting instantaneous strain will display a similar level of complexity and show contrasted finite strain field (not presented here) between the different scenarios tested but also within each of the simulations.

These simplified simulations underlined the large spatial and temporal variations in the direction taken by linear and planar fabrics resulting from such variable local stress fields. These variations will be emphasized by complex sets of superimposed structures comparable to those collected on the field. The significance of the genetic and spatial relationship existing between the various simulations and the field data collected for the Southern Cross is currently being investigated and will be presented in further details.

References

Bierlein F.P., Groves D.I., Goldfarb R.J. & Dube B., 2006, Lithospheric controls on the formation of provinces hosting giant orogenic gold deposits, Mineralium Deposita, 40, 874–886.

Bloem E.J.M., Dalstra H.J., Ridley J.R. & Groves D.I., 1997, Granitoid diapirism during protracted tectonism in an Archaean granitoid-greenstone belt, Yilgarn Block, Western Australia. Precambrian Research, 85, 147–171.

Collins W.J., Van Kranendonk M.J. & Teyssier C., 1998, Partial convective overturn of Archaean crust in the east Pilbara Craton, Western Australia: driving mechanisms and tectonic implications, Journal of Structural Geology, 20, 1405–1424.

Groves D.I., Gebre-Mariam M., Hagemann S.G. & Robert F., 1998, Orogenic gold deposits: a proposed classification in the context of their crustal distribution and relationship to other gold deposit types, Ore Geology Reviews, 13, 7–27.

Moresi L., Dufour F. & Mulhaus H., 2003, A Lagrangian integration point finite element method for large deformation modelling of viscoelastic geomaterials, Journal of Computational Physics 184, 476–497.

Mueller A. & McNaughton N., 2000, U-Pb ages constraining batholith emplacement, contact metamorphism and the formation of gold and W-Mo Skarns in the Southern Cross area, Yilgarn Craton, Western Australia, Economic Geology, 95, 1231–1257.

Neumayr P., Walshe J., Hagemann S., Petersen K., Roache A., Frikken P., Horn L. & Halley S., 2008, Oxidized and reduced mineral assemblages in greenstone belt rocks of the St. Ives gold camp, Western Australia: vectors to high-grade ore bodies in Archaean gold deposits? Mineralium Deposita, 43, 363–371.

Ramsay J.G. & Huber M.I., 1987, *The techniques of modern structural geology: Folds and fractures*, Academic Press.

Ridley J. & Diamond L.W., 2000, Fluid chemistry of orogenic lode gold deposits and implications for genetic models, in *Gold in 2000*, Reviews in Economic Geology Volume 13, Hagemann S.G. & Brown P.E. eds, Society of Economic Geologists, 141–162.

Snowden P., 1984, Non-Diapiric Batholiths in the North of the Zimbabwe Shield, in *Precambrian Tectonics Illustrated*, Kroner A. & Greiling R., eds, Sehweizerbart, Stuttgart, Germany, 135–146.

Van Kranendonk M.J., Collins W., Hickman A., Pawley M.J., 2004, Critical tests of vertical vs. horizontal tectonic models for the Archaean East Pilbara Granite-Greenstone Terrane, Pilbara Craton, Western Australia. Precambrian Research, 131, 173–211.

Williams P. & Curie K., 1993, Character and regional implications of the sheared Archaean granite-greenstone contact near Leonora, Western Australia, Precambrian Research, 62, 343–365.

THE PONGOLA SUPERGROUP - A MESOARCHEAN ANALOGUE OF ANDEAN MAGMATISM AND TECTONICS

A.H. Wilson

School of Geosciences, University of the Witwatersrand, Johannesburg, 2050, South Africa allan.wilson@wits.ac.za

The c.3.0 Ga Pongola Supergroup is one of the most extensive and best preserved volcano-sedimentary terrains of the Mesoarchean period. It is located close to the eastern boundary of the Kaapvaal Craton in South Africa and in Swaziland and extends for over 300 km in a roughly N-S direction (Gold, 2006). The volcanic rocks have for long been known to possess a marked crustal signature and the sedimentary basins formed initially from braided river systems which gradually subsided to form a deepening epicontinental epeiric sea. While early studies proposed that the entire Pongola Supergroup formed in an intra-continental rift (Burke *et al*., 1985) this is not supported by field observations and compositions of the volcanic rocks and Matthews (1990) suggested a plate tectonic model relating to an active continental margin with associated rifting. The precise tectonic setting has been debated for over 30 years with little final agreement. The type sections in the northern sector of the belt are gently dipping and essentially undeformed but the belt becomes intensely deformed in the south where it also undergoes a major facies transition.

The lower dominantly volcanic section is the Nsuze Group (maximum thickness 4500 m), and the upper dominantly sedimentary succession is the Mozaan Group (maximum thickness 5000 m). By 3 Ga southern African Archaean crustal development had established the granite – greenstone terrain of the Barberton greenstone belt and its southern and western equivalents, and had undergone intense deformation, but association of these older terrains to the onset of modern-style plate tectonics is unknown. Other greenstone terrains, such as those in Zimbabwe, were yet to become established at the time of deposition of the Pongola Supergroup. In relation to the Kaapvaal Craton the Pongola Supergroup represents the start of a long period of development of major sedimentary basins and therefore provides a critical glimpse of Earth history at the earliest stage of crustal stabilization and continent formation and possibly the oldest example of a modern-style continental plate tectonic setting. Other volcano-sedimentary successions in the Kaapvaal Craton were also becoming established at the same time. The volcanic rocks of the Dominion Group (at the base of the Witwatersrand Supergroup) (Marsh, 2006) are located in the central part of the Kaapvaal Craton and are of the same approximate age (but appreciably older), and have been lithologically correlated with the Nsuze Group. Although there are some similarities between the Dominion Group and Nsuze Group, the accepted simple lithological correlation may have obscured understanding of the real tectonic settings of these terrains.

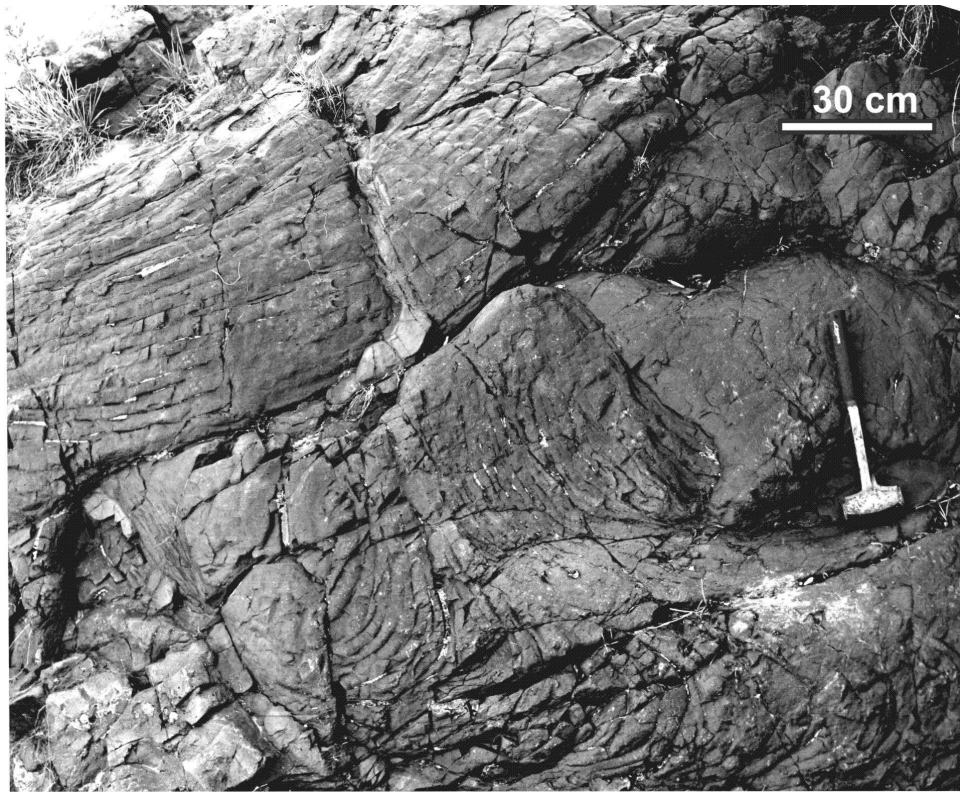

Figure 1. Intersecting pahoehoe lava lobes, together with break-outs, in the White Mfolozi inlier.

Figure 2. Slab showing interaction of contrasting magmas (dacite and basaltic andesite) which erupted simultaneously, and possibly even from the same vent. It is noticeable from the detailed textures that the magmas did not mix readily.

This study reports on detailed field observations and compositions of volcanic rocks from several areas of the Nsuze Group that are particularly well preserved, over a period of 30 years, together with new mapping and the precise analysis of nearly 400 samples. These areas include the type section of volcanic stratigraphy that has a wide range of rock types from basalt to felsic volcanic rocks, as well as the White Mfolozi and Nkandhla inliers in the south. Primary textures and structures (many indicative of shallow water and subaerial environments) include pillow lavas, pyroclastic deposits and pahoehoe lobes with exceptionally well preserved ropey lava tops (Fig. 1). In spite of its extensive lateral development the Pongola Supergroup is relatively poorly represented in the southern section because of its cover by Mesozoic sediments of the Karoo Supergroup. However, recent mapping and careful interpretation of lithogeochemistry indicates that specific volcanic centres can be identified each having their own unique signature, compositional distribution and eruptive style.

Broad major and trace element geochemical trends are identified for the complete suite of samples and can be superficially modelled by fractionation as observed in more limited previous studies. The extensive data set from this study indicates that single stage fractionation to explain the spectrum of rock types is simplistic and cannot be modelled rigorously. The various volcanic domains are considered separately in terms of source and fractionation processes thereby allowing a better control on the complex interrelated processes, such as would occur in arc environments, in the relative roles of source and differentiation of magmas (Davidson & Wilson, 2009). There is abundant evidence that magma mixing or intermingling took place both from the distribution of lava compositions and field evidence that contrasting magmas were erupted simultaneously (Fig. 2), possibly even from the same vents. Composite feeder dykes are also observed to have contrasting compositions.

A bimodal distribution of compositions is observed for the volcanic rocks (peaks at 0.7% and 5% MgO; 74% and 56% SiO_2), with the most abundant rock type being basaltic andesite to andesite (Fig. 3). There is no geochemical break over the entire compositional spectrum. While a strong crustal signature for Nsuze Group rocks is well established, various sections have quite different lineages and different coherent fields for major and trace elements. Previous data sets of limited extent (Armstrong *et al*., 1982; Crow *et al*., 1989) showed broad and generally scattered trends which permitted rudimentary fractionation modeling from a single primary magma combined with crustal contamination. The new data (including ratios of highly incompatible elements and REE) show distinctly different fields relating to individual volcanic vents tapping a wide range of source materials which included both underlying crustal rocks as well as primitive Archaean mantle. Fractionation processes linking the entire suite of samples cannot be rigorously modelled, even for individual volcanic domains.

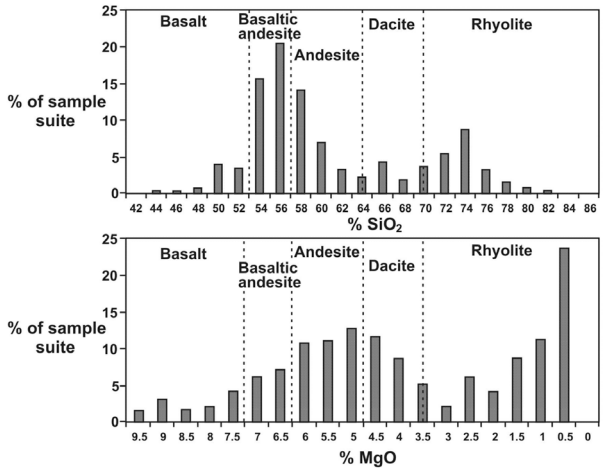

Figure 3. Bimodal distribution of rock compositions for volcanic rocks of the Pongola Supergroup.

While there is no clear indicator of a specific tectonic setting, the over-riding conclusion is that the magmas were generated from melting of a wide variety of sources, most of which had a strong crustal affinity, and these magmas underwent mixing to varying degrees as well as fractionation in high level magma chambers which fed numerous coeval dykes. On the basis of the range and coherence of magma compositions, the continental rifted environment, post emplacement tectonics, as well the presence of late-orogenic granitoid bodies, an analogue of the Andean model best represents the tectonic setting and magmatism of the Pongola Supergroup. Further

analysis of the data set will assist in distinguishing the various facies of the belt as either most closely allied to an inland continental back-arc setting or the landward side of an active continental margin.

References

Armstrong N.V., Hunter D.R. & Wilson A.H., 1982, Stratigraphy and petrology of the Archaean Nsuze Group, northern Natal and southeastern Transvaal, Precambrian Research, 19, 75–107.

Burke K., Kidd W.S.F. & Kusky T.M., 1985, The Pongola structure of southeastern Africa: The world's oldest preserved rift? Journal of Geodynamics, 2, 35–49.

Crow C., Condie K.C., Hunter D.R. & Wilson A.H., 1989, Geochemistry of volcanic rocks from the Nsuze Group, South Africa: arc-like volcanics in a 3.0 Ga intracratonic rift, South African Journal of Earth Science, 9, 589–597.

Davidson J. & Wilson M., 2009, The relative roles of source vs differentiation in determining the characteristics of arc magmas, Goldschmidt Conference, Davos, A267.

Gold D.J.C., 2006, The Pongola Supergroup, in *The Geology of South Africa*, Johnson M.R., Anhaeusser C.R. & Thomas R.J., eds, Johannesburg, The Geological Society of South Africa, 135–147.

Marsh J.S., 2006, The Dominion Group, In *The Geology of South Africa*, Johnson M.R., Anhaeusser C.R. & Thomas R.J., eds, Johannesburg, The Geological Society of South Africa, 149–154.

Matthews P.E., 1990, A plate tectonic model for the late Archaean Pongola Supergroup in Southeastern Africa, in: *Crustal Evolution and Orogeny*, Sychanthavong S.P.H., ed, New Delhi, Oxford Publishers, 41–72.

GROWTH OF ARCHEAN LOWER CONTINENTAL CRUST: AN ARC ACCRETION MODEL

B.F.Windley[1], A.A. Garde[2] & K. Sajeev[3]

[1]Department of Geology, University of Leicester, Leicester LE1 7RH, UK
[2]Geological Survey of Denmark and Greenland (GEUS), Østervoldgade 10, Copenhagen DK-1350, Denmark
[3]Centre for Earth Sciences, Indian Institute of Sciences, Bangalore 560012, India

The Meso-Neoarchean lower crust in two key regions, West Greenland and the Scourian of NW Scotland, underwent fundamentally similar modes of evolution, except that the last two were also subducted to eclogite depths. We first describe in detail the crust in West Greenland, then layered complexes in Scotland emphasizing their high-pressure assemblages, then some modern analogues, and finally discuss the implications worldwide of these findings.

West Greenland

Recent synthesis of the voluminous data on the Meso-Neoarchean crust of West Greenland has led to the following re-evaluation and model (Garde, 2007; Windley and Garde, 2009). The ca. 700 km long, Archean craton of West Greenland consists of six Meso-Neoarchean (ca. 3000–2720 Ma) shear zone - bounded crustal blocks that display similar cross-sections; from south to north Ivittuut, Kvanefjord, Bjørnesund, Sermilik, Fiskefjord, Maniitsoq. Each block has a southerly upper and a northerly lower zone, thus each faces upwards to the south. Upper zones have prograde amphibolite facies mineralogy and have never been in the granulite facies, whereas lower zones reached granulite facies and were partly retrogressed to amphibolite facies. Upper and lower zones consist predominantly of tonalite-trondhjemite-granodiorite (TTG) orthogneisses; geochemistry suggests generation by slab melting in subduction settings of active continental margins. The gneisses contain km-thick metavolcanic amphibolite layers typically bordered by km-thick layers containing anorthosite and leucogabbro. Most upper zones contain upper greenschist to amphibolite facies metavolcanic belts including volcaniclastic, andesitic rocks. The two most-prominent metavolcanic belts have supra-subduction zone island arc or proto-arc geochemical signatures (Garde, 2007; Polat et al, 2008).

The 2 km-thick (c. 2970 Ma) Fiskenæsset Complex comprises chromite-layered anorthosites (An_{75}–An_{95}), leucogabbros, gabbros (with meta-igneous amphiboles) and peridotites, and contains local roof pendants from overlying metavolcanic tholeiitic amphibolites. Trace element systematics suggest a genetic link between the Fiskenaesset Complex and the bordering basaltic rocks ranging from mid-ocean ridge basalt to island arc basalt. Overall the data suggest derivation from a hydrous magma of an oceanic island arc (Polat et al., 2009).

The style of deformation changes downwards within crustal blocks; upper zones are characterised by linear metavolcanic belts deformed by mostly one major phase of isoclinal folding, and lower zones by kilometre-scale double-triple fold interference patterns. Everywhere TTG protoliths have intruded anorthositic and volcanic rocks typically along ductile shear zones, in places so extensively that only anorthositic or amphibolitic lenses are preserved. The Meso–Neoarchean crust was thickened by a combination of thrusting, isoclinal folding and continual TTG injection. Dissimilarities in the proportions of anorthositic and metavolcanic rocks in the six blocks suggest that they evolved in several different microcontinents, but by similar processes. Confirmation of this model is provided by the presence of a 400 m-wide shear zone with mylonitic, cataclastic and augen gneisses on the proposed boundary between the bottom of the Bjørnesund block and the top of the Sermilik block; this is a late cataclastic shear on a suture zone between different types of gneisses of these two crustal blocks. The Greenland crustal blocks provide an exceptional, well-exposed example of how crustal growth took place in the Meso-Neoarchean from island arcs to continental margin arcs, and finally by collision tectonics to produce an amalgamated continent. The linear Paleoarchean Akilia-Isua block (Nutman et al., 2007) was trapped between the Sermilik and Fiskefjord blocks and thus incorporated into the Meso-Neoarchean continent.

NW Scotland

The Scourian complex on the mainland of NW Scotland consists predominantly of c. 3.0 Ga granulite facies tonalitic to granodioritic gneisses that contain many remnant layers up to several hundred metres thick of former layered gabbro-ultramafic complexes that contain peridotites, gabbros, garnet gabbros, garnet leucogabbros, garnet wehrlites, and garnet websterites (Bowes et al., 1964). O'Hara (1961) estimated a P of 17 kbar and T of 1000°C, but later studies of the granulite facies mafic rocks were in the range of 8-11 kbar and 850-1000°C. In one area (near the village of Achiltibuie), with the best-preserved assemblages, we discovered (unpublished) a garnet-clinopyroxene association with only a minor overprint of amphiboles. Inclusions of clinopyroxene within garnet are omphacitic (X_{Jd} up to 20.1 [Na-Fe^{3+}-2Ti]*100). The petrology, mineral chemical signatures and phase diagram results demonstrate high *P-T* conditions of *c*. 21-23 kbar and 1050°C. Specifically, an isochemical phase diagram calculated in the CaO-Na_2O-K_2O-FeO-MgO-TiO_2-Al_2O3-SiO_2-H_2O system for a calculated bulk chemical composition for the peak ga rnet+omphacite+clinopyroxene+rutile assemblage with a minor amphibole-plagioclase symplectite indicates the high-P stability of the assemblage. Precise metamorphic conditions were estimated based on the compositional isopleths of the peak mineral compositions (X_{Mg} [Mg/

(Fe+Mg)] and X_{Grs} [Ca/(Fe+Mg+Ca)] isopleths for garnet and X_{Mg} and X_{Jd} [Na/(Ca+Na)] for clinopyroxene).
We interpret the available data from Achiltibuie to indicate that the rocks were subducted to eclogite-facies c. 70-75 km depths and during exhumation were equilibrated in the granulite facies at about 3.0 Ga. In so far as the remainder of the 100 km-long Scourian complex contains abundant similar relict layered igneous complexes with similar garnet-rich assemblages that it is likely that garnets elsewhere contain omphacite inclusions and that the a large area/volume of the crust was deeply subducted in the Neoarchean.

Modern Analogues

Comparable modern analogues to the rocks described above are in the Peruvian Andes, the Southern California batholith, Kohistan in the Himalaya of Pakistan, and Fiordland in New Zealand. Whereas the upper crustal levels of the batholiths of the Andes and Cordillera of western America typically with diapiric granitic plutons are not comparable to the deeper crustal levels exposed in West Greenland, the deep sections of these mountain ranges do present remarkably analogous profiles. In Patagonia and British Columbia (the Coast plutonic complex) sheets of calc-alkaline hornblende-bearing tonalite, trondhjemite, granodiorite or diorite intruded along thrusts and shear zones, became foliated to gneisses, were metamorphosed in the high amphibolite or granulite facies at 9–10 kbar, and underwent partial melting to produce migmatites. These high-grade gneissic rocks and structures developed during crustal thickening in active continental margins in association with sub-horizontal thrust-nappe tectonics in the Mesozoic or Tertiary. Confirmation of the gneissic character of the deep Andes comes from crustal xenoliths in Columbia that consist of hornblende tonalitic gneisses, granulite facies gneisses, pyroxenites, pyribolites (two pyroxene amphibolites) and pyriclasites (two pyroxene–biotite–plagioclase schists).

The Cretaceous western Peninsular Ranges batholith in southern California is made up of hundreds of mid-crustal plutons of hornblende–biotite tonalite and granodiorite, intruded into island arc-type volcanic and volcaniclastic rocks, some emplaced as foliated and gneissose sheets along ductile shear zones during synkinematic amphibolite facies metamorphism. Tonalitic gneisses and tonalites contain bodies of locally layered and graded norite, gabbro, gabbro anorthosite and anorthosite that consist of very calcic cumulate plagioclase An_{70-96} and inter-cumulus magmatic hornblende; they were derived from a high-alumina basaltic magma. This western batholith formed as a root of a primitive island arc on oceanic lithosphere at a convergent plate margin. Lee et al. (2007) constructed a model for generation of the Peninsular Ranges batholith as follows: in the Triassic a fringing island arc was created off the Paleozoic continental margin of North America, in late Jurassic to early Cretaceous times the back-arc basin closed and this fringing arc was accreted onto the edge of the North American continent, and in the early Cretaceous farther eastwards subduction gave rise to new basaltic arc magmas, which gave rise to the main tonalitic–granodioritic batholiths that were emplaced into the accreted island arc on the active continental margin. They went on to suggest that this environment was applicable along the entire Cordilleran margin from Alaska to Chile and as a general mechanism even to the Archean. One example is the Jurassic Border Ranges complex in Alaska, which is composed of ultramafic cumulates, massive and cumulate gabbronorites that represent the plutonic core of an intra-oceanic island arc, an overlying andesitic volcanic rocks. The gabbroic rocks contain calcic plagioclase (An75–100), iron-rich pyroxene and magnetite. These plutonic and volcanic island arc rocks were intruded by calc-alkaline plutons of tonalite, granodiorite and quartz diorite in batholithic proportions. In the Cordillera Occidental of the Peruvian Andes late Cretaceous plutons of the tonalitic–granodioritic Coastal Batholith were emplaced into volcanic rocks of the Albian Casma Basin and their broadly coeval basic plutonic complexes. The 6 km-thick Casma volcanic pile consists of pillow-bearing basalts, hyaloclastites, basaltic andesites, dacites and rhyolites; the volcanic rocks have low Zr/Y vs. low Zr values characteristic of oceanic arcs. The basic complexes comprise anorthosite (with cumulate plagioclase up to An94) and gabbro with inter-cumulus hornblende that is secondary after clinopyroxene, but derived from a late volatile-rich residual melt. The complexes occur in layers and lenses up to 5 km wide, and 40 km long, but grouped in "clusters indicating the former presence of substantial bodies that prior to fragmentation may have approached 1000 km2 in area". The tonalitic– granodioritic plutons were emplaced into the volcanic–plutonic rocks with the result that many of the latter now occur as lenses and inclusions within the tonalites and granodiorites. Similarities in mineralogy, and major and trace element patterns suggest that the volcanic rocks represent the liquid fraction after cumulate crystallization of the basic complexes, both generated from tholeiitic magmas in the mantle. The tonalitic–granodioritic plutons include primary magmatic hornblendites, and layered gabbros with cumulate plagioclase and inter-cumulus magmatic hornblende that indicate that these complexes crystallized under a very high fluid pressure; extrusive equivalents are pyroclastic and basaltic–andesitic volcanic rocks. The Cordilleran batholiths in North and South America provide a viable modern analogue for the arc-generated crustal growth in West Greenland (Windley et al., 1981).

The Cretaceous Kohistan island arc (Pakistan) consists of calc-alkaline volcanic and volcaniclastic rocks and an associated Chilas complex of layered norites and noritic gabbros that formed the root or magma chamber of the arc. The island arc was accreted to the southern margin of the Asian continent, and in consequence magmatism changed from oceanic to continental leading to emplacement of the tonalitic-granodioritic Trans-Himalayan batholith into the island arc in an Andean-type continental margin setting.

Discussion

In the modern examples quoted above, island arcs were able to accrete to margins of continents, because continents existed in the Mesozoic and Cenozoic, but

in West Greenland, or anywhere else worldwide, there were no major continents in existence in the Meso to Neoarchean. However, e.g. in West Greenland there were many island arcs available to mutually accrete and amalgamate into microcontinents, around which other fringing island arcs could begin the conversion to continental arc magmatism. These speculations imply that the processes of continental growth from island arc magmatism to continental arc/ cordilleran magmatism were broadly similar throughout much of Earth history, and for this reason, tectonic blocks of different ages can be found with similar crustal sections and with broadly comparable components and age relations. Both experimental work and geochemical studies have indicated that there was a change from generation of tonalite–trondhjemite- to granodiorite-dominated continental crust at the end of the Archean, as direct partial melting of the subducting slab became less feasible as the Earth became cooler. The Archean gneisses of the North Atlantic craton and the Paleoproterozoic Julianehåb batholith in South Greenland actually provide a good example of this geochemical change. However, it would seem that this transition did not have other fundamental influences on the magmatic and tectonic accretion of new continental crust over time as discussed above. The results of this study, based on West Greenland and a variety of Archean and modern analogues, suggest that continental growth through time has commonly taken place by processes dominated by arc generation.

The examples from NW Scotland demonstrate that not only were subduction processes possible in the Meso-Neoarchean in order to produce calc-alkaline island arcs and active continental margins, but that they were also able to transport material to eclogite facies depths, as today. However, it is important to look for the differences as well as the similarities between ancient and modern rocks and environments. One significant difference is that, whereas in the Phanerozoic subduction has produced low-temperature eclogitic rocks, in the Meso-Neoarchean plate subduction gave rise to high-temperature eclogite facies assemblages, a difference that may readily be ascribed to changes in thermal gradients with time.

References

Bowes D.R., Wright A.E. & Park R.G., 1964, Layered intrusive rocks in the Lewisian of the north-west Highlands of Scotland, Quarterly Journal of the Geological Society of London, 120, 153–191.

Garde A.A., 2007, A mid-Archaean island arc complex in the eastern Akia terrane, Godthabsfjord, southern west Greenland, Journal of the Geological Society of London, 164, 565–579.

Lee C-T.A., Morton D.M. Kistler, R.W. & Baird A.K., 2007, Petrology and tectonics of Phanerozoic continent formation: from island arcs to accretion and continental arc magmatism, Earth and Planetary Science Letters, 263, 370–387.

Nutman A.P., Friend C.R.L., Horie K. & Hidaka H., 2007, The Itsaq Gneiss Complex of southern West Greenland and the construction of Eoarchean crust at convergent plate boundaries, in *Earth's Oldest Rocks*, Van Kranendonk M.J., Smithies R.H. & Bennett V.C., eds, Elsevier, 187–218.

O'Hara, M. 1961, Zoned ultrabasic and basic gneiss masses in the early Lewisian metamorphic complex of Scourie, Sutherland, Journal of Petrology, 2, 248–276.

Polat A., Frei, R., Appel P.W.U., Dilek Y., Freyer B., Ordóñez-Calderón J.C. & Yang Z., 2008, The origin and composition of Mesoarchean oceanic crust: evidence from the 3075 Ma Ivisartoq greenstone belt, SW Greenland, Lithos, 100, 293–321.

Polat A., Appel. P.W.U., Fryer B., Windley B., Frei R., Samson I.M. & Huang H., 2009, Trace element systematics of the Neoarchean Fiskenaesset anorthosite complex and associated meta-volcanic rocks, SW Greenland: evidence for a magmatic arc origin, Precambrian Research, 175, 87–115.

Windley B.F. & Garde A.A., 2009, Arc-generated blocks with crustal sections in the North Atlantic craton of west Greenland: crustal growth in the Archean with modern analogies, Earth Science Reviews, 93, 1–30.

Windley B.F., Bishop F.C. & Smith J.V., 1981, Metamorphosed layered igneous complexes in Archean granulite-gneiss belts, Annual Reviews in Earth and Planetary Science, 9, 175–198.

GEOCHEMICAL CHARACTERISTICS OF THE NE MURCHISON TERRANE, WESTERN AUSTRALIA

D.A. Wyman[1] & R. Kerrich[2]

[1]School of Geosciences, The University of Sydney, Sydney, NSW, 2006, Australia
[2]Department of Geological Sciences, The University of Saskatchewan, Saskatoon, SK, 57N 5E2, Canada

Introduction

A new lithostratigraphic scheme established by the Western Australia Geological Survey (Van Kranendonk & Ivanic, 2009) provides context for a geochemical and isotopic study in the Meekatharra – Mt Magnet area of the northeast Murchison terrane. The stratigraphic relationships of many map units in the area, however, remain ambiguous. Nonetheless, the associations of tholeiitic arc basalts, andesites and rhyolites of the 2814 – 2800 Ma Norie Group and komatiites, tholeiites, depleted tholeiites and rhyolites of the overlying 2800 – 2733 Ma Polelle Group allow for important comparisons with similar lithostratigraphic associations elsewhere in the Yilgarn Craton and the Superior Province, Canada. Many of those other terranes are characterised by lower plume- or plateau-type sequences and (conformably) overlying arc-like sequences. Therefore, the northeast Murchison provides an important demonstration of the natural variability of mid- to late-Archean geodynamics that must be accommodated in generic conceptual models of tectonic processes at that time. Although not observed in outcrop, the presence of a c 2950 Ma Group "basement" is indicated by xenocrystic and detrital zircons (Van Kranendonk & Ivanic, 2009). Potential contamination effects are assessed in this study by Sm-Nd isotopic analysis of select samples.

Geochemical Results

2814 Ma – 2733 Ma volcanic and shallow-level intrusive rocks of the Norie Group were sampled in Cue – Mt. Magnet area are. Volcanic samples extend from basaltic to rhyolitic. Sporadic high Th/La ratios in some samples indicate that crustal contamination has locally been significant. Other basalt and andesite samples display no such enrichments and are geochemically comparable to examples documented in juvenile Neoarchean arc terranes, such as the south – central Abitibi belt (Fig. 1).

High-Mg bodies in the Norie Group (15 – 33 wt.% MgO) are most plausibly feeder magmas for the overlying Pollele Group. Based on compatible element systematics and REE fractionation, the majority of these bodies are related to komatiitic units of the Polelle Group (Fig. 2). The intrusions rarely exhibit pronounced Th enrichments. Nonetheless, one sample displayed a shift in $\varepsilon Nd_{T=2.8Ga}$ from an "expected" mantle value near +5 to +0.5. The result is most plausibly related to contamination processes by c. 2950 Ma material at deeper crustal levels than represented by present exposures.

Barley et al. (2000) reported geochemical data for the Ti-rich, Al-deleted Gabanintha komatiite that are now assigned to the Polelle Group. New results from the present study encompass many of the other igneous rock types in the Group. Many tholeiitic basalts of the Pollele Group exhibit MREE-HREE fractionations ($[Tb/Yb]_N$ = 0.7 – 0.8) indicative of a refractory mantle source as well as LREE depletions. Some of these basalts qualify as "low-Ti" varieties (TiO_2 = 0.4 – 0.7 wt.% at SiO_2 = 49 – 52 wt.%; Al_2O_3/TiO_2 = 18 -34). Although they are not as compositionally extreme as occurrences noted in proximity to the Kidd Creek massive sulphide body in the southern Abitibi belt, they are analogous to other deleted tholeiites documented further east in the Kidd-Munroe assemblage (Wyman, 1999). As in the case of the Canadian examples, the Polelle depleted tholeiites are readily shown not to be fractionation products of the spatially associated komatiites, which in this area exhibit features such as LREE enrichments as well as distinct trends involving TiO_2, MgO, etc (Fig. 2).

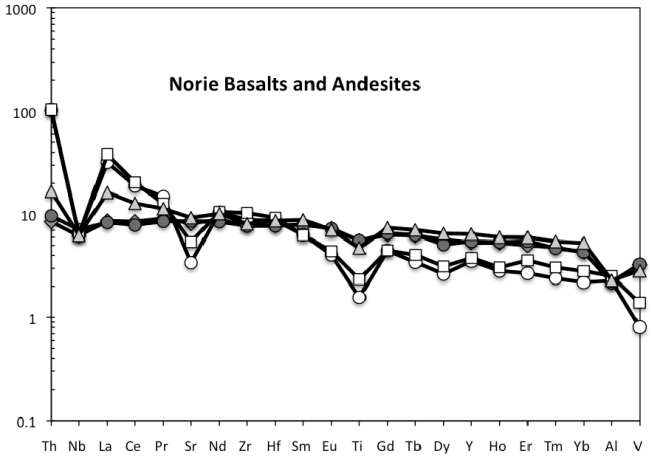

Figure 1. Primitive Mantle-normalised plot of Norie Group basalts and andesites.

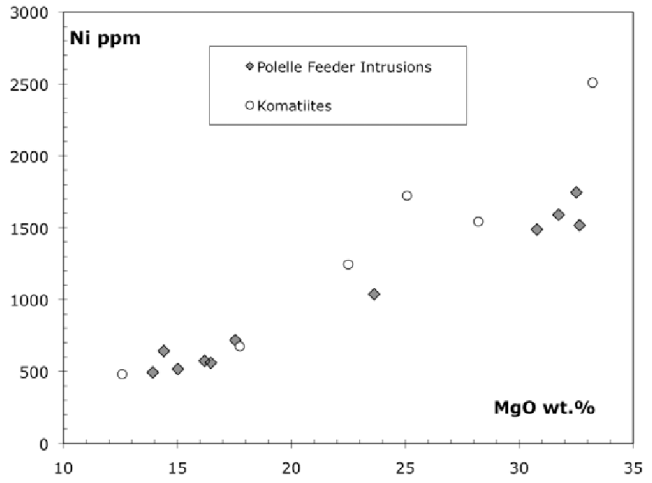

Figure 2. MgO-Ni plot for Polelle (Gabanintha) komatiites and Norie Group high-Mg bodies.

At least two types of basaltic-andesites and andesites occur in the Polelle Group. One type is characterised by flat patterns on mantle-normalised multi-element plots and appears to be differentiates of "plateau-basalt" or MORB-like basalts. The patterns lack any evidence that crustal contamination has occurred in these magmas. The other type is more typical of andesites associated with Archean massive sulphide-bearing sequences. They are classed as tholeiitic, based on La-Nb-Yb criteria employed in the Abitibi belt. Extensive contamination would likely have driven the magmas into the calc alkaline field. They are characterised by normalised multi-element patterns that are moderately LREE-enriched with minor negative Nb anomalies and moderate Th enrichments comparable to Noranda Mine Sequence examples of the Abitibi belt.

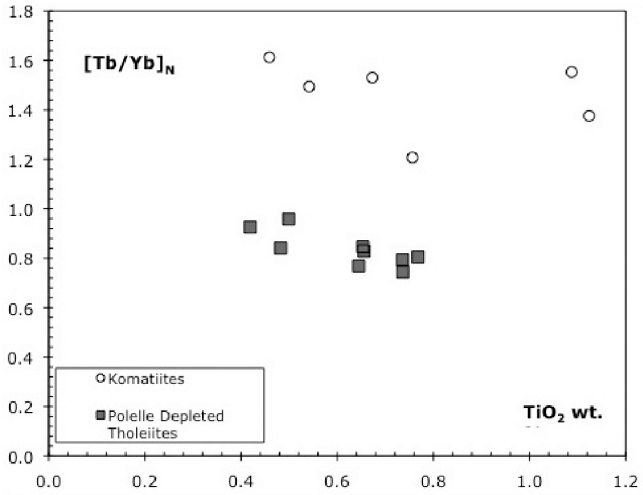

Figure 3. Discrimination of Polelle (Gabanintha) komatiites from depleted tholeiites.

Presently available Sm-Nd isotopic data for the northeast Murchison samples span $\varepsilon Nd_{2.8Ga}$ values between +4.6 and -2.1, illustrating variable degrees of crustal contamination effects and differences in the mantle sources of the volcanic suites (Fig. 4). Irrespective of crustal contamination, it is clear that volcanic sequences in the area reflect variable magma sources through time. Their chemical and isotopic compositions are most plausibly accounted for by an interval of mantle plume geodynamics imposed upon a form of subduction-style tectonic regime.

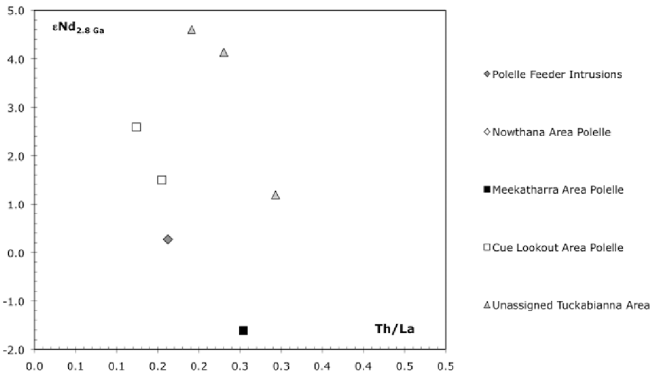

Figure 4. Variation in Sm-Nd isotopic composition versus Th/La for volcanic and subvolcanic rocks of the northeast Murchison terrane.

References

Barley M.E., Kerrich R., Reudavy I., & Xie Q., 2002, Late Archean Ti-rich, Al-depleted komatiites and komatiitic volcaniclastic rocks of the Murchison Terrane in Western Australia, Australian Journal of Earth Sciences, 47, 873–883.

Van Kranendonk M.J. & Ivanic T.J. 2009, A new lithostratigraphic scheme for the northeastern Murchison Domain, Yilgarn Carton, Geological Survey of Western Australia, Annual Review 2007-08, 34–53.

Wyman D.A., 1999, A. 2.7 Ga depleted tholeiite suite: evidence of plume-arc interaction in the Abitibi Greenstone Belt, Canada, Precambrian Research, 97, 27–42.

METAMORPHISM EVOLUTION OF THE KHONDALITE BELT, THE NORTH CHINA CRATON

C. Yin[1], G. Zhao[1], C. Wei[2], & M. Sun[1]

[1]Department of Earth Sciences, The University of Hong Kong, Pokfulam Road, Hong Kong
[2]School of Earth and Space Sciences, Peking University, Beijing 100871, China

Introduction

The Qianlishan Complex in conjunction with the adjoining the Helanshan, Daqingshan, Wulashan and Jining Complexes is considered to represent a Paleoproterozoic collisional orogen, named the Khondalite Belt, along which the Yinshan Block in the north and the Ordos Block in the south were amalgamated to form the Western Block of the North China Craton at ~1.95 Ga (Fig 1, 2; Zhao et al., 2005; Santosh et al., 2007; Xia et al., 2006). The Western Block then collided with the Eastern Block along the NS-trending Trans-North China Orogen to form the coherent basement of the North China Craton at ~1.85 Ga (Zhao et al., 1999, 2000; Guo et al., 2005; Wilde et al., 2002; Kroner et al., 2005; Faure et al., 2007; Trap et al., 2009). It thus has now become increasingly clear about the ~1.85 Ga collisional event which led to the formation of the Trans-North China Orogen, with details of the pre-collisional architecture of the crust that became incorporated into the orogen. In contrast, the Khondalite Belt has drawn few attentions and not much work has been done on it. This forms the justification for this study in which we carried out detailed metamorphic and geochronological studies on high-grade Al-rich gneisses of the Qianlishan Complex, one of the westernmost complexes in the Khondalite Belt, in order to understand the tectonic evolution of the Qianlishan Complex. Combined with previous data on other complexes, the results of this study provide important insights into understanding of the tectonic evolution of the Khondalite Belt.

Approaches

1. Field investigation: Investigating field outcrops of khondalite series rocks (Fig. 3) of the Qianlishan Complex; and collecting samples from the Khondalite Belt;
2. Petrographic examination: Determining mineral assemblages, textures and reaction relations in the Al-rich gneisses in the Khondalite Belt (Fig. 4);
3. P-T path reconstruction: Revealing the metamorphic evolution and processes by petrographical study and constructing corresponding P-T pseudosections;
4. Geochronology study: Determining the age of metamorphic event by using the LA-ICP-MS U-Pb zircons dating method.

Results

Results of metamorphism

The petrological evidence from khondalite series rocks in Qianlishan Complexes indicates four stages of metamorphic evolution: the prograde metamorphic stage (M_1) is represented by quartz + plagioclase + muscovite + biotite inclusions within the core of large garnet porphyroblasts; The peak metamorphic stage (M_2) is marked by the second growth of garnet porphyroblasts and matrix sillimanite, K-feldspar, biotite, plagioclase, quartz, with little amount of accessory minerals such as rutile; This is then followed by the post-peak metamorphic stage (M_3) represented by the formation of

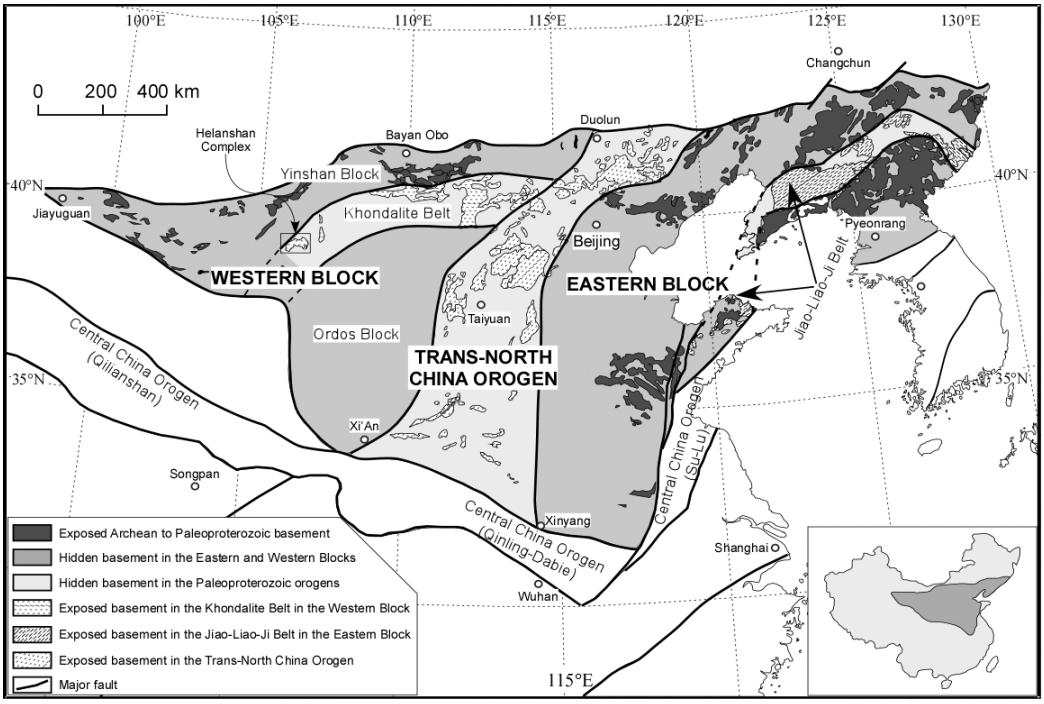

Figure 1. Tectonic Subdivision of the North China Craton (Zhao et al., 2005).

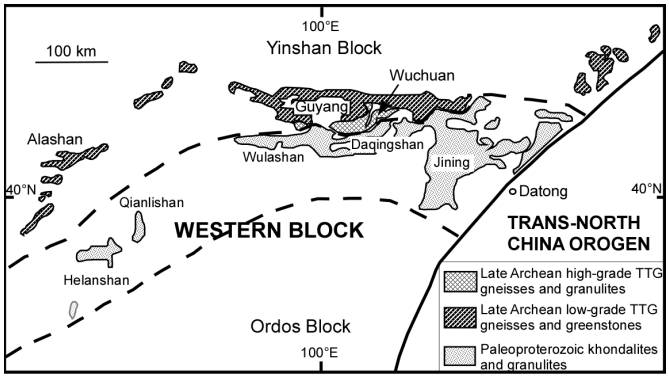

Figure 2. Tectonic Subdivision of the Western Block (after Zhao et al., 2005).

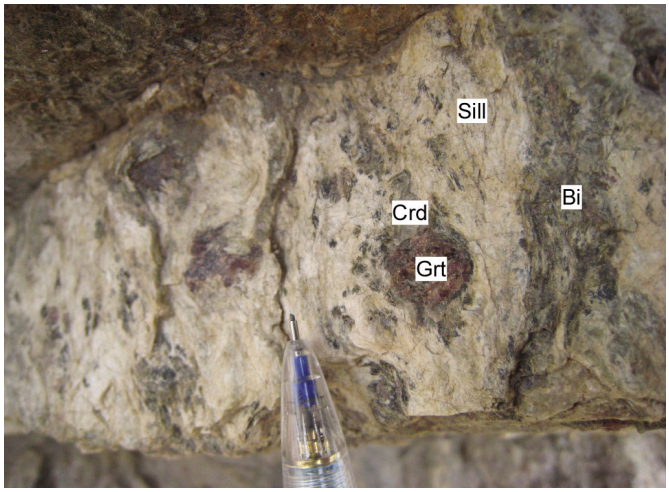

Figure 3. Cordierite-Garnet-Sillimanite Gneiss in Qianlishan Complex.

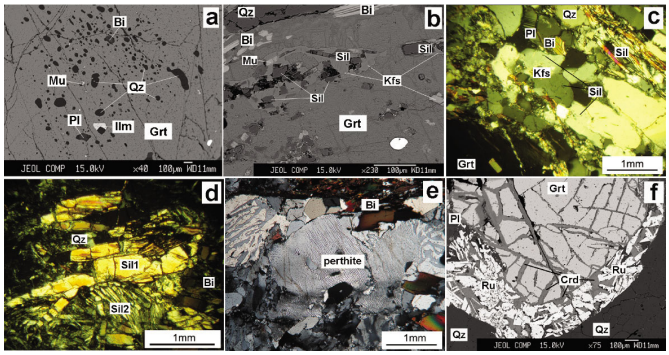

Figure 4. Photomicrographs of sillimanite-garnet gneiss (cross-polarized light and BSE). (a) Mineral inclusions within the core of garnet porphyroblast. (b) Some K-feldspar inclusions within mantle of garnet included sillimanite aggregates which remain minor small grained relic muscovite. (c) Matrix mineral assemblage, some small fibrous sillimanite inclusions within K-feldspar and quartz. (d) The matrix coarse sillimanite (sil1) could be from kyanite and very fine-grained sillimanites (sil2) which are developed within or around the biotite flakes. (e) K-feldspar containing thin lamellae of plagioclase as perthite. (f) Cordierite coronas surrounding garnet grains or in the cracks of garnet porphyroblasts.

cordierite coronas surrounding rims or in the cracks of garnet porphyroblasts in response to a decompressional process.

These mineral assemblages and their P-T estimates using THERMOCALC (Version 3.26) define a clockwise P-T path involving nearly isothermal decompression, similar to a P-T path based on the mineral assemblage's stability fields of P-T pseudosection constructed in NCKFMASH system for representative rock composition (Fig. 5).

Metamorphic P-T paths of the khondalite series rocks from other complexes in the Khondalite Belt, Western Block are shown in Figure 6.

Results of geochronology

Metamorphic zircons yield two age populations with one at ~1.95 Ga and another at ~1.92 Ga (Fig. 7), of which the former is interpreted as the timing of the collision between the Yinshan and Ordos blocks to form the Western Block, whereas the later is considered to be the age of subsequent post-orogenic extensional event.

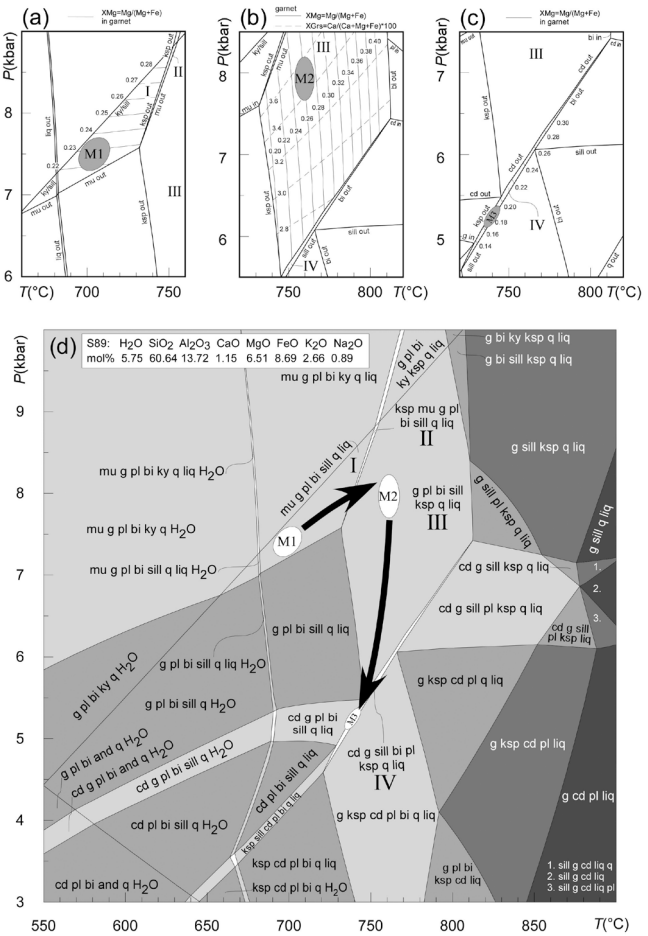

Figure 5. P-T pseudosection in NCKFMASH. Bulk composition (in mol. %) is SiO_2: 62.67; Al_2O_3:15.75; CaO: 1.40; MgO: 8.21; FeO: 8.21; K_2O: 2.71; Na_2O: 1.05 (Samples from the Qianlishan Complex). The P-T pseudosection calculated for bulk rock composition of garnet-sillimanite-cordierite gneiss. (a-c), Enlarged and simplified parts (fields I-IV) of the pseudosection with calculated isopleths of mineral composition and molar proportions; (d), the clockwise P-T path is derived by comparing the modelled assemblages and isopleths with assemblages, chemistry and zoning of minerals observed in the sample.

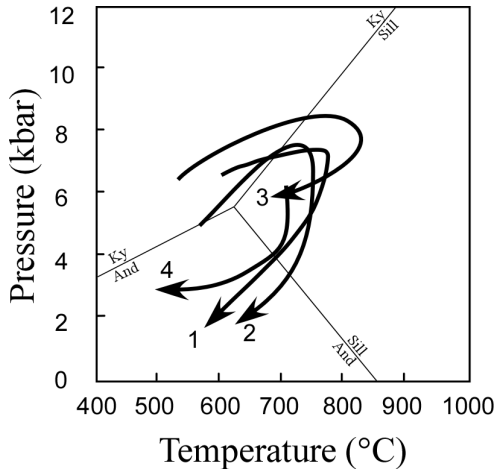

Figure 6. (1) Helanshan-Qianlishan Complex (Zhao et al., 1999); (2) Daqingshan-Wulashan Complex (Jin et al., 1991; Liu et al., 1993); (3) The first metamorphic event in the Jining Complex (Lu and Jin, 1993); (4) The second metamorphic event in the Jining Complex (Lu and Jin, 1993).

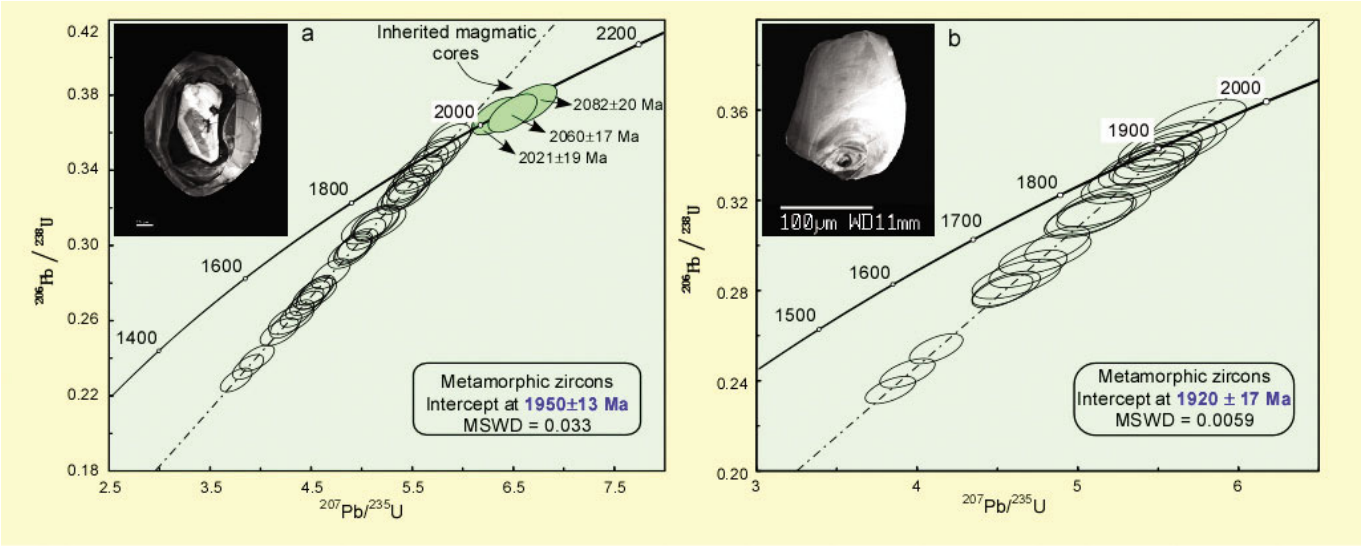

Figure 7. U-Pb isotopic compositions for zircons from the Qianlishan Complex. (a) Concordia diagram on inherited magmatic cores and metamorphic overgrowth rims. (b) Concordia diagram on metamorphic overgrowth rims.

Conclusion

1. The clockwise P-T paths of khondalite series rocks from the Qianlishan Complex and other complexes of the Khondalite Belt, combined with available structural and geochronological considerations, provide the first constraint of the tectonothermal events, involving the the amalgamation of the Yinshan and Ordos blocks to form the Western Block during a collisional orogeny.
2. At ~1.95 Ga, the Yinshan Block in the north collided with the Ordos Block in the south to form the east-west-trending Khondalite Belt. During the continent-continent collision, the Paleoproterozoic sedimentary rocks along the passive continental margin of the Ordos Block were subducted beneath the active-type continental margin of the Yinshan Block. The collision caused crustal-scale folding, thrusting and thickening, and resulted in granulite facies metamorphism and the formation of the khondalite series rocks at the lower crustal levels.
3. At ~1.92 Ga, possibly due to the slab-break off or some other tectonic mechanism, the Khondalite Belt experienced post-collisional extension with widespread emplacement of mafic dykes, which caused the UHT metamorphism of the khondalite series rocks in local areas (e.g. the Jining and Daqingshan Complexes).

Acknowledgements

This research was financially supported by Hong Kong RGC GRF grants (7063/06P, 7066/07P and 7053/08P). A HKU postgraduate studentship to Changqing Yin is greatly acknowledged.

References

Faure M., Trap P., Lin W., Monie P. & Bruguier O., 2007, Polyorogenic evolution of the Paleoproterozoic Trans-North China Belt, new insights from the Lüliangshan-Hengshan-Wutaishan and Fuping massifs, Episodes, 30, 1–12.

Guo J.H., Sun M., Chen F.K. & Zhai, M.G., 2005, Sm-Nd and SHRIMP U-Pb zircon geochronology of high-pressure granulites in the Sanggan area, North China Craton: timing of Paleoproterozoic continental collision. Journal of Asia Earth Science, 24, 629-642.

Kröner A., Wilde S.A., Li J.H. & Wang K.Y., 2005, Age and evolution of a late Archean to Paleoproterozoic upper to lower crustal section in the Wutaishan/Hengshan/Fuping terrain of northern China, Journal of Asia Earth Science, 24, 577–595.

Liu X.S., Jin W., Li S.X. & Xu X.C., 1993, Two types of Precambrian high-grade metamorphism, Inner Mongolia, China, Journal of Metamorphic Geology, 11, 499–510.

Lu L.Z. & Jin S.Q., 1993, P-T-t paths and tectonic history of an early Precambrian granulite facies terrane, Jining district, southeastern Inner Mongolia, China, Journal of Metamorphic Geology, 11, 483–498.

Santosh M., Wilde S.A., Li J.H., 2007, Timing of Paleoproterozoic ultrahigh-temperature metamorphism in the North China Craton: Evidence from SHRIMP U-Pb zircon geochronology, Precambrian Research, 159, 178–196.

Trap P., Faure M., Lin W., Monie P., Meffre S. & Melleton J., 2009, The Zanhuang Massif, the second and eastern suture zone of the Paleoproterozoic Trans-North China Orogen, Precambrian Research, 172, 80–98.

Wilde S.A., Zhao G.C. & Sun M., 2002, Development of the North China Craton during the late Archean and its final amalgamation at 1.8 Ga: Some speculations on its position within a global Palaeoproterozoic supercontinent, Gondwana Research, 5, 85–94.

Xia X.P., Sun M., Zhao G.C., Wu F.Y., Xu P., Zhang J.H. & Luo Y., 2006, U–Pb and Hf isotopic study of detrital zircons from the Wulashan khondalites: Constraints on the evolution of the Ordos Terrane, Western Block of the North China Craton, Earth and Planetary Science Letters, 241, 581–593.

Zhao G.C., Wilde S.A., Cawood P.A. & Lu L.Z., 1999. Tectonothermal history of the basement rocks in the western zone of the North China Craton and its tectonic implications, Tectonophysics, 310, 37–53.

Zhao G.C., Wilde S.A., Cawood P.A. & Lu L.Z., 2000, Petrology and P–T path of the Fuping mafic granulites: implications for tectonic evolution of the central zone of the North China Craton, Journal of Metamorphic Geology, 18, 375–391.

Zhao G.C., Sun M., Wilde S.A. & Li S.Z., 2005, Late Archean to Paleoproterozoic evolution of the North China Craton: key issues revisited, Precambrian Research, 136, 177–202.

ARCHEAN GRANITES IN THE LAKE AUSTIN REGION, MURCHISON DOMAIN, YILGARN CRATON: CRYSTALLIZATION OF MAGMA PULSES IN A DYNAMIC TECTONIC SETTING.

I. Zibra

Geological Survey of Western Australia, Mineral House, 100 Plain Street, East Perth WA 6004, Australia

Introduction

The northeastern Murchison Domain forms part of the Youanmi Terrane within the Archean Yilgarn Craton (Cassidy et al., 2006). It includes a typical Archean association with arcuate greenstone belts lying between large areas of granitic rocks. In the Lake Austin area, the studied granitic suite includes several lithologies ranging from homogeneous to porphyritic monzogranite, mafic (biotite-rich) granodiorite, and microleucogranite.

Outcrop-scale evidence of synmagmatic deformation

Several meso-scale structures suggest that pluton crystallization occurred in a dynamic environment. This contribution mainly illustrates some representative outcrop-scale features.

In the Lake Austin region, different granites commonly show amoeboid to crenulate intrusive contacts and share a vertical, roughly north–south-trending magmatic foliation, compositional layering and schlieren fabric. Such a pluton-scale trend is evident in the total magnetic intensity image. Magmatic lineation is rarely detectable due to poor exposure. However, good exposures in a few localities suggest that a sub-horizontal to shallowly south-dipping magmatic lineation appears dominant in all granite types.

Compositional layering (figure 1) is characterized by decimetre-thick, along-strike continuous layers displaying average monzogranite composition with slightly different proportions of biotite, quartz and feldspars. At the microscale, the main fabric is marked by aligned subhedral to euhedral feldspar crystals, surrounded by recrystallized quartz aggregates. Microstructures suggest that quartz recrystallization occurred at a temperature close to the granite solidus. The layering is truncated locally by magmatically foliated microgranite veins displaying crenulate boundaries against host rocks, which are displaced by synmagmatic faults. These features suggest that the compositional layering has a magmatic origin and developed before the full crystallization of the granitic suite.

Schlieren fabric is characterized by thin trails of biotite, generally discontinuous along strike, and concordant with the large-scale, N-S trending structures. The biotite-rich layers do not separate granites with different compositions. Due to the sub-vertical orientation and the lack of pervasive plastic deformation at microscale, this fabric likely derives from flow sorting during intense magmatic flow within a single batch of magma.

Figure 1. Well-defined planar fabric in porphyritic monzogranite, due to tonalite to leucogranite sheets aligned parallel to the magmatic foliation. The base of photo is about one metre.

K-feldspar cumulates occur as steep tabular bodies concordant with the magmatic foliation, displaying strong shape preferred orientation of euhedral K-feldspar crystals (figure 2). They are interpreted as dykes, diapirs and tubes that intruded the host granites during magmatic shearing due to mechanical and thermal instabilities that induced mobility of accumulated crystals (Vernon and Paterson, 2008). Tiling and brittle deformation of euhedral K-feldspar crystals may reflect alignment and shearing of mobilized cumulates during intense magmatic flow.

Magmatic folds (i.e. hypersolidus folding of magmatic fabric: Paterson et al., 1998) commonly occur within different granitic types and are best observable within the compositionally-layered granites (figure 3). At the microscale, the axial plane foliation is marked by the strong alignment of undeformed igneous feldspars, indicating that its origin is primarily magmatic (e.g.

Paterson et al., 1989). Quartz grains are elongated parallel to the foliation and display chessboard subgrain patterns, suggesting that minor deformation occurred in the high-quartz field (Kruhl, 1996) at a temperature close to the granite solidus. Quartz grain boundaries are consistently deeply sutured, suggesting recrystallization through grain boundary migration at high-temperature (Stipp et al., 2002).

Figure 2. Sharp intrusive boundary between homogeneous monzogranite (at right) and a K-feldspar-rich layer, interpreted as cumulate dyke intruded into host monzogranite.

Figure 3. Magmatic fold displaying similar geometry in a magmatically foliated, biotite-bearing schlieren monzogranite. Magmatic foliation is parallel to the axial plane of the fold.

Schlieren fabric, compositional layering, and magmatic boundaries are frequently offset along magmatic faults (figure 4). Fault planes are commonly associated with aplitic to pegmatitic material interpreted as former melt accommodating synmagmatic shearing. Within the shear planes, leucogranitic material typically displays a weak magmatic alignment, and no subsolidus deformation is visible at grain scale. Magmatic faults can generally be traced for a few metres to a few tens of metres along strike. They typically occur at low to moderate angles (10–45°) from the main magmatic fabric, displaying both dextral and sinistral displacement. The observed offset varies from few centimetres to few tens of metres. Some outcrops show complex relations between subsequent episodes of magma injection and synmagmatic faulting, likely reflecting the construction of a magma chamber in an active tectonic setting.

Figure 4. Melt-filled dextral shear zone, highlighted by the displaced schlieren fabric in the host monzogranite.

Discussion and future outlook

Preliminary observations summarized here suggest that most of the granites from the 'Austin Suite' may be roughly coeval, possibly representing subsequent magma pulses that crystallized in an active tectonic setting. The pattern of the magmatic fabric, consistently oriented N–S in most of the study area, suggests that it could be the expression of the regional stress field at the time of igneous crystallization, rather than representing internal processes related to the construction of the magma chamber. The observed compositional layering could result from multiple sheeted injections along sub-vertical planes during synmagmatic shearing.

Preliminary microstructural investigations indicate that several microfabrics, ranging from (sub-) magmatic, to high- and moderate-temperature solid state are recorded in the studied granites.

The age of the 'Austin Suite' is still poorly constrained. U–Pb ages of about 2650 to 2680 Ma have been obtained of east of the area discussed here (Schiøtte and Campbell, 1996), where a heterogeneous granitic suite similar to the "Austin Suite" is enclosed within two distinct greenstone belts. In this area, most of the granites have been affected by pervasive greenschist-facies shearing along the Meekatharra structural zone (Spaggiari, 2006). Therefore, a correlation between these sheared granites and the "Austin Suite" is not straightforward. Thus, new geochronology has been planned for the "Austin Suite" in order to constrain the timing of the pluton crystallization in the context of the regional deformation.

Acknowledgements

This contribution is published with the permission of the Executive Director, Geological Survey of Western Australia.

References

Cassidy K.C., Champion D.C., Krapez B., Barley M.E., Brown S.J.A., Blewett R.S., Groenewald P.B. & Tyler I.M., 2006, A revised geological framework for the Yilgarn Craton, Western Australia, Geological Survey of Western Australia, Record 2006/8, 8p.

Kruhl J.H., 1996, Prism- and basal-plane parallel subgrain boundaries in quartz: a microstructural geothermobarometer, Journal of Metamorphic Geology, 14, 581–589.

Paterson S.R., Fowler Jr. T.K., Schmidt K.L., Yoshinobu A.S., Yuan E.S. & Miller R.B., 1998, Interpreting magmatic fabric patterns in plutons, Lithos, 44, 53–82.

Paterson S.R., Vernon R.H. & Tobisch O.T., 1989, A review of criteria for the identifications of magmatic and tectonic foliations in granitoids, Journal of Structural Geology, 11, 349–363.

Schiøtte, L., & Campbell, I.H., 1996, Chronology of the Mount Magnet granite–greenstone terrain, Yilgarn Craton, Western Australia: implications for field based predictions of the relative timing of granitoid emplacement, Precambrian Research, 78, 237–260.

Spaggiari C.V., 2006, Interpreted bedrock geology of the northern Murchison Domain, Youanmi Terrane, Yilgarn Craton, Geological Survey of Western Australia, Record 2006/10, 19p.

Stipp M., Stünitz H., Heilbronner R. & Schmid S.M., 2002, The eastern Tonale fault zone: a "natural laboratory" for crystal plastic deformation of quartz over a temperature range of 250 to 700°C, Journal of Structural Geology, 24, 1861–1884.

Vernon R.H. & Paterson S.R., 2008, Mesoscopic structures resulting from accumulation and melt movement in granite, Transaction of the royal society of Edinburgh, Earth Sciences, 97, 369–381.

THEME 3

UNIQUE MINERAL SYSTEMS?

KEYNOTE & INVITED SPEAKERS

THE LITHOSPHERE, GEODYNAMICS AND METALLOGENY OF EARLY EARTH

G.C. Begg[1,2], W.L. Griffin[2], S.Y. O'Reilly[2] & L. Natapov[2]

1Minerals Targeting International PL, Suite 26, 17 Prowse St, West Perth, WA 6005, Australia
2GEMOC, Macquarie University, NSW 2109, Australia

Relationship of ore deposits to plate tectonics

Ore systems are closely linked to processes resulting from plate tectonics and global dynamics (e.g. Mitchell & Garson 1981, Sawkins 1984, Windley 1995, Kerrich et al. 2005). A robust understanding of the genetic controls on ore deposit formation means that deposits themselves can be sensitive indicators of geologic process (e.g. Meyer 1988, Groves & Bierlein 2007). In this paper we explore the lithospheric and geodynamic controls on ore deposits in the early Earth prior to the Mesoproterozoic, and attempt to discover why there are so few significant deposits older than 3 Ga. Mantle plume activity related to a cooling Earth, the onset of plate tectonics, the evolution of the continental crust and sub-continental lithospheric mantle, the rise of atmospheric oxygen, and biological evolution are some of the factors that are likely to have influenced the genesis and preservation of deposits through time. The latter two are not considered further here.

Earliest evidence for plate tectonics and related ore deposits

Cooling of the Earth is primarily through the action of plate tectonics (linked with mantle convection) and the melting of mantle plumes to form large igneous provinces. Modelling of a hot early Earth suggests that plume dynamics may have been the dominant mode until at least the Neoarchean. Analysis of paleomagnetic, geochemical, tectonostratigraphic, isotopic and seismological evidence indicates that plate tectonics has operated since at least 3.2 Ga (Cawood et al. 2006, Dilek & Polat 2008), but possibly as early as the Hadean (summarized in Condie & Kroner 2008, Shirey et al. 2008). The earliest preserved crust that is indicative of probable plate tectonic processes is the Eoarchean 3.8 Ga Isua greenstone belt, Greenland (Dilek & Polat 2008). Both vertical forces related to gravitational equilibration of the crust, and horizontal forces related to plate tectonics, appear to have operated throughout the Paleo- to Neoarchean, with the former declining in significance with time and with cooling of the lower crust (e.g. Bedard 2003, Van Kranendonk et al. 2007). Plate tectonics has been dominant since at least the Late Neoarchean (Cawood et al. 2006), building cratons via accretionary and collisional processes (e.g. Kerrich & Polat 2006, Polat et al. 2005).

Rare well-preserved remnants of Paleo- and Mesoarchean upper crust indicate that mineralizing processes were active at this time. The 3.315 Ga Spinifex Ridge Porphyry Cu-Mo deposit and 3.24 Ga Sulphur Springs VHMS deposit, both in the Pilbara craton, are among the oldest preserved deposits of their type. Both formed at a time when vertical tectonics was locally dominant (Van Kranendonk et al. 2007), and may not be direct genetic correlatives of similar deposits in post-Archean convergent margin environments elsewhere. The 2.95 Ga orogenic gold deposits in the Barberton Greenstone Belt appear to be associated with late orogenic lateral (plate) tectonics, similar to later deposits of this type (e.g. Goldfarb et al. 2005). Ca 2.92 Ga nickel sulphide deposits of the Yilgarn craton may be associated with a cratonic margin, similar to younger deposits of this type (Begg et al., submitted). The size of 2.89-2.82 Ga placer gold deposits of the peri-cratonic foreland Witswatersrand Basin, indicates that the Mesoarchean (and possibly earlier) processes were considerably more efficient at extracting and concentrating gold from the mantle than the later Earth (Frimmel 2008).

Abundant high-quality Neoarchean metal deposits are preserved. Witswaterand gold aside, does the generally smaller size and relative paucity of older deposits indicate a change in Earth processes, or does it merely reflect poor preservation of the upper crust? Was there something fundamentally different about plate tectonic processes or metal source regions?

Growth of Sub-Continental Lithospheric Mantle (SCLM)

Integration of geophysical, geological, and geochemical data on the crust and lithospheric mantle has generated a map of lithospheric composition and architecture that suggests ca 70% of the existing SCLM may have an Archean parentage. Modelling of zircon Hf-isotope data from GEMOC's worldwide database concludes that a similar percentage (>60%) of continental crust had formed by the end of the Archean (Belousova et al., in prep). Of particular significance is the inference that most preserved Proterozoic crust overlies Archean SCLM that has been variably refertilised and metasomatised by mantle melts associated with convergent margin, post-collisional, and mantle plume processes (Begg et al. 2009a, Griffin et al. 2009). These interpretations suggest that consideration of lithospheric preservation and recycling is crucial to understanding Earth evolution. Pristine Archean SCLM comprises highly depleted (Fe-poor) dunite/harzburgite that most likely formed by high degree partial melting of large, hot mantle plumes (Griffin et al. 2009). Re-Os isotopic studies of sulphides from SCLM peridotites (e.g. Griffin et al. 2004) indicate that most of this Archean SCLM formed between 3-3.5 Ga ago (Griffin et al, this volume), a finding consistent with isotopic and trace element data from mafic-ultramafic crustal rocks (Shirey et al. 2008), and the record of PGE contents in komatiites (Maier et al. 2009). It is likely

therefore that the geodynamic environment during this period was dominated by particularly vigorous mantle plume activity and possibly major mantle overturns (e.g. Davies 1995).

In a recycling model, depleted, rigid, bouyant Archean SCLM survives the rifting and accretionary processes of supercontinent cycles, while the juvenile, fertile, dense SCLM typical of island arcs is removed. At least 20% of existing SCLM may be such fertile SCLM that has yet to be recycled. Although geochronological and isotopic (Hf, Nd) studies indicate that juvenile Proterozoic crust may be less extensive than previously believed, a recycling model must still account for significant amounts of juvenile Proterozoic crust. Accretionary events and rifting at margins may add or subtract variable thicknesses of crust via obduction or detachment, respectively. Also, crustal re-surfacing with juvenile mantle-derived products, and development of cover sequences, make detection of older crust difficult.

Interaction between Plate tectonics and SCLM

Formation of a buoyant, anhydrous (stiff) SCLM represents a milestone in Earth dynamics as it will have had a profound interaction with, and influence on, plate tectonics. Amalgams of lithospheric blocks form rigid cratons, dictating a minimum plate size, localizing subduction on their margins, and facilitating the transfer of stress during accretionary and collisional events. Lateral plate motions involving intra-continental rifting or subduction at a convergent margin represent opportunities to thin crust, and to dissect continents and cratons. In particular, subduction rollback facilitates the formation of backarc basins, which are first documented at 3.0 Ga and are widespread by 2.7 Ga (Condie & Kroner 2008). Fragmentation of brittle cratonic lithosphere may result in the development of intracratonic basins with high geothermal gradients. Far field stresses may reactivate old boundaries within the SCLM, or form new translithospheric faults. Significantly, the appearance of this cratonic SCLM enabled the formation of supercontinents, forcing a new organizing framework on a coupled plate tectonic-mantle convection system.

.

Linking the Lithosphere and Geodynamics to Ore Deposits in the Early Earth

A coupled whole-lithosphere and geodynamic approach can help us understand secular and spatial controls on metallogeny, within the larger framework and macro control of the supercontinent cycles. In the modern Earth, the polarity of subduction, disruption of subduction, and rate of convergence conspire to determine the metallogenic fertility of Cu and Au source regions in both the convecting mantle and SCLM (e.g. Solomon 1990, Richards 2009). This probably also applied to Archean plate tectonics. Many giant ore deposits of all ages are located on or near translithospheric faults, implying either a direct or indirect mantle role in their genesis. Examples of the former include deposits of magmatic Ni-Cu-PGE sulphides, porphyry Cu-Mo-Au, and Iron-Oxide-Copper-Gold. AS well as enabling the passage of melts, translithospheric faults may exert an influence on crustal structure (fault arrays, basins, topographic highs) and thermal architecture, and hence the location of deposits related to hydrothermal fluid systems (e.g. SEDEX Ag-Pb-Zn, polymetallic VHMS).

The collisional climaxes heralding supercontinents that lasted from ca 2.65-2.45 Ga and ca 1.85–1.65 Ga were characterized by peaks in mantle plume activity. In the Neoarchean, Banded Iron Formations (BIF) precipitated from the resultant Fe-rich seawater in narrow ocean basins. The variable thickness of SCLM resulted in plume melting being focused in areas of thin lithosphere at cratonic margins, forming giant magmatic Ni-Cu-PGE deposits of the Yilgarn (Neoarchean) and Superior (Paleoproterozoic) cratons (Begg et al. 2009b, Begg et al., submitted). Collision of arcs, cratons, and microcontinental fragments of depleted SCLM created a smorgasboard of opportunities for convergent margin-related ore deposits. The effects of delamination of denser (e.g. oceanic) lithosphere and crustal thickening at accretionary/collisional margins made magmatic arc-related deposits (epithermal gold, porphyry copper, VHMS base metal) the victims of uplift and erosion, explaining their paucity in the ancient record. In contrast, those backarcs protected from major crustal thickening by underlying or outboard microcontinents, preserve some of the syn-volcanic deposits (e.g. VHMS deposits of the southern Superior or nickel sulphide deposits of the Yilgarn and Zimbabwe cratons), and were prime locations for the generation and preservation of late-stage orogenic gold deposits (southern Abitibi and Eastern Goldfields provinces in the Archean; Birrimian Province in the Paleoproterozoic). Similarly, peri- or intra- cratonic settings will enhance the preservation potential of a range of other deposits types, including platform-hosted BIF (e.g. Sao Francisco and Pilbara cratons), sediment-hosted base metals (e.g. SEDEX of northern Australia, Broken Hill Ag-Pb-Zn of eastern Australia), Iron-Oxide-Copper-Gold of the Gawler craton, “stratiform” sediment-hosted Cu, and placer deposits of gold (Witswatersrand) and diamonds.

Conclusions

There is a strong case for early Archean, and possibly Hadean subduction. This must have provided an environment favourable for the formation of many convergent-margin-related ore deposits, but not the environment required to preserve them. A period of major mantle plume activity (possibly in response to earlier subduction) created thick, depleted, buoyant and stiff SCLM in the Paleo- to Mesoarchean, paving the way for craton formation. It also created a captive potential metal source region. Cratonic lithosphere, coupled with plate tectonics, provided suitable lithospheric and geodynamic settings for ore- forming processes and the preservation of the resultant deposits. These settings include: craton margins with their changes in lithospheric thickness and associated translithospheric faults; stable continental shelves; intracratonic basins; backarc basins. In particular, it is proposed that the creation of backarc basins involving fragmentation of cratonic lithosphere preferentially along pre-existing sutures, was a KEY development in metallogenic evolution, in terms of both enhanced metallogenic fertility AND high crustal-

preservation potential. Magmatic arcs on continental/ cratonic margins are capable of forming many large ore deposits, but these deposits rarely survive the uplift and erosion attendant with accretion/collision-related crustal thickening.

The appearance of cratonic lithosphere dictated a re-organisation of plate tectonics, and likely resulted in the onset of the supercontinent cycle which is still with us today. Changing geodynamic conditions implicit through these cycles are a macro control on metallogenesis.

We have found that continents are dominantly (ca 70%) built on Archean SCLM. This implies that there may have been a great number more Archean ore deposits than are preserved. Archean and Paleoproterozoic ore deposits have only survived on cratons that:- a) have remained large entities on the order of 1000 km across; b) have mostly, if not exclusively, remained as lower plates during post-deposit plate interactions.

References

Bedard J.H., Brouillette P., Madore L., & Berclaz A., 2003, Archaean cratonization and deformation in the northern Superior Province, Canada: an evaluation of plate tectonic versus vertical tectonic models, Precambrian Research, 127, 61–87.

Begg G.C., Hronsky J.M.A., Arndt N.T., Griffin W.L., O'Reilly S.Y. & Hayward N., submitted, Lithospheric, Cratonic, and Geodynamic Setting of Ni-Cu-PGE Sulfide Deposits.

Begg G.C., Griffin W.L., Natapov L.M., O'Reilly S.Y., Grand S.P., O'Neill C.J., Hronsky J.M.A., Poudjom Djomani Y., Swain C.J., Deen T. & Bowden P., 2009a, The lithospheric architecture of Africa: Seismic tomography, mantle petrology and tectonic evolution. Geosphere 5, 23-50.

Begg G.C., Hronsky J.M.A., O'Reilly S.Y., Griffin W.L. & Hayward N., 2009b, Plumes, Cratons and Nickel Sulphide Deposits, in Smart Science for Exploration and Mining: Proceedings of the 10th Biennial SGA Meeting of The Society for Geology Applied to Mineral Deposits, Townsville, Australia, Williams P.J., ed., 1, 147–148.

Cawood P.C., Kröner A. & Pisarevsky S., 2006, Precambrian plate tectonics: Criteria and evidence, GSA Today, 16, no.7, 4–11.

Condie K.C., and Kröner A., 2008, When did plate tectonics begin? Evidence from the geologic record, in When Did Plate Tectonics Begin on Planet Earth? Condie, K.C., & Pease, V., eds, Geological Society of America Special Paper 440, 281–294.

Davies G. F., 1995, Punctuated tectonic evolution of the earth, Earth and Planetary Science Letters, 136, 363–379.

Dilek Y. & Polat A., 2008, Suprasubduction zone ophiolites and Archean tectonics, Geology, 36, 431–432.

Frimmel H.E., 2008, Earth's continental crustal gold endowment, Earth and Planetary Science Letters, 267, 45–55.

Goldfarb R.J., Baker T., Dubé B., Groves D.I., Hart C.J.R. & Gosselin P., 2005, Distribution, Character, and Genesis of Gold Deposits in Metamorphic Terranes, Economic Geology 100th Anniversary Volume, 407–450.

Griffin W.L., Graham S., O'Reilly S.Y. & Pearson N.J., 2004, Lithosphere evolution beneath the Kaapvaal Craton. Re-Os systematics of sulfides in mantle-derived peridotites. Chemical Geology 208, 89–118.

Griffin W.L., O'Reilly S.Y., Afonso J.C. & Begg G., 2009, The composition and evolution of lithospheric mantle: A re-evaluation and its tectonic implications, Journal of Petrology, 50, 1185–1204.

Kerrich R., Goldfarb R.J., & Richards J.P., 2005, Metallogenic Provinces in an Evolving Geodynamic Framework, Economic Geology 100th Anniversary Volume, 1097–1136.

Kerrich R. & Polat A., 2006, Archean greenstone-tonalite duality: Thermochemical mantle convection models or plate tectonics in the early Earth global dynamics? Tectonophysics, 415, 141–164.

Maier W.D., Barnes Stephen J., Campbell I.H., Fiorentini M.L., Peltonen P., Barnes Sarah-J & Smithies R.H., 2009, Progressive mixing of meteoritic veneer into the early Earth's deep mantle, Nature, 460, 620–623.

Mitchell A.H.G. & Garson M.S., 1981, Mineral deposits and global tectonic settings, New York, Academic Press, 405p.

Polat A., Kusky T.M., Li J.H., Fryer B., Kerrich R. & Patrick K., 2005, Geochemistry of Neoarchean (ca 2.55-2.50 Ga) volcanic and ophiolitic rocks in the Wutaishan greenstone belt, central orogenic belt, North China craton: Implications for geodynamic setting and continental growth, Geological Society of America Bulletin, 117, 1387–1399.

Richards J.P., 2009, Postsubduction porphyry Cu-Au and epithermal Au deposits: Products of remelting of subduction-modified lithosphere, Geology, 37, 247-250.

Sawkins F.J., 1984, Metal Deposits in Relation to Plate Tectonics, Berlin, Springer, 325p.

Shirey S.B., Kamber B.S., Whitehouse M.J., Mueller P.A. & Basu A.R., 2008, A review of the isotopic and trace element evidence for mantle and crustal processes in the Hadean and Archean: Implications for the onset of plate tectonic subduction, in When Did Plate Tectonics Begin on Planet Earth? Condie K.C. & Pease V., eds, Geological Society of America Special Paper 440, 1–29.

Solomon M., 1990, Subduction, arc reversal, and the origin of porphyry copper-gold deposits in island arcs, Geology, 18, 630–633.

Van Kranendonk M.J., Smithies R.H., Hickman A.H., & Champion D.C., 2007, Review: secular tectonic evolution of Archean continental crust: interplay between horizontal and vertical processes in the formation of the Pilbara Craton, Australia, Terra Nova, 19, 1–38.

Windley B.F., 1995, The evolving continents, 3rd ed., New York, Wiley, 526p.

EARLY EARTH METALLOGENY: LITHOSPHERE-BOUNDARY LAYER-MANTLE INTERACTIONS

R. Kerrich

Geological Sciences, University of Saskatchewan, Saskatoon, Canada S7N 5E2

Geodynamic Framework

Archean mantle lithosphere is thick (~250 km), refractory, and buoyant, becoming progressively thinner, less refractory, and less buoyant relative to the asthenosphere through the Proterozoic to Phanerozoic eras (Artemieva 2009). These trends likely reflect a progressively decreasing temperature of melting in mantle plumes, and growth of Archean crust by migrating arcs capturing thick ocean plateaus, and their imbrication, with buoyant coupling of plume residue to imbricated crust forming the continental mantle lithosphere [CLM] (Wyman & Kerrich 2009). Mantle plumes cannot melt at ~ 250 km under Archean CLM, but are "steered" to the thinner transition from Archean to Proterozoic CLM, typically marked by translithospheric faults, where decompressional melting occurs at ~150 km. Archean CLM has been metasomatised in domains by hydrous fluids from subducting slabs at CLM margins; melting of these domains by impingement of plumes generates norites, erupted prevalently over 2.9-1.4 Ga, that superficially resemble crustally contaminated plume melts but are enriched in incompatible elements. Between the convecting asthenosphere and conductive CLM is the thermal boundary layer (TBL), seismically defined as the low-velocity layer, and composed of low-degree partial melts enriched in incompatible elements.

Mantle superplumes erupted in ocean basins forming ocean plateau, and large igneous provinces (LIP's) on cratons, at ~ 2.9 Ga, 2.7 Ga, 2.4 Ga, 1.9 Ga, 1.4 Ga, 800 Ma, 250 Ma, and 120 Ma (Islay & Abbott, 1999; Ernst et al. 2008). Four supercontinents, Kenorland, Columbia, Rodinia, and Pangea assembled at respectively ~ 2.7 Ga, 1.9 Ga, 1.0 Ga, and 300 Ma, dispersing at ~~ 2.2 Ga, 1.3 Ga, 750 Ma and <200 Ma respectively (Condie & Aster 2010). Supercontinents were stitched together either by accretionary orogens or continent-continent orogens. The Archean-Proterozoic transition was diachronous and marked by: (1) thinner CLM; (2) preservation of Paleoproterozoic passive margin sequences of Kenorland; and (3) decreased thermal gradients at convergent margins recorded in a transition from slab melting tonalite-trondhjenite-granodiorite (TTG) to continental margin arc slab dehydration-wedge melting basalt-andesite-dacite-rhyolite (BADR) magma series.

Kenorland

2.7 Ga plume-CLM interaction: Ni-Cu-PGE Deposits

In areas where komatiites from the 2.7 Ga superplume erupted through continental lithosphere, sulfur-saturation was induced by assimilation of high-silica crust, noritic magmas from melting of the lithospheric mantle, and/or sulfur-rich sedimentary rocks. Examples include deposits of the Abitibi terrane and Yilgarn craton (Arndt et al. 2005)

2.7 Ga oceanic arc to back-arc settings: VMS and Algoman-type BIF deposits

Volcanism in the Superior Province occurred from 3.1 to 2.7 Ga, yet volcanic-hosted base metal (Cu-Zn-Pb) massive sulphide (VMS) deposits are restricted to the period 2720-2700 Ma. Major VMS provinces are present at Kidd Creek, Noranda, Val d'Or, and Mattagami. It is likely that the 2.7 Ga superplume rearranged plate geometry, perhaps inducing oceanic back-arc rifting, which is intrinsically favorable for VMS deposit generation and ocean-crust obduction, as was the case for the better documented Cretaceous superplume event that was coeval with opening of backarcs around the Pacific margin of Asia. The giant Kidd Creek deposit is the best-preserved Archean example of a VMS deposit in a magmatic-arc sequence with coeval eruption of plume lavas (Wyman & Kerrich 2009). Some VMS deposits, exemplified by the Horne deposit, Noranda, are gold rich. Relatively thin banded-iron formations (BIFs), the so-called Algoman-type BIFs, are prominent in greenstone belts that host VMS deposits, possibly because those also include plume lavas (Kerrich et al. 2005). The BIFs were precipitated during periods of volcanic quiescence and from warm seawater discharge. Carbonaceous horizons are present in units containing both VMS and Algoman BIFs.

2.7 Ga accretionary orogens: Orogenic Au deposits

Orogenic gold deposits are located in sutures of ~2.7 Ga accretionary orogens associated with the assembly of Kenorland. The deposits formed from metamorphic-hydrothermal fluids that were generated as subcreted, hydrated juvenile crust was heated during terminal transpressive accretion across sutures (Goldfarb et al. 2005; Kerrich et al. 2005). The distribution of globally contemporaneous orogenic gold provinces favors a Kenorland supercontinent configuration, rather than the distinct Sclavia and Vaalbara cratonic reconstructions.

2.4 Ga plume-Kenorland dispersal: BIF

Numerous Superior-type BIFs were located on the Paleoproterozoic passive margins of Kenorland during supercontinent break-up, notably those of the Hamersley Basin and counterparts in the Kaapvaal craton. The conjunction of factors leading to their generation was: (1) the presence of the first extensive passive margins, which were stabilized and preserved by Archean CLM; and (2) the 2.4 Ga superplume that generated oceanic plateaus and continental flood basalts. Reduced ocean bottom waters cooled the submarine lava fields, dissolving Fe^{2+} and Si, which were precipitated in oxygenated waters of continental shelves.

Paleoproterozoic Columbia

Geodynamic overview

About 500 m.y. after the breakup of Kenorland, a superplume at ~2.0 Ga preceded assembly of the second supercontinent, Columbia, at ~2-1.8 Ga. Columbia was assembled first by closure of internal oceans, expressed as oceanic arc complexes, and then stitched by continent-continent type orogens. Final assembly of Laurentia was at ~ 1.7 Ga when the Yavapai and Mazatzal provinces accreted to the rest of North America (Vigneresse 2005). Intra-continental rifting that initiated dispersal of Columbia was marked by extensive belts of the intrusive association rapakivi granites-anorthosite-mangerite-charnokite; this association involves crustal and asthenosphere-derived melts, with melts from the thermal boundary layer (Vigneresse 2005). Dispersal of Columbia at ~1.6-1.4 Ga was likely diachronous, the younger age corresponding to a superplume (Zhao et al. 2004).

1.9 Ga superplume: BIF, phosphorites, hydrocarbons, and magmatic Ni

Several types of ore deposits are associated with this mantle plume-lithosphere interaction. On the circum-Superior Province cratonic passive margin, extensive BIFs were formed, notably in the Lake Superior region and Labrador trough. These were coeval with those on the Siberian craton passive margin that include the Krivoy Rog BIF. Phosphorite deposits, with significant amounts of uranium, are present in the 1.95-1.85 Marquette Range Supergroup, Minnesota, a passive margin sequence of the ~2.0 Ga Penokean orogen. The oldest preserved oilfield occurs in a thick succession of 2.0 Ga siliciclastic and volcanic rocks along a rifted passive margin of Kenorland in northwestern Russia. The estimated carbon reserve is 25 x 10^{10} tonnes, which is present as shungite and carbonaceous shales (Melezhik et al. 2004). Most large mantle plume events have associated BIF and hydrocarbon deposits stemming from the biosphere sequestering greenhouse gases degassed from the plume.

Ultramafic and mafic rock-hosted nickel deposits, part of plume LIPs, are also located on the craton margins, including those of the Thompson belt and the 1.8 Ga Sudbury deposits, central Canada. Host rocks to Sudbury include extensive norites, the result of melting of metasomatized peridotite of the CLM by some combination of impact and associated asthenospheric decompressional melting. "Steering" mantle plumes to CLM margins accounts for the circum-Superior distribution of magmatic nickel deposits.

~1.7 Ga oceanic arc to back-arc settings: VMS deposits

Arc, or back-arc, sequences, reflecting assembly of Columbia, include significant base metal VMS provinces. The largest and best preserved in North America are Jerome in the 1.8-1.69 Ga Yavapai Province of Arizona and Flin Flon in the Amisk Group of Manitoba. Globally correlative examples include Boliden of the Skellefte district in central Sweden, and Otukampu, Finland, both in arc volcanic sequences that are possibly extensions of the ~ 1. 7 Ga Trans Hudson orogen of Laurentia.

Paleoproterozoic orogens and ~1.8-1.7 Ga foreland basins: Au and U deposits

Paleoproterozoic orogens that stitched Columbia together were dominantly of the continent-continent type. However, sectors of those orogens have accretionary characteristics and these contain orogenic gold deposits. The largest deposits are the 1.7 Ga Homestake gold deposit (1,100 tonnes Au) in the South Dakota sector of the Trans-Hudson orogen, deposits of the 2.1 Ga Birimian orogen of West Africa, and equivalent orogenic gold deposits in the Sao Francisco craton of Brazil (Goldfarb et al. 2005).

Foreland basins developed inboard of the continent-continent orogens that stitched Columbia together. Unconformity type uranium deposits developed in siliciclastic sequences, proximal to unconformities of the Athabasca Supergroup, a foreland basin to the Trans-Hudson orogen. Equivalent basins are McArthur River in the foreland of the Barrimundi orogen in Australia's Northern Territory, and those of the foreland basin of the Eburnean orogen in western Africa. Foreland basins evolved into intracontinental basins. The critical conjunction of geological processes is: (1) transition from TTG (high Th/U) to BADR (lower Th/U) magma series; (2) foreland basins on unconformities above basement that included Fe^{2+} facies; (3) high preservation potential on or peripheral to Archean CLM; and (4) mixing of meteoric water aquifers in the basement and sedimentary rocks proximal to the unconformities (Kerrich et al. 2005).

1.7-1.5 Ga "anorogenic" rift magmatism

Magmatic deposits of Fe-Ti-V-P are associated with gabbro-anorthosite complexes of this age, and include the Mealy Mountains (New York), Kiglapait (Canada), and Smaalands-Taberg (Sweden) deposits. Magmatic deposits of Sn-Be-W-Zn-Cu are present in 1.7-1.5 Ga Rapakivi granites of Missouri, Fennoscandia, and Brazil; the granites include crustal and mantle signatures, where enrichment of incompatible elements involved melts from the thermal boundary layer induced by rifting of Columbia (Vigneresse 2005).

~1.8-1.4 Ga intracontinental rift basins: IOCG and SEDEX deposits

Intracontinental basins developed on several cratons during disaggregation of Columbia. The Olympic Dam Fe-oxide-Cu-Au-REE (IOCG) deposit is associated with 1.6 Ga A-type granites in the Adelaide intracontinental rift of South Australia. In North America, younger Mesoproterozoic counterparts are present in A-type granites, including Rapakivi granites, in Missouri. Magmatism carries signatures of depleted mantle, the thermal boundary layer at the base of the CLM, and lower crust. Whereas A-type granites are widespread in many Mesoproterozoic terranes, the specific conjunction of geological processes responsible for IOCG deposits in association with just a few terranes has been unconstrained. It is notable that the Rapakivi magmatic association and IOCG deposits are largely restricted to the Proterozoic, likely involving a well developed TBL under Archean CLM, the source of low-degree melts during rifting of Kenorland and Columbia.

Giant siliciclastic-hosted Pb-Zn deposits occur in intracontinental rifts that pre-dated the break-up of Columbia. The giant Sullivan deposit, British Columbia, formed in a 1.4 Ga mafic sill-sediment complex of the Belt-Purcell Supergroup. The Belt-Purcell basin subsequently evolved into the Meso-Neoproterozoic passive margin of Laurentia as rifting progressed to open new oceans. In reconstructions of Columbia, eastern Australia is interpreted to be adjacent to western Laurentia, and the Mt. Isa Pb-Zn deposit of Queensland may be correlative with deposits of the Laurentian passive margin (Kerrich et al., 2005). For the Belt-Purcell Supergroup, intracontinental extension involved thinning lithosphere, upwelling asthenosphere, and intraplate mafic magmas driving hydrothermal systems. For the 1.8 Ga McArthur River SEDEX in Australia, back-arc extension above a subduction zone is inferred.

Conclusions

VMS and orogenic gold deposits formed in geodynamic settings of backarcs and sutures of accretionary orogens, respectively, that have changed little through time. Rare Precambrian porphyry-Cu deposits occur, but are associated with sparse BADR magma series rather than prevalent TTG. Collectively, their preservation reflects thick, refractory, Archean CLM. Rapakivi granites and IOCG are both prevalent in the Proterozoic likely due to involvement of melts from a well developed thermal boundary layer under Archean CLM during rifting of Kenorland and Columbia. In the Archean, Mississippi Valley Pb-Zn and SEDEX deposits are not known given some combination of poor development of foreland basins and intracontinental rifts, and high sea level stands from abundant mantle plumes. For similar reasons, Archean passive margin sequences are rarely preserved. The secular distribution of magmatic-Ni and BIF deposits reflect the time series of mantle plumes. Restriction of large unconformity U deposits to the Paleo- to Mesoproterozoic remains enigmatic: possibly, younger foreland basins were not developed on Archean basement with reduced facies.

Acknowledgements

Kevin Cassidy and Ian Tyler are thanked for the invitation to present a keynote at the 5th IAS. This paper is an outgrowth of a 2008 paper co-authored with R. Goldfarb, J. Cline, and D. Leach.

References

Arndt N.T., Lesher C.M. & Czemanske G.K., 2005, Mantle-derived magmas and magmatic Ni-Cu-(PGE) deposits, Economic Geology, 100th Anniversary Volume, 5–23.

Artemieva, I. M., 2009, The continental lithosphere, Lithos, 109, 23–46.

Condie,K.C. & Aster R.C., 2010, Episodic zircon age spectra of orogenic granitoids: The supercontinent connection and continental growth, Precambrian Research, 180, 227–236.

Ernst R.E., Wingate M.D.T., Buchan K.L. & Li Z.X., 2008, Global record of 1600-700 Ma Large Igneous Provinces (LIP's), Precambrian Research, 160, 159–178.

Goldfarb R. J., Baker T., Dube B., Groves D.I., Hart C.J.R. & Gosselin P., 2005, Distribution, Character, and Genesis of Gold Deposits in Metamorphic Terranes, Economic Geology, 100th Anniversary Volume, 407–450.

Islay A.E. & Abbott D.H., 1999, Plume-related mafic volcanism and the deposition of banded iron formations, Journal of Geophysical Research, 104, 15,461–15,477.

Kerrich R., Goldfarb R.J. & Richards J.P., 2005, Metallogenic Provinces in an evolving geodynamic framework, Economic Geology, 100th Anniversary Volume, 1097–1136.

Melezhik V.A., Filippov M.M. & Romashkin A.E., 2004, A giant Paleopoterozoic deposit of shungite in NW Russia, Ore Geology Reviews, 24, 135–154.

Vigneresse J.L., 2005, The specific case of the Mid-Proterozoic rapakivi granites and associated suite within the context of the Columbia supercontinent, Precambrian Reseach, 137, 1–34.

Wyman D. & Kerrich R., 2009, Plume and arc magmatism in the Abitibi subprovince: Implications for the origin of Archean continental lithospheric mantle, Precambrian Research, 168, 2–22.

Zhao G., Sun M., Wilde S.A. & Li S., 2004, A Paleo-Mesoproterozoic supercontinent, Earth Science. Reviews, 67, 91–123.

MASS INDEPENDENT FRACTIONATION OF SULPHUR ISOTOPES, IMPLICATIONS FOR ARCHAEAN TO PALAEOPROTEROZOIC MINERAL SYSTEMS

B.A. Wing

Department of Earth and Planetary Sciences, McGill University, 3450 University Street, Montreal, Quebec, H3A 2A7 CANADA

Introduction

Multiple sulphur isotope analyses provide a unique perspective on Archaean and Palaeoproterozoic (and younger) mineral systems. Measurements of $\delta^{33}S$, $\delta^{34}S$, and $\delta^{36}S$ values sedimentary rocks have revealed that mass-independent isotope fractionation ($\delta^{33}S \neq 0.515 \times \delta^{34}S$, $\delta^{36}S \neq 1.9 \times \delta^{34}S$) is a defining characteristic of the pre-2.45 Ga Earth surface system. Laboratory experiments and photochemical modelling highlight atmospheric oxygen levels as a positive control on the production and preservation of mass-independent sulphur isotope fractionation. Under this interpretation, oxygen was a trace gas in the pre-2.45 Ga atmosphere (Farquhar et al. 2000). Tracking the sulphur isotope anomalies (quantified as $\Delta^{33}S \approx \delta^{33}S - 0.5 \times \delta^{34}S$ and $\Delta^{36}S \approx \delta^{36}S - 2 \times \delta^{34}S$) in Archaean and Palaeoproterozoic rocks has revealed a sustained and vigorous microbial sulphur-recycling program (Kaufman et al. 2007, Ueno et al. 2008) under an Archaean atmosphere with apparent variations in a number of trace gases (SO_2 - Farquhar et al. 2007; CH_4 and CO_2 - Domagal-Goldman et al. 2008; OCS - Ueno et al. 2009).

While ore-forming processes in mineral systems may fractionate sulphur isotopes, theoretical arguments (Hulston & Thode, 1965) and examinations of modern mineralizing environments (Ono et al. 2006) demonstrate this fractionation will not be characterized by isotopic anomalies. Except for extremely rare reservoirs (e.g., source regions for some eclogitic diamonds - Farquhar et al. 2002), sulphur outside the Earth surface system appears to be isotopically normal. Non-zero $\Delta^{33}S$ and $\Delta^{36}S$ values in Archaean and Palaeoproterozoic (and younger) mineral systems, therefore, immediately imply an interconnected sulphur cycle between the site of mineralization and a source of Archaean and Palaeoproterozoic surface sulphur. In this presentation I will highlight three areas where mass independent fractionation of sulphur isotopes has provided new constraints on Archaean and Palaeoproterozoic (and younger) mineral systems.

Tracers

The most straightforward application of multiple sulphur isotope measurements in mineral systems is to identify and quantify contributions from surface sulphur to the source of sulphide mineralization. This approach has been used to monitor Archaean/Palaeoproterozoic sedimentary sulphur in diamond formation regions (Farquhar et al, 2002), seawater sulphate in Archaean volcanic massive sulphide (VMS) deposits (Jamieson et al. 2006), and assimilated Archaean/Palaeoproterozoic crustal sulphur in magmatic platinum-group-element deposits (Penniston-Dorland et al. 2008). A recent iconic example highlights the state-of-the-art: nominally magmatic komatiite-hosted Ni deposits exhibit the complete structure of the Archaean sedimentary multiple sulphur isotope record, although in a greatly telescoped form (Bekker et al. 2009).

Temperatures

In addition to fingerprinting sulphur sources, multiple sulphur isotope analyses can evaluate consistency with the hypothesis of ore mineral crystallization under equilibrium conditions (Jamieson et al. 2006). The philosophy of the approach is based on the three-isotope exchange method used to constrain equilibrium isotope fractionation factors (Matsuhisa et al. 1978). If the bulk composition of a system is characterized by a non-zero $\Delta^{33}S$ value, that value will act as a pivot point for the isotopic evolution of all the sulphur-bearing minerals in the system. The simple consequence is that sulphur-bearing minerals cannot be in equilibrium unless they have the same $\Delta^{33}S$ and $\Delta^{36}S$ values. This condition can be used to screen sulphur-bearing mineral pairs for application of sulphur isotope thermometers, making a notoriously unreliable technique much less so (Jamieson et al. 2006).

Total Environment

In combination with other geochemical measurements, multiple sulphur isotope analyses have the potential to constrain the total ore-forming environment of Archaean and Palaeoproterozoic mineral systems. As a result, sulphur isotope anomalies enable investigations of how mineralizing fluid regimes may have evolved over Earth's history. Multiple sulphur isotope analyses from ore sulphides of the ~2.7 Ga Kidd Creek VMS deposit, Canada, together with metal ratios and oxygen isotopic gradients, point to sulphate-poor ore-forming fluids in the late Archaean. Similarly, multiple sulphur isotope analyses from VMS ore sulphides of the Noranda Camp, Canada, when combined with a large suite of trace element data, indicates that ore-forming fluids of seawater origin had a distinctive cobalt and nickel-rich character.

Acknowledgements

I acknowledge the colleagues who have made it a blast to work together on multiple sulphur isotopes in Archaean to

Palaeoproterozoic mineral systems, John Jamieson, Libby Sharman, Sarah Penniston-Dorland, James Farquhar, Ian Jonasson, Bruce Taylor, Mark Hannington, and Andrey Bekker.

References

Bekker A., Barley M.E., Fiorentini M.E., Rouxel O.J., Rumble D. & Beresford S.W., 2009, Atmospheric sulfur in Archean komatiite-hosted nickel deposits, Science, 326, 1086–1089.

Domagal-Goldman S.D., Kasting J.F., Johnston D.T. & Farquhar J., 2008, Organic haze, glaciations and multiple sulfur isotopes in the Mid-Archean Era, Earth and Planetary Science Letters, 269, 29–40.

Farquhar J., Bao H.M. & Thiemens M., 2000, Atmospheric influence of Earth's earliest sulfur cycle, Science, 289, 756–758.

Farquhar J., Wing B.A., McKeegan K.D., Harris J.W., Cartigny, & Thiemens M.H., Kaufman 2002, Mass-independent sulfur of inclusions in diamond and sulfur recycling on early Earth, Science, 289, 2369–2372.

Farquhar J., Peters M., Johnston D. T., Strauss H., Masterson A., Wiechert U. & Kaufman A. J., 2007, Isotopic evidence for Mesoarchaean anoxia and changing sulphur chemistry, Nature, 449, 706–709.

Hulston J.R. & Thode H.G., 1965, Variations in ^{33}S, ^{34}S and ^{36}S contents of meteorites and their relation to chemical and nuclear effects, Journal of Geophysical Research, 70, 3475–3484.

Jamieson J.W., Wing B.A., Hannington M.D. & Farquhar J., 2006, Evaluating isotopic equilibrium among sulphide mineral pairs in Achaean ore deposits, case study from the Kidd Creek VMS deposit, Ontario, Canada, Economic Geology, 101, 1055–1061.

Kaufman A. J., Johnston D. T., Farquhar J., Masterson A., Lyons T. W., Bates S., Anbar A. D., Arnold G. L., Garvin J. & Buick R., 2007, Late Archean Biospheric Oxygenation and Atmospheric Evolution, Science, 317, 1900–1903.

Matsuhisa Y., Goldsmith J.R., & Clayton R.N., 1978, Mechanisms of hydrothermal crystallization of quartz at 250°C and 15 kbar, Geochimica et Cosmochimica Acta, 42, 173–182

Penniston-Dorland S.C., Wing B.A., Nex A.M., Kinnaird J.A., Farquhar J., Brown M., & Sharman E.R., 2008, Multiple sulfur isotopes reveal a primary magmatic origin for the Platreef PGE deposit, Bushveld Complex, South Africa, Geology, 36, 979–981.

Ueno Y., Ono S., Rumble D., Maruyama S., 2008, Quadruple sulfur isotope analysis of ca. 3.5 Ga Dresser Formation, New evidence for microbial sulfate reduction in the early Archean, Geochimica et Cosmochimica Acta, 72, 5675–5691.

Ueno Y., Johnson M.S., Danielache S.O., Eskebjerg C., Pandey A., & Yoshida N., 2009, Geological sulfur isotopes indicate elevated OCS in the Archean atmosphere, solving faint young sun paradox, Proceedings of the National Academy of Science, 106, 14784–14789.

DIVERSITY OF Ni-Cu DEPOSIT STYLES: IS THE ARCHEAN UNIQUE?

S.W. Beresford

MMG (Minerals and Metals Group), Southbank, Victoria 3006, Australia

Introduction

The last decade's major advances in Ni-Cu geoscience have resulted from a push away from forensic science on how deposits formed, to predictive geoscience focussing on where they form. The most significant advances in the last decade have been the realisation of a diversity of komatiite-hosted Ni-Cu deposits (Beresford et al 2007), and a step change in our ability to predict the location of Ni-Cu deposits, the most significant being the development of GLAM (Geodynamic lithospheric Architecture Mapping), a multidisciplinary predictive dataset developed by WMC and GEMOC (and the topic of the preceding talk by Graham Begg).

In this presentation we focus on recent advances in our understanding of deposit scale diversity. These advances have been driven from within industry, and are largely a function of the development of 3D models and the integration of geology, potential fields data, and 3D seismic. The latter tools having enabled imagery of entire ore deposits and ore systems. Our idealized ore deposit schematics are forever changed.

We adopt a modified version of the magmatic Ni-Cu deposit classification of Naldrett (2004) and divide Ni-Cu deposits into three types:

1. Komatiite-hosted Ni-Cu deposits
2. Komatiitic basalt Ni-Cu-PGE deposits
3. Mafic-hosted Ni-Cu-(PGE) deposits.

Komatiite-hosted Ni-Cu deposits

Country rock variation is the key variable in controlling emplacement and differentiation, and crucially ore style and localization. We adopt a variant of the classification scheme of Marston (1984) which reflects this key control on deposit variation. The major advance in the last decade has been the recognition that komatiitic dunite deposits are not simply larger versions of Kambalda style komatiitic peridotite deposits and that everything from host rocks, ore style, to exploration strategies is different.

Komatiitic dunite e.g. Mt Keith, Perseverance-Progress,Cosmos-Alec Mairs

The largest komatiite-hosted Ni-Cu deposits form as shallow sills emplaced into a komatiite-felsic volcanic facies association. These dunite deposits have huge disseminated sulphide haloes and complex poddy massive sulfides. The geological and geochemical and geophysical characteristics of these deposits is a significant departure from Kambalda-style deposits.

A key advance in our understanding of these deposits came from the discovery of the Black Swan and Cosmos-Alec Mairs complexes. Massive sulphide distribution is complex and not restricted to the basal contact but present as poddy secondary channels spatially associated with the master channel but not necessarily at the base of the master channel (Fig. 1). This advance has transformed exploration strategies and discovery success. Post emplacement modification of these secondary channels has locally resulted in strongly relocated massive sulfides eg Emily Ann, Harmony (e.g. Duuring et al., 2004).

Barnes et al (2006) comparison of komatiitic-hosted Ni-Cu deposits in the Yilgarn and Abitibi highlighted that the key control on the volume of Ni metal in the Yilgarn was the volume of channelized komatiites. Unfortunately identification of komatiitic channels is seldom possible at district scale exploration targeting (as detailed datasets do not exist) so a key question is what controls the volume of komatiite channels and can this be identified in pre-competitive datasets.

World class non Archean Ni-Cu-PGE deposits have long been known to form marginal to Archean cratons (Begg previous talk) due to focussing of magma along the margin of thick, rigid, buoyant cratonic lithosphere. The Agnew-Wiluna Belt, the world's largest komatiitic Ni camp, sits in a an intercratonic position but along the outboard margin of the resilient proto-Yilgarn Craton at 2.71 Ga as inferred in multiple datasets and best exemplified by gridded granitoid Sm-Nd model ages (Champion and Cassidy 2007). The Agnew-Wiluna Belt sits along the eastern margin of the Yilgarn Craton snap shot at 2.7 Ga in an analogous position to the setting of post-Archean Ni-Cu-PGE deposits.

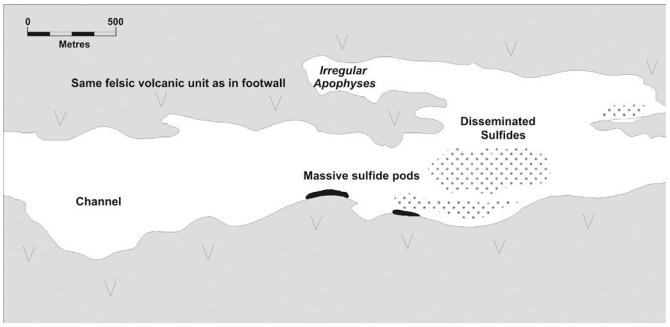

Figure 1. Schematic komatiitic-dunite-hosted Ni-Cu deposit illustrating complex massive and disseminated sulphide distribution. Note the scale.

The Agnew-Wiluna Belt is characterised by a typical Boorara domain stratigraphy (Cassidy et al. 2006). A notable feature of the stratigraphy is the presence of multiple komatiite horizons, the lower horizon which forms a komatiite-felsic volcanic facies association. What is the significance of such an association and what makes the Agnew-Wiluna Belt (AWB) so special (in terms of Ni endowment)?

- Proximal facies felsic volcanic rocks are present discontinuously along the AWB long axis (Beresford et al. 2007).
- Low temperature pyritic exhalative sulfides are spatial associated with the axis of the AWB and felsic volcanics and are absent from the northern, southern and lateral portions of the AWB. Bekker et al (2009) utilised multiple S isotopes to confirm that the low temperature pyritic exhalative sulfides are the S source for the komatiitic Ni-Cu deposits and not sedimentary sulfides.
- Thick channelised dunites often have ambiguous structurally modified contacts with their country rocks preventing accurate determination of the intrusive or extrusive origin. Rare pit exposures at Mt Keith indicate the Mt Keith dunite has abundant apophyses along the top and bottom contact confirming an intrusive origin (Rosengren et al. 2006). An invasive flow origin can be ruled out because of the nature of the coherent felsic volcanic rocks. The absence of extrusive facies in any of the dunitic units in the AWB and Boorara domain suggests a similar origin (Trofimovs et al., 2004).
- The subvolcanic channelized komatiite sills are present only in thick felsic volcanic succession (Fiorentini et al. 2007). Away from the axis of the AWB the komatiitic sills are tabular/sheet like, have chromitite seams, and are barren of Ni-Cu mineralisation.
- Using isopach variations in volcanic stratigraphy, geochemical proxies, palinspastic stratigraphic reconstruction, potential field data interpretation, komatiite facies analysis, and analogs Beresford et al (2007) hypothesised that the axis of the AWB represents an inverted (back arc?) rift and the locus for voluminous proximal komatiite volcanism. The presence of felsic volcanism and associated low temperature VHMS occurrences are proxies for vents along this rift and can be identified in pre-competitive datasets.

Komatiitic peridotite eg Kambalda

Komatiitic peridotite deposits are a well understood ore deposit style, characterised by basal contact massive sulfides overlain by matrix and disseminated sulfides. Massive sulfides are hosted by fold or fault bounded embayments termed trough structures. Each massive sulfide ore deposit commonly forms ribbon like shoots. A clear distinction is made between troughs (structures hosting sulfides) and channels (structure hosting hangingwall volcanic facies; Stone et al., 2005). The two features are vastly different in size and origin. Unfortunately there remains continued confusion in the literature. We believe this is the single most important concept in 'brownfields' Nickel exploration and any misunderstanding is a serious inhibitor to future exploration success.

Komatiitic-basalt Ni-Cu-PGE deposits eg Raglan, Collurabbie

Komatiite-hosted Ni-Cu deposits represent a distinct subclass of magmatic Ni-Cu-(PGE) deposits (Naldrett 2004). This subclass represents a point along the continuum from high MgO komatiites (parent magmas up 32wt% MgO) through transitional komatiites to komatiitic basalts (12-18wt% MgO). Komatiitic basalt hosted Ni-Cu-(PGE) deposits are better known from the post-Archean Circum Superior eg Raglan. In recent years komatiitic basalt and transitional style of deposits have been recognised in the Yilgarn and Abitibi Greenstone Belts eg Collurabbie, Shebandawan. This is an important observation for exploration as these deposits differ from komatiite-hosted deposits senso stricto in numerous practical ways including MgO content, Ni:Cr and Pd:Ir with implications for lithogeochemical targeting approaches to exploration. Komatiitic basalt exploration plays have been rejected in the past because of high Cr and low MgO values!

Komatiite-hosted Ni-Cu-(PGE) deposits represent a continuum of parent magma compositions, viscosities, mineralogy, and magmatic temperatures. Variations in these parameters have resulted in variations in sulfide mineralogy, grade, and geophysical expression.

Mafic-hosted Ni-Cu-(PGE) deposits

We divide mafic Ni-Cu deposits into four descriptive subclasses:

1. Breccia pipes eg Aguablanca, Carr Boyd
2. Chonoliths eg Noril'sk, Double Eagle
3. Dyke blows eg Voisey's Bay
4. Disseminated giants eg Santa Rita, Duluth, Platreef

The major deposit scale advances in the last decade have come from Voisey's Bay, where over a decade of descriptive work has highlighted that Voisey's Bay is not a feeder to a layered intrusion but rather a complex series of blows along a dyke. The Eastern Deeps intrusion is a red herring. A key insight from Voisey's Bay has now been extrapolated to all mafic deposits. Massive sulfides rarely (if ever?) form by gravitational settling in contrast to komatiitic systems and Sudbury (i.e. low viscosity and superheated melts). Massive sulfides are thus not restricted to the basal contacts of mafic-Ni deposits, again in sharp contrast to komatiitic deposits.

Recent advances have highlighted that mafic Ni-Cu deposits do not exclusively form from country rock S addition but a complex range of processes including felsic assimilation, mixing, and sometimes S addition. This is in marked contrast to komatiitic deposits which form from S addition (Bekker et al 2009). This recognition has led to exploration success, the ultimate test of ideas.

Is the Archean unique?

In the past decade we have identified that komatiite-hosted Ni-Cu deposits senso stricto are restricted to the Archean but that komatiitic basalt deposits are not restricted to the Proterozoic as previously thought.

A crucial remaining question is why don't we get world class mafic Ni-Cu deposits in the Archean?

Conclusions

1. The Archean does contain a unique ore deposit style (Komatiite-hosted Ni-Cu) reflecting the

secular cooling of the Earth and the absence of high MgO komatiites (Parent magmas > 25% MgO) since the Archean. However komatiitic basalt-hosted Ni-Cu deposits are now known to occur in the Archean.

2. Komatiite and mafic Ni-Cu deposits represent strongly contrasting deposit styles with very few similarities albeit they represent end members of a continuum. Criteria from each end of the spectrum should not be combined in genetic or exploration models.
3. The diversity of magmatic Ni-Cu deposits should be thought of as a continuum. However the end members of this continuum represent significant variations in parent magma MgO content (range of 25% MgO) and at least 4 orders of resultant variation in dynamic viscosity. These viscosity variations impart the key (from a genetic model and exploration) variations in deposit styles.

Acknowledgements

The author acknowledges permission of MMG to publish. I wish to acknowledge discussions in academia and industry with numerous past and present colleagues on the geology of Ni-Cu deposits, genesis and exploration. In particular I'd like to acknowledge Dawn Evans-Lamswood, and Ben Grguric who's work on Voisey's Bay and Mt Keith respectively remains the unheralded benchmark in nickel deposit research.

References

Barnes S.J., Lesher C.M. & Sproule, R.A., 2008, Geochemistry and petrogenesis of komatiites and komatiitic basalts in the Eastern Goldfields Superterrane, Western Australia and the Abitibi Greenstone Belt, Canada, and implications for the distribution of associated Ni-Cu-PGE deposits, Institution of Mining and Metallurgy, 116, 167–187.

Bekker A., Barley M.E., Fiorentini M.L., Rouxel O.J., Rumble D. & Beresford S.W., 2009, Atmospheric Sulfur in Archean komatiite-hosted Nickel deposits, Science, 29, 1086-1089.

Beresford S.W., Fiorentini M., Hronsky J.M.A., Rosengren N., Bertuch D.I., Saleem A., Cas R.A.F., Stone W.E., Duuring, P., Bekker A. & Barley M., 2007, Komatiite-hosted Ni-Cu-(PGE) deposits: understanding deposit and camp footprints, Geoscience Australia Record 2007/14, 159–163.

Cassidy KF, Champion DC, Krapež B, Barley ME, Brown SA, Blewett RS, Groenewald PB, & Tyler IM, 2006, A revised geological framework for the Yilgarn craton, Western Australia, Western Australia Geological Survey Record 2006/8, 8p.

Champion D.C. & Cassidy K.F., 2007, An overview of the Yilgarn Craton and its crustal evolution, Geoscience Australia Record 2007/14, 13–35.

Duuring P, Bleeker W. & Beresford SW, 2007, Structural modification of the komatiite-associated Harmony nickel sulfide deposit, Leinster, Western Australia, Economic Geology, 102, 277–297.

Evans-Lamswood D.M., Butt D.P., Jackson R.S., Lee D.V., Muggridge, M.G., Wheeler, R.I., & Wilton, D.H.C., 2000, Physical controls associated with the distribution of sulphides in the Voisey's Bay Ni-Cu-Co deposit Labrador, Economic Geology, 95, 749–770.

Fiorentini M.L, Rosengren N, Beresford S.W, Grguric B, & Barley M.E, 2007, Controls on the emplacement and genesis of the MKD5 and Sarah's Find Ni-Cu-PGE deposits, Mount Keith, Agnew-Wiluna belt, Western Australia, Mineralium Deposita, 42, 847–877

Grgruic B. & Riley T., 2006. An integrated geometallurgical approach to optimize business outcomes at the MKD5 Nickel deposit, Mount Keith, Western Australia, Society of Economic Geologists special Publication, 12, 311–329.

Marston R.J. 1984. Nickel mineralization in Western Australia, Geological Survey of Western Australia, Mineral Resources Bulletin 14.

Naldrett A.J., 2004, Magmatic Sulfide Deposits: Geology, Geochemistry and Exploration, Springer Verlaag, 728pp.

Rosengren N.M., Beresford S.W., Grguric B. & Cas R.A.F., 2005, An intrusive origin for the giant komatiitic MKD5 nickel deposit, Mount Keith, Western Australia, Economic Geology, 100, 49–156.

Stone W.E. , Beresford S.W. & Archibald N.J. 2005 Structural Setting and Shape Analysis of Nickel Sulfide Shoots at the Kambalda Dome, Western Australia: Implications for Deformation and remobilization, Economic Geology 100, 1441–1455

Trofimovs J, Davis B.K., & Cas R.A.F., 2004, Contemporaneous ultramafic and felsic intrusive and extrusive magmatism in the Archaean Boorara Domain, Eastern Goldfields Superterrane, Western Australia, and its implications, Precambrian Research, 131, 283–304.

MAPPING THE FOOTPRINTS OF HYDROTHERMAL SYSTEMS

S.W. Halley

Mineral Mapping Pty. Ltd.

Introduction

Low detection limit ICP-MS and new infra-red reflectance technologies allow the full extent of chemical and mineralogical footprints of hydrothermal systems to be quantified. The spatial extent of the hydrothermally modified rocks measured with these methods is orders of magnitude larger than would have been interpreted from visual observations of the rocks. The patterns are controlled by solid solution substitutions within pyrite, sericite, chlorite, feldspar and carbonate.

Within each geological province, local climatic, topographic and regolith factors determine which sample medium is most effective for regional reconnaissance geochemistry. For example, we could use laterite geochemistry in West Africa, lake sediment or hydrogeochemistry from still-stand lakes in the Abitibi, soil geochemistry from Brazil or a fine-fraction from talus in Chile. With the right choice of sample medium, a sample spacing of 1km by 1km is easily sufficient the recognise the footprint of a large hydrothermal system. Rapid reconnaissance sampling like this allows a mineral explorer to quickly and cheaply decide which part of a geological province to explore, or to decide between different provinces.

Once an alteration cell has been recognised, chemical zonation within that system can usually be recognised with surprisingly widely spaced samples. Metals will precipitate from a hydrothermal fluid in response to a change in temperature, redox, pH etc. The changes in these chemical parameters produce zoned metal distributions and zoned patterns of sericite, chlorite, feldspar and carbonate solid solutions that can be measured chemically or spectrally.

Chemistry should not be interpreted in isolation from the geology. Both faults and stratigraphy have a major influence on fluid flow patterns, and the influence of stratigraphy is commonly underestimated. In some environments, the host stratigraphy has a major influence on buffering redox and/or pH, and this chemical control goes beyond a simple wallrock reaction process.

The principles of mapping hydrothermal footprints and the chemical gradients within them can be applied to all sorts of hydrothermal deposit types, VMS, porphyry Cu, Unconformity U, etc; not just Archean gold systems.

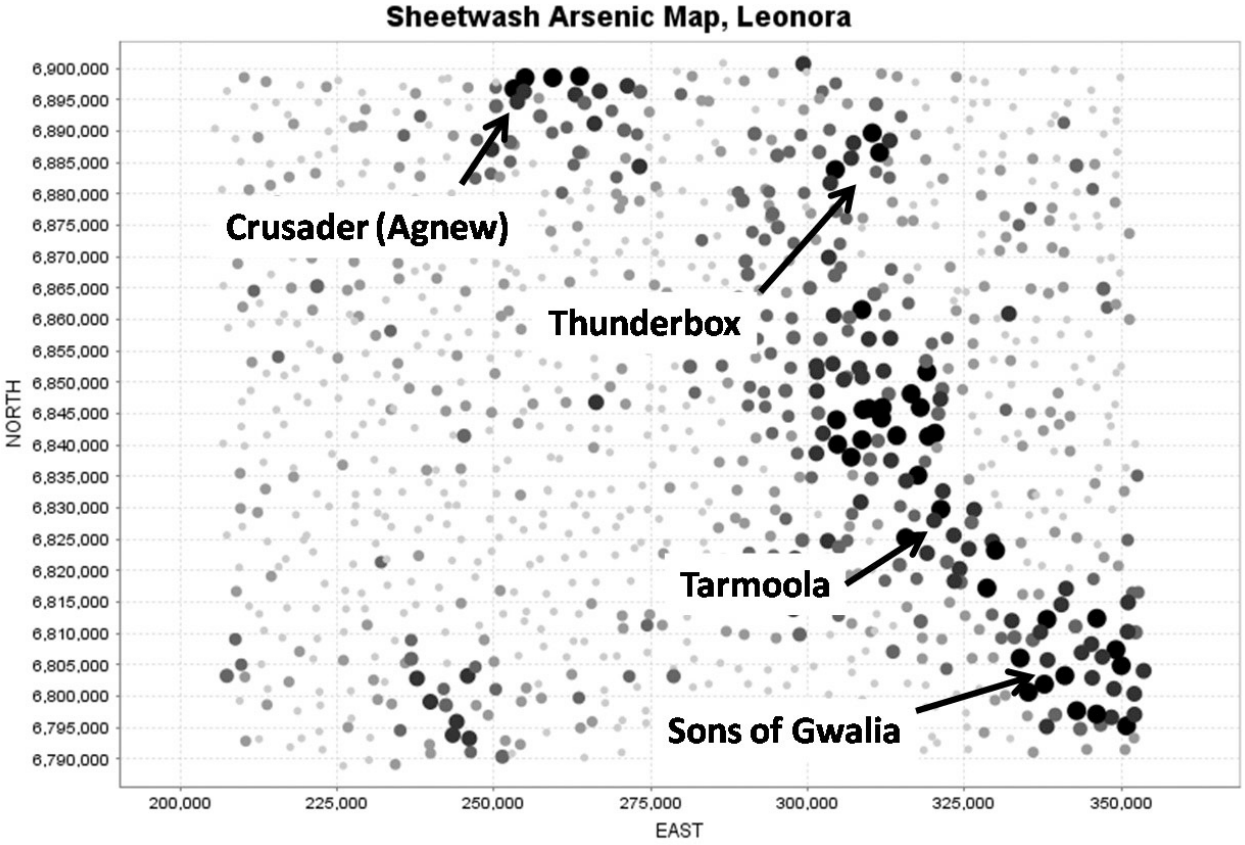

Figure 1. Geochemistry of sheetwash samples from the Leonora 1:250,000 map sheet. This data set includes around 1,000 samples, with a nominal sample density of 1 per 15 square kilometres. The signature of the known gold systems within this area is clearly mapped by Au, As and Sb responses (Bradley, et al, 1995).

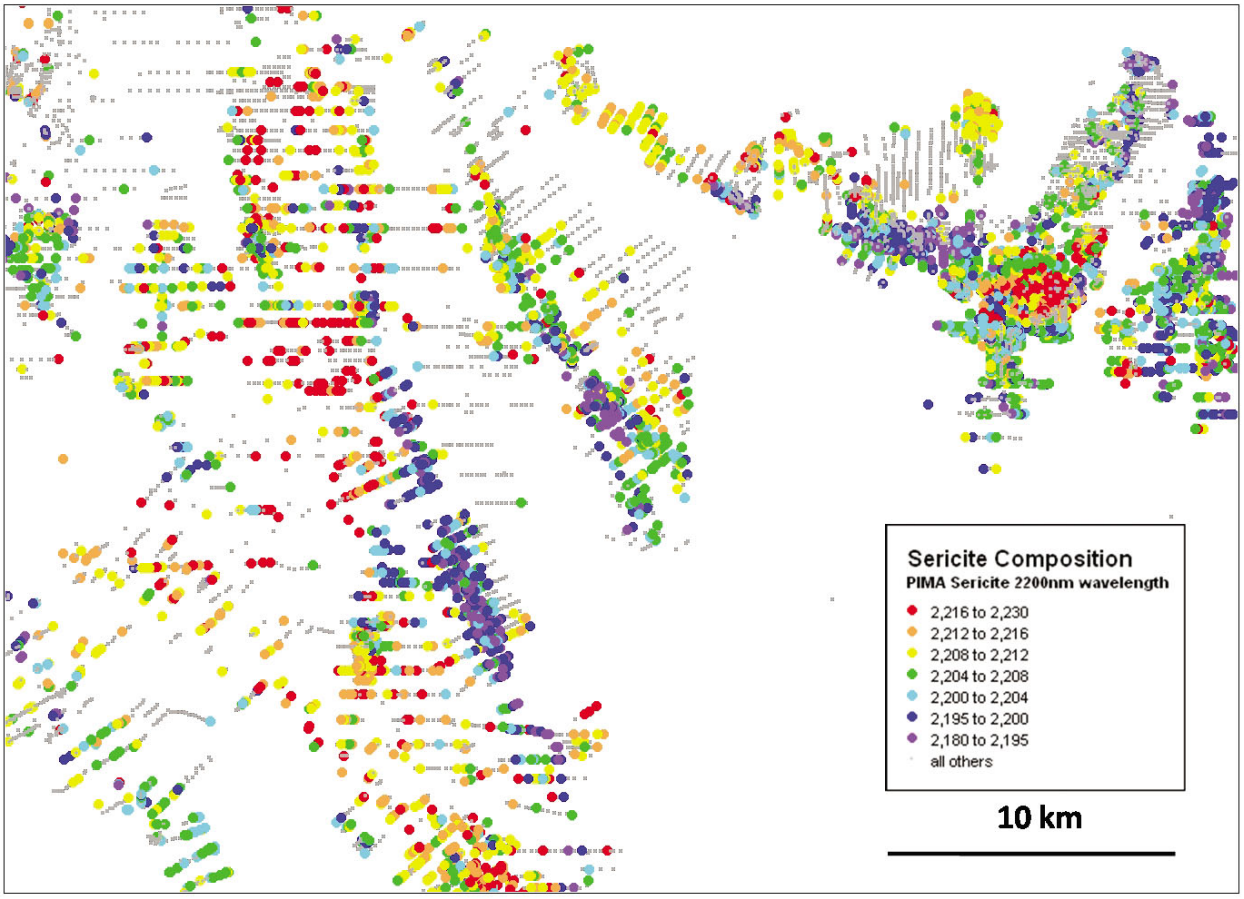

Figure 2. White mica chemistry from the Kalgoorlie region. The points on this map show the wavelength at the minimum point for the 2200nm feature in white micas, measured with PIMA on bottom-of-hole RAB samples. Short wavelengths are indicative of acid fluids, and long wavelengths of alkaline fluids. The map pattern is the result of fluid-driven pH reactions, coupled with the buffering capacity of the host rocks.

Acknowledgements

I wish to acknowledge the contribution of current colleagues at Triton Gold Ltd. and former colleagues from Placer Dome.

Reference

Bradley J.J., Sanders A. J., Varga Z. S. & Storey J.M., 1995, Geochemical mapping of the Leonora 1:250 000 sheet. Western Australia Geological Survey, 1:250 000 Regolith Geochemistry Series Explanatory Notes, 61p.

IMAGING WHOLE ARCHAEAN MINERAL SYSTEMS

D.B. Snyder

Geological Survey of Canada, Ottawa, Ontario

The question why large ore systems form involves all geological factors that control the generation and preservation of mineral deposits over all scales and all time. Here the emphasis will be on two end-members: the large lithospheric scales at the oldest possible times, when cratons and their lithosphere were first forming. Although geodynamical, geochemical, and pressure-temperature histories of the mineral systems are all important, the geophysical methods discussed here are able to more directly address questions of overall system architecture and specific fluid pathways and reservoirs. The subject seismic and magnetotelluric surveys originally were applied to aid terrane and area selection in diamond exploration. The current working hypothesis that carbonated, hydrated or otherwise metasomatised lithospheric peridotite represents a multi-stage source region for both diamonds and kimberlites also has important applications and relevance to the fluid sources and metallogeny of Archaean mineral systems.

One source of fabric that causes seismic wave anisotropy within the mantle of the Slave craton of northwest Canada is newly interpreted to be fluid conduits that form a macroscopic stockwork of carbonated, hydrated or otherwise metasomatised peridotite dykes within depleted harzburgite (Snyder & Lockhart 2009). These metasomatised peridotite conduits probably are composed of rocks such as pyroxenites or wehrlites and occupy 10% of the mantle where present. Using teleseismic anisotropy to reliably locate and predict the alignment of these dyke stockworks in the mantle lithosphere beneath known diamondiferous kimberlites has general application for informed target selection, both for diamond and for kimberlite exploration. In addition, reduced bulk shear wave speeds near these stockworks may be diagnostic of their presence deep in the sub-continental lithospheric mantle.

Nearly a decade ago major- and trace-element data on garnet concentrates from kimberlites and related volcanic rocks were used to construct cross sections and mantle maps showing the lithosphere thickness, thermal state, composition and structure (Griffin et al. 2004). More recently, mantle conductivity structure, controlled primarily by temperature and composition, was hypothesized to represent another indicator of mantle state (Jones et al. 2009). A third method of characterizing properties of the mantle, propagation parameters of seismic S- and surface waves generated by earthquakes, has been used even longer to locate continental keels and to define shield areas (see references in Bedle & van der Lee 2009). Other methods of analysing teleseismic waves at higher spatial resolution help characterize the cratonic cores of continental shields. Key cratons (Kaapvaal, Zimbabwe, Slave, Superior, Aldan) locally have the best-understood mantle properties because of both extensive diamond exploration and resultant large populations of mantle xenoliths and xenocrysts. Seismic methods enable indirect outward extrapolation from these select known cratonic regions via similarities in seismic properties such as anisotropy or strong discontinuities that can be assumed to be plate margins when placed in the context of known surface geology (e.g. Snyder 2008)

Seismic wave-speed variations at continental scale due to mantle heterogeneity and anisotropy have been variably attributed to thermal and compositional variations (Griffin et al. 2004, Artemieva 2009). Lithospheric thickness beneath oceans and younger parts of the continents is widely assumed to be temperature controlled. Within continental interiors and shield areas, temperature estimated via available heat flow measurements does not vary sufficiently to explain all seismic S-wave variation so that perhaps half is attributable to compositional variation (Artemieva 2009). Some of the regional variations may also be due to compositional fabric. Study of teleseismic wave propagation indicates that wave-speed anisotropy nearly doubles within the Lac de Gras kimberlite field in NW Canada when compared to surrounding parts of the Slave craton (Snyder 2008). The implied increase in structural fabric in the lithospheric mantle cannot be explained entirely by stronger alignment of minerals or temperature effects beneath the kimberlite field and forward modelling of the observed anisotropy implies the superposition of an additional fabric related to kimberlite eruption. The source of this fabric is interpreted to be fluid conduits that form a macroscopic stockwork

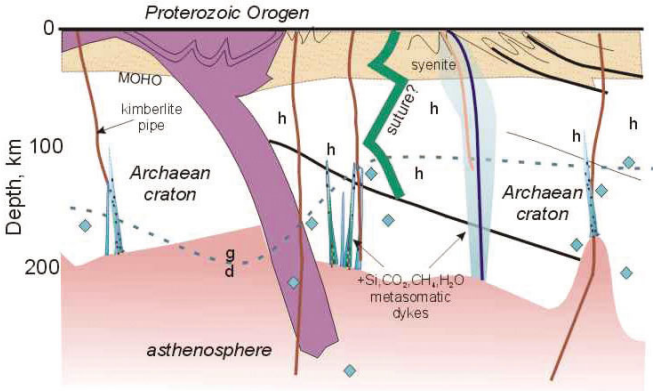

Figure 1. Schematic cross section illustrating diamond-bearing mantle beneath generic parts of shields and where metasomatic stock works might form. Horizontal scale is arbitrary. Light lines sketch important generic lithospheric structures such as the Moho discontinuity, plate sutures and former subduction zones. Dotted line labelled g:d marks the graphite-diamond equilibrium boundary. Solid diamond symbols indicate mantle depths at which paleobarometry on diamond inclusions indicates the diamond formed; similarly, h indicates harzburgitic mantle composition determined from the geochemistry of inclusions, xenoliths and xenocrysts. Kimberlitic and syenitic magmas may originate from within the metasomatic stockworks or in the asthenosphere.

of carbonated, hydrated or otherwise metasomatised peridotite dykes within depleted harzburgite (Malkovets et al. 2007, Snyder & Lockhart 2009). The superimposed fabric is thus composed of residual rocks that record the source or the passage of kimberlite clan rocks formed from <1% partial melts of carbonated lherzolite. These metasomatised peridotite conduits probably are composed of rocks such as pyroxenites or wehrlites and occupy 10% of the mantle where present. Dense stockworks of metasomatized kimberlitic mantle may only occur, or only be currently recognized, beneath populous kimberlite fields such as Lac de Gras. Within some cratons or continental shields such stockworks could exist, but have few dykes or pipes that reached the present surface. The metasomatized peridotite volumes beneath Lac de Gras of 10–30% should, however, produce sufficient variation is P- or S-wave velocities to cause anomalies on regional- or continental-scale velocity models. Such anomalies do occur within 3-D P-wave velocity models beneath the central Slave craton (Snyder & Lockhart 2009) and may be recognizable on some continental-scale surface wave models (Bedle & van der Lee 2009) in that the Slave craton is not underlain by the highest velocities within North America. The cause of this metasomatism remains uncertain and not necessarily related to subduction of crust and mantle lithosphere.

Although metasomatised mantle has been generally thought a possible source for important mineral systems, these mantle stockworks can be hypothesized directly from seismic observations to form a source or reservoir for magmas such as kimberlites, or late-orogenic syenites. Gold-bearing, mantle-derived monzodiorites-syenites are now widely recognized within the Superior craton to have been emplaced during a period of late extension and substantial uplift at ~2678 Ma (Beakhouse et al. 2005). Slightly younger (~2665 Ma) syenites are similarly recognized in like settings in the Yigarn craton (Duuring et al. 2000). Crustal-scale seismic surveys document architecture and structural geometries of how these magmas, coeval metasomatic fluids, and their economic cargo became deposited within the crust. As has been recognized in Western Australia and elsewhere, crustal-penetrating fault zones with attendant damage zones and upper-crustal antiforms are two important classes of structure in this regard. Clear examples of such pathway structures are also available from the Slave and Superior cratons in Canada.

Regional seismic reflection profiles within the southern Abitibi greenstone belt of Ontario targeted specific metallogenically important features such as the Porcupine-Destor deformation zone (Snyder et al. 2008). Interpretation of these profiles individually and in a composite north-south transect revealed a number of prominent bands of reflectors within the upper 15-km of the crust that define a series of folds or antiformal stacks of thrust nappes. Structures and stratigraphy mapped at the surface confirm structural culminations in these locations. At depths greater than 10 km the reflectors have generally shallower dips implying broad folding. Major ore deposits such as those at the Kidd Creek, Hollinger, McIntyre and Dome mines are located on the northern, steeply dipping limbs of these antiformal stacks, implying that the fold structures at least partly focused mineralizing fluids within the upper crust into the near-surface. The Porcupine-Destor deformation zone is proximal to the large gold deposits near Timmins and was revealed by the seismic data to be a composite of early fold structures and late transpressive fault arrays and damage zones.

Diverse seismic observations in Canada and elsewhere have thus provided key insights into component structures and overall architecture throughout the entire sub-Archaean continental lithosphere today. By stripping off known Proterozoic and younger structures using geochronological constraints, one can infer some characterisitics of the original mineral system at 2660-2680 Ma at all of its levels. Key components include underthurst/subducted lithosphere, randomly(?) metasomatised mantle regions, crustal- or even mantle-penetrating faults, and crustal antiforms. These various characteristic features are more and more widely recognized on diverse cratons and continents and are perhaps now beginning to appear characteristic components of whole Archaean mineral systems.

Acknowledgements

Acquisition of the teleseismic data was made possible by support from the POLARIS consortium and the Natural Science & Environment Research Council in Canada. This work contributes to the Geo-mapping for Energy and Minerals and Targeted Geoscience Initiative programs of Natural Resources Canada.

References

Artemieva I., 2009, Compositional variations in the continental lithosphere constrained by non-geochemical data, Lithos, 109, 23–46.

Beakhouse G.P., 2007, Structurally controlled, magmatic hydrothermal model for Archean lode gold deposits; a working hypothesis, Open File Report - Ontario Geological Survey, Toronto, ON, Canada, 133p.

Bedle H. & van der Lee S., 2009, S-velocity variations beneath North America, Journal Geophysical Research, 114, B07308, doi:10.1029/2008JB005949.

Duuring P., Hagemann S.G., & Groves D.I., 2000, Structural setting, hydrothermal alteration, and gold mineralization at the Archaean syenite-hosted Jupiter Deposit, Yilgarn Craton, Western Australia, Mineralium Deposita, 35, 402–421.

Griffin W.L., O'Reilly S.Y., Doyle B.J., Pearson N.J., Coopersmith H., Kivi K., Malkovets V., & Pokhilenko N., 2004, Lithosphere mapping beneath the North American plate, Lithos, 873–922.

Jones A.G. Evans R.L., Muller M.R., Hamilton M.P., Miensopust M.P., Garcia X., Cole P., Ngwisanyi T., Hutchins D., Fourie C.J.S., Jelsma H., Evans S., Aravanis T., Pettit W., Webb S., Wasborg J., & The SAMTEX Team, 2009, Area selection for diamonds using magnetotellurics: Examples from southern Africa, Lithos, 112S, 83–92.

Malkovets V.G., Griffin W.L., O'Reilly S.Y. & Wood B.J., 2007, Diamond, subcalcic garnet, and mantle metasomatism: kimberlite sampling patterns define the link, Geology 35, 339–342.

Snyder D.B., 2008, Stacked uppermost mantle layers within the Slave craton of NW Canada as defined by anisotropic seismic discontinuities, Tectonics, 27, TC4006, doi:10.1029/2007TC002132.

Snyder D.B. & Lockhart G.D., 2009, Does seismically anisotropic subcontinental mantle lithosphere require metasomatic wehrlite-pyroxenite dyke stockworks? Lithos, 112S, 961–965.

Snyder D. B., Bleeker W., Reed L.E., Ayer J.A., Houle M.G. & Bateman R., 2008, Tectonic and metallogenic implications of the Discover Abitibi regional seismic reflection profiles in the Timmins mining camp, Economic Geology, 103, p. 1135–1150.

ELECTRICAL IMAGES OF ARCHEAN CRATONS: LINKS TO MINERALISED ZONES

S.F. Evans

Moombarriga Geoscience

Introduction

Developing a model of Archean craton formation through the integration of different geoscientific datasets has long been a difficult task. The problem that exists is there are only a small number of techniques that are able to reveal information about the Earth's lower crust and upper mantle. Most Archean cratons throughout the world have not been extensively studied enough to prove or disprove hypotheses on craton formation. Direct detection methods rely on samples of the Earth being brought to the surface by volcanic events, mainly kimberlite pipes. These samples known as xenoliths, which also include diamond, are then analysed for their chemical composition and radiogenic ratios in an effort to determine ages and physical conditions at the time of crystallisation. There are two natural source geophysical techniques that can be utilised to image geometrical and physical properties of the Earth; seismic tomography and magnetotellurics. Herein, I present an overview of the magnetotelluric technique and controls on electrical conductivity within the continental lithosphere.

The Magnetotelluric Method

Deep crustal electromagnetic investigations have become more precise in their imaging of subsurface electrical conductivity distribution, both laterally and vertically, in recent years. This is due to technological advances in the acquisition, processing and interpretation of natural-source electromagnetic data using the magnetotelluric (MT) method. The MT method measures the time-variations in the natural electromagnetic (EM) field at the surface of the Earth. Low-frequency variations (1 – 0.0001 Hz) in the EM field are primarily caused by solar wind interacting with the terrestrial magnetic field, whereas high-frequency variations (>1 Hz) are caused by distant lightning storms. The EM field comprises a magnetic field and an associated electric field. By Faraday's Law of induction, this time-varying magnetic field induces an electric field within the Earth, and, in turn, described by Ohm's Law the electric field generates an electric current. The scaled magnitude ratio of the electric and magnetic fields, as well as the phase differences between the electric and magnetic fields, at a number of sites are utilized to determine the sizes and locations of zones of enhanced conductivity.

The Electrical Resistivity of the Earth

The electrical resistivity (or it's reciprocal, conductivity) of rocks can vary by over eight orders of magnitude (>100,000 – <0.001 Ωm) (see figure 1). Typically, competent, un-fractured, crystalline rocks within the continental crust have a high resistivity (~100,000 Ωm), but values less than this are often observed. Regions of low resistivity can be attributed to the presence of interconnected conductive material that is, typically, a minor component of the whole rock. Electrical conduction within the Earth can be attributed to either ionic conduction (movement of charged particles) or electronic conduction (movement of electrons). Ionic conduction may be due to the presence of partial melts along grain boundaries or saline water filling pore space or intruding along fracture zones (Jones, 1992). Electronic conduction generally occurs when interconnected graphite, sulphide or iron ores occur within a rock.

Laboratory studies have shown that the primary control of electrical conductivity in the upper mantle is temperature and follows the Arhenuis solid state equation (Constable & Duba, 1990, Shankland & Duba, 1990, Constable et al., 1992). The Magnesium content (Mg#) in mantle minerals is also known to contribute to conductivity changes such that a decrease in Mg# (increase in Fe) will result in an increase in the electrical conductivity. The Mg# is a secondary control on the electrical conductivity in the mantle with other factors such as composition, pressure and oxygen fugacity having an insignificant effect (Jones et al., 2009). Conveniently, seismic velocity is control by temperature and Mg# so direct comparison can be made.

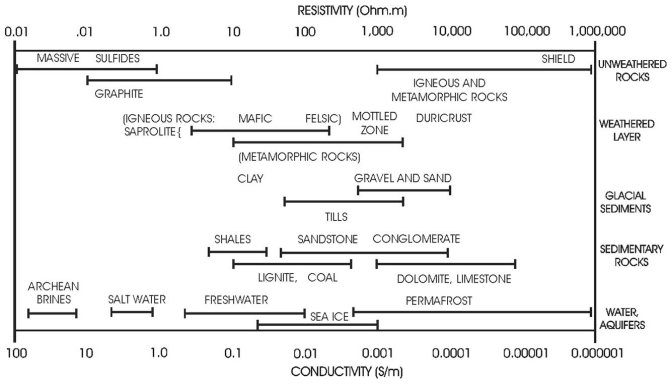

Figure 1. Electrical conductivity (and resistivity) values for different rock types.

Magnetotelluric Observations of Archean Cratons

Given the laboratory studies discussed previously and the fact that Archean cratons are typically depleted in iron (and other elements) and have a lower geothermal gradient when compared to younger terrains, one would expect that Archean lithospheric mantle to be electrical resistive (>1000Ωm). This, in fact, is what has been observed by MT surveys throughout the world over the last ~20 years. Extensive studies of the Slave craton (Jones, 2001), the Fennoscandian shield (Korja & Hjelt), the Gawler craton (Heinson et al., 2006, Maier et al., 2007) and more recently the Kaapvaal craton (Jones et al., 2009) have reported Archean upper-mantle to be electrically resistive relative to adjoining, younger or reworked geologic entities.

It is uncommon for an Archean craton to be imaged as a single homogeneous resistive block. Within the cratonic area zones of low electrical resistivity are often observed. In the upper mantle these zones of low resistivity are often attributed to the presence of fertile mantle material, a thin lithosphere which would then accommodate a higher geothermal gradient or the presence of a piece of ancient subducted slab. In the crust, zones of low resistivity are often attributed to terrain boundaries and major faults where graphite and/or sulphides have been mineralized.

I present a number of case studies where regional MT studies focusing on Archean cratons have mapped anomalous zones of low resistivity within or proximal to Archean lithosphere. These anomalous zones are spatially coincident with significant mineral deposits and suggest a link between large scale electrical features and localized mineralisation.

References

Constable S.C. & Duba A., 1990, Electrical conductivity of olivine, a dunite, and the mantle, Journal of Geophysical Research, 95, 6967–6978.

Constable S., Shankland T.J. & Duba A., 1992, The electrical conductivity of an isotropic olivine mantle, Journal of Geophysical Research, 97, 3397–3404.

Korja T. & Hjelt S.E., 1993, Electromagnetic studies in the Fennoscandian shield — Electrical conductivity of Precambrian crust, Physics of the Earth and Planetary Interiors, 81, 107–138.

Jones A.G., 1992, Electrical conductivity of the continental lower crust, in *Continental lower crust*, Fountain D.M., et al., eds, New York, Elsevier, 81–143.

Jones A.G., Ferguson I.J., Chave A.D., Evans R.L. & McNeice G.W., 2001, Electric lithosphere of the Slave craton, Geology, 29, 423–426.

Heinson G.S., Direen N. and Gill R., 2006, Magnetotelluric evidence for a deep-crustal mineralising system beneath the giant Olympic Dam Iron-Oxide Copper Gold deposit, southern Australia, Geology, 34, 573–576.

Maier R., Heinson G., Thiel S., Selway K., Gill R. & Scroggs M., 2007, A 3D lithospheric electrical resistivity model of the Gawler Craton, Southern Australia, Applied Earth Science (Transactions of the Institute of Mining and Metallurgy B), 116, 13–21.

Shankland,T.J. & Duba A. G., 1990, Standard electrical conductivity isotropic, homogeneous olivine in the temperature range 1100–1500 C, Geophysics Journal International, 103, 25–31.

THE ECONOMIC AND STRATIGRAPHIC IMPORTANCE OF DEPOSITIONAL GAPS IN ARCHEAN GREENSTONE BELT STRATIGRAPHY

P.C. Thurston[1], G.J. Baldwin[1], B.S. Kamber[1] & D. Stone[2]

[1] Laurentian University, Sudbury ON, Canada;
[2]Ontario Geological Survey, Sudbury ON, Canada

Archean greenstone belt stratigraphy worldwide is largely intact with upper structural levels consisting of dome and keel geometry with granitoids concentrated in structural domes and supracrustal rocks in intervening synclinoria e.g., in the Superior(Percival, 2007) and Pilbara (Van Kranendonk et al., 2002) cratons. Evidence for autochthonous construction consists of: 1) xenocrystic zircons in young greenstones were derived from older, underlying units in the belt (e.g. the Abitibi belt/Superior craton) (Ayer et al., 2005); 2) dikes and mafic intrusions coeval with younger units cut older greenstones (Abitibi and N. Caribou terrane e.g., Rogers, 2000); 3) trace element evidence for contamination by older granitoids is found in mafic volcanics across the Superior craton (Thurston, 2002). This evidence reinforces the notion that greenstone belts developed autochthonously with rare notable exceptions (Tomlinson et al., 1996).

Broadly, Archean greenstone belts consist of volcanic sequences unconformably overlain by successor basins. We recognize the following types of lithotectonic assemblages:

1. Basal quartzite-komatiite units. These units were deposited unconformably above granitoids or older greenstones, representing shallow water sedimentation followed by rift-related komatiite-tholeiite sequences. These units are generally small and poorly preserved with examples in the Superior craton (Thurston & Chivers, 1990), the Baltic shield (Thurston, 2001), and the Yilgarn craton. This type of unit represents an early response to orogeny and these units develop along the margins of major cratonic blocks.
2. Komatiite-tholeiite units. These units represent plume-related volcanism commonly developed as mafic plain style volcanism. These sequences underlie many arc sequences world-wide. Their basal contact is either intrusive or unconformable. They are commonly capped by chemical and minor clastic metasediments (Sproule et al., 2002).
3. Basalt-rhyolite volcanic cycles. These are dominated by Plinian style ash-flows, flows and related domes. The basal contacts are generally conformable and the units are capped by chemical and minor clastic sedimentary rocks. Geochemically these sequences display calc-alkaline geochemistry with Ti-Nb-Ta anomalies typical of arc petrogenesis.
4. Continental margin sequences. A small number of greenstone belts consist of thrust-telescoped volcanic and sedimentary strata adjacent to against older terranes (Tomlinson et al., 1996).

The youngest units in most greenstone belts are pull-apart successor basins consisting of fine marine clastics to alluvial-fluvial metasediments and minor calc-alkaline to alkaline volcanics. The successor basins usually have a basal subaerial unconformity (Ayer et al., 2005). In general, the volcanic assemblages (1-4 above) are superposed one on another with no sign of a subaerial unconformity marked by a zone of weathering, a paleosol or an angular unconformity. These assemblage types are generally capped by a meter-scale thicknesses of chemical and clastic metasediments or a sedimentary interface zone (SIZ) (Thurston et al., 2008). These SIZ units are dominated by chemical sediments (BIF) which show a variety of origins.

Field and textural studies have shown that iron oxides in BIF are largely diagenetic and the chert component is primary or diagenetic (Krapez et al., 2003). Major cherts in some greenstones are silicified precursor units e.g. in the Barberton (Lowe, 1999) and the northern part of the eastern Pilbara (Van Kranendonk, 2006). There is field evidence for hydrothermal cherts i.e. chert dikes cutting BIF (Van Kranendonk, 2006). Si isotopic studies distinguish silicification of precursor volcanic rock types (high Al_2O_3, high $\delta^{30}Si$), seawater (low Al_2O_3, high $\delta^{30}Si$) and hydrothermal (low Al_2O_3, low $\delta^{30}Si$) sources for chert in iron formation (van den Boorn et al., 2007). Trace element studies show BIF cherts are produced by replacement of precursor rock types or derived from seawater or hydrothermal fluids (Baldwin, 2009; Bolhar et al., 2005). The trace element studies rely upon the presence of positive anomalies in La, Eu, Gd, and Y and general LREE depletion indicating seawater origin whereas hydrothermally derived cherts display HREE depletion. The cherts at Mt. Goldsworthy show stratigraphic trends from initial closed basin units to deeper water, open ocean deposition (Sugahara et al., 2009). Cherts representing silicification of precursor rock types will generally display relatively flat REE patterns.

In the Abitibi belt of the Superior craton, 7 volcanic assemblages span 2750-2695 Ma (Ayer et al., 2005). In the western Abitibi, the 2730-2724 Ma Deloro assemblage is overlain by the 2710-2704 Ma Tisdale assemblage a ~14 My depositional gap. The Deloro assemblage consists of basal basalts overlain by rhyolite and within the rhyolitic upper part of the assemblage are three iron formations. Earlier work had speculated that the top of the Deloro assemblage represented a regional unconformity. To better understand the nature of the 14-20 My depositional gap, mapping of the SIZ units and geochemistry of the chert component was carried out in

an area with minimal structural complications (Baldwin, 2009). Iron formation units originating by replacement have flat REE profiles. Other parts of the middle iron formation demonstrated a seawater and a hydrothermal trace element signature. Unlike studies of the Mt Goldsworthy cherts in the Pilbara, there was no clear stratigraphic trend to the variation in chert geochemistry documented. It is interesting to note that some strata-bound, stratiform chert breccia units yielded seawater signatures suggesting long term rock-water interaction followed by fluid overpressure producing the chert breccia.

The middle iron formation is about 50 m thick with about 10 m representing mass flows. The underlying rhyolite is 2728.1±1.6 Ma and the overlying rhyolite is 2724.5±1.5 Ma representing a time gap of 0.5-6.7 My for deposition of 40 m of iron formation yielding an average depositional rate of 0.006-0.08 mm/yr. the best evidence for slow sedimentation is the occurrence of stratabound chert breccias in which the quasi-tabular chert clasts indicate they were pre-brecciation chert bands that were sufficiently lithified (likely hardgrounds produced by extended rock-water interaction/diagenesis) to preserve their shape upon brecciation. Some sedimentologically similar chert breccias interacted with hydrothermal fluid to produce a hydrothermal signature in the cherts. Some cherts preserve structures indicative of soft-sediment loading (flame structures, ball & pillow structures) likely associated with rapid sedimentation supported by seawater trace element patterns.

The iron formations at the Deloro-Tisdale contact indicate extended periods of water-rock interaction interspersed with rapid sedimentation. The lack of a consistent stratigraphic control on the various chert types (cf. Sugahara et al., 2009) suggests variable seawater composition. The lack of large volumes of clastic sediment and the slow depositional rate indicates a restricted, starved basin. The low depositional rate constrained by the ages, the evidence for extended water-rock interaction producing hard grounds, and the lack of clastic detritus in the SIZ are all consistent with slow deposition i.e., condensed sections. As this BIF is well removed from terrigenous sedimentation, these BIFs are records of simple hiatuses in volcanism or paraconformities. The SIZ units capping other Abitibi assemblages may be similar but beyond U-Pb zircon system resolution given the common presence of chert breccia units .The depositional gaps marked by BIF of great lateral extent represent a hiatus in volcanism and thus a time in which hydrothermal fluids may circulate in the volcanic pile giving rise to syngenetic VMS or komatiite-associated nickel deposits. For example, each of the SIZs capping lithotectonic assemblages in the Abitibi greenstone belt include VMS style mineralization produced during a hiatus in volcanism as shown in Table 1.The assemblages/episodes (Table 1) re roughly equivalent to stratigraphic groups. At a more detailed scale, individual chert horizons capping formations or members within the Blake River Group in the Noranda area form stratigraphic markers at and below which are found the numerous VMS deposits of the Noranda camp(Thurston et al., 2008).

BIF has been considered a potential stratigraphic marker in Archean greenstones. This study raises the issue as to whether other BIFs represent paraconformities (Table2). The presence of a regional unconformity in northeastern Quebec (Maurice et al., 2009) raises speculation about the importance of the correlative depositional gap at Steeprock in shield wide correlation.

Table 1.

Assemblage	Episode/Age	Deposits	References
Blake R.	2704-26957	Rouyn-Noranda Kamkotia	(Gibson & Watkinson, 1990) (Ayer et al., 2005)
Tisdale	2710-2704	Val d'Or	(Chartrand & Cattalani, 1990)
Kidd-Munro	2719-2711	Kidd Ck. Potter	(Ayer et al., 2005)
Stoughton-Roquemaure	2723-2720	Estrades	Chartrand & Cattalani 1990
Deloro	2734-2724	Hunter	(Thurston et al., 2008)
Pacaud	2750-2735	Gemini-Turgeon	(Thurston et al., 2008)

Table 2.

Area/craton	Ages below to above IF	Possible Depositional Gap	Reference
Bartlett dome/Superior	2728.1±1.6/2724.5±1.5	0.5-6.7 My	(Baldwin, 2009)
Steeprock/Superior	2780/2735	45 My	(Stone 2010)
Confederation/Superior	2880/2771	~109 My	(Rogers, 2000)
Kostomuksha/Baltic	2843/2757	114 My	(Puchtel et al., 1998)

References

Ayer J., Thurston P.C., Bateman R., Dubé,B., Gibson H.L., Hamilton M.A., Hathway B., Hocker S.M., Houlé M., Hudak G. J., Ispolatov V., Lafrance B., Lesher C.M., MacDonald, P.J., Péloquin, A.S., Piercey, S.J., Reed, L.E. & Thompson P. H., 2005, Overview of Results from the Greenstone Architecture Project: Discover Abitibi Initiative, Open File Report 6154, Ontario Geological Survey, 125p.

Baldwin, G.J., 2009, The sedimentology & Geochemistry of BIF - Deloro Assemblage, MSc thesis, Laurentian, 116p.

Bolhar R., Van Kranendonk M.J. & Kamber, B.S., 2005, A trace element study of siderite-jasper banded iron formation in the 3.45 Ga Warrawoona Group, Pilbara craton-Formation from hydrothermal fluids and shallow seawater, Precambrian Research, 137, 93–114.

Chartrand F., & Cattalani S., 1990, *Massive sulfide deposits in NW Quebec*, CIM Special Paper 43, 77–91.

Gibson H.L. & Watkinson D. H., 1990, VMS deposits of the Noranda Cauldron, CIM Special Paper. 43, 119–132.

Krapez B., Barley M.E. & Pickard A. L., 2003, Hydrothermal and resedimented origins of the precursor sediments to banded iron formation: sedimentological evidence from the Early Palaeoproterozoic Brockman supersequence of Western Australia, Sedimentology, 50, 979–1011.

Lowe D. R., 1999, Petrology and sedimentology of cherts and related silicified sedimentary rocks in the Swaziland Supergroup, Special Paper - Geological Society of America, 329, 83–114.

Maurice C., David J., Bedard J. H. & Francis D., 2009, Evidence for a widespread mafic cover sequence and implications for continental growth in the NE Superior Province, Precambrian Research, 168, 45–65.

Percival J. A., 2007, Geology and Metallogeny of the Superior Province, Canada, Special Publication No. 5, Geological Association of Canada Mineral Deposits Division, 903–928.

Puchtel I. S., Hofmann A. W., Mezger K., Jochum K. P., Shchipansky A. A. & Samsonov, A. V., 1998, Oceanic plateau model for continental crustal growth in the Archaean; a case study from the Kostomuksha greenstone belt, NW Baltic Shield, Earth and Planetary Science Letters, 155, 57–74.

Rogers N., McNicoll V., van Staal C.R. and Tomlinson K.Y., 2000, Lithogeochemical studies in the Uchi-Confederation greenstone belt, northwestern Ontario: implications for Archean tectonics., Current Research Part C, Geological Survey of Canada, 1–11.

Sproule R.A., Lesher C.M., Ayer J.A., Thurston P.C. & Herzberg, C.T., 2002, Secular variation in the Geochemistry of Komatiitic rocks from the Abitibi Greenstone belt, Canada, Precambrian Research, 115, 153–186.

Sugahara H., Sugitani K., Mimura K., Yamashita F. & Yamamoto K., 2009, A systematic rare-earth elements and yttrium study of Archean cherts at the Mount Goldsworthy greenstone belt in the Pilbara Craton: Implicaions for the origin of microfossil-bearing black cherts, Precambrian Research.

Thurston P., Ayer J., Goutier J. & Hamilton M.A., 2008, Depositional Gaps in Abitibi Greenstone Belt Stratigraphy: a key to exploration for syngenetic mineralization, Economic Geology, 103, 1097–1134.

Thurston P.C., 2002, Autochthonous development of Superior Province greenstones? Precambrian Research. 115, 11–36.

Thurston P.C. & Kozhevnikov V.N., 2001, An Archean quartz arenite-andesite association in the eastern Baltic Shield, Russia, Precambrian Research, 101, 313–340.

Thurston P.C. & Chivers K.M., 1990, Secular variation in greenstone sequence development emphasizing Superior Province, Canada: Precambrian Research, 46, 21–58.

Tomlinson K. Y., Hall R. P., Hughes D. J. & Thurston P. C., 1996, Geochemistry and assemblage accretion of metavolcanic rocks in the Beardmore-Geraldton greenstone belt, Superior Province, Canadian Journal of Earth Sciences, 33, 1520–1533.

van den Boorn S.H.J.M., van Bergen M.J., Nijman W. & Vroon P.Z., 2007, Dual role of seawater and hydrothermal fluids in Early Archean chert formation: Evidence from silicon isotopes, Geology, 35, 939–942.

Van Kranendonk M.J., 2006, Volcanic degassing, hydrothermal circulation and the flourishing of early life on Earth: Pilbara Supergroup, Pilbara Craton, Western Australia, Earth-Science Reviews, 74, 197–240.

Van Kranendonk, M.J., Hickman, A.H., Smithies, R.H., & Nelson, D.R., 2002, Geology and tectonic evolution of the Archean North Pilbara Terrain, Pilbara Craton, Western Australia, Economic Geology. 97: 695–732.

THEME 3

UNIQUE MINERAL SYSTEMS?

ORAL & POSTER ABSTRACTS

BIF-RELATED IRON ORE IN THE YILGARN CRATON, WESTERN AUSTRALIA: GEOLOGICAL SETTING AND ORE FORMING PROCESSES

T. Angerer, P. Duuring, D.F. Lascelles & S.G. Hagemann

Centre for Exploration Targeting, School of Earth and Environmental Science, M006, University of Western Australia, 35 Stirling Highway, Crawley, WA 6009, (tangerer@cyllene.uwa.edu.au)

Introduction

Many Paleo- to Mesoarchean greenstone belts in the Narryer and Youanmi terranes of the Yilgarn craton host Banded Iron Formation (BIF, ~30% Fe), some of which contain high-grade magnetite-, hematite- and/or goethite-rich ore deposits (58 - 68% Fe) of about 10 to 200 Mt in size. In recent years, numerous small to medium-sized exploration and mining companies are focussing on understanding controls on greenstone belt-hosted iron ore and exploiting the increasing number of delineated resources (for a complete overview of deposits refer to Greentree & Lord 2007, Cooper & Flint 2009). As a result, several industry-sponsored studies of greenstone belt-hosted iron deposits in the Yilgarn are currently being undertaken by the Centre for Exploration Targeting, UWA, in order to characterise the "iron upgrade" processes in these deposits, the timing of mineralisation with respect to the terrain history, structural control of ore bodies and fluid sources. This contribution is an overview of Archean BIF-hosted iron ore in the Yilgarn, based on field observations and preliminary data on fluid-rock interaction. It is believed that the deposits described in this abstract represent a good cross section of the various lithostratigraphic and tectonometamorphic settings of greenstone belts in the Yilgarn. Therefore, we attempt to identify common Archean ore-forming processes in the Yilgarn that can then be compared with BIF-hosted ore from other geological settings, such as the Proterozoic deposits of the Hamersley Province, Western Australia.

The geological setting of selected BIF-related iron ore deposits in the Yilgarn

Koolyanobbing (Koolyanobbing greenstone belt, Southern Cross domain)

The Koolyanobbing iron ore deposits in the Koolyanobbing greenstone belt are hosted in greenschist facies metamorphosed quartz-magnetite BIF within the ~3.05-2.93 Ga, lower succession (Cassidy et al. 2006). Hydrothermal alteration and iron ore formation at Koolyanobbing took place in four stages (Angerer & Hagemann *in revision*), commencing with an early Fe-Mg(±Ca?) metasomatism, which caused localised alteration of quartz-magnetite BIF to Fe-rich carbonate-magnetite BIF. This was followed by a syn-orogenic mobilisation of gangue minerals producing "mass-negative" enrichment of mostly magnetite protore (a partially mineralised or carbonate-altered rock, which was subject to further alteration). Localised hydrothermal quartz-magnetite mineralisation in reverse fault breccias and fractures occurred afterwards and was followed by strike-slip fault-controlled late hydrothermal alteration that involved the formation of specular hematite and martitisation.

Windarling (Marda-Diemals greenstone belt, Southern Cross domain)

The Windarling deposits in lower-greenschist facies metamorphosed parts of the Marda-Diemals greenstone belt coincide with 10 to 50 m-thick, metachert-magnetite/martite BIF of the lower succession. Martite-lepidoblastic hematite-goethite ore bodies are commonly arranged in an en-echelon series. Unweathered magnetite-hematite ore is commonly enclosed by carbonate-rich magnetite BIF, in which metachert has been replaced by hydrothermal carbonate. High-Mg basalt wall rocks are incipiently deformed, with cleavages associated with late-stage shear zones; BIF bands locally show internal tight folding with an axial planar, micro- lepidoblastic hematite foliation. Late-stage specular hematite is restricted to quartz-carbonate veins occurring in high-Mg basalts, BIF, and ore.

Wiluna West (Joyner's Find greenstone belt, Southern Cross domain)

The Wiluna West iron ore deposit comprises a number of small high-grade microplaty hematite ore bodies within tightly folded, greenschist to lower-amphibolite facies metamorphosed BIF of the Joyner's Find greenstone belt. The proximity of the greenstone belt to the northern boundary of the Yilgarn Craton, where it is overlain by two Paleoproterozoic transgressional successions (i.e. Glengarry Group Finlayson Formation and Earaheedy Group Yelma Formation) resulted in an unusual series of ore-forming processes at the Wiluna West deposit (Lascelles 2009). The microplaty-hematite and anhedral hematite/martite/goethite ore bodies are associated with multiple Paleoproterozoic weathering events that predate deposition of the Glengarry and Earaheedy groups. Several episodes of hydrothermal fluids interacting with BIF resulted in the deposition of specular hematite.

Mount Gibson (Retaliation greenstone belt, Murchison domain)

The Mount Gibson BIF lies within the (~3 Ga) Windanning Formation of the Luke Creek Group (Watkins & Hickman 1990). The quartz-magnetite BIF is now subvertical and defines upright, isoclinal folds. Two distinct Archean ore/protore-forming processes took place: (1) Removal of silica during diagenesis resulted in magnetite protore, which then has been modified by recent weathering to martite-goethite ore.

(2) Low- to medium-grade magnetite protore formed by hydrothermal replacement of chert by ferroan calcite, which was subsequently leached by recent weathering, forming magnetite-goethite ore.

Weld Range (Weld Range greenstone belt, Murchison domain)

The greenschist facies metamorphosed Weld Range greenstone belt hosts two known high-grade hematite-magnetite deposits, Madoonga and Beebyn, which are located in separate quartz-magnetite BIF units of the ~2752 Ma Wilgie Mia Formation. At the Beebyn deposit, steeply dipping BIF units with minor interbedded shale are bound by mafic volcanic rocks that intruded the original Wilgie Mia Formation. These rocks have been complexly deformed to produce at least three generations of folds with ductile shear zones, and several later generations of brittle faults (Duuring & Hagemann 2010). High-grade Fe mineralisation in BIF is the product of at least three main episodes of hydrothermal fluid alteration: (1) the replacement of quartz-rich bands by ferroan dolomite, (2) the dissolution of the ferroan dolomite, followed by the local addition of hydrothermal magnetite-carbonate, and (3) the deposition of coarse-grained chlorite with specular hematite in fault zones, together with the martitisation of earlier magnetite-rich bands. The stratigraphic footwall contact between the BIF and mafic volcanic rocks is the location of the most intense hydrothermal alteration and corresponding high-grade Fe mineralisation.

Ore-forming processes with respect to the geological settings in the Yilgarn craton

Archean iron ore deposits in the Yilgarn Craton display striking similarities, but also important differences in terms of their ore-forming processes. Deposits at Koolyanobbing, Windarling, Weld Range, and Mount Gibson share very similar hydrothermal alteration histories responsible for mineralisation (Fig. 1). The steps for iron-enrichment include carbonate alteration that preferentially replaces original quartz bands in BIF. Subsequent hydrothermal leaching of these carbonate and/or iron oxides coincided with the deposition of secondary magnetite. This style of alteration is well-developed in zones of high permeability, such as reactivated fault and shear zones, which commonly form along the margins of the BIF. Specular hematite±carbonate±quartz alteration is usually late and hosted by strike-slip dominated faults, that probably formed during late transpressional to transtensional deformation in the Yilgarn Craton (Chen et al. 2001). In the Mount Gibson deposit differs this last style of alteration is not expressed. The Mount Gibson and Wiluna West deposits display the greatest differences to other deposits in the Yilgarn Craton. Diagenetic processes in parts of the Mount Gibson deposit resulted in a chert-free protore without the involvement of carbonate alteration. The Wiluna West deposit was strongly affected by Proterozoic weathering and is the only example in the Yilgarn Craton of ancient weathering that produced microplaty hematite.

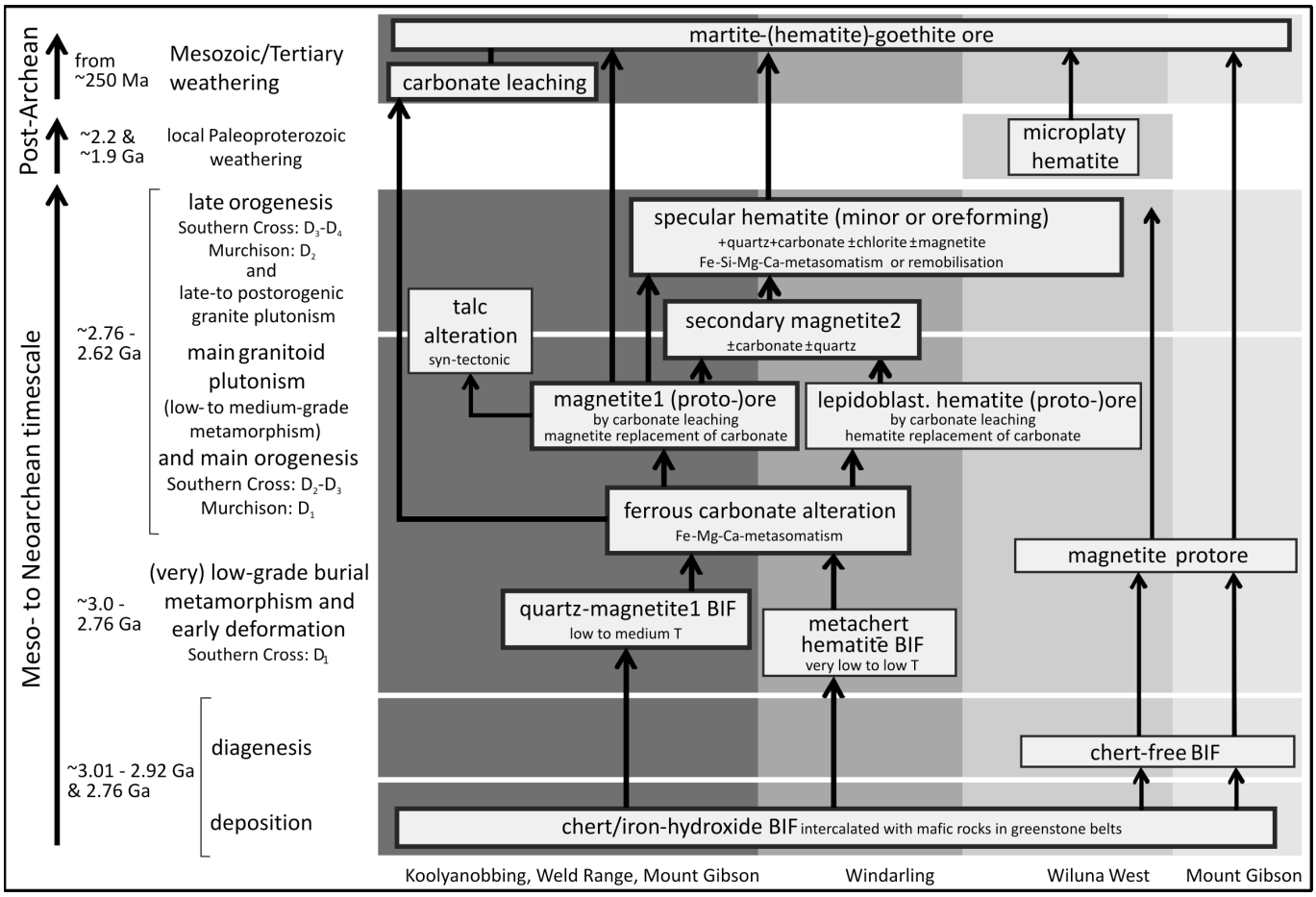

Figure 1. Integrated flow chart that shows iron mineralisation processes for the selected BIF-hosted deposits in the Yilgarn craton. The grey shaded backgrounds correspond to the series of iron-enrichment steps displayed by specific deposits. The most common series is represented by the bold boxes. (Age dates mainly based on Cassidy et al. 2006)

Ore-forming processes appear not to be greatly influenced by the peak metamorphic facies conditions affecting the BIF (examples described here range from lower-greenschist to lower-amphibolite facies), nor its age of deposition. The remarkably similar hydrothermal alteration styles and ore genesis processes at Koolyanobbing, Weld Range, and Mount Gibson may, at least in part, be caused by their comparable BIF depositional facies (i.e. thin BIF units surrounded by mafic volcanic rocks) and their similar tectonic evolution.

Comparison with Proterozoic Hamersley basin deposits

Iron deposits hosted by BIF in the Yilgarn Craton share many similarities with Proterozoic, basin-hosted BIF deposits of the Hamersley basin. They both display similar mineralogical and geochemical (i.e., Fe/Si ratio) characteristics, although deposits in the Yilgarn Craton may have been metamorphosed to higher conditions (i.e. up to amphibolite facies, compared with lower-greenschist facies conditions in the Hamersley basin, (Gole 1981).

Although there is no unifying model for all major hypogene-supergene microplaty hematite iron ore deposits in the Hamersley basin (e.g. Mt. Whaleback, Mt. Tom Price, Paraburdoo), a common theme for high-grade ore genesis is the presence of hydrothermal iron-rich carbonate±magnetite caused by basinal brines that originated from underlying dolomite strata. Microplaty hematite replaced early carbonate minerals, with local ankerite co-precipitation, due to convection of a deep meteoric-water fluid. These alteration mineral assemblages are modified by recent supergene events (Thorne et al. 2008, and references within). Structures that controlled fluid flow in the Hamersley basin were mainly late-Ophthalmian (~2.2 Ga) low-angle extensional faults. A thorough comparison with mineralising fluids responsible for deposits in the Yilgarn Craton cannot yet be made due to the lack of available data. However, it is possible that metamorphic devolatilization of mafic country rocks and/or interaction with magmatic fluids derived from nearby granitoids played a role for the introduction of magnesium, calcium, and probably iron, during the early-stages of carbonate-magnetite alteration. Late-stage fluids responsible for carbonate-specular hematite-quartz alteration probably originated from late- to post-orogenic granitoid magmatism and/or meteoric waters. Fluids were channelled by ductile to brittle structures formed within compressive to transpressive deformation events between 2.73 and 2.62 Ga (Cassidy et al. 2006).

Conclusion

Important BIF-hosted iron ore deposits in the Yilgarn Craton are a product of several hypogene ore-forming stages, which in most cases took place throughout the orogenic cycle during Meso- to Neoarchean time. These processes included early iron-rich carbonate alteration followed by carbonate leaching and replacement by hydrothermal magnetite and/or hematite. In many deposits, late-stage strike-slip fault-controlled specular hematite mineralisation took place. In rare examples, diagenetic leaching of amorphous silica produced iron-oxide-rich (proto-)ore, whereas Paleoproterozoic weathering is associated with microplaty hematite ore. Recent supergene events were also important in modifying the hydrothermal ore bodies. These Archean deposit examples display remarkable similarities to Proterozoic Hamersley basin-type iron deposits, despite their obvious differences in age, geological setting, and deformational histories. Future work will concentrate on constraining hydrothermal fluid characteristics and possible sources for BIF-hosted deposits in the Yilgarn Craton.

Acknowledgment

The authors like to thank Cliffs NR, Sinosteel Midwest Corp., Golden West Resources Ltd, Mount Gibson iron ore, Ltd, for their financial and logistic support and for their permission to publish this abstract.

References

Angerer T. & Hagemann S. G., *in revision*, The BIF-Hosted High-Grade Iron Ore Deposits in the Archean Koolyanobbing Greenstone Belt, Western Australia: Structural Control on Syn-orogenic and Weathering related Magnetite-, Hematite- and Goethite-rich Iron Ore, Economic Geology.

Cassidy K.C., Champion D.C., Krapez B., Barley M.E., Brown S.J.A., Blewett R.S., Groenewald P.B. & Tyler I.M., 2006, A revised geological framework for the Yilgarn craton, Western Australia, Geological Survey of Western Australia, Record 2006/8, 8p.

Chen S. F., Libby J. W., Greenfield J. E., Wyche S. & Riganti A., 2001, Geometry and kinematics of large arcuate structures formed by impingement of rigid granitoids into greenstone belts during progressive shortening, Geology, 29, 283–286.

Cooper R.W. & Flint D.J., 2009, Iron Ore Deposits of the Yilgarn Craton — 2009 (1:1 500 000), Geological Survey of Western Australia.

Duuring P. & Hagemann S. G., 2010, High-grade iron mineralisation at the Beebyn deposit, Weld range, W.A., 5th International Archean Symposium.

Gole M. J., 1981, Archean banded iron-formations, Yilgarn Block, Western Australia, Economic Geology, 76, 1954–1974.
Greentree M.R. & Lord D., 2007, Iron mineralization in the Yilgarn craton and future potential, in *Proceedings of Geoconferences (WA) Inc. Kalgoorlie '07 Conference*, Bierlein F. P. and Knox-Robinson C. M. eds, 25–27 September 2007, Kalgoorlie, Western Australia. 70–73.

Lascelles D. F., 2009, Microplaty Hematite in the Yilgarn: The Wiluna West Iron Ore Deposit, in: *Proceedings of the 10th Biennial SGA Meeting of The Society for Geology Applied to Mineral Deposits Townsville Australia 17th - 20th August 2009*, Williams P. J. ed, SEG.

Thorne W. S., Hagemann S. G., Webb A. & Clout J., 2008, Banded Iron Formation-related Iron Ore Deposits of the Hamersley Province, Western Australia, in *Banded Iron Formation-related High-grade Iron Ore*, Hagemann S. G., Rosière C. A., Gutzmer J. and Beukes N. J., eds, 197–222.

Watkins K. P. & Hickman A. H., 1990, Geological evolution and mineralization of the Murchison province, Geological Survey of Western Australia Bulletin, 137, 267p.

KOMATIITE-HOSTED NICKEL SULFIDE DEPOSITS: WHAT'S SO SPECIAL ABOUT THE KALGOORLIE TERRANE?

S.J. Barnes[1] & M.L. Fiorentini[2]

[1]CSIRO Earth Science and Resource Engineering, steve.barnes@csiro.au.
[2]Centre for Exploration Targeting, University of Western Australia.

Nickel sulfide ores have been found associated with komatiites in most Archaean cratons in which komatiites occur, but the global distribution of these deposits is very strongly skewed in favour of the greenstone belts of the Kalgoorlie Terrane (KT). Approximately 50% of the world's sulfide nickel resource in komatiites, komatiite basalts and ferropicrites of Archaean or Proterozoic age, and about 90% of the Archaean total, is contained within this single 500 km long greenstone trend. This raises the question posed in the title.

The komatiite assemblage of the Kalgoorlie Terrane is distinctive in containing a very high proportion of very strongly olivine-enriched lithologies, particularly in comparison with the Abitibi terrane of the Superior Province, and with the eastern terranes (Kurnalpi, Burtville) of the Yilgarn craton. This is illustrated in Figure 1, which shows the data distributions of komatiitic rocks from these various terranes expressed in terms of FeO-MgO variations (Barnes et al., 2004), and filtered to exclude over-represented localities (Barnes et al., 2007). The Kalgoorlie Terrane is distinctive amongst greenstone belts worldwide in containing a high proportion of extremely olivine-rich cumulate rocks with original olivine compositions of 93 mol % or more forsterite. These compositions imply parent magmas in excess of 25% MgO, but this is not a unique feature. Many other greenstone belts (including those represented on Figure 1) contain magmas of this composition, but few contain abundant olivine mesocumulates and adcumulates derived from these magmas.

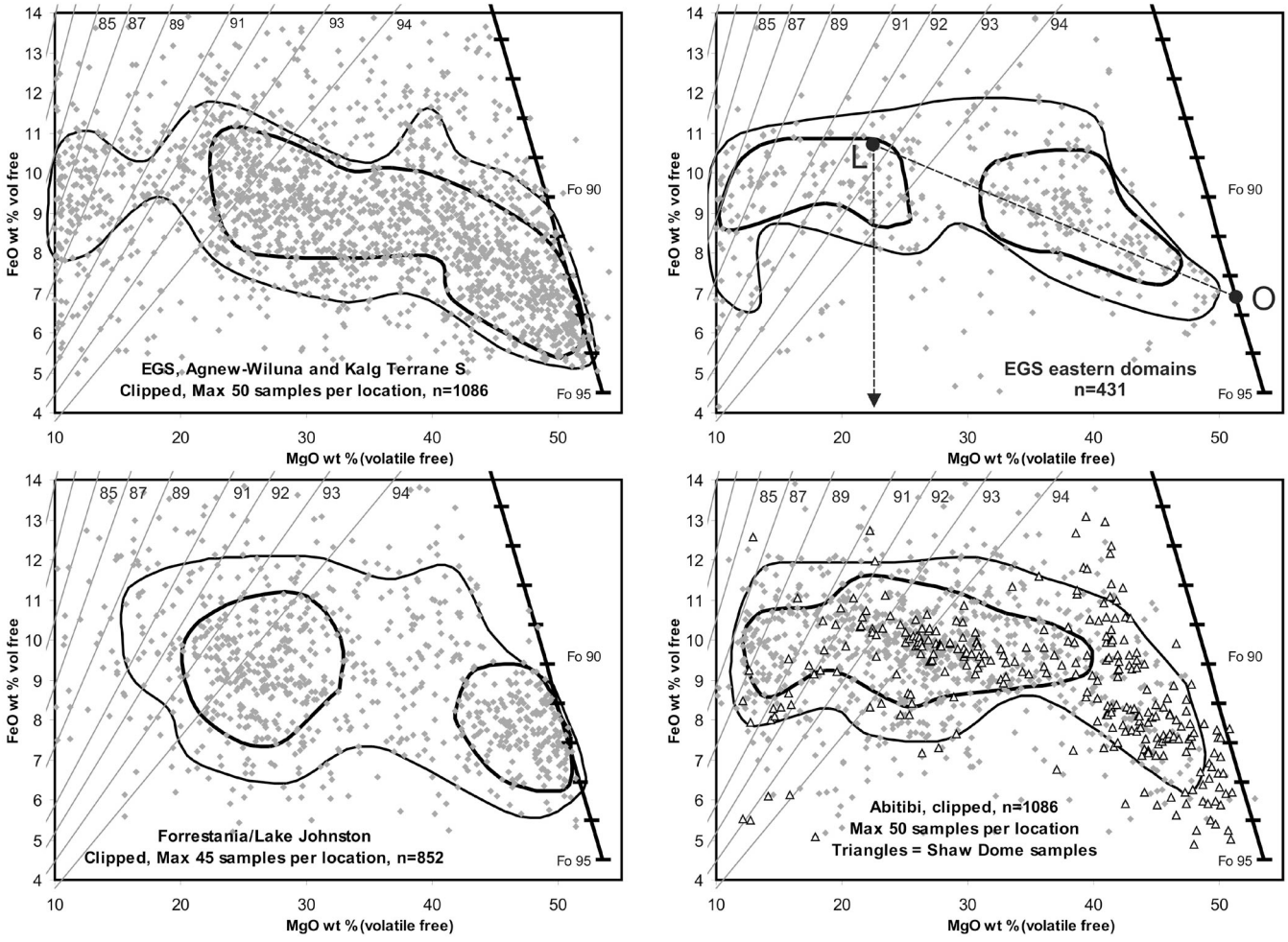

Figure 1. Plots of volatile-corrected FeO vs MgO in komatiite samples from (clockwise from top left) the Kalgoorlie Terrane, the eastern terranes of the Eastern Goldfields Superterrane (EGS),the Abitibi domain of the Superior Province, and the Forrestania and Lake Johnston greenstone belts of the Youanmi Terrane of the Yilgarn Craton. Contours contain the densest 50 and 80% of the data. Sloping heavy diagonal line is pure olivine with forsterite (Fo) content shown. Sloping light diagonal lines show liquid compositions in equilibrium with olivine of given Fo content.

The extreme olivine adcumulates of the Agnew-Wiluna trend in the northern part of the KT are associated with the largest deposits (Mt Keith and Perseverance). Beresford et al., (2004) and Rosengren et al. (2005) interpreted these large olivine adcumulate bodies as subvolcanic sills, emplaced in proximal settings. Comparable rocks are very rare, the only other widespread occurrence in a komatiitic volcanic setting being in the Forrestania and Lake Johnston greenstone belts, which also show distinctive data distributions on the MgO-FeO plots (Fig. 1). Significantly, these two (probably correlative) belts are the only known example of nickel sulfide mineralisation in Al-depleted (Barberton-type) komatiites, excluding some minor occurrences in South Africa and Brazil.

The presence of large bodies of highly-olivine rich cumulates is a critical controlling factor in making the East Yilgarn environment special. Whether or not this is a consequence of magma and source compositions, or other on-geochemical factors, can be tested further by considering some other aspects of the chemistry of the parent komatiite magmas, using a comprehensive global database of all available published whole-rock geochemistry on komatiites and associated rocks (Barnes et al., 2007).

The komatiites of the KT have a wide range of REE and other incompatible trace element abundances ranging from values typical for Al-undepleted (Munro-type) komatiites, to patterns indicative of high degrees of crustal contamination. In some but by no means all cases, these contamination signals are closely associated with sulfide mineralisation. Less endowed belts, notably Abitibi and the eastern terranes of the EGS, contain substantially lower proportions of strongly contaminated komatiites.

A similar relationship applies to platinum-group element concentrations. The KT komatiite array as a whole contains a higher proportion of samples showing anomalous PGE enrichments and depletions, but outside the immediate ore environments there is no evidence that the KT komatiites were any more or less enriched or depleted in PGEs than typical komatiites of this type and age worldwide (Fiorentini et al., 2010) (Fig 2). There is clear evidence, from the general lack of systematic PGE depletion anywhere outside ore-bearing flows, that the KT komatiites were erupted sulfide-undersaturated in almost all cases, and the pattern of PGE and incompatible trace element chemistry is entirely consistent with, and strongly supportive of, a substrate erosion model for local derivation of sulfur by supracrustal or near-surface assimilation of sulfidic sedimentary rocks (Bekker et al., 2009). There is no evidence within the komatiite data array for any role for anomalous lithosphere interactions, as suggested for other mineralised LIPs by Zhang, et al. (2008) or any other mantle-related geochemical process in controlling the chemistry of the KT komatiites.

The anomalously high Ni endowment of the terrane is related to the physical conditions of magma ascent and emplacement. Specifically, the formation of large bodies

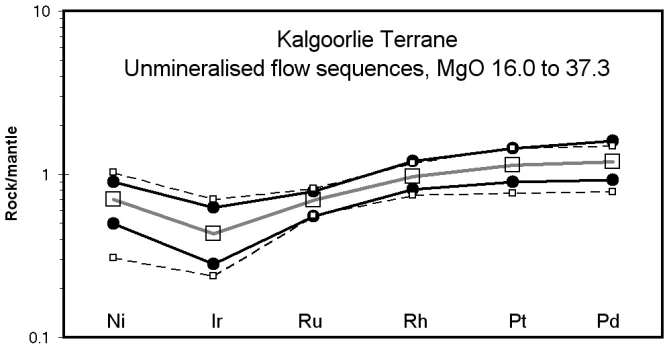

Figure 2. Chalcophile element mantle-normalised spidergram comparing Ni and PGE abundances in 37 samples of komatiites from unmineralised flows in the KT (20th and 80th percentiles, black lines with closed circles), with 230 samples of unmineralised 2.7 Ga-old Munro-type komatiites worldwide (20th, 50th, 80th percentiles, square symbols) over similar MgO range, data from Barnes and Fiorentini (2008) and sources cited therein.

of extremely olivine-rich, high-T cumulates requires high, prolonged magma fluxes through long-lived, focussed conduit systems or distributory flow pathways (Hill et al., 1995; Lesher et al., 1984). Establishment of such environments requires high rates and continuity of supply of high-T komatiite magma through the crust; a difficult condition to satisfy given that komatiite magmas are denser than typical crustal rocks. Overcoming the buoyancy problem requires existence of a complete interconnected column of magma through the crust and into deep mantle source regions, a condition which requires the presence of long-lived deep crust-mantle penetrating fracture systems coupled with very high magma production rates in the source.

Further insight can be gained from the associated stratigraphy. Komatiites of the Agnew-Wiluna Belt are closely associated with felsic/intermediate volcanics of unclear affinity, which may have played a crucial role during the ore-forming process (Fiorentini et al., 2007). They are unlike modern arc magmas, and have possible affinity with TTG suite magmas. The komatiites form part of a complex multi-modal volcanic assemblage, and were emplaced very close in time with the felsic rocks. Komatiites from the Black Swan area were erupted simultaneously with dacite lavas of undoubted TTG affinity, which by common consensus derive from melting of mafic lower crustal sources. At Kambalda and Widgiemooltha, felsic lavas are absent and komatiites were erupted on top of thick tholeiite package with strong geochemical and volcanological similarities to modern oceanic plateau tholeiites (Arndt et al., 2008). This range of associations, coupled with evidence for emplacement of a large volume of komatiite magma over a restricted time span (Nelson, 1997) is strong evidence for a plume origin, and for interaction of plume tail magmas with whatever local environment happened to be developed at the intersection of the surface with the main trans-crustal feeder system (Arndt et al., 2008). Komatiites do not appear to be very discriminating in the environments in which they erupt.

Explanations for the high endowment of the Kalgoorlie Terrane call on evidence for a preferential location at the edge of an older Archaean cratonic nucleus or "Archon" (Begg et al., 2009). According to this view, the margin of the Archon effectively channels the passage of the plume and the magmas it produces. The craton margin model implies a common tectonic affinity between the KT and many other younger nickel sulfide provinces which have conclusively been shown to be associated with Archon margins, particularly the Proterozoic Thompson and Raglan Belts of the Superior Craton margin. The critical features of the KT – high magma fluxes, deep mantle-tapping structures, and association with felsic-intermediate magmas of TTG affinity – are all explicable within this framework. A large mantle plume accounts for high magma flux, and the presence of plateau-type basaltic sequences derived from the plume head. High flux of extremely hot plume-derived mantle magmas through long lived deep-tapping structures allows for very efficient advective transfer of plume heat into the crust, giving rise to localised melting of older mafic-underplated material in the lower crust to form TTG magmas, which locally exploit the same structures. The less productive komatiite-arc association of the Kurnalpi terrane reflects a more or less random juxtaposition of distal portions of extensive komatiite flow fields with supracrustal environments beyond the immediate thermal influence of the plume tail; magma fluxes within this environment are insufficient to establish major ore-forming systems.

Productive komatiite packages need high magma fluxes, favoured by the interaction of mantle plumes with long-lived Archon margins. This environment is also suitable for generation and channelling of deep crustal melts relating to the passage of high komatiite magma fluxes. The komatiite magmas of the Kalgoorlie Terrane are not particularly unusual or distinctive. What is special is the rate at which unusually large volumes of plume-generated komatiite magma were emplaced through the crust.

Acknowledgements

The PGE data reported in this contribution were collected as part of AMIRA project P710a, funded by BHP Billiton Ltd., Norilsk Nickel Australia Ltd., Lion Ore Australia NL, Independence Group NL and MERIWA.

References

Arndt N.T., Lesher C.M., & Barnes S.J., 2008, *Komatiite*, Cambridge, Cambridge University Press, 467 p.

Barnes S.J. & Fiorentini, M.L., 2008, Iridium, ruthenium and rhodium in komatiites: Evidence for iridium alloy saturation: Chemical Geology, 257, 44–58.

Barnes S.J., Hill R.E.T., Perring C.S. & Dowling S.E., 2004, Lithogeochemical exploration for komatiite-associated Ni-sulfide deposits: strategies and limitations, Mineralogy and Petrology, 82, 259–293.

Barnes S.J., Lesher C.M. & Sproule R. A., 2007, Geochemistry of komatiites in the Eastern Goldfields Superterrane, Western Australia and the Abitibi Greenstone Belt, Canada, and implications for the distribution of associated Ni-Cu-PGE deposits, Applied Earth Science (Transactions of the Institute of Mining and Metallurgy Series B), 116, 167–187.

Begg G.C., Hronsky J.M.A., O'Reilly S., Griffin W.L. & Hayward N., 2009, Plumes, Cratons and Nickel Sulphide Deposits: SGA Biennial meeting, Townsville, Qld., 2009, 147–148.

Bekker A., Barley M.E., Fiorentini M.L., Rouxel O.J., Rumble D. & Beresford S.W., 2009, Atmospheric Sulphur in Archaean Komatiite-Hosted Nickel Deposits, Science, 326, 1086–1089.

Beresford S.W., Fiorentini M., Rosengren N.M., Duuring P., Barley M.E. & Bleeker W., 2004. The structural and stratigraphic architecture of the Agnew-Wiluna greenstone belt, Western Australia, AMIRA P710 Final Report.

Fiorentini M.L., Barnes S.J., Lesher, C.M., Heggie G., Keays R.R. & Burnham, O.M., 2010, Platinum-group element geochemistry of mineralized and non-mineralized komatiites and basalts, Economic Geology, accepted, minor revisions.

Fiorentini M.L., Rosengren N., Beresford S.W., Grguric B., Barley M.E., 2007. Controls on the emplacement and genesis of the MKD5 and Sarah's Find Ni-Cu-PGE deposits, Mount Keith, Agnew-Wiluna Greenstone Belt, Western Australia. Mineralium Deposita, 42, 847–877.

Hill R.E.T., Barnes S.J., Gole M.J., & Dowling S.E., 1995, The volcanology of komatiites as deduced from field relationships in the Norseman-Wiluna greenstone belt, Western Australia, Lithos, 34, 159–188.

Lesher C.M., Arndt N.T. & Groves, D.I., 1984, Genesis of komatiite-associated nickel sulphide deposits at Kambalda Western Australia: a distal volcanic model, in *Sulphide deposits in mafic and ultramafic rocks* in Buchanan D.L., & Jones M.J., eds, London, Institute of Mining and Metallurgy, 70–80.

Nelson D.R., 1997, Evolution of the Archaean granite-greenstone terranes of the Eastern Goldfields, Western Australia: SHRIMP U-Pb zircon constraints, Precambrian Research, 83, 57–81.

Rosengren N.M. Beresford S.W. Grguric B.A & Cas R.A.F. 2005. An intrusive origin for the komatiitic-dunite hosted Mount Keith disseminated nickel sulphide deposit, Western Australia, Economic Geology, 100 149–156.

Zhang M., O'Reilly S., Wang K.-L., Hronsky J. & Griffin W., 2008, Flood basalts and metallogeny: the lithosphere mantle connection, Earth Science Reviews, 86, 145–174.

THE STRATIGRAPHIC SUCCESSION AT THE JAGUAR VHMS DEPOSIT

S.M. Belford, G.J. Davidson, J. McPhie & R.R. Large

ARC Centre of Excellence in Ore Deposits (CODES COE), The University of Tasmania, TAS, 7005 Australia

Introduction

Jaguar, an Archean Cu-Zn-rich volcanic-hosted massive sulfide deposit, is situated in the Teutonic Bore volcanic complex in the Eastern Goldfields of the Yilgarn Craton, Western Australia. The Jaguar deposit is one of only three VHMS deposits that have been mined in the Eastern Goldfields. The deposit is hosted in a succession dominated by coherent facies and their associated volcaniclastic facies, with minor non-volcanic facies. The rocks (c. 2.69 Ga) have been affected by regional greenschist facies metamorphism and deformation, and hydrothermal alteration is intense around the massive sulfide orebody.

Using only drillcore across a 1 km x 1.6 km area, twenty-five principal lithofacies have been recognised in the study area and are organised into five groups: 1) coherent rhyolite, dacite, andesite, basalt and dolerite facies; 2) monomictic volcanic breccia and conglomerate; 3) polymictic volcanic breccia and conglomerate; 4) volcanic sandstone and mudstone; and 5) non-volcanic mudstone and chemical facies. The environment of deposition was submarine and below-storm-wave-base.

The stratigraphy at Jaguar has been reconstructed using observations and interpretations based on facies analyses and relationships, rock fabric and microstructure that are supported by the application of immobile element geochemistry. The succession is split into Footwall (FW), Mineralised Package (MP) and Hangingwall (HW) units.

The Footwall

The FW, up to 450 metres below the ore, is divided into four volcanic lithofacies having distinctive composition. From the base these units are informally named: the Deep Andesite (DFA), the Footwall Rhyolite (FF), the Footwall Andesite (FA) and the Footwall Basalt (FB). The eruptive sequence is marked by an absence of sedimentation and only minimal reworking of the volcaniclastic breccias. Limited exposure of the footwall units and their contacts means the relationships are not tightly constrained. The oldest unit, the DFA, consists of massive coherent andesite with a fine-grained, vesicle-rich top, and is interpreted as a shallow sub-volcanic sill or lava. The morphology and physical characteristics of the FF indicate that it is a lava dome comprising coherent and associated volcaniclastic facies. The FA comprises andesite lava that consists of massive coherent andesite core and a thick hyaloclastite carapace. This andesite was possibly coeval with the still growing rhyolite dome. The FB, which conformably overlies the FA, comprises coherent basalt, dominantly pillowed, intercalated with hyaloclastite and pillow-fragment breccia. The early FB lavas were topographically lower than the rhyolite dome summit, and debris flow deposits originating on the dome are locally intercalated among the basalt lavas. The debris flows may have been the result of collapse of unstable dome carapace or tectonically unstable scarps of growth faults. The FB constructed a seafloor having an irregular topography comprising unstable mounds of pillow basalts surrounded by talus aprons of basalt breccia and conglomerate. The paleo-depth of water is poorly constrained. Today, the volcanic facies can occur through a wide range of water depths. The minimal evidence for reworking indicates that the depth is likely to have been below storm wave base.

The Mineralised Package

The MP is a complex assemblage of intercalated coherent, autoclastic, resedimented volcaniclastic and non-volcanic lithofacies divided into six sub-units: 1) the Dacite MP (MPF) comprising coherent dacite, monomictic dacite breccia and monomictic pumice-rich breccia facies; 2) the Conglomerate MP (MPC) comprising polymictic dacite breccia, polymictic conglomerate and pillow-fragment basalt breccia facies; 3) the Pumice-rich MP (MPT) comprising polymictic pumice-rich breccia and pumice granule sandstone facies; 4) the Laminated MP (MPS) comprising laminated volcanic mudstone, non-volcanic mudstone and black shale, polymictic conglomerate, volcanic sandstone and chert facies; 5) the Laminated Chert MP (MPH) comprising chert facies; and 6) the Sulfide ore (MPO).

The basal unit of much of the MP is the MPH, a laminated chert which directly overlies the FB. Chemical deposition of the chert occurred on the sea floor as a mantling exhalite immediately prior the eruption of the MPF. In places, plastic deformation and brecciation occurred during contemporaneous local seismic events (growth faulting), which locally exposed the FB. The plastic deformation indicates that the chert was a still a semi-gel at this time and that it is not the result of later silicification of clastic sediments (a common feature in Archean areas of low sedimentation rate). The length of time that the chert took to form is not known, but was probably not long. This chemical deposition of the chert, free of epiclastic input, implies that a circulating hydrothermal system was developing in the footwall and that virtually no external sediment input was occurring at this time. At about this time the dacite (MPF) was erupted on to the seafloor as a series of small domes or lava flows. The dacite was the last product of the fractionated magmas of the FW magma chamber. The eruption was concomitant with increasing tectonic instability. Local development of growth fault scarps likely exposed the underlying basalt breccias. Growing, small domes of dacite produced pumiceous carapace breccias by means

of non-explosive, quench fragmentation of the pumiceous dacite lava or dome Grain flows originating from the carapace breccia in places incorporated the still gel-like chert as clasts among the pumiceous dacite fragments. Pumiceous mass-flow deposits are a particularly good host for the development of economic VHMS deposits because they are originally highly porous and permeable.

Away from the dacite domes, more distal, finer-grained pumice breccia was deposited overlying either the chert or basalt breccia (where exposed by removal of the chert mantle due to slumping and scouring associated with the growth faults). Ongoing seismic activity and development of growth faults also generated debris flows, which locally incorporated the still plastic chert as clasts, and more rarely, basalt clasts exposed by the fault scars. These debris flows, along with the dome-spall massflows, formed the MPC. The wedge shape of many of the breccia and conglomerate lenses supports the interpretation that active growth faults were contemporaneous with deposition, although their orientations are poorly constrained. The polymetallic sulfide orebody was formed in this environment. Within the MPC, primary sulfide clasts indicate that the sulfide body was forming contemporaneously with the MP. Tectonic instability and growth faulting exposed the growing massive sulfide to erosion. This instability and associated slumping, caused elutriation of finer-grained particles into the water column where they were moved about by water and weak currents before settling out of suspension (MPS). As deposition of the MP continued, dacite dome activity reduced and the last dacite magmas were probably emplaced as cryptodomes within the growing, unconsolidated, volcaniclastic pile. Throughout this activity, the seafloor topography was irregular and constantly changing.

The Orebody

A low strain window is the primary source of evidence that the deposit was syn-volcanic and formed predominantly, but not entirely beneath the seafloor. The evidence of the infill of open space textures, the colloform intergrowths of sulfide and chert, the sulfide replacement of glass spherulites plus replacement fronts within the dacite all support this conclusion. There is no evidence for presence of chimneys or the presence of a seafloor mound accumulation. There is no obvious conduit that demonstrates a constrained focus of the mineralising hydrothermal fluids and the fluids are considered to have moved up the inferred growth faults. The ascending hydrothermal fluids were probably focused at depth by these syn-volcanic growth faults and/or volcanic vent structures, but lost focus and dispersed within the porous volcaniclastic facies in both the upper FB and MP. The water depth at the time of mineralisation is difficult to determine but geological data are generally consistent with sulfide accumulation in a relatively deep-water (below storm-wave base) environment.

By the end of the MP times, only suspension sedimentation was occurring, eruptions had ceased, as had major hydrothermal activity. The sedimentation rate was very low but weak low-temperature hydrothermal activity persisted, manifested as thin layers (< 2 cm) of hydrothermal chert among mudstone laminae and uncommon beds of black carbonaceous shale. Sulfide is present as disseminated, fine-grained pyrite grains within mudstone laminae and may have precipitated from buoyant fluids venting at the seafloor, or have grown in situ. As the laminated mudstone at the top of the MP shows no evidence of widespread silicification developed 'hardground', the overall exposure time of this unit to silica-rich Archean waters was not long.

The Hangingwall

The HW is a constructional sequence of coherent and associated volcaniclastic lithofacies interbedded with laminated volcanic and non-volcanic mudstone facies. It is divided into four major volcanic units, defined by packages of associated volcanic lithofacies having distinctive composition. From the base of the hangingwall, these units are informally named: the Hangingwall Andesite (HA), the Hangingwall Basalt (HB), the Upper Porphyritic Andesite (HUA) and the Upper Quartz Rhyolite (HUR). The HA and the HB have been further subdivided into separate mappable units, assisted in the case of the HA, by distinct geochemical characteristics.

Early Hangingwall

The onset of HW times was signalled by the eruption of new magma. The relatively viscous HA1 lava flowed across and intruded down into the slowly accreting mudstone that was the top of the MP. The HA1 lava formed as a low aspect coulee and although twice the thickness of the HA2 and HA3 lavas, it had more restricted areal extent, which was most likely a function of viscosity. A period of sedimentation (HA1S) followed emplacement of the HA1. The HA2 was erupted onto the seafloor and partially burrowed into the unconsolidated sediments of HA1S. Ambient sedimentation continued and the HA2S mudstone and black shale was laid down, forming a passive conformable contact over the occurrences of HA2 carapace breccias. Extension-generated growth faulting and related subsidence in the south continued. HA3, the upper andesite was then erupted onto the seafloor, in parts a pillow lava, elsewhere a massive lava with a hyaloclastite carapace. The lower contacts of HA3 are in places peperitic and elsewhere conformably overlie mudstone, whereas the upper contacts are marked by a hyaloclastite carapace that overlies massive or pillowed andesite. In turn, the HA3 is passively overlain by laminated mudstone and black shale (HA3S) which signalled the end of the calc-alkaline HA magmas. The geometry of the HA unit suggests that throughout its deposition there was gradual subsidence, most likely the result of extension-generated growth faulting.

The HB lavas which followed the HA formed by a voluminous outpouring of tholeiitic basalt that formed six mappable units. These compositionally monotonous basalts included pillowed and massive facies, plus hyaloclastite and one facies dominated by fire-fountain clasts. An initial lava, HB0, was of low volume and limited in extent, being restricted to the southern area, and the likelihood is that this was a topographic low at

the time of formation. The HB1 which followed, is the thickest of the HB units and it is also wedge shaped to the south. The HB1 and HB2 units consist of pillow lavas and extensive hyaloclastite carapaces. A widespread fluidal-clast breccia facies is associated with the HB1 carapace, and indicates that there were several fountaining vents along a fissure. The greatest concentration of fluidal clasts is likely to be close to the vent, although the local mass flows could have distributed the fluidal clasts over a wider area, mixing with the hyaloclastite clasts and filling any depression in the seafloor. Subsidence appeared to continue in the southern area during the eruption of the HB1 and HB2 lavas. At about the time of the eruption of the HB3 lava, the external stress regime appears to have changed from extensional to compressional resulting in a change from extrusive to intrusive igneous emplacement styles. The dolerite sills were emplaced coeval with the HB3 to HB5 lavas at stratigraphic levels up to HB2. The strikingly similar composition, and contact relationships between the HB and the D, indicate that they were both co-magmatic and coeval, and most likely the D sills were part of the feeders to the HB lavas. The stress regime switch to compression meant that melts more readily propagated sub-parallel to layering rather than erupting. The upper three units (HB3, HB4 and HB5) were progressively less extensive in volume, and had only minor carapace breccias in comparison to HB1 and HB2.The aggregate inflation of the succession due to sill intrusion was between 150 and 200 m. The inflation was probably not uniform; more magma intruded in the south of the area and likely caused tilting to the north. During the HB outpouring, there was minimal deposition of sediment although rare instances of black mudstone occur in peperite along the base of some lava flows.

Late Hangingwall

When the prodigious outflow and sill intrusion that generated the hangingwall basalts and dolerites had ceased, a volcanic hiatus allowed an accumulation of mud-dominated sediment (HUS1). The unit geometry indicates that the original depositional surface was tilted to the north, i.e. in the opposite direction to earlier times. As with the earlier mudstones in the MP, there is no evidence of prolonged exposure to silica-rich water that would have resulted in silicification developed 'hardground', therefore this unit was probably not exposed to silica-rich Archean waters for very long. A short time interval is further supported by the peperitic margins on apophyses extending from the overlying andesite body. The emplacement of the HUA andesite followed. The HUA, a series of submarine lavas, was dominated by coherent andesite associated with autoclastic facies. Feldspar-phyric andesite apophyses intruded into the underlying HUS1 unit. The peperite margins attest to the semi-consolidated nature of the underlying mudstone at the time of eruption. The composition of this andesite is similar to the HA andesites, but is more felsic and more calc-alkaline than the HA. Another volcanic hiatus saw the deposition of the HUS2, a mudstone dominated unit which passively overlies the HUA. A basal conglomerate with clasts of HUA andesite indicates that locally, the lower HUS2 contact was erosive. Immediately overlying the HUS2 is the HUR, a quartz-phyric rhyolite unit. The base of the HUR is marked by polymictic rhyolite breccia that includes a small proportion of clasts derived from the underlying mudstone and which grades upwards into coherent rhyolite. Underlying the rhyolite and intruded into the HUS2, a body of dominantly coherent rhyolite with peperite margins is interpreted as either an apophysis or feeder dyke of the HUR. The composition of the HUR is similar to the HB, which suggests that it is a fractionated part of same source magma. The top of the sequence is not seen.

Post-Lithification Evolution

The lateral continuity of almost all units, and the lack of repetition of sequence, does not support the presence of subtle thrust ramp repetitions. All the sedimentary younging evidence unequivocally indicates younging to the west, indicating no obvious major folds. The deformation of the sequence is not significant enough to influence stratigraphic reconstruction. That the Jaguar succession has been deformed is manifest in the durchebewgung textures in ductile sulfides and the rare graphite layers. Locally there are also zones of brittle deformation where fault breccias, plus or minus fault gouge, occur. It has not been possible to correlate between these zones of fault breccia or gouge because of the absence of any kinematic indicators. Therefore the extent and the direction of movement, if any exists, is unknown. In the study area, fault movement is assumed to have been minor due to the planar nature of the succession as evident in the upper hangingwall and the ability to readily correlate the succession across these fault zones.

Acknowledgements

This study was done as part of SMB's PhD at CODES, University of Tasmania. We thank Jabiru Metals for their financial and logistical support and Dr N. Martin for all his help. SMB's PhD was funded by an ARC APAI scholarship, which was negotiated with the help of Mr Peter Ellis (deceased).

ARCHAEAN GOLD MINERAL SYSTEMS IN THE EASTERN YILGARN CRATON: NEW RESEARCH CONTRIBUTIONS FROM THE *pmd**CRC

R.S. Blewett and the *pmdCRC team**

Geoscience Australia, GPO Box 378, Canberra, ACT, 2601, Australia

Introduction

The Eastern Goldfields Superterrane (EGST) in the eastern Yilgarn Craton of Western Australia is Australia's premier gold and nickel province, and has been the focus of geological investigations for over a century. The Predictive Mineral Discovery Cooperative Research Centre (*pmd**CRC) was a collaborative government-industry initiative (2001–2008) that was designed to answer key questions, test established paradigms, and to advance the geological understanding of this metal-endowed Archaean region. This paper presents a summary of some of the highlights and new findings from this research, many of which challenge established paradigms (Y4 Project team 2008, and references therein). Although a Yilgarn-based study, there are general implications for understanding the tectonics and gold mineral systems of other Archaean terranes.

Geodynamic setting and thermo-baric evolution

In order to better constrain the competing hypotheses of the geodynamics of the Yilgarn Craton, and Archaean tectonics in general, the *pmd**CRC synthesised the main elements of the orogenic system into a new integrated framework in time and space. Elements considered included the greenstone stratigraphy, magmatic history, metamorphism, mineralisation, and structural geology, together with extensive geological and geophysical maps. The synthesis highlighted the strong interdependence where a change in one element saw all elements change. The constraints from this integrated 4D framework suggest an overall extensional margin dominated the geodynamic evolution of the eastern Yilgarn Craton.

Fundamental map patterns were revealed with improvement to the Sm-Nd database by the *pmd**CRC. A new crustal age map shows the EGST consists of NNW-striking elongate Sm-Nd patterns, where are interpreted to mark variable degrees of crustal contamination from an extended underlying Younami Terrane basement. These fundamental map patterns challenge the exotic strike-slip terrane and allocthonthous obduction settings, and support simpler rifting/back-arc extensional settings.

One of the most significant advances from the *pmd**CRC relates to the metamorphic evolution of the EGST. Previously, the EGST was thought to record significant crustal overthickening during collision, developing a single prograde cycle with a post-kinematic peak that was overprinted by retrogression and alteration. In contrast, the *pmd**CRC showed that five discrete thermo-baric events occurred in time and space, with large variations in peak metamorphic crustal depths (12 to 31 km). The metamorphic evolution can viewed with stages of crustal growth (Ma and M1), thermal priming of the crust (M2), lithospheric extension (M3b), and finally inversion and reactivation (M3b).

Structural evolution

Taking advantage of the improved geochronological framework, a revised structural/deformational history was developed by the *pmd**CRC. The new history also better integrates the stratigraphic evolution and the 3D architecture. The new revised history highlights seven key deformation events (D1 to D7), many of which were of extensional mode. From this new understanding a series of observations and interpretations are made.

- D1 extension was dominantly E- to ENE-directed, and likely reflected the shape of the eastern continental margin. Extension dominated the period 2720–2670 Ma, and was responsible for establishing the fundamental NNW-trending architecture of the EGST. The D1 extensional event also influenced all subsequent deformational events, as well as the early Ni and later Au mineralisation.

- Short periods of convergence late in the history (<2665 Ma) inverted this system. Most of the convergence direction was ENE perpendicular to the margin (D2, D4a), with a short period (2650 Ma) when there was a far-field stress switch to an ESE orientation (D4b). This stress switch was also responsible for north-directed thrusts (previously called D1), which developed along dome hinges as accommodation of regional sinistral strike-slip faulting (D4b) within mostly inter-dome high-strain shear zones.

- Contractional deformation was diachronous with events around 5 My younger in the SW compared to the NE, which was interpreted as oblique far-field convergence zone to the eastern margin of the system.

- A major lithospheric extensional event (D3) occurred between two periods of coaxial contraction (D2, D4a). The extension was possibly driven by the delamination of a lower crustal eclogitic restite from the earlier voluminous tonalite-trondjhemite-granodiorite magmatism. The main locus extension was the Ida and Ockerburry Fault Systems (bounding structures of the Kalgoorlie Terrane), with late basins developed in the hanging wall, and intrusion of magmas from a metasomatised mantle source. These late basins are a feature of many granite-greenstone belts (e.g. in Superior, Slave, Pilbara, Barberton, and

West African cratons), and they are commonly syn-gold.

- The D1/D3 extension ruptured the crust, and developed a deep-penetrating fault system that facilitated access to metasomatised mantle melts (as seen in deep seismic profiles and magnetotellurics). Numerical modelling showed that these extensional events were able to draw fluids downwards, facilitating mixing with chemically contrasting fluids from depth.

- The faster the rate and the greater volume of new crust formation and its transition to cratonisation the more favourable the terrane/province (fast/voluminous and slow/less voluminous: cf. EGST and Younami; Yilgarn/Superior and Pilbara/Barberton).

- Structurally, texturally and mineralogically these systems record a number of gold mineralisation events and yet commonly only the youngest dated ages are quoted in the literature (e.g. at St Ives, Agnew and Laverton). With a better understanding of the structural and mineralisation paragenesis, a renewed effort should be made to date the various paragenetic stages within the deposits. New techniques, such as 3D scanning of veins, show that some mineralised veins are multiphase, with reactivation throughout the mineralisation history.

Lithospheric architecture

The last decade has seen a dramatic increase in the availability of high quality geophysics, especially seismic reflection and passive seismic data. Software and hardware advances now permit realistic 3D inversions of the potential field data, and the results visualised in 3D on a standard desktop computer. By integrating these geophysical datasets with the geological mapping of the Geological Survey of Western Australia and Geoscience Australia, a series of new 3D geological maps were constructed by the *pmd**CRC. These maps delineate the granite-cored domes which dominate the regional architecture. Granite domes also occur beneath the deepest greenstone basins, are no more than 7 km from the surface. Many of these domes nucleated about D1 growth faults that controlled the greenstone stratigraphy. Such faults, when inverted, became the location of major gold deposits, such as Kalgoorlie, Wallaby and Kanowna Belle.

Major crustal breaks are associated with all the main gold districts, with the golden corridor from Kambalda to Wiluna linked to a regional anticlinorium whose limbs are defined by outward dipping shears that connect to deep faults. Convex domes are nested within this regional structure, providing a favourable focussing architecture for deep fluids. This architecture is not the 'Y-front' shape popularised in the earlier literature. The seismic character of the much of the crust is dominated by extensional features – such as core complexes. This reinterpretation contrasts with earlier seismic interpretations of contraction and thrust duplexes above a contractional detachment.

The architecture of upper mantle was delineated by the *pmd**CRC, with tools such as broad-band seismology and magnetotellurics. These datasets show anomalous structure in the upper mantle beneath the main gold camps. The upper mantle fast shear-wave velocity body is interpreted as a delaminated eclogitic lower crust. The delamination was interpreted to have started in the east (2665 Ma), with younging to the west (2655 Ma).

Relationship of gold mineralisation to the structural history

Gold deposits are traditionally described from contractional settings, and late in the tectonic history. However, the *pmd**CRC mapped gold in all events up to D5, with the highest grade and tonnage occurring from D3 times onwards. This is the time the metasomatised mantle was accessed and late basins developed. Orogenic gold occurs in extensional shear zones. The *pmd**CRC mapped these zones at Leonora, Lancefield, Leinster and at Kunanalling; all developed by extensional exhumation of large granite domes. The deposits are restricted to the shear planes (C and C') of the extensional foliations and have very deep extents down the stretching direction. These are a new gold play and have been under-explored. All of the major deposits/camps have D1 growth faults within them (e.g. Golden Mile, Agnew-Lawlers, Sunrise Dam and St Ives), and these structures were subsequently inverted and mineralised.

Relationship of gold mineralisation to metamorphism

Gold mineralisation and late-stage metamorphism of the greenstone sequences have been traditionally linked in the orogenic gold model. The *pmd**CRC has made a significant advance in the thermo-baric evolution of the EGST, with the spatial and temporal definition of five discrete events. The highest pressures attain 8.7 kb, in rocks with low geothermal gradients. These M1 assemblages occur in the oldest greenstone sequences adjacent to granite domes, and in the footwall of extensional detachments. High-temperature (M*a*) granulites are likely to have developed beneath an arc, in a region of high geothermal gradients. The main regional moderate pressure and temperature M2 metamorphic event probably accounts for much of the available metamorphic fluid, and was generated before the main gold events (suggesting that this was not a major fluid source). The D3 extensional event was associated with tight anticlockwise M3a PT*t* paths in the upper plate that exhumed older higher pressure (with clockwise path) assemblages in the footwall. Regional exhumation during D4 to D5 times is recorded by widespread low-pressure M3b assemblages (~1 kb) and was associated with regional retrogression and alteration. Maps of redox of the alteration mineralogy illustrate the regional scale of these hydrothermal systems.

Low-Ca potassic granites are crustal melts that were emplaced at high levels across the entire craton and mark decompression and uplift of the exposed crust to high crustal levels (<1 kb), commencing 10–15 My after the inferred delamination of the eclogitic restite imaged in the tomography, and resulting in the final cratonisation

of the craton. This time delay is consistent with the thermal diffusivity through the known crustal thickness of the Yilgarn.

Relationship of gold mineralisation to magmatism

The timing of gold, the number of discrete gold events, and the role of the evolving magmatic system has long been a source of controversy. The first significant gold event was synchronous with the major D3 extensional event (e.g. Lancefield, Kalgoorlie, Sunrise Dam, Leonora and St Ives). This event introduced small volume melts, of syenite and Mafic-type granite (sanukitoids), interpreted to have been sourced from a metasomatised mantle wedge. Many deposits have mineralisation ages younger (10+ My) than the porphyries that host the deposit, implying no direct temporal connection with these intrusions.

3D mapping by the *pmd**CRC show that multi-phase granite-cored domes lie at varying depths beneath all the giant gold deposits. Most of the granites (and especially the late-stage Low-Ca granites) do not intrude into the greenstones; rather they crystallise at the lower basalt or komatiite levels in the stratigraphy. These vertically zoned systems may have provided fluids from depth in the cores of the domes through the same pathways that earlier, small-magma volumes (e.g. deposit-scale porphyries) had passed. The early architecture was critical in facilitating early magma emplacement which in turn set up local sites of anisotropy which localised strain during the multiple phases of reactivation.

Gold and fluid source(s)

The suggested gold sources include metamorphic, magmatic and mantle reservoirs. Lamprophyres and metasomatised mantle melts (sanukitoid porphyries and syenites) are temporally associated with major gold mineralisation in other Archaean terranes (e.g. Abitibi, Pilbara). The first significant gold in the EGST was deposited synchronous with the emplacement of metasomatised mantle magmas (2665–2655 Ma). A possible gold source was the metasomatised mantle, and the magmas reflect a melt fraction and common pathway with the gold from this source. Once gold is deposited in the system it can be later remobilised. For example, Proterozoic reworking on the northern margin of the Yilgarn Craton redeposited gold at Plutonic. It is not clear if the remobilisation of D3 gold in the EGST occurred within a few million years (i.e. D4 and D5 events) within the same deposit, or whether multiple gold sources for each event occurred. The addition of base metals together with gold suggests basinal input (late basin inversion) and tellurium suggests magmatic input (Low-Ca granites and High-Ca crustal melts post 2655 Ma) for associated metals. These deposits are the same ones that host classical orogenic gold and yet could be classified as anomalous-metal association and intrusion-related deposits respectively. The coincidence in space (separated in time) suggests that classifying these deposits into different types is not helpful in understanding the gold mineral system.

The fluid associated with orogenic gold has traditionally been considered metamorphic in origin. The *pmd**CRC attempted to define the fluid source(s), challenged the traditional view, and showed that at least three fluids were present. Modelling revealed that the devolatilisation of greenstones releases only short-duration low-volume fluids. The resultant rock mass is left dry and unable to subsequently contribute fluid to any later event. The multiple gold events observed mean that metamorphic fluids may have been the source for one of the gold events, but not all. Furthermore, metamorphic studies show that the regional M2 metamorphism of the greenstones occurred prior to the first significant gold event. Considering the mineralogy, simple geochemical modelling required at least two fluids–a mafic fluid and a granitic fluid. Furthermore, the presence of multiple gold events and their differences in PT conditions, redox, mineralogy and metal associations, together with wall rock alteration all indicate an evolving system of fluid sources. This metamorphic-only source contrasts with voluminous magmatic and mantle fluid sources. The *pmd**CRC defined three end-member fluids to account for the extreme range of O, S, C stable isotopes, the range of redox inferred from these, and from the chemistry of the alteration mineralogy. Within vein systems, fluid dominates over wall rock so that the chemistry reflects different sources of fluids and not necessarily the influence of reactions with local wall rocks. An emerging picture of the role of possible mantle fluid reservoirs is provided by studies of the noble gases, especially those in D4b gold-bearing veins at St Ives and Sunrise Dam. This is a significant finding. How indicative this is to other deposits remains to be determined.

Depositional mechanisms

There are four main ways to deposit gold (phase separation, fluid-rock reaction, vapour condensation and mixing across chemical gradients). All four processes have been documented in the EGST. The question remains what makes the giant deposits and the high grades. Research from the *pmd**CRC suggests that fluid mixing across chemical gradients was the most efficient method, and the range of data showing gradients in operation with multiple fluid sources are now very compelling.

Predictive mineral discovery

The *pmd**CRC developed a process-based understanding of the gold mineral system, and translated this understanding into mappable proxies of the process. The maps were then integrated in a GIS, resulting in the generation of a new target map of gold without the input of any gold layer. The map ‘discovered’ 75% of the known gold in <5% of the area, a verification of the process understanding. Importantly, the map identified all the major gold camps. This result revealed the critical geological elements in terms of process that are needed to form a giant gold deposit. The necessary datasets for identifying these processes are also defined. The map also revealed a number of areas that were not known for hosting large deposits, but had all the favourable ingredients – these represent new opportunities.

Cooperative not competitive research: a better working model

The *pmd**CRC was successful in bringing together government and university researchers with industry. Despite the obvious cultural differences, the working model was very much based on cooperation and collaboration. The results described above stand for themselves. The enduring legacy is also with the participants, the *pmd**CRC changed, for the better, the way we think and operate.

Acknowledgements

I wish to acknowledge the team members of the *pmd**CRC, the sponsors of the centre, and the centre management. Reviews by David Champion and Dean Hoatson improved the paper. Published with permission of the CEO Geoscience Australia. Geocat number 70128.

References

Y4 Project team, 2008, Concepts to targets: a scale-integrated mineral systems study of the Eastern Yilgarn Craton. pmd*CRC Y4 project Final Report, Parts I-II 162 pp Parts IV-V, 391pp (http://www.pmdcrc.com.au/final_reports_projectY4.html).

HIGH-GRADE IRON MINERALISATION AT THE BEEBYN DEPOSIT, WELD RANGE, WESTERN AUSTRALIA

P. Duuring & S.G. Hagemann

Centre for Exploration Targeting, School of Earth and Environment, University of Western Australia, Crawley, WA 6009, Australia

Introduction

Late-Archean, Algoma-type Banded Iron Formation (BIF)-hosted deposits in the Yilgarn Craton of Western Australia are comparatively less well-studied and explored compared with their larger cousins, which are the Paleoproterozoic, Superior-type BIF-hosted deposits of the Hamersley Province (Western Australia), Transvaal Basin (South Africa), and the Quadrilatero Ferrifero (Brazil). At least in Western Australia, iron exploration strategies are increasingly being geared towards the discovery of Algoma-type deposits since they represent an opportunity to find under-explored, low-tonnage, high-grade iron ore bodies. The Weld Range greenstone belt, located about 60 km NNW of Cue in the Murchison Domain of the Yilgarn Craton, hosts two known Algoma-type, high-grade hematite-magnetite deposits, Madoonga (68 Mt resource at 57.7 wt.% Fe) and Beebyn (62 Mt resource at 59.6 wt.% Fe, ASX announcement 2008). The aim of this abstract is to document the geology of the Beebyn deposit, interpret its deformation history, and comment on important controls for the genesis of its high-grade (>45 %) iron mineralisation.

Regional geology

The Murchison Domain lies in the western part of the Youanmi Terrane, in the Yilgarn Craton of Western Australia (Cassidy et al. 2006). The oldest recognised supracrustal rocks in the Murchison Domain formed after 3034 Ma, although, unexposed supracrustal rocks might be older because granitoids in the area locally host xenocrystic zircons that have ages older than ~4000 Ma. The oldest granitoids have ages that range from about 3050 to 2919 Ma (Van Kranendonk & Ivanic, 2009 and references therein). The north-eastern area of the domain, which is the subject of a recent re-interpretation by Van Kranendonk & Ivanic (2009), includes Murchison Supergroup supracrustal rocks that can be divided into: (1) Norie Group, 2814 to 2800 Ma, mafic volcanic rocks, felsic volcaniclastic sandstones, and BIF, (2) Polelle Group, 2785 to 2734 Ma, mafic volcanic rocks, felsic volcanic and volcaniclastic sedimentary rocks, and BIF, and (3) Glen Group, 2724 to 2700 Ma, coarse clastic sedimentary rocks and komatiitic basalt. An older, ca. 2950 Ma group occurs in the Mount Gibson-Golden Grove area to the south. All supracrustal rocks were intruded by granitic rocks during distinct episodes of magmatism taking place from about 2716 to 2592 Ma, resulting in several granitoid suites (Van Kranendonk & Ivanic 2009).

Peak metamorphic facies conditions vary across the Murchison Domain, but are commonly influenced by their proximity to granitoids. For example, the Murrouli basalt, located at the base of the Norie Group in the north-eastern part of the domain near Meekatharra, is metamorphosed to amphibolite facies, but grades to upper-greenschist facies with distance from the intrusive contact with the Nannine tonalite (Van Kranendonk & Ivanic 2009). Major structural features in the domain include at least two generations of regional folds that deform supracrustal rocks of the Norie, Polelle, and Glen groups. The first generation of folds are E-trending and isoclinal. They are re-folded by more open and upright, NE-trending folds that plunge shallowly to moderately to the NE or SW. Van Kranendonk (2008) describes two deformation events that control geological relationships in the Cue-Meekatharra area of the Murchison Domain. The D_1 event produced E-trending folds and contemporaneous granitoid emplacement at about 2676 Ma, whereas broadly E-W shortening during the D_2 event from about 2660 to 2637 Ma resulted in N- to NNE-trending folds, foliations, and lineations, as well as NNW-striking sinistral shear zones and NE-striking dextral shear zones. In addition to high-grade, Algoma-type BIF-hosted deposits, the domain hosts volcanic massive-hosted sulphide (ca. 2950 Ma, Golden Grove, Mt Gibson), magmatic PGE and V-Ti (ca. 2780 Ma, Windimurra, Barrambie, Weld Range), magmatic W-Mo (ca. 2767, Ma Mt Mulgine), and orogenic Au deposits (ca. 2650 to 2630 Ma, Mt Gibson, Reedy's, Big Bell, Noongal).

Weld Range greenstone belt

The Weld Range study area coincides with a 3 to 5 km-wide, ~70 km-long, series of parallel ridges that trend mainly ENE, but curves to a more northerly trend in eastern areas of the district where the rocks are structurally juxtaposed against the Illigalara monzogranite (Ivanic, 2009). Oldest exposed supracrustal rocks in the Weld Range greenstone belt are steeply S-dipping, S-facing rocks of the 2800 to 2730 Ma Polelle Group that crop out to the north of the Weld Range series of ridges. These rocks include komatiite, komatiitic basalt, and tholeiitic basalt of the lower Meekatharra Formation. The lower stratigraphic position of the komatiite is truncated in the north by post-tectonic monzogranite of the Bald Rock Supersuite (ca. 2637 to 2592 Ma) (Van Kranendonk & Ivanic 2009). The komatiite comprises several repeated flow sequences of basal olivine adcumulate-textured zones that grade up-sequence and to the south into olivine mesocumulate-, orthocumulate-, and randomly-oriented olivine spinifex-textured komatiite. Andesitic to rhyolitic volcanic and volcaniclastic rocks of the Greensleeves Formation overlie the komatiite flows. Rhyolitic

pyroclastic breccia that crops out near the inferred upper stratigraphic contact with the mafic/ultramafic volcanic sequence is very coarse-grained (5 to 50 cm), poorly sorted, and comprises angular clasts of mostly coherent, porphyritic rhyolite, with minor fragments of fine-grained mafic to ultramafic volcanic rocks. Farther south, the Greensleeves Formation becomes finer-grained and well-sorted, and is conformably overlain by ~2752 Ma (Wang, 1998) BIF, tuffaceous siltstones, and felsic rocks of the Wilgie Mia Formation. This formation contains three main BIF sequences that include, from north to south, the Madoonga, Lulworth, and Wilgie Mia BIF. Felsic rocks that once separated the BIF are now mostly replaced by mafic volcanic units that range in texture from basaltic to gabbroic, with doleritic textures being most common. Tectonised contacts are mainly preserved between these BIF and mafic volcanic units. The Wilgie Mia Formation and intervening mafic volcanic rocks are overlain by undifferentiated felsic volcanic and volcaniclastic rocks, and subsequently by schistose pelite and psammite of the Ryansville Formation, which are locally intruded by Yalgowra Suite (Austin Downs Supersuite) gabbronorite, gabbro, and dolerite (Ivanic 2009).

Supracrustal rocks in the Weld Range greenstone belt are metamorphosed to upper-greenschist to lower-amphibolite facies (300 ± 50° C) at pressures of < 2-3 kbars (Gole 1980). District-scale structures in the belt include ENE-trending, isoclinal folds that have an axial planar foliation oriented subparallel to bedding in supracrustal rocks (Spaggiari 2006). A moderately SW-plunging syncline (located to the south of the main series of ridges at the Weld Range) is defined by the folding of bedding contacts and a bedding-parallel foliation displayed by rocks of the Ryansville Formation (Ivanic 2009). A NNE-trending fault (i.e., Carbar Fault, Spaggiari 2006) defines the eastern margin of the Weld Range greenstone belt. Conflicting interpretations about the movement sense along the fault include reverse-sinistral (Spaggiari 2006) and dextral displacements (Van Kranendonk 2008). Late, NW- to N-trending, steeply dipping, brittle faults displace the Weld Range greenstone belt with lateral displacements of < 1 km.

Methodology

Detailed lithological, structural, and alteration outcrop mapping were performed at a 1:2,000 scale over the 8 km-strike length of the Beebyn deposit. Outcrop is mostly confined to a <100 m-wide, <50 m-high, ENE-trending ridge. Core from six diamond drill holes that cover the strike length of the deposit was studied with emphasis on the relationship between unweathered rock types, structures, hydrothermal alteration, and iron mineralisation. The holes were drilled from surface to the NNW at moderate to steep angles. Examples of least-altered/weathered rocks were collected in conjunction with their more altered and weathered variants for the purpose of thin-section and carbonate-staining studies.

Geology of the Beebyn deposit

The Beebyn deposit stratigraphy trends ENE, is steeply SSE-dipping, and includes BIF, basalt, dolerite, and gabbro, with minor chloritic shale or siltstone interbedded with the BIF. Three main BIF units (the "North", "Central", and "South" BIF) in the deposit are bounded by mafic volcanic rocks. All major lithological contacts between BIF and mafic volcanic rocks are deformed. Only narrow (<3 m-thick) intervals of mafic volcanic rocks placed within the North BIF have intrusive contacts, thereby supporting at least local emplacement of mafic sills within BIF. Chloritic shale or siltstones are minor constituents of the North and Central BIF. Stratigraphic younging directions are not displayed by any rock types at Beebyn. The North BIF is the thickest BIF and hosts the widest zones of high-grade iron mineralisation. These zones are most commonly located along the stratigraphic footwall contact of the North BIF. The depth of weathering varies over the strike length of the Beebyn deposit, averaging about 120 m below the present surface, but extending to considerably greater depths (~200 m) along lithological contacts or within steeply-dipping fault zones.

The North BIF and nearby mafic volcanic rocks experienced several episodes of structurally-controlled, hydrothermal fluid alteration prior to near-surface weathering. These alteration events significantly changed the primary mineralogy, texture, chemistry, and more specifically, the iron content of the BIF. The earliest hydrothermal alteration event affecting the North BIF involved the channelling of hydrothermal fluids along the footwall contact of the North BIF. Primary silica-rich mesobands were replaced by hydrothermal Fe-rich dolomite and minor magnetite. The product is a BIF that has retained its primary texture and iron content, but has a lower abundance of silica. Reactivation of the North BIF footwall contact aided the introduction of a second hydrothermal fluid that leached Fe-rich dolomite bands. The removal of the carbonate mineral gangue produced a BIF that has a higher proportion of residual Fe oxide-rich mesobands, a greater abundance of Fe, and textures that include collapse breccias and the crenulation of Fe oxide-rich bands. Locally, spaces created by the dissolution of carbonate-rich bands are filled by a later generation of fine-grained, euhedral, hydrothermal magnetite and carbonate minerals. A third episode of hydrothermal alteration is associated with reactivation of the footwall contact, but also with the formation of discrete, 1 m-wide, bedding-parallel shear zones located near the middle of the North BIF. Coarse-grained chlorite and specular hematite are concentrated within these shear zones. Wallrock to the shear zones displays varying degrees of oxidation of the magnetite-rich bands to hematite (formation of martite), whereas remnant carbonate-rich bands are replaced by chlorite. These hydrothermal alteration mineral assemblages in BIF are locally cut by several generations of carbonate(-rich)-quartz±magnetite±martite±chlorite veins. Discrete overprinting hydrothermal alteration episodes are less obvious in footwall mafic volcanic rocks, which are very fine-grained and intensely altered to talc-chlorite. Grain size in mafic volcanic rocks increases with distance from the footwall contact. Supergene-related goethite and hematite overprint hydrothermal alteration mineral assemblages within 200 m of the present surface.

Deformation events

Five main deformation events are preserved at Beebyn. The first deformation event (D_{B1}) involved E-W shortening and resulted in the formation of isoclinal, recumbent F_1 folds that have axial planes oriented subparallel to the now ENE-trending, multiply-folded stratigraphy. F_1 fold axes observed within the BIF have variable plunge directions; however, they mainly plunge moderate to steeply to the NE. Reverse shear zones or faults occur along folded limbs and locally displace fold hinges.

The second deformation event (D_{B2}) coincided with N-S shortening and caused the refolding of F_1 folds. These F_2 folds are tight, upright, ENE-trending, and mainly plunge shallow to moderately to the WSW. Rare centimetre-scale examples of refolded F_1 folds are exposed in the North BIF. Asymmetric, Z-shaped parasitic F_2 folds (in plan) are commonly defined by mesobands in BIF and correspond with asymmetric, north-limb-down F_2 folds in cross-section. These parasitic fold relationships suggest the existence of a synclinal fold hinge to the south of the broadly S-facing Beebyn deposit stratigraphy (perhaps corresponding with the synclinal fold hinge within the Ryansville Formation mapped to the south of the Weld Range, Ivanic 2009). In the centre of the Beebyn deposit, Z-shaped F_2 folds result in en echelon, SE-stepping, of ~3 m-thick, lenses of hematite-magnetite-altered BIF. Locally, 10 cm to 3 m-diameter pods of specular hematite are concentrated in the hinge zones of metre-scale F_2 folds, suggesting that Fe-rich hydrothermal fluids were focused towards F_2 fold hinges during or after F_2 folding.

A third deformation event (D_{B3}) involving E-W shortening resulted in re-folding of the stratigraphy and the formation of F_3 folds in BIF. These folds are open to tight, trend N-S, and plunge steeply to the N or S. The F_3 folds contribute to the large variation in the orientation of F_1 and F_2 fold hinges at Beebyn.

Subsequent deformation at Beebyn (D_{B4} and D_{B5}) corresponds with the transition from ductile to brittle styles of deformation. North-south shortening during D_{B5} resulted in NNW- to NNE-trending, subvertical, brittle faults that cut the folded Beebyn stratigraphy. These faults commonly host extensional quartz veins and are spatially associated with zones of intense goethite-weathering of BIF horizons. Displacement indicators are rare, but where they exist they indicate mostly dextral displacements of up to 20 m. Based on the interpretation of aeromagnetic data, it is possible that dextral fault displacements may be even greater (<400 m). A resumption of E-W shortening during D_{B6} resulted in the centimetre-scale, dextral displacement of N-trending faults and extensional quartz veins by ENE-trending, bedding-parallel, brittle faults.

Conclusions

The Weld Range greenstone belt in the Murchison Domain of Western Australia hosts several examples of Algoma-type, BIF-hosted iron deposits. The Beebyn deposit displays complex hydrothermal alteration and structural relationships in BIF and surrounding mafic volcanic rocks that strongly influence the occurrence, positioning, and morphology of high-grade hematite-magnetite ore bodies. Understanding these key relationships is vital for interpreting the major controls on the ore body and for predicting the occurrence of other ore bodies in the greenstone belt.

Acknowledgements

This study is financially supported by Sinosteel Midwest Corporation Ltd. Weld Range exploration geologists are thanked for their generous logistical support.

References

Cassidy K.C., Champion D.C., Krapez B., Barley M.E., Brown S.J.A., Blewett R.S., Groenewald P.B. & Tyler I.M., 2006, A revised geological framework for the Yilgarn Craton, Western Australia, Geological Survey of Western Australia, 8p.

Gole M.J., 1980, Mineralogy and petrology of very-low-metamorphic grade Archaean banded iron-formations, Weld Range, Western Australia, American Mineralogist, 65, 1–2.

Ivanic T., 2009, Madoonga, WA Sheet 2444, 1:100 000 Geological Series, Geological Survey of Western Australia.

Spaggiari C.V., 2006, Interpreted bedrock geology of the northern Murchison Domain, Youanmi Terrane, Yilgarn Craton Western Australian Geological Survey, 19p.

Van Kranendonk M.J., 2008, New evidence on the evolution of the Cue-Meekatharra area of the Murchison Domain, Yilgarn Craton, Geological Survey of Western Australia Annual review for 2007–08, 39–49.

Van Kranendonk M.J., & Ivanic T.J., 2009, A new lithostratigraphic scheme for the northeastern Murchison Domain, Yilgarn Craton, Geological Survey of Western Australia, Annual review for 2008–09, 35–53.

Wang Q., 1998, Geochronology of the granite-greenstone terranes in the Murchison and Southern Cross Provinces of the Yilgarn Craton, Western Australia. Unpublished PhD Thesis, Australian National University, Canberra.

GOLD MINERALIZATION DURING GNEISS DOME EXHUMATION IN THE MESOARCHAEAN: THE BARBERTON GREENSTONE BELT, SOUTH AFRICA

A. Dziggel[1], M. Poujol[2], A.F.M. Kisters[3], A. Otto[1], M. Trieloff[4], W.H. Schwarz[4] & F.M. Meyer[1]

[1]Institute of Mineralogy and Economic Geology, RWTH Aachen University, Wuellnerstraße 2, 52062 Aachen, Germany
[2]Géosciences Rennes UMR CNRS 6118, Université Rennes 1, 35024 Rennes Cedex, France
[3]Department of Geology, University of Stellenbosch, Private Bag X1, Matieland, 7602 Stellenbosch, South Africa
[4]Institut für Geowissenschaften, Im Neuenheimer Feld 234-236, 66120 Heidelberg, Germany

Introduction

The Barberton greenstone belt in South Africa is one of a few Palaeo- to Mesoarchaean greenstone belts that host economically significant gold deposits older than ca. 3000 Ma (Goldfarb et al., 2001). The majority of gold deposits, including the Sheba and Fairview mines, occur along the southern contact of the ca. 3227 ± 1 Ma Kaap Valley pluton (Kamo and Davis, Figure 1), and are hosted by greenschist facies supracrustal rocks. In contrast to these greenschist facies deposits, the gold mineralization at the New Consort gold mine is situated in the immediate hanging wall of an exhumed, composite gneiss dome known as the Stentor pluton (Figure 1). The granitoid-greenstone contact is characterized by a major high-strain zone that separates the mid-crustal gneisses from the low grade greenstone belt. The mineralized shear zones are hosted by distinctly higher-grade metamorphic rocks, ranging from upper greenschist facies (ca. 520°C and 4 kbar) to upper amphibolite facies conditions (ca. 600-700°C and 6-8 kbar; Otto et al. 2007). The ore and alteration assemblages in the ore bodies change progressively with metamorphic grade, pointing to a causal relationship between the gold mineralization and the juxtaposition of the Stentor gneiss dome against

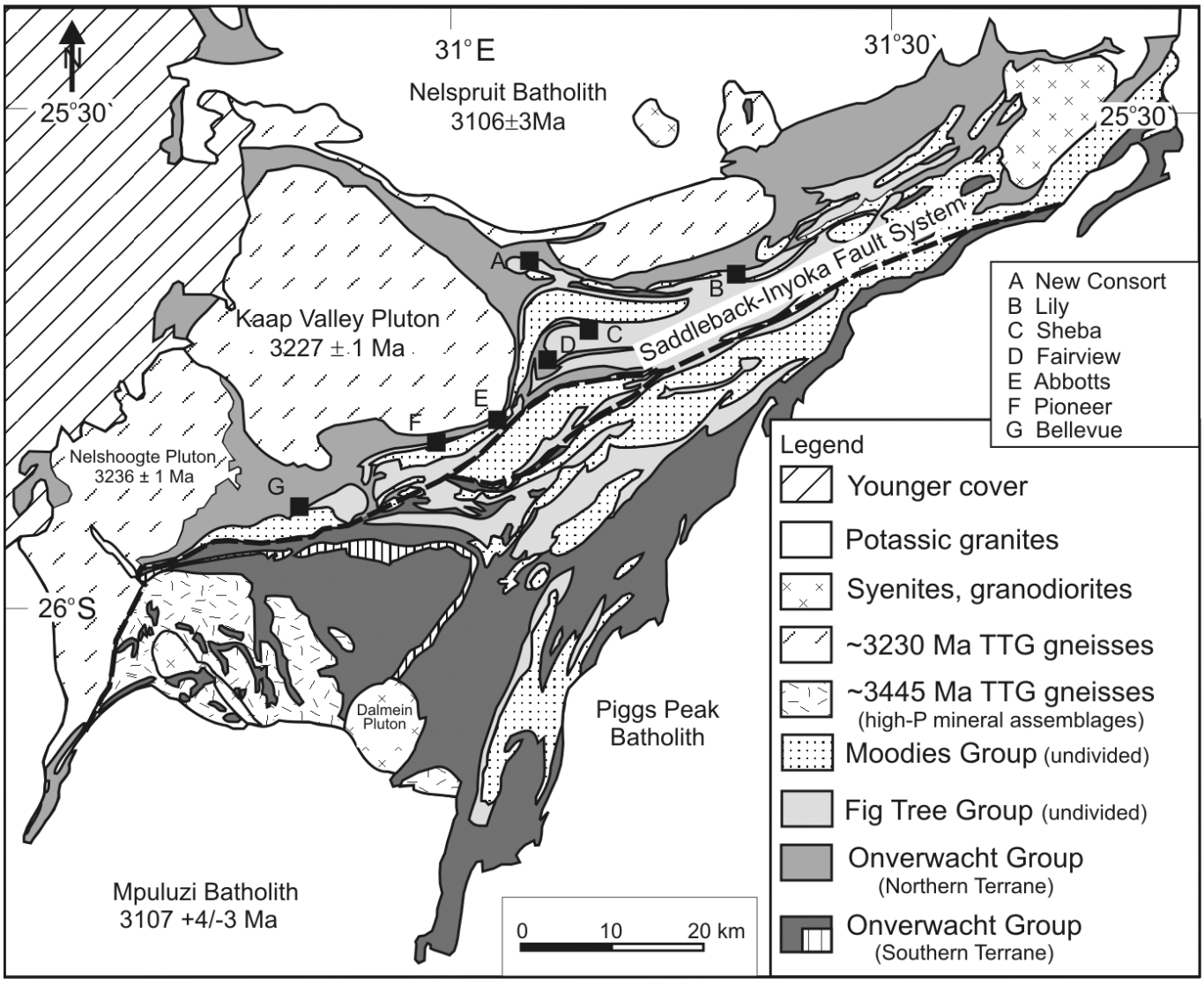

Figure 1. Geological map of the Barberton Mountain Land.

the overlying greenstone belt. In order to elucidate the timing relationships between regional metamorphism, gneiss dome exhumation, and the gold mineralization at the New Consort gold mine, we carried out U-Pb zircon and titanite and hornblende Ar-Ar dating.

Geological Setting

The ca. 3500-3200 Ma Barberton greenstone belt and surrounding granitoid terrane are situated in the eastern part of Mpumalanga Province, South Africa. The granitoid-greenstone terrain is characterized by a prolonged and polyphase tectono-magmatic history, and records major tectono-magmatic events at ca. 3450 Ma, 3230 Ma, and 3100 Ma (e.g., de Ronde and de Wit, 1994). Geochronological data indicate that the greenstone belt consists of at least two different terranes that are separated by the Saddleback-Inyoka fault system in the centre of the belt (Figure 1). The terrane juxtaposition is interpreted as a consequence of northwest-ward subduction and crustal convergence between ca. 3300 and 3230 Ma (de Ronde and de Wit, 1994; Moyen et al., 2006; Kisters et al., 2010), followed by extensional shearing and solid state doming of granitoid gneiss domes to the south and west of the greenstone belt (e.g., Kisters et al., 2003). Gold introduction has been interpreted to be temporally linked with the emplacement of a major suite of ca. 3100 Ma potassic, sheet-like granites (e.g., de Ronde and de Wit, 1994; Schoene et al., 2008). The age of the gold mineralization has been estimated based on a ca. ca. 3126 ± 21 Ma porphyry dyke that predates the greenschist facies mineralization at Fairview mine (Figure 1), and a ca. 3084 ± 18 Ma age for hydrothermal rutile from the same deposit (de Ronde et al., 1991).

The New Consort gold mine

Since the beginning of gold production in 1884, the New Consort gold mine has produced more than 2.1 million ounces of gold. Gold mineralization is mainly structurally controlled, and is associated with the so-called "Consort Bar", a relatively thin mylonitic shear zone at the contact between the amphibolites and ultramafic schists of the ca. 3280 Ma Ma Onverwacht Group and the overlying metapelites and metapsammites of the ca. 3260-3230 Ma Fig Tree Group. The supracrustal sequence has been folded into two major synclines, namely the 3 Shaft and Top Section Synclines (Figure 2). Three phases of deformation have been distinguished (e.g. Dziggel et al., 2006; Otto et al., 2007). It should be noted that the sequence of deformation events refers to the local structural evolution and does not correspond to any regional tectonic event. The earliest deformation event (D_1) is characterized by the development of a moderately south dipping S_{1A} foliation, and predates the gold mineralization. The PT-conditions of the D_1 formation have been estimated at ca. 600-700°C and 5 ± 1 kbar. Based on overprinting relationships, the S_1 folation has been subdivided into an early S_{1A} and a late S_{1B} stage. The early foliation characterizes the Stentor gneisses and immediately overlying amphibolite facies supracrustal rocks. It is associated with a mineral stretching lineation that plunges at shallow to moderate angles to the SW and W. Kinematic indicators within the gneisses suggest a top-to-the-southwest movement with a dextral strike slip component (Schoene et al., 2008). This early deformation has been interpreted to have formed due to syn- to post-collisional extensional shearing following the main accretionary event in the centre of the greenstone belt.

The S_{1B} foliation overprints the earlier fabric, and is best developed in a ca. 1 km wide, contact-parallel high-strain zone to the north of the Top Section Syncline (Dziggel et al., 2006; Figure 2). The initial shearing along the Consort Bar was coeval with this early deformation event. The S_{1B} foliation is generally parallel to S_{1A}, however, it is recorded in both amphibolites and retrograde greenschist facies mylonites. The L_{1B} lineation is either downdip, or plunges at shallow to moderate angles to the SE. The D_{1B} deformation has been linked to progressive unroofing and solid state doming of the Stentor gneisses. An early high-T mineralization in upper amphibolite facies rocks in the footwall of the Consort Bar correlates with this deformation event. This early mineralization is associated with loellingite and pyrrhotite, and the temperature of mineralization has been estimated at ca. 680 ± 25 °C.

The second and main stage of gold mineralization correlates with the local D_2 deformation. The D_2 deformation is marked by a reactivation of early structures and the development of the NNW trending, steeply dipping Shires shear zone system in the central parts of the mine. The ore bodies formed during this event are hosted by discrete mylonitic shear zones within, or in close vicinity to, the Consort Bar. In the deeper parts of the mine, the mineralized D_2 shear

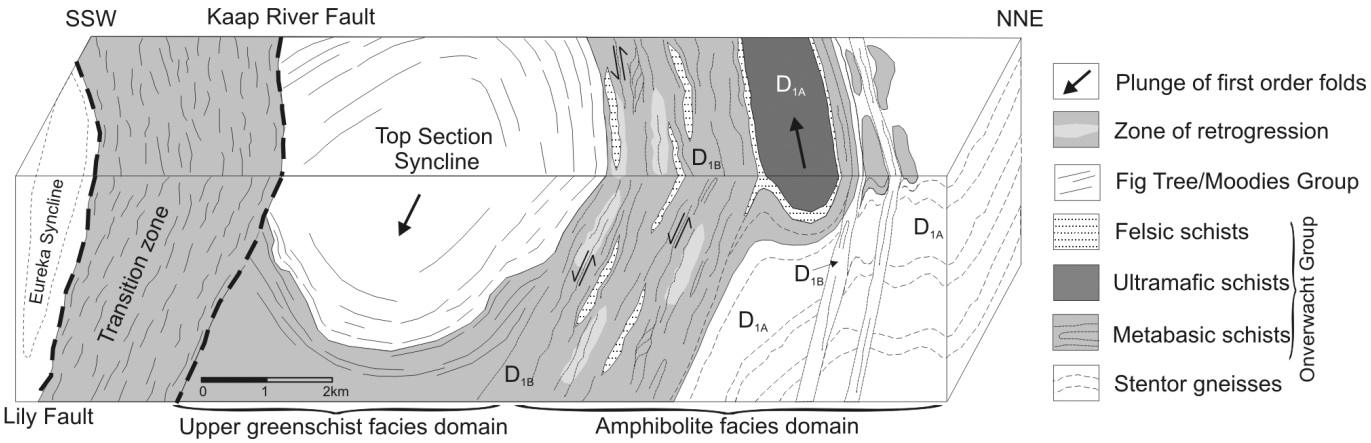

Figure 2. Geological cross-section though the granitoid greenstone contact at the New Consort gold mine.

zones are characterized by numerous synkinematic pegmatite dykes, indicating magmatism coeval with the mineralization. Petrological and thermometric data from the three main ore bodies indicate increasing temperatures with increasing structural depth, ranging from ca. 520°C in the Fig Tree Group, to ca. 600°C in the basal Onverwacht Group. The increasing temperatures are also indicated by a progressive change in sulfide assemblages, from arsenopyrite + pyrite + pyrrhotite in the structurally highest, to arsenopyrite + pyrrhotite + chalcopyrite + loellingite in the deeper parts of the mine (Otto et al., 2007). Significantly, the main stage of mineralization was syn-peak metamorphic with respect to the Fig Tree Group, but postdates the peak of metamorphism in the underlying Onverwacht Group.

Geochronology

In order to establish the timing of tectonic events in the mine area, several different approaches were used. U-Pb zircon dating of a late-tectonic granite intrusion crosscutting the earliest (D_{1A}) fabrics yields an age of 3250 ± 30 Ma. This age is, within error, similar to the terrane accretion event in the Barberton greenstone belt, suggesting that the early extensional shearing correlates with this event. Phase diagram modelling indicates that the early shearing was followed by near-isothermal decompression to conditions of ca. 500-600°C and 1-3 kbar (Dziggel et al., 2006). The retrogression is marked by the development of greenschist facies mylonites in the later high-strain belt, and by a partial replacement of the peak assemblage in the earlier deformation domain. U-Pb dating of retrograde titanite from an amphibolite from the earlier deformation domain gives an age of 3046 ± 27 Ma, suggesting that the final exhumation of the Stentor gneiss dome postdates the earlier shearing by ca. 200 million years. The age is also similar to a 3027 ± 7.5 Ma age on hydrothermal titanite from the mineralization in the footwall of the Consort Bar, as well as a ca. 3040 Ma Ar-Ar hornblende age (corrected for present decay constant bias, see e.g. Schwarz and Trieloff, 2007) for an amphibolite from the D_{1A} deformation domain. This suggests that 1) the extensional exhumation and gold mineralization were more or less contemporaneous, and that 2) ductile shearing was associated with a second metamorphic event that led to a complete resetting of the hornblende Ar-Ar age in the earlier deformation domain.

Conclusions

The gold mineralization at the New Consort gold mine was coeval with NE-SW extensional exhumation and solid state doming of the Stentor gneiss dome at ca. 3030-3040 Ma. This late-stage mineralization is considerably younger than the gold mineralization in the greenschist facies gold deposits of the Barberton greenstone belt, which has previously been dated at ca. 3080 Ma. In conjunction with previously published ages, the data indicate the gold mineralization in the Barberton greenstone belt to have occurred during, at least, two mineralization episodes at ca. 3080 Ma and 3040 Ma. The data point to a prolonged period of hydrothermal activity during the end of an either protracted or episodic structural and thermal evolution that may have lasted some 200 million years.

Acknowledgements

The management of Barberton Mines Ltd. is thanked for access to underground workings and sample material. Marc Poujol thanks Mike Tubrett for his assistance during ICP-MS data acquisition. Alex Otto acknowledges support from the German Academic Exchange Service (DAAD) and the Society of Economic Geology.

References

de Ronde C.E.J. & de Wit M.J., 1994, Tectonic history of the Barberton greenstone belt, South-Africa - 490 million years of Archean crustal evolution, Tectonics, 13, 983–1005.

Dziggel A., Knipfer S., Kisters A.F.M. & Meyer F.M., 2006, P-T and structural evolution during exhumation of high-T, medium-P basement rocks in the Barberton Mountain Land, South Africa, Journal of Metamorphic Geology, 24, 535–551.

Goldfarb R.J., Groves D.I. & Gardoll S., 2001, Orogenic gold and geologic time: a global synthesis, Ore Geology Reviews, 18, 1-75.

Kamo S.L. & Davis D.W., 1994, Reassessment of Archaean crustal development in the Barberton Mountain Land, South Africa, based on U-Pb dating, Tectonics, 13, 165–192.

Kisters A.F.M., Stevens G., Dziggel A. & Armstrong R.A., 2003, Extensional detachment faulting at the base of the Barberton greenstone belt: evidence for a 3.2 Ga orogenic collapse, Precambrian Research, 127, 355–378.

Kisters A.F.M., Belcher R.W., Poujol M. & Dziggel A., 2010, Continental growth and convergence-related arc plutonism in the Mesoarchaean: evidence from the Barberton granitoid-greenstone terrain, South Africa, Precambrian Research, in press.

Moyen J.F., Stevens G. & Kisters A.F.M., 2006, Record of mid-Archaean subduction from metamorphism in the Barberton terrain, South Africa, Nature, 442, 559–562.

Otto A., Dziggel A., Kisters A.F.M. & Meyer F.M., 2007, The New Consort gold mine, Barberton greenstone belt, South Africa: Orogenic gold mineralization in a condensed metamorphic profile, Mineralioum Deposita, 42, 715–735.

Schoene B., de Wit M.J. & Bowring S.A., 2008, Mesoarchean assembly and stabilization of the eastern Kaapvaal craton: a structural-thermochronological perspective, Tectonics, 27, doi:1029/2008TC002267.

Schwarz W.H. & Trieloff M., 2007, Revising the K decay constant, Meteoritics and Planetary Science, 42, A138.

METAMORPHISM, FLUID DYNAMICS AND GOLD MINERALISATION, EASTERN GOLDFIELDS OF W.A.

R.K. Fagan

Department of Mining Geology, W.A. School of Mines, Locked Bag 22, Kalgoorlie Western Australia 6433

Regional metamorphic isograd patterns for the largely distal marine Archaean greenstone succession in the Eastern Goldfields of W.A., provide some useful insights into the fluid dynamics of regional metamorphism and late-stage gold mineralisation in this world-scale gold province. Metamorphic grades vary from sub-greenschist facies up into the high-grade granulite facies, in a largely post-tectonic regional scale metamorphic event. Metamorphic thermal gradients and the resulting three dimensional metamorphic zonal sequences vary systematically, reflecting a range of geothermal gradients, geometrically arranged about a number of thermal highs and lows which in turn reflect the systematic but irregular distribution of up-welling and down-welling geothermal convective cells respectively in this substantial crustal block.

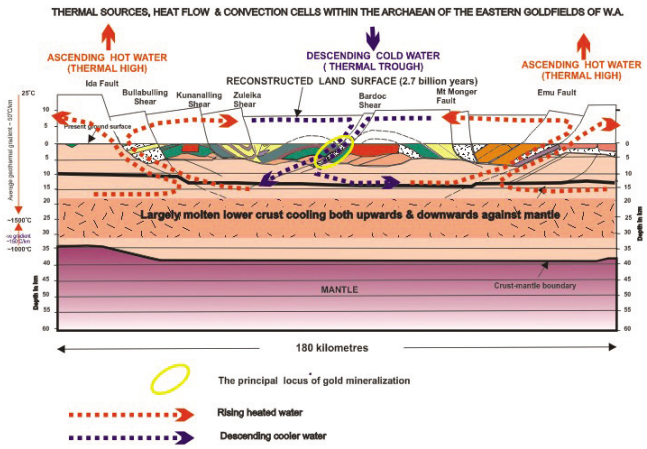

Figure 1. An East-West Reconstruction of the Archaean Crust Section North of Kalgoorlie along the 1994 Seismic Line.

In excess of seven metamorphic zones in pelitic assemblages are defined ranging from prehnite-pumpellyite facies through to the sillimanite-K-feldspar zone of the amphibolite facies. Granulite facies conditions may also be presented and are generally restricted to narrow bands representing the bases of more deeply unroofed keel structures. The overall geothermal gradient of 50°C/km is the equivalent of that experienced in high heat-flow regions such as present day volcanic arc environments and evidence is presented that suggests that this may well have been widespread and the continental norm in the late Archaean. The metamorphic gradients however range from around 25°C/km to around 75°C/km about fairly regularly distributed crustal hot and cold spots. The resulting metamorphic zonal sequences vary systematically around these widely spaced thermal highs and lows in what appears to be a substantial, very thick, dominantly marine sequence that was metamorphosed after having been obducted and shunted several hundred kilometres over an adjacent very thick and very hot Archaean emergent continental crustal block. Extrapolation of radiogenic elemental abundances in continental crusts back into the Late Archaean provides convincing arguments supporting these significantly elevated temperatures as a likely norm for continental crustal slabs of these dimensions and age.

In three dimensions the isograd and metamorphic zonal distribution is one of a series of very low amplitude, (higher grade) domes and (lower grade) basins, situated above the locus of crustal thermal highs and lows respectively (Figure 1). These in turn reflect the distribution of crustal-scale hydrothermal convection cells, controlled in large part by the distribution of regional fault systems transecting a continental crust substantially heated from within by the four-fold enrichment of radiogenic potassium that existed at this time (two half lives ago).

Under the described geothermal convective cell geometry, fluid flow in the upper portions of the convection cells would be from high-metamorphic grade (up-welling) sites to low metamorphic grade (down-welling) sites and in the reverse in the lower crustal portions of these convection cells. The predominance of giant-scale gold deposits (million ounce plus deposits) in the lower metamorphic grade regions of the Eastern Goldfields suggests that the gold mineralising fluids were descending in down-welling convection sites at the time of mineralisation and not ascending and cooling as is the more generally accepted model of mesothermal gold deposition. This would require a precipitation mechanism in keeping with fluid descent rather than ascent.

Since the late Archaean some 10-15 km of the upper crust has been removed by erosion. Most of this erosion followed quickly after orogeny and uplift of a substantial mountainous terrene as the largely marine Archaean sequence was pushed up and over an adjacent continental crustal slab, and was multiply deformed and regionally metamorphosed. Much of the extensive erosion responsible for the present subdued landscape dates from this period.

PLATINUM-GROUP ELEMENT GEOCHEMISTRY OF MINERALIZED AND NON-MINERALIZED ARCHAEAN AND PROTEROZOIC KOMATIITES AND BASALTS

M. Fiorentini[1], S.J. Barnes[2], C. M. Lesher[3], G. Heggie[1], R.R. Keays[3,4] & O.M. Burnham[3,5]

[1]Centre for Exploration Targeting, University of Western Australia, Crawley, WA 6009, Western Australia
[2]CSIRO Earth Science and Resource Engineering, Kensington, Perth, 6151 Western Australia
[3]Mineral Exploration Research Centre, Department of Earth Sciences, Laurentian University, Sudbury, Ontario P3E2C6 Canada
[4]School of Geosciences, Monash University, Melbourne, Victoria 3800, Australia
[5]Ontario Geoscience Laboratories, Sudbury, Ontario P3E6B5 Canada

Introduction

The magmatic hypothesis for the formation of Ni-Cu-(PGE) deposits requires that a sulfide melt reacts with a silicate magma, and that this process depletes the silicate magma in highly chalcophile elements such as Co, Ni, Cu, and the platinum-group elements (PGE) to varying degrees (see review by Naldrett, 2004). The sulfide melt may segregate directly from the magma, but in most cases sulfur is derived from crustal rocks by devolatilization, incongruent melting, or wholesale melting (Lesher et al., 1984). The PGE are particularly sensitive to depletion during equilibration with sulfide melt owing to their extremely high partition coefficients, as measured experimentally (Fleet & Stone, 1991; Fonseca et al. 2009) and inferred from the composition of natural sulfide ore magmas (Campbell & Barnes, 1984; Peach and Mathez, 1996; Barnes & Lightfoot 2005). A number of studies over the last 25 years have used the differential partitioning of PGEs into sulfides as the basis for lithogeochemical indicators of sulfide saturation and segregation (Barnes et al., 1988. Keays, 1995; Maier et al., 1998).

The abundances and distribution of PGE in mafic and ultramafic melts are influenced by a complex combination of factors, including the silicate:sulfide mass ratio (Campbell & Naldrett, 1979), the compositions and abundances of other phases in the system (Lesher & Burnham, 2001), the physical volcanology and nature of the ore-forming process (Lesher et al., 2001) and their influence on temperature, composition, fO_2/fS_2, and metal partitioning (Fiorentini et al., 2004; Lesher & Campbell, 1993), alloy saturation effects (Barnes & Fiorentini, 2008; Puchtel et al., 2004), and secular evolution of the mantle source composition (Maier et al., 2009).

Localized PGE depletion has been recognized in several mineralized areas (cf. Fiorentini et al., 2010), including Noril'sk, Perseverance, Kambalda, Raglan, Thompson, and the Abitibi belt, but PGE depletion was not observed at Black Swan. This methodology has also been applied to the evaluation of flood basalt sequences in Greenland and China, and to intrusive and extrusive suites in the Svecofennian Vammala and Kotalahti belts in Finland. These studies have shown that PGE depletion is generally very local and restricted to specific units, indicating that most mafic-ultramafic magmas are undersaturated in sulfide on eruption and that the observed PGE depletion is related to localized syn-eruption equilibration with externally-derived sulfide melts within very restricted parts of the volcanic system.

Fiorentini et al. (2008) looked into the variability of ruthenium in sulfide-saturated and undersaturated chromite-saturated komatiites. This approach relied on the idea that ruthenium is highly chalcophile but also displays some degree of compatibility in chromite (e.g. Fiorentini et al., 2004). Accordingly, the Ru content of chromites from sulfide-saturated and undersaturated systems should be different and detectable, as borne out by the presence of elevated levels of Ru in chromite-rich rocks from barren komatiitic cumulates.

Identifying the spatial and genetic relationship between PGE variation and Ni-Cu-(PGE) mineralization requires 1) a large quantity of high-quality whole-rock PGE analyses from systems displaying a wide range of ages, locations, tectonic and volcanic settings, and Ni-Cu-(PGE) mineralization styles and endowments in order to establish the expected "background" PGE concentrations (Lesher & Campbell, 1993; Maier et al., 2009); 2) careful geological control on sampling, recognizing the dynamic channelized nature of magmatic ore-forming systems (Lesher et al., 2001), and 3) advances in our basic understanding of PGE geochemistry, particularly the factors influencing the partitioning of PGE into silicates, sulfides, and alloys.

This paper presents a large body of new data on the PGE abundances of mineralized and non-mineralized komatiites, komatiitic basalts, and basalts, focusing on komatiites and komatiitic basalts associated with Type I (stratiform basal massive-disseminated) and Type II (stratabound internal disseminated) Ni-Cu-(PGE) deposits (Arndt et al., 2008; Lesher et al., 2001). The principal objective is to establish the validity and effectiveness of using PGE depletions/enrichments as regional and local scale vectors toward Ni-Cu-(PGE) mineralization.

The new data set incorporates high-precision PGE analyses of komatiites, komatiitic basalts, and high-Fe komatiites from non-mineralized and variably mineralized belts and terranes, including newly-generated data for the Proterozoic Raglan and Thompson Nickel Belts in Canada and the Eastern Goldfields

Superterrane in Western Australia, and other high-quality data on komatiites and basalts from a wide range of other published sources. Baseline PGE concentrations in non-mineralized komatiites for different komatiite types from different ages and localities have been established by Maier et al. (2009).

For this approach to be of practical use in Ni-Cu-PGE exploration, it is essential that it should work in areas of sparse data availability, where magmatic sulfides have not already been sampled within potentially mineralized host rocks. In other words, PGE anomalies must be recognizable in rocks which otherwise display no indication of presence of magmatic sulfides. It is also desirable that PGE lithogeochenmistry should provide haloes of anomalism within mineralized systems which extend beyond the extent of accumulated sulfides; this would then permit PGE data to be used as a vector towards ore, more effective than relying purely on Ni or S anomalism. The data set used in this study has been filtered with this in mind, as discussed in more detail below.

Discussion and conclusions

Platinum-group element depletion associated with Ni-Cu-(PGE) ore-forming processes is recorded in host rocks to a number of deposits. However, PGE depletion is not as common as expected: generally, samples displaying extreme degrees of PGE depletion represent less than ten per cent of any given data set from any location. In addition, a number of mineralized komatiite suites, Black Swan being a prime example, record no evidence of depletion at all. In addition, the degree of PGE depletion is commonly less than expected based on modeling and on experimentally-derived D values.

The most notable features related to a sulfide segregation PGE signal in magmatic systems are 1) the high degree of PGE concentration scatter in any given data population, in the absence of sulfide-rich samples, with both highly depleted and enriched values spanning various orders of magnitude; and 2) the geochemical co-variance of all PGE. However, different PGE signatures are found at different localities. The common occurrence of false negatives exposes the limitations of the application of a whole-rock PGE-based lithogeochemical method in exploration. No depletion signal at all is observed for certain deposits, which in most cases (such as Black Swan) are high-R factor systems where the volume of sulfide liquid was very small compared with the volume of the host komatiite flow field.

Platinum-group element enrichment signals are commonly recognized from known ore environments in S-poor samples lacking detectable Ni anomalism. Such samples are typically more common and aerially widespread than depleted samples, and in many cases extend some hundreds of meters beyond the limits of known mineralization, thus serving to enlarge the immediate geochemical halo around a deposit.

If we consider mineralized versus unmineralized belts as a whole, then with a sufficiently large population of samples it is possible to discriminate prospectivity. The Agnew-Wiluna greenstone belt and the southern Kalgoorlie terrane of the Yilgarn Craton both show distinct signals of PGE enrichment and depletion. The Raglan greenstone belt in particular stands out, particularly in the presence of PGE depletion within the unmineralized basaltic section of the stratigraphy. This signal extends well beyond the ore-bearing units and would be a significant prospectivity indicator in the absence of detailed knowledge of the ore-bearing horizon.

These results are significant in re-enforcing the conclusion that komatiites are almost universally sulfide-undersaturated on eruption (or emplacement into near-surface intrusions) and that mineralization processes are restricted to highly localized environments in dynamic magma conduits and feeder pathways. The ultramafic rocks now found closely associated with the ores represent undepleted magmas unrelated to the ore-forming process, subsequently juxtaposed with the previously-formed ore as a result of continuing flow through the same conduit. Depleted magmas representing the distal ends of mineralizing systems are evidently very rare, or at least are very rarely sampled. This is not surprising in view of the relatively low R factors associated with komatiite-hosted deposits, which imply that the volume of magma interacting with sulfide liquid is typically very small compared with the overall volume of komatiite flow fields.

The komatiite data provide a template for applying discriminants of sulfide-related PGE depletion to basalts. Tholeiitic and komatiitic basalts show a more complex pattern of variation, which can broadly be divided into three categories: consistent PGE depletion at high Mg#, increasing PGE depletion with decreasing Mg#, and scattered PGE depletion uncorrelated with a range of Mg#. We interpret as the result of the three processes of, respectively, source saturation and retention of sulfide in the mantle (MORBs); “cotectic saturation”, found mostly in LIP-related basalts; and post-eruption ore-forming sulfide assimilation and segregation (Raglan komatiitic basalts) as outlined above. Superimposed on the cotectic trend are signals of episodic batch sulfide segregation in the case of the Greenland and Siberian LIP flood basalt suites.

Acknowledgements

This research was supported through grants by AMIRA, MERIWA and ARC to SJB, MF and GH, two CAMIRO grants to CML and RRK, and NSERC grants to CML and RRK. We are very grateful to Inco (now Vale Inco), Falconbridge (now Xstrata), Billiton and WMC Resources (now BHP-Billiton), Independence Group, Noril’sk Nickel Australia and Hudson Bay Exploration (now Anglo-American) for supporting the project and providing access to mines, exploration properties, and diamond drill cores. We have benefited greatly from discussions with many colleagues. The manuscript greatly benefitted from the insightful and thorough reviews of Steve Beresford and Sarah-Jane Barnes.

References

Arndt N.T., Lesher C.M. & Barnes S.J., 2008, Komatiite: Cambridge, Cambridge University Press, 467p.

Barnes Sarah.-J., Boyd R., Nilsson L.P., Often M., Pedersen R.B., & Robins, B., 1988, The use of mantle normalisation and metal ratios in discriminating between the effects of partial melting, crystal fractionation and sulphide segregation on platinum group metals, gold, nickel and copper: examples from Norway, in *Geo-Platinum '87*, Prichard H.M., Potts P.J., Bowles J.F.W., & Cribbs, S.J., eds, London, Elsevier Science Publishers Ltd., 113–139.

Barnes, Sarah-J., & Lightfoot, P.C., 2005, Formation of magmatic nickel sulfide deposits and processes affecting their copper and platinum-group element contents, Economic Geology 100th anniversary volume, 179–214.

Barnes, Stephen J. & Fiorentini, M.L., 2008, Iridium, ruthenium and rhodium in komatiites: Evidence for iridium alloy saturation, Chemical Geology, 257, 44–58.

Campbell I.H. & Barnes S.J., 1984, A model for the geochemistry of the platinum-group elements in magmatic sulphide deposits, Canadian Mineralogist, 22, 151–160.

Campbell I.H. & Naldrett A.J., 1979, The influence of silicate:sulphide ratios on the geochemistry of magmatic sulphides, Economic Geology, 74, 503–1505.

Fiorentini M.L., Barnes S.J., Lesher, C.M., Heggie, G.J., Keays, R.R., & Burnham, O.M., 2010, Platinum-group element geochemistry of mineralized and non-mineralized komatiites and basalts, Economic Geology, accepted.

Fiorentini M.L., Beresford S.W. & Barley M. E., 2008, Ruthenium-chromium variation, a new lithogeochemical tool in the exploration for komatiite-hosted Ni-Cu-(PGE) deposits, Economic Geology, 103, 431–437.

Fiorentini M., 2004, PGE geochemistry of komatiites, Agnew-Wiluna Belt (WA): implications for NiS ore genesis and composition of the Archaean mantle, University of Western Australia, 280p.

Fleet,M.E., Stone W.E. and Crocket J.H., 1991, Partitioning of palladium, iridium and platinum between sulfide liquid and basalt melt: effects of melt composition, concentration and oxygen fugacity, Geochimica et Cosmochimica Acta, 55, 2545–2554.

Fonseca R.O.C., Campbell I.H., O'Neill H.S.C. & Allen, C.M., 2009, Solubility of Pt in sulphide mattes: Implications for the genesis of PGE-rich horizons in layered intrusions, Geochimica et Cosmochimica Acta., 73, 5764–5777.

Keays R. R., 1995, The role of komatiitic and picritic magmatism and S-saturation in the formation of ore deposits, Lithos, 34, 1–18.

Lesher C.M., & Burnham O.M., 2001, Multicomponent elemental and isotopic mixing in Ni-Cu-(PGE) ores at Kambalda, Western Australia, Canadian Mineralogist, 39, 421–446.

Lesher C. M., Burnham O.M., Keays R.R., Barnes S.J. & Hulbert L., 2001, Trace-element geochemistry and petrogenesis of barren and ore-associated komatiites, Canadian Mineralogist, 39, 673–696.

Lesher C. M., and Campbell I. H., 1993, Geochemical and fluid dynamic modeling of compositional variations in Archean komatiite-hosted nickel sulfide ores in Western Australia, Economic Geology, 88, 804–816.

Lesher C.M., Arndt N.T. & Groves D.I., 1984, Genesis of komatiite-associated nickel sulphide deposits at Kambalda Western Australia: a distal volcanic model, in *Sulphide deposits in mafic and ultramafic rocks*, Buchanan D.L., & Jones, M.J., eds, London, Institute of Mining and Metallurgy, 70–80.

Maier W.D., Barnes, Stephen J., Campbell I.H., Fiorentini M.L., Peltonen P., Barnes Sarah-J. & Smithies, H., 2009, Mantle magmas reveal progressive mixing of meteoric veneer into the early Earth's deep mantle, Nature, 460, 620–623.

Maier W.D., Barnes Sarah-J. & Dewaal, S.A., 1998, Exploration for magmatic Ni-Cu-PGE sulphide deposits - a review of recent advances in the use of geochemical tools, and their application to some South African ores, South African Journal of Geology, 101, 237–253.

Naldrett A.J., 2004, *Magmatic Sulfide Deposits: Geology, Geochemistry and Exploration*, Heidelberg, Springer, 727p.

Peach C.L. & Mathez E.A., 1996, Constraints on the formation of platinum-group element deposits in igneous rocks, Economic Geology, 91, 439–450.

Puchtel I.S., Humayun M., Campbell A.J., Sproule R.A., Lesher C. M., 2004, Platinum-group element geochemistry of komatiites from the Alexo and Pyke Hill areas, Ontario, Canada, Geochimica Et Cosmochimica Acta, 68, 1361–1383.

DEFORMATION/MINERALIZATION COUPLING WITHIN THE MURCHISON GREENSTONE BELT, SOUTH AFRICA: FROM TECTONICS TO STRUCTURAL TRAPS

D. Gapais[1], J. Jaguin[1], P. Boulvais[1], M. Poujol[1] & G. Ruffet[1]

[1]Géosciences Rennes, UMR CNRS 6118, Université de Rennes 1, Campus de Beaulieu, 35042 Rennes Cedex, France

Introduction

The study of structures within greenstone belts and surrounding gneissic basement is a first-order tool to understand deformation modes that operated during Archaean times. Furthermore, these domains host some of the main ore deposits, which emphasizes the importance of providing constrains to better understand how structures may have controlled mineralization processes. The study area, the Murchison Greenstone Belt, hosts large Sb deposits mined in different locations along a linear structure, the so-called Antimony line, as well as VMS-type copper-zinc and emerald mineralization.

Geological setting

The 3.09-2.97 Ga old east-northeast-trending Murchison Greenstone Belt (MGB), located within the Kaapvaal Craton of southern Africa, is a volcanic and sedimentary belt that can be traced from the Drakensberg Escarpment to the west, for a distance of some 140km to the east where it is truncated by Phanerozoic Karoo rocks of the Lebombo Range (Fig. 1). Five units can be recognized from north to south, corresponding to different crustal level (Vearncombe, 1987):

1. The Rooiwater Complex is a thick layered igneous complex of mainly gabbros and anorthosites metamorphosed in the greenschist to amphibolite facies. The Complex is considered as a 2.74 Ga mafic intrusion that emplaced tectonically into its present position (Poujol et al., 1996).
2. The Silwana amphibolites represent strongly deformed hornblende-plagioclase-epidote schists (Frippe et al, 1980) whose age is still unknown.
3. The Rubbervale Formation is made of quartz schists, silicified tuffs and felsic lavas that were metamorphosed in the greenschist facies. This unit is pervasively deformed and was dated at 2.971±10 Ga (Poujol et al, 1996). It hosts VMS type deposits that formed the so-called Copper-Zinc-Line (Schwarz-Schampera et al., 2010).
4. The Murchison low-grade (greenschist facies) ultramafic, mafic, carbonated and metasedimentary schists, cover a large part of the belt. They host the narrow ENE trending Antimony Line where antimony-gold deposits occur. Volcanic rocks of the Weigel Formation were dated at 3.087 ±10 Ga (Poujol, 1996).
5. The La France Formation is a domain made of two main types of rocks, fushitic quartzites and aluminous quartz-mica schists affected by amphibolite-facies metamorphism.

The Murchison belt is in contact with the Groot-Letaba gneiss to the north. Its southern border is marked by leucogranites that intrude both the belt and the surrounding ca. 3.063 Ga Makhutswi gneisses (Poujol & Robb, 1999).

Structural patterns

The MGB is a narrow elongate and long structure (140 km × 20 km) trending ENE with greenschist facies rocks in the center and amphibolite facies rocks in both the northern and southern parts of the belt (Silwana amphibolites and La France Formation, Block & Moyen, this volume).

The belt is marked by a strong and pervasive foliation. Strain estimates by Vearncombe et al. (1992) yielded amounts of shortening between 40% and 75 % is strongly marked with shortening between 41% and 75% (Vearncombe et al, 1992). Foliation planes strike around ca. 80°N, with generally steep dips ranging from 52° to 90° (Vearncombe et al, 1992). The foliation bears a stretching lineation that is generally steeply plunging (lineation pitch mostly higher than 50°). Similar structures are observed in the gneisses to the north of the belt. Foliations and lineations are associated with sinistral-transpressional (top to the south) shear sense indicators throughout the belt.

Structures within Archaean greenstone belts and Palaeoproterozoic deformation belts have been often interpreted in terms of initially flat foliations associated with nappe emplacement that were subsequently transposed into steeply dipping fabrics (e.g. Bleeker, 1991; Choukroune et al. 1997).

Alternatives models have emphasized the first order involvement of the thermal state of the lithosphere on structure that may develop during compression (see reviews in Chardon et al., 2009 and Gapais, 2009). They in particular argued that a weak and hot lithosphere favoured distributed homogeneous crustal shortening combined with downward motion of the upper crust into the weak material leading to dome and basin geometries (Cagnard et al, 2006; Chardon et al., 2009). Several arguments may support this interpretation for the MGB.

- The overall geometry, with a narrow and long greenstone belt quenched between two gneissic basements, which does straightforward suggest thrust and nappe tectonics.
- The overall asymmetric synformal geometry (Viljoen

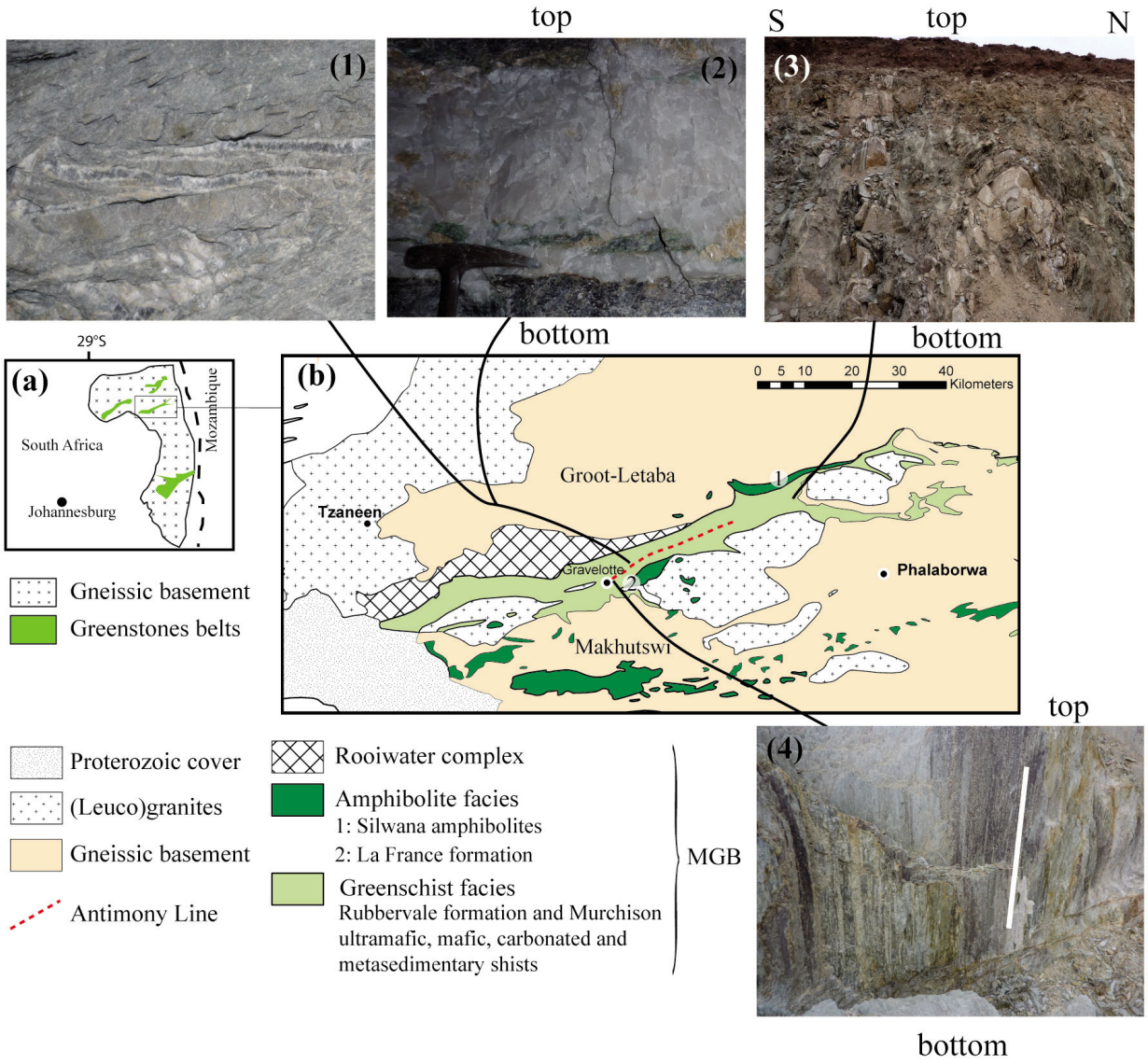

Figure 1. (a) Localisation of the MGB on the east part of the Kaapvaal Craton (b) Map of the belt and surroung gneisses and granitoids. Also presented pictures: (1) tension tracks filled by Quartz and Stibnite in greenschist (1-2 cm wide) (2) massive quartz-carbonate-fuschite vein (3) Fold within schistose greenschist (4) steeply plunging stretching lineation (underline in white) in greenschist, Malati Pump.

et al, 1978), with central greenschist facies units bounded by amphibolite facies ones that suggest downward relative motions of the central part of the belt.

- Distributed deformations throughout the belt.
- Steeply dipping foliations.
- Steeply plunging lineations.

In addition, as observed in many Archaean or Palaeoproterozoic belts, the lastest structures are compressive, with no evidence for syn- to post-thickening extension.

During the deformation, two-mica granites emplaced to the south of the MGB. Consistently, some of them show well-developed SC fabrics (Berthé et al, 1979) that attests for syn-cooling deformation (Gapais, 1989) with top to the south motion. These granites will be dated both by ^{40}Ar-^{39}Ar and U-Pb in order to get information on the age of the deformation.

Deformation/mineralization relationships

Mineralization in antimony (mostly stibnite) is hosted along the 35 km long and 250m wide Antimony Line that corresponds to a major shear zone (Vearncombe et al, 1987) located in the core of the belt. At the outcrop scale, mineralization occurs principally in quartz-carbonate veins within carbonates and talc rocks (Vearncombe et al, 1992). The underground observations show that there are at least two different generations of veins, some early deformed veins folded or boudinaged in the foliation, and late veins cross-cutting the foliation at high angle. According to Boocock (1984) and Maiden & Boocock (1984), the dominant style of mineralization occurs in early brittle fractures (syn-D1, Boocock, 1984; Vearncombe et al, 1992), but minor mineralization are found disseminated or in a wide range of vein types (pre-D1 to post-D2 of Vearncombe et al, 1992). So precipitation of stibnite must have occurred during rather a long time span. Besides, authors have suggested a hydrothermal character of the deposits with several potential origins

for the fluid: either seawater or magmatic (Smith, 1986; Boese 1964) or metamorphic fluid (Pearton & Viljoen, 1986; Willson & Viljoen, 1986), or fluids related to the emplacement of granitic bodies within the antimony line (Kedda et al, 1990, Poujol et al, 1997).

The position of the late veins that have a high angle with the foliation, with tension gashes orientations, underlines the direct link between spaces created by deformation and mineralization. The Antimony Line acted as structural traps for the mineralizing fluid(s), likely associated with fluid channeling along this localized shear zone (Boese, 1964). The Antimony line is marked by the local development of subhorizontal stretching lineation associated with sinistral strike-slip components. This underlines that the Antimony line is a shear zone where strike-slip components concentrated during progressive deformation. Strain localization and preferred fluid channeling within the Antimony line must be closely related processes.

^{40}Ar-^{39}Ar of fuschitic metasomatism associated with the mineralizing fluids will allow us to specify the relationships between fluid circulation and regional geological events (deformation, magmatism, metamorphism), especially by comparing these ages with the U-Pb ages obtained on the granitoid intrusions within the Antimony Line and to the south of the belt. Combined C and O isotopes analyses on quartz-carbonates veins and host rocks will allow us to constrain the rock-fluids interactions and the source(s) of the fluid(s).

References

Barton J.M., 1984, Timing of ore emplacement and deformation, Murchison and Sutherland greenstones belts, Kaapvaal Craton, in Gold 82: the geology, geochemistry and genesis of gold deposits, Foster R.P. ed, Proceedings of the symposium gold 82, University of Zimbabwe, 629–644.

Berthe D., Choukroune P. & Jegouzo P., Orthogneiss, mylonite and non coaxial deformation of granites: the example of the South Armorican Shear Zone, in Journal of Structural Geology, 1, 31-42.

Bleeker W.,1990, Newstructural-metamorphic constraints on Early Proterozoic oblique collision along the Thompson Nickel Belt, Manitoba, in Geological Association of Canada, Special Paper 37, 57–73.

Block S. & Moyen J.-F., 2010, the Murchison Greenstone Belt, South Africa: Accreted Slivers with contracting metamorphic conditions, this volume.

Boese R., 1964, Die Antimoglanzgänge von Gravelotte in der Murchison Range on Nordost-Transvaal, PhD thesis, University of Hamburg, 85p.

Boocock C.N., 1984, Ore genesis along the Antinomy Line, Murchison Range, North-eastern Transvaal, M.Sc. thesis, University of the Witwatersrand, 193p.

Cagnard F., Brun J.-P. & Gapais D., 2006, Modes of thickening of analogue weak lithospheres, Tectonophysics, 421, 145–160.

Chardon D., Gapais D. & Cagnard F., 2009, Flow of ultra-hot orogens: A view from the Precambrian, clues for the Phanerozoic, Tectonophysics, 477, 105–118

Choukroune P., Ludden J.N., Chardon D., Calvert A.J. & Bouhallier H., 1997, Archaean crustal growth and tectonic processes: a comparison of the Superior Province, Canada and the Dharwar craton, India, in Orogeny through Time, Burg J.-P. & Ford M., eds, Geological Society of London, Special Publication 121, 63–98.

Fripp R.E.P., Van Nierop D.A. & Callow M.J., Lilly P.A. & Du Plessis L.U., 1980, Deformation in part of the Archaean Kaapvaal Craton, South Africa, Precambrian Research, 13, 241–251.

Gapais D., 1989, Shear structures within deformed granites: Mechanical and thermal indicators, Geology, 17, 1144–1147.

Gapais D., Cagnard F., Gueydan F., Barbey P. & Ballèvre M., 2009, Mountain Building and exhumation processes through time: inferences from nature and models, Terra Nova, 21, 188–194.

Jaguin J., Moyen J.-F., Boulvais P. & Poujol M., 2010, Mid-Archaean granites south of the Murchison Greenstone Belt, South Africa: the oldest large biotite-muscovite leucogranites bodies, this volume.

Kedda S. W., Robb L.J., Meyer F.M. & Verhagen B.T., 1990, Gold mineralization associated with albitized felsic intrusions in the Murchison greenstone belt, South Africa, in 3rd IAS Abstracts volume, Perth, Australia.

Maiden K.J. & Boocock C.N., 1984, Deformational and metamorphic features of antimony ores of the Murchison Antimony line, north-eastern Transvaal, Transactions of the Geological Society of South Africa, 87, 327–333.

Pearton T.N. & Viljoen M.J., 1986, Antimony mineralization in the Murchison greenstone belt – an overview, in Mineral Deposits of Southern Africa, Anhaeusser C.R. and Maske S., eds, Geological Society of South Africa, 293–320.

Poujol M., Robb L.J., Respaut J.P. & Anhaeusser, C.R., 1996, 3.07-2.97 Ga Greenstone Belt formation in the northeastern Kaapvaal Craton: Implications for the origin of the Witwatersrand Basin, Economic Geology, 91(8): 1455–1461.

Poujol M., Respaut J.P., Robb L.J., Anhaeusser C.R., 1997, New U-Pb and Pb-Pb data on the Murchison greenstone belt, South Africa and their implications for the origin of the Witwatersrand Basin, Information circular No 319, Economic Geology research Unit, University of the Witwatersrand, Johannesburg.

Poujol M., 2001, U-Pb isotopic evidence for episodic granitoid emplacement in the Murchison greenstone belt, South Africa, Journal of African of Earth Sciences, 33, 155–163.

Schwarz-Schampera U., Terblanche H. & Oberthür, T., 2010, Volcanic-hosted massive sulfide deposits in the Murchison greenstone belt, South Africa, Mineralium Deposita, 45(2), 113–145.

Smith H.S., 1986, Evidence from δ13C and δ18O isotopes in carbonate minerals for the origin of fluids in Archaean greenstone belt metamorphic and mineralization processes, Extended Abstracts, Geocongress 1986, Johannesburg : Abstract volume of the Geological Society of South Africa, 341–344.

Vearncombe J. R., Jr, Cheshire P. E., De Beer J. H., Killick A., Mallison W.S., McCourt S. & Stettler E.H., 1987, Structure related to the Antimony Line, Murchison schist belt, Kaapvaal Craton, South Africa, in Tectonophysics, 154, 285–308.

Vearncombe J. R., Barton J. M., Jr, Cheshire P. E., De Beer J. H., Stettler E. H. & Brandl G., 1992, Geology, geophysics and mineralization of the Murchison schist belt, Rooiwater complex and surrounding granitoids, Memoirs of the Geological Survey of South Africa (now Council for Geosciences), 139.

Viljoen M.J., VanVuuren C.J.J., Pearton T.N., Minnitt R.C.A. Muff R. & Cilliers P., 1978, The regional geological setting of the mineralization in the Murchison Range with particular reference to antimony, in Special publication of the Geological Society of South Africa, 4, 55–76.

Willson C. & Viljoen M.J., 1986, The Athens antimony ore body, Murchison greenstone belt, in Mineral Deposits of Southern Africa, Anhaeusser C.R. and Maske S., eds, Geological Society of South Africa, 333–338.

PLUTONIC GOLD MINE, WESTERN AUSTRALIA: AN ARCHAEAN MINERAL SYSTEM

M.F. Gazley[1,2], J.K. Vry[1], E. du Plessis[2], J.A. Baker[1], M.R. Handler[1] & J.C. Boorman[1]

[1]Victoria University of Wellington, PO Box 600, Wellington, New Zealand
[2]Barrick Gold of Australia, Locked Bag 12, Cloisters Square, Perth 6085, Western Australia

Introduction

Plutonic Gold Mine (Plutonic), owned and operated by Barrick Gold of Australia, is located ~800 km north-east of Perth, Western Australia, at the south-western margin of the Plutonic Well Greenstone Belt (PWGB), in the Marymia Inlier. This paper asks, based on data from Plutonic, what can recent advances in hand-held X-Ray fluorescence (XRF) and modelling of metamorphosed mafic rocks allow us to learn about gold mineralising systems?

Geological Setting

The PWGB is a northeast-southwest trending, ~50 km long, ~10 km wide Archaean granite-greenstone terrane that is located between the Pilbara and Yilgarn cratons in Western Australia. Since 1990, over four million ounces of gold have been produced, largely from the main Plutonic mine, and a large number of significantly-smaller deposits throughout the belt. Known economic concentrations of gold at Plutonic occur mainly within the Mine Mafic Package. This consists predominantly of amphibolite-facies metabasaltic rocks, with thin (typically <1 m), discontinuous intraformational metasediments, including metashales, graphitic metashales and metacherts. The typical peak metamorphic assemblage in the metabasaltic rocks is hbl-plag-ttn-ilm-ep-qtz. Early thrust stacking of the greenstone sequences of the PWGB (Bagas, 1999; Rowe et al., 2002), is thought to be the cause of this metamorphism.

Gold Mineralisation

The main episode of gold mineralisation at Plutonic occurred late during, or probably slightly after the metamorphic peak (e.g. Vickery, 2004). The resulting thin (~1 – 3 m thick) biotite-bearing lodes (brown lode), contain gold in association with qtz-bt-chl-amph-ttn-ep-carb-asp-po±ccp. Where these gold-bearing horizons are well developed, they tend to be near-parallel to the stratigraphy, as marked by the rare metasedimentary horizons, and to the dominant foliation. Other styles of gold mineralisation also occur at the Plutonic deposit in lesser amounts (e.g. rare muscovite-rich lodes, late-stage quartz-carbonate-pyrrhotite dominated veins, and shear-hosted lode). As in many greenstone-hosted gold deposits that have been metamorphosed to high temperatures (amphibolite facies or above), none of the gold mineralisation is marked by a wide alteration halo.

Geochronology

The Mine Mafic Package was deposited at 2900 – 2720 Ma, based on U-Pb dating of zircons in cross-cutting felsic intrusions (e.g. McMillan, 1996; Vickery, 2004), and subsequently underwent several episodes of metamorphism and deformation. Peak metamorphic conditions were attained between 2660 – 2630 Ma (Vielreicher & McNaughton, 2002), based on geochronological data from the Plutonic deposit and the PWGB. At about the same time, an early episode of gold mineralisation at ~2650 Ma occurred at a number of deposits in the north of the PWGB (McMillan, 1996; Vielreicher et al., 2002). As yet, no geochronological data has confirmed whether this early episode of gold mineralisation also affected rocks in the region of the Plutonic deposit, where three episodes of gold mineralisation have been identified, at ~2100 Ma, ~1850 Ma, and ~1680 Ma (McMillan, 1996; MFG unpub. data). The data from the wider region is consistent with the interpretation of previous workers (e.g. McMillan, 1996; Vielreicher et al., 2002; Vickery, 2004) that the main early gold mineralisation at Plutonic was synchronous with, or slightly followed the regional metamorphic peak – an assertion that we are willing to maintain at this stage. A late-stage hydrothermal event at 1719 ± 14 Ma (U-Pb dating of a metamorphic overgrowth on zircons), may or may not be associated with gold mineralisation (Vielreicher et al., 2002). This age is confirmed by a Pb-Pb age of 1725 ± 26 Ma of hydrothermal titanite in a late-stage chlorite-carbonate vein (MFG, unpub. data), that, at the location of the sample, was not associated with gold.

Host Rock Geochemical Stratigraphy

Until recently, only a general stratigraphy of the Mine Mafic Package existed (e.g. Rowe et al., 2002). A detailed stratigraphy had proven difficult to resolve as there are very few distinct and continuous marker horizons traceable over any significant distance, either from drill hole to drill hole or within underground development. Visual recognition of flow unit boundaries in diamond drill core from Plutonic is extremely difficult, and is based on recognition of subtle features such as pillow margins or amygdules, or slight changes in mineralogy, a change in the abundance of ilmenite/titanite at a hand-sample scale. To further complicate interpretation of the stratigraphy, the thickness of the Mine Mafic Package is highly variable (<20 m to >300 m) and the deformation history is complex, with eight recognised deformation events (Rowe et al., 2002).

Figure 1 shows our trace element data for a ~180 m thick section through the Mine Mafic Package. Elemental concentration data is presented for K, Ti, Cr, Fe, Zr and Au (in ppm) with all but the latter analysed on pulverised diamond drill core samples with an Innov-X Omega hand-held XRF with a 10 – 40 kV (10 – 50 μA) X-ray tube which was corrected and standardised using internal

standards and international basalt standard JB-1. Au was analysed by fire assay at Ultra Trace Laboratories, Perth; the same lab provided conventional XRF analyses for four samples as a check of the concentrations measured by the hand-held XRF. This data is represented by large stars on Figure 1.

The results of the hand-held XRF data presented in Figure 1 show that at Plutonic: (1) a geochemical stratigraphy in which individual lava flows are recognisable on the basis of element concentrations (most obviously in Cr and Zr data); (2) the most evolved basalts are at the base (Cr-poor, Zr- and Ti-rich), and the least evolved at the top of the sequence (Cr-rich, Zr- and Ti-poor), confirming pre-existing evidence that the sequence is overturned, and demonstrating for the first time that the presented section does not involve significant structural repetition; (3) gold concentrations in the presented section are independent of Fe concentration in the host rocks, contrary to previous expectations (c.f. Phillips et al., 1996); and that instead; (4) gold commonly occurs along basalt flow boundaries, where K concentrations indicate that an invisible alteration halo exists around many ore zones that cannot be recognised without this data. These haloes probably indicate minor biotite alteration that is not evident during core logging.

P-T determinations from mafic rocks

The early thrust stacking of Archaean greenstone sequences that has been reported for the PWGB (e.g. Rowe et al., 2002), as well as in nearby parts of the Yilgarn and Pilbara cratons (e.g. Swager & Griffin (1990); and references therein), probably produced the amphibolite-facies metamorphism at 2660 – 2630 Ma (Vielreicher & McNaughton, 2002). Evidence for changing metamorphic conditions is found within the pronounced growth zoning in hornblende crystals in metabasalt rocks of the Mine Mafic Package from Plutonic. The zoning is best seen in back-scatter electron images, and suggests either rapidly changing metamorphic conditions or that the P-T path crossed a reaction boundary. Recent advances in modelling amphibole compositions (e.g. Diener et al., 2007; Bhadra & Bhattacharya, 2007) that are now incorporated in petrologic forward modelling tools such as THERMOCALC v. 3.31, can help show how metabasaltic rocks respond to changes in metamorphic conditions, and provide insights into the geological and/or geodynamic setting at the time. Given that a high percentage of the world's gold is hosted within greenstone sequences, understanding the geodynamic and *P-T* conditions that the rocks of these sequences have experienced is important for better understanding and ultimately predicting gold mineralisation therein.

Our new *P-T* data shows that the rocks of the Plutonic area have been subjected to a rapid increase in pressure, from about 2 – 3 kbar to 10 kbar, at temperatures ~600 °C, followed by rapid exhumation from these depths. Previous workers reported metamorphism at near-constant pressures of ~4 kbar (e.g. Vickery, 2004). Given the steep nature of the *P-T* paths that are predicted by our THERMOCALC modelling, and the sharp change in pressure recorded by our traditional

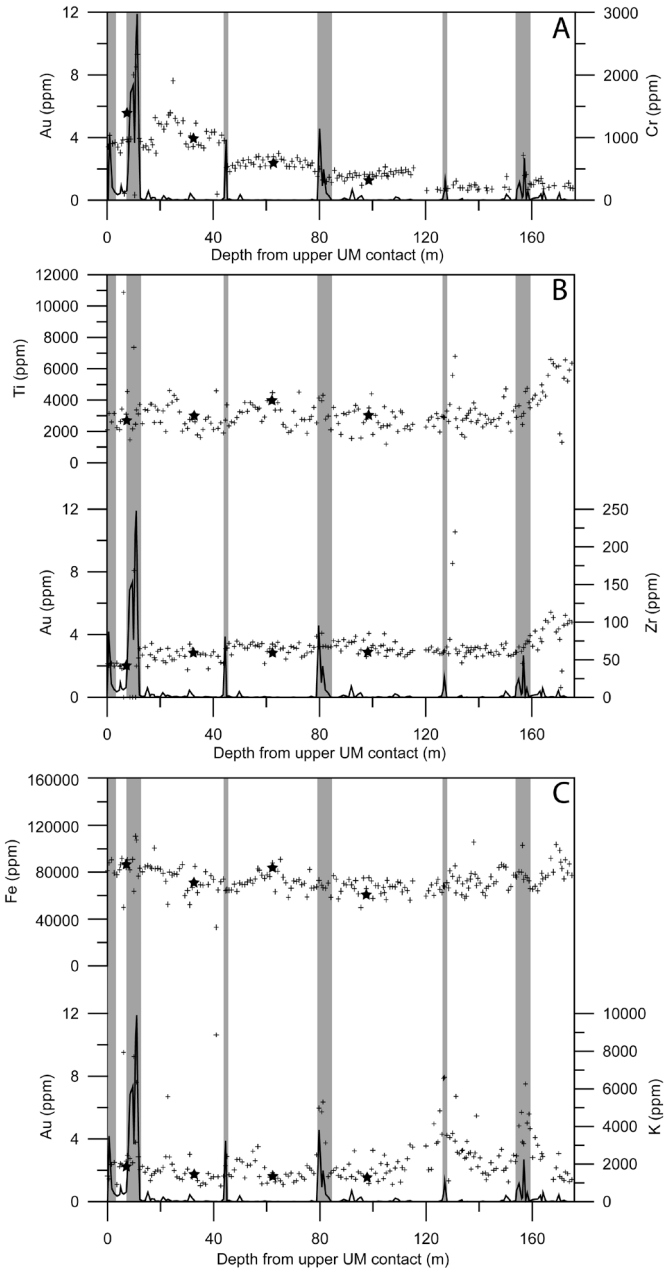

Figure 1. Hand-held XRF data for a representative section through the Mine Mafic Package showing basalt flow unit boundaries. Down-core depth is measured from the contact with the overlying ultramafic (UM) rocks with younging direction to the right (down-section), and shaded bands mark high gold concentrations. Conventional XRF analyses are indicated by stars for the same samples; all analyses match our data well except for the Cr data point at 7 m. (a) Cr (ppm) values are indicated by stars, Au (ppm) values are connected with a line. Abrupt changes in Cr concentration are interpreted to mark flow unit boundaries, where gold appears also to be concentrated. A gold-mineralised fault and shear zone occur at 1 m and ~11 m, respectively, and there is a gap in the data from 116-120 m. (b) Ti and Zr concentrations (in ppm) show magma fractionation trends and influxes of magma into the system at ~20 m and ~155 m. (c) Au, K and Fe concentrations (in ppm), show that Au is independent of Fe and instead tends to be associated with high K at the flow unit boundaries.

geothermobarometry, we suggest that it is most likely that over-thrusting was responsible for the onset of peak metamorphism and possibly provides a mechanism for overturning the rocks of the belt. This interpretation is consistent with the results of previous structural studies by Rowe et al. (2002) who suggested that significant portions of the PWGB were overturned early during the geological history of the area. Our results indicate that peak metamorphism occurred at 10 kbar and ~600 °C, some 6 kbar higher than previously recognised, and was followed by a major episode of gold mineralisation at temperatures that were either syn- or post-peak at ~575 °C, approximately 100 °C higher than previously recognised (c.f. Vickery, 2004).

Conclusions

The methods that we have described here in applying hand-held XRF analyses to unravel the stratigraphy of greenstone rocks are readily applied, and have the potential to reveal otherwise unclear stratigraphy and its control on mineralisation in many different types of deposits worldwide. On the basis of the hand-held XRF data we contend that at Plutonic: (1) the variations in thickness of the Mine Mafic Package are the result of changes in primary stratigraphy and not the result of a structural process; (2) different lava flow units are clearly identifiable on the basis of the elemental concentrations; (3) contrary to conventional theory, the Fe composition of different units within the Mine Mafic Package does not result in favourable gold mineralisation in the more Fe-rich units, instead the primary stratigraphy of the sequence appears to be a more fundamental control.

Our use of new advances in modelling mafic rocks shows that it is possible to obtain very useful *P-T* data from metabasaltic rocks, which can be invaluable in piecing together the geological history of an auriferous greenstone sequence and the driving forces that ultimately lead to gold mineralisation.

Acknowledgements

This work represents part of the first author's PhD research at Victoria University of Wellington, New Zealand. Funding for this research comes from Barrick Gold of Australia. JKV and MFG are extremely grateful for the support and assistance they have received from the mine geologists during their time on site. K. Evans, J. Diener, R. Powell, S. Murray, M.-A. Millet and L. Brisbout are gratefully acknowledged for their input on various aspects of this research.

References

Bagas L., 1999, Early tectonic history of the Marymia Inlier and correlation with the Archaean Yilgarn Craton, Western Australia, Australian Journal of Earth Science, 46, 115–125.

Bhadra S., Bhattacharya A., 2007, The barometer tremolite + tschermakite + 2 albite = 2 pargasite + 8 quartz: Constraints from experimental data at unit silica activity, with application to garnet-free natural assemblages, American Mineralogist, 92, 491–502.

Diener J.F.A., Powell R., White R.W. & Holland T.J.B, 2007, A new thermodynamic model for clino- and orthoamphiboles in the system Na_2O-CaO-FeO-MgO-Al_2O_3-SiO_2-H_2O-O, Journal of Metamorphic Geology, 25, 631–656.

McMillan N.M., 1996, Late-Archaean, syn-amphibolite facies, lode-gold deposits overprinted by Palaeoproterozoic deformation, metasomatism and hydrothermal activity at Marymia, Western Australia, Unpublished PhD thesis, University of Western Australia.

Phillips G.N., Groves D.I., Kerrich R., 1996, Factors in the formation of the giant Kalgoorlie gold deposit, Ore Geology Reviews, 10, 295–317.

Rowe R.J., Awan A.W., McCuaig T.C., Sauter P.C.& Vickery N.M., 2002, Structural Geology of the Plutonic Gold Mine, Applied Structural Geology for Mineral Exploration and Mining Symposium, Kalgoorlie, WA, 180–185.

Swager C. & Griffin T.J., 1990, An early thrust duplex in the Kalgoorlie-Kambalda greenstone belt, Eastern Goldfields Province, Western Australia, Precambrian Research, 48, 63–73.

Vickery N.M., 2004. The Plutonic Gold Deposit, Western Australia: Geology and Geochemistry of an Archean Orogenic Gold System. PhD dissertation, University of New England.

Vielreicher N.M., Ridley J.R., Groves D.I., 2002. Marymia: an Archean, amphibolite facies, hosted orogenic lode-gold deposit overprinted by Palaoproterozoic orogenesis and base metal mineralisation, Western Australia. Miner Deposita, 37, 737.64.

Vielreicher N.M., McNaughton N.J., 2002. SHRIMP U-Pb geochronology of magmatism and thermal events in the Archaean Marymia Inlier, central Western Australia. International Journal of Earth Science, 91, 406.432.

MAPPING THE MINERAL SYSTEM: TRACE ELEMENT ANOMALY RESIDENCE IN THE REGOLITH AT SMALL SCALES

R. Hough, R. Anand, J. Cleverley & C. Ryan

CSIRO, Minerals Down Under Flagship, Earth Science and Resource Engineering, PO Box 1130, Bentley, WA 6102

Mapping the mineral system is a challenging task in areas of cover. Understanding trace element residence and provenance of near-surface geochemical anomalies in heterogeneous regolith, including transported overburden is crucial for both exploration and environmental geochemistry. Synchrotron based X-Ray Fluorescence and Proton Microprobe element mapping have been used to constrain element distributions and speciation variation within regolith from the Moolart Well, Rose dam and Mount Gibson gold deposits (e.g. Figure 1). We have been able to spatially resolve the distribution of trace metals and relate these directly to the petrographic context displayed by the samples, including distinguishing transported from in-situ signatures of metal dispersion. Minerals precipitated from groundwaters in the upper sediments of regolith profiles could provide an interesting sample medium to search for hydromorphic dispersion from underlying, and deeply buried mineralisation. Alunite appears to be one such mineral occurring in the regolith profile of the Enterprise pit, Mount Gibson that contains appreciable Au, Cu, Pb and As. This illustrates the potential of such studies to establish true residence of geochemical anomalies in cover and the potential to identify new minerals as mineral exploration sampling media.

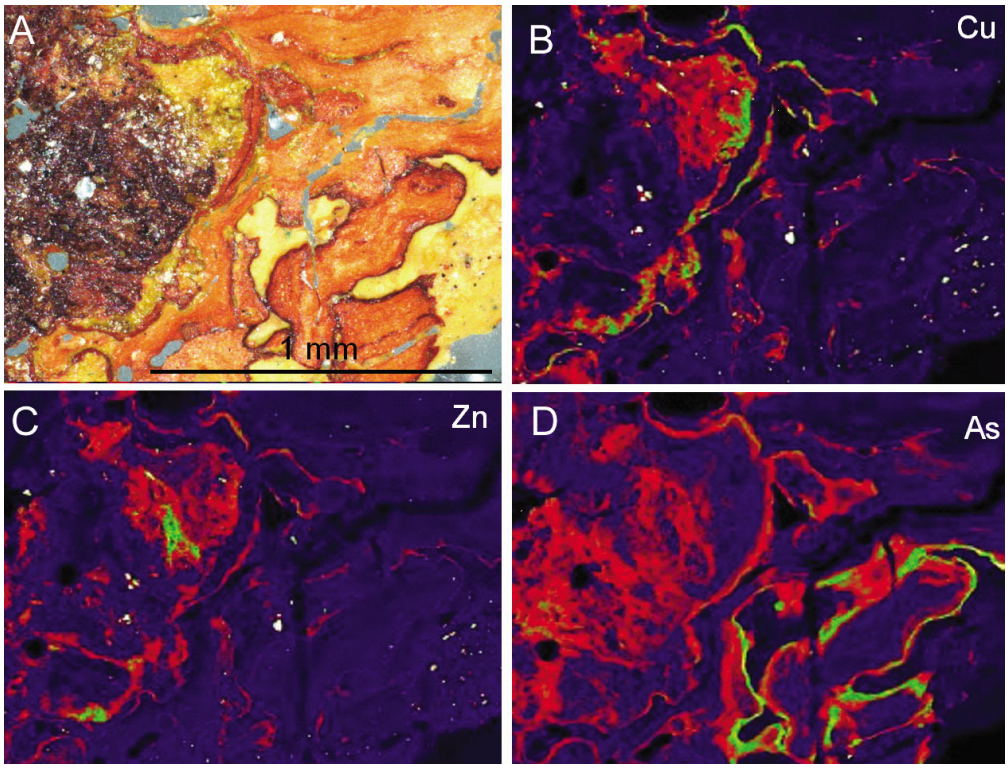

Figure 1. Synchrotron XRF element maps of an iron oxide nodule from the Moolart Well gold deposit.

ARCHEAN METAL SOURCES OF MESOPROTEROZOIC Mn DEPOSITS, WOODIE WOODIE, EAST PILBARA

S.A. Jones[1] & N.J. McNaughton[2]

[1]Consolidated Minerals Pty Ltd, [2]John de Laeter Centre, Curtin University of Technology

Introduction

High-grade manganese has been mined in the Woodie Woodie area since the mid 1950s with an average grade of 48% Mn and 5% Fe. The manganese was considered for many years to have a supergene origin with an Oligocene age obtained by Ar^{40}-Ar^{39} dating (Dammer et al., 1994). However, subsequent mapping has shown that the manganese deposits are much older as they are commonly truncated by a Mesoproterozoic sandstone unit and appear to have a strong structural control (Fig. 1a), suggesting a hydrothermal origin.

Major and trace element geochemistry of manganese samples from Woodie Woodie is also consistent with a hydrothermal rather than a supergene origin. The source of the manganese was thought to be from the Carawine Dolomite, due to elevated manganese values in the dolomite. However, recent geochemical studies suggest a more mafic source for metals carried by the mineralising fluids, most likely Archean basalts of the underlying Fortescue Group and older greenstones. The age of manganese deposition at Woodie Woodie is estimated to be confined to the period ca. 840 - 1150 Ma based on Pb isotopes from Pb-rich manganese ore and is consistent with field studies indicating that manganese deposition is closely associated with growth faults during Mesoproterozoic basin development and sedimentation. The Oligocene age obtained by Dammer et al. (1994) is now considered to reflect the timing of weathering and lateritization.

Geological setting and style of Woodie Woodie manganese deposits

Woodie Woodie manganese deposits are typically located close to the unconformity between Archean Carawine Dolomite and the overlying Mesoproterozoic Manganese Subgroup. Minor manganese deposits are also located along the basal contact of the dolomite and within the underlying Jeerinah Formation (Fortescue Group). The dolomite is overlain by a thick carapace of chert breccia (Pinjian Chert Breccia) that developed over a billion year period of weathering between deposition of the dolomite in the Archean and deposition of the Mesoproterozoic Manganese Subgroup (Noldart & Wyatt, 1962). Carawine Dolomite forms the eastern part of the Hamersley Group, and the Manganese Subgroup forms part of the Collier Group of the Bangemall Supergroup (Martin & Thorne, 2004).

Manganese ore is predominantly hosted by dolomite, chert breccia (including *in-situ* chert breccia and fault-related chert breccia formed from the breakdown of dolomite by hydrothermal fluids) and in places, basal units of the Mesoproterozoic Manganese Subgroup. At Woodie Woodie, Manganese orebodies are commonly truncated by the Waltha Woora Sandstone (Manganese Subgroup), although in the northern part of the Woodie Woodie mine corridor, this sandstone is overprinted by manganese mineralisation. The metamorphic grade throughout the Woodie Woodie region is typically lower greenschist facies.

Manganese orebodies are generally irregular in shape, ranging from steeply dipping irregular sheet-like to plug-like bodies (fault-hosted manganese) that are commonly overlain by stacked bedding-parallel lenses (stratabound manganese). The orebodies range in size from 0.2 to 5.5 Mt, with an average size of 0.5 Mt and are generally 50-100m wide and about 100-600m in length. The average ore grades at Woodie Woodie are 41% Mn, 6% Fe and 16% SiO2 and the average Mn:Fe ratio is 6:1. The dominant manganese minerals at Woodie Woodie comprise fine grained to coarsely bladed pyrolusite or polianite (MnO_2), braunite (Mn_2O_3), stubby crystals of hausmannite (Mn_3O_4; $MnFe_3O_4$) and finely banded or colloform cryptomelane ($K(Mn^{+4},Mn^{+2})_8O_{16}$). The manganese ore is generally surrounded by a Fe-rich halo of hematite, goethite and limonite. Vuggy infill textures of ore minerals are observed in some ore samples.

Structural controls on manganese mineralisation

The manganese at Woodie Woodie is typically associated with major faults that down-throw the Pinjian Chert Breccia into extensional basins which have then been infilled with basal Manganese Subgroup sedimentary breccias, sandstone and siltstone (Fig. 1b). Marked facies changes in stratigraphic units and a thickening of the overlying Manganese Subgroup across many of the mineralised structures at Woodie Woodie indicate that basin formation and sedimentation of the Manganese Subgroup was synchronous with movement on these faults (i.e., growth faults). In the mine corridor, growth faults have been recognised in the Radio Hill, Austin, Chris D, Bells, and Greensnake pits. At Greensnake (Fig. 1c), the weathered carapace of *in situ* chert breccia has been down thrown on large normal faults and is preserved in an early basin. To the west of the Greensnake pit, at the edge of the basin, the weathered chert breccia has been eroded off and Waltha Woora Sandstone is deposited directly onto dolomite.

Growth faults can represent significant fluid conduits for ore-bearing fluids and in the mine corridor manganese appears to be preferentially deposited close to the edges of fault-controlled basins (Fig. 1b). A structural model

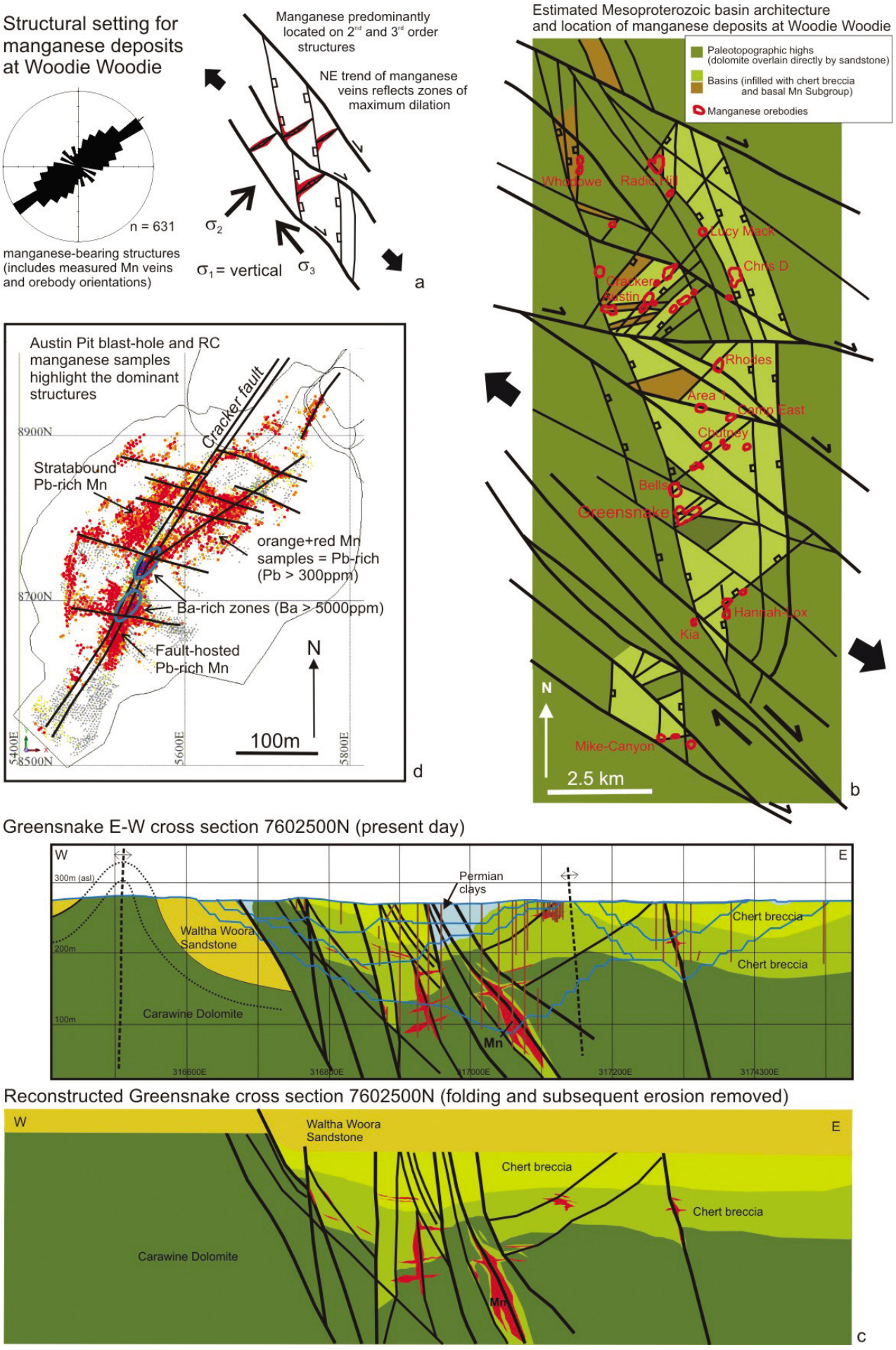

Figure 1a, Structural controls on manganese deposition; b: Estimated basin geometry of the Woodie Woodie mine corridor; c: Present day E-W cross section of Greensnake Pit above and reconstructed section removing the effects of deformation and erosion; d: Pb-rich and Ba-rich Mn samples in Austin Pit delineate major structures.

of the Woodie Woodie area shows that manganese is predominantly located on 2nd and 3rd order NNE- to ENE-striking faults adjacent to major NNW- and NE-striking growth faults (Fig. 1a). The dominance of steep NE-trending manganese veins reflects maximum dilation along these structures during NW-SE extension. Fault orientations and kinematics at Woodie Woodie indicate that the manganese deposits developed in a dextral transpressive regime adjacent to major NW-oriented transfer faults.

The fault pattern at Woodie Woodie represents the reactivation of a pre-existing structural framework established during rifting and deposition of the Fortescue and Hamersley Groups. Subsequent deformation events throughout the region have resulted in multiple reactivation and inversion of many normal faults. A deformation history is now established for the Woodie Woodie region and includes: $\mathbf{D_1}$ extension associated with rifting and deposition of the Fortescue and Hamersley Groups; $\mathbf{D_{2a+b}}$ prolonged NW-SE extension and development of local Manganese Subgroup basins (associated with manganese deposition); $\mathbf{D_3}$ NE-SW compression produced tight to open WNW- to NNW-oriented upright folds in Archean units and the overlying Manganese Subgroup. This folding is truncated by the flat-lying ca. 850 Ma Googenhama Conglomerate of the basal Officer Basin (Grey et al., 2005) and may be related to the 1030-950 Ma Edmundian Orogeny (Sheppard et al., 2007); $\mathbf{D_4}$ E-W extension and formation of late NE- and NW-oriented grabens throughout the Woodie Woodie region; $\mathbf{D_5}$ N-S compression produced open E- to ENE-oriented folds and warps. Although the Woodie Woodie region has undergone multiple extension and compression episodes, the original Mesoproterozoic basin architecture is largely preserved and gives important clues to the location of manganese.

Woodie Woodie manganese geochemical and Pb-isotope characteristics

The manganese at Woodie Woodie is associated with elevated Ba, Zn, Pb, V, Ba, Cu, Mo and As and displays a clear hydrothermal signature on Co+Ni vs As+Cu+Mo+Pb+V+Zn diagrams that discriminate between hydrothermal and supergene deposits (e.g. Nicholson, 1992). All manganese ore samples plot well within the hydrothermal field. There is a strong fractionation between manganese and iron, with Mn:Fe ratios typically 6:1, and in general there is a negative correlation between Mn and Fe, with the iron forming a halo around the manganese deposits. REE patterns show a marked difference between weathered surface manganese and manganese at depth. The weathered surface samples display a marked enrichment in all REE, and in particular the LREE to MREE (La, Ce, Pr, Nd and Sm). The REE patterns for the weathered samples at Woodie Woodie are similar to other supergene deposits such as Groote Eylandt (e.g., Pracejus et al., 1990). These weathered samples also plot at the edge of the supergene field on the Co+Ni vs As+Cu+Mo+ Pb+V+Zn discrimination diagrams.

Elements such as Pb and Ba are highly variable throughout the Woodie Woodie mine corridor, but within individual deposits, can be used to map out structures and intersection zones between major faults. For example, in the Austin orebody (Fig. 1d), two areas along the major Cracker Fault, display markedly higher Ba (>5000 ppm) and correspond with intersection zones of mapped faults. These Ba-rich zones appear to highlight areas of structural complexity that may represent zones of major fluid flow.

Elevated Pb concentrations are observed in some manganese ores throughout the Woodie Woodie mine corridor and a Pb-rich manganese oxide mineral, coronadite, has been identified by XRD and SEM petrography. Wholerock Pb-isotope studies of Pb-rich ore samples have provided a range of possible model Pb ages ($t_{7/6}$) from 840 to 1150 Ma. This variability may reflect a long-lived mineralising system and/or multiple Archean sources for the Pb. These ages are consistent with coeval manganese deposition and Mesoproterozoic basin formation and sedimentation. Manganese orebodies are generally truncated by Mesoproterozoic sandstone, but in the northern part of the mine corridor, Mesoproterozoic sandstone is overprinted by manganese mineralisation, suggesting multiple mineralization events and long-lived extension and basin formation.

The source of the manganese was thought to be from the Carawine Dolomite due to elevated Mn values (up to 4 wt. %) but a more likely source is the underlying Archean Fortescue Group basalts and/or basement rocks. Modelling the Pb isotopic composition of ore samples suggests an Archean Pb source, from 2.7 to 3.5 Ga in age, with typical crustal μ-values ($^{238}U/^{204}Pb$) and Th/U higher than typical crust, favouring the dominance of a basaltic source over medium to high metamorphic grade basement rocks. The Mn-content of basaltic rocks is typically higher than felsic granitoids and gneisses, suggesting that the Mn is mainly sourced from basaltic rocks such as the Fortescue Group and/or the older greenstones. The Pb isotope modelling precludes a single Pb source and/or time of mineralization, whereas the variable Pb-content in ore samples suggests Pb and Mn are not necessarily from the same source.

Manganese deposition is predominantly governed by changes in Eh-pH and Mn^{2+} is highly soluble except under strongly oxidising conditions (e.g., Maynard, 2007). Therefore a reduced hydrothermal fluid could deposit Mn oxides during interaction with oxidised groundwater and/or seawater in near-surface environments. At Woodie Woodie, the marked spatial association between dolomite and manganese also suggests that there is a strong pH control on ore deposition.

Conclusions

The strong structural control on the style and location of manganese orebodies, the elevated As+Cu+Mo+ Pb+V+Zn values in the manganese and the marked contrast in REE element patterns between manganese ores at surface and at depth indicates a hydrothermal rather than supergene origin for much of the manganese at Woodie Woodie. The timing of manganese deposition is

broadly constrained by field relationships and Pb-isotope modelling and is clearly associated with Mesoproterozoic extension and basin formation. Manganese is most likely sourced from the underlying Archean basement, particularly basalts of the Fortescue Group and the older greenstones.

References

Dammer D., McDougall I., & Chivas A.R., 1994, 40Ar-39Ar dating of cryptomelane-hollandite from regolith, Western and Northern Australia, Australian National University Research School of Earth Sciences, Annual Report 1994, 130–132.

Grey K., Hocking R.M., Stevens M.K., Bagas L. Carlsen G.M., Irimies F., Pirajno F., Haines P.W., & Apak S.N., 2005, Lithostratigraphic nomenclature of the Officer Basin and correlative parts of the Paterson Orogen, Western Australia, Geological Survey of Western Australia, Report 93, 89p.

Martin D.M. & Thorne A.M., 2004, Tectonic setting and basin evolution of the Bangemall Supergroup in the northwestern Capricorn Orogen, Precambrian Research, 128, 385–409.

Maynard J.B., 2007, Manganiferous sediments, rocks, and ores, Treatise on Geochemistry, Chapter 7.11, 289–308.

Nicholson K., 1992, Contrasting mineralogical-geochemical signatures of manganese oxides: Guides to metallogenesis, Economic Geology, 87, 1253–1264.

Noldart A.J. & Wyatt J.D., 1962. The geology of portion of the Pilbara Goldfield covering the Marble Bar and Nullagine 4-mile map sheets, Western Australia Geological Survey Bulletin 115, 199p.

Pracejus B., Bolton B.R., Frakes L.A. & Abbot M., 1990, Rare-earth element geochemistry of supergene manganese deposits from Groote Eylandt, Northern Territory, Australia.

Sheppard S., Rasmussen B., Muhling J.R., Farrell T.R. & Fletcher I.R., 2007. Grenvillian-aged orogenesis in the Palaeoproterozoic Gascoyne Complex, Western Australia, 1030-950 Ma reworking of the Proterozoic Capricorn Orogen, Journal of Metamorphic Geology, 25, 477–494.

CONTROLS ON QUARTZ ± GOLD VEIN FORMATION AND HYDROTHERMAL ALTERATION IN THE FÆRINGEHAVN AND TASIUSARSUAQ TERRANES, SOUTHERN WEST GREENLAND

J. Kolb[1], D.M. Schlatter[1], B.M. Stensgaard[1] & A. Dziggel[2]

[1]Department of Economic Geology, Geological Survey of Denmark and Greenland, Øster Voldgade 10, DK-1350 Copenhagen K, Denmark
[2]Institute of Mineralogy and Economic Geology, RWTH Aachen University, Wüllnerstr. 2, 52064 Aachen, Germany

Introduction

Archaean orogenic gold mineralization is associated with crustal-scale shear zones, such as the Boulder-Lefroy shear zone (Yilgarn Craton, Western Australia, e.g. Golden Mile) and the Cadillac tectonic zone (Superior Province, Canada, e.g. Val d'Or) (Goldfarb et al. 2001). In the Nuuk region of southern West Greenland, gold occurrences, such as Storø, Qussuk, Bjørneøen, and SW Isua, are spatially associated with the transcurrent Ivinnguit fault (IVF) (Stensgaard et al. 2006), separating the Akia terrane (AT) from a complex zone of various amalgamated terranes in the south. A similar major structural break, the Qarliit Nunaat fault (QNF), separates the Tasiusarsuaq terrane (TT) to the south from the complex zone of amalgamated terranes in the Nuuk area.

In this paper, we use structural, petrological, and age data from the TT and the Færingehavn terrane (FT) in order to establish a tectono-metamorphic model for the terrane evolution. We implement the structural control and hydrothermal alteration of barren and auriferous quartz veins and discuss the control of hydrothermal fluid migration and gold concentration.

Regional Geology

The study area is situated in the North Atlantic craton, southern West Greenland. The area has been subdivided into various terranes based on U-Pb zircon ages of protolith formation and metamorphism. From north to south, the Akia, Isukasia, Færingehavn, Kapisilik, Tre Brødre and Tasiusarsuaq terranes are distinguished (Nutman & Friend 2007). The TT was thrust north between ca. 2720-2700 Ma and amalgamated with the other terranes except the AT. This terrane juxtaposition was followed by the collision with the AT along the IVF between 2650-2600 Ma. The earlier structures were reactivated by ca. 2565 Ma shearing in the Færingehavn straight belt. The Qôrqut granite intruded late-to post-tectonically as a sheet-like intrusion at 2530 ± 30 Ma (Moorbath et al. 1981).

The lode gold mineralization at Storø is associated with deformation along the Storø shear zone, a higher order splay of the IVF. Gold mineralization in quartz veins was dated at ca. 2630 Ma (van Gool et al. 2007, Nutman et al. 2007) and is, thus, contemporaneous with terrane collision and deformation at the IVF.

Geology of the Tasiusarsuaq (TT) and Færingehavn (FT) terranes

The TT consists mainly of 2920-2810 Ma TTG gneiss. Supracrustal rocks occur as small lenses and belts and are dominated by amphibolite and mafic granulite with minor meta-sedimentary and -ultramafic rocks. In the south, mostly conformable layers of 2835 ± 10 Ma porphyritic granitoids, the Ilivertalik granite, occur in a zone that extends about 50 km in an E-W direction and 20 km in a N-S direction (Pidgeon & Kalsbeek 1978).

The FT forms a ca. 30 km wide, mainly NE-SW trending belt and is dominated by ca. 3850-3600 Ma quartzo-feldspatic gneiss that was intruded by a Palaeoarchaean swarm of mafic dykes. The gneiss is in tectonic contact with a variety of ca. 2840 Ma supracrustal rocks, including meta-ultramafic rocks, amphibolite, and aluminous, mostly sillimanite-bearing paragneiss.

Metamorphism

Granulite facies peak metamorphism at ca. 2.8 Ga in the TT was followed by amphibolite facies retrogression until ca. 2670-2610 Ma. Retrogression was most extensive in a several km wide zone at the northern terrane boundary. Greenschist facies metamorphism is associated with faults and Palaeoproterozoic (ca. 1890 Ma) dolerite dikes and marks the youngest tectono-metamorphic overprint.

An early low- to medium-pressure granulite facies metamorphic event in the FT was proposed at ca. 3650-3400 Ma. This was followed by high-pressure metamorphism at ca. 2715 Ma (Grt-Cpx-Hbl-Pl-Qtz in mafic granulite). The exhumation of the FT and the supracrustal rocks was associated with widespread low-pressure amphibolite facies metamorphism, and immediately followed the high-pressure metamorphic event.

Structural geology

The general map pattern is characterized by open to close folds with SE to S trending axial traces and is surprisingly similar in both terranes. In detail, the rock fabrics indicate four different deformation stages (D_1-D_4).

D_1 fabrics are preserved in low strain gneiss enclaves, where a S_1 foliation and/or S_1-parallel aplitic dikes are preserved. In the TT, the S_1 foliation is defined by Cpx

and Opx, which suggests that the D_1 deformation stage occurred under granulite facies conditions at about 2.8 Ga.

During D_2, the S_1 foliation was isoclinally folded (F_{2a}) and an axial planar S_2 foliation developed. The isoclinal F_{2a} folds form rootless, intrafolial folds in S_2 or, in low strain enclaves, up to 50 cm wide (half wavelength) rootless folds. The F_{2a} fold axes are variable and show no distinct orientation maximum. The S_2 foliation is the penetrative foliation and is mainly closely spaced. It is, together with the moderately SE- to S-plunging mineral stretching lineation (L_2), defined by amphibolite facies mineral assemblages. However, in the FT, the D_2 fabrics are locally associated with the high-pressure granulite facies assemblage. Shear sense indicators point to a reverse sense of movement broadly to the N-NW. In low strain zones, the S_2 foliation is folded into upright, open to close F_{2b} folds with a wavelength of up to 3 km. The F_{2b} fold axis is oriented approximately perpendicular to the mineral stretching lineation and plunges at shallow angle to the E-ENE. This deformation stage is common to both terranes and is mainly characterized by N- to NW-vergent thrusting in the amphibolite facies probably between 2.77 and 2.70 Ga.

During D_3, the S_2 foliation is folded into upright, open to tight folds with N-S to NW-SE trending axial traces on a km-scale. Higher order folds down to cm-scale are abundant. The F_3 fold axes mainly plunge at shallow to moderate angles (5°-25°) S-SE, but non-cylindrical folds were also observed with F_3 plunging both SE and at around 20° NW. The F_3 folds show a repeated, progressive decrease in wavelength from gentle to isoclinal, which is connected to an increase in amplitude at various scales. The limbs of the tight to isoclinal F_3 folds are sheared off. This is also observed at all scales: higher order folds are sheared off by up to 2 m wide shear zones, whereas map-scale folds are sheared off by 20-100 m and, locally, up to 1 km wide shear zones. The most abundant shear zones are characterized by a closely spaced, near vertical, NW-SE trending S_3 foliation. The L_3 mineral stretching lineation, defined by Hbl, Bt, and Pl, plunges predominantly at 5°-20° to the SE. Shear sense indicators are often ambiguous and both sinistral and dextral senses of shear may be indicated in the same zone. An axial planar pegmatite was dated at 2672 ± 5 Ma in the TT.

The D_4 stage is characterized by several sets of faults that both cross cut and are intersected by Palaeoproterozoic dolerite dikes.

Hydrothermal Mineralisation and Alteration

Numerous quartz veins were observed in both terranes. They are 1-20 cm wide and are continuous along strike and down dip over several m to up to 200 m. Besides Qtz they contain minor Po, Py and Ccp. In general, most of the veins are parallel to S_2 on the limbs of F_3 folds or they are parallel to S_3 in the D_3 shear zones. They often form at lithological contacts. Some of the quartz veins formed in an a-c orientation of F_3 folds and are, in places, deformed into sigmoidal veins. Locally, a striation on the quartz vein surface of S_3 parallel veins is observed to be parallel to the L_3 mineral stretching lineation.

The quartz veins are surrounded by a 5 cm to 1 m wide alteration halo. Composite systems of several parallel quartz veins together with alteration zones can be 50-200 m wide and can be followed along strike and down dip to up to 250 m if the outcrop situation allows that.

In the TTG-gneiss, the hydrothermal alteration comprises Ms, Qtz, Bt, Ccp and Po. In the amphibolite a Bt, Qtz, Act, Po and Ccp alteration formed, locally with Ms and Ep. The mafic granulites in the central part of the map sheet have a slightly different alteration containing Bt, Di, Tm, Qtz, Po, Py and Ccp, whereas the alteration assemblage in nearby gneiss is the same to that described above.

Structural control of quartz veins

The quartz veins and associated halos are developed (1) parallel to S_3 in the steep limbs of F_3 folds and D_3 shear zones, (2) occupy m-scale dilational jogs in parasitic F_3 z-folds, (3) parallel to S_2 in recumbent F_3 folds with thicker veins in the steep limb, (4) as extension veins linking stepping D_3 deformation zones in dilational jogs, very similar to the structure described in (2) but cross cutting the S_2 foliation, and (5) as en-echelon sigmoidal veins displaying a dextral sense of rotation on the south-western limb of F_3 synclines, which is explained by dextral shear deformation on the limb during F_3 flexural slip. The quartz veins are either parallel to S_3 or directly related to F_3 folding. All these structural controls are consistent with the interpretation that the quartz veins and the associated hydrothermal alteration formed synchronous with the D_3 deformation. In the recumbent folds, where the quartz veins appear to be parallel to S_2 the relationship to D_3 is explained by reactivation of S_2 during F_3 flexural slip. This is supported by the observation of thicker quartz veins in the steep limbs that are in a local extensional site in the D_3 regime.

Regional control of mineralization

On a regional scale, the F_3 folds change systematically from open to tight in cross-section over several km. Very tight folds are sheared off by near vertical, NW-SE trending shear zones. Quartz veins and alteration zones are, in general, more abundant in the tight F_3 folds spatially associated with the D_3 strike-slip shear zones. The F_3 folds and, therefore, the hydrothermal quartz veins were dated at 2672 ± 5 Ma about 50 km SW of the 2720-2700 Ma QNF and about 75 km SW of the 2650-2600 Ma IVF. About 40 km SW of the IVF, a NNW-SSE trending shear zone probably represents a D_3 strike-slip shear zone and was dated at ca. 2630-2610 Ma (Nutman & Friend 2007). This age distribution (ca. 2670-2600 Ma) is interpreted to represent a progressive deformation during the D_3 stage propagating from the S to the N closer to the terrane boundary (IVF). The ca. 2630 Ma lode-gold occurrences such as Storø are genetically linked to the IVF.

Although the quartz veins formed in the same structural environment, are similar in size and mineralogy, and have

similar amphibolite facies alteration halos, they have different gold contents. Quartz veins further away from the QNF and IVF contain 2-20 ppb gold, whereas closer to these major structures 100-800 ppb are recorded. Stream and soil sediment samples show a similar tendency to higher gold values close to the IVF. There is a trend that younger quartz veins and those closer to the crustal break record higher gold concentrations.

Discussion

The quartz vein hosted gold mineralization at Storø formed at about 2630 Ma and is, thus, spatially and genetically linked to terrane collision and deformation along the IVF at 2650-2600 Ma. Several other gold occurrences located along the strike extent of the IVF are probably also related to that tectono-metamorphic event. The IVF may, therefore, represent a high permeability zone where hydrothermal fluid flow is concentrated. Structurally controlled gold mineralization occurs in higher order splays that may have acted as favorable deposit sites.

Quartz veins in the study area that are closest to the IVF have the highest gold concentrations, which would be in favor of a model based on focused auriferous hydrothermal fluid migration along the IVF. However, quartz veins of similar structural setting, similar timing, and similar hydrothermal alteration 20 km SW of the IVF are barren of gold. Possible explanations for the lack of gold in these veins are: (1) the fluids were different and contained no gold; and (2) gold didn't precipitate from the fluid. The most important precipitation mechanisms are phase separation, fluid-rock interaction, and fluid mixing. The hydrothermal quartz veins have the same structural control and very similar wall rocks, excluding fluid-rock interaction and structurally induced phase separation as a possible explanation. The similar hydrothermal alteration systematics associated with mineralized and barren veins indicate that the fluid composition must have been rather similar. Therefore, a different fluid source and modification of the fluid by fluid mixing are regarded as unrealistic processes to explain our observations.

We propose a model for the area in which the hydrothermal system evolved during the tectono-metamorphic evolution and terrane collision. Early (2670 Ma) quartz veins formed away from the terrane collision zone by a developing orogenic hydrothermal fluid system. During terrane collision between 2650-2600 Ma, the fluid system matured and concentrated gold. The development of the IVF as a transcrustal structure was a prerequisite for focused fluid migration along that high permeability zone. Orogenic gold mineralization culminated around 2630 Ma (e.g. Storø) in higher order splays from the IVF in favorable deposit sites along the strike extent of the IVF. Gold precipitated most probably due to phase separation in the quartz veins and fluid-rock interaction in the alteration zones.

Acknowledgements

Financing of field work in Greenland in a joint GEUS-BMP project is gratefully acknowledged. The paper is published with the permission of the Director of the Geological Survey of Denmark and Greenland (GEUS).

References

Goldfarb R.J., Groves D.I. & Gardoll S., 2001, Orogenic gold and geologic time: a global synthesis, Ore Geology Reviews, 18, 1–75.

Moorbath S., Taylor P.N. & Goodwin R., 1981, Origin of granitic magma by crustal remobilisation: Rb-Sr and Pb/Pb geochronology and isotope geochemistry of the late Archaean Qorqut Granite Complex of southern West Greenland, Geochimica et Cosmochimica Acta, 45, 1051–1060.

Nutman A.P. & Friend C.R.L., 2007, Adjacent terranes with ca. 2715 and 2650 Ma high-pressure metamorphic assemblages in the Nuuk region of the North Atlantic Craton, southern West Greenland: Complexities of Neoarchaean collisional orogeny, Precambrian Research, 155, 159–203.

Nutman A.P., Christiansen, O. & Friend C.R.L., 2007, 2635 Ma amphibolite facies gold mineralisation near a terrane boundary (suture?) on Storø, Nuuk region, southern West Greenland, Precambrian Research, 159, 19–32.

Pidgeon R.T. & Kalsbeek F., 1978, Dating of igneous and metamorphic events in the Fiskenæsset region of southern West Greenland, Canadian Journal of Earth Sciences, 15, 2021–2025.

Stensgaard B.M., Rasmussen T.M. & Steenfelt A., 2006, An integrative and quantitative assessment of the gold potential of the Nuuk region, West Greenland, Geological Survey of Denmark and Greenland Bulletin, 10, 37–40.

van Gool J.A.M., Scherstén A., Østergaard C. & Neraa T., 2007, Geological setting of the Storø gold prospect, Godthåbsfjord region, southern West Greenland; Results of detailed mapping, structural analysis, geochronology and geochemistry, Danmarks og Grønlands Geologiske Undersøgelse Rapport, 2007/83, København

CAMP-SCALE CONTROLS ON WORLD CLASS GOLD SYSTEMS IN THE YILGARN CRATON

J.M. Miller[1], T.C. McCuaig[1], B. Duggan[1] & G. Adams[2]

[1]Centre for Exploration Targeting, University of Western Australia, Crawley, W.A., 6009
[2]Focus Minerals Ltd, PMB 3, Coolgardie, W.A. 6429

Introduction

In the last 20 years models for the formation of world class gold systems have focussed on structural and host-rock control models, with the Crustal Continuum model widely applied as a unifying theory in the 1990's (Groves, 1993). Recent research into Archean gold systems in the Yilgarn Craton has assessed the role of fluids and also the relative importance of magmatic systems. The significance of the oxidation state for the alteration assemblages associated with gold mineralisation has been debated. Arguments range from whether oxidised assemblages are linked to fluid sourced from a deep mantle source or intrusion (e.g. Neumayr et al., 2008; Mueller et al, 2008) or do they reflect wall rock buffering (e.g., Evans et al., 2006) and/or fluid unmixing (e.g. Hodkiewicz et al., 2009). Some models still argue for the metamorphic fluid model (Phillips and Powell, 2009). However, mantle-derived fluids or melts (e.g., Mueller et al., 2008), and the location of zones of upper mantle fertility (Hronsky & Groves, 2009), are key components of many recent genetic gold models. If correct, these models imply understanding the nature of mantle tapping architecture is critical. The importance of unravelling the nature of the fluids, and associated alteration, is relevant to exploration targeting as fluid proxies can potentially be mapped using alteration assemblages via mineral identification, use of hyperspectral methods and also isotopic data. This paper highlights new insights into the formation of several world class gold deposits and camps by integrating structural geology and alteration with an understanding of the early architecture. This provides an improved insight into the structural style and alteration footprint associated with major gold systems at a camp-scale.

Camp-scale architectural controls

World class gold systems occur adjacent to reactivated crustal-scale deformation zones (e.g. Goldfarb et al., 2003), and these structures have been identified via field mapping, geochronology, and the use of geophysical data (predominantly magnetic, gravity and seismic data). Apart from physically identifying the location of crustal scale zones, unravelling the early event history along these structures is critical to understanding the formation of the currently mappable fault geometries because early rift architecture may have exerted a fundamental control. The role of early formed architecture has been well documented in Porphry Copper-Gold deposits with arc-transfer faults controlling the location of major mineral deposits (Garwin et al., 2005). The link between early extensional architecture in the Yilgarn Craton, and the current map patterns, was first highlighted by several studies in the early 1990's (e.g., Hammond & Nisbet, 1992; Williams and Whitaker, 1993). In the world class St Ives Gold Field, recent integrated geological and geophysical studies indicate that the architecture controlling the gold mineral systems at 2650-2630 Ma was already established as a 3D network of normal and oblique transfer faults at the time of volcanism, some 70 to 50 Ma earlier (Miller et al., 2009). This architecture controlled the emplacement of the komatiite units, the key host dolerite units, and also later intrusions. The early rift geometry is interpreted to have been a series of early WNW-trending relay faults associated with oblique rifting along an older NNW-trending basement boundary. During later D2 inversion a series of N-trending linking thrusts developed between the WNW-trending relay faults that later became critical contractional jogs during the main stage gold event. This example highlights the importance of seeing through various deformation events to early fundamental crustal architecture, and how this impacts on targeting orogenic gold mineralization at the camp scale. The role of early fault architecture is as important a process as the focussing of fluids and deformation around regional domes, which have also been highlighted to be a key control on the localisation of mineralisation (e.g. Davis et al., 2010).

Models for gold mineralisation associated with mafic and syenite intrusions

The Yilgarn Terrane underwent multiple phases of magmatism with a distinct phase of syenite and mafic mantle-derived intrusives that were emplaced coevally with the formation of late-stage sedimentary basins (Champion & Sheraton, 1997; Cassidy & Champion, 2002). Several papers have emphasised the role of these late-orogenic mafic and syenite intrusions with respect to gold mineralisation. Gold mineralisation is inferred to have had a direct link to mantle derived magmatism at Granny Smith and the world class Wallaby deposit (e.g. Mueller et al., 2008). However, U-Pb geochronology on these deposits indicates that only some of the gold mineralisation was coeval with magmatism, with high grade orogenic-style gold lodes associated with a reduced sericite–dolomite–albite assemblage that formed after the emplacement of the intrusive rocks (Salier et al., 2004; Mueller et al., 2008). Mafic magmas associated with the world class Kanowna-Belle deposit have also been inferred to be indicators of fertility for gold, and may have been the primary source for much of the metal endowment in that system (Davis et al., 2010).

In most deposits hydrothermal alteration associated with mineralisation overprints mafic dykes and larger intrusive bodies. One exception is the world class Jundee gold deposit that has strike-slip lodes that over print an

earlier series of mafic intrusives, but are cross-cut and truncated by mafic granodiorites. The formation of this deposit is bracketed by the emplacement of mantle derived intrusives, providing strong spatial and temporal relationships with this phase of magmatism, and the formation of a world class ore body. The Jundee deposit also contains unusual colloform vein textures indicative of mineralisation forming at an inferred shallow level with evidence for only one major phase of gold introduction i.e. there is no evidence for multiple phases of major gold introduction at Jundee.

Structural Geology integrated with alteration – evidence for multiple gold events

Many deposits show evidence for multiple phases of gold mineralisation. The Wallaby and Sunrise Dam gold deposits are located within 30km of each other. The Wallaby gold deposit is within an actinolite-magnetite-epidote-calcite alteration zone associated with a pipe-like syenite body that intruded a massive late basin conglomerate unit (Salier et al., 2004). Syenite dykes within the deposit, and associated mineralised steep-dipping calcite veins (with pyrite, biotite), have a radial distribution that implies vein emplacement during magmatism. The syenite dykes and calcite veins were over printed by N-S and NW-SE shortening associated with hematite-associated gold mineralization with low angle lodes. The hematite-associated lodes were then overprinted by a distinct phase of NE- to E-dipping sinistral oblique-slip faults linked to NW-SE shortening that define the major gold event and have reduced orogenic-style lodes with quartz, sericite, pyrite, dolomite, calcite ± fuchsite. The proposed model for Wallaby is that the earlier phase of gold mineralization associated with radial calcite veins (followed by the low angle hematite-associated lodes) was genetically linked to the syenite intrusives (Mueller et al., 2008). These lodes have been cross-cut by later orogenic-style lodes that were not coeval with the emplacement of the intrusives, but were linked to a deeper level fluid (i.e. Salier et al., 2004). The Sunrise Dam deposit is hosted by variable lithologies including volcanic rocks, BIF's, and felsic porphyries, and has initial low gold grades associated with early ductile shearing linked to a N-S trending mineral lineation, and the development of low angle W-dipping ductile shear zones with steeper dipping linking faults. These structures are over printed by E-W shortening with associated BIF-style gold mineralization and upright folding. Later sinistral-slip deformation was linked to NW-SE shortening with the associated formation of arsenic-rich lodes (Nugus et al., 2005), and this phase of gold correlates with the end-stage of orogenic gold at Wallaby. The Sunrise Dam structures are also further reactivated as late-stage dextral faults during ENE-WSW shortening with additional very high-grade gold mineralisation that at the end-stage is associated with base metals, tellurides and crustiform veins (Nugus et al., 2005).

The majority of major lodes within the world class St Ives Gold Field have classic orogenic-styles of mineralisation (e.g. quartz-calcite-albite-pyrite-sericite) with evidence indicating the major lodes are linked to one main stress field. However, the early WNW-trending transfer faults within the gold field have an earlier phase of actinolite and epidote growth over printed by oxidised alteration associated with low gold grades - that has marked similarities to the early alteration at Wallaby.

In the Coolgardie Goldfield there were two major phases of mineralisation that produced economic quantities of gold. These are associated with different structural kinematics and alteration styles. An early high-temperature phase (e.g. Knight et al., 2000) is linked to NW-SE shortening and sinistral-reverse kinematics with supralithostatic fluid over pressure associated with low angle quartz-vein arrays with arsenopyrite. The fault-vein arrays associated with this earlier phase of gold are geometrically similar to the quartz vein arrays in mafic rocks within the St Ives Goldfield. The second phase of gold mineralisation at Coolgardie over prints the earlier high-temperature phase and is linked to NE-SW shortening, dextral kinematics and lower temperature mineral assemblages with a strong base-metal association.

Summary

The key observations from the Wallaby, Sunrise Dam and Coolgardie deposits are that; 1) multiple gold events can occur that can be correlated regionally (although with major differences in endowment), 2) stress switches (marked by changes in fault kinematics and fault/extension vein geometries) are linked to changes in alteration assemblage. The interpretation is that stress switches changed the fluid flow pathways producing the sudden observed changes in alteration by: 1) accessing different fluid reservoirs and/or, 2) channelling fluid through, and equilibrating with, different rock types. In most areas distinct differences in alteration that can be mapped at meso- to macro-scale are linked to different structural events. The observed complexity within the deposits is inferred to reflect small total strains and much of the deformation may be driven by fluid over pressure linked to gold mineralization. Structural geology and reactive host rocks are critical aspects to the gold mineral system, particularly ore shoots. However, a key question is why do multiple phases of gold occur in same location irrespective of structural kinematics? Sunrise Dam was a transpressional and dilational jog at different points in the geological evolution with associated high grade mineralization. Furthermore, orogenic and magmatic-associated lodes have developed in the same locality (Wallaby). No matter what the genetic model, multiple pulses of fluids are evident in several deposits, particularly world class systems. There is evidence that some deposits have a strong association with mafic intrusions (Jundee), but orogenic-style lodes that post-date these intrusives are the dominant type (Salier et al., 2005). Models of multiple distinct events enriching a system to create a world class deposit need to be tempered by the observation that some deposits have one distinct phase of gold (e.g. Jundee).

Many deposits have a link to early architecture inferred from mantle-derived mafic intrusives (and by inference late-basin stage faulting with mafic intrusives occurring

where major vertical conduits existed), or variations in the host stratigraphy (e.g. dolerite and ultramafic thickness variations). The prevalence of gold deposits associated with dolerite is inferred to reflect not just a key host rock type, but the location of early architecture associated with the emplacement of the dolerite (and later gold-bearing fluids). Areas where variation in the strike of major faults occurs may indirectly highlight areas where the early fault architecture has created complexity (resulting in regional fault jogs being prospective). These relationships suggest there were architecturally favourable zones within a belt (e.g. transfer-normal fault intersections that formed pipe-like conduits) that were repeatedly reactivated via repeated fluid fluxing. Reactivation was to an extent independent of kinematics with strike-slip and compressional stress fields both associated with gold mineralisation. Mafic melts, previously linked to gold fertility (e.g. Davis et al., 2010), potentially produced gold-enriched crustal or lithospheric columns along architecturally favourable zones (or domes), to provide gold-rich segments of a belt creating an indirect link to orogenic gold lodes, although some gold is directly linked to this magmatism. Multiple phases of fluids are inferred to have fluxed along these enriched columns, and potentially there was more than one fluid type linked to gold lode development resulting in the observed mineralogical complexity, with possible different rates of fluid fluxes in different areas (e.g. a one phase gold system versus multiple gold events). Similar fluid fluxes may have occurred outside the gold-enriched areas.

Large zones of oxidised and reduced assemblages most commonly reflect distinct alteration events (and, in most cases, not fluid mixing). However, such alteration gradients potentially map zones where multiple phases of fluid flow have occurred. Oxidised assemblages may also map out older intrusive associated mineralisation (and possible precursor enrichment), and if mineral assemblage mapping is combined with architectural structural interpretation, it may provide a powerful method to map potential gold camps. Research focused on understanding the link between architecture, magmatism, and fluid flow through time, and how this is expressed in practical exploration data sets under cover, will be critical to using a mineral systems approach in the discovery of world class deposits.

Acknowledgements

This work evolved from pmd*CRC work. We would like to acknowledge discussion with David Groves, Jon Hronsky, Stephen Cox, Ed Baltis, Mike Nugus, Janet Tunjic, Richard Blewett, Rick Squire, Damien Keys, Matt Crawford, Paul Henson.

References

Cassidy K.F, Champion D.C., Fletcher I.R., Dunphy J.M., Black L.P. & Claoue-Long J.C., 2002, Geochronological constraints on the Leonora–Laverton transect area, northeastern Yilgarn craton, Geoscience Australia, Record 2002/18, 31–54.

Champion D.C. & Sheraton J.W., 1997, Geochemistry and Nd isotope systematics of Archaean granites of the Eastern Goldfields, Yilgarn craton, Australia: implications for crustal growth processes, Precambrian Research 83, 109–132.

Davis B.K, Blewett R.S., Squire R., Champion D.C., Henson P.A., 2010, Granite-cored domes and gold mineralisation: Architectural and geodynamic controls around the Archaean Scotia-Kanowna Dome, Kalgoorlie Terrane, Western Australia, Precambrian Research, in press.

Evans K.A., Phillips G.N. & Powell R., 2006, Rock-buffering of auriferous fluids in altered rocks associated with the golden mile-style mineralization, Kalgoorlie Gold Field, Western Australia, Economic Geology, 101, 805–817.

Garwin S., Hall R. & Watanabe Y., 2005, Tectonic setting, geology and gold and copper mineralization in Cenozoic magmatic arcs of Southeast Asia and the west Pacific, Economic Geology 100th Anniversary Volume, 891–930.

Goldfarb R.J., Baker T., Dubé B., Groves D.I., Hart C.J.R. & Gosselin P., 2005, Distribution, character, and genesis of gold deposits in metamorphic terranes, Economic Geology 100th anniversary volume, 407–450.

Groves D.I., 1993. The crustal continuum model for late-Archaean lode-gold deposits of the Yilgarn Block, Western Australia, Mineralium Deposita, 28, 366–374.

Hammond R.L. & Nisbet B.W., 1992, Towards a structural and tectonic framework for the Norseman –Wiluna Greenstone belt, Western Australia, in *The Archaean: Terrains, Processes and Metallogeny,* Glover J.E. & Ho S.E., eds, University of Western Australia Publication 22, 39 – 50.

Hodkiewicz P.F., Groves D.I., Davidson G.J., Weinberg R.F. & Hagemann S.G., 2009, Influence of structural setting on sulphur isotopes in Archean gold deposits, eastern Goldfields Province, Yilgarn, Western Australia, Mineralium Deposita, 44, 129–150.

Hronsky J. & Groves D.I., 2009, Towards a unified model for magmatic Gold metallogeny with implications for orogenic gold, *Smart Science for Exploration and Mining, 10th Biennial SGA Meeting of The Society for Geology Applied to Mineral Deposits, Townsville Australia, August 2009,* Williams P.J., ed, 102–104.

Knight J.T., Ridley J.R., & Groves D.I., 2000, The Archean amphibolite facies Coolgardie Goldfield, Yilgarn Craton, Western Australia: Nature, controls, and gold field-scale patterns of hydrothermal wall-rock alteration. Economic Geology, 95, 49–84.

Miller J., Blewett R. & Tunjic J., 2009,. The role of early formed structures on the development of a major gold system: St Ives gold camp, Kambalda, Yilgarn Craton, W.A., *Smart Science for Exploration and Mining, 10th Biennial SGA Meeting of The Society for Geology Applied to Mineral Deposits, Townsville Australia, August 2009,* Williams P.J., ed, 951–953.

Mueller A.G., Hall G.C., Nemchin A.A., Stein H.J., Creaser R.A. & Mason D.R., 2008. Archean high-Mg monzodiorite–syenite, epidote skarn, and biotite–sericite gold lodes in the Granny Smith–Wallaby district, Australia: U–Pb and Re–Os chronometry of two intrusion-related hydrothermal systems, Mineralium Deposita, 43, 337–362.

Neumayr P., Walshe J., Hagemann S., Petersen K. Roache A. Frikken P., Horn L. & Halley S. 2008, Oxidised and reduced mineral assemblages in greenstone belt rocks of the St. Ives gold camp, Western Australia: vectors to high-grade ore bodies in Archaean gold deposits? Mineralium Deposita, 43, 363–371.

Phillips G.N., Powell R., 2009, Formation of gold deposits: Review and evaluation of the continuum model, Earth Science Reviews 94, 1–21.

Salier B.P., Groves D.I., McNaughton N.J., Fletcher I.R., 2004, The world-class Wallaby gold deposit, Laverton, Western Australia: An orogenic-style overprint on a magmatic-hydrothermal magnetite-calcite alteration pipe? Mineralium Deposita 39, 473–494

Salier B.P., Groves D.I., McNaughton N.J., Fletcher I.R., 2005, Geochronological and stable isotope evidence for widespread orogenic gold mineralization from a deep-seated fluid source at ca 2.65 Ga in the Laverton Gold Province, Western Australia, Economic Geology, 100, 1363–1388.

Williams P.R. & Whitaker, RA.J., 1993, Gneiss domes and extensional deformation in the highly mineralised Archaean Eastern Goldfields Province, Western Australia, Ore Geology Reviews, 8, 141–162.

GEOCHEMICAL DEPTH-PROFILING OF LATE-STAGE MELTS FROM THE ~ 2.8 Ga WINDIMURRA IGNEOUS COMPLEX, WESTERN AUSTRALIA

O. Nebel[1], J.A. Mavrogenes[1], R.J. Arculus[1], T. Ivanic[2] & R. Langford[3]

[1]Research School of Earth Science, Australian National University, ACT 0200, Canberra
[2]Geological Survey of Western Australia, Department of Mines and Petroleum, WA 6060, Perth
[3]Flinders Mines Ltd, WA 6000 Perth

Introduction

Layered mafic intrusions (LMI) are large igneous bodies predominantly of mantle origin. The majority of these complexes are of Archean to mid-Proterozoic age and are only preserved in old cratons (Maier, 2005). Hence, their great ages and characteristics inherited from their ultimate sources in the upper mantle constitute unique windows into the genesis of cratonal roots and the evolution of the depleted mantle. In addition, the often preserved sequence from ultramafic to highly evolved magmas makes these bodies ideal for the study of mantle melting and subsequent crystallisation processes. Another notable aspect of LMIs is the occurrence of > 95% of the world's accessible noble metal resources, predominantly concentrated in reef horizons in the lower sequences of these bodies. Due to these important features, LMIs have been the subject of intense research for decades. However, despite numerous attempts, there are some fundamental issues associated with LMI that remain unsolved. Their origin is still a matter of debate, i.e., if mantle melting was triggered by a hot mantle plume, or by de-compressional melting in an extensional tectonic setting (Ernst & Buchan, 2001; Maier et al., 2008), even possibly related to subduction activity. Closely linked to the origin debate concerns the unusually high, bulk Si contents of these intrusions manifest by the early appearance of orthopyroxene in the crystallisation sequence. The silicate crystallisation sequence of the volumetrically most abundant, relatively dry, mantle-derived basaltic magmas (e.g., mid-ocean ridge basalts) is: olivine>plagioclase>clinopyroxene with late-stage orthopyroxene. In contrast, in many of the oldest and largest LMI, orthopyroxene is the next phase to appear after olivine. Only an origin for the parental melt from a highly depleted mantle source (harzburgitic) or via extensive contamination with silica-rich melts can explain this critical feature. Another important but yet open question is the cause of reef-type PGE deposits in some LMI whereas others appear to lack these economically important horizons.

In this contribution, we study the upper sequence of one of the planet's largest LMI, the Windimurra igneous complex with major and trace element analyses of whole rocks and minerals. We intend to place constraints on the genesis of late-stage melts in LMI, and voluminous mantle derived melts in general. A better understanding of mechanisms that control element distributions in the latest stage of voluminous mantle melts is essential in future ore prospecting and the formation of mafic crust.

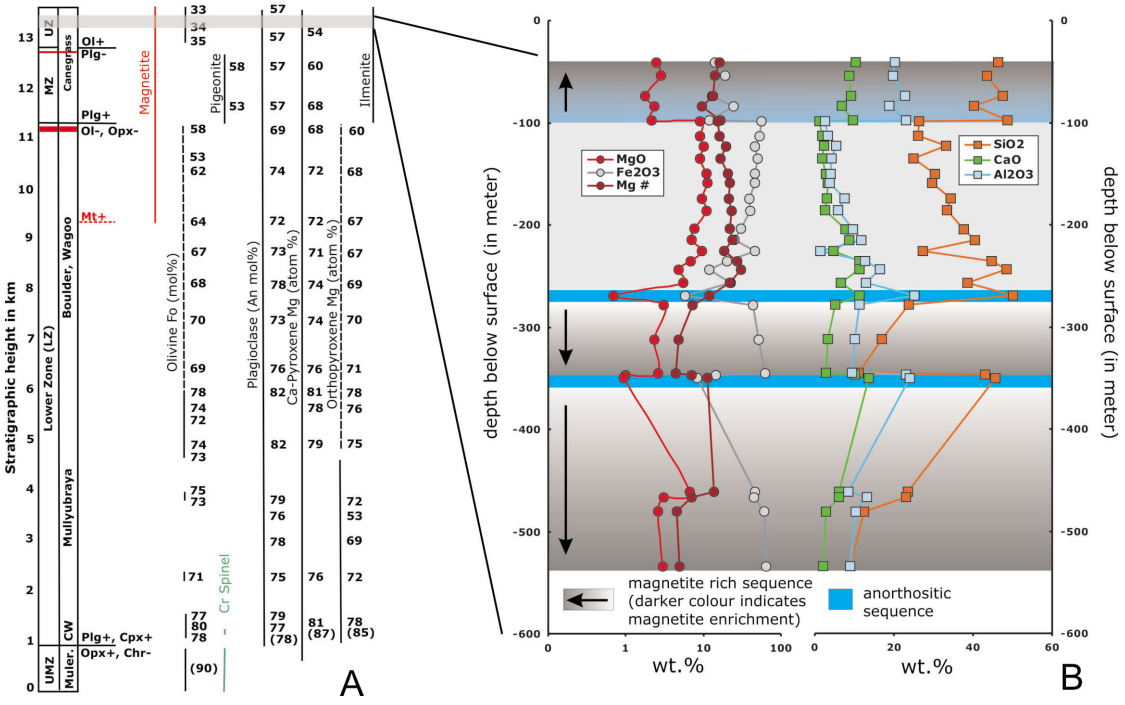

Figure 1. A: Stratigraphic series of the Windimurra Complex; modified from Ahmat (1986). B: Downhole major element variations of the studied drill core series. Note that figure B shows the uppermost part of figure A.

Geologic background

The Windimurra igneous complex (WIC) in Western Australia is similar in size to the Stillwater Complex, USA. It outcrops over a present surface area of >2000 km², southeast of Mount Magnet. The WNC consists of two major units, i.e., the Windimurra and the Narndee intrusions, both of which are composed of a series of ultramafic, mafic, and feldspathic rocks similar to other LMIs. The age of the WIC is 2.80 Ga as constrained by U-Pb SHRIMP analyses of zircon from the Narndee complex (Ivanic et al., 2010). Both complexes as part of the Murchison Domain intruded the Archean Yilgarn Craton with ambient plutonic rocks that are in no apparent relation to the actual complexes (Ivanic et al., 2010). Despite similar apparent emplacement ages of the two complexes, previous petrological investigations have suggested individual intrusion histories for both bodies and a later tectonic juxtaposition. The major difference between the two complexes is emplacement under relatively hydrous versus dry magma conditions. The Narndee Complex is characterised by elevated water contents with abundant igneous mica and amphiboles, and a basal amphibole cumulate unit (Scowen, 1991). In marked contrast, the Windimurra Complex contains no primary hydrous minerals, pointing to overall dry emplacement conditions derived from upper mantle sources, even in the evolved upper zone sequences (Ahmat, 1986). Along with these differences in water contents, previous Sr isotope investigations of the Windimurra Complex show depleted mantle isotope signatures with no or very minor crustal contamination.

Sample description & results

Drill core samples for the present study are taken from two boreholes located in the centre of the Windimurra Complex. The drill cores (MNDD002/3) are two of three boreholes that were drilled by Maximus Resources, in collaboration with the Western Australian Geologic Survey. The cores comprise a continuous sequence of 540 m of ultramafic, mafic and troctolitic layers of the upper section of the 'magnetic anomaly' located in the SW of the complex. The core can be subdivided into two major sequences with olivine-phyric gabbroic rocks in more shallow levels underlain by denser and magnetite-rich layers down-hole. The chemical compositions of the rocks are characterised by mafic to ultramafic successions with large variations in silica and total iron contents. The range is from oxide-rich layers to gabbroic and ultramafic compositions, depending on phase assemblage, with bulk silica contents between 9.0-50 wt.%. The phase assemblages are consistent with cumulate assemblages formed from evolving, parental tholeiitic magmas.

Discussion

Genetic model

The extreme Fe-enrichment observed in the uppermost Windimurra rock series conforms overall with an origin from late-stage tholeiitic melts in the absence of water. The late-stage character is confirmed by the occurrence of apatite-magnetite layers, and the reappearance of Fe-rich olivine, as reported from upper sequences of other LMI. However, the major difference of the Windimurra Complex compared with other LMI is the extreme Fe-enrichment after magnetite saturation. In the two lower sequences iron contents decrease up sequence, while in the upper series this trend reverses with iron concentrations increasing with increase height. The Fe-enrichment trend is decoupled from the modal abundance of magnetite and calls for an alternative mechanism. One way to achieve extreme Fe-enrichment in late stage melts of LMI is liquid immiscibility, as e.g., observed in the Skaergaard LMI (Jakobsen et al., 2005). In this model, a late-stage melt splits into a Si-rich, granitic component, and a Fe-rich part. However, based on recent experimental results (Schmidt et al., 2006), immiscible Fe-rich liquid preferentially incorporate Nb over Ta. Therefore, Nb/Ta, which is typically constant in any consanguineous magmatic system, would exhibit elevated Nb/Ta with increasing Fe contents in immiscible liquids. In Figure 2, Nb/Ta is projected versus FeO*, and shows the opposite trend of decreasing Nb/Ta with increased FeO*. Whilst this trend can be attributed to Fe-Ti oxide fractionation with low Nb/Ta in the normal series, the overall bulk silicate Earth-like Nb/Ta of the uppermost Fe-rich suite is inconsistent with liquid immiscibility, and so can be excluded here. A second possible cause of Fe-enrichment after magnetite saturation is magmatic differentiation under dry and low redox conditions. An early model of differentiation in late-stage melts of LMIs predicted strong silica enrichment after Fe-Ti oxide crystallization (Toplis & Carroll, 1995). However, as outlined by (Thy et al., 2009), this is only true for a large, and probably unrealistic amount of magnetite fractionation and accumulation. This is in contrast with observations

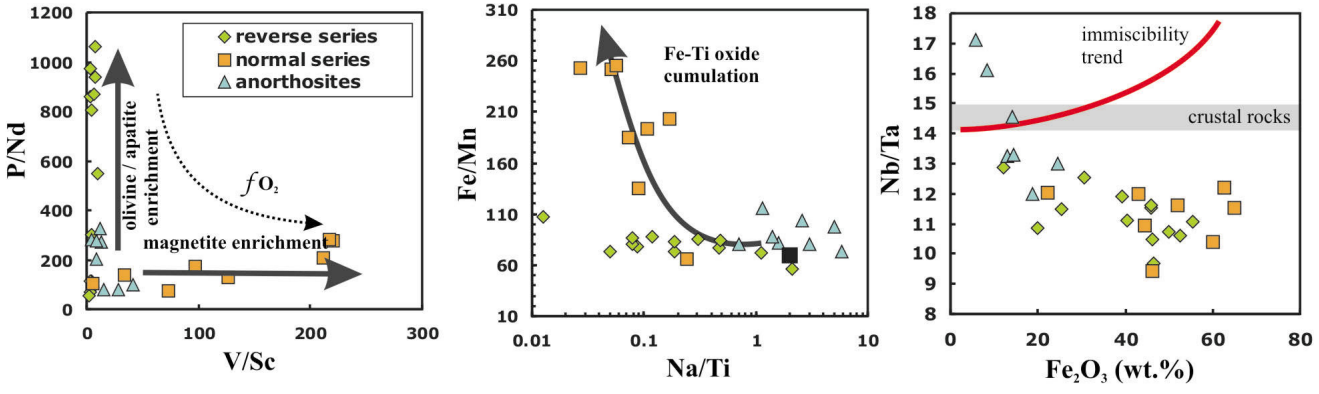

Figure 2. Major and trace element variation of drill cores MNDD002/3

of modal mineral abundances in late stage melts from the Skaergaard LMI, where magnetite fractionation modeling can causes redox conditions by -2Δ FMQ log units.

The modal magnetite abundances in the basal series of our studied drill core are extreme. However, the absolute amount of magnetite is probably on the order of ~30%, if the abundance is normalized to the entire suite, including the interstitial olivine-rich and roof anorthositic layers. Hence, the continuous enrichment in Fe in melts with 'low' magnetite abundance overlying the basal magnetite series is in general agreement with geochemical modeling results of (Thy et al., 2009). While the Fe enrichment in the reverse series can be caused by magnetite crystallization, a second, physical separation process needs to be considered. Accordingly, the opposing Fe enrichments trends (cumulus enrichment to the base vs. roof enrichment in the interstitial layers, as observed in Fig 1B) in these late stage melts of the Windimurra upper zone sequence are interpreted here as the result of dynamic crystallization and changes in fO2 within one magma chamber and subsequent physical separation of phases. The series of events can be drawn as follows: 1) Fe-rich late-stage magma intruded and started to crystallize magnetite. 2) Magnetite crystallization triggered physical magnetite accumulation on the base of a larger magma chamber, whilst a buoyant anorthositic liquid-crystal mush was floating up. Interstitial liquid remained at intermediate levels. 3) Extensive magnetite crystallization initiated a change in the ferric-ferrous ratio in the residual, interstitial magma. After consumption of the vast majority of Fe3+ by magnetite formation, the remaining liquid was Fe2+-rich, hence more reduced 4) After magnetite cumulus formation, decreased DFMQ in the remaining liquid-crystal mush sequence triggered fayalite-rich olivine (>Fa90) crystallization, which itself suppressed extensive orthopyroxene formation (as evident from subsolidus orthopyroxene exsolution) 5) Ferric-ferrous ratios were buffered by olivine crystallization, which consumed Fe2+ until ΔFMQ was high enough for equilibrium magnetite+opx crystallization. 6) The last stage involved physical filter-pressing of residual liquid out of base magnetitite and roof anorthosite until final crystallization. The depth gradient of Fe in the reverse series can be attributed to final density distributions of minerals in a crystal mush.

Concluding remarks and future outline

An extreme tholeiitic fractionation trend in the latest stages of fractional crystallization in the absence of water explains this series seen at Windimurra. Hence our suite is interpreted here to represent one pulse of magma recharge, hence being one large, dry Fe-rich magma chamber. The latter is confirmed by the absence of primary hydrous minerals, which are often present in other LMI. Thus, the Windimurra complex exhibits an extraordinary example of pure, extensive mantle melting and extreme Fe enrichment. Most importantly, it can be demonstrated that redox conditions can undergo dramatic changes in a closed magmatic system. In summary, we conclude that the absence of water plays a critical role on large scale mantle melt solidification scenarios, and implies that in a dry system, extensive magnetite formation is the controlling factor for the redox state of the melt. Future work, including stable and radiogenic isotope studies, are require to further refine our suggested hypothesis, and has the potential to unravel long standing questions in LMI research. In light of the absence of large PGE deposits in the Windimurra complex, we suspect that the water-poor environment may place constraints on the enrichment of PGE in reef horizons, which may require hydrous crustal assimilation. Accordingly, the early occurrence of orthopyroxene in the Windimurra sequence is not related to hydrous mantle melting, such that Si-enrichment in LMI is most likely related to their source rather than to crustal assimilation.

References

Ahmat A.L., 1986, Petrology, structure, regional geology and age of the gabbroic Windimurra Complex, Western Australia, PhD thesis, University of Western Australia.

Ernst R. E. & Buchan K. L., 2001, Large mafic magmatic events through time and links to mantle plume heads, in *Mantle Plumes: Their Identification through Time*, Ernst R.E. & Buchan K.L. eds.

Ivanic T.J., Wingate M.T., Van Kranendonk M.J., Kirkland C.L., and Wyche S., 2010, Age and significance of voluminous mafic-ultramafic magmatic events in the Murchison Domain, YIlgarn Craton, this volume.

Jakobsen J.K., Veksler I.V., Tegner C. & Brooks C. K., 2005, Immiscible iron- and silica-rich melts in basalt petrogenesis documented in the Skaergaard intrusion, Geology, 33, 885–888.

Maier W.D., 2005, Platinum-group element (PGE) deposits and occurrences: Mineralization styles, genetic concepts, and exploration criteria, Journal of African Earth Sciences, 41, 165–191.

Maier W.D., Barnes S.J., Bandyayera, D., Livesey, T., Li, C. & Ripley, E., 2008, Early Kibaran rift-related mafic-ultramafic magmatism in western Tanzania and Burundi: Petrogenesis and ore potential of the Kapalagulu and Musongati layered intrusions, Lithos**,** 101, 24–53.

Schmidt M.W., Connolly J.A.D., Gunther D. & Bogaerts M., 2006, Element partitioning: The role of melt structure and composition, Science, 312, 1646–1650.

Scowen P.A.H., 1991, The geology and geochemistry of the Narndee intrusion, Western Australia, PhD thesis, The Australian National University.

Thy P., Lesher C.E. & Tegner, C., 2009, The Skaergaard liquid line of descent revisited, Contributions to Mineralogy and Petrology, 157, 735–747.

Toplis M.J. & Carroll, M.R., 1995, An experimental study of the influence of oxygen fugacity on Fe-Ti oxide stability, phase relations and mineral-melt equilibria in ferro-basaltic systems, Journal of Petrology, 36, 1137–1170.

EPIDOTE-CLINOZOISITE AS A HYPERSPECTRAL TOOL IN ARCHEAN EXPLORATION

T.J. Roache[1], J.F. Huntington[2], M.A. Quigley[2], K. Yang[2], J.L. Walshe[1], B.W. Bil[3] & K.L. Blake[4]

[1]CSIRO ESRE, 26 Dick Perry Avenue, Kensington, WA, 6151, Australia.
(email tony.roache@csiro.au)
[2]CSIRO ESRE, 11 Julius Avenue, North Ryde, NSW, 2113, Australia.
[3] AGH-University of Science and Technology, A. Mickiewicza 30 Ave, Krakow, 30-059, Poland.
[4]Advanced Analytical Centre, James Cook University, Townsville, QLD, 4811, Australia.

Introduction

For twenty years mineral exploration has used short wavelength infrared (SWIR) hyperspectral data in the search for resources (e.g. Hauff et al. 1989, Hermann et al. 2001, van Ruitenbeek et al. 2005), but fresh-rock alteration mapping over this period has been predominantly restricted to white mica and to a lesser degree chlorite. White mica composition is the most well accepted hyperspectral index for characterizing alteration (cf. Scott & Yang 1997), but where white mica is only present in small amounts – lithologically and metamorphic dependent – proxies for other alteration minerals must be used. Chlorite composition (Pontual et al. 1997) is another spectral index that is used to differentiate proximal from distal alteration, and within Archean gold provinces may be used in tandem with white mica composition to affectively map alteration (e.g. Halley & Walshe 2006). It is proposed within this paper that end-member mineral phases within the solid solution series epidote-clinozoisite are representative of separate alteration styles. A hyperspectral index that acts as a proxy for this compositional difference will be presented in conjunction with textural and compositional evidence to show the relevance of this index to mineral exploration. The epidote-clinozoisite index is aimed at supplementing and supporting data derived from other hyperspectral indices that target gold mineralization, in this case within the lithologically-diverse mafic sequences of the Eastern Yilgarn Craton, Western Australia.

Methodology

A routinely-applied practice in the creation of and ongoing use of hyperspectral indices is to validate the mineral/s in question through a number of means including electron microprobe (EMPA), x-ray diffraction (XRD) and petrography. However, in a mineral system context, further information on mineral parageneses and spatial validation of the hyperspectral indices with respect to isotope, trace-element and lithogeochemistry is critical to be able to confidently map alteration minerals. The first part of the mineral systems methodology – mineral assemblage/parageneses and hyperspectral characterization/validation – will be detailed within this paper.

An understanding of the alteration minerals present within the mineral system is the first step in the methodology. This process involves petrographic description and EMPA, including back-scattered electron (BSE) images for additional textural reference. Alteration-related minerals were classified on the basis of being vein-hosted, but in a large number of cases matrix-hosted alteration that is defined by "metamorphic-like" concentric zoning were classified as metasomatic-related when grains:

- are fractured, infilled and commonly accompanied by brecciation;
- are contained within the selvage to veins;
- with patchy overgrowths are associated with veins; and
- contain rims of similar composition and habit to grains within adjacent veins.

To create a hyperspectral index that is of general interest to explorationists within the Yilgarn, SWIR spectra and associated samples for validation were analysed from seven different gold deposits within the eastern Yilgarn Craton. Qualitative mineral abundances from thin section description provided reference for spectral interpretation from thin section blocks. Two SWIR spectra were averaged to represent a bulk spectrum for each thin section block. Epidote and clinozoisite compositions were collected from the JXA 8200 EPMA at James Cook University, Townsville, using 15 kV acceleration voltage, 20 nA probe current and Jeol CITZAF (based on Armstrong method matrix correction). Additional analyses were obtained from a SEM-EDS Hitachi S-4700 with Thermo Noran Vantage analytical system at the Institute of Earth Science, Jagiellonian University, Cracow and a FEI Quanta 200 FEG with Schattky field emission gun at the Department of Economic Geology, AGH University, Cracow. Both Polish SEM devices used 15 kV acceleration voltage and 10 nA probe current.

Spectral interpretation and index creation within The Spectral Geologist™ (TSGCore™) software focussed on those minerals associated with most or all of the deposits. Indices were tested using a combination of visual validation via the spatially referenced spectra and drill core image facility within TSGCore™, and correlation plots involving EMPA compositions and proxy compositions derived from SWIR spectra.

Results

Mineral assemblages and parageneses

Epidote and clinozoisite have both been recognized as a metasomatic alteration mineral in the Archean Yilgarn Craton, but the latter has previously been identified as being metasomatic in origin at only one deposit (Clark *et al.* 1989). Detailed sampling and analyses at each of the seven deposits has revealed that clinozoisite is a common metasomatic phase at most sites, and is also spatially- and temporally-related with one of the dominant styles of gold mineralization at the Plutonic mine. Clinozoisite

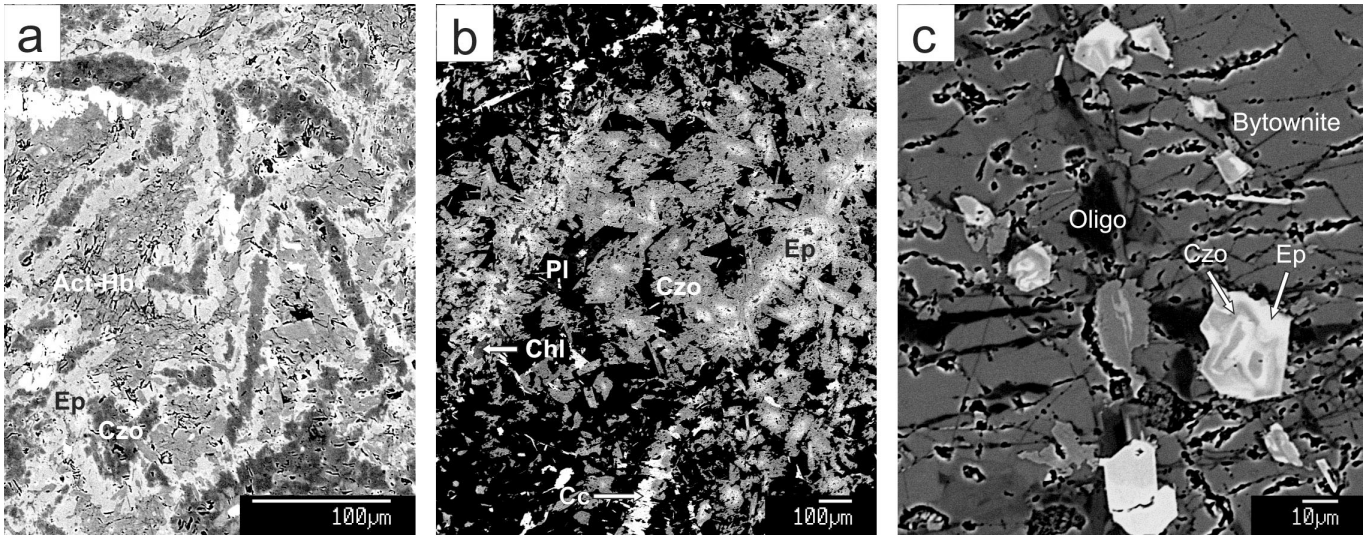

Figure 1. BSE images of multi-phase epidote-clinozoisite. a) Detailed image of the Ep-Czo+Act-Hb zone within figure 7a. Zoned, elongate accumulations of clinozoisite (Czo) and epidote (Ep) are surrounded by actinolitic hornblende (Act-Hb). Sample M400-098; Darlot. b) Zoned clinozoisite (Czo) and epidote (Ep) after bytownite (Pl). Epidote is concentrated within veins that also contain chlorite (Chl) and calcite (Cc). Sample M400-079; Lawlers. c) Bytownite was cross-cut by oligoclase (Oligo) -bearing veins that are also associated with oscillatory-zoned epidote (Ep) and clinozoisite (Czo). Sample M400-073; Lawlers.

is associated with a single clinozoisite+quartz±chlorite±biotite±carbonate±tourmaline±prehnite±pyrrhotite alteration assemblage, and epidote is associated with at least two alteration events characterized by epidote±actinolite±chlorite±albite±K-feldspar±anhydrite±biotite±carbonate±pyrite.

Given the textural criteria outlined in the methodology, the parageneses of epidote and clinozoisite may be summarized in the following:

- Metamorphic actinolite and/or plagioclase (oligoclase) was replaced by epidote;
- Metamorphic hornblende and/or calcic plagioclase (bytownite) altered to clinozoisite;
- Within tschermakite-bearing rocks, clinozoisite is the main epidote-series phase;
- Epidote is only present within tschermakite-bearing rocks where it was overgrown by the latter; and
- If there is neither clinozoisite nor any preserved metamorphic actinolite cores within a tschermakite-bearing sample, there is no epidote overprint.

If there is another paragenetic step involved, or if there are multiple epidote-clinozoisite phases within a sample, the parageneses become increasingly complicated:

- Where epidote-bearing veins overprint metamorphic hornblende or calcic plagioclase, epidote generally rims clinozoisite within the wall-rock (e.g. Fig. 1a), or in some circumstances may be rimmed by the latter (eg. Fig. 1b); and
- Generally, chlorite+quartz is associated with clinozoisite replacement of epidote and albite+K'spar±muscovite is associated with epidote replacement of clinozoisite.

In extreme cases, mutually overprinting vein-hosted epidote and clinozoisite are associated with oscillatory-zoned epidote-clinozoisite grains (Fig. 1c).

Mineral compositions and hyperspectral indices

Epidote-clinozoisite microprobe compositions from the seven gold deposits collectively define a broadly bimodal distribution. Each population is approximately separated by an epidote molecule content pistazite (Ps) of 15. A Ps of 15 distinguishes epidote (>15) from clinozoisite (<15) (Deer *et al.* 1996).

Observation from pure epidote and clinozoisite spectra (Clark et al. 2007) reveal that a change in the position of the 1550 nm absorption feature from relatively low to high wavelengths is related to a shift from epidote to clinozoisite, respectively. Other mineral spectra – including chlorite – that contain a weak absorption feature at 1550 nm may be filtered out using the depth of the latter, as epidote and clinozoisite contain a relatively deep 1550 nm absorption feature. The combination of the wavelength position and depth of the 1550 nm absorption feature – defined here as the epidote-clinozoisite index – is used to spectrally characterize the epidote-clinozoisite solid solution series. Comparison of the with epidote and/or clinozoisite compositions yields a subdivision of epidote- and clinozoisite-bearing samples based on a threshold of 1552.5 nm (Figure 2a). Inconsistencies in the classification are related to samples that contain both epidote and clinozoisite, as indicated by the spread of EMPA compositions in some samples. Petrography reveals that regardless of the EMPA compositional range, samples classified as epidote and clinozoisite on the basis of the epidote-clinozoisite index predominantly contain the corresponding phase. In many cases the subordinate phase represent relict porphyroblast cores (Figure 1a) and/or isolated veins (Figure 1b).

Epidote and clinozoisite commonly coexist with chlorite within mafic rocks, therefore in an effort to draw paragenetic links between end-member mineral phases that have been hinted through petrographic observation and EMPA compositions, epidote-clinozoisite and chlorite composition indices were compared from

samples that only contain coexisting chlorite and/or clinozoisite. Correlation of indices shows that epidote and clinozoisite coexist with Mg-rich chlorite and Fe-rich chlorite, respectively (Figure 2b).

Discussion

The most probable reason why the calculated from multi-phase epidote- and clinozoisite-bearing samples does not reflect the broad compositional ranges measured by EMPA, is because the SWIR spectra are derived from a large area (1 cm diameter) compared to the EMPA spot size. The difference in sample size was handled so that one averaged SWIR spectrum per sample was plotted against the range of EMPA compositions from the one sample, therefore eliminating the subjectivity in assigning variable epidote-clinozoisite index values to particular EMPA analyses. The apparent inconsistency in the assignment of epidote and clinozoisite to their respective domains would be improved by reducing the diameter of the hyperspectral lens to approach the spot size of the EMPA, but in terms of applying the epidote-clinozoisite index to mapping at drill hole-, mine- and exploration-scales, the general correlation between SWIR and EMPA is more than sufficient to delineate broad alteration domains. Differentiation between metamorphic- and metasomatic-derived epidote-clinozoisite may require the mapping of structurally controlled fluid pathways (Roache 2008) combined with lithogeochemistry, but the increasing integration of mineralogically-validated hyperspectral indices – as shown by the correlation of chlorite composition and epidote-clinozoisite indices – will result in a robust measure of metasomatic mineral assemblages that uniquely map Archean mineral system architecture.

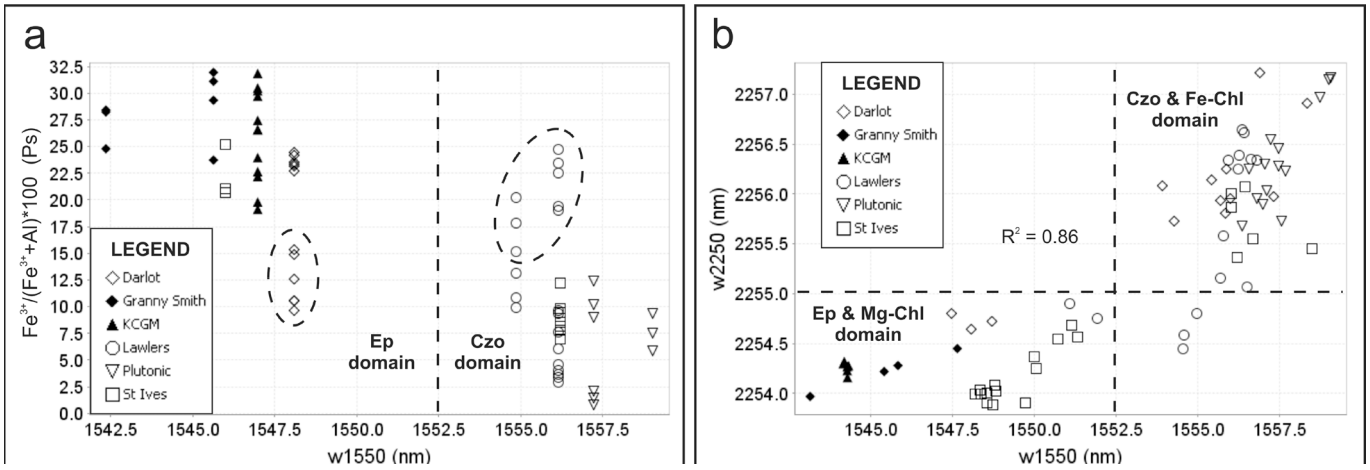

*Figure 2. Epidote, clinozoisite and chlorite compositional relationships from six of the seven studied gold deposits within the eastern Yilgarn Craton. a) Scatter plot of (Fe^{3+}/[Fe^{3+}+Al]*100) – epidote molecule content pistazite (Ps) – versus the epidote-clinozoisite index (w1550). Wavelength in nanometres (nm). Classification of epidote (Ep) and clinozoisite (Czo) is differentiated by a threshold value of 1552.5 nm. Samples that contain values below or near to 15 Ps within the epidote domain represent subordinate clinozoisite (Fig. 1a) and samples with values above 15 Ps within the Czo domain represent subordinate epidote (Fig. 1b). Al and Fe^{3+} were calculated on the basis of 12.5 O. b) Scatter plot of the chlorite composition index (w2250) versus the epidote-clinozoisite index (w1550). Wavelength in nanometres (nm). Samples selected for comparison contained chlorite and epidote/clinozoisite, and defined a linear relationship with correlation coefficient (R^2) of 0.86. Thresholds of 2255 nm and 1552.5 nm differentiate epidote (Ep) and Mg-rich chlorite (Mg-Chl) from clinozoisite (Czo) and Fe-rich chlorite (Fe-Chl). Most samples fall within each mineralogical domain.*

Acknowledgements

Thanks to MERIWA, M400 project sponsors and the CSIRO Minerals Down Under National Research Flagship for financial support. B.W. Bil samples were analysed thanks to a AGH-UST scientific grant: BS-11.11.140.562. Tests upon the Polish SEM devices were performed by Adam Gawel.

References

Clark M.E., Carmichael D.M., Hodgson C.J. & Fu M., 1989, Wall-rock alteration, Victory Gold Mine, Kambalda, Western Australia: processes and P-T-X_{CO2} conditions of metasomatism, in *The Geology of Gold Deposits: The perspective in 1988*, Keays R.R., Ramsay W.R.H. & Groves D.I., eds, Economic Geology Monograph, 6, 445–459.

Clark R.N., Swayze G.A., Wise R., Livo E., Hoefen T., Kokaly R. & Sutley S.J., 2007, USGS digital spectral library splib06a, U.S. Geological Survey Digital Data Series, 231, http://speclab.cr.usgs.gov/spectral.lib06.

Deer W.A., Howie R.A. & Zussman J., 1997, *Rock-forming minerals volume 1B: disilicates and ring silicates*, The Geological Society of London, 629p.

Halley S. & Walshe J., 2006, Alteration vectors to blind high grade gold ore bodies, in *Outcrop to Orebody – Innovative Geoscience in Exploration and Mining: Kalgoorlie,* Neumayr P., ed, AIG Bulletin, 44, 87–88.

Hauff P.L., Kruse F.A. & Madrid R.J., 1989, Gold exploration using illite polytypes defined by X-Ray diffraction and reflectance spectroscopy, in *Gold Forum on Technology and Practices -'World Gold 89' Proceedings, Littleton, Colorado,* Society for Mining, Metallurgy and Exploration, 76–82.

Herrmann W., Blake M., Doyle M., Huston D., Kamprad, J., Merry N. & Pontual S., 2001, Short Wavelength Infrared (SWIR) Spectral Analysis of Hydrothermal Alteration Zones Associated with Base Metal Sulfide Deposits at Rosebery and Western Tharsis, Tasmania, and Highway-Reward, Queensland, Economic Geology, 96, 939–955.

Pontual S., Merry N. & Gamson P., 1997, Spectral Interpretation Field Manual: Ausspec International Pty. Ltd., Kew, Victoria 3101, Australia, Spectral Analysis Guides for Mineral Exploration G-Mex Version 1.0, 169p.

Roache T., 2008, Hyperspectral modelling in mining and exploration: advances in the understanding of structurally-controlled mineralization, Geological Society of Australia, Abstracts 89, 276.

Scott K.M. & Yang K., 1997, Spectral reflectance studies of white micas, AMIRA, 439R, 35p.

van Ruitenbeek J.A., Cudahy T., Hale M. & van der Meer F.D., 2005, Tracing fluid pathways in fossil hydrothermal systems with near infrared spectroscopy, Geology, 33, 597–600.

THE UNDEREXPLORED ARCHEAN CRATON IN SOUTH EAST GREENLAND

B.M. Stensgaard, J. Kolb & T.F.D. Nielsen

Department of Petrology and Economic Geology, Geological Survey of Denmark and Greenland, Øster Voldgade 10, DK-1350 Copenhagen K, Denmark

Introduction

South East Greenland between 62°N and 67°N is one of the lesser-known regions in Greenland, having seen only limited geological investigations and no systematic sampling programmes (Nielsen 2009). The region encompasses the Archean North Atlantic craton (62°–64°30'N), the Palaeoproterozoic Ammassalik mobile belt (64°30'–67°N), and around 66°–67°N the Palaeogene intrusions of the Kialeq region.

Systematic data are essential as a basis for geological models and evaluation of the mineral potential. To open up the region for exploration, the Bureau of Minerals and Petroleum (BMP) has financed a two-year (2009 and 2010) systematic sampling program. In 2009, the program focused on the North Atlantic craton in South East Greenland (NAC-SEG). The initial program is focused on sediment sampling for geochemistry and indicator mineral analysis. Supplementary to this, surface water samples for chemical analysis were taken and radiometric spectra of representative lithologies were measured. In conjunction with the above objectives, the geology of selected key areas was reconnaissance. The initial sampling program will be followed by a genuine geological investigation program and assessment of the mineral potential. This program will incorporate the Geological Survey of Denmark and Greenland (GEUS), BMP and international research groups.

Here, we summarise the collected data and present the first results of the 2009 sampling program. In addition, we present a preliminary evaluation of the mineral potential and compare the geochemical and geological data with the better known Archean terranes in South West Greenland.

Regional geology of the North Atlantic craton in South East Greenland

The NAC-SEG consists mainly of gneisses interleaved with supracrustal belts that are up to 1 km wide and continue several kilometres along strike (Fig. 1, Andrews et al. 1973, Escher & Nielsen 1983). The gneisses comprise an early tonalitic-granodioritic generation, which is intruded by syn- to late-tectonic granitic to granodioritic sheets. The gneisses and supracrustal rocks are deformed and affected by amphibolite- to granulite-facies metamorphism. Late- to post-tectonic alkaline intrusions (2700–2660 Ma) belong to the Skjoldungen Alkaline Province (SAP) in the central part of the NAC-SEG (Rosing et al. 1988, Blichert-Toft et al. 1995). The province comprises at least 20 intrusions of variable size and composition. The most alkaline being the late-tectonic Singertât carbonatite complex in the fjord Kassortoq. Syenitic gneiss south and west of Kassortoq and at the western part of the island Skjoldungen are common. Based on the lithological variation and the regional structural grain, the NAC-SEG is subdivided into the Northern Zone (NZ), the central Skoldungen Alkaline Province (SAP), and the Southern Zone (SZ, Fig. 1). The present view on the tectno-metamorphic evolution is summarised in Figure 2.

Systematic sampling program

The preferred sample medium for the sediment samples was fine-fraction stream sediment from first- or second-order streams. Sediments from glacial overburden (consolidated or fresh) or cliff-scree sediments were collected in areas without drainage systems. A total of 506 sediment samples were taken. The sediments were dried, sieved and split before the fine-fraction (<0.1 mm) was sent for geochemical analysis. The samples have been analysed for 62 elements with a combination of INAA, Total Digestion (four acids) - ICP, Lithium Metaborate/ Tetraborate Fusion - ICP and ICP/MS methods. An average sample density of one sample per ca. 18–20 km^2 was achieved in costal and less glaciated areas, whereas the sample density was one sample per ca. 36–40 km^2 in more glaciated areas.

For indicator mineral analysis 138 coarse-grained sediment samples were collected. The material was sieved through a 6.35 mm screen in the field until a sample weight of about 8–10 kg was reached. The samples is being processed and picked for kimberlite and Au-Ni-Cu-PGE indicator minerals.

In places with suitable drainage systems, the sediment samples were supplemented by collection of two surface water samples from streams. Conductivity and pH were measured on one sample in the field. The second water sample was acidified before storage and later shipped for geochemical analysis. A total of 379 water samples were collected and have been analysed for 64 elements using a High Resolution Magnetic Sector ICP/MS.

When possible, measurements of radiometric spectra using a handheld multi-channel gamma-ray spectrometer were undertaken at suitable sample locations, determining the concentration of total gamma radiation, K, U and Th for rock units that were found to be representative for the area.

As part of the geological reconnaissance, rock samples of the representative lithology and, locally, mineralised rocks were sampled for geochemistry, petrology and age dating.

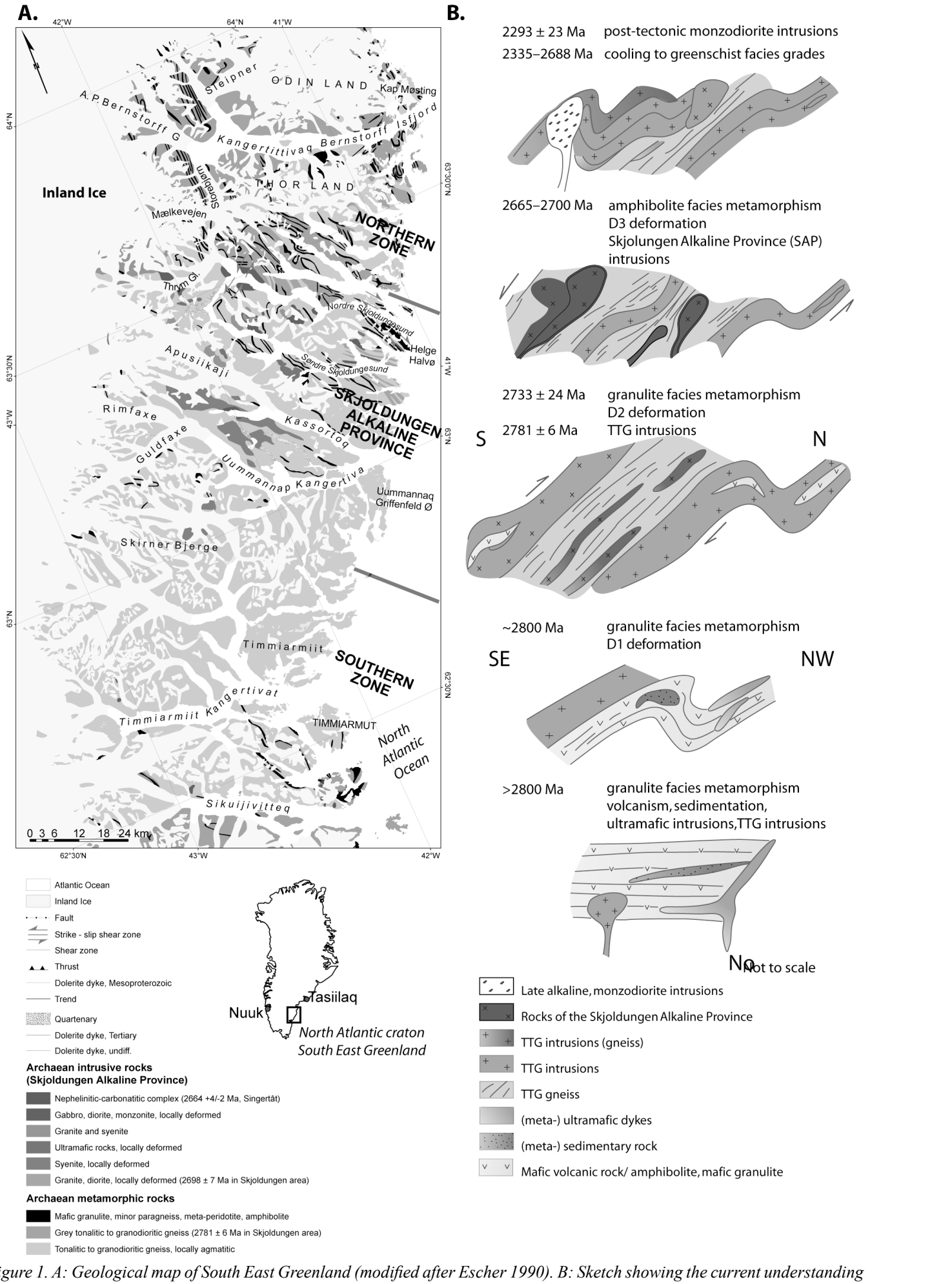

Figure 1. A: Geological map of South East Greenland (modified after Escher 1990). B: Sketch showing the current understanding of the geological evolution in the North Atlantic craton of South East Greenland.

Preliminary results

The sediment sample and surface water geochemistry, and the coarse-grained sediment indicator mineral data are confidential until April 1, 2010, were they will be released to the public. The complete data set from South East Greenland will be presented at the symposium in September 2010.

Preliminary results from the geochemistry point out areas that are anomalous in Ni, Cr, Au, Sn, In and REE. The first batch of indicator mineral samples comprises orthopyroxene, clinopyroxene, hornblende, olivine, chromite, garnet, pyrite, chalcopyrite and, locally, a few grains of gold. This assemblage is expected for the granulite-facies terrane with only few supracrustal belts intruded by ultramafic rocks. The samples are exceptionally fresh so that sulphide minerals are represented and can be used for mineral potential analysis. Olivine, chromite, Cr-diopside and Cr-andradite indicate an ultramafic source that may be fertile for Ni-Cu-PGE mineralisation.

The pH and conductivity of surface water and the radiometric measurements provided evidence for significant regional variations. Even though the range of both pH and conductivity is limited, likely due to the dominance of pristine glacial water sources, the data show clear correlation with known syenite from the Skjoldungen Alkaline Province at Kassortoq and the western part of the island Skjoldungen (Fig. 1). The regional correlation of high pH and conductivity with alkaline rocks possibly reflects preferential input into the surface water from these rock units. The SAP is also enriched in radiometric measured K. Elevated pH, conductivity and radiometric K content is also seen in the eastern parts of the Kassortoq and Skjoldungen areas, to the south at Timmiarmiut, and in the north at Nordre Skjoldungensund to spatially overlap with alkaline rocks. Their distribution in the Archean craton appears to be much more wide-spread than previously recognised.

Mineral potential

Based on the results from geological reconnaissance and the preliminary data of sediment and surface water geochemistry and sediment indicator mineral analysis, the following types of potential mineralisation have been identified.

Orthomagmatic systems with Ni-Cu-Cr-PGE-Au potential: Small, metre-scale lenses of metamorphosed ultramafic rocks are hosted in mafic rock units (supracrustal units) in the NZ (Fig. 1). These lenses generally show elevated concentrations of Ni, Cu and Cr. Several gossan horizons, up to tens of metres wide and continuous along strike for tens of kilometres, are seen within the rock sequence and may also hold a potential for Ni-PGE and Au. Within the SAP massive sulphide (pyrrhotite-pentlandite-chalcopyrite) mineralisation, 2–5 m wide and continuous along strike for several kilometres, have been encountered. The massive sulphide occurrences are hosted within meta-ultramafic rocks and may represent orthomagmatic mineralisation.

Hydrothermal quartz vein systems with Au potential: Quartz veins surrounded by hydrothermal alteration zones (pyrrhotite-chalcopyrite-quartz-biotite-garnet) in the SAP and the SZ are 10–20 m wide and traceable for 100 m to several kilometres along strike. The hydrothermal quartz veins and alteration zones in the SAP are structurally controlled by shear zones that are probably related to a pronounced 2.7 Ga thrust-shear zone that correlates with a world-wide peak of orogenic gold formation in Archean cratons.

Alkaline and carbonatite intrusions with REE, Sn, In and diamond potential: The Singertât carbonatite complex in the SAP yields a combined REE content of about 2500 ppm from grab rock samples. Sediment chemistry from other areas within the SAP, adjacent to alkaline rock units, have anomalous REE, Sn and In content and may indicate potential for these elements. However, the geological settings and rock units of the SAP are thought to be permissive for Nb, Th and U mineralisations these have not been encountered so far. Also, the syn-tectonic gabbros, granites and syenites of the SAP are generally very magnetite-rich, and the general geological setting is permissive for iron oxide copper-gold deposits. In the SZ, up to 2 m wide ultramafic dykes form a conjugate set. These dykes can be followed for several hundred metres along strike but represent calc-alkaline ultramafic rocks leaving only a low potential for diamond mineralisation.

Comparison with the geochemical signature of southern West Greenland

Stream sediment geochemistry data have successfully been used for the North Atlantic craton in southern West Greenland to interpret crustal configuration and mineralising systems (Steenfelt 2001, Steenfelt, pers. comm.). Most of the known lithologies and different crustal domains in southern West Greenland are distinguished from each other in one single or in a combination of geochemical parameters. For example, granulite facies tonalitic orthogneiss areas are found to be elevated in Sr, whereas areas with granodioritic to granitic rocks is associated with elevated Rb. Elevated combinations of both have been interpreted to indicate younger granites intruding older granulite facies terrain. Granitic components are further marked by combined high values of lithophile elements Cs, Rb, U and Th in the stream sediment geochemistry. Areas with elevated Ni concentrations in stream sediment geochemistry reflects areas with belts of mafic igneous infra- and supracrustal rocks or a high density of enclaves of such rocks in gneiss. Belts with high amount of igneous mafic rocks are associated with high Ni/Mg ratio, which have interpreted to reflect sea-floor alteration (Nielsen et al. 2006). Supracrustal belts associated with elevated Rb in the stream sediment geochemistry are attributed sedimentary rocks being present in the sea floor and basin environment. Ultramafic bodies are revealed by high Ni and Cr concentrations. The used of stream sediment geochemistry in the assessment of the potential for gold mineralising systems have also been applied successfully. Beside the use of traditional gold-pathfinder elements such as elevated As, Sb and Bi also elevated Cs

have been used as an indication of permissive ground for gold mineralisation associated with granite-related hydrothermal alteration (Steenfelt 2000). Also high Ni/Mg ratio, Rb, La, Th, and U have been shown to be indicative for gold mineralising systems (Stensgaard et al. 2006). A comparison between above established parameters from West Greenland and the new data from South East Greenland will be presented at the symposium in September 2010 when the data have been released.

References

Andrews J.R., Bridgwater D., Gormsen K., Gulson B., Keto L. & Watterson J., 1973, The Precambrian of Southeast Greenland, in *The Precambrian of Scotland and Related Rocks of Greenland*, Tarney J. & Park R.G., eds, Birmingham University Press, 143–156.

Blichert-Toft J., Rosing M.T., Lesher C.E. & Chauvel, C., 1995, Geochemical constraints on the origin of the Late Archean Skjoldungen alkaline igneous province, SE Greenland, Journal of Petrology, 36, 515–561.

Escher J.C. 1990: Skjoldungen 62°30'–67°00'N; 35°50'–43°15'W. Geological map of Greenland 1:500 000 (Geologisk kort over Grønland), Geological Survey of Denmark and Greenland.

Escher J.C. & Nielsen T.F.D., 1983, Archaean gneisses and supracrustal rocks of the Tingmiarmiut region, South-East Greenland, Rapport Grønlands Geologiske Undersøgelse, 115, 79–82.

Nielsen B.M., Steenfelt A. & Rasmussen T.M., 2006, Gold potential of the Nuuk region based in multi-parameter spatial modelling, Progress 2005, Danmarks og Grønlands Geologiske Undersøgelse Rapport 2006/27, 207p.

Nielsen T.F.D., 2009, Geological overview of the Region, in Preparations for a mineral resource assessment programme in South-East Greenland (MRAPSEG), (Confidential – Fortrolig), Thorning, L., ed. Danmarks og Grønlands Geologiske Undersøgelse Rapport 2009/5, 7–11.

Steenfelt A., 2001, Geochemical atlas of Greenland - West and South Greenland, Danmarks og Grønlands Geologiske Undersøgelse Rapport 2001/46, 39p.

Steenfelt A., 2000, Geochemical signatures of gold provinces in South Greenland, Transactions Institution of Mining and Metallurgy, section B, Applied Earth Science 109, B14–B22.

Stensgaard B.M., Rasmussen T.M. & Steenfelt A., 2006, An integrative and quantitative assessment of the gold potential of the Nuuk region, West Greenland, in *Review of Survey activities 2005*, Geological Survey of Denmark and Greenland Bulletin 10, Sønderholm M. & Higgins A.K., eds, 37-40.

THEME 4

ESTABLISHING A HABITABLE PLANET

KEYNOTE & INVITED SPEAKERS

TURBULENT LIFESTYLE: CYANOBACTERIA ON EARTH'S SANDY BEACHES – TODAY AND 3 BILLION YEARS AGO

N. Noffke

Old Dominion University; Ocean, Earth & Atmospheric Sciences; Norfolk, Virginia; USA
nnoffke@odu.edu

Introduction

Cyanobacteria are photoautotrophic microorganisms that form algal mats in marine environments. Algal mats are also termed microbial mats. These coherent organic carpets are very well adapted to harsh hydraulic conditions. If the microbes are covered by sediment, the mobile trichomes move towards the new depositional surface. They baffle and trap sand grains. If jet-like bottom currents cross the seafloor, the microbes respond by biostabilization.

Influences of microbial mats on marine sediments are generally understood as biogeochemical processes generating stromatolites in carbonate environments. In sandy environments, however, the interaction of microbial mats with physical sediment dynamics is dominant agent (Noffke & Paterson, 2008). Precipitation of minerals does not take place.

Our work in modern siliciclastic settings showed, that the microbial-physical interaction originates characteristic 'microbially induced sedimentary structures (MISS)'. Examples for such MISS are 'multidirected ripple marks', 'erosional remnants and pockets', 'oriented grains', and many others. The structures do not resemble stromatolites at all. They come in a great variety of shapes and morphologies. MISS are classified as own, separate group of sedimentary structures (Noffke et al., 2001b; Noffke 2009).

MISS occur not only today in modern marine environments. In systematic studies, we explored their occurrence in shallow-marine sandstones of all Earth ages. The structures record that extensive photoautotrophic microbial mats covered large areas of the ancient seafloor throughout Earth history (Noffke, 2000; Noffke et al., 2002; 2003b; 2006a, b). The mats most likely have been constructed by cyanobacteria. The oldest structures were found in the 3.2 Ga old Moodies Group, South Africa (Noffke et al., 2006b).

Biofilm-Catenae

Microbial mats are not distributed at random. Different types of mats develop in response to the long-term hydraulic pattern of an area. Because hydraulic reworking is function of morphology of the sea floor, we term lateral successions of different mat types 'biofilm-catenae' (Noffke, 1997; Noffke & Krumbein, 1999; Noffke et al. 2008). This was shown for example for the shelf of the Ordovician of the Montagne Noire in France (Noffke, 2000). Thick, epibenthic microbial mats grow at sites of calm dynamic conditions. Thin-endobenthic microbial mats grow at sites that are regularly reworked by storms.

In modern tidal flats, different types of microbial mats establish from the low to the high water lines (Noffke & Krumbein, 1999). In the lower intertidal zone, biofilms overgrow the sands. Biofilms are organic envelopes that cover each individual sand grains. The main biofilm-formers are coccoid cyanobacteria. In the upper intertidal zone, thin, endobenthic microbial mats develop. The mats are composed by the highly mobile filamentous species *Oscillatoria limosa*. In the lower supratidal zone, thick, epibenthic microbial mats can be found. These mats are formed by *Microcoleaus chthonoplastes*, a filamentous cyanobacterium well adapted to long periods of subaerial exposure. The same biofilm-catena was detected in a fossil tidal flat of the 2.9 Ga Pongola Supergroup, South Africa (Noffke et al., 2008).

Biostabilization of Sand

Quantitative measurements documented biostabilization of microbial mats and biofilms. Biostabilization is sand fixation by microorganisms. Microbially overgrown sandy surfaces are protected against erosion. The biostabilization of biofilms, endobenthic and epibenthic microbial mats was measured (Noffke & Paterson, 1995-1996, Mellum Island, Germany, and 2003 – 2007, Outer Banks, USA).

Biofilms do not much affect sedimentary processes (Noffke & Krumbein, 1999). Close to the low water line, biofilm-coated sand grains are swirled around by constant turbulence. The photoautotrophic cyanobacteria escape lethal burial, because the microbial-mineral aggregates stay longer in suspension than non-colonized grains. They settle at least and always accumulate on top of the sedimentary surface. Endobenthic microbial mats stabilize sandy substrates 3 – 5 times compared to sterile sand. Epibenthic microbial mats stabilize sand up to 12 magnitudes.

The response by benthic cyanobacteria to the hydraulic conditions was quantified in field experiments using a portable MANZENRIEDER flume chamber (Cady & Noffke, 2009).
This experiment produced a water current that crossed microbial mat surfaces. A digital system analyses the first release of sand grains from the mat surface. This

first release indicates the start of erosion of the microbial mat. The effect of the microbial mat on biostabilization of the sandy deposits was illustrated in a Shield's diagram (Noffke, 1997; Cady & Noffke, 2009). Endobenthic microbial mats colonize the uppermost millimeter of the sandy tidal surface and reduce the erosive forces of the currents significantly. The mat-covered sand withstands currents of up to 0.90 cm/s. The biostabilization effect is caused by the lower degree of roughness of the mat-interwoven depositional surface. Epibenthic microbial mats cover the tidal sands like a carpet. Their smooth surfaces reduce the erosive forces up to magnitudes of 12. As a consequence, such thick mats withstand currents of up to 1.60 m/s. This biostabilization effect prevents the direct influence of turbulent waters on the sand grains. This microbial effect can be expressed by a simple modification of the Shield's relation for sediment movement:

$$Q = r u^{*2} / (r s - r f)\, g\, \underline{Dn},$$

where u^* is the shear velocity; rf is the density of fluid; rs is the density of sediment; g is the gravity constant; D is the actual grain diameter under the influence of biostabilization; and n is the exponent to which D is raised for the data to comply to the Shield's relationship.

Comparison of modern with fossil MISS: the key to the past

The 2.9 billion years old Archean Pongola Supergroup, South Africa, records a sandy tidal flat originally located in a temperate clime zone. This ancient tidal flat may be compared to the modern tidal flats we find along the present North Sea coast. This ancient tidal flat includes exceptionally preserved MISS. These structures record microbial mats of high diversity. Detailed comparison of the ancient MISS in the Pongola with modern MISS of the North Sea tidal flats revealed that the nearly 3 billion years old microbial mats have been of same types like these colonizing our modern tidal flats today (Fig. 1). Our comparative study showed that the MISS in the Pongola Supergroup are of identical morphologies to those of the modern MISS in present tidal areas. The fossil MISS have the same pattern of distribution as the modern MISS. The same structures occur in exactly the same tidal zones in both modern and ancient tidal flats. The microscopic close-up reveals that both fossil and modern microbial mats include identical textures. This concurrence of morphologies, distributions, and internal microtextures in both modern and ancient mats permits suggestions on the original mat-forming microbiota. Most probably, the exceptionally well preserved microbial mats of the Pongola Supergroup include the oldest known cyanobacteria in Earth's history. Because the preserved microbiota are highly divers, this finding suggests an earlier rise of cyanobacteria than generally assumed. It is not likely that other prokaryotic groups would have formed the identical MISS with identical microtextures in the identical tidal zones like cyanobacteria do today. In conclusion, cyanobacteria possibly have been at least 2.9 Ga around (Margulis, 2009).

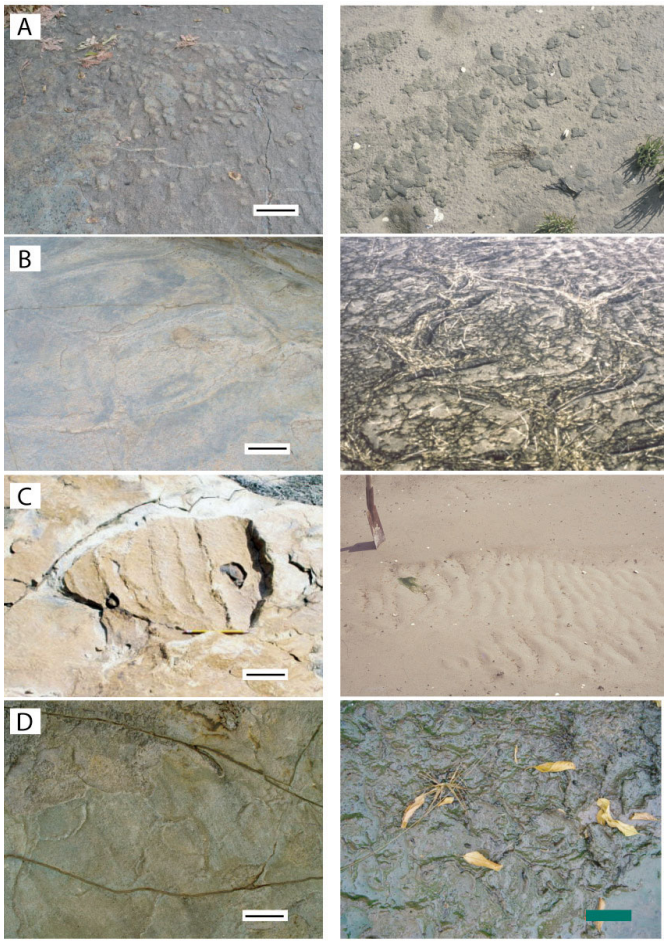

Figure 1. Microbially induced sedimentary structures (MISS). Photos on left show fossil MISS from 2.9 Ga Pongola Supergroup, South Africa. Photos on right show modern counterparts from east coast of USA and from Tunisia. A: Mat chips; scale 10 cm. Mat chips are fragments of microbial mats. They were ripped off their parent site and redeposited elsewhere. B: Polygonal oscillation cracks; scale: 15 cm. Such a polygonal crack pattern records alternating dry and wet seasons in a semi-arid, hopt climate zone. C: Erosional pocket; scale: 18 cm. Erosional pockets are gabs in microbial mats, where erosion has exposed the depositional surface beneath the mats. D: Dessiccation cracks in microbial mat; scale: 15 cm. Such cracks form in tidal areas of periodical exposure of mat surfaces.

Acknowledgements

Funding provided by National Science Foundation, NSF, Sedimentary Geology and Paleobiology Program; NASA Exobiology Program; and NASA Mars Exploration Rover Program.

References

Cady S. & Noffke N., 2009, Geobiology: Evidence for Early Life on Earth and the Search for Life on other Planets, GSA Today, 19, 4–10.

Margulis l, 2009, Pavements along memory lane and castles of sand long before "Man", Earth Science Reviews, 96, 5–6.

Noffke N., 2009, The criteria for biogeneicity of microbially induced sedimentary structures (MISS) in Archean, sandy deposits.- Earth Science Reviews, 96, 173–180.

Noffke N., Beukes N., Hazen R. & Swift D., 2008, Exceptionally preserved microbial mats of Meso-Archean age: the Sinqueni Formation, Pongola Supergroup, South Africa, Geobiology, 6, 5–20.

Noffke N. & Paterson D., eds., 2008, An actualistic perspective: Biotic-physical interaction of benthic microorganisms and the significance for the biological evolution of Earth, Geobiology, Special Issue, 6, 93.

Noffke N., Beukes N. & Hazen R., 2006a, Microbially induced sedimentary structures in the 2.9 Ga old Brixton Formation, Witwatersrand Supergroup, South Africa, Precambrian Research, 146, 35–44.

Noffke N., Hazen R., Eriksson K. & Simpson E., 2006b, A new window into early life: Microbial mats in a siliciclastic early Archean tidal flat (3.2 Ga Moodies Group, South Africa), Geology, 34, 253–256.

Noffke N., Hazen R. & Nhleko N., 2003, Earth's Earliest Microbial Mats in a Siliciclastic Marine Environment (Mozaan Group, 2.9 Ga, South Africa), Geology, 31, 6, 673–676.

Noffke N., Knoll A.H. & Grotzinger J., 2002, Sedimentary Controls on the Formation and Preservation of Microbial Mats in Siliciclastic Deposits: A Case Study from the Upper Neoproterozoic Nama Group, Namibia, Palaios, 17, 1–12.

Noffke N., Gerdes G., Klenke Th. & Krumbein W.E., 2001, Microbially induced sedimentary structures – a new category within the classification of primary sedimentary structures, Journal of Sedimentary Research, 71, 649–656.

Noffke N., 2000, Extensive microbial mats and their influences on the erosional and depositional dynamics of a siliciclastic cold water environment (Lower Arenigian, Montagne Noire, France), Sedimentary Geology, 136, 207–215.

Noffke N. & Krumbein W.E., 1999, A quantitative approach to sedimentary surface structures contoured by the interplay of microbial colonization and physical dynamics, Sedimentology, 46, 417–426.

ISOTOPIC EVIDENCE FOR EVOLVING ATMOSPHERIC AND OCEANIC CHEMISTRY AND THE EARLY EVOLUTION OF LIFE ON EARTH

J. Farquhar

Department of Geology and ESSIC, University of Maryland, College Park, Maryland, 20742, USA

Introduction

Numerous aspects of the evolution of Earth's atmosphere, oceans, and early evolution of life are captured by the records of light stable isotopes. Some of these observations were made more than 25 years ago, and others have been made only recently. This talk will examine the information provided by stable isotopes with a specific emphasis on the record of sulfur isotopes as they relate to the longer term evolution of Earth's surface environments and biosphere.

The record of sulfur isotopes include a (stepwise) change in the magnitude of variability for sulfur isotopes expressed by $\delta^{34}S$ measurements starting early in Earth history (e.g., Canfield 2004 – Figure 1). The oldest sequences exhibit a small range of variability (generally smaller than 15-30 ‰ for $\delta^{34}S$) and increases first to approximately 60 ‰ in the early Paleoproterozoic and then again to ~75‰ in the latest Precambrian. The origin of these changes has been attributed to changes in the role of sulfate reducing bacteria in the oceans at ~2.4 Ga and to changes in the sulfur cycle (possibly related to bioturbation) that occur near the end of the Precambrian.

Another type of change is expressed using $\Delta^{33}S$ as a change from a large mass-independent signal that disappears in the early Paleoproterozoic to a small signal attributable to metabolic processes associated with sulfate reduction and ultimately sulfur disproportionation. The change in $\Delta^{33}S$ in the early Paleoproterozoic is thought (1) to signal the rise in atmospheric oxygen, which impacted the production and transfer of isotope signals of atmospheric origin to the rock record and (2) to signal the rise of oceanic sulfate which allowed for the expression of isotope fractionations by sulfate reducing bacteria.

A closer look at the Archean record of $\delta^{34}S$ and $\Delta^{33}S$ reveals periods when the variability of $\delta^{34}S$ is small and that the $\Delta^{33}S$ is large (Eoarchean and Paleoarchean), periods when the variability of $\delta^{34}S$ and $\Delta^{33}S$ are both small (Mesoarchean), and periods when the variability of $\delta^{34}S$ and $\Delta^{33}S$ is as high as 10‰ (Neoarchean). The reason for this evolution has been discussed by a number of authors (Ohmoto et al. 2006; Farquhar et al., 2007; Domagol Goldman et al., 2009; Ueno et al., 2009; Halevey et al., 2010), and have generally been attributed to either changes in the source reactions that produce the mass-independent signal or (more recently) to changes in the cycling of sulfur between the atmosphere and the oceans.

A further feature of the sulfur isotope record is provided by $\Delta^{36}S$, which appears to be correlated with $\Delta^{33}S$, but in different ways during different intervals in the Archean, early Proterozoic (Farquhar et al., 2007). These changes have also been interpreted in the context of changing source reactions, and in some cases, apparent overprints by biological activity (Shen et al., 2009; Philippot et al., 2007; Kaufman et al., 2007).

While these features have provided new insights, they have also raised a number of questions. These include: (1) debates about the presence or absence of biological imprints on top of mass-independent signals early in Earth's history; (2) uncertainty about the relative roles of self shielding (which would be a necessary consequence of photolysis) and primary mass-independent isotope effects in producing the signal; and (3) uncertainty in the pathways that this sulfur isotope signal is transferred and transformed during the operation of the sulfur cycle. These aspects of the sulfur isotope record and its interpretation will be discussed.

References

Canfield, D.E., 2004, The evolution of the Earth surface sulfur reservoir, American Journal of Science, 304, 839–861.

Domagal-Goldman S.D., Kasting J.F., Johnston D.T. & Farquhar J. 2008, Organic haze, glaciations and multiple sulfur isotopes in the Mid-Archean Era, Earth and Planetary Science Letters, 269(1-2), 29–40.

Farquhar J., Peters M., Johnston D.T., Strauss H., Masterson A., Wiechert U. & Kaufman A.J. 2007, Isotopic evidence for Mesoarchaean anoxia and changing atmospheric sulphur chemistry, Nature 449(7163), 706-U5.

Farquhar J., Wu N.P., Canfield, D.E. & Oduro, H., 2010, Connections between sulfur cycle evolution, sulfur isotopes, sediments, and base metal sulfide deposits, Economic Geology, 105, in press.

Halevey I., Johnston D.T. & Schrag D.P., 2010, Explaining the structure of the Archean Mass-independent sulfur isotope record, Science Express 10.1126/ science.1190298.

Ohmoto H., Watanabe Y., Ikemi H., Poulson S.R. & Taylor B.E., 2006, Sulphur isotope evidence for an oxic Archaean atmosphere, Nature 442(7105), 908–911.

Shen Y. N., Farquhar J., Masterson A., Kaufman A.J. & Buick R., 2009, Evaluating the role of microbial sulfate reduction in the early Archean using quadruple isotope systematic, Earth and Planetary Science Letters, 279(3-4), 383–391.

Thomazo C., Ader M., Farquhar J. & Philippot P., 2009, Methanotrophs regulated atmospheric sulfur isotope anomalies during the Mesoarchean (Tumbiana Formation, Western Australia), Earth and Planetary Science Letters, 279(1-2), 65–75.

Ueno Y., Johnson M.S., Danielache S.O., Eskebjerg C., Pandey A. & Yoshida N., 2009, Geological sulfur isotopes indicate elevated OCS in the Archean atmosphere, solving faint young sun paradox, Proceedings of the National Academy of Sciences of the United States of America, 106(35), 14784–14789.

Ueno Y., Ono S., Rumble D. & Maruyama S., 2008, Quadruple sulfur isotope analysis of ca. 3.5 Ga Dresser Formation: New evidence for microbial sulfate reduction in the early Archean, Geochimica et Cosmochimica Acta, 72(23), 5675–5691.

ARCHEAN ISOTOPIC RECORDS: PALEO-OCEAN PROXIES OR MICROBIAL CYCLING?

C.M. Johnson

Department of Geoscience, University of Wisconsin, Madison, WI 53705, USA

Introduction

Interpretations of the isotopic compositions of ancient marine sedimentary rocks often divide into two groups; one, where these compositions are taken to reflect direct proxies for ancient seawater, and a second, where early authigenic mineral formation and soft-sediment diagenesis are thought to control the measured isotopic compositions, providing insight into microbial metabolisms. The large Fe isotope excursion that is seen in Neoarchean and Paleoproterozoic marine sedimentary rocks (Figure 1) are an excellent example of this debate. Iron isotopes have drawn great interest because the largest isotopic fractionations are produced by redox changes, and the occurrence of extensive iron-rich deposits such as iron formations of Archean and Proterozoic age indicates that large quantities of iron were cycled in ancient marine environments.

Iron and sulphur isotope records in ancient marine sedimentary rocks

The zero to positive δ^{56}Fe values for rocks >3.5 Ga in age, which to date only include banded iron formations (BIFs), are generally accepted to reflect partial oxidation of marine hydrothermal Fe^{2+}_{aq}, suggesting that the amount of oxidant was limited (e.g., Dauphas et al., 2004; Johnson & Beard, 2006; Whitehouse & Fedo, 2007). More controversial, however, is the Fe isotope record between ~3 and 2.5 Ga, where δ^{56}Fe values decrease to the lowest values yet measured in marine sedimentary rocks (Figure 1). Importantly, this shift occurs several hundred m.y. before the initial increase in atmospheric O_2. Focusing only on Fe isotope data from rocks younger than 2.8 Ga, Rouxel et al. (2005) and Anbar & Rouxel (2007) proposed that oxidation of marine hydrothermal Fe^{2+}_{aq} during BIF genesis, or oxide precipitation on continental shelves, produced negative δ^{56}Fe values in seawater, which was directly incorporated into sulphide-rich marine sedimentary rocks. The shift to negative δ^{56}Fe values is interpreted by these authors to record reservoir effects during abiologic oxide precipitation before free oxygen was available. Difficulties with this proposal lie in the isotopic compositions of earlier Archean rocks, which, so far, are essentially devoid of negative δ^{56}Fe values (Figure 1). If abiologic oxidation in the absence of free oxygen is the explanation for negative δ^{56}Fe values in rocks of 2.5 to 2.7 Ga age, why is this not recorded in older rocks, particularly the BIFs of >3.5 Ga in age?

In contrast, Yamaguchi et al. (2005) and Johnson et al. (2008a; 2008b) do not generally interpret the Fe isotope compositions to be a direct proxy for seawater and instead favour microbial iron cycling as an explanation for the Fe isotope variability. Mobilization of low-δ^{56}Fe aqueous Fe(II) by microbial dissimilatory iron reduction (DIR), and transport to sulfidic sinks in Neoarchean basins, has been proposed as a mechanism for shifting the δ^{56}Fe values of bulk-rock samples, a model referred to as an "Fe isotope basin shuttle" (Severmann et al., 2008). One of the arguments in favour of DIR as a mechanism for producing the negative δ^{56}Fe values in iron-rich shales and iron formations is that DIR produces *large* quantities of low-δ^{56}Fe aqueous Fe(II), whereas abiologic oxidation produces *small* quantities of low-δ^{56}Fe aqueous Fe(II) (Johnson et al., 2008b). Moreover, Johnson et al. (2008b) highlighted the fact that the negative δ^{56}Fe excursion occurs before an increase in the spread of δ^{34}S values for sedimentary sulphides (Figure 1), indicating that marine sulphate contents were limited prior to ~2.4 Ga; this in turn would favour DIR over bacterial sulphate reduction (BSR). The inferred rise in seawater sulphate at ~2.4 Ga corresponds with a decrease in the Fe isotope excursion (Figure 1), and Johnson et al. (2008b) proposed that this reflects a contraction in the extent of DIR relative to BSR. If the negative δ^{56}Fe excursion reflected an expansion of DIR, which is an anaerobic process that requires ferric hydroxides as an electron donor, this expansion should had occurred before free oxygen was available, reflecting the fact that oxygen sinks (e.g., conversion of ferrous to ferric Fe) would need to be first filled before a rise in free O_2 could occur; this explanation is consistent with the observation that oxygenic photosynthesis preceded the rise of atmospheric O_2 by several hundred m.y.

If the negative δ^{56}Fe excursion is due to DIR, and, importantly, its disappearance after ~2.2 Ga records an expansion of BSR, δ^{56}Fe and δ^{34}S values should be anti-correlated. As is well shown in modern marine systems, high sulphate contents inhibits DIR, because the sulphide that is produced by BSR effectively titrates reactive ferric (and ferrous) iron, eliminating its availability to DIR. DIR is most active in modern marine environments where sulphate is limited. Generally, δ^{56}Fe and δ^{34}S values are anti-correlated in Archean and Paleoproterozoic black shales (Yamaguchi et al., 2004), providing an important test of the microbial model for the negative δ^{56}Fe excursion, although an exception can be found for sulphides from the 2.7 Ga Belingwe sedimentary basin, where δ^{56}Fe and δ^{34}S values are positively correlated (Archer & Vance, 2006).

Adding other isotopes to the mix: C, O, and Sr

Marine carbonates are often proposed as the best candidates for a direct proxy for ancient seawater, although interpretation of C isotopes has been controversial. For example, the highly negative δ^{13}C values for iron formation carbonates have been interpreted by some studies to record microbial oxidation of organic matter (Baur et al., 1985; Becker & Clayton, 1972; Beukes

& Gutzmer, 2008; Fischer et al., 2009), whereas other studies called upon an ocean that was stratified in C isotope compositions to explain the data (Beukes et al., 1990; Winter & Knauth, 1992). By combining multiple isotopes, Heimann et al. (2010) showed that the C, O, and Fe isotope compositions of siderite from the 2.5 Ga Kuruman BIF could not reflect precipitation from seawater, but instead reflects the C, O, and Fe pathways involved with DIR. In addition, initial $^{87}Sr/^{86}Sr$ ratios determined on the same Kuruman BIF siderites confirm they did not form in equilibrium with seawater but instead reflect microbial diagenesis (Ludois et al., 2010) This is not to say that all Archean and Proterozoic marine carbonates were produced by microbial processes; indeed, all evidence indicates that Ca-Mg carbonates, unlike Fe-rich carbonates, that have $\delta^{13}C$ values near zero and low initial $^{87}Sr/^{86}Sr$ ratios likely formed in equilibrium with seawater, and therefore their Fe isotope compositions also likely reflect those of seawater (e.g., Czaja et al., 2010; Von Blanckenburg et al., 2008).

Can the Cretaceous provide insight into the Archean?

If redox cycling of Fe was driven by microbial processes in the soft sediment in Neoarchean and Paleoproterozoic basins, effectively decoupling Fe isotope variations from ambient conditions with regard to atmospheric oxygen, as favoured here, but in contrast to the proposals of Rouxel et al. (2005) and Anbar and Rouxel (2007), this may be tested by studies of Phanerozoic marine sediments that were deposited during periods of low seawater sulphate, when DIR would be expected to be relatively active. The Cretaceous oceans had low sulphate contents (likely <5 mM; Adams et al., 2010; Demicco et al., 2005; Lowenstein et al., 2003; Wortmann & Chernyavsky, 2007), in part due to massive evaporite deposition in the proto-South Atlantic (Wortmann & Chernyavsky, 2007). As a consequence, DIR may have replaced BSR as the dominant C degradation pathway in poorly oxygenated marine environments. In fact, Fe isotope data from a segment of Cretaceous strata encompassing Oceanic Anoxic Event (OAE) 2 (Jenkyns et al., 2007) suggests high rates of DIR prior to the event (Figure 1). Note that the negative $\delta^{56}Fe$ values, taken as a signal of DIR, occur before OAE-2, when seawater sulphate contents are inferred to have been lowest, but disappear at OAE-2 and later, when sulphate contents are inferred to have increased. This trend is accompanied by a decrease in $\delta^{34}S$ values for sulphides up to OAE-2, remarkably similar to the Fe-S isotope variations in the Neoarchan and Paleoproterozoic. A small step up in $\delta^{34}S$ values for sulphate at OAE-2 is also consistent with an increase in sulphate contents at OAE-2 (Figure 1), which would inhibit DIR.

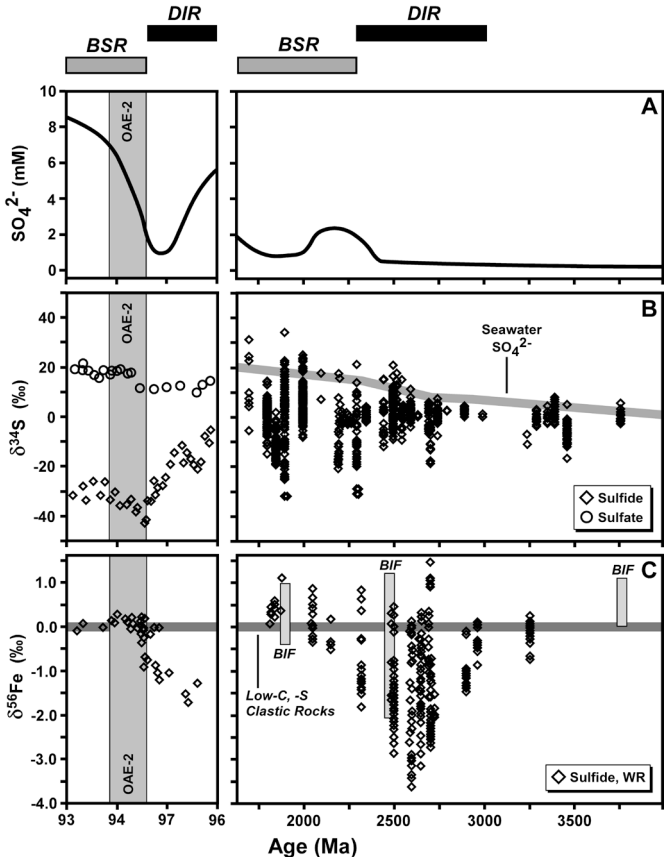

Figure 1. Temporal variations in seawater sulphate (A), $\delta^{34}S$ (B), and $\delta^{56}Fe$ (C) values for the Archean and Proterozoic (right side) and Cretaceous (left side). Adapted from Johnson et al. (2008b), with additional data (Adams et al., 2010; Habicht et al., 2002; Jenkyns et al., 2007; Kah et al., 2004; Schröder et al., 2008).

Conclusions

Anaerobic microbial processes such as DIR may be decoupled from ambient seawater and atmospheric conditions, and a record of this is seen in Fe isotope excursions in the Neoarchean and Paleoproterozoic, as well as the Cretaceous. In many, but not all, cases, the Fe isotope record for Fe-rich (BIF) and C-rich (black shales) units may not reflect seawater processes if microbial diagenesis was the last process to occur in the sediment prior to lithification. Although not useful as a paleo-ocean proxy in such cases, the Fe isotope data provide an important marker for the appearance of DIR on Earth. Because DIR requires a source of organic carbon and ferric Fe, its establishment at perhaps ~3 Ga requires photosynthesis (oxygenic or anaerobic) to have been established even earlier.

Acknowledgements

Collaborations with many researchers been important in forming the ideas discussed here, including, but not limited to, Brian Beard, Nic Beukes, Heidi Crosby, Andy Czaja, Jenn Eigenbrode, Robert Handler, Adriana Heimann, Andreas Kappler, Chris Kennedy, Kase Klein, Jim Ludois, Ken Nealson, Dianne Newman, Hiroshi Ohmoto, Eric Roden, Michelle Scherer, Silke Severmann, Joe Skulan, George Tangalos, John Valley, Sue Welch, Rene Wiesli, Lingling Wu, and Kosei Yamaguchi.

References

Adams D.D., Hurtgen M.T. & Sageman B.B., 2010, Volcanic triggering of a biogeochemical cascade during Oceanic Anoxic Event 2, Nature Geoscience, p. doi:10.1038/NGEO743.

Anbar A.D. & Rouxel O., 2007, Metal stable isotopes in paleoceanography, Annual Review of Earth and Planetary Sciences, 35, 717–746.

Archer C. & Vance D., 2006, Coupled Fe and S isotope evidence for Archean microbial Fe(III) and sulfate reduction: Geology, 34, 153–156.

Baur M.E., Hayes J.M., Studley S.A. & Walter M.R., 1985, Millimeter-Scale Variations of Stable Isotope Abundances in Carbonates from Banded Iron-Formations in the Hamersley Group of Western-Australia, Economic Geology, 80, 270–282.

Becker R.H. & Clayton R.N., 1972, Carbon isotopic evidence for the origin of a banded iron-formation in Western Australia, Geochimica et Cosmochimica Acta, 36, 577–595.

Beukes N.J. & Gutzmer J., 2008, Origin and paleoenvironmental signficance of major iron formations at the Archean-Paleoproterozoic boundary, Society of Economic Geologists SEG Reviews, 15, 5–47.

Beukes N.J., Klein, C., Kaufman A.J. & Hayes J.M., 1990, Carbonate Petrography, Kerogen Distribution, and Carbon and Oxygen Isotope Variations in an Early Proterozoic Transition from Limestone to Iron-Formation Deposition, Transvaal Supergroup, South-Africa, Economic Geology and the Bulletin of the Society of Economic Geologists, 85, 663–690.

Czaja A.D., Johnson C.M., Beard B.L., Eigenbrode J.L., Freeman K.H. & Yamaguchi K.E., 2010, Iron and carbon isotope evidence for ecosystem and environmental diversity in the ~2.7 to 2.5 Ga Hamersley Province, Western Australia, Earth and Planetary Science Letters, in press.

Dauphas N., van Zuilen M., Wadhwa M., Davic A. M., Marty B., and Janney, P.E., 2004, Clues from Fe isotope variations on the origin of Early Archean BIFs from Greenland, Science, 306, 2077–2080.

Demicco R.V., Lowenstein T.K., Hardie L.A. & Spencer R.J., 2005, Model of seawater composition for the Phanerozoic, Geology, 33, 877–880.

Fischer W.W., Schroeder S., Lacassie J.P., Beukes N.J., Goldberg T., Strauss H., Horstmann U.E., Schrag D.P. & Knoll A.H., 2009, Isotopic constraints on the Late Archean carbon cycle from the Transvaal Supergroup along the western margin of the Kaapvaal Craton, South Africa, Precambrian Research, 169, 15–27.

Habicht K. S., Gade M., Thamdrup B., Berg P. & Canfield D.E., 2002, Calibration of sulfate levels in the Archean Ocean, Science, 298, 5602, 2372–2374.

Heimann A., Johnson C.M., Beard B.L., Valley J.W., Roden E.E., Spicuzza M.J. & Beukes N., 2010, Fe, C, and O isotope compositions of banded iron formation carbonates demonstrate a major role for dissimilatory iron reduction in ~2.5 Ga marine environments, Earth and Planetary Science Letters, in press.

Jenkyns H.C., Matthews A., Tsikos H. & Erel, Y., 2007, Nitrate reduction, sulfate reduction, and sedimentary iron isotope evolution during the Cenomanian-Turonian oceanic anoxic event, Paleoceanography, 22, PA3208, doi:10.1029/2006PA001355.

Johnson C.M. & Beard B.L., 2006, Fe isotopes: an emerging technique in understanding modern and ancient biogeochemical cycles., GSA Today, 16, 4–10.

Johnson C.M., Beard B.L., Klein C., Beukes N.J. & Roden E.E., 2008a, Iron isotopes constrain biologic and abiologic processes in Banded Iron Formation genesis, Geochimica et Cosmochimica Acta, 72, 151–169.

Johnson C.M., Beard B.L. & Roden E.E., 2008b, The iron isotope fingerprints of redox and biogeochemical cycling in the modern and ancient Earth, Annual Review in Earth and Planetary Sciences, 36, 457–493.

Kah L.C., Lyons T.W. & Frank T.D., 2004, Low marine sulphate and protracted oxygenation of the Proterozoic biosphere, Nature, 431, 834–838.

Lowenstein T.K., Hardie L.A., Timofeeff M.N. & Demicco R.V., 2003, Secular variation in seawater chemistry and the origin of calcium chloride basinal brines, Geology, 31, 857–860.

Ludois J.M., Heimann A., Johnson C.M., Beard B.L., Valley J.W., Roden E.E. & Spicuzza M.J., 2010, Strontium isotopes of banded iron formation carbonates: An argument against iron carbonates precipitating from seawater, Astrobiology Science Conference: Houston, TX, Lunar and Planetary Institute.

Rouxel O.J., Bekker A. & Edwards K. J., 2005, Iron isotope constraints on the Archean and Paleoproterozoic ocean redox state, Science, 307, 1088–91.

Schröder S., Bekker A., Beukes N.J., Strauss H. & van Niekerk H.S., 2008, Rise in seawater sulphate concentration associated with the Paleoproterozoic positive carbon isotope excursion: evidence from sulphate evaporites in the ~2.2-2.1 Gyr shallow-marine Lucknow Formation, South Africa, Terra Nova, 20, 108–117.

Severmann S., Lyons T.W., Anbar A., McManus J. & Gordon G., 2008, Modern iron isotope perspective on the benthic iron shuttle and the redox evolution of ancient oceans, Geology, 36, 487–490.

Von Blanckenburg F., Mamberti M., Schoenberg R., Kamber B.S. & Webb G.E., 2008, The iron isotope composition of microbial carbonate, Chemical Geology, 249, 113–128.

Whitehouse M.J. & Fedo C.M., 2007, Microscale heterogeneity of Fe isotopes in >3.71 Ga banded iron formation from the Isua Greenstone Belt, southwest Greenland, Geology, 35, 719–722.

Winter B.L. & Knauth L.P., 1992, Stable isotope geochemistry of cherts and carbonates from the 2.0 Ga Gunflint iron formation: implications for the depositional setting, and the effects of diagenesis and metamorphism, Precambrian Research, 59, 283–313.

Wortmann U.G. & Chernyavsky B.M., 2007, Effect of evaporite deposition on Early Cretaceous carbon and sulphur cycling, Nature, 446, 654–656.

Yamaguchi K.E., Johnson C.M., Beard B.L. & Ohmoto H., 2004, Iron-sulfur-carbon contents and isotope systematics of 2.7 Ga shallow and deep facies black shales from the Hamersley Basin, Australia, Geochimica et Cosmochimica Acta, 68, A795–A795.

Yamaguchi K.E., Johnson C.M., Beard B.L. & Ohmoto H., 2005, Biogeochemical cycling of iron in the Archean-Paleoproterozoic Earth: Constraints from iron isotope variations in sedimentary rocks from the Kaapvaal and Pilbara Cratons, Chemical Geology, 218, 135–169.

ARE THERE SIGNS OF LIFE IN THE ~3,400 MA STRELLEY POOL FORMATION?

D. Wacey

Centre for Microscopy, Characterisation & Analysis, and School of Earth & Environment, The University of Western Australia, 35 Stirling Highway, Crawley, WA 6009

Introduction

The 3426-3350 Ma Strelley Pool Formation (SPF) is a silicified, dominantly sedimentary unit within the Pilbara Supergroup, Western Australia. It is found widely across the East Pilbara Terrane forming a prominent marker horizon in numerous greenstone belts, separating the largely volcanic 3520–3427 Ma Warrawoona and 3350–3315 Ma Kelly Groups (Hickman 2008). It has become one of the key formations for the study of early life following reports of some of the world's oldest stromatolites in the East Strelley (e.g. Lowe 1980) and Panorama (e.g. Hofmann et al. 1999) greenstone belts. The biogenicity of these stromatolites has been heavily debated and while large parts of the scientific community now appear to accept the biogenicity of at least the Panorama examples, others remain to be convinced (see Wacey 2010).

More recently, the basal sandstone member of the SPF has been investigated in some detail in the East Strelley greenstone belt. Here, these findings will be summarised and three types of microstuctures will be highlighted that suggest that life may have already colonised the shallow water environment of Strelley Pool prior to stromatolite formation.

Putative biosignals from the basal sandstone member of the SPF

1. Biofilms on detrital pyrite grains

Wacey et al. (2010a) describe rounded detrital pyrite grains occurring in dark-grey to black bedded sandstone at the base of the SPF, and in reworked intraclasts of black sandstone 1-2 m higher in the SPF. These form placer concentrates of heavy minerals with chromite, rutile and zircon. The rounded pyrite grains are coated with black carbonaceous material that is often laminated and becomes more diffuse away from pyrite surfaces (Fig. 1a). Surface channels and spherical to elliptical pits within the pyrite surface are systematically associated with the carbonaceous material (Fig. 1b). Wacey et al. (2010a) used high-resolution geochemical techniques [nano-scale secondary ion mass spectrometry (NanoSIMS), transmission electron microscopy (TEM), laser Raman micro-spectroscopy] to determine

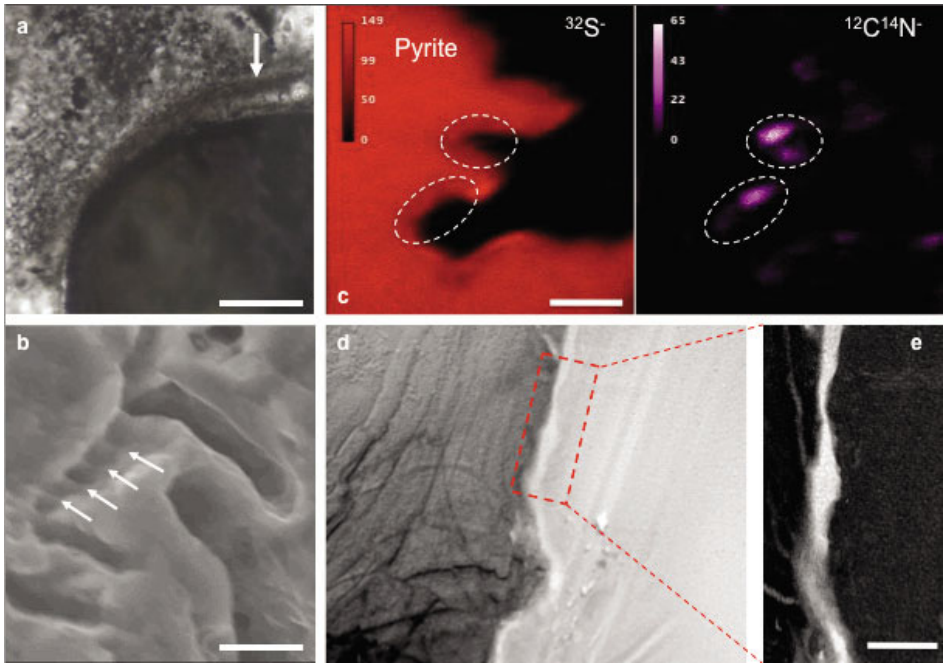

Figure 1. Biofilms on detrital pyrite grains. (a) Optical photomicrograph of a detrital pyrite grain coated with carbonaceous biofilm. The biofilm is crudely laminated near to the pyrite surface (arrowed) and more diffuse distant to the pyrite. (b) Secondary electron SEM image of microbially-mediated channels within pyrite grains. Note the evenly spaced indentations along the edges of a channel (arrowed) suggestive of attachment by chains of cells. (c) NanoSIMS elemental maps of sulfur (left; measured as $^{32}S^-$ to indicate pyrite) and nitrogen (right; measured as $^{12}C^{14}N^-$) showing localised concentrations of nitrogen associated with microbial pits within the pyrite surface. (d) Bright field TEM image showing pyrite (dark grey; left), silica-rich cement (light grey; right), and narrow band of low mass material (white; centre) at the pyrite-silica boundary. (e) Energy-filtered TEM elemental map of carbon distribution within the boxed area in (d). Scale bar is 30 μm for (a); 4 μm for (b); 2 μm for (c); 500 nm for (e).

whether these structures were biological in nature and to constrain their age. NanoSIMS elemental analysis showed localised enrichments of nitrogen within pits and channels (Fig. 1c). TEM and Raman confirmed the presence of carbonaceous grain coatings (Fig. 1d) and showed that the carbon structure was consistent both with a biological origin and with the metamorphic history of the sandstone. TEM and Raman also revealed a number of mineral deposits systematically associated with the pyrite surfaces and carbonaceous coatings. For example, a ~1 μm thick layer of amorphous silica and iron-aluminium-silicate occurs in a discrete band between the carbonaceous coatings and a pure microcrystalline silica cement, and nano-grains of iron oxide are present both within the carbonaceous layers and associated with the amorphous layer. Small (1-2 μm) grains of pyrite also occur separate from the main detrital pyrite grains, often within the carbonaceous coatings.

The grain-selective nature of the carbonaceous coatings, their lamination, association with micron-sized rounded pits/channels in the pyrite surfaces, the structure of the carbon, and lack of evidence for local hydrothermal activity lead Wacey et al. (2010a) to interpret the coatings as the remains of ancient biofilms. The pits and channels on pyrite surfaces are clustered and have dimensions typical of living microbes, leading Wacey et al. (2010a) to interpret them as microbial trace fossils. In particular, the spacing of indentations within some of the channels (Fig. 1b) and spatial restriction of nitrogen to their immediate vicinity strongly suggests microbial attachment to pyrite surfaces by chains of cells or filaments. Directly comparable microbially-mediated structures have been documented in younger rocks (e.g. from the Proterozoic of Montana (Schieber 2002) and from the modern bio-erosion of pyrite by Fe- and S-oxidising microbes (Bennett & Tributsch 1978). Similarly, oxidation of pyrite by extant Fe- and S-oxidising microbes results in precipitation of insoluble Fe-hydroxides that, on geologic timescales, dehydrate to Fe-oxides (Posth et al. 2008), consistent with observations of nano-iron oxides from the SPF. The 1-2 μm grains of pyrite observed within the biofilms have been interpreted as the products of localised bacterial sulfate-reduction, suggesting an entire microbial sulfur cycle operating on the micro-scale (Wacey et al. 2010a). This interpretation is supported by sulfur isotope data (see below). In summary, this work provides evidence for reduced forms of iron and sulfur functioning as electron donors for microbial oxidation reactions on the early Earth.

2. Microfossils

Two further types of carbonaceous microstructures are found in well-preserved black sandstone. These occur within pore spaces and coating framework quartz grains, surrounded by and infilled with microcrystalline silica cement. Cell-like microstructures are typically 2 μm to 5 μm in diameter and occur as clumps and chains (Fig. 2a). Tubular sheath-like structures occur in association with the 'cells' and are up to 10 μm in diameter and up to 50 μm long (Fig. 2a). Both types of microstructures are numerous and often occur in the same black sandstone samples as the detrital pyrite grains described above. A number of hypotheses are currently being tested for their formation: H1 – They are bona fide cells and sheaths that are indigenous to the sandstone; H2 – They originate from non-biological self-organisation of carbonaceous material during the growth and re-crystallisation of spherulites (cf. Brasier et al. 2005); H3 – They are younger contamination. Preliminary geochemical data indicate the following:

- Raman imaging and micro-spectroscopy shows that the microstructures are found below the surface of thin sections (i.e. they are not sample preparation artefacts). They are composed of carbon that has a structure consistent with both a biological precursor and having experienced lower greenschist facies metamorphism. The microstructures cannot, therefore, be modern contaminants. However, since metamorphism occurred up to ~2.9 Ga, this Raman signal does not allow discrimination between microstructures that are 3.4 Ga (i.e. indigenous to the SPF) from those which may have been introduced between 3.4 and 2.9 Ga.

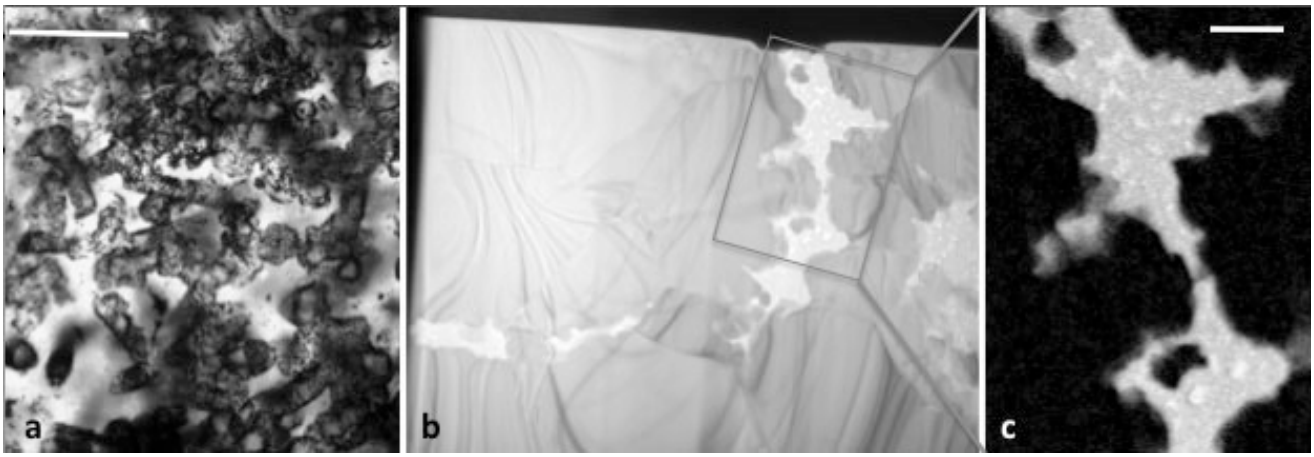

Figure 2. Putative microfossils from the Strelley Pool sandstone. (a) Optical photomicrograph showing cell- and sheath-like microstructures. (b) Bright field TEM image from an ultrathin FIB section showing a cross-section through approximately one quarter of a putative coccoid cell wall (light grey) within a microcrystalline quartz matrix (dark grey). The interior of the 'cell' is to the top left of the image and is composed of numerous interlocking micro-quartz grains. (c) Energy-filtered TEM elemental map showing the distribution of carbon within the boxed area in (b). Scale bar is 50 μm for (a) and 500 nm for (c).

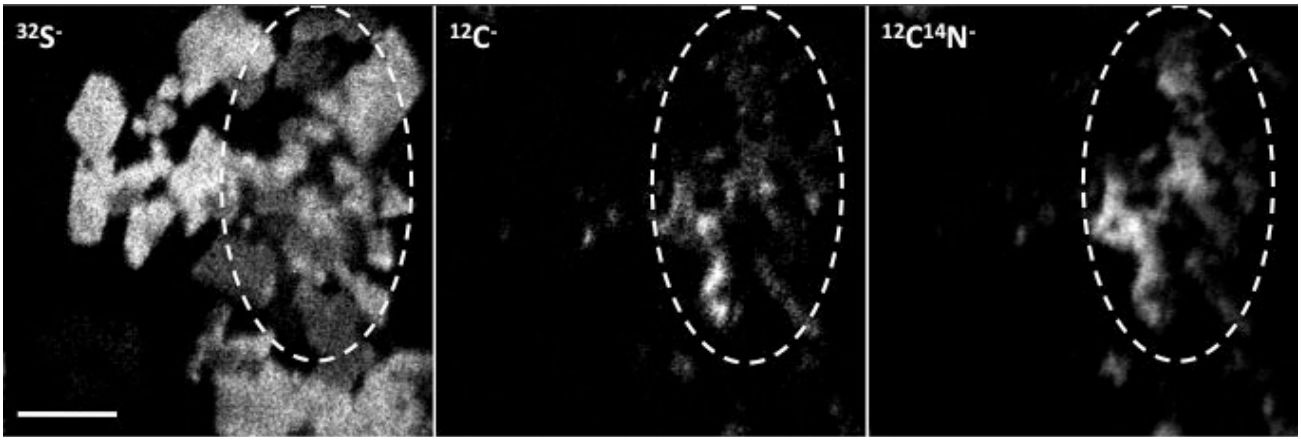

Figure 3. NanoSIMS secondary ion images of pyrite (left; measured as $^{32}S^-$), and associated organic material (centre $^{12}C^-$, and right $^{26}CN^-$). Dashed ovals represent identical areas in each image and highlight those areas with highest carbon and nitrogen values. Scale bar is 2μm.

- TEM data from focussed ion beam (FIB) milled ultrathin sections confirm the carbonaceous composition of the microstructures and confirms that they extend well below the surface of the thin section (Fig. 2b, c). This data also allows H2 to be rejected since the carbon does not coat spherulitic quartz grains (Fig. 2b).

In situ isotopic data is currently being obtained together with 3D analysis of the microstructures to further constrain their origin.

3. Pyrite biominerals

Micron-sized pyrite grains coat many of the detrital framework quartz grains within pockets of well-preserved black sandstone, and also in reworked black intra-clasts higher up in the sandstone member. Two suites of geochemical data obtained using NanoSIMS suggest a biological formation mechanism (Wacey et al. 2010b):

- NanoSIMS elemental mapping shows that these tiny pyrite grains are systematically associated with carbon and nitrogen (Fig. 3). The highest relative concentrations of C and N are often associated with the smallest and least well-formed (in terms of crystal shape) pyrite grains. C and N are two vital biological elements. The mere presence of C and N does not necessarily indicate the former presence of biological activity because they can be formed non-biologically, for example, through Fischer-Tropsch type synthesis (McCollum & Seewald 2006). However, this requires not only high temperatures but, especially in the case of nitrogen, very specific reactants and catalysts. The depositional setting and early diagenetic history of the Strelley Pool sandstone is inconsistent with such conditions, hence the systematic co-occurrence of C and N with micron-sized pyrites strongly suggests a biological input to pyrite formation the SPF.
- NanoSIMS $\delta^{34}S$ values range from ~ -12 to +6‰ (mean -2.5‰) within a single thin section, with a spread of 18‰ and a maximum fractionation of ~15‰ from inferred early Archean seawater sulfate and ~12‰ from inferred elemental sulfur in the early Archean ocean. This micron-scale variation could not have been resolved using conventional analyses, and the bulk mean value of -2.5‰ would likely have been interpreted as a hydrothermal or volcanogenic signature. In contrast, the NanoSIMS data suggests this pyrite formed by microbial sulfur processing on the early Earth. The range in $\delta^{34}S$ values is of a similar magnitude to putative reports of biological sulfur processing in other early Archean sediments (e.g. Shen et al. 2001), and to average fractionation factors for microbial sulfur processing reactions observed today (e.g. Habicht & Canfield 2001).

Multiple sulfur isotope analysis is currently underway to attempt to further constrain sulfur cycling within these sediments.

Acknowledgements

I wish to acknowledge Martin Brasier, Matt Kilburn & Martin Saunders who have collaborated on much of this work, and Arthur Hickman & Martin van Kranendonk who have provided invaluable advice regarding sample collection and the regional geology of the Pilbara. This work was funded by the Australian Microscopy and Microanalysis Research Facility, and The University of Western Australia.

References

Bennett J.C. & Tributsch H., 1978, Bacterial leaching on pyrite crystal surfaces, Journal of Bacteriology, 134, 310–317.

Brasier M.D., Green O.R., Lindsay J.F., McLoughlin N., Steele A. & Stoakes C., 2005, Critical testing of Earth's oldest putative fossil assemblage from the ~3.5 Ga Apex Chert, Chinaman Creek, Western Australia, Precambrian Research 140, 55–102.

Habicht K.S. & Canfield D.E., 2001, Isotope fractionation by sulfate-reducing natural populations and the isotopic composition of sulfide in marine sediments, Geology, 29, 555–558.

Hickman A.H., 2008, Regional review of the 3426-3350 Ma Strelley Pool Formation, Pilbara Craton, Western Australia, Geological Survey of Western Australia, Record, 2008/15.

Hofmann H.J., Grey K., Hickman A.H. & Thorpe R., 1999, Origin of 3.45 Ga coniform stromatolites in Warrawoona Group, Western Australia, Geological Society of America Bulletin, 111, 1256–1262.

Lowe D.R., 1980, Stromatolites 3,400-Myr old from the Archean of Western Australia, Nature, 284, 441–443.
McCollum T.M. & Seewald J.S., 2006, Carbon isotope composition of organic compounds produced by abiotic synthesis under hydrothermal conditions, Earth and Planetary Science Letters, 243, 74–84.
Posth N.R., Hegler F., Konhauser K.O. & Kappler A., 2008, Alternating Si and Fe deposition caused by temperature fluctuations in Precambrian oceans, Nature Geoscience, 1, 703–708.
Schieber J., 2002, Sedimentary pyrite: A window into the microbial past, Geology, 30, 531–534.
Shen Y., Buick R. & Canfield D.E., 2001, Isotopic evidence for microbial sulphate reduction in the early Archaean era, Nature, 410, 77–81.
Wacey D, Kilburn M.R., McLoughlin N., Parnell J., Stoakes C.A. & Brasier M.D., 2008, Using NanoSIMS in the search for early life on Earth: ambient inclusion trails in a c.3400 Ma sandstone, Journal of the Geological Society of London, 165, 43–53.
Wacey D., 2010, Stromatolites in the ~3400 Ma Strelley Pool Formation, Western Australia: examining biogenicty from the macro- to the nano-scale, Astrobiology (in press).
Wacey D., Saunders M. & Kilburn M.R., 2010a, Primitive life colonised pyrite on the early Earth, Nature Geoscience (in review).
Wacey D., Boyce A.J. & Kilburn M.R., 2010b, Sulphur isotope analysis using NanoSIMS: an example from the early Archean of Western Australia, Precambrian Research (in review).

THE GREAT OXIDATION EVENT RECORDED BY TRANSITION ELEMENT ABUNDANCES IN BANDED IRON FORMATIONS

K.O. Konhauser* & S.V. Lalonde

Department of Earth and Atmospheric Sciences, University of Alberta, Edmonton, AB, Canada.
**corresponding author: kurtk@ualberta.ca*

Summary
Banded Iron Formations, ancient marine deposits originally consisting of iron- and silica-rich chemical sediments, preserve a record of the evolution of seawater by shifts in their composition over time. The Great Oxidation Event some 2.4 – 2.2 billion years ago (Ga) is recorded in the BIF rock record by dramatic excursions in the abundances of certain redox-sensitive trace elements such as molybdenum, chromium, and copper. In this work we present data from new analyses of several BIF as well as from an extensive literature compilation, all of which point towards profound changes in the supply of redox-sensitive trace elements coincident with the first accumulation of free oxygen in Earth's atmosphere.

Introduction
Before the evolution of silica biomineralization and oxygenation of the deep oceans circa 0.5 Ga, dissolved silica and iron accumulated in seawater at times past the point of saturation, precipitating out as chemical muds that thickly accumulated over large areas of the deep ocean floor to be preserved as BIF. The BIF rock record is extensive, spanning every continent and encompassing sediments from as young as 0.5 Ga to as far back as Earth's earliest known marine deposit (~3.8 Ga BIF in Greenland). Crucially, as pure chemical sediments free of detrital contamination, the precipitates that formed BIF effectively captured elemental and isotopic signatures of evolving ancient seawater by sorption and co-precipitation reactions; it is this property of BIF that arguably makes them one of the richest records of marine geochemistry on the ancient Earth.

Methods
In-situ trace element analyses were performed on BIF samples at the University of Alberta using a quadrupole ICP-MS coupled to laser ablation system. NIST 610 and 612 standards and BIF samples were ablated using identical conditions with spot sizes of either 20 µm or 60 µm, 5 Hz repetition rate and energy density of ~13 J/cm^2. Quantitative results were obtained via the calibration of relative element sensitivities against the NIST 610 and 612 standards. Data reduction and concentration determinations were obtained using the GLITTER® (XP version, New Wave Research) laser ablation software.

Results/Conclusion
Banded iron formations deposited prior to the Great Oxidation Event generally possess very low abundances of molybdenum and chromium, in accordance with the low mobility of these elements under anoxic or reducing conditions. Approximately concomitant with independent evidence for the first appearance of free oxygen circa 2.5 Ga, the abundance of these elements in BIF increases dramatically as they became increasingly mobile at Earth's surface as the result of oxidation processes. The BIF record is not entirely straightforward, however; some non-redox-sensitive trace elements also show excursions at this time, and may reflect novel geochemical consequences of the newly-available O_2 that have been previously overlooked. Related proxies (e.g., black shales) should provide much needed additional insight into this enigmatic period of Earth's history.

THEME 4

ESTABLISHING A HABITABLE PLANET

ORAL & POSTER ABSTRACTS

IRON ISOTOPE EVIDENCE FOR AN ABIOLOGICAL ORIGIN OF A BIF FROM THE YILGARN CRATON

A.D. Czaja[1,2], C.M. Johnson[1,2], B.L. Beard[1,2] & M.J. Van Kranendonk[3,4]

[1]Department of Geoscience, 1215 W. Dayton Street, University of Wisconsin, Madison, WI 53706, USA
[2]NASA Astrobiology Institute, University of Wisconsin, Madison, WI 53706, USA
[3]Geological Survey of Western Australia, Department of Mines and Petroleum, 100 Plain Street, East Perth, WA, 6004, Australia
[4]School of Earth and Environment, University of Western Australia, 35 Stirling Highway, Crawley, WA, 6009 Australia

Introduction

Banded iron formations (BIFs) are important geologic features of the Precambrian Earth, in large part because the accumulation of such vast quantities of iron represents iron cycling on a scale not seen today, and therefore these units can provide insights into element cycling in the ancient atmosphere–biosphere–hydrosphere system. Although no consensus yet exists on the conditions necessary to form BIFs, all models infer deposition in a marine setting and a role for Fe-rich fluids from anoxic bottom waters, magmatic fluids, or hydrothermal fluids (e.g., Klein 2005). Depositional and tectonic settings undoubtedly influence BIF formation, and consideration of the dominant Fe-bearing mineralogy is also necessary (e.g., James 1954). Gross (1965) distinguished volcanogenic BIFs as "Algoma" type, and BIFs deposited in stable continental margins as "Superior" type, where the latter is represented by the well-known BIFs of the 2.5 Ga Hamersley Basin.

Fe isotope geochemistry potentially provides a direct measurement of iron pathways involved in BIF genesis (Johnson et al. 2003, Dauphas et al. 2004, Rouxel et al. 2005, Dauphas et al. 2007a, 2007b, Frost et al. 2007, Whitehouse & Fedo 2007, Johnson et al. 2008a, Vaalas-Hyslop et al. 2008, Planavsky et al. 2009, Steinhoefel et al. 2009, Heimann et al. 2010, Steinhoefel et al. 2010). For BIFs >3.7 Ga in age, δ^{56}Fe values (see Fig. 1 caption for definition) are generally positive, which have been interpreted to reflect partial oxidation of hydrothermally-sourced Fe^{2+}_{aq}, possibly by oxygenic or anoxygenic photosynthesis (Dauphas et al. 2004, 2007a, 2007b, Whitehouse & Fedo 2007). Strikingly, 2.5 Ga BIFs from the Hamersley (e.g., Dales Gorge Member of the Brockman Iron Formation) and Transvaal basins (e.g., Kuruman Iron Formation) have highly negative δ^{56}Fe values, mimicking the temporal changes seen in contemporaneous marine sedimentary materials including black shales, carbonates, and sedimentary sulphides (Rouxel et al. 2005, Yamaguchi et al. 2005, Archer & Vance 2006, Czaja et al. 2010). Some workers have interpreted the appearance of negative δ^{56}Fe values to record the emergence of Fe cycling by dissimilatory iron-reducing bacteria (e.g., Johnson et al. 2003, 2008a, 2008b, Heimann et al. 2010, Steinhoefel et al. 2010), but others have interpreted the data to reflect extensive oxide precipitation (Rouxel et al. 2005, Anbar & Rouxel 2007). In contrast, BIFs of 1.9 Ga age in the Lake Superior region (e.g., Gunflint and Biwabik formations) tend to have positive δ^{56}Fe values, also mimicking the temporal trend in marine sedimentary rocks, and these have been broadly interpreted to record partial oxidation, possibly linked to photosynthesis (e.g., Frost et al. 2007, Vaalas-Hyslop et al. 2008, Planavsky et al. 2009). Here we report on new Fe isotope data from a 2.75 Ga BIF that has isotopic compositions that deviate strongly from those of the known marine sedimentary record. Because the Weld Range BIF is of the "Algoma" type, this study offers an opportunity to study Fe isotope variations in a BIF system that was likely dominated by hydrothermal processes.

Geologic setting and materials

Samples were collected from three stratigraphic positions in a single diamond drill core recovered from the 2.75 Ga Wilgie Mia Formation of the Murchison Supergroup from the Weld Range, western Youanmi Terrane, Yilgarn Craton, Western Australia. BIFs in this unit conformably overlie subaerially deposited volcaniclastic rocks and are interpreted to be part of a collapsed felsic volcanic caldera system. These units were regionally metamorphosed to ~300 °C (Gole 1980, Watkins & Hickman 1990). The samples are composed of jaspilitic chert interbedded with magnetite and occasional pyrite grains (Fig. 1A, B). Petrographic and hand sample-scale relationships show that magnetite and then pyrite crosscut bedded jaspilitic chert, which indicate that magnetite and pyrite are secondary, formed by movement of Fe-rich fluids, likely of hydrothermal origin, along bedding planes. A major effort was made to obtain pure samples of individual Fe-bearing phases, namely hematite, magnetite, and pyrite, to test for formation in Fe isotope equilibrium. A tungsten carbide scribe was used to collect samples of each Fe phase from individual mm-scale bands (hematite-jaspilite and magnetite) or mm-scale grains (pyrite); in all cases, the Fe-bearing minerals sampled are estimated to be >90% pure by this sampling method. These powders were dissolved and the Fe purified using ion-exchange chromatography. Iron isotope measurements were made using MC-ICP-MS at the University of Wisconsin-Madison.

Results and Conclusions

All three Fe phases studied have positive δ^{56}Fe values that occur over relatively narrow ranges and the average values of each phase increase in the order magnetite–hematite–pyrite (Fig. 1C). The Fe contents of the layers in which these phases reside are also very different; Fe comprises 1–7 wt. % of the jaspilitic chert layers (as hematite), 55–71 wt. % of the magnetite layers, and 12–41 wt. % of the pyrite grains. Based on petrographic

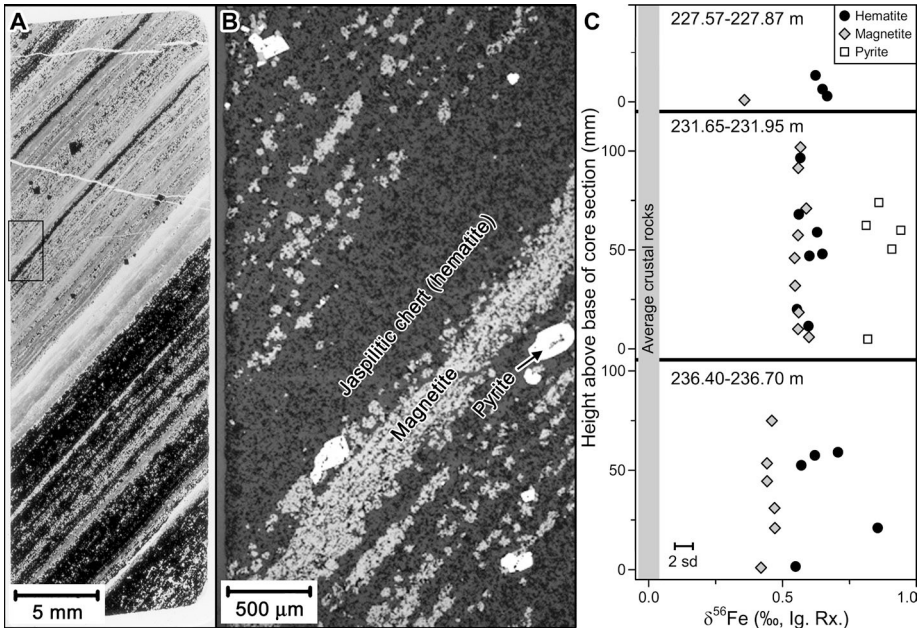

Figure 1. Spatial relations and Fe isotope compositions of the Fe mineral phases in the Weld Range BIF. A) Photograph of a thin section of a core sample in transmitted light (black outline indicates the area pictured in part B). B) Photomicrograph in reflected light showing the variety of Fe phases present in the BIF and their spatial relations. C) $\delta^{56}Fe$ values measured for each Fe phase from three core samples collected from different depths (indicated in each sub-panel). The error bar in part C is 2 s.d. for replicate analyses. $\delta^{56}Fe$ is defined as ((56Fe/54Fe)Sample/(56Fe/54Fe) Ig Rxs - 1) x 103 and the IRMM-014 standard has a value of -0.09 ‰ on this scale.

relations, hematite, or poorly-crystalline ferric hydroxide precursors, is the closest to a primary precipitate in the samples. The low-Fe contents and $\delta^{56}Fe$ values that range from 0.54 to 0.72 ‰ of the hematite in the chert layers are consistent with incomplete oxidation of Fe^{2+}_{aq}, followed by Fe oxide precipitation, suggesting the oxidant was limited. Later-formed magnetite has similar, though slightly lower $\delta^{56}Fe$ values that range from 0.37 to 0.60 ‰; such compositions could reflect net addition of Fe^{2+}-rich fluids into the semi-consolidated jaspilitic chert layers. The $\delta^{56}Fe$ values for pyrite, which formed after the magnetite, range from 0.81 to 0.94 ‰, some of the highest values yet reported for sedimentary rocks, and probably reflect interaction between dissolved sulphide and excess Fe^{2+}_{aq}.

The fact that all Fe-bearing phases have positive $\delta^{56}Fe$ values, relative to the likely near-zero $\delta^{56}Fe$ values of hydrothermal Fe^{2+}_{aq} sources (e.g., Johnson et al. 2008b), indicates that the Fe inventory in the Weld Range BIF was probably small relative to the hydrothermal flux, based on simple isotopic mass balance. Moreover, the fact that the relative $\delta^{56}Fe$ values of hematite–magnetite–pyrite follows that expected for Fe isotope equilibrium (Polyakov & Mineev 2000, Polyakov et al. 2007, Blanchard et al. 2009) suggests formation by entirely abiologic pathways from a major, probably common reservoir of Fe^{2+}_{aq}; where biological cycling has been inferred based on Fe isotope compositions of BIFs, one of the key lines of evidence has been Fe isotope disequilibrium among the phases (Johnson et al. 2008a, Heimann et al. 2010). Although the equilibrium Fe isotope fractionations between hematite, magnetite, and pyrite remain uncertain, predicted fractionations at 100–300 ºC are $\Delta^{56}Fe_{magnetite\text{-}hematite} \sim +0.2$ to +0.5 ‰ and $\Delta^{56}Fe_{pyrite\text{-}magnetite} \sim +1.5$ to +0.5 ‰, which are consistent with those measured in this study. Broadly, our results are similar to those obtained by Steinhoefel et al. (2009) in their study of the "Algoma" type iron formation from the Old Wanderer Formation, Zimbabwe, although pyrite was not analysed in that study. Collectively, these results suggest that Archean volcanogenic, or "Algoma" type BIFs may form by significantly different pathways than those involved in the large "Superior" type BIFs of late Archean and early Proterozoic age such as the Brockman and Kuruman iron formations, which included a major component of biological Fe cycling.

References

Anbar A.D. & Rouxel O., 2007, Metal stable isotopes in paleoceanography, Annual Reviews of Earth and Planetary Sciences, 35, 717–746.

Archer C. & Vance D., 2006, Coupled Fe and S isotope evidence for Archean microbial Fe(III) and sulfate reduction, Geology, 34, 153–156.

Blanchard M., Poitrasson F., Méheut M., Lazzeria M., Mauria F. & Balana E., 2009, Iron isotope fractionation between pyrite (FeS_2), hematite (Fe_2O_3) and siderite ($FeCO_3$): A first-principles density functional theory study, Geochimica et Cosmochimica Acta, 73, 6565–6578.

Czaja A.D., Johnson C.M., Beard B.L., Eigenbrode J.L., Freeman K.H. & Yamaguchi K.E., 2010, Iron and carbon isotope evidence for ecosystem and environmental diversity in the ~2.7 to 2.5 Ga Hamersley Province, Western Australia, Earth and Planetary Science Letters, doi: 10.1016/j.epsl.2010.01.032.

Dauphas N., van Zuilen M., Wadhwa M., Davic A.M., Marty B. & Janney P.E., 2004, Clues from Fe isotope variations on the origin of Early Archean BIFs from Greenland, Science, 306, 2077–2080.

Dauphas N., van Zuilen M., Busigny V., Lepland A., Wadhwa M. & Janney P.E., 2007, Iron isotope, major and trace element characterization of early Archean supracrustal rocks from SW Greenland: protolith identification and metamorphic overprint, Geochimica et Cosmochimica Acta, 71, 4745–4770.

Dauphas N., Cates N.L., Mojzsis S.J. & Busigny V., 2007, Identification of chemical sedimentary protoliths using iron isotopes in the >3750 Ma Nuvvuagittuq supracrustal belt, Canada, Earth and Planetary Science Letters, 254, 358–376.

Frost C.D., von Blanckenburg F., Schoenberg R., Frost B.R. & Swapp S.M., 2007, Preservation of Fe isotope heterogeneities during diagenesis and metamorphism of banded iron formation, Contributions to Mineralogy and Petrology, 153, 211–235.

Gole M.J., 1980, Mineralogy and petrology of very-low-grade metamorphic grade Archean banded iron-formations, Weld Range, Western Australia, American Mineralogist, 65, 8–25.

Gross G.A., 1965, Geology of iron deposits in Canada: General geology and evaluation of iron deposits, Vol. 1, Geologic Survey of Canada, Economic Geology Report 22.

Heimann A., Johnson C.M., Beard B.L., Valley J.W., Roden E.E., Spicuzza M.J. & Beukes N.J., 2010, Fe, C, and O isotope compositions of banded iron formation carbonates demonstrate a major role for dissimilatory iron reduction in ~ 2.5 Ga marine environments, Earth and Planetary Science Letters, in press.

James H.L., 1954, Sedimentary facies of iron-formation, Economic Geology, 49, 235–293.

Johnson C.M., Beard B.L., Beukes N.J., Klein C. & O'Leary J.M., 2003, Ancient geochemical cycling in the Earth as inferred from Fe isotope studies of banded iron formations from the Transvaal Craton, Contributions to Mineralogy and Petrology, 144, 523–547.

Johnson C.M., Beard B.L., Klein C., Beukes N.J. & Roden E.E., 2008a, Iron isotopes constrain biologic and abiologic processes in Banded Iron Formation genesis, Geochimica et Cosmochimica Acta, 72, 151–169.

Johnson C.M., Beard B.L. & Roden E.E., 2008b, The iron isotope fingerprints of redox and biogeochemical cycling in modern and ancient earth, Annual Reviews in Earth and Planetary Sciences, 36, 457–493.

Klein C., 2005, Some Precambrian banded iron formations (BIFs) from around the world: their age, geologic setting, mineralogy, metamorphism, geochemistry, and origin, American Mineralogist, 90, 1473–1499.

Planavsky N., Rouxel O., Bekker A., Shapiro R., Fralick P. & Knudsen A., 2009, Iron-oxidizing microbial ecosystems thrived in late Paleoproterozoic redox-stratified oceans, Earth and Planetary Science Letters, 286, 230–242.

Polyakov V.B., Clayton R.A., Horita J. & Mineev S.D., 2007, Equilibrium iron isotope fractionation factors of minerals: reevaluation from the data of nuclear inelastic resonant X-ray scattering and Mossbauer spectroscopy, Geochimica et Cosmochimica Acta, 71, 3833–3846.

Polyakov V.B. & Mineev S.D., 2000, The use of Mossbauer spectroscopy in stable isotope geochemistry, Geochimica et Cosmochimica Acta, 64, 849–865.

Rouxel O.J., Bekker A. & Edwards K.J., 2005, Iron isotope constraints on the Archean and Paleoproterozoic ocean redox state, Science, 307, 1088–1091.

Steinhoefel G., Horn I. & von Blanckenburg F., 2009, Micro-scale tracing of Fe and Si isotope signatures in banded iron formation using femtosecond laser ablation, Geochimica et Cosmochimica Acta, 73, 5343–5360.

Steinhoefel G., von Blanckenburg F., Horn I., Konhauser K.O., Beukes N.J. & Gutzmer J., 2010, Deciphering formation processes of banded iron formations from the Transvaal and the Hamersley successions by combined Si and Fe isotope analysis using UV femtosecond laser ablation, Geochimica et Cosmochimica Acta, doi: 10.1016/j.gca.2010.01.028.

Valaas-Hyslop E., Valley J.W., Johnson C.M. & Beard B.L., 2008, The effects of metamorphism on O and Fe isotope compositions in the Biwabik Iron Formation, northern Minnesota, Contributions to Mineralogy and Petrology, 155, 313–328.

Van Kranendonk M.J. & Ivanic T.J., 2009, A new lithostratigraphic scheme for the northeastern Murchison Domain, Yilgarn Craton, Geological Survey of Western Australia Annual Review for 2007–08, 34–53.

Watkins K.P. & Hickman A.H., 1990, Geological evolution and mineralization of the Murchison Province, Western Australia, Geological Survey of Western Australia Bulletin 137, 267p.

Whitehouse M.J. & Fedo C.M., 2007, Microscale heterogeneity of Fe isotopes in >3.71 Ga banded iron formation from the Isua Greenstone Belt, southwest Greenland, Geology, 35, 719–722.

Yamaguchi K.E., Johnson C.M., Beard B.L. & Ohmoto H., 2005, Biogeochemical cycling of iron in the Archean-Paleoproterozoic Earth: constraints from iron isotope variations in sedimentary rocks from the Kaapvaal and Pilbara Cratons, Chemical Geology, 218, 135–169.

COMBINING Ge/Si RATIOS AND Si ISOTOPES TO CONSTRAIN THE ORIGIN OF A MESOARCHEAN BANDED IRON FORMATION

C. Delvigne[1,2], D. Cardinal[2], A. Hofmann[3] & L. André[2]

[1]Department of Earth Sciences and Environment, Université Libre de Bruxelles, Brussels, Belgium
[2]Department of Geology and Mineralogy, Royal Museum of Central Africa, Tervuren, Belgium
[3] School of Geological Sciences, University of KwaZulu-Natal, P/Bag X54001, Durban, South Africa

Introduction

Banded iron formations (BIFs) are chemical precipitates limited to the Precambrian and typically characterized by alternation of iron-rich and amorphous silica-rich layers whose origin is highly controversial. Many hypotheses have been proposed for their genesis, but the mechanism of deposition is still unresolved. To address this issue, much of the previous work on BIFs has focused on the sources of Fe2+ and the oxidation and precipitation processes. It is generally accepted that the Fe component of Precambrian BIFs has its origin in hydrothermal alteration of oceanic crust (e.g. Jacobsen & Pimentel-Klose 1988, Klein & Beukes 1989, Alibert & McCulloch 1993, Bau & Dulski 1996, Bau et al. 1997). Proposed mechanisms of oxidation and subsequent precipitation of ferric iron are debated. They include abiotic photo-oxidation, direct oxidation by Fe(II)-oxidizing anoxygenic photoautotrophic bacteria, and O2-mediated indirect oxidation by oxygenic photosynthetic bacteria. Surprisingly, only a few studies have been directed to the source of silica. In recent studies, it has been proposed that silica is either derived from continental sources (Hamade et al. 2003, Frei & Polat 2007) or originated from seafloor hydrothermal fluids (André et al. 2006, Lascelles 2007, Steinhoefel et al. 2009, Wang et al. 2009).

Based on the relation between Ge/Si ratios and silica content of mesobands of 2.3 Ga Hamersley BIFs, Hamade et al. (2003) concluded to a mixing scenario involving two compositionally different water masses that interacted with each other: high Ge/Si bottom waters and low Ge/Si ambient surface waters. These authors considered that silica was predominantly derived from weathering of continental landmass, whereas iron was regarded to be of hydrothermal origin. This was supported by the study of Frei & Polat (2007) on 3.8 Ga Isua BIF that combined Ge/Si ratios and REE data. This is however moderated by the possibility that the Ge/Si variability could also be explained by a preferential adsorption of Ge onto Fe-oxyhydroxides.
This contrasts with the study of André et al. (2006) who concluded that negative δ30Si signatures converge with Fe isotopes to support a hydrothermal origin of silica in 3.8 Ga Isua BIFs. Moreover, they precluded any major change in the degree of mixing of hydrothermal waters with ambient seawater, since no correlation was found between δ30Si and Eu/Eu*. More recently, Steinhoefel et al. (2009) concluded that heavy bulk Fe and light Si isotopic compositions of Neoarchean BIFs from Zimbabwe suggest rapid precipitation events from an episodically recharged hydrothermal fluid. They further suggested that the variability of the Si isotope composition might reflect modifications of hydrothermal fluids with distance to the venting site caused by Rayleigh distillation and/or mixing with ambient seawater.

To investigate the different hypotheses of genesis, we have undertaken a multi-tracer approach combining REE+Y, Ge/Si ratio and Si isotopes (δ30Si) of stratigraphically resolved layers of ca. 2.95Ga BIF from the Pongola Supergroup, South Africa, to investigate the time-related geochemical changes of this BIF deposit.

Samples and methods

Sample material was obtained from a ca. 3m thick BIF horizon from the ca. 2.95Ga Sinqeni Formation (Mozaan Group, Pongola Supergroup) in the White Imfolozi Inlier, South Africa. Ge and REE+Y concentrations were analysed by HR-ICP-MS of powdered mesobands dissolved by a borate fusion using a flux with a 99,999% purity. Major elements were analysed by ICP-AES.

For Si isotopes a NaOH alkaline attack and chromatographic purification was carried out (Georg et al. 2006). To achieve a complete dissolution, only 1-5 mg of powdered rock was used.

Si isotopic compositions were then measured using a Nu Plasma multicollector plasma source mass spectrometer (MC-ICP-MS) operating in dry plasma mode, with an external Mg doping to correct mass bias (Cardinal et al. 2003, Abraham et al. 2008). Data were obtained by the sample-standard bracketing technique relative to the NBS28 silica sand standard for silicon isotopes.

Results

REE+Y data

REE+Y patterns of individual mesobands, normalized against Post-Archean Australian Average Shale (PAAS) are characterized by positive La and Eu anomalies (from 1.26 to 4.81 and 0.84 to 2.20, respectively). Y is significantly enriched in all mesobands relative to Ho, yielding high Y/Ho ratios (from 21.90 to 56.71 with an outlier at 14.98). Based on the REE characteristics, BIFs exhibit typical hydrothermal features (positive Eu anomalies) as well as seawater signature with Y/Ho ratio and positive La anomaly similar to modern marine precipitates.

Ge/Si ratios

Ge/Si ratios range from 3.13 to 20.57µmol/mol with an outlier at 49.79µmol/mol. This range is in accordance with data from 2.3Ga Hamersley BIF (from 0.82 to 21.63µmol/mol, Hamade et al. 2003). However, more pure cherts (98% SiO2) show Ge/Si ratios of 3.98 and 4.30µmol/mol. This contrasts with the ratio of 0.82µmol/mol obtained by Hamade et al. (2003). Ge/Si ratios in Si-rich layers average 3.92µmol/mol, whereas Fe-rich layers average 20.06µmol/mol. In agreement with these authors, we observe a clear hyperbolic relationship in which increasing silica is accompanied by a lowering of Ge/Si ratios.

Si isotope composition

Preliminary results indicate that δ30Si varied between -2.27‰ and -0.81‰ in Si-rich mesobands and between -1.52‰ and -1.19‰ in Fe-rich mesobands. As suggested by Figure 1, the Si isotopic composition changes with stratigraphic position: δ30Si composition increases stratigraphically upwards. This trend can be observed for both Si- and Fe-rich mesobands, but to a lesser extent for the latter. It is worth mentioning that the isotopic difference between the Fe- and Si-rich members decreases from the base to the top of the Sinqeni BIF sequence.

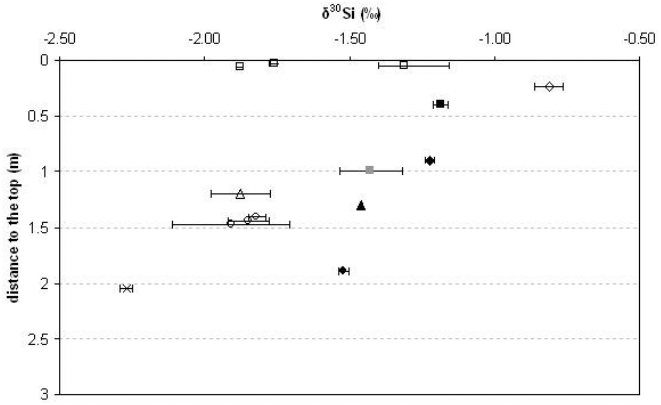

Figure 1. Si isotopic compositions in relation with sample stratigraphic position (distance of sample from the top of the sequence). Si-rich mesobands (empty symbols and cross); Fe-rich mesobands (black symbols); intermediate mesobands (grey symbols). Each symbol type represents a different stratigraphic level. Symbols are the average value of two complete replicates with standard deviation from different samples.

Discussion

The overall Si isotope composition of our BIF samples are within the observed range of previously investigated BIFs (André et al. 2006, van den Boorn et al. 2007, Steinhoefel et al. 2009,). Both Si- and Fe-rich mesobands display an overall light Si isotopic signature that is compatible with a hydrothermal origin. Indeed, silica-rich deposits precipitated around oceanic smokers present a δ30Si signature of -1.6±0.7‰ (Ding et al. 1996). This is in accordance with REE patterns showing a positive Eu-anomaly which is interpreted as a hydrothermal signature.

This seems to be at odds with low Ge/Si ratios in Si-rich layers that would suggest continental weathering as a contributing source for the silica. Alternatively, the Ge/Si variability could also be explained by the selective adsorption of Ge onto Fe-oxyhydroxides (Pokrovski et al. 2006). Similarly, a Si-isotopic fractionation is induced by selective adsorption of light isotopes onto Fe-oxides (Delstanche et al. 2009, Opfergelt et al. 2009). As Ge/Si and δ30Si show an inverse relationship during abiotic process (Pokrovski et al. 2006, Delstanche et al. 2009, Opfergelt et al. 2010), it would be expected that Fe-rich mesobands exhibit lighter δ30Si signatures than Si-rich mesobands, just the inverse of what is observed. As Fe-rich mesobands show heavier isotopic compositions, we therefore conclude that preferential Ge adsorption onto Fe-oxyhydroxides would not be responsible for the observed Ge/Si variability. An experimental study has demonstrated a temperature-related increase of the Ge/Si ratio in fluids that are in contact with Ge-bearing silicates with temperature (Pokrovski & Schott 1998). The Ge/Si ratio increases by more than one order of magnitude when the temperature is raised from 25 to 500°C. Data from a more recent study show that the temperature effect on Ge/Si ratios in hydrothermal fluids is even larger, since it varies from 0.73µmol/mol to 15-62µmol/mol from cold (<10°C) to warmer (30-70°C) hydrothermal systems (Wheat & Mc Manus 2008). From this, we can suggest that low Ge/Si ratio do not necessarily imply a continental weathering, but may also reflect hydrothermal inputs spanning a large range of temperature characteristics.

The heavier Si isotopic compositions of Fe-rich mesobands compared to Si-rich mesobands were also observed in Neoarchean BIFs (Steinhoefel et al. 2009). They explained such results by an episodically active hydrothermal system in which silica precipitation occurred at periods of low plume activity from a largely unaffected fluid causing strong negative δ30Si values, whereas Fe oxide precipitation involved high hydrothermal activity and a fluid that has been previously modified by Rayleigh distillation and/or by mixing with seawater. Our data do not show any correlation between δ30Si and Eu/Eu* or Y/Ho, excluding mixing with seawater. Moreover, the relation between δ30Si and the sample stratigraphic position is in favour of a gradually modified fluid by a Rayleigh process. The bottom of the sequence corresponding to the beginning of the process would reflect pristine hydrothermal fluids with clear light signature that became heavier due to ongoing precipitation of isotopically light products. The shift towards light signature at the top of the sequence may be due to an episode of a recharge event.

As underlined by Frei and Polat (2007), it is too early at this stage to further elaborate on the effects and mechanisms of Si isotopic and Ge/Si fractionation during BIF precipitation and a more detailed discussion will have to await further studies.

Conclusion

The light Si isotopic composition of Pongola BIF suggests a hydrothermal origin, and the relationship between the isotopic signature and the sample stratigraphic position may reflect modification of the fluid, likely by a

Rayleigh process. Mixing with seawater seems unlikely, as no correlation between δ30Si and Eu/Eu* or Y/Ho is evident. A heavier Si isotopic composition of Fe-rich mesobands compared to Si-rich mesobands suggests that high Ge/Si ratios in Fe-rich layers are probably not due to a preferential Ge adsorption onto Fe-oxyhydroxides. A large range of Ge/Si values measured in hydrothermal fluids (Wheat & Mc Manus 2008) suggests that low Ge/Si ratio do not necessarily imply continental weathering, but may also reflect hydrothermal input.

Acknowledgements

C. Delvigne would like to acknowledge the «Fonds pour la formation à la Recherche dans l'Industrie et dans l'Agriculture» (FRIA) for funding.

References

Abraham K., Opfergelt S., Fripiat F., Cavagna A., de Jong J., Foley S., André L. & Cardinal D., 2008, d30Si and d29Si Determinations on USGS BHVO-1 and BHVO-2 Reference Materials with a New Configuration on a Nu Plasma Multi-Collector ICP-MS, Geostandards and Geoanalytical Research, 32, 193–202.

Alibert C. & McCulloch M., 1993, Rare earth element and neodymium isotopic compositions of the banded iron-formations and associated shales from Hamersley, Western Australia, Geochimica et Cosmochimica Acta, 57, 187–204.

André L., Cardinal D., Alleman L. & Moorbath S., 2006, Silicon isotopes in~ 3.8 Ga West Greenland rocks as clues to the Eoarchaean supracrustal Si cycle, Earth and Planetary Science Letters, 245, 162–173.

Bau M. & Dulski P., 1996, Distribution of yttrium and rare-earth elements in the Penge and Kuruman iron-formations, Transvaal Supergroup, South Africa, Precambrian Research, 79, 37–55.

Bau M., Höhndorf A., Dulski P. & Beukes N., 1997, Source of Rare-Earth Elements and Iron in Paleoproterozoic Iron-Formations from the Transvaal Supergroup, South Africa: Evidence from Neodymium Isotopes, Journal of Geology, 1997, 105, 121–130.

Cardinal D., Alleman L., Jong J., Ziegler K. & André L., 2003, Isotopic composition of silicon measured by multicollector plasma source mass spectrometry in dry plasma mode, Journal of Analytical Atomic Spectrometry, 18, 213–218.

Delstanche S., Opfergelt S., Cardinal D., Elsass F., André L. & Delvaux B., 2009, Silicon isotopic fractionation during adsorption of aqueous monosilicic acid onto iron oxide, Geochimica et Cosmochimica Acta, 73, 923–934.

Ding T., Jiange S., Wan D., Li Y., Li J., Song H., Liu Z. & Yao X.,1996, Silicon Isotope Geochemistry, Geological Publishing House, Beijing, China.

Frei R. & Polat A., 2007, Source heterogeneity for the major components of similar to 3.7 Ga Banded Iron Formations (Isua Greenstone Belt, Western Greenland): Tracing the nature of interacting water masses in BIF formation, Earth and planetary science letters, 253, 266–281.

Georg R.B., Reynolds B.C., Frank M. & Halliday A.N., 2006, New sample preparation techniques for the determination of Si isotopic compositions using MC-ICPMS, Chemical Geology, 235, 95–104.

Hamade T., Konhauser K., Raiswell R., Goldsmith S. & Morris R., 2003, Using Ge/Si ratios to decouple iron and silica fluxes in Precambrian banded iron formations, Geology, 31, 35–38.

Jacobsen S.B. & Pimentel-Klose M.R., 1988, Nd isotopic variations in Precambrian banded iron formations, Geophysical Research Letters, 15, 393–396.

Klein C. & Beukes N.J., 1989, Geochemistry and sedimentology of a facies transition from limestone to iron-formation deposition in the early Proterozoic Transvaal Supergroup, South Africa, Economic Geology, 84, 1733.

Lascelles D.F., 2007, Black smokers and density currents: A uniformitarian model for the genesis of banded iron-formations, Ore Geology Reviews, 32, 381–411.

Opfergelt S., de Bournonville G., Cardinal D., André L., Delstanche S. & Delvaux B., 2009, Impact of soil weathering degree on silicon isotopic fractionation during adsorption onto iron oxides in basaltic ash soils, Cameroon, Geochimica et Cosmochimica Acta, 73, 7226–7240.

Opfergelt S., Cardinal D., André L., Delvigne C., Bremond L.& Delvaux B., 2010, Variations of d30Si and Ge/Si with weathering and biogenic input in tropical basaltic ash soils under monoculture, Geochimica et Cosmochimica Acta, 74, 225–240.

Pokrovski G. & Schott J., 1998, Thermodynamic properties of aqueous Ge (IV) hydroxide complexes from 25 to 350°C: Implications for the behavior of germanium and the Ge/Si ratio in hydrothermal fluids, Geochimica et Cosmochimica Acta, 62, 1631–1642.

Pokrovsky O., Pokrovski G., Schott J. & Galy A., 2006, Experimental study of germanium adsorption on goethite and germanium coprecipitation with iron hydroxide: X-ray absorption fine structure and macroscopic characterization, Geochimica et Cosmochimica Acta, 70, 3325–3341.

Steinhoefel G., Horn I. & von Blanckenburg F., 2009, Micro-scale tracing of Fe and Si isotope signatures in banded iron formation using femtosecond laser ablation, Geochimica et Cosmochimica Acta, 73, 5343–5360.

Van den Boorn S., van Bergen M., Nijman W. & Vroon P., 2007, Dual role of seawater and hydrothermal fluids in Early Archean chert formation: Evidence from silicon isotopes, Geology, 35, 939–942.

Wang Y., Xu H., Merino E. & Konishi H., 2009, Generation of banded iron formations by internal dynamics and leaching of oceanic crust, Nature Geoscience, 2, doi:10.1038/NGEO652.

Wheat C. & McManus J., 2008, Germanium in mid-ocean ridge flank hydrothermal fluids, Geochemistry, Geophysics, Geosystems, 9, Q03025, doi:10.1029/2007GC001892.

GEOCHEMICAL AND Fe ISOTOPE FINGERPRINTS FOR BIF AND OTHER PRECAMBRIAN CHEMICAL SEDIMENTARY ROCKS?

C.M. Fedo[1], M.M. Hage[1], B.S. Kamber[2], R. Schoenberg[3] & M.J. Whitehouse[4]

[1]Dept. of Earth & Planetary Sciences, University of Tennessee, Knoxville, TN 37996 USA
[2]Dept. of Earth Sciences, Laurentian University, Sudbury, ON P3E 2C6 Canada
[3]Center for Geobiology & Dept. of Earth Science, University of Bergen, Bergen, Norway
[4]Laboratory for Isotope Geology, Swedish Museum of Natural History, Stockholm Sweden

Introduction

Since the original claim for the presence of chemofossils in a supposed banded iron formation (BIF) on Akilia, southwest Greenland (Mojzsis et al. 1996), many attempts have been made at refining geochemical (Fedo & Whitehouse 2002, Mojzsis & Harrison 2002, Friend et al. 2002, Bolhar et al. 2004, Cates & Mojzsis 2006, Friend et al. 2008) and iron isotope (Dauphas et al. 2004, Whitehouse & Fedo 2007, Dauphas et al. 2007) fingerprints capable of clearly identifying BIF and other hydrogenous sedimentary rocks in poly deformed Archean terranes.

As high-quality data sets continue to grow, more clarity is emerging with regards to compositional ranges and the veracity of specific geochemical, largely trace element, and iron isotope fingerprints. As part of a broad study investigating the geochemistry and iron isotope composition of BIF from 3.8 Ga to 1.9 Ga, we have also investigated a second group of samples that, based on their geological relationships, likely did not form as chemical sedimentary precipitates, but mineralogically and/or texturally resemble sediments. In this early progress report, we present data from these two groups in order to test the veracity of the "fingerprints."

Genuine BIF samples in our study include those from (1) the >3.7 Ga Isua Greenstone Belt (Fedo et al. 2001), (2) the ~3.0 Ga Buhwa Greenstone Belt, Zimbabwe (Fedo & Eriksson 1996); and (3) the ~ 1.9 Ga Gunflint Iron Formation, Minnesota and Ontario (Fralick et al. 2002). Our non sedimentary group of samples includes banded jasper+magnetite rock from the ~2.7 Ga Hunter Mine Group, Abitibi Greenstone Belt, Québec, interpreted as "hydrothermal iron formation" (Chown 2000, Mueller & Mortensen 2002), carbonate veins and disseminated carbonate from different locales in the >3.7 Ga Isua Greenstone Belt, SW Greenland, well known for abundant carbonate metasomatism of mafic and ultra mafic rocks (Rose et al. 1996, Rosing et al. 1996), and mixed quartz+amphibole+pyroxene±feldspar rock from Innersuartuut, southwest Greenland that closely resembles controversial (cf. Mojzsis et al. 1996, Fedo & Whitehouse 2002) ~3.6 Ga banded rocks on nearby Akilia.

Geochemistry

Chemical sedimentary rocks that precipitate from sea water should carry a distinct trace element chemistry related to the compositional inventory of the water column and processes that fractionate elements in low temperature aqueous systems (Bau & Moller 1993, Bau 1996, Kamber & Webb 2001, Lawrence & Kamber 2006). Some of the most useful elements in recognizing these processes include the dominantly trivalent lanthanide (rare earth) group elements (REE), Y, and some high field strength elements such as Zr and Hf. In modern sea water, factors such as source composition (mantle hydrothermal v. terrestrial), particle-solution interactions, water depth, and water redox/salinity determine the trace element composition (Lawrence & Kamber 2006). A consequence of the geochemistry of the REE working in concert with these factors is that distinct fractionations occur that are not generally observed in high-temperature (magmatic) rocks, for which Bau (1996) coined the term CHARAC (charge and radius controlled). In CHARAC characterized systems, twin-pair elements such as Y/Ho and Zr/Hf behave coherently and so maintain chondritic values. In aqueous systems, by contrast, other processes like chemical complexation also determine trace element behaviour (Bau, 1996) and lead to superchondritic values for Zr/Hf and Y/Ho. The result should be a geochemical fingerprint characterized by: shale-normalized positive La, Gd, Eu, and Y anomalies, shale normalized negative Ce anomalies, and superchondritic values for Y/Ho and Zr/Hf.

Genuine BIF samples from our three localities that span approximately two billion years have most of the characteristics of chemical sediments, but there are samples that do not. For example, a number of samples from the Gunflint BIF do not have positive La anomalies and most have chondritic values for Y/Ho. BIFs from Zimbabwe have a majority of the REY characteristics, except for a few samples with virtually no La anomaly, and like the Gunflint Iron Formation samples, most have chondritic, rather than superchondritic sedimentary Y/Ho ratios. Samples of BIF from the Isua Greenstone Belt, as a whole, have the most complete set of geochemical characteristics expected in hydrogenous sediments.

Our sample of jasper+magnetite (Hunter Mine Group, Abitibi Greenstone Belt) is interpreted to have formed from progressive hydrothermal alteration of hyaloclastite (e.g., Chown et al. 2000) and has a major element composition dominated by SiO2 (66.69 %) and Fe2O3(T) (29.78 %) with very low abundance of Al2O3 (0.46 %). The REE+Y (REY) pattern for this

sample carries all the signatures of a chemical sediment, including positive, shale-normalized La, Eu, Gd, and Y anomalies, no Ce anomaly (calculated using expressions in Lawrence & Kamber 2006) and elevated Y/Ho. Two samples of vein carbonate (ferroan dolomite) and an ~50 cm layer of ferroan dolomite mixed with quartz hosted in metamorphosed mafic rock from the Isua Greenstone Belt possess positive La, Eu, Y anomalies, a very slight negative Ce anomaly (0.9), and superchondritic Y/Ho. Additionally, two samples of finely disseminated carbonate within anthophyllite have flat to slightly positive La anomalies, and positive Eu and Y anomalies, although Y/Ho is chondritic at 26 and 30. Our three samples from Innersuartuut share few geochemical characteristics with hydrogenous sediment.

Fe Isotopes

Similar to the observations made for trace-element distribution of sediments precipitated from sea water, the iron isotope record of chemical sediments, and that of BIF with δ^{56}Fe ratios ranging from -2 to +1.5 ‰ (e.g., Johnson and Beard 2006) in particular, stands in marked contrast with the overwhelming majority of iron reservoirs on Earth, including lithospheric mantle, continental crust, and clastic sediments, all of which have δ^{56}Fe values of essentially 0 ‰. Exceptions to this phenomenon have been the recognition of isotopic variability in altered ocean crust (δ^{56}Fe > 0 ‰) and associated alteration products (δ^{56}Fe < 0 ‰; Rouxel et al. 2003), and high variability in δ^{56}Fe between -0.38 and +0.25 ‰ for metasomatized mantle rocks (Williams et al. 2005). Given the very restricted range of lithologies with non-zero δ^{56}Fe values, it should be possible to fingerprint BIF merely from its Fe isotope composition, which would be a powerful tool for recognizing protoliths in deformed and metamorphosed rocks where primary textures and minerals have been replaced (e.g., Dauphas et al. 2004, 2007).

All of the genuine BIF samples studied so far have bulk-rock Fe isotope compositions that are consistent with a chemical sedimentary "fingerprint" (-0.239 ‰ < δ^{56}Fe < +1.046 ‰). However, examination of Fe isotope signatures of the non chemical sedimentary samples yields unexpected results. The banded jasper+magnetite rock from the Abitibi Greenstone Belt has δ^{56}Fe = +1.25 ‰, the heaviest value measured in our samples thus far, but lies within the expected confines for a chemical sediment. Our only measurement for a relatively pure metasomatic carbonate sample (0.09 weight % SiO_2) has δ^{56}Fe = -0.350 ‰, again far from the expected zero value. The three samples from Innersuartuut have a mineral assemblage inconsistent with a sedimentary origin, but have some REY characteristics of a chemical sediment, and have fractionated negative δ^{56}Fe values ranging from -0.206 to -0.188 ‰. Although this is opposed to the typically positive δ^{56}Fe values of early Archean Isua BIFs and the Akilia rocks, based on which the latter have been suggested to be of chemical sedimentary origin (Dauphas et al. 2004), one of our high iron (48.63 wt. % Fe_2O_3(T)) quartz+magnetite BIF samples from Isua has a δ^{56}Fe = -0.239 ‰.

Interpretations and Conclusions

Our combined study of genuine BIF samples that span in time across the Great Oxidation Event and a non sedimentary group of samples reveals unexpected complexities for developing fingerprints for chemical sedimentary rocks. The importance of being able to accurately identify sediments that formed in equilibrium with sea water is a cornerstone for interpreting Earth's earliest surface conditions. Furthermore, as the controversy over the origin of the rocks on Akilia demonstrates, BIF (or other chemical sediment) could be an important component in the search for relicts of the nascent biosphere. In this progress report, we conclude that the full suite of geochemical and Fe isotope fingerprints does exist in many BIF samples. However, there are important exceptions in some samples, rendering it clear that all BIFs do not carry a diagnostic suite of geochemical characteristics, even though there is a consistent fractionation of Fe isotopes as is expected.

Perhaps more importantly, our group of non sedimentary samples variably possess critical components of a sedimentary geochemical "fingerprint," and all that have been analysed thus far have fractionated (positive and negative) bulk-rock Fe isotopes. The remarkable occurrence of unquestionably secondary carbonate veins, lenses, and disseminations hosted by a number of lithologies at Isua poses the possibility that the clear sedimentary signature was perhaps remobilized from a subsurface, shallow-water, sedimentary facies not presently exposed in the otherwise deep-water succession there (Fedo 2000, Fedo et al. 2001).

Samples dominated by quartz+amphibole+pyroxene±feldspar from Innersuartuut that look very similar to rocks exposed on nearby Akilia do not have a majority of components typical of chemical sedimentary rocks. By contrast, all three samples have fractionated Fe isotopes that might easily be mistaken for having a sedimentary origin. Repeated deformation (and likely metasomatism) has compromised protolith geochemical signatures.

The Abitibi Greenstone Belt sample carries all of the geochemical characteristics that typify BIF and has a fractionated Fe isotope composition making it a perfect candidate to be "fingerprinted" as BIF. Although it has been interpreted as having formed via hydrothermal alteration of a volcanic rock in a caldera complex, the complete geochemical and isotopic coincidence with hydrogenous sediments warrants continued laboratory and field work to confirm its interpreted high-temperature geologic setting.

It would be easy to misidentify some other rock as BIF in a complexly deformed and metasomatized setting, and we urge caution in the application of these techniques to determine protoliths like those on Akilia in which composition may have been disturbed multiple times in its history. The best situation for interpreting the origin of such rocks relies on an integrated approach that utilizes the geology in connection with geochemistry and isotopes.

Acknowledgements

This research supported by NASA grant EXOB08-0063 awarded to CMF. It has also been supported by the following grants awarded to MMH: Precambrian Research Center Student Grant, Geological Society of America Student Research Grant, Institute of Lake Superior Geology Student Research Grant, and American Philosophical Society and NASA Astrobiology Institute's Lewis and Clark Fund for Exploration and Field Research in Astrobiology. MJW acknowledges support from the Swedish Research Council (Vetenskapsrådet).

References

Bau, M., 1996, Controls on the fractionation of isovalent trace elements in magmatic and aqueous systems: evidence from Y/Ho, Zr/Hf, and lanthanide tetrad effect, Contributions to Mineralogy and Petrology, 123, 323-333.

Bau, M. & Möller, P., 1993, Rare earth element systematics of the chemically precipitated component in Early Precambrian iron formations and the evolution of the terrestrial atmosphere-hydrosphere-lithosphere system, Geochimica et Cosmochimica Acta, 57, 2239-2249.

Bolhar R., Kamber B., Moorbath S., Fedo C. & Whitehouse M., 2004, Characterization of early Archean chemical sediments by trace element signatures, Earth and Planetary Science Letters, 222, 43-60.

Cates, N. & Mojzsis, S., 2006, Chemical and isotopic evidence for widespread Eoarchean metasedimentary enclaves in southern West Greenland, Geochimica et Cosmochimica Acta, 70, 4229-4257.

Chown, E., N'Dah, E., & Mueller, W., 2000, The relation between iron-formation and low temperature hydrothermal alteration in an Archean volcanic environment, Precambrian Research, 101, 263-275.

Dauphas, N., van Zuilen, M., Busigny, V., Lepland, A., Wadhwa, M., & Janney, P., 2007, Iron isotope, major and trace element characterization of early Archean supracrustal rocks from SW Greenland: Protolith identification and metamorphic overprint, Geochimica and Cosmochimica Acta, 71, 4745-4770.

Dauphas, N., van Zuilen, M., Wadhwa, M., Davis, A., Marty, B., & Janney, P., 2004, Clues from Fe isotope variations on the origin of Early Archean BIFs from Greenland, Science, 306, 2077-2080.

Fedo, C.M., 2000, Setting and origin for problematic rocks from the >3.7 Ga Isua Greenstone Belt, southern West Greenland: Earth's oldest coarse clastic sediments, Precambrian Research, 101, 69–78.

Fedo C. & Eriksson K., 1996, Stratigraphic framework of the ~3.0 Ga Buhwa Greenstone Belt: a stable-shelf succession unique in the Zimbabwe Archean Craton, Precambrin Research, 77, 161–178.

Fedo C. & Whitehouse M., 2002, Metasomatic origin of quartz-pyroxene rock, Akilia, Greenland, and implications for Earth's earliest life, Science, 296, 1448–1452.

Fedo C., Myers J., & Appel P., 2001, Depositional setting and paleogeographic implications of Earth's oldest supracrustal rocks, the >3.7 Ga Isua Greenstone Belt, West Greenland, Sedimentary Geology, 141–142, 61–77.

Fralick P., Davis D. & Kissin S., 2002, The age of the Gunflint Formation, Ontario, Canada: single zircon U-Pb age determinations from reworked volcanic ash, Canadian Journal of Earth Science, 39, 1085–1091.

Friend, C.R.L., Nutman, A.P., & Bennett, V.C., 2002, Origin and significance of Archean quartzose rocks at Akilia, Greenland, Science, Technical Comments, 298, 917a.

Friend C., Nutman A., Bennet V. & Norman M., 2008, Seawater-like trace element signatures (REE + Y) of Eoarchean chemical sedimentary rocks from southern West Greenland, and their corruption during high-grade metamorphism, Contributions to Mineralogy and Petrology, 155, 229–246.

Johnson C., & Beard B., 2006, Fe isotopes: An emerging technique for understanding modern and ancient biogeochemical cycles, GSA Today, 16, 4–10.

Kamber B. & Webb G., 2001, The geochemistry of late Archean microbial carbonate: implications for ocean chemistry and continental erosion history, Geochimica et Cosmochimica Acta, 65, 2509–2525.

Lawrence M.G., & Kamber B.S., 2006, The behaviour of the rare earth elements during estuarine mixing – revisited, Marine Chemistry, 100, 147–161.

Mojzsis S., Arrhenius G., McKeegan K., Harrison T., Nutman A., & Friend C., 1996, Evidence for life on Earth before 3,800 million years ago, Nature, 384, 55–59.

Mojzsis S.J., & Harrison T.M., 2002, Origin and significance of Archean quartzose rocks at Akilia, Greenland, Science, Technical Comments, 298, 917a.

Mueller W. & Mortensen J., 2002, Age constraints and characteristics of subaqueous volcanic construction, the Archean Hunter Mine Group, Abitibi greenstone belt, Precambrian Research, 115, 119–152.

Rose N.M., Rosing, M.T., & Bridgwater, D., 1996, The origin of metacarbonate rocks in the Archaean Isua supracrustal belt, West Greenland, American Journal of Science, 296, 1004–1044.

Rosing M., Rose N., Bridgwater D., & Thomsen H., 1996. Earliest part of Earth's stratigraphic record: A reappraisal of the > 3.7 Ga Isua (Greenland) supracrustal sequence: Geology, 24, 43–46.

Rouxel O., Dobbek N., Ludden J., & Fouquet Y., 2003, Iron isotope fractionation during oceanic crust alteration, Chemical Geology, 202, 155–182.

Whitehouse M. & Fedo C., 2007, Microscale heterogeneity of Fe isotopes in >3.71 Ga banded iron formation from the Isua Greenstone Belt, southwest Greenland, Geology, 35, 719–722.

Williams H.M., Peslier A.H., McCammon C., Halliday A.N., Levasseur S., Teutsch N., & Burg J.-P., 2005, Systematic iron isotope variations in mantle rocks and minerals: the effects of partial melting and oxygen fugacity, Earth and Planetary Science Letters, 235, 435–452.

DOES THE NEOARCHAEAN FORTESCUE GROUP RECORD THE EARLIEST EVIDENCE FOR OXYGENIC PHOTOSYNTHESIS?

D.T. Flannery[1], J.M. Coffey[1], S.C. George[1, 2] & M.R. Walter[1]

[1]Australian Centre for Astrobiology, University of New South Wales, Sydney, Australia. dtf@student.unsw.edu.au
[2]Department of Earth and Planetary Science, Macquarie University, Sydney, Australia.

While it is generally accepted that our atmosphere was oxygenated at around 2.45 to 2.32Ga during what is known as the Great Oxidation Event (GOE), considerable controversy still surrounds the timing of the origin of cyanobacteria and the beginning of oxygenic photosynthesis. Some see evidence for oxygenic photosynthesis and oxic environments tens of millions (Anbar et al., 2007), or more than a billion (Rosing and Frei, 2004) years prior to the GOE. Others hold that there is no reliable evidence for a considerable delay between the evolution of cyanobacteria and the oxygenation of the atmosphere and that these two events occurred contemporaneously (Rasmussen et al., 2008). Here we report evidence for the presence of cyanobacteria at the time of deposition of the ~2.7Ga Tumbiana Formation in the Pilbara region.

The Tumbiana Formation is a thin unit of stromatolite-bearing clastic and carbonate rocks hosted within the Fortescue Group of the Pilbara Craton (Figure 1). The sedimentary successions of the Meentheena Member of the Tumbiana Formation were laid down in the Neoarchean, some ~300 million years before the Great Oxidation Event. They are remarkably well preserved, having undergone only prehnite-pumpellyite facies metamorphism. The palaeoenvironment appears to be one that would have been conducive to the growth of cyanobacteria. Previous palaeoenvironmental studies of the member have seen researchers divided into two main camps: those who favour a shallow marine palaeoenvironment (e.g. Thorne and Trendall, 2001; Sakurai et al., 2005), and those who favour a lacustrine interpretation (e.g., Walter, 1983; Buick, 1992; Bolhar and Van Kranendonk, 2007; Awramik and Buchheim, 2009). Earlier workers have highlighted the local geochemistry (Buick, 1992), and morphological features of poorly preserved microfossils (Schopf and Walter, 1983) as evidence for oxygenic photosynthesis. The Tumbiana stromatolites are also ideal candidates for hydrocarbon extraction and cyanobacterial biomarkers (2α-methyl hopanes) have been successfully isolated from the overlying Maddina and Jeerinah Formations (Brocks, *et al.,* 1999). These results have since been questioned (Rasmussen, 2008).

Work already completed for our study has confirmed a lacustrine interpretation of the palaeoenvironment and reinforced the original biomarker results of Brocks et al. (1999). The lacustrine interpretation is based on abrupt and significant lateral facies changes, cyclic repetition of facies, basement topography, REE+Y analysis and sedimentological features, primarily the

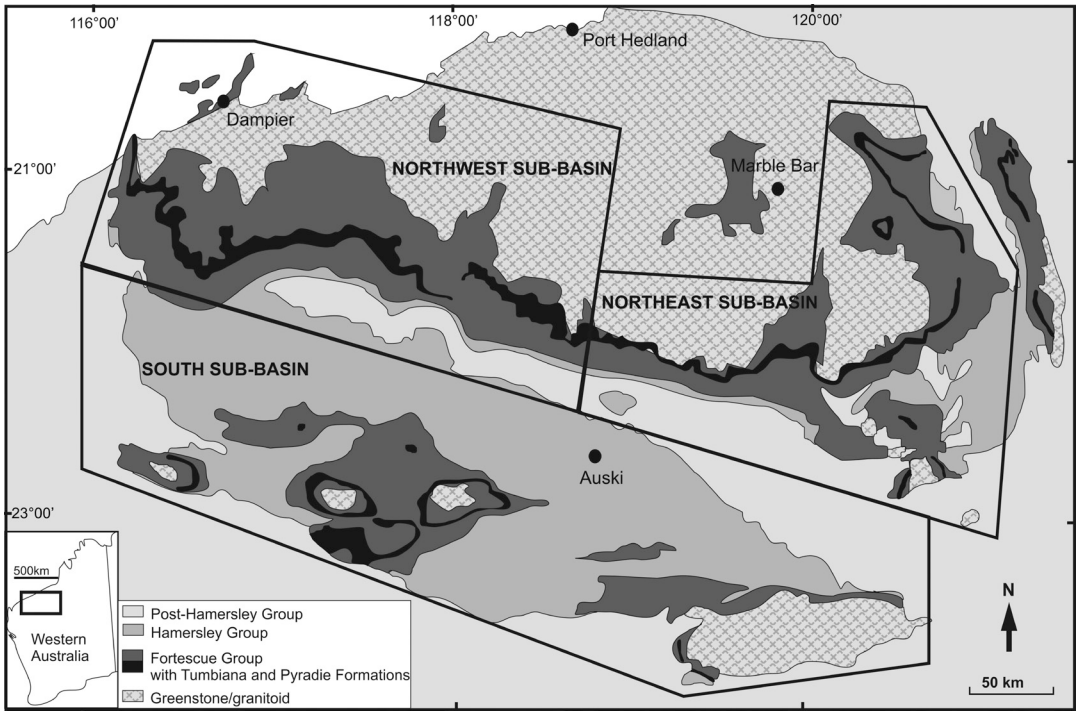

Figure 1. A map of the Pilbara Craton in Western Australia showing the extent of the Tumbiana Formation. After Thorne and Trendall, 2001.

Figure 2. Conical Stromatolites from which cyanobacterial biomarkers were obtained.

presence of climbing symmetrical ripples and a general lack of features commonly associated with marine environments. Mature hydrocarbons were obtained directly from outcrops of conical stromatolites (Figure 2), negating the possibility of contamination by drilling fluids (an earlier concern). Molecular signatures characteristic of anthropogenic contamination were not observed. Biomarkers varied between outcrop samples and showed an increase in hydrocarbon concentrations towards the centres of stromatolites. They included hopanes, steranes and aromatic steranes, consistent with the results of Brocks et al. (2003).

More detailed sedimentological, geochemical and palaeobiological studies are continuing. However, it seems at this stage that the weight of evidence indicates that cyanobacteria and therefore most probably oxygenic photosynthesis had evolved by ~2.7Ga. Why some geochemical indicators of an oxygenated atmosphere do not appear for another 300 million years remains to be explained.

Acknowledgements

This work is supported by grants from the Australian Research Council.

References

Anbar A.D., Duan Y., Lyons T.W., Arnold G.L. , Kendall B., Creaser R.A., Kaufman A.J., Gordon G.W., Garvin J. & Buick R, 2007, A whiff of oxygen before the great oxidation event, Science, 317, 1903–1906

Awramik S.M. & Buchheim H.P., 2009, A giant, Late Archean lake system: The Meentheena Member (Tumbiana Formation; Fortescue Group), Western Australia, Precambrian Research, 174, 215–240.

Bolhar, R. & Van Kranendonk M.J., 2007, A non-marine depositional setting for the northern Fortescue Group, Pilbara Craton, inferred from trace element geochemistry of stromatolitic carbonates, Precambrian Research, 155, 229–250.

Buick R., 1992, The antiquity of oxygenic photosynthesis: evidence from stromatolites in sulphate-deficient Archaean lakes, Science, 255, 74–77.

Thorne A.M. & Trendall A.F., 2001, Geology of the Fortescue Group, Pilbara Craton, Western Australia, Geological Survey of Western Australia, Memoir 144, 249p.

Rasmussen B., Fletcher I.R., Brocks J.J. & Kilburn M.R. 2008. Reassessing the first appearance of eukaryotes and cyanobacteria, Nature, 455, 1101–1104.

Rosing M.T. & Frei R., 2004, U-rich Archaean sea-floor sediments from Greenland - indications of >3700 Ma oxygenic photosynthesis, Earth and Planetary Science Letters, 217, 237–244.

Sakurai R., Ito M., Ueno Y., Kitajima K. & Maruyama S., 2005, Facies architecture and sequence-stratigraphic features of the Tumbiana Formation in the Pilbara Craton, north western Australia: Implications for depositional environments of oxygenic stromatolites during the Late Archean, Precambrian Research, 138, 255–273.

Schopf J. W. & Walter M. R., 1983, Archean microfossils: new evidence of ancient microbes, in The Earth's Earliest Biosphere: Its Origin and Evolution, Schopf, J.W., ed, Princeton University Press, Chapter 9, 214–239.

Walter M.R., 1983, Archean stromatolites: evidence of the Earth's earliest benthos, in The Earth's Earliest Biosphere: Its Origin and Evolution, Schopf, J.W., ed, Princeton University Press, Chapter 8, 187-213.

WHAT DO MANTLE ROCKS TELL US ABOUT THE EVOLUTION OF THE ATMOSPHERE?

S.F. Foley

Earth System Science Research Centre and Institute for Geosciences, University of Mainz, Germany

Little is known about the composition of the atmosphere in the Hadean and Archaean. The Earth has 21% oxygen and 78% nitrogen, but neither is typical of the terrestrial planets. Much has been written in the last few years to the early Proterozoic great oxidation event, examining and explaining the rise of oxygen between 2.4 and 2.1 Ga, but the other 80 to >99% of the atmosphere has received relatively little attention. Approaches taken to estimate the composition of the early atmosphere are from comparative planetology, the need for a suitable environment for the origin of life on Earth, and the need to avoid global Archaean glaciation in the presence of the "faint young sun". Noble gas isotopes indicate early degassing of trace species, but do not constrain the nature of the major species greatly.

The "faint young sun" arguments require a much greater effect of greenhouse gases. A higher methane concentration has been suggested, and linked to irreversible oxidation of the Earth by hydrogen loss to space, thus possibly explaining the later oxidation of the Earth's surface and atmosphere close to the Archaean-Proterozoic boundary (Catling et al., 2001). Higher CO_2 concentrations have been invoked in many scenarios (e.g. Owen et al., 1979), but are difficult to reconcile with palaeosol data (Sheldon, 2006). A more recent suggestion sees a higher pressure atmosphere dominated by nitrogen: in this scenario, Goldblatt et al. (2009) address the later removal of nitrogen from the atmosphere with three fundamental questions "where is the nitrogen now?", "how did it get from the atmosphere to its present location?" and "when did this transfer take place?", but do not consider how the N_2 got there in the first place.

The composition and chemical evolution of the atmosphere is inextricably linked to degassing of the Earth by volcanoes, and so to the oxidation state of the upper mantle and long-term recycling of surface material into the mantle as a function of time. The moon and Mars are useful analogies for the the mantle of the early Earth because they were initially volcanically active but became stalled tectonically at different times in their histories. The best estimates of the oxidation states of their volcanic sources are an order of magnitude below iron-wüstite (IW-1) for the moon, and IW to IW+2 for Mars (Wadhwa, 2008), both considerably lower than continental mantle samples from the Earth. The sources of Archaean volcanics are frequently said to be no different in oxidation state from those of modern basalts (Delano, 2001; Li and Lee, 2004). Here I argue that the Earth's mantle was more reduced in the Hadean and Archaean, and explore the implications for the composition of degassed species and the composition of the early atmosphere.

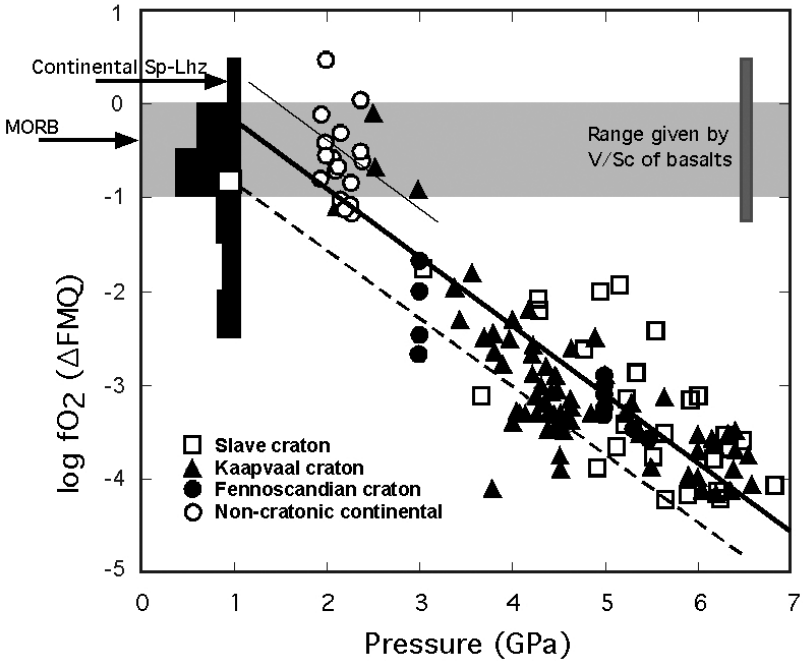

Figure 1. Oxidation state of lithospheric and asthenospheric mantle as a function of time and tectonic environment. Modern oceanic mantle (dashed line) is considerably more reduced than non-cratonic continent (thin solid line). Older continents (thick solid line) lie in between and have probably been oxidized by later metasomatic events.

Oxidation state of the Hadean and Archaean mantle

Most information on the oxidation state of the mantle comes from oxygen barometry, which reconstructs mantle fO_2 from the distribution of iron as Fe^{3+} and Fe^{2+} between component minerals of peridotite (O'Neill and Wall, 1987). Most data is available for the continental mantle lithosphere, with a further bias in favour of garnet-bearing peridotites sampled by kimberlites from the cratonic mantle. These cratonic garnet peridotites have mostly been part of the lithosphere since the mid- to late Archaean (Pearson, 1999), and range in fO_2 mostly between 1.5 and 4.5 log units below the FMQ buffer (Fig.1). Ballhaus and Frost (1994) calculated that the fO_2 of peridotites should decrease by ca. 0.7 ΔFMQ units per 1 GPa increase in pressure; this is represented by the slope of the solid line in Fig.1, indicating that the data array may be explained largely by the effect of pressure. However, it has frequently been shown that later metasomatism of peridotites caused by the infiltration of melts leads to an increase in the apparent fO_2 of the peridotites (McGuire et al, 1991; Frost and McCammon, 2008), so that the position of the solid line in Fig.1 would be slightly lower if it is to represent the original pre-metasomatic redox state.

A number of studies have suggested that the oxidation state of the mantle has not changed since at least 3.5Ga. In addition to those based on oxygen barometry, the V/Sc ratios (Li and Lee, 2004) and Cr contents (Delano, 2001) of volcanic rocks have been used to conclude that the source regions of Archaean basalts were no different in oxidation state to modern basalts. However, this overlooks the fact that oxidation state of the mantle varies between continental and oceanic environments on the modern Earth (Fig.1). Non-cratonic continental peridotites (Ionov and Wood, 1992; Foley et al., 2006) are more oxidized than simple down-pressure projection of cratonic peridotites (Fig.1) and supra-subduction arc wedge peridotites may be still more oxidized, ranging from FMQ to FMQ+2 log units. Abyssal peridotites indicate more reducing conditions than under continents (Bryndzia et al., 1989); the average value for abyssal peridotites of FMQ-0.88 can be extrapolated to higher pressures to form an array for the convecting sub-oceanic asthenosphere (dashed line in Fig.1) that is about 0.7 log units below that of the cratonic lithosphere and 1.2-1.3 log units below the non-cratonic continental lithosphere.

Eclogite xenoliths can also be used as sensors for the oxidation state of the mantle in the late Archaean. The V/Sc ratios of those eclogites shown by a correlation of oxygen isotopes with major element chemistry to represent subducted basaltic ocean crust, and dated at 2.5-2.7 Ga (Jacob, 2004), is lower than the average for modern MORB, indicating slightly more reducing conditions in the late Archaean. Given additionally that cratonic peridotites are more reducing than non-cratonic ones, and that their oxidation states have been raised by later metasomatism, it appears acceptable to conclude that the Archaean asthenospheric mantle was more reduced than the current sub-ridge mantle, and that the record of Archaean basalts is biased towards continental regions. This is a very important conclusion given the probability that the amount of continental crust, and thus also sub-continental lithospheric mantle, was much smaller until about 2.7-2.5 Ga. Furthermore, the ages of cratonic peridotites and eclogites that give the evidence for more reducing Archaean conditions are almost entirely from the late Archaean (2.9-2.5 Ga), raising the possibility that the mantle had progressively oxidized during the Hadean and Archaean before this.

Degassing from the mantle at various oxidation states

The relevance of the oxidation state of the mantle to volcanic gases is controlled by the availability of volatile species and their solubilities in melts. Fig.2 illustrates the stable C-O-H species in equilibrium with solid carbon at 30 kbar and 1200°C as a function of oxygen fugacity, corresponding to conditions at depths of about 100km in the upper mantle and thus likely conditions for the formation of melts in the presence of volatile species. Fig.2 indicates that H_2O+CO_2 mixtures are likely under the more oxidizing conditions of the non-cratonic mantle, whereas fluid species would consist of H_2O and CH_4 with minor H_2 and C_2H_6 at IW to IW+2. CO_2 is essentially absent at these conditions, and CO does not feature at high pressures at any oxygen fugacities (Taylor et al., 1987).

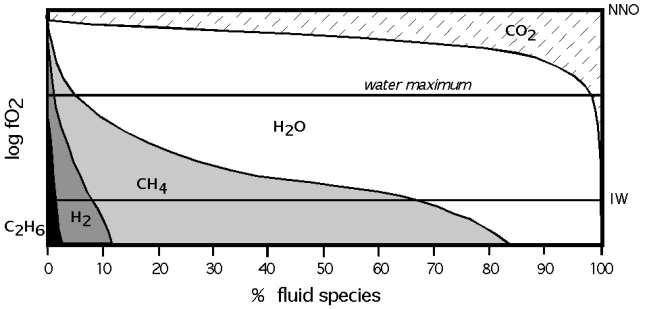

Figure 2. C-O-H fluid speciation as a function of oxygen fugacity over the range likely during the evolution of the Earth's upper mantle. An early reduced mantle contained no CO_2, and reduced forms of C and N.

The solubilities of all volatile components increase with increasing pressure, meaning that degassing occurs by release of dissolved volatiles as melts move towards the surface. The key to the composition of volcanic gas species is the content of the various volatile species in melts during melting. The volatile components CO_2, H_2O, H_2S and SO_2 are all incompatible components with high solubilities in melts at mantle pressures, meaning that they will be preferentially taken up in the melt. The case is less clear for CH_4 and nitrogen species, which appear to have solubilites that are strongly dependent on the oxidation state. In the case of carbon, more than 20 wt% CO_2 is soluble in silicate melts at 100km depth (Wyllie & Huang, 1976), whereas the solubility of reduced carbon is limited to 0.2 wt%, with a maximum of 0.5 wt% if melts are strongly depolymerized (Taylor et al., 1987; Mysen et al., 2009). Less is known about nitrogen, but available data indicate that solubilities are very low at relatively high and intermediate oxygen fugacities where N_2 is stable, but increase at least five times at low oxygen

fugacities that are typical of the deep mantle and may have prevailed in the upper mantle during the first 2.000 million years of Earth history. The reason lies in the different solution mechanisms; molecular N_2 dissolves only in spaces between silicate network components, whereas reduced nitrogen dissolves as NH_2 units in the silicate structure itself (Libourel et al., 2003; Mysen et al., 2008).

Coupled with the evidence for progressive oxidation of the mantle throughout the Hadean and Archaean, these solubility data mean that early rapid degassing of CO_2 is not realistic, because melts would have contained little carbon. In contrast, early, reduced conditions would have mobilized nitrogen in melts, and volcanic gases would have been much richer in nitrogen than in any tectonic environments on the modern Earth. Thus, the conclusion that the oxidation state of the mantle has increased through time is consistent with an early nitrogen-rich atmosphere (Goldblatt et al, 2009). Furthermore, before the atmosphere became oxygen-bearing, a higher content of the trace gas CH_4 was likely from the point of view of volcanic gas compositions, and this should have also contributed to the gradual oxidation of the Earth's surface and atmosphere (Catling et al., 2001).

Acknowledgments

This research is financed by the Mainz Earth System Science Research Centre (Geocycles).

References

Ballhaus C. & Frost B.R., 1994, The Generation of Oxidized CO_2-Bearing Basaltic Melts from Reduced CH_4-Bearing Upper-Mantle Sources, Geochimica et Cosmochimica Acta, 58, 4931–4940.

Bryndzia L., Wood B. & Dick H., 1989, The oxidation state of the Earth's sub-oceanic mantle from oxygen thermobarometry of abyssal spinel peridotites, Nature, 341, 526–527.

Catling D.C., Zahnle K.J. & McKay C.P., 2001, Biogenic methane, hydrogen escape, and the irreversible oxidation of early Earth, Science, 293, 839–843.

Foley S.F., Andronikov A.V., Jacob, D.E. & Melzer S., 2006, Evidence from Antarctic mantle peridotite xenoliths for changes in mineralogy, geochemistry and geothermal gradients beneath a developing rift, Geochimica et Cosmochimica Acta, 70, 3096–3120.

Frost D.J. & McCammon C.A., 2008, The redox state of Earth's mantle, Annual Review of Earth and Planetary Sciences, 36, 389–420.

Goldblatt C., Claire M.W., Lenton T.M., Matthews A.J., Watson A.J. & Zahnle K.J., 2009, Nitrogen-enhanced greenhouse warming on early Earth, Nature Geoscience, 2, 891–896.

Ionov D.A. & Wood B., 1992, The oxidation state of subcontinental mantle: oxygen thermobarometry of mantle xenoliths from central Asia, Contributions to Mineralogy and Petrology, 111, 179–193.

Jacob D.E., 2004, Nature and origin of eclogite xenoliths from kimberlites, Lithos, 77, 295–316.

Li Z.X.A. & Lee C.T.A., 2004, The constancy of upper mantle fO_2 through time inferred from V/Sc ratios in basalts, Earth and Planetary Science Letters, 228, 483–493.

Libourel G., Marty B. & Humbert F., 2003, Nitrogen solubility in basaltic melt. Part I. Effect of oxygen fugacity, Geochimica et Cosmochimica Acta, 67, 4123–4135.

McGuire A.V., Dyar M.D. & Nielson J.E., 1991, Metasomatic Oxidation of Upper Mantle Peridotite, Contributions to Mineralogy and Petrology, 109, 252–264.

Mysen B.O., Yamashita S. & Chertkova N., 2008, Solubility and solution mechanisms of NOH volatiles in silicate melts at high pressure and temperature-amine groups and hydrogen fugacity, American Mineralogist, 1760–1770.

Mysen B.O., Fogel M.L., Morrill P.L. & Cody G.D., 2009, Solution behavior of reduced C-O-H volatiles in silicate melts at high pressure and temperature, Geochimica et Cosmochimica Acta, 73, 1696–1710.

O'Neill H. & Wall V., 1987, The olivine-orthopyroxene-spinel oxygen geobarometer, the nickel precipitation curve, and the oxygen fugacity of the Earth's upper mantle, Journal of Petrology, 28, 1169–1191.

Owen T., Cess R.D. & Ramanathan V., 1979, Enhanced CO_2 greenhouse to compensate for reduced solar luminosity on early Earth, Nature, 277, 640–642.

Pearson D. G., 1999, The age of continental roots, Lithos, 48, 171–194.

Sheldon N.D., 2006, Precambrian paleosols and atmospheric CO_2 levels, Precambrian Research, 147, 148–155.

Taylor W.R. & Green D.H., 1987, The petrogenetic role of methane, in *Magmatic processes: physicochemical principles*, Mysen B.O. ed, Washington D.C., Geochemical Society, 121–138.

Wadhwa M., 2008, Redox conditions on small bodies, the Moon and Mars, Reviews in Mineralogy and Geochemistry 68, 493–510.

Wyllie P.J. & Huang W.L., 1976, High CO_2 solubilities in mantle magmas, Geology, 21–24.

INTEGRATION OF OBSERVATIONAL AND ANALYTICAL METHODOLOGIES TO CHARACTERIZE ORGANIC MATTER IN EARLY ARCHAEAN ROCKS: DISTINGUISHING BIOLOGICAL FROM ABIOTICALLY SYNTHESIZED CM STRUCTURES

M. Glikson[1], A. Hickman[2], L. Duck[1], S. Golding[1] & R. Webb[3]

[1]School of Physical Sciences, University of Queensland Brisbane Australia,
[2]Geological Survey of Western Australia, 100 Plain Street, Perth, Australia,
[3]Centre for Microscopy and Microanalysis, University of Queensland Brisbane Australia.

Transmission Electron Microscopy (TEM) was applied to observe and characterize carbonaceous materials (CM) extracted from black cherts and argillite in drill core from the Warrawoona Group of the Pilbara Craton, Western Australia. The black chert came from 'white smoker type' deposit in the ca.3.5 Ga (model Pb/Pb ages=3.49-3.51Ga) Dresser Formation, whereas the black argillites were obtained from the 3.46 Ga Apex Basalt. The samples were observed and analyzed in TEM combined with electron dispersive spectral analysis (EDS), high resolution TEM (HRTEM) to determine molecular ordering, and C-isotope geochemistry. The TEM and HRTEM observations revealed significant morphological and structural differences between the carbonaceous materials of the Dresser and Apex samples enabling interpretations in terms of primary and secondary origins, biological as well as abiotic formation, as well as metamorphic history.

Organic petrology using reflected light microscopy was used on whole rock samples to observe mineral – organic matter relationship and CM structure relative to host rock texture. The results support insitu, syn-depositional origin for the Dresser Formation CM. Reflectance % (Ro) of CM determined on polished whole rock samples and polished resin-embedded CM-concentrates enabled the reconstruction of thermal history. Several Ro populations were identified in the Dresser Formation samples: probable microbial cells preserved in fluid inclusions within quartz crystals, severely thermally degraded CM originally belonging to microbial cells, CM coating mineral grains and reworked CM particles which can be traced to grain coating. The two latter occurrences of CM are attributed to abiotic origin. The Apex Basalt samples yielded consistently very high Ro values corresponding to graphite stage organic metamorphism. The weak optical anisotropy of the graphite is inconsistent with graphite mineral forming during regional metamorphism. Two main graphite forms were identified, namely a platy and a tubular. In HRTEM the tubular form showed nano-tubes and fullerenes within mono-layered spheres. Furthermore, TEM and HRTEM show that the void enclosed mono-layered carbon nano-spheres are more often detached from tubular graphite, forming clusters outside the nano-tubes. These forms are a key to the distinction between biologically and abiotically synthesized CM bodies, both by their small size, perfect outline, their formation and very high temperature, and especially their resistance to thermal degradation.

Dresser Formation samples are isotopically light in the range of -32.1 to -38.2‰ supporting a biological source. Although TEM indicated four distinct types of CM, C-isotope analysis was undertaken on mixed CM concentrates. Nevertheless, the isotopically lighter samples contained a notable input from non thermally degraded microbial cells entombed within fluid inclusions, liberated during the de-mineralizing process. On the other hand the "heavier' samples contained predominantly thermally degraded high Ro CM.

C-isotope compositions of the Apex CM are generally heavier than Dresser samples, between 22.5 and 28.6‰ consistent with high thermal stress. The samples show a C-isotope trend in which CM at 143m depth is "lighter" whereas above and below this level CM becomes increasingly and consistently isotopically heavier. The upper part of the section is dominated by platy graphite with rare nano-tubes. Predominantly tubular graphite and fullerenes characterize sample SAL-13 at 142m depth coinciding with the isotopically lightest values. Below 143m. CM is less well preserved, predominantly of fragmented platy graphite type, becoming increasingly "heavier" signifying close association with peridotite intrusion. Two types of graphite identified in TEM are also distinguished isotopically as a primary tubular graphite and a secondary type of re-melting and solidifying of primary graphite.

PRESERVATION OF GEOCHEMICAL AND Fe ISOTOPE FINGERPRINTS OF BANDED IRON FORMATION THROUGH PROGRADE METAMORPHISM

M.M. Hage[1], C.M Fedo[1], B. Kamber[2] & R. Schoenberg[3]

1Department of Earth and Planetary Sciences, University of Tennessee, Knoxville, TN 37996, USA
2Department of Earth Sciences, Laurentian University, Sudbury, Ontario P3E 2C6, Canada
3Center for Geobiology & Department of Earth Science, University of Bergen, N-5020 Bergen, Norway

Introduction

Banded iron formation (BIF) is a chemical sedimentary rock that carries profound implications about early Earth history because (1) it is found within the oldest fragments of supracrustal material, and all through the Precambrian when fundamental changes in Earth's physical, biological and chemical evolution occurred, and (2) its geochemistry preserves a record of the environment in which it formed (Klein 2005, Ohmoto et al. 2006). Recent work has applied characteristics of BIF geochemistry in a metamorphosed rock sequence to investigate the proposed oldest life on Earth and possible environments of formation (cf. Friend et al. 2008, Fedo et al., 2006, Bolhar et al. 2004, Fedo & Whitehouse 2002). Central to this debate is the notion that BIF records the presence of a retained hydrosphere and so could host biological fragments. "Fingerprinting" of BIF via geochemical and isotopic methods has been used as a powerful way of recognizing it even if the rock has been significantly metamorphosed or altered since deposition.

A concern when studying BIF is how well it can retain distinct original, or near original, compositions through progressive metamorphism. The ~ 1.9 Ga Gunflint Iron Formation (Fralick et al. 2002) outcrops along a NE-SW-trending belt that extends approximately 175 km from Thunder Bay, Ontario, where the unit is unmetamorphosed, to ~19 km west of the Gunflint Trail in northern Minnesota, where it is truncated and separated from the correlative, Biwabik Formation by the intrusion of the 1.1 Ga Duluth Complex. This intrusion developed a contact aureole within the iron formations, with peak metamorphism reaching upper amphibolite-facies. Both unmetamorphosed and metamorphosed samples of predominantly oxide-facies BIF were examined by detailed petrographic, geochemical and isotopic analyses to test the veracity of signatures acquired during precipitation.

Sample Description

At field scale, the main lithologies of the amphibolite-grade Gunflint BIF located along the Gunflint Trail include finely banded magnetite-quartz BIF and coarsely banded magnetite-quartz BIF, with less common centimeter-scale chert-dominated layers containing rip-up clasts of magnetite-rich layers. In thin section, samples range between Fe-silicate and oxide facies BIF, and contain varying amounts of quartz, magnetite, and amphibole. Quartz occurs as equant grains with 120º interlocking grain boundaries, which suggests recrystallization, and range in size from ~50 μm to 500 μm. Magnetite typically occurs as anhedral grains, ranging in size from ~ 10 μm to 200 μm, and occurs either has disseminated grains between quartz or amphibole grains or as distinct bands. Amphiboles are found in all samples and typically occur as a clotted mass of fine (< 50 μm) equant grains or needles with a few larger (~ 200 μm) grains also present. Similar to the magnetite, the amphiboles occur either as disseminated grains and needles in-between quartz and magnetite grains, or as distinct layers.

The unmetamorphosed Gunflint BIF as observed in the Thunder Bay region represents a shallower-water facies than is found in the high-grade BIF of northern Minnesota, with hummocky cross-stratification, silicified microbial mats and carbonate-rich iron formation all being present. Samples contain varying degrees of quartz, magnetite, hematite, ankerite, and calcite. Most quartz grains are anhedral and <100 μm, with some grains up to ~300 μn in size. Magnetite, hematite and carbonate grains are typically anhedral and may or may not occur in distinct bands.

Geochemistry

The major element chemistry of Gunflint BIF is typical of other BIFs, regardless of metamorphic grade, and is dominated by SiO_2 (~ 7 to 90 wt%) and Fe_2O_3(T) (~ 10 to 67 wt%), with much lesser amounts of CaO (~ 0.6 to 12 wt%), MgO (~ 0.2 to 6 wt%), MnO (~ 0.04 to 3.4 wt%), Al_2O_3 (~0.2 to 2.8 wt%), P_2O_5 (~0.1 to 1.0 wt%), Na_2O (~ 0.1 to 0.5 wt%), and K_2O (~ 0.1 to 0.4 wt%). Although no evidence for abundant clastic contamination was observed in outcrop or thin section scale, the geochemistry indicates slightly elevated abundances, relative to other very pure chemical sediments, of trace elements typically related to clastic detritus, such as Sc (0.3 to 5 ppm), Th (0.19 to 2.1 ppm), Hf (0.1 to 0.8 ppm), Zr (3 to 54 ppm), and Rb (0.1 to 35 ppm) (Bau & Dulski 1996).

It has been suggested that Archean and Proterozoic hydrogenous sediments, such as BIFs free from clastic contamination, can be discriminated on the basis of variations in their rare earth element (REE) signatures. Both Archean and post Great Oxidation Event (GOE) BIFs, regardless of provenance and metamorphic grade

should show: LREE depletion relative to the source and positive La_{SN}, Gd_{SN}, and Y_{SN} anomalies. Archean BIF typically have no Ce_{SN} anomaly while post GOE BIF have variably positive and negative Ce anomalies and reduced Eu anomalies compared to their Archean counterparts (Bau & Dulski 1996, Bolhar et al. 2004).

The PAAS-normalized REE + Y plots of all Gunflint samples (Figure 1A) are relatively flat and there is no obvious correlation between Y/Ho and degree of LREE depletion. The flatness of the REE profiles is thus not a function of degree of clastic contamination but reflects a relatively local dissolved REE source with a very steeply negative REE pattern (such as Archean TTG). Similar situations have been described in Zimbabwean microbial carbonates (Kamber et al., 2004). This finding argues strongly for deposition in a semi-restricted basin. The inferred depositional setting is also compatible with only modest positive Eu anomalies, ranging from 1.0-1.96 in high-grade samples and 1.20-1.74 in low-grade samples, suggesting only minor hydrothermal input into the depositional basin (Klein 2005) and isolation from open ocean deep water. In agreement with their post GOE age, the BIFs show both positive and slightly negative Ce anomalies, ranging from 0.93-1.31 in high-grade rocks and 1.01-1.86 in low-grade rocks, and some samples lack any anomaly ($Ce/Ce^* = 1.0$). The co-existence of samples with negative and positive Ce anomalies suggests deposition above and below a redox chemocline, supporting the widely held notion that the Paleoproterozoic deep ocean was not ventilated. Both positive and negative La_{SN} anomalies (0.77-1.88) are recorded in the metamorphosed samples, however only positive La_{SN} anomalies (1.06-1.99) were found in the unmetamorphosed rocks. In all of the samples, only one has a slightly positive Gd_{SN} anomaly (1.05). Other BIF "fingerprints" are found in some of the Gunflint samples, with $(La/Sm)_{CN}$ values ranging from 0.87 to 7.9, $(Sm/Yb)_{SN}$ values ranging from 0.61 to 2.2, and $(Eu/Sm)_{SN}$ values ranging from 1.03 to 2.2.

Fe Isotopes

High-grade samples have δ56Fe values ranging from -0.127 to +0.871 ‰, with an average isotopic composition of +0.483 ‰, while low-grade samples have δ56Fe values ranging from -0.205 to +0.541 ‰, with an average isotopic composition of +0.160‰ (Figure 1B). These values are in agreement with the previously published Fe isotope values for the correlative Biwabik Iron formation, where bulk layers range from -0.75 to +0.80 ‰ (Frost et al. 2007). Moreover, the trend of the low-grade carbonate-rich Gunflint samples towards lighter bulk-rock Fe isotope compositions, when compared to the high-grade magnetite-rich Gunflint BIF, agrees with observations made for the Biwabik iron formation (Frost et al. 2007). Frost et al. (2007) noted that in the lowest grade samples, there was a consistent sequence in which δ56Fe of magnetite > silicate ≥ carbonates, however, because no mineral Fe isotope data were obtained for this study, it is not possible to test this observation in the Gunflint Iron Formation.

Conclusions

The similarity in the major, trace, and rare earth geochemistry between the amphibolite-facies and unmetamorphosed samples from the Gunflint Iron Formation suggests that original, or near original, signatures acquired during precipitation and/or diagenesis are preserved throughout prograde metamorphism. This data also introduces the possibility that traditional BIF "fingerprints" may not be as viable as original thought, such as the presence of a negative Ce anomaly and positive La and Gd anomalies, which were not found in all of the samples analysed here.

Although the high-grade samples have an average Fe isotopic value that is enriched in ^{56}Fe relative to the low-grade samples, there is enough overlap in the range of compositions between the two groups to suggest that the short duration of contact metamorphism in this area allowed near original (i.e. diagenetic) compositions to be preserved during prograde metamorphism, which concurs with the findings of Frost et al. (2007) for the correlative Biwabik Iron Formation.

Acknowledgements

We thank Martin Whitehouse for helpful discussions on BIF. This research supported by NASA grant EXOB08-0063 awarded to CMF and the following grants awarded to MMH: Precambrian Research Center Student Grant, Geological Society of America Student Research Grant, and Institute of Lake Superior Geology Student Research Grant.

References

Bau M. & Dulski P., 1996, Distribution of yttrium and rare-earth elements in the Penge and Kuruman iron-formations, Transvaal Supergroup, South Africa, Precambrian Research, 79, 37–55.

Bolhar R., Kamber B., Moorbath S., Fedo C. & Whitehouse M., 2004, Characterization of early Archean chemical sediments by trace element signatures, Earth and Planetary Science Letters, 222, 43–60.

Fedo C. & Whitehouse M., 2002, Metasomatic origin of quartz-pyroxene rock, Akilia, Greenland, and implications for Earth's earliest life, Science, 296, 1448–1452.

Fedo C., Whitehouse M. and Kamber B., 2006, Geological constraints on detecting the earliest life on Earth: a perspective from the Early Archean (older than 3.7 Gyr) of southwest Greenland, Philosophical Transactions of The Royal Society B, 361, 851–876.

Fralick P., Davis D. & Kissin S., 2002, The age of the Gunflint Formation, Ontario, Canada: single zircon U-Pb age determinations from reworked volcanic ash, Canadian Journal of Earth Science, 39, 1085–1091.

Friend C., Nutman A., Bennet V. & Norman M., 2008, Seawater-like trace element signatures (REE + Y) of Eoarchean chemical sedimentary rocks from southern West Greenland, and their corruption during high-grade metamorphism, Contributions to Mineralogy and Petrology, 155, 229–246.

Frost C., von Blanckenburg F., Schoenberg R., Frost B. & Swapp S., 2007, Preservation of Fe isotope heterogeneities during diagenesis and metamorphism of banded iron formation, Contributions to Mineralogy and Petrology, 153, 211–235.

Johnson C., Beard B. & Roden E., 2008, The iron isotope fingerprints of redox and biogeochemical cycling in modern and ancient Earth, Annual Review of Earth and Planetary Sciences, 36, 457–493.

Kamber B., Bolhar R. and Webb G., 2004, Geochemistry of late Archean stromatolite from Zimbabwe: evidence for microbial life in restricted epicontinental seas, Precambrian Research, 132, 379–399.

Klein C., 2005, Some Precambrian banded iron-formations (BIFs) from around the world: Their age, geologic setting, mineralogy, metamorphism, geochemistry, and origin, American Mineralogist, 90, 1473–1499.

Ohmoto H., Watanabe Y., Yamaguchi K., Naraoka H., Haruna M., Kakegawa T., Hayashi K. & Kato Y., 2006, Chemical and biological evolution of early Earth: Constraints from banded iron formation, in *Evolution of Early Earth's Atmosphere, Hydrosphere, and Biosphere – Constraints from Ore Deposits*, Kesler, S. and Ohmoto, H., eds, Geological Society of America Memoir 198, 291–331.

Schoenberg R. & von Blanckenburg F., 2006, Modes of planetary-scale isotope fractionation, Earth and Planetary Science Letters, 252, 342–359.

IN SITU $\delta^{18}O$ ANALYSES IN QUARTZ AND MAGNETITE FROM THE DALES GORGE BIF

J.M. Huberty[1], N.T. Kita[1], P.R. Heck[1,2], R. Kozdon[1], J.H. Fournelle[1], H. Xu[1] & J.W. Valley[1]

[1]WiscSIMS & NAI, Dept. of Geoscience, Univ. of Wisconsin, Madison, WI 53706, USA
[2]present address: Dept. of Geophysical Sciences, Univ. of Chicago, Chicago, IL 60637, USA

Introduction

Banded Iron Formations (BIFs) are Precambrian chemical marine sediments commonly composed of quartz and iron oxides. The Dales Gorge BIF formed at the Archean-Proterozoic transition during the peak of BIF production which has been suggested to reflect oxygenation of the atmosphere and oceans. Iron isotope ratios ($\delta^{56}Fe$) have been measured from the Dales Gorge BIF and negative $\delta^{56}Fe$ values for magnetite have been attributed to a mixture between a biological source of iron produced by dissimilatory iron reducing bacteria and hydrothermal fluids (Johnson et al. 2008). Oxygen isotope ratios ($\delta^{18}O$) have been previously analyzed for the Dales Gorge BIF but the results have been contradictory, with reports of average $\delta^{18}O$ values for quartz of 21.2±0.6‰ VSMOW (2SD, 20-22‰, Becker & Clayton, 1976) and ~19‰ VSMOW (10 to 23‰, Hayashi et al. 2008). Values of $\delta^{18}O$ for magnetite from 0 to 5‰ VSMOW are reported by Becker & Clayton (1976).

Geologic Setting

The ~2.5 Ga Dales Gorge Member of the Brockman Iron Formation, Hamersley Group, Western Australia is one of the most well-studied BIFs due to its spectacularly laminated banding from the macro- to micro-scale. Classic important works (Trendall & Blockley 1970, Ayres 1972, Morris 1980, Ewers & Morris 1981, Trendall 1993) give detailed mineralogical descriptions, and recent sedimentological (Krapez et al. 2003), radiogenic isotope (Trendall et al. 2004) and petrographic studies (Pecoits et al. 2009) provide new understanding of these rocks. The Dales Gorge Member is subdivided into 33 alternating shale and BIF macrobands (0.5-15 m thick) – the latter are composed of cm-scale mesobands which are in turn made up of numerous sub-mm microbands. Microband was originally defined as a quartz and iron oxide couplet which have been suggested to reflect seasonal varves or oscillations in hydrothermal activity. Microbands can be further divided thus the term is avoided here and laminae is used to describe sub-mm bands of magnetite.

Results and Discussion

High precision *in situ* analyses of oxygen isotope ratios ($^{18}O/^{16}O$) by Secondary Ion Mass Spectrometry (SIMS) were obtained for quartz and single crystals of magnetite from the Dales Gorge BIF using a Cameca IMS-1280 at the WiscSIMS laboratory, UW-Madison. Figure 1 shows 208 new analyses of quartz from 32 samples in 7 BIF macrobands (DB4-5 & 12-16) with an average $\delta^{18}O$ value of 22.0±1.3‰ VSMOW (2SD, 20-26‰). These values are in good agreement with the average $\delta^{18}O$ value of 21.2±0.6‰ VSMOW (2SD, 20-22‰) found by Becker & Clayton (1976) for mineral concentrates and contrast with the average $\delta^{18}O$ value of ~19‰ (11-23‰) measured by Hayashi et al. (2008) by laser ablation after a complex chemical leaching process. The samples described in Hayashi et al. (2008) come from outcrops near Tom Price whereas samples in Becker & Clayton (1976) and in this study come from drill cores at Wittenoom and Paraburdoo respectively. Hayashi et al. (2008) analyzed laser trenches 100 µm x 2 mm in size – larger than the quartz grains in Figures 3 & 4 from Hayashi et al. (2008) and in all samples from this study. New *in situ* SIMS analyses have resolved $\delta^{18}O$ values for single crystals of quartz and magnetite with a 10 µm spot size, and previous *in situ* analyses with a larger spot size cannot be reproduced and thus appear in error. SIMS analyses of $\delta^{18}O$ for quartz were made in mesobands with a dominant mineralogy of magnetite, carbonate, stilpnomelane, and seven $\delta^{18}O$ analyses from 23 to 26‰ were found in carbonate- and stilpnomelane-rich areas though typical values of 22‰ were found in these same areas (Fig. 1).

Magnetite mesobands in the Dales Gorge BIF are composed of individual ~100 µm laminae. Previous studies have identified these laminae as magnetite overgrowths on hematite. Backscatter Electron Scanning Electron Microscopy (BSE-SEM) and Orientation Contrast (OC) Imaging reveal these layers are actually composed of silician magnetite overgrowths on magnetite. No magnetite overgrowths on hematite were identified in any of the samples for this study, and no evidence is seen of hydrothermal alteration to concentrated hematite ore. Electron Probe Microanalysis (EPMA) shows that silician magnetite contains up to 2 wt% SiO_2 and is zoned with the highest amounts of Si at the boundary between magnetite and silician magnetite. Three distinct textures of silician magnetite are seen in the Dales Gorge BIF: (1) Sinuous internal lamellae of magnetite with overgrowths of silician magnetite, (2) recrystallized magnetite with a core of Si-poor magnetite and a rim of silician magnetite, and (3) a complex intergrowth at the µm-scale of magnetite (Mt) and silician magnetite (Si-Mt). Figure 2a shows a BSE image where the brightness and contrast in the SEM have been adjusted so grey-scale values are distributed to show only magnetite. Quartz, carbonate, and stilpnomelane are present but appear black in this image. Internal magnetite lamellae contain numerous µm to sub-µm inclusions of carbonate and quartz whereas silician magnetite overgrowths are devoid of mineral inclusions (Fig. 2a). All three textures are found within ~100 µm-thick magnetite laminae from macrobands DB4-5, and DB12-16 of drill core DDH-44 from Paraburdoo (Ewers & Morris 1981). Electron Backscatter Diffraction (EBSD) and *in situ* X-ray micro-

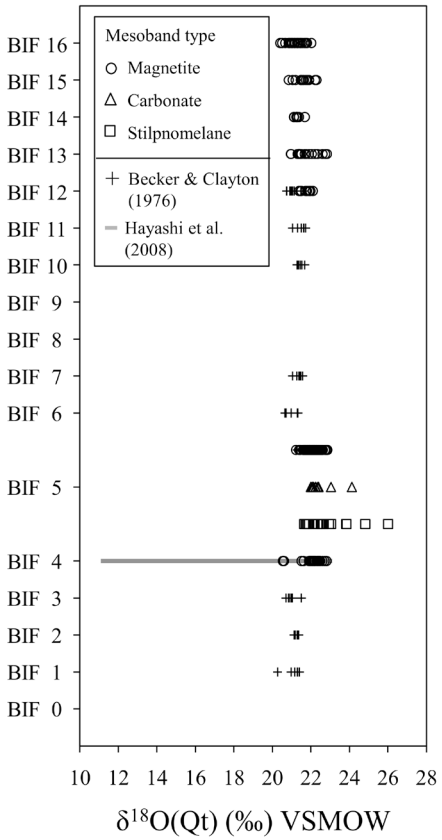

Figure 1. 208 in situ analyses of quartz have an average $\delta^{18}O$ value of 22.0±1.3‰ VSMOW (2SD,20 26‰) and are in good agreement with an average $\delta^{18}O$ value of 21.2±0.6‰ (20-22‰) found by Becker and Clayton (1976) for quartz concentrates. These values contrast with an average $\delta^{18}O$ value of ~19‰ VSMOW (10-23‰) reported by Hayashi et al. (2008) for in situ analysis by laser fluorination. Quartz analyses were made in mesobands with a dominant mineralogy of magnetite, carbonate, stilpnomelane, and seven $\delta^{18}O$ analyses from 23 to 26‰ were found in carbonate- and stilpnomelane-rich areas though typical values of ~22‰ were found within these same areas.

diffraction (XRD, ~50 μm beam size) confirm that the internal lamellae are magnetite and not hematite. Because silicon decreases the reflectivity relative to pure magnetite, this may explain the misinterpretation of this texture as magnetite overgrowths on hematite in previous studies. Silicon is not present in silician magnetite as discrete crystals of quartz >10 nm (Field Emission Gun SEM) but may be present as a γ-Fe_2SiO_4 component either in solid solution or as mixed layers with magnetite.

Oxygen isotope analyses of magnetite are not yet calibrated to the VSMOW scale due to crystal orientation effects on instrumental bias of $\delta^{18}O$ for magnetite by SIMS (Huberty et al. 2009, 2010). The average precision of $\delta^{18}O$ is ±0.4‰ (2SD) within single grains of magnetite standard 5830 (Magnet Cove, Arkansas, USA), close to ±0.3‰ (2SD) obtained for multiple grains of UWQ-1, a homogeneous quartz standard (Kelly et al. 2007). In contrast, the average grain-to-grain precision for magnetite 5830 is five times worse, ±2‰ (2SD) reflecting variation in instrumental bias due to differences in crystal orientation between randomly mounted grains. Several tests were conducted in order to improve accuracy of $\delta^{18}O$ for magnetite, and the grain-to-grain precision improves from ±2.9‰ to ±0.8‰ (2SD, n=26 grains) for analyses of magnetite 5830 made at routine analytical conditions and the new improved analytical condition (Huberty et al. 2010). Crystal orientation effects on bias of $\delta^{18}O$ have also been identified for hematite at similar levels as for magnetite (Huberty et al. 2010), as well as for $\delta^{56}Fe$ in magnetite and $\delta^{34}S$ in sphalerite and galena (Kita et al. 2010, Kozdon et al. 2010). Importantly, crystal orientation effects have not been identified for $\delta^{18}O$ in quartz, other silicates or for most minerals analyzed by WiscSIMS.

While quartz is relatively homogeneous in $\delta^{18}O$, magnetite analyses vary at the <100 μm scale from -10 to +4‰ and are significantly more variable than $\delta^{18}O$ values of 0 to +5‰ VSMOW found by Becker & Clayton (1976). Figure 2b shows 138 new analyses of $\delta^{18}O$ for magnetite

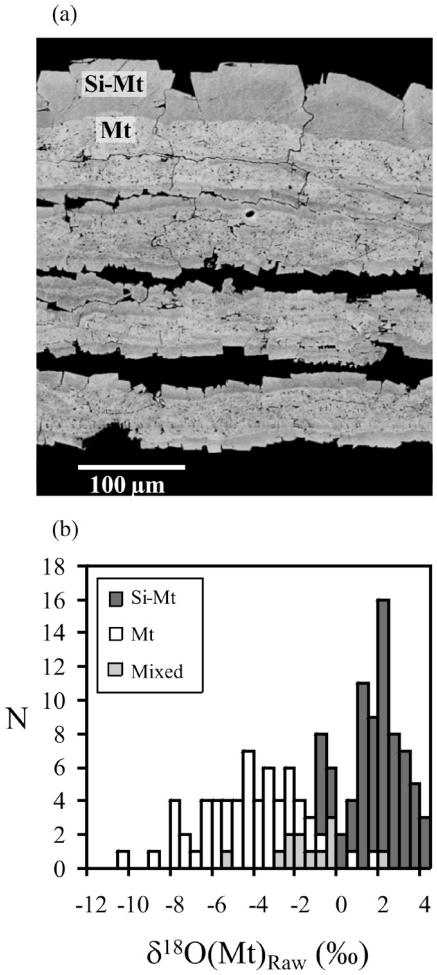

Figure 2. (a) BSE image with grey-scale values distributed to show only magnetite. Quartz, carbonate, and stilpnomelane appear black in this image. Magnetite laminae ~100 μm wide are composed of silician magnetite overgrowths (Si-Mt, darker grey) on magnetite (Mt, lighter grey). Magnetite lamellae contain numerous μm to sub-μm inclusions of carbonate and quartz whereas silician magnetite overgrowths are devoid of mineral inclusions >10 nm. (b) 138 in situ analyses of $\delta^{18}O$ for magnetite laminae: magnetite (white bars, n=55), silician magnetite (dark grey bars, n=71), and mixed analyses (light grey bars, n=12). Values of $\delta^{18}O$ for magnetite vary at the <100 μm scale from -10 to +4‰ and are significantly more variable than $\delta^{18}O$ values of 0 to +5‰ VSMOW found by Becker & Clayton (1976).

laminae: magnetite (white bars, n=55), silician magnetite (dark grey bars, n=71), and mixed analyses (light grey bars, n=12). Raw measured values of $\delta^{18}O(Mt)_{Raw}$ are bracketed by a precision of ±2‰ (2SD) due to crystal orientation effects. The average $\delta^{18}O(Mt)_{Raw}$ value is -4.9‰ for magnetite and +1.4‰ for silician magnetite. EBSD patterns show that misorientations are ~5° within individual magnetite laminae, and silician magnetite is epitaxial to magnetite. Thus, the large variability in $\delta^{18}O$ for magnetite is not the result of differences in crystal orientation, and the average difference of 6.3‰ between silician magnetite and magnetite is a real bi-modal distribution not attributable to crystal orientation effects. Measured values of $\delta^{18}O(Mt)_{Raw}$ from -10‰ to +4‰ are within ±2‰ of the corrected values relative to VSMOW, and these values are not expected to change significantly once $\delta^{18}O$ values are measured more accurately at the improved analytical condition. The homogeneity of $\delta^{18}O$ values for quartz likely reflects exchange during metamorphism whereas the variability of $\delta^{18}O$ for magnetite (-10 to +4‰) reflects differences in temperature and fluid composition during BIF formation.

Conclusions

Oxygen isotope ratios have been analyzed *in situ* by SIMS for quartz and magnetite in the Dales Gorge BIF. Quartz is nearly homogeneous with an average $\boldsymbol{\delta}^{18}O$ value of 22.0±1.3‰ VSMOW (2SD, 20-26‰). These values are in good agreement with an average $\boldsymbol{\delta}^{18}O$ value of 21.2±0.6‰ VSMOW (2SD, 20-22‰) found by Becker & Clayton (1976) on quartz concentrates and contrast with an average $\boldsymbol{\delta}^{18}O$ value of ~19‰ VSMOW (11-23‰) reported by Hayashi et al. (2008) from laser trenches 100 **µm** x 2 mm in size. Thus, values of $\boldsymbol{\delta}^{18}O$ from Hayashi et al. (2008) are not representative for samples from the Dales Gorge BIF. BSE and OC imaging, EPMA, EBSD, and XRD analyses show that magnetite laminae ~100 µm wide are composed of silician magnetite overgrowths on magnetite and not magnetite overgrowths on hematite as has been commonly reported. In contrast to quartz, values of $\boldsymbol{\delta}^{18}O$ for magnetite vary from -10 to +4‰ (within ±2‰ of VSMOW) and are significantly more variable than $\boldsymbol{\delta}^{18}O$ values of 0 to +5‰ VSMOW found by Becker & Clayton (1976). Values of $\boldsymbol{\delta}^{18}O$ for magnetite at present have a precision and accuracy of ±2‰ (2SD) due to crystal orientation effects by SIMS. The average $\boldsymbol{\delta}^{18}O(Mt)_{Raw}$ value for magnetite is 6.3‰ lower than for silician magnetite and reflects differences in temperature and fluid composition during BIF formation. Thus the oxygen isotope ratios for quartz and magnetite in these samples cannot be used to interpret the temperature or composition of seawater.

Acknowledgements

We thank Takayuki Ushikubo for assistance in SIMS analysis, Hiromi Konishi for assistance with XRD analysis, Brian Hess for sample preparation, and Jim Kern for technical assistance. This study was funded by the NASA Astrobiology Institute, NSF-EAR (0509639, 0838058) and DOE (93ER 14389). WiscSIMS is partly supported by NSF-EAR (0319230, 0516725, 0744079).

References

Ayres D.E., 1972, Genesis of iron-bearing minerals in banded iron formation mesobands in the Dales Gorge member, Hamersley Group, Western Australia, Economic Geology, 67, 1214–1233.

Becker R.H. & Clayton R.N., 1976, Oxygen isotope study of a Precambrian banded iron-formation, Hamersley Range, Western Australia, Geochimica et Cosmochimica Acta, 40, 1153–1165.

Ewers W.E. & Morris R.C., 1981, Studies of the Dales Gorge Member of the Brockman Iron Formation, Western Australia, Economic Geology, 76, 7, 1929–1953.

Hayashi K.-I., Naraoka H. & Ohmoto H., 2008, Oxygen Isotope Study of Paleoproterozoic Banded Iron Formation, Hamersley Basin, Western Australia, Resource Geology, 58, 43–51.

Huberty J.M., Kita N.T., Heck P.R., Kozdon R., Fournelle J.H., Xu H. & Valley J.W., 2009, Crystal orientation effects on bias of $\delta^{18}O$ in magnetite by SIMS, Geochimica et Cosmochimica Acta, Suppliment 73, A562.

Huberty J.M., Kita N.T., Kozdon R., Heck P.R., Fournelle J.H., Xu H. & Valley J.M., 2010, Crystal Orientation Effects in $\boldsymbol{\delta}^{18}O$ of Magnetite and Hematite by SIMS, Chemical Geology, in preparation.

Johnson C.M., Beard B.L., Klein C., Beukes N.J. & Roden E.E., 2008, Iron isotopes constrain biologic and abiologic processes in banded iron formation genesis, Geochimica et Cosmochimica Acta, 72, 151–169.

Kelly J.L., Fu. B., Kita N.T. & Valley J.W., 2007, Optically continuous silcrete quartz cements of the St. Peter sandstone: High precision oxygen isotope analysis by ion microprobe, Geochimica et Cosmochimica Acta, 71, 15, 3812–3822.

Kita N.T., Huberty J.M., Kozdon R., Beard B.L. & Valley J.W., 2010, High precision SIMS oxygen, sulfur and iron stable isotope analyses of geological materials: Accuracy, surface topography and crystal orientation, Surface and Interface Analysis, in press.

Kozdon R.K., Kita N.T., Huberty J.M., Fournelle J.H. & Valley J.W., 2010, *In situ* sulfur isotope analysis of sulfide minerals by SIMS: Precision and accuracy, Chemical Geology, in review.

Morris R.C., 1980, A Textural and Mineralogical Study of the Relationship of Iron Ore to Banded Iron-Formation in the Hamersley Iron Province of Western Australia, Economic Geology, 75, 184–209.

Morris, R.C., 1993, Genetic modelling for banded iron-formation of the Hamersley Group, Pilbara Craton, Western Australia, Precambrian Research, 60, 243-286.

Pecoits E., Gringas M.K., Barley M.E., Kappler A., Posth N.R. & Konhauser K.O., 2009, Petrography and geochemistry of the Dales Gorge banded iron formation: Paragenetic sequence, source and implications for palaeo-ocean chemistry, Precambrian Research, 172, 163–187.

Trendall A.F. & Blockley J.G., 1970, The iron formations of the Precambrian Hamersley Group, Western Australia with special reference to the associated crocidolite, Western Australia Geological Survey Bulletin 119.

Trendall A.F., Compston W., Nelson D.R., De Laeter J.R. & Bennet V.C., 2004, SHRIMP zircon ages constraining the depositional chronology of the Hamersley Group, Western Australia, Australian Journal of Earth Sciences, 51, 5, 621–644.

Valley J.W. & Kita N.T., 2009, *In situ* Oxygen Isotope Geochemistry by Ion Microprobe, in Secondary Ion Mass Spectrometry in the Earth Sciences, Fayek M. ed, MAC Short Course 41, 19–63.

WEATHERING INTENSITY ON LAURENTIA DURING THE MESOPROTEROZOIC: EVIDENCE FROM THE BELT-PURCELL SUPERGROUP, WESTERN NORTH AMERICA

R. Kerrich[1] & I. González-Álvarez[2,3,4]

[1]Department of Geological Sciences, University of Saskatchewan, Saskatoon, SK S7N 5E2, Canada
[2]ABM Resources NL, Nedlands 6009, Perth, Western Australia
[3]Centre for Exploration Targeting, School of Earth and Environment, University of Western Australia, Crawley 6009, Western Australia
[4]Now at: CSIRO, Australian Resources Research Centre, Geology and Geochemistry, Kensington, WA 6151, Australia

Abstract

Argillites and sandstones of the Belt-Purcell Supergroup sampled at three localities spanning over ~17 km of stratigraphic section display systematic negative anomalies of Eu/Eu* relative to post-Archaean Upper Continental Crust (PA-UCC). The Chemical Index of Alteration (CIA), corrected for diagenetic K-addition, spans 63 to 85 compared to Post-Archaean Australian Average Shale (PAAS) at 70. Argillites average at 73 and sandstones at 68. These results, in conjunction with low absolute contents of Sr, Ca and Na, high Rb/Sr and K/Cs ratios, and covariations of CIA-Eu/Eu*, collectively could be viewed as a combination of intense chemical weathering and a recycled sedimentary component in the provenance. Such geochemical relationships and CIA values are in keeping with large modern river systems such as the Ganges, Mekong or Amazon rivers that drain intensely weathered provenances.

The Belt-Purcell basin was part an intracontinental rift system with developing spreading centres, which developed as the Mesoproterozoic supercontinent Columbia dispersed at ~1,500 Ma, possibly due to plume impingement. Intense weathering in the source region may be associated with elevated levels of atmospheric CO_2 degassed from the mantle plume and new spreading centres.

Introduction

Proterozoic paleoclimates and their driving forces are controversial. Severe swings in climate caused at least two low-latitude glacial periods, at ~2,400-2,200 and ~800-600 Ma, and inferred pronounced changes in atmospheric oxygen levels at ~ 2.4-2.2 Ga. Siliciclastic sediments may record chemical signatures of weathering intensity in the source area, which in turn reflect paleoclimate. Feldspar and quartz constitute ~80% of the modal mineralogical composition of the upper continental crust (Taylor & McLennan, 1985 and references therein). Hydrolysis of feldspars and ferromagnesian minerals, accompanied by the depletion of mainly alkali- and alkaline-earth metals in the residual bedrock, are the most common features of the weathering process. Based on these principles, the chemical index of alteration (CIA) was formulated by Nesbitt and Young (1982) using a geochemical approach to study paleoclimate: $CIA=[Al_2O_3/(Al_2O_3+CaO+Na_2O+K_2O)]*100$; where CaO is associated with the silicate fraction of the rock. The CIA varies from 100 in severely weathered residual clays to ~50 in unweathered rocks. Values of CIA in Post Archaean upper continental crust (PA-UCC) and Post Archaean Australian Shale composite (PAAS) are 50 and 70, respectively (Taylor & McLennan, 1985). Peaks in the CIA at 2,700-2,500 Ma, ~1,900 Ma, and 800-600 Ma may imply an unusually warm paleoclimate (Condie et al., 2001). Some of the CIA peaks (~2,700 and ~1,900 Ma) are attributed to an increase in atmospheric CO_2 levels produced by mantle superplume events (Condie et al., 2001). This study addresses weathering intensity for the interval ~1,500-1,400 Ma for which there is little data, especially K-corrected values for CIA.

This study also attempts to ascertain the original geochemical signature of weathering in the catchment of the Belt-Purcell Supergroup in order to assess paleoclimate between the two main glacial periods in the Mesoproterozoic.

Geologic setting

The Belt-Purcell Supergroup (BPS) is a remnant of an extensive ~17 km thick, dominantly siliciclastic sequence (e.g. Whipple et al., 1984). It outcrops over 500 km in length, from southwestern Montana to southeastern British Columbia (Fig. 1A). This large volume of siliciclastic detritus is divided mainly into two main lithologies: (1) argillites; and (2) sandstones. The Belt-Purcell Supergroup comprises four stratigraphic divisions: the lower Belt; the Ravalli Group; the middle Belt; and the Missoula Group (e.g., Whipple et al., 1984).

The tectonic setting for the Belt-Purcell Basin is interpreted to be part of an intracontinental rift system that formed at ~1,500 Ma, associated with dispersal of the supercontinent Columbia. Sedimentation spanned ≤75 Ma, with a maximum age of sedimentation constrained at 1,469 ± 3 Ma by U-Pb dating of zircons in synsedimentary sills situated near the base of the Supergroup, to a minimum age estimated at 1,401 ± 6

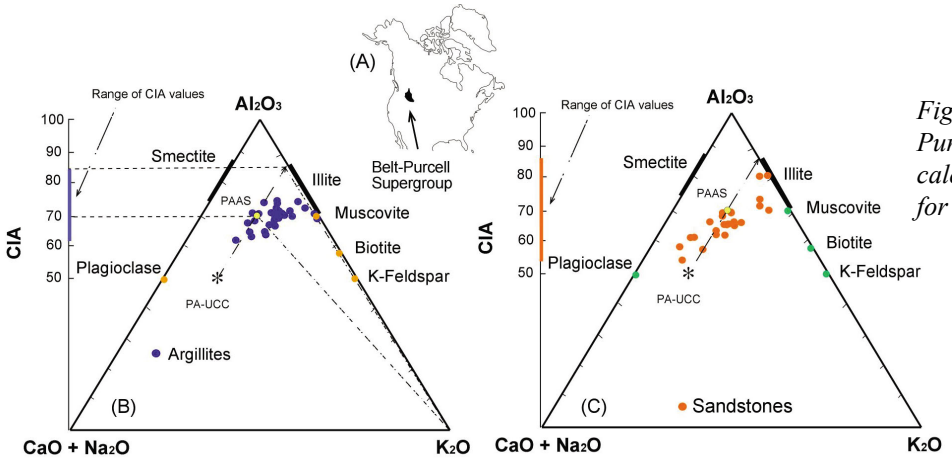

Figure 1. (A) Location of the Belt-Purcell Supergroup; (B) and (C) CIA calculation correcting to K-addition for argillites and sandstones.

Ma from a tuff horizon in the upper Missoula Group. Metamorphic grade is lower greenschist facies at the three localities sampled for this study.

Intensity of weathering in the source area

K-addition

An important factor to take into account when calculating CIA values is possible diagenetic addition of K into the rock/sediment. Post-depositional potassic alteration has been described previously as a widespread feature in many Precambrian siliciclastic sedimentary sequences and saproliths. This diagenetic addition of K has been factored by Fedo et al. (1995) into a corrected CIA. In Al_2O_3-CaO+Na_2O-K_2O coordinate-space, unweathered rocks plot at a CIA of 50 on the plagioclase-K-feldspar join. Chemical weathering generates a trend from a point representing unweathered PA-UCC, parallel to the CN-A axis. Corrected CIA values are calculated by projecting from the K apex (100%) through data points to the weathering trend, then read off the CIA y-axis (Fedo et al., 1995).

K_2O contents in argillites are enriched by a factor of 1.12 on average, but up to 35% addition relative to PA-UCC. Diagenetic potassic addition is supported by the illite-rich matrix in argillites. Given K enrichment due to diagenetic addition of K by basinal fluids, corrected CIA values range from 63 to 85, and from 55 to 80 for argillites and sandstones, respectively. Most of the argillites CIA values are >67, with an average of 73, and for sandstones >65, with an average of 68 (Fig. 1B). Diagenetic brines were intermittently active over >1 Ga, as recorded by diagenetic monazites, and fractionated REE and HFSE, but did not significantly perturb Al_2O_3-CaO-Na_2O relationships (Gonzalez-Alvarez et al. 2006).

Eu/Eu and CIA correlation*

Negative correlations between CIA and Eu/Eu*, and Sr and Eu/Eu*, are found worldwide in different tectonic settings associated with modern deep-sea sediments. Gao & Wedephol (1995) interpreted the covariation of decreasing Eu/Eu* with increasing CIA values as due to decreasing contributions of juvenile terranes but larger siliciclastic input from older recycled sediments from larger provenances. This is based on the premise that juvenile crustal terranes from local sources are decomposed very little due to short transport, whereas long transport or large catchment areas with an important recycling component develop deeper Eu anomalies, and hydrolysis of feldspar and ferromagnesian silicates due to more intense decomposition.

Other trace and major element proxies

The Belt-Purcell argillites and sandstones with <4 wt% LOI (loss on ignition) values display pronounced negative CaO, Na_2O and Sr anomalies as low as 0.1 for Sr relative to PA UCC, consistent with intense chemical weathering of the source terrane(s) (Bhat & Ghosh, 2001), but high Rb/Sr ratios relative to PA-UCC. This geochemical feature has been reported in several Archaean and Proterozoic metasedimentary sequences (Bhat & Ghosh, 2001). The data are consistent with deeply weathered cratonic rocks, where Sr is lost from the weathered regolith, whereas Rb is retained in the clay fraction. Elevated Rb/Sr may also result as well from diagenetic addition of Rb along with K.

Ratios of K/Cs in this database are mostly lower than the PA-UCC average value of 7600, consistent with an intensely weathered source where Cs is preferentially retained over K in the weathering profile. Fractionation of K/Cs may also stem from diagenetic introduction of K. There is no robust test for weathering versus diagenetic influence for the measured K/Cs values; however, the simplest interpretation given the combination of covariant CIA versus Eu/Eu*, Sr and K/Cs is in terms of weathering intensity. Like CIA values, K/Cs could be viewed as some combination of contemporaneous weathering intensity in the catchment and any proportion of recycled sedimentary rocks in the provenance from a previous weathering-sedimentation cycle.

In summary, the corrected CIA values, low absolute contents of Sr, Ca and Na, with high Rb/Sr, and K/Cs ratios, as well as covariations of CIA-Eu/Eu*, Sr-Eu/Eu* and K/Cs-CIA, suggest an intensely weathered provenance under hot, wet climate for the argillites and sandstones of the Belt-Purcell Supergroup.

The drainage system

The Belt-Purcell Basin could have been drained by a Mississippi-scale river system (e.g., Rainbird et al., 1997). Modern large river systems, classified as tropical-wet rivers, that drain areas that are intensely weathered, include the Mekong, Congo and Amazon rivers. The geochemistry of their suspended sediment features large

negative anomalies in Ca, Na and Sr relative to PA-UCC. In addition, other studies comparing the geochemistry of sand from modern rivers and the Archaean Witwatersrand siliciclastic rocks report CIA values of sands of tropical rivers of 75 (Orinoco River) and 68 (Ganges River). These values are comparable with the range and average CIA of 73 and 66 for argillites and sandstones of the Belt-Purcell Supergroup, respectively.

Accordingly, negative correlations between CIA and Eu/Eu*, Sr and Eu/Eu*, and pronounced depletions in Sr, Ca and Na in the Belt-Purcell rocks, could be interpreted as consistent with the results from previous studies that postulate the existence of a major river system that drained a large catchment area, supplying a substantial amount of weathered sediments to the Belt-Purcell basin.

Proterozoic climate and geodynamics

Condie et al. (2000) have shown common time series for mantle plumes, CIA values, black shales, percentage of shale to total sediments, and iron formations from ~2,500 to 1,700 Ma. They proposed that mantle plumes released large quantities of CO_2 through volcanic gases that intensified silicate weathering on the continents. Values of CIA span 67-88 in black shales at ~1,900 Ma, albeit uncorrected for diagenetic K addition (cf. Fedo et al., 1995) which corresponds to a possible superplume event (Condie et al., 2001). Major perturbations in the atmosphere-hydrosphere-biosphere have also been linked to the Cretaceous superplume.

The Mesoproterozoic supercontinent Columbia assembled at ~1,900-1,800 Ma and then dispersed by ~1,500 Ma due to plume impingement. The Belt-Purcell Basin was part of a system of intracontinental rifts that developed ~1,500 Ma associated with that dispersal, and the basal sections have tholeiitic gabbro sills compositionally consistent with intra-plate magmatism. Weathering intensity of the Belt-Purcell Supergroup catchment provides a test for perturbation of atmospheric CO_2 associated with the inferred ~1,500 Ma coupled plume-rifting of the Mesoproterozoic supercontinent. Condie et al. (2001) showed a minor peak of CIA at ~1,500 Ma. The average CIA of BPS argillites is 73, extending to 85, compared to ~75 for shales associated with the ~1,900 Ma superplume and 70 for PAAS. These results are consistent with moderate to high intensities of chemical weathering, in a hot and wet climate, for the catchment of the intracratonic rift Belt-Purcell Basin.

Condie et al. (2001) linked the total percentage of shale in the sedimentary sequences with plume activity. Release of gases due to magmatism associated with plumes would intensify chemical weathering by silicate hydrolysis and be responsible for larger shale volumes in the sedimentary record. The plume-shale time series peaks at ~1,900 Ma, and has time correlating values of CIA that extend to 88, and shales at ~36% of total sedimentary sequences. In the Belt-Purcell sequence at ~1,470-1,400 Ma, CIA extends to ~80 (this study), and total-shale thickness percentage is 40% (Condie et al., 2001 and references therein), suggesting that the Belt-Purcell Supergroup could be associated with the same weathering-plume relationship. Most paleomagnetic, paleoclimatic and sedimentary data are consistent with deposition of the Belt-Purcell Supergroup sediments at low latitudes between 10° and 35°. Alternatively, weathering-alteration studies, coupled with petrographic observations of feldspars, hematitic clasts and evaporites in the Belt-Purcell rocks, as well as geochemical studies, have been interpreted as reflecting semi-arid to arid climate with intermittent wetter intervals. Other independent potential evidence for hot climate during deposition of the Belt-Purcell Supergroup is in halite casts, and abundant scapolite, which are potential sources of the salts in the inferred hypersaline basinal brines.

Conclusions

Calculated CIA values in the Belt-Purcell Supergroup argillites, corrected for diagenetic K-addition, span 63 to 85, averaging 73, versus 50 and 70 for PA-UCC and PAAS respectively. These data in conjunction with low absolute contents of Sr, Ca and Na, together with high Rb/Sr and K/Cs ratios, and covariations of CIA-Eu/Eu*, Sr-Eu/Eu* and K/Cs-CIA, collectively are commensurate with a moderate to intensely weathered provenance in a prevalently hot, wet climate. Such geochemical relationships and CIA values are in keeping with large modern river systems such as the Ganges, Mekong and Amazon. Intense weathering of the provenance may be associated with elevated levels of atmospheric CO_2 degassed from volcanoes associated with the mantle plume implicated in rifting of the supercontinent Columbia.

Acknowledgements

The staff of Waterton-Glacier International Peace Park is thanked for their enduring support. R. Kerrich acknowledges NSERC MFA support of the ICP-MS facility, and the George McLeod endowment to the Department of Geological Sciences, University of Saskatchewan, Canada. T. Prokopiuk is thanked for his insights.

References

Bhat M.I. & Ghosh S.K., 2001, Geochemistry of the 2.51 Ga old Rampur Group pelites, western Himalayas: implications for their provenance and weathering, Precambrian Res., 108, 1–16.

Condie K.C., Des Marais D.J. & Abbott D., 2000, Geologic evidence for a mantle superplume event at 1.9 Ga, Geochemistry,. Geophysics, Geosystems, 1, 2000GC000095.

Condie K.C., Des Marais D.J. & Abbott D., 2001, Precambrian superplumes and supercontinents: a record in black shales, carbon isotopes, and paleoclimates? Precambrian Research, 106, 239–260.

Fedo C.M., Nesbitt H.W. & Young G.M., 1995, Unraveling the effects of potassium metasomatism in sedimentary rocks and paleosols, with implications for paleoweathering conditions and provenance, Geology, 23, 921–924.

Gao S. & Wedepohl K.H., 1995, The negative Eu anomaly in Archaean sedimentary rocks: implications for decomposition, age and importance of their granitic sources, Earth and Planetary Scence Letters, 133, 81–94.

González-Álvarez I., Kusiak M.A. & Kerrich R., 2006 A trace element and chemical Th-U total Pb dating study in the lower Belt-Purcell Supergroup, western North America: provenance and diagenetic implications, Chemical Geology, 230, 140–160.

Nesbitt H.W. & Young G.M., 1982, Early Proterozoic climates and plate motions inferred from major element chemistry of lutites, Nature, 299, 715–717.

Rainbird R.H., McNicoll V.J., Thériault L.M., Abbott J.G., Long D.G.F. & Thorkelson D.J., 1997, Pan-continental river system draining Grenville orogen recorded by U-Pb and Sm-Nd geochronology of neoproterozoic quartzarenites and mudrocks, northwestern Canada, Journal of Geology, 105, 1–17.

Taylor S.R. & McLennan S.M., 1985, *The continental crust: its composition and evolution*. Blackwell, Oxford, U.K.

Whipple J.W., Connor J.J., Raup O.B. & McGrimsey R.G., 1984, Preliminary report on the stratigraphy of the Belt Supergroup, Glacier National Park and adjacent Whitefish Range, Montana, in *Northwest Montana and Adjacent Canada*, McBane, J.D., Garrison, P.B., eds, Montana Geological Society Guidebook, 1984 Field Conference and Symposium, 33–50.

MESOARCHEAN HYDROTHERAMAL OCEANIC SEDIMENTATION AND ENVIRONMENT: DXCL-DRILLNG, WEST PILBARA, AUSTRALIA

S. Kiyokawa[1], T. Ito[2], M. Ikehara[3], K. Yamaguchi[456], H. Naraoka[1], R. Sakamoto[1], S. Koge[1], K. Hosoi[3] & Y. Suganuma[7]

1. Department of Earth and Planetary Science, Kyushu University, 6-10-1, Hakozaki, Higashiku, 812-8581, JAPAN.
2. Faculty of Education, Ibaraki University, 2-1-1, Bunkyo, Mito, Ibaraki, 310-8512, JAPAN.
3. Centre for Advanced Marine Core Research, Kochi University, 200, Monobe-otsu, Nankoku, Kochi, 783-8502, JAPAN.
4. Department of Chemistry, Toho University, 2-2-1, Miyama, Funabashi, Chiba, 274-8510, JAPAN.
5. Japan Agency for Marine-Earth Science and Technology, 3173-25, Showa-machi, Kanazawaku, Yokohama, Kanagawa, 236-0001, JAPAN.
6. NASA Astrobiology Institute, U.S.A.
7. National Institute of Polar Research, 10-3, Midorimachi, Tachikawa, Tokyo, 190-8518, JAPAN.

Introduction

During the Neoarchean to Paleoproterozoic, atmospheric conditions varied from low oxygen contents to oxic conditions, especially at 2.5 Ga, identified as the Great Oxidation event (e.g. Canfield, 2005). A strong MIF anomaly is identified in Neoarchean time, however it was lower before 2.8 Ga (e.g. Farquhar et al., 2007). A small rise in MIF value during the Mesoarchean has been suggested as representing early oxygenation at this time (Ohomoto et al., 2006, Kump 2008). To understand this hypothesis, it is important to identify basic geological evidence, such as lithology, stratigraphy and geochemical evidence, of the sedimentary rock records at this age. In the Mesoarchean, iron rich sedimentary rocks have been recognized as hydrothermal siliceous sequences. Many places have been recognised as a sequence of black chert to iron rich sediments above a volcanic sequence (e.g. Marble Bar Chert 3.5 Ga, Sulfer Spring 3.2 Ga, Dixon Island –Cleaverville formations 3.2 Ga, Masauri Chert 3.3 Ga). These sedimentary sequences contain the clues to the understanding of the Archean ocean and earth surface environments.

Here, we will focus the Dixon Island and Cleaverville formations, which are among the best preserved Archean hydrothermal sedimentary sequences in the world, to describe the detailed stratigraphy and interpreted relatively deep ocean (immature island arc setting) environment (Kiyokawa & Taira, 1998, Kiyokawa et al., 2006). These formations contain 3195±12Ma felsic tuff, metamorphosed at below the prehnite-pumpellyite facies and preserving a more than 900 m thick stratigraphy (Fig. 1).

During the summer of 2007, we carried out scientific drilling, called "DXCL drilling project", to get continuous and flesh samples (Yamaguchi et al., 2009). This drilling project selected two coastal sites; (CL 1 and CL2) in the lower part of the Cleaverville Formation, and another site (DX) in the upper Dixon Island Formation (Fig. 1). A systematic combination of stratigraphical, sedimentological, geochemical, and geobiological approaches were applied to the fresh samples. From these core samples and good coastline outcrops, we will try to understand Mesoarchean deep ocean sedimentation, and

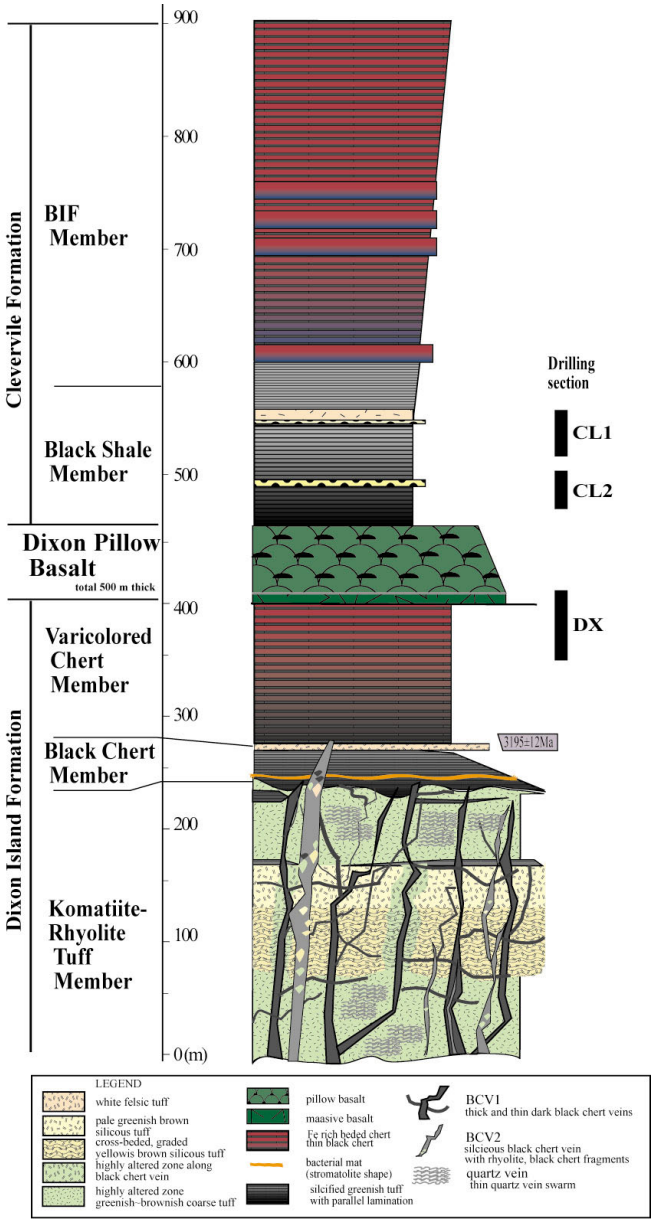

Figure 1. Simplified stratigraphic column of the Dixon Island – Cleaverville formations and drilling levels (after Yamaguchi et al. 2009)

the formation of banded iron formation in the lower-most submarine hydrothermal environment at that time. Here we will show the recent results from the Dixon Island-Cleaverville sequence, which will be key evidence for understanding the nature of the middle Archean (3.2 Ga) marine environment influenced by hydrothermal activity and biogenic activity.

Stratigraphy of Dixon Island –Cleaverville formations

Continuous exposure of the Dixon Island and Cleaverville formations occurs along the Dixon Island and Cleaverville beach, and we made various scale geologic maps, such as a 1/5000 map of the 5 km long island, 1/1000 map in a 1 km long continuous section, and 100 m 1/100 and 1/20 scales maps in stratigraphic transitional zones. Based on this mapping, we identified the deformational history (Kiyokawa et al., 2002), detailed stratigraphic relationships, later stage volcanic intrusion and strike-slip (D_2) related sedimentary basin development. From this work, we restored the 900 m thick volcano-sedimentary sequence of the Dixon Island-Cleaverville formations (Fig. 1).

The Dixon Island Formation, which is approximately 350 m in thick, is composed of Komatiite-Rhyolite Tuff, Black Chert and Varicolored Chert members. The Komatiite-Rhyolite Tuff member is 200 m thick. It is composed of highly silicified greenish-altered komatiite and white felsic tuff containing laminated coarse to medium-grained felsic tuff. Spinifex-textures are well developed (splashed-pattern) in this highly altered zone. Numerous black-chert vein swarms are one of the most distinctive characteristics of the Komatiite-Rhyolite Tuff member. They consist of individual veins that range from a few millimetres to two metres in thickness and contains many fine carbonaceous particles.

The Black Chert member overlies the Komatiite-Rhyolite Tuff member with irregular contact. This member forms a 15~20 m thick stratified sequence which is composed of massive black, well-laminated black and tuffaceous laminated chert. The massive black chert has carbonaceous particles which are quite similar with those in the black chert veins. Well-laminated black chert contains a brown colored small-scale stromatolite-like wavy layer which is 10~20 cm thick and continuous over an area more than 1 km wide. The black chert veins suddenly disappear in the Black Chert member.

The 100 ~ 150 m thick Varicolored Chert member is comprised of well laminated thin ferruginous-red chert and bedded black-white-green chert. Partly preserved black chert layers contain wavy laminated biomat textures. The thick pillow basalt of the Dixon Pillow Basalt conformably overlies this member.

The Cleaverville Formation, which is more than 400 m in thickness, conformably overlies the pillow basalt. This formation is composed of Black Shale and BIF members. The Black Shale member contains thick massive black shale with some thin volcaniclastic (pyroclastic) layers. These rocks are highly weathered in outcrop. Partly preserved, well-bedded cherty beds occur in these weathered massive shales. The BIF member conformably overlies the Black Shale member. Iron bed content gradually increase towards the top. BIF is formed by well laminated, less than 1 cm thick iron beds, white chert and red chert with some weathered red shales. There are some magnetite beds within red hematite iron beds. The top of this formation is in fault contact within a large scale fold axis. After the folding, shallow water sediments were deposited unconformably on the Dixon Island – Cleaverville formations.

DXCL drilling

The drilling angle was 52º and total core length was 200m. In this location, the weathering zone i at least 40m deep. Stratigraphic thickness of the DX, CL1 and CL2 cores are 61, 36 and 27 m respectively.

The DX core is well stratified and contains thin alteration of very thin laminated black shale and thin pyrite lamination, which are less than 5mm in thickness. From petrographic observations, very fine lamination is present, less than 0.05 mm thick, with organic carbon bearing black, fine grained chert and pyrite layers. Pyrite layers are well banded and form pinch-swell structures. There are fine grained pyrites in the massive black chert. 10-20 cm thick massive pyrite veins are preserved in the deformed zone of the deepest core.

The CL 1 and CL2 cores are partly fragmented by D_2 strike-slip deformation an observation consistent with outcrop. They mainly consist of organic-rich massive black shale beds (20cm in thickness) with few cross-laminated fine volcaniclastic sandstones. Petrographic observation shows the black shale is mostly silt size grains and contains fine grained pyrite. Well banded pyrite layers are not well preserved in the CL core. Sulfide-containing black chert and shale are not found in surface weathered outcrops, and therefore is the first discovery of this lithology in these geologic units.

Geochemical analysis

We did total organic carbon, carbon isotope and pyrite S isotopic analysis on black chert and black shale. Total organic carbon concentration of each samples are over 0.5 wt.% and the DX core is especially rich with an average of 1.2 wt.% and the maximum value reaches over 3.0 wt.%. Total organic carbon concentration of DXCL cores is much higher than those of averaged contents (0.1 to 0.2 wt.%) of black chert bed in exposed Dixon Island Formation (Kiyokawa et al. 2006). Carbon isotope ($\delta^{13}C$) compositions of organic matter in drill core range from -32 to -26‰ in most samples. On the other hand, new data from the lower part of the Black Chert member of the Dixon Island Formation contains lighter value (-43 to 35‰).

Sulfur isotope composition from the black shale and black chert is $\delta^{34}S$: -1.9 to +12.9 ‰ in the DX core and +0.9 to +25.9 ‰ in CL core (Sakamomto et al., this volume).

Sedimentary environment

The Dixon Island Formation contains komatiite volcanism-related, organic matter-containing hydrothermal activity. The black chert and iron rich chert in this formation is identified as deposited in anoxic calm conditions, forming a thick stagnant water layer at the bottom of the sea. After basaltic volcanic activity in this area, the sedimentary environment of the Cleaverville Formation was slightly shallower than that of the Dixon Island Formation. It is affected by distal pyroclastic volcanism and had higher sedimentation. Banded iron formation was deposited gradually on the thick black chert beds. This stratigraphic change shows a stratified ocean cross section from stagnant anoxic to shallower oxic condition at the top. This changing stratigraphy, from an organic rich sequence to iron formation, is a quite similar stratigraphy to that of other banded iron formations, such as the Marra Mamba and Brockman Iron formations of the Hamersley Basin.

Lighter carbon (-40‰) contents of black chert above a vent system might be affected by hydrothermal related bacteria (methanogen). According to the relationship between the distribution of the black chert veins and the occurrence pattern of microfossils in the black chert, many microbial colonies were produced around hydrothermal vents. On the other hand, carbon isotope values above the Black Chert member is mostly about 30 ‰. Therefore the origin of organic carbon in most of the Dixon Island and Cleaverville formations was mainly contributed by phototroph (i.e. cyanobacteria), which is dropped and deposited on the bottom of the ocean floor.

Wide and heavy $\delta^{34}S$ values support the activity of sulfate reduction bacteria and suggest that the sedimentary environments are highly closed spaces with limited sulfate supply. It is assumed that sulfate reduction and pyrite crystallization took place in a thick stagnant organic layer on the sediment.

Conclusion

We suggest the Dixon Island and Cleaverville formations preserve one of the best examples of oceanic slope conditions from relatively deep ocean to the oxygenic portion around an immature island arc setting in the Mesoarchean. In this time, the ocean might have been well stratified. The lower portion is the anoxic and stagnant bottom of the ocean floor, which is partly influenced by hydrothermal activity. The activity of sulfur reducing bacteria occurs in the anoxic closed bottom - lower sequence of the water column. On the other hand, the ocean surface might contain cyanobacteria activity that partly started oxygenation and formed an oxic layer. When the sedimentation level reached shallowing oxic water layers, iron formation was deposited at the top of this sequence. In this way, the Dixon Island and Cleaverville formation might be a well preserved oxygen producing system of the early oxygenation event in the Mesoarchean.

Acknowledgements

We thank Arthur Hickman and Mike Doepel for organising the DXCL drilling project. We acknowledge support from JSPS foundation (No.18253006, No.1434053).

References

Canfield D.E., 2005, The early history of atmospheric oxygen. Annual Review of Earth and Planetary Sciences, 33, 1–36.

Farquhar J., Peters M., Johnston D. T., Strauss H., Masterson A., Wiechert U. &, Kaufman A.J., 2007, Isotopic evidence for Mesoarchean anoxia and changing atmospheric sulphur chemistry, Nature, 449, 11, 706–710.

Kiyokawa S. & Taira A., 1998, The Cleaverville Group in the West Pilbara Coastal Granioid-Greenstone Terrain of Western Australia: an example of a Middle Archean immature oceanic island-arc succession, Precambrian Research, 88, 109–142.

Kiyokawa S., Taira A., Byrne T., Bowring S. & Sano Y., 2002, Structural evolution of the middle Archean coastal Pilbara terrane, Western Australia, Tectonics, 21, 5, 1044–1068.

Kiyokawa S., Ito T., Ikehara M. & Kitajima F., 2006, Middle Archean volcano-hydrothermal sequence: Bacterial microfossil-baring 3.2 Ga Dixon Island Formation, coastal Pilbara terrane, Australia, Geological Society of America Bulletin, 118, 3–22.

Kump L.R., 2008, The rise of atmospheric oxygen, Nature, 451, 17, 277–278.

Ohmoto H., Watanabe Y., Ikemi H., Poulson S. R. & Taylor B.T., 2006, Sulphur isotope evidence for an oxic Archean atmosphere, Nature, 442, 24, 908–911.

Yamaguchi K.E., Kiyokawa S., Ito T., Ikehara M., Kitajima F. & Suganuma Y., 2009, Clues of Early Life: Dixon Island-Cleaverville Drilling Project (DXCL-DP) in the Pilbara craton of Western Austraria, Scientific Drilling, 7, 34–37

HYDROTHERMAL ACTIVITY AND IRON SEDIMENTATION IN NAGAHAMA BAY, SATSUMA IWO-JIMA ISLAND, KAGOSHIMA, JAPAN

T. Nagata[1], S. Kiyokawa[1], M. Ikehara[2], K. Oguri[3], S. Goto[4], T. Ito[5], K. Yamaguchi[6,7,8], R. Sakamoto[1] & M. Takehara[1],

[1]Department of Earth and Planetary Science, The University of Kyushu, 6-10-1 Hakozaki Higashiku, Fukuoka, 812-8581, Japan
[2]Center for Advanced Marine Core Research, The University of Kochi, 200 Monobe-otsu, Nankoku, Kochi, 783-8502, Japan
[3]Earth and Life History Research Program, Institute of Biogeosciences, Japan Agency for Marine-Earth Science and Technology, 2-15 Natsushima, Yokosuka, Kanagawa, 237-0061, Japan
[4] Fuel Resource Geology Research Group, Institute for Geo-Resources and Environment, National Institute of Advanced Industrial Science and Technology, Tsukuba Central 7, 1-1-1 Higashi, Tsukuba, Ibaraki, 305-8567, Japan
[5] Faculty of Education, The University of Ibaraki, 2-1-1 Bunkyo, Mito, Ibaraki, 310-8512, Japan
[6] Faculty of Science Department of Chemistry, The University of Toho, 2-2-1 Miyama, Hunabashi, Chiba, 274-8510, Japan
[7]Precambrian Ecosystem Laboratory, Japan Agency for Marine-Earth Science & Technology, 3173-25, Showa-machi, Kanazawaku, Yokohama, Kanagawa, 236-0001, Japan
[8] NASA Astrobiology Institute, USA

Introduction

Banded Iron formation (BIF) is a unique sedimentary rock in earth history. However, they are not well understood, because there is no modern example of BIF sedimentation (e.g. Konhauser et al., 2007). Before discussing "banded" iron rocks, it is very important to understand the behaviour of iron hydroxide sedimentation. We try to observe iron hydroxide sedimentation in Satsuma Iwo-jima in Southern Kyushu Japan and to understand the iron precipitation and sedimentation from a modern shallow ocean.

Satsuma-Iwojima is a 6km wide and 3km long volcanic island, located 38 km south of Satsuma Peninsula. This island is located on the northwest rim of the Kikai caldera (23km wide and 16km long), and the caldera rim surrounds the west and northwest parts of island. It contains active rhyolitic Iwo-dake and old basaltic Inamura-dake (Ono et al., 1982). Many hot springs are present along the shore of Iwo-dake. Brown to creamy white waters, which formed by the mixing of hot water and seawater, are identified along coast of Iwo-dake. The reddish brown colored water is formed by neutralization of the highly acidic hot spring. It formed from dissolved Fe^{2+} ions in the acidic hot spring becoming red colored ferrihydrite (Fe^{3+}) (Shikaura & Tazaki, 2001). Especially, in Nagahama Bay is located one of best and most active hot spring discharges and the best preserved reddish color ocean in Iwo-Jima. The half cleidoic environment of the Nagahama Bay has preserved a high rate sedimentation of iron oxide. In Nagahama Bay, red color iron-rich water is affected by tidal currents, but sedimentation of the ferric deposit (iron hydroxide) is confirmed in the sea bottom (Ninomiya & Kiyokawa, 2009). In this study, to understand the iron sedimentation in Nagahama Bay, we did 1) Sediment core samples (core sketch, CT scan, 3D analysis), 2) Sediment trap (using 1m cylindrical containers), 3) Time-series of turbidity measurement of cross section in the bay (using multiple sensor: HORIBA WX-22), 4) Long term temperature analysis (using fixed-point thermometer in sea floor), 5) Hourly observations of the seafloor by, diving, OGURI-View system (an automatic underwater digital camera system: Oguri et al. 2006), 6) Hourly observation of color changes in the surface water by automatic digital and the on-land camera system,

Results and Discussion

1. Core sample: Thickness of the sediment in the bay was 1.5m. We collected 1m long core samples by push core by diving. About 5cm from the top layer is an unformed iron rich deposit, below this layer is weakly consolidated iron-rich orange colored mud, organic-rich black mud and 6 volcanic ash layers up to 6.5 cm thick. The cross stratification and ferruginous fine-grained sediment layers were confirmed by CT scan and 3D analysis. Layers of fine-grained volcanic ash have the feature of fining-upward and gradual change to iron hydroxide beds. The bottom part has distinctive layers of pink ash which fell in 1997 (based on report in Mishima Village). Therefore, the average rate of deposition of these core samples is 8 cm/year, including ash layers.

2. Sediment trap: The unformed iron deposit accumulated 7.5 cm during 82days (2009/07/12 ～2009/10/03). Approximate deposition rate of red ferrihydrite is 2.8 cm/month (33.3 cm/year).

3. Turbidity measurement: Daily changes of the degree of turbidity of seawater were confirmed as due to tidal currents. Seawater entered the bottom of the bay at high tide. Spring tide was the most active current and preserved ripple bed forms on the surface of the soft iron sediments. The longest turbidity times were during neap tides. Sometimes, unusual mixing was induced by strong Typhoon and heavy rain (Ninomiya & Kiyokawa, 2009).

4. Long term temperature: The temperature of seawater in the Nagahama bay shows similar fluctuations to that of the air temperature during the measurement period. Lowest temperatures occurred in the middle of February. There are 6°C fluctuations (from 46 –

40°C) identified in the sea bottom temperature. These temperature fluctuations followed the tidal current. The higher temperature was identified at low tide and lower temperature is seen at low tide. Seawater temperature changed from 27ºC (September) to 17ºC (February) with the seasons, but the hot spring temperature remained constant regardless of the season.

Figure 1. Nagahama Bay.

Conclusion

The 1m long core samples from Nagahama Bay have records covering 12 years and show average deposition rate is 8 cm/year. There are 6 volcanic ash layer in the middle to lower part, and cross stratification is well preserved. Therefore, the ash layers were affected by wave and water current. The fine-grained iron deposit layer without ash was deposited during a quite period.

To compare the temperature shift of hot spring and tide, we confirmed that temperature is low at high tide, and high at low tide, and temperature shift change maximum is at the spring tide, and minimum at the neap tide. In other words, the amount of discharge of hot spring and the amount of seawater inflow varies inversely. If the hot spring contains high content of iron oxides, spring tide and lower tide time might be the best conditions to precipitate iron hydroxide in the ocean. During this time, however, the iron sedimentation was not as great because of high-speed inflow at these time (Ninomiya and Kiyokawa, 2009).

Moreover, the sediment trap shows iron hydroxide deposition rate is 2.8 cm/month (33.3 cm/year). On the other hand, estimates of deposition rate from core samples are 8 cm/year. These differences suggest that there is at least 4-8 times more hydroxide iron than we expected from the sedimentary record. More than 80% of hydroxide iron coming from the hot spring of Nagahama Bay might flow out to the open sea during tidal and storm effects.

The fine-grained iron hydroxide in the Nagahama Bay is provided and deposited at neap tide because neap tide is relatively quiet and there is enough supply of hot spring water. After that, most of iron hydroxide beds that form stratification in the core are mostly influenced by mixing by typhoons and heavy rain. The iron oxide of the upper part of a graded bed is formed by these mingling events. In addition, these modern iron hydroxide sediments suggest that the sedimentation of BIF in shallow oceans might be contracted by tidal (neep tide) and storm events.

Acknowledgements

We thank T. Ohyama and other Mishima village people. We acknowledge support from JSPS foundation (No.18654086).

References

Konhauser K.O., Amskold L., Lalonde S.V., Posth N.R., Kappler A. & Anbar A., 2007, Decoupling photochemical F(II) oxidation from shallow-water BIF deposition, Earth and Planetary Science Letters, 258, 87–100.

Oguri K., Kitazato H. & Glud R.N. 2006, Platinum octaetylporphyrin based planar optodes combined with an UV-LED excitation light source: An ideal tool for high-resolution O2 imaging in O2 depleted environment, Marine Chemistry, 100, 95–106.

Ono K., Soya T. & Hosono T., 1982, Geology of the Satsuma-Io-jima district, Quadrangle series, scale 1:50000, Geological Survey, Japan, 80p, (in Japanese with English abstract).

Ninomiya T. & Kiyokawa S., 2009, Time-series measurements of the colored volcanic vent seawaters during a tidal cycle in Nagahama Bay, Iwo-jima Island, Kagoshima, Japan., Memoirs of the Faculty of Sciences, Kyushu University, Series D, Earth and Planetary Sciences, 32, 2, 1–14.

Shikaura H. & Tazaki K., 2001, Cementations of sand grains are accelerated by microbes – Formation of bio-terrace at Satsuma Iwo-Jima Island., Clay Science Japan, 40, 229–241 (in Japanese with English abstract).

ON THE ORIGINS OF CARBONACEOUS MATERIAL ASSOCIATED WITH APATITE IN BANDED IRON FORMATIONS

D. Papineau

Geophysical Laboratory, Carnegie Institution of Washington

Introduction

Banded iron formations (BIFs) represent the main economic source of iron on Earth, yet their origin is still not well understood. Recent experimental work suggests that microorganisms likely played a key role in the formation of these common Precambrian rocks, which is significant because the oldest terrestrial sedimentary rocks are BIFs. If microorganisms were indeed involved in BIF formation, a hypothesis is that organic and/or other remains of their past presence in BIFs should be present. However, diagenetic and metamorphic processes affect the crystal structure and geochemical composition of carbonaceous material in BIFs. In particular, during sedimentation and early diagenesis of BIFs, anaerobic heterotrophic oxidation of organic carbon can result in the liberation of phosphate and of ^{13}C-depleted carbonate in pore water solutions. Diagenetic recycling of organic carbon in BIFs can act to concentrate phosphate in such micro-environments and eventually to the occurrence of carbonaceous material associated with phosphate minerals, as commonly seen in phosphorites. In fact, biogenic carbonaceous material in Paleoproterozoic stromatolitic phosphorites is intimately associated with apatite, which implies that micro-organisms in such microbial ecosystems directly participated in the accumulation and biomineralization of apatite. However, the application of this mineral association as a biosignature to other rock types, especially Eoarchean BIFs, has not been systematically studied and other processes also have to be considered.

In an effort to document the spatial distribution of carbonaceous material associated with apatite in BIFs and to address the possibility of an abiogenic origin for these mineral associations, several surveys of apatite grains were performed in BIF thin sections spanning a range of ages and metamorphic grades. Surveys of apatite occurrences have so far been performed on dozens of polished BIF thin sections and apatite grains have been found in almost all of them. Optical microscopy, Raman micro-spectroscopy, and scanning electron microscopy revealed that carbonaceous material is commonly associated with apatite grains in BIFs, but that these mineral associations are not always found. In one occurrence of graphite associated with apatite from an upper amphibolite facies BIF from the Eoarchean Nuvvuagittuq Supracrustal Belt, a thin graphite particle occurred in contact with a nanoscopic multi-phase sulfide (sphalerite and chalcopyrite) and was embedded in an amphibole that coated an apatite grain. From such a mineral association and petrological context, it is likely that hydrothermal metamorphic fluids were involved in producing these mineral associations and therefore graphite associations with apatite may also form from fluid-deposition in addition to the recrystallization of diagenetic mineral assemblages. These observations do not exclude a possible biogenic origin of the carbon in this fluid-deposited graphite, but raise a cautionary note on the interpretation of graphite + apatite mineral associations in BIFs as biosignatures.

Acknowledgements

The NASA Exobiology and Evolutionary Biology Program, the NASA Astrobiology Institute, the Geophysical Laboratory of the Carnegie Institution of Washington, and the Carnegie of Canada are thanked for continuous support. I also thank B. De Gregorio for his contributions in this work and interesting discussions into the origin of Precambrian organic matter

LINKING CONTINENTAL WEATHERING AND METHANOGEN FAMINE TO THE PALEOPROTEROZOIC GLACIATION

E. Pecoits, N.R. Aubet & K.O. Konhauser

Department of Earth and Atmospheric Sciences, University of Alberta, Edmonton T6G 2E3, Canada

Although the sun was substantially less bright, multiple lines of evidence favour a "liquid" ocean during the Archean (i.e., the "faint young Sun paradox"). Elevated atmospheric CO_2 levels were long considered to be the most parsimonious solution for the warm Archean climate (Walker et al., 1981). Most recently, methane has arguably been invoked as an important atmospheric constituent and green house gas throughout much of the Precambrian (e.g., Kasting, 2005). Whereas small amounts of methane could have formed abiotically (e.g., serpentinization), much larger concentrations should have been produced and maintained by methanogenic bacteria in an anoxic world. Once free oxygen became an important atmospheric gas, the atmospheric lifetime of methane likely became short, and its abundance would have decreased significantly. In this regard, geochemical modeling of the late Archean and early Paleoproterozoic atmosphere have focused on the oxidative conversion of atmospheric methane to carbon dioxide, a less efficient greenhouse gas, during the rise of atmospheric oxygen (Pavlov et al., 2000). Thus, it has been proposed that the rise of O_2 at ca. 2.4 Ga (the so-called "Great Oxidation Event") should have caused a drastic decrease in atmospheric CH_4 concentrations and may have triggered the Paleoproterozoic glaciation (Bekker et al., 2005). But, did a large-scale demise in methanogenesis due to increasing environmental oxygenation really occur? Oxidative weathering of terrestrial sulphides, increased oceanic sulphate, and the ecological success of sulphate-reducing microorganisms over methanogens has been proposed as a possible cause for the methane collapse (Zhanle et al., 2006), but this explanation is difficult to reconcile with the rock record. Recent studies (Konahuser et al., 2009; Pecoits et al., 2009) revealed a decline in the molar nickel to iron ratio recorded in banded iron formations about 2.7 Ga ago, which is mainly attributed to a reduced continental weathering of nickel to the oceans, a consequence of cooling upper-mantle temperatures and decreased eruption of nickel-rich (ultra-)mafic rocks at the time. Nickel is a key metal cofactor in several enzymes of methanogens and the authors proposed that its decline would have stifled their activity in the ancient oceans and disrupted the supply of biogenic methane. A decline in biogenic methane production therefore could have occurred before increasing environmental oxygenation and not necessarily be related to it. As documented in the sedimentary record (e.g. Bekker et al., 2005), this transition resulted in surface refrigeration at a time of low solar luminosity. Hence, a diminishing supply of volcanic nickel links the demise of methanogens to the redox state of the atmosphere where the glacial epoch might ultimately represent climatic adjustments which paved the way to an atmosphere with CO_2 acting as a major greenhouse gas.

References

Bekker A., Kaufman A.J., Karhu J.A. & Eriksson K.A., 2005, Evidence for Paleoproterozoic cap carbonates in North America, Precambrian Research, 137, 167–206.

Kasting J.F., 2005, Methane and climate during the Precambrian era, Precambrian Research, 137, 119–129.

Konhauser K.O., Pecoits E., Lalonde S.V., Papineau D., Nisbet E.G., Barley M.E., Arndt N.Y., Zahnle K. & Kamber B.S., 2009, Oceanic nickel depletion and a methanogen famine before the Great Oxidation Event, Nature, 458, 750–54.

Pavlov A.A., Kasting J.F., Brown L.L., Rages K.A. & Freedman R., 2000, Greenhouse warming by CH4 in the atmosphere of early Earth, Journal of Geophysical Research, 105(E5), 11981–11990.

Pecoits E.; Gingras M.K.; Barley M.E.; Kappler A.; Posth N.R. & Konhauser K.O., 2009, Petrography and geochemistry of the Dales Gorge banded iron formation: Paragenetic sequence, source and implications for palaeo-ocean chemistry, Precambrian Research, 172, 163–187.

Walker J.C.G., Hays P.B. & Kasting J.F., 1981, A negative feedback mechanism for the long-term stabilization of Earth's surface temperature. Journal of Geophysical Research, 86, 9776–9782.

Zahnle K.J., Claire M.W. & Catling D.C., 2006, The loss of mass-independent fractionation of sulfur due to a Paleoproterozoic collapse of atmospheric methane, Geobiology, 4, 271–283.

DISSIMILATORY MICROBIAL IRON REDUCTION IN SIMULATED ARCHEAN CONDITIONS

E.M. Percak-Dennett[1], E.E. Roden[1] & C.M. Johnson[1]

[1]Department of Geoscience, The University of Wisconsin Madison, Madison, WI 53715, USA

Introduction

Banded Iron Formations (BIFs) are composed of alternating layers of Fe-bearing minerals and chert. Fe-rich BIF strata contain minerals such as hematite, magnetite, siderite, and various Fe-silicate phases (Klein, 2005). In some cases, these minerals have unique stable Fe isotope compositions that are thought to reflect pathways of BIF formation (Johnson et al., 2008b). Dissimilatory microbial iron oxide reduction (DIR) coupled to oxidation of organic matter codeposited with Fe(III) oxides has been identified as a mechanism for the production of Fe(II)-bearing minerals such as magnetite and siderite (Konhauser et al., 2005; Nealson and Myers, 1990; Walker, 1984), and recent studies have provided insight into how DIR may have influenced the Fe isotope composition of BIF minerals (Crosby et al., 2007; Johnson et al., 2008a). However, the exact role that DIR may have played in BIF mineral genesis is not fully understood.

Experimental Work

This experimental research seeks to better define the potential for DIR to generate Fe-bearing BIF minerals and/or their less- or non-crystalline precursors in reaction systems that mimic conditions that are thought to have been present in Archean oceans. In order to test the idea put forward by Walker (Walker, 1984) that more Fe(II)-rich minerals (siderite and Fe-silicates) will be generated with increasing organic carbon input to DIR systems, experiments were conducted using varying inputs or organic carbon into a system (electron donor) with a constant amount of electron acceptor. Since the ultimate goal was to mimic conditions seen (or thought to be seen) in the Archean, all bacterial growth was conducted in Artifical Archean Sewater (AAS). A modern artificial seawater recipe (Kester et al., 1967) was modified to produce an AAS by removing most of the sulfate (ca. 200 μM remain) and contains ca. 2 mM dissolved silica. This media also contains low phosphate levels (between .25 and 1 μM)

A novel Fe(III) oxide-silica coprecipitate was produced to serve as an electron acceptor for DIR in AAS medium. The coprecipitate, which is formed through oxidation of ferrous chloride in a sodium bicarbonate-buffered solution oversaturated with silicic acid species, is analogous to what is expected to have been present Archean ocean surface sediments. The coprecipitate was examined by x-ray diffraction (XRD) and transmission electron microscopy (TEM) and found to be amorphous and to have a very small particle size (less than 5 nm). This electron acceptor has been found to be very readily reducible by both enrichment cultures and a pure culture of the marine DIRM *Desulfuromonas acetoxidans*, with this coprecipitate being reduced both faster and to a greater total extent compared to silica-free amorphous Fe(III) oxide.

A marine enrichment culture was developed and sustained in AAS with the novel co-precipitation serving as the electron acceptor, and acetate as the electron donor and carbon source. The source for this enrichment a marine mud flat sample, and initial inoculation occurred over one year ago. This culture has been transferred and maintained for over one year, to ensure a robust and active consortium of acetate-oxidizing iron-reducing bacteria. This enrichment culture has been analysed using 454 pyrosequencing, and over 97% of the reads were Desulfuromonaceae.

Experiments were completed using between 70 and 100 mM iron-silica co-precipitate and either 1, 5, 10 or 20 mM of acetate in AAS media with a sodium bicarbonate buffer. Experiments were conducted at pH 7, and at pH 6.5, with the lower pH due to an (intended) increase in the partial pressure of CO_2 in the headspace of the culture bottles. Bacterial inoculation was made using the previously mentioned marine enrichment culture growing under acetate-limiting conditions to minimize the amount of acetate carried over during inoculation. On days 0, 1, 2, 3, 5, 7, 10, 15, 20 both solid-phase (0.5M HCl extraction) and aqueous Fe(II) were measured using Ferrozine. Parallel aliquots were taken under sterile anaerobic conditions for use in isotopic analysis. Fe(II) levels remained stable from 10 to 20 days, and cultures were moved to an oven in order to undergo simulated diagenesis at day 20. This "diagenesis" took place between 90 and 120°C. Each week Fe(II) and aqueous Fe(II) were measured as described previously, and aliquots were removed, dried under anaerobic conditions, and analysed by XRD to detect the emergence of any mineralogical signature.

After 20 days, the percentage of iron reduced ranges from 15% for cultures with 1mM of acetate to 50-75% for cultures with 5-20 mM of acetate, and aqueous Fe(II) increased over the 20 day inoculation as well. No definitive minerals were seen even after 6 weeks of incubation at elevated temperatures. However, there was a small-scale increase in the profile corresponding to where peaks would be for 2-line ferrihydrite. Once all experiments are complete, the Fe isotope composition of aqueous and solid-phase components will be determined through multicollector inductively coupled plasma mass spectrometry.

References

Crosby H.A., Johnson C.M., Beard B.L. & Roden E.E., 2007, The mechanisms of iron isotope fractionation produced during dissimilatory Fe(III) reduction by *Shewanella putrefaciens* and *Geobacter sulfurreducens*, Geobiology, 5, 169–189.

Johnson C.M., Beard B.L., Klein C., Beukes N.J. & Roden E.E., 2008a, Iron isotopes constrain biologic and abiologic processes in banded iron formation genesis, GCA, 72, 151–169.

Johnson, C.M., Beard, B.L., & Roden, E.E., 2008b, The iron isotope fingerprints of redox and biogeochemical cycling in the modern and ancient Earth: Annual Reviews in Earth and Planetary Sciences, 36, 457–493.

Kester D. Duedall I. Connors D. & Pytkowic. RM, 1967, Preparation of Artificial Seawater, Limnology and Oceanography, 12, 176.

Klein, C., 2005, Some Precambrian banded iron-formations (BIFs) from around the world: Their age, geologic setting, mineralogy, metamorphism, geochemistry, and origin, American Mineralogist, 90, 1473–1499.

Konhauser K.O., Newman D.K. & Kappler A., 2005, The potential significance of microbial Fe(III) reduction during deposition of Precambrian banded iron formations, Geobiology, 3, 167–177.

Nealson K.H., and Myers C.R., 1990, Iron reduction by bacteria: A potential role in the genesis of banded iron formations, American Journal of Science, 290, 35–45.

Walker J.C.G., 1984, Suboxic diagenesis in banded iron formations, Nature, 309, 340–342.

EVOLUTION OF THE PALEOARCHEAN MARINE SULFATE RESERVOIR

D.L. Roerdink[1], P.R.D. Mason[1], J. Farquhar[2] & T. Reimer[3]

[1]Department of Earth Sciences, Utrecht University, 3584 CD Utrecht, The Netherlands
[2]Department of Geology and ESSIC, University of Maryland, College Park, Maryland, 20742, USA
[3]Bernhard-May-Str. 43, Wiesbaden, 65203, Germany

Introduction

The Archean sulfur cycle was considerably different from that operating today. Significant mass-independent sulfur isotope fractionation in Archean sedimentary rocks indicates atmospheric oxygen concentrations of less than 10^{-5} times present day levels (Farquhar et al., 2000; Pavlov & Kasting, 2002). Under these anoxic conditions, sulfide minerals such as detrital pyrite were stable (Rasmussen and Buick, 1999) because sulfide weathering did not occur. Volcanic degassing of SO_2 was thus the only significant source of sulfate to the ocean (Canfield, 2004). Low marine sulfate concentrations are also supported by the small magnitude of sulfur isotope effects in Archean pyrites relative to seawater sulfate (<200 µM; Habicht et al., 2002). Despite this, Archean barite deposits from South-Africa, Australia and India suggest localized elevated concentrations of sulfate between 3.5 and 3.2 Ga (Huston and Logan, 2004). It remains unclear how this reservoir of oxidized sulfur species was generated, most likely through atmospheric photolysis reactions. Here, we present multiple sulfur isotope data ($\delta^{34}S$, $\Delta^{33}S = \delta^{33}S - 1000 \times (1 + \delta^{34}S/1000)^{0.515}$, and $\Delta^{36}S = \delta^{36}S - 1000 \times (1 + \delta^{34}S/1000)^{1.90}$) of 3.55-3.23 billion year old barites from different localities in the Barberton greenstone belt, South-Africa, to discuss the origin and evolution of the sulfate reservoir in the Paleoarchean.

Paleoarchean barites from the Barberton greenstone belt

Samples were collected from four barite deposits across the Barberton greenstone belt, covering the entire time span from which barite occurrences are known in the Palaeoarchean. Locations are shown on figure 1. The oldest barite deposit (Londozi) occurs in the southeastern part of the greenstone belt, and belongs to the Theespruit Formation of the lower Onverwacht group (Reimer, 1980). Felsic volcanics adjacent to the Londozi barite were dated at 3.55 Ga (Kröner et al., 1996), suggesting this is the oldest barite currently identified in the geological record. Samples from this deposit consist of 1-5 cm thick layers of fine crystalline barite interbedded with chert. The area around the Londozi barite has experienced up to amphibolite facies metamorphism (Kröner et al., 1996), which is considerably higher than the sub-greenschist to greenschist facies reached elsewhere in the greenstone belt (Stevens & Moyen, 2007).

Slightly younger barites (upper Onverwacht group) occur in the westernmost part of the greenstone belt near Farm Vergelegen (Vergelegen barite). The exact age of the deposit is unknown, but the thin barite bed is closely associated with an extension of the Buck Ridge

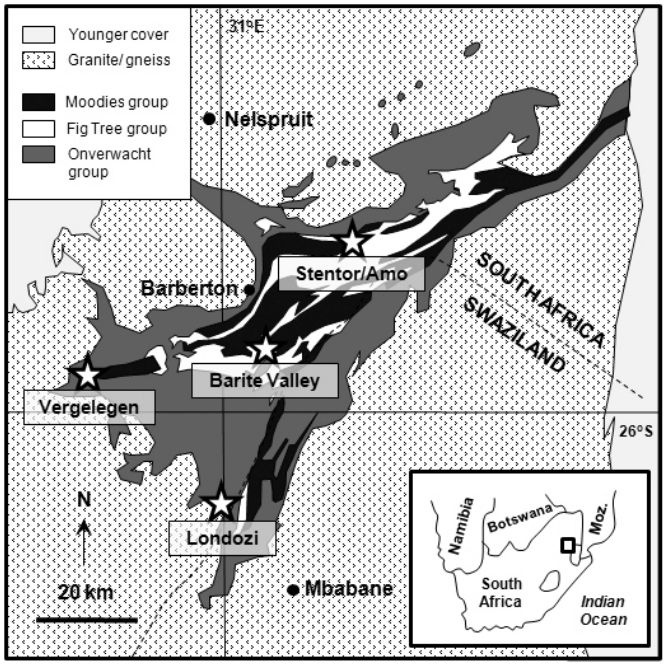

Figure 1. Geologic map of the Barberton greenstone belt showing locations of Paleoarchean barite deposits sampled in this study.

chert (Reimer, 1980), and the age is estimated to be between 3.4 and 3.5 Ga. Vergelegen barites consist of coarse crystalline barite, and become strongly deformed towards the western part of the outcrop.

In the northeast of the greenstone belt, two closely associated deposits occur near the Stentor pluton (Stentor and Amo deposit). Both deposits belong to the Bien Venue Formation of the Fig Tree group (3.26 Ga) and consist of sugary, fine grained barite.

The largest barite deposit occurs in the central part of the Barberton greenstone belt in the Barite Valley. It belongs to the Mapepe Formation of the Fig Tree group (3.23 Ga) and consists primarily of reworked green barite sands and bedded barite associated with chert (Heinrichs & Reimer, 1977).

Analytical procedures

Barite powders were obtained by microdrilling and reduced to sulfide using a Thode reduction solution (Forrest and Newman, 1977). The produced hydrogen sulfide was trapped in a silver nitrate solution to precipitate silver sulfide. At the University of Maryland stable isotope laboratory, the silver sulfide was reacted with approximately 10 times excess F_2 at 250°C in Ni-reaction vessels for 8 hours. The product SF_6 was purified by cryogenic and gas chromatographic methods, and the

final purified gas was analyzed by a ThermoFinnigan MAT 253 with a precision (2σ) of 0.1‰ on $\delta^{34}S$, 0.02‰ on $\Delta^{33}S$ and 0.2‰ on $\Delta^{36}S$.

Results

The total $\delta^{34}S$ variation in Paleoarchean barite was apparently very limited. Average values of $\delta^{34}S$ are 5.62 ± 1.20‰ for the 3.55 Ga Londozi deposit, 4.16 ± 0.68‰ for the 3.4-3.5 Ga Vergelegen deposit, 4.40 ± 1.00‰ for the 3.26 Ga Amo and Stentor deposits and 4.75 ± 1.70‰ for the Barite Valley deposit (errors given as 1 standard deviation). Individual layers of barite in samples from the Londozi deposit show a variation of up to 3‰ per sample, whilst $\Delta^{33}S$ and $\Delta^{36}S$ are homogeneous.

Distinctive temporal variations were observed for $\Delta^{33}S$ and $\Delta^{36}S$. The 3.55 Ga Londozi deposit is characterized by a $\Delta^{33}S$ value of -1.03 ± 0.07‰ and $\Delta^{36}S$ value of 1.03 ± 0.01‰, whereas $\Delta^{33}S$ = -0.75 ± 0.21‰ and $\Delta^{36}S$ = 0.76 ± 0.16 ‰ in the barite from the 3.4-3.5 Ga Vergelegen deposit. The youngest deposits display even smaller magnitudes of mass-independent sulfur isotope signatures, with a $\Delta^{33}S$ value of -0.52 ± 0.06‰ and $\Delta^{36}S$ = 0.41 ± 0.13‰ at Amo and Stentor (3.26 Ga), and $\Delta^{33}S$ = -0.524 ± 0.14‰ and $\Delta^{36}S$ = 0.51 ± 0.19‰ for the Barite Valley samples (3.23 Ga). The entire dataset defines a trend of $\Delta^{36}S = -1.03\Delta^{33}S - 0.03$, which is very similar to the Archean array ($\Delta^{36}S/\Delta^{33}S$ = -0.9) defined by Farquhar et al. (2000) as well as the results obtained in SO_2 photolysis experiments at 193 nm UV-radiation ($\Delta^{36}S/\Delta^{33}S$ = -1.1; Farquhar et al., 2001).

Origin of the barite-sulfate

Based on the consistency between the slope in $\Delta^{36}S$ versus $\Delta^{33}S$ space defined by our samples and the expected slope for SO_2 photolysis, we confirm the conclusion by Bao et al. (2007) that early Archean barites contain sulfate of photolysis origin, as no other process is known to result in similar effects for both $\Delta^{33}S$ and $\Delta^{36}S$. However, our data does not support the suggestion by Bao et al. (2007) that atmospheric sulfate is mixed with hydrothermal sulfate with zero $\Delta^{33}S$ and $\Delta^{36}S$. Explaining our data by such a mixing trend would require an endmember with $\delta^{34}S$ up to 32‰. Although these values are similar to the sulfur isotopic composition of Phanerozoic seawater, no such heavy reservoir is known for the Archean. The absence of any mixing trend towards the mantle sulfur reservoir suggests that direct magmatic or hydrothermal input is absent and all of the sulfate is derived from volcanic degassing of SO_2 that underwent photolysis in the atmosphere.

Evolution of the Paleoarchean marine sulfate reservoir

Our data shows that the magnitude of mass-independent sulfur isotope fractionation observed in marine sulfate decreased significantly throughout the Paleoarchean, whereas the magnitude of mass-dependent fractionation remained the same. An increasing amount of volcanic sulfur contributing to the marine sulfate reservoir from 3.5 to 3.2 Ga is unlikely to explain this trend, as mixing would also affect δ34S values. A change in atmospheric chemistry, such as locally increased oxygen levels or an organic haze (cf. Domagal-Goldman et al., 2008), are possible explanations for the changing isotope composition. The limited variability in δ34S within individual deposits is probably related to reservoir effects following the extraction of light δ34S into sulfide during abiotic or microbial sulfate reduction. Such processes would also explain the small-scale variations in δ34S observed on the sample scale.

References

Bao H., Rumble Iii D., & Lowe D.R., 2007, The five stable isotope compositions of Fig Tree barites: Implications on sulfur cycle in ca. 3.2 Ga oceans, Geochimica et Cosmochimica Acta, 71, 4868–4879.

Canfield D.E., 2004, The evolution of the Earth surface sulfur reservoir, American Journal of Science, 304, 839–861.

Domagal-Goldman S.D., Kasting J.F., Johnston D.T. & Farquhar J., 2008, Organic haze, glaciations and multiple sulfur isotopes in the Mid-Archean Era, Earth and Planetary Science Letters, 269, 29–40.

Farquhar J., Bao H., & Thiemens M., 2000, Atmospheric Influence of Earth's Earliest Sulfur Cycle, Science, 289, 756–758.

Farquhar, J., Savarino, J., Airieau, S., & Thiemens, M.H., 2001, Observation of wavelength-sensitive mass-independent sulfur isotope effects during SO2 photolysis: Implications for the early atmosphere, Journal of. Geophysical Research, 106, 32829–32839.

Forrest, J. & Newman, L., 1977, Silver-110 Microgram Sulfate Analysis for the Short Time Resolution of Ambient Levels of Sulfur Aerosol, Analytical Chemistry, 49, 1579–1584.

Habicht K. S., Gade M., Thamdrup B., Berg P., & Canfield D.E., 2002, Calibration of sulfate levels in the Archean ocean, Science, 298, 2372-2374.

Heinrichs T. K. & Reimer T., 1977, A sedimentary barite deposit from the Archean Fig Tree Group of the Barberton Mountain Land (South Africa), Economic Geology, 72, 1426–1441.

Huston D.L. & Logan G.A., 2004, Barite, BIFs and bugs: evidence for the evolution of the Earth's early hydrosphere, Earth and Planetary Science Letters, 220, 41–55.

Kröner A., Hegner E., Wendt J.I., & Byerly G.R., 1996, The oldest part of the Barberton granitoid-greenstone terrain, South Africa: evidence for crust formation between 3.5 and 3.7 Ga, Precambrian Research, 78, 105–124.

Pavlov A.A. & Kasting J.F., 2002, Mass-independent fractionation of sulfur isotopes in Archean sediments: Strong evidence for an anoxic Archean atmosphere, Astrobiology, 2, 27–41.

Rasmussen B. & Buick R., 1999, Redox state of the Archean atmosphere: Evidence from detrital heavy minerals in ca. 3250-2750 Ma sandstones from the Pilbara Craton, Australia, Geology, 27, 115–118

Reimer T.O., 1980, Archean sedimentary baryte deposits of the Swaziland Supergroup (Barberton Mountain Land, South Africa), Precambrian Research, 12, 393–410.

RECONSTRUCTION OF 3.2 Ga OCEAN FLOOR ENVIRONMENT FROM CORES OF DXCL DRILLING PROJECT, PILBARA, WESTERN AUSTRALIA: RESULTS OF STRATIGRAPHIC ANALYSIS AND SULFUR ISOTOPE ANALYSIS

R. Sakamoto[1], S. Kiyokawa[1], T. Ito[2], M. Ikehara[3], H. Naraoka[1], K.E. Yamaguchi[4,5,6] & Y. Suganuma[7]

1. Department of Earth and Planetary Science, Kyushu University, 6-10-1, Hakozaki, Higashiku, 812-8581, JAPAN.
2. Faculty of Education, Ibaraki University, 2-1-1, Bunkyo, Mito, Ibaraki, 310-8512, JAPAN.
3. Center for Advanced Marine Core Research, Kochi University, 200, Monobe-otsu, Nankoku, Kochi, 783-8502, JAPAN.
4. Department of Chemistry, Toho University, 2-2-1, Miyama, Funabashi, Chiba, 274-8510, JAPAN.
5. Precambrian Ecosystem Laboratory, Japan Agency for Marine-Earth Science and Technology, 2-15 Yokosuka, Kanagawa, 237-0061, JAPAN.
6. NASA Astrobiology Institute, U.S.A.
7. National Institute of Polar Research, 10-3, Midorimachi, Tachikawa, Tokyo, 190-8518, JAPAN.

Introduction

The 3.2 Ga Dixon Island - Cleaverville formations in the coastal Pilbara terrane, Western Australia, is one of the most complete and best preserved examples of middle Archean sedimentary sequences in an oceanic arc setting (Kiyokawa et al., 2006). To understand the relative deep marine environments in these formations at 3.2 Ga Mesoarchean (Kiyokawa et al., 2006), we did detailed mapping and identified well-stratified oceanic sections of that age (Kiyokawa & Taira, 1998, Kiyokawa et al., 2002). In the summer of 2007, we conducted scientific drilling (DXCL drilling project) at Cleaverville Beach in the West Pilbara to understand stratigraphic continuity that was unclear in lithologies from land outcrops, and collect continuous fresh samples for geochemical analysis (Yamaguchi et al., 2009). In DXCL, we obtained three fresh drill cores (DX, CL2 and CL1 in ascending order) which are 200 m long in total and 130 m in stratigraphic thickness. Here we report the results of detailed lithology, stratigraphy and stable sulfur isotope analysis of these core samples.

Lithology of DXCL drilling core

We measured the thickness of beds and counted the number of over 5 mm beds and laminations in non-deformed parts (DX: 45 m, CL2: 23 m, CL1: 30 m). In the DX core, black shale, laminated pyrite and gray chert are identified as 1705, 1395 and 298 layers in order. In CL1 and CL2 cores, black shale, laminated pyrite and volcaniclastic sandstone are identified as 495 (CL2: 219, CL1: 276 layers), 181 (CL2: 44, CL1: 137 layers) and 37 (CL2: 10, CL1: 27 layers, with nothing in DX layers. Only a volcanic sedimentary sequence was identified in CL core. We formed rock type ratio diagram for each 1 m of the cores (Fig. 1) to identify lithological changes through the cores.

The DX core, totalling 100m long and covering the upper part of the Dixon Island Formation, is constructed by black shale, gray chert and pyrite. Gray chert contains very fine lamination of chert and black organic layers, 10 to 300 μm in thickness. Pyrite is well preserved in black shales. Pyrite is divided into three types as follows; massive, graded and isolated types. The massive type formed thin-bedded pyrite layer constructed by strongly concentrated fine pyrite grains. Graded type is formed an upward condensed very fine and euhedral grains from massive black shale. Isolated type is uniform grains within laminated and massive black shale.

DX core is divided into four units. Unit 1 forms alternating

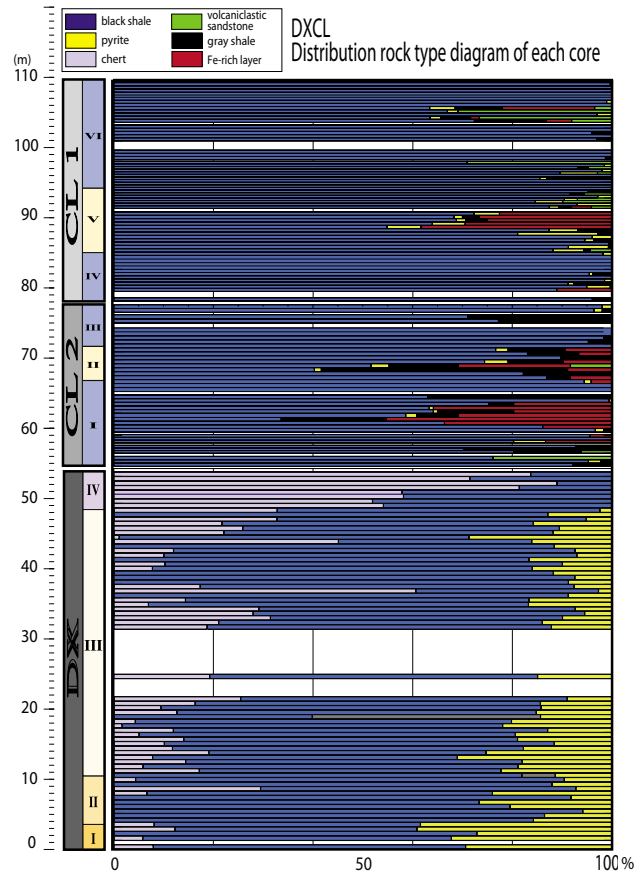

Figure 1. Diagram of containing ratio of each rock in DX, CL1 and CL2. Each bar graph shows distribution of rock type in 1m core.

laminated black shale and many thicker pyrite beds. Unit 2 consists of a few cm thick massive black shale and thin pyrite layers. Unit 3 is alternating thin-laminated black shale and pyrite layers. Unit 4 is well-laminated black shale and bedded chert. This unit does not contain pyrite beds.

CL1 and CL2 cores, which are 100m long, are mainly constructed by massive black shale, banded pyrite and thin volcanic sandstone. Massive black shale is thicker than that of the DX cores and composed of siltstone with organic matter. Partly preserved thin pyroclasitic layers were constructed by fine grained volcaniclastics with cross-lamination. Partially preserved graded type and isolated type pyrite layers occur in this core.

Characteristics of lithological change in the DX to CL cores are as follows; 1) black shale layers are thickening upward from DX to CL1 (2.1 cm to 14.4 cm in average), 2) pyrite layers in DX core are thinning upward from bottom to the top (10 cm to 3 cm in average) and CL core contains only few thinner layers (0.6 cm to 0.3 cm on average) and 3) thin volcaniclastic layers appear and increase in upper part of CL core.

Sulfur Isotope analysis

We analysed $\delta^{34}S$ sulfur isotope of 63 bulk black shales in each core. Data of these black shales is -1.9 to +12.9 ‰ in DX core, +1.7 to +24.9 ‰ in CL1 core and +4.4 to +26.8 ‰ in CL2 core. The range of values is widely extended over more than 27‰. Wide and heavy $\delta^{34}S$ values indicate the very active microbial sulfate reduction at the ocean floor, which has to limit the sulfate supply closed condition.

Sedimentary environment

From detailed observation of lithology, the 3.2 Ga Dixon Island-Cleaverville formations evolved from calm and deeper anoxic condition to relatively shallower conditions with weak volcanism. There was a stagnant anaerobic layer at the sea floor during that time. It is assumed that sulfate reduction and pyrite crystallization proceeded in the stagnant organic deep ocean at 3.2 Ga.

Acknowledgements

We thank Arthur Hickman and Mike Doepel for organising the DXCL drilling project. We acknowledge support from JSPS foundation (No.18253006, No.1434053).

References

Kiyokawa S., Taira, A., 1998, The Cleaverville Group in the West Pilbara Coastal Granioid-Greenstone Terrain of Western Australia: an example of a Middle Archean immature oceanic island-arc succession, Precambrian Research, 88, 109–142.

Kiyokawa S., Taira A., Byrne T., Bowring S. & Sano Y., 2002. Structural evolution of the middle Archean coastal Pilbara terrane, Western Australia. Tectonics, 21, 1044–1068.

Kiyokawa S., Ito T., Ikehara M. & Kitajima F., 2006, Middle Archean volcano-hydrothermal sequence: Bacterial microfossil-baring 3.2 Ga Dixon Island Formation, coastal Pilbara terrane, Australia, Geological Society of America Bulletin, 118, 3–22.

Yamaguchi K.E., Kiyokawa S., Ito T., Ikehara M., Kitajima F. & Suganuma Y., 2009, Clues of Early Life: Dixon Island-Cleaverville Drilling Project (DXCL-DP) in the Pilbara craton of Western Australia, Scientific Drilling, 7, 34–37

ALKALINE HYDROTHERMAL FLUIDS IN THE EARLY ARCHEAN OCEAN

T. Shibuya[1], T. Komiya[2], K. Nakamura[1], K. Takai[1] & S. Maruyama[3]

[1]Precambrian Ecosystem Laboratory, Japan Agency for Marine-Earth Science and Technology, 2-15 Natsushima-cho, Yokosuka 237-0061, Japan
[2]Department of Earth Science and Astronomy, University of Tokyo, 3-8-1 Komaba, Meguro-ku, Tokyo 153-8902, Japan
[3]Department of Earth and Planetary Sciences, Tokyo Institute of Technology, 2-12-1 Ookamaya, Meguro-ku, Tokyo 152-8551, Japan

Introduction

A detailed study focusing on the carbonatization of Archean greenstones has the potential to reconstruct the physico-chemical condition of Archean hydrothermal systems because hydrothermal calcite generally registers temperature, pH, and isotopic composition of coexisting fluid in its carbon and oxygen isotopes (Zhen & Hoefs, 1993). Thus, the isotopic composition of calcite and its depth variation in the Archean oceanic crust can provide new insights into the physico-chemical condition of the Archean subseafloor hydrothermal system. In this study, we report the degree of carbonatization, the stable carbon and oxygen isotopes of calcite, and their stratigraphic variations recorded in the greenstones of the middle Archean Cleaverville area, Pilbara Craton, Western Australia, where seafloor hydrothermal alteration of an oceanic crust is preserved (Shibuya et al., 2007). These data provide the thermal structure of the hydrothermal system and the pH condition of the hydrothermal fluid.

Results and Discussion

The Cleaverville greenstone underwent various amounts of hydrothermal carbonatization but the degree of carbonatization decreases with depth below the overlying chert/BIF horizon. Calcite in the greenstone mainly replaces igneous minerals and vein- and/or vesicle-filling calcite is minor. These geological and mineralogical occurrences of calcite indicate that the hydrothermal carbonatization took place at an Archean mid-ocean ridge. The $\delta^{13}C$ of calcite changes from positive, through negative, to near zero with depth, while $\delta^{18}O$ gradually decreases stratigraphically downward. Based on the modeling under various conditions, it is suggested that the depth variations of the measured $\delta^{13}C$ and $\delta^{18}O$ were produced by the increase in temperature with depth. Especially, the positive shift of $\delta^{13}C$ from the middle to lower part of the greenstone sequence strongly suggests that the downwelling hydrothermal fluid became alkaline with increasing temperature. Thermodynamic modelling of hydrothermal reactions between basaltic rocks and CO_2-rich seawater also predicts formation of alkaline high-temperature hydrothermal fluids in the Archean oceanic crust. The chemically reactive mixing zones between alkaline hydrothermal fluids and more acidic seawater are characterized by the inverse pH and chemical polarity of modern systems, leading to extensive deposition of silica and iron (hydr)oxides on the seafloor. The results shows there is sufficient silica influx to Archean oceans required from mass balance models, and provides a new solution of pH-controlled generation of Archean BIF that has been interpreted mainly by the redox chemistry in the Archean ocean.

Acknowledgements

This research was partially supported by the 21st Century COE Program “How to build habitable planets,” Tokyo Institute of Technology, sponsored by the Ministry of Education, Culture, Sports, Technology and Science, Japan.

References

Zheng Y.F. & Hoefs J., 1993, Carbon and oxygen isotopic covariations in hydrothermal calcites: Theoretical modeling on mixing processes and application to Pb–Zn deposits in the Harz Mountains, Germany, Mineralium Deposita, 28, 79–89.

Shibuya T., Kitajima K., Komiya T., Terabayashi M., & Maruyama S., 2007, Middle Archaean ocean ridge hydrothermal metamorphism and alteration recorded in the Cleaverville area, Pilbara Craton, Western Australia, Journal of Metamorphic Geology, 25, 751–767.

EARLY EVOLUTION OF NON-MARINE ECOSYSTEM: IMPLICATIONS FROM THE PILBARA CRATON

H. Sugahara[1], K. Sugitani[1], K. Mimura[1], F. Yamashita[2] & K. Yamamoto[1]

[1]Graduate School of Environmental Studies, Nagoya University, Nagoya 464-8601, Japan
[2]Graduate School of Science, Nagoya University, Nagoya 464-8601, Japan

Introduction

Morphologically diverse fossil-like microstructures were recently reported from black cherts from the ca. 3.0 Ga Farrel Quartzite in the Goldsworthy greenstone belt, the Pilbara Craton of Western Australia (Sugitani et al. 2007). They are of special interest in the context of the early evolution of life, because the structures are composed of diverse morphological types and many of specimens are characterized by large (> 20μm) size and complex morphologies. Their biogenicity was inferred from the indigenousness and syngenicity, the sedimentary origin of the host chert, and narrow size range, chemical composition, evidence of flexible and/or breakable walls, apparent taphonomic features and the presence of colony-like aggregations (Sugitani et al., 2007). This is supported by the facts that the structures are organic-walled (Grey & Sugitani, 2009), and that the structures are enriched in nitrogen and sulphur as well as carbon (Oehler et al., 2009). While their biogenicity seems to be nearly confirmed, the origin of the host black cherts has been poorly understood. Their deposition in a shallow to sub-aerial depositional environment was suggested (Sugitani et al., 2003), but detailed studies have not yet been performed. In this study, we report the results of systematic rare-earth and yttrium (REE+Y) analyses of black cherts of various lithologies including microfossil-bearing chert of the Farrel Quartzite collected from the Goldsworthy greenstone belt and place constraints on their origins and depositional environment.

Samples and methods

Fifty-one samples were collected from the Goldsworthy greenstone belt (Mount Grant and Mount Goldsworthy). The samples include four lithological types; laminated to banded chert (LC), vein chert (VC), and stratiform chert associated with evaporites (CE1 and CE2) (Fig.1). Among these four groups, only CE2 samples contain microfossils. LC samples (n=29) are from the Cleaverville Formation at Mount Grant (n=9) and at Mount Goldsworthy (n=20). VC samples (n=5) are from altered mafic volcanic rocks of the Warrawoona Group at Mount Grant. CE1 samples (n=4) are from the Farrel Quartzite at Mount Grant. CE2 samples are also from the Farrel Quartzite at Mount Grant (n=10) and at Mount Goldsworthy (n=3). The analysis of rare-earth and yttrium compositions of each sample followed the method of Yamamoto et al. (2004). Major element concentrations were also determined by X-ray fluorescence spectrometer (XRF) in order to evaluate clastic contamination.

Results

All the chert samples are characterized by low concentrations of TiO_2 and Al_2O_3 (TiO_2=0.002-0.062%, Al_2O_3=0.02-1.13%), representative of clastic components. Furthermore, there can be seen no relationships of total REE concentrations and REE patterns with the concentrations of these clastic components. Thus, REE-patterns discussed below are thought to reflect geochemical characteristics of water masses from which the cherts were precipitated. Characteristics of PAAS (Post Archean average shale)-normalized REE+Y patterns and Y/Ho ratios of the four lithological groups are as follows. VC samples show slightly light REE (LREE) -enriched patterns with slight to moderate positive La and Eu anomalies (1.26-1.70 for La calculated by $[La/\{Pr(Pr/Nd)^2\}]_{PAAS}$ and 1.52-1.63 for Eu calculated by $[Eu/(2/3Sm+1/3Tb)]_{PAAS}$). Y/Ho ratios are chondritic to slightly super-chondritic (Y/Ho=25.3-31.9). CE1 samples are characterized by relative enrichment of LREE and MREE, slight to moderate positive La and Eu anomalies (1.16-1.95 for La and 1.41-1.78 for Eu), and chondritic to slightly super-chondritic Y/Ho ratios (Y/Ho=29.0-34.3). CE2 samples have different features from VC and CE1; slightly HREE-enriched patterns with positive La and Eu anomalies (1.15-4.00 for La and 1.29-3.76 for Eu) and slightly super-chondritic Y/Ho ratios (Y/Ho=25.8-39.2). LC samples from both at Mount Grant and Mount Goldsworthy have HREE-enriched patterns with positive La and Eu anomalies (1.28-3.16 for La and 1.34-2.56 for Eu). Y/Ho ratios are super-chondritic (Y/Ho=32.0-68.4).

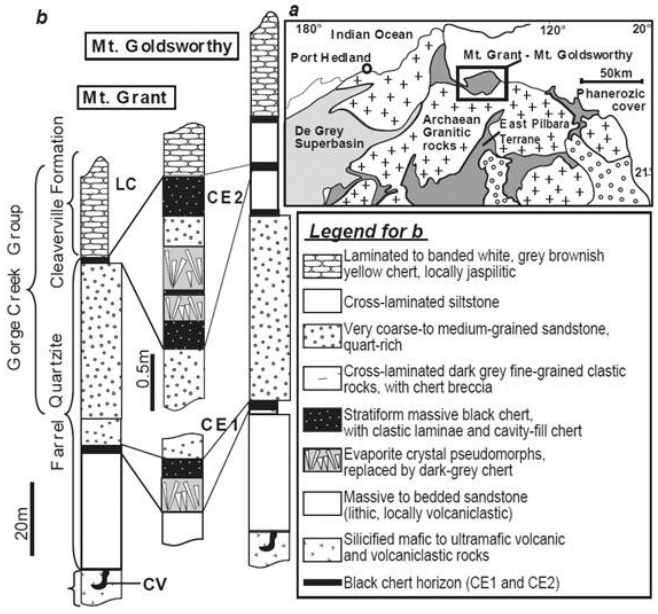

Figure 1. (a) Geology of the northeastern Pilbara Craton and the location of the Goldsworthy greenstone belt (Mt. Grant and Mt. Goldsworthy) (after Smithies et al., 2004, Sugitani et al., 2007). (b)Simplified stratigraphic column at Mt. Grant (left column) and Mt.Goldsworthy (right column) indicating chert samples (LC, CE1, CE2 and VC) in the stratigraphy.

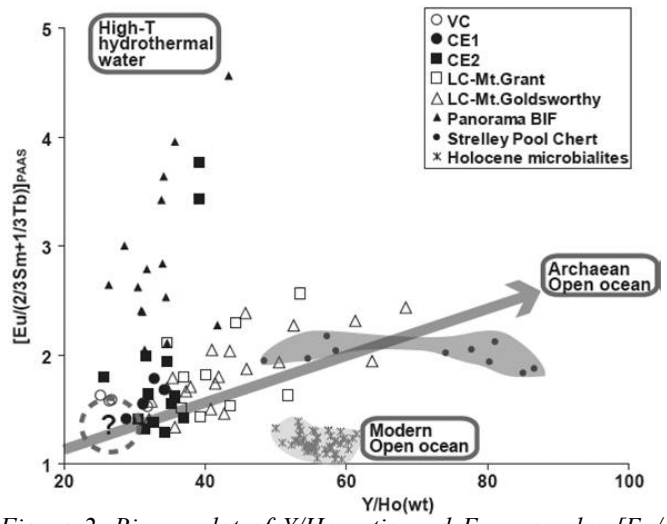

Figure 2. Binary plot of Y/Ho ratio and Eu anomaly; $[Eu/(2/3Sm+1/3Tb)]_{PAAS}$. There can be seen a positive correlation array.

Discussion

The shale-normalized REE features of LC samples from the deepening upward Cleaverville Formation are characterized by HREE-enriched patterns and positive La anomaly, similar to modern seawater and seawater-derived chemical or biological precipitates. The LC samples have weak positive Eu anomalies and chondritic to super-chondritic Y/Ho ratios. Although positive Eu-anomaly is often regarded as high temperature hydrothermal signatures, it is not always the case for Archean chemical precipitates. Rather, it can be an Archean normal seawater signature (e.g. Danielson et al., 1992). Modern seawater and its derivatives are characterized by super-chondritic Y/Ho ratios, implying that the LC samples were not solely from seawater. In a Y/Ho-Eu-anomaly diagram (Fig. 2), LC samples show a positive correlation between these indices. This increasing trend of Y/Ho ratios and Eu positive anomaly coincides with the deepening upward stratigraphic trend of the Cleaverville Formation (Sugitani et al., 2003). Namely, the stratigraphic trends of Y/Ho ratios and Eu-positive anomalies in LC samples represent an increasing of seawater influence. On the other hand, CE1 and fossil-bearing CE2 samples are plotted within a relatively narrow area of chondritic to slightly super-chondritic Y/Ho ratios with negligible positive Eu anomalies. Namely, their features are distinct from the supposed contemporaneous seawater signatures. CE1 and CE2 black cherts are closely associated with evaporite deposits (Fig. 1) and are considered to have deposited in a closed to semi-closed basin at continental margin setting (Sugitani et al., 2003, 2007). Thus, the water mass, from which these cherts were precipitated, were likely influenced by non-marine water such as continental run-off, ground water or geothermal water. REE+Y signatures suggest that such the influence of non-marine water was more significant for CE1 cherts. It should be noted that REE+Y features of VC samples are distinct from the microfossil-bearing CE2 cherts. Although their origins are not constrained, it is unlikely that they are products of high-temperature hydrothermal activities.

Conclusions

A systematic REE+Y study was performed on the black carbonaceous cherts of four lithological types including microfossil-bearing cherts collected from the Mount Goldsworthy greenstone belt in the Pilbara Craton, Western Australia. In the Y/Ho-Eu-anomaly diagram, laminated to banded cherts (LC) from the Cleaverville Formation show a clear stratigraphic trend of increasing Y/Ho ratio and Eu positive anomaly. This trend suggests the increase of seawater influence with the deepening upward stratigraphic trend. Stratiform massive cherts associated with evaporites (CE1 and CE2) from the Farrel Quartzite are characterized by chondritic to slightly super-chondritic Y/Ho ratios and negligible positive Eu-anomalies. These features are distinct from the supposed contemporaneous seawater signatures, and suggest contribution of non-marine components. The results of this study and their close association with evaporite deposits suggest that the microfossil-bearing black cherts (CE2) and their equivalents (CE1) were deposited in a closed to semi-closed basin where influx of non-marine water was significant. It can be implied that non-marine ecosystems composed of diverse microorganisms were already flourished at least 3.0 Ga.

Acknowledgements

This study was supported by a grant-in-aid support by the Japan Society for the Promotion of Science (No. 19340150). We specially express our gratitude to Dr. K. Grey for her support to our fieldwork in the Pilbara Craton and to Dr. M.J. Van Kranendonk for his helpful comments on interpretations of geology of Mount Grant and Mount Goldsworthy area and for constructive comments.

References

Danielson A., Moller P. & Dulski P., 1992, The europium anomalies in banded iron formations and the thermal history of the oceanic crust, Chemical Geology, 97, 89–100

Grey K. & Sugitani K., 2009, Palynology of Archean microfossils (ca. 3.0 Ga) from the Mount Grant area, Pilbara Craton, Western Australia: further evidence of biogenicity, Precambrian Research, 173, 60–69

Oeher D.Z., Robert F., Walter M.R., Sugitani K. Allwood A., Meibom A., Mostefaoui S., Selo M., Thomen A. & Gibson E.K., 2009, NanoSIMS: insights to biogenicity and syngeneity of Archaean carbonaceous structures, Precambrian Research, 173, 70–78

Smithies R.H., Van Kranendonk M.J. and Hickman A.H., 2004, De Grey, W.A. Sheet 2757 (Version 2.0), Western Australia Geological Survey, 1:100 000 Geological Series.

Sugitani K., Grey K., Allwood A., Nagaoka T., Mimura K., Minami M., Marshall C.P., Van Kranendonk M.J. & Walter M.R., 2007, Diverse microstructures from Archaean chert from the Mount Goldsworthy-Mount Grant area, Pilbara Craton, Western Australia: Microfossils and dubiofossils, pseudofossils? Precambrian Research, 158, 228–262

Sugitani K., Mimura K., Suzuki K., Nagamine K. & Sugisaki R., 2003, Stratigraphy and sedimentary petrology of Archean volcanic-sedimentary succession at Mt. Goldsworthy in the Pilbara Block, Western Australia: implications of evaporite (nahcolite) and barite deposition, Precambrian Research, 120, 55–79

Yamamoto K., Itoh N., Matsumoto T., Tanaka T. & Adachi M., 2004, Geochemistry of Precambrian carbonate intercalated in pillows and its host basalt: implications for the REE composition of circa 3.4 Ga seawater, Precambrian Research, 135, 331–344

NEW INSIGHTS INTO THE EARLY EVOLUTION OF LIFE: EVIDENCE FROM THE PILBARA CRATON

K. Sugitani[1], K. Grey[2, 5], K. Mimura[1], M. Van Kranendonk[2, 5], D.Z. Oehler[3], E.J. Javaux[4], K. Lepot[4] & M.R. Walter[5]

[1]Graduate School of Environmental Studies, Nagoya University, Nagoya 464-8601, Japan
[2]Geological Survey of Western Australia, Department of Mines and Petroleum, East Perth, Australia
[3]Astromaterials Research and Exploration Science, NASA - Johnson Space Center, TX 7705, USA
[4]Department of Geology, University of Liège, Liège 4000, Belgium
[5]Centre for Astrobiology, University of New South Wales, Sydney, Australia

Introduction

Sugitani et al. (2007) reported carbonaceous microstructures with diverse morphologies from the ca. 3.0 Ga Farrel Quartzite of the Gorge Creek Group, Pilbara Craton, Western Australia, and suggested a highly probable to possible biogenic origin for them. The results of that study have been supported by new geochemical and paleontological lines of evidence (Grey & Sugitani, 2009; Sugahara et al., 2010; Sugitani et al., 2009a,b; Oehler et al., 2009a, b), in addition to the continued accumulation of data from more than 2000 specimens. In this study, we summarize the results of our studies on the Farrel Quartzite microfossil assemblage and report the presence of similar-shaped structures in the ca. 3.4 Ga, stromatolite-bearing Strelley Pool Formation. Several unresolved problems of these structures are discussed, in order to propose a potential research strategy for revealing their significance to the early evolution of life.

The Farrel Quartzite microfossil assemblage

The Farrel Quartzite microfossil assemblage is contained in stratiform black chert ca. 30cm thick in the uppermost portion of the ca. 3.0 Ga Farrel Quartzite in the Mount Goldsworthy greenstone belt. The black chert is closely associated with evaporite beds and was probably deposited in a closed to semi-closed basin. Similar microfossil assemblages have been found from more than 10 localities along a continuous strike length of 7 km. Five major morphological types of microfossils have been identified, including threads, film-like structures, small (<15μm) spheroids often comprising colony-like clusters, relatively large (>15μm) solitary spheroids, and lenticular to spindle-like structures. Spheroids and spindles are up to 80μm or more in maximum dimension. Biogenicity of these microstructures was inferred from the indigenousness and syngenicity, the sedimentary origin of the host chert, and narrow size range, chemical composition, evidence of flexible and/or breakable walls, apparent taphonomic features and the presence of colony-like aggregations (Sugitani et al., 2007). This was supported by the facts that the structures are organic-walled and can be extracted by palynological processes (Grey & Sugitani, 2009), and that the structures are enriched in nitrogen and sulfur as well as carbon (Oehler et al., 2009a, b). A systematic rare-earth element and yttrium study showed that the host carbonaceous cherts were deposited in a moderate and habitable environment, but not in a high-temperature hydrothermal environment (Sugahara et al. 2010). Sugitani et al. (2009a) also reconstructed three-dimensional images of selected specimens and demonstrated the three-dimensionally preserved complex morphologies represented by a flange-like appendage surrounding the body of spindle-like structure, providing further evidence for the biogenicity of the Farrel Quartzite assemblage.

Microstructures from the Strelley Pool Formation

The Strelley Pool Formation (Hickman, 2008), formerly named the Strelley Pool Chert, is known to contain well-preserved and morphologically diverse stromatolites (e.g., Allwood et al., 2006). Results of our recent microscopic study show that carbonaceous black chert associated with stromatolites and evaporites in this formation also contains structures morphologically similar to the Farrel Quartzite assemblage, from three remote and far-separated sites in the Panorama, Warralong, and Mount Goldsworthy greenstone belts. Spheroids and lenticular to spindle-like structures have been identified from all the three sites, and film-like structures from two sites. Large spheroids (>15μm) are not abundant and tend to be solitary (Fig. 1a), or rarely in pairs (Fig. 1b). Small spheroids of similar size (<10μm) occur as colony-like clusters, occasionally with a fluffy envelope or film-like structures (Fig. 1c). The majority of lenticular to spindle-like structures range from 40 to 60 μm along the major axis. They are solitary in many cases (Fig. 1d), although several colony-like clusters and pairs have been identified (Fig. 1e). Some spindle-like structures appear to have flange-like appendage, like those found from the Farrel Quartzite assemblage.

Discussion

Unresolved problems of the Farrel Quartzite microfossil assemblage

While the biogenic origin of the Farrel Quartzite microstructures seems to be nearly established, some fundamental problems remained unresolved. Namely, taxonomy and phylogeny of the Farrel Quartzite assemblage are poorly understood. In other words, it is not clear whether the morphological diversity actually correlates to biotic diversity, and it is difficult to explain why many specimens have unusually large size (> 20μm, and occasionally up to 80μm along the major axis), unexpected for Archean prokaryotic microfossils. In order to solve these problems, Sugitani et al. (2009b) focused on complex structures, such as 1) pair of attached spheroids or spindles (Fig.1g, h); 2)

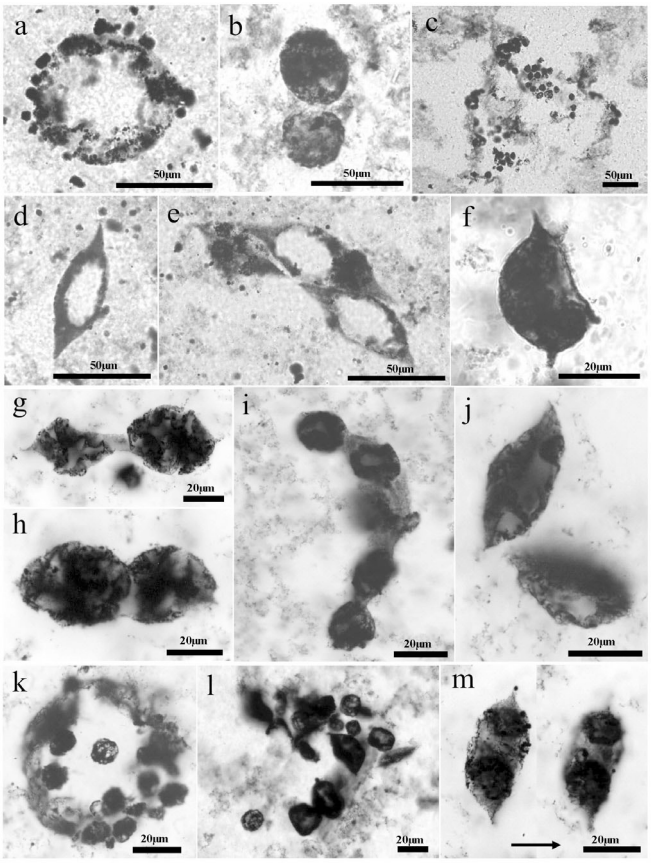

Figure 1. Photomicrographs of microstructures from the Strelley Pool Formation (a-f) and the Farrel Quartzite (g-m).

chain-like arrangement of multiple lenticular structures (Fig. 1i); 3) oblique arrangement of two lenticular to spindle-like structures (Fig.1j); 4) colony-like cluster composed of a single large spheroid and multiple small spheroids, or mixture of spheroids and spindles (Fig. 1k, l); and 5) spheroid or spindle-like structure with an inner object (Fig. 1m). Some of these complex structures and occurrences were interpreted to represent reproductive or resting stages of cells. The authors suggested the possibility that the morphological variations of the Farrel Quartzite assemblage are at least partially attributed to life cycle variants, although statistical analyses of these complex structures are still insufficient.

Features of the Strelley Pool microstructures and suggested further studies

Microstructures from the Strelley Pool Formation are embedded within a microcrystalline quartz matrix. Film-like structures and walls of spheroids and lenticular to spindle-like structures are composed of black to dark brown material. They are variable in appearance, ranging from hyaline to granular, and in some cases are deformed or partially broken (Fig. 1a, d, f). Morphologies of these structures are independent of crystal boundaries of the matrix chert. Some specimens are found cut by veins. They appear to have been locally subjected to the same alteration events such as silicification and ferruginization as their matrix. Carbon isotopic values of host cherts are light, less than 30 per mil. These features imply the possibility that they are biogenic structures, like the Farrel Quartzite assemblage. At this stage, however, their origins have not yet fully and rigorously discussed. Further detailed studies will be required in order to confirm their biogenicity. Statistic analyses of their size are indispensable, in order to know whether they have a narrow size range or not. In addition, Raman data of the individual structures should be obtained, in order to confirm their carbonaceous compositions.

Conclusion

The ca. 3.0 Ga Farrel Quartzite and the ca. 3.4 Ga Strelley Pool Formation in the Pilbara Craton, Western Australia seem to provide quite important information about the early evolution of life. They contain large (~80μm) and complex structures that are unexpected for Archean microfossils, such as lenticular to spindle-like structures with a flange-like appendage. Also complex structures similar to reproductive cells are common. Though the whole picture of the Farrel Quartzite microfossil assemblage has not yet been fully revealed and the biogenicity of microstructures of the Strelley Pool Formation is still under consideration, further studies that include developing and involving new techniques and methodologies should solve these problems. If these studies do corroborate both biogenicity and syngeneity, we could suggest that Archean life might have been more evolved and comprised more complex ecosystems than generally expected. Finally, it should be noted that spheroidal and spindle-like carbonaceous structures, similar or even larger in size than the Farrel Quartzite microfossils, were previously reported from the Barberton greenstone belt, South Africa, almost contemporaneous with the Strelley Pool Formation (Walsh, 1992), although this finding has been controversial. Recently large (up to 300 μm) spheroidal organic-walled microfossils have been reported from the 3.2 Ga Moodies Group shales, the Barberton greenstone belt (Javaux et al, 2010). Comparative studies of these four assemblages from different cratons and ages also would provide new insights into the early evolution of life and the biotic diversity in the Archean.

Acknowledgements

K.S. wishes to acknowledge Mr. T. Nagaoka for preparing many thin sections indispensable for this study, and financial support from the Japan Society for the Promotion of Science (a grant-in-aid, No. 19340150). Kath Grey publishes with the permission of the Executive Director, Geological Survey of Western Australia.

References

Allwood A.C., Walter M.R., Kamber B.S., Marshall C. & Burch, I., 2006, Stromatolite reef from the Early Archean era of Australia, Nature, 441, 714–718.

Grey K., Sugitani K., 2009, Palynology of Archean microfossils (c. 3.0 Ga) from the Mount Grant area, Pilbara Craton, Western Australia: further evidence of biogenicity, Precambrian Research, 173, 60–69.

Hickman, A.H., 2008, Regional review of the 3426-3350 Ma Strelley Pool Formation, Pilbara Craton, Western Australia, Geological Survey of Western Australia, Record 2008/15.

Javaux E.J., Marshall C.P., Bekker A., 2010, Organic-walled microfossils in 3.2-billion-year-old shallow-marine siliciclastic deposits", Nature, (AOP), http://dx.doi.org/10.1038/nature08793

Oehler D.Z., Robert F., Walter M.R., Sugitani K., Allwood A., Meibom A., Mostefaoui S., Selo M., Thomen A. & Gibson E.K., 2009a, NanoSIMS: insights to biogenicity and syngeneity of Archaean carbonaceous structures, Precambrian Research, 173, 70–78.

Oehler D.Z., Robert F., Walter M.R., Sugitani K., Meibom A., Mostefaoui S. &, Gibson E.K., 2009b, Diversity in the Archaean biosphere: New insights from NanoSIMS, Astrobiology, under review.

Sugahara H, Sugitani K., Mimura K., Yamashita F. & Yamamoto K., 2010, A systematic rare-earth elements and yttrium study of Archean cherts at the Mount Goldsworthy greenstone belt in the Pilbara Craton: Implications for the origin of microfossil-bearing black cherts, Precambrian Research, 177, 73–87.

Sugitani K., Grey K., Allwood A., Nagaoka T., Mimura K., Minami M., Marshall C.P., Van Kranendonk M.J., Walter M.R., 2007, Diverse microstructures from Archaean chert from the Mount Goldsworthy-Mount Grant area, Pilbara Craton, Western Australia: Microfossils, dubiofossils, or pseudofossils? Precambrian Research, 158, 228–262.

Sugitani K., Grey K., Nagaoka T. & Mimura K., 2009a, Three-dimensional morphological and textural complexity of Archean putative mmicrofossils from the northeastern Pilbara Craton: Indications of biogenicity of large (>15µm) spheroidal and spindle-like structures, Astrobiology 9, 603–615.

Sugitani K., Grey K., Nagaoka T., Mimura K. & Walter M., 2009b, Taxonomy and biogenicity of Archaean spheroidsl microfossils (ca. 3.0 Ga) from the Mount Goldsworthy-Mount Grant area in the northeastern Pilbara Craton, Western Australia, Precambrian Research, 173, 50–59.

Walsh M.M., 1992, Microfossils and possible microfossils from Early Archean Onverwacht Group, Barberton Mountain Land, South Africa, Precambrian Research 54, 271–292.

THE ROLE OF KOMATIITE IN GOVERNING BANDED IRON FORMATIONS IN THE EARLY EARTH

H. Xu[1], Y. Wang[2] & H. Kosnishi[1]

[1]NASA Astrobiology Institute, Department of Geoscience, University of Wisconsin – Madison, Madison, Wisconsin 53706, USA
[2] Sandia National Laboratories, P. O. Box 5800, Albuquerque, New Mexico 87185, USA

Banded iron formation (BIFs) that occurred only episodically in time and sporadically in space offer clues to the environment of the early Earth. In general, BIFs were formed between ~3.8 and ~1.65 billion years ago at what was then the bottoms of the ocean and sea (Trendall & Blockley, 1970; Meyer, 1985; Trendall, 2002; Klein, 2005). The BIFs contain alternating layers of silica-rich chert layer and iron-rich minerals like hematite and magnetite (Fig. 1). Banded iron formations (BIFs) carry important information on the early evolution of the Earth (Ohmoto et al., 2004; Canfield, 2005; Kasting, & Howard, 2006). Unfortunately, the actual mechanism for their formation still remains controversial. Our new results show that the predominant occurrence of BIFs in the Achaean-Paleoproterozic period may be controlled by the compositional changes in the oceanic crust. BIF formation requires Fe-Si-rich geologic fluids. Such fluids can be generated only from the early oceanic crust (Al-poor komatiite) through hydrothermal leaching by seawater (Fig. 2) (Wang et al., 2009).

Komatiites are very-low-Al, Fe-bearing basalts. Komatiites erupted in a large variety of tectonic settings. Most were emplaced in an oceanic environment, some as parts of the oceanic crust but the majority within oceanic plateaus (Arndt et al, 2008). They have spatial and temporal links with Banded Iron Formations. Figure 3 clearly indicates that BIFs and komatiites both occurred roughly in the same span of time from 3.8 to 1.7 Ga. Even more interestingly, Isley & Abbott (1999) provided a detailed analysis for the temporal correlation between BIFs and komatiites (an indicator of mantle plume activity). They have compiled ages of 37 komatiites, 36 mafic dike sequence, 21 layered ultramafic intrusions, 5 Archean/ paleoproterozic basalt sequences, and 54 BIFs. Over this time period, the ages of komatiites, and those of global plumes, correlate strongly, at the 99% confidence level, with the ages of banded iron formations (BIFs) (Isley & Abbott, 1999). This strong temporal correlation between BIFs and komatiites can clearly be seen in Figure 3.

Close spatial links between BIFs and komatiites are commonly observed, especially in the Algoma-type of BIFs. It is reported in the Mauranipur greenstone belt in Central India, BIFs overlying metasediments are surrounded by basaltic komatiites (Malviya et al., 2006). A similar spatial relationship can be seen in Kostomuksha greenstone belt, NW Baltic Shield. In the Rio Das Vehas greenstone belt in Brazil, komatiitic basalts are intercalated with abundant BIFs (Zucchetti et al., 2000). In the eastern belt of the Archean Yigarn Block in Western Australia, BIFs are intimately associated with komatiites (Barnes et al., 1993).

Although the dominant igneous rock type in all BIF regions were tholeitic basalt, the tholeitic basalts in Archean greenstone sequences are usually interlayered with komatiitic flows (Campbell et al., 1989). This close association between the two is attributed to the unique nature of mantle plumes originating in a much hotter Archean mantle. The fluid dynamic calculation carried out by Campbell et al. (1989) indicates that komatiites could form by melting in the high-temperature axis (the tail) of a mantle plume while basalts would form by melting in the cooler head. Isley & Abbott (1999) have

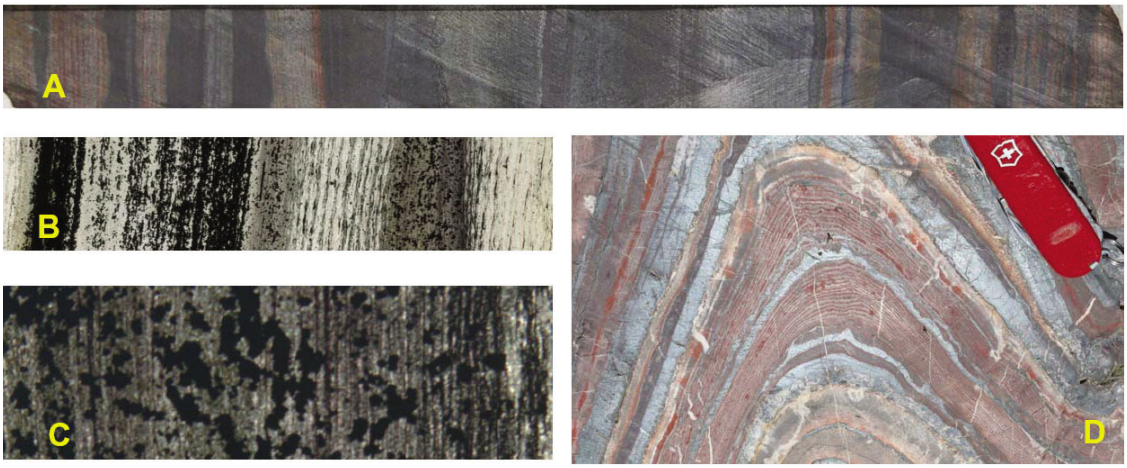

Figure 1. Photographs of banded iron formations (BIFs). One Hamersley core sample exhibits both meso-bands and mm-scale micro-bands in core sample (A) and thin section (B-C). The length for the samples in (A), (B) and (C) are 21.5 cm, 4 cm, and 0.56 cm, respectively. Similar features are also observed in an Achaean BIF nearby Mine Building of Soudan Underground Mine State Park, Soudan, Minnesota (D). See Supplementary Information for a large area view of the exposed BIF.

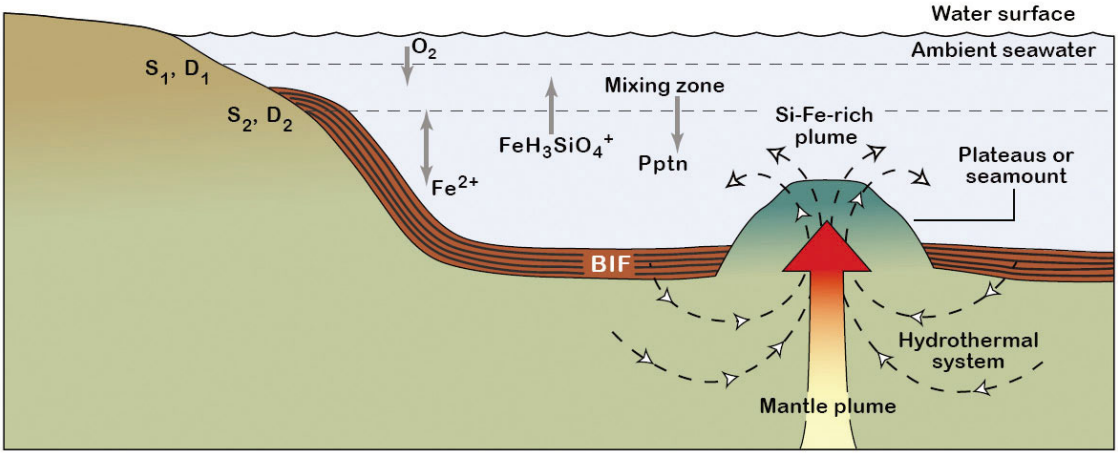

Figure 2. Precipitation of banded iron formations (BIFs) from a hydrothermal system. The ambient seawater could be either oxic or anoxic (only the former is shown here). Komatiitic rocks formed as a part of plateaus or seamounts above a deep mantle plume. Periodic precipitation of iron oxide and silica was induced through a self-organization mechanism. Pptn – mineral precipitation; S_1, D_1 – the area of the upper surface of the mixing zone and the corresponding mass exchange coefficient for mixing, respectively; S_2, D_2 – the area of the lower surface of the mixing zone and the corresponding mass exchange coefficient for mixing, respectively.

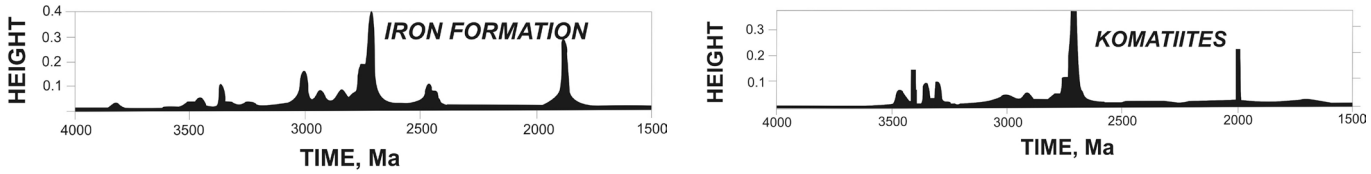

Figure 3. Time series of occurrences of banded iron formations (A) and komatiites (B) (Modified from Isley and Abbott, 1999).

shown that three of four Archean and Paleoproterozic flood basalt sequences that they have compiled contain komatiitic units. Furthermore, mantle plumes beneath oceanic lithosphere are generally expressed by the formation of oceanic plateaus and seamounts (e.g., Isley & Abbott, 1999). Fe and Si leached from those hydrothermal systems may be transported away from the plateaus/seamounts and deposited on the surrounding oceanic floor or continental shelf. BIFs did not have to deposit directly on their original source rocks – komatiitic rocks.

Later enrichment of Al in the oceanic crust leads to the formation of Fe(II)-bearing chlorite during the leaching and the depletion of Fe2+ in leaching fluids, thus preventing BIF formation in recent geological time periods. We further show that periodic precipitation of iron and silica minerals can be induced by positive feedbacks among relevant chemical reactions as a Fe-Si-rich fluid mixes with its ambient seawater (Wang et al., 2009). Complexation of Fe2+ with silicic acid plays an important role in the whole process. Unlike previous hypotheses, the mechanism proposed here attributes BIF micro-bandings to the internal dynamics of the chemical system, rather than to an outside force such as surface temperature variations. Therefore, BIFs are expected to occur in both shallow and deep water environments, as observed.

Previous hypotheses about band formation involved seasonal fluctuations, temperature shifts, or periodic blooms of microorganisms, all of which left many open questions about how BIFs dominated the global marine landscape for two billion years and why they abruptly disappeared ~ 1.65 billion years ago (e.g., Trendall, & Blockley, 1970; Posth et al., 2009). Our newly developed a BIF formation model that offers a more complete picture of the environment at the time, including interactions between rocks, water, and air. The lithosphere affects the hydrosphere, the hydrosphere affects the atmosphere, and all those eventually affect the biosphere on the early Earth. Their absence in more recent rocks indicates that the earth conditions changed around 1.65 billion years ago. This change likely had wide-ranging effects on the physical and biological composition of the Earth. For example, the end of BIF deposition would have starved iron-dependent bacteria and shifted in favor of microbes with sulfur-based metabolisms. In addition, chemical changes and pH rise in the ocean, and rising atmospheric oxygen may have allowed the emergence and widespread distribution of organisms that entirely depend on the use of molecular oxygen.

References:

Arndit N.T., Lesher C.M. & Barnes S.J, 2008, *Komatiite*, Cambridge University Press.

Barnes S.J., Hill R.E.T., Kauahikaua J. & Perring C.S., 1993, Thermomechanical erosion by lava flows and the genesis of komatiite-hosted nickel sulphide deposits, Abstract for Kalgoorlie 93 Conference.

Canfield D.E., 2005, The Early History of atmospheric oxygen: Homage to Robert M. Garrels, Annual Reviews in Earth and Planetary Science, 33, 1–36.

Champbell I.H., Griffiths R.W. & Hill, R. I., 1989, Melting in an Archean mantle plume: heads it's basalts, tails it's komatiites, Nature, 339, 696–699.

Holm N.G., Dumont M., Ivarsson M. & Konn C., 2006, Alkaline fluid circulation in ultramafic rocks and formation of nucleotide constituents: a hypothesis, Geochemical Transactions, 7, 7.

Isley A.E. & Abbott D.H., 1999, Plume-related mafic volcanism and the deposition of banded iron formation, Journal of Geophysical Research 44(B7), 15461–15477.

James H.L. & Sims P.K., 1973, Precambrian iron-formations of world. Economic Geology, 68, 913–914.

Kasting J.F. & Howard M.T., 2006, Atmospheric composition and climate on the early Earth, Philosophical Transactions of the Royal Society, B, 361, 1733–1742.

Klein C., 2005, Some Precambrian banded iron-formations (BIFs) from around the world: Their age, geologic setting, mineralogy, metamorphism, geochemistry, and origin. American Mineralogist, 90, 1473–1499.

Meyer, C., 1985, Ore metals through Geologic history, Science, 227, 1421–1428.

Ohmoto H., Watanabe Y. & Kumazawa, K., 2004, Evidence from massive siderite beds for CO_2-rich atmosphere before ~1.8 billion years ago. Nature, 429, 395-399.

Posth N R., Hegler F., Konhauser K.O. & Kappler, A., 2008, Alternating Si and Fe deposition caused by temperature fluctuations in Precambrian oceans, Nature Geoscience, 1, 703–708.

Trendall A.F. & Blockley J.G., 1970, The iron formations of the Precambrian Hamersley Group, Western Australia, Geological Survey of Western Australia, Bulletin 119, 1–366.

Trendall A.F., 2002, The significance of iron-formation in the Precambrian stratigraphic record. 3rd International Association of Sedimentologists, Special Publication, 33, 33–66.

Wang Y., Xu H., Merino E., & Konishi H., 2009, Generation of banded iron formations by internal dynamics and leaching of oceanic crust, Nature Geoscience, 2, 781–784.

ENRICHMENT OF MOLYBDENUM IN MESOARCHAEAN BLACK SHALES: A PREIMINARY RESULT OF DXCL-DP (DIXON ISLAND-CLEAVERVILLE DRILLING PROJECT), PILBARA, WESTERN AUSTRALIA

K.E. Yamaguchi[12,3], R. Sakamoto[4], K. Hosoi[5], S. Kiyokawa[4], H. Naraoka[4], M. Ikehara[5] & T. Ito[6]

[1]Geochemical Laboratory, Department of Chemistry, Toho University, 2-2-1 Miyama, Funabashi , Chiba, Japan
[2]Precambrian Ecosystem Laboratory, Japan Agency for Marine-Earth Science and Technology, 2-15 Natsushima, Yokosuka, Kanagawa, Japan
[3]NASA Astrobiology Institute
[4]Department of Earth and Planetary Sciences, Kyushu University, Hakozaki, Fukuoka, Japan
[5]Center for Advanced Marine Core Research, Kochi University, Monobe, Nankoku, Kochi, Japan
[6]College of Education, Ibaraki University, Mito, Ibaraki, Japan

Introduction

Degree of enrichment of redox-sensitive metals in carbonaceous sediments and sedimentary rocks (i.e., black shales) and their association with organic carbon and sulfide have been used to indicate paleoredox conditions of the oceans and atmosphere (e.g., Holland, 1984, 1994). Molybdenum is one of such metals, and takes different valence states (and different solubilities in fluids) in the Earth's surface environments, depending on their surrounding redox conditions (i.e., dissolved O_2 content of weathering fluids). Biogeochemical cycle of Mo is redox-dependent. Molybdenum-bearing sulfides in continental rocks are, through oxidative weathering (dissolution), the major source of Mo into the ocean. Therefore, the weathering flux of Mo from continent depends on the redox state of the atmosphere. Carbonaceous sediments and sedimentary rocks are commonly enriched in Mo relative to average shales (Vine & Toutelot, 1970; Leventhal, 1993; Arthur & Sageman, 1994; Wignall, 1994). This is because organic matter and biologically produced sulfide in marine sediments (and later sedimentary rocks) are the major sink of dissolved Mo (or redox-sensitive metals in general) in the ocean (e.g., Morford & Emerson, 1999).

There are numerous studies on the geochemistry of redox-sensitive metals in modern sediments and Phanerozoic sedimentary rocks (e.g., Cretaceous blacks shales); however, there are only a limited number of studies for Precambrian sedimentary rocks (e.g., Naraoka *et al*., 2001; Yamaguchi & Ohmoto, 2001a, 2001b, 2002; Yamaguchi, 2002; Yamaguchi *et al*., 2004; Anbar *et al*. 2007; Scott *et al.* 2008). It has been widely believed that the pO_2 of the atmosphere drastically changed from the pre-GOE value of $<10^{-6}$ PAL to post-GOE value of $>10^{-2}$ PAL (GOE; Great Oxidation Event; e.g., Holland, 1994, 2002; Bekker *et al.*, 2004; PAL: present atmospheric level). To further evaluate the inferred GOE that has been believed to have occurred at 2.3 Ga ago, potential differences in the geochemistry of redox-sensitive metals in black shales before and after the GOE are apparently very important. Naraoka *et al*. (2001) first reported significant enrichment of Mo and correlations with contents and stable isotopic compositions of organic carbon and sulfide in the 2.5 Ga black shales (drillcores) of the Mt. McRae Shale, Hamersley Group, Pilbara, Western Australia. Several years later, discovery of Naraoka *et al.* (2001) was confirmed by a similar study by Anbar *et al*. (2007). They suggested that oxygenation of the atmosphere at around the GOE could have been earlier, by a few hundred million years, than commonly thought. Yamaguchi (2002) (also see Yamaguchi & Ohmoto, 2001a, b) reported positive correlation among Mo, organic carbon (C_{org}), and S in the Archean–Paleoproterozoic (3.2 ~ 2.2 Ga) drillcore black shales, and suggested that, based on data from 3.2 Ga black shales from the Fig Tree Group in the Barberton Greenstone Belt in South Africa, atmospheric oxygenation had possibly occurred much earlier. These discoveries need to be confirmed by different samples sets of the same or older ages.

Importance of drillcore samples

Surface weathering of sulfide-bearing black shales would result in oxidative dissolution of Mo-bearing sulfide minerals to generate sulphuric acid, which further accelerate weathering reactions. Some organic matter would also be decomposed by oxidative weathering. Therefore, in order to evaluate the degree of Mo enrichment in black shales, it is absolutely essential to obtain and use modern-weathering-free, high-quality fresh drillcore samples, rather than surface outcrop samples. This is especially true for samples in the early Earth.

Dixon Island – Cleaverville Drilling Project (DXCL-DP)

In order to newly obtain fresh drillcore samples of Mesoarchean black shales with negligible modern weathering, in summer 2007, we conducted continental drilling at Cleaverville coast in northwestern Pilbara region, Western Australia. We could recover 3.2 Ga sulfidic black shales of the Cleaverville Group from three drillholes (~200m in total), namely DX, CL1, and CL2. The age of the samples, ~3.2 Ga, is very important for the studies of the evolution of early Earth's environments, because it is much older, by several hundred million years,

than the period of the inferred GOE (2.3-2.4 Ga; e.g., Holland, 1994, 2002; Bekker *et al.*, 2004); no significant enrichment of Mo was expected to occur in the before-GOE black shales if pO_2 was as low as $<10^{-6}$ PAL. The second reason why we targeted this geologic unit is, as previously noted, to confirm the results of Yamaguchi (2002) that reported enrichment of Mo, associated with that of C_{org} and S, in the contemporaneous 3.2 Ga drillcore black shales from South Africa. Basic information on the geology of the drilling site and that on the DXCL-DP has been reported by Kiyokawa *et al.* (2006) and Yamaguchi *et al*. (2009), respectively. More detailed stratigraphy and carbon isotope geochemistry are to be reported in Kiyokawa *et al*. (2010) and Sakamoto *et al*. (2010). In this study, we report the discovery of Mo enrichment in the 3.2 Ga DXCL-DP black shales.

Preliminary Results and Discussion

We analyzed total chemical compositions of forty black shale samples from drillcore DX and fifty-six of those from CL1 and CL2, utilizing ICP-AES and ICP-MS methods following total decomposition of the samples by alkali fusion and mixed acid digestion Molybdenum concentrations for DX samples are from 0.3 to 12.9 ppm, with an average value of 1.8 ppm ($1\sigma = 1.9$), and those for CL1 and CL2 (combined) are from 0.8 to 3.3 ppm, with an average value of 1.4 ppm ($1\sigma = 0.4$). The highest concentration of Mo occurs in C_{org}-rich sample, and is comparable to that of the contemporaneous Fig Tree Group in South Africa (Yamaguchi & Ohmoto, 2001a, 2001b, 2002; Yamaguchi, 2002). The highest concentration of Mo in the DXCL-DP samples, ~13 ppm, is lower than that found in the 2.5 Ga Mt. McRae Shale of the Hamersley Group, Western Australia (maximums are ~17 ppm by Naraoka *et al*, 2001, and ~40ppm by Anbar *et al*., 2007). However, it is much higher, by thirteen times, than the average Mo concentration in the Phanerozoic shales (1 ppm; Vine & Toutelot, 1970). Therefore, we suggest that the 3.2 Ga old DXCL-DP black shales are enriched in Mo.

We also analyzed stable isotope compositions of organic carbon and sulfur contained in the same sample suites. Details are to be presented by Sakamoto *et al.* (2010). We suggest, based on the variable $\delta^{34}S$ values (–1.9 ~ +26.8 ‰), that bacterial sulfate reduction was so extensive in the 3.2 Ga relatively deep marine sediments that utilization of sulfate by sulfate-reducers was near completion. Depositional environments for laminated shales in general should have been deep enough to accumulate very fine-grained sediments in calm environments, typically below the wave-base. Production of bacteriogenic sulfide would have enhanced fixation of dissolved Mo into sulfide minerals in sediments. This is rather a common process occurring in oxygen-depleted environments in the modern ocean overlain by an oxic atmosphere (e.g., Morford & Emerson, 1999). A combined enrichment of Mo, C_{org}, and S, together with high $\delta^{34}S$ values for a sedimentary formation may be used as a strong evidence for operation of modern-day style mechanism of sedimentary Mo enrichment. This further implies that oxygenation of the atmosphere and (at least the surface) oceans was significant during deposition of the sediments. Therefore, such oxygenation could have already started by at least 3.2 Ga ago, ~800 Ma earlier than commonly thought (e.g., Holland, 1994, 2002; Bekker *et al.*, 2004).

Surface oceans should be generally oxic if the overlying atmosphere is oxic. Locally, dissolved oxygen is often depleted in mid-depth oxygen-minimum zone (OMZ). In contrast, deep ocean can be temporarily anoxic on a global scale, as it probably happened in the Cretaceous (known as OAE: Oceanic Anoxic Event). Oxygenation of atmosphere, once occurred, is a global phenomenon and could not have been a reversible process, as Lasaga & Ohmoto (2002) suggest based on a dynamic numerical model for geochemical cycle of oxygen. Anbar et al. (2007) suggested that there was a whiff of oxygen into the 2.5 Ga atmosphere (before the inferred GOE at 2.3 Ga), based on the previously-mentioned confirmation of the results of Naraoka et al. (2001) for Mo enrichment in the black shales of the 2.5 Ga Mt. McRae Shale. If atmospheric oxygenation is irreversible while oceanic oxygenation is reversible, then it comes to that the global oxygenation could have started by at least 2.5 Ga. The present study, based on a similar data set of Anbar et al. (2007), may push back this important age of global oxygenation to 3.2 Ga ago. We suggest that OAE-type of redox structure of the ocean, i.e., oxygenated surface ocean is overlain by an oxic atmosphere and underlain by oxygen-depleted deep ocean, could have been the case for the Earth's surface environment 3.2 Ga ago. Operation of present-day style geochemical cycle of Mo in the Mesoarchean surface environments suggests early evolution of atmosphere, oceans, and microbial biosphere.

Acknowledgements

Arthur Hickman, Hiroshi Ohmoto, Yumiko Watanabe, Munetomo Nedachi, and Takeshi Kakegawa are thanked for their continued contributions to many aspects related to DXCL-DP. This study was financially supported by the Grant-in-Aid for Scientific Research from MEXT (Japanese Ministry of Education, Culture, Sports, Science and Technology) and JSPS (Japan Society for the Promotion of Science).

References

Anbar A.D., Duan Y., Lyons T.W., Arnold G.L., Kendall B., Creaser R.A., Kaufman A.J., Gordon G.W., Garvin J. & Buick R., 2007, A Whiff of Oxygen Before the Great Oxidation Event, Science, 317 1903–1906.

Arthur M.A. & Sageman B.B., 1994, Marine black shales: Depositional mechanism and environments of ancient deposits. Annual Reviews in Earth and Planetary Science, 22, 499–551.

Bekker A., Holland H.D., Wang P.L., D. Rumble III, H.J. Stein, J.L. Hannah, L.L. Coetzee & N.J. Beukes, 2004, Dating the rise of atmospheric oxygen, Nature, 427: 117–120.

Holland H.D., 1984, The chemical evolution of the atmosphere and oceans, Princeton University, Press, Princeton.

Holland H.D., 1994, Early Proterozoic atmospheric change. in *Early Life on Earth*, Novel Symposium No. 84, Bengston S., ed., Columbia University Press, New York.

Holland H.D., 2002, Volcanic gases, black smokers, and the great oxidation event. Geochimica et Cosmochimica Acta, 66: 3811–3826.

Kiyokawa S., Ito T., Ikehara M., Kitajima F., 2006, Middle Archean volcano-hydrothermal sequence: Bacterial microfossil-bearing 3.2 Ga Dixon Island Formation, coastal Pilbara terrane, Australia, Geological Society of America Bulletin, 118, 3–22.

Kiyokawa S., Ito T., Ikehara M., Yamaguchi K.E., Naraoka H., Sakamoto R., Koge S., Hosoi K. & Suganuma Y., 2010, Mesoarchean hydrothermal oceanic sedimentation and environment: DXCL Drilling Project, West Pilbara, Australia. This volume.

Naraoka H., Kakegawa T., Ohmoto H., 2001, C, S, and N isotope excursions of biogenic products in the 2.7 Ga Jeerinah Formation, Hamersley district, Western Australia. 4th International Archaean Symposium, Perth.

Lasaga A.C., Ohmoto H., 2002, The oxygen geochemical cycle: dynamics and stability. Geochimica Cosmochimica Acta, 66, 361–381.

Leventhal J., 1993, Metals in Black Shales, in *Organic Geochemistry: Principles and Applications*, Engel M.H. & Macko S.A., eds, 581–592.

Morford J.L., Emerson S., 1999, The geochemistry of redox sensitive trace metals in sediments, Geochimica et Cosmochimica Acta, 63: 1735–1750.

Sakamoto R., Kiyokawa S., Ito T., Ikehara M., Naraoka H., Yamaguchi K.E., Suganuma Y., 2010, Reconstruction of 3.2 Ga ocean floor environment from cores of DXCL Drilling Project, Pilbara, Western Australia: Results of stratigraphic analysis and sulfur isotope analysis, this volume.

Scott C., Lyons T. W., Bekker A., Shen Y., Poulton S. W., Chu X. and Anbar A. D., 2008, Tracing the stepwise oxygenation of the Proterozoic ocean, Nature, 452, 456-459.

Vine J.D., Tourtelot E.B., 1970, Geochemistry of black shale deposits: A summary report, Economic Geology, 65, 253–272.

Wignall P.B., 1994, *Black Shales*, Oxford University Press, Oxford, 127p.

Yamaguchi K.E., Ohmoto H., 2001a, Molybdenum and organic carbon in Archean black shales, Evidence for aerobic ocean, in *Earth System Processes*, Edinburgh.

Yamaguchi K.E., Ohmoto H., 2001b, Organic carbon, S, Mo, U, and V in Archean and Paleoproterozoic black shales, Astrobiology, 1, 414.

Yamaguchi K.E., 2002, Geochemistry of Archean-Paleoproterozoic black shales: Early Evolution of the atmosphere, oceans, and biosphere, Ph.D. dissertation, The Pennsylvania State University, 485p.

Yamaguchi K.E., Ohmoto H., 2002, Molybdenum geochemical cycle in the Archean, Geological Society of America Annual Meeting, Denver.

Yamaguchi K.E., Johnson C.M., Beard B.L., Ohmoto H., 2004, Iron isotope perspective for Molybdenum enrichment in the Archean Lewin shales and Carawine dolomites of the eastern Hamersley Basin, Western Australia, International Journal of Astrobiology, 1, 45.

Yamaguchi K.E., Kiyokawa S., Ito T., Ikehara M., Kitajima F., Suganuma Y., 2009, Clues of Early Life: Dixon Island - Cleaverville Drilling Project (DXCL-DP) in the Pilbara Craton of Western Australia, Scientific Drilling, 7, 34–37.

This Record is published in digital format (PDF) and is available online at <www.dmp.wa.gov.au/GSWApublications>.
Laser-printed copies can be ordered from the Information Centre for the cost of printing and binding.

Further details of geological products produced by the Geological Survey of Western Australia can be obtained by contacting:

Information Centre
Department of Mines and Petroleum
100 Plain Street
EAST PERTH WESTERN AUSTRALIA 6004
Phone: (08) 9222 3459 Fax: (08) 9222 3444
www.dmp.wa.gov.au/GSWApublications